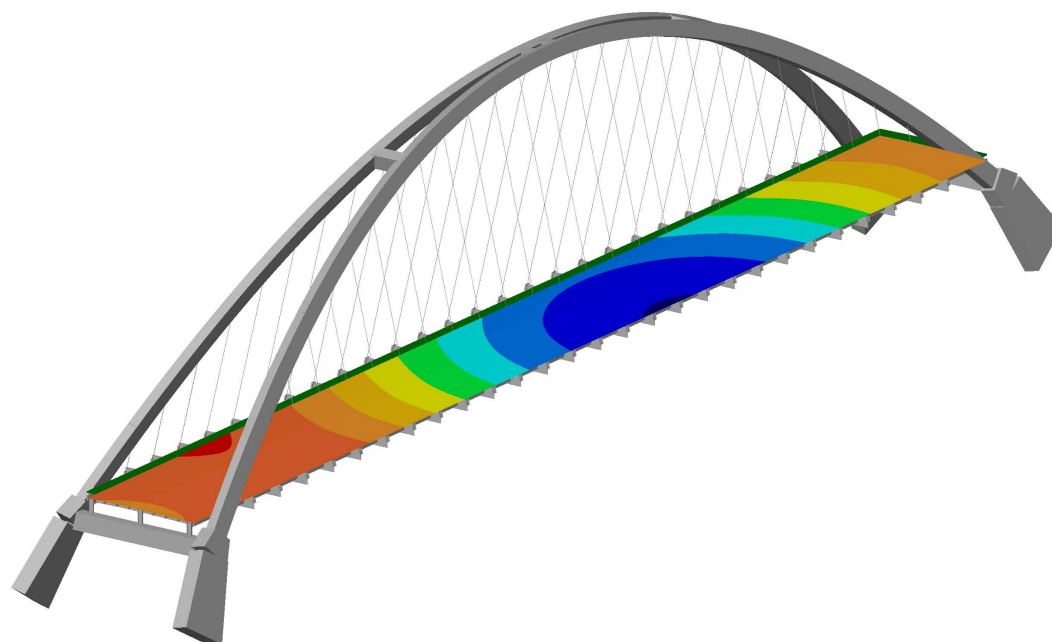


Manual for Refined Analysis in Bridge Design and Evaluation

May 2019



U.S. Department of Transportation
Federal Highway Administration

Sponsored by

Federal Highway Administration
Office of Infrastructure
FHWA-HIF-18-046

Foreword

This manual provides technical guidance on using refined methods of analysis for design and evaluation of highway bridges, to supplement the provisions and commentary of the AASHTO specifications. The application of refined methods is needed when a bridge design falls outside of the limits for the approximate methods in the AASHTO specifications or when refined methods can provide a more rigorous treatment to appropriately account for unique details and/or behaviors. Refined methods can also be used to achieve a more effective design or a more accurate load rating. To generate confidence, this manual includes seven case study analysis examples and provides trusted results that can be used by software providers and engineers to verify their modeling techniques.

The hard and competent work of Modjeski and Masters, Inc. in producing this manual is gratefully acknowledged. In addition, the quality of the final product benefitted from key contributions of reviewers including Brandon Chavel (National Steel Bridge Alliance), Duncan Paterson (HDR), Don White (Georgia Tech Univ.), Toorak Zokaie (Caltrans), and Sue Hida (Caltrans).



Joseph L. Hartmann, Ph.D., P.E.
Director, Office of Bridges and Structures

Notice

This document is disseminated under the sponsorship of the U.S. Department of Transportation (USDOT) in the interest of information exchange under Task 2 of the FHWA Cooperative Agreement DTFH61-11-H-00027. The U.S. Government assumes no liability for the use of the information contained in this document.

The U.S. Government does not endorse products or manufacturers. Trademarks or manufacturers' names appear in this report only because they are considered essential to the objective of the document. They are included for informational purposes only and are not intended to reflect a preference, approval, or endorsement of any one product or entity.

Quality Assurance Statement

The Federal Highway Administration (FHWA) provides high-quality information to serve Government, industry, and the public in a manner that promotes public understanding. Standards and policies are used to ensure and maximize the quality, objectivity, utility, and integrity of its information. FHWA periodically reviews quality issues and adjusts its programs and processes to ensure continuous quality improvement.

TECHNICAL REPORT DOCUMENTATION PAGE

1. Report No. FHWA-HIF-18-046	2. Government Accession No.	3. Recipient's Catalog No.	
4. Title and Subtitle Manual for Refined Analysis in Bridge Design and Evaluation		5. Report Date May 2019	
		6. Performing Organization Code	
7. Author(s) Andrew Adams, Nohemy Galindez, Travis Hopper, Thomas Murphy, Philip Ritchie, Vanessa Storlie, Jared Weisman		8. Performing Organization Report No.	
9. Performing Organization Name and Address Modjeski and Masters 100 Sterling Parkway, Suite 302 Mechanicsburg, PA 17050		10. Work Unit No.	
		11. Contract or Grant No. DTFH61-11-H-00027	
12. Sponsoring Agency Name and Address Federal Highway Administration Office of Infrastructure – Bridges and Structures 1200 New Jersey Ave., SE Washington, DC 20590		13. Type of Report and Period Covered	
		14. Sponsoring Agency Code	
15. Supplementary Notes Work funded by Cooperative Agreement "Advancing Steel and Concrete Bridge Technology to Improve Infrastructure Performance" between FHWA and Lehigh University. FHWA Technical Manager: Brian M. Kozy PhD, PE			
16. Abstract This manual provides guidance on performing refined analysis of bridges. The manual describes "refined analysis" and the methods allowed by AASHTO LRFD. Guidance for the modeling of typical girder bridges at various levels of complexity are provided. Additional guidance is provided for modeling prestressed and post-tensioned concrete girder bridges, fatigue and mechanical connections in steel bridges, and modeling of substructures as well as for more advanced topics such as soil-structure interaction and nonlinear and dynamic analyses. Methods and examples of verifying and validating the output from an analysis software are provided. Discussion of the various loads bridges are subjected to and how to apply the loads in refined analyses is included. The last chapter discusses how to take the results from the refined analysis and go forward to the design of a structure. Also included are seven example problems and comparison of the results from different levels of analysis. The seven examples are: 1. Three-span, Precast Concrete I-Girder Bridge made continuous for live load, 2. Three-span Continuous Steel I-Girder Bridge, 3. Three-span Continuous Curved Steel I-Girder Bridge on skewed supports, 4. Three-span Continuous Concrete Box Girder Spine Beam, 5. Dynamic Analysis of a Curved Steel Girder Bridge, 6. Stability Analysis of a Tall Concrete Pier Column, 7. Four-span Continuous, Precast Segmental Concrete Box Girder Bridge.			
17. Key Words refined analysis, FEA, finite element analysis, modeling, bridge design, bridge analysis		18. Distribution Statement No restrictions. This document is available to the public online and through the National Technical Information Service, Springfield, VA 22161.	
19. Security Classif. (of this report) Unclassified	20. Security Classif. (of this page) Unclassified	21. No of Pages 709	22. Price Free

(This page intentionally left blank)

SI* (MODERN METRIC) CONVERSION FACTORS

APPROXIMATE CONVERSIONS TO SI UNITS

Symbol	When You Know	Multiply By	To Find	Symbol
LENGTH				
in	inches	25.4	millimeters	mm
ft	feet	0.305	meters	m
yd	yards	0.914	meters	m
mi	miles	1.61	kilometers	km
AREA				
in ²	square inches	645.2	square millimeters	mm ²
ft ²	square feet	0.093	square meters	m ²
yd ²	square yard	0.836	square meters	m ²
ac	acres	0.405	hectares	ha
mi ²	square miles	2.59	square kilometers	km ²
VOLUME				
fl oz	fluid ounces	29.57	milliliters	mL
gal	gallons	3.785	liters	L
ft ³	cubic feet	0.028	cubic meters	m ³
yd ³	cubic yards	0.765	cubic meters	m ³
NOTE: volumes greater than 1000 L shall be shown in m ³				
MASS				
oz	ounces	28.35	grams	g
lb	pounds	0.454	kilograms	kg
T	short tons (2000 lb)	0.907	megagrams (or "metric ton")	Mg (or "t")
TEMPERATURE (exact degrees)				
°F	Fahrenheit	5 (F-32)/9 or (F-32)/1.8	Celsius	°C
ILLUMINATION				
fc	foot-candles	10.76	lux	lx
fl	foot-Lamberts	3.426	candela/m ²	cd/m ²
FORCE and PRESSURE or STRESS				
lbf	poundforce	4.45	newtons	N
lbf/in ²	poundforce per square inch	6.89	kilopascals	kPa

APPROXIMATE CONVERSIONS FROM SI UNITS

Symbol	When You Know	Multiply By	To Find	Symbol
LENGTH				
mm	millimeters	0.039	inches	in
m	meters	3.28	feet	ft
m	meters	1.09	yards	yd
km	kilometers	0.621	miles	mi
AREA				
mm ²	square millimeters	0.0016	square inches	in ²
m ²	square meters	10.764	square feet	ft ²
m ²	square meters	1.195	square yards	yd ²
ha	hectares	2.47	acres	ac
km ²	square kilometers	0.386	square miles	mi ²
VOLUME				
mL	milliliters	0.034	fluid ounces	fl oz
L	liters	0.264	gallons	gal
m ³	cubic meters	35.314	cubic feet	ft ³
m ³	cubic meters	1.307	cubic yards	yd ³
MASS				
g	grams	0.035	ounces	oz
kg	kilograms	2.202	pounds	lb
Mg (or "t")	megagrams (or "metric ton")	1.103	short tons (2000 lb)	T
TEMPERATURE (exact degrees)				
°C	Celsius	1.8C+32	Fahrenheit	°F
ILLUMINATION				
lx	lux	0.0929	foot-candles	fc
cd/m ²	candela/m ²	0.2919	foot-Lamberts	fl
FORCE and PRESSURE or STRESS				
N	newtons	0.225	poundforce	lbf
kPa	kilopascals	0.145	poundforce per square inch	lbf/in ²

*SI is the symbol for the International System of Units. Appropriate rounding should be made to comply with Section 4 of ASTM E380.
(Revised March 2003)

(This page intentionally left blank)

TABLE OF CONTENTS

List of Figures.....	xv
List of Tables	xxvii
List of Abbreviations	xxxix
CHAPTER 1. PREFACE	1
1.1 Background.....	1
1.2 What is Refined Analysis?	2
1.3 Why use a Refined Analysis?	3
1.4 Evolution of Structural Analysis Methods.....	4
1.5 State of Practice	6
1.6 Scope of Manual	7
1.7 Summary	9
CHAPTER 2. REFINED METHODS OF ANALYSIS.....	11
2.1 Methods of Analysis Permitted by AASHTO LRFD	11
2.2 Refined Methods of Analysis Referenced in AASHTO LRFD and AASHTO MBE ..	12
2.3 Essentials of Finite Element Analyses	13
2.3.1 General Capabilities of Modern Finite Element Software.....	13
2.3.2 Gauss Points, Shape Functions and Degrees of Freedom.....	14
2.3.3 Typical Input and Output	16
2.3.4 Typical Element Families and Usage.....	17
2.3.4.1 Point Elements, Constraints, and Rigid Links	17
2.3.4.2 Line Elements.....	17
2.3.4.2.1 Bar or Truss Elements.....	18
2.3.4.2.2 Beam Elements	18
2.3.4.3 Surface Elements.....	20
2.3.4.4 Volume Elements.....	21
2.3.5 Boundary Conditions	22
2.3.6 Submodeling.....	23
2.4 Definitions, Comparison and Applicability of One-, Two-, and Three-Dimensional Analysis.....	25
2.4.1 Definitions	25
2.4.2 One-Dimensional Analysis	26
2.4.3 Two-Dimensional Analysis	30
2.4.3.1 Basic Grid Analysis.....	30
2.4.3.2 Improved Grid Analysis	31
2.4.4 Three-Dimensional Analysis	33
2.5 Refined Methods of Analysis and Reliability.....	35
2.5.1 Evaluation of the LRFD Reliability Index.....	35
2.5.2 Effect of Refined Analysis on Calibration	36
2.5.3 Effect of Refined Analysis on Achieved Reliability	37
CHAPTER 3. GENERAL GIRDER BRIDGE MODELING.....	39
3.1 Introduction	39
3.2 Mesh Generation	40
3.2.1 Manual	40
3.2.2 Automatic	41
3.2.2.1 Free Mesh	41

3.2.2.2	<i>Mapped Mesh</i>	41
3.2.3	<i>Semi-Automatic</i>	42
3.2.4	<i>Transition Meshes</i>	42
3.3	Material Properties	43
3.4	One-Dimensional Analysis	43
3.5	Two-Dimensional Analysis	46
3.5.1	<i>Basic Grid Analysis</i>	46
3.5.1.1	<i>Elements and Geometry</i>	46
3.5.1.2	<i>Section Properties</i>	51
3.5.1.3	<i>Loading and Results</i>	53
3.5.2	<i>Plate with Eccentric Beam</i>	54
3.5.2.1	<i>Elements and Geometry</i>	54
3.5.2.2	<i>Section Properties</i>	56
3.5.2.3	<i>Loading and Results</i>	56
3.5.3	<i>Diaphragm / Cross-frame Stiffness</i>	57
3.5.4	<i>Handling Torsional Stiffness in 2D Models</i>	62
3.5.4.1	<i>Thin-walled Open Section Girder Grid Systems</i>	63
3.5.4.2	<i>Stocky Open Section and Closed Section Girder Grid Systems</i>	66
3.5.4.3	<i>Quasi-Closed Sections</i>	66
3.5.5	<i>Modeling Composite Construction</i>	67
3.6	THREE-DIMENSIONAL ANALYSIS	68
3.6.1	<i>Element Types and Usage</i>	68
3.6.1.1	<i>Bar (Truss) Elements</i>	68
3.6.1.2	<i>Beam Elements</i>	68
3.6.1.3	<i>Surface (Shell) Elements</i>	68
3.6.1.4	<i>Volume Elements</i>	69
3.6.1.5	<i>Constraints and Rigid Links</i>	69
3.6.1.6	<i>Spring and Point Elements</i>	69
3.6.2	<i>Geometry</i>	69
3.6.2.1	<i>Girder Location</i>	69
3.6.2.2	<i>Concrete Slab Location</i>	72
3.6.2.3	<i>Cross-Frame/Diaphragm Locations</i>	72
3.6.2.4	<i>Bearing/Support Location</i>	73
3.6.3	<i>Number of Elements</i>	73
3.6.3.1	<i>Element Aspect Ratio and Geometric Distortion</i>	74
3.6.3.2	<i>Girder Flanges</i>	74
3.6.3.3	<i>Girder Webs</i>	75
3.6.3.4	<i>Cross-Frames and Diaphragms</i>	75
3.6.3.4.1	<i>Cross-Frames</i>	75
3.6.3.4.2	<i>Diaphragms</i>	76
3.6.3.5	<i>Deck Slabs</i>	76
3.6.3.6	<i>Stiffeners</i>	76
3.6.4	<i>Interpreting Analysis Results</i>	76
3.7	Boundary Conditions	77
3.7.1	<i>Idealized Boundary Conditions</i>	77
3.7.2	<i>Idealized Versus Actual Boundary Conditions</i>	78

3.7.3	<i>Bearings</i>	79
3.8	Service Versus Strength Limit States Models	79
3.9	Construction Sequence / Staged Loading	80
CHAPTER 4. CONCRETE/STEEL GIRDER BRIDGE MODELING		83
4.1	Concrete Bridges	83
4.1.1	Modeling Guidelines	83
4.1.1.1	<i>Concrete Material Models</i>	83
4.1.1.2	<i>Concrete Beam Element Moment of Inertia</i>	83
4.1.1.3	<i>Modeling Non-Prismatic Cross-Sections</i>	85
4.1.1.4	<i>Shear Lag Effects</i>	85
4.1.1.5	<i>Modeling Diaphragms in Concrete Box Girders</i>	87
4.1.1.6	<i>Boundary Condition Considerations</i>	88
4.1.2	Time-Dependent Non-Linear Effects	88
4.1.3	Prestressing and Post-Tensioning	91
4.1.3.1	<i>Equivalent Load Method</i>	92
4.1.3.1.1	<i>Straight Strands</i>	92
4.1.3.1.2	<i>Harped Strands</i>	93
4.1.3.1.3	<i>Draped Strands</i>	94
4.1.3.1.4	<i>General Strand Configurations</i>	95
4.1.3.1.5	<i>Non-Prismatic Cross-Sections</i>	96
4.1.3.1.6	<i>Prestress Losses</i>	96
4.1.3.1.7	<i>Actual Tendon Layout vs. Idealized Tendon Layout</i>	96
4.1.3.1.8	<i>External/Unbonded Tendons</i>	98
4.1.3.2	<i>Including Tendons in Analysis Model</i>	98
4.1.3.3	<i>Other Approaches</i>	101
4.1.4	Analysis Issues vs. Design Issues	101
4.1.4.1	<i>Vertical Component of Prestressing</i>	101
4.1.4.2	<i>Strategies for Thermal Force Effects</i>	101
4.1.4.3	<i>Web Shear Distribution</i>	101
4.2	Steel Bridges	102
4.2.1	Proper Modeling of Geometry and Stiffness	102
4.2.2	Fatigue	103
4.2.2.1	<i>Load Induced Fatigue</i>	103
4.2.2.2	<i>Distortion Induced Fatigue</i>	104
4.2.2.3	<i>Local Structural Stress Approach</i>	106
4.2.2.4	<i>Modeling Cut-Outs</i>	111
4.2.2.5	<i>Distortion Induced Fatigue Stress Range Reduction</i>	112
4.2.3	Bolted/Riveted Steel Connections	113
4.2.3.1	<i>Modeling Bolted Splice Connections</i>	114
4.2.3.2	<i>Modeling Gusset Plate Connections</i>	115
4.3	Substructure and Foundation Modeling	118
4.3.1	Integral Construction	118
4.3.2	Continuous Construction	119
4.3.3	Overall Interaction	120
CHAPTER 5. MODELING ADVANCED TOPICS		123
5.1	Introduction	123

5.2 Soil-Structure Interaction.....	123
5.2.1 <i>General Information</i>	123
5.2.2 <i>Shallow Foundations</i>	124
5.2.3 <i>Deep Foundations</i>	126
5.2.3.1 <i>Depth to Fixity Method</i>	126
5.2.3.2 <i>Substructuring-Iterative Method</i>	127
5.2.3.3 <i>Direct Iterative Method</i>	133
5.2.3.4 <i>Direct Nonlinear Method</i>	135
5.2.4 <i>Summary</i>	136
5.3 Nonlinear Analyses.....	137
5.3.1 <i>Modeling Levels</i>	138
5.3.2 <i>Sources of Nonlinearities</i>	140
5.3.2.1 <i>Material Nonlinearity</i>	140
5.3.2.1.1 <i>Stress-Strain Relationships</i>	140
5.3.2.1.2 <i>Nonlinear Joints</i>	147
5.3.2.1.3 <i>Time-Dependent Effects</i>	150
5.3.2.2 <i>Geometric Nonlinearity</i>	151
5.3.2.2.1 <i>Main Aspects of Geometric Nonlinear Analyses for Bridges</i>	151
5.3.2.2.2 <i>Requirements for an Advanced Geometric Nonlinear Analysis</i>	155
5.3.2.2.3 <i>Inelastic Behavior</i>	156
5.3.2.3 <i>Boundary Condition and Tension/Compression Only Nonlinearity</i>	157
5.3.3 <i>Aspects of the Numerical Solution</i>	157
5.3.3.1 <i>Incremental Methods</i>	157
5.3.3.2 <i>Numerical Solvers</i>	160
5.3.4 <i>General Recommendations for Nonlinear Analyses</i>	161
5.4 Dynamic Analyses.....	161
5.4.1 <i>General Information</i>	161
5.4.2 <i>Modeling for Dynamic Analyses</i>	162
5.4.2.1 <i>Modeling Mass</i>	162
5.4.2.2 <i>Modeling Damping</i>	166
5.4.2.3 <i>Modeling Stiffness</i>	168
5.4.2.4 <i>Model Discretization</i>	169
5.4.3 <i>Multi-Modal Response Spectrum Analysis</i>	169
5.4.3.1 <i>Input</i>	169
5.4.3.2 <i>Solution</i>	170
5.4.3.3 <i>Output</i>	171
5.4.4 <i>Time-History Analysis</i>	172
5.4.4.1 <i>Input</i>	172
5.4.4.2 <i>Solution</i>	172
5.4.4.2.1 <i>Time-Stepping Methods</i>	172
5.4.4.2.2 <i>Modal Time-History Analysis</i>	173
5.4.4.3 <i>Output</i>	174
CHAPTER 6. VERIFICATION/VALIDATION.....	175
6.1 Introduction	175
6.2 Software Verification	176
6.3 Design Model Verification	177

6.3.1	<i>Example Comparison to Alternative Methods of Analysis</i>	178
6.3.2	<i>Verification of Time Dependent Analysis – Creep</i>	181
6.3.2.1	<i>Description of the Problem</i>	181
6.3.2.2	<i>Verification Process</i>	181
6.3.2.3	<i>The Simple Test Case</i>	181
6.3.2.4	<i>Bounding the Solution</i>	183
6.4	Validating Models of Existing Bridges	186
6.4.1	<i>Introduction</i>	186
6.4.2	<i>Field Validated Model Example</i>	187
6.5	Ramifications of Incorrect Boundary Conditions	192
CHAPTER 7. LOAD APPLICATION		195
7.1	Applying Loads	195
7.2	Dead Loads	195
7.2.1	<i>Modeled Components</i>	195
7.2.2	<i>Non-Modeled Components</i>	196
7.3	Live Loads	197
7.3.1	<i>AASHTO LRFD Requirements</i>	197
7.3.2	<i>Additional Requirements</i>	197
7.3.3	<i>Modeling Vehicle Live Loads</i>	197
7.3.4	<i>From Wheels to Loads</i>	199
7.3.5	<i>Live Load Optimization</i>	200
7.3.6	<i>Wind Loads</i>	203
7.3.7	<i>Centrifugal and Braking Forces</i>	204
7.3.8	<i>Thermal Loads</i>	204
7.3.9	<i>Loading Substructures</i>	205
7.3.10	<i>Verifying Live Loads</i>	206
7.4	Prestressing Loads	207
7.5	Loading Nonlinear Models	208
CHAPTER 8. ANALYSIS TO DESIGN		209
8.1	Compatibility of Analysis and Specification Provisions	209
8.2	Analysis Results to Design Inputs	210
8.2.1	<i>Integrating Stresses</i>	211
8.2.2	<i>Non-Composite Construction</i>	212
8.2.3	<i>Composite Construction</i>	212
8.2.4	<i>Concrete Girder Bridges</i>	214
8.2.5	<i>Steel Girder Bridges</i>	215
8.2.6	<i>Spine Beam Models</i>	219
8.2.7	<i>Deflection and Camber</i>	221
8.2.8	<i>Volume Elements</i>	221
8.2.9	<i>Nonlinear Behavior</i>	222
8.2.10	<i>Stability</i>	222
8.2.10.1	<i>Beam Columns</i>	222
8.2.10.2	<i>Lateral-Torsional Buckling</i>	224
8.2.11	<i>Dynamic Behavior</i>	224
CHAPTER 9. EXAMPLES		227

9.1 Example 1 – Three-span, Precast Concrete I-Girder Bridge (Continuous for Live Load)	227
9.1.1 ID Line Girder Analysis	229
9.1.1.1 Step 1 – Determine Non-Composite and Composite Section Properties.....	230
9.1.1.1.1 Non-Composite Section Properties – Interior and Exterior Girders.....	230
9.1.1.1.2 Composite Section Properties for Interior Girders	231
9.1.1.1.3 Composite Section Properties for Exterior Girders	232
9.1.1.2 Step 2 – Determine Approximate Live Load Distribution Factors	232
9.1.1.2.1 Interior Girder Moment Distribution Factors	232
9.1.1.2.2 Exterior Girder Moment Distribution Factors	234
9.1.1.3 Step 3 – Determine Dead Loads	237
9.1.1.3.1 Self-Weight of Girder, w_{sw}	237
9.1.1.3.2 Weight of Stay-in-Place Forms, w_{sip}	237
9.1.1.3.3 Weight of Concrete Deck Slab, w_{deck}	237
9.1.1.3.4 Weight of Concrete Haunches	237
9.1.1.3.5 Weight of Intermediate Diaphragms.....	238
9.1.1.3.6 Weight of Barriers.....	238
9.1.1.3.7 Weight of Future Wearing Surface	239
9.1.1.3.8 Summary of Dead Loads	239
9.1.1.4 Step 4 – Develop Analysis Models.....	239
9.1.1.5 Step 5 – Develop Moment, Shear, and Deflection Diagrams	240
9.1.2 Plate and Eccentric Beam Analysis	247
9.1.2.1 Step 1 – Create Non-Composite Dead Load Model.....	249
9.1.2.1.1 Step 1a – Define Girder and Intermediate Diaphragm Locations.....	249
9.1.2.1.2 Step 1b – Define Girder and Intermediate Diaphragm Cross-Sections	250
9.1.2.1.3 Step 1c – Define Material Properties for Girders and Intermediate Diaphragms	251
9.1.2.1.4 Step 1d – Define Support Conditions	251
9.1.2.1.5 Step 1e – Define Non-Composite Loads	251
9.1.2.1.6 Step 1f – Define Load Cases.....	251
9.1.2.1.7 Step 1g – Ensure Correct Attributes Are Assigned to Components	251
9.1.2.1.8 Step 1h – Run Analysis and Verify Results using Simplified Methods	252
9.1.2.1.9 Step 1i – Extract Required Results from Analysis Software	252
9.1.2.2 Step 2 – Create Composite Dead Load Model.....	252
9.1.2.2.1 Step 2a – Define Girder, Diaphragm, and Concrete Deck Slab Location ..	253
9.1.2.2.2 Step 2b – Define Diaphragm Cross-Sections and Concrete Deck Slab Thickness	255
9.1.2.2.3 Step 2c – Define Material Properties for the Concrete Deck Slab	256
9.1.2.2.4 Step 2d – Define Support Conditions	256
9.1.2.2.5 Step 2e – Define Dead Loads Applied to Composite Structure.....	257
9.1.2.2.6 Step 2f – Define Load Cases.....	257
9.1.2.2.7 Step 2g – Ensure Correct Attributes Are Assigned to Components	257
9.1.2.2.8 Step 2h – Run Analysis and Verify Results using Simplified Methods	258
9.1.2.2.9 Step 2i – Extract Required Results from Analysis Software	258
9.1.2.3 Step 3 – Create Live Load Model	259
9.1.2.3.1 Step 3a – Determine Optimized Live Load	259

9.1.2.3.2	Step 3b – Run Analysis and Verify Results using Simplified Methods	259
9.1.2.3.3	Step 3c – Extract Required Results from Analysis Software	260
9.1.2.4	Step 4 – Combine Analysis Results	261
9.1.3	Finite Element Model and Analysis	268
9.1.3.1	Step 1 – Develop Non-Composite Model	269
9.1.3.1.1	Step 1a – Define Geometry for Girders and Diaphragms	269
9.1.3.1.2	Step 1b – Define Cross-Section Properties	271
9.1.3.1.3	Step 1c – Define Material Properties	272
9.1.3.1.4	Step 1d – Define Support Conditions	272
9.1.3.1.5	Step 1e – Define Non-Composite Loads	273
9.1.3.1.6	Step 1f – Define Load Cases	273
9.1.3.1.7	Step 1g – Ensure Correct Attributes Are Assigned to Components	273
9.1.3.1.8	Step 1h – Run Analysis and Verify Results	273
9.1.3.1.9	Step 1i – Extract Required Results from Analysis Software	276
9.1.3.2	Step 2 – Create Composite Dead Load Model	276
9.1.3.2.1	Step 2a – Create Geometry for Girders, Diaphragms, and Deck Slab	277
9.1.3.2.2	Step 2b – Define Cross-Sections for Girders, Diaphragms, and Concrete Deck Slab	277
9.1.3.2.3	Step 2c – Define Material Properties for Girders, Diaphragms, and Deck Slabs	278
9.1.3.2.4	Step 2d – Define Support Conditions	278
9.1.3.2.5	Step 2e – Define Loads Applied to Composite Structure	278
9.1.3.2.6	Step 2f – Define Load Cases for Composite Dead Loads	278
9.1.3.2.7	Step 2g – Ensure Correct Attributes Are Assigned to Components	278
9.1.3.2.8	Step 2h – Run Analysis and Verify Results Using Simplified Methods	279
9.1.3.2.9	Step 2i – Extract Analysis Results	283
9.1.3.3	Step 3 – Create Composite Live Load Model	283
9.1.3.3.1	Step 3a – Determine Optimized Live Load	283
9.1.3.3.2	Step 3b – Run Analysis and Verify Results using Simplified Methods	284
9.1.3.3.3	Step 3c – Extract Required Results from Analysis Model	285
9.1.3.4	Step 4 – Combine Analysis Results	285
9.1.4	Comparison of 1D, 2D, and 3D Analysis Results	292
9.1.4.1	Interior Girder	292
9.1.4.1.1	Moment	292
9.1.4.1.2	Shear	295
9.1.4.1.3	Deflection	298
9.1.4.2	Exterior Girder	300
9.1.4.2.1	Moment	300
9.1.4.2.2	Shear	303
9.1.4.2.3	Deflection	306
9.1.4.3	Conclusions	308
9.2	Example 2 – Three-span Continuous Steel I-Girder Bridge	311
9.2.1	1D Line Girder Analysis	313
9.2.1.1	Step 1 – Determine Non-Composite and Various Composite Section Properties	313
9.2.1.1.1	Non-Composite Section Properties – Interior and Exterior Girders	313
9.2.1.1.2	Long-Term Composite Section Properties for Interior Girders	314

9.2.1.1.3	Short-Term Composite Section Properties for Interior Girders.....	314
9.2.1.1.4	Long-Term and Short-Term Composite Section Properties for Exterior Girders	315
9.2.1.2	<i>Step 2 – Determine Approximate Live Load Distribution Factors</i>	315
9.2.1.2.1	Interior Girder Distribution Factors	315
9.2.1.3	<i>Step 3 – Determine Dead Loads on a “Per Girder” Basis</i>	316
9.2.1.3.1	Self-Weight of Girder, w_{sw}	316
9.2.1.3.2	Weight of Stay-in-Place Forms, w_{sip}	316
9.2.1.3.3	Weight of Concrete Deck Slab, w_{deck}	316
9.2.1.3.4	Weight of Concrete Haunches	316
9.2.1.3.5	Weight of Intermediate Cross-Frames and Connection Plates	317
9.2.1.3.6	Weight of Barrier	317
9.2.1.3.7	Weight of Future Wearing Surface	317
9.2.1.3.8	Summary of Dead Loads	317
9.2.1.4	<i>Step 4 – Develop Analysis Models</i>	318
9.2.1.5	<i>Step 5 – Develop Moment, Shear, and Deflection Diagrams</i>	318
9.2.2	<i>Plate and Eccentric Beam Analysis</i>	325
9.2.2.1	<i>Step 1 – Create Non-Composite Dead Load Model</i>	327
9.2.2.1.1	Step 1a – Define Girder and Intermediate Cross-Frame Locations	327
9.2.2.1.2	Step 1b – Define Girder and Cross-Frame Cross-Sections.....	327
9.2.2.1.2.1	Intermediate Cross-Frames	328
9.2.2.1.2.2	Pier Cross-Frames	331
9.2.2.1.3	Step 1c – Define Material Properties for Girders and Cross-Frames	332
9.2.2.1.4	Step 1d – Define Support Conditions	332
9.2.2.1.5	Step 1e – Define Non-Composite Loads	332
9.2.2.1.6	Step 1f – Define Load Cases.....	332
9.2.2.1.7	Step 1g – Ensure Correct Attributes Are Assigned to Components	332
9.2.2.1.8	Step 1h – Run Analysis and Verify Results using Simplified Methods	333
9.2.2.1.9	Step 1i – Extract Required Results from Analysis Software	334
9.2.2.2	<i>Step 2 – Create Composite Dead Load Model</i>	334
9.2.2.2.1	Step 2a – Define Concrete Deck Slab Location.....	334
9.2.2.2.2	Step 2b – Define Concrete Deck Slab Thickness	335
9.2.2.2.3	Step 2c – Define Material Properties for Concrete Deck Slab	335
9.2.2.2.4	Step 2d – Define Support Conditions	335
9.2.2.2.5	Step 2e – Define Loads Applied to Composite Structure	335
9.2.2.2.6	Step 2f – Define Load Cases.....	336
9.2.2.2.7	Step 2g – Ensure Correct Attributes Are Assigned to Components	336
9.2.2.2.8	Step 2h – Run Analysis and Verify Results using Simplified Methods	336
9.2.2.2.9	Step 2i – Extract Required Results from Analysis Software	337
9.2.2.3	<i>Step 3 – Create Live Load Model</i>	337
9.2.2.3.1	Step 3a – Define Material Properties for Concrete Deck Slab	337
9.2.2.3.2	Step 3b – Determine Optimized Live Load	337
9.2.2.3.3	Step 3c – Run Analysis and Verify Results using Simplified Methods	338
9.2.2.3.4	Step 3d – Extract Required Results from Analysis Software	338
9.2.2.4	<i>Step 4 – Combine Analysis Results</i>	338
9.2.3	<i>3D Finite Element Analysis</i>	346

9.2.3.1	<i>Step 1 – Create Non-Composite Dead Load Model</i>	347
9.2.3.1.1	Step 1a – Create Geometry for Girders and Cross-Frames.....	347
9.2.3.1.2	Step 1b – Define Cross-Section Properties.....	348
9.2.3.1.3	Step 1c – Define Material Properties for Girders and Cross-Frames	349
9.2.3.1.4	Step 1d – Define Support Conditions	349
9.2.3.1.5	Step 1e – Define Non-Composite Dead Loads	349
9.2.3.1.6	Step 1f – Define Load Cases.....	350
9.2.3.1.7	Step 1g – Ensure Correct Attributes Are Assigned to Components	350
9.2.3.1.8	Step 1h – Run Analysis and Verify Results using Simplified Methods	350
9.2.3.1.9	Step 1i – Extract Required Results from Analysis Software	352
9.2.3.2	<i>Step 2 – Create Composite Dead Load Model</i>	353
9.2.3.2.1	Step 2a – Create Geometry for the Concrete Deck Slab.....	353
9.2.3.2.2	Step 2b – Create Geometric Sections for the Concrete Deck Slab	353
9.2.3.2.3	Step 2c – Define Material Properties for Steel and Concrete	353
9.2.3.2.4	Step 2d – Define Support Conditions	353
9.2.3.2.5	Step 2e – Define Composite Dead Loads	353
9.2.3.2.6	Step 2f – Define Load Cases.....	354
9.2.3.2.7	Step 2g – Ensure Correct Attributes Are Assigned to Components	354
9.2.3.2.8	Step 2h – Run Analysis and Verify Results with Simplified Methods.....	354
9.2.3.2.9	Step 2i – Extract Required Results from Analysis Software	355
9.2.3.3	<i>Step 3 – Create Live Load Model</i>	355
9.2.3.3.1	Step 3a – Define Material Properties for Concrete Deck Slab	355
9.2.3.3.2	Step 3b – Determine Optimized Live Load	355
9.2.3.3.3	Step 3c – Run Analysis and Verify Results using Simplified Methods	355
9.2.3.3.4	Step 3d – Extract Required Results from Analysis Software	356
9.2.3.4	<i>Step 4 – Combine Analysis Results</i>	356
9.2.4	<i>Comparison of 1D, 2D, and 3D Analysis Results</i>	364
9.2.4.1	<i>Interior Girder</i>	364
9.2.4.1.1	Moment.....	364
9.2.4.1.2	Shear	367
9.2.4.1.3	Deflection.....	370
9.2.4.2	<i>Exterior Girder</i>	372
9.2.4.2.1	Moment.....	372
9.2.4.2.2	Shear	375
9.2.4.2.3	Deflection.....	378
9.2.4.3	<i>Conclusions</i>	380
9.3	Example 3 – Three-span Continuous Curved Steel I-Girder Bridge with Skewed Supports	381
9.3.1	<i>1D Line Girder Analysis</i>	384
9.3.2	<i>2D Plate and Eccentric Beam Analysis</i>	384
9.3.2.1	<i>Step 1 – Create Non-Composite Dead Load Model (explicit deck)</i>	386
9.3.2.1.1	Step 1a – Define Girder, Intermediate Cross-Frame, and Concrete Deck Slab Locations	386
9.3.2.1.2	Step 1b – Define Girder, Intermediate Cross-Frame, and Concrete Deck Slab Cross-Sections.....	386

9.3.2.1.3	Step 1c – Define Material Properties for Girders, Intermediate Cross-Frames, and Concrete Deck Slab	389
9.3.2.1.4	Step 1d – Define Support Conditions	390
9.3.2.1.5	Step 1e – Define Non-Composite Loads	390
9.3.2.1.6	Step 1f – Define Load Cases.....	390
9.3.2.1.7	Step 1g – Ensure Correct Attributes Are Assigned to Components	390
9.3.2.1.8	Step 1h – Run Analysis and Verify Results using Simplified Methods	391
9.3.2.1.9	Step 1i – Extract Required Results from Analysis Software	393
9.3.2.1.10	Step 1j – Perform supplemental hand calculations (flange lateral bending moments)	393
9.3.2.2	<i>Step 2 – Create Composite Dead Load Model.....</i>	393
9.3.2.2.1	Step 2a – Define Location of Girders, Cross-Frames, and Concrete Deck Slab	393
9.3.2.2.2	Step 2b – Define Section Properties for Girders, Cross-Frames, and Concrete Deck Slab	393
9.3.2.2.3	Step 2c – Define Material Properties for Girders, Cross-Frames, and Concrete Deck Slab.....	394
9.3.2.2.4	Step 2d – Define Support Conditions	394
9.3.2.2.5	Step 2e – Define Composite Dead Loads	394
9.3.2.2.6	Step 2f – Define Load Cases.....	394
9.3.2.2.7	Step 2g – Ensure Correct Attributes Are Assigned to Components	394
9.3.2.2.8	Step 2h – Run Analysis and Verify Results using Simplified Methods	395
9.3.2.2.9	Step 2i – Extract Required Results from Analysis Software	396
9.3.2.2.10	Step 2j – Perform supplemental hand calculations (flange lateral bending moments)	396
9.3.2.3	<i>Step 3 – Create Composite Live Load Model</i>	396
9.3.2.3.1	Step 3a – Define Material Properties for Concrete Deck Slab	396
9.3.2.3.2	Step 3b – Determine Optimized Live Load	396
9.3.2.3.3	Step 3c – Run Analysis and Verify Results using Simplified Methods	397
9.3.2.3.4	Step 3d – Extract Required Results from Analysis Software	398
9.3.2.3.5	Step 3e – Perform supplemental hand calculations (flange lateral bending moments)	398
9.3.2.4	<i>Step 4 – Combine Analysis Results</i>	398
9.3.3	<i>3D Finite Element Model and Analysis</i>	412
9.3.3.1	<i>Step 1 – Create Non-Composite Dead Load Model.....</i>	413
9.3.3.1.1	Step 1a – Create Geometry for Girders, Cross-Frame, and Concrete Deck Slab	413
9.3.3.1.2	Step 1b – Define Cross-Section Properties.....	413
9.3.3.1.3	Step 1c – Define Material Properties	414
9.3.3.1.4	Step 1d – Define Support Conditions	414
9.3.3.1.5	Step 1e – Define Non-Composite Dead Loads	414
9.3.3.1.6	Step 1f – Define Load Cases.....	414
9.3.3.1.7	Step 1g – Ensure Correct Attributes Are Assigned to Components	414
9.3.3.1.8	Step 1h – Run Analysis and Verify Results using Simplified Methods	415
9.3.3.1.9	Step 1i – Extract Required Results from Analysis Software	416
9.3.3.2	<i>Step 2 – Create Composite Dead Load Model.....</i>	416

9.3.3.2.1	Step 2a – Create Geometry for Girders and Cross-Frames.....	416
9.3.3.2.2	Step 2b – Define Cross-Section Properties.....	416
9.3.3.2.3	Step 2c – Define Material Properties.....	416
9.3.3.2.4	Step 2d – Define Support Conditions.....	416
9.3.3.2.5	Step 2e – Define Composite Dead Loads.....	416
9.3.3.2.6	Step 2f – Define Load Cases.....	416
9.3.3.2.7	Step 2g – Ensure Correct Attributes are Assigned to Components.....	416
9.3.3.2.8	Step 2h – Run Analysis and Verify Results using Simplified Methods.....	417
9.3.3.2.9	Step 2i – Extract Required Results from Analysis Software.....	418
9.3.3.3	<i>Step 3 – Create Live Load Model.....</i>	<i>418</i>
9.3.3.3.1	Step 3a – Define Material Properties for Concrete Deck Slab.....	418
9.3.3.3.2	Step 3b – Define Optimized Live Load.....	418
9.3.3.3.3	Step 3c – Run Analysis and Verify Results using Simplified Methods.....	418
9.3.3.3.4	Step 3d – Extract Required Results from Analysis Software.....	420
9.3.3.4	<i>Step 4 – Combine Analysis Results.....</i>	<i>420</i>
9.3.4	<i>Comparison of 2D and 3D Analysis Results.....</i>	<i>433</i>
9.3.4.1	<i>Girders.....</i>	<i>433</i>
9.3.4.2	<i>Cross-Frames.....</i>	<i>458</i>
9.3.4.2.1	Cross-Frame Forces.....	458
9.3.4.2.1.1	Net Axial Force.....	458
9.3.4.2.1.2	Shear.....	462
9.3.4.2.1.3	Moment.....	467
9.3.4.3	<i>Conclusions.....</i>	<i>472</i>
9.4	Example 4 – Three Span Continuous Concrete Box Girder Spine Beam.....	475
9.5	Example 5 – Dynamic analysis of a curved steel girder bridge.....	481
9.5.1	<i>Methodology.....</i>	<i>482</i>
9.5.2	<i>Step 1 – Model for Dynamic Analysis.....</i>	<i>483</i>
9.5.2.1	<i>Step 1a - Model Geometry and Mesh.....</i>	<i>483</i>
9.5.2.2	<i>Step 1b – Cross Section Properties.....</i>	<i>484</i>
9.5.2.3	<i>Step 1c – Material Properties.....</i>	<i>485</i>
9.5.2.4	<i>Step 1d – Boundary Conditions.....</i>	<i>486</i>
9.5.2.5	<i>Step 1e – Natural Frequency Analysis.....</i>	<i>486</i>
9.5.2.6	<i>Step 1f – Response Spectrum Analysis.....</i>	<i>486</i>
9.5.2.7	<i>Step 1g – Soil Structure Interaction.....</i>	<i>488</i>
9.5.2.8	<i>Step 1h – Run Analysis.....</i>	<i>491</i>
9.5.2.9	<i>Step 1i – P-Δ Check.....</i>	<i>492</i>
9.5.3	<i>Step 2 – Model for Pushover Analysis.....</i>	<i>495</i>
9.5.3.1	<i>Step 2a – Calculate Displacement Demand.....</i>	<i>495</i>
9.5.3.2	<i>Step 2b – Model Geometry and Mesh.....</i>	<i>496</i>
9.5.3.3	<i>Step 2c – Column Plastic Moment Capacity.....</i>	<i>497</i>
9.5.3.4	<i>Step 2d – Pushover Analysis.....</i>	<i>500</i>
9.5.3.5	<i>Step 2e – Displacement Demand vs. Capacity Check.....</i>	<i>500</i>
9.5.3.6	<i>Step 2f – Results Verification.....</i>	<i>505</i>
9.5.4	<i>Conclusions.....</i>	<i>507</i>
9.6	Example 6 – Stability Analysis of a Tall Concrete Pier Column.....	509
9.6.1	<i>Methodology.....</i>	<i>509</i>

9.6.2	Step 1 – Model Description	510
9.6.2.1	Step 1a – Model Geometry and Mesh.....	510
9.6.2.2	Step 1b – Material Properties.....	510
9.6.2.3	Step 1c – Cross-Section Properties.....	512
9.6.2.4	Step 1d – Boundary Conditions.....	515
9.6.2.5	Step 1e – Loads.....	516
9.6.3	Step 2 – Moment Magnification Procedure	519
9.6.3.1	Step 2a – Linear Static Analysis.....	520
9.6.3.1.1	Load Cases.....	520
9.6.3.1.2	Analysis and Results Verification.....	520
9.6.3.1.3	Results.....	522
9.6.3.2	Step 2b – Eigenvalue Analysis.....	523
9.6.3.2.1	Loads.....	524
9.6.3.2.2	Analysis and Results Verification.....	524
9.6.3.2.3	Effective Length Factor.....	526
9.6.3.3	Step 2c – Moment Magnification.....	527
9.6.4	Step 3 – Large Deflection Non-linear Analysis	531
9.6.4.1	Step 3a – Non-linear Analysis Model.....	531
9.6.4.1.1	Member Stiffness.....	531
9.6.4.1.2	Loads and Load Cases.....	532
9.6.4.1.3	Non-linear Controls.....	532
9.6.4.1.4	Analysis and Results Verification.....	532
9.6.5	Step 4 – Comparison of Results	534
9.6.5.1	Step 4a – Magnified Moment.....	534
9.6.6	Step 5 – Capacity	535
9.6.6.1	Step 5b – Capacity vs. Demands.....	536
9.6.7	Conclusions	537
9.7	Example 7 – Four-Span Continuous, Precast Segmental Concrete Box Girder Bridge.	
	539
9.7.1	Spine Beam Model Analysis – Using Equivalent Load Method	542
9.7.1.1	Step 1 – Dead Load Model.....	543
9.7.1.1.1	Step 1a – Define Girder Location.....	543
9.7.1.1.2	Step 1b – Define Girder Cross-Sections.....	543
9.7.1.1.3	Step 1c – Define Material Properties for Girders.....	544
9.7.1.1.4	Step 1d – Define Support Conditions.....	545
9.7.1.1.5	Step 1e – Define Dead Loads Applied to Structure.....	546
9.7.1.1.6	Step 1f – Model Staged Construction.....	548
9.7.1.1.7	Step 1g – Run Analysis and Verify Results.....	552
9.7.1.1.8	Step 1h – Extract Required Results from Software.....	553
9.7.1.2	Step 2 - Post-Tensioning Model.....	556
9.7.1.2.1	Step 2a – Modify Material Properties.....	556
9.7.1.2.2	Step 2b – Tendon Section Properties.....	556
9.7.1.2.3	Step 2c – Calculate and Define Post-Tensioning Equivalent Loads.....	556
9.7.1.2.3.1	Friction Losses.....	557
9.7.1.2.3.2	Anchor Set Losses.....	559
9.7.1.2.3.3	Elastic Shortening Losses.....	562

9.7.1.2.3.4	Relaxation Losses	563
9.7.1.2.3.5	Creep Losses	563
9.7.1.2.3.6	Shrinkage Losses	566
9.7.1.2.3.7	Tendon Forces after Losses	570
9.7.1.2.3.8	Equivalent Loads Applied to Beam Elements	571
9.7.1.2.4	Step 2d – Run Analysis and Verify Results.....	577
9.7.1.2.5	Step 2e – Extract Required Results from Software	578
9.7.1.3	<i>Step 3 – Live Load Analysis</i>	584
9.7.1.3.1	Step 3a – Create Live Load Analysis Model	584
9.7.1.3.2	Step 3b – Modify Model for Linear-Elastic Analysis.....	584
9.7.1.3.3	Step 3c – Determine Optimized Live Loads.....	584
9.7.1.3.4	Step 3d – Run Analysis and Verify Results.....	585
9.7.1.3.5	Step 3e – Extract Required Results from Analysis Software	585
9.7.1.4	<i>Step 4 – Combine Analysis Results</i>	585
9.7.2	<i>Shell Element Model Analysis – Using Explicitly Modeled Tendons</i>	586
9.7.2.1	<i>Step 1 – Dead Load Model</i>	587
9.7.2.1.1	Step 1a – Create Geometry for Girders, Tendons, and Diaphragms	587
9.7.2.1.2	Step 1b – Define Section Properties	588
9.7.2.1.3	Step 1c – Define Material Properties	589
9.7.2.1.4	Step 1d – Define Support Conditions	590
9.7.2.1.5	Step 1e – Define Dead Loads applied to Structure	590
9.7.2.1.6	Step 1f – Model Staged Construction	591
9.7.2.1.7	Step 1g – Run Analysis and Verify Results.....	591
9.7.2.1.8	Step 1h – Extract Required Results from Software	593
9.7.2.2	<i>Step 2 – Post-Tensioning Model</i>	596
9.7.2.2.1	Step 2a – Create Analysis Model for Post-Tensioning Loads	596
9.7.2.2.2	Step 2b – Modify Material Properties.....	596
9.7.2.2.3	Step 2c – Calculate and Define Post-Tensioning Loads.....	596
9.7.2.2.4	Step 2d – Run Analysis and Verify Results.....	597
9.7.2.2.5	Step 2e – Extract Analysis Results	598
9.7.2.3	<i>Step 3 – Live Load Analysis</i>	604
9.7.2.3.1	Step 3a – Create Live Load Analysis Model	604
9.7.2.3.2	Step 3b – Modify Model for Linear-Elastic Analysis.....	604
9.7.2.3.3	Step 3c – Determine Optimized Live Loads.....	604
9.7.2.3.4	Step 3d – Run Analysis and Verify Results.....	604
9.7.2.3.5	Step 3e – Extract Required Results from Analysis Software	605
9.7.2.4	<i>Step 4 – Combine Analysis Results</i>	605
9.7.3	<i>Comparison of Spine Beam and Shell Element Model Results</i>	607
9.7.3.1	<i>Moment</i>	607
9.7.3.2	<i>Shear</i>	608
9.7.3.3	<i>Comparison of Strength I Factored Loads</i>	608
	REFERENCES	615
	APPENDIX 2A – REFERENCES TO REFINED ANALYSIS IN AASHTO LRFD	620
	APPENDIX 2B – REFERENCES TO REFINED ANALYSIS IN AASHTO MBE	638
	APPENDIX 7A – REFERENCES TO REFINED ANALYSIS IN AASHTO LRFD	641
	APPENDIX 7B – REFERENCES TO REFINED ANALYSIS IN AASHTO MBE	643

APPENDIX 9A - EXAMPLE 2 LIVE LOAD DISTRIBUTION FACTORS.....	645
Interior Girder Distribution Factors.....	645
Exterior Girder Distribution Factors.....	646
APPENDIX 9B – EXAMPLE 2 GEOMETRY.....	651
APPENDIX 9C - EXAMPLE 2 EQUIVALENT PIER CROSS-FRAME CALCULATIONS.	655
APPENDIX 9D - EXAMPLE 3 GIRDER SECTION PROPERTIES	659
GLOSSARY OF TECHNICAL TERMS.....	661

LIST OF FIGURES

Figure 1. Illustration. Six degrees of freedom (DOF) at a point, or node.....	14
Figure 2. Graph. Schematic illustration of the relationship between DOF, accuracy, and computational effort.....	15
Figure 3. Illustration. Bar or truss element.	18
Figure 4. Illustration. Beam element.....	18
Figure 5. Illustration. Plate element.....	20
Figure 6. Illustration. Shell element.....	20
Figure 7. Illustration. Typical surface element geometries.....	20
Figure 8. Illustration. Typical shapes for volume elements.....	22
Figure 9. Illustration. Example of increasing levels of submodeling.	24
Figure 10. Illustration. General progression from a 1D model to a 3D model.	26
Figure 11. Illustration. Plan and typical sections for three-span continuous steel girder bridge for Example 2.	27
Figure 12. Illustration. 1D model of three-span continuous steel girder bridge for Example 2. ..	27
Figure 13. Illustration. Plan and elevation of a torsionally stiff curved single concrete box beam bridge (Nutt et al., 2008).....	28
Figure 14. Illustration. Typical cross-section (Nutt et al., 2008).....	28
Figure 15. Illustration. 1D spine beam model.....	29
Figure 16. Illustration. 2D grid model of three-span continuous steel girder bridge for Example 2.	31
Figure 17. Illustration. 2D PEB model of three-span continuous steel girder bridge for Example 2, with internally offset girders and cross-frames bolded.....	32
Figure 18. Illustration. 3D model of three-span continuous steel girder bridge for Example 2. ..	34
Figure 19. Illustration. Example of a free mesh.....	41
Figure 20. Illustration. Example of a mapped mesh.	42
Figure 21. Illustration. Examples of transition meshes.....	43
Figure 22. Illustration. Definition of central angle (adapted from AASHTO, 2014).	45
Figure 23. Illustration. Three-dimensional spine model of curved concrete box girder bridge (adapted from AASHTO, 2014).	46
Figure 24. Illustration. Grid model with element at longitudinal girder lines.	47
Figure 25. Illustration. Grid model with additional elements between longitudinal girder lines.	48
Figure 26. Illustration. Grid model with additional stiffening elements along the edge of deck.	49
Figure 27. Illustration. Curved grid model.	50
Figure 28. Illustration. Orientation of transverse grid lines.....	51
Figure 29. Illustration. Typical concrete diaphragms.	52
Figure 30. Illustration. Typical steel cross-frames.....	53
Figure 31. Illustration. Portion of typical concrete slab on girder bridge and PEB model with explicit shear connection elements (diaphragms not shown for clarity).....	54
Figure 32. Illustration. Orthogonal mesh.....	55
Figure 33. Illustration. Skewed mesh.	55
Figure 34. Illustration. Intermediate cross-frame model - flexural stiffness.	58
Figure 35. Illustration. Intermediate cross-frame model - shear stiffness.	59
Figure 36. Illustration. Intermediate cross-frame model - flexural stiffness.	60
Figure 37. Illustration. Intermediate cross-frame model - shear stiffness.	61

Figure 38. Illustration. Calculating equivalent Saint-Venant torsion stiffness for I-sections.....	65
Figure 39. Illustration. Actual Flange-web intersection.	70
Figure 40. Illustration. Modeled flange-web intersection.....	70
Figure 41. Illustration. Flange thickness transition.....	70
Figure 42. Illustration. Flange thickness transition modeling.....	71
Figure 43. Illustration. Modeling web depth.	72
Figure 44. Illustration. Aspect ratio = 1:1.....	74
Figure 45. Illustration. Aspect ratio = 5:1.....	74
Figure 46. Graph. Example of the moment-curvature relationship for a given axial force.....	84
Figure 47. Illustration. Box girder cross-section (Corven Engineering, 2016).	86
Figure 48. Graph. Axial stresses on top face of box girder top flange.	86
Figure 49. Illustration. Tendons crossing over at pier.	88
Figure 50. Graphs. Compound figure showing subfigures showing stress vs. time and strain vs. time for the effect of creep.....	89
Figure 51. Graph. Creep deformation vs. age at loading.	90
Figure 52. Graph. Creep deformation vs. time for different applied loadings.....	91
Figure 53. Illustration. Straight strands.....	93
Figure 54. Illustration. Simplified model for straight strands.....	93
Figure 55. Illustrations. Compound illustration showing beams with harped strands and varying number of harp points.	94
Figure 56. Illustrations. Compound illustration showing simplified beam models for beams with harped strands and varying number of harp points.	94
Figure 57. Illustration. Beam with draped strands.	95
Figure 58. Illustration. Simplified model for beam with draped strands.	95
Figure 59. Illustration. General beam scenario.	95
Figure 60. Illustration. Idealized strand layout in continuous beam.....	97
Figure 61. Illustration. Actual strand layout in continuous beam.....	97
Figure 62. Illustration. Simplified beam model for actual strand layout.	98
Figure 63. Graph. AASHTO fatigue resistance curves including horizontal constant amplitude fatigue limit (CAFL).	104
Figure 64. Illustration. Distortion at web gap between flange and stiffener connection plate. ..	105
Figure 65. Illustration. Structural details and structural stress (adapted from IIW, 2008).	106
Figure 66. Illustration. Example of determination of structural stress by extrapolation (adapted from IIW, 2008).	107
Figure 67. Illustration. Types of LSS (adapted from IIW, 2008).....	107
Figure 68. Illustration. Shell element and solid element models (adapted from IIW, 2008).....	108
Figure 69. Illustration. Extrapolation reference points for various meshes (adapted from IIW, 2008).	108
Figure 70. Graph. Comparison of LSS baseline curves.....	110
Figure 71. Illustration. Dimensions for root fatigue stress range resistance reduction (adapted from AASHTO, 2014).	111
Figure 72. Illustration. Typical orthotropic ribs, with and without cut-out (adapted from FHWA, 2012).....	112
Figure 73. Graph. Shear force-displacement relationship for common connectors (Ocel, 2013).	114

Figure 74. Graph. Typical full stress-strain relationship for Grades 50 and 100 steel (Ocel, 2013).	115
Figure 75. Photo. Example of a typical truss gusset plate connection.	116
Figure 76. Illustration. Examples of typical truss gusset plate connections (Ocel, 2013).	117
Figure 77. Illustration. Behavior of integral substructures.	118
Figure 78. Illustration. Developing superstructure force effects for an integral abutment bridge by bounding the solution.	119
Figure 79. Illustration. Continuous span arrangements with fixed bearings at tall, slender piers	120
Figure 80. Illustration. Example of modeling the substructure with the superstructure, including bearings and rigid links to achieve correct locations of superstructure beams (deck not shown).	120
Figure 81. Graphs. Nonlinear behavior – essentially linear vs. mildly nonlinear vs. significantly nonlinear.	123
Figure 82. Illustration. Winkler spring model for SSI of a shallow foundation (adapted from FHWA, 2006).	125
Figure 83. Illustration. 2D plane strain model of a slab on grade.	125
Figure 84. Illustration. Pile lateral deformations and depth to fixity model.	126
Figure 85. Illustration. Compound figure showing two models coupled at a point to account for SSI effects.	127
Figure 86. Graph. Example p-y curves at varying depths along the pile.	128
Figure 87. Equation. 6 x 6 SSI stiffness matrix.	130
Figure 88. Illustration. Example calculation of stiffness terms for 6 x 6 SSI stiffness matrix.	131
Figure 89. Illustration. Model developed from inputs into a foundation program.	132
Figure 90. Illustration. Inputting 6 x 6 SSI stiffness matrix into superstructure / substructure model. (Note: The example reflects a specific program. Other programs might require a different methodology.)	133
Figure 91. Illustration. Compound figure example of directly modeling the SSI with the bridge superstructure.	134
Figure 92. Graphs. Example of comparing pile results of the foundation program used to develop the support spring stiffness values for the FEA model and the results of the FEA model.	135
Figure 93. Illustration. Use of joint elements to model nonlinear soil support conditions.	136
Figure 94. Illustration. Fiber-based modeling approach for line and surface elements.	141
Figure 95. Illustration. Representative stress-strain behavior of various typical structural steels (adapted from AASHTO, 2011).	142
Figure 96. Illustration. Typical tensile stress-strain relationship of reinforcing steel (adapted from AASHTO, 2011).	142
Figure 97. Illustration. Typical tensile stress-strain relationship of stainless compared to carbon steel (adapted from BSSA, 2018).	143
Figure 98. Illustration. Typical tensile stress-strain relationship of prestressing strand (adapted from AASHTO, 2011).	144
Figure 99. Illustration. Hardening Rules for Metals (adapted from ANSYS, 2010).	144
Figure 100. Illustration. Typical concrete stress-strain curve, including tension and compression portions (adapted from Vercher, 2015).	146
Figure 101. Illustration. Confined and Unconfined Concrete Stress-Strain Relationships (adapted from AASHTO, 2011).	146

Figure 102. Illustration. Idealized elastic plastic moment curvature curve.	149
Figure 103. Illustration. Example of nonlinear elastic material behavior.....	150
Figure 104. Illustration. Force-displacement relationship of a typical isolation bearing (adapted from AASHTO, 2010).	150
Figure 105. Illustration. Stiffness softening effect due to initial eccentricities in a compressive member.	152
Figure 106. Illustration. Global and local P-Delta effect.....	153
Figure 107. Graph. Iterative method of converging on incremental solution using a constant load level.....	158
Figure 108. Graph. Iterative method of converging on incremental solution using arc-length..	159
Figure 109. Illustration. 3D deck truss model with non-structural masses modeled.....	164
Figure 110. Illustration. Example of an analysis model of a curved bridge using a spine beam superstructure.....	165
Figure 111. Illustration. Spine model modified to use eccentrically placed masses to result in the proper mass moment of inertia for the superstructure.	165
Figure 112. Graph. Example Rayleigh (proportional) damping curve.	168
Figure 113. Graph. Example of the shape of a seismic response spectrum.....	170
Figure 114. Illustration. Example pier cap.....	179
Figure 115. Illustration. Principal stress field.....	180
Figure 116. Illustration. Example strut and tie model.	180
Figure 117. Graph. Loading history for test problem.	182
Figure 118. Graph. Comparison of displacements due to creep.	183
Figure 119. Illustration. Shell element model of the apron region.	184
Figure 120. Illustration. Lattice model of apron region.....	185
Figure 121. Graph. Comparison of results for edge girder without creep.	186
Figure 122. Graph. Comparison of results for edge girder after creep of 10,000 days.	186
Figure 123. Illustration. Circles showing locations of typical fatigue cracks on welded floorbeams.....	188
Figure 124. Illustration. Isometric view of three-dimensional finite element model.	188
Figure 125. Graph. Two trucks – unit V (three-dimensional model).	189
Figure 126. Illustration. Comparison of field-measured vs. calculated frequencies and mode shapes.....	189
Figure 127. Illustration. Finite element model of first level submodel.	190
Figure 128. Illustration. Field vs. calculated strain time histories.....	191
Figure 129. Graph. Quarter point displacements for unmodified and retrofitted structure.	192
Figure 130. Illustration. Framing plan and moment diagrams for Girder 1.	193
Figure 131. Illustration. AASHTO standard vehicle loadings (AASHTO, 2017).....	198
Figure 132. Illustration. HS20 Truck with tandem axles and wheel patch loads with 30' spacing between 32k axles (AASHTO, 2017).	199
Figure 133. Illustration. Influence surface for vertical bending moment at the circled location, Node 24 (Grubb, 2011).	201
Figure 134. Illustration. Wheel-load model of the fatigue live load positioned on influence surface to maximize the positive vertical bending moment at Node 24 (Grubb, 2011).	201
Figure 135. Illustration. Various permit lane and truck loading configurations (Grubb, 2011).	202
Figure 136. Illustration. Calculated moment envelopes.	207
Figure 137. Illustration. Determining moments from FEA stress output.	211

Figure 138. Illustration. Deck system in which the effective flange width set equal to the tributary width may result in an underestimation of force effects for the larger section.....	213
Figure 139. Illustration. Analysis and design section for a concrete member in positive bending.	215
Figure 140. Illustration. Steel girder analysis and design sections (note that in some circumstances the longitudinal deck steel reinforcement which is not illustrated may be taken as part of the design section in negative moment regions).	217
Figure 141. Illustration. Steps required to determine design stresses from stress output in negative moment regions	218
Figure 142. Illustration. Conventional practices for determination of cross-frame member forces from 2D-grid analysis results (adapted from White et al., 2012).	219
Figure 143. Illustration. Shear flow due to torsion in single cell box girder (Corven, 2015).....	220
Figure 144. Illustration. Shear flow due to torsion in multicell box girder (Corven, 2015).....	220
Figure 145. Illustration. Shear flow due to major-axis shear in single cell box girder with inclined webs (Corven, 2015).....	221
Figure 146. Illustration. Example 1 framing plan.....	228
Figure 147. Illustration. Example 1 bridge cross-section.	228
Figure 148. Illustration. Components of AASHTO Type VI prestressed beam.....	231
Figure 149. Illustration. Dimensions of AASHTO Type VI prestressed beam.....	231
Figure 150. Illustration. Lever rule dimensions.....	234
Figure 151. Illustration. Barrier dimensions and weight calculation.....	238
Figure 152. Graph. 1D moment diagram and live load envelope for interior girder.....	241
Figure 153. Graph. 1D shear diagram and live load envelope for interior girder.....	242
Figure 154. Graph. 1D deflection diagram for interior girder.	243
Figure 155. Graph. 1D moment diagram and live load envelope for exterior girder.	244
Figure 156. Graph. 1D shear diagram and live load envelope for exterior girder.....	245
Figure 157. Graph. 1D deflection diagram for exterior girder.	246
Figure 158. Illustration. Girder and intermediate diaphragm location.	247
Figure 159. Illustration. Diaphragm eccentricity.....	250
Figure 160. Illustration. PEB model.	256
Figure 161. Illustration. PEB moment calculation.....	260
Figure 162. Graph. 2D moment diagram and live load envelope for interior girder.....	262
Figure 163. Graph. 2D shear diagram and live load envelope for interior girder.....	263
Figure 164. Graph. 2D deflection diagram for interior girder.	264
Figure 165. Graph. 2D moment diagram and live load envelope for exterior girder.	265
Figure 166. Graph. 2D shear diagram and live load envelope for exterior girder.....	266
Figure 167. Graph. 2D deflection diagram for exterior girder.	267
Figure 168. Illustration. Modeling of web depth.	270
Figure 169. Illustration. Non-composite 3D FEA model.	271
Figure 170. Illustration. Girder flanges for 3D FEA model.	271
Figure 171. Illustration. Element force effects in non-composite concrete girder	274
Figure 172. Illustration. Surface definitions for Span 1 of composite model.....	277
Figure 173. Illustration. Deck slab element forces in composite concrete girder.....	280
Figure 174. Illustration. Element force effects in composite concrete girder.....	281
Figure 175. Illustration. Critical lane loading.	284
Figure 176. Illustration. Critical truck loading.	284

Figure 177. Graph. 3D moment diagram and live load envelope for interior girder.....	286
Figure 178. Graph. 3D shear diagram and live load envelope for interior girder.....	287
Figure 179. Graph. 3D deflection diagram for interior girder.	288
Figure 180. Graph. 3D moment diagram and live load envelope for exterior girder.	289
Figure 181. Graph. 3D shear diagram and live load envelope for exterior girder.....	290
Figure 182. Graph. 3D deflection diagram for exterior girder.	291
Figure 183. Graph. Comparison of moments for interior P/S concrete girder.	293
Figure 184. Graph. Comparison of factored moments for interior P/S concrete girder.	294
Figure 185. Graph. Comparison of shears for interior P/S concrete girder.	296
Figure 186. Graph. Comparison of factored shears for interior P/S concrete girder.	297
Figure 187. Graph. Comparison of deflections for interior P/S concrete girder.....	299
Figure 188. Graph. Comparison of moments for exterior P/S concrete girder.....	301
Figure 189. Graph. Comparison of factored moments for exterior P/S concrete girder.....	302
Figure 190. Graph. Comparison of shears for exterior P/S concrete girder.	304
Figure 191. Graph. Comparison of factored shears for exterior P/S concrete girder.	305
Figure 192. Graph. Comparison of deflections for exterior P/S concrete girder.....	307
Figure 193. Illustration. Example 2 framing plan.....	311
Figure 194. Illustration. Example 2 bridge cross-section.	311
Figure 195. Illustration. Example 2 girder elevation.	312
Figure 196. Illustration. Haunch area for interior girders.....	316
Figure 197. Graph. 1D moment diagram and live load envelope for interior girder.....	319
Figure 198. Graph. 1D shear diagram and live load envelope for interior girder.....	320
Figure 199. Graph. 1D deflection diagram for interior girder.	321
Figure 200. Graph. 1D moment diagram and live load envelope for exterior girder.	322
Figure 201. Graph. 1D shear diagram and live load envelope for exterior girder.....	323
Figure 202. Graph. 1D deflection diagram for exterior girder.	324
Figure 203. Illustration. Girder and intermediate cross-frame location.....	325
Figure 204. Illustration. Intermediate cross-frame model – flexural stiffness.....	329
Figure 205. Illustration. Intermediate cross-frame model – shear stiffness.....	330
Figure 206. Illustration. Deck eccentricity.	335
Figure 207. Graph. 2D moment diagram and live load envelope for interior girder.....	340
Figure 208. Graph. 2D shear diagram and live load envelope for interior girder.....	341
Figure 209. Graph. 2D deflection diagram for interior girder.	342
Figure 210. Graph. 2D moment diagram and live load envelope for exterior girder.	343
Figure 211. Graph. 2D shear diagram and live load envelope for exterior girder.....	344
Figure 212. Graph. 2D deflection diagram for exterior girder.	345
Figure 213. Illustration. 3D non-composite geometry visualized.....	348
Figure 214. Graph. 3D moment diagram and live load envelope for interior girder.....	358
Figure 215. Graph. 3D shear diagram and live load envelope for interior girder.....	359
Figure 216. Graph. 3D deflection diagram for interior girder.	360
Figure 217. Graph. 3D moment diagram and live load envelope for exterior girder.	361
Figure 218. Graph. 3D shear diagram and live load envelope for exterior girder.....	362
Figure 219. Graph. 3D deflection diagram for exterior girder.	363
Figure 220. Graph. Comparison of moments for interior steel girder.	365
Figure 221. Graph. Comparison of factored moments for interior steel girder.	366
Figure 222. Graph. Comparison of shears for interior steel girder.....	368

Figure 223. Graph. Comparison of factored shears for interior steel girder.....	369
Figure 224. Graph. Comparison of deflections for interior steel girder.	371
Figure 225. Graph. Comparison of moments for exterior steel girders.....	373
Figure 226. Graph. Comparison of factored moments for exterior steel girders.....	374
Figure 227. Graph. Comparison of shears for exterior steel girders.....	376
Figure 228. Graph. Comparison of factored shears for exterior steel girders.....	377
Figure 229. Graph. Comparison of deflections for exterior steel girder.....	379
Figure 230. Illustration. Example 3 framing plan.....	381
Figure 231. Illustration. Example 3 bridge cross-section.	381
Figure 232. Illustration. Example 3 elevation of Girder 1 (G1).	382
Figure 233. Illustration. Example 3 elevation of Girder 2 (G2).	382
Figure 234. Illustration. Example 3 elevation of Girder 3 (G3).	383
Figure 235. Illustration. Example 3 elevation of Girder 4 (G4).	383
Figure 236. Illustration. Equivalent flexural stiffness model, example cross-frame (CF1).	388
Figure 237. Illustration. Equivalent shear area model, example cross-frame (CF1).	389
Figure 238. Illustration. Sample truck loading configuration.....	397
Figure 239. Graph. 2D moment diagram and live load envelope for Girder 1.....	400
Figure 240. Graph. 2D shear diagram and live load envelope for Girder 1.	401
Figure 241. Graph. 2D deflection diagram for Girder 1.	402
Figure 242. Graph. 2D moment diagram and live load envelope for Girder 2.....	403
Figure 243. Graph. 2D shear diagram and live load envelope for Girder 2.	404
Figure 244. Graph. 2D deflection diagram for Girder 2.	405
Figure 245. Graph. 2D moment diagram and live load envelope for Girder 3.....	406
Figure 246. Graph. 2D shear diagram and live load envelope for Girder 3.	407
Figure 247. Graph. 2D deflection diagram for Girder 3.	408
Figure 248. Graph. 2D moment diagram and live load envelope for Girder 4.....	409
Figure 249. Graph. 2D shear diagram and live load envelope for Girder 4.	410
Figure 250. Graph. 2D deflection diagram for Girder 4.	411
Figure 251. Illustration. Sample truck loading configuration.....	419
Figure 252. Graph. 3D moment diagram and live load envelope for Girder 1.....	421
Figure 253. Graph. 3D shear diagram and live load envelope for Girder 1.	422
Figure 254. Graph. 3D deflection diagram for Girder 1.	423
Figure 255. Graph. 3D moment diagram and live load envelope for Girder 2.....	424
Figure 256. Graph. 3D shear diagram and live load envelope for Girder 2.	425
Figure 257. Graph. 3D deflection diagram for Girder 2.	426
Figure 258. Graph. 3D moment diagram and live load envelope for Girder 3.....	427
Figure 259. Graph. 3D shear diagram and live load envelope for Girder 3.	428
Figure 260. Graph. 3D deflection diagram for Girder 3.	429
Figure 261. Graph. 3D moment diagram and live load envelope for Girder 4.....	430
Figure 262. Graph. 3D shear diagram and live load envelope for Girder 4.	431
Figure 263. Graph. 3D deflection diagram for Girder 4.	432
Figure 264. Graph. Comparison of 2D moments to 3D moments for Girder 1.....	434
Figure 265. Graph. Comparison of factored moments for Girder 1.	435
Figure 266. Graph. Comparison of 2D shears to 3D shears for Girder 1.	436
Figure 267. Graph. Comparison of factored shears for Girder 1.	437
Figure 268. Graph. Comparison of 2D deflections to 3D deflections for Girder 1.	438

Figure 269. Graph. Comparison of 2D flange lateral bending moments to 3D flange lateral bending moments for Girder 1.....	439
Figure 270. Graph. Comparison of 2D moments to 3D moments for Girder 2.....	440
Figure 271. Graph. Comparison of factored moments for Girder 2.	441
Figure 272. Graph. Comparison of 2D shears to 3D shears for Girder 2.	442
Figure 273. Graph. Comparison of factored shears for Girder 2.....	443
Figure 274. Graph. Comparison of 2D deflections to 3D deflections for Girder 2.....	444
Figure 275. Graph. Comparison of 2D flange lateral bending moments to 3D flange lateral bending moments for Girder 2.....	445
Figure 276. Graph. Comparison of 2D moments to 3D moments for Girder 3.....	446
Figure 277. Graph. Comparison of factored moments for Girder 3.	447
Figure 278. Graph. Comparison of 2D shears to 3D shears for Girder 3.	448
Figure 279. Graph. Comparison of factored shears for Girder 3.....	449
Figure 280. Graph. Comparison of 2D deflections to 3D deflections for Girder 3.....	450
Figure 281. Graph. Comparison of 2D flange lateral bending moments to 3D flange lateral bending moments for Girder 3.....	451
Figure 282. Graph. Comparison of 2D moments to 3D moments for Girder 4.....	452
Figure 283. Graph. Comparison of factored moments for Girder 4.	453
Figure 284. Graph. Comparison of 2D shears to 3D shears for Girder 4.	454
Figure 285. Graph. Comparison of factored shears for Girder 4.....	455
Figure 286. Graph. Comparison of 2D deflections to 3D deflections for Girder 4.....	456
Figure 287. Graph. Comparison of 2D flange lateral bending moments to 3D flange lateral bending moments for Girder 4.....	457
Figure 288. Graph. Comparison of cross-frame DC1 forces – G1-G2 cross-frames.	458
Figure 289. Graph. Comparison of cross-frame DC1 forces – G2-G3 cross-frames.	459
Figure 290. Graph. Comparison of cross-frame DC1 forces – G3-G4 cross-frames.	459
Figure 291. Graph. Comparison of cross-frame DC2+DW forces – G1-G2 cross-frames.	460
Figure 292. Graph. Comparison of cross-frame DC2+DW forces – G2-G3 cross-frames.	460
Figure 293. Graph. Comparison of cross-frame DC2+DW forces – G3-G4 cross-frames.	461
Figure 294. Graph. Comparison of cross-frame LL forces – G1-G2 cross-frames.	461
Figure 295. Graph. Comparison of cross-frame LL forces – G2-G3 cross-frames.	462
Figure 296. Graph. Comparison of cross-frame LL forces – G3-G4 cross-frames.	462
Figure 297. Graph. Comparison of cross-frame DC1 forces – G1-G2 cross-frames.	463
Figure 298. Graph. Comparison of cross-frame DC1 forces – G2-G3 cross-frames.	463
Figure 299. Graph. Comparison of cross-frame DC1 forces – G3-G4 cross-frames.	464
Figure 300. Graph. Comparison of cross-frame DC2+DW forces – G1-G2 cross-frames.	464
Figure 301. Graph. Comparison of cross-frame DC2+DW forces – G2-G3 cross-frames.	465
Figure 302. Graph. Comparison of cross-frame DC2+DW forces – G3-G4 cross-frames.	465
Figure 303. Graph. Comparison of cross-frame LL forces – G1-G2 cross-frames.	466
Figure 304. Graph. Comparison of cross-frame LL forces – G2-G3 cross-frames.	466
Figure 305. Graph. Comparison of cross-frame LL forces – G3-G4 cross-frames.	467
Figure 306. Graph. Comparison of cross-frame DC1 forces – G1-G2 cross-frames.	467
Figure 307. Graph. Comparison of cross-frame DC1 forces – G2-G3 cross-frames.	468
Figure 308. Graph. Comparison of cross-frame DC1 forces – G3-G4 cross-frames.	468
Figure 309. Graph. Comparison of cross-frame DC2+DW forces – G1-G2 cross-frames.	469
Figure 310. Graph. Comparison of cross-frame DC2+DW forces – G2-G3 cross-frames.	469

Figure 311. Graph. Comparison of cross-frame DC2+DW forces – G3-G4 cross-frames.	470
Figure 312. Graph. Comparison of cross-frame LL forces – G1-G2 cross-frames.	470
Figure 313. Graph. Comparison of cross-frame LL forces – G2-G3 cross-frames.	471
Figure 314. Graph. Comparison of cross-frame LL forces – G3-G4 cross-frames.	471
Figure 315. Illustration. NCHRP 620 comprehensive example (Nutt et al., 2008).	475
Figure 316. Illustration. Analysis model geometry.	476
Figure 317. Illustration. Typical section, Section X-X (Nutt et al., 2008).	476
Figure 318. Illustration. Pier section, Section Y-Y (Nutt et al., 2008).	477
Figure 319. Graph. Spine beam shear.	478
Figure 320. Graph. Spine beam moment.	479
Figure 321. Graph. Spine beam torsion.	480
Figure 322. Illustration. Pier details.	481
Figure 323. Illustration. Foundation details.	482
Figure 324. Illustrations. Compound figure showing substructure geometry.	484
Figure 325. Chart. Effective flexural stiffness of cracked reinforced concrete circular sections (AASHTO Guide Specifications for LRFD Seismic Design, 2011).	485
Figure 326. Graph. Design response spectrum.	487
Figure 327. Illustration. Support member naming convention.	489
Figure 328. Graph. Bent column interaction diagram.	494
Figure 329. Illustration. Location of column plastic hinge nodes.	497
Figure 330. Graph. Reinforced concrete moment-curvature model.	499
Figure 331. Illustration. Pier 1 transverse pushover deformed shape at load factor = 2.0.	501
Figure 332. Illustration. Pier 1 transverse pushover deformed shape at load factor = 4.0.	501
Figure 333. Illustration. Pier 1 transverse pushover deformed shape at load factor = 6.0.	502
Figure 334. Illustration. Pier 1 transverse pushover deformed shape at load factor = 8.0.	502
Figure 335. Illustration. Pier 1 transverse pushover deformed shape at load factor = 10.0.	502
Figure 336. Illustration. Pier 1 transverse pushover deformed shape at load factor = 11.0.	503
Figure 337. Illustration. Pier 1 transverse pushover deformed shape at load factor = 12.0.	503
Figure 338. Illustration. Pier 1 transverse pushover deformed shape at load factor = 12.23.	503
Figure 339. Illustration. Pier 1 transverse pushover deformed shape at load factor = 12.31.	504
Figure 340. Illustration. Pier 1 transverse pushover deformed shape at load factor = 12.35.	504
Figure 341. Illustration. Deformed shape for the transverse pushover analysis of Pier 1 at failure.	505
Figure 342. Illustration. Assumed transverse collapse mechanism of Pier 1.	506
Figure 343. Illustration. Pier plan, elevation, and reinforcement details.	511
Figure 344. Illustration. User defined nodes.	512
Figure 345. Illustration. (a) Incorrect and (b) correct definition of pier cap cross section vertical eccentricity.	515
Figure 346. Illustration. Application of bearing reactions on the pier cap for linear static analysis.	519
Figure 347. Illustration. Overlap of pier cap and column elements.	522
Figure 348. Graphs. Compound figure showing axial load and bending moment diagrams from the linear static analysis.	523
Figure 349. Illustration. Applied loads on the pier cap for eigenvalue analysis.	524
Figure 350. Illustration. Deflected shape of the column (in grey) corresponding to the Euler buckling load.	525

Figure 351. Graph. Comparison of column bending moments from linear static analysis, magnified moment procedure, and non-linear analysis.	535
Figure 352. Graphs. Compound figure showing interaction diagrams for the pier shaft and drilled shaft.	536
Figure 353. Graphs. Compound figure comparing the capacity and demand for the (a) pier shaft and (b) drilled shaft.	537
Figure 354. Illustration. Typical segment cross-section.	539
Figure 355. Illustration. Deviator segment cross-section.	539
Figure 356. Illustration. Continuity pier segment cross-section.	540
Figure 357. Illustration. Expansion pier segment cross-section.	540
Figure 358. Illustration. Elevation view of pier segments.	540
Figure 359. Illustration. Span 1 elevation.	541
Figure 360. Illustration. Span 2 elevation.	541
Figure 361. Illustration. Segment elevations.	541
Figure 362. Illustration. Support conditions.	545
Figure 363. Illustration. Changing support conditions.	546
Figure 364. Illustration. Pier diaphragm areas.	547
Figure 365. Illustration. Expansion diaphragm areas.	547
Figure 366. Illustration. Stage #1.	548
Figure 367. Illustration. Stage #2.	549
Figure 368. Illustration. Stage #3.	549
Figure 369. Illustration. Stage #4.	550
Figure 370. Illustration. Stage #5.	550
Figure 371. Illustration. Stage #6.	551
Figure 372. Illustration. Stage #7.	551
Figure 373. Illustration. Stage #8.	551
Figure 374. Graph. Dead load moment vs. distance along span for various construction stages.	554
Figure 375. Graph. Dead load shear vs. distance along span for various construction stages. ..	555
Figure 376. Illustration. Tendon schematic.	557
Figure 377. Illustration. Tendon force variation.	560
Figure 378. Graph. Creep losses at different stages vs. location – Span 1 tendons.	566
Figure 379. Graph. Creep losses at different stages vs. location - Span 2 tendons.	566
Figure 380. Graph. Shrinkage losses at different stages vs. location - Span 1 tendons.	569
Figure 381. Graph. Shrinkage losses at different stages vs. location - Span 2 tendons.	569
Figure 382. Illustration. Equivalent load free-body diagram.	572
Figure 383. Illustration. Free-body diagram - Point ①.	572
Figure 384. Illustration. Free-body diagram - Point ②.	572
Figure 385. Free-body diagram - Point ③.	573
Figure 386. Illustration. Free-body diagram - Point ④.	573
Figure 387. Illustration. Free-body diagram - Point ⑤.	573
Figure 388. Illustration. Free-body diagram - Point ⑥.	574
Figure 389. Illustration. Shears due to PT and dead loads - Model 1.	578
Figure 390. Illustration. Shears due to PT and dead loads - Model 2.	578
Figure 391. Graph. Moment due to post-tensioning vs. distance along span for various construction stages.	579

Figure 392. Graph. Secondary PT moments vs. distance along span for various construction stages.....	580
Figure 393. Graph. Shear due to post-tensioning vs. distance along span for various construction stages.....	582
Figure 394. Graph. Secondary PT shears vs. distance along span for various construction stages.....	583
Figure 395. Illustration. Optimized loading for maximum moment over Pier 2.....	584
Figure 396. Illustration. Selected locations for design moments.....	586
Figure 397. Illustration. Selected locations for design shears.	586
Figure 398. Illustration. Point locations.....	588
Figure 399. Illustration. Perimeter definition.	589
Figure 400. Illustrations. Compound figure showing varying support conditions.	590
Figure 401. Illustration. Deviator areas for weight calculations.....	592
Figure 402. Illustration. Temporary PT anchor block areas for weight calculations.	592
Figure 403. Graph. Dead load moment vs. distance for various construction stages.	594
Figure 404. Graph. Dead load shear vs. distance for various construction stages.....	595
Figure 405. Graph. Post-tensioning moments vs. distance for various construction stages.....	600
Figure 406. Graph. Secondary post-tensioning moments vs. distance for various construction stages.....	601
Figure 407. Graph. Shears due to post-tensioning vs. distance for various construction stages.	602
Figure 408. Graph. Shears due to secondary PT moment vs. distance for various construction stages.....	603
Figure 409. Illustration. Selected design moment locations.	605
Figure 410. Illustration. Selected locations for design moments and live load for Span 2 maximum positive moment.....	606
Figure 411. Illustration. Selected design shear locations.....	606
Figure 412. Illustration. Selected locations for design shears and truck loading for maximum shear near Pier 1.....	607
Figure 413. Graph. Comparison of dead load and post-tensioning moments from spine beam and shell element models at $t = 100$ days.	609
Figure 414. Graph. Comparison of dead load and post-tensioning moments from spine beam and shell element models at $t = 1,000$ days.	610
Figure 415. Graph. Comparison of dead load and post-tensioning moments from spine beam and shell element models at $t = 10,000$ days.	611
Figure 416. Graph. Comparison of dead load and post-tensioning shears from spine beam and shell element models at $t = 100$ days.	612
Figure 417. Graph. Comparison of dead load and post-tensioning shears from spine beam and shell element models at $t = 1,000$ days.	613
Figure 418. Graph. Comparison of dead load and post-tensioning shears from spine beam and shell element models at $t = 10,000$ days.....	614
Figure 419. Illustration. Lever rule dimensions.....	647
Figure 420. Illustration. Pier cross-frame - flexural stiffness model.	655
Figure 421. Illustration. Pier cross-frame - shear stiffness model.	655
Figure 422. Illustration. Pier cross-frame - axial stiffness model.....	656

LIST OF TABLES

Table 1. Effective shear areas of common shapes.	19
Table 2. Comparison of reliability indices.	36
Table 3. Equivalent loads for actual tendon layout.	97
Table 4. Recommended meshing and extrapolation (see also Figure 69) (IIW, 2008).	109
Table 5. Examples of different modeling levels for nonlinear analyses.	139
Table 6. Recommended Values for Parameters of the Stress-Strain Relationship of Reinforcing Steel (FHWA, 2014).	143
Table 7. Recommended damping ratios (Chopra, 2017).	167
Table 8. Live load reactions.	193
Table 9. Non-composite section property calculation.	230
Table 10. Composite section property calculation – interior girder.	232
Table 11. Composite section property calculation – exterior girder.	232
Table 12. Bridge characteristics for distribution factor equations.	233
Table 13. Interior girder moment distribution factors.	234
Table 14. Exterior girder moment distribution factors.	235
Table 15. Exterior girder distribution factor summary.	237
Table 16. Dead loads on a per girder basis.	239
Table 17. Coordinates for girder and intermediate diaphragm ends.	249
Table 18. Intermediate diaphragm section properties.	250
Table 19. Concrete material properties.	251
Table 20. Coordinates for girder and diaphragm ends.	254
Table 21. Coordinates of concrete deck slab corners.	255
Table 22. Pier and abutment diaphragm section properties.	255
Table 23. Concrete material properties.	256
Table 24. Girder flange section properties.	272
Table 25. Concrete material properties.	272
Table 26. Abutment, intermediate, and pier diaphragm section properties.	277
Table 27. Concrete material properties.	278
Table 28. Example 2 non-composite section properties.	313
Table 29. Example 2 interior girder long-term composite section properties.	314
Table 30. Example 2 interior girder short-term composite section properties.	314
Table 31. Example 2 exterior girder long-term composite section properties.	315
Table 32. Example 2 exterior girder short-term composite section properties.	315
Table 33. Example 2 distribution factors.	315
Table 34. Example 2 girder self-weight.	316
Table 35. Dead loads on a per girder basis.	318
Table 36. Girder section properties from the software.	328
Table 37. Intermediate cross-frame centroid calculation.	330
Table 38. Equivalent cross-frame properties.	331
Table 39. Equivalent pier cross-frame properties.	332
Table 40. Steel material properties.	332
Table 41. Coordinates of concrete deck slab corners.	334
Table 42. Material properties.	335
Table 43. Deck slab concrete material properties.	337
Table 44. Girder flange properties.	348

Table 45. Cross-frame member section properties.	349
Table 46. Steel material properties.	349
Table 47. Concrete material properties.	353
Table 48. Deck slab concrete material properties.	355
Table 49. G1-1 section properties.	387
Table 50. Example 3 cross-frame equivalent flexural stiffness.	388
Table 51. Example 3 cross-frame equivalent shear area.	389
Table 52. Example 3 non-composite material properties.	390
Table 53. Summary of Example 3 support conditions.	390
Table 54. Unfactored concrete deck slab reactions from 2D PEB model.	392
Table 55. Unfactored FWS reactions from 2D PEB model.	395
Table 56. Unfactored truck reactions (including multiple presence) from 2D PEB model.	398
Table 57. Unfactored concrete deck slab reactions from 3D FEA model.	415
Table 58. Unfactored FWS reactions from 3D FEA model.	417
Table 59. Unfactored truck reactions (including multiple presence) from 3D FEA model.	419
Table 60. 2D/3D ratios for maximum positive major-axis bending moment.	472
Table 61. 2D/3D ratio for maximum negative major-axis bending moment.	472
Table 62. 2D/3D ratios for shear.	472
Table 63. 2D/3D ratios for deflection.	473
Table 64. 2D/3D ratios for flange lateral bending moment.	473
Table 65. Spine beam section properties.	477
Table 66. Column section properties.	477
Table 67. Soil properties.	482
Table 68. Substructure section properties.	485
Table 69. Concrete material properties.	486
Table 70. Support stiffness matrices for final SSI iteration.	489
Table 71. Natural frequency analysis results.	491
Table 72. Factored axial load on columns.	492
Table 73. Elastic seismic displacement demands on columns.	493
Table 74. Column P- Δ check summary.	495
Table 75. Seismic displacement demands at the top of the columns.	496
Table 76. Column moment-curvature model values.	499
Table 77. Column displacement capacity check.	504
Table 78. Pier 1 transverse plastic rotation and displacement capacities.	506
Table 79. Material properties.	510
Table 80. Gross section properties.	512
Table 81. Effective section properties.	514
Table 82. Unfactored bearing reactions.	518
Table 83. Strength I load combination factored loads.	519
Table 84. Linear static analysis load cases.	520
Table 85. Effective moment of inertia values of the column.	532
Table 86. Moment and stiffness comparison at the base of the drilled shaft.	533
Table 87. Comparison of calculated moments at the base of the drilled shaft.	538
Table 88. Girder section properties from software.	544
Table 89. Concrete material properties – dead load model.	545
Table 90. Diaphragm, deviator, and anchor block weights.	547

Table 91. PT material properties.....	556
Table 92. PT section properties.	556
Table 93. Friction losses in Span 2 Tendon T1.	558
Table 94. Friction and wobble losses for Span 1.	558
Table 95. Friction and wobble losses for Span 2.	558
Table 96. Anchor set losses for Spans 1 and 2 without friction.	560
Table 97. Anchor set losses for Span 2 with friction.	562
Table 98. Span 1 tendon T1 forces.	570
Table 99. Span 1 tendon T2 forces.	570
Table 100. Span 1 tendon T3 forces.	570
Table 101. Span 1 tendon T4 forces.	570
Table 102. Span 2 tendon T1 forces.	571
Table 103. Span 2 tendon T2 forces.	571
Table 104. Span 2 tendon T3 forces.	571
Table 105. Span 2 tendon T4 forces.	571
Table 106. Equivalent loads for model.	575
Table 107. Discrete point load definition for Span 2 – Tendon T1 (Stage 8).....	577
Table 108. Flexure results for selected locations at 10,000 days.....	586
Table 109. Shear results for selected locations at 10,000 days.....	586
Table 110. Girder shell section properties.	588
Table 111. Diaphragm section properties.	589
Table 112. Tendon section properties.	589
Table 113. Tendon forces for Span 1.....	596
Table 114. Tendon forces for Span 2.....	596
Table 115. Temperature changes for Span 1.	597
Table 116. Temperature changes for Span 2.	597
Table 117. Flexure results for selected locations at 10,000 days.....	606
Table 118. Shear results for selected locations at 10,000 days.....	607
Table 119. Comparison of Factored Strength I Loads.....	608
Table 120. Bridge characteristics for distribution factor equations.....	646
Table 121. Interior girder moment distribution factors.	646
Table 122. Exterior girder moment distribution factors based on AASHTO LRFD.....	648
Table 123. Exterior girder moment distribution factor summary.....	649
Table 124. Coordinates for girder and cross-frame ends – Span 1.....	651
Table 125. Coordinates for girder and cross-frame ends – Span 2.....	652
Table 126. Coordinates for girder and cross-frame ends – Span 3.....	653
Table 127. Example 3 Girder G1 section properties.....	659
Table 128. Example 3 Girder G2 section properties.....	659
Table 129. Example 3 Girder G3 section properties.....	659
Table 130. Example 3 Girder G4 section properties.....	660

LIST OF ABBREVIATIONS

1D	One-dimensional
2D	Two-dimensional
3D	Three-dimensional
AASHTO	American Association of State Highway and Transportation Officials
ACI	American Concrete Institute
AISC	American Institute of Steel Construction
API	American Petroleum Institute
ASTM	American Society for Testing and Materials
BrIM	Bridge Information Modeling
CAFL	Constant Amplitude Fatigue Limit
COV	Coefficient of Variation
CQC	Complete Quadratic Combination
DOF	Degrees of Freedom
DSM	Direct Stiffness Method
FEA	Finite Element Analysis
FHWA	Federal Highway Administration
FWS	Future Wearing Surface
GUI	Graphical User Interface
IIM	International Institute of Welding
LRFD	Load and Resistance Factor Design
LSS	Local Structural Stress
MBE	Manual for Bridge Evaluation
MDOF	Multi-Degree of Freedom
NCHRP	National Cooperative Highway Research Program
NLF	No Load Fit
NSBA	National Steel Bridge Alliance

PEB	Plate on Eccentric Beam
POC	Point of Contraflexure
PT	Post-Tension
SDLF	Steel Dead Load Fit
SDOF	Single Degree of Freedom
SIP	Stay-In-Place
SRSS	Square-Root-Sum-of-Squares
SSI	Soil Structure Interaction
TDLF	Total Dead Load Fit

CHAPTER 1. PREFACE

1.1 Background

Over the last few decades significant advances have occurred in the way that bridge engineering analysis *can be* carried out. Engineering practitioners of today, with the aid of ever-advancing computer technology, are able to solve engineering problems of great complexity, and produce designs/evaluations which are more refined and more reliable than in the past. However, our nation's governing bridge design specifications and the profession as a whole have not yet fully exploited the capabilities of this new generation of engineering design professionals and analytical tools.

The generic term “refined analysis” is often used to describe a more detailed, sophisticated structural modeling approach, which typically involves computerized finite element analysis (FEA). The ability to perform FEA is within the skill set of most engineers today, and software tools are widely available to most engineering firms. *However, “refined analysis” is largely undefined in the design specifications, and is employed loosely and sometimes ambiguously in the specification provisions.* In addition, there is limited guidance in the literature on the proper application of such analytical techniques.

In 2009, an international technology scan entitled “Assuring Bridge Safety and Serviceability in Europe” was sponsored by Federal Highway Administration (FHWA), American Association of State Highway and Transportation Officials (AASHTO), and National Cooperative Highway Research Program (NCHRP). The scan team determined that U.S. engineers need advanced tools and protocols to better assess and assure safety and serviceability of bridges (Hida et al, 2010). The team recommended increased use of refined analysis for bridge design and evaluation, and encouraged the use of refined analysis to avoid unnecessary posting, rehabilitation, or replacement. Unfortunately, practical implementation of these recommendations has been limited.

Many bridge engineers appear to favor a general philosophy of keeping analyses as simple as possible to minimize errors or to remain true to the accepted, proven engineering practices, and consequently have avoided embracing regular use of refined analysis methods. However, this approach, while comfortable, comes at a cost to our nation and may not foster the most effective use of limited resources. The current AASHTO LRFD Bridge Design Specifications feature a reliability-based approach to bridge design, and include formulas for various aspects of load distribution and limit state design with conservatism built in to envelope the limits of applicability and consider all the relevant parameters. Conservatism always adds unnecessary cost, which may have serious implications for owner-agencies with limited budgets.

At the same time, the perceived complexity of the AASHTO provisions encourages designers to focus on developing and using complex automated calculation tools to execute the necessary code checks rather than performing meaningful structural modeling to better understand behavior and address the limit states that are being evaluated. This often hides the controlling factors and hinders the development of new bridge innovations in general.

A properly and efficiently executed refined analysis can provide substantially better information about the state of stress in a bridge and allow for more cost-effective and reliable design.

However, if approached improperly, a refined analysis can involve excessive engineering effort and increased possibility for error. Refined analysis models are often more sensitive to the input parameters and the mathematical assumptions which are employed by the software, and so must be used with care. The engineer must understand the assumptions to ensure correct application. Furthermore, the results of refined analyses can be misleading, making it all the more important that the engineer verify the results by independent calculations. The complexity of the model may make this difficult, so special procedures must be employed to verify accuracy.

The solution to these concerns is to provide standard modeling guidelines and benchmark solutions to guide engineers and provide a consistent set of results for verification, which is the main goal of this manual.

Note that in everyday usage, verify and validate have very similar meanings. However, when it comes to refined analysis, they have different meanings. Verification refers to making sure the analysis is performing correctly, that it is giving the correct results to the input given. Validation refers to making sure that the input is correct, and the results reflect the behavior of the actual structure being modeled.

This manual was developed to provide guidance to bridge engineers regarding the use of finite elements as a refined analysis method for designing or evaluating typical concrete deck slab on girder highway bridges. Complex structure types, such as cable stayed, suspension, or arch bridges are not specifically addressed. The AASHTO LRFD Bridge Design Specifications (AASHTO LRFD) (AASHTO, 2014) allow for many different types of analysis, but generally only provide detailed guidance on the application of approximate methods, such as distribution factors for right straight multi-girder bridges, leaving the details of refined analysis up to the bridge design engineer. When a structure falls outside the limits of applicability of an approximate method, AASHTO LRFD essentially requires refined analysis without providing much guidance as to how it should be carried out.

1.2 What is Refined Analysis?

Refined analysis often means different things. A definition of refined analysis is needed to explain more clearly what this manual addresses. Perhaps a good way to define what something is, is to start with what it is not. By noting where the AASHTO LRFD states “in lieu of a refined analysis...,” an idea of what is not considered refined analysis can be developed. This would include:

- Line girder analysis using distribution factors
- Single step moment magnification procedure for compression elements
- Curved spine beam analyses
- Strut and tie models of concrete elements
- Strip method of deck analysis and design
- Cross-sectional frame analysis for box girders
- V-load for curved I-girder bridges
- M/R method for curved bridges
- Equations for effective flange width of composite decks

Having listed some of what refined analysis is not, a definition of what refined analysis might include can begin to be constructed. *A refined analysis might:*

- *Account for shear lag in deck and planar elements*
- *Account for the distortion of a cross-section*
- *Explicitly model cross-frames*
- *Explicitly model the deck as a plate (rather than a grid) in two dimensions*
- *Distribute load to girder lines based on interconnecting stiffness*
- *Assess capacity through the use of plastic hinges, such as by pushover analysis.*

Refined analyses are more sophisticated, and when correctly applied, generally more accurate than the current approximate methods contained in the AASHTO Specifications.

1.3 Why use a Refined Analysis?

In some cases refined analysis is *required* to complete the design according to AASHTO LRFD. These are instances for which the specification approximate methods do not apply. *Furthermore, there are reasons why using a refined analysis might be advantageous, including but not limited to:*

- *Capturing behavior not adequately accounted for by approximate methods and/or outside the limits of the Specifications. Even within the limits of applicability, approximate methods can give erroneous indications of a structure's true behavior.*
- *Obtaining more accurate, and less conservative, demands for existing structures, especially when approximate methods result in conservative demands which in turn result in extensive repair or replacement of structures.*

The potential payoff for widespread implementation of refined analysis in the bridge engineering industry is considered broad, but difficult to quantify. This Manual promotes a fundamental change in the practice of bridge engineering and attempts to move our industry past the use of simplistic design specifications to achieve more optimal solutions. It can be said that if merely one bridge is saved from replacement by the application of refined analysis in an evaluation, then any additional engineering effort is justified. If only five percent material savings could be realized in every new design across the nation, then potential savings in taxpayer money would easily be in the tens of millions of dollars *every year*.

Practitioners indicate that refined analysis of most bridge structures can be done for only a small premium over conventional, simplified techniques with currently available computer technology. The practice of bridge engineering in the future is expected to take a more holistic approach, where the design, fabrication, construction, inspection, and management will be much more integrated by digital information exchange. Refined analysis is expected to become routine as software vendors develop “translator” and “wizard” tools to communicate with database records and generate detailed structural models for engineering analysis. This Manual is seen as an essential component to defining proper criteria for software vendors to follow and for engineers to demand from their tools.

Refined analysis in bridge engineering has the potential to provide the following benefits in the engineering design and evaluation of our nation's infrastructure:

- Improved structural safety by more rigorous assessment of limit states
- Increased economy by going beyond use of approximate, conservative design formulae
- Increased safety and economy by accurate modeling of system or local behavior
- Improved safety evaluation by full consideration of condition data such as section losses or as-built geometry
- Increased sustainability by more frequent salvaging of existing infrastructure
- Accelerated innovation development as industry gains deeper understanding of bridge behavior

Note that while a general theme of the reasons for refined analyses is greater design economy, there are also cases where refined analysis does not result in savings, but an improved, more uniform level of safety, by providing deeper insight into actual structural load paths. An example would be where an element carries a greater percentage of total load than adjacent similar elements, and designing them all for an average load would lead to a higher probability of progressive failure.

1.4 Evolution of Structural Analysis Methods

Structural mechanics has its roots in the mid-nineteenth century. Over the next several decades numerous “classical methods” of structural analysis were developed, including Castigliano’s 1st and 2nd theorems, slope-deflection, three moment equation, conjugate beam, moment area, virtual work, moment distribution, and many others. In general, a linear analysis technique needs to satisfy equilibrium, compatibility, and the stress-strain relationship of the component material(s). Some classical methods solve specific geometrical problems, while others have more general application.

Matrix algebra also has its roots in the same time period in the mid-nineteenth century. But it wasn’t until about 1930 that the aerospace industry started to develop modern matrix methods of structural analysis (Felippa, 2001). There are essentially two matrix analysis techniques, the compatibility, or flexibility method, where the unknowns are forces, and the equilibrium, or stiffness method, where the unknowns are displacements. For about the next 30 years matrix methods were simply another tool for performing structural analyses, along with the numerous classical methods, due to the limitations of the “human computers” and the calculating devices such as the slide rule or mechanical calculators available to them. The required solution of simultaneous equations, often by matrix inversion calculations for structures involving more than a handful of members, quickly became unwieldy. The flexibility method, which required selection of appropriate redundant force patterns, was embraced by the aerospace industry, as the selection of redundants for the lattice skeleton of aircraft was well understood, resulting in simpler solutions to the problems they faced.

In 1951, the first electronic commercial computers, the UNIVAC1, were manufactured. Although much too expensive for the average consultant design office, early computers represented a gigantic leap forward in calculating power. Throughout the 1950s what were eventually referred to as “mainframe” computers continued to be developed. In the late 50s, the FORTRAN programming language was developed making it much easier to program the computers to solve scientific and engineering problems. Then, in 1959, M. J. Turner, head of the Structural Dynamics Unit at Boeing and an expert in aeroelasticity, presented the first paper on

the Direct Stiffness Method (DSM) (Felippa, 2001). R. W. Clough coined the term Finite Element Method in a paper authored in 1960 (Clough, 1960) which eventually replaced DSM by about 1965 as the terminology for the analysis method.

For the DSM, element stiffness matrices are generated in local reference systems, then transformed to a global reference system and directly assembled together to create the overall structure stiffness matrix. The assembly method is insensitive to element type and works no matter how many nodes comprise an element. This allows the programs to easily accommodate essentially unlimited additions of new types of elements as they are developed. The analysis method is linear elastic and small deflection, since the matrices are assembled based on initial geometry and elastic properties and remain unchanged throughout the analysis, but nonlinear problems could be solved iteratively using a series of linear steps by revising the stiffness matrix at the beginning of each step.

The DSM was perfectly suited for solving general boundary value problems using digital computers. But general purpose direct stiffness finite element programs did not develop overnight. Even though computers were becoming more powerful and were being acquired by more design offices, early computerization consisted mainly of custom automating the classical methods that were in use at the time, which generally limited the solutions to specific problems or geometries. Not to mention that the aerospace industry still was invested in the flexibility method. By about 1970, however, the DSM had carried the day, and become the standard solver technique for what we know today as general purpose finite element programs.

One of the first matrix structural analysis packages available to bridge design engineers was “STRESS,” for STRuctural Engineering System Solver, developed by S. J. Fenves and others at M.I.T. and supported on the IBM 1130, a powerful and relatively inexpensive computer marketed in the mid 1960s. This line element software enabled engineers to solve systems of two- and three-dimensional truss and beam elements. The key difference between this software and the custom written programs of the time was that this program could solve problems of any geometrical configuration. Using this program bridge designers were able to analyze multi-girder bridges using grillages or space frames to arrive at a system solution rather than rely on approximate distribution factors.

Programs such as STRESS, written to solve static first-order problems, soon were used by creative engineers as a calculation engine to compute trial and error deflections necessary to use iterative methods such as the Newmark process for calculating frequencies, mode shapes, buckling loads, and second order deflected shapes of relatively complex structures. Engineers used their understanding of structural theory and structural behavior to overcome the hardware and software limitations of the time. This continues today, for instance an equivalent Saint-Venant torsional constant can be used to account for warping, an effective modular ratio can be used to adjust section properties to account for concrete creep under sustained loads, or an effective stiffness is used to approximate cross frame behavior with a single element.

In the 1970s general purpose finite element programs started to become more widely available to design engineers in the form of programs such as NASTRAN, SAP, and STRUDL. These packages added enormous analytic capabilities to the engineer’s tool kits. Element libraries contained not only beam and truss elements, but plate bending elements, shell elements, and plane-stress and plane-strain triangles and quadrilaterals as well as three-dimensional brick

elements. This enabled engineers to solve continuum-type three-dimensional problems with relative ease.

Over the last 40+ years there have been many advances in the capabilities of finite element analysis (FEA) programs including:

- Improvements in pre-processing
 - Graphical user interfaces (GUIs)
 - Large element libraries
 - Model generation wizards/automatic model generation
- Improvements in solver capabilities
 - Multiple solver choices depending on model/elements
 - Matrix optimization
 - Non-linear iterative capabilities
- Improvements in post-processing
 - Report generation
 - Stress visualizations
 - Animations

It should be noted that most of these advances are essentially “bells and whistles” for improving speed and user-friendliness. The DSM of the 1970s continues to be the standard solver technique in use today. The main advantage of the programs of today over those of yesterday is the increase in computing capacity. Structures can be modeled and analyzed today in a day that would have taken weeks to run 40 years ago, if they could have been analyzed at all. Furthermore, it is expected that structures which engineers would never attempt to model today, will be easily modeled and analyzed in the future.

1.5 State of Practice

The standard method of analysis for typical multi-girder bridges in the United States has for years been a line girder analysis with the use of distribution factors. In this type of approximate analysis, each girder is analyzed as a stand-alone component. Assumptions are made regarding the distribution of dead loads among the girders, while distribution factors account for the transverse distribution of live loads. If the bridge is continuous, or otherwise indeterminate, an analysis program is usually used to determine the shears and moments in the girders based on the distributed loads applied.

There are many advantages to this approach to bridge analysis, among them ease of use and repeatability of results. However, there are some disadvantages, not the least of which is the limited range of applicability. The method begins to break down when the bridge becomes skewed and/or curved. In these cases, the cross-frames between girders become part of the primary load resisting system, and accounting for them in the analysis requires additional approximate calculations such as the V-load method, or M/R method for curved bridges. The accuracy of these approximations degrades as the degree of skew and/or curvature increases.

Also, even for straight non-skewed structures, use of AASHTO LRFD distribution factors tends to introduce a degree of conservatism that usually results in more total design live load than lanes on the bridge, and the use of more material in the design than necessary. Using refined analysis

to distribute the live load more accurately has the potential to provide more economical new bridges and/or improved load ratings for existing bridges.

The trend in refined analysis has been a decreasing additional cost in time and effort versus traditional approximate methods. Developments in available software continue to decrease the differential analysis cost such that this will not be a significant factor in the decision of which method to use in the very near future, if in fact it has not already occurred for some classes of structures.

In the United States, certain bridge types have been designed using refined methods of analysis for at least 40 years. In fact, approximately in 1988, when the framework for the AASHTO LRFD was developed, the development team proposed to the Panel guiding the work that distribution factors not be part of the Specifications, but rather that the requirement would be a two- or three-dimensional refined analysis. At the time this suggestion was roundly rejected as beyond the capability of most practicing engineers. Now many more practicing engineers have had some education and/or experience with the refined methods of analysis, computer programs to perform such analyses are more widely available, and the computing power required to run them is easily affordable. *Currently, for most cases of design of concrete deck slab on girder highway bridges, a 2-D plate on eccentric beam (PEB) would be the recommended refined analysis procedure* (for more on PEB see Sections 2.4.3.2 and 3.5.2).

Modeling issues, in particular boundary conditions and loading, are sources of problems in the application of refined methods such as FEA, not to mention that different acceptable models can yield somewhat different results. It is not the purpose of this manual to legislate the use of models for particular types of bridges, but to direct the engineer in developing reasonable models which will produce more consistency in the application of these refined methods. This is particularly true for bridges with complex geometry such as curved and skewed bridges in which the quantification of the forces and distortions in some of the members cannot be accurately predicted with the approximate methods for load distribution in Section 4 of the AASHTO LRFD. This is why references are made at various places within the specification as to when refined methods are particularly appropriate.

1.6 Scope of Manual

The approach presented by this manual is to relate refined analysis techniques to those currently addressed in the AASHTO LRFD, to highlight what an engineer needs to consider when moving to a refined analysis, and to ground the process in basic engineering fundamentals and practical, experience-based guidelines. Guidance on the applicability of one-, two-, and three-dimensional analysis are provided. References to specific proprietary software packages are avoided if possible.

Also addressed are some of the unique issues of analyzing existing structures, such as the need to know the construction method and sequence in order to properly account for the distribution of dead load and locked-in stresses. For example:

- A girder bridge erected as simply supported for dead load but made continuous for live load.

- Segmental concrete girders erected by the cantilever method acting like cantilevers for dead load but continuous girders for live load.

It is not the aim of this manual to cover material that can be found in other existing publications. A partial list of publications that supplement/extend the information presented here are:

- NCHRP Report 725 – Guidelines for Analysis Methods and Construction Engineering of Curved and Skewed Steel Girder Bridges
- NCHRP Report 620 – Development of Design Specifications and Commentary for Horizontally Curved Concrete Box-Girder Bridges
- AASHTO/NSBA Steel Bridge Collaboration – G 13.1 Guidelines for Steel Girder Bridge Analysis, 2nd Edition
- FHWA Orthotropic Deck Design Manual
- NHI Course No. 130095 – Analysis and Design of Skewed and Curved Steel Bridges with LRFD – Reference Manual
- NSBA Skewed and Curved Steel I-Girder Bridge Fit (Chavel et al., 2016)
- FHWA Post-Tensioned Box Girder Design Manual (Corven, J., in development)

Throughout the following chapters, references to the seven examples developed as part of this manual are included. These examples are provided in Chapter 9. The seven examples include four general bridge analysis examples:

- (1) Example 1 - a straight, three-span, composite precast concrete I-girder concrete deck slab bridge with square supports, simply supported for dead load made continuous for live load;
- (2) Example 2 - a straight, three-span continuous, composite steel I-girder concrete deck slab bridge with square supports;
- (3) Example 3 - a curved, three-span continuous, composite steel I-girder concrete deck slab bridge with skewed supports; and
- (4) Example 4 - a curved, three-span continuous, concrete box girder spine beam.

Also provided are three more specifically targeted examples on more advanced topics:

- (5) Example 5 - a dynamic linear multimode response spectra analysis of the curved multi-girder steel bridge from Example 3 including soil structure interaction, pushover, and dynamic deflections;
- (6) Example 6 - a stability analysis of a tall concrete pier incorporating geometric nonlinearity and utilizing cracked/uncracked section properties where appropriate;
- (7) Example 7 - a staged, construction analysis of a four span 660' long continuous concrete box girder bridge with external tendons, focusing on global design forces including concrete creep and shrinkage.

Multiple methods are used in the examples in order to compare the results of increasing refinement in the analyses.

1.7 Summary

To support advancement in the practice of bridge engineering in the U.S., this Manual provides guidelines and examples for the proper use of refined analysis in bridge engineering. The expected outcome is a move toward widespread use of more refined, modern analytical techniques to improve economy, safety and performance of our nation's infrastructure now and in the future. Some engineers may be uncomfortable moving away from the predictable and conservative load distribution factor method of design to refined methods that result in potentially lower and more variable design force effects. However, as long as the refined model is representative of the designed structure, the target Reliability Index of the AASHTO LRFD Design Specification will still be obtained. In other words, the design will still satisfy the intent of the Specifications, meeting all limit states and achieving constructability, safety, and serviceability, through use of a more efficient design with less conservatism.

To achieve this goal, this manual strives to provide sound technical guidance, but to not overly constrain designers. Often there is more than one valid path to correct results, while there are certainly also potential pitfalls leading to incorrect results. The intent of this manual is to educate engineers, making them more aware of both the pitfalls and valid paths, without prescribing an overly restrictive approach to refined analysis.

This manual provides guidance on the following topics:

- *Reviewing the basics of the finite element method.*
- *Choosing the appropriate level of refinement, i.e. 1D, 2D, or 3D model for the problem at hand.*
- *Assembling the chosen model(s), including element types, meshing, and boundary conditions.*
- *Loading the model(s) in accordance with the AASHTO LRFD Specifications.*
- *Verification/Validation of both the model and loading.*
- *Extraction of usable results.*

Preventing misuse of the FEA method, while maximizing flexibility so designers can choose the most appropriate implementation for the structure and client at hand, is the goal. The manual is written such that a bridge engineer who has just received licensing as a professional engineer, and is familiar with the general aspects of bridge design and analysis, but who may not have had much exposure to the finite element analysis method as applied to bridges, can utilize it to perform routine bridge analyses. Important concepts are highlighted using *italics*. Some advanced topics are also provided for more experienced engineers to help in performing more sophisticated refined analyses.

CHAPTER 2. REFINED METHODS OF ANALYSIS

2.1 Methods of Analysis Permitted by AASHTO LRFD

Article 4.4 of the AASHTO LRFD establishes the most basic requirements for any analysis applied to bridges or any other structures as meeting the requirements of equilibrium, compatibility, and appropriate material constitutive relationships. Along with FEA, Article 4.4 of the AASHTO LRFD lists the following acceptable analysis methods but does not preclude the possibility of others:

- Classical force and displacement methods as might be utilized in pier analysis, development of influence lines and other cases where methods such as virtual work, moment distribution or slope deflection still occasionally yield efficient solution methods.
- Finite difference method, which is a numerical means of evaluating a differential equation for either a boundary value problem or a time-dependent problem. This has been largely supplanted by the finite element method, but can occasionally still be used efficiently as an independent check.
- Folded plate method using the theory of elasticity. Several solution methods have been developed. One method, developed by Goldberg and Leve, combines the equations of classical plate theory for loads normal to the plane of the plates with the elasticity equations defining the plane stress problem for loads in the plane of the plates. While hand calculation is tedious, Scordelis (Scordelis, 1960) adapted the method to a matrix method amenable to computer solution.
- Finite strip method, which is a semi-analytical finite element method suitable for problems whose properties are uniform in one or more directions, allowing for a discretization into strips. The solution is approximated by using a continuous harmonic function series which satisfies the boundary conditions in one direction, and piecewise polynomial interpolation in the other directions. Useful for solving plate, folded plate, shell, and bridge deck problems.
- Grillage analogy method involving models built of line elements interconnected in a manner to be relatively faithful to the structure geometry. These are also often called “grid methods.” They have been implemented both using grid-specific software and using beam elements to develop the grid in a finite element analysis.
- Series or harmonic methods are applicable primarily to the solution of dynamic issues and have had historic application to stability and suspension bridge analysis. These methods are also largely supplanted by finite element analysis but still form the basis of many textbook or handbook solutions to certain types of problems which have continued value as a means of checking computer-oriented solutions.
- Methods based on the formation of plastic hinges which, while lacking continuity, replace that virtue with a mechanism which permits relative rotations at the hinges to be determined so that external work can be estimated. Pushover analyses, or capacity protection as a seismic design strategy, are applications of methods using plastic hinges.

- Yield line theory extends the formation of plastic hinges to continuum-type problems where the inelastic rotation is idealized along lines much like a piano hinge. The design methods permitted for a test specimen of a railing system are based on a yield line approach.

In addition to the applications identified above, other analysis methods, such as Fiber Element Modeling, a nonlinear section modeling method, have been utilized by bridge designers as well as researchers developing provisions for the AASHTO LRFD.

Despite the existence of these other methods, the finite element method has become the method of choice for most refined analyses of bridge structures. Reasons for this include flexibility of application, ease of use, and continuing increase in the computing power available to bridge designers. As such, when this manual refers to “refined analysis” it typically means the finite element method. The continued listing of these other methods provides continuity with past research, and also provides independent techniques to verify refined analyses, even though most current work is performed with finite element analysis.

Article 4.4 also establishes that it is the responsibility of the designer to properly implement the analysis method and correctly interpret the results, no matter what method is used.

2.2 Refined Methods of Analysis Referenced in AASHTO LRFD and AASHTO MBE

There are many references to refined analyses in the AASHTO LRFD (AASHTO, 2014) and the AASHTO Manual for Bridge Evaluation (AASHTO MBE) (AASHTO, 2011). See Appendix 2A for a compilation of references to refined analysis found in the 7th Edition of AASHTO LRFD and Appendix 2B for a compilation of references to refined analysis found in the 2nd Edition of AASHTO MBE.

As mentioned in Section 2.1, Article 4.4 of the AASHTO LRFD lists some, but by no means all, of the refined analysis methods available. Articles 4.5 and 4.6 contain recommendations on modeling and analysis using refined methods and in addition to this manual should be the starting place for an analyst contemplating performing a refined analysis. Guidance is provided on when to perform a refined analysis and what level of refinement is necessary in given situations. Article 4.6.3 is specifically about refined methods of analysis and much of the information specific to FEA in the AASHTO LRFD can be found there. Other references to refined analyses throughout the AASHTO LRFD are more generic.

A significant number of references to refined analyses are along the lines of “in lieu of a more refined analysis, the following can be used,” implying that a refined analysis should be considered if more accuracy is required, but the given simplified method is usually sufficient for routine bridge design. In AASHTO LRFD Sections 5 and 6, the sections devoted to design of concrete and steel respectively, refined analyses are often recommended for the design of specific elements in specific situations.

There are relatively fewer references to refined analyses in the AASHTO MBE. Most of the references to refined analyses in the AASHTO MBE recommend when such an analysis should be performed, but do not give any further guidance or recommend a specific refined method.

2.3 Essentials of Finite Element Analyses

2.3.1 General Capabilities of Modern Finite Element Software

FEA software ranges from basic inexpensive software that can model linear elastic behavior of frame structures composed of beam elements, to expensive software that can model nonlinear inelastic behavior of complex structures and can utilize large libraries of specialty elements. Over time, the capabilities of FEA software have increased, while the licensing costs have decreased. Though some of the improved capability is related to the solvers, i.e. iterative nonlinear solvers, much of the improvement has been in the ease of use and the tailoring of the software for bridge design. FEA programs have also benefitted from advances in computer processing speed and memory.

Utilizing high-end FEA programs, such as those employed in aerospace design, is not cost effective for most routine bridge designs, since typical bridge designs do not require the advanced capabilities of those programs. Additionally, while powerful, high-end programs tend to be more general purpose, and not tailored to producing bridge models.

The bridge design industry generally uses midlevel FEA software for typical bridge design tasks. These are programs with point, line, surface, and volume elements. Although mostly used for linear elastic analyses, the programs usually have some material and geometric nonlinear capabilities. The more advanced of the midlevel programs have modules tailored for bridge design, making bridge model creation, loading, and analysis easier.

Model generation currently can be performed through graphical interfaces, with the resulting models viewed graphically on a monitor, rather than the text input and output files of the past. Text files, however, still have their place, and can often be utilized to quickly generate new models, change current model properties, or to check model inputs.

There are many different solvers with various exotic sounding names used in FEA programs. Sometimes a single program will use different solvers for different size models, models utilizing certain elements, or models requiring iterative solutions. They are all essentially variations on the Direct Stiffness Method, however. The different solvers handle solution of the N stiffness equations, to facilitate solving certain classes of models more efficiently. For instance, a small model where N is relatively small may invert the full $N \times N$ stiffness matrix during solution without performing any optimization, while a large model may employ optimization techniques (referred to as sparse solvers) that take advantage of the large number of zeros in the stiffness matrix that can be ignored, such that the equations are solved more efficiently.

Some of the tools available in current software packages include model creation wizards, geometry based modeling, section property databases and generators, automatic meshing, bridge live loading generators, and specification checkers. In short, it is becoming easier than ever to generate and run complex bridge models. More complex models, however, mean more potential for errors which can be more difficult to find.

Bridge Information Modeling (BrIM) systems are expected to be the next step in the evolution of structural bridge models. BrIM is defined as the process of documenting all bridge information, such as materials, geometry, foundations, traffic, and other data, from project conception through the entire life cycle of the structure using a data centric 3D model. Full 3D bridge models can be

used for more than just structural analysis and design. The models will be part of the database of information about the bridge and can be used to aid in other tasks downstream of design, such as fabrication, construction, and operation.

2.3.2 Gauss Points, Shape Functions and Degrees of Freedom

The finite element method is a numerical matrix solution technique for finding approximate solutions to boundary value problems. The method entails using a series of elements to approximate a continuum. Individual elements use polynomial functions called shape functions to describe the deflected shape between the element connections, or nodes. For a given level of meshing, the more accurately the shape functions approximate the actual deflected shape, the better the agreement with the actual behavior.

Integration is used to calculate the element stiffnesses as well as for element state determination (e.g., recovery of element internal stresses and nodal forces for a given set of element displacements). The integration proceeds by evaluating the function at specific points, applying an appropriate weighting factor, and summing results. Gauss numerical integration, or Gaussian Quadrature, is the most commonly used technique in generating element matrices. This technique minimizes internal integration points and locates them so as to minimize integration error when the integrand is a general polynomial. Systematically combining all of the individual elements into a global system of equations leads to the solution of the overall model. Often finite element programs provide output at the gauss points of elements as well as the nodes. For further information on the finite element method, see texts such as (Bathe, 1976) and (Zienkiewicz, 2005).

Displacements of a point, or node, can be characterized with up to six quantities in Cartesian coordinates: translation and rotation for each of the three axes, as illustrated in Figure 1. The possible movements of a node due to the structure loading are referred to as degrees of freedom (DOF). The DOF of a model corresponds to the sum of all the DOF at all the nodes in the model, although not all finite elements incorporate all six DOF at the nodes in their formulations. For instance, members modeled using truss elements that do not incorporate rotational degrees of freedom can have incompatible rotations at connecting nodes. Another example would be two dimensional planar elements that do not incorporate out-of-plane DOF. Generally the more DOF in a model, the more computational effort is required to solve the equations. For example a truss modeled as pin-connected using two force bar elements will require less computational effort than the same truss modeled using beam elements with full fixity at the joints.

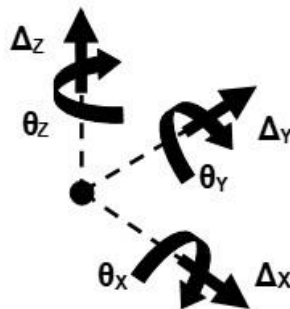


Figure 1. Illustration. Six degrees of freedom (DOF) at a point, or node.

One way to minimize the DOF is to minimize the number of nodes in the model. Conversely, as the number of nodes and corresponding DOF increase, generally so does the accuracy of the solution. Figure 2 schematically illustrates the relationship between increasing DOF, increasing accuracy, and computational effort. Note that there is a diminishing rate of increased accuracy, and increasing the DOF beyond a certain point results in very little increase in accuracy, but the computational effort continues to increase. There is no absolute criteria for determining the optimum number of DOF for any given problem.

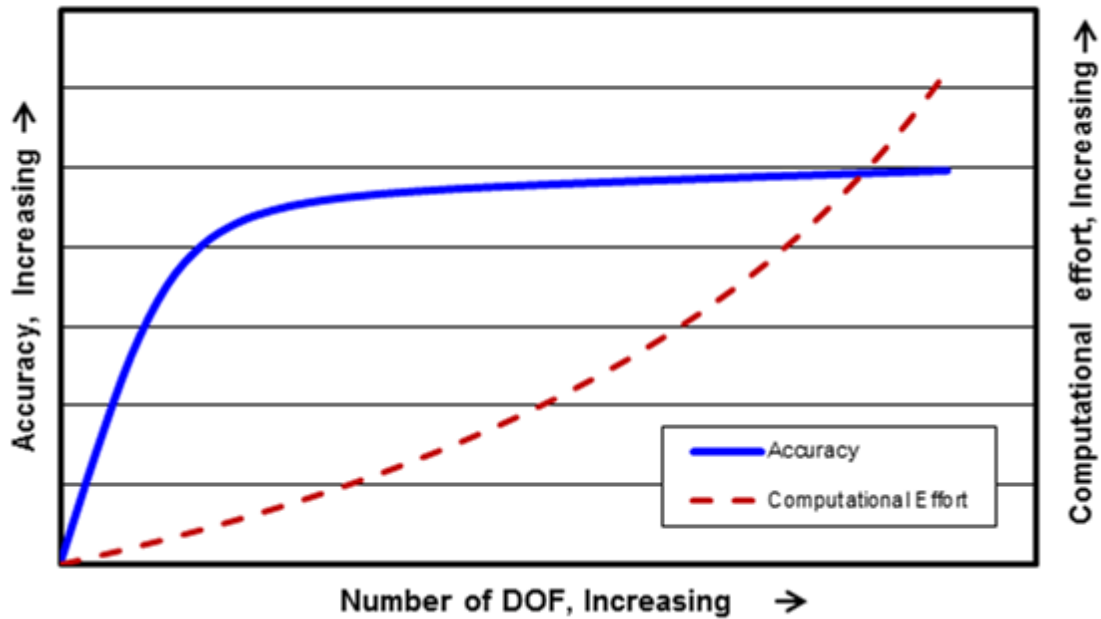


Figure 2. Graph. Schematic illustration of the relationship between DOF, accuracy, and computational effort.

As mentioned previously, different finite elements also incorporate different DOF in their shape functions. Choosing the element that captures the significant DOF of the problem to be solved is also important, since choosing an element that does not have sufficient DOF will result in a less accurate solution, while choosing an element with extra DOF will require more solution time. For instance, choosing a plate element to model a composite deck will result in errors, since plate elements do not support a membrane DOF and therefore will not carry axial forces in-plane.

Note that erring on the side of extra DOF is preferable to not enough, as long as inappropriate restraint is not being provided, since current computer processor speeds can often render the extra solution time inconsequential, and taking extra solver time is better than getting inaccurate solutions. Generating more output data may increase the time required to interpret the results, however.

Different elements with the same DOF can also have different internal formulations such that behavior and results are different. For instance Timoshenko beam elements are formulated to include shear deformation, while Bernoulli beam elements do not (for more on this see Section 2.3.4.2.2).

A certain amount of experience and good judgment is required to optimize the DOF such that computational effort is minimized while the desired accuracy is achieved.

2.3.3 Typical Input and Output

As mentioned previously, input can usually be performed using a graphical user interface. For large models it may be easier to generate all or many elements of the model using spreadsheet generated text files. Changing element geometrical properties and/or loadings in a large model is also often easier using spreadsheet generated text files. Many FEA software packages have features that aid in the creation of models, and specifically aid in the creation of bridge models.

Input begins with geometrical discretization and assigning model attributes. The first step is to define node locations, choose the type of elements to be used, and generate a mesh that reflects the geometry of the structure being modeled. Paying attention to element connectivity and DOF is important, including constraints such as rigid links in order to construct a stable model and avoid mechanisms. Next, geometrical properties of the elements, i.e. area, moments of inertia, etc. are assigned. Many programs make this easier with libraries of common rolled shapes and section property calculators.

Material properties can then be assigned to the elements. Young's modulus and Poisson's ratio, from which the shear modulus can be calculated, are sufficient for many analyses employing only isotropic materials. Anisotropic materials require additional parameters. Mass density or unit weight, depending on the software, is required if dead loads are to be automatically generated. Getting the mass correct is particularly important if a dynamic analysis is being performed. The coefficient of thermal expansion is required if thermal analyses are to be performed or expansion/contraction capabilities are to be utilized, for instance when using thermal expansion/contraction as a surrogate for explicit lengthening/shortening when cambering. For higher order analyses, such as those with steel yielding, concrete cracking, or soil non-linearity, more material parameters are required. Again, many programs make this easier with libraries of commonly used materials, and default values for common material behaviors. *Getting the relative member stiffnesses correct in a refined analysis model is key to getting a representative distribution of force effects.*

Next, stable boundary conditions need to be applied. Boundary conditions are restraints that prevent movement in specified directions at specified points. In order to be stable, sufficient boundary conditions must be present to prevent rigid body motion of the model in any of the three translational or three rotational directions. In the past, most programs would fail to run if one attempted to solve an unstable structure. Some current solvers will give (incorrect) results for an unstable structure. Often this is easily recognized due to obviously wrong forces or deflections.

Finally, loadings can be applied. Current programs are very flexible with regard to loadings. Point, distributed, area, thermal, and displacement loadings among others can be applied to the model. Care should be taken when assigning loads between nodes to ensure that the nodal loads generated by the program are approximately statically equivalent to the actual loads being applied.

Once the model has been assembled and the program run, various outputs are generated. Load cases can often be combined and factored within the programs if desired. Note that factored combinations are only appropriate in cases where superposition is valid, such as linear elastic analyses, and not for nonlinear results. Usually all of the outputs can be viewed graphically as well. It is suggested that the deflected shape and reactions be examined initially. Often errors can be easily identified when the model deflects or reactions are distributed in unexpected ways. Other typically utilized outputs are forces and/or stresses. These can usually be viewed as graphs or contours, or exported in the form of tables for further post-processing. Note that outputs are not always in a form that can be directly utilized for AASHTO LRFD (see Chapter 8 for more on utilizing analysis results).

2.3.4 Typical Element Families and Usage

There are four typical element families used in bridge design: Point, line, surface, and volume. There are many elements with different formulations, different capabilities, and different DOF within each family of elements. They range from specialty elements with very specific application, to more generic elements with more general application. Constraints and rigid links are arguably a fifth class of elements. Constraints and rigid links can provide appropriate connectivity within a model, such as composite action. It is the user's responsibility to make sure the elements comprising a model are compatible and have the appropriate DOF and capabilities for the problem at hand.

2.3.4.1 Point Elements, Constraints, and Rigid Links

Point elements are zero, or near zero, length elements which interconnect other elements in a model, usually at coincident nodes. Point elements are often used between elements to release certain degrees of freedom. Point elements can also be used to provide linear or nonlinear support conditions, to add a point mass for dynamic analyses, or to connect multiple nodes by springs with translational and rotational stiffness. Some FEA packages have interface point elements that can be used for instance as tension only, or contact elements, or in between layers of composite materials.

Point elements are not typically used in models for routine slab-on-girder bridge design, but may be utilized to model bearings using releases or spring stiffnesses between superstructures and substructures within a model.

Constraints and rigid links are methods of constraining or releasing the movement of geometric or nodal freedoms within a model. They can be used to set up a relationship between nodal freedoms, maintaining defined compatibilities. Often, they are preferable to using stiff elements when connecting nodes rigidly, as overly stiff elements can result in solver errors due to an ill-conditioned stiffness matrix. They also allow the flexibility of constraining any combination of the six DOF at a node.

2.3.4.2 Line Elements

Line elements are used to model bars, beams, cables or other structural elements where the length of the element is generally much greater than the depth and the width. For line elements, transverse through-thickness normal stresses are negligible, with normal stresses generated only along the longitudinal axis of the element. Line elements are attractive for use in bridge design,

as the forces typically used for bridge component design; axial forces, bending moments, and shear forces, are directly output.

2.3.4.2.1 Bar or Truss Elements

Bar or truss elements are two-force members capable of resisting deformation only in the longitudinal member direction (see Figure 3). This resistance is associated with axial force in the member. This type of element is used where members are subjected to primarily axial forces, such as trusses or cross-frames. In some programs, bar elements are a special case of a beam element, with all rotational degrees of freedom released. Some programs allow tension only or compression only bar elements.

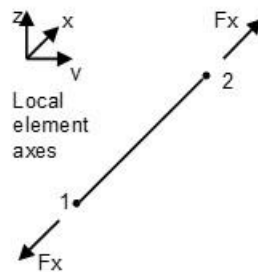


Figure 3. Illustration. Bar or truss element.

2.3.4.2.2 Beam Elements

Depending on the element formulation, beam elements can have stiffness and transmit loads corresponding to all six DOF at each node as illustrated in Figure 4. Beam elements are therefore capable of modeling components that resist not only axial forces but also biaxial shear, biaxial moment, and torsion. Most programs allow the release of individual DOF such that elements with any combination up to six DOF at each node are possible. Beam section properties can also be manipulated to effectively release DOF. There are two formulations of beam elements, Euler-Bernoulli beam elements and Timoshenko beam elements. The formulations for these two types of elements can be found in various texts, including (Hughes, 2012).

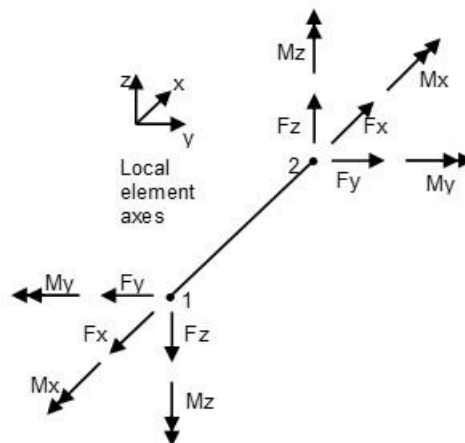


Figure 4. Illustration. Beam element.

Euler-Bernoulli beam elements are typically used when capturing deformation due to shear is not required. Shear deformation is generally negligible in cases where the span to depth ratio of the beam is greater than about 8. For most cases, modeling bridge girders using this type of beam element will produce satisfactory results.

Timoshenko beam elements are capable of capturing shear deformation. This element should be used when shear deformations are not negligible. An effective shear area must be provided in the section properties in order to formulate the Timoshenko beam element shear stiffness matrix. The effective shear area corresponds to the area for which the strain energy from a uniform shear stress equals the strain energy that would be present in the non-uniform shear stress of the beam shape being analyzed.

The effective shear area of a section depends on the shape of the section, but is always smaller than the cross-sectional area in a given plane, such as the approximation using the area of the web rather than the total cross-sectional area as the effective shear area for wide flange beams loaded about the strong axis. Effective shear areas of common shapes such as those listed in Table 1 are often provided in FEA program manuals, but can also be found in some reference books. A general treatment for calculating the effective shear area is found in (Meek, 1971), or a section property calculator can be utilized to find the effective shear area of a given shape.

Table 1. Effective shear areas of common shapes.

Description	Effective Shear Area
Solid Rectangular Section – dimensions b x d	$5/6 bd$
Thin-walled Hollow Rectangular Section	$2 tD$
Solid Circular Section	$0.9 \pi R^2$
Thin-Walled Hollow Circular Section	$\pi R t (=A/2)$
I-beam (along web direction)	A_{web}
I-beam (along flange direction)	$A_{flanges}$
No Shear Deformation	$1000A^*$

Note: In some programs a value of zero for the shear area results in shear deformations being neglected. Consult the software user manual for more information.

Although using Euler-Bernoulli beam elements for girders is generally sufficient, using Timoshenko beam elements will generally provide more accurate results, with little increase in computational effort, no difference in the mesh, and no increase in the amount of output data. Timoshenko beam elements should always be used when shear deformations are not negligible, such as when modeling short deep members or when large concentrated loads are applied close to a support. In general, a reasonable shear area must be assigned to Timoshenko beam elements to achieve valid results, although in some programs assigning a value of zero to the shear area results in shear deformations being neglected.

Most current finite element beam element formulations include only the Saint-Venant torsion while ignoring the warping torsion because the available six degrees of freedom can only accommodate planar behavior. Some programs may include beam element formulations which include a seventh degree of freedom to allow inclusion of warping torsional stiffness directly.

2.3.4.3 Surface Elements

Surface elements such as plates and shells are used to model situations where the thickness is generally much less than the dimensions of the other two orthogonal directions. The main difference between plates and shells is that shells include axial membrane stresses in the plane of the elements, as well as the bending and shear stresses carried by plate elements. Figures 5 and 6 show a plate and a shell element respectively. The shell element includes the membrane forces indicated by $\sigma_{x,m}$ and $\sigma_{y,m}$.

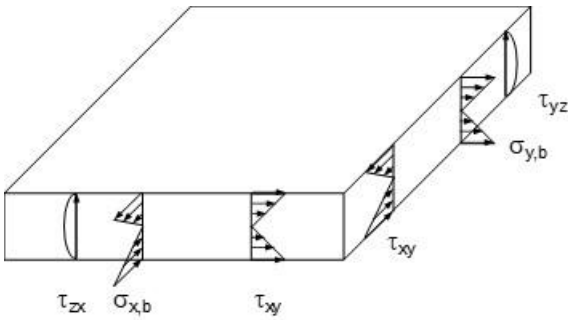


Figure 5. Illustration. Plate element.

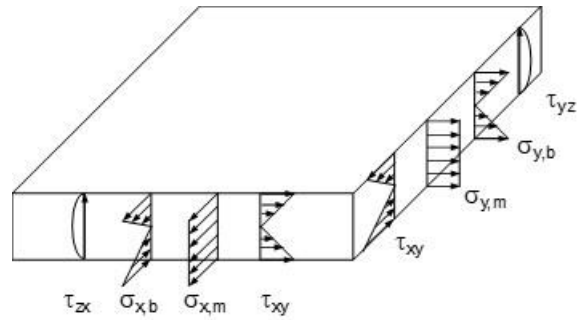


Figure 6. Illustration. Shell element.

Surface elements are generally modeled as triangles or quadrilaterals as illustrated in Figure 7. Quadrilaterals are typically used for the regular shaped areas in finite element analysis of bridges though triangles may be used, especially for transition meshes and irregular shapes. Usually some minimal out-of-flatness is tolerable, as is having curved edges when a midside node is present. For more information on out-of-flatness for surface elements, see (Cook, 2002).

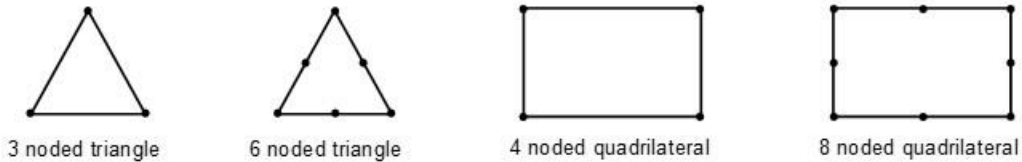


Figure 7. Illustration. Typical surface element geometries.

Finite element software sometimes offers the choice between Kirchhoff-Love formulation plates or shells and Mindlin-Reissner plates or shells. The difference between Kirchhoff-Love and Mindlin-Reissner surface elements is similar to the difference between Euler-Bernoulli and Timoshenko beam elements as described in Section 2.3.4.2.2. Mindlin-Reissner elements include through thickness shear deformations, while Kirchhoff-Love elements do not.

The Mindlin-Reissner shell formulation is recommended in general because it tends to be more accurate, even for thin shell bending problems in which shear deformation is negligible. *As with beam elements, including shear deformations will almost always provide more accurate results if modeled correctly, with little increase in computational effort, no difference in the mesh, and no increase in the amount of output data.* When the mesh is coarse, and shear deformation is negligible, Mindlin-Reissner elements tend to be slightly stiffer than Kirchhoff-Love elements. When the mesh is sufficiently fine, the Mindlin-Reissner elements tend to be more flexible than

Kirchhoff-Love elements due to the additional shear deformation. The accuracy of the Mindlin-Reissner formulation deteriorates when there is mesh distortion and large aspect ratios, and therefore Kirchhoff-Love elements should be used in such cases when shear deformation is known to be small.

Depending on the formulation, shell elements may only resist five of the six degrees of freedom at their nodes, with the in-plane rotation, often referred to as the “drilling” DOF, unconstrained. Sometimes this can cause numerical instabilities resulting in errors.

A second phenomenon that can affect several element types, but may be more prevalent in shell formulations, is known as “shear locking” or “parasitic shear.” The problem manifests itself when shear strains become vanishingly small compared to bending strains, such as in cases of pure bending, and results in overly stiff behavior of the elements. Many finite element programs have implemented improved element formulations in order to minimize this effect. While problems due to “shear locking” are expected to be rare, the analyst should be aware of the effect, and be able to adjust the number or type of elements accordingly.

“Membrane locking” is another phenomenon can occur in curved shell and beam elements. It is characterized by spurious membrane strains in beam and shell elements in a state of pure bending. The effect can be avoided by use of flat shell elements and the spurious effect decreases quickly in curved shell elements with mesh refinement.

2.3.4.4 *Volume Elements*

Volume elements, also referred to as solid or brick elements, are used to model general three-dimensional behavior at the element level of an analysis, such as when through thickness normal stresses along all three axes are important. Because the mesh size of volume elements is driven by the thickness of components due to aspect ratio considerations, modeling girders or bridge deck slabs with volume elements can result in fine meshes with high numbers of degrees of freedom resulting in potentially long solution times.

The nodes of volume elements typically only have stiffness and transmit forces corresponding to the three translational degrees of freedom, no rotational constraint is provided. Care needs to be taken when mixing elements with rotational degrees of freedom such as beams with volume elements. Volume elements can take various shapes. Some of the common ones are illustrated in Figure 8. As with surface elements, some minimal out-of-flatness of surfaces can often be tolerated, and curved sides are possible when midside nodes are present.

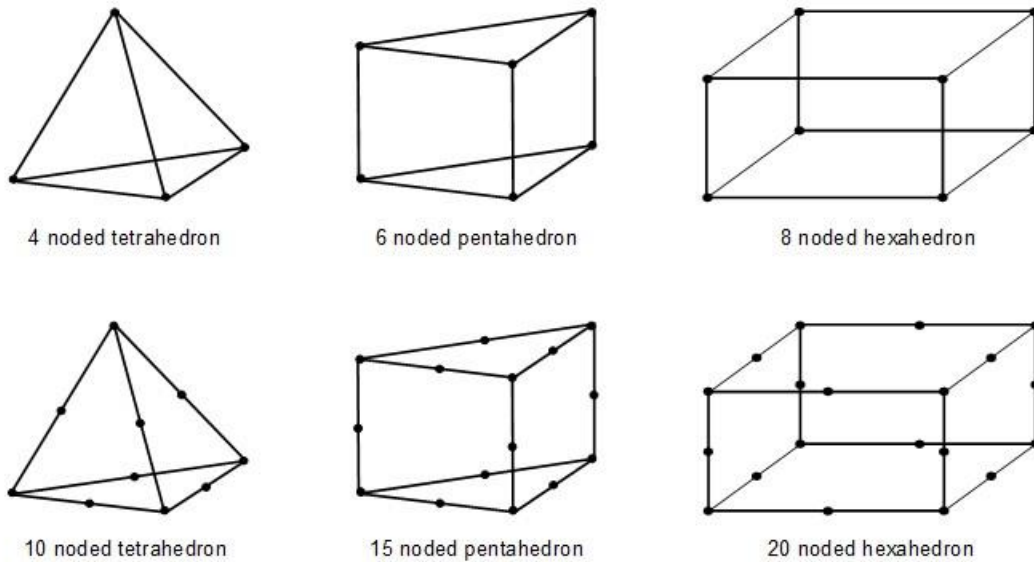


Figure 8. Illustration. Typical shapes for volume elements.

Historically, volume elements have been used for localized analyses, such as stress concentrations in a welded steel connection or stresses in disturbed (D) regions of concrete bridges, and rarely used in routine bridge design due to the high computational effort and difficulty in extracting useful specification design forces. Line and surface elements are usually capable of approximating the behavior of bridge components sufficiently for design purposes when stresses in the through thickness direction are not required. With increases in computing power and advances in software, use of volume elements for routine design may become more common in the future.

2.3.5 Boundary Conditions

Boundary conditions refer to the supports and restraints applied to models. As mentioned previously, the boundary conditions should result in a stable model, such that unrestrained rigid body displacements are prevented. Restraints are commonly located at bearings if the substructure of the bridge is not part of the model, but they also can be located at the foundation or the interface between the foundation and the rock or soil in more detailed models.

The most commonly used boundary conditions are idealized supports giving full fixity to either translation or rotation. Actual supports are never fully fixed or fully pinned, but approximating them as such is often sufficient. More advanced analyses can utilize friction or non-linear behavior such as compression only or tension only supports if program capabilities permit. *Modeling the supports incorrectly, such as misalignment of the orientation of fixity, can have a major influence on solution results even if the difference in the supports appears minor.* This can be particularly true when the structural geometry near the supports is complex, for instance at bearings of curved or skewed bridges (see Section 6.5).

Partially restrained supports modeled with springs can be used as well, as long as the support stiffness is approximately known. Simple “diagonal” springs, so called because only the

diagonal of the stiffness matrix is populated, are used when the stiffnesses of the various degrees of freedom are independent. For more complex cases, some programs have user programmable springs that permit cross-coupling of stiffnesses for cases when the degrees of freedom are not independent. This is often necessary when including the foundation stiffness in a model as a spring stiffness at the base of piers or abutments. An accurate representation of the foundation stiffness will have coupling between the DOF, and require a full 6x6 stiffness matrix. If the support stiffness is not known, bounding the problem by running analyses first with an unrestrained (or flexible) support and then with a fixed support can sometimes be employed to envelope the solution.

More information on typical bridge design boundary conditions can be found in Section 3.7.

2.3.6 Submodeling

Submodeling, also known as substructuring (not to be confused with the substructure of a bridge), refers to the FEA technique of creating a finer mesh model of a particular portion of a finite element model where more accurate results are desired. A larger coarse model is used to find the global forces and/or displacements at the boundaries of the refined area. These global forces/displacements are then applied to the finer submodel to determine the local effects in that particular area.

An example of submodeling is illustrated in Figure 9 where the connection of a floorbeam to the tie girder of a tied arch is examined in much greater detail. At the bridge level, a coarse line element model is appropriate. A more detailed shell element model (A) can be used to represent a portion of the tie girder and the end of a floorbeam. Further submodeling of the top and bottom halves of the tie girder floorbeam connection using shell elements can be modeled as in (B) and (C). Finally, solid element modeling of the corner details can be used for example to determine fatigue stresses (D), (E), (F), and (G).

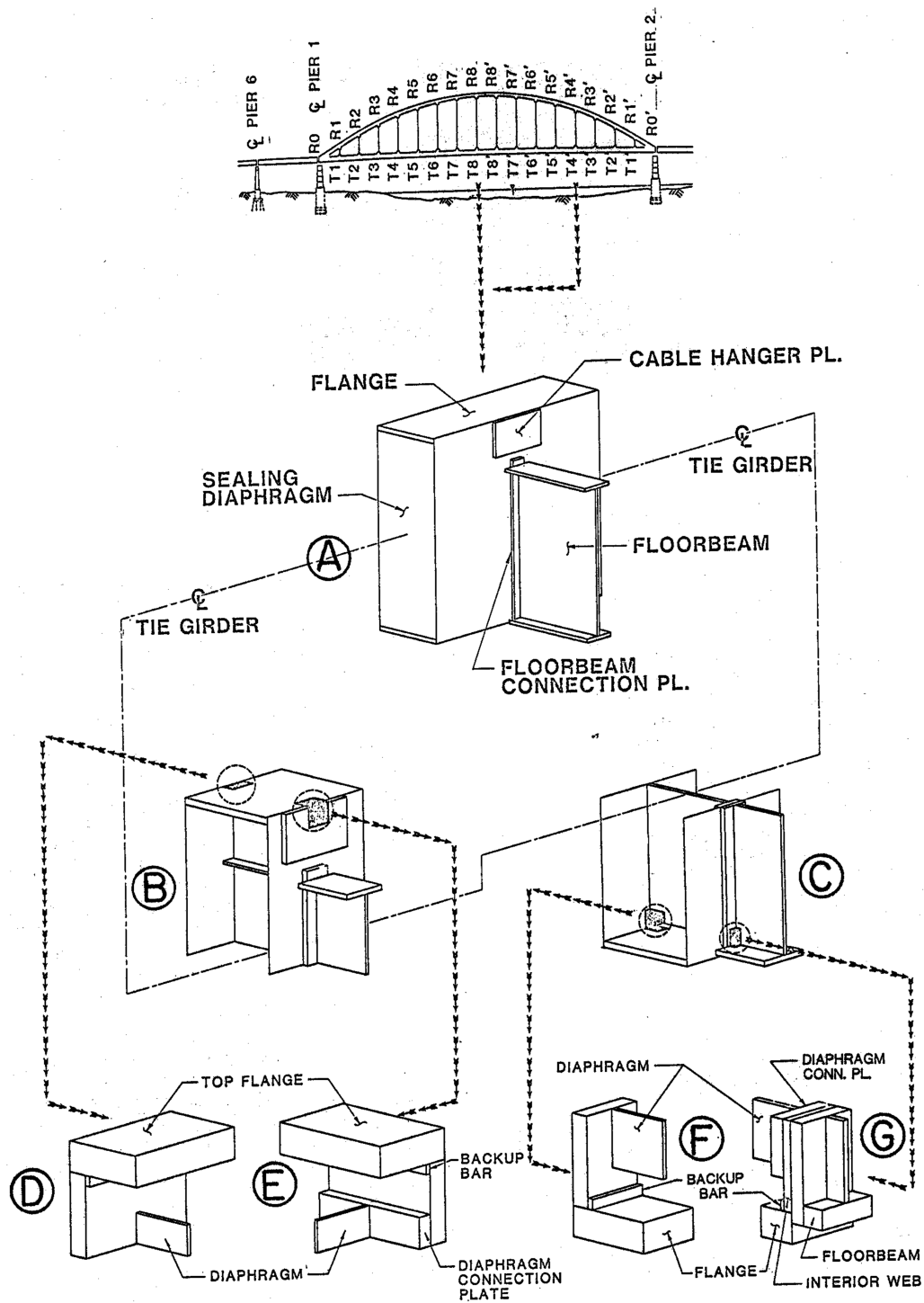


Figure 9. Illustration. Example of increasing levels of submodeling.

This technique results in a much more efficient computational effort than using a fine mesh for the entire structure. Close attention needs to be paid to the boundary conditions and loading/displacements of the submodel, in order to achieve valid results. Submodeling is not

typically employed in routine bridge design, but may be appropriate in certain cases such as forensic or detailed fatigue analyses.

2.4 Definitions, Comparison and Applicability of One-, Two-, and Three-Dimensional Analysis

2.4.1 Definitions

An analysis will often be described as a 1D, 2D, or 3D analysis (where the D refers to dimensions), as a way of describing the level of refinement of the analysis. In order to avoid confusion, a definition of what constitutes each of these analyses is needed. It is also important to distinguish between system and member dimensions. The number of dimensions used to classify the analysis does not necessarily correspond to the type of elements used in the analysis; i.e. a 2D analysis may require three dimensional elements in the analysis program. Conversely, a truss bridge might be analyzed as a 3D assemblage, but still be constructed of two force truss elements.

For the purposes of this manual, a 1D analysis is one in which the resultant quantities (moments, shears, axial loads, deflections, etc.) are a function of only one spatial dimension. For a curving structure, that dimension may be measured along the curved axis; i.e. the reference dimension does not have to be straight. Examples of a 1D analysis include a line girder analysis of a straight bridge or a spine beam model of a curved concrete box structure.

Similarly, 2D analysis results are a function of two spatial coordinates. Examples would include a grid (also sometimes referred to as grillage) analysis (see Section 3.5.1), or a plate with eccentric beam (PEB) analysis (see Section 3.5.2).

A 3D analysis requires three coordinates to define results. Generally in a 3D concrete slab on beam bridge model, the girders and the cross-frames/diaphragms are modeled with explicit depth. Note that for a 3D analysis, there are still many variations possible, with a wide range of refinements available. A girder bridge modeled with plate elements for girder webs, but with beam elements representing the flanges would be a 3D analysis, as would one with solid elements used for the flanges and webs of the girders. Both are 3D analyses, but there is a very large difference in refinement between them.

Figure 10 illustrates a general progression in the level of refinement of an analysis for a continuous plate girder bridge.

Note that it is usually not necessary to model the cross-slope, superelevation, and/or vertical curve in a typical beam girder bridge analysis. In some cases it may make sense to include these variations, such as when net axial forces are present or when modeling variable depth transverse members that follow the cross-slope in a 3D analysis.

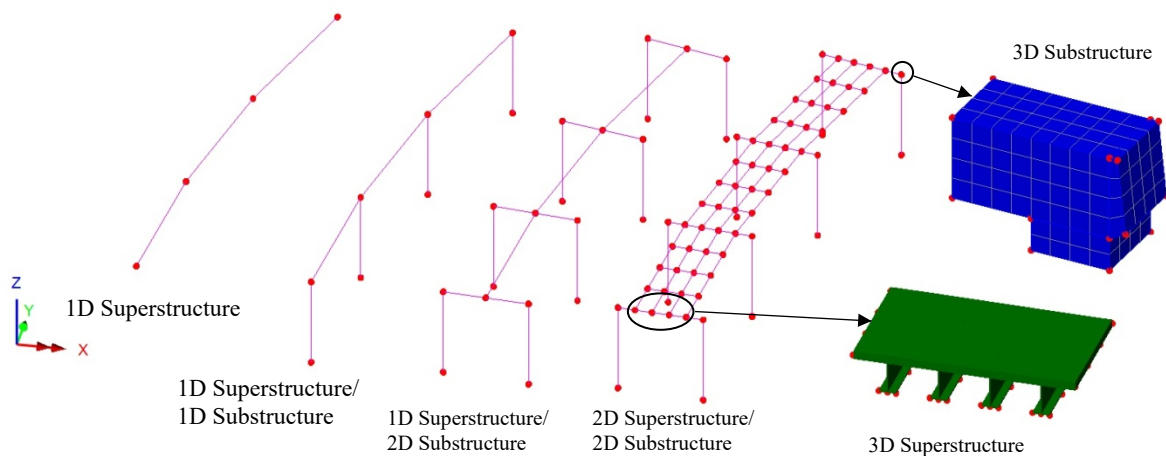


Figure 10. Illustration. General progression from a 1D model to a 3D model.

2.4.2 One-Dimensional Analysis

One-dimensional analysis replaces the structure with a single series of line elements that follow the geometry of the structure as seen in plan view. One-dimensional analyses are typically linear elastic, small deflection, and consist of a single material transformed section. Varying section properties can be handled with stepped section properties in the models, or by explicitly varying the section properties along the length in more advanced programs.

A design based on the distribution factors in Section 4 of the AASHTO LRFD usually represents the structure as a single beam and is, therefore, a type of one-dimensional analysis. Figure 11 shows the plan and typical cross-sections of the steel girder three span continuous bridge that is analyzed in Example 2 (see Chapter 9). Figure 12 illustrates a single representative girder model. In order to utilize the approximate distribution factors, the bridge must satisfy the limitations listed in the AASHTO LRFD. In general, the distribution factors are applicable to straight parallel multi-girder right bridges, although skews up to 60° can be accommodated with the correction factors in Articles 4.6.2.2.2e and 4.6.2.2.3c. Note that the skew angle is defined in AASHTO as the angle between the centerline of a support and a line normal to the roadway centerline. Minimal skews and curvatures can be approximated as straight for one-dimensional analyses.

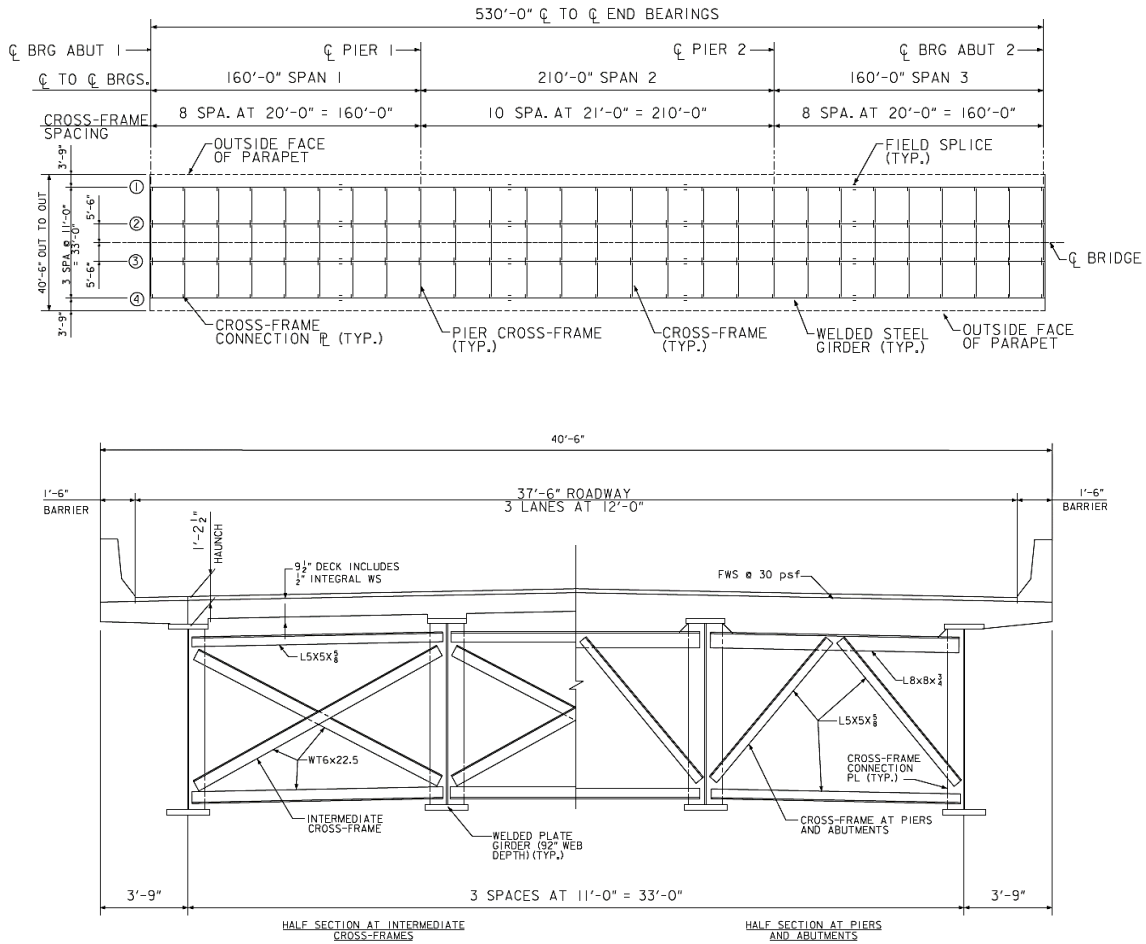


Figure 11. Illustration. Plan and typical sections for three-span continuous steel girder bridge for Example 2.

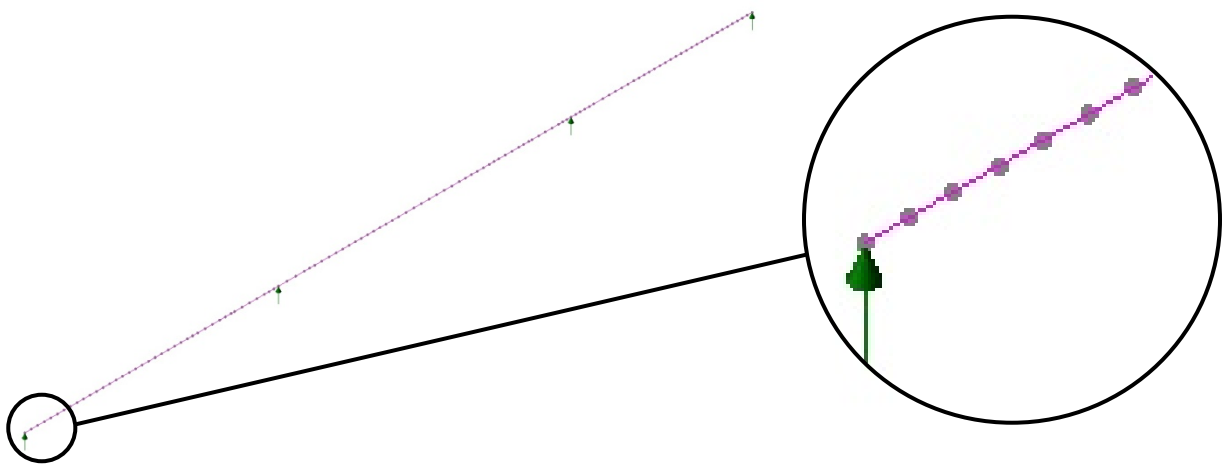


Figure 12. Illustration. 1D model of three-span continuous steel girder bridge for Example 2.

Structures which have large torsional rigidity and for which the Saint-Venant response is dominant, such as single box girders, can also be efficiently modeled as a single series of line elements. Figures 13 through 15 from Example 4 illustrate a one-dimensional spine beam model. According to Article 4.6.1.1 of AASHTO LRFD, if the span length of a bridge superstructure with torsionally stiff closed cross-sections exceeds 2.5 times its width, the superstructure may be idealized as a single-spine beam. This restriction does not apply to cast-in-place multicell concrete box girders, so smaller aspect ratios are permitted. Article 4.6.1.2.2 extends the limitation of Article 4.6.1.1 to curved torsionally stiff single steel box girder systems.

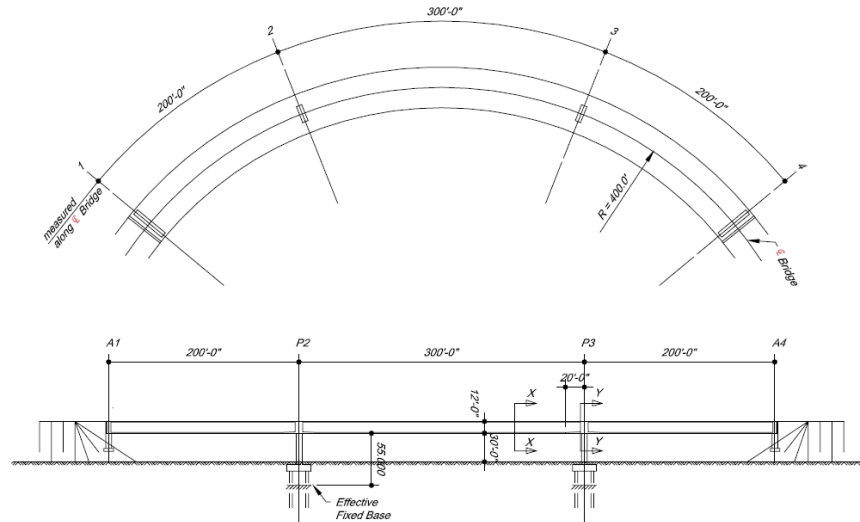


Figure 13. Illustration. Plan and elevation of a torsionally stiff curved single concrete box beam bridge (Nutt et al., 2008).

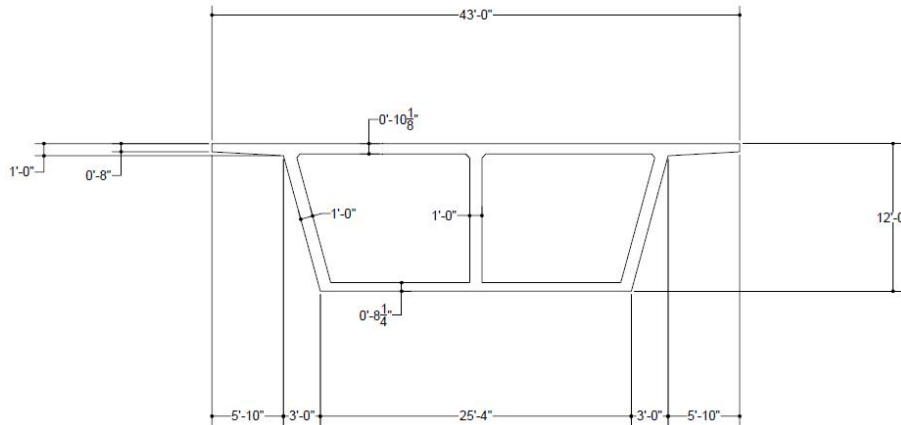


Figure 14. Illustration. Typical cross-section (Nutt et al., 2008).

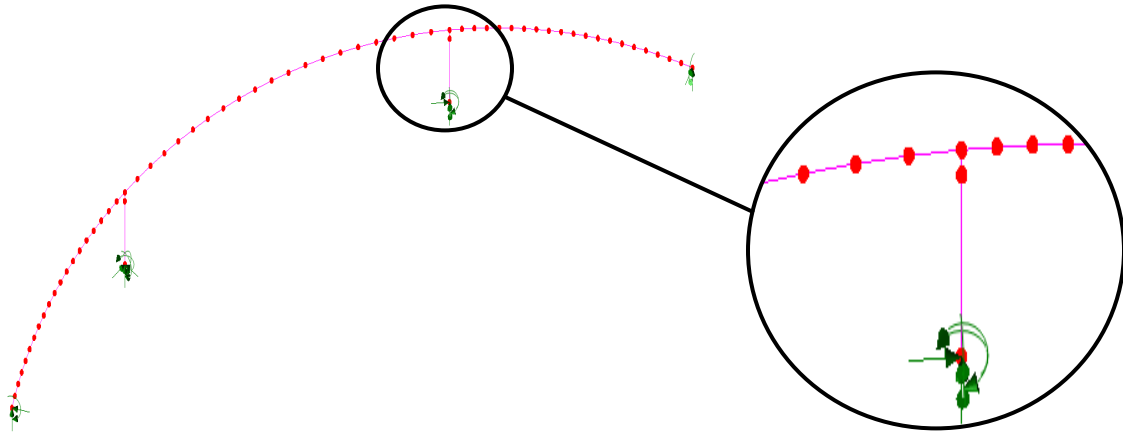


Figure 15. Illustration. 1D spine beam model.

In regard to skew, Chapter 12 of the PCI Bridge Design Manual (PCI, 2011) states that skew angles greater than 20° result in significant bending moment and shear effects in the exterior beams of concrete girder bridges. It goes on to warn that seismic effects can also be significantly altered by skew. The skew correction factors in the PCI Manual mirror those in AASHTO LRFD, however.

In NCHRP Report 725, White et al. (White et al., 2012) define a skew index for steel multi-girder bridges, based on span aspect ratio and skew angle, as Equation (1).

$$I_s = \frac{w_g \tan \theta}{L_s} \quad (1)$$

where:

- I_s = skew index
- w_g = width of bridge between fascia girders
- L_s = span length at the bridge centerline
- θ = skew angle (measured from transverse axis)

In continuous span bridges, the index is determined for each span. In spans with unequal skews at the bearing lines, θ is taken as the larger skew angle.

For straight steel girder bridges, a skew index of about 0.30 differentiates bridges in which skew effects of flange lateral bending, cross-frame forces, and girder layovers are important from those where skew effects are less significant. When the skew index exceeds a second limit of 0.65, the vertical displacements and major axis bending moments are affected more significantly by the skew.

For curved structures, Articles 4.6.2.2.4 and C4.6.2.2.4 of AASHTO LRFD permits the use of the V-load and M/R approximate methods for steel I-girder and box girder bridges, respectively. This provides a method of extending one-dimensional line girder results to the analysis of curved

multi-girder bridges. Many limitations are listed and minimal guidance is provided on applicability. It is left to the Engineer to determine when their use is appropriate.

According to Article 12.4.2.1 in the PCI Bridge Design Manual, bending moments in curved concrete beams from longitudinal flexure are virtually the same as those for a straight beam of span equal to the arc length between supports and therefore straight beam analysis can be used for preliminary design. The same cannot be said for torsional moments, which are related to the flexural moment divided by the radius of curvature, or M/R . Article 4.6.1.2.4b of AASHTO LRFD contains a similar provision regarding multi-girder steel superstructures, but places additional restrictions on use, presumably since it is not limited to preliminary design.

1D analyses can be an efficient choice when designing essentially straight, right, regular multi-girder bridges or torsionally stiff box girder spine beam bridges, where lateral and torsional responses are not critical. 1D analyses are not appropriate in cases with:

- large cross-frame or diaphragm forces such as from load distribution in multi-girder bridges with large skew and/or curvature,
- geometrical sources of stiffness such as force couples from flange lateral bracing or multiple bearings under box girders,
- significant lateral effects in multi-girder bridges.

For guidance on modeling one-dimensional analyses, see Section 3.4.

2.4.3 Two-Dimensional Analysis

Often referred to as grid methods, two-dimensional analysis methods consist at minimum of an interconnected series of beam elements that represent the major flexural members of a bridge superstructure and sometimes include the substructure. The deck slab can be either distributed and included with beam properties or explicitly modeled with shell elements. 2D analyses can be used simply to determine girder distribution factors with one-dimensional methods used to complete the design, or utilized to determine both dead load and live load envelopes for subsequent factoring and limit states checks.

Because 2D models explicitly account for live load distribution based on geometry and element stiffnesses, loads are more accurately distributed, and resulting designs are potentially less conservative than those based on the approximate distribution factors in a 1D design. Skew factors also do not need to be applied, as skew effects are explicitly modeled. See Examples 1 and 2 in Chapter 9 for a comparison of 1D versus 2D design.

2.4.3.1 Basic Grid Analysis

Early grid analyses used networks of line elements in a single plane, as illustrated in Figure 16. Approximate girder distribution factor methods could be replaced with a method to explicitly distribute loads based on actual longitudinal and transverse member stiffnesses. The transverse member stiffnesses in the grid often require the use of an effective stiffness value, for instance when modeling steel cross-frames, since vertical geometry is not modeled.

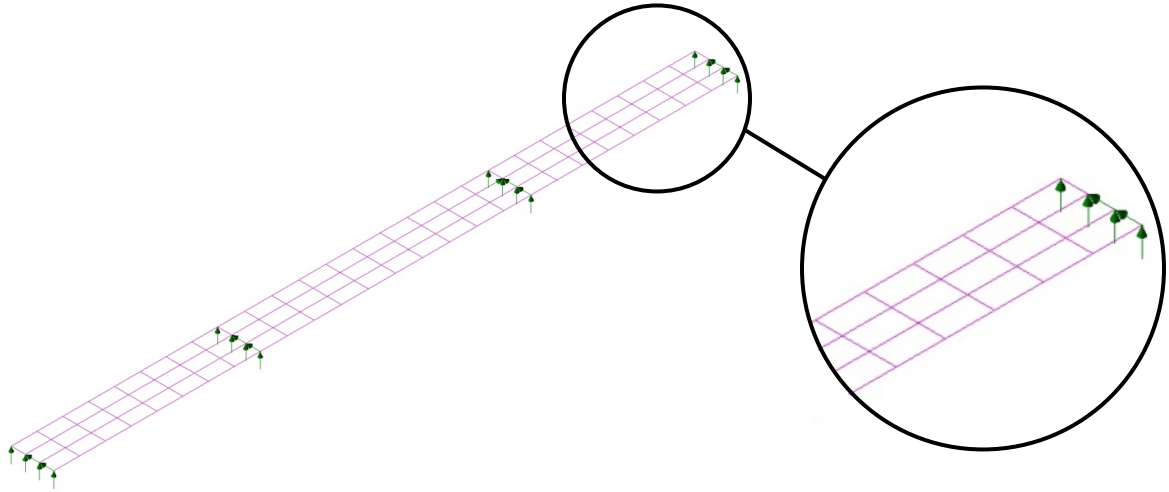


Figure 16. Illustration. 2D grid model of three-span continuous steel girder bridge for Example 2.

A grid requires the development of member properties that proportionally assign the material in the bridge to the mesh of line elements. By approximating the deck properties into line elements, the grid analysis does not fully model the membrane stiffness of the deck, but the outputs of shear, moment, and axial force are compatible with AASHTO design equations. For guidance on modeling basic grid analyses, see Section 3.5.1.

Even though basic grid analysis is a step up in rigor from a 1D analysis, it still suffers from many of the same limitations. In some cases, a grid analysis may be acceptable for member design, but not for calculating camber and deflections at intermediate construction stages. Basic grid analyses are not appropriate in cases with:

- Large second-order effects, such as compression flange lateral bending stresses,
- Geometrical sources of stiffness such as force couples from flange lateral bracing (pseudo box) or multiple bearings under box girders,
- Significant lateral effects in multi-girder bridges,
- Significant torsional effects in open section girders,
- When other than no load fit is used with steel cross frames,
- When large shear membrane forces are present in the plane of analysis.

However, improved grid analysis techniques have been developed to overcome many of these limitations.

2.4.3.2 Improved Grid Analysis

Over the years, both program enhancements and modeling techniques, not to mention increased computing power, have resulted in improvements to the basic grid analysis. *The plate with eccentric beam (PEB) model is now commonly used to model multi-girder bridges.* This model combines a line element girder and cross-frame/diaphragm grid with a shell element deck including the geometric offset of the deck from the girder centroids. A typical PEB model is illustrated in Figure 17.

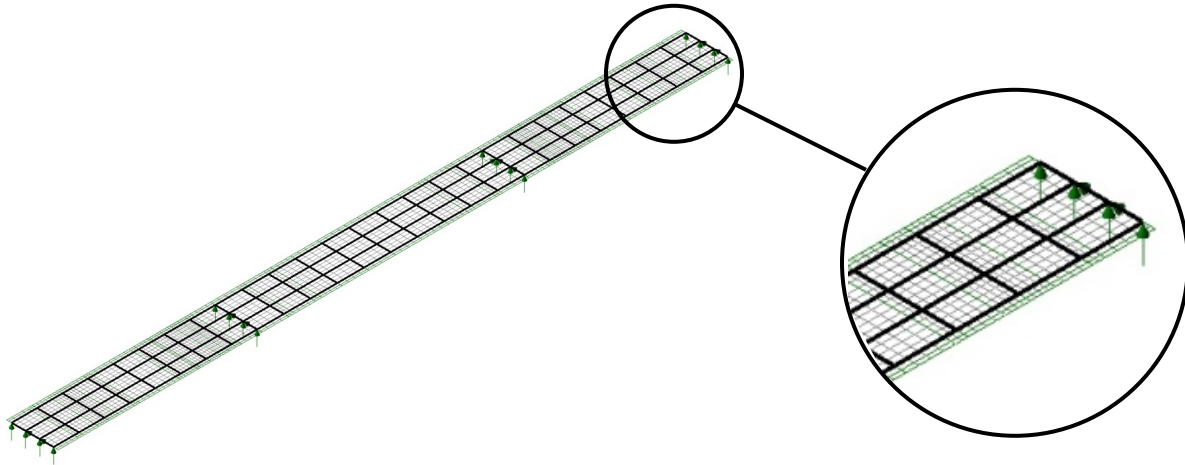


Figure 17. Illustration. 2D PEB model of three-span continuous steel girder bridge for Example 2, with internally offset girders and cross-frames bolded.

Improved grid models are still typically linear elastic and small deflection, but no longer require a single material transformed section. Models can use actual gross section material properties, and explicitly assign separate material properties to the girders and the deck. Varying section properties in the girders are still usually handled with stepped section properties in the models.

Some programs now have beam elements with definable offsets such that the deck and girders can be modeled in a single plane, with the offsets providing the geometrical eccentricity, although rigid links are also effective when the offsets need to be modeled explicitly.

Timoshenko beam elements that include shear deformations allow for improved cross-frame stiffness approximations, and in some programs, “exact” cross-frame stiffness properties can be programmed into user defined elements.

Techniques have been developed to calculate effective torsional constants in order to account for warping stiffness in thin-walled open sections (see Section 3.5.4.1). Use of such techniques allows calculation of camber and deflections during construction of thin-walled open section multi-girder steel bridges.

One of the biggest advantages of PEB models is that they can explicitly model the behavior of structures with large skew or curvature. A PEB analysis requires less compromise and fewer assumptions in defining the elements of the mesh, and does model the membrane stiffness of the deck. Modeling the deck as a continuum explicitly captures accurate transverse load distribution and torsional behavior more easily than a basic grid analysis, where the transverse load distribution is concentrated at the transverse grid members and the torsional behavior must be distributed among multiple grid members. Also eliminated is the requirement of assigning an “effective width” of deck to each girder in order to calculate effective composite stiffness. Separating the deck from the girders for a composite structure does require the design force outputs to be aggregated in order to utilize the component based AASHTO LRFD.

Although modeling the deck and girders separately makes extracting design forces a little more difficult, improved grid analysis is accurate enough to use for design of most multi-girder bridges. The improved analysis is not appropriate in cases with:

- Large second-order effects,
- Geometrical sources of stiffness such as force couples from flange lateral bracing (pseudo box) or multiple bearings under box girders,
- Thermal gradient analyses.

For guidance on modeling PEB analyses, see Section 3.5.2.

2.4.4 Three-Dimensional Analysis

As computing power has increased, the ability to run analyses incorporating larger numbers of elements has increased as well. This permits more explicit modeling of the members of multi-girder bridge structures. Now not only can the concrete deck be modeled explicitly, but instead of using a single line element to model a girder, the web and flanges of a girder can be explicitly modeled at very accurate geometries. Cross-frames can also be explicitly modeled with multiple elements instead of single lines of elements with effective stiffnesses. Individual material properties can be assigned. By modeling thin-walled open sections with multiple elements, both warping and Saint-Venant torsional stiffnesses can be explicitly accounted for, and corresponding stresses can be output. Section properties are explicitly modeled, so no stepwise approximations need be used.

By using a 3D model and explicitly modeling the elements of a bridge, geometrical effects are accounted for, and reflected automatically in the results. While small deflection analyses are typical, geometric nonlinearity can be analyzed either within the program, or by running iterative analyses. Linear elastic material properties are also typical, although many programs can now automatically iteratively solve nonlinear material problems. If desired, second-order effects such as web buckling can be determined at a subcomponent level. A typical 3D model is illustrated in Figure 18. For guidance on modeling 3D analyses, see Section 3.6.

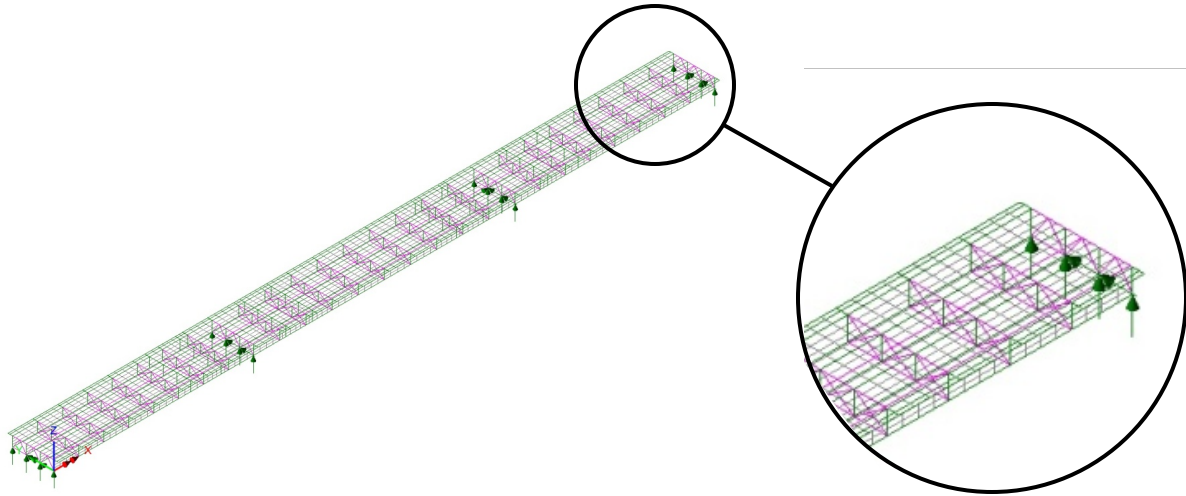


Figure 18. Illustration. 3D model of three-span continuous steel girder bridge for Example 2.

So why not use 3D analysis for every design? At present, it is not always the most efficient solution. Although the effort involved in constructing and running a 3D analysis is not much greater than for 1D or 2D analyses, to then proceed to produce a design from the output is more of a challenge. One of the main hurdles is that AASHTO LRFD is a limit states design specification, and often nonlinear behavior such as steel yielding and concrete cracking is permitted at strength limit states. AASHTO LRFD is also mostly a component design specification, and extracting compatible design forces from a 3D analysis is still cumbersome for most programs. In many practical cases the improved accuracy is insignificant and not worth the additional effort. See comparisons of examples in Chapter 9 of this manual. For most typical concrete slab on girder bridges, a PEB analysis is still the recommended approach.

3D modeling should be used when more “exact” behavior is desired, and for submodels, such as:

- Local analyses such as details and points of interconnection in the structure where stress concentrations are apt to be present.
- Warping torsional stiffness needs to be considered.
- Complex dynamic analyses, when modeling the stiffness and/or the distribution of mass more accurately is required.
- Complex stability analyses, both global and local.
- Cases where flange lateral bending is significant.
- Staged construction/fit-up analyses.

Eventually, it is expected that the FEA programs and/or the AASHTO Design Specifications will evolve to the point where a 3D analysis and design will require negligible additional effort over a 1D or 2D method. At that time, the grid analysis will probably be relegated to one of the checking methods. Until that time, however, 3D analysis can still be an important tool, whether for new designs, ratings, or forensic investigations.

2.5 Refined Methods of Analysis and Reliability

Two issues arise regarding refined analysis and reliability: the impact of using refined analysis instead of distribution factors on the calibration of the AASHTO LRFD Specifications, and *the effect on achieved reliability for a bridge designed using refined analysis*. The AASHTO LRFD Specification live load and resistance models were calibrated to achieve a target reliability utilizing the calculated distribution factors in the specification. If a refined analysis such as 3D finite element analysis (FEA) or plate and eccentric beam (PEB) grillage analysis is used resulting in different load effects and different size design sections, a different reliability will be realized. The following sections explore the effects of refined analyses on the design reliability indices, and what, if anything, should be done about it.

2.5.1 Evaluation of the LRFD Reliability Index

In the case of the resistance, R , and the load effect, Q , both being normal random variables and satisfying certain limits on the sizes of their coefficients of variation, COV's, the reliability index, β , can be calculated using Equation (2):

$$\beta = \frac{\bar{R} - \bar{Q}}{\sqrt{\sigma_R^2 + \sigma_Q^2}} \quad (2)$$

where: \bar{R} = mean or expected value of the resistance

\bar{Q} = mean or expected value of the load

σ_R = standard deviation of the resistance

σ_Q = standard deviation of the load

This equation is a simple expression for the reliability index and can be used to make qualitative assessments of the effect of varying the method of analysis of live load. The actual calibration equations used in the development of AASHTO LRFD, based on the Rackwitz and Fiessler (1978) procedure, were more complex, more general and subject to fewer limitations than the equation presented here. They are treated further in Nowak (1999) and Kulicki et al. (2007).

The quantitative assessment of the effect of varying the method of analysis of live load presented here was developed using the same process used in the development of AASHTO LRFD. It is worth noting that modern calibration calculations usually use the Monte-Carlo method. A comparison showed that the Monte-Carlo method applied to the full set of bridges used in the LRFD calibration gave virtually identical reliability indices determined during the original calibration of AASHTO LRFD (Kulicki et al., 2007).

In specification calibration it is common to assume that the provided resistance of sample bridges exactly satisfies the code requirements. Using this assumption enables the sum of the specified factored loads to be used instead of calculating the resistance of sample bridges. The loads represented by Q in the reliability equation are statistically projected based on nominal loads, biases and coefficients of variation. The live load is based on extrapolating measured data to the design life which is 75 years in the case of AASHTO LRFD. Another assumption inherent in the calibration is that the analysis doesn't introduce any shifts in the bias factors, or otherwise affect

the load and resistance distributions, i.e., it's a perfect mapping from load (probabilistic and notional) to force effects.

2.5.2 Effect of Refined Analysis on Calibration

Several cases are presented to illustrate the effect of changing the method of analysis used in AASHTO LRFD on the calibration. *The qualitative difference in the reliability index is deduced from the reliability equation and a quantitative assessment is illustrated for a representative sample of bridges from the original LRFD calibration.*

Case 1 – Design by Simplified Methods: Design with 7th Edition of AASHTO LRFD. This is the base case. Quantitative results are shown in Table 2 for comparison to the remaining cases.

Case 2 – Design by Refined Analysis: Design with simulated refined analysis results assumed to be 80 percent of the values from AASHTO LRFD girder distribution factors for both load and resistance. This illustrates assuming that the refined analysis yielded 80 percent of the live load moment that the distribution factors yield. In terms of calibration, analysis is a mapping of both the probabilistic load model (load), as well as the notional loading (resulting in a provided resistance), to design effects such as moment and shear. For this case, the assumption is that the refined analysis is used to calculate the effects of the probabilistic load model and the notional load model.

These changes would affect both R and Q in a similar way in the reliability equation so the differences compared to the base case would be expected to be small. This is confirmed in Table 2 by comparing the reliability indices for Case 1 and Case 2. There are slight differences because the factored HL93 loading, while trend-wise similar to the projected live load, is not identical to it. Additionally, there are statistical factors applied to the projected live load.

Case 3 – Evaluation by Refined Analysis for Load Effects: Design (provided resistance) based on the AASHTO LRFD including the use of the current specification supplied distribution factors but the projected live load on the load side was based on simulated refined analysis assumed to yield 80 percent of results from AASHTO LRFD girder distribution factors. This simulates an AASHTO LRFD design evaluated by refined analysis of HL93 loading. Considering the reliability equation it would be expected that since Q is decreased by use of the reduced distribution factors, the reliability indices in the case should be higher than Case 1. This is confirmed in Table 2.

Table 2. Comparison of reliability indices.

Bridge Properties			Reliability Index		
Girder Type	Span (ft)	Spacing (ft)	Case 1	Case 2	Case 3
Prestressed Concrete	60	8	3.76	3.76	4.96
Prestressed Concrete	60	12	3.75	3.75	4.94
Prestressed Concrete	120	8	3.64	3.55	4.26
Prestressed Concrete	120	12	3.64	3.56	4.27
Composite steel	60	8	3.71	3.70	4.74
Composite steel	60	12	3.71	3.69	4.69
Composite steel	120	8	3.58	3.51	4.12
Composite steel	120	12	3.55	3.47	4.05

The results are as would be expected:

- Since the analytical method used in calibration shows up on both sides of the calibration equation in Case 2, it has little impact on the results compared to the base case;
- When more conservatism than used in calibration is present in the design, either through live load distribution factors as assumed in Case 3, or through design resistance, the Reliability Index increases compared to the base case.

2.5.3 Effect of Refined Analysis on Achieved Reliability

The question that may be most relevant to the use of refined analysis in bridge design is: How does the use of refined analysis during the design phase of a bridge impact the safety of the constructed bridge? Clearly, if the method of analysis used results in less material in the structural members, and thus lower resistance, there has been a change in the level of reliability provided. In order to explore this issue, the difference between the target reliability index, and the achieved reliability for any particular bridge can be evaluated.

The AASHTO LRFD Specifications are intended to address the design of a broad range of bridge components. Some, such as a simply supported girder in a two-girder cross-section, are statically determinate in both the longitudinal and transverse directions, and thus the load effects can be easily determined through simple statics. Others, such as a continuous girder in a multi-girder cross-section, are statically indeterminate in both the longitudinal and transverse directions. In the first instance, any analysis method should produce a result that is essentially identical and result in the target reliability. For the second example, the use of approximations and simplifications can introduce differences between calculated and actual load effects. *The framers of the specifications were very careful to ensure that what differences do develop result in conservative estimates of design effects when using these approximate methods, such as the distribution factor method. As a result, the use of approximate methods will generally cause the achieved reliability index of a structure to be higher than the target value.*

Referring to Case 3 above, if an approximate analysis results in a resistance being 25 percent higher than required to achieve a target reliability index of 3.5, the achieved reliability index can range from about 4.0 to almost 5.0. There are many instances in the AASHTO LRFD Specifications, and the Standard Specifications before them, where an approximate method is given in lieu of a more refined one, with the understanding that the approximate method will produce more conservative results. This occurs both in terms of analysis of load effects as well as determination of resistances. *When a designer chooses to use an approximate method, the design force effects will tend to be conservative, resulting in larger design forces. It should come as no surprise that the design will have an increased resistance, and therefore a higher reliability, due to the higher ratio of resistance to actual demand.*

It is important at this point to consider the degree of conservatism that may or may not be present in the distribution factor method. The examples contained in this manual do show that a relatively significant amount of savings is available when more refined analysis methods are used, but previous studies have indicated smaller differences (Zokaie, 2000). LRFD distribution factors tend to be more conservative resulting in greater differences with refined analysis distribution when the lever rule is used or at the limits of applicability of the LRFD distribution factors (Yousif, 2007). In any event, *for structures that have less indeterminacy, the achieved*

reliability index has always been closer to the minimum target level, and that has been deemed acceptable, and there has not been any indication that the level of achieved reliability has resulted in problems.

The replacement of an approximate method during the design process with a presumably more accurate refined method can thus be thought of as moving the achieved reliability of the structure toward the target minimum reliability index from a higher value. A question can be raised regarding whether this is beneficial overall. The target strength reliability index of 3.5 was set based on successful past design practice. *It could be argued that the effects of the approximate method of analysis (distribution factor and line girder analysis) were inherent in setting the target level, and thus any reduction in the conservatism of those methods would result in unacceptably low values of the reliability index.* However, as noted above, the level of reliability would be approaching that of simpler structures for which the calculation of load effects are more straightforward, and these have historically performed well.

The discussion thus far has been regarding the use of refined analysis in determining the load effects on a structure. The same arguments also apply for the case when refined methods are used to determine the resistance of a structure or component.

In summary, the effect of utilizing refined analysis in the design of a bridge does reduce the achieved reliability, however the target value of 3.5 is approached from above, resulting in a structure with an acceptable level of reliability. *Assuming the analysis is performed correctly, a reduction in reliability should not be a reason to avoid using refined methods.*

CHAPTER 3. GENERAL GIRDER BRIDGE MODELING

3.1 Introduction

Finite element modeling and analysis of a bridge can provide fast, accurate, easily modified results, but also can become a time and resource intensive process. The following assumptions commonly made in routine bridge engineering analysis are not necessary to perform a finite element analysis, but often are employed to make the design process more efficient:

- Isotropic, linear elastic materials
 - Properties are the same in all directions
 - Stress and strain are related by a constant, the modulus of elasticity, E , no material nonlinearities
- Plane sections remain plane and section properties remain constant
 - Shear deformations are small enough to be neglected
 - Torsional warping is small enough to be neglected
 - Sections do not change due to cracking or yielding during analysis
- Boundary conditions are considered either fully restrained or fully unrestrained
 - Each of the 6 degrees of freedom are generally either unyielding or free to move, although in some cases partial restraint and/or prescribed displacements may be utilized
 - Restraints applied at bearing locations and joints between members
- Loads remain constant in direction and magnitude
 - Second-order effects are small enough to be neglected or
 - Second-order effects are accounted for using correction factors – no geometric nonlinearities
- Superposition of loads is valid since material or geometric nonlinearities are negligible, effects are load path independent.
 - Load effects can be factored
 - Load effects can be added
- Bridge live loadings can be approximated with concentrated point and distributed loads

Not adhering to the above assumptions can result in a more accurate analysis, but at a cost of more effort, especially when the analysis becomes nonlinear. Linear analyses, when extrapolation and superposition are valid, allow a number of loadcases to be checked based on a handful of analyses. A nonlinear analysis, where extrapolation and superposition are not valid, can only evaluate a single loadcase. The analyst must determine when the increased accuracy is worth the increased effort. The optimal model is the one that provides the desired accuracy, with the minimal amount of refinement. A certain amount of accuracy is required to avoid compromise of the design reliability index, β . With refinement, comes increased effort and chance for error in the analysis. Good judgment is required not only when balancing accuracy of results versus computational effort, but when assessing whether the results obtained are reasonably accurate.

The following sections will provide generalized guidelines to use when modeling slab-girder bridges to determine bending moments, shears, and displacements for use in conjunction with the AASHTO LRFD.

3.2 Mesh Generation

The mesh, the nodes and elements connecting them, of a finite element model is arguably its most important aspect. It should go without saying that the mesh should allow the geometrical aspects and stiffness of the structure to be modeled. Keep in mind, however, that the model is a numerical representation. While it generally may “look” like the structure being modeled, the important aspect is that it “behaves” like the structure being modeled. This means getting the stiffness and load effects of the model correct, and it may include elements superimposed on each other, or placed where they would “interfere” with each other in the actual structure.

In general, nodes should be located as close to the centroids of elements being modeled as possible, although some programs allow eccentricities to be used to place element centroids at the correct location. Meshing models consisting only of line elements is fairly simple with nodes along element centroids, at intersections with other elements, and at boundaries. Meshing models with plate or shell elements should place nodes at the mid-plane of the elements in a regular rectangular grid if possible. Meshes should be kept as simple and regular as practicable.

Proper meshing can result in efficiencies in both solving and interpreting results of a model. As mentioned in Section 2.3.2, the number of nodes and corresponding degrees of freedom (DOF), have a direct effect on computation effort. The mesh should have sufficient nodes and elements to provide sufficient accuracy without extra computational effort. Advice on number of elements in models to try to achieve this goal is given in the following sections. Secondary considerations which would lead the analyst to control mesh generation include:

- Locating nodes where loads are to be applied,
- Locating nodes where output is desired,
- Locating nodes to facilitate interfacing with adjacent elements, such as diaphragms in concrete bridges, or stiffeners and cross-frames in steel bridges.
- Locating nodes where it is anticipated that a later iteration of the model will require a node, or
- Orienting the mesh in order to obtain stresses in a specific direction.

In general, meshing of line elements is less critical than meshing of surface or volume elements, due to the number of DOF involved. *The mesh can be generated either manually by the user or automatically by the finite element program or a combination of the two.*

3.2.1 Manual

Manually generating the mesh can be a long, tedious process depending on the size and complexity of the model. In this method, the engineer manually generates every node and every element. Although potentially time-consuming and error prone, manual generation ensures that the mesh is exactly the way it is intended, as every node and element is individually generated. The process can be expedited by using spreadsheet generated text input files. Use of this method has decreased for complex models due to improvements in automatic meshing features.

3.2.2 Automatic

Many finite element programs are capable of automatically generating nodes and elements. Automatic meshing has the potential of increasing the economy of the analysis as the time-consuming process of generating many of the nodes and elements is done by the software. Automatic meshing is particularly suited for generating large areas, especially large irregularly shaped areas of plate or shell elements. Two methods of automatic meshing exist, free meshing and mapped meshing.

3.2.2.1 Free Mesh

Free meshes have no restrictions on element shape (i.e., both triangles and quadrilaterals may appear in the mesh) and the elements do not necessarily appear to be in any particular recognizable pattern. A free mesh can be applied to regularly and irregularly shaped surfaces. Figure 19 is an example of a free mesh; all of the elements happen to be quadrilaterals but no pattern is visible in the elements.

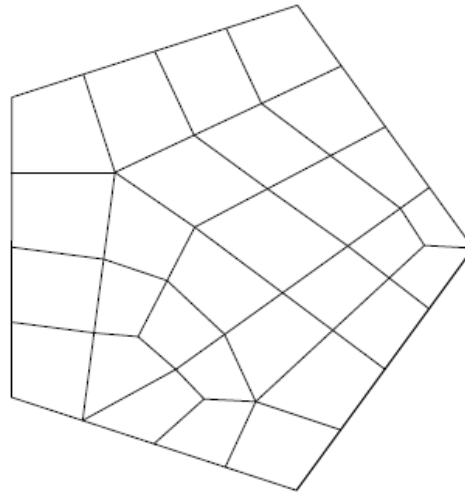


Figure 19. Illustration. Example of a free mesh.

3.2.2.2 Mapped Mesh

A mapped mesh uses only one element shape (i.e., all triangles or all quadrilaterals) and the elements appear to follow a pattern. If a mapped mesh is desired, developing surfaces with regular shapes will aid in the meshing of the surface. Figure 20 is an example of a mapped mesh; all elements are quadrilaterals and are in obvious rows of elements. To use a mapped mesh, it may be necessary to define the number of elements along each edge of the surface. Mapped meshes are commonly used for bridges due to the regularly shaped surfaces of girder webs and concrete decks.

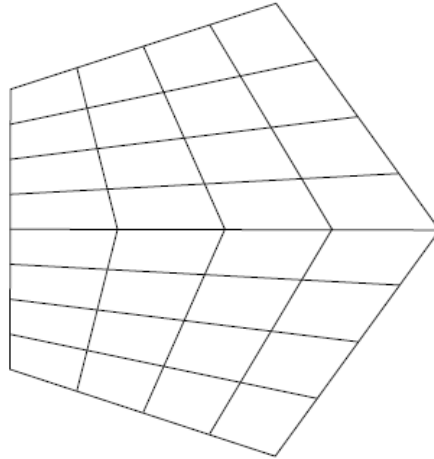


Figure 20. Illustration. Example of a mapped mesh.

3.2.3 *Semi-Automatic*

Semi-automatic refers to a combination of manual generation, possibly by text input, combined with automatic local mesh refinement. This combines the ease and speed of automatic generation with the control of manual generation.

3.2.4 *Transition Meshes*

Often refined models are used when stresses are desired at localized regions of a large bridge. *Rather than modeling the entire structure with a fine mesh for such localized results, the mesh can be transitioned into a much coarser mesh away from the area of interest.* This can greatly decrease solution times for the model while maintaining accuracy. Figure 21 illustrates some examples of transition meshes.

Another method of transitioning is to use multi-point constraints to enforce compatibility between a denser and coarser mesh across a common edge or surface boundary. An example of this would be transitioning from a shell element mesh to a line element mesh of a wide flange beam. Constraints can be used to enforce compatibility between the single node at the end of the line element and the multiple nodes at the end of the shell element mesh.

For advanced users, some programs may have additional methods of transitioning between meshes. Program literature should be consulted and models verified when using program specific techniques.

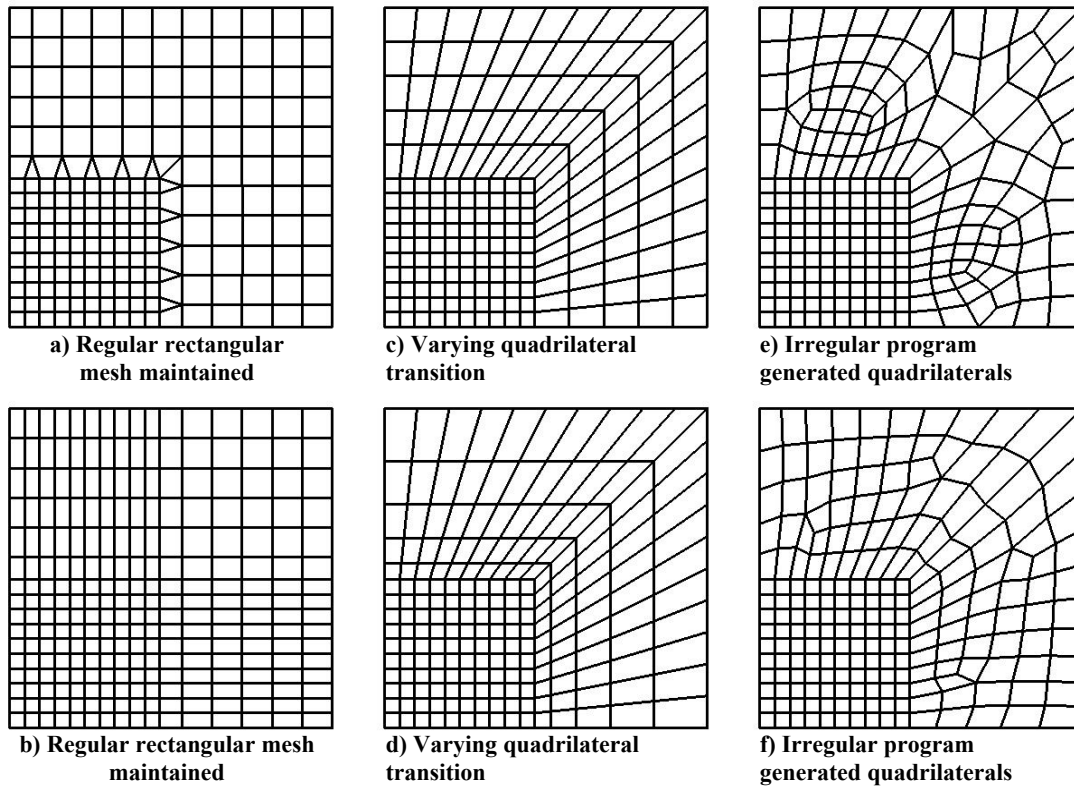


Figure 21. Illustration. Examples of transition meshes.

3.3 Material Properties

The two most commonly used materials in bridge construction, steel and concrete, are typically assumed to be isotropic materials for the purposes of analysis. An isotropic material is considered to have the same material properties (Young's Modulus, Poisson's ratio, etc.) in all directions. Although reinforced concrete in reality is orthotropic, differences that arise in load effects from ignoring the reinforcing and assuming isotropic gross section properties can be safely neglected in most analyses.

Anisotropic materials have different material properties depending on the orientation of the material. Wood or fiber reinforced composites are examples of anisotropic materials. For an anisotropic material it is important that the material properties are oriented along the appropriate member axes. Anisotropic materials are not considered herein.

For typical design, only linear-elastic material behavior is required, but many programs also have non-linear and inelastic material property capabilities for modeling such things as yielding of steel or creep in concrete.

3.4 One-Dimensional Analysis

For bridges that satisfy the AASHTO LRFD limitations, one dimensional analyses are fairly simple to create. *Typically there are two types of bridges where a one-dimensional analysis may*

be appropriate; multi-girder bridges where a single representative girder is analyzed, and bridges that have a torsionally stiff cross-section and can be analyzed as a single spine beam. In spine beam analyses, beam elements located at the centroid of the section are used to follow the geometry of the girder or bridge cross-section as seen in plan. An effective girder section is normally utilized for a one dimensional analysis with the deck area contribution transformed into an equivalent area of girder material using short term or long term modular ratios as appropriate. Multiple models can be used for various stages of construction.

Multi-girder structures modeled as a single representative girder are typically analyzed using a single lane of traffic loading, applying appropriate approximate distribution and multiple presence factors to the load effects to achieve a conservative design. AASHTO LRFD Article 4.6.2.2 contains equations for distribution for most common design cases, which are generally based on girder spacing, aspect ratio of girder spacing to length of span, and ratio of longitudinal stiffness to transverse stiffness. Additional correction factors contained in AASHTO LRFD Article 4.6.2.2 can be applied to account for skew.

In most cases using distribution and multiple presence factors assumes the same loading in all lanes. For cases where special loads such as permit or legal loads are mixed with regular traffic, force effects can be determined using the proportional distribution method described in AASHTO LRFD Article 4.6.2.2.5.

Straight girders can be analyzed with any continuous beam analysis program, as well as general purpose finite element programs. *The suggested minimum number of elements per span is eight. Often getting results at the tenth points is required, so using at least ten elements per span is recommended.* Loads are applied to the model at nodal locations, so using more elements will result in more accurate results, at little additional expense, but the increased accuracy is generally negligible. As always, engineering judgment is required.

As stated earlier in Section 2.4.2, according to Article 12.4.2.1 in the PCI Bridge Design Manual, bending moments in curved concrete beams from longitudinal flexure are virtually the same as those for a straight beam of span equal to the arc length between supports and therefore straight beam analysis can be used for preliminary design. Similarly per AASHTO LRFD Article 4.6.1.2.4b-1, curved steel multi-girder bridges that rely on transfer of load between girders to resist torsion can be analyzed as straight for major axis bending and shear with a span length equal to the arc length if the following conditions are met:

For I-girders:

- Girders are concentric
- Bearing lines are not skewed more than 10 degrees from radial
- The stiffness of the girders is similar – This requirement is to ensure that there is relatively equal sharing of loads among girders, but AASHTO provides little guidance on what the difference can be. If there is suspicion that girders are not similar enough, a simple curved girder refined model can be used to check load distribution. When in doubt, use a curved girder model rather than the straight approximation described here.
- For all spans, the arc span divided by the girder radius in feet is less than 0.06 radians, where the arc span L_{as} , is taken as:

- Arc length of the girder for simple spans
- 0.9 times the arc length for end spans of continuous members
- 0.8 times the arc length for interior spans of continuous members

For box girders:

- Girders are concentric
- Bearing lines are not skewed
- The girder depth is less than the width of the box at mid-depth
- For all spans, the arc span divided by the girder radius in feet is less than 0.3 radians, where the arc span L_{as} , is taken as:
 - Arc length of the girder for simple spans
 - 0.9 times the arc length for end spans of continuous members
 - 0.8 times the arc length for interior spans of continuous members

The AASHTO LRFD gives some guidance on modeling curved spine beams. Multiple straight elements can be used to approximate the curvature of curved structures in plan. AASHTO LRFD Article 4.6.1.2.2 applies to horizontally curved torsionally stiff single girder superstructures except concrete box girders.

For concrete box girders, Article 4.6.1.2.3 of the AASHTO LRFD states that horizontally curved concrete box girders may be designed with straight segments, for central angles (see Figure 22) up to 12 degrees within one span, unless concerns about other force effects dictate otherwise. It also states that horizontally curved nonsegmental concrete box girder bridge superstructures may be analyzed and designed for global force effects as single-spine beams with straight segments, for central angles up to 34 degrees within one span.

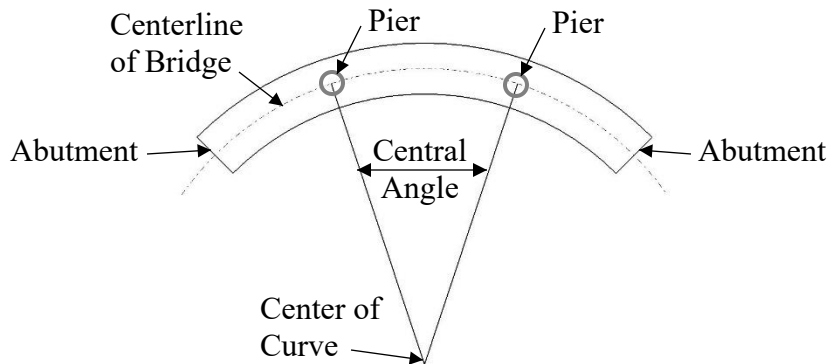


Figure 22. Illustration. Definition of central angle (adapted from AASHTO, 2014).

Article 4.6.1.2.3 of AASHTO LRFD also states that horizontally curved segmental concrete box girder superstructures meeting the requirements of AASHTO LRFD Article 4.6.1.1, and whose central angle within one span is between 12 degrees and 34 degrees may be analyzed as a single-spine beam comprised of straight segments provided no segment has a central angle greater than 3.5 degrees as shown in Figure 23. For both segmental and non-segmental box girder bridges with central angles exceeding 34 degrees within any one span, or for bridges with a maximum

central angle in excess of 12 degrees with unusual plan geometry, the bridge should be analyzed using 6 degrees of freedom in a proven three-dimensional analysis method.

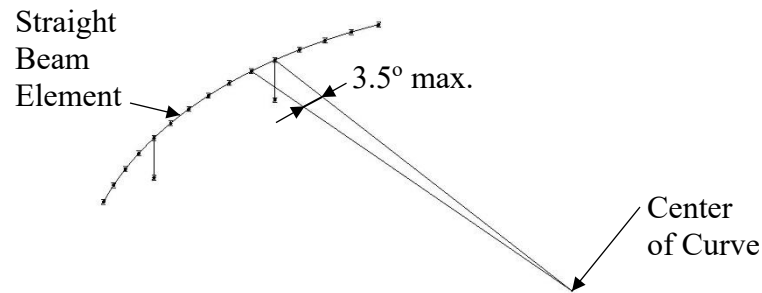


Figure 23. Illustration. Three-dimensional spine model of curved concrete box girder bridge (adapted from AASHTO, 2014).

Section 9.4 shows an example of the analysis of a cast-in-place concrete box girder spine beam. The example problem reproduces the results of an example problem in NCHRP Report 620 (Nutt et al., 2008). For more detailed information, see NCHRP Report 620.

3.5 Two-Dimensional Analysis

3.5.1 Basic Grid Analysis

Performing a grid analysis consists of concentrating the longitudinal and transverse stiffness properties of the bridge structure into a network of line elements in a plane. *Grid analyses can be used to model slab and voided slab bridges, but this manual will concentrate on grid models for slab-on-girder bridges. Any slab-on-girder bridge with any support conditions, skew or curved, can be analyzed.* For more information on grid analysis see (Hambly, 1976), and (O'Brien and Keogh, 1999).

There are essentially four steps in grid analysis:

- Idealize the structure into an appropriate equivalent grid of line elements.
- Calculate and assign section properties to achieve equivalent approximate longitudinal and transverse structure stiffness.
- Apply loads.
- Analyze and extract distribution factors or design force effects.

Multiple grid models can be utilized to analyze bridges for different stages of construction.

3.5.1.1 Elements and Geometry

Beam elements are used to model the network of longitudinal and transverse lines in the planar grid. At minimum the number and location of longitudinal grid lines should be coincident with the number and location of longitudinal girders, as illustrated in Figure 24. Additional longitudinal lines can be added between widely spaced girder lines to improve live load placement accuracy, and is recommended to account for the full area of deck if the effective

width of deck used in calculating section properties is significantly less than the actual spacing of girders, as shown in Figure 25.

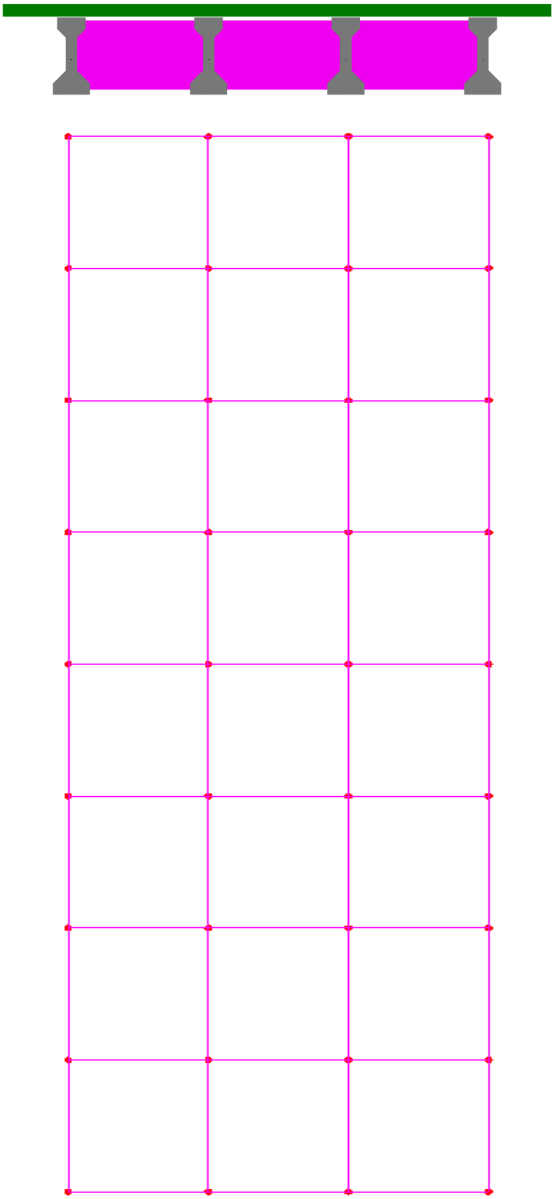


Figure 24. Illustration. Grid model with element at longitudinal girder lines.

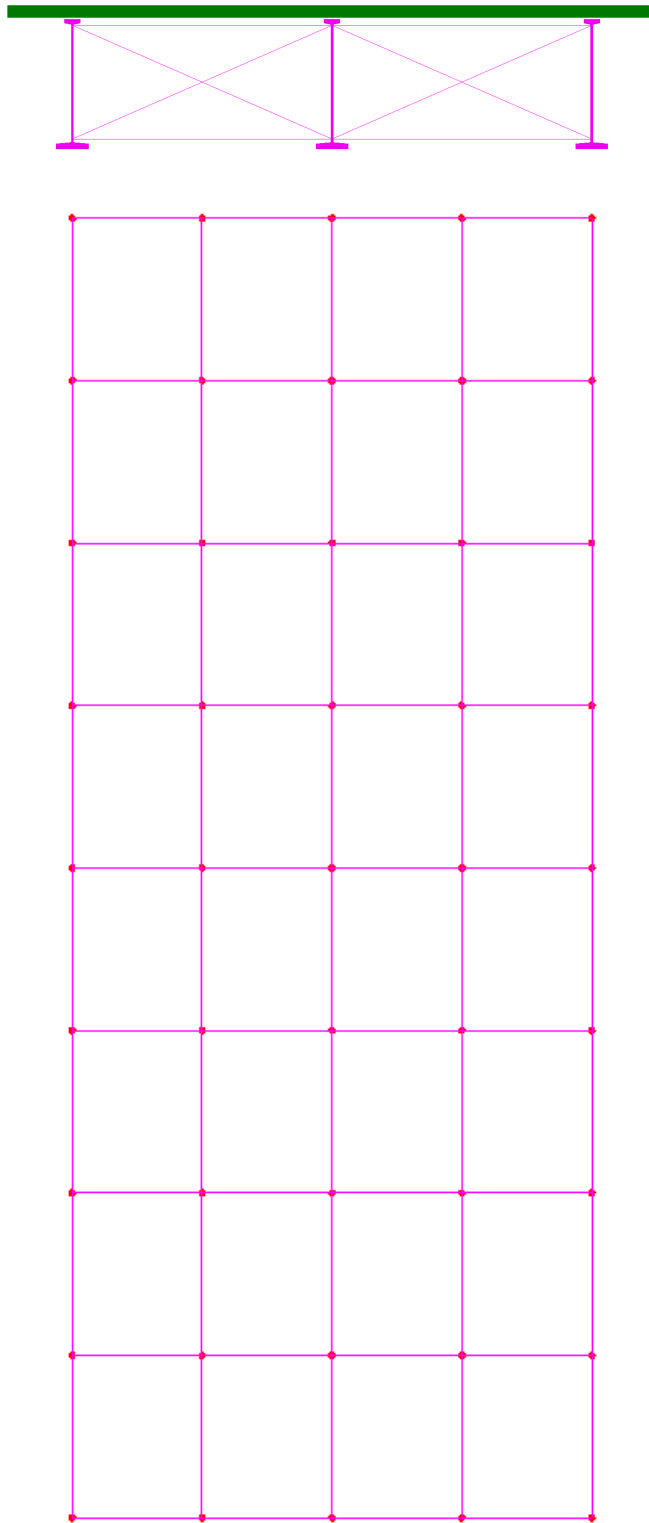


Figure 25. Illustration. Grid model with additional elements between longitudinal girder lines.

Edge lines can be provided at or near the edge of the deck when integral barriers or edge stiffening is present, as illustrated in Figure 26. For bridges with sidewalks, longitudinal lines should be provided at the center of the sidewalks, although the contribution of the sidewalk to the stiffness of the bridge may or may not be neglected, depending on the analysis.

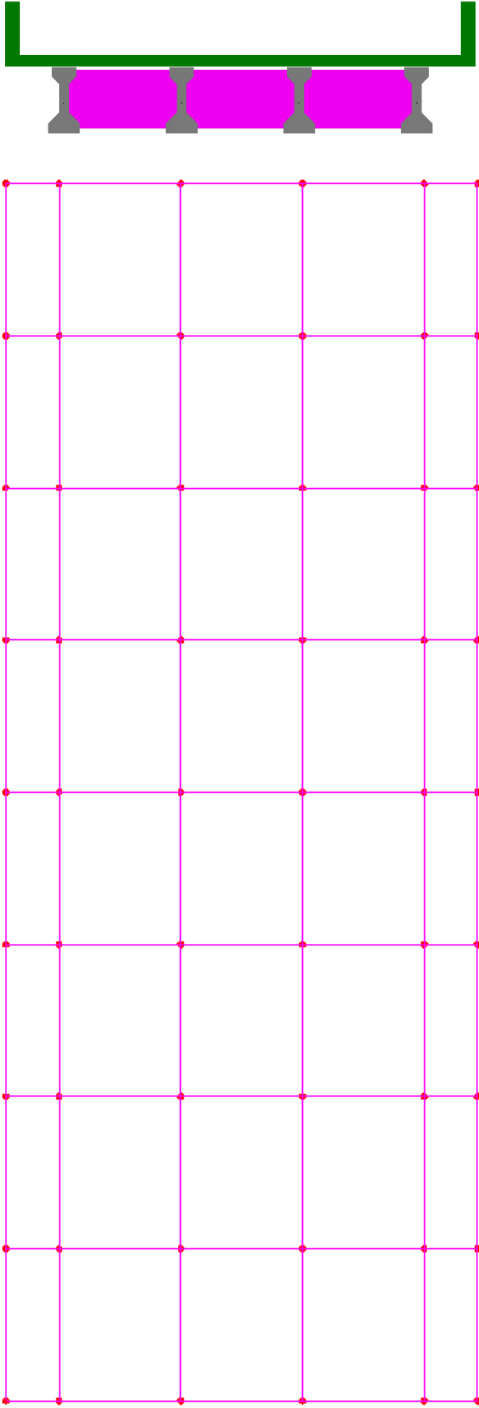


Figure 26. Illustration. Grid model with additional stiffening elements along the edge of deck.

Curved structures can be modeled either with curved elements or approximated with a series of straight elements between transverse lines, as shown in Figure 27. When using straight elements to approximate a curved beam the maximum recommended central angle for the elements is 3.5 degrees, similar to spine beams as illustrated in Figure 23.

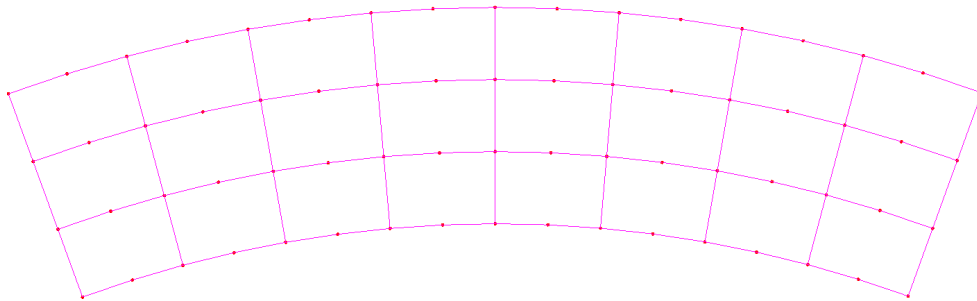


Figure 27. Illustration. Curved grid model.

At minimum, transverse lines should be provided at all cross-frame/diaphragm locations, including at supports. As with the longitudinal elements, when the effective width of deck included with the cross-frames/diaphragms does not encompass the full length of deck, additional lines can be added between cross-frames/diaphragms in order to account for the full area of deck slab. Additional transverse lines may also be required at intersections of straight elements approximating a curved structure. If no cross-frames/diaphragms are present, the transverse line spacing is somewhat arbitrary, but recommendations in the literature range from 1/4 to 1/9 of the effective span length.

Recommended spacing of transverse grid lines ranges from the longitudinal girder spacing for small aspect ratio bridges (short/wide) to twice the longitudinal girder spacing for large aspect ratio bridges (long/narrow). The recommended number of transverse lines per span is preferably odd (even number of spacings), with a minimum of seven (Wong, 2010). Often it is convenient to place nodes at the tenth points of each span, as forces and deflections are often required at those locations. Transverse lines preferably should run full width of the grid, but adjustments can be made for staggered cross-frames.

The orientation of transverse lines preferably should be normal to the longitudinal lines of the grid. For skewed bridges when the angle of skew is less than 20 degrees, transverse lines should be parallel to supports, although transverse section properties can be calculated as if lines run orthogonal to longitudinal girders, see Figure 28(a). For skews greater than 20 degrees, the transverse lines should run parallel to the supports for small aspect ratio bridges, and orthogonal to the span for large aspect ratio bridges, as shown in Figures 28(b) and (c) (Wong, 2010). Transverse lines do not need to be equally spaced, but regular spacing contributes to simpler analyses.

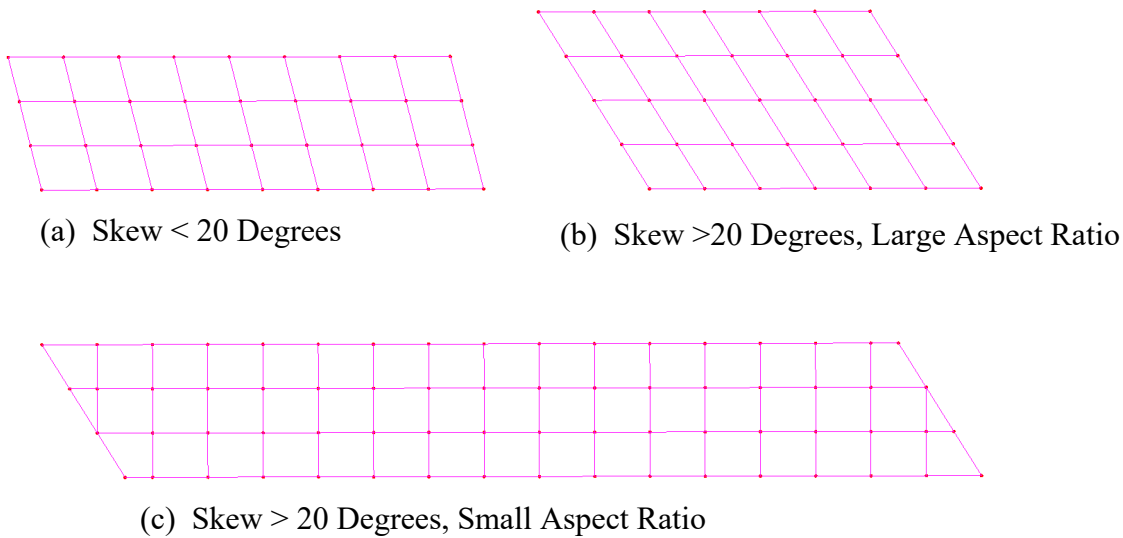


Figure 28. Illustration. Orientation of transverse grid lines.

Supports should be placed at the locations of bearings. *Support conditions can be very important, especially for highly skewed bridges, as small reactions and potential uplift can occur at acute corners, and large reactions at obtuse corners can result in having to design for large shear forces.* While it is conservative to design for these large forces, modeling supports with spring stiffnesses approximating the actual bearing stiffness rather than using unyielding supports will distribute the load more realistically and can reduce the extreme reactions (see Section 3.7.2). Reactions may also be reduced by adjusting cross-frame geometry (see Section 3.5.3).

3.5.1.2 Section Properties

Longitudinal section properties are calculated about the centroid of the composite transformed section. Note that even though the centroids of all longitudinal lines may not lie in the same plane, they are still modeled as such. Section properties are generally based on the gross uncracked concrete properties for girders and decks, although the effective width of deck based on AASHTO LRFD Article 4.6.2.6 or a rational analysis should be used. In some regions, such as over interior supports of a composite concrete deck steel girder bridge, cracked section properties can be used, although it is generally not necessary. If using cracked section properties over an interior support, the properties should extend approximately 15 percent of the length into each span.

Because the longitudinal properties are represented in the longitudinal lines and the transverse properties in the transverse lines, basic grid models can easily accommodate orthotropic properties if desired. When dissimilar materials are used, a transformed area using modular ratios based on short term or long-term properties may also be appropriate.

Torsional stiffness is important in a grid analysis, as the model geometry does not provide the appropriate stiffness utilizing moment couples separated by structure width/depth, especially for the contributory width of deck in each element. The torsional stiffness of each longitudinal line

is equal to the sum of the torsional stiffnesses of each girder and contributory width of deck. The girder torsional stiffness can be calculated using the equations of AASHTO LRFD Article C4.6.2.2.1 (also see Section 3.5.4 of this manual). The contribution of a width, b , of deck thickness, d , to the torsional stiffness is half that of the typical theoretical value for a thin-walled beam element, i.e. $J = bd^3/6$ (Hambly, 1976). The reason is because the slab includes only the contributions of shear flow at the top and bottom faces, while for a discrete element the shear flows at the ends are included as well. Note that the modular ratio needs to be applied when mixing dissimilar materials.

Transverse section properties are calculated similarly to the longitudinal properties. If no cross-frames/diaphragms are present, the contributory width of concrete deck slab is used to calculate moment of inertia and torsional constant. When a cross-frame/diaphragm is present, an estimate of the effective width of deck slab acting with the cross-member needs to be made. A reasonable estimate is that the effective width is 0.3 of the distance between longitudinal members (Hambly, 1976), with any remaining portion of deck represented in additional cross-members. For a diaphragm, such as the typical concrete diaphragms from Example 1 shown in Figure 29, calculating the section properties is straightforward, similar to a longitudinal member. For cross-frames, such as the typical steel cross-frames from Example 2 illustrated in Figure 30, the stiffness of the multi-member cross-frame must be approximated by a single line element. Several methods of approximating the stiffness are detailed in Section 3.5.3 of this manual.

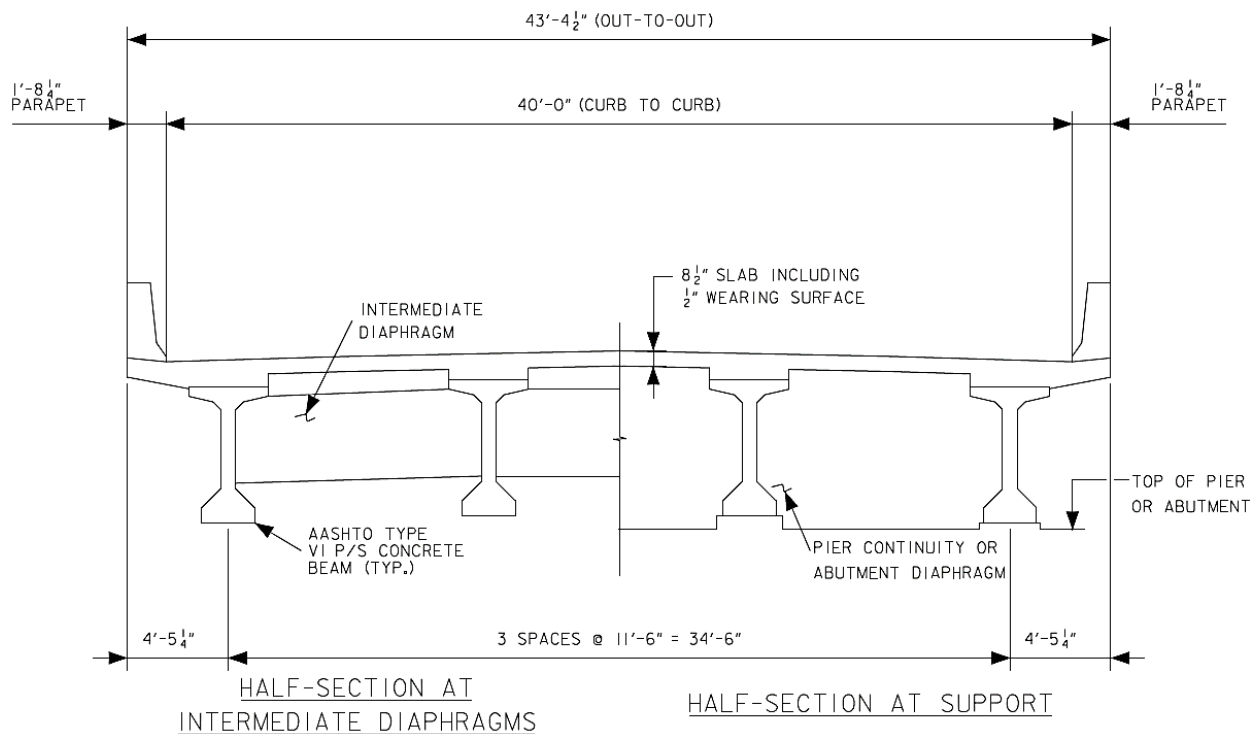


Figure 29. Illustration. Typical concrete diaphragms.

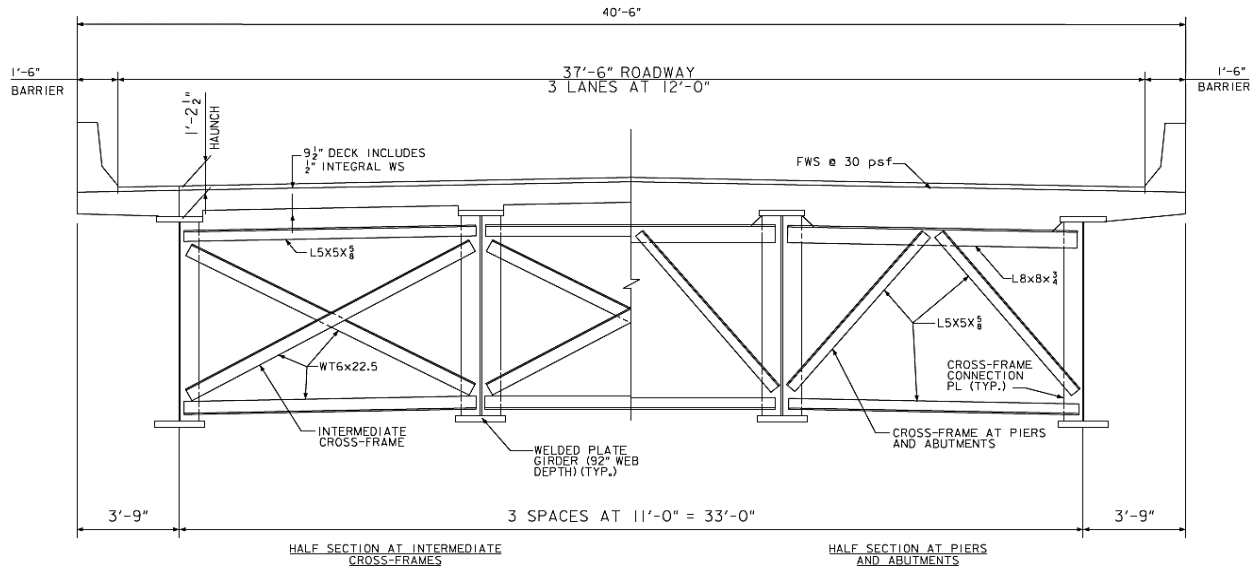


Figure 30. Illustration. Typical steel cross-frames.

3.5.1.3 Loading and Results

A grid model is generally loaded with vertical loads only which can be placed at the nodes or along the elements. Dead loads should be distributed to grid elements based on tributary distances, with care being taken to not double count by assigning the same load to both longitudinal and transverse members. *Live loads that fall in between grid elements can be distributed to the nodes. Ideally a statically equivalent loading should be applied, but in practice, distributing vertical loads to adjacent nodes based on ratios of geometric distance is usually sufficient, although shear forces near supports may be underestimated due to the distribution of the nodal load directly to the support.* Some programs can automatically distribute live loads to the grid, greatly reducing the modeling effort required. See Chapter 7 of this manual for more information on loading.

Once the analysis has been performed, design loads must be extracted. Due to the torsional resistance of the transverse members, there will be “steps” in the moment diagrams of the longitudinal girders. If the node is a location of a transverse cross-frame/diaphragm, use the actual output moment values. If the node is a location where the transverse member only represents the slab, average the girder bending moments on either side of the node (Hambly, 1976).

Shortcomings of the basic grid analysis include (Hambly, 1976):

- Transfer of shear between longitudinal girders through the deck cannot be effectively modeled. Some effects of this are:
 - Shear forces in the deck slab are underestimated.
 - Load distribution and resulting axial forces in the girders are incorrect as longitudinal inter-beam shear and axial forces which would result in couples reducing the moment in loaded beams and increasing moments elsewhere cannot be transferred.

- Warping torsion not modeled.
- 3D cross-frame behavior is approximated with single line elements.

3.5.2 Plate with Eccentric Beam

A PEB analysis is a refinement of the basic grid analysis that explicitly models the deck slab and girders separately. The depth of the structure is accounted for by locating the deck slab “plate” and the longitudinal girder “beams” at their respective centroids, such that the girders are “eccentric” to the deck plate as illustrated in Figure 31.

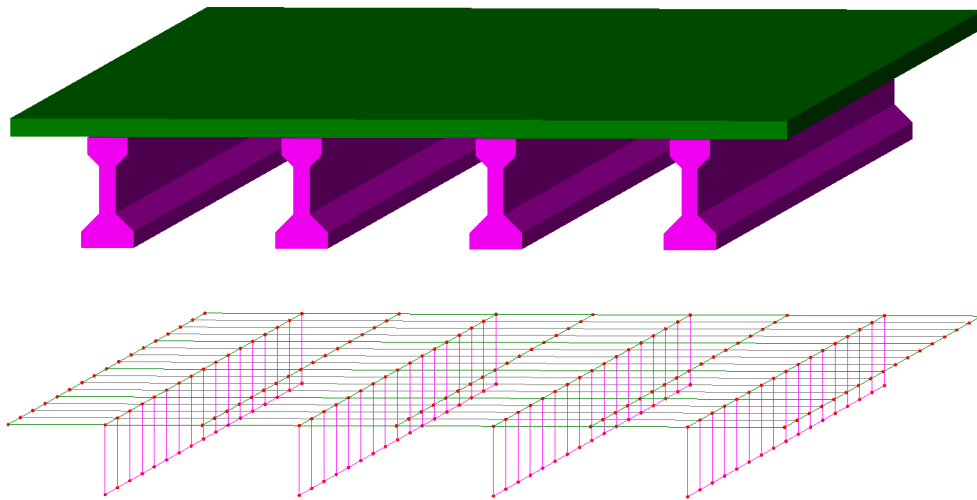


Figure 31. Illustration. Portion of typical concrete slab on girder bridge and PEB model with explicit shear connection elements (diaphragms not shown for clarity).

The PEB analysis eliminates some of the shortcomings of the basic grid analysis and improves the stiffness properties of the model. The presence of a continuous deck in a PEB analysis enforces compatibility between girders and allows the transfer of longitudinal shear forces between girders. Explicitly modeling the deck also means that composite behavior no longer needs to be approximated using effective widths and modular ratios. Given an appropriate mesh size it will be automatically modeled using the material properties and geometry of the deck and girders. Modeling the deck explicitly does make it harder to assign orthotropic properties such as cracked section properties in one direction to the deck if so desired. For long term loads an effective modular ratio factor may still need to be accounted for in the model as well.

For routine design of most typical concrete slab on beam bridges when accuracy beyond the approximate distribution factor approach is desired, the PEB is the recommended refined analysis model. The PEB may also be appropriate in cases where a structure exceeds the limits of applicability of the approximate distribution factors.

3.5.2.1 Elements and Geometry

The PEB model locates beam elements along the centroids of longitudinal girder lines. Beam elements are also used to connect the longitudinal elements transversely at cross-

frame/diaphragm locations, if present. Shell elements are used to model the concrete deck over the entire length edge to edge. Volume elements could also be used, but would result in an inefficient solution due to the large increase in DOF and minimal increase in accuracy involved.

Although the deck and the girders/cross-members are modeled eccentric to each other in the PEB model, depending on the software being used, and the connectivity of the deck, lines may be in the same plane, or in different planes. If the software supports element eccentricities, the eccentricity can be defined in the element properties and all lines can be in the same plane. If element eccentricities are to be explicitly modeled, elements or links can be used to connect the deck and the girders/cross-members, and the deck lines and the girders/cross-member lines can be located in different planes.

The number of elements used to model the girders and the deck are interrelated, as the two are connected at nodal locations. *At a minimum, nodes should be located at the tenth points of each span, as forces and deflections are often required at those locations. The number of elements used along the length of the bridge for the deck slab should be the same as that for the longitudinal girder elements where composite action is to be modeled. The number of longitudinal elements should be such that a reasonable aspect ratio is obtained. Up to 5 to 1 is usually acceptable, although approaching 1 to 1 is best. At minimum there should be two shell elements between each line of girders in order to capture shear lag behavior.*

A deck on a skewed bridge can be oriented as a skewed mesh or an orthogonal mesh (see Figures 32 and 33). Typically element orientation is not critical as the shell elements are isotropic in-plane. For simplicity the deck elements are usually oriented in the same direction as the cross-frames or diaphragms. The node locations of the mesh must be compatible with the node locations of other elements of the model. Quadrilateral elements will provide good results until they become highly skewed, e.g. corners more acute than 45° , at which point triangular elements become more appropriate.

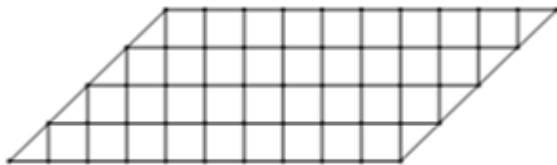


Figure 32. Illustration. Orthogonal mesh.

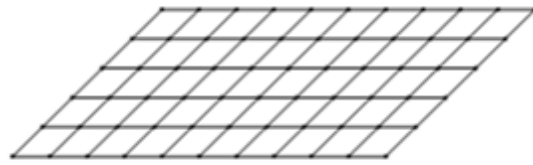


Figure 33. Illustration. Skewed mesh.

When full composite action is to be modeled, the girder elements should be rigidly connected to the deck slab elements. If the deck slab is modeled at the same elevation as the girders and an offset used to achieve the correct location, composite action will be automatically achieved through the use of common nodes. Otherwise the composite behavior can be accomplished by using rigid link constraints or stiff beam elements, with one element per location of corresponding nodes connecting the girder elements and the slab elements. Care should be taken when using stiff beam elements, as overly stiff elements can introduce calculation errors in some cases. For non-composite girders, link elements with little shear resistance can be used. Elements with no shear resistance can be used if steps such as providing shear resistance at a single point are also taken to avoid a mechanism, i.e. zero resistance in a given direction.

While the vertical eccentricity of the girders and deck is explicitly considered, the vertical eccentricity of the support conditions may or may not be explicitly modeled. For vertical loadings, modeling the vertical eccentricity of the supports is typically not important (see Section 3.7.2).

3.5.2.2 Section Properties

Girder section properties are calculated about the centroid of the longitudinal girders. Section properties are generally based on the gross uncracked properties for concrete girders. In some regions, such as over interior supports, cracked or effective section properties can be used if a reduced stiffness is more realistic. Deck section and stiffness properties are calculated by the program based on geometry and material properties with no need for transformed properties.

Transverse member properties are calculated about the centroid of diaphragms, even though the transverse member connects the centroids of the longitudinal members. For cross-frames, the stiffness of the multi-member cross-frame must be approximated by a single line element. As mentioned previously, several methods of approximating the stiffness are detailed in Section 3.5.3 of this manual. As with the longitudinal members, deck section and stiffness properties are calculated by the program based on geometry and material properties.

Torsional stiffness is important in a PEB analysis, although not quite as important as in a grid analysis, as the model geometry provides the appropriate stiffness contribution of the deck automatically. The girder and diaphragm torsional stiffnesses can be calculated using the equations of AASHTO LRFD Article C4.6.2.2.1 (also see Section 3.5.4 of this manual).

3.5.2.3 Loading and Results

A PEB model can be loaded with both vertical and horizontal loads, although boundary conditions should be modeled at their correct elevation if horizontal loads are to be applied. Dead loads can be assigned automatically based on cross-sectional areas, or using concentrated, line, or area loadings. Live loads that fall in between nodes of shell elements can be distributed to the nodes, either automatically or manually. As previously mentioned, ideally a statically equivalent loading should be applied, but in practice, distributing vertical loads to adjacent nodes based on ratios of geometric distance is usually sufficient, although shear forces near supports may be underestimated due to distribution of nodal load directly to the support. See Chapter 7 for more information on loading.

Once the analysis has been performed, load effects must be extracted. *In a PEB analysis, composite forces in the discretized girder and deck elements must be summed back to the shears, moments, and axial forces for each composite member of the bridge as recognized by the AASHTO LRFD.* Integrating stresses over the contributory deck width to determine forces, and summing force outputs of the deck and girders, may be required to calculate the design load resultants, or the demands on a given component, in order to compare to AASHTO LRFD limit states. For more information see Chapter 8 of this manual.

As with the basic grid, if the transverse members have torsional resistance, there will be “steps” in the moment diagrams of the longitudinal girders.

Shortcomings of the PEB analysis include:

- Warping torsion not modeled, although approximations can be made.
- 3D cross-frame behavior is approximated with single line elements.

3.5.3 Diaphragm / Cross-frame Stiffness

Steel or concrete diaphragms can be modeled simply by using beam elements representative of the entire diaphragm cross-section. An element formulation that includes shear deformation is recommended, especially for short deep members. Depending on the element formulation, one element may be sufficient to capture the forces in the diaphragm, with more elements required to capture the deflected shape.

Steel truss-type cross-frames are open web members consisting of a bottom chord, one or more (often two) diagonals, and possibly a top chord. *In a grid or PEB analysis, the entire cross-frame is represented by a single member.* While this single member should approximate the behavior of the actual cross-frame as closely as possible, accurately modeling the stiffness is more important for curved or skewed bridge geometries than for straight square bridges.

Cross-frames in skewed bridges can act as alternative load paths and distribute vertical loads transversely. Depending on the skew and the width-to-span ratio, the effects of the transverse load distribution due to this “nuisance stiffness” can be quite severe (Coletti, 2011). Orienting the cross-frame on the skew, or staggering cross-frames in adjacent bays can help mitigate this problem (Krupicka, 1993).

NCHRP Report 725 details various methods for calculating equivalent section properties in order to represent cross-frames with a single member (White et al., 2012). The methods include:

- Assume cross-frame is loaded predominantly in flexure and calculate an equivalent moment of inertia,
- Assume cross-frame is loaded predominantly in shear and calculate an equivalent moment of inertia,
- Assume cross-frame has both significant flexural and significant shear deformations and approximate both the moment of inertia and an effective shear area, and
- Calculate the exact equivalent stiffness and define the entire stiffness matrix of a user programmable element.

The flexural stiffness method models the cross-frame as a propped cantilever subject to a moment at the propped end to determine the cross-frame stiffness properties. The moment is modeled by a unit force couple as shown in Figure 34. The model utilizes truss elements for the cross-frame members. The left side of the cross-frame is restrained both vertically and horizontally at the top and bottom, while on the right side the nodes are only restrained vertically.

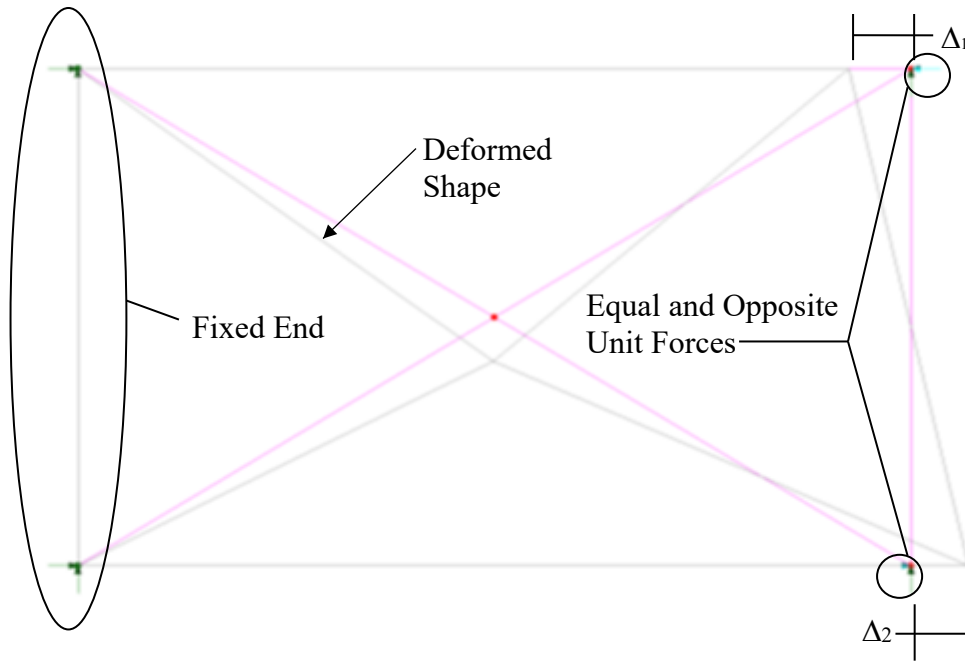


Figure 34. Illustration. Intermediate cross-frame model - flexural stiffness.

The rotation, θ , is calculated using the sum of the horizontal deflections (from the analysis model) divided by the height of the cross-frame; this is equal to $(\Delta_1 + \Delta_2)/\text{depth}$ for small deflections. The effective bending stiffness of a single element I_b is determined using Equation (1):

$$I_b = \frac{ML}{4E\theta} \quad (1)$$

where: I_b = equivalent moment of inertia
 M = moment due to unit force couple = $1 \times \text{depth}$
 L = length between girders
 E = steel modulus of elasticity
 θ = rotation due to unit force couple = $(\Delta_1 + \Delta_2)/\text{depth}$

The shear stiffness method models the cross-frame as a cantilever fixed at one end and free to deflect vertically but not rotate at the other end to determine the cross-frame stiffness properties. A unit load is applied to the end that is free to deflect as shown in Figure 35. The model utilizes truss elements for the cross-frame members. The left side of the cross-frame is restrained both vertically and horizontally at the top and bottom, while on the right side the nodes are only restrained horizontally.

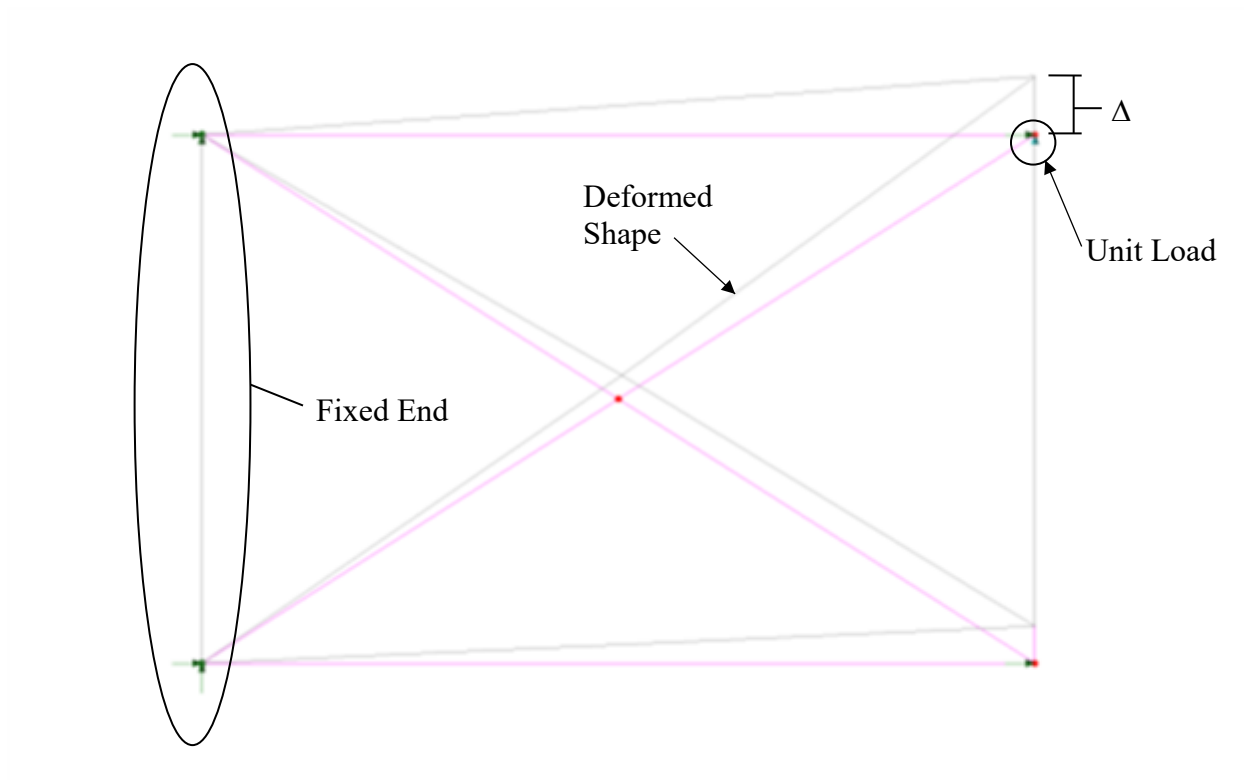


Figure 35. Illustration. Intermediate cross-frame model - shear stiffness.

The effective bending stiffness of a single element I_s is determined using Equation (2):

$$I_s = \frac{PL^3}{12E\Delta} \quad (2)$$

where: I_s = equivalent moment of inertia
 P = unit force
 L = length between girders
 E = steel modulus of elasticity
 Δ = vertical deflection

For programs where beam elements incorporating shear deformations (Timoshenko formulation) are available, a second independent variable, the shear area, can be used to more accurately model the cross-frame. The following method can be used to determine an effective bending stiffness and an effective shear area.

The effective bending stiffness based on an effective moment of inertia is determined by modeling the cross-frame as a cantilever, similar to Figure 34 but with no restraints on the free end, and subjecting it to a force couple as illustrated in Figure 36.

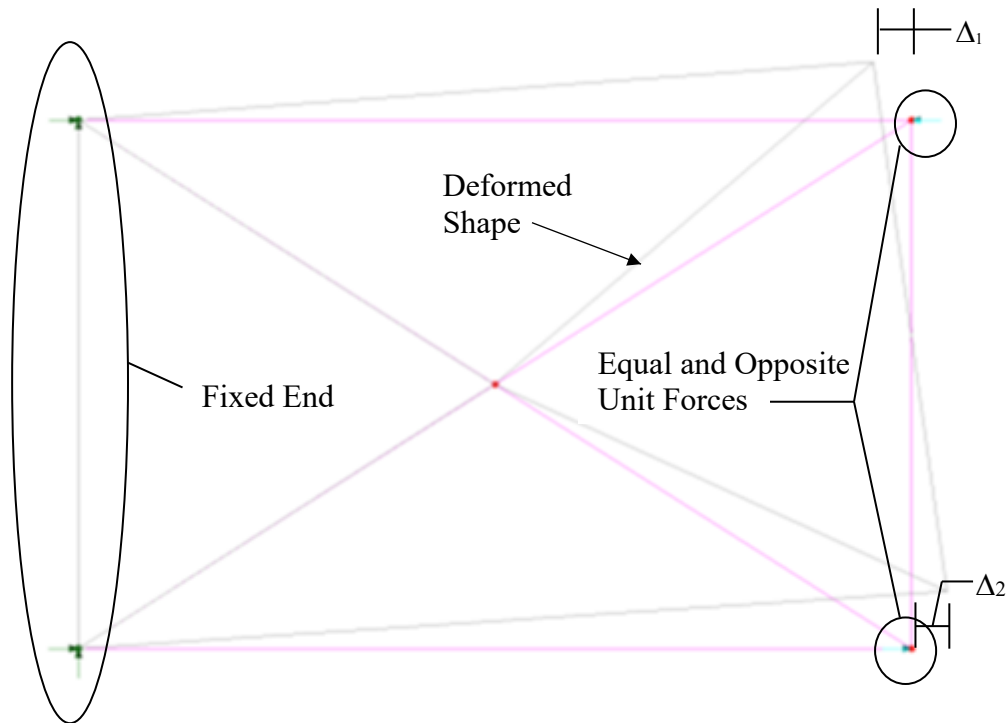


Figure 36. Illustration. Intermediate cross-frame model - flexural stiffness.

The rotation, θ , is calculated using the sum of the horizontal deflections (from the analysis model) divided by the height of the cross-frame; this is equal to $(\Delta_1 + \Delta_2)/\text{depth}$. In the shear-deformable beam approach I_{eq} is determined using Equation (3):

$$I_{eq} = \frac{ML}{E\theta} \quad (3)$$

- where:
- I_{eq} = equivalent moment of inertia
 - M = moment due to unit force couple = $1 \times \text{depth}$
 - L = length between girders
 - E = steel modulus of elasticity
 - θ = rotation due to unit force couple = $(\Delta_1 + \Delta_2)/\text{depth}$

The equivalent shear area is determined by modeling the cross-frame as a cantilever, similarly to Figure 35 but with no restraints on the free end, and subjecting it to a unit vertical shear at the free end, as illustrated in Figure 37.

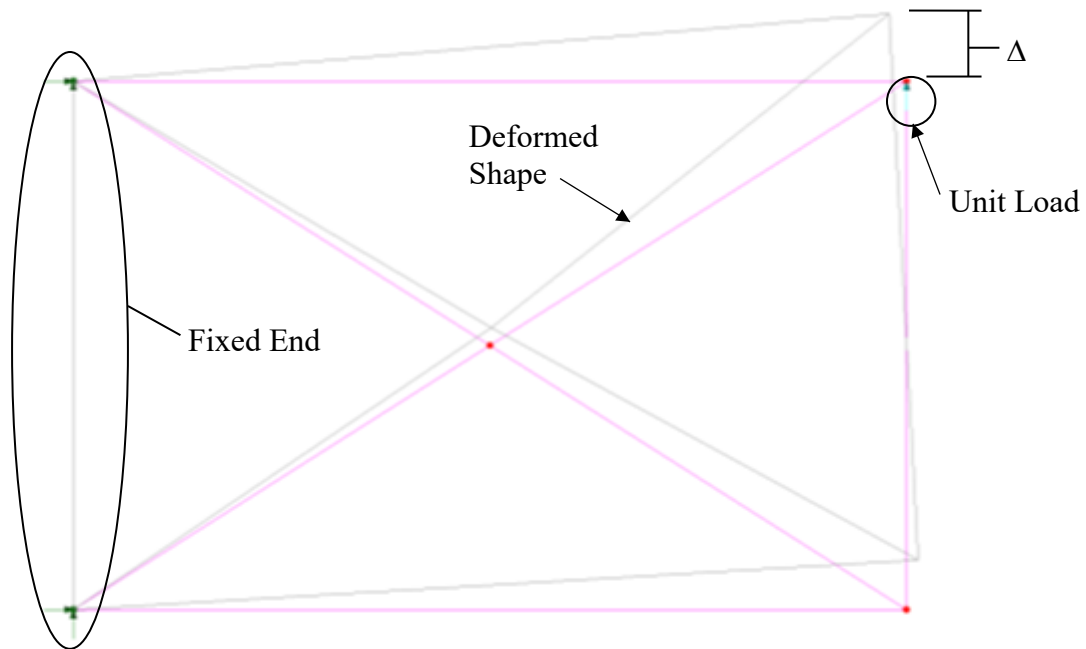


Figure 37. Illustration. Intermediate cross-frame model - shear stiffness.

The equivalent shear area is then calculated using Equation (4):

$$A_{eq} = \frac{VL}{G \left(\Delta - \frac{VL^3}{3EI_{eq}} \right)} \quad (4)$$

where: A_{eq} = equivalent area
 Δ = deflection due to unit force
 V = unit force
 L = length between girders
 E = steel modulus of elasticity
 I_{eq} = equivalent moment of inertia
 G = shear modulus of elasticity = $E/[2 \times (1 + \nu)]$
 ν = Poisson's ratio

Connection stiffness and second-order stiffness softening can also be taken into account per AASHTO LRFD Article C4.6.3.3.4 (Wang et al., 2012). In lieu of a more accurate analysis, the equivalent stiffness $(AE)_{eq}$ of equal leg single angles, unequal leg single angles connected to the long leg, and flange connected tee-section members may be taken as $0.65AE$ in whichever effective beam analysis is chosen.

The choice of which equivalent element to use depends on the elements available, the cross-frame geometry, and level of accuracy required. Using the bending stiffness or the shear stiffness method is common if the program being used only has Euler-Bernoulli beam elements, and bending stiffness EI is the only adjustable variable. Generally, the flexural method should

be used when the cross-frame is relatively long and shallow and dominated by bending behavior, and the shear method should be used when the cross-frame is relatively short and deep and dominated by shear behavior. It is ultimately up to the judgment of the engineer, who best understands the type of deformation occurring at the cross-frame, to choose the most appropriate model for that specific behavior.

When available, the shear deformable (Timoshenko) beam approach utilizing both I_{eq} and A_{eq} is recommended for modeling cross-frame stiffness for routine bridge design. If an “exact” element is required, the procedure to define the entire element stiffness matrix of a user defined element is detailed in NCHRP Report 725 (White et al., 2012). The additional effort required for the use of an “exact” element is rarely justified, but for bridges with high skews or curvature, calculating accurate forces in cross-frames is important. In order to determine the forces in the multiple cross-frame members based on the forces in an equivalent single member, see Section 8.2.5.

3.5.4 Handling Torsional Stiffness in 2D Models

The method by which torsion is handled in 2D finite element models is important because of the two sources of torsional stiffness, Saint-Venant and warping. Saint-Venant torsion theory assumes the following:

- Torsion is constant
- Each cross-section rotates as a rigid body (no distortion of cross-section shape)
- Rate of twist is constant
- Cross-sections are free to warp, i.e. displace, in the longitudinal direction but the warping is the same for all cross-sections

With Saint-Venant torsion, only shear stresses are produced. Warping torsional restraint occurs when the cross-sections are not free to warp in the longitudinal direction, and normal stresses develop.

Although influenced by boundary conditions, loading, and length, generally stocky sections such as concrete I-girder and closed sections such as thin wall box girders resist torsion mainly by Saint-Venant torsion, while thin wall open sections such as wide flange beams resist torsion mainly by warping restraint. Historically, thin walled open sections have been steel, but as concrete sections continue to become more slender, the contribution of warping rigidity may need to be checked. The concrete deck generally resists torsion by Saint-Venant stiffness as well, and the contribution of the deck to torsional stiffness is described in Section 3.5.1.2 of this manual.

In most FEA programs line beam elements only model Saint-Venant torsional stiffness (GJ), they do not capture warping torsional stiffness (EC_w). In order to capture the warping behavior a line beam element would have to be higher order and the program would need to accommodate a warping DOF in addition to the nodal displacement and nodal rotation DOF.

If torsional stiffness is important in a line element model having open sections or other sections where warping stiffness is significant, either an effective torsion constant that incorporates both the warping stiffness and the Saint-Venant stiffness should be utilized, or the sections can be

discretized further to capture the correct behavior. One method of determining an effective torsion constant is discussed in Section 3.5.4.1. For wide flange beams discretely modeling the flanges and web with multiple elements, rather than using a single line element, would capture the warping behavior. Discrete modeling would require the model to incorporate more DOF, resulting in a greater computational effort, not to mention more output data to reduce.

Modeling torsional stiffness is more important when significant torsional loads are present, such as in curved and/or skewed bridges.

3.5.4.1 Thin-walled Open Section Girder Grid Systems

In many cases neglecting the contribution of the warping torsional stiffness of thin-walled open sections in longitudinal girders in an FEA grid model results in negligible error when determining design force effects. Exceptions to this are for skewed or curved bridges when a stability analysis or deflection analysis is being performed on the non-composite structure. In these cases, including the warping torsional stiffness can result in a significant improvement of the accuracy of the model. Discretely modeling the entire cross-section with shell elements is one method to capture the warping behavior, but it also results in a much more complicated model, with an accompanying increase in computational effort.

Alternatively, in NCHRP Report 725 White et al. (White et al., 2012), determined that an equivalent torsion constant, J_{eq} , could be used in place of the actual Saint-Venant torsion constant J , for line elements in 2D grid models to obtain results that approximated the results of more sophisticated 3D models. The equivalent torsion constant was based on equating the stiffness GJ_{eq}/L_b with the analytical torsional stiffness associated with assuming warping free conditions at simply supported ends and warping fixity at intermediate cross-frame locations in a bridge girder.

The assumption of warping fixity at cross-frame locations is certainly an approximation, but it leads to reasonably accurate characterization of the girder torsional stiffness pertaining to the overall deformations of the bridge as long as:

- There are at least 2 I-girders connected together, and
- They are connected by enough cross-frames such that the connectivity index I_C is less than 20, where $I_C = 15000 / [R(n_{cf}+1)m]$, where R is the minimum radius of curvature at the centerline of the bridge cross-section in feet throughout the length of the bridge, n_{cf} is the number of intermediate cross-frames in the span, and m is a constant taken equal to 1 for simple-span bridges and 2 for continuous-span bridges. In bridges with multiple spans, I_C is taken as the largest value obtained from any of the spans.

The equation for J_{eq} given an unbraced length L_b between intermediate cross-frames with assumed warping fixity at each end is given by Equation (5).

$$J_{eq} = J \left[1 - \frac{\sinh(pL_b)}{pL_b} + \frac{[\cosh(pL_b) - 1]^2}{pL_b \sinh(pL_b)} \right]^{-1} \quad (5)$$

Similarly, the equation for J_{eq} for the end panel between the bearing and the first cross-frame with warping fixity at one end and warping free boundary at the other end is given by Equation

(6).

$$J_{eq} = J \left[1 - \frac{\sinh(pL_b)}{pL_b \cosh(pL_b)} \right]^{-1} \quad (6)$$

where $p^2 = GJ/EC_w$

For more information, see NCHRP Report 725. In lieu of a more precise analysis, J and C_w may be calculated using the following equations.

Article C4.6.2.2.1 of AASHTO LRFD gives an approximate formula (Equation (7)) for calculating J for thin-walled open section beams:

$$J = \frac{1}{3} \sum bt^3 \quad (7)$$

where: b = width of plate elements (in.)
 t = thickness of plate elements (in.)

Article C6.9.4.1.3 of AASHTO LRFD gives an approximate formula (Equation (8)) for calculating C_w for singly symmetric steel I-beams:

$$C_w = \frac{t_f h^2}{12} \left\{ \frac{b_1^3 b_2^3}{(b_1^3 + b_2^3)} \right\} \quad (8)$$

where: b_1, b_2 = individual flange widths (in.)
 h = distance between flange centroids (in.)
 t_f = flange thickness (in.) Use an average thickness if the flange thicknesses differ.

Alternately, C_w can be calculated using Equation (9):

$$C_w = \frac{h^2 I_{y1}}{\frac{I_{y1}}{I_{y2}} + 1} \quad (9)$$

where: h = distance between flange centroids (in.)
 I_{y1}, I_{y2} = moments of inertia of the flanges about a vertical axis in the plane of the web (in⁴).

An alternate, approximate, method for calculating an equivalent torsional stiffness of an I-section is to ignore the web and idealize the flanges of the I-shape as beams, not necessarily the same size, spanning laterally the length L_b between cross-frames (see Figure 38). Assuming the girder is restrained from warping at internal cross-frames and is unrestrained from warping at its ends results in the idealized beams having fixed-fixed against rotation but free to deflect end conditions for an internal length of girder and fixed-free end conditions for an end length of girder.

Apply a unit load at one end of each flange, equal but in opposite directions, and allow the flanges to displace laterally. Rotation is restrained in the internal case. The applied torque will be the unit load multiplied by the distance between the flanges, $T=1 \cdot h$, and assuming small displacements the rotation will be a sum of the two displacements divided by the distance between flanges. Dividing the torque by the rotation gives the torsional stiffness of the system. Equate that to $GJ_{additional}/L_b$, and solve for $J_{additional}$ where $J_{additional}$ is the approximate contribution of warping to the torsional stiffness. The total equivalent torsional stiffness J_{eq} will be the calculated Saint-Venant stiffness J plus $J_{additional}$.

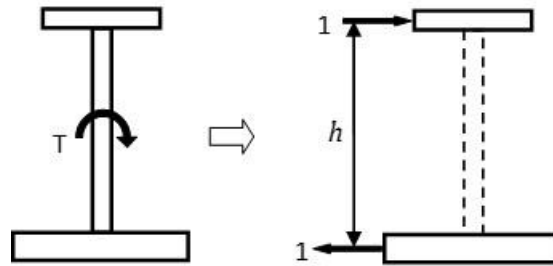


Figure 38. Illustration. Calculating equivalent Saint-Venant torsion stiffness for I-sections.

For the general case the equation is:

$$J_{eq} = J + \frac{L_b h^2}{2G(\Delta_1 + \Delta_2)} \quad (10)$$

where: L_b = Length between cross-frames (in)

h = Distance between flange centroids (in)

G = Shear modulus of elasticity = $E/[2 \times (1 + \nu)]$ (ksi)

E = Modulus of elasticity (ksi)

ν = Poisson's ratio

Δ_1, Δ_2 = Deflection of top and bottom flanges, respectively (in)

For an internal panel with equal size flanges, the equation will be:

$$J_{eq} = J + \frac{6EIh^2}{GL_b^2} \quad (11)$$

For an end panel and with equal flanges the equation would be:

$$J_{eq} = J + \frac{3EIh^2}{2GL_b^2} \quad (12)$$

where: I = Moment of inertia of a flange about a vertical axis (in^4)

For relatively large cross-frame spacing, the results of this approximate method can produce equivalent torsional stiffnesses on the order of about 10 percent smaller compared to the

equations in NCHRP Report 725. However, this method provides a much better feel to the engineer about how the structure is behaving.

3.5.4.2 Stocky Open Section and Closed Section Girder Grid Systems

For stocky open sections and closed section grid models, warping stiffness can generally be neglected, as Saint-Venant torsional stiffness dominates. In FEA grid models utilizing line elements, the torsional stiffness is explicitly defined, and simply requires the correct Saint-Venant torsional inertia, J , to be utilized. In lieu of a more precise analysis, Article C4.6.2.2.1 of AASHTO LRFD gives approximate formulae for calculating J for open stocky sections and closed thin-walled shapes:

Stocky open sections:

$$J = \frac{A^4}{40.0I_p} \quad (13)$$

Closed thin-walled shapes:

$$J = \frac{4A_o^2}{\sum \frac{s}{t}} \quad (14)$$

where: A = area of cross-section (in.²)
 I_p = polar moment of inertia (in.⁴)
 A_o = area enclosed by centerlines of elements (in.²)
 s = length of a side element (in.)
 t = thickness of plate elements (in.)

3.5.4.3 Quasi-Closed Sections

When designing steel tub girders, top flange lateral bracing is required to help provide lateral and torsional stability until the composite slab is in place. While not strictly a closed section, the torsional stiffness of tub girders with top lateral bracing can be thought of as effectively a closed section. Depending on bracing configuration, the following equations convert the truss bracing into an equivalent plate thickness, which can then be used to calculate the effective J using the closed thin-walled shape equation above (FHWA, 2012B):

Warren Type:

$$t_{eq} = \frac{2.60sw}{\left[\frac{L_d^3}{A_d} + \left(\frac{s^3}{3} \right) \left(\frac{2}{A_t} \right) \right]} \quad (15)$$

Pratt Type:

$$t_{eq} = \frac{2.60sw}{\left[\frac{L_d^3}{A_d} + \left(\frac{s^3}{3} \right) \left(\frac{2}{A_t} \right) \right]} \quad (16)$$

X- Type:

$$t_{eq} = \frac{2.60sw}{\left[\frac{L_d^3}{2A_d} + \left(\frac{s^3}{12} \right) \left(\frac{2}{A_t} \right) \right]} \quad (17)$$

where: t_{eq} = equivalent plate thickness

s = spacing between struts

w = width between flanges

L_d = diagonal length

A_d = area of diagonal

$A_t = A_f + A_w/4$

A_f = area of one top flange

A_w = area of one web

A_s = area of strut

3.5.5 Modeling Composite Construction

Composite construction can be modeled in different ways, depending on the behavior the designer wishes to capture. Up to three different models may be required in order to model the differing stiffnesses of the girder only, long term composite, and short term composite sections for AASHTO LRFD Strength load case design. For concrete construction, creep calculations depend on the time the deck becomes composite. Models can also differ depending on the direction of loading. As long as the stiffness is correct in the plane being loaded, for example the vertical stiffness is correct for a model subjected to gravity loads only, the model should give accurate results. Linear elastic models are typically used to determine design forces, even though nonlinear plastic capacities can be utilized in design.

With regard to the properties of concrete decks, per Articles 4.5.2.2 and C6.10.1.5 of AASHTO LRFD, generally the deck is assumed to be uncracked and active over the entire length of the bridge, including tensile portions, when modeling the distribution of loads in a bridge, but the tensile strength is ignored when designing the members for those loads. In some cases a cracked concrete or effective concrete stiffness in the model may be appropriate, such as in the case of an existing bridge analysis where inspection indicates extensive transverse cracking in the deck above interior supports.

Extracting the load effects required for design is also a consideration. Because AASHTO LRFD treats composite girders as a unit at the component level, forces on the composite section are required. The more discretely the elements are modeled, the more accurate the results, but the more difficult it can be to extract the cross-section design forces.

The simplest model is the beam element model with composite section properties included in the section properties, either a single beam in 1D or a grid in 2D. These are good choices for straight bridges with predominately gravity loading. It is the easiest for design because the differing stiffnesses of the various design models are simply reflected in the beam element section properties, and design moments and shears for the members can be directly obtained. In order to calculate the section properties an effective width of deck must be assumed, usually based on the design effective width. The concrete deck is usually transformed to the material of the girders using modular ratios. Note that stresses in a transformed section cannot be directly obtained from the transformed section itself; they must be calculated using the modular ratio.

The PEB model consists of beam elements for girder sections and shell elements for the deck slab. The slab and the beams are modeled in their geometrically correct positions, while still being compositely connected along their entire length. This model can provide more accurate

design forces as the effective width of concrete does not need to be assumed, since the stiffness of the deck slab determines the force carried by the concrete. *The stiffness of the deck for the various models can be adjusted using an effective thickness or an effective modulus of elasticity (recommended) for the concrete deck slab.* Obtaining the design forces can be more challenging, since the forces in the girder and the concrete deck slab must be combined to find the design moments and shears for the composite member. For more information on extracting force effects for a composite member see Section 8.2.

3.6 THREE-DIMENSIONAL ANALYSIS

3.6.1 Element Types and Usage

There are many types of elements that can be used in a 3D finite element model. The types of elements and where they may be used in the modeling of a slab-girder bridge are described in the following sections. Keep in mind that when mixing multiple element types, compatible element DOF need to be ensured at common nodes. For instance, connecting a beam element with rotational stiffness to a solid element with only translational stiffness will not result in moments being transferred across the joint.

3.6.1.1 Bar (Truss) Elements

Two force truss elements are the simplest members available. For a slab-girder bridge, this type of element is typically used for steel cross-frame diagonals.

3.6.1.2 Beam Elements

Beam elements are typically used for steel cross-frame top and bottom chords, girder flanges, diaphragm flanges, diaphragms (if the web is not modeled using shell elements), and when modeled, longitudinal and transverse stiffeners. Depending on how the concrete slab is modeled, beam elements may also be used as shear connectors.

3.6.1.3 Surface (Shell) Elements

Bridge components where surface elements are typically used include: concrete deck slabs, girder flanges and webs, especially for box members, and plate diaphragms. Surface elements may also be used for stiffeners and diaphragms. Note that generally bridge components carry membrane forces, so shell elements rather than plate elements are usually more appropriate. Also, note that other than cases where stress output is desired, I-section flanges, stiffeners, and cross-frames can typically be modeled sufficiently and more easily using beam elements.

3.6.1.4 Volume Elements

Volume, also known as brick or solid, elements have the advantage of being able to model explicitly three-dimensional geometry, and capture a full three-dimensional stress field. Volume elements are rarely used in routine bridge design, even in 3D analyses, due to the large number of DOF associated with modeling large flat relatively thin surfaces with volume elements and the resulting high computational effort, and the difficulty in extracting useful design forces.

3.6.1.5 Constraints and Rigid Links

Constraints such as rigid links can be used to rigidly connect elements whose nodes are not coincident. Some examples of uses for rigid links include modeling composite action between girders and deck slabs, modeling the offset between the centroid and the surface of an element where a second element connects, and modeling elements that are very rigid compared to surrounding elements, such as integral concrete bent caps.

3.6.1.6 Spring and Point Elements

Spring and point elements can be used at interfaces or boundary conditions, such as where bearings are present, or to model substructure/foundation stiffnesses.

3.6.2 Geometry

The advantage of a 3D finite element model over line girder, grid, and Plate and Eccentric Beam (PEB) analyses is that interaction between girders, cross-frame behavior, and distribution of live load can be explicitly modeled. This can be important as the degree of geometric complexity increases, for instance as with highly skewed or curved bridges. Increased accuracy is obtained by a combination of correct geometry and correct stiffnesses, including placing the deck slab at the correct elevation, modeling diaphragms and/or cross-frames at actual locations, distributing loads via element stiffness, and by modeling bearings i.e. boundary conditions correctly. The increase in modeling accuracy leads to an increase in accuracy for dead and live load force effects to be used in the design.

3.6.2.1 Girder Location

Girders should be spaced at their proposed center-to-center distance, often determined during a previous preliminary design phase, or in the case of an existing bridge, at the actual center-to-center distance measured in the field.

Girder flanges are typically modeled at the elevation associated with the centroid of each flange. The girder web is typically modeled at the girder centerline. The web depth used in the model can either be the actual web depth or the distance between flange centroids. *It is recommended to use the distance between flange centroids such that the flanges are at the correct location; if the flanges are not at the proper location, the underestimated stiffness can be important, especially for shallow girders, defined as less than 50" deep (Grubb et al., 2011).*

Figure 39 shows the top flange-web intersection of a steel girder to be constructed while Figure 40 shows how this intersection could be modeled in a 3D finite element model. The additional area due to extending the web to the flange centroid is typically not significant and can be

considered as representative of the flange-web weld in welded plate girders or the fillet of rolled shapes, which are not typically included in a 3D model.

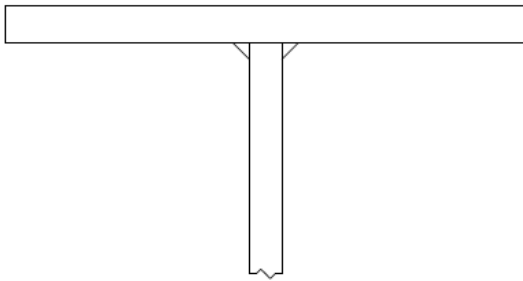


Figure 39. Illustration. Actual Flange-web intersection.

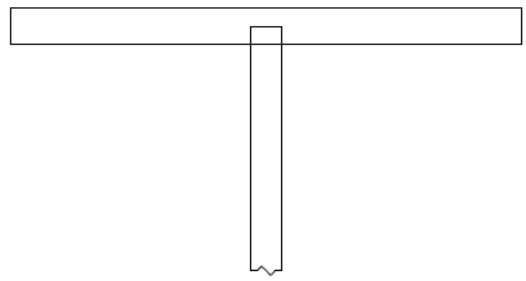


Figure 40. Illustration. Modeled flange-web intersection.

The approach described above works best when constant thickness flanges are used for the entire length of the girder. If the girder has a constant web depth but varying flange plate thicknesses, the distance between flange centroids will vary, requiring the model to have a step in the depth at the flange thickness transition (see Figure 41). This step, depending on how it is modeled, can result in a transition zone with poor aspect ratios and/or stress concentrations in the web shell elements (see Figure 42(a)). The simplest way to account for the transition is to keep the web depth a constant average and use an abrupt flange thickness transition as illustrated in Figure 42(b). This is typically sufficient and the generally recommended way to model a flange depth transition. Alternately, a constant average web depth can be used along with a transition section, tapering from the smaller flange depth at the transition, to the deeper flange depth a short distance away as illustrated in Figure 42(c). The distance should be chosen to be consistent with the web mesh. The most accurate solution is dependent upon the analysis software being used; some analysis software allows the element cross-section to be offset from its defined mesh axis line. This allows the flanges to be shifted to their correct locations while maintaining the correct web depth which is typically constant, as illustrated in Figure 42(d).

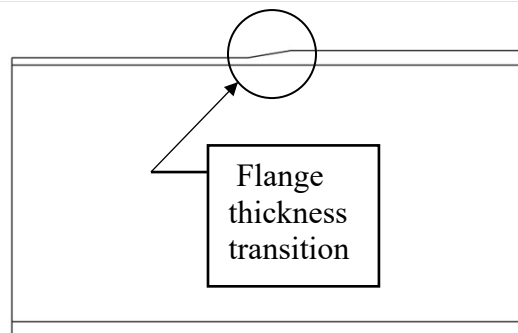
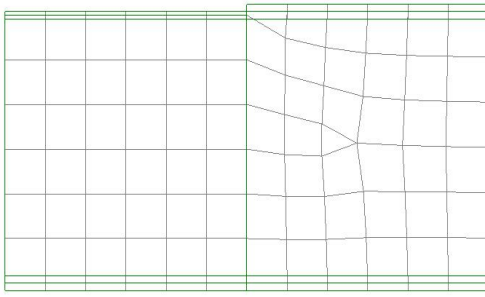
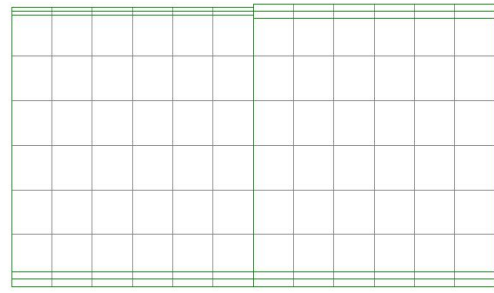


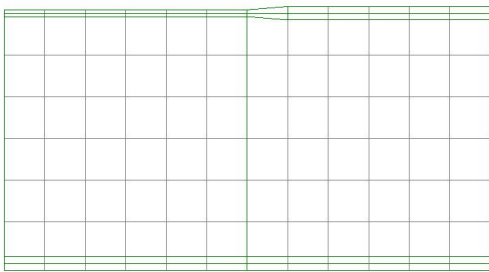
Figure 41. Illustration. Flange thickness transition.



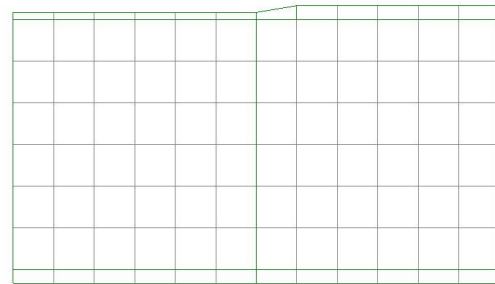
(a) Poor



(b) Good



(c) Better



(d) Best

Figure 42. Illustration. Flange thickness transition modeling.

In Figure 43 three different ways of modeling the web of a concrete I-section are shown. In Figure 43(a), the web is assumed to only be the rectangular portion of the girder. In Figure 43(b), the web is assumed to extend from the centroid of the top flange to the centroid of the bottom flange, with the fillets included in the flanges. Figure 43(c) assumes the web extends from the top of the top flange to the bottom of the bottom flange.

Modeling the web as illustrated in Figure 43(c) is recommended, with nodes placed at the locations of the centroids of the remaining area of the top and bottom flanges such that the flanges are at their correct positions. Modeling the full depth of the web also allows diaphragms to be modeled full depth and the support to be placed at the approximately correct elevation.

Modeling as in Figure 43(b) would be the second choice, but requires iteratively solving for the centroid of the remaining area of the flanges and the end of the web in order to be as accurate as possible. Modeling as in Figure 43(a) is not recommended as it has to account for a discontinuity between the top and bottom of the web and centroids of the flanges.

No matter which method is chosen, care should be taken to avoid “double counting” any portion of the cross-sectional area.

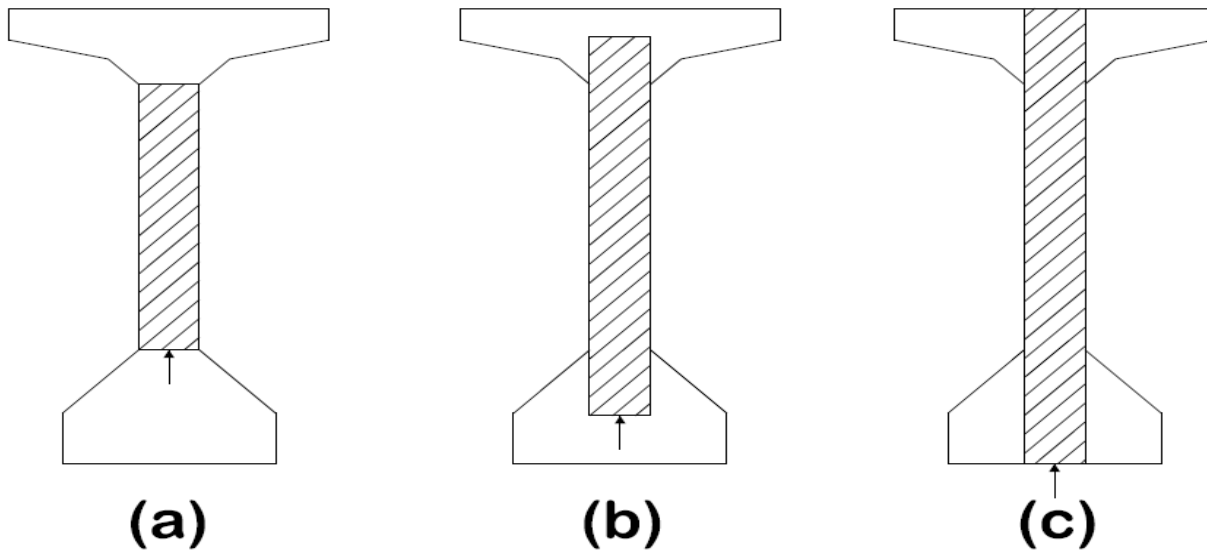


Figure 43. Illustration. Modeling web depth.

3.6.2.2 Concrete Slab Location

The concrete slab is modeled such that the centroidal elevation is at the correct location. This can be achieved by either: modeling the mid-thickness of the slab at the correct elevation and connecting the flange to the slab by various methods such as rigid links, or by modeling the slab at the same elevation as the girder top flange and using an offset to achieve the correct location, as some FEA programs allow.

3.6.2.3 Cross-Frame/Diaphragm Locations

Cross-frames and diaphragms are members that span between longitudinal girders. Cross-frames are open web truss configurations of steel members, often X or K configurations, while diaphragms are solid web members, either full or partial girder depth. In straight non-skewed bridges, cross-frames and diaphragms may only function as bracing prior to the composite deck being cast. In curved and skewed bridges, cross-frames and diaphragms also function as primary structural members, distributing loads transversely between girders. *It is recommended that cross-frames/diaphragms only be modeled when they are being counted on to redistribute load, otherwise it is recommended that they be conservatively omitted from the model.*

Since a 3D finite element model explicitly models the girder depth, the cross-frames/diaphragms can also be modeled explicitly. For simplicity, full depth steel cross-frame members can be connected at nodes along the top and bottom of the girder webs, which although not necessarily precisely correct, is acceptable for typical design of straight non-skewed bridges as long as the cross-frame stiffness is adjusted if necessary to account for the greater modeled depth. The designer may need to adjust any force results from the model to account for the changed geometry. When the connection plates/stiffeners are also explicitly modeled, it is possible to place the cross-frame/diaphragm members at their exact geometrical location. *It is recommended that connection plates/stiffeners be typically included in 3D models, and nodes located along the depth in order to place the cross-frames/diaphragms at the correct geometry, especially for*

partial depth cross-frame/diaphragms. If for whatever reason the cross-frames/diaphragms are not located at their correct geometry, it is up to the analyst to ensure that the member stiffnesses are such that results are acceptable.

If connection eccentricities, connection stiffness, and second-order amplification of the corresponding steel cross-frame member transverse deflections are not explicitly modeled, they can be taken into account using an effective area (Wang et al., 2012). In lieu of a more accurate analysis, the equivalent stiffness $(AE)_{eq}$ of equal leg single angles, unequal leg single angles connected to the long leg, and flange connected tee-section members may be taken as $0.65AE$.

3.6.2.4 Bearing/Support Location

Idealized supports in the 3D finite element model are typically located at a node at the web-flange intersection where the bearing stiffener (or diaphragm in the case of tub girders) is located. This point support is generally sufficient for typical designs. When local stresses are required, modeling a more accurate bearing area on the flange would be more appropriate.

3.6.3 Number of Elements

The number of elements required varies depending upon the type of analysis being performed, the elements being used, and the desired accuracy. Analysis of the gross structure to determine bending moments, shears, and displacements for routine design purposes requires fewer elements than when examining specific details such as localized stresses in coped webs of steel beams or dapped ends of concrete beams. The focus of this manual is on the gross structure; details regarding analysis of localized areas can be found elsewhere. The number of elements required also varies depending on the behavior of the member.

As discussed previously in Section 2.3.2, for a given element formulation, the number of elements required is a balance between accuracy and efficiency. Using many elements provides more accurate results but also requires more time to construct, analyze, and process the model. Using few elements results in a very quick analysis but the accuracy of the results may be compromised. Varying the mesh size over a given model can also achieve efficiency. A fine mesh can be used in an area of interest where more accurate results are required transitioning to a coarser mesh elsewhere in the model.

The guidelines provided below should aid in arriving at a reasonably accurate solution without being time and resource intensive. Running a few sensitivity analyses early in the design process can also help in developing an efficient model, and in general should always be performed when conducting a refined analysis. *As a rule of thumb, if increasing the number of elements results in a difference of less than five percent, the coarser mesh is sufficient.*

One thing to keep in mind is that elements must connect at nodes. This should be considered when defining the model geometry, to ensure that nodes are located where they are needed or may be needed in future analysis models. Examples are nodes located where concentrated loads are to be applied, or along line or shell element girders where shell deck elements connect in order to achieve acceptable aspect ratios, or along shell element girders where cross-frames or stiffeners may need to be explicitly modeled.

Another consideration to keep in mind is the compatibility of the mesh at the interface between different element types. Make sure the degrees of freedom of the elements being connected are compatible. *“Floating” nodes or nodes that are not connected to other elements should generally be avoided at interfaces as displacement incompatibilities such as gaps or elements occupying the same space can result.*

3.6.3.1 Element Aspect Ratio and Geometric Distortion

The aspect ratio of an element is the ratio of the longest side to the shortest side. Figures 44 and 45 show single surface elements with aspect ratios of 1:1 and 5:1 respectively. In an ideal situation, all elements would have an aspect ratio of 1:1, but for irregular shapes this is impossible to achieve, not to mention the aspect ratio also affects the number of elements and consequently degrees of freedom in a model. In addition to the aspect ratio, the angle between adjacent edges of an element should ideally be as close to uniform as possible. For instance a quadrilateral element would ideally have 90° angles in each corner.

It is generally believed that an aspect ratio of up to 5:1 will provide accurate results in most cases, and Article 4.6.3.3.1 of AASHTO LRFD sets 5:1 as the maximum limit. A recommended rule of thumb is that the interior angles of elements should be equal to the ideal angle plus or minus 60 percent. Depending on the element formulation, the application, and the solver being used, larger aspect ratios and geometric distortion may be acceptable, but as always, the results should be verified. Note that the aspect ratio/geometric distortion is more important for elements in a varying stress field, and for elements in close proximity to an area for which numerical results are desired. For more on mesh refinement see (Bathe, 2006)



Figure 44. Illustration.
Aspect ratio = 1:1.



Figure 45. Illustration. Aspect ratio = 5:1.

3.6.3.2 Girder Flanges

The number of elements along the girder length for the flange should be equal to the number of elements along the length of the web such that the nodes align and interconnect. *AASHTO Article C4.6.3.3.1 recommends a minimum of 5, and preferably at least nine nodes per beam span.* The locations of cross-frames or diaphragms also affect the spacing and placement of nodes.

Depending on the type of element used, the number of elements required for the flange width will vary. If the flanges are modeled using beam elements, the beam element will have the geometric properties of the entire flange area/plate. *Modeling the flanges using beam elements is recommended for I-shaped girders. If shell elements are used, at least two elements are needed to define the flange width for I-girders, one on each side of the web centerline. For box girders, at least two elements are needed and four are recommended to capture shear lag effects.*

Consideration of the element aspect ratios of both the flanges and the web should be included in determining the number of shell elements required.

3.6.3.3 Girder Webs

Available literature indicates that the number of shell elements required to model the girder web depth can be anywhere from one to twelve elements. The number of elements required depends on the behavior the designer wishes to capture. One element may not be able to accurately capture the desired behavior while twelve elements will result in a significant increase in the analysis time with limited increase in accuracy.

To capture the parabolic shear behavior in a typical bridge design, it is recommended to use at least four elements throughout the depth of the web, but this number can be reduced if capturing the parabolic shear behavior is unimportant. The number of web shell elements along the length of the girder often depends on the number of elements in the flanges. Locations of longitudinal and vertical stiffeners may be a consideration in the location and number of elements in the web.

The number of web elements can also be influenced by the element aspect ratio in both the web and the flanges. As mentioned previously, the ideal aspect ratio of 1:1 will often result in many elements. This ratio can typically be increased up to 5:1 with little loss of accuracy. Depending on the element formulation, the application, and the solver being used, differing aspect ratios and corresponding numbers of elements may be appropriate.

3.6.3.4 Cross-Frames and Diaphragms

3.6.3.4.1 Cross-Frames

Cross-frame diagonals are typically modeled using bar (truss) elements. *Only one element is necessary for each diagonal as only axial force is considered.*

Cross-frame top and bottom chords are typically modeled using beam elements but may also be modeled using shell elements when local stresses are being investigated. If shell elements are used, one element per angle leg or two elements for a WT-shape flange and one element for the WT-shape stem are reasonable. *For shell elements, the number of elements along the length of the chord member should provide a reasonable element aspect ratio. If beam elements are used, depending on element formulation, one element may be sufficient to capture the behavior of the chord member. If the top chord is composite with the deck, the number of elements should be consistent with the number of deck elements.*

3.6.3.4.2 Diaphragms

Diaphragms for 3D models, similarly to girders, can be defined using shell elements for the web and beam elements for the flanges for steel diaphragms. *Four elements are recommended for full depth of diaphragms, with a minimum of two elements in partial depth diaphragms, keeping in mind that the number of elements used in the web should provide a reasonable aspect ratio, and should be compatible with the girder webs. The number of elements for the flanges should be consistent with the number used along the length of the web and the concrete deck slab if composite.*

It is recommended that the shell elements of full depth rectangular section solid diaphragms in concrete bridges also be modeled with four elements. The number of elements should be compatible with the depth of the connected girders, and the number of elements along the length should be compatible with the number of deck elements. As always, the aspect ratio should be kept within reasonable limits.

3.6.3.5 Deck Slabs

The deck slab for a 3D model is modeled similarly to the deck slab in a PEB model, see Section 3.5.2.1. The main difference is that the centroid of the deck slab is attached to the girder flange elements in the 3D model rather than the respective centroids of the deck and the girder line elements being attached as in the PEB.

3.6.3.6 Stiffeners

Transverse stiffeners are rarely modeled in routine bridge design. If modeling stiffeners is required, transverse stiffeners can typically be modeled with beam elements extending from the top flange to the bottom flange. Longitudinal stiffeners can also be modeled using beam elements. The number of elements along the length of the stiffeners should match the number of elements along the web where the stiffener is located. If local stresses are required, or cross-frame/diaphragm connection locations need to be modeled explicitly, shell elements can be used to model stiffeners.

3.6.4 Interpreting Analysis Results

When using refined analysis techniques, especially as models become more complex, behavior is captured that historically has been ignored or overlooked. Forces and displacements arising from these behaviors are usually not significant to the design of the structure, but can cause confusion when the engineer's frame of reference is a line girder analysis.

It is important to note that these behaviors are typically not spurious, but represent actual conditions of the structure. And while sometimes these effects can be accounted for through conservative assumptions, they should not be disregarded just because they do not appear when using simplified analysis techniques. Recognizing the associated forces is essential in providing load paths and satisfying static equilibrium associated with the model behavior.

As an example, in three-dimensional analysis of a multi-girder bridge when truck loads are placed such that the rotations of the girders at a fixed pier vary significantly across the bridge width, longitudinal forces can develop at the bearings. This occurs due to the vertical distance

between the bearing and the neutral axis, such that rotations induce a longitudinal displacement at the bearings. If the rotations are different for different girders, there will be differences in the longitudinal displacements, which will induce varying longitudinal loads.

Similarly, when parapet weights are applied at their physical locations, diaphragms will tend to act as points of support along the fascia girders. The force effects generated in three-dimensional analysis will be quite different than if one were to assume equal load sharing and a uniform distribution along each girder. The loads generated are typically small, and the simplifying assumption will result in an adequate design, but the behavior from a three-dimensional model will be significantly different than expected if the engineer is unfamiliar with this behavior.

Another effect that often arises in shell element models is localized stress concentrations. These can be actual stress concentrations due to geometric discontinuities in the bridge, or they may be artifacts of the analysis model, for instance where a line element is assumed to be attached at a single node of a shell element rather than distributed over an area. Other conditions that may result in stress concentrations include but are not limited to:

- Re-entrant corners
- Steel connections/splices
- Bearings on concrete
- Applied concentrated loads
- Point interfaces

Dealing with these stress concentrations is up to the judgment of analyst, but in many cases they can be safely ignored, particularly when good detailing practices have been followed.

3.7 Boundary Conditions

As stated earlier in Section 2.3.5, boundary conditions are restraints usually applied at the bearings of bridge members, or the foundations of substructures, in global coordinates such that the model is only allowed to deform in the prescribed manner at the given restraints when load is applied. *The boundary conditions should replicate the behavior of the bearings, abutments, piers, or foundation as required.*

The boundary conditions can reflect, among other considerations:

- The amount of tolerance to movement in restrained directions in a typical bearing,
- Whether there is accommodation of transverse temperature expansion,
- The longitudinal displacement of bearings due to girder rotation,
- Potential support settlement,
- Substructure stiffness,
- Soil-structure interaction, if present.

When unable to approximate the behavior of the substructure or foundation with idealized boundary conditions, other techniques can be utilized, with appropriate restraints or interface elements to model the connectivity at the bearings or foundation.

3.7.1 Idealized Boundary Conditions

Modeling and analysis used in design generally assume idealized boundary conditions which are usually not possible to achieve in actual construction. These idealized boundary conditions usually consist of preventing some combination of translations and/or rotations along the three orthogonal axes. *In many cases, using idealized boundary conditions provides a sufficient approximation of actual boundary conditions.* The following is a list of idealized boundary conditions that typically also assume that the supports are rigid in the vertical direction:

- Pinned – A “pinned” boundary condition is used when the girder is allowed to rotate about an axis transverse to the support. Translation is not allowed in any of the orthogonal directions. Depending on the type of bearing used, rotation about the longitudinal axis and the vertical axis of the bridge may be permitted. Note that when a girder is described as having a “fixed” end with respect to expansion, a “pinned” support is usually intended.
- Fixed – A “fixed” boundary condition is applied when the girder is not allowed to translate or rotate about any axis.
- Unrestrained – An “unrestrained” boundary condition is applied when the girder end is allowed to translate and rotate in the longitudinal and transverse directions.
- Guided Expansion – A “guided expansion” boundary condition is used when the girder is allowed to rotate about an axis transverse to the guide, and translate along an axis longitudinal to the guide, but is fixed against transverse translation. Depending on the type of bearing used, rotation about the longitudinal and vertical axes may be permitted. Guided expansion is usually intended when an “expansion” bearing is specified.

It is critical to ensure that the movements permitted at the boundary conditions used in the analysis sufficiently match those in the actual bridge; discrepancies between the actual and modeled supports can significantly impact forces in girders or substructures. For instance, in curved structures, the direction of thermal movement is not necessarily parallel to the longitudinal axis of the bridge. If expansion bearings in a continuous segment are not oriented along rays from a single point, thermal forces will result, and should be designed for. Care should also be exercised when fully restraining bearings transversely, which in some cases can lead to overestimation of lateral forces.

3.7.2 Idealized Versus Actual Boundary Conditions

Because of real world considerations such as friction and limited stiffnesses of connected elements, actual boundary conditions usually lie somewhere between the fully pinned, fully fixed, or fully unrestrained idealized conditions described in Section 3.7.1. Geometrically, supports such as bearings are generally not located at the centroids of girders, although often they are modeled as such. For vertical bearing reactions of straight unskewed bridges, assuming substructures and foundations are unyielding is adequate for typical superstructure analyses.

Sometimes it may be necessary to model the boundary conditions more accurately. *For instance modeling supports with spring stiffnesses approximating the actual bearing stiffness rather than using unyielding supports can result in more realistic distribution of reaction forces, especially in significantly skewed or curved bridges.* In bridges with significant horizontal curvature and/or skew, it is generally a bad idea to model the horizontal bearing conditions as rigid. The resulting horizontal force effects can be unreasonably large. Even if the bearing stiffness is unknown,

modeling the stiffness as an extremely large finite value, instead of an infinite (unyielding) value can often result in much better force effect estimations.

When the effect of substructure stiffnesses on bearing reactions is significant, it is recommended that that piers and abutments be modeled explicitly. Beam elements are typically sufficient to model such elements with little additional computing effort.

Including foundation stiffnesses such as soil-structure interaction can range from simple to complicated. Foundation stiffnesses can be computed and input into the superstructure model as spring stiffnesses. Simple diagonal springs can be used when each degree of freedom is modeled as fully independent. More advanced analyses can utilize a fully coupled 6x6 spring stiffness matrix including off diagonal terms, obtained from an independent foundation analysis program (for more information see Section 5.2).

3.7.3 Bearings

When only the superstructure is being modeled, boundary conditions are usually modeled at the locations of bearings. In these cases, bearings are modeled as described in Sections 3.7.1 and 3.7.2. *When substructures are modeled along with superstructures, bearings should be modeled as interface elements between the superstructure and the substructure.*

There are multiple methods of modeling such interface elements, from simple truss elements to model transmission of vertical forces only, to advanced nonlinear elements that can model lift-off or stick-slip friction (see Section 5.3.1.3). *In most cases, a zero length six degree of freedom spring interface element is recommended.* Assignments of low or zero stiffness are made in directions of permitted movement. *Assignments of high stiffness, usually about three orders of magnitude larger than adjacent elements is appropriate, in directions where movement is restrained.*

As stated previously for boundary conditions, it is critical to ensure that the movements permitted by interface elements used in the analysis sufficiently match those in the actual bearings. Care should be taken especially when interfaces are modeled as fully rigid, particularly in the transverse direction.

3.8 Service Versus Strength Limit States Models

In AASHTO LRFD, a distinction is made between service limit states and strength limit states, with different load factors and different resistances employed. Exceeding a service limit state may result in maintenance issues, vibration, or some minor damage to the structure, while exceeding a strength limit state would result in failure of the structure or a component of the structure. From a probabilistic standpoint, a limited number of the former may be acceptable, while the latter should have a vanishingly small probability.

This distinction carries over into modeling. *In many cases, different models should be utilized for service and strength limit states.* For instance, there are elements on a bridge that are deemed non-structural, or non-load carrying, yet definitely add stiffness and carry loads in service. Examples would be concrete parapets and integral wearing surfaces. For strength limit state analyses, these typically would not be modeled, and their weight would be applied with line or

area loads. For service limit state analyses, such as deflection or fatigue, these elements would be modeled and their stiffnesses included in the analysis. Additionally, service limit state analyses almost always utilize linear elastic models. While linear elastic models are often sufficient for strength limit state analyses, sometimes more advanced models are required to investigate nonlinear/inelastic behavior such as concrete cracking, steel yielding, or stability at the strength limit state.

3.9 Construction Sequence / Staged Loading

Often in bridge design the entire structure is initially assumed to be constructed in a minimum of steps, with no regard to sequence. Girders are modeled complete end-to-end of the bridge. Wet deck concrete weight is applied abutment to abutment in a single step as well. Then superimposed loads are placed on the full composite structure. This is not how bridges are actually constructed.

There are many different ways that a bridge can be constructed, each with a unique loading sequence. It may be the case that the most critical load case occurs at some point during construction, for example stability of a composite girder bridge prior to the concrete deck hardening. For this reason, a construction sequence analysis should be performed to make sure the bridge will not exceed any limit state at any point during construction, as well as reaching the desired stress state in the final condition. The construction analysis required depends on the contract language and delivery type. Often only the proposed construction sequence on the contract plans needs be checked sufficiently to demonstrate that the bridge is constructible. Contractors wishing to deviate from the proposed sequence would provide their own analysis demonstrating adequacy.

Although permanent bridge dead loads are well defined for a constructability analysis, temporary construction loadings are not well defined by AASHTO LRFD, making constructability checks more difficult. One of the reasons is that construction loadings are so variable and bridge specific, depending not only on the type of bridge, but also the method of erection. The designer should make every effort to ensure that the loadings of the constructability analysis are consistent with the assumed method of construction.

Historically, in order to perform a constructability check of a relatively complex bridge, a “deconstruction” analysis was performed. The bridge was modeled in its final condition and then a series of analyses were run removing single or groups of elements. Temporary supports or bracing could also be added and/or removed in the models as necessary. This process not only permitted a check of the stresses at each step of construction, but also allowed for calculation of elevations and camber such that the bridge ended up in the correct final position, since that is where it “started.”

Another common series of analyses are the deck pour sequence. Typically, the deck is not poured all at once. Due to the large volume of concrete required, it is cast in stages. Therefore, the first pour is partially hardened and composite for loads from the second pour. The first and second pours are partially hardened and composite for loads from the third pour. And so on until the entire deck is cast. The modulus of the deck concrete can be adjusted for each pour in each analysis if desired to reflect the time of curing. Running multiple analyses with maximum and minimum properties, for instance regarding composite action, can also be useful in bounding the

response. Again, not only can stresses be checked at each stage, but by summing the deflections of the entire sequence, required camber due to the deck weight can be calculated.

A similar sequential redecking analysis may also be prudent during the initial design of a bridge. During a redecking, keeping a portion of the bridge open to traffic may be necessary/desireable. A sequence that permits a staged redecking of a bridge while maintaining a given level of both construction and traffic loading should be performed during design on bridges where redecking at some point is considered likely.

Cantilever construction also requires a series of analyses. Temporary fixity must be applied at the pier, and an analysis run for each segment of bridge added to the structure. The pier needs to be checked at each stage to ensure that the load does not become too unbalanced. Displacements determined at each analysis stage can be used to ensure that the final condition matches the desired profile grade.

Bridge girders are sometimes initially simply supported for dead loads, and then made continuous for live loads. Multiple models reflecting the correct connectivity for the loading would be required. Deflections from the simply supported models would be used for determining camber.

Many current software packages have simplified the construction sequence/staged loading process. No longer do separate models need to be analyzed and processed individually. Solving sequentially and “adding”/“subtracting” elements in various load steps, a single model can be utilized for the entire sequence.

For slab-on-girder bridges, the contract plans require camber diagrams or tables for each girder, so that the desired profile grade is achieved under dead loads. In order to calculate the camber, it is necessary to correctly model all sources of stiffness such that deflections are determined with sufficient accuracy. Note there is no such thing as a “conservative” calculation of displacements, since achieving the profile grade within tolerance is the goal. This is particularly important in curved or skewed bridges since transverse load distribution and torsional behavior are significant contributors. Such model(s) may or may not be the same model(s) used for performing strength design.

For steel girder erection, fit-up of the cross-frames can affect not only the final geometry of the bridge, but can contribute to locked-in stresses as well. There are three possible fit-up conditions: No load fit (NLF) where the girder webs are vertical and cross-frames are unstressed in the unloaded geometry, steel dead load fit (SDLF) where the girder webs are vertical and the cross-frames are unstressed under steel only load, or total dead load fit (TDLF), where the webs are vertical and the cross-frames unstressed under the full dead load of the bridge.

NLF is the easiest to design and often to construct, but can result in out-of-plumb girders and locked-in forces in curved and skewed bridges. SDLF and TDLF can diminish or eliminate the out-of-plumbness and locked-in forces, but may require the cross-frames to be force-fit initially, in order that they are unstressed at the appropriate displacement. Choosing the appropriate fit-up is important, as it be the difference between erection being simple and easy, and difficult or impossible for the contractor.

Per AASHTO, the designer is responsible for the fit-up method specified for construction. In some cases a more refined analysis may be warranted, especially for curved or highly skewed bridges. If a refined analysis of the bridge has been done, modeling the installation of the cross-frames for the desired fit condition is often the simplest and most accurate method of obtaining cross-frame forces. For more information on cross-frame fit-up see G 13.1 Guidelines for Steel Girder Bridge Analysis (AASHTO/NSBA, 2011), NCHRP Report 725 (White et al., 2012), NCHRP 20-07/Task 355 (White et al., 2015), and Skewed and Curved Steel I-Girder Bridge Fit (Beckman et al., 2016, Chavel et al., 2016).

CHAPTER 4. CONCRETE/STEEL GIRDER BRIDGE MODELING

4.1 Concrete Bridges

The following sections provide material specific guidelines to use when modeling concrete girder bridges. Some guidance is also given on using the results to design in accordance with AASHTO LRFD.

4.1.1 Modeling Guidelines

4.1.1.1 Concrete Material Models

For most routine concrete bridge design, linear elastic concrete material properties should be utilized. Typically, the minimum properties that need to be assigned to a linear elastic material model are modulus of elasticity and Poisson's ratio. AASHTO LRFD Article 5.4.2.4 provides a formula for the modulus of elasticity based on unit weight and f'_c . AASHTO LRFD Article 5.4.2.5 assigns a value of 0.2 for Poisson's ratio unless determined by physical testing. Computer programs will often have a material library and simply choosing the concrete material corresponding to the design f'_c is all that is necessary for AASHTO properties.

For more advanced analyses, more sophisticated material models may be required with additional concrete material characteristics. Material characteristics related to creep and shrinkage or concrete cracking are examples of more sophisticated material models. AASHTO LRFD Article 5.4 should serve as a starting point in defining some of these material properties but program documentation and research literature can also be helpful in choosing appropriate values for the material variables. For more guidance on advanced material models, see Section 5.1.2.1.

4.1.1.2 Concrete Beam Element Moment of Inertia

The flexural stiffness of a concrete member can vary with the applied load. When modeling concrete members with beam elements, the various stiffness options are best handled by using a constant modulus of elasticity and adjusting the beam element moment of inertia. Up until the cracking moment is reached, the flexural stiffness is best modeled by the use of the gross moment of inertia based on the full concrete cross-section.

At the point where the reinforcement has reached first yield, the stiffness is best modeled by the cracked moment of inertia, which is calculated by ignoring all concrete on the tension side of the neutral axis and transforming the area of steel on the tension side, all determined at the ultimate moment state.

For analyses where the cracking moment is exceeded, but the steel has not yielded, such as determining live load deflections, an effective moment of inertia is appropriate. This is because cracks occur at discrete locations, and the stiffness is greater than the cracked stiffness in between the cracks. AASHTO LRFD Article 5.7.3.6.2 provides a method for calculating an effective moment of inertia for determining deflections and camber of flexural members. AASHTO LRFD Article 5.7.4.3 provides a method for calculating an effective stiffness for evaluating slenderness effects in compression members with certain slenderness ratios. ACI 318

provides a more accurate method for calculating the effective stiffness for evaluating slenderness effects.

The gross and the ultimate cracked moments of inertia are two bounds to the stiffness of a concrete element that are dependent on the force effects, which are initially unknown. It should be noted that axial force effects will also affect the values for the cracking and yield moment, and hence the stiffness of the element, adding additional complications.

Figure 46 shows the moment-curvature relationship for a circular reinforced concrete column. The moment-curvature relationship is developed in Example 5 using Mander's model for confined and unconfined concrete (Mander, 1988), and the steel model developed by Raynor et al. (Raynor, 2002). The unconfined and confined concrete models and steel models are discussed further in Section 5.3.2.1. The moment-curvature relationship shown below is used to define the plastic hinge behavior of one of the columns in Example 5; behavior of plastic hinges is also discussed further in Section 5.3.2.1.

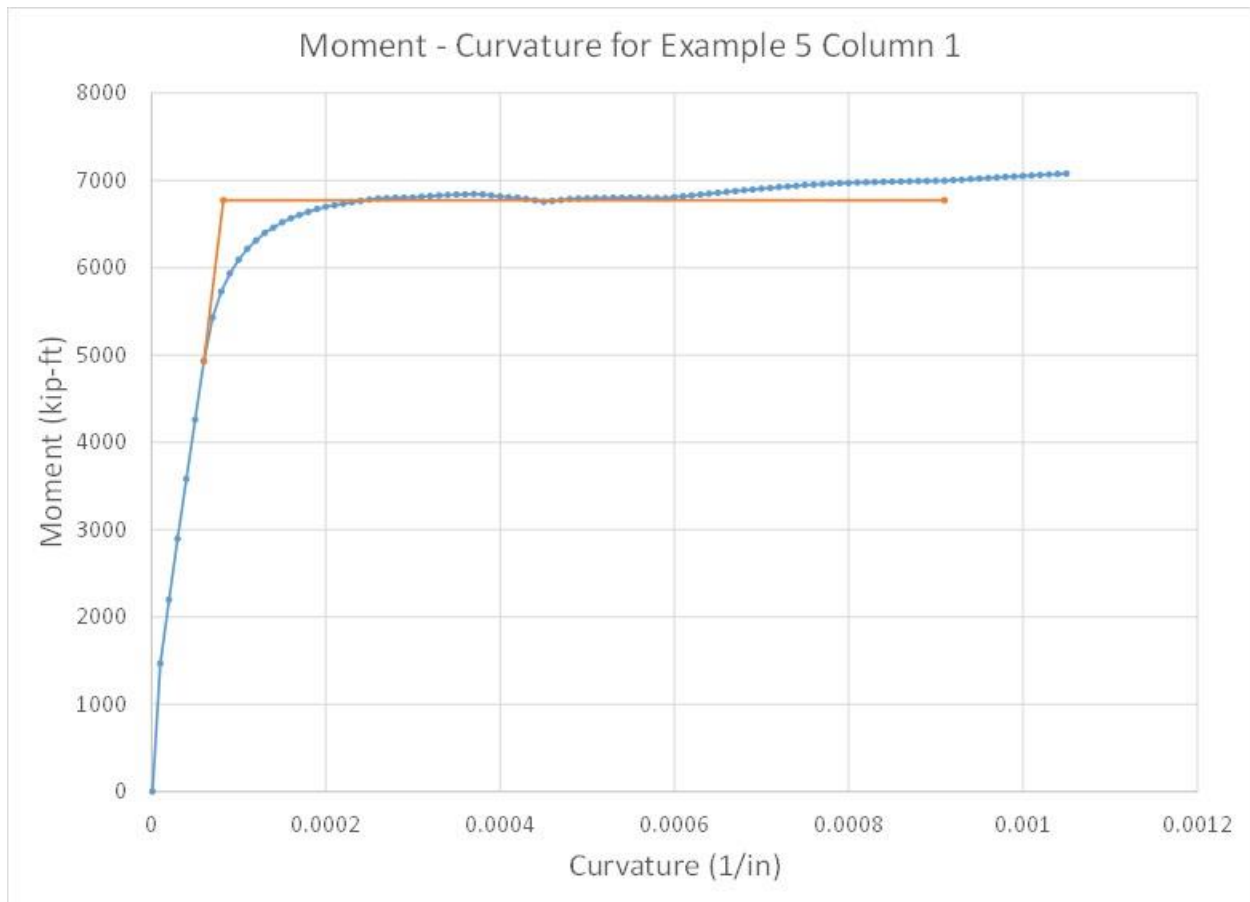


Figure 46. Graph. Example of the moment-curvature relationship for a given axial force.

Determining which stiffness to use will depend on the type of analysis being performed. The additional accuracy of the resulting force effects, gained through use of an iterative adjustment of the stiffness along the length of the concrete members based on those same force effects, is usually not worth the additional effort. As such, a constant value of the moment of inertia is

typically appropriate. *For strength limit state dead and live load analyses of bridge structures, it is recommended that the gross concrete stiffness be used throughout the model.*

For seismic analyses, where plastic hinging and significant nonlinear material behavior is expected, additional consideration is required. If a displacement based design method is being utilized, a lower stiffness is typically conservative. In these cases, effective or even cracked stiffness values should be used. For force based methods, it may be more conservative to use gross section properties.

Several publications provide charts relating effective stiffness to gross stiffness as a function of reinforcement ratio and axial load. Two common sources for these are the AASHTO Guide Specifications for LRFD Seismic Bridge Design, and the FHWA Seismic Retrofitting Manual for Highway Structures. These provide reasonable estimates of the reduced stiffness of concrete members and are very easy to implement.

If stresses are being determined directly from the refined analysis, using the appropriate stiffness is even more important. A further variation in flexural stiffness that can be used is to account for creep behavior with a reduced effective modulus of concrete. An example of this approach is the use of the effective $2n$ modular ratio for permanent loads and prestress at the service limit state in concrete girders, and the effective $3n$ modular ratio for permanent loads at all limit states on composite concrete-steel girders. If the model is being used only to determine load effects (moments and shears), the effective section properties can be used to calculate stresses during design.

4.1.1.3 Modeling Non-Prismatic Cross-Sections

For girders with variable cross-sections, it is necessary to accommodate the variation in girder centroid. For models using beam elements, the location of the line(s) used to define the beam element should be located at the centroid of the typical section. At locations where the cross-section varies from the typical section, eccentricities will need to be applied such that the geometry aligns (see Figure 345 in Section 9.6.2.3 for an example). When shell elements are used, the cross-section should be divided into regions of constant thickness and regions of varying thickness as shown in Figure 398 of Section 9.7.2.1.1. Where the thickness varies, an average thickness should be determined; eccentricities may be needed to align the surfaces appropriately.

4.1.1.4 Shear Lag Effects

Shear lag refers to the effect of in-plane shear stiffness and how it alters the normal stress distribution from that predicted by simple beam theory. For example, in a box girder, the axial stresses due to bending will tend to be larger in the flange at the connection to the web. The stresses will tend to decrease toward the middle of the flange between the webs and toward the flange tips of overhangs due to in-plane shear deformations. Thus, these areas “lag” behind in stresses due to shear. Figure 48 shows the axial stress distribution in the top flange of the concrete box girder (shown in Figure 47) both with and without accounting for shear lag. The effect is largest when the moment is changing rapidly along the length of a member, which is another way of saying when the shear forces are large. The more points of connection among the elements of a cross-section, the smaller the shear lag effect.

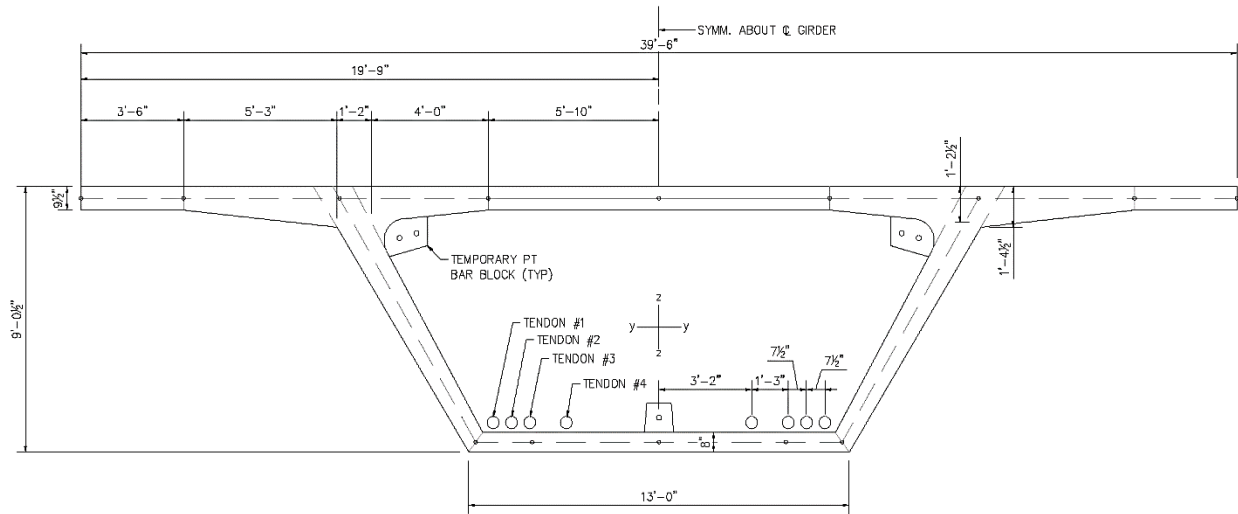


Figure 47. Illustration. Box girder cross-section (Corven Engineering, 2016).

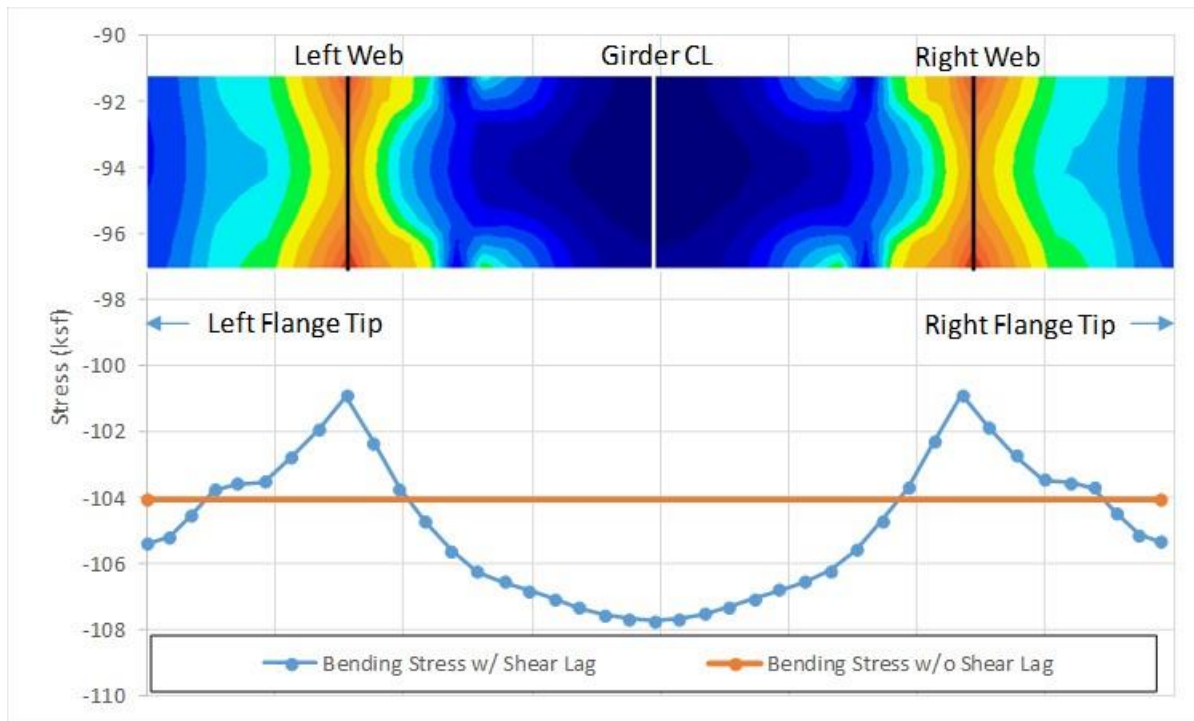


Figure 48. Graph. Axial stresses on top face of box girder top flange.

To accurately capture shear lag effects, shell or solid elements are required to model the cross-section. There are ways of modifying a grillage model to capture shear lag, but it is rarely worth the effort when higher order elements are available.

4.1.1.5 Modeling Diaphragms in Concrete Box Girders

The internal diaphragms are present over a small percentage of the overall member length; therefore, it is not necessary to account for the stiffness of the internal diaphragms in a beam element model. The weight of the internal diaphragms can be accounted for using applied loads.

When a shell element model is used, including the diaphragms in the model avoids fictitious large stresses at the supports if a single point (or a pair of points) is used to model the bearings. Explicitly modeling the support diaphragm also provides a location for the tendons to be anchored for explicitly modeled prestressing tendons. Modeling the diaphragms in the shell element model can be done using either shell elements or solid elements. The advantage of shell elements is that the analysis remains less complex but the disadvantage is that shell elements are typically used where the thickness of the component is significantly less than the other dimensions which is not always the case with the internal concrete diaphragms. Using solid elements allows for the actual diaphragm geometry to be modeled but the analysis becomes increasingly complex.

In Example 7 of Chapter 9, the continuity tendons cross over the interior supports and are anchored in the adjacent span. In this example, a diaphragm was placed at each tendon anchorage location and inflection point resulting in a series of diaphragms. Figure 49 shows an elevation view of the tendons crossing over an interior pier used in Example 7. The dashed lines in Figure 49 represent the diaphragms that were included in the shell element model to anchor the different tendons. The shell elements used to model the pier diaphragm are given a thickness equal to the diaphragm thickness shown on the plans. Anchorage diaphragms are defined at the points where the tendon changes direction and points where the tendons are anchored; these diaphragms are used to connect the tendons to the box girder. The anchorage diaphragm thickness is sufficient to minimize the deflection under the tendon loads; elastic material properties with no self-weight are used as the pier diaphragm accounts for the weight.

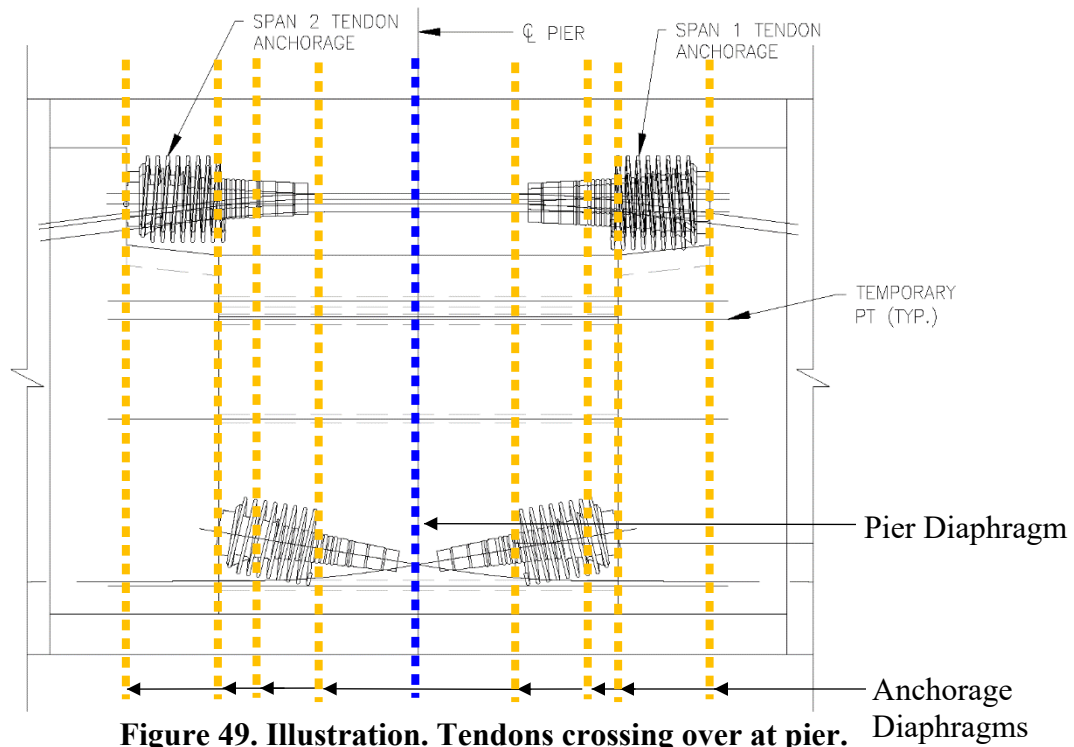


Figure 49. Illustration. Tendons crossing over at pier.

4.1.1.6 Boundary Condition Considerations

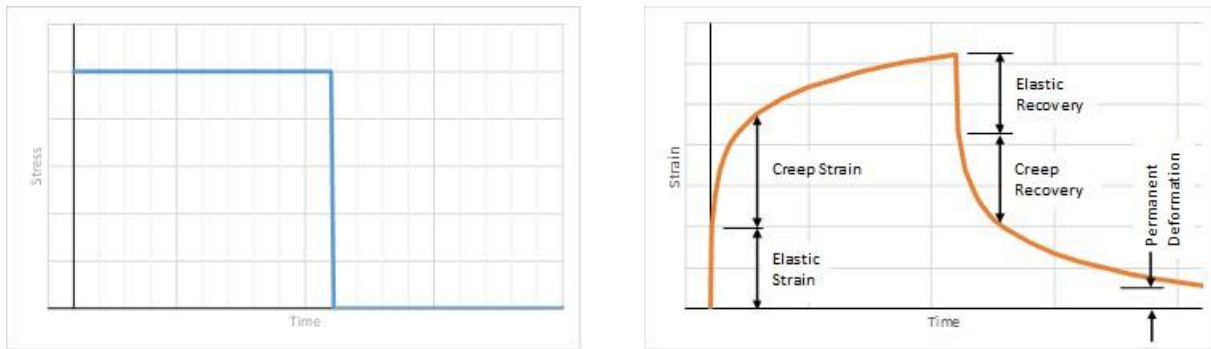
The boundary conditions for concrete bridges may vary depending on the type of construction. For concrete girders set on bearings, the superstructure and substructure can be designed separately. For concrete girders that are integral with the substructure, typical of cast-in-place concrete construction, appropriate modeling of the substructure and foundation stiffness is necessary to accurately predict the superstructure force effects. See Section 4.3 for more information about modeling substructure and foundation components.

4.1.2 Time-Dependent Non-Linear Effects

Concrete undergoes changes in strain with time due to two processes: shrinkage and creep. Creep and shrinkage result in volumetric changes to concrete elements and both are very hard to predict accurately. Of particular note is a sentence in the commentary of the AASHTO LRFD, Article C5.4.2.3.1: “Without specific physical tests or prior experience with the materials, the use of the empirical methods referenced in these Specifications cannot be expected to yield results with errors less than ± 50 percent.”

Shrinkage is a volumetric change caused for the most part by loss of adsorbed water during the curing process and is independent of applied load. It is affected by the ratio of the surface area to the volume of the concrete element, the relative humidity of the air around the element, stiffness of the aggregate, and the water-to-cement ratio, among other factors. Several equations have been developed to model the development of shrinkage with time. AASHTO LRFD Article 5.4.2.3.3 provides one example of the equations used to calculate the volumetric change due to shrinkage; the equations from the CEB-FIP model code and ACI 209 may also be used.

Similar to shrinkage, creep is a volumetric change in a concrete element over time but is dependent on the applied stress. Load applied to a concrete element will result in an initial elastic deformation plus an additional creep deformation that increases with time. The creep deformation is a function of the total duration of the applied load as well as the age of the concrete at the time of loading. If the load is then removed, the structure will experience creep recovery, i.e. it will creep back towards its initial undeformed condition. If the load was applied for a significant time duration and then removed, there will be a permanent deformation to the structure that will never fully be recovered. Figure 50 (a) and (b) show the time history for a member under a compression load, illustrating both creep and creep recovery. The same factors that influence the amount of shrinkage also influence creep deformations. AASHTO LRFD Article 5.4.2.3.2 presents equations to estimate the amount of creep, but also allows the use of CEB-FIP and ACI 209 formulations.



(a) Subfigure showing the applied stress vs. time. (b) Subfigure showing the strain due to applied stress vs. time. (based on MacGregor & Wight 6th Edition Figure 3-22b)

Figure 50. Graphs. Compound figure showing subfigures showing stress vs. time and strain vs. time for the effect of creep.

Figure 51(a) shows the amount of creep deformation for four identical columns loaded at four different ages: 1 day, 7 days, 28 days, and 120 days. Both columns are four-foot in diameter, 4 ksi concrete compressive strength is used, and the bases are assumed to be fixed (see Figure 51(b)). A load of 500 kips is applied at the top of the column. Figure 51(a) shows that the age at time of loading has a significant effect on the amount of creep deformation and the rate at which the creep deformation plateaus. The creep deformation for the column loaded at 7 days is approximately 75 percent of that for the column loaded at one day. Loading applied at 28 days results in approximately 60 percent of the creep deformation while loading at 120 days results in about 50 percent of the creep deformation.

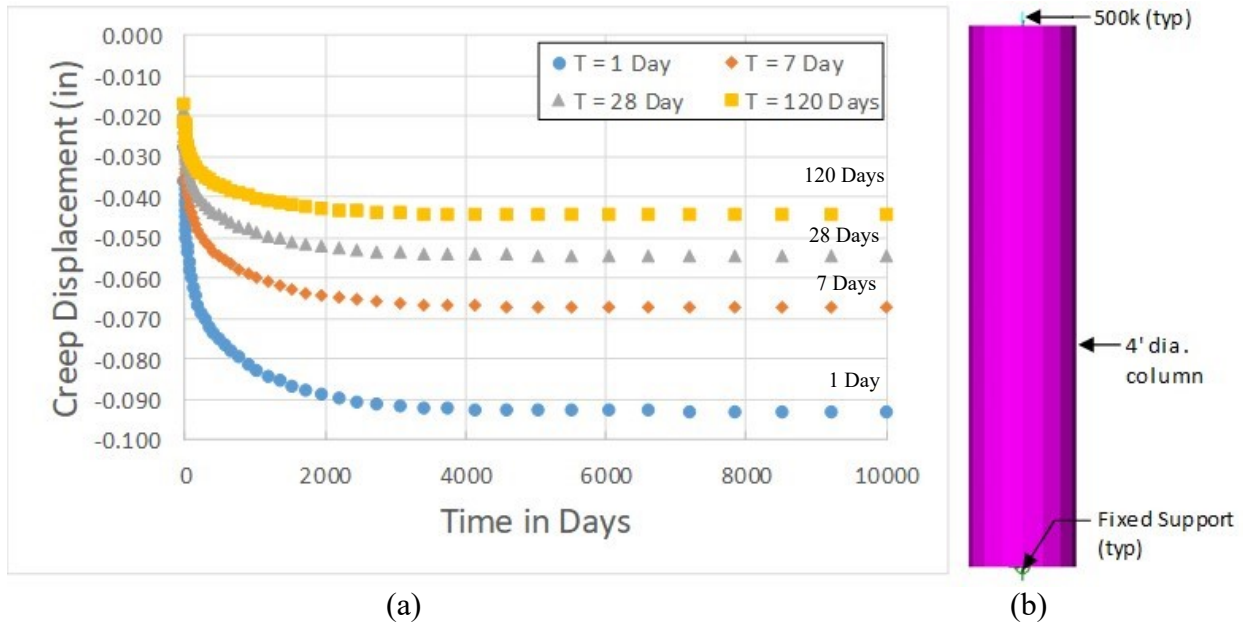


Figure 51. Graph. Creep deformation vs. age at loading.

An additional effect of creep is the reduction of loads induced by other deformations of the structure. For example, in a bridge with integral piers, the shortening of the superstructure due to shrinkage will induce moments in the piers, but these will be relieved by the creep of the pier concrete such that the final forces that must be considered in the design will be significantly reduced.

Several analysis programs of varying complexity include the ability to model shrinkage and creep of concrete structures using nonlinear material properties. Care should be taken when taking advantage of program features to understand what the program is doing, whether it is modeling creep behavior, or performing a calculation of post-tensioning losses due to creep. For the analyst, the key points to consider when deciding whether to include these effects in an analysis are:

- Concrete structures that experience a change in the statical system after loads are applied will generally be more susceptible to the effects of creep in that the load effects will vary over time due to creep. The statical system refers to how the bridge is supported at various construction stages. For example, a bridge constructed by the balanced cantilever method is transformed into a continuous girder when the midspan closure pour is made, and hence is susceptible to creep effects.
- The actual creep experienced by a structure may be significantly different from that calculated during the design phase. The effects of variation in creep on the structure should be investigated by bounding the creep calculations and ensuring the structure can accommodate a range of creep magnitudes.
- Usually the designer is concerned with two stages in a structure's life: during/just after construction and after all long term effects have occurred. A typical value of 10,000 days (30 years) is used as a 'reasonable' end time when no further additional effects from creep are expected. For the four-foot diameter column described above, loaded at 120

days, the effect of applied load on creep deformation is shown in Figure 52 below. As the applied load increases, the creep deformation also increases.

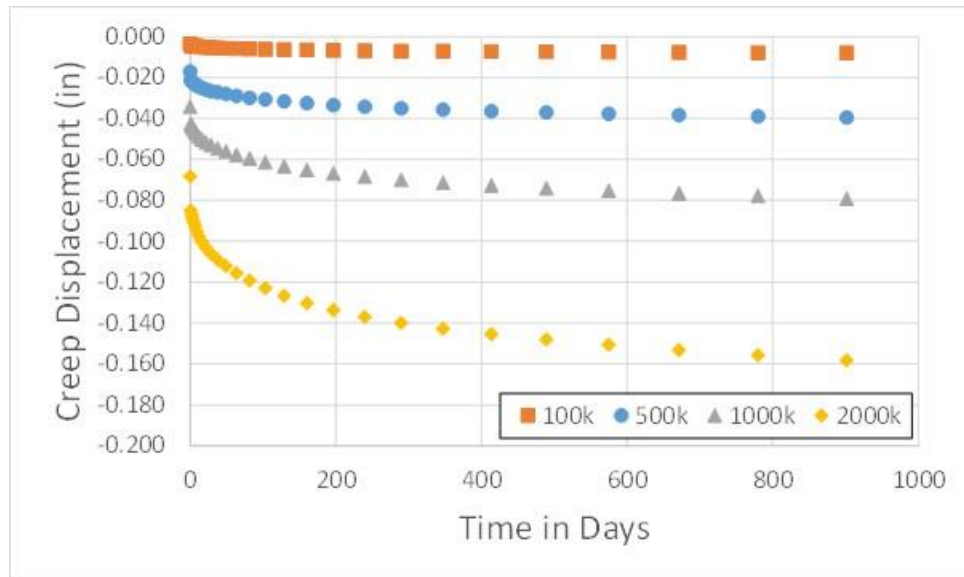


Figure 52. Graph. Creep deformation vs. time for different applied loadings.

- A very useful simple check on the results of a creep analysis is to calculate the effective creep coefficient. This is the ratio of the creep deformations to the initial elastic deformation, and is generally between 0.5 and 4.0, with a value of 2.0 being common. If a refined analysis including creep effects results in ratios beyond this range, or even at the outer limits of the range, a careful review of the inputs and results is in order. See Section 9.7 for an example of creep modeling and Section 6.3.2 for an example of verification of creep.
- The default creep model in a specific analysis program may work better for some types of elements than others; i.e. beam elements rather than shell elements. Depending on the program, the input for the nonlinear material property may automatically be calculated for certain types of elements while the designer must calculate the values for other types of elements.

The compressive strength, and hence the modulus of elasticity, of concrete also varies with time. However, the increase of strength is relatively rapid, and unless the analysis includes construction staging where load is applied to very recently cast concrete, the variations in compressive strength and modulus of elasticity are typically ignored and constant values are assumed.

4.1.3 Prestressing and Post-Tensioning

Including the effects of prestressing and post-tensioning in an analysis model is not necessarily straight forward especially when the tendon layout is complex. It is important to note that unlike typical hand analysis for prestressing, primary and secondary prestressing forces are not calculated separately; rather the prestressing is applied to the model, and the software solves for the total effect. Primary moments are due to tendon eccentricity, i.e. $P \times e$. Secondary moments

develop due to supports of indeterminate structures constraining free movement under prestressing. If desired, the primary prestressing effects can be solved for separately (perhaps by hand), and subtracted out to determine secondary effects. However, with refined analyses there is usually little reason to do this, especially if creep is included in the model behavior. Several methods for incorporating prestressing into an analysis model are presented in the following sections.

4.1.3.1 Equivalent Load Method

The equivalent load method is an approach in which the prestressing/post-tensioning force is represented by external loads that produce load effects equivalent to the prestressing. In this method, since the strand layout and *jacking* force is already known, this information is used to determine equivalent loads that can be applied to the structure in the analysis model, and will have the same effect as the tendons without having to model the individual tendons. A key point to remember is that the loads used to model the prestressing force must be self-equilibrating, meaning that there should be no net reactions when looking at the whole structure.

The following notation applies to all figures in Section 4.1.3.1:

- c.g.c = center of gravity of concrete (ft)
- c.g.s = center of gravity of strands (ft)
- P = effective prestressing force (kips)
- e = eccentricity between c.g.c and c.g.s (ft)
- L = distance between bearing centerlines (ft)

The equivalent load method can be used for analysis of beam lines (1D analysis) as shown in the following sections. Additionally, the equivalent load method can be used in grid/PEB (2D) analyses as well as 3D analysis. In certain cases where the designer is looking at localized effects, such as bursting stresses in anchorage zones, the equivalent load method should not be used.

The advantages of this method include its theoretical simplicity and relative ease of verifying the correct prestressing is applied. Drawbacks include the inability to determine changes in prestress force due to applied loads, and the need to account for prestress losses independently.

4.1.3.1.1 Straight Strands

The simplest strand layout is one where the strands are placed parallel to the center of gravity of concrete. The strands are often placed eccentrically in order to efficiently utilize the compressive strength of the concrete and the tensile strength of the strands, to counteract the applied loading.

Figure 53 shows a beam with straight strands placed eccentrically. To analyze this beam using the equivalent load method, the effect of the prestressing is incorporated by applying an axial load, equal to P, at the centroid of the beam section and end moments, $M = P \times e$, at the beam ends as shown in Figure 54. Note that the moments due to eccentricity are only applied at the ends.

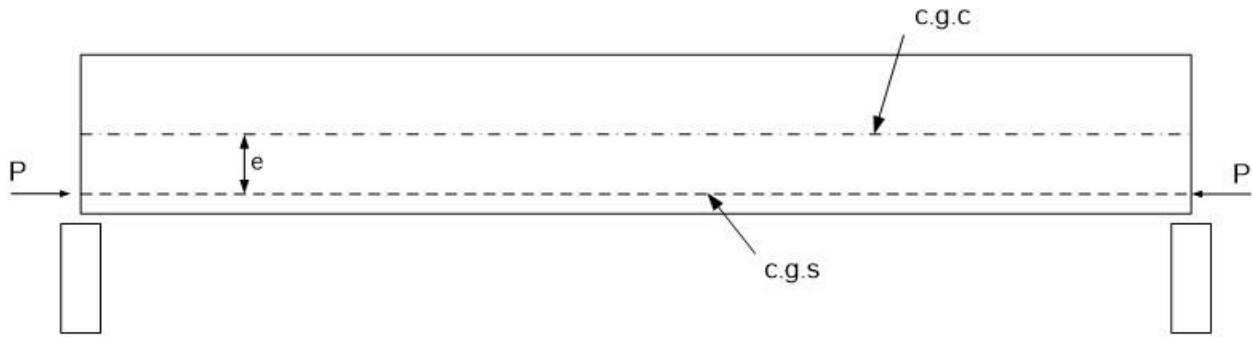


Figure 53. Illustration. Straight strands.

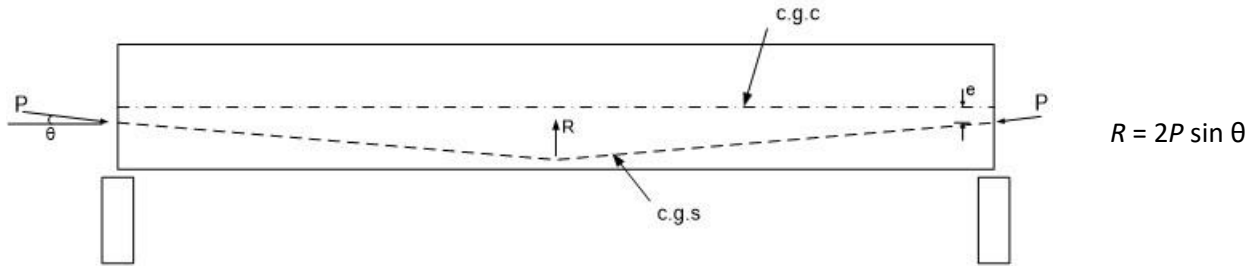


Figure 54. Illustration. Simplified model for straight strands.

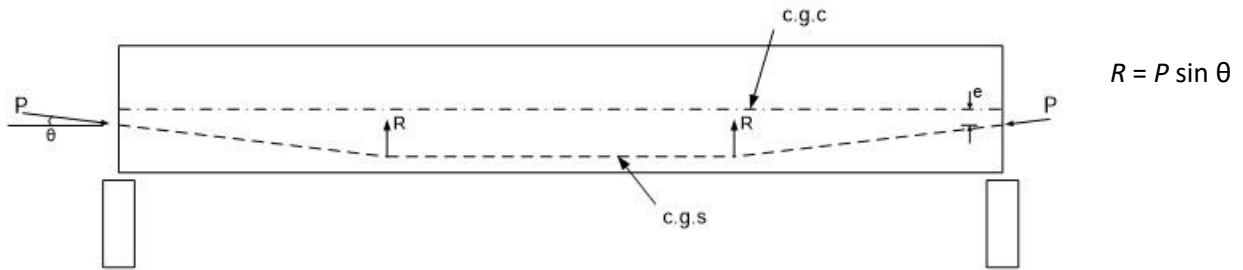
4.1.3.1.2 Harped Strands

Harped strands are those that are kinked, typically at one or two hold down points, along the beam as shown in Figure 55. At each hold down point, there is an upward force due to the angle of the strand changing. In Figure 55, the hold down point at midspan must resist the total vertical component of the prestressing force, P . In Figure 55(b), each hold down point resists one-half of the total vertical component of the prestressing force, P , since the hold down points are symmetric.

Figure 56 shows how the effects of the prestressing force are applied using the equivalent load method; the axial load is applied concentrically to the beam element and a point load is applied at each hold down point in an upward direction. Figures 55 and 56 show the general case in which the center of gravity of strands does not coincide with the center of gravity of concrete; therefore, an end moment, $M = P \times e$, is also applied.

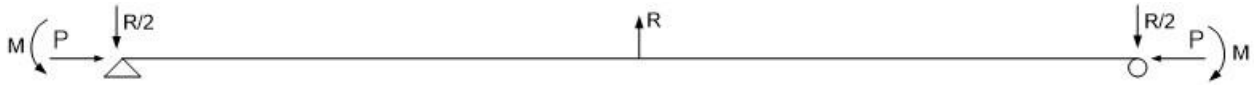


(a) Subfigure showing one harp point.



(b) Subfigure showing two harp points.

Figure 55. Illustrations. Compound illustration showing beams with harped strands and varying number of harp points.



(a) Subfigure showing one harp point.



(b) Subfigure showing two harp points.

Figure 56. Illustrations. Compound illustration showing simplified beam models for beams with harped strands and varying number of harp points.

4.1.3.1.3 Draped Strands

Draped strands are similar to harped strands except they form a continuous arc as shown in Figure 57. The vertical effect of the prestressing force from draped strands is a uniformly distributed load equal to w_b , which is approximated by Equation (20) (Lin and Burns, 1981). Figure 58 shows how the effects of the prestressing force are applied using the equivalent load method; the axial force is applied concentrically to the beam and the prestressing force is calculated using Equation (20) and applied to the beam as a uniformly distributed load. Figures 57 and 58 show the general case where the center of gravity of strand and center of gravity of concrete are not aligned; as shown in Figure 58, an end moment, $M = P \times e_1$, is applied at the beam ends.

$$w_b = \frac{8P(e - e_1)}{L^2} \quad (20)$$

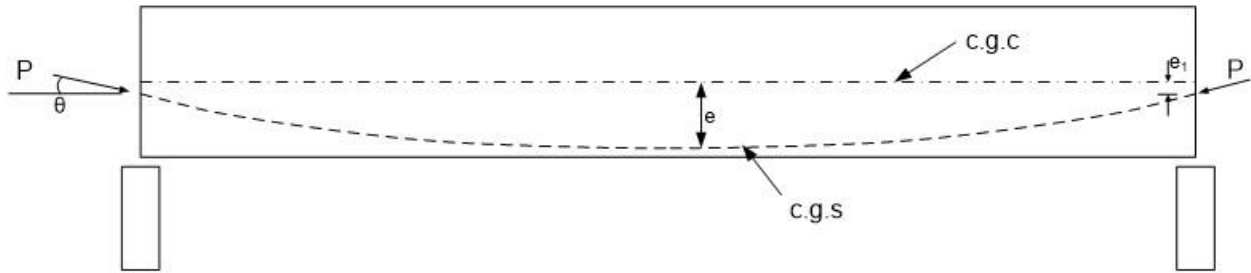


Figure 57. Illustration. Beam with draped strands.

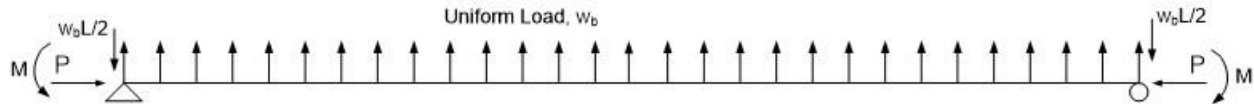


Figure 58. Illustration. Simplified model for beam with draped strands.

4.1.3.1.4 General Strand Configurations

The cases described above are shown for simple spans but the equivalent load method can also be used for other span configurations. The concept can be extended for beams with multiple spans, varying span lengths, and with varying strand profiles. The equivalent loads are calculated for each parabolic segment using Equations (21) and (22) for each harp point and applied to the analysis model. Figure 59 illustrates a general scenario with the equivalent loads.

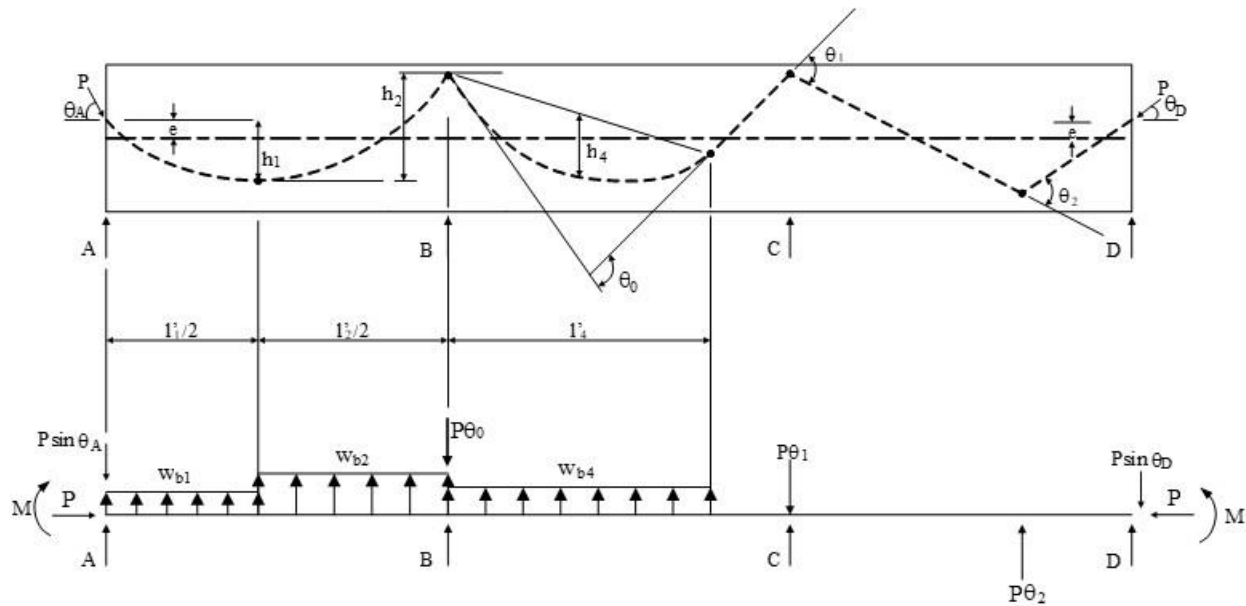


Figure 59. Illustration. General beam scenario.

$$w_{bi} = \frac{8Ph_i}{L_i^2} \quad (21)$$

$$R = P\theta_i \quad (22)$$

4.1.3.1.5 Non-Prismatic Cross-Sections

The previous sections assumed that the beam cross-section is constant along the length of the beam. This is often the case for simple span beams but may not be the case for continuous spans where it may be necessary to increase the section depth to carry the negative moment near the interior support(s). The determination of the equivalent loads for a non-prismatic cross-section is similar to the method for prismatic cross-sections. Equivalent loads are dependent on the tendon profile not the cross-section properties of the concrete member.

4.1.3.1.6 Prestress Losses

When determining the correct prestressing forces to be used in the equivalent load method, losses need to be accounted for. Creep, shrinkage, elastic shortening, strand relaxation, anchorage set, and (curvature) friction and wobble (additional friction due to deviation of ducts from specified profile) reduce the force in the strands. The losses due to creep, shrinkage, elastic shortening, and strand relaxation, are typically assumed to be constant over the girder length and their effects are incorporated by reducing the equivalent loads by the ratio of the final force to the initial force. If the concrete material property considers losses due to creep and shrinkage, these do not need to be calculated and included in the equivalent loads.

For post-tensioned construction, the losses that vary along the length of a member such as friction and wobble need to be addressed. The number of locations along the beam where these losses need to be determined depends upon the tendon profile. For a parabolic profile, Aalami (2001) recommends that the tendon be divided into 20 segments per span. For a harped profile, the number of locations is reduced as the tendon is not constantly changing direction. For an example of prestress loss calculations, see Example 7 in Chapter 9.

Many software packages include utilities that are capable of calculating the prestress loss for a given tendon layout and material or allow the user to input losses calculated separately. The equivalent loads may include the effect of creep, shrinkage, elastic shortening, strand relaxation and anchorage set in addition to the effect of friction and wobble. These software packages are also typically capable of performing time-step analyses to account for loading in different stages. It is important to note that if an analysis includes deformations due to creep behavior and the equivalent load method of modeling prestressing is being used, prestress losses due to creep and shrinkage must be calculated separately in order to reduce the equivalent loads accordingly.

4.1.3.1.7 Actual Tendon Layout vs. Idealized Tendon Layout

As shown in the previous sections, the ideal strand layout for continuous spans is typically two parabolas intersecting. While ideal, this layout is very difficult to physically create and the strands would have to be bent sharply at the intersection. Instead of a sharp intersection (see Figure 60), the strand layout is typically a series of parabolic segments that form a smooth curve as shown in Figure 61. The intersection point (P.I.) should be near an inflection point and lie on a line, as shown by the dash-double dot line in Figure 61, connecting two known points along the strand layout.

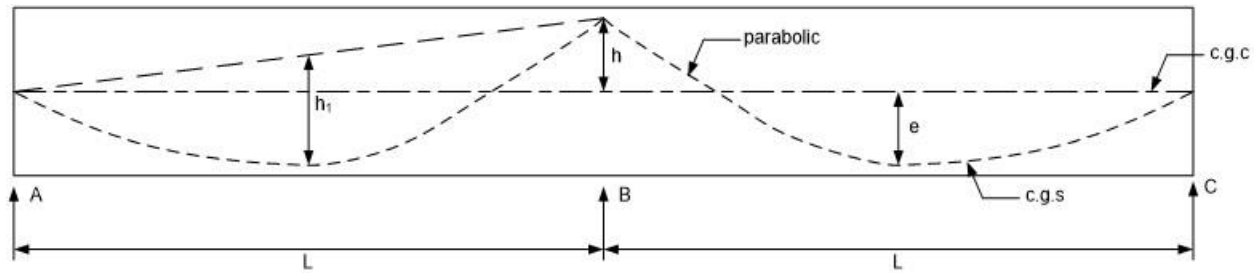


Figure 60. Illustration. Idealized strand layout in continuous beam.

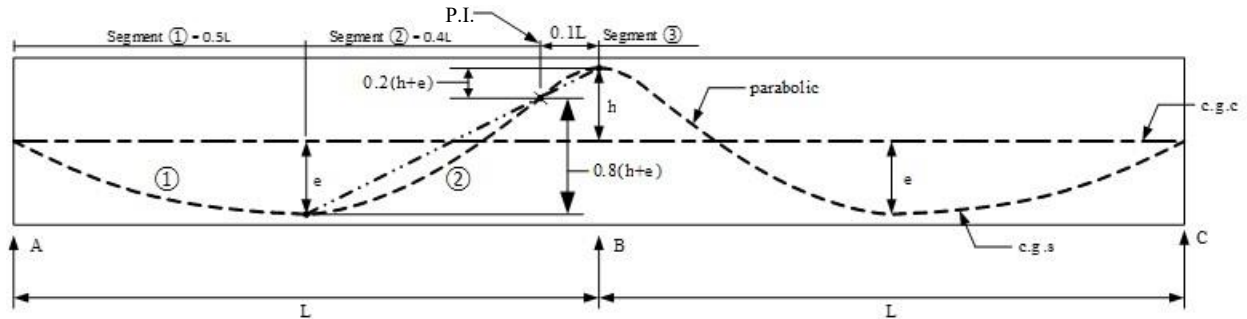


Figure 61. Illustration. Actual strand layout in continuous beam.

The equivalent loads for the actual strand layout are calculated using Equation (23) for each segment ①, ②, and ③ where e is the vertical variation in the strand location for each parabolic segment and ℓ is the length of each parabolic segment, not the length of the span. For segment ①, ℓ is the distance from A to the low point or $L/2$. For segment ②, ℓ is the distance from the low point to the point of intersection, or $0.4L$ for the case shown. For segment ③, ℓ is the distance from the point of intersection to the high point over the support, or $0.1L$ for the case shown. The equivalent loads are given in Table 3 and shown on a simple 1D beam model as Figure 62.

$$w_b = \frac{8Pe}{(2\ell)^2} \quad (23)$$

Table 3. Equivalent loads for actual tendon layout.

Segment	Uniform Load
①	$w_{b①} = \frac{2eP}{(2(0.5L))^2}$
②	$w_{b②} = \frac{8(0.8(h+e))P}{(2(0.4L))^2}$
③	$w_{b③} = \frac{8(0.2(h+e))P}{(2(0.1L))^2}$

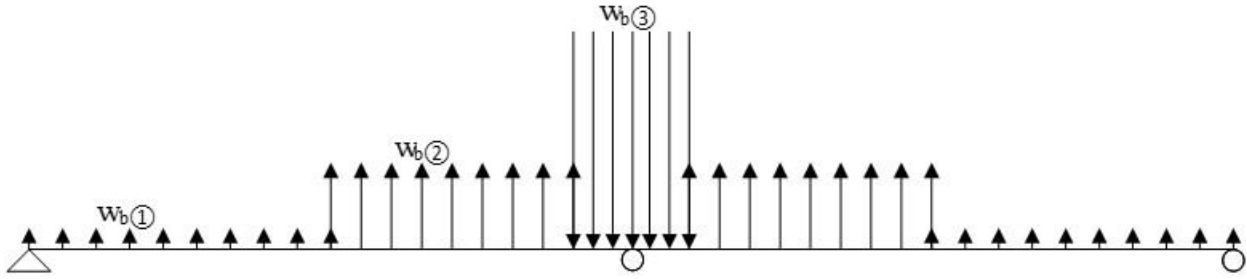


Figure 62. Illustration. Simplified beam model for actual strand layout.

4.1.3.1.8 External/Unbonded Tendons

External tendons are placed outside of the concrete member cross-section. External tendons tend to be run in the voids of concrete box girders. In general, all external tendons are unbonded. Unbonded tendons are tendons running through ducts within the concrete but the ducts are not filled with grout. External/unbonded tendons are connected to the concrete member at discrete points along the tendons. The physical ramification of being unbonded is that strain compatibility is no longer valid. The strain in the tendons tends to be uniform between connection points.

Modeling of girders with external/unbonded tendons using the equivalent load method is similar to that of bonded straight or harped tendons, with equivalent loads applied at anchorage and deviator locations as well as inflection points. The equivalent load method, because it does not account for changes in prestress force due to deformations of the section, does not distinguish between bonded and unbonded tendons.

4.1.3.2 Including Tendons in Analysis Model

Another method for including the effects of prestressing and post-tensioning is to explicitly include the tendon in the analysis model. In this method, bar or beam elements are defined along the path of the tendon, and the chosen element is assigned the material and geometric properties of the tendon. Important factors to consider include:

- Curved tendon layouts may have to be approximated with straight segments depending on software. If straight segments are necessary, the curve must be divided up into small enough segments to accurately represent the tendon. Specific guidance on the number of segments is not available but a central angle of 3.5° , similar to that used for the element length in modeling curved spine beam models, may be considered appropriate;
- The location of the tendons may control the mesh of the concrete girder; if the tendon layout changes, the entire model may need to be remeshed;
- The bond between the concrete and steel will be considered a perfect bond unless bond behavior is considered in the model; and
- Possibly having to account for the variation in load in the tendon due to losses along the tendon length.

The force in the strands can be applied using several different approaches. These approaches include the use of equivalent (fictitious) temperature changes or initial strains which correspond to the tendon tensile force. To induce compression in the concrete adjacent to the tendon, a negative temperature change can be applied to the element(s) representing the tendon. The decrease in temperature causes the tendon to contract but since the tendon is restrained, the temperature change causes stresses to be applied to the cross-section. The temperature change necessary to reach a given force in the tendon can be calculated using Equation (24).

$$\Delta T = -\frac{P}{\alpha EA_{ps}} \quad (24)$$

where: P = required force in tendons (kips)
 α = coefficient of thermal expansion (in/°F)
 E = modulus of elasticity of prestressing steel (ksi)
 A_{ps} = area of tendon (in²)

The effect of elastic shortening of the concrete is not included in Equation (24), therefore an iterative approach may be required to achieve the desired prestress with elastic shortening. This can be done using a spreadsheet to calculate the required temperature change based on the desired force, initial estimate of the temperature change, and the tendon force from the model as shown by Equation (25). Alternatively, since the tendon force is linearly related to the temperature change, a load factor equal to the ratio of the required tendon force divided by the tendon force from the model can be calculated and then applied to the temperature change. The load factor will likely vary for each segment of the tendon.

$$\Delta T_N = \Delta T_O \frac{P_{Req}}{P_{Model}} \quad (25)$$

where: ΔT_N = new value for ΔT
 ΔT_O = old value for ΔT
 P_{Req} = desired force in tendons
 P_{Model} = force in tendons due to ΔT_O

The prestress losses described in Section 4.1.3.1.6 must still be considered when the tendon is explicitly included in the analysis model. If the concrete material model used has the capability of considering creep and shrinkage effects, and the model built can capture the interaction between the tendon element and the surrounding concrete element, then creep and shrinkage losses could be automatically calculated. If the concrete model does not account for creep and shrinkage, these losses must be accounted for separately. Additionally, strand relaxation must be considered in the analysis either automatically by the program or calculated according to AASHTO LRFD and incorporated into the analysis. These losses are typically uniform along the length of the beam; therefore, an effective value of P, that accounts for these losses, can be used in Equation (24) or to calculate an initial strain value. The friction and wobble losses as well as anchorage seating losses can be included in a similar manner except that the value of P will vary along the length of the beam. Since the value of P varies along the length, the temperature change or initial strain will also vary along the length.

In a typical pre-tensioned analysis, or after grouting in a post-tensioned analysis, it is acceptable to assume that the concrete and steel tendons are perfectly bonded together. If the bond behavior is to be considered, one of several different methods, as described below, may be used. One method is to use springs to represent the bond between materials. Another method is to use a bond-link element where the element has six (three displacement and three rotational) degrees of freedom at each node to connect the concrete and steel elements; slip is assumed to act only along the longitudinal axis of the reinforcement. Bond-link elements can model full, partial, or no bond between the concrete and the reinforcement. Interface or contact elements may also be used to prevent one component from penetrating another component. They can also capture slip when the stress between the two components becomes greater than the limit strength. In situations where the line defining the tendon is the same line as the edge of the concrete elements, a perfect bond would be assumed if one of the other methods isn't used.

For a post-tensioned girder, the behavior of the tendons relative to the girders/ducts varies depending on the stage of construction. Prior to stressing, the tendons are independent of the girder and it is not necessary to include them in the model. During stressing, the tendons may be assumed to be frictionless allowing the tendon to slip freely or the tendons may be assumed to experience friction due to the curvature of the ducts. Once the tendons have been grouted, the bond between the tendon and the duct can be assumed to be perfect and no slip will occur. The behavior of the tendon during these different stages can be modeled using the bond-link or interface/contact elements described above. The bond between steel and concrete can be defined using the Coulomb friction law. Modeling the changing conditions of the tendons and the bond between steel and concrete is typically beyond that required for determining force effects used to design a bridge.

Accounting for the variation in the tendon force due to losses is dependent on how the software accommodates the losses. If the losses are calculated by the software along the length of the tendon, then this would not be an issue. However, if the software does not calculate losses, and they need to be calculated by hand and applied along the length, it could become complicated. The tendon forces would have to be calculated for each stage of construction and applied to the appropriate model.

In the case where explicitly modeled tendons are used to represent both the temporary and permanent post-tensioning, the designer must investigate whether the elements representing the temporary PT carry compression forces when the permanent post-tensioning is stressed. The temporary PT is typically not able to carry any compression force and once the tension force was removed would become loose. If this is the case, those particular elements would need to either be removed at the stage where the permanent PT is applied or set such that they don't contribute to the stiffness. One alternative may be to use an element that is capable of carrying tension only.

When explicitly modeling tendons, ideally bar (axial load only) elements would be used to represent the tendons. If it is desired to utilize available slicing functions within an analysis package to determine shears and moments from a shell element, it may be necessary to use beam elements with moment releases at each end instead of bar elements. Additionally, when using the slicing functions, it may be necessary to have the elements representing the tendons turned off or become invisible such that they don't counteract the force in the concrete member.

4.1.3.3 Other Approaches

A third method to include the effects of prestressing and/or post-tensioning is to use a smeared or embedment approach where the steel is distributed throughout the concrete and is not defined using the edge of a concrete element but goes through the element. The reinforcement contribution is determined numerically. The prestressing force is applied to the concrete beam either uniformly along the length or variably along the length if the tendon stress varies. The embedment approach typically considers that there is perfect bond between the steel and concrete. There are methods to incorporate bond-slip behavior between materials while using the embedment approach; these methods typically involve adding extra nodes along the length of the reinforcement and the nodes are used to define the bond behavior. In the smeared approach, the reinforcement is typically considered to be uniformly distributed while in the embedment approach this is not the case. In this approach, the tendon relaxation is accounted for in the prestressing loads when they are calculated by hand. If the analysis program calculates the prestressing loads, the tendon relaxation may already be included. Use of the smeared or embedment approaches are program dependent. Consult program user literature for more guidance.

4.1.4 Analysis Issues vs. Design Issues

4.1.4.1 Vertical Component of Prestressing

In harped or draped prestressing strand profiles, a vertical prestressing force, V_p , develops due to the vertical location in the tendon changing and typically opposes the shear forces due to gravity loads. V_p will appear in the analysis results but is also present in the AASHTO LRFD shear capacity equations. Therefore, the designer must decide whether they are going to use V_p on the capacity side of the equation or if V_p will be included on the load side of the equation. It should not be included on both sides of the equation, but should be included on the side which results in a more conservative design. It is noted the load factor and resistance factor are not equal.

4.1.4.2 Strategies for Thermal Force Effects

Thermal force effects are typically determined using either uniform temperature changes or temperature gradients; methods for determining thermal loads are described in Section 7.3.8 of this manual. Thermal force effects may be large and control the design of certain bridge components. The difficulty in designing for thermal force effects is that the design changes necessary to reduce these loads are not straightforward and are counterintuitive; when demands are high, increasing the section dimensions is the typical solution but for thermal loads doing so may result in even larger demands.

4.1.4.3 Web Shear Distribution

Classical analytical techniques are available that can be used to determine shear flow in multi-cell boxes. These techniques utilize shear and torsion results from a spine beam model. Using the shear and torsion results, the shear stresses in each web can be calculated and integrated over the web to determine the shear force in each web. Alternatively, a simple shell element model can be created and the shear and torsion forces from a spine beam model applied. The shear stresses in the shell elements can be summed to determine the shear force in each web.

Depending on the analysis package, modelling the entire structure using shell elements may be the most straightforward way to determine the shear in each web.

4.2 Steel Bridges

The following sections provide material specific guidelines to use when modeling slab on steel girder bridges. Guidance is also given on using the results to design in accordance with AASHTO LRFD.

4.2.1 Proper Modeling of Geometry and Stiffness

As steel girder bridge models become more complex, modeling the geometry correctly becomes more critical. Although getting the geometry 100 percent “exactly” correct is more trouble than it is worth, efforts should be made to include all forces due to eccentricities that are present, while minimizing spurious forces due to eccentricities introduced by modeling approximations. Running parametric analyses with simplified models can be helpful in determining if contemplated approximations significantly affect results. Experience and judgment are also invaluable in determining which modeling approximations result in negligible differences.

Depending on the design objective, correctly modeling the stiffnesses of both the main and secondary elements can be extremely important, such as when deflected geometry is required. Steel girders tend to be relatively flexible, especially open section steel girders, prior to cross-frames being installed and/or the deck hardening. *Modeling the initial geometry and the construction sequence correctly can be critical, particularly with curved and skewed girders.*

Modeling cross-frame geometry and stiffness correctly can be a challenge, due to the inherent eccentricities associated with typical single angle cross-frame connections. In straight non-skewed bridges, where cross-frames and diaphragms only function as bracing prior to the composite deck being cast, the modeled stiffness should be less than or equal to the actual stiffness to avoid overestimating the load distribution among girders. In many cases omitting the cross-frame/diaphragms from the analysis is conservative. In a 3D analysis when the cross-frames/diaphragms are being counted on to distribute loads to adjacent girders, such as when maximizing a rating, they always should be included.

In curved and skewed bridges, cross-frames and diaphragms also function as primary structural members, distributing loads transversely between girders. *When analyzing cross-frames and diaphragms for curved and/or skewed bridges, the modeled stiffness should be less than or equal to the actual stiffness when calculating girder load effects, and greater than or equal to the actual stiffness when calculating cross-frame/diaphragm load effects.* For guidance on modeling cross-frame geometry and stiffness see Sections 3.5.3, 3.6.2.3, and 3.6.3.4.

When modeling open section curved steel girders with line elements, accounting for the warping torsional stiffness is important. This can be accomplished using an effective Saint-Venant torsional stiffness constant. See Section 3.5.4 for guidance.

For highly skewed and curved bridges, design of initial fit-up of the structural steel can be crucial. Differential cambering such that the girders are at the correct final elevation can lead to force fitting of cross-frames during construction and/or locked-in forces in the final condition in cross-frames. See Section 3.9 for guidance on the construction fit-up of steel girders.

For most routine designs of typical steel girder bridges, second-order effects are negligible and are ignored. In rare cases, such as bridges with tall slender piers, second-order effects can be significant. When the design parameters fall outside the second-order approximations of the AASHTO Specification, a nonlinear analysis may be appropriate. See Section 5.3.1.2 for guidance on performing geometric nonlinear analyses.

4.2.2 Fatigue

Refined analysis has long been used for fatigue evaluations in order to provide better insight into structure behavior and to validate approaches used to address fatigue issues either during initial design, or more commonly during development of a fatigue retrofit. It is arguably the best method to evaluate one class of fatigue behavior, distortion induced fatigue.

Fatigue is defined in AASHTO LRFD as the initiation and/or propagation of cracks due to a repeated variation of normal stress with a tensile component, typically referred to as the live load stress range. Designing for fatigue is analogous to a Service Limit State since fatigue fractures occur due to repeated applications of stress that are lower than the nominal capacity of a section, and are commonly insensitive to permanent (dead load) stress magnitude.

An important aspect of fatigue with regard to finite element modeling is that it usually is only an issue at a location of stress concentration, rarely in base metal in the middle of flanges or webs. In steel bridges stress concentrations typically are located at regions of geometric discontinuity which occur mostly at welded attachments, but base metal is also susceptible, for instance at copes or cutouts.

The AASHTO LRFD distinguishes between two types of fatigue:

- Load induced fatigue defined as fatigue effects due to in-plane stresses for which components and details are explicitly designed.
- Distortion induced fatigue defined as fatigue effects due to secondary stresses not normally quantified in the typical analysis and design of a bridge.

The distinction between these two types of fatigue is arbitrary, and only a convention for design purposes. At the material level the mechanism for forming and growing cracks is the same. In general fatigue evaluations consist of comparing a measured or calculated stress range against an allowable stress range. There are various approaches to this task, ranging from very simple to extremely complex.

4.2.2.1 Load Induced Fatigue

Designing for AASHTO load induced fatigue requires calculation of the nominal stress range due to fatigue loading, choice of the appropriate detail category, and check of the corresponding allowable stress range. Categories for various details can be found in Table 6.6.1.2.3-1 of AASHTO LRFD. The “detail category” is based on full scale laboratory testing and accounts for several parameters that are highly variable and difficult to quantify in practice (for example, local stress concentrations and initial discontinuity size). The AASHTO fatigue resistance can be determined according to Article 6.6.1.2.5 of AASHTO LRFD and the curves are illustrated in Figure 63.

The nominal stress range is determined in the same manner as that used in strength design and is readily calculated using member properties and simple mechanics principles for most common bridge components. Force effects for calculating the nominal stress range need not be determined by a finite element analysis, but a 1D, 2D or 3D analysis would all suffice to determine the axial and bending forces needed to calculate the nominal stress, if not the nominal stress directly, for any given member detail.

A common application for refined analysis in relation to fatigue evaluations is to provide a less conservative estimate of the applied live load stress range at a given detail. When compared to field measured data, stress ranges calculated using approximate methods such as distribution factors often have been found to be significantly conservative. This should come as no surprise, as distribution factors were developed to be conservative for strength design. Refined analyses can provide a better estimate of live load distribution and resulting nominal stress ranges, particularly when non-structural sources of stiffness such as barriers and wearing course are included. The use of refined analysis to develop more accurate stress ranges when evaluating fatigue details can provide substantial benefits to the designer and owner, especially when correlated to field measurements.

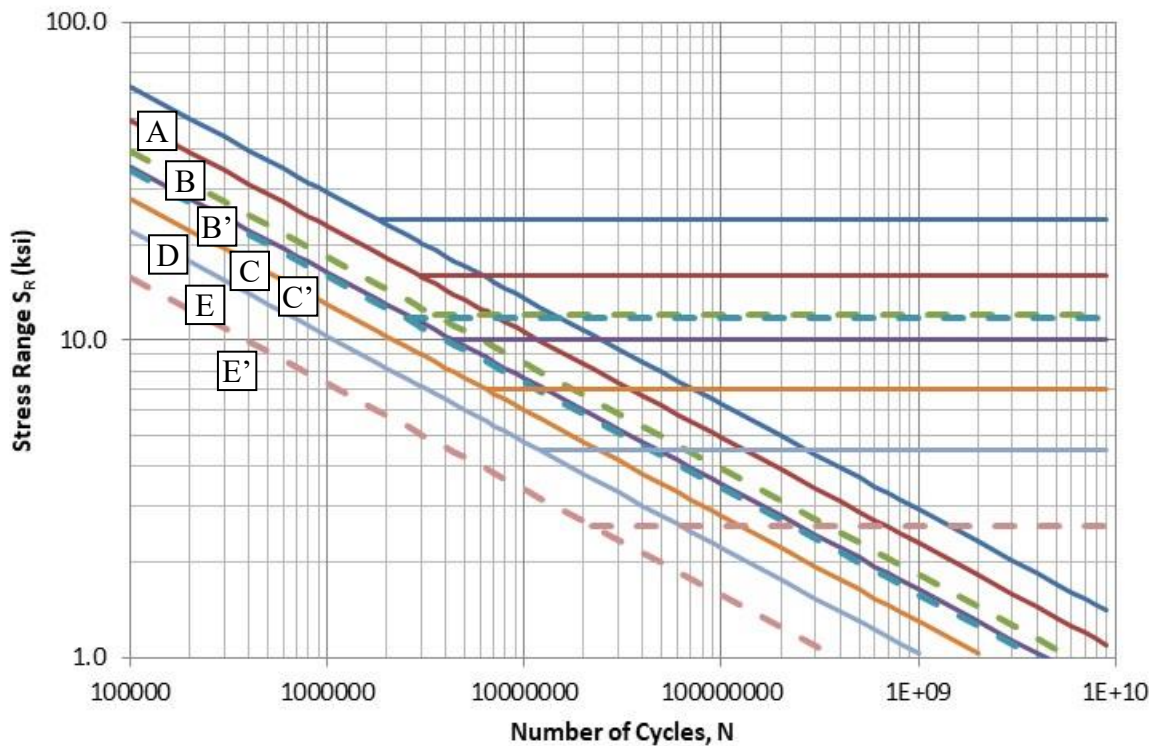


Figure 63. Graph. AASHTO fatigue resistance curves including horizontal constant amplitude fatigue limit (CAFL).

4.2.2.2 Distortion Induced Fatigue

Distortion induced fatigue, on the other hand, can occur at just about any location where differential displacements exist and are not definable to a given detail and/or a nominal stress range. For example, a common location for distortion induced fatigue is the web near the flange

at the location of a stiffener connection plate that is not attached to the flange, referred to as the web gap and illustrated in Figure 64. Differential deflections in adjacent girders can result in stresses due to distortion in the web gap. The stiff cross-frame distorts under load pulling the flexible web out of plane, while the stiff deck restrains the top flange, thus the web gap provides a small point of high flexibility.

Since such stresses are not easily calculated or quantified in typical bridge design, AASHTO LRFD deals with distortion induced fatigue by stipulating “proper” detailing practices in Article 6.6.1.3. AASHTO LRFD Article 6.6.1.3.1 indicates that connection plates in straight bridges should be welded or bolted to both the compression and tension flanges, and in the absence of better information, designed to resist a “rule of thumb” minimum 20 kip lateral load. Following these good detailing practices is generally effective in preventing distortion induced fatigue in typical straight new designs without requiring additional stress analysis.

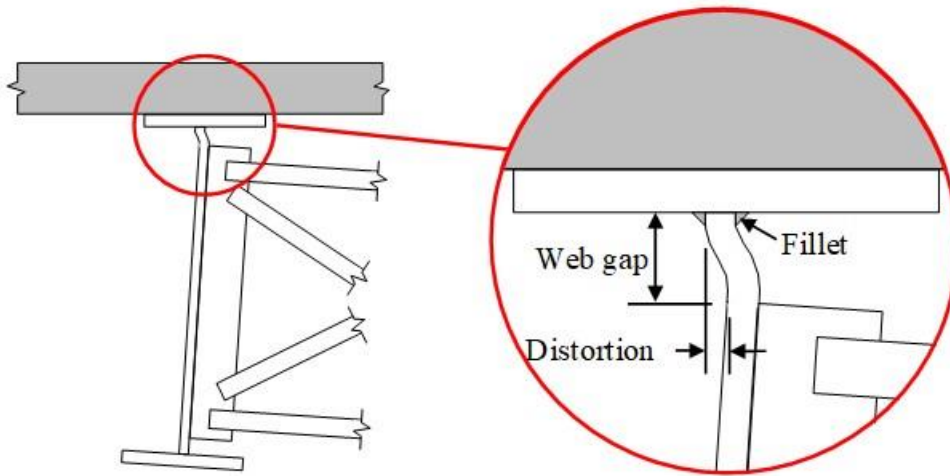


Figure 64. Illustration. Distortion at web gap between flange and stiffener connection plate.

While the LRFD Specification design methods should be used when possible, there are analysis cases when the specification provisions are not applicable, such as when a detail does not correspond to any of the detail categories, or when the geometry of a detail does not have a well-defined easily determined nominal stress, such as the previously mentioned web gap in an existing bridge. In situations such as these, where a localized fatigue evaluation is required, one must either perform full scale testing or perform a refined analysis.

The refined analysis approach as defined herein is similar to methods developed by the American Petroleum Institute (API) and American Welding Society (AWS) and is well documented in publications available from the International Institute of Welding (IIW) (IIW, 2008). It is consistent with the Level 3 analysis method described in the *Manual for Design, Construction, and Maintenance of Orthotropic Steel Deck Bridges* (FHWA, 2012A), which provides comprehensive information on fatigue analysis of orthotropic deck details. It is used extensively for the fatigue evaluation of tubular structures and plate-type structures with complex geometries by various industries, where there is no clearly defined nominal stress due to complicated geometric effects. It is appropriate for use in cases where a crack initiates at the toe of a weld, or

at a free edge of a plate such as a hole or cut-out. It is not appropriate for cases where the crack initiates at the root of a weld, or in a uniform stress field such as a full penetration weld connecting flange plates.

4.2.2.3 Local Structural Stress Approach

The local structural stress (LSS) approach, a version of the “hot spot” method, attempts to quantify the maximum structural stress in the vicinity of the detail using a refined analysis rather than addressing it through classification. The maximum structural stress is dependent on the global dimensional and loading parameters of the component excluding effects due to the local weld profile itself. The non-linear peak stress caused by the local discontinuity, i.e. the weld toe, is excluded from the structural stress. Examples of structural discontinuities and details together with the structural stress distribution are illustrated in Figure 65.

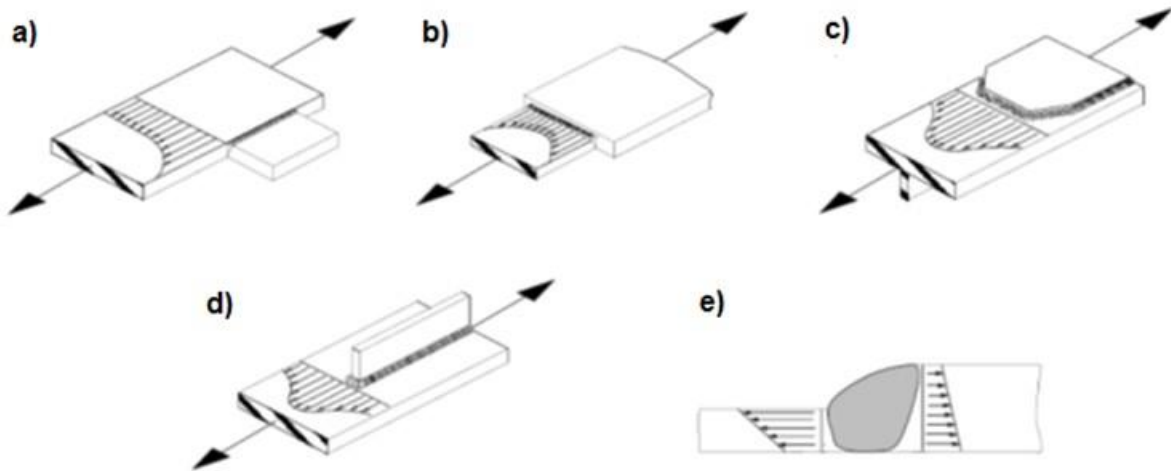


Figure 65. Illustration. Structural details and structural stress (adapted from IIW, 2008).

The LSS method is based on the assessment of the surface stress precisely at the weld toe of the detail under investigation. Shell or solid element FE models can be utilized. Due to the sharp point of discontinuity at the weld toe, the stress gradients become steep and sensitive to the mesh size of an FE model used in analysis. *In order to avoid errors due to the stress gradient, the structural stress on the surface at the weld toe is extrapolated from reference points on the surface of the plate as illustrated in Figure 66.* The number and location of the reference points can vary depending on which design codes or research recommendations are used. The recommendations here are consistent with those in the orthotropic deck design manual (FHWA, 2012A) based on the guidance provided by IIW (IIW, 2008).

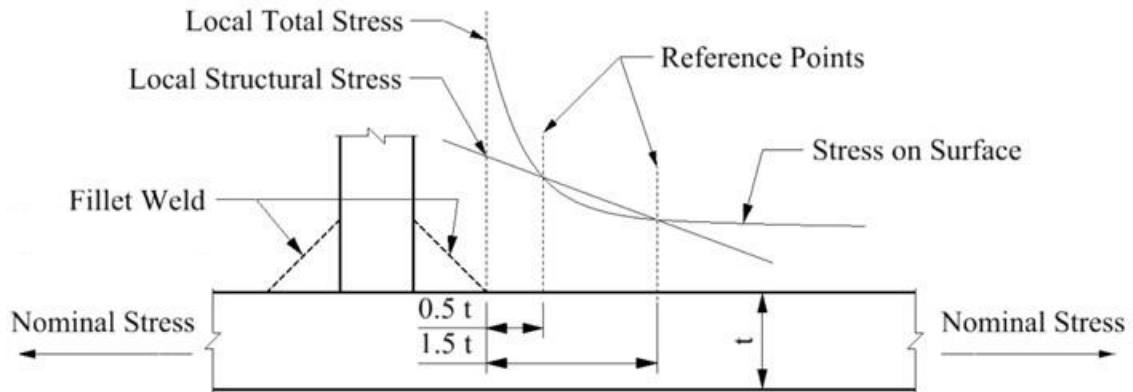


Figure 66. Illustration. Example of determination of structural stress by extrapolation (adapted from IIW, 2008).

IIW differentiates between two types of LSS according to their location on the plate and their orientation with respect to the weld toe as illustrated in Figure 67. Type (a) is located on a plate surface, and type (b) on a plate edge. In most cases the recommended stress to consider is that perpendicular to the toe, the exception being to use the principal stress if it is less than 60° inclined to the line perpendicular to the toe.

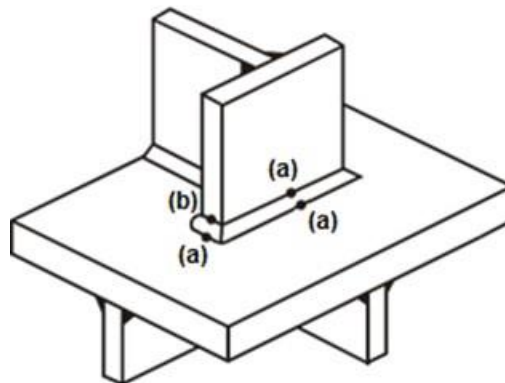


Figure 67. Illustration. Types of LSS (adapted from IIW, 2008)

For a shell element model, where the elements are located at the centroid of the component as illustrated on the left in Figure 68, 8-noded elements are recommended especially in regions of steep gradients. In most cases the welds need not be modeled, the exception being when there is eccentricity leading to local bending at the weld. If the weld is not modelled, extrapolation to the structural intersection point is recommended in order to avoid stress underestimation due to the missing stiffness of the weld.

For more complex cases, isoparametric 20-node solid elements with mid-side nodes at the edges are recommended. Although a multi-layer arrangement of solid elements can be used, one element is usually sufficient to model the thickness of a plate. Modeling of the weld profile is recommended for solid element models as illustrated in Figure 68 on the right.

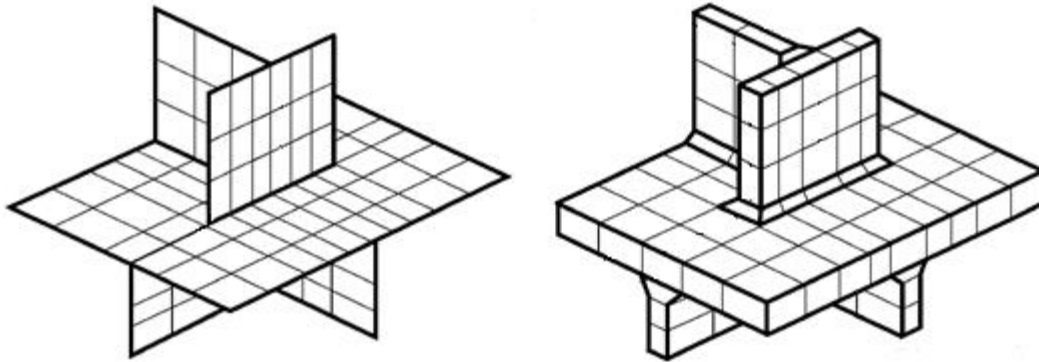


Figure 68. Illustration. Shell element and solid element models (adapted from IIW, 2008).

Typical extrapolation paths are shown by the arrows in Figure 68. Element sizes are important when using extrapolation, since nodes must be located at the reference points in order to obtain the stresses needed for extrapolation. The width a solid element or two shell elements in front of an attachment should not exceed the attachment width 'w' as illustrated in Figure 68 on the right. Figure 69 illustrates and Table 4 lists the IIW recommended locations of extrapolation points for relatively fine and coarse meshes for type a) and type b) locations.

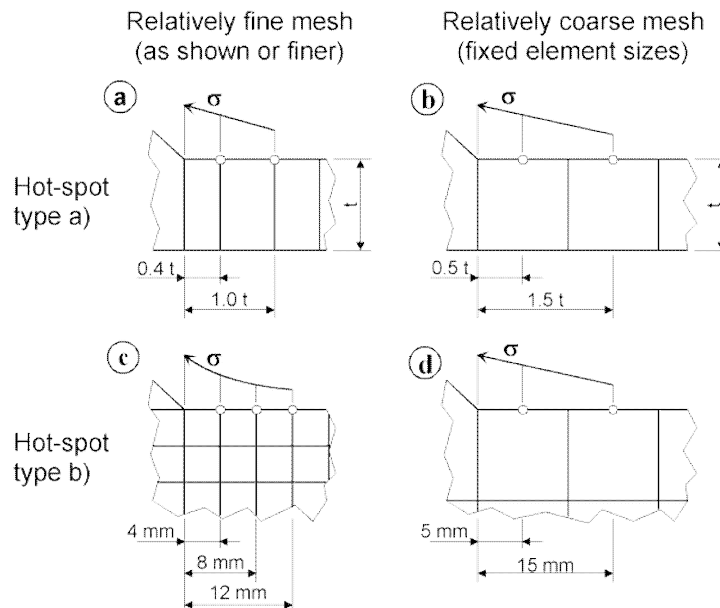


Figure 69. Illustration. Extrapolation reference points for various meshes (adapted from IIW, 2008).

Table 4. Recommended meshing and extrapolation (see also Figure 69) (IIW, 2008).

Type of model and weld toe		Relatively Coarse Models		Relatively Fine Models	
		Type (a)	Type (b)	Type (a)	Type (b)
Element Size	Shells	t x t max t x w/2*	10 x 10 mm (0.4 x 0.4 in)	$\leq 0.4 t \times t$ or $\leq 0.4 t \times w/2$	$\leq 4 \times 4$ mm ($\leq 0.16 \times 0.16$ in)
	Solids	t x t max t x w	10 x 10 mm (0.4 x 0.4 in)	$\leq 0.4 t \times t$ or $\leq 0.4 t \times w/2$	$\leq 4 \times 4$ mm ($\leq 0.16 \times 0.16$ in)
Extrapolation Points	Shells	0.5 t and 1.5 t mid-side points**	5 and 15 mm (0.2 and 0.6 in) mid-side points	0.4 t and 1.0 t nodal points	4, 8, and 12 mm (0.16, 0.32, and 0.48 in) nodal points
	Solids	0.5 t and 1.5 t surface center	5 and 15 mm (0.2 and 0.6 in) surface center	0.4 t and 1.0 t nodal points	4, 8, and 12 mm (0.16, 0.32, and 0.48 in) nodal points
* w = longitudinal attachment thickness + 2 weld leg lengths					
** surface center at transverse welds, if the weld below the plate is not modeled					

The guidance provided is intended for modeling of the local region in the vicinity of the specific location of interest. For the remainder of the model using a similar mesh refinement would be inefficient. Two approaches are possible to improve efficiency of the model:

- Submodeling as described in Section 2.3.6 of this manual; and
- Use a significantly coarser global model away from the region of interest.

While both of these methods are acceptable, if a refined global model is being utilized anyway, it is recommended that it be locally refined, as local boundary stiffnesses will be automatically satisfied. For a submodel, the local boundary stiffnesses will need to be approximated.

The LSS resistance model is based on calibration between refined stress analysis and test data. Eurocode LSS category resistance curves are either the 90 or 100 N/mm² curve depending on the detail, labeled according to the allowable stress range at 2,000,000 cycles. *The corresponding AASHTO curve is the Category C curve, which envelopes the European curves, and is recommended as the baseline curve for the LSS method* (see Figure 70). Recall that misalignment and the corresponding local bending stresses are not accounted for when using the LSS method, they must be modeled explicitly.

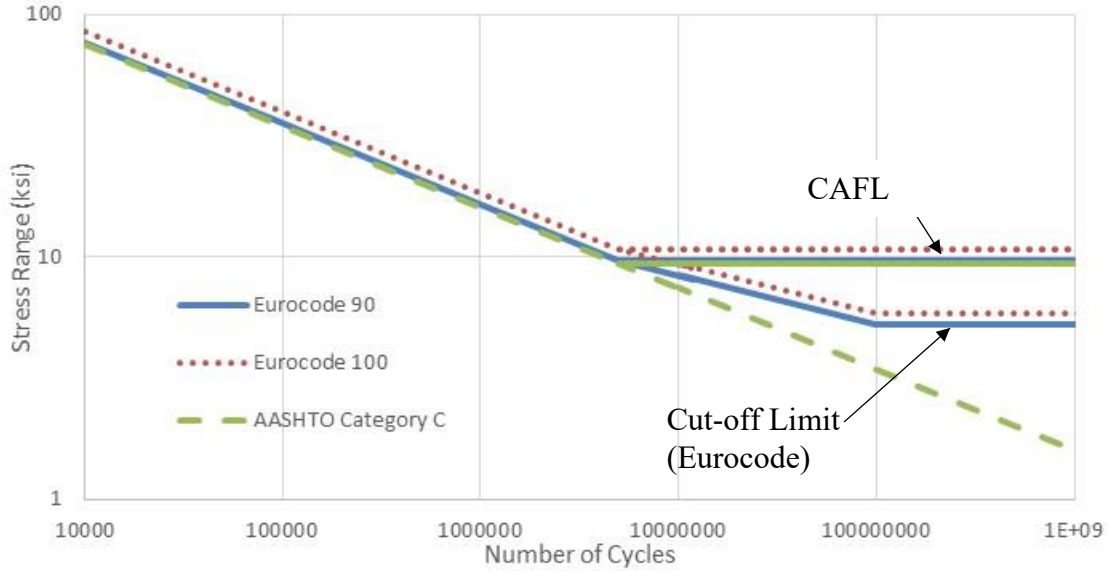


Figure 70. Graph. Comparison of LSS baseline curves.

Weld root fatigue cracking is not directly addressed by the LSS method. However, AASHTO LRFD Equation 6.6.1.2.5-4 (Equation (26)) can be used to check whether root cracking is an issue. The geometrical parameters of the weld as illustrated in Figure 71 are used to reduce the Category C stress range curve if necessary:

$$(\Delta F)_n = (\Delta F)_n^c \left(\frac{0.65 - 0.59 \left(\frac{2a}{t_p} \right) + 0.72 \left(\frac{w}{t_p} \right)}{t_p^{0.167}} \right) \leq (\Delta F)_n^c \quad (26)$$

- where:
- $(\Delta F)_n^c$ = Nominal fatigue resistance for Detail Category C.
 - $2a$ = Length of the non-welded root face in the direction of the thickness of the loaded plate (in). For fillet welded connections $(2a/t_p)$ shall be taken equal to 1.0.
 - t_p = Thickness of loaded plate (in).
 - w = Leg size of the reinforcement or contour fillet, if any, in the direction of the thickness of the loaded plate (in).

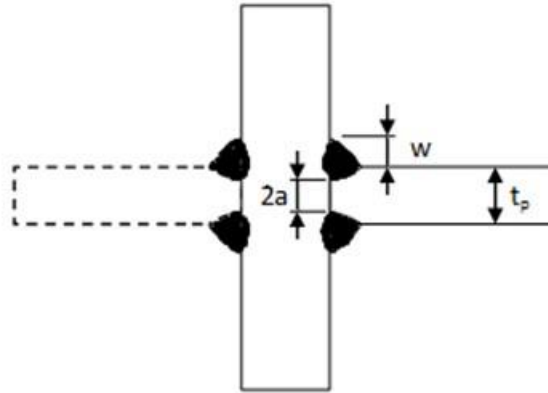


Figure 71. Illustration. Dimensions for root fatigue stress range resistance reduction (adapted from AASHTO, 2014).

Note that Category C fatigue resistance of the toe of the weld can be made to control the design by adjusting the plate and weld parameters if desired.

4.2.2.4 Modeling Cut-Outs

A sufficiently refined mesh must be used to determine the stress range in base metal tangent to a cut-out, such as the one illustrated in Figure 72. To be more consistent with both potential laboratory tests and other refined analyses, finite element results should be evaluated a small distance from the edge of the mesh. A 6 mm (1/4 inch) offset, similar to that proposed for orthotropic plate analysis, is recommended. Use of this offset value will place a node at this location and drive the mesh size at the edge of the cut-out, although the mesh can be transitioned to a larger size away from the area of interest. As long as the edge preparation of the cut-out is consistent with the requirements prescribed for Category A as contained in AASHTO LRFD, the S-N curve for Category A can be used to assess the stress range.

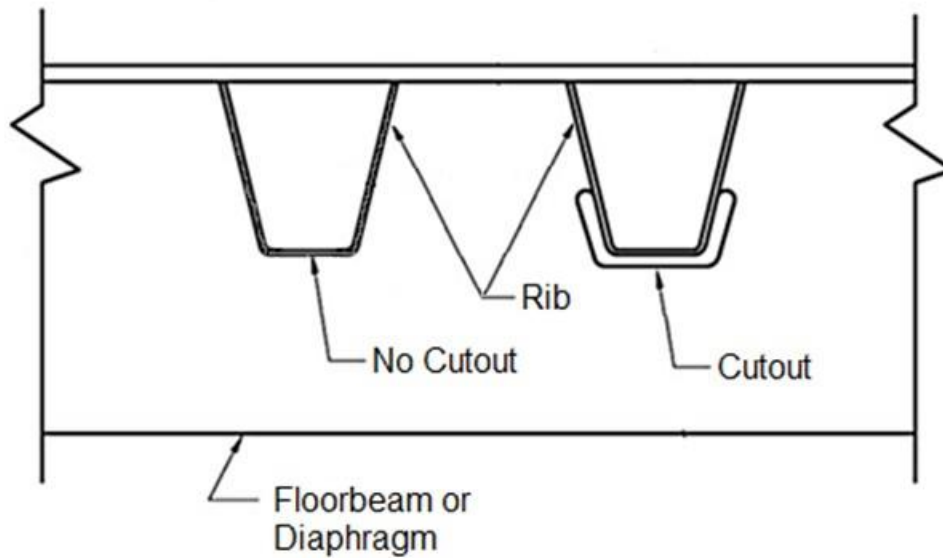


Figure 72. Illustration. Typical orthotropic ribs, with and without cut-out (adapted from FHWA, 2012)

4.2.2.5 Distortion Induced Fatigue Stress Range Reduction

Keep in mind that stress ranges calculated using refined analyses are very sensitive to the stiffnesses of various aspects of the models. When possible, models should be calibrated to measured values on a full-scale test specimen or actual bridge member. In the absence of such calibration, evaluation of the accuracy of the model is up to the judgment of the analyst. For retrofit cases, even if the absolute value of the stress range is not known with great accuracy, the relative performance of alternative stress range reduction strategies can be assessed.

When a refined model indicates that the stress range at a specific fatigue prone detail is greater than allowable, parametric analyses can be performed to determine what needs to be done to reduce the stress range. Depending on the situation, the allowable stress range may correspond to a finite life or an infinite life case. New designs typically aim for infinite life, while for existing bridges calculating a remaining finite life is often sufficient. Note that the AASHTO loadings for these two cases differ. *There are two design approaches that can reduce stresses, the strength approach and the flexibility approach.* The strength approach increases the amount of material and/or provides a more direct load path resulting in a lower stress range. The flexibility approach removes material making the detail less stiff such that alternate more desirable load paths are utilized resulting in a lower stress range.

An example would be the distortion induced stress in the web gap illustrated in Figure 64. If a strength solution is explored, the model would examine the effect of attaching the stiffener connection plate to the flange of the girder. If a flexibility solution is explored, the model might investigate increasing the depth of the gap until the stress range decreased to an acceptable value. The *Manual for Repair and Retrofit of Fatigue Cracks in Steel Bridges* (FHWA, 2013) provides many approaches for addressing fatigue issues in bridges.

4.2.3 Bolted/Riveted Steel Connections

Connections are one of the most expensive features of steel structures. Additionally, connections can be difficult to retrofit or repair. Therefore, any method that results in reductions in size or complexity of connections, or results in an increased rating capacity, will potentially result in large savings. Simplified methods exist to perform conservative steel connection designs using hand calculations, and should typically be used for routine designs. Such methods usually require that equilibrium is satisfied using linear approximations, and that compatibility will be satisfied through contained plastic flow in the steel plates, if necessary.

Up through the 7th Edition of AASHTO LRFD, the most common hand calculation method for eccentric loading has been the Elastic (or Vector) Method which is considered to be lower bound conservative. *The Elastic Method assumes equilibrium about the centroid of the bolt pattern and ignores compatibility of deformations.* Concentric force effects are equally distributed to bolts in the Elastic Method, while force effects due to moments are distributed linearly with the distance from the centroid perpendicular to the radius. Stiffness effects such as loading the first row of bolts more heavily are addressed implicitly in the specification by reducing bolt capacity, and ductility of connectors/connected material is assumed to redistribute forces more evenly.

A more accurate, less conservative method is the Ultimate Method (Crawford and Kulak, 1971) which assumes that:

- The connected plate under eccentric load rotates about an instantaneous center of rotation
- The deformation which occurs at each fastener varies linearly with its distance from the center of rotation and acts in a direction perpendicular to the radius from the fastener to the instantaneous center of rotation.
- The ultimate strength of the group is reached when the ultimate strength of the fastener furthest from the center of rotation is reached.

The main differences from the Elastic Method are that the center of rotation is no longer assumed to be at the centroid of the bolt group, and although the deformation still varies linearly with the distance from the center of rotation, the force/deformation relationship, or stiffness, can be but need not be linear. The main drawback of the Ultimate Method is that it is iterative, approaching the “exact” solution from an upper bound. An instantaneous center must be assumed, and then equilibrium checked.

The Ultimate Method can be easily performed using a refined analysis, without iterations if a linear bolt force/deformation relationship is used, such as the initial slope of the curves in Figure 73. Not only will the center of rotation be automatically utilized, the deformations of the connected material and unequal force distribution will be explicitly accounted for based on the stiffnesses of the connected materials. When the bolt force-deformation relationship is modeled as linear, the ultimate method produces the same result as the classical elastic method.

Refined connection analyses can range from simple linear elastic to advanced material and geometric nonlinear depending on the situation. Also note that although most bolted bridge connections are designed as “slip-critical,” with bolt pretension resulting in friction between steel plies, connection design rarely incorporates this friction directly. It is assumed that the friction is

overcome when a prescribed force is distributed to the most highly stressed bolt in the connection.

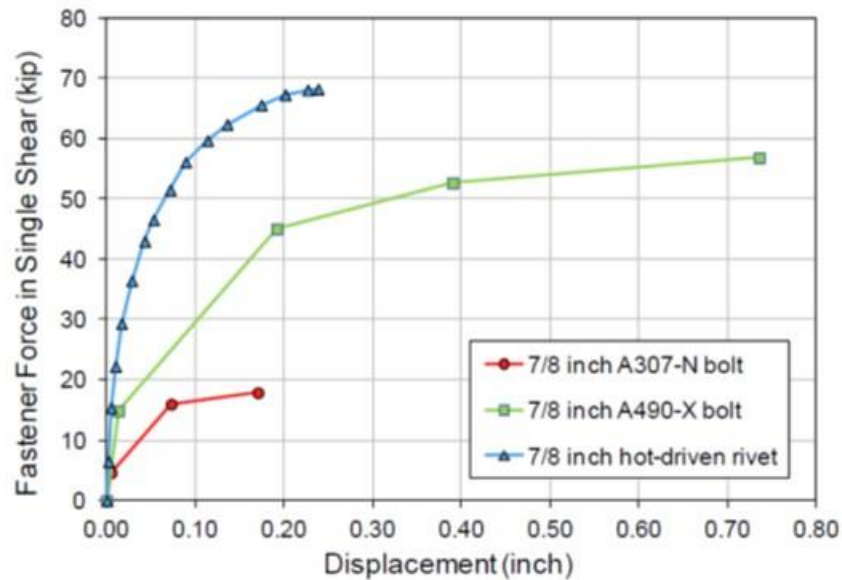


Figure 73. Graph. Shear force-displacement relationship for common connectors (Ocel, 2013).

As described in Article C6.13.2.7 of AASHTO LRFD, the equations for bolt resistance in AASHTO LRFD Article 6.13.2.7 include a 20 percent reduction to account for the unequal distribution of forces due to deformations of the connected material, so if the bolt resistance for a refined analysis is being calculated by AASHTO LRFD, consideration can be given to increasing the resistance by 20 percent. Note that in a refined analysis, stress concentrations may develop in the main material of the model, but as mentioned previously, it is assumed that ductility will distribute the forces more evenly, so localized stress concentrations can generally be ignored.

4.2.3.1 Modeling Bolted Splice Connections

To model splice connections, shell elements are used to model the splice plates and a limited length of the member flange and web plates at the connection. Main member shell elements should ideally extend two to three times the largest dimension of the member beyond the splice. Beyond this length, beam elements can be used to model the remainder of the member. At the intersection of the shell and beam elements, constraints, rigid links, or rigid elements can be used to ensure compatibility.

There should be a node located at the center of each connector (rivet or bolt) in each connected shell mesh, and ideally a spring element should be used to connect the nodes, although beam elements can be used as well. The spring (or beam) stiffness should model the shear load-displacement characteristics of the connectors, based on the material and diameters of the bolts or rivets. Examples of the full shear load-displacement relationships for common connectors are illustrated in Figure 73. While non-linear examples are shown, and can be used when the appropriate spring elements are available, linear approximations are sufficient for cases when the

connection plate or the main members rather than the connectors controls the capacity. The axial stiffness assigned to the connectors should be essentially rigid, generally three orders of magnitude stiffer than the shear load-displacement is sufficient.

A maximum mesh size of the splice plates, and the members within the splice, generally in the range of 3-4 inches, is driven by the spacing of the connectors, as each connector requires a node. The splice plate and the member within the splice mesh size should be fairly uniform. Member shell element mesh sizes can increase as distance from the splice increases, but may be limited by other features such as perforations.

For linear material analyses, only the modulus of elasticity of steel is required for the main material. If material nonlinear analyses are desired, depending on the software, the full stress-strain relationship can be utilized to define the material as illustrated in Figure 74. Often using a bilinear approximate curve with minimal strain hardening is both simpler and conservative, while avoiding issues with convergence and excessive localization of plastic strain.

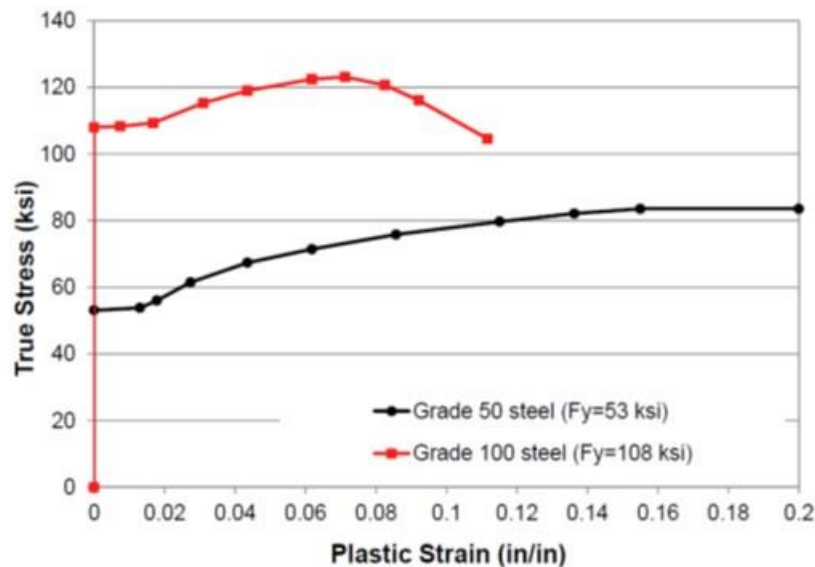


Figure 74. Graph. Typical full stress-strain relationship for Grades 50 and 100 steel (Ocel, 2013).

Although the model boundary conditions can represent the actual structure, it is only necessary to ensure that the supports are sufficiently distant from the connection that the reactions do not influence the stress field in the connection portion of the model, and that the bending moment, shear, and axial force are representative of the design forces over the length of the splice.

4.2.3.2 Modeling Gusset Plate Connections

Due to the failure of the gusset connection on the I-35W truss bridge in Minnesota, gusset connections in existing trusses have recently come under increased scrutiny. When conservative simplified hand procedures for designing and rating gusset plates (FHWA, 2009) indicate insufficient capacity, less conservative more accurate refined analyses can be utilized to verify

capacity and avoid costly retrofits. Many of the previous recommendations for splices are based on analysis models developed by the FHWA for gusset plate design and rating and which were calibrated with full scale experiments (Ocel, 2013), and similar techniques can be applied to other bolted connections, for both linear and non-linear analyses. Typical models could include:

- A 3D shell element model in the vicinity of the connection is constructed
- Nonlinear material properties
- Nonlinear geometric properties
- Nominal out-of-straightness is included

Figure 75 shows a typical riveted gusset plate connection with five members framing in, two chords, two diagonals and a vertical.



Figure 75. Photo. Example of a typical truss gusset plate connection.

To model gusset connections such as these, shell elements are used to model the gusset plates, splice plates, and a limited length of the member cross-section framing in to the connection. Lacing can either be modeled with shell or beam elements. NCHRP 12-84 (Ocel, 2013) recommends that the shell element portion of the members should extend a minimum of 200 inches beyond the edge of the gusset plate, but two to three times the largest dimension of the member should be sufficient. As with the previously mentioned splices, beyond this length, beam elements can be used to model the remainder of the member with multi-point constraints enforcing compatibility at the intersection of the beam element representation of the member with the shell element portion of the model. At all beam intersections other than at the gusset plate, pinned joints can be used. For simplicity, gusset submodels should include the truss panels on each side of the joint, as illustrated in Figure 76, to sufficiently represent the equilibrium and compatibility conditions at the joint.

All joints that are braced laterally should be restrained from moving out-of-plane. The statically determinate nature of trusses means that the free body of the joint and the truss panels can be modeled as simply supported in-plane. In Figure 76 the supports are located at U1 and U3, but due to the statically determinate nature of the model, any two joints other than the joint under consideration can be used as long as the correct loadings can be applied.

In geometric nonlinear analyses, to facilitate buckling geometric imperfections should be incorporated not only on the gusset plates but also on the diagonal compression member. If the out-of-straightness has not been measured, the shape of this initial out-of-straightness can be determined by a separate linear elastic analysis of the joint model by applying pressure loads on the gusset plates and out-of-plane displacements to the end of the compression diagonal at the gusset (Ocel, 2013). The out-of-straightness generated typically looks like the first mode buckling behavior of the gusset plate which would represent the lower bound of the resistance in a buckling analysis.

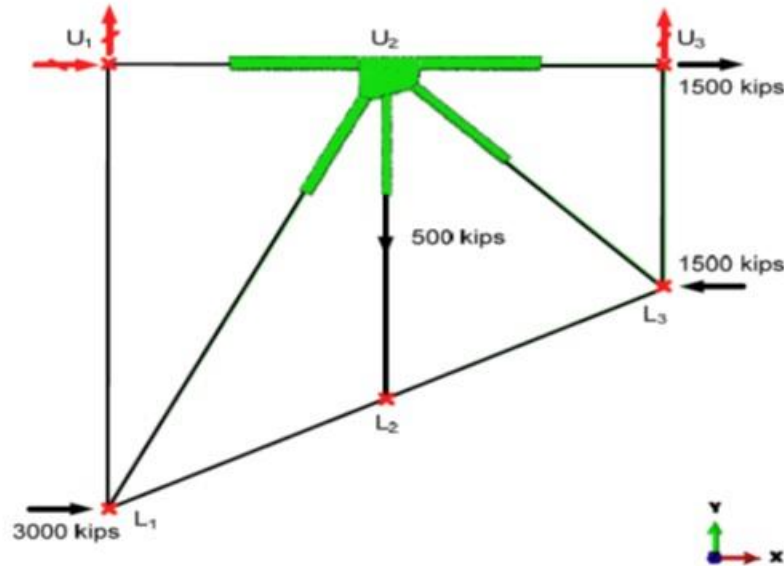


Figure 76. Illustration. Examples of typical truss gusset plate connections (Ocel, 2013).

After the deformed shape is obtained, the deformations are scaled such that the maximum magnitude of the out-of-straightness of gusset plates equals $L_{max}/150$ and the out-of-plumbness of a diagonal member equals $0.10 \cdot L_{gap}$ where L_{max} is the maximum length of free edges adjacent to the compression diagonal and L_{gap} is the smallest length of the gap between the compression diagonal and the adjacent members. There is little guidance on the limits of out-of-straightness permitted in gusset plate design, so the limits are somewhat arbitrary, but previous research has found that once the modeled gusset out-of-straightness exceeds approximately 0.06 inches, the effect of additional deformation on the buckling resistance is relatively small (Ocel, 2013). Once a model is constructed, parametric studies can be performed to confirm the effect of initial imperfections, if desired.

Loading is applied in the plane of the truss to the appropriate nodes such that the connection is in equilibrium under the desired loading. When the analysis is non-linear, superposition does not apply and load effects cannot be factored and/or added. The factored dead load should be applied first and then the live load should be increased proportionately until maximum capacity is achieved. When performing a rating, the factor by which the live load is increased is equal to the rating factor.

A 3D shell model utilizing non-linear material properties, non-linear geometric properties, and initial out-of-straightness can identify the following failure modes of a gusset plate connection:

- Buckling
- Shear yielding
- Chord splice failure

Since bolt holes are not typically modeled, net section and block shear failures cannot be identified, but these modes are easily checked with LRFD Specification provisions. For more guidance on nonlinear analyses, see Section 5.3.

4.3 Substructure and Foundation Modeling

Modeling of the substructures in the same analysis model as the superstructure can be done for any model, but it is only required when the interaction between them affects the overall behavior. For non-integral bridge superstructures, the behavior of the superstructure is often independent of the behavior of the substructure, and therefore the substructure need not be included in the superstructure model. In that case, the support conditions for the superstructure can be applied at the locations of the bearings and the substructures are then analyzed separately using the appropriate bearing reaction forces found from the superstructure analysis. Live loadings to determine substructure extreme force effects can sometimes be a challenge.

For guidance on modeling of bearings see Section 3.7.3. Additional guidance on the application of live load to substructures can be found in Section 7.3.9. Cases where the effects of the substructures on the superstructure need to be accounted for include bridge structures with integral bent caps, integral abutment bridges, seismic analyses, and continuous bridges with variable substructure stiffnesses.

4.3.1 Integral Construction

With an integral bent cap connection between the superstructure and substructure, the system behaves like a frame. Figure 77 exaggerates the range of behaviors caused by the relationship between the bending stiffnesses of the superstructure and substructures. In Figure 77(a), the columns of the substructure are relatively tall and slender such that the response of the superstructure to the applied loads is similar to a continuous beam with vertical supports placed at the bearing locations (i.e. little to no moment restraint from the substructures). In Figure 77(b), the substructure columns are much stiffer, which results in the superstructure response being similar to that of a fixed ended beam.

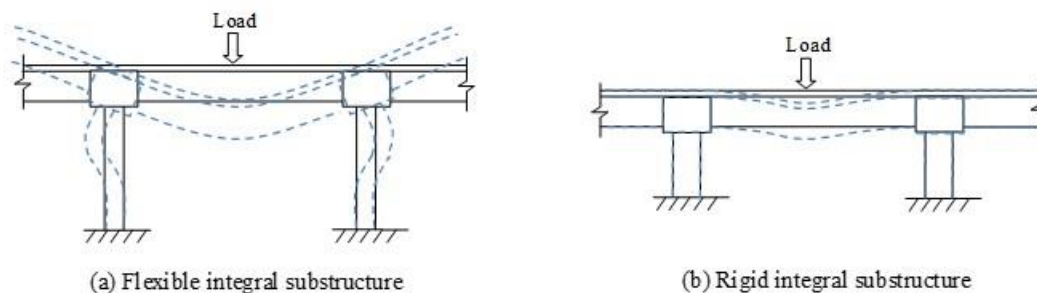


Figure 77. Illustration. Behavior of integral substructures.

For cases such as integral abutment bridges (Figure 78), the behavior of the soil impacts the behavior of the substructure and superstructure. In lieu of performing an analysis which accounts for the soil-structure interaction, the design force effects due to dead and live loads for the superstructure beams can be fully bounded as shown in Figure 78(a). The superstructure is assumed to be simply supported to determine the positive moments (Figure 78(b)), and then fixed boundary are assumed at the base of the abutments or at the ends of the beams to determine the negative moment values to use for design (Figure 78(c)). The force effects arising from temperature loadings and their interaction with the effects due to other load types should be investigated by accounting for the effects of soil-structure interaction. Refer to Section 5.2 for more information on modeling soil-structure interaction.

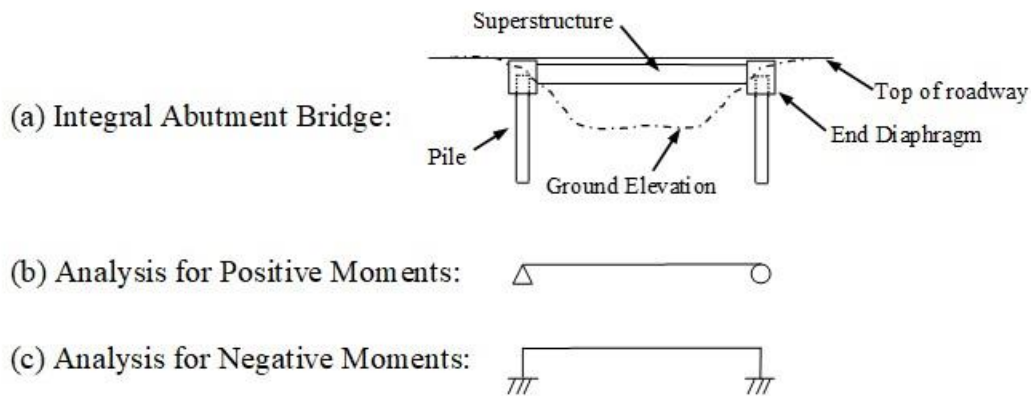


Figure 78. Illustration. Developing superstructure force effects for an integral abutment bridge by bounding the solution.

4.3.2 Continuous Construction

For continuous superstructures, the behavior of the substructures in the vertical and lateral directions should be examined to determine if their effects should be included in the analysis. If the substructures can be considered sufficiently rigid in the vertical direction then it is acceptable to use vertically rigid supports for the bearings under the superstructure. When there are substructures that are vertically flexible then the substructure stiffness should be accounted for.

There are no set rules regarding what constitutes being “sufficiently rigid,” however it is apparent that substructures types such as a typical concrete hammerhead pier can be considered to provide a rigid vertical support. On the other hand, a wide steel beam straddle bent would likely have sufficient flexibility to cause a shift in moments from those determined by assuming the vertical supports are rigid. The vertical stiffness at each beam in the cross-section at the straddle bent will vary as well, since the vertical stiffness at beams near the mid-span of the straddle bent will be less than for those near the columns. When in doubt, often a simple beam element frame model will give insight into the rigidity of the substructure.

Additionally, at locations where longitudinal forces are transferred from the superstructure into the substructure, the longitudinal stiffness of the substructures may impact the superstructure design forces, and therefore should be considered in the analysis model. An example of this

would be a continuous deck system on tall piers as depicted in Figure 79. In this arrangement, at the fixed bearings the flexibility of the piers in the longitudinal directions are used to accommodate the thermal movements and the flexibility of these piers will affect the moments in the adjacent spans.

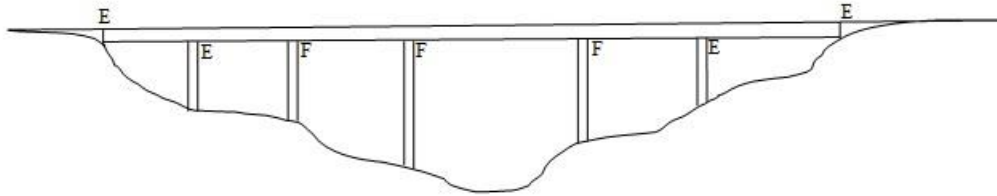
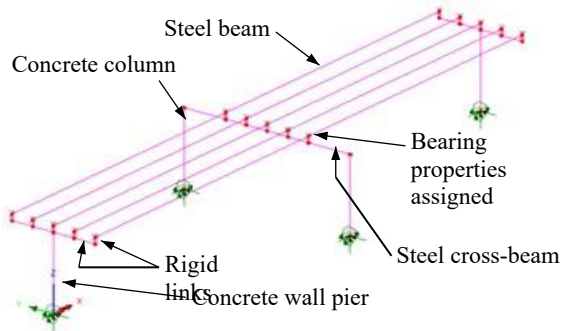


Figure 79. Illustration. Continuous span arrangements with fixed bearings at tall, slender piers

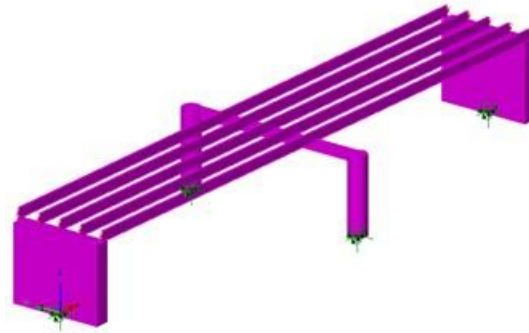
4.3.3 Overall Interaction

While substructures do not typically need to be modeled in cases other than these, they can be added to any analysis model to simplify the determination of the substructure force effects. The most straightforward way to account for the influence of the substructure on the superstructure is to explicitly include both in the same analysis model. When substructures are explicitly modeled, it must be ensured that the bearings are modeled to achieve the appropriate behavior (e.g. fixed vs. expansion vs. guided expansion), and that components are modeled at their correct spatial locations. For more on the modeling of bearings, see Section 3.7.3.

To simplify the extraction of the required output, typically the substructure will be modeled using beam line elements. Even substructure types such as wall piers can be modeled using beam elements if shear deformations are accounted for in the element formulation and appropriate geometric properties are assigned. To connect superstructure members to the substructure at the correct elevations and transverse locations, rigid links or constraints can be used. Figure 80 demonstrates the modeling of a two-span continuous superstructure and substructures, utilizing beams elements, rigid links, and elements for the bearings.



(a) Line element model



(b) Line element model with fleshed member cross-sections

Figure 80. Illustration. Example of modeling the substructure with the superstructure, including bearings and rigid links to achieve correct locations of superstructure beams (deck not shown).

The appropriate boundary conditions are placed at the bottom of the modeled substructure components, typically at the top of the footing. For situations where the foundation-soil interaction is not required, fixed or free support conditions can be assigned as needed. Typically, all translational directions would be restrained, and moment restraints would be assigned based on the type/size of the foundation present. Narrow footings would dictate the use of moment releases about an axis perpendicular to the short direction, while moments can likely be considered to be restrained about an axis perpendicular to the wide direction. If it is unclear whether the support conditions should be considered fixed or free, then the solution should either be bounded or a soil-structure interaction analysis, as described in Section 5.2 should be used to quantify the level of fixity.

Further information regarding modeling and analysis of substructures can be found in Section 3.14.3 of G.13.1 Guidelines for Steel Girder Bridge Analysis (AASHTO/NSBA, 2014).

CHAPTER 5. MODELING ADVANCED TOPICS

5.1 Introduction

The following sections provide guidance for performing advanced analyses including soil-structure interaction, nonlinear, and dynamic analyses for use in conjunction with, or in addition to, AASHTO LRFD.

5.2 Soil-Structure Interaction

5.2.1 General Information

In most circumstances, the effects of soil-structure interaction (SSI) do not have a significant impact on the behavior of the superstructure and substructure of bridges, and therefore they do not need to be considered for typical bridge analysis problems. Situations where effects of SSI likely do need to be accounted for include:

- Seismic analysis
- Refined analysis of integral abutment bridges
- Design or evaluation of shallow foundations supported by relatively soft soil
- Design or evaluation of deep foundations

Note that an in-depth discussion of seismic analyses is beyond the scope of this document, and details on SSI for seismic analysis can be found in (NHI, 2011) and (FHWA, 2006).

Additionally, it should be noted that much of the published literature regarding SSI is in regards to seismic analyses, however the methods discussed in these sources are typically applicable to non-seismic load cases, with adjustments or simplifications made to the procedures as necessary.

The actual behavior of soil under loading is often nonlinear. Before selecting a method to use to account for SSI, the degree of nonlinear behavior of the foundation for the specific structure and load levels under investigation should be estimated. From this finding, a decision on the type of SSI analysis to utilize can then be made. For instance, examine Figure below, where a generic nonlinear load-response curve (for instance pile lateral load vs. lateral displacement) is shown with equivalent linear stiffnesses indicated for several points along the curve.

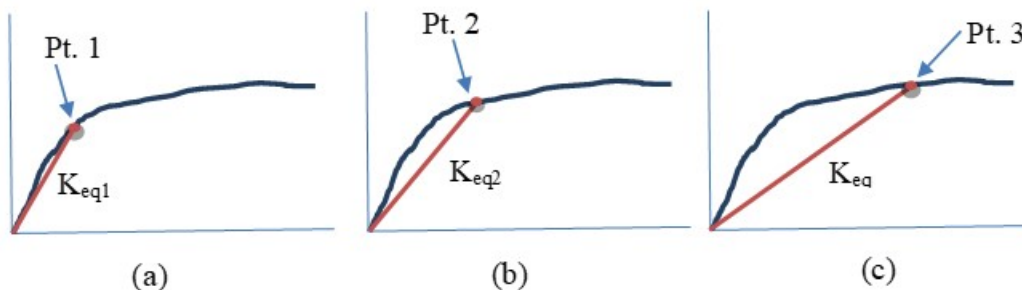


Figure 81. Graphs. Nonlinear behavior – essentially linear vs. mildly nonlinear vs. significantly nonlinear.

The response up to Point 1 is essentially linear, and therefore K_{eq1} can be utilized for any load level up to this point. Linear methods described in subsequent sections would be suitable to model this behavior. Past Point 1, the response becomes nonlinear, however K_{eq2} is not significantly different than K_{eq1} , indicating mildly nonlinear behavior which can likely be approximated using one of the iterative methods described. Moving past Point 2 towards Point 3, the difference between K_{eq3} and K_{eq1} becomes much greater, indicating significant nonlinear response is occurring. For loads on this part of the curve, it may be difficult to converge on the correct stiffnesses when using one of the iterative methods. In this case, the nonlinear methods which are presented may be more suitable.

As for how the SSI can be accounted for in the analysis, there are two general types of methodologies: substructuring methods and direct methods. In substructuring methods, the behavior of the SSI is investigated outside of the analysis model which is used for the rest of the bridge. The effects of the SSI are then determined and input as boundary conditions in the bridge analysis model. On the other hand, direct methods involve modeling the interaction between the structure and the soil in the same model as the rest of the bridge.

Lastly, it must be kept in mind that analysis results are only as good as the properties input, therefore using inaccurate values can defeat the purpose of performing a refined analysis. Because subsurface properties can be so variable, consultation with geotechnical engineers is recommended when determining subsurface properties to utilize in an analysis considering SSI. Even when subsurface conditions are well documented, behavior can be difficult to precisely model. For most of the methods described below, it may often be prudent to run parametric studies using a range of properties to obtain a bounded solution. At the very least, the engineer should be aware of the effect of the various input parameters on the results, and therefore a sensitivity analysis is highly encouraged.

5.2.2 *Shallow Foundations*

Typically these types of foundations rest on bedrock or competent soil and therefore undergo only small displacements, under which soil behaves essentially in a linear manner with minimal cross-coupling between the translational and rotational degrees of freedom (DOF). Use of fixed boundary conditions for the 3 translational DOF and for rotation about the vertical axis is common. The decision regarding the use of fixed or free restraint for the other 2 rotational DOF is often based on the footing dimensions. Wide footing widths often provide sufficient restraint against rotation such that a fixed condition is appropriate. On the other hand, a footing width which is relatively narrow likely warrants assuming there is no rotational restraint about the axis perpendicular to the narrow dimension.

If SSI for a shallow foundation needs to be accounted for, a rigid plate method, such as the one described in Section 9.5 of (NHI, 2011) or Section 6.2.2.1 of (FHWA, 2006) can be used to determine the stiffness values for each of the degrees of freedom. In this method, the foundation is assumed to be a rigid plate embedded in an elastic medium (soil), and the stiffness coefficients are developed using equations involving the soil stiffness, the foundation dimensions and the embedment depth of the footing in the soil. While not typically required, more in depth methods may need to be utilized if the shallow foundation geometry, soil properties, or loading are such that the rigid plate method is not applicable (for instance, if the footing is relatively flexible such that its stiffness may influence the overall behavior). These types of methods would involve

modeling the footing and then accounting for the effect of the soil using either Winkler springs, as shown in Figure 82, or by modeling a portion of the soil continuum using finite elements, as shown in Figure 83.

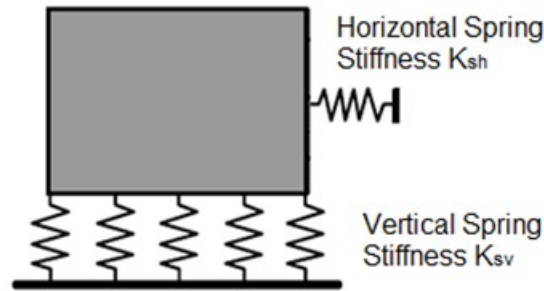


Figure 82. Illustration. Winkler spring model for SSI of a shallow foundation (adapted from FHWA, 2006).

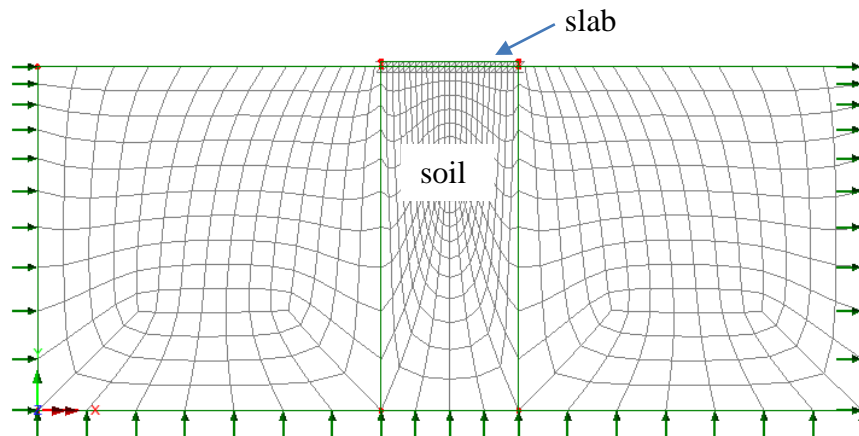


Figure 83. Illustration. 2D plane strain model of a slab on grade.

Winkler springs idealize the soil supporting the foundation as a system of independent, closely spaced, discrete springs, analogous to a beam on elastic foundation analysis. The stiffness properties input can be either elastic, elasto-plastic, or fully nonlinear, although if elastic properties are used then it must be ensured that the soil is behaving primarily in its linear-elastic range. In the soil continuum approach, 2D or 3D elements are used to represent a region of soil in the vicinity of the structure. The modeling of the interface between the soil and structure can be adjusted as needed to capture the behaviors which occur. For instance, if there is no uplift between the structure and soil, then the two portions of the model can be directly connected. However, if uplift occurs then the connection between soil and structure may need to be modeled with interface or joint elements to permit the separation to occur. Additionally, some study must be undertaken to ensure that a large enough region of soil is modeled such that the boundary conditions applied at the edges of the modeled soil do not significantly influence the results near the structure.

Both of these types of methods could be implemented by either adding the footing and soil effects in the bridge analysis model (a direct approach), or by creating a separate model to determine elastic or elasto-plastic spring stiffnesses to use as boundary conditions in the bridge

model (a substructuring approach). Developing spring stiffnesses using a substructuring approach is discussed in greater detail in Section 5.2.3.2 in reference to deep foundations, and the methodology can be equally applied to shallow foundations.

5.2.3 Deep Foundations

Methods for including SSI in an analysis of a bridge with deep foundations can be broadly categorized into one of four methods: depth to fixity method, substructuring-iterative method, direct iterative method, and direct nonlinear method. The iterative methods mimic a nonlinear analysis by performing iterations of linear analyses, changing the stiffnesses based on the determined displacements. In the substructuring method, the complexity of the overall analysis effort is reduced by using separate analysis models (and often separate analysis programs) for global structure analysis and for the SSI analysis. The direct nonlinear method is the most refined methodology, and is necessary for circumstances where the nonlinear behavior is prevalent and the use of iterative methods would be unwieldy.

5.2.3.1 Depth to Fixity Method

The depth to fixity method requires the use of either empirical formulas/charts or a foundation program such as COM624, LPILE, or FB-MultiPier to determine an effective length of the piles. This effective length represents the depth to fixity for a simplified analysis where the piles are modeled in the FEA model as beam-columns, using fixed supports at the bottom nodes and no support along their length. This is shown in Figure 84. Depending on the goals of the analysis, the depth to fixity can be selected to either provide the correct peak pile moments (useful for design/evaluation of the piles), or the correct substructure stiffness (which will generate the correct force effects in the rest of the bridge structure).

Depending on the detailing of the pile connection to the pile cap, fixed or pinned boundary conditions are used to connect the top of the pile to the rest of the analysis model. Typically, an embedment into the pile cap of 2-3 times the pile diameter provides sufficient rigidity that a fixed condition can be assumed. Otherwise a pinned connection should be assumed, or the solution should be bounded, examining force effects and displacements using both assumptions.

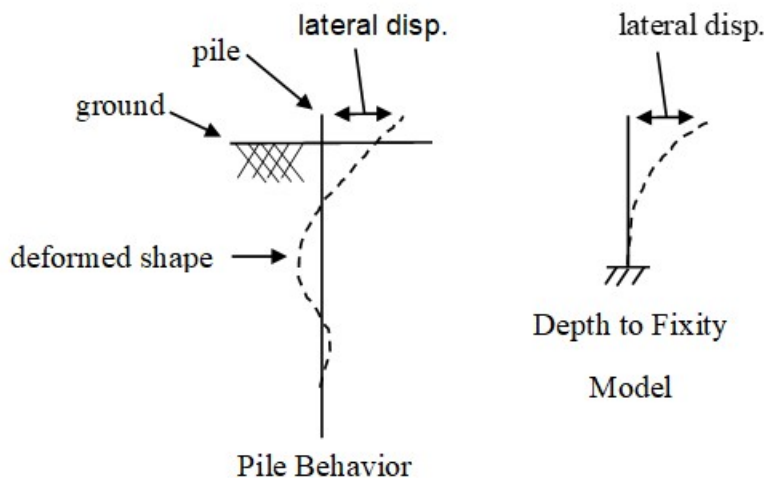


Figure 84. Illustration. Pile lateral deformations and depth to fixity model.

Empirical formulas/charts should only be used to determine the depth to fixity for preliminary studies, since the behavior/interaction of the soil and structure is grossly oversimplified and the possibility exists of generating unconservative results. When using a foundation program to determine the depth to fixity, the resulting analysis can be considered as being more refined, however if undertaking that level of effort, then one of the substructuring or direct approaches described below is likely a better option.

5.2.3.2 Substructuring-Iterative Method

In the substructuring-iterative method, the stiffness of the foundation and soil is represented by a support stiffness matrix in the bridge analysis model. An example of this methodology is provided in Example 5, where a seismic response spectrum analysis is performed. A separate model of the foundation and soil, often developed using specialized software, is used to determine the values of the stiffness matrix. The two models are thus coupled together at a single point, as depicted in Figure 85. If the behavior of the soil for the loading under consideration is nonlinear, then iterations between the foundation program and the global FEA model are required to arrive at the correct stiffness values, as described at the end of this section.

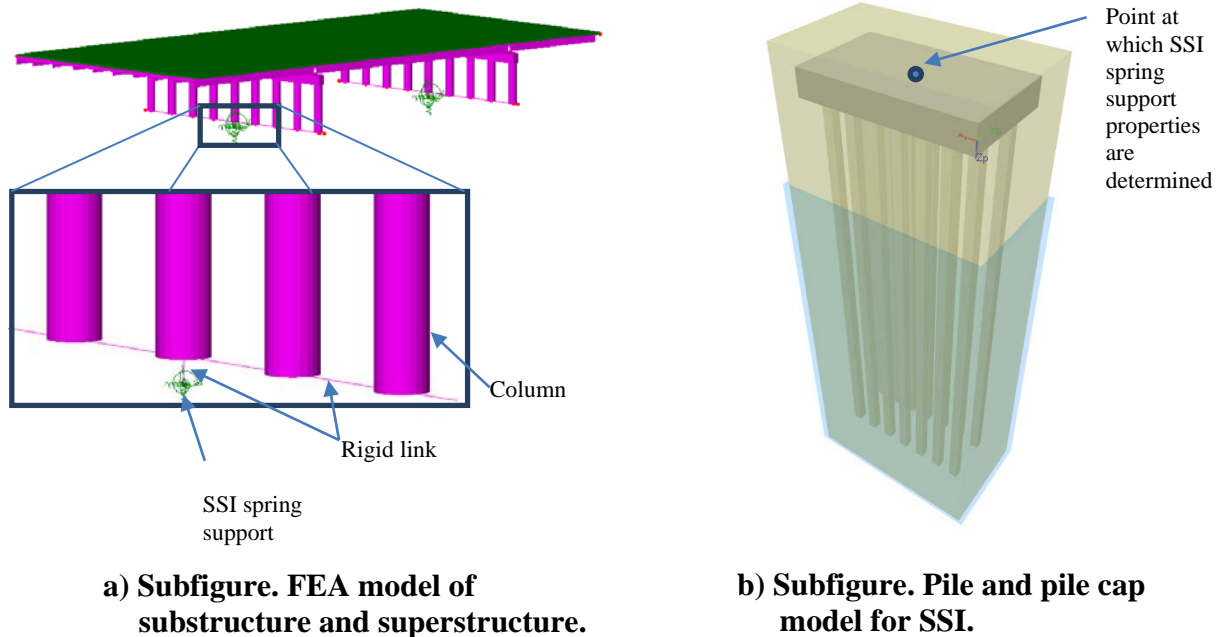


Figure 85. Illustration. Compound figure showing two models coupled at a point to account for SSI effects.

In certain circumstances there can be significant coupling between the six degrees of freedom, a typical example being footings with battered piles. In these cases, when condensing the SSI effects to a single node in the analysis model, the six terms (one for each DOF – Δ_x , Δ_y , Δ_z , θ_x , θ_y , θ_z) which are typically input for the support stiffnesses may not be sufficient to capture the full behavior. To account for the coupling effects, the full 6 x 6 matrix of stiffness values, with off-diagonal terms, should be developed and input into the analysis model of the bridge. Since

FEA programs each have their own methodology, refer to the program's user manual for more information regarding the input of coupled stiffnesses. It is recommended that test cases with simple models be run to ensure the behavior obtained from the coupling element is as expected.

There are three methods typically used to develop a SSI stiffness matrix for use in the FEA program: 1) hand calculate the stiffness of a single deep foundation element, 2) model a single foundation element in specialized software to develop the stiffness of that component, or 3) model the entire foundation in the specialized software. For methods 1 and 2, the total stiffness of the foundation is found by summing the effects of each deep foundation element, while also accounting for any group effects which reduce the total stiffness.

Section 10.6 of (NHI, 2011) or Section 6.2.2.2 of (FHWA, 2006) provide methods for hand calculating the effects of the interaction between soil and piles, but it is more typical to use specialized foundation programs to determine the stiffness values for use in the superstructure/substructure analysis model. Examples of foundation programs include FB-MultiPier, COM624, LPILE, or GROUP (all of which utilize beam on elastic foundation/p-y curve methods) or those similar to DFSAP (which utilizes a strain wedge model, where the pile is assumed to be supported continuously by a wedge of soil).

The foundation analysis programs mentioned above can model deep foundations (or just portions of deep foundations) and have a wide variety of soil models available to represent the site specific soil conditions. The remainder of this section will focus on a discussion of modeling SSI for pile supported foundations using p-y analysis. In a p-y analysis, Winkler springs are placed along the length of the pile to represent the stiffness of the soil.

The curves which relate the soil pressure to pile lateral displacements are referred to as p-y curves, so named for the axes of the plot of load vs. displacement. Example p-y curves are shown in Figure 86 for various depths along the length of a pile, with the p-y curves changing with depth due to the variances in soil type and soil pressure from above. Generally the p-y curves will show increasing stiffness with increased depth, although varying soil conditions along the length of the pile may result in this not being the case.

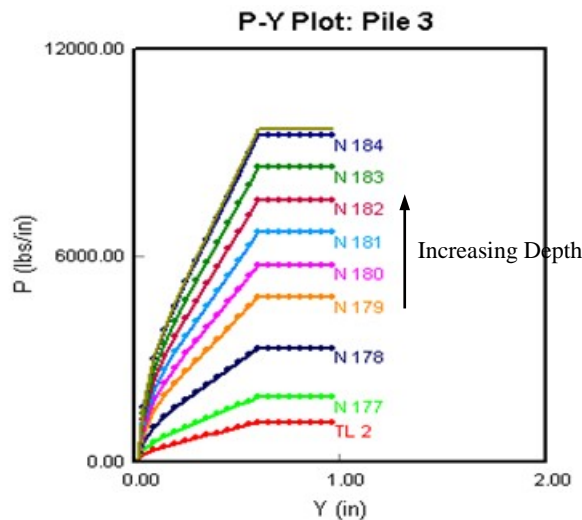


Figure 86. Graph. Example p-y curves at varying depths along the pile.

There are also curves for axial and torsional responses, typically referred to as t-z curves for vertical skin friction, Q-z curves for vertical end bearing, and T- Φ curves for torsional effects. For the most part these curves were originally developed from test data and adjusted based on factors such as pile diameter, depth along the pile, ultimate soil resistance, internal friction angle, and load type (static vs. cyclic).

In typical foundation programs, selecting a soil model and inputting the relevant properties (such as unit weight, friction angle, etc.) results in the generation of the nonlinear response curves for p-y, t-z, Q-z, and T- Φ effects for each pile node. For more information regarding the nonlinear curves used to model the behavior of soil, refer to the foundation program's user manual. When the properties of the soil present are not constant throughout the depth, the soil should be broken up into layers, with each soil layer defined separately in the program. If it is expected that the pile cap will always be embedded in soil, then the effect of the embedded pile cap on the lateral stiffness may be considered.

Along with soil properties, structural dimensions and material properties for the piles need to be input. An assumption regarding the behavior of the connection between the top of the pile and the pile cap should be made based on the detailing present, as described in 5.2.3.1.

Either a single pile or a group of piles can be modeled and analyzed. If a single pile is modeled, then the stiffness matrix for the group will need to be developed from the results. For more information on this procedure, refer to (NHI, 2011) and (FHWA, 2006). Regardless of whether a single pile or the full group of piles is modeled, accounting for the group effects (P-multipliers) based on the spacing between piles is required.

There are several types of SSI stiffness matrices which can be developed when utilizing foundation programs and p-y analysis. The selection of which type is most appropriate to use is dependent on the load levels under investigation and whether or not coupling between DOF needs to be considered.

At load levels which the behavior is expected to be relatively linear, an equivalent linear stiffness matrix can be developed using superposition. In the foundation program, relatively small unit loads or displacements (such that all responses are in the approximately linear elastic range of the p-y and other curves) are applied at the top of the piles in each DOF separately, with the other DOF restrained for each case. The stiffness coefficients along the diagonal of the matrix can then be determined by dividing the applied or induced force effects by the displacement. If there is coupling between DOF while in the linear elastic range of the soil, then off-diagonal terms can be determined by dividing the restraining force by the displacement, resulting in an equivalent linear coupled stiffness matrix.

The 6 x 6 matrix including the cross-coupling terms for lateral displacement and rotation is shown in Figure 87. A table depicting the calculation of stiffness terms is shown in Figure 88.

$$[K] = \begin{bmatrix} K_{11} & 0 & 0 & 0 & K_{15} & 0 \\ 0 & K_{22} & 0 & K_{24} & 0 & 0 \\ 0 & 0 & K_{33} & 0 & 0 & 0 \\ 0 & K_{42} & 0 & K_{44} & 0 & 0 \\ K_{51} & 0 & 0 & 0 & K_{55} & 0 \\ 0 & 0 & 0 & 0 & 0 & K_{66} \end{bmatrix} = \begin{bmatrix} \frac{P_x}{\Delta_x} & 0 & 0 & 0 & \frac{P_{Rx}}{\theta_y} & 0 \\ 0 & \frac{P_y}{\Delta_y} & 0 & \frac{P_{Ry}}{\theta_x} & 0 & 0 \\ 0 & 0 & \frac{P_z}{\Delta_z} & 0 & 0 & 0 \\ 0 & \frac{M_{Rx}}{\Delta_y} & 0 & \frac{M_x}{\theta_x} & 0 & 0 \\ \frac{M_{Ry}}{\Delta_x} & 0 & 0 & 0 & \frac{M_y}{\theta_y} & 0 \\ 0 & 0 & 0 & 0 & 0 & \frac{M_z}{\theta_z} \end{bmatrix}$$

where:

K_{ij} = stiffness terms

x, y = horizontal directions

z = vertical direction

Δ_i = displacement in i direction

θ_i = rotation about i axis

P_i = applied force

M_i = applied moment

PR_i = restraining force

MR_i = restraining moment

Figure 87. Equation. 6 x 6 SSI stiffness matrix.

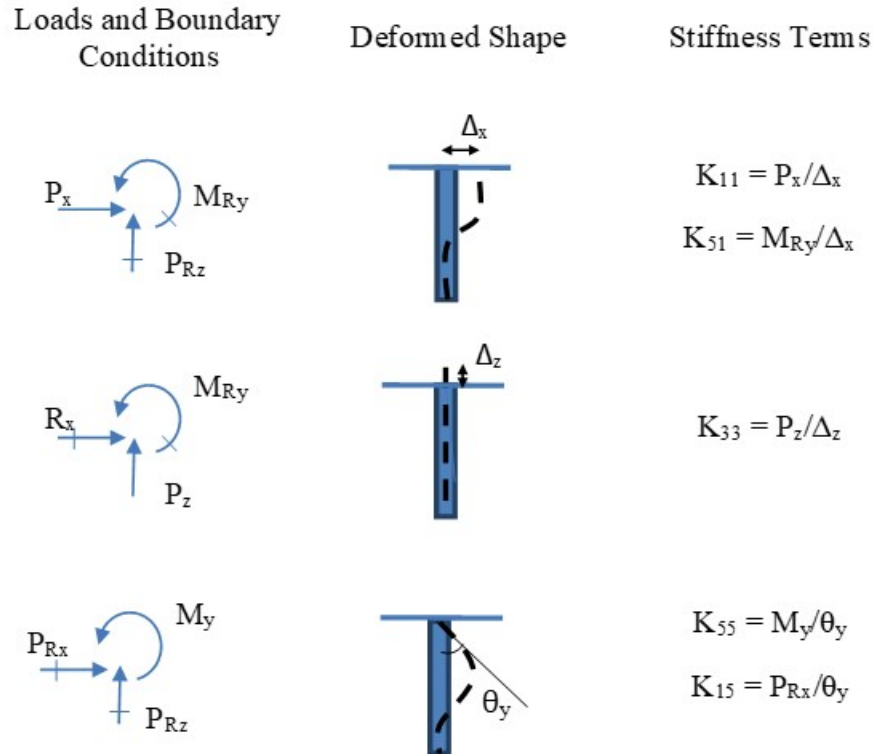


Figure 88. Illustration. Example calculation of stiffness terms for 6 x 6 SSI stiffness matrix.

Note that the matrix should be symmetric, i.e. $K_{15} = K_{51}$ and $K_{24} = K_{42}$. Furthermore, care must be taken to ensure the off-diagonal terms have the proper sign. With the typical right-hand-rule sign convention, displacement in the x direction will result in a $-M_{ry}$ value, and the rotation θ_y will result in a $-P_{rx}$ value. Therefore, the stiffness terms K_{15} and K_{51} should be negative.

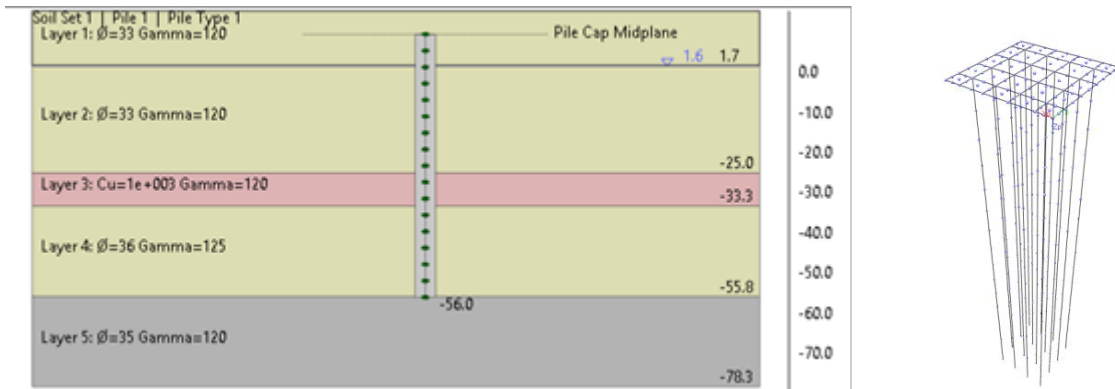
Whether or not the off-diagonal terms are significant for the case being investigated can be determined by running test cases, which may include determining how much the coupling effect changes as the applied loads used to determine the stiffness coefficients are changed, and/or examining how much the global model FEA results change from inclusion or exclusion of the off-diagonal terms.

Care needs to also be taken to ensure that the assumptions in the modeling of the foundation match the behavior under the applied loadings. The superposition method should not be used for cases where nonlinear soil behavior is encountered. In this case, a separate coupled stiffness matrix should be developed for every load case that is being investigated. At the least, the load cases should be broken up into groups with similar magnitudes of loading so that separate sets of stiffnesses can be determined for each group. The coupled stiffness matrices can be developed by applying all of the loads for the load case under consideration simultaneously in the foundation analysis program. The six diagonal terms of the stiffness matrix can then be developed by dividing the applied force by the calculated displacement or rotation. These six diagonal terms will include the cross-coupling effects (i.e. the off-diagonal terms are not needed), which may simplify the input of stiffnesses into the analysis model of the

superstructure. Alternatively, some foundation programs will determine and directly output a 6 x 6 stiffness matrix with off-diagonal terms based on the input loads.

Regardless of the type of stiffness matrix that is used, the point at which the stiffness matrix was extracted or developed from the soil-foundation model needs to be consistent with the location where the stiffness matrix is input in the superstructure/substructure model. Additionally, it must be ensured that consistent units and sign conventions are maintained when using the output from one program for development of inputs into another program.

Figure 89 depicts a graphical representation of some of the inputs for a foundation program, which include the pile type, length, and layout, the pile cap and water table elevations, and the soil properties, including unit weight, friction angle, and others as required by the program. In Figure 89(a), the pile cap can be seen to be embedded in the top soil layer, and the piles extend down through various cohesionless soil layers (Layers 1, 2, and 4) and a cohesive soil layer (Layer 3) until they reach the rock layer (Layer 5). In Figure 89(b), the pile cap, piles, and nodal locations are shown.



(a) Soil layers.

(b) Pile cap and piles.

Figure 89. Illustration. Model developed from inputs into a foundation program.

Figure 90 depicts one manner in which the 6 x 6 stiffness matrix representing the SSI can be input into the superstructure/substructure model. For the program which was utilized to develop the figure, the 6 x 6 stiffness matrix is assigned to the element connecting the fixed support node (fixed in all 6 DOF at the bottom node) to the independent geometrically coincident node at the base of the column. For this example, the stiffness matrix was extracted from the foundation program at the top of the pile cap/bottom of the column. Had the stiffness matrix been extracted from another location in the substructure, rigid links or constraints would need to be used to connect the base of the column to the location of the extracted stiffness matrix.

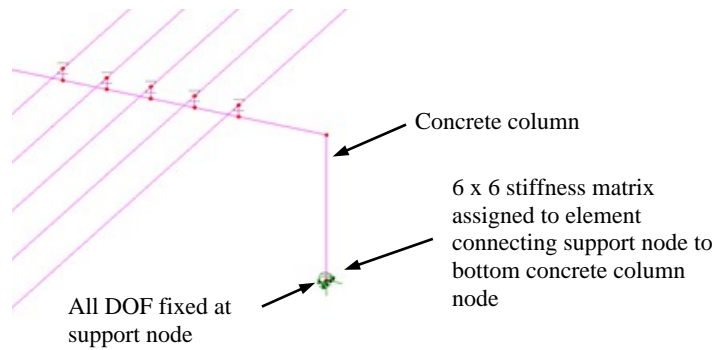


Figure 90. Illustration. Inputting 6 x 6 SSI stiffness matrix into superstructure / substructure model. (Note: The example reflects a specific program. Other programs might require a different methodology.)

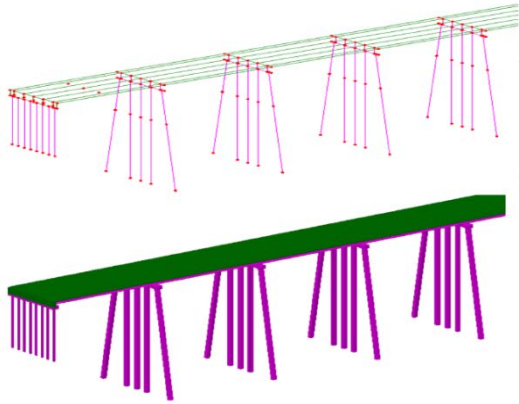
To iterate and determine the correct stiffness values, a procedure as outlined below would be utilized:

1. Estimate demands on foundation
2. Apply demands to foundation model
3. Run foundation model and determine stiffnesses
4. Apply stiffnesses in global FEA model
5. Run global FEA model and determine foundation demands
6. Repeat steps 1-5 until convergence is achieved (change in results \leq roughly 10 percent)

Alternatively, the procedure could start at Step 4 by estimating the stiffness values to use in the global FEA model during the first iteration. Unlike in a seismic analysis, where the loads will depend on the stiffness developed from the foundation's interaction with the soil, for non-seismic analyses the changes in input stiffnesses are not likely to have as dramatic of an impact, and therefore convergence should be achieved quite quickly. However, if this is not the case, then a nonlinear procedure may be more practical, especially if there are many load cases to investigate.

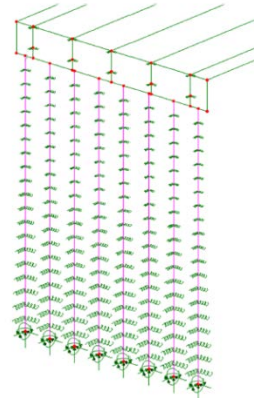
5.2.3.3 Direct Iterative Method

Direct iterative methods involve modeling the foundation elements in the same model as the rest of the bridge structure and utilizing linear springs to model the effects of the soil. Similar to the substructuring iterative method, to correctly capture the nonlinear effects of the soil behavior, iterations are required to obtain the correct support stiffnesses to assign in the model. While initially requiring more effort than the substructuring iterative method, due to having to input the varying spring stiffnesses along the length of the deep foundation elements, this method does not require the continual transfer of information from one model to another while performing the iterations required. This is advantageous when many load cases need to be examined. An example model for an integral abutment bridge is shown in Figure 91.



a) Subfigure. Continuous span integral abutment bridge model

- top: line and shell elements
- bottom: fleshed cross-sections



b) Subfigure. Close-up view of the integral abutment, piles and assigned support conditions.

Figure 91. Illustration. Compound figure example of directly modeling the SSI with the bridge superstructure.

For the structure in Figure 91, the abutment piles are founded on hard rock, and fixed boundary conditions are used at the bottom nodes in the model. Alternatively, springs representing the end bearing behavior, with an equivalent stiffness determined using Q-z curves, could be applied to the bottom nodes if appropriate. All pile nodes other than those at the bottom of the piles have spring stiffnesses assigned in the transverse and longitudinal directions. The stiffness values assigned along the length of the piles vary due to their depth below the top of soil, the soil type present at each node, and due to the displacements found for the load case under consideration. Care must be taken to ensure that the correct stiffness values are assigned based on the tributary length of pile associated with each node. For this example, the detailing at the pile cap is such that fixity is expected, resulting in the connection between the pile and the pile cap being defined as fixed. If piles are only minimally embedded in the cap, then hinges should be placed at the tops of piles.

When modeling friction piles, vertical support stiffnesses determined using t-z curves are assigned to the pile nodes to represent the skin friction behavior. Torsional SSI (represented by T- Φ curves) is not typically influential in these types of analyses and is therefore usually neglected.

Typically a separate foundation program is used to develop the spring stiffness values for use in the global FEA model. Using a foundation program such as those mentioned previously, p-y curves can be developed for nodes at each depth in the FEA model. The p-y curves used to develop the stiffness values should include the group effects (P-multipliers). An initial estimate of the expected displacements can be made for each load case under consideration using the foundation program, and then the spring stiffnesses for use in the global FEA model can be developed using these displacements and the p-y curves. Once convergence is achieved

(changes in response values \leq roughly 10 percent), the results from the FEA model and the foundation program should be compared to ensure similar behaviors are occurring. Small differences may be present due to differences in assumptions in the FEA and foundation programs. An example comparison is shown in Figure 92, where good agreement between the pile lateral displacement (Figure 92(a)) and pile moments is observed (Figure 92(b)).

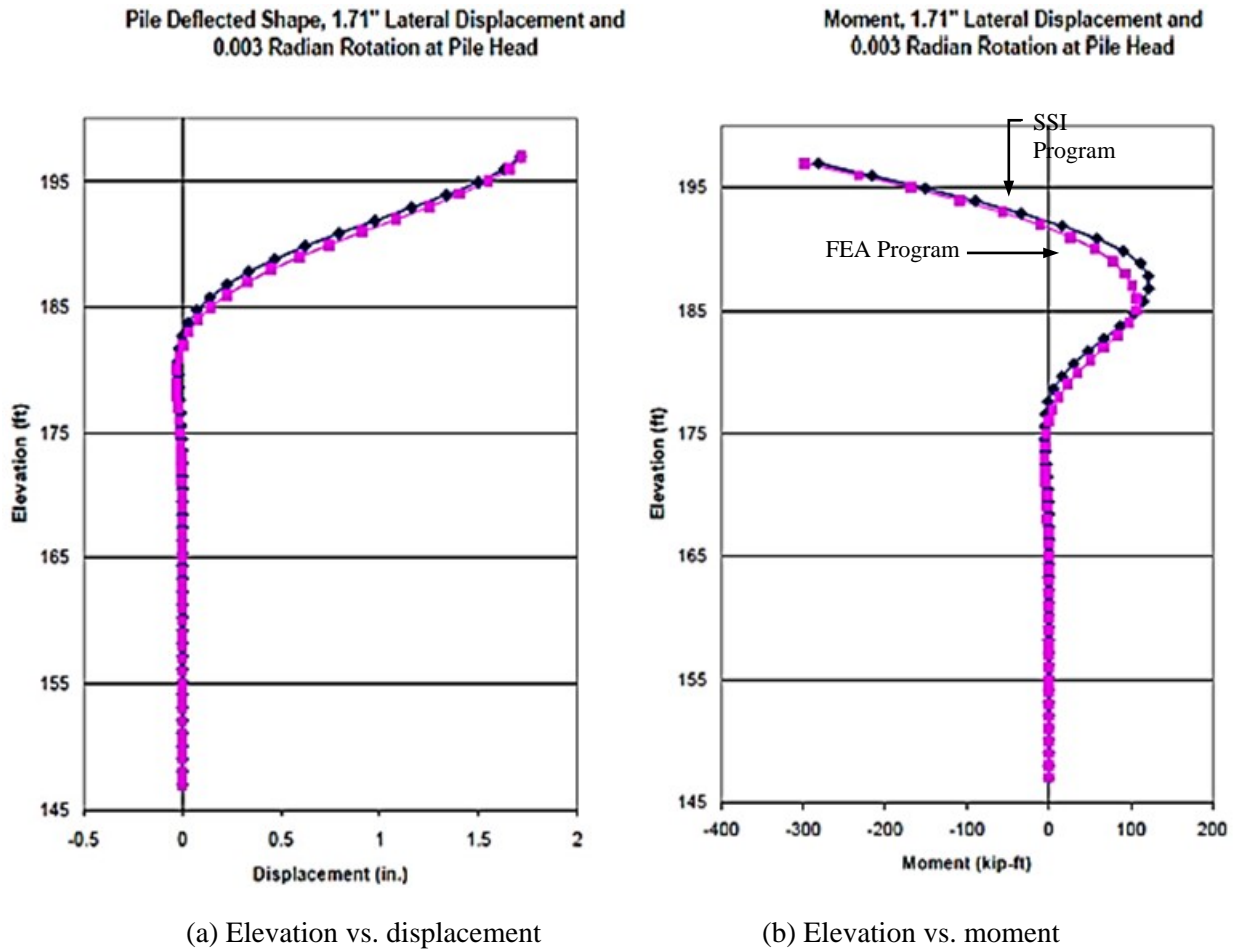


Figure 92. Graphs. Example of comparing pile results of the foundation program used to develop the support spring stiffness values for the FEA model and the results of the FEA model.

Further refinements can be made to the main FEA model and foundation model described above to examine the influence of other potentially key design variables, such as the backwall soil pressure, use of pre-augered holes with selected fill material, or the pile to pile cap fixity.

5.2.3.4 Direct Nonlinear Method

This method is similar to the direct iterative method as described in the preceding section, except that the nonlinear soil effects are accounted for directly by using nonlinear support spring elements and performing a nonlinear analysis. Nonlinear analyses are discussed further in Section 5.3. An example of the use of nonlinear elements to model the desired behavior is shown below in Figure 93. Note that the mesh and the nodes are essentially identical to what

one would use in a direct iterative analysis. The only difference is that nonlinear spring elements with nonlinear stiffness properties are used between pile nodes and fixed support nodes.

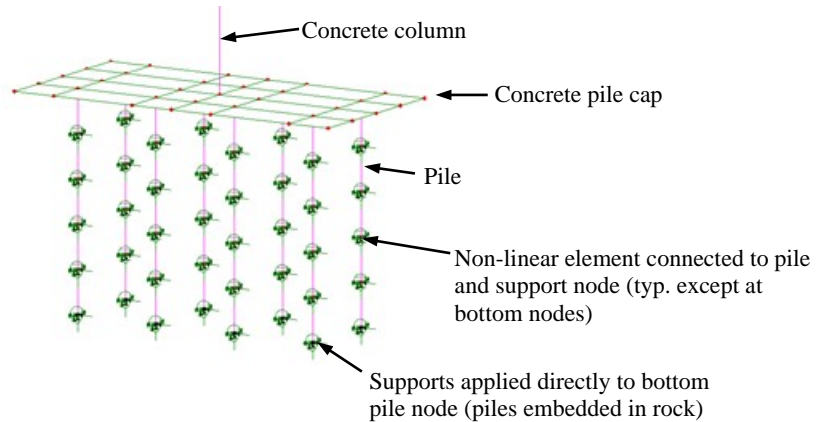


Figure 93. Illustration. Use of joint elements to model nonlinear soil support conditions.

Each soil element needs to be assigned the appropriate p-y curve in the lateral directions, and potentially a t-z curve in the vertical direction to account for skin friction, based on its location along the length of the pile and the soil type/condition. As described in Section 5.2.3, these curves may be developed using a foundation program. Care must be taken to ensure that the supports are close enough together to be able to mimic the continuous support provided by the soil. If necessary, a sensitivity study should be undertaken. As with the iterative method, the results from the FEA should be confirmed by checking against the results from a foundation program.

5.2.4 Summary

In summary, analysis methods for shallow and deep foundations were presented to account for soil structure interaction. The methods for each foundation type were presented in order of their complexity. The following points below are emphasized and should be noted when deciding on a methodology to use.

For all SSI investigations:

- Initial simplified analyses and/or sensitivity analyses are helpful in gaining an understanding of the behavior and determining the amount of non-linearity to expect. This in turn helps with selection of an appropriate SSI analysis methodology, if one is required. In addition, sensitivity analyses can be used to examine which soil parameters most significantly affect the soil-structure interaction response.
- Increases in complexity do not always result in improved accuracy, as the output can only be as good as the input, and assumptions often have to be made when interpreting soil data. Consultation with geotechnical engineers to assist with developing soil properties for use in the analysis is recommended.

For shallow foundations:

- SSI typically does not need to be accounted for, since the use of fixed boundary conditions for vertical and horizontal degrees of freedom and either fixed or free boundary conditions freedom (dependent on the dimensions of the footing) for rotational degrees is sufficient to model the behavior of the structure.
- In situations where SSI does need to be accounted for, often the rigid plate method, as described in Section 6.2.2 of (FHWA, 2006), is appropriate.

For deep foundations:

- The depth to fixity method (Section 5.2.1) provides a simple way to account for the effects of deep foundations. While easy to implement and useful in estimating the effects of SSI on the superstructure and substructure of bridges, the simplifications involved in this method potentially result in significant aspects of the actual soil-structure interaction behavior being neglected. In some circumstances this can produce unconservative results.
- With similar inputs, the other three methods presented in Sections 5.2.2 through 5.2.4 should produce similar results, although with different levels of effort required.
 - Use of the substructuring-iterative method or direct iterative method is recommended when non-linear behavior of the soil is not expected to play a significant role in the behavior of the structure.
 - When significant amounts of soil non-linearity are present or expected, and its effect needs to be accounted for, use of the direct non-linear method is recommended. Note that when used in this circumstance, the amount of effort required may actually be less than if an iterative approach were used. This is due to the large number of analysis iterations which may be required to converge on the correct equivalent elastic stiffnesses and structural response if the response is significantly nonlinear.

5.3 Nonlinear Analyses

For the majority of analyses required in bridge engineering, especially for design of typical slab on girder bridges, a linear elastic analysis is all that is needed. Nonlinear behavior is typically either ignored as insignificant or conservatively accounted for by AASHTO LRFD. Examples where AASHTO LRFD takes nonlinearity into account would be the Whitney stress block for concrete beam capacity or the single step moment magnification equations for column compression. For most bridge designs, little economic advantage can be gained from any material savings that might be achieved by using a more complex nonlinear analysis over a linear analysis. In some cases economies can be realized, for example by confirming the capacity of an existing structural member or system, such that repair or replacement is not required and resources can be directed elsewhere. Care should be exercised when such an analysis is performed, making sure that all Specification considerations are accounted for.

Often nonlinear behavior is associated with complex longer span structures such as suspension bridges and slender arches. Other common bridge design situations where nonlinear analyses may be called for include seismic demands, stability and redundancy evaluations, or forensic studies. In general, nonlinear analyses are recommended when one or more of the assumptions

used in linear analyses (See Section 3.1) are no longer sufficient to accurately depict the structural behavior. As a result, the response deviates from a linear load-dependent relationship *and the analysis solution(s) can no longer be extrapolated or superposed*. Additionally, if the material relationship enters the inelastic range, the structure behavior becomes load history dependent. Typical factors that contribute to the nonlinear response of a bridge include:

- Stresses exceeding the linear limits of inelastic materials, e.g., yielding of metals, crushing of concrete under compression, cracking of concrete under tension
- Nonlinear-elastic material behavior, e.g. hyperelastic materials such as elastomers, commonly used for bearings
- Time-dependent behavior, e.g., creep and shrinkage of concrete
- Large changes in initial geometry, e.g., buckling, cable behavior
- Changing boundary conditions, e.g., friction, lift-off from supports, restrainers

Seismic design is the area where most of the literature/guidelines on nonlinear analyses has been focusing (FHWA, 2014), (Aviram et al., 2008), (FHWA, 2006), (Akkari and Duan, 2000). Although seismic applications are also assessed here, the main focus of this section is to identify additional practical situations in bridge design where a nonlinear analysis might be required. Guidance is provided regarding the assumptions and common modeling techniques needed to perform an efficient analysis with reasonable accuracy. Some simplifications and intrinsic limitations of typically available software are also discussed.

When constructing a nonlinear model, it is strongly recommended that a linear model be initially constructed and run, to ensure there are no problems with geometry, mesh refinement, and connectivity. Once the functioning linear model is constructed, nonlinear behavior can be introduced as required. By gradually adding complexity and checking the model at intermediate steps, sources of error can be narrowed down more easily when troubleshooting problems. Cross-slope, superelevation, and the vertical curve only need be modeled if the eccentricity caused by the geometric variations affect the nonlinear results.

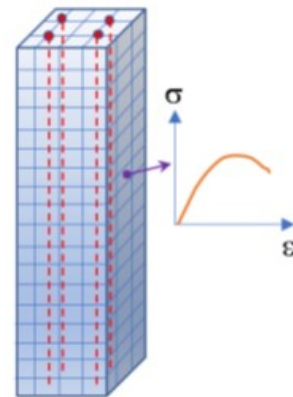
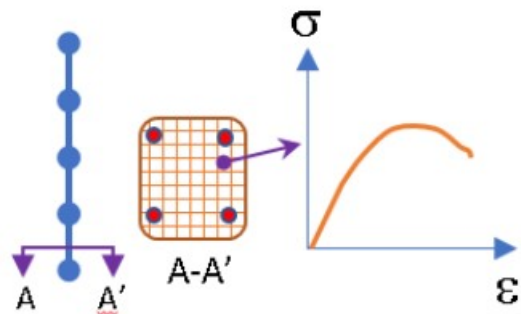
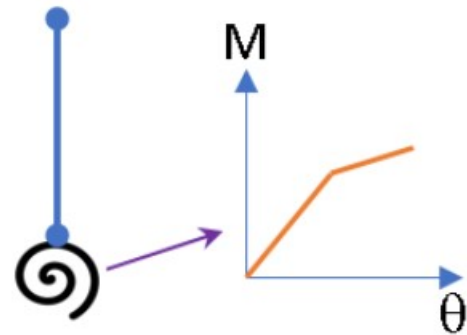
5.3.1 Modeling Levels

When a nonlinear analysis is needed, a finite element analysis is typically the easiest and most efficient method, able to address any geometry and most sources of non-linearity. There are different modeling or analysis approaches that can be followed depending on the desired level of accuracy of the results, which is basically defined by the element type and analysis capabilities of the software, and the specific structural problem to be assessed. Table 5 shows some of the typical modeling levels that can be followed to address a common structural problem involving nonlinear behavior. For nonlinear analyses in general, it is recommended to start with a simple modeling approach and increase the complexity gradually.

Table 5. Examples of different modeling levels for nonlinear analyses.

Problem	Modeling Level	Description
Plastic hinge at base of concrete column	Basic	Line element with an end spring (joint) including a bilinear moment-rotation relationship (2D or 3D).
	Intermediate	Nonlinear line elements with cross section discretization to incorporate the stress-strain relationships of steel and concrete (2D or 3D).
	Advanced	Concrete solid elements with embedded reinforcement line elements, compatible with nonlinear material definitions (3D).

Visualization



Since programs differ in their nonlinear options for analyses, material, and element formulations, it is recommended that program literature be consulted to identify which materials/elements have nonlinear capabilities and their limitations, and how they can be activated during the analysis. Often the manuals include step-by-step practical examples that provide helpful guidance, especially for users without previous experience with nonlinear modeling. Performing tests of the software with easily verified simplified theoretical problems is also recommended.

5.3.2 Sources of Nonlinearities

Sources of nonlinearity are generally classified into three categories: material, geometric and boundary condition (also included in this category is tension/compression only situations). A structure can experience one or a combination of these effects simultaneously. In a program, the definition of nonlinearities is also dependent on the element formulation, which is chosen according to the desired response and level of complexity of the model, as discussed in 5.3.1.

5.3.2.1 Material Nonlinearity

In structural analysis, the material mechanical properties are defined by the relationship between stress and strain. When this relationship is linear, the stress is directly proportional to the strain, and the stiffness or Modulus of Elasticity (E) is a constant. For nonlinear problems, the stiffness varies with the degree of deformation and/or damage experienced by the structure. Programs often add advanced features to the linear definitions of typical materials to incorporate nonlinear behavior into certain robust elements (e.g. plasticity for fiber-based elements). Software packages also have pre-defined nonlinear material models with parameters that the user can easily adjust for particular applications (e.g. CEB/FIP Model Code 90 for creep in concrete). Non-linear behavior may also be included directly in the element formulation without the need of defining a separate material (e.g. specialized joints).

Ideally, the properties utilized in a nonlinear material analysis should be based on test results of the actual materials being used in the structure. Often this is not possible, and reliance on typical presumed representative/conservative values from the literature must be relied upon. It is up to the analyst to ensure that the material properties used in the analysis accurately reflect those in the actual structure.

The following presents a further discussion of these common approaches used to address material nonlinearity in a refined analysis.

5.3.2.1.1 Stress-Strain Relationships

A nonlinear stress-strain curve based on material properties can be defined based on recommendations in the design specifications or information from uniaxial tension/compression tests and can be utilized when the object (e.g. structure, member) is modeled as a continuum (e.g. plane-strain problems), or when the element formulation itself is able to accommodate the continuum behavior of the material (e.g. fiber-based elements).

The *fiber-based* approach is a technique for addressing material nonlinear behavior in a line (e.g. beam) or surface (e.g. shell) element. In this approach, the element cross section is divided internally into multiple sub elements (fibers for line elements or layers for surface elements, see Figure 94), each one having an independent stress-strain behavior according to the nonlinear definition of the material but complying with the strain compatibility of the element cross section assuming that plane sections remain plane after loading effects. Most programs do not include shear behavior in the stress-strain response of the fiber deformations and assume that shear stresses remain linear. The fiber forces are summed up to get the cross section internal forces (i.e. axial force and moment) used in design.

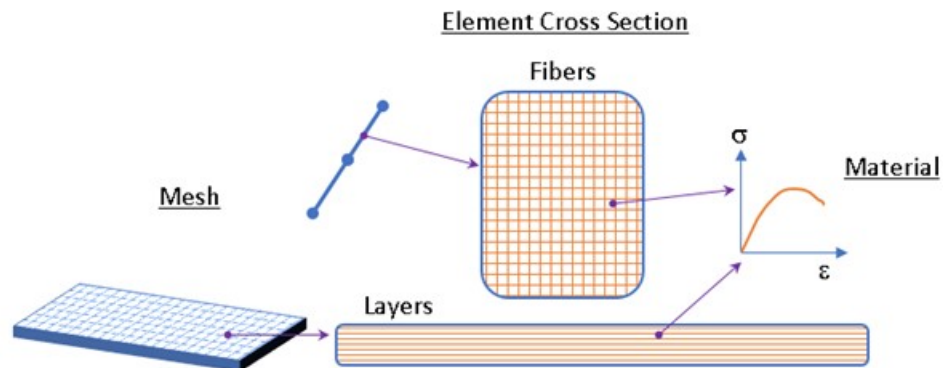


Figure 94. Illustration. Fiber-based modeling approach for line and surface elements.

Examples of typical materials used in bridge construction with nonlinear characteristics are:

- **Steel:** The stress-strain relationship of steel is typical of a ductile material characterized by similar behavior under tensile or compression stresses. It has a constant modulus of elasticity of about 29,000 ksi below the elastic limit, and the yield strength and strain hardening varies according to the chemical composition, heat treatment and forming processes as illustrated in Figure 95 for different structural steels. The typical stress-strain relationship of reinforcing steel is illustrated in Figure 96. With the use of stainless steel increasing in bridges, it should be noted that the stress-strain behavior of stainless steel differs from that of carbon steel. As illustrated in Figure 97, carbon steel exhibits linear elastic behavior up to the yield stress and a plateau before strain hardening, while stainless steel has a more rounded response with no well-defined yield stress. Stainless steel “yield” strength is generally defined by the 0.2 percent strain offset. In the absence of specific test information, the values shown in Table 6 are recommended for seismic design (FHWA 2014, Raynor et al. 2002). Figure 98 shows the stress-strain curves for prestressing strands according to (AASHTO, 2011).

For metals, ductile behavior is based on plasticity theory characterized mainly by negligible volumetric change when the elastic limit of the stress-strain curve is exceeded (i.e. incompressible material). Yielding in ductile materials is often defined in terms of the Maximum Distortional Energy theory commonly referred to as the von Mises Criterion. In this theory, yielding in a multiaxial stress state occurs when the energy of distortion reaches the corresponding value from a uniaxial tension test. Another common and more conservative failure criterion is Tresca, which is based on the maximum Shear Stress instead of the Distortional Energy.

In most practical cases, modeling the steel as a bilinear material is sufficient, but it is recommended that some nominal post-yield stiffness be included to aid in convergence and avoid multiple equilibrium positions for a given load. A kinematic hardening rule is recommended for ductile materials under small strains and reversal loading, while isotropic hardening is applicable for monotonic loads or larger strain problems (see Figure 99). For problems that require addressing post-ultimate behavior, some programs

allow the definition of the full stress-strain curve of the steel, including the unloading portion. In such cases, the user manual should be consulted to define the solution strategy and avoid numerical issues (See Section 5.3.3 for further details regarding the numerical solution).

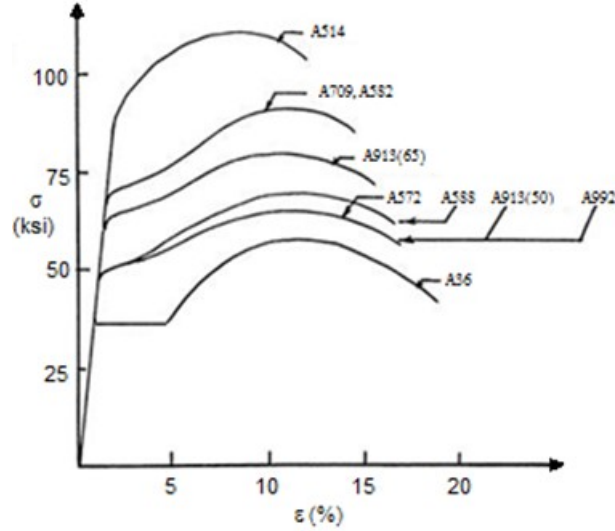


Figure 95. Illustration. Representative stress-strain behavior of various typical structural steels (adapted from AASHTO, 2011).

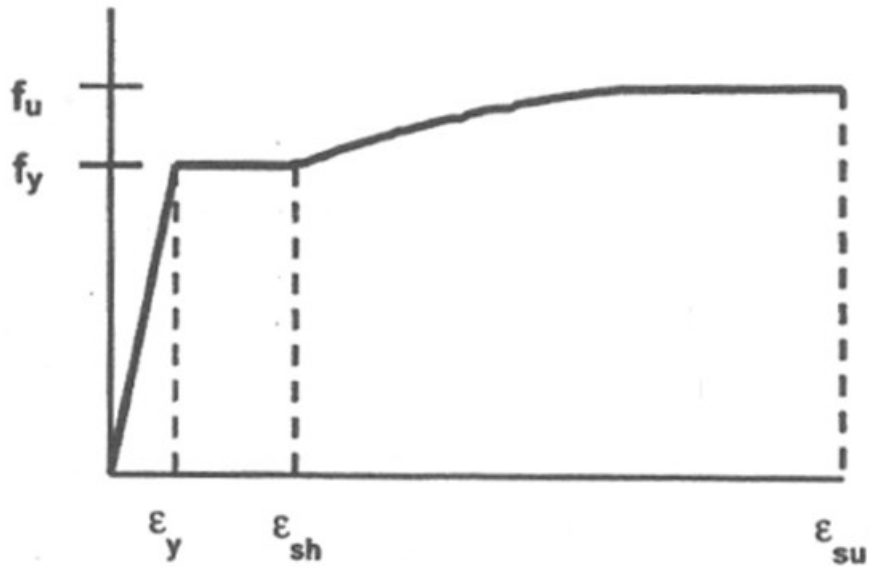


Figure 96. Illustration. Typical tensile stress-strain relationship of reinforcing steel (adapted from AASHTO, 2011).

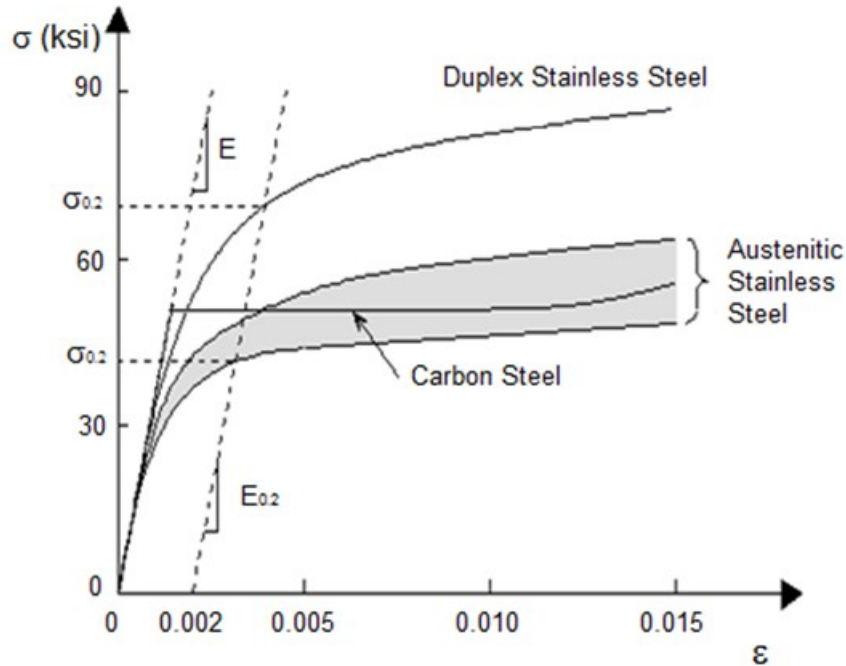


Figure 97. Illustration. Typical tensile stress-strain relationship of stainless compared to carbon steel (adapted from BSSA, 2018).

Table 6. Recommended Values for Parameters of the Stress-Strain Relationship of Reinforcing Steel (FHWA, 2014).

Property	Notation	Bar Size	ASTM A706	ASTM A615 Grade 60
Specified minimum yield stress (ksi)	f_y	#3 - #18	60	60
Expected yield stress (ksi)	f_{ye}	#3 - #18	68	68
Expected tensile strength (ksi)	f_{ue}	#3 - #18	95	95
Expected yield strain	f_{ye}	#3 - #18	0.0023	0.0023
Onset of strain hardening	ϵ_{sh}	#3 - #8	0.0150	0.0150
		#9	0.0125	0.0125
		#10 & #11	0.0115	0.0115
		#14	0.0075	0.0075
		#18	0.0050	0.0050
Reduced ultimate tensile strain	ϵ_{su}^R	#4 - #10	0.090	0.060
		#11 - #19	0.060	0.040
Ultimate tensile strain	ϵ_{su}	#4 - #10	0.120	0.090
		#11 - #19	0.090	0.060

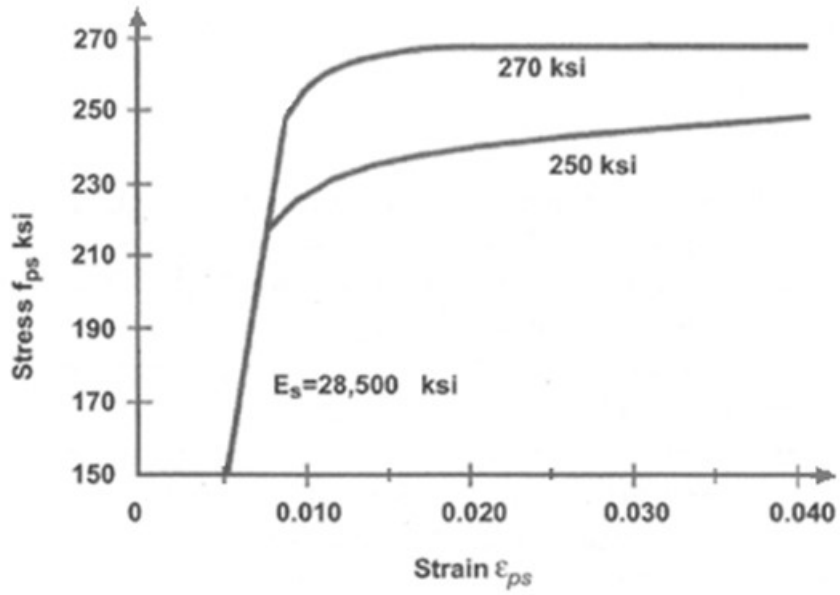


Figure 98. Illustration. Typical tensile stress-strain relationship of prestressing strand (adapted from AASHTO, 2011).

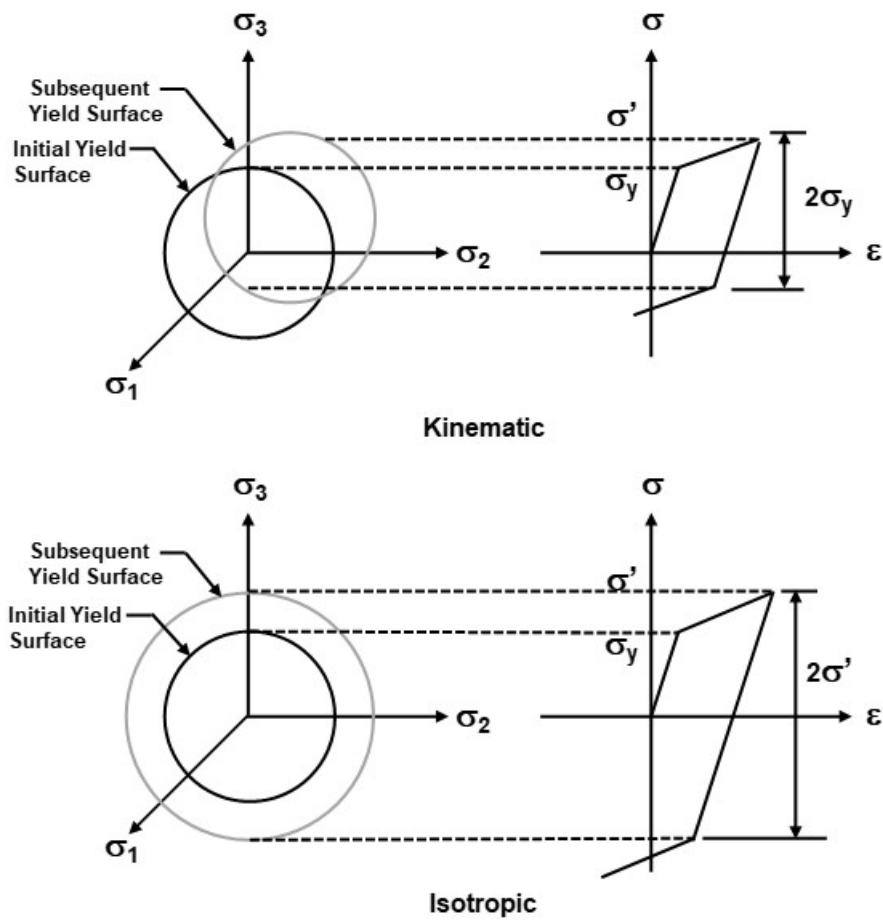


Figure 99. Illustration. Hardening Rules for Metals (adapted from ANSYS, 2010).

- Concrete: Concrete is a complex material that responds differently under tensile and compressive stresses. A typical inelastic concrete stress-strain curve is illustrated in Figure 100. Although the linear elastic portion of the curve is limited, using line elements with linear elastic concrete material properties and an effective member moment of inertia to approximate the tangent stiffness, is sufficient for most analyses. When the stiffness varies too much to “linearize” using a tangent modulus, a nonlinear material approach is recommended.

Most advanced software packages handle concrete behavior with a plasticity-based stress-strain relationship that covers a tension softening zone, to account for cracking including reinforcement effects, and a compressive crushing capacity in terms of the maximum strength, σ_{cu} . Failure criteria in these advanced models are often defined as a function of damage variables that represent the loss or degradation of stiffness in the material.

Several nonlinear material models have been proposed to describe the response of concrete. For seismic evaluation of frame structures, the constitutive relationship developed by Mander et al. (1988a, 1988b) has gained recognition due to its capability to directly address confined and unconfined conditions in columns. The differing behavior of confined versus unconfined concrete is illustrated in Figure 101. Additional guidance on Mander’s concrete material models is provided in Mander et al. (1998) and Priestley et al. (1996).

Care should be exercised when taking advantage of the advanced parameters of complex concrete material models. Material variables that are unfamiliar to the typical design engineer, such as dilatancy, may be utilized in the models. In these cases, programs usually set default values for the parameters that describe the inelastic behavior of a typical concrete, and their range limits and assumptions for applicability are generally included in the documentation of the program. It is recommended to work with these default values unless a very particular problem is assessed. As previously recommended, consulting the program user manual and verifying behavior in simple models prior to attempting to analyze more complex models is always a good practice.

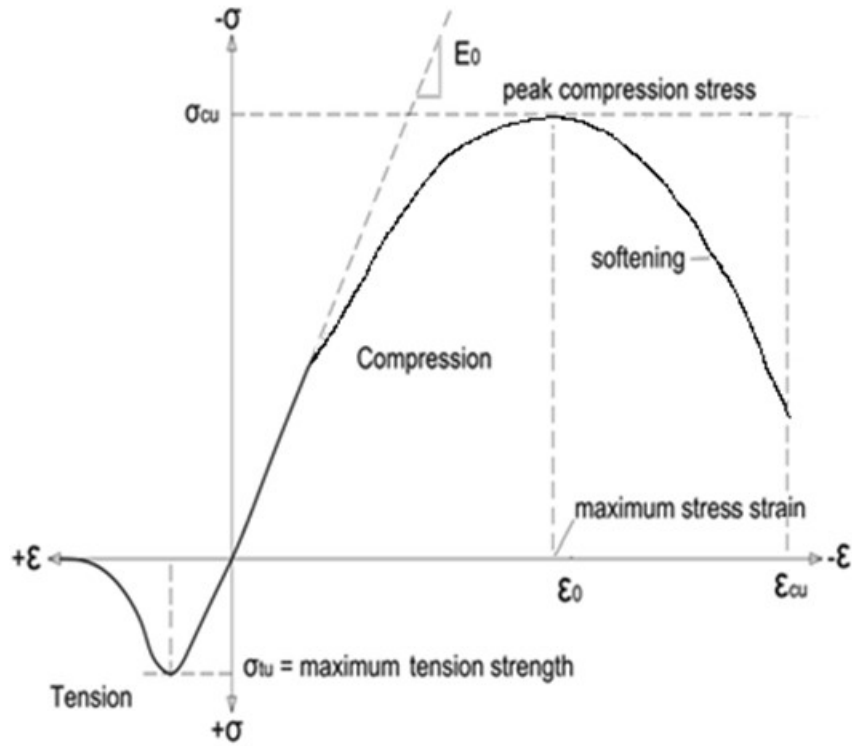


Figure 100. Illustration. Typical concrete stress-strain curve, including tension and compression portions (adapted from Vercher, 2015).

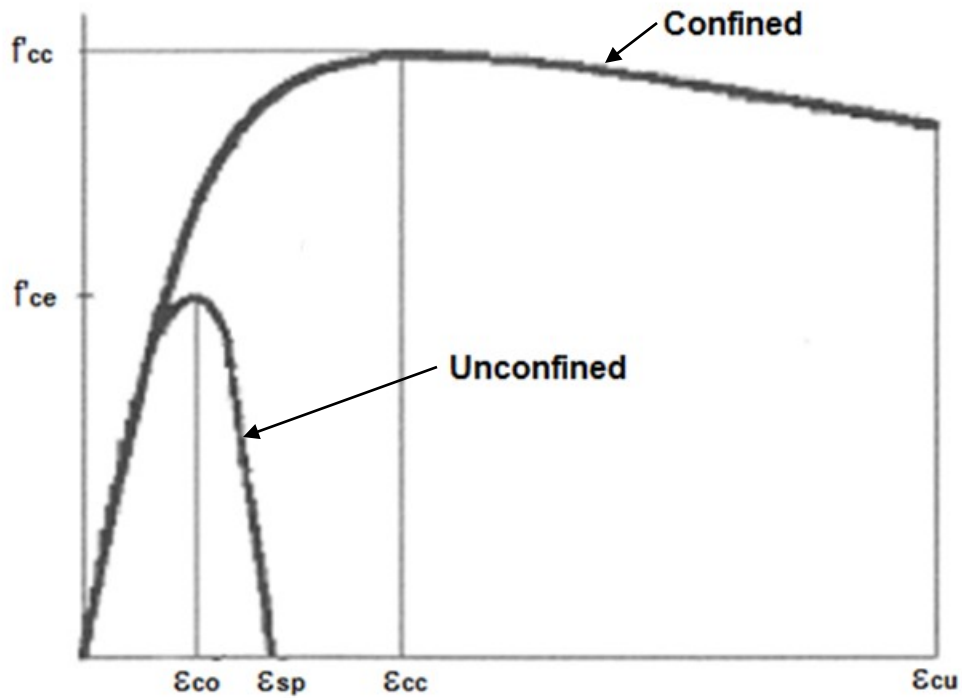


Figure 101. Illustration. Confined and Unconfined Concrete Stress-Strain Relationships (adapted from AASHTO, 2011).

- Soil: This is another example of a material with complex behavior. In structural analysis, it is often assumed that the structures are rigidly supported at the foundation level and that the stiffnesses of the underlying soil and foundation do not significantly affect the superstructure response. However, for certain structural evaluations that require accuracy in the estimation of the responses (especially displacements), the analysis needs to include the effects of the soil-structure interaction, as discussed in Section 5.2. The soil effects can be introduced into the model using several techniques ranging from simplified nonlinear joints to continuum elements with complex nonlinear models. The selection depends on the structure to be modeled and the target responses (e.g., a 3D bridge with foundation springs vs. a 2D culvert with surrounding continuum soil).

5.3.2.1.2 Nonlinear Joints

Use of nonlinear joints is a simplified technique commonly used in structural modeling to introduce material nonlinearity into models with simplified line or surface elements. The nonlinear behavior of the joints is directly defined in terms of an internal force-effect relationship, e.g. moment/rotation or force/deformation. The discrete location of the joints is explicitly defined (or modeled) by the user which requires insight into the problem. Typical applications include: indeterminate structure mechanism analyses (i.e. plastic hinges), partially restrained connections, bearings, and soil-structure interaction. Further description of some of these applications are presented next.

- Plastic Hinges: Historically, plastic hinges have been used in piecewise linear analyses to calculate the mechanism load for indeterminate structures in plastic design. A mechanism analysis to find ultimate capacity can be easily run using joint elements with the simplest and most conservative relationship of an elastic-perfectly plastic curve, neglecting strain hardening, as illustrated in Figure 102 for a moment-curvature relationship. Although the implementation of this approach is relatively straightforward, the discrete joints need to be located at the positions where hinging action is expected to occur in the structure. It is recommended that an initial linear analysis be performed to identify the critical locations where the maximum stresses are exhibited, particularly when these locations are not evident.

Current implementations of these types of joints can be more sophisticated, with the post-yield, ultimate and failure behavior directly included in the nonlinear function of the joint. This permits analysis of not only the mechanism load, but the displacement capacity and post-ultimate behavior as well, including softening due to hysteresis in some cases. Performing such analyses requires knowledge of the member properties, such that the discrete hinge behavior can be programmed to approximate the behavior of the member. Values that might be utilized include yield capacity, ultimate capacity, residual capacity, and rotation limit (beyond which capacity equals zero).

Since rotations are the most common source of inelastic behavior in frame structures, a plastic hinge is usually defined as a discrete nonlinear rotational spring at a particular cross section along a column or beam. In addition to uncoupled moment, torsion, axial force and shear hinges may also be available. Coupled axial force moment hinges which

yield based on the interaction of axial force and/or bi-axial bending moments at the hinge location may also be available. Coupled hinges are appropriate when significant axial force as well as bending is present, typically in columns.

Member bending deformation is generally expressed as a function of moment and curvature. When curvature is used as the independent variable of the nonlinear curve, a definition of the hinge length (i.e. spread of plasticity) is required over which the curvature is integrated to get the corresponding member rotations and deflections. Using a zero-length hinge can be thought of as a simplification of the cross-sectional fiber analysis described at the beginning of this section. That is, if the integrated moment across the section is expressed as a function of the corresponding linear strain slope (i.e. curvature) from a fiber-based approach, the resultant graph could be utilized in a more simplified model using a nonlinear joint.

A similar situation applies when the axial force (or shear) is defined in terms of strains. For steel sections, hinge rotation capacity is typically controlled by the local stability of the cross-section. Characteristic length of plastic hinges for compact steel sections can be taken as the smaller of 1/8 of the clear height of a column or 1.5 times the member depth. For concrete sections, these lengths are dependent on the dimensions and reinforcing. Guidelines for choosing characteristic length for concrete members are provided in FEMA 356 - Prestandard and Commentary for the Seismic Rehabilitation of Buildings (ASCE, 2000) and for concrete and steel members in AASHTO Guide Specifications for LRFD Seismic Bridge Design, 2nd Edition (AASHTO, 2011).

For programs that allow the definition of coupled internal forces for nonlinear joints, the most common case is the axial force-biaxial moment interaction. The interaction equations can be developed for the particular section using the fiber-based approach that accounts for the stress-strain curves of the materials combined with the equilibrium and strain compatibility equations. For practical applications, common approximate methods included in AASHTO LRFD such as Bresler's Reciprocal Load Equation for concrete members, or the Load Contour Method for steel sections, can be used to create the yielding surfaces.

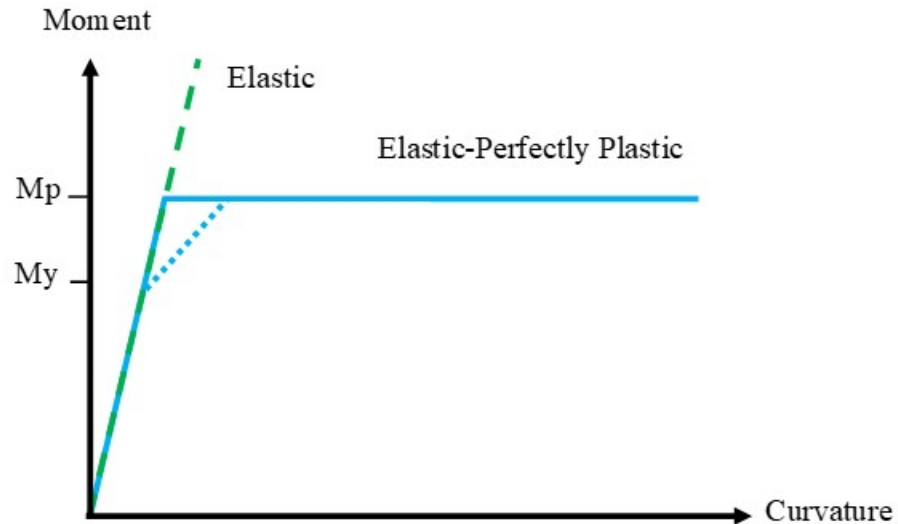


Figure 102. Illustration. Idealized elastic plastic moment curvature curve.

- Elastomeric bearings: Although most nonlinear material behavior is also inelastic, there may be rare cases when an elastic nonlinear material is needed for an analysis. Rubber, an elastomer, is in a class of materials known as hyperelastic. These materials are characterized by the elastic nonlinear behavior illustrated in Figure 103.

The most common application of this material in bridges is elastomeric bearings and seismic isolators. Often the nonlinear elastic behavior of the bearings can be sufficiently approximated by linear elastic behavior in the range that the materials see under typical bridge loadings. When more accurate behavior is required outside of that range, usually under seismic demands, it is recommended to model the global behavior of the connection with joint elements instead of explicitly modeling the bearing itself. In that case, a bilinear force-displacement relationship, as shown in Figure 104, is suggested by the guidelines for Seismic Isolation Design (AASHTO, 2010) to represent the bearing behavior. Those Specifications also recommend performing refined nonlinear analyses for very flexible structures (Effective Periods > 3s) and when the damping ratio of the isolation system exceeds 30 percent.

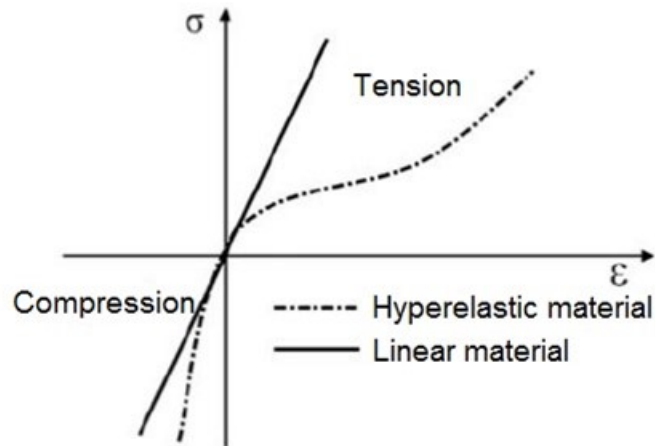


Figure 103. Illustration. Example of nonlinear elastic material behavior.

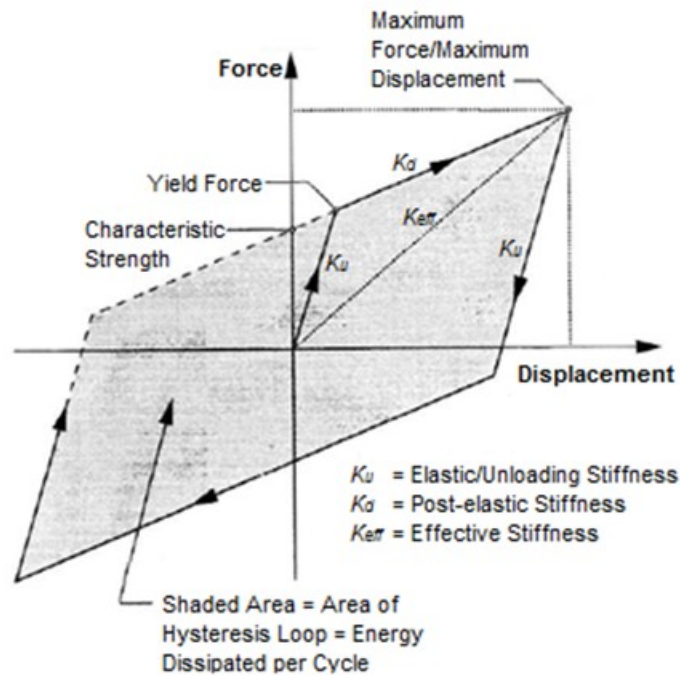


Figure 104. Illustration. Force-displacement relationship of a typical isolation bearing (adapted from AASHTO, 2010).

5.3.2.1.3 Time-Dependent Effects

Material time-dependent effects such as creep, shrinkage, aging of concrete, and relaxation of steel can also be assessed with nonlinear analyses. Programs that can model these effects will generally include specialized materials specifically for that purpose. Modeling of these effects is discussed in Section 4.1.2.

5.3.2.2 *Geometric Nonlinearity*

A geometric nonlinear analysis considers the equilibrium of the structure and its components in their deformed or deflected geometry. This is required when the applied loads and/or generated displacements are large enough to induce additional internal forces as a result of the eccentricities between the final and original geometry of the structure (also known as second order effects). Most structures with typical loading scenarios do not require this type of advanced analysis, since the resultant displacements are so small that the secondary effects are negligible or can be conservatively accounted for by the approximate moment amplification factors recommended by the specifications. However, a refined analysis may be preferred in order to get more accurate estimates of the demands, or may be required when large displacements fall outside the range limits of the approximate methods in the specifications.

A small-strain deformation theory is usually sufficient to characterize most of the structural situations in bridges where geometric nonlinearities are exhibited. Although large displacements and rotations may be experienced by slender members (e.g. cables, arches, thin plates), the strains continue to be within the small range (<5 percent). Large strains are found in very few cases and are often related to material nonlinearities, such as in rubber members or metal forming. It is very rare that a large strain analysis would be required in bridge engineering practice.

5.3.2.2.1 Main Aspects of Geometric Nonlinear Analyses for Bridges

When a member in a structure experiences large compressive forces (e.g. columns, piers) and is also subject to transverse displacements caused by either lateral (with respect to the member) or eccentric loads, fabrication imperfections, or even construction tolerances, a detrimental softening effect occurs in the force-displacement relationship, due to the eccentricity between the actual position of the applied loads and the deformed geometry. This is illustrated in Figure 105. This softening effect can be accounted for by using a geometric term in the stiffness matrix of the analysis, which is a function of the axial load of the element. An analog situation is observed in tensile members (e.g. cables, arch ties) which exhibit a beneficial stiffening effect with increasing tensile force. In an analysis using the geometric stiffness matrix formulation, a set of loads is applied to the model, the program determines the geometric stiffness matrix based on those applied loads, combines it with the normal stiffness matrix, and solves for the displacements.

With this formulation, it is possible to solve for the bifurcation (buckling) load by the use of an eigenvalue solution, which determines the factor on the geometric stiffness matrix resulting in a zero stiffness in the structure. This is termed an eigenvalue buckling analysis, and is very useful in finding bifurcation loads. As above, a set of loads is applied to the model, resulting in the calculation of the geometric stiffness matrix. An eigenvalue solution is then applied to determine the factor on the applied loading that will result in an instability. The eigenvalue is the factor applied to the loading to find the buckling load, and the eigenvector is the buckled shape.

These analyses are relatively easy to perform, and normally are sufficient when investigating a buckling behavior. However, they do have limitations that need to be understood. Because an eigenvalue solution is essentially a linear problem, other sources of nonlinear behavior such as material and boundary conditions, are not accounted for. Additionally, these solutions work best

when the behavior is closest to a sharp bifurcation. Problems where large displacements occur prior to reaching the buckling load are not good candidates for this type of analysis. The classic example is a snap-through buckling of a shallow arch. In this instance, the flat arch is very sensitive to small displacements, and an eigenvalue solution will not correctly capture the structural behavior.

The alternative to an eigenvalue buckling analysis is an iterative large displacement analysis which tracks the load-deflection behavior of the structure by updating the stiffness matrix at each load increment. This type of analysis is able to include all sources of nonlinearity, and model even the most complex structural behavior. However, it is generally time intensive, and requires post-processing in order to obtain the results of interest.

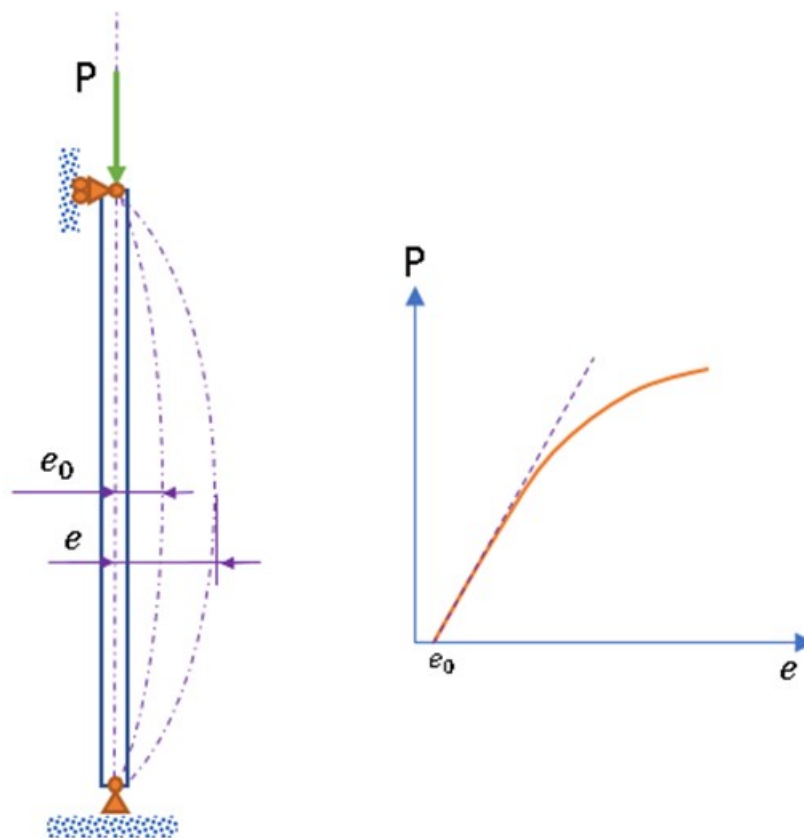


Figure 105. Illustration. Stiffness softening effect due to initial eccentricities in a compressive member.

In practice, the treatment of geometrically nonlinear behavior has been classified in the building field differently if it involves the relative lateral displacement of floors of a building, as opposed to localized displacements of a column between floors. In terms of general structural behavior, this can cause significant confusion, as the effect described is the same: additional moment due to the deflections. The two terms will be discussed herein, as several software packages utilize this terminology.

If the structural compressive member is subject to a relative end lateral displacement (Δ) produced by the global deformation of the structural system, additional overturning moments are generated along the member. This global behavior is commonly referred to as “P- Δ ,” as illustrated in Figure 106 for a cantilever short column under axial (P) and lateral (H) loads. The more the column deforms laterally as a result of the horizontal force, the larger the moment is at the base due to the additional bending produced by the vertical load. This behavior is typical of columns in unbraced frames, including single column bents, where the lateral displacement is either unrestrained or just partially restrained due to the coupled lateral stiffness action of other members such as the deck system.

To account for P- Δ effects in a refined model with line elements (e.g. beams, frames), at least one element needs to be defined between locations where the lateral displacements are expected to be significant, for example, at lateral concentrated forces or where important inertial force effects are developed (i.e. large tributary mass). The common practice of defining one element per level is usually enough to capture the global P- Δ effects from a frame structure. Examples of loading sources inducing lateral movements, Δ , in bridges include: earthquakes, wind, temperature and centrifugal effects.

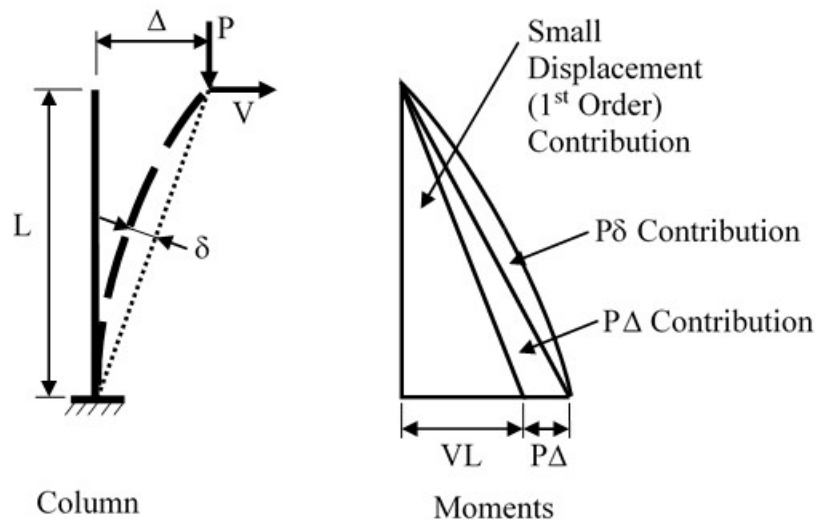


Figure 106. Illustration. Global and local P-Delta effect.

An application of the P- Δ concept is found in stability evaluations. For steel frame buildings, AISC uses the concept of “notional loads” to incorporate the initial out-of-straightness “ Δ ” effects in the structure under gravity load combinations (Griffis, L. and White, D., 2013). These are small lateral loads, proportional to the gravity loads in the load combination, such that the resultant deformed profile represents an initial global imperfect geometry from which second-

order effects are calculated. In modeling bridges, a similar method could be utilized if the notional loads that result in the appropriate deformed geometry are determined. In the absence of such notional loads, initial out-of-straightness can be modeled directly, based on maximum permissible fabrication and erection tolerances (see Section 5.3.2.2.2).

A compressive member can also experience local deflections (δ) along its length, as illustrated in Figure 106, which are a function of the internal moments along the length of the member. Compression members that are subject to lateral deformations, Δ , often develop internal moments, and thus need to account for the P- δ effects as well. This can either be handled separately, by the amplification of the internal moments using a moment magnification equation, or directly in the analysis through consideration of geometrically nonlinear effects. For such an analysis, including additional nodes along the length of the member is usually sufficient. A mesh refinement study is always recommended to ensure that the local effects along the member are accounted for within satisfactory tolerances (e.g. force changes of less than 5 percent between two mesh refinement levels). Running benchmark analyses as described in Section 6.2 can provide a feel for needed mesh refinement.

For the analysis of classic suspension bridges, the very large tension force in the cables acts to stiffen the bridge, leading to lower deflections and reduced bending demands of the stiffening truss or girder. Each different loading case on a bridge will result in a different value for the tension force in the cable, and thus requires its own nonlinear solution. In practice, many suspension bridges are so dead load dominated, that the variation in cable force due to live load is relatively small. For these cases, the stiffness can be considered constant based on the dead load tension only, and typical live load optimization methods that assume linear behavior can be applied. The stiffness is thus considered “linearized” about the dead load state. This is also the method typically used to find modal frequencies and shapes for these bridges.

For the analysis of cable stayed bridges, there are two main sources of geometrically nonlinear behavior: cable sag and deck compression. In the case of cable sag, the effect of gravity pulling down on the cable tends to decrease the stiffness. In cables with small sag values ($<1/600$, Podolny and Scalzi, 1986), the flexibility introduced by the cable weight can be neglected. These are typically cables oriented mostly vertically, or relatively short cables. In other cases, i.e long, more horizontally oriented cables, AASHTO LRFD recommends a modified modulus of elasticity, E_{MOD} (Eqns. 4.6.3.7-1 and -2), to account for this effect. These are known as the Ernst equations. When the force in a cable does not vary significantly, the use of this modified modulus along with a single element modeling the cable length is typically adequate. A single value for the cable stiffness is used for multiple loadings. However, if the load on the cable, and therefore the sag, changes significantly, then other methods should be used.

Some programs include specialized nonlinear cable elements that account for the sag and tension-stiffening effect of the cable. For cases where the tension in the cables is reduced and sag becomes significant, e.g. $\text{sag} > L/600$ (Podolny & Scalzi 1986), a large-displacement analysis with multiple nonlinear elements per cable could be more effective. *Experience has indicated that in these situations, a minimum of four elements per cable are sufficient when regular nonlinear beam elements are used in lieu of a specialized cable formulation, which would only require one element.*

Even though very large compressive loads develop in the deck of a cable stayed bridge, the stiffness provided by the stays typically limits the magnitude of the compression induced loss of bending stiffness in the deck. For most analyses of the final configuration of typical cable stayed bridges, consideration of this nonlinear behavior is not required. However, for analyzing more extreme conditions, such as loss of a cable, or behavior of the bridge during erection, this nonlinear behavior may become significant.

5.3.2.2.2 Requirements for an Advanced Geometric Nonlinear Analysis

A more advanced geometric nonlinear approach is recommended for members prone to exhibit large displacements and rotations under loads. This includes very slender compressive members and some cable structures. A large-displacement analysis is also recommended when a post-failure analysis needs to be conducted to identify alternative loading paths in the structure, such as in a redundancy analysis for a fracture critical member. Since this local behavior depends on a highly deformed geometry, there needs to be a sufficiently refined mesh (number of elements) in areas of significant deformation to accurately capture the corresponding change in geometry and to keep the incremental rotations small within the elements, which is a requirement in some nonlinear geometric formulations, e.g. within force increments of an Updated Lagrangian formulation. In any case, the user must verify that the elements in the model not only support nonlinear geometric capabilities but also large-displacement behavior.

Arches without a tie member (e.g. true arches) are a clear example of where the global vertical in-plane $P-\delta$ effects are significant. Although bending amplification due to live loads in these arches is addressed in AASHTO LRFD, a refined approach may be recommended to account for the stiffness of the deck. This could represent economical savings in the design of a new arch or increase the capacity for the rating of an existing structure.

For suspension bridges, AASHTO LRFD requires use of a large-displacement analysis due to the large change in geometry of the main cable as the live loads are applied to the structure. One element (cable or nonlinear beam) is generally sufficient to model the main cable between hangers and the hangers themselves.

When investigating buckling behavior, performing at least one large-displacement analysis for a load combination of interest related with unstable postbuckling behavior is recommended, which may not necessarily be controlling for design. For example, in a deck arch, the controlling buckling mode typically corresponds to an asymmetric loading condition, but for the out-of-plane mode, a full deck loading becomes more critical. The resultant critical loads are compared with the forces from a linear eigenbuckling analysis to identify if initial deformations affect the stability of the member. For specific buckling modes that involve sudden changes in geometry, such as snap-through of shallow arches, a large-displacement analysis is required with a displacement-control method defined for the solution. For more guidance on stability, see Section 8.2.10.

In general, a large-displacement analysis requires more computational effort to get a solution when compared to a small-deflection analysis due to the need to capture higher deformations with smaller load increments. This is only accomplished by defining smaller force (or displacement) increments and tighter solution tolerances. It is important to remember that when performing a nonlinear analysis for a particular loading combination, all loads need to be

simultaneously applied in the proportion dictated by the combination since superposition is not valid.

5.3.2.2.3 Inelastic Behavior

For most slender members that undergo geometric nonlinearity, the strains are so small that nonlinear material properties are typically not required. However, at the strength limit level of intermediate members (i.e. not slender, not short), inelastic material behavior often occurs accompanied by second order effects. If both nonlinearities are considered in the model, the displacements will be more pronounced resulting in larger moments.

Steel beam-column members are particularly susceptible to experience both inelastic and second order effects due to their capacity to sustain large forces with relatively small cross sections. However, since the nominal compressive resistance equations for steel members included in AASHTO LRFD already account for the effects from residual stresses during the rolling process and an initial out-of-straightness of the member of $L/1500$ (δ), the material inelasticity and initial geometric imperfections should not be included in the structural analysis for design purposes. What needs to be considered for design is the additional geometric P- Δ , or P- δ effects when δ is significant (e.g. arches under live load). There are basically two ways to account for these second order effects in steel members, as mentioned previously:

- Apply the code amplification factors to the first-order elastic moments, or
- Use directly the second-order moments from a geometric nonlinear (but elastic) analysis.

Additionally, the compression-flexure interaction equations for steel members have been calibrated to give a close but conservative estimate of the capacity of the member when the amplification factors are used. For a complete discussion about how AASHTO LRFD handles the axial-flexure loading interaction in steel beam-column members, the reader is referred to White (2015).

For concrete beam-column members, the need to account for the interaction of inelastic and geometric nonlinear effects is less frequent due to the lower levels of slenderness exhibited by these members. AASHTO LRFD recommends an effective reduced stiffness (Eqns. 5.7.4.3-1 and -2) to compute the buckling load utilized in the amplification factor equations. Initial unintended eccentricities are accounted for with a reduction factor (0.8 or 0.85 for tie or spiral transverse reinforcement) applied to the nominal axial resistance of the concrete beam-column member.

For forensic studies or performance-based evaluations (e.g. displacement-controlled seismic analyses), where the objective is to replicate a failure mode, all sources of nonlinearity should be included in the analysis in order to get a reliable approximation of the behavior of the structure. Some stability methods (e.g. Direct Analysis Method by AISC) specify stiffness reduction factors instead of completely modeling the material inelasticity to account for additional deformations (see Appendix 1 of AISC, 2016). The Direct Analysis Method works well modeling progressive plastic hinge formation.

5.3.2.3 *Boundary Condition and Tension/Compression Only Nonlinearity*

Boundary condition and tension/compression only nonlinearities are easy to identify physically but may be difficult to implement in a model. These nonlinearities can be present within the structure or only at supports. Some of the common situations that fall within this category are:

- Lift-off at bearings
- Opening and closing of expansion joints
- Pounding of adjacent structures
- Behavior of seismic isolation bearings
- Friction between sliding surfaces, including stick-slip
- Behavior of cable restrainers
- Behavior of tension only members such as bracing or counters

For less advanced programs, some of these effects can be modeled using multiple linear elastic analyses, such as removing supports with negative reactions and rerunning to model lift-off at bearings. Using such techniques can become onerous when moving loads are considered, however.

More advanced programs usually handle this nonlinearity by adding fictitious elements such as joints or spring lines/surfaces between the boundaries that undergo or are prone to have contact. The behavior of these elements is characterized by a nonlinear curve where gaps and changes of stiffness at a determined level of displacement can be defined, as described in Section 5.3.2.1b. Some programs have specific elements for some of these situations, such as tension only or compression only elements. Consult the program user guide to determine capabilities.

5.3.3 *Aspects of the Numerical Solution*

Nonlinear static analyses typically require an iterative solution technique (e.g. standard or modified Newton-Raphson) which converges on the correct answer. The “correct” answer is the one that satisfies the conditions of equilibrium, compatibility, and material stress-strain relationships. Software typically applies convergence criteria to determine when to stop iterating, when the answer is within predefined numerical tolerances that result in insignificant changes between iterations. The degree of convergence is important, as the final state of the model for a given increment is used as the starting point for the next increment.

5.3.3.1 *Incremental Methods*

The first step in performing an iterative analysis is choosing a reasonable load/displacement increment. Smaller increments can lead to faster convergence, while larger increments can reduce overall computation time. Increments can be varied, such as large increments used initially, and then smaller increments later for more nonlinear portions of the analysis. Small increments can sometimes be used to traverse a particularly difficult to converge portion of an analysis. Some programs can adjust increments automatically, based on convergence in the previous step.

The default iterative solution procedures in FEA programs typically iterate at a constant applied load level, that is, the load level is incremented and the program seeks a displacement solution at each new level. This means that for a constant force increment a unique displacement solution is

assumed to be found (see Figure 107). Convergence difficulties arise when this approach is used to solve limit load problems, where the load-displacement curve exhibits local maximums or minimums. This can occur due to the model reaching its limit of resistance due to a combination of material and/or geometric nonlinearity. “Snap-through” buckling of shallow structures is one class of problem of this nature. In these cases, it is recommended that an arc-length solution procedure be employed, and some programs will automatically switch to such a solution procedure under such scenarios. Arc length methods provide an additional constraint on the solution process that allows the applied load to vary during the iterations, thus allowing the navigation of limit loads in the solution (see Figure 108). Displacement-control methods are one class of arc length methods.

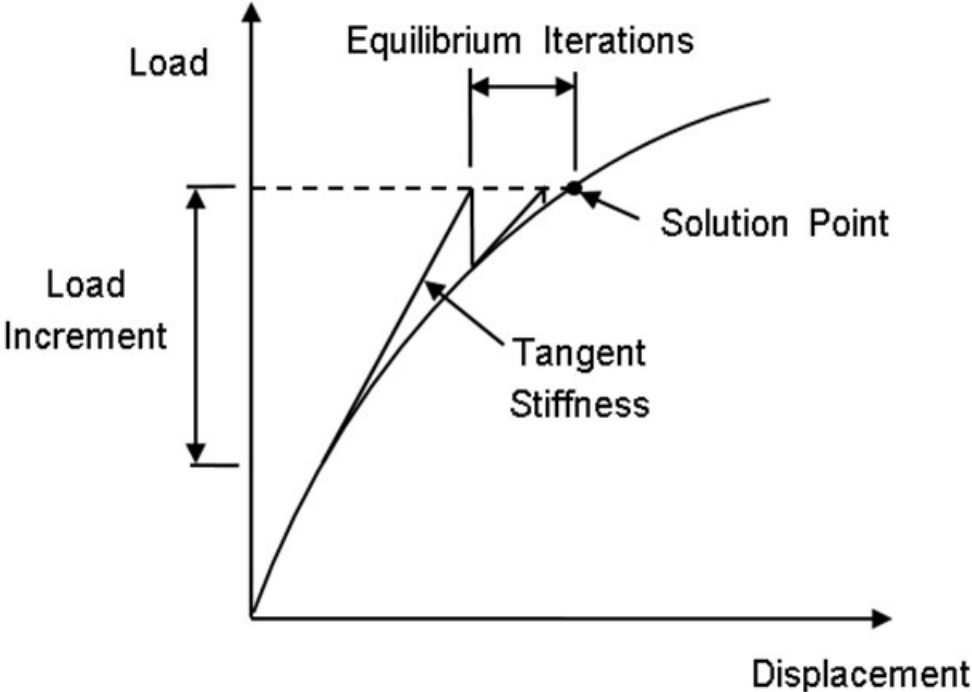


Figure 107. Graph. Iterative method of converging on incremental solution using a constant load level.

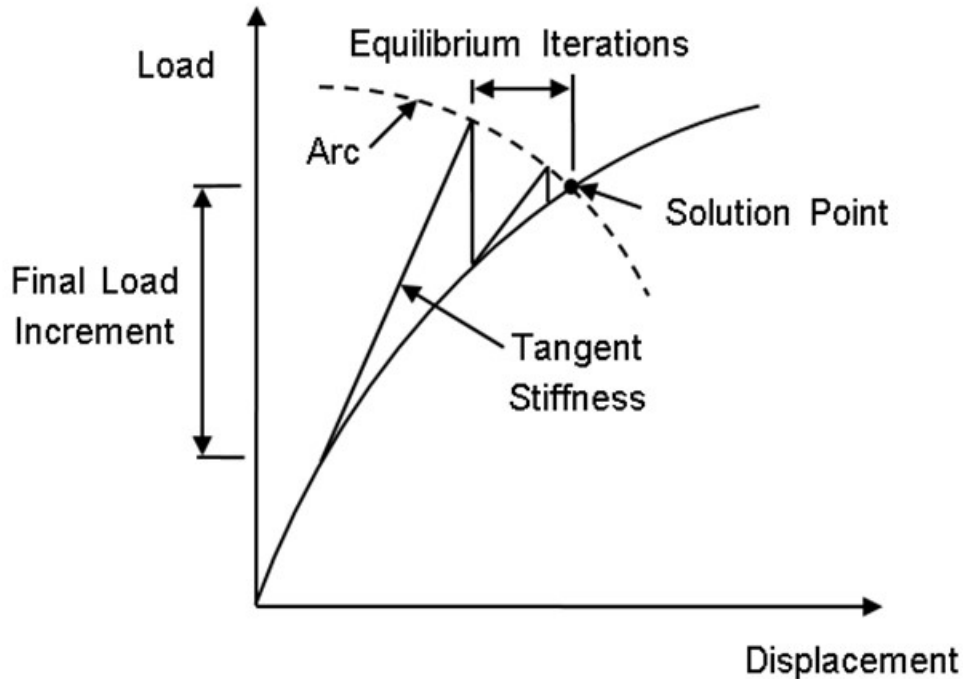


Figure 108. Graph. Iterative method of converging on incremental solution using arc-length.

One of the most common problems with nonlinear solutions is nonconverging increments. In addition to the aforementioned zero stiffness issue, other numerical issues such as small or zero load increments can also result in nonconvergence. There are several strategies that can be effective in getting a troublesome model to converge on a solution, including:

- Use of imposed displacements rather than loads.
- Reducing the increment at the portion of the solution where the model is having trouble converging.
- Slightly adjusting stiffness properties to avoid horizontal portions of load-deflection curve solutions, such as providing for some nominal strain hardening in steel properties.
- Adjusting program solution technique, and/or convergence criteria (usually defined in terms of allowable residual forces, displacements, and/or work compared to the “exact” equilibrium solution).

For user adjustable convergence criteria, a program user manual will often provide advice on the range recommended for a given criteria, from “tight” to “loose.” Assigning “tight” criteria will result in a more accurate answer, but may require more iterations and smaller increments to achieve convergence. “Loose” criteria achieve convergence more quickly for a given increment, but the answer may not be as accurate, and may make it more difficult to converge the following increment. There can be a large number of user adjustable variables in an iterative solution technique and associated convergence criteria.

It can take significant time and effort on the engineer’s part to coax a program into convergence to the correct solution of a nonlinear problem, especially when several different types of nonlinear behavior are present. A thorough understanding of the software’s particular solution

methodology is recommended, and even then substantial time may be required with various tries with different solution parameters to obtain convergence in some problems. If the program provides for it, examining the results, such as the deflected shape, for the unconverged analysis increment can often provide clues as to how to address the problem. It is also useful to perform an eigenvalue analysis and look for odd modal shapes that can reveal the location of the issue.

Some programs may only be able to solve problems with positive slope of the load deflection curve, or increasing loading. For programs such as these, identifying the point at which the program cannot converge on a solution can be sufficient in determining a maximum load for which the model is stable. Other programs may be able to solve for decreasing load portions, and provide unloading curves such as post-buckling behavior as well.

Not all physical behaviors resulting in nonlinear responses need be assessed using an iterative analysis. Some computer programs have the capability to “linearize” certain problems by applying either numerical techniques or simplifying assumptions that allow obtaining a more efficient solution. In frame analysis problems for example, a classic simplified geometric nonlinear problem occurs when the axial forces in the structural members do not change significantly during loading, such as gravity forces in robust piers or bents under lateral forces with small displacements. In that case, the contribution to the geometric stiffness matrix, K_g , from the stiffness terms associated with the lateral loads are negligible, and only the terms corresponding to the axial forces are used to create K_g without the need of iterations (Wilson, 2002). Therefore, in similar situations, it is convenient to run a concatenated analysis where the initial step corresponds to the “Gravity + Notional” Loads including the nonlinear geometric effects followed by the transient lateral loads which are analyzed linearly with the modified stiffness.

5.3.3.2 Numerical Solvers

There are two basic types of solvers in FEA software: direct and iterative. It should be noted that an iterative *analysis* should not be confused with an iterative *solver* as discussed next.

Direct solvers are based on the Gaussian elimination method, where for each load case, X equations are used to solve for X unknowns, where X corresponds to the number of degrees of freedom. Although they are stable and applicable to any type of analysis, these solvers become computationally expensive when dealing with complex models with large numbers of DOF. However, several optimization methods have been developed to reduce the computational time of the solution. A direct solver is generally recommended for most practical structural problems, especially those dealing with nonlinear behavior.

Conversely, iterative solvers find an approximate solution using an iterative process that minimizes errors through a convergence criterion, requiring less computational storage. Care must be taken when using iterative solvers with less than favorably conditioned models because the solution provided may diverge from the real behavior of the structure. The key to a good iterative solver is a good preconditioner that results in a better conditioned problem. The problem typically should be positive definite resulting in a unique solution. Iterative solvers are generally recommended for linear analyses of very large well-conditioned models. For more on the specifics of iterative solvers consult the documentation of the program being utilized.

5.3.4 General Recommendations for Nonlinear Analyses

- Elements: Nonlinear analyses often utilize specialized elements different than the typical ones used in linear elastic analyses. Elements with nonlinear material or large-deflection capabilities may need to be used depending on the problem to be modeled.
- Mesh: Although the mesh refinement is a key aspect in the accuracy of any finite-element analysis, it is essential in the evaluation of nonlinear behaviors where large displacements or rotations are exhibited along the members (e.g. P- δ behavior).
- Materials: Start with linear material models, especially when other nonlinearities are included in the analysis, to have as a baseline for comparisons when the nonlinear materials are introduced. For the nonlinear materials, verify in the program manual the ranges where the input parameters are valid and vary them accordingly.
- Increments: Use smaller increments and/or a displacement-based approach if convergence issues arise during the analysis.
- Convergence: Adjust the convergence criteria limits following the program manual recommendations to prevent loss of accuracy in the results.
- Solver: Use a direct solver for nonlinear analysis.

5.4 Dynamic Analyses

Per Article 4.7 of AASHTO LRFD, dynamic analysis may be required to investigate wind or vehicle induced vibrations, the effects of seismic loads, or the effects of blast loads. Dynamic analyses may also be appropriate for investigating vehicle impact or behavior of structures subject to vessel or vehicle collisions. Of these types of problems, seismic analyses are encountered most frequently and therefore will be a focus in many of the following discussions. Additionally, Example 5 describes a multi-mode response spectrum seismic analysis. Although seismic loads tend to be longer duration than the pulse loads of other dynamic effects, much of the information provided in reference to seismic analysis is also applicable to other types of dynamic analysis problems.

Dynamic analyses can be broken into two broad categories: modal analyses and direct integration analyses. For modal analyses, the behavior of the structure is determined by adding together the response of the structure's individual vibration modes. This can be done in the frequency domain, as with a response spectrum analysis, or in the time domain, with a modal time history analysis. For this approach, the frequencies and mode shapes of the structure must first be found through an eigenvalue analysis, and then combined to determine the structure's response.

The direct integration approach, also called a time-stepping analysis, solves the global dynamic equations of motion at each time step. This method is able to account for numerous sources of nonlinearity, and is most commonly used for nonlinear time history analyses.

5.4.1 General Information

The equations for static and dynamic equilibrium may be written generally as Equations (27) and (28), respectively.

$$\text{Static:} \quad [K]\{u\} = \{P\} \quad (27)$$

$$\text{Dynamic:} \quad [M]\{\ddot{u}(t)\} + [C]\{\dot{u}(t)\} + [K]\{u(t)\} = \{P(t)\} \quad (28)$$

where: M = mass matrix;

C = damping matrix;

K = stiffness matrix;

P = vector of loads;

\ddot{u} , \dot{u} , and u , = vectors of acceleration, velocity, and displacement, respectively; and

(t) indicates that the vectors are a function of time.

The dynamic equation above indicates that the characteristics of the load, mass, stiffness, and damping of the structure all influence how significant the dynamic effects are to the overall response of a structure. For some transient loads such as live load and wind load, adjustment factors to account for the dynamic portion of a structure's response have been developed, and therefore a static analysis is sufficient to determine the response of the structure and member force effects. However, for cases involving these or other loading types where the interaction between the loads, mass, damping, and stiffness characteristics of the structure result in complex dynamic behaviors, a full dynamic analysis is warranted.

To determine the dynamic structural response, the equations for dynamic equilibrium are solved using modal analysis, step-by-step direct integration, or sometimes a combination of the two. These will be discussed further in subsequent sections when examining two types of dynamic analysis: response spectrum analysis and time-history analysis.

5.4.2 Modeling for Dynamic Analyses

To carry out a dynamic analysis the mass, damping, and stiffness of the structure all need to be modeled, unlike a linear static analysis which only requires the correct modeling of the stiffness of the structure. The following sections discuss the modeling of each of these parameters as well as the issue of model size as it relates to solving dynamic analyses and post-processing results.

5.4.2.1 Modeling Mass

Finite element analysis uses one of two methods, or sometimes a combination of the two, to develop the mass matrix for the structure. In the lumped mass formulation, the mass matrix is formed by assuming that all of the mass is located at the nodes, and the resulting mass matrix is diagonal. Conversely, a consistent mass matrix is developed by assuming that mass is distributed throughout the elements, resulting in a symmetric matrix with off diagonal terms.

The method implemented is dependent on the software and the element type being used, and can have an effect on the results. Therefore, the engineer should be aware of the formulation being used in their software, and the influence it may have. For instance, if a lumped mass matrix is utilized, it is populated only along the diagonal and is easily inverted, resulting in computational advantages. However, additional elements may be required to better distribute the mass in the model and more accurately capture the dynamic behavior, which increases the computational effort. In general, use of consistent mass matrices tends to bound the structure's natural frequencies from above, while the opposite is typically true for lumped mass matrices. Use of consistent mass matrices is more accurate for flexural type problems, while lumped mass matrices are more accurate for wave propagation problems, such as analysis of blast or impact

loadings (Cook, 2002). This is due to the lumped masses resulting in fewer spurious oscillations, and also has the added benefit of being less computationally intensive than use of a non-diagonal consistent mass matrix.

In a static analysis, a combination of applied loadings and gravity (body force) can be used to represent the dead load of the structure. Typically the weight of the modeled components are accounted for by assigning proper material mass densities and specifying the gravitational acceleration, while the weight of non-modeled components (i.e. components which are typically considered to not contribute to the stiffness of the structure, such as wearing surfaces, barriers, and utilities) are accounted for by applying point, line or surface loads.

For dynamic analyses, the use of loads to account for mass is not appropriate. Instead, all mass must be explicitly defined such that when gravity is assigned, the full weight of the structure, with the correct distribution of weight, is present. Therefore, the mass of components which are not explicitly modeled needs to be included. Additionally, it should be ensured that elements used in the model which are not a part of the actual structure (such as rigid links between members) are assigned a negligible mass density.

In finite element programs there are typically several ways to account for the mass of components which are not modeled. Two methods are outlined below and examples are given for the 3D deck truss model shown in Figure 109.

- (1) Use point, line, or area masses.

Example: Assign a point mass at each joint to represent the mass of the gusset plates

- (2) Develop an equivalent mass density which accounts for the non-structural components to assign to a nearby modeled structural component.

Example: Assign an equivalent mass density to the deck which accounts for the mass of the wearing surface:

$$\rho_{eq} = (t_{deck} \rho_{conc} + t_{ws} \rho_{ws}) / t_{deck}$$

where: ρ_{eq} = equivalent mass density;
 t_{deck} = deck thickness;
 ρ_{conc} = concrete mass density;
 t_{ws} = wearing surface thickness; and
 ρ_{ws} = wearing surface mass density.

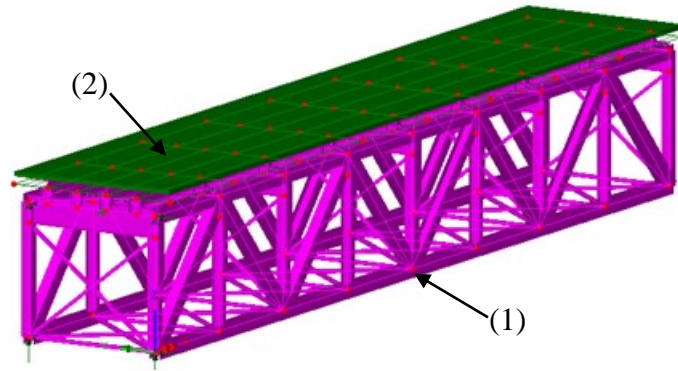


Figure 109. Illustration. 3D deck truss model with non-structural masses modeled.

Regardless of the methodology used, the total weight of the structure should always be verified. Checking the weight versus a previous version of the analysis model which utilized typical material densities and applied loads to account for the weight of non-modeled components is recommended.

In addition to accurately modeling the total mass, the distribution of mass and how it interacts with the structure must also be modeled correctly. Mass moment of inertia is a value describing the body's resistance to angular acceleration under an applied torque. Therefore, it is the angular equivalent of mass, i.e.:

For linear motion: $F = ma$

For rotational motion: $T = I_m \alpha$

where:

F = force;

m = mass;

a = acceleration;

T = torque;

I_m = mass moment of inertia; and

α = angular acceleration.

The mass moment of inertia depends on the spatial distribution of the mass about an axis. Refer to a standard dynamics textbook, for example (Beer, et al., 2016), for the equations of the mass moment of inertias for various shapes. While the total mass may be easily accounted for in an analysis model, unless care is taken the mass moment of inertia may not accurately represent the actual structure.

The torsional response of most typical bridges is not critical to the overall dynamic behavior. However, for sharply curved bridges there can be significant vertical and lateral coupling with the torsional response of the bridge. Additionally, in aeroelastic evaluations the torsional response is very important, and it is critical that the mass moment of inertia is properly modeled.

As an example, consider the curved bridge being modeled as a spine beam shown in Figure 110. An equivalent mass density can be assigned to the spine elements to account for the full mass of the superstructure, however the software program may assume that all of the mass is located along the beam elements or at the nodal locations (depending on the use of a consistent or lumped mass matrix). As a result of neglecting the fact that there is mass that is eccentric to the beam line, the dynamic torsional response of the structure will not be correct.

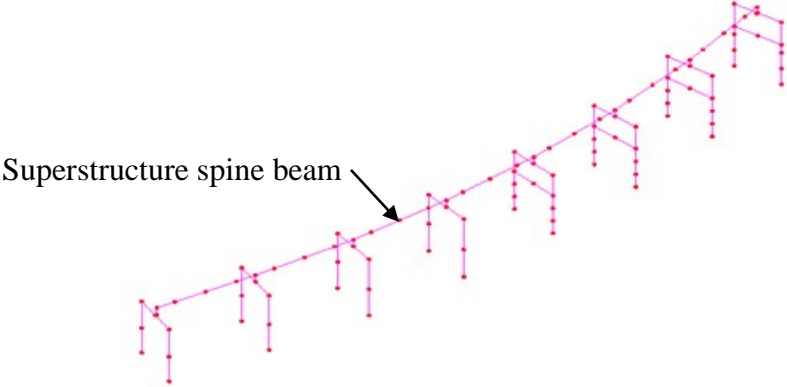


Figure 110. Illustration. Example of an analysis model of a curved bridge using a spine beam superstructure.

To remedy this, the mass moment of inertia of the superstructure about the longitudinal axis can be determined, and the model can be modified to have a similar mass moment of inertia value. Depending on the software being used, this can be accomplished by employing eccentrically placed masses, as shown in Figure 111, or by assigning masses with rotational components along the spine beam.

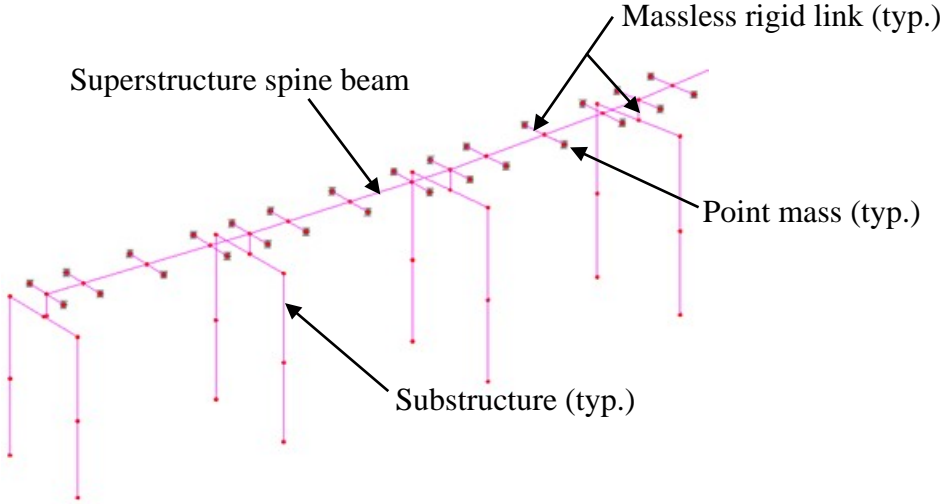


Figure 111. Illustration. Spine model modified to use eccentrically placed masses to result in the proper mass moment of inertia for the superstructure.

Results from a simplified version of the spine model (for instance, utilizing only one span) could be compared with a simplified PEB model of the deck system to ensure that the modeling of the mass moment of inertia is appropriately capturing the behavior of the structure. Often it will not

be apparent what, if any, mass moment of inertia is included in a given software package's beam element formulation. Information such as this is sometimes missing from a program's documentation. For such a case, it is recommended to create some simple dynamic models and back-calculate the included mass moment of inertia, then determine what additional inertia needs to be added.

5.4.2.2 *Modeling Damping*

Damping acts to reduce the motions of the system and dissipate the energy which is input. The damping in actual structures is due to a multitude of interactions. At small displacements, behaviors such as friction between components, micro-cracking of concrete, hysteretic material behavior, localized yielding of steel, slip of steel connections, and others all contribute to the damping. At large displacements, the yielding of components and formation of hinges further add to the amount of energy dissipated from the system.

The actual damping behavior of structures tends to be complex, nonlinear, and amplitude but not frequency dependent. However for simplicity, damping is typically accounted for using equivalent viscous damping (sometimes referred to as classical damping). In this formulation, damping is proportional to velocity, as was shown previously in the dynamic equilibrium equation. Despite being a simplification of the actual behavior, it has been shown that use of equivalent viscous damping produces reasonable results for typical structures. Furthermore, the use of equivalent viscous damping greatly reduces the computational effort and permits the problem to be solved by modal analysis methods. This is in large part due to the classical damping matrix, C , being diagonal.

The magnitude of the equivalent viscous damping is expressed as a percentage of the critical damping value (often referred to as the damping ratio, ζ). The critical damping value is the smallest amount of damping which will inhibit oscillation completely. The damping ratio for use in an analysis should be selected based on collected data of similar structure types, or based on the material, construction type, and stress levels expected for the analysis being performed. AASHTO LRFD C.4.7.1.4 recommends damping ratios of one percent, two percent, and seven percent for welded or bolted steel construction, concrete construction, and timber construction, respectively. Additional recommended damping ratios are shown in Table 7. It should be noted that these values were obtained from studies on buildings. Bridges, especially medium to long-span ones, can often have damping ratios smaller than those shown.

Table 7. Recommended damping ratios (Chopra, 2017).

Stress Level	Type and Condition of Structure	Damping Ratio (%)
$\leq \frac{1}{2}$ yield stress	Welded steel	2-3
	Prestressed concrete	
	Reinforced concrete w/ slight cracking	
	Reinforced concrete w/ considerable cracking	3-5
	Bolted or riveted steel	5-7
	Wood with nailed or bolted joints	
At or just below yield	Welded steel	5-7
	Prestressed concrete w/o complete loss in prestress	7-10
	Reinforced concrete	
	Prestressed concrete w/ no prestress left	
	Bolted or riveted steel	10-15
	Wood with bolted joints	
	Wood with nailed joints	15-20

For modal analysis, which will be described further below, typically the damping ratio can be input directly, either for specific modes or for all modes utilized. For time-history analysis, a formulation called Rayleigh damping is often used, in which the damping matrix is developed as a linear combination of the mass and stiffness matrices, as illustrated in Equation (29):

$$[C] = a_0[M] + a_1[K] \quad (29)$$

where: $[M]$, $[C]$, and $[K]$, are the mass, damping, and stiffness matrices, respectively, a_0 is the mass-proportional damping coefficient, and a_1 is the stiffness proportional damping coefficient.

With this method, the amount of damping can be selected to approximate the actual or desired amount damping with the proper selection of the values a_0 and a_1 . This methodology has been shown to be reasonably accurate for structures with relatively low damping (less than roughly 15 percent of the critical damping value). To determine the mass-proportional and stiffness-proportional damping coefficients, the desired damping ratio is selected at two frequencies and Equations (30) and (31) are solved simultaneously.

$$\frac{1}{2}(\frac{1}{\omega_i}a_0 + \omega_i a_1) = \xi_i \quad (30)$$

$$\frac{1}{2}(\frac{1}{\omega_j}a_0 + \omega_j a_1) = \xi_j \quad (31)$$

where: ω_i and ω_j are the frequencies selected to have the percentage of critical damping values ξ_i and ξ_j .

Typically, the frequencies of the highest and lowest contributing modes are selected to determine a_0 and a_1 . The engineer should plot ξ vs. frequency to understand how the amount of damping varies with frequency and to ensure important vibration modes are not inadvertently over or underdamped. The two proportional damping coefficients can then be adjusted as necessary to achieve the desired damping effect.

As an example, say it is desired to obtain a target damping of 2.5 percent in the range from 0.75 Hz to 5 Hz. Solving for a_0 and a_1 using the known ω values and ξ_i and ξ_j values both equal to 2.5 percent results in the plot shown in Figure 112.

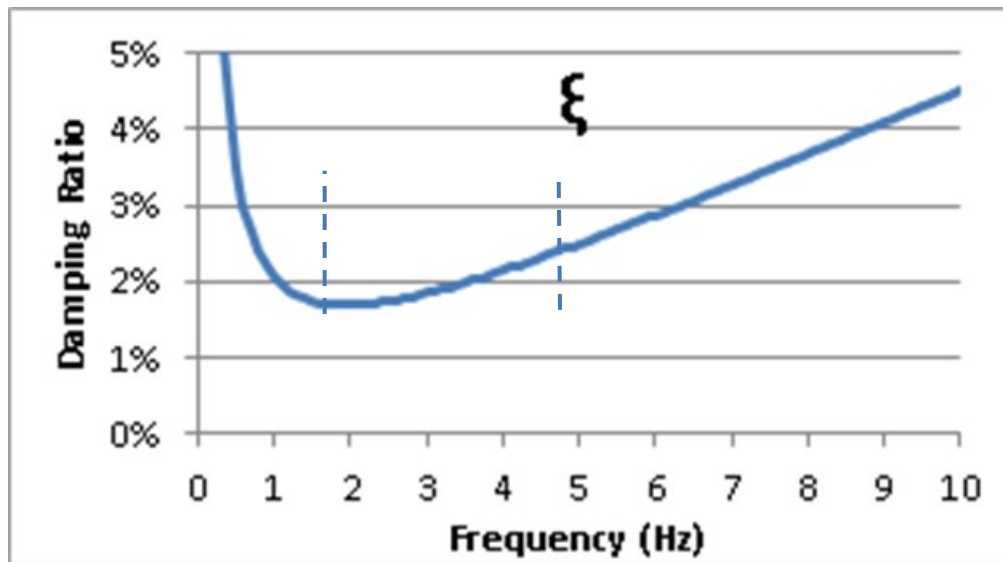


Figure 112. Graph. Example Rayleigh (proportional) damping curve.

At the two selected frequencies the damping ratios are equal to the desired value. At frequencies above and below the range of interest (i.e. < 0.75 Hz and > 5 Hz), the developed relationship provides damping ratios greater than the target value of 2.5 percent. Within the range of interest (0.75 Hz-5 Hz) damping ratios less than the target value are obtained (in this case with a minimum value of 1.68 percent at a frequency of 2 Hz). Once plotted, the range of interest or target damping ratios can be manipulated to adjust the curve and obtain the desired effect. The curve will always have a shape similar to what is shown above, with a damping ratio that varies with frequency. It is not possible to obtain a truly constant damping ratio with Rayleigh damping.

5.4.2.3 Modeling Stiffness

Typical procedures for modeling stiffness in static analyses apply equally well for dynamic analyses. Section 3 provides guidance regarding proper modeling of beams, cross-frame stiffness, torsional stiffness, boundary conditions, etc.

When a linear elastic dynamic analysis is performed for a structure and the elastic limit is likely to be exceeded, then the stiffness used for a dynamic analysis can be modified to account for this. An example of this would be concrete columns in a seismic analysis. For static analysis the columns may be modeled using gross section properties, however for a seismic analysis the stiffness should be reduced if cracking of the concrete is likely to occur. For more information, refer to Section 7.3.2 of FHWA (2006).

5.4.2.4 Model Discretization

For a given model, the computational effort required to solve a dynamic analysis is often greater than for a static analysis. For large analysis models, a reduction in the model size from that used for static analyses may be required so that the model can run efficiently and the results files do not become impractically large. However the effects on the output of reducing model size need to be considered, and the layout of the mesh needs to at least meet the requirements of any relevant specifications (for instance: AASHTO LRFD BDS, AASHTO Guide Specifications for LRFD Seismic Bridge Design, or FHWA, 2006).

For modal analysis, natural mode shapes of the structure are required. The number of modes that can be solved for is equal to the number of degrees of freedom in the model, however the number of modes needed for accurate results is usually significantly less than this. This is appropriate since not all modes, particularly the very high frequency ones, contribute significantly to the response of the structure. While not all modes need to be utilized to determine the response of the structure, it must be ensured that enough modes are present to obtain an accurate representation of the actual behavior. This is done by examining mass participation factors, which indicate how much of the mass is participating in each mode and in each direction. These values can be output from the analysis program, and it needs to be ensured that the sum of values for each direction is a sufficient amount of the mass of the structure (typically given as 90 percent). With larger models, more modes are required to reach the 90 percent level.

For time-history analyses, it must be remembered that output at each element/node will be stored for each time-step, which can result in a large pool of data which may be difficult to work with, both in terms of storage and file manipulation, as well as processing, evaluating and understanding the results. For both response spectrum and time-history analysis, there are times when it is appropriate to utilize a “lower order” model for dynamic analyses than what was used for static analyses. For instance, a bridge modeled using a PEB model for static analysis may best be modeled as a spine beam to perform the seismic analysis. This is especially true if the critical interests for the seismic analysis are the connection forces between the substructure and the superstructure (i.e. stresses in the girders are not paramount). In other cases, a condensation procedure may be appropriate to simplify a portion of the structure and reduce the number of degrees of freedom.

One option available in some programs to reduce the computational effort for modal analyses is to selectively include only modes with significant amounts of modal mass when determining the structural response. Another option that may be available is a Guyan (static condensation) reduction feature, which allows the software to condense the available degrees of freedom of the model into a smaller subset, either chosen by the user or automatically chosen by the software (Cook, 2001). Great care should be taken to ensure that important modes of vibration are not inadvertently condensed out, which would cause the resulting analysis to be in error.

5.4.3 Multi-Modal Response Spectrum Analysis

5.4.3.1 Input

The primary input to a response spectrum analysis is the relationship between acceleration and modal period. A response spectrum is constructed by recording the peak response, usually acceleration, of a single degree of freedom (SDOF) oscillator when subjected to an earthquake's ground motion. The peak acceleration of the SDOF is then plotted against the period (or frequency) of the oscillator, which is varied to produce the full spectrum curve.

A design response spectrum typically represents the combined hazard of many different potential earthquake events, and is smoothed. Figure 113 shows an example of the shape of a response spectrum curve, with the acceleration expressed as a percentage of gravity (g).

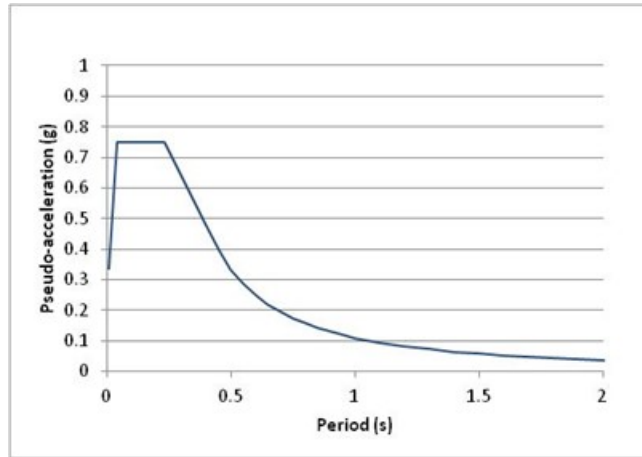


Figure 113. Graph. Example of the shape of a seismic response spectrum.

The response spectrum depicted in Figure 113 is the typical shape used for design, with a plateau at lower period/high frequency values and a tail which asymptotically approaches zero at infinite period. It should be noted that damping is typically accounted for in the response spectrum itself, and therefore does not need to be included in the model.

The response spectrum is input into an FEA model by discretizing the curve. Finite element programs typically use a linear interpolation between the input points, so enough data points must be input such that the linear interpolation appropriately represents the actual curve. The LRFD Specifications require that the response spectrum be applied in the longitudinal and the transverse directions. For curved structures the longitudinal direction is generally taken as along the chord between supports.

5.4.3.2 Solution

The problem is transformed from n coupled equations (according to the equation for dynamic equilibrium in Section 5.4) into m uncoupled equations, where n is the number of degrees of freedom and m is the number of mode shapes considered in the modal analysis. For each mode shape, there is an associated frequency, determined by performing an eigenvalue analysis prior to the response spectrum analysis.

All modes do not contribute equally to the response of the structure, so while the upper limit of m is n , generally m can be significantly less than n . The appropriate number of modes to use is determined by examining the mass participation factors output from the eigenvalue analysis.

The total mass participation in each direction should be 90 percent or greater. If the total mass participation is less than 90 percent, then either more modes need to be considered or the model needs to be adjusted. Methods of adjustment include reducing the number of DOF in the model or artificially reducing the number of DOF for the eigenvalue analysis by Guyan Reduction (also see Section 5.4.1.4). Consult the manual for the software being used to determine how this procedure is implemented.

Combining the mode shapes and the mass properties of the system allows a set of inertia “forces” to be developed for each mode. When these are applied to the structure and multiplied by an acceleration value, the dynamic response of the mode undergoing that acceleration can be determined. Since the response spectrum provides the peak acceleration values over the duration of the seismic loading for different frequencies, the peak response for each mode is simply the effects of the inertia “forces” multiplied by the response spectrum ordinate associated with the frequency of the mode. Then by combining the effects of all modes, the total response of the structure is found. Since effectively each mode is treated as a SDOF system with an already known peak acceleration (from the response spectrum), this procedure greatly reduces the computational requirements when compared with time-stepping methods which are described in Section 5.4.4.2.1.

The peak responses of each mode do not necessarily occur at the same time, so an accurate estimate of the overall response of a structure requires some method of modal combination that accounts for this. Studies have shown that estimates of peak response found by using methods such as the Square-Root-Sum-of-Squares (SRSS) method and the Complete Quadratic Combination (CQC) method provide values which are sufficiently accurate for design purposes. Generally the CQC method is preferable, especially if the modes of the structure are closely spaced. When no damping is specified for the CQC method, it reverts to the SRSS method.

5.4.3.3 *Output*

Response spectrum analysis results are the peak output values, not values at specific times. Due to the manner in which the responses of the various modes are combined, the sign of the response is lost, and therefore all values in the results are positive. Because of these two facts, care must be taken when utilizing the analysis output. The responses determined are not concurrent, and therefore base reactions cannot be summed, since that would overestimate the value due to the peak reactions likely occurring at different time instances. Likewise, the relative displacement between nodes cannot be determined from the response spectrum output, since the peak displacements of two nodes may not coincide with the occurrence of their peak relative displacement. Therefore, all responses of interest, such as relative displacements or combinations of forces, must be calculated prior to combining modal results. The analysis model can be modified as necessary to ensure that this occurs. For instance, a joint element with very low stiffness can be added between nodes so that the peak change in length of the joint element will be recorded by the program.

As mentioned previously, the response spectrum is input in the transverse and longitudinal directions. The responses in these directions are then combined to arrive at the design force effects and displacements. Generally the 30 percent rule is used, wherein the maximum response is determined from either $1.0L+0.3T$ or $0.3L+1.0T$, where L and T represent the responses due to the spectrum applied in the longitudinal and transverse directions, respectively. This requires

selecting the longitudinal and transverse directions. The Caltrans CQC3 procedure removes this feature by requiring the 30 percent rule to be run for all orientations, creating an envelope of seismic motions in all directions. This can be done by selecting a longitudinal/transverse orientation and then performing the analysis in angle increments up to 90 degrees to determine the most severe force effect for each component.

5.4.4 Time-History Analysis

5.4.4.1 Input

The inputs for a seismic time-history analysis are sets of ground motions, typically specified as acceleration vs. time. Often these come from actual recorded earthquakes, although they also can be artificially generated. The selected time-history data can be altered using spectrum matching to result in input motions with characteristics similar to the desired design response spectrum. Spectrum matching is typically performed using specialized software such as RspMatch and is beyond the scope of this manual.

The time-history input is assigned to each support location in the model. If the model represents a long structure (about 2 miles or longer), then some of the time-histories input in the model may need to be modified to account for the seismic wave not occurring at all locations simultaneously. Further guidance can be found in other seismic specific sources such as (FHWA, 2006). Per the AASHTO LRFD Specifications a minimum of 3 time-histories must be utilized in the longitudinal, transverse, and vertical directions. For curved structures the longitudinal direction is taken as along the chord between supports. Use of 7 or more time-history analyses can allow for the use of mean output values instead of maximum values for design purposes. Different states and agencies may have slightly different requirements.

For other types of dynamic time-history analysis problems, the input loading will often be a set of forces that vary through time in location and/or in magnitude. An example would be a truck crossing over a bridge. The loading may be modeled with either a constant force for each of the wheel loads, or with variable forces which account for the impact resulting from the dynamic interaction of the truck suspension system with the bridge.

5.4.4.2 Solution

For a multi-degree of freedom (MDOF) system with n degrees of freedom, the equation for dynamic motion given in Section 5.4.1 results in n coupled differential equations. The methods of solution of these equations falls into one of two categories: time-stepping methods involving step-by-step integration or modal analysis. Time-stepping methods must be used to handle the most complex problems, including nonlinear time-history analysis and systems with non-classical damping. Modal analysis has the benefit of being much more numerically efficient than time-stepping methods, but its use is limited to assumptions of linear elastic behavior and classical damping.

5.4.4.2.1 Time-Stepping Methods

For time-stepping methods the equations of dynamic equilibrium are solved at discrete time-steps by use of the initial conditions, values at previous time-steps, and assumptions regarding how the values vary between time-steps. Two types of time-stepping methods are typically

available in finite element analysis programs: explicit and implicit. The two methods differ in how the dynamic equilibrium equations are solved, which results in different characteristics relating to the maximum useable time-step size, accuracy, convergence, stability, and computational demands. The specific time-stepping methods of the program being used should be understood so that the one most applicable and best suited to the problem at hand can be selected.

When using explicit methods, the solution at the next time-step is determined by satisfying the dynamic equilibrium equations at the current time-step. This solution scheme results in the decoupling of the equations of equilibrium, such that the stiffness matrix does not need to be inverted at each time-step. However, it also results in the solution being only conditionally stable, meaning that a solution can only be obtained if the time-step utilized is less than the critical time-step. With time-steps larger than the critical value, the responses of the higher frequencies will not be evaluated correctly, resulting in the errors accumulating until the solver “crashes.” The critical time-step can be defined as 2 divided by ω_{\max} , where ω_{\max} is the maximum circular frequency of the system. Often explicit methods are used for wave propagation problems, for instance the examination of stress waves from blast or impact loading (i.e. very short duration, pulse loadings). In these circumstances, with a uniform mesh present, the critical time-step can be estimated as S/c , where S is the distance between nodes and c is the wave propagation speed of the material, which can be taken as the square root of E divided by ρ .

For implicit methods, the solution at the next time-step is determined by satisfying the equilibrium equations at the next time-step. Unlike the explicit method, this scheme requires inverting the stiffness matrix at each time-step (a very computationally demanding endeavor), but the solution is unconditionally stable and therefore the choice of time-step is dependent only on accuracy considerations. To accurately account for all of the high frequency modes, the time-step would need to be less than the critical time-step described above, however, implicit methods are typically used when lower frequency components are more influential to the response, such that the effects of higher modes can be neglected. This is typically the case for analysis of problems such as seismic loading or vibrations due to live loads, which have loadings that are not pulse-like in nature. With high frequencies not contributing significantly to the response, use of fewer time-steps which are much larger than the critical time-step is often acceptable. This mitigates the computational demands of the stiffness matrix needing to be inverted at each time-step. A time-step of $1/10^{\text{th}}$ - $1/20^{\text{th}}$ of the period of the highest mode which influences the total response is recommended.

Finite element software programs may have their own methods to select an appropriate time-step for both explicit and implicit solution methods. The documentation for the program being utilized should be examined to gain an understanding of what is occurring “under the hood.” Additionally, regardless of the method used, upon completion of the initial time-history analysis, the analysis should be performed again utilizing a smaller input time-step to ensure that the solution is not being significantly affected by the selected value.

5.4.4.2.2 Modal Time-History Analysis

Modal time-history analysis requires the determination of mode shapes and frequencies, as described above for response spectrum analysis, however some FEA programs will utilize load-dependent mode shapes (Ritz vectors) instead of the free vibration mode shapes. Once the

modes and equivalent static forces have been determined, time-stepping methods are used to solve the SDOF system associated with each mode. The responses of the modes are then combined for each time-step.

The solution using modal analysis requires the selection of a time-step, and it is usually sufficient to use $1/10^{\text{th}}$ – $1/20^{\text{th}}$ of the period of the highest mode utilized. A larger value can be utilized if the higher modes do not contribute significantly to the behavior of the structure. As mentioned above, modal analysis is limited to examining problems with linear elastic behavior and classical damping.

5.4.4.3 Output

Time-history analyses determine the response at all time-steps. This can result in extremely large sets of output data. In some cases it may be acceptable to run the analysis utilizing a small time-step, but have the program save the results using a larger time-step. In this way, accuracy of the results can be assured while reducing the size of the output files, however care needs to be taken to ensure that this down sampling does not result in missing important peak values in the response. An envelope of the force effects from the analysis can often be utilized in lieu of the large post-processing effort which would be required to sort through the data and summarize each maximum and minimum force effect with its concurrent effects at each node of interest.

CHAPTER 6. VERIFICATION/VALIDATION

6.1 Introduction

Analysis and design software has become almost ubiquitous throughout the bridge design community. Some packages are now available which can create the model from limited input with modeling “wizards,” code-check the sections and produce reports with many figures and diagrams all in a single afternoon. Unfortunately, the one task the software will not do is take responsibility for any of the results. Below is a disclaimer typical of those found in software manuals or licensing materials.

Considerable time, effort and expense has gone into the development and documentation of [the programs]. The programs have been thoroughly tested and used. By using the programs, however, the user accepts and understands that no warranty is expressed or implied by the developers or the distributors on the accuracy or the reliability of the programs.

The user must explicitly understand the assumptions of the programs and must independently verify the results.

As software does more and more, the need for independent verification increases. The multi-colored plots of stress contours, three-dimensional deformed meshes, and reams of computer produced design checks have become so convincing that even the most well-grounded engineer begins to respond to the siren’s call of advanced graphics and quantity of data. But the analyst must always be aware that errors do occur and checking results is as important as ever.

There are two sources of inaccurate computer results; user input errors, and internal software bugs. User input errors include errors in input data (the venerable GIGO, Garbage In = Garbage Out, observation) as well as misapplication of the software stemming from an incomplete understanding of the software’s capabilities and operational details. These types of errors are very familiar to most engineers, although that does not make them any less troubling.

Perhaps more troubling though are the errors resulting from software bugs. When learning to use a software package, analysts become accustomed to incorrect results coming from incorrect modeling and input errors. The default assumption on the part of the analyst, as it should be, is that errors are due to the user. Because software bugs are so rare, substantial effort is made looking for the misplaced decimal point, or the incorrectly connected element. When it becomes clear that the input is correct, and the problem lies with the software’s execution, the analysts confidence in the ability of the software is greatly shaken.

Why do software bugs persist? Many of the base codes contained in commercial software packages are many decades old. It would seem that by now any possible error in the algorithms would have been discovered, especially considering the extensive verification problem sets that are used by the developers. The answer appears to be in the implementation of new features and capabilities, and their interaction with the existing code structure. A beam formulation may perform flawlessly, but when an eccentricity feature is added errors may arise when temperature loading is applied or when torsional properties are required.

It should be noted that when referring to finite element analyses, verification and validation are not the same thing. Verification refers to making sure that the model is behaving as intended and giving the results that are expected. For instance, if you were modeling a column to determine the Euler buckling load, it should give you the same answer as performing a hand calculation of the Euler buckling load. Validation means confirming that the model is behaving the same as an actual structure.

Examples of model verification from actual designs are presented in this section involving:

- the use of alternative methods of static analysis;
- the verification of time dependent effects; and
- the results of incorrect boundary conditions of live load analyses of a girder bridge

Finally, when the models are being developed to repair or rehabilitate an existing structure then the opportunity exists to measure something in the field and compare the results to the finite element analysis, thus validating the model. Several examples of this type of approach are presented in more detail later in this section dealing with comparisons of FEA results with measured live load response using:

- deflections;
- mode shapes and frequencies; and
- strain gauge results.

Although several of the examples deal with models of complex bridges beyond the scope of this manual, they are not intended as examples of how to model those complex structures, but as examples of how to approach the process of verification/validation.

6.2 Software Verification

When starting with a new finite element analysis package or an update for that matter, it is important to become confident that the software works, or, on the contrary, to find out what is wrong with it. It is often convenient to start with the simple question “does a symmetric problem subject to symmetric loads yield symmetric results?” Is it possible to do a problem simple enough that one can determine that the sum of the vertical reactions is, in fact, equal to the sum of the vertical loads?

Start with something which can be solved by hand whenever possible and analyze it with the software. If one is about to embark on a second-order analysis, it might be prudent to check if one can solve a simple Euler column before proceeding further. Add complexities and observe trends. Analyze a model for which some form of alternative solution exists. For example, one might build a plate model and compare the results to tables based on the theory of plates and shells in some of the classic texts or handbooks. To this end the model should be faithful to the requirements of the closed form solution. Likewise, there are equations or tabular results available for plane stress/plane strain analysis in texts on the theory of elasticity.

One should start with symmetrical problems and symmetrical loadings to facilitate the confirmation of symmetric results are part of the vetting process. Similarly, one might use boundary conditions that facilitate the accumulation of reactions to determine whether

equilibrium is present. Once a basic skill set is established, the models can be made more complicated and the trend in results verified, even if closed form solutions do not exist.

Running benchmark problems such as those in Appendix C of AISC Design Guide 25 (Kaehler et al., 2015) can not only provide assurances that the software is working properly, but can also give a feel for the meshing requirements for the elements being used.

6.3 Design Model Verification

Engineers have to perform professional due-diligence regarding the checking of the results of a refined analysis. It is certainly possible to do a line-by-line check of input files, or element by element check through a graphical interface, since often having a second set of eyes check the model will catch obvious modeling errors, and such a check should typically be performed, but that type of check does not confirm the functionality of the software.

When models are built as part of a design or review process to represent a structure which does not yet exist, the analysis results should be verified. *Model verification can take several different forms depending on what the models are going to be used for.* For most models, it is probably not likely that closed form or tabular form solutions exist, but they should be used if available. It is also unlikely that a checker will perform a hand analysis using classical methods, although it is certainly valid when used appropriately. In some cases it may be possible to draw analogies between tabulated influence lines of continuous beams to formulate a check, for instance see (Anger, 1956) or the beam tables in the AISC Manual of Steel Construction. Influence surfaces of plates available in (Homberg et al., 1963), (Homberg, 1968) and (Pucher, 1977) are commonly used in concrete design. In many cases a simpler FEA will be used to verify results of a more complicated FEA.

For routine design of typical slab girder bridges, even those with curvature or skew, comparing the design moments and shears to an appropriate line girder analysis done using a trusted program can provide confidence that the results are reasonable. *Simply examining results by looking at the deflected shape or the shapes of shear and moment diagrams, and the magnitudes of the extreme force effects, can provide confidence when they satisfy the intuitive sense of the experienced bridge designer.* Sometimes a comparison with the results of a strength based mechanism solution or simple statically determinate load proportioning can be used to gain confidence in an FEA solution and may even qualify as an independent check.

For models utilizing surface (shell) or volume elements, stress contours should be viewed as well as the deflected shape. Although there are a number of different stresses that can be viewed, start with the normal stress in the direction of loading. Viewing principal stresses can also be helpful. Often the default contours are averaged or interpolated, typically referred to as smoothing. *Ideally, the unsmoothed results should be examined for highly discontinuous contours between elements, indicating modeling issues that typically require a more refined mesh.*

One of the issues facing analysts utilizing 2- or 3-dimensional analyses is cross-frame/diaphragm designs. With 2D or 3D analyses, the analyst is explicitly provided with cross-frame/diaphragm forces that a 1D analysis cannot provide. In some cases, these forces may be much larger than the cross-frames/diaphragms the analyst is accustomed to providing can carry. This may be due

to analysts ignoring second-order softening effects and over-estimating the stiffness of cross-frames/diaphragms in their models. In some cases there may be a feedback loop established where as the cross-frames/diaphragms get larger and stiffer more load is attracted, requiring the cross-frames/diaphragms to get still larger and stiffer.

In situations where the cross-frames/diaphragms are not being counted on to distribute forces, but are merely present during construction to provide stability, the cross-frames/diaphragms can be conservatively omitted from the model, or the stiffnesses of the cross-frames/diaphragms adjusted such that little or no force is carried by them. In all other situations such as curved or skewed structures where the cross-frames/diaphragms are being counted on to distribute forces, the analyst should attempt to provide the correct stiffness of the cross-frames/diaphragms in the model, such that the forces are representative of the actual bridge.

In some cases, it may be prudent to bound the solution, and design the girders as if no cross-frame distribution is occurring, but design the cross-frames as if the maximum distribution is occurring. At a minimum the structure should be designed to provide the assumed load path provided by the analysis. For instance, do not use an analysis model with large forces in the cross-frames/diaphragms to provide design forces for the girders, and then disregard the large forces when designing the cross-frames/diaphragms. *If incompatible assumptions are employed in determining the design forces for different members, make sure they are conservative.*

On projects of a scope that make it feasible to employ more than one finite element package, vetting the results by comparing two analyses using totally different packages has proved effective but not fool-proof in past projects. If two models quickly produce very comparable results then the vetting can be efficient. However, there have been more than a few cases where results were sufficiently different that a considerable amount of time and effort had to be devoted to resolve the differences between programs. This is probably more apt to be the case where dynamic analyses, stability analyses, or automated applications of the AASHTO live load are involved. Considerable care is required to make sure that the applied loading is the same for both of the models and that the boundary conditions are identical.

Time and budget permitting, especially for complex analyses, it is strongly recommended that independent models using different finite element programs be used to verify results.

6.3.1 Example Comparison to Alternative Methods of Analysis

Strut and tie modeling is a lower bound analysis methodology covered in AASHTO LRFD Article 5.6.3 that is essentially an extension of the truss analogy used in beams. It is used in disturbed regions, also referred to as “discontinuous” or “D” regions, which are those that do not adhere to typical plane stress assumptions. The regions are given an assumed load path consisting of compression struts and tension ties to form a stable structural system. Tension ties represent areas requiring steel reinforcement while the compression struts represent an area of concrete effective in carrying the load. Points where struts and ties meet are referred to as nodes, and are designed based on the number of struts and ties framing in.

Due to the unrestricted nature of this process, a number of acceptable models can be created for a given problem. However, engineering judgment should be exercised to determine a reasonable and logical flow of forces. As a general rule, strut and tie models should minimize the number of

ties (for greater efficiency) and generate stresses similar to those found in an elastic distribution. The creation and use of a strut and tie model for the concrete pier cap illustrated in Figure 114 is detailed in the following example.

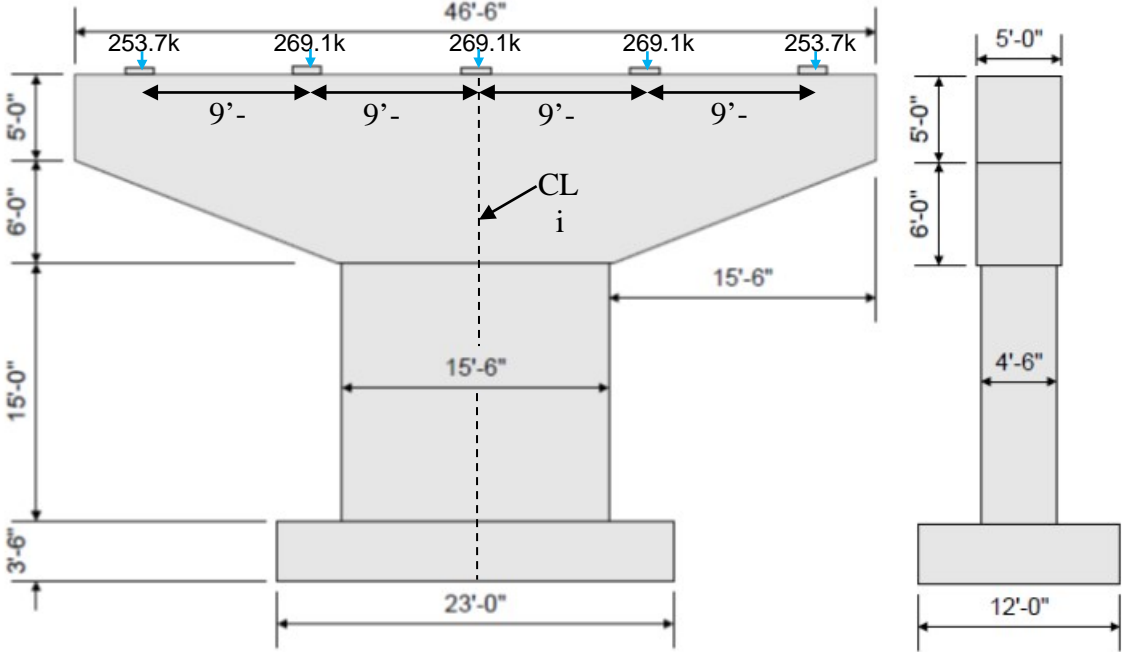


Figure 114. Illustration. Example pier cap.

To aid in the creation of a strut and tie model it can be helpful to first observe the principal stress fields (trajectories) in a plane stress model. Figure 115 shows the results of such an analysis, which can then be used to identify appropriate configurations of struts and ties or to validate results from a refined finite element analysis.

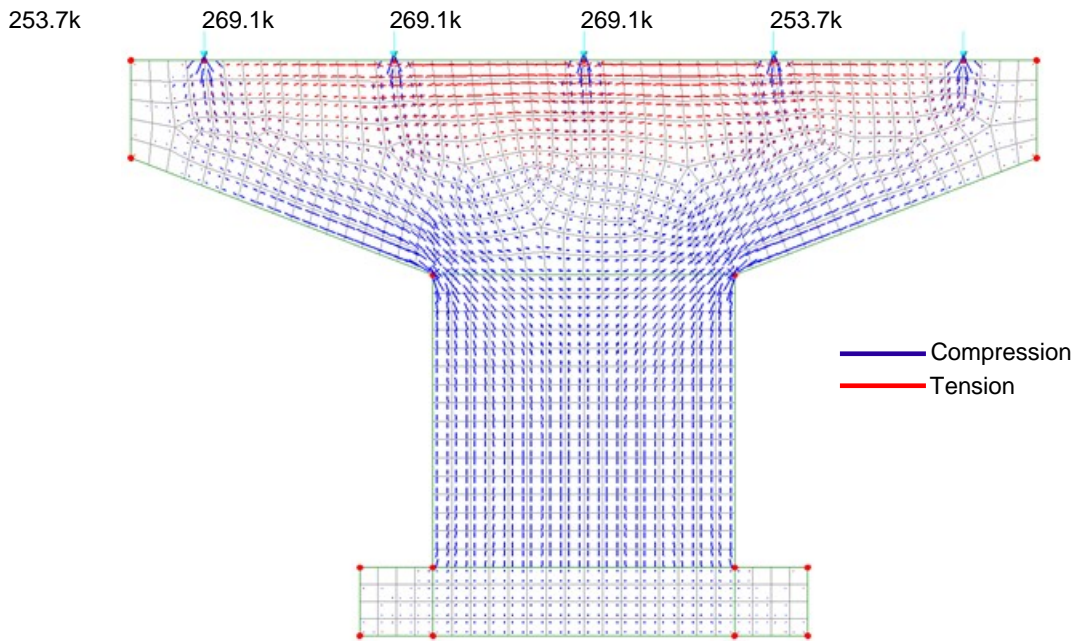


Figure 115. Illustration. Principal stress field.

Using Figure 115 as a guide to the anticipated flow of forces, a strut and tie model is constructed using idealized lines and is shown in Figure 116. It should be noted that without doing the aforementioned analysis first, one may arrive at a different, yet equally valid (in terms of AASHTO LRFD compliance) strut and tie geometry. However, the incorporation of this step will result in forces that more closely reflect actual behavior and therefore produce a more efficient design.

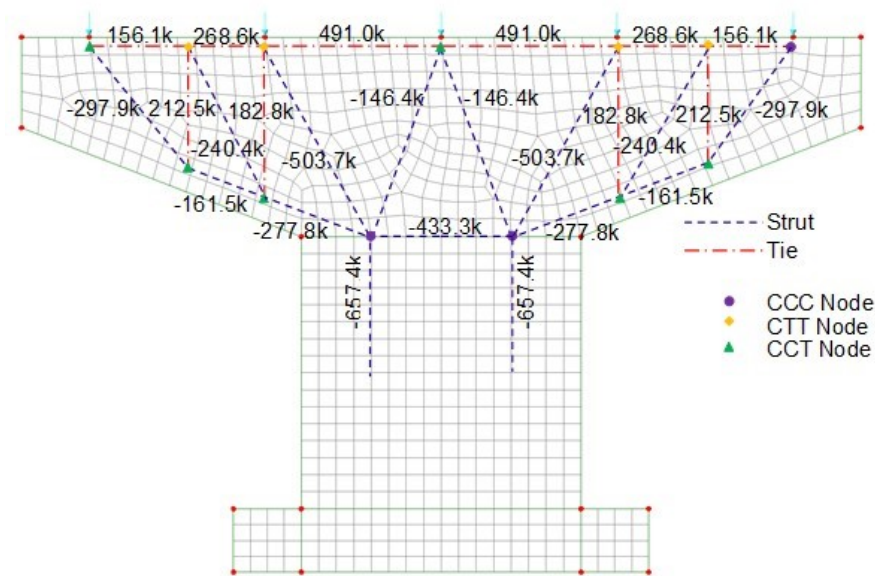


Figure 116. Illustration. Example strut and tie model.

After the model is created, forces in the struts, ties, and nodes can be determined via analysis. A model that is statically determinant is preferable so that member stiffnesses, which are difficult to accurately estimate, can be ignored and forces can be easily calculated and/or checked by hand.

Once forces are determined, ties can be designed and stress levels in struts and nodes can be checked in accordance with the AASHTO provisions (5.6.3.3-5.6.3.5). If the required rebar and strut area are compatible with the assumed geometry (i.e. they can fit within the location), then no further iterations are required. However, it may be necessary to modify the model and recalculate forces to accommodate the design. Once a design compatible geometry is set, final checks on anchorage and crack control can be made.

6.3.2 Verification of Time Dependent Analysis – Creep

6.3.2.1 Description of the Problem

Often times when dealing with highly stressed concrete structures, or those that experience changes in the statical system over time, correctly accounting for the effects of creep and shrinkage is required to produce a robust design. The following example uses the challenge of modeling creep effects in a concrete structure to highlight some of the methods that should be used by engineers to validate the results of complex analyses. The specific details of the problem should not be the focus, but rather the process of verification and the general approach. Time-dependent properties, such as those associated with creep and shrinkage, can be an especially vexing problem. It has been found that starting with a relatively simple problem that has a known load, a known age of loading, a period under sustained load and an unloaded period, and comparing that to analytic results can be helpful.

For complex structures, or structures exhibiting complex behavior, it is usually impossible to perform check calculations by hand to verify all of the results of a refined analysis. However, the software can still be verified to be handling the class of problem correctly, and by performing multiple analyses using very different approaches, the overall results can be verified to be converging toward a single solution.

6.3.2.2 Verification Process

The approach taken was a two-pronged attack: verify the ability of the software to handle a basic creep problem correctly and use two different methods of analysis to provide an estimate of the variability of the results. The first line of attack was used to vet different software packages available to determine which could or could not appropriately handle the creep problem, and to build a deeper understanding of the issues surrounding long-term deformations in concrete. The second method was applied to the final analyses of the structure and the determination of the design forces.

6.3.2.3 The Simple Test Case

The first step was to conceive of a simple problem which would exhibit all of the complex creep behavior expected in the structure. Because the construction timeline of the structure would extend over several years, and the loads on it can change dramatically throughout the

construction to include cycles of loading and unloading, the problem must accommodate changes in loading over time. It was found that a simple column with a variable loading history would encompass the behaviors of interest.

To most engineers, creep is a rather strange effect, and the deeper one digs into the behavior, the stranger it gets. It is almost as if concrete has a memory for loads, and never forgets what loads have been applied, even when they are removed. This is a very difficult behavior to include into a software package, and in fact various programs have been found to not correctly handle it.

The simple problem is as follows: A column 5 feet tall, with a one foot square cross section is subjected to a 150 kip axial load which is removed and then reapplied. The goal is to match the deflection versus time plot with that calculated by hand using the methods contained in the CEB-FIP 90 Specification. Figure 117 shows the loading history applied.

The problem was solved by FEA, once using beam elements and once using shell elements, as the software handles creep differently in the two element types. Adjusting the modulus of elasticity over time was found to have little effect on this example. The results are shown in Figure 118. The beam and the hand calculations based on the CEB-FIP equations look to be very similar, however it does not appear that the shells are creeping after unloading. Further investigations showed that indeed, the shell elements were not displaying true creep behavior, and were not continuing to creep after the loads were removed.

When elements are suspected of providing such erroneous results, the software vendor should be notified. Once the “bug” is confirmed, then the problem becomes what to do? Waiting for the corrected element formulation in the next software release typically would result in unacceptable delays. The best solution would be to find a software package that handles the problem correctly, but often this is not a practical option. Better vendors will provide assistance but much of the time it is up to the analyst to develop an acceptable workaround.

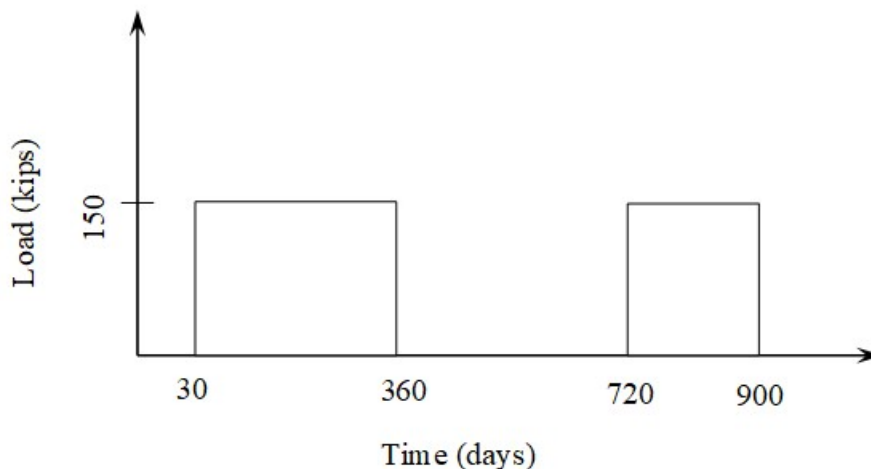


Figure 117. Graph. Loading history for test problem.

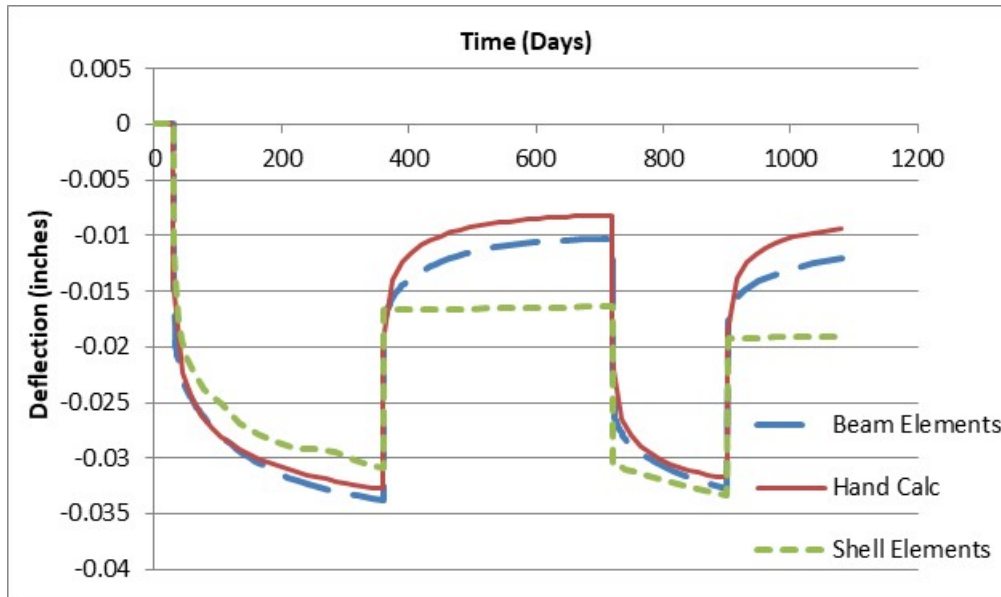


Figure 118. Graph. Comparison of displacements due to creep.

6.3.2.4 Bounding the Solution

The results of the software vetting process indicated that beam elements could adequately approximate the creep behavior contained in CEB-FIP 90, but that shell elements were not as good. However, the structure in question is a variable depth, multi-cellular concrete structure with loadings both in and out-of-plane which is best modeled with shell elements. The solution adopted was to model the structure twice, once using shell elements and again using a “McHenry Lattice” approach, which is a way of modeling shell structures using only beam and truss elements.

Figure 119 shows the shell element model of the structure. This model was used to investigate localized stresses and to obtain the loads for design. Each slab and wall was modeled explicitly, including the variations in slab thickness and overall structure depth. Creep analyses were also done with this model. The shell element results were integrated to obtain axial force, shears, and bending moments on notional beams which were made up of a wall and associated top and bottom slab widths. These forces were then used to design the notional beams using methods from the AASHTO LRFD.

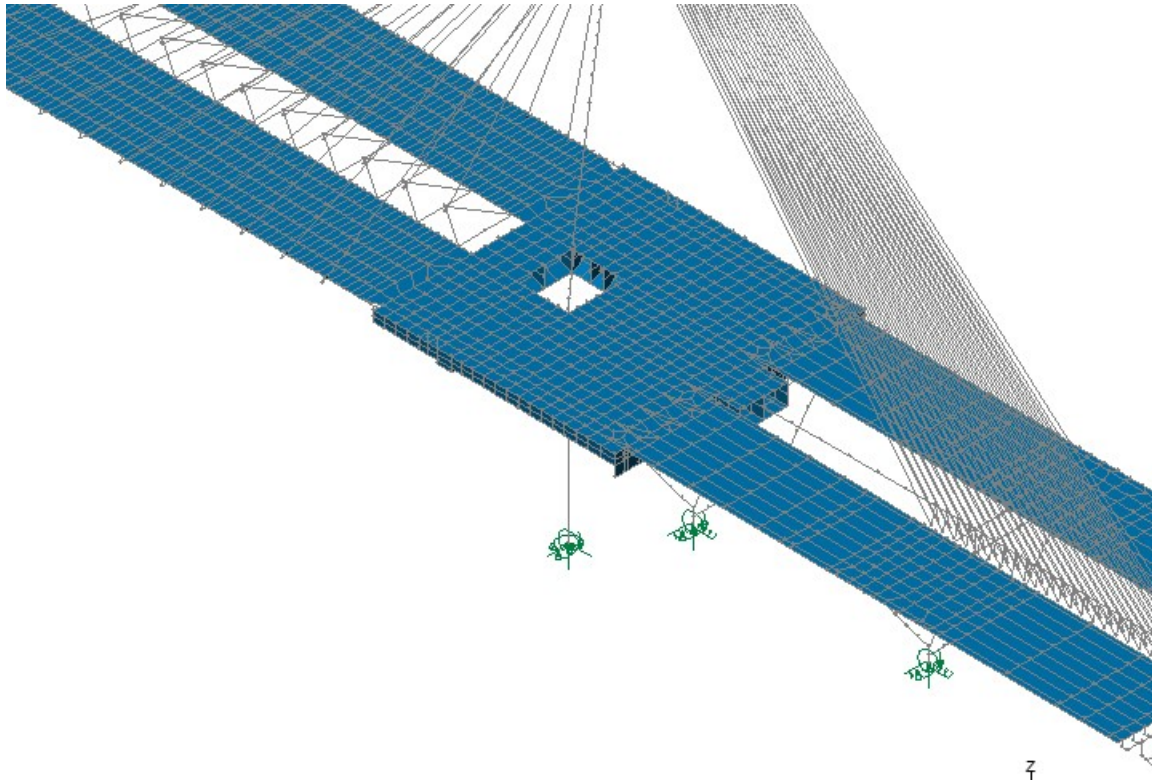


Figure 119. Illustration. Shell element model of the apron region.

The McHenry lattice model is shown in Figure 120. Details on using a McHenry lattice are contained in “Bridge Deck Behavior” (Hambly, 1976). In general, the method can be described as replacing shell elements by a number of frames containing beam elements around the frame perimeters and X-bracing across the frame centers. The perimeter beams replace the bending and axial stiffness of the slab, while the X-bracing replaces the shear stiffness and a portion of the axial stiffness. This method was originally proposed in 1943 as a way to model shell structures prior to the development of finite element analysis methods.

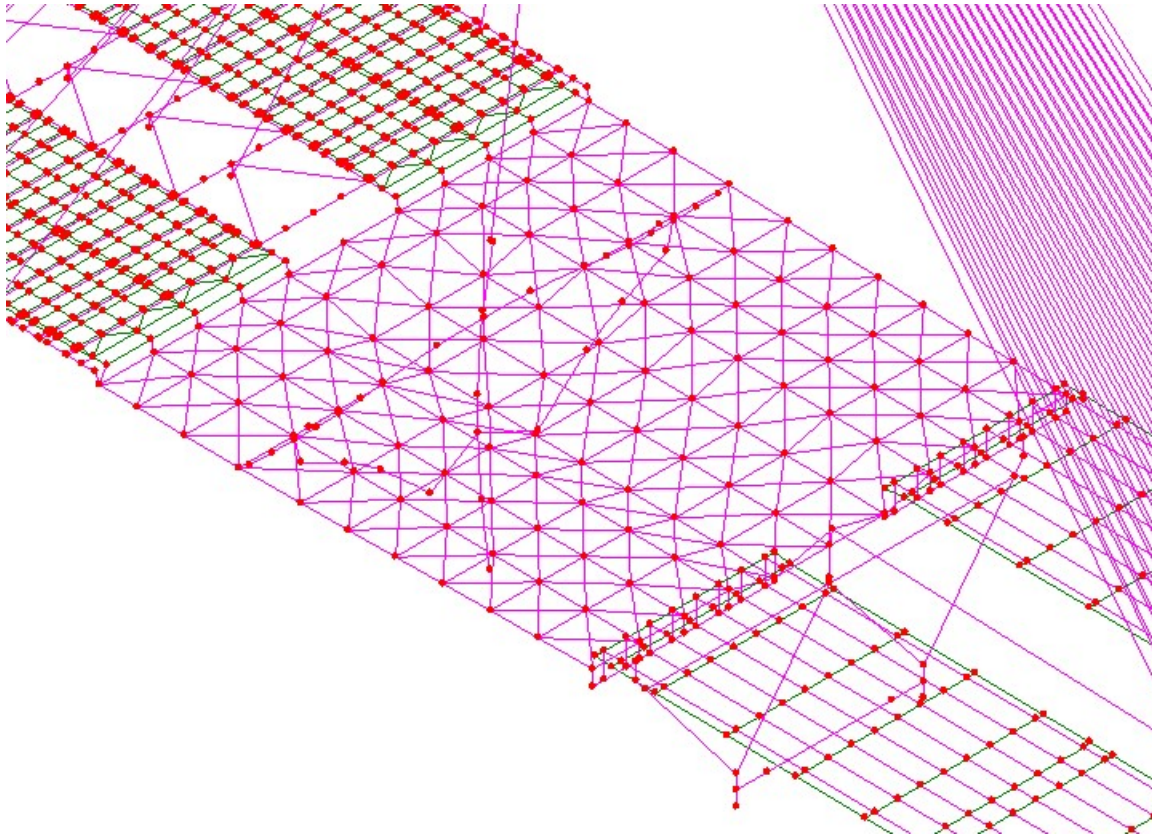


Figure 120. Illustration. Lattice model of apron region.

The McHenry lattice model was used to investigate the global behavior of the bridge, and to determine the effects of the different creep formulation in shell elements and beam elements. One distinct advantage of the McHenry lattice over the shell element model was the greatly reduced degrees of freedom in the model which greatly improved processing time and allowed quick parametric analyses of alternative configurations of the structure.

The results from the McHenry lattice were integrated into beam forces, as with the shells, and compared to the integrated shell results. For analyses without creep, they generally closely matched, with the shell element results displaying a much greater refinement and better accounting for localized behavior. Figure 121 shows results for one of the exterior longitudinal notional beams. The agreement in this example is very good, with the lattice (here called grillage) results displaying a coarser, but accurate plot of the axial load.

When creep is included, shown in Figure 122, the results begin to diverge. The shell element model does not display as much change in the forces due to creep as the grillage model. In fact, a substantial increase in the axial load is shown in the grillage model that is not accounted for in the shell element model. *Therefore, the use of multiple models based on different assumptions permitted the incorporation of creep into the analysis, resulting in a significantly different, and substantially more accurate, design for this structure.*

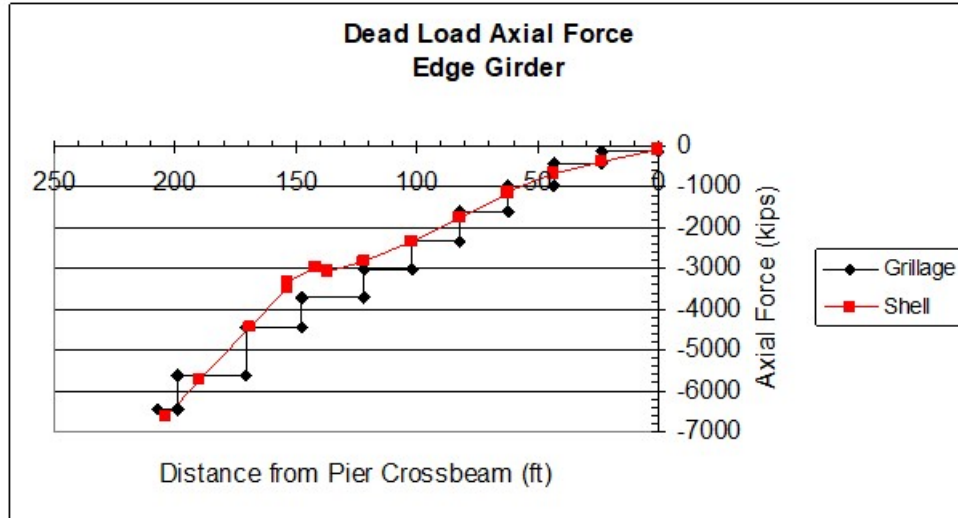


Figure 121. Graph. Comparison of results for edge girder without creep.

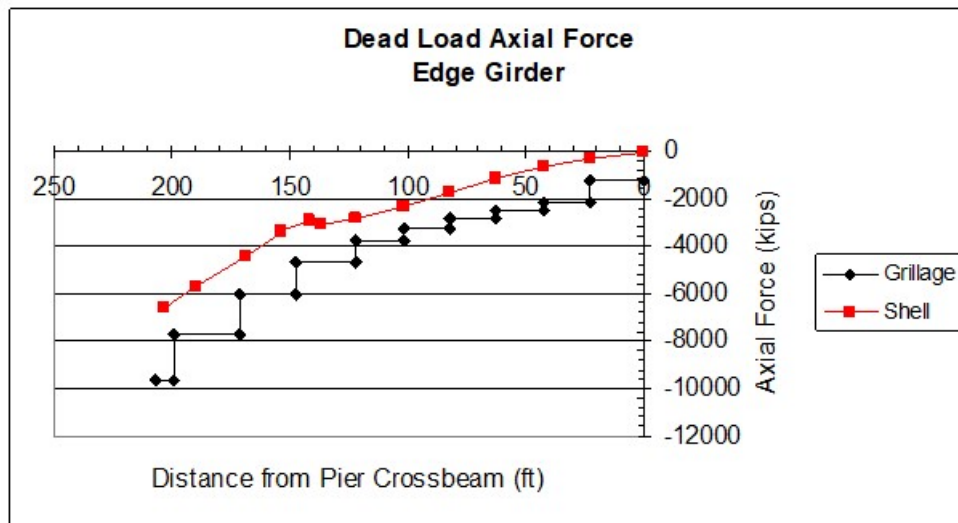


Figure 122. Graph. Comparison of results for edge girder after creep of 10,000 days.

6.4 Validating Models of Existing Bridges

6.4.1 Introduction

Retrofitting an existing bridge presents a unique circumstance in that a physical entity already exists. *Often the original designer's calculations or at least a stress sheet are available. It is important to compare initial results to the designer's estimate.* Even though the design may have been done pre-computer, there is a very good chance the designer developed a reasonably good indication of the primary loads. Recently an analysis was performed of a large bridge in which the analyst got results radically different from the stress sheet. In fact, they differed so much that the owner was alerted to a possible safety issue. The analysis had been done using truss members in a three-dimensional frame work. Unfortunately, one of the section properties

was incorrect on one of the truss diagonal members, reflected in four elements due to symmetry. When this was found and corrected, the results obtained agreed very closely with those calculated by the designers.

As illustrated in some of the analyses of existing structures presented herein, it is very appropriate to try to measure something, a displacement, force, mode shape, or stress, in order to compare with the finite element analysis. The fact that the structure exists, as distinguished from new design, provides an invaluable opportunity to ascertain that the finite element analysis is operating correctly. Of course, existing bridges have been subject to wear and tear, which may make their analysis a little more difficult. This may be particularly true on older bridges that have pin wear. The advent of gap elements and one-way elements in the newer finite element packages has been a tremendous advantage to engineers trying to solve these kinds of problems. These elements have also added realism to seismic analyses of certain classes of structures.

Finally, try to find out how the existing bridge was built. This involves the erection method and the degree to which camber was accounted for. One might start with the assumption that the two-dimensional design model may have been statically determinate, e.g., a cantilever truss, and, therefore, camber is not significant in determining the stresses. However, if that same structure is now analyzed as a three-dimensional model, it will be vitally important that the camber in the primary members and the camber, or lack thereof, in the secondary members be accounted for. Similarly, structures are sometimes erected so that in the partial stage of erection the articulation is different than it is in the final condition. For example, it is not too unusual to erect steel true arch bridges using pins at the crown and the spring lines. One or more of these pinned connections may be spliced with bolted plates to create moment connections after the steel is erected to make the structure statically indeterminate for other applied loads. Failure to recognize this would result in an improper dead load analysis.

6.4.2 Field Validated Model Example

The case of a bow string arch bridge with a very slender tie and a large arch rib which serves as the primary bending element will be examined (Kulicki, 1988). This particular bridge exhibited relatively large and long lasting vibrations under the passage of isolated trucks. The resultant problems were two-fold. The global vertical displacement field of the tied-arch spans was excessive and, due to the public's loss of confidence in the bridge, intolerable. Secondly, out-of-plane distortions of the floorbeams, which were related to the global displacement, had resulted in ever-increasing fatigue cracking in the webs of the welded floorbeams at locations shown in Figure 123.

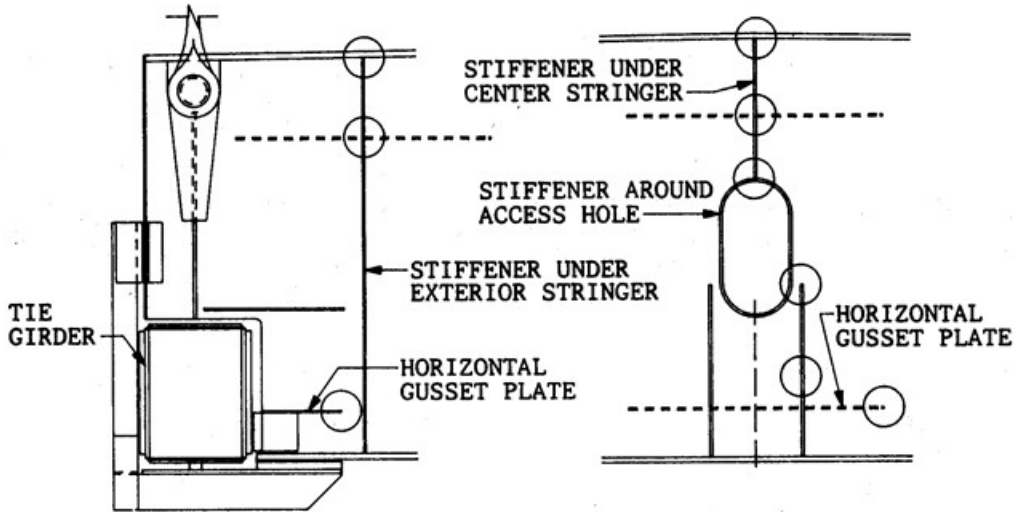


Figure 123. Illustration. Circles showing locations of typical fatigue cracks on welded floorbeams.

A combined field and analytic approach was taken as it was clear that field verified computer models would provide the most confident basis for evaluating proposed retrofits on the bridge, which had a history of prior problems. Since the observed problems were dynamic in nature, investigations began with field studies using accelerometers and strain gauges. Analytic studies utilized extensive finite element time history dynamic modeling and sub-structuring. The finite element models used to study the global dynamics were three-dimensional assemblages of plate bending, beam and truss elements as shown in Figure 124.

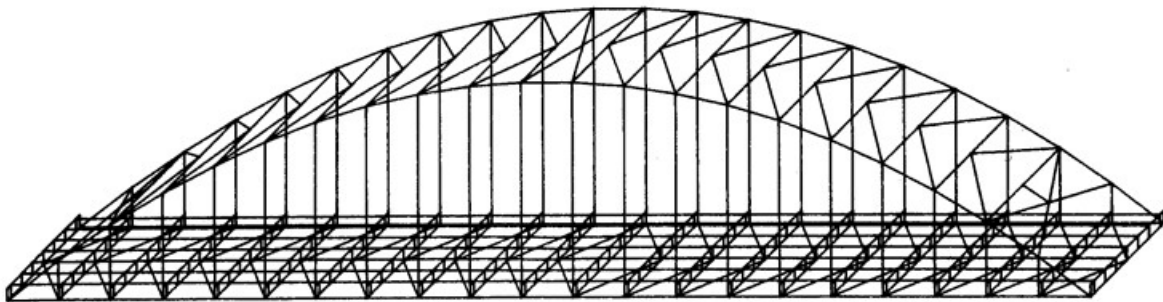


Figure 124. Illustration. Isometric view of three-dimensional finite element model.

Figure 125 is a comparison of analytically-obtained displacements compared to field-estimated displacements for two test trucks moving northbound and two test trucks moving southbound. Field data on displacements were obtained by estimating vertical displacement by sighting from a pier cap to a bolt pattern five panels away using a transit. While this type of measurement was quick and convenient, more accurate measurements could be taken with LIDAR, lasers and sometimes string potentiometers. Despite the expedient nature of the measurements taken in this case they were sufficient to produce confidence in the global model.

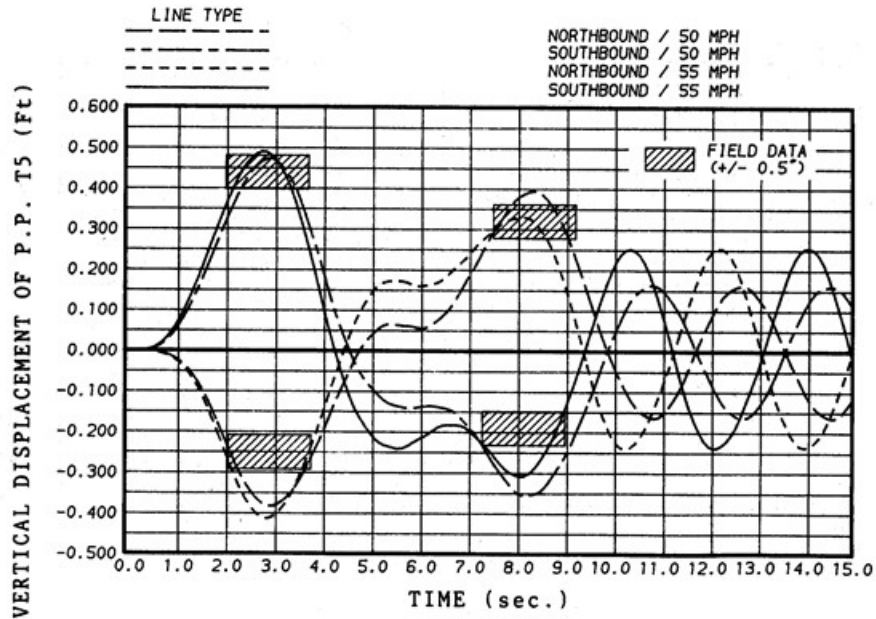


Figure 125. Graph. Two trucks – unit V (three-dimensional model).

Measured frequencies and mode shapes under imposed or ambient excitation provide a more comprehensive comparison assessment of the accuracy of a computer model because they combine the effects of stiffness and mass. Additionally, while the frequencies represent an integrated response, the mode shapes can sometimes point to local deficiencies or errors in a model. A comparison of field-measured and calculated frequencies and mode shapes for the arch bridge under consideration are shown in Figure 126. In this figure, the closed circles represent measured normalized amplitudes at the discrete accelerometer locations, while the continuous solid lines represent calculated mode shapes. Note that the mode numbers indicate that not all of the theoretical modes are significantly excited by the controlled truck traffic used in the field studies.

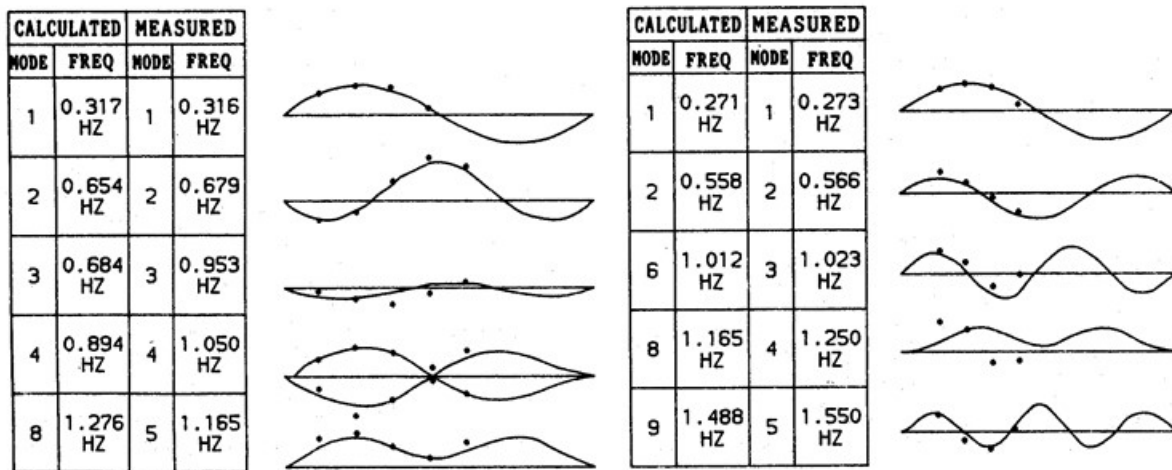


Figure 126. Illustration. Comparison of field-measured vs. calculated frequencies and mode shapes.

The measurement of strains made under vehicles of known weight and under random traffic can be particularly useful where behavior of an individual member or detail is being investigated as may often be the case in fatigue or cracking investigations.

In the current case strain measurements were compared to analytic results obtained using a submodel shown in Figure 127, which contains 670 plate bending elements, 541 beam elements, 14 truss elements and 156 boundary elements interconnecting 592 joints, resulting in 5,690 degrees of freedom. For a given instant of the time-history obtained using the global model shown in Figure 124, the displacement field surrounding the submodel was applied, which was then allowed to take the deformation pattern and, hence strains required to accommodate the global displacements. Figure 128 shows a comparison of field-measured and calculated strain histories from the submodel at four locations in unwelded gaps between plates. These gaps were cope size, i.e. about an inch in length.

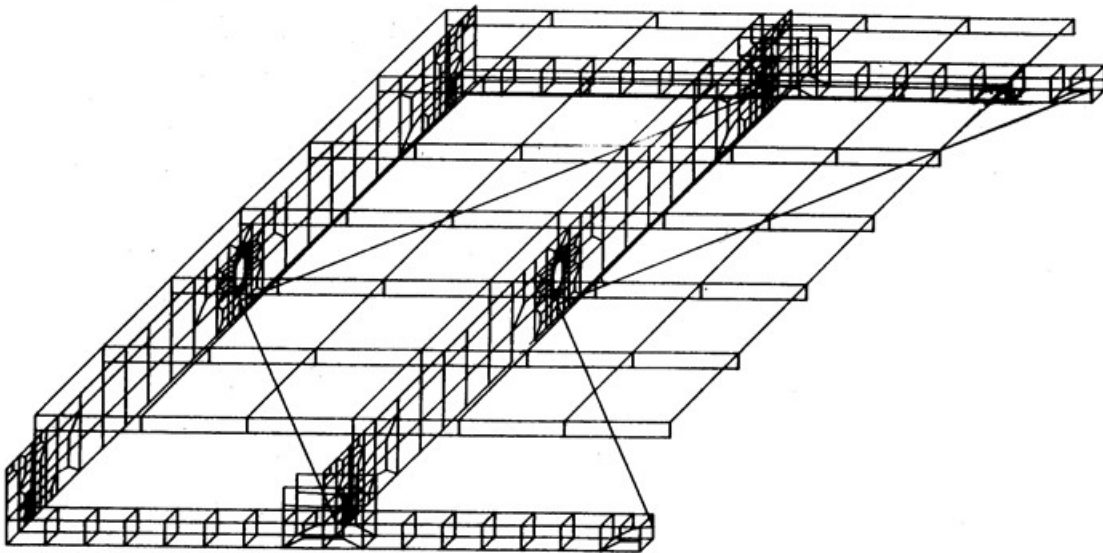


Figure 127. Illustration. Finite element model of first level submodel.

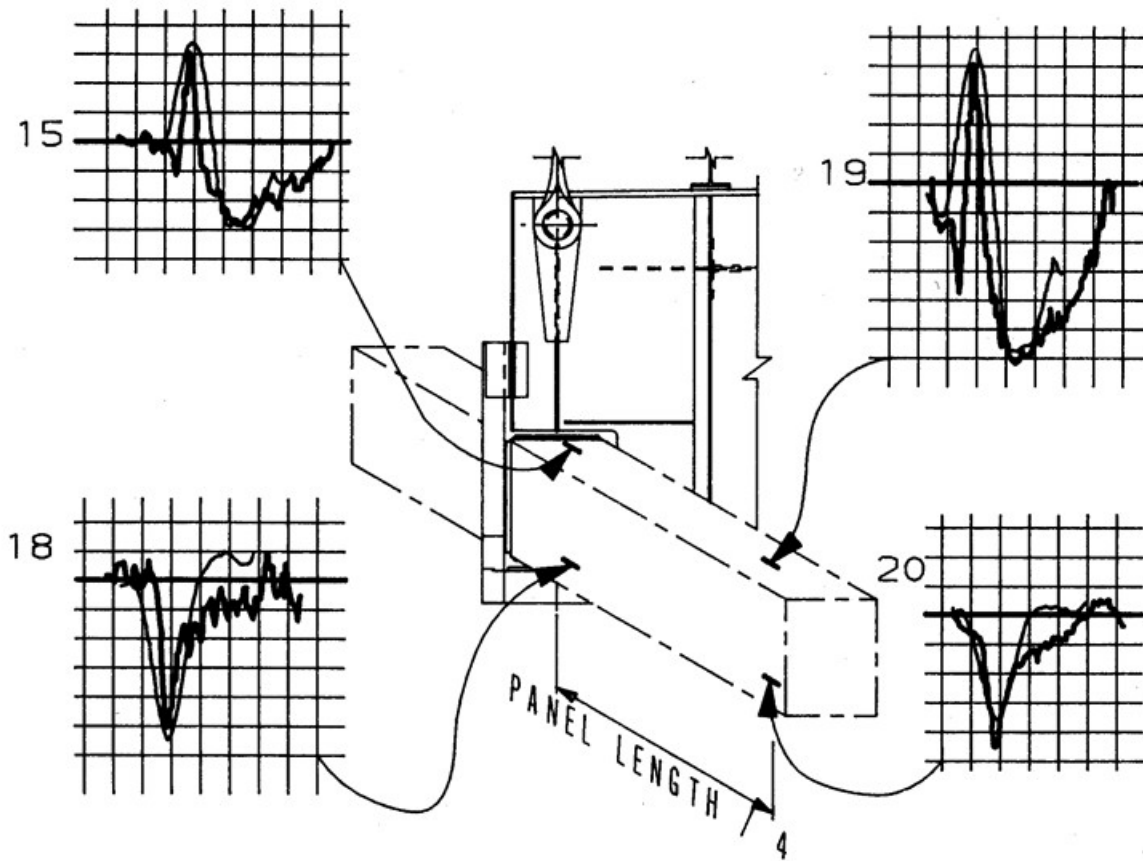


Figure 128. Illustration. Field vs. calculated strain time histories.

The comparison of field and analytic results indicates that the computer modeling accurately represents the physical situation. This step provided a confident base onto which various retrofits could be superimposed.

Often investigations such as those described above involving a field verified computer model are important not only in understanding the problem at hand, but also in evaluating potential retrofits. In the case at hand, the effect of two promising retrofit concepts on the dynamic response under vehicular traffic were studied using the three-dimensional finite element models. A typical comparison of the two concepts and the original response is shown in Figure 129. This comparison shows the time history of quarter point displacements under truck passage calculated for the original configuration and hypothetical retrofits based either on adding inclined hangers or conversion of the tie into a stiffening truss. The results of these studies indicate that while both were quite effective in reducing the unacceptable vertical displacement, the stiffening truss retrofit concept was more effective in reducing the crack-inducing distortion of the welded floorbeams.

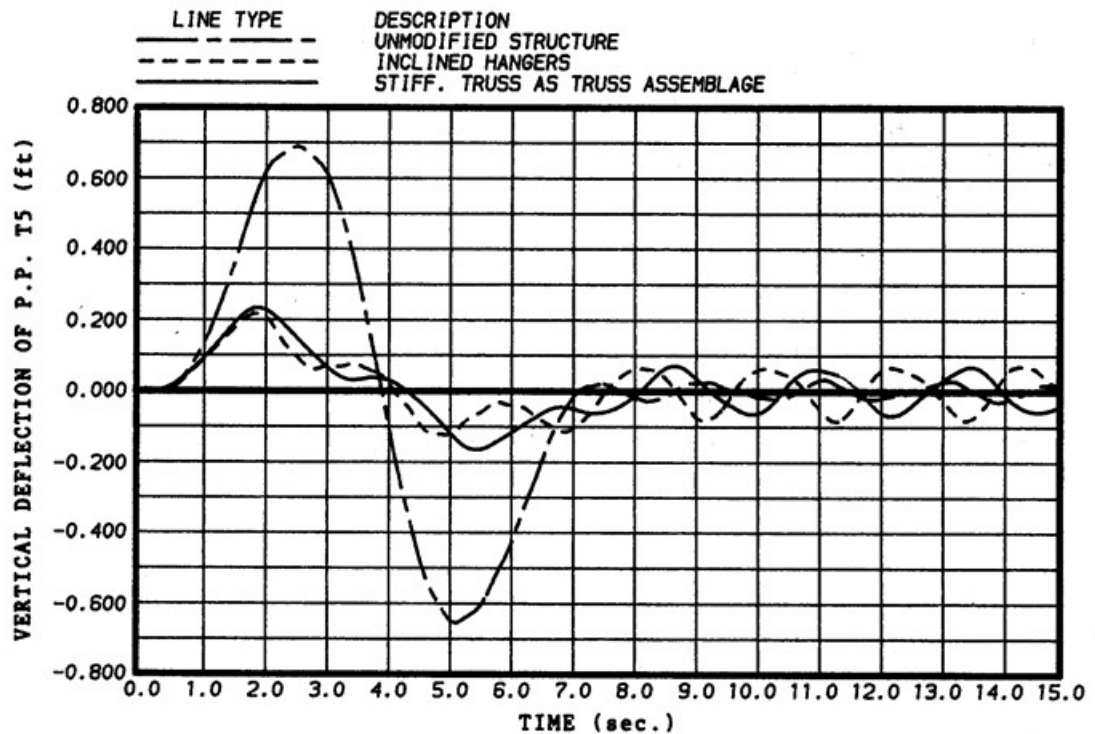


Figure 129. Graph. Quarter point displacements for unmodified and retrofitted structure.

In this case, the implemented solution involved the addition of a stiffening truss under traffic using the original tie girder as the bottom chord, and the addition of numerous gap closing plates and angles. Field tests after retrofit indicated that the reduction in displacement was almost exactly as predicted in the computer simulations.

6.5 Ramifications of Incorrect Boundary Conditions

Boundary conditions are a recurring problem in FEA. Consider the structure shown in Figure 130. This was a relatively straightforward bridge designed by grid analysis. The designer had a good model for this structure, except that the rotational degree of freedom corresponding to the global "X" axis was fixed instead of being released at all of the bearings. This did not allow the diaphragms at the piers and abutments to respond correctly to the imposed loadings and deformations, and also had the effect of producing artificially stiff ends on the girders by virtue of vector resolution between global and local systems. The effect of this condition on the reactions obtained at the abutments and piers was dramatic.

For brevity, Table 8 shows only results for the far abutment. It can be seen that the reactions are quite non-uniform, with a very substantial uplift reported at the acute angle. Note the moments at the pinned ends of the girders in the moment diagram reflecting the incorrect reactions shown in Figure 130. Also shown in Table 8 are the correct reactions determined when the structure was modeled as a grid with proper boundary conditions at the supports using a generic computer program for matrix structural analysis. In this case, a positive reaction is found at all bearings, and a significantly different moment diagram also resulted as shown in Figure 130.

The modeling of the degrees of freedom at the lines of support on this structure was also investigated utilizing a relatively complete three-dimensional finite element analysis. The deck slab, girders and cross-frames were modeled in their proper relative positions. The comparison of reactions obtained with the grid and FEA models was excellent.

Table 8. Live load reactions.

FAR ABUTMENT (FA) SUPPORT REACTIONS				
GIRDER NO.	"GRID" CORRECT SUPPORT CONDITION	DESIGNER'S INCORRECT REACTIONS	"GRID" INCORRECT SUPPORT CONDITIONS USING DESIGNER'S ASSUMPTIONS	
	(VERTICAL - k)	(VERTICAL - k)	(VERTICAL - k)	(MOMENT X k-ft)
1	66.68	223.61	223.24	811.24
2	64.36	47.07	47.14	1231.35
3	64.93	86.29	85.49	1229.66
4	66.62	117.94	117.94	1237.95
5	69.46	-81.63	-81.51	813.37

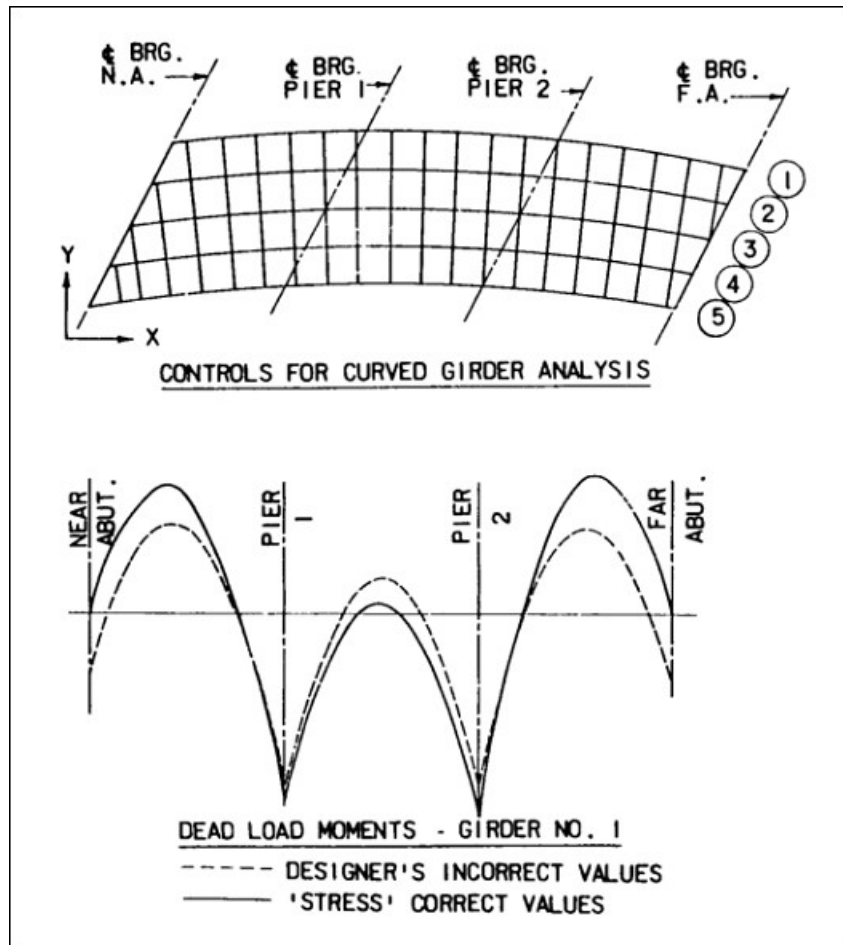


Figure 130. Illustration. Framing plan and moment diagrams for Girder 1.

Boundary condition errors in models can be easily overlooked, as point support problems typically are not something easily seen visually in graphic displays, unlike connectivity or geometry. This example illustrates the importance of verifying that the boundary conditions of the model represent the support conditions of the structure. It is essential that the proper restraint is provided at boundaries, including the orientation.

Model boundary conditions can be verified in a number of ways. Reactions can be viewed to determine if values are as expected. If moments are found at pinned supports, or force effects in directions intended to be released, then the boundary condition parameters should be revised. Articulation of the support can be investigated by viewing the deflected shape. Verify that the translations and rotations are as expected. A simplified loading can be assigned to the model and reactions verified to be in the range expected.

CHAPTER 7. LOAD APPLICATION

7.1 Applying Loads

Applying structural loadings in finite element programs can range from specifically defining the load at each node in the model, to taking advantage of automatic load generators to apply predefined truck loadings automatically. Most bridge analysis programs will have the capabilities to apply not only concentrated loads, but varying distributed or pressure loads, temperature changes resulting in thermal expansion/contraction (strains), prescribed displacements, and accelerations to mass resulting in force effects, e.g. acceleration due to gravity. Many will also allow defining combinations of concentrated and distributed loads to simulate various truck and lane loadings.

While most programs will permit defining the location of loadings between nodes, how they apply the defined load to the model is important, and may vary depending on what elements are being utilized. For instance, if the transformation involves simply proportioning the loads to the adjacent nodes based on geometry, i.e. lumped (simple beam) distribution to the nearest nodes, it can result in errors in the load effects, especially when the mesh is relatively coarse, and the resulting nodal loads are not statically equivalent to the defined loads. For instance, say a simple span beam is modeled using three equal length elements. The applied loading is a concentrated load P at midspan, for which we know the resulting maximum moment, $PL/4$. The given model applies a load of $P/2$ at each of the third point nodes, resulting in a maximum moment of $PL/6$, or an error of 50 percent.

General recommendations for applying loads:

- *A node should be present at locations of unmoving concentrated loads.*
- *The mesh should be fine enough to approximate the static equivalent load effects for distributed loads, automatic gravity loads, and moving loads in cases where only lumped nodal loads are calculated and always verify how loads are being applied.*

The finer the mesh, the more accurately the model load effects will reflect the applied loadings, due to node proximity to the applied loads and the nodal loading approaching the statically equivalent loading. Mesh refinement needs to be balanced against computational effort, however. The analyst should verify that the loading is accurately reflected in the model, by checking how the loading is approximated and adjusting the mesh and/or loading such that the load effects are sufficiently correct.

7.2 Dead Loads

7.2.1 Modeled Components

Incorporating the dead load of modeled components can be relatively easy in a refined analysis. Since the length/width of an element and the cross-sectional area/thickness are available to the program, it can automatically calculate the dead load of modeled elements using the material density and applying the acceleration due to gravity. For elements that incorporate dissimilar materials using modular ratios to alter some of the dimensions, an effective density can be utilized to achieve the correct loading. Alternatively, the applied acceleration can be altered to account for differences. Note that all of the inputs should be checked for accuracy when taking

advantage of this capability, and as a further check the load effects and reactions can be examined as well.

7.2.2 Non-Modeled Components

Non-modeled components are elements that are present on the bridge, but which the designer does not wish to contribute to the stiffness of the structural model. Non-modeled components may include but are not limited to connection plates, integral wearing surface, future wearing surface, haunches, barriers, and utilities.

The dead load of non-modeled components can be included in a number of ways, depending on the accuracy of the analysis required. The easiest way is to include it via the modeled components, by increasing the effective material density or the effective gravitational acceleration. Usually this is performed in preliminary design, by adding an additional 5-10 percent for concrete bridges and 10-20 percent for steel bridges to the weight of the modeled components.

A second more accurate way to add the dead weight of non-modeled components is through the use of concentrated or distributed loadings on the model. This requires the calculation of the dead loads of all the non-modeled components, but has the advantages of not only applying more accurate weights but also of applying the loads closer to the specific location of the component.

While evenly distributing barrier loads to all girders can be appropriate for a 1D analysis, barrier weights can be modeled as distributed line loads applied at their actual locations in 2D and 3D analyses. For 2D and 3D models applying the load to the edge of the deck where a barrier is present, not necessarily through the barrier centroid, is usually sufficient. Similarly, utility loads can be applied as distributed line loads at their actual locations in 2D and 3D analyses. Haunch weight can be applied as distributed line loads along girder lines. Integral and future wearing surfaces can be applied as distributed line loads on 1D models and 2D grid models, or pressure distributed loads on the deck surface of 2D PEB models or 3D models. Gusset and connection plate loads can be applied as concentrated loads at the location of the connections.

An alternate way to add the dead load of elements whose stiffness the analyst wishes to neglect is to explicitly model them but assign a negligible stiffness to them. This is a good technique to use with elements whose stiffness is desired in certain analyses, but is neglected in others, such that a single base model can be utilized. Examples would be stiffnesses of an integral wearing surface or barriers that the analyst wishes to conservatively neglect in a strength limit state analysis, but include in a service limit state, such as deflection, analysis.

It may be tempting to the analyst to neglect the weight of non-modeled components such as connection plates or stiffeners as insignificant. For final design in particular, it is strongly advised that calculations be performed confirming that dead loads are indeed insignificant prior to neglecting them.

7.3 Live Loads

7.3.1 AASHTO LRFD Requirements

Section 3.6 of AASHTO LRFD contains most of the provisions pertaining to application of live loads in bridge design. *The live loads are generally the same no matter what method of analysis is used.* A search through the Seventh Edition of AASHTO LRFD identified provisions related to the magnitude and application of live load in refined analyses. The articles are listed in Appendix 7A. Most of the provisions relate to correct application of live load to refined models and when a refined model can/should be used to get a more accurate distribution of live load. Some relief is provided in the form of a reduced load factor when the fatigue stress range is maximized by placing the truck in two different positions laterally on the bridge.

A similar search of the Second Edition of AASHTO MBE yielded the provisions listed in Appendix 7B. The MBE provides for the use of site specific loadings as well as permit checks and AASHTO Legal Loads. Reduced load factors are specified for fatigue analyses based on refined analyses.

7.3.2 Additional Requirements

No specification can cover every situation a designer may encounter. There are places where unique situations occur and designers have to be alert as it may require additional, site-specific, evaluation of live load. AASHTO LRFD provides some examples of such situations in Articles C3.6.1.2.1 and C3.6.1.3.1. From the perspective of this manual these caveats flag the possible need for the analyst to provide a description of one or more custom vehicle configurations and/or custom line or surface loads, and to ensure that such custom loads are properly defined and applied to the appropriate analysis model(s).

7.3.3 Modeling Vehicle Live Loads

For various provisions in AASHTO LRFD the live load is modeled as a uniform line load, concentrated loads, a distributed pressure load, and individual patch loads. *The basic HL-93 loading involves the design truck, the uniform load, and the design tandem, all of which are shown in Figure .* The HL-93 Truck Train is also included in Figure , which consist of two HL-93 Trucks. 100 percent of the truck axle loads are shown in the figure for visualization; however, only 90 percent of the effect of the two trucks is used when applying the load in accordance with AASHTO LRFD. Where dimensions of the elements of the structure under design are large relative to the spacings of the vehicle wheel/axle loads, concentrated point loads for wheels and/or axles are adequate. In reality, most truck trailers would be twin axles with wheel patch loads as illustrated in Figure 132, but for many analysis models this refinement has little effect.

There are applications where point loadings are insufficient. This would be the case for example with local fatigue effects, orthotropic decks, grid decks, closely spaced joists, certain timber decks, and buried culverts and pipes. In these cases, the single axle may be represented as twin axles and the point loads may be represented by patches. Figure 132 shows the refined truck which uses both twin axles and patch loads representing the wheels. This configuration should be used when the actual tire pressure area and tire spacing could affect the results. It is the responsibility of the user to make sure that the software adequately represents the configuration

of the vehicle being used for the element under design, or at least as a conservative representation of it. The effect of superelevation or centrifugal force should be considered as well as they may unbalance the lines of wheel loads.

Amplification of live loadings due to dynamic effects are accounted for through the application of the Dynamic Load Allowance of AASHTO LRFD Article 3.6.2. For most elements and limit states this factor is 33 percent, applied to vehicle loads only, not sidewalk or distributed lane loads. This factor is most easily applied by increasing the vehicle loads in the analysis, but it can also be applied to the force effects afterward, as long as vehicle and lane effects are kept separate.

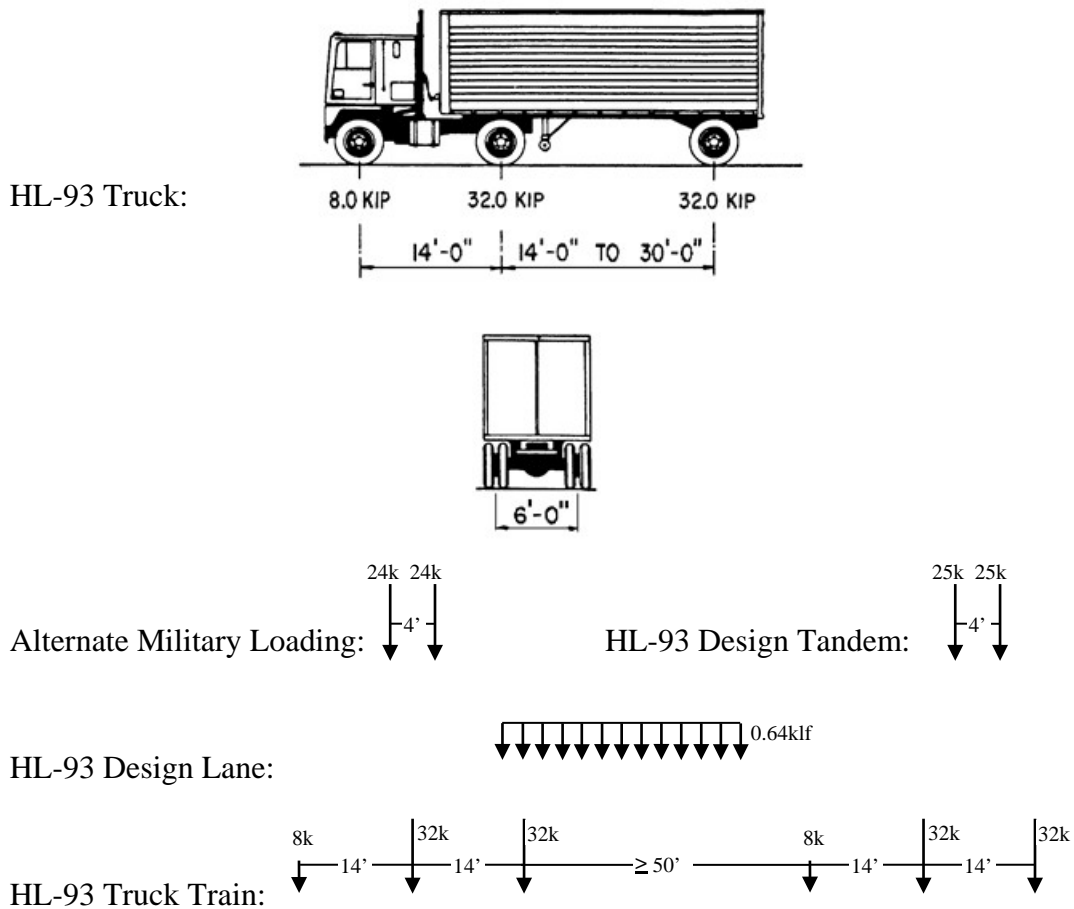


Figure 131. Illustration. AASHTO standard vehicle loadings (AASHTO, 2017).

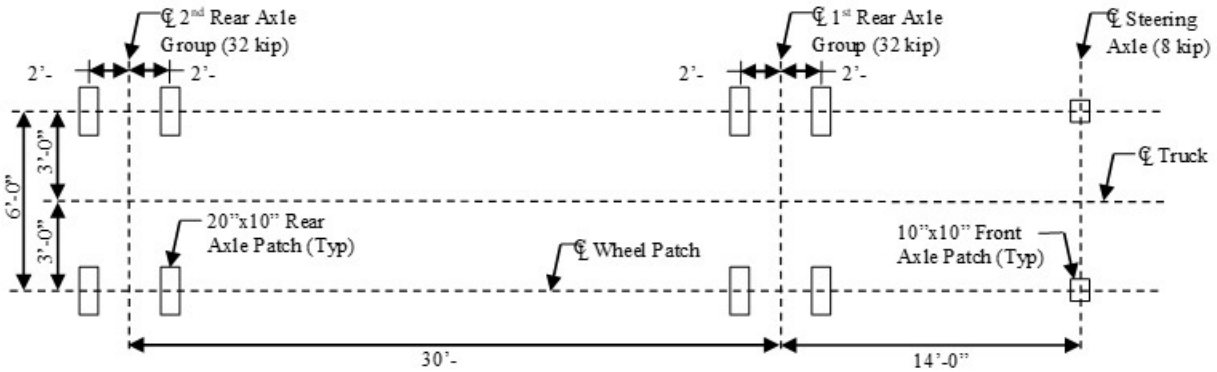


Figure 132. Illustration. HS20 Truck with tandem axles and wheel patch loads with 30' spacing between 32k axles (AASHTO, 2017).

Fatigue loading consists of a single HL-93 truck or axles thereof with a constant spacing of 30' between the 32-kip axles. A dynamic load allowance of 15 percent is applied to the fatigue load per Article 3.6.2.1 of AASHTO LRFD. The truck should be placed both longitudinally and transversely to create the extreme stress range effect. In some cases, the maximum stress range in a detail such as a cross-frame or orthotropic rib will be obtained by placing trucks in two different transverse positions on the deck. Previous editions of AASHTO LRFD dealt with this situation by applying a 75 percent factor to the stress range. This has been changed in the 2015 Interim Revisions to using the single transverse location that results in the largest stress range. Note that two longitudinal positions may still be used to generate the largest stress range.

Sidewalks or shared use paths, the designation for sidewalks that also accommodate bicycle traffic, are often present along with vehicular travel lanes on bridges. AASHTO LRFD treats these as an additional travel lane with respect to multiple presence, and prescribes a design pedestrian live load of 75 psf in Article 3.6.1.6. Also according to Article 3.6.1.6, vehicles are to be considered on the sidewalk when they can mount it, but not concurrently with pedestrian loads. Some owners may require vehicle loads be applied to sidewalks/paths, sometimes on a site specific basis, for instance to allow for future widening. When the path is separated from the roadway, judgment may be required to determine what vehicles, if any, should be used for path design.

7.3.4 From Wheels to Loads

Once the live loadings have been defined, they must be applied appropriately to the model. This can be harder than it appears. Given that generally the model does not have a node at every point where one wishes to locate a wheel, the mesh size and the method used to apply patch or concentrated loads is important. Even though FEA programs will typically allow loads to be applied between nodes, often the effective loading applied to the model is simply the given loading proportionately distributed to the adjacent nodes. As mentioned previously, this approximation can be significantly wrong if the mesh is coarse, especially near supports.

The AASHTO recommended lane width is twelve feet, which typically should be used in modeling. The exception to this is when the bridge is striped for narrower lanes, then the narrower lane width should also be used in modeling and design. The lane load is ten feet wide

and vehicle loads are typically six feet between wheel lines. The lane load and truck load should be placed transversely within the lane in order to obtain the extreme force effect in the member under consideration. Truck loads are typically limited to the center eight feet of each lane, the exception being for design of overhangs, where the wheel load is placed one foot from the face of curb or railing. Lanes should be positioned to produce the extreme force effect in the member under consideration, which may not correspond with the striped lanes.

Typically, 1D models do not account for lateral or torsional force effects. The exception is the spine beam model, where the entire bridge cross-section is modeled with a single line element. To model the effects correctly, the eccentricity causing torsional effects due to transverse placement of lanes, wind on live load, or centrifugal loads needs to be included. This can be accomplished either by providing dummy elements at the location of the load, and attaching them to the spine beam with rigid links, or more easily by including the torsional effect as a torsional moment or couple as part of the applied load.

Another confounding provision is the multiple presence factor. AASHTO LRFD Article 3.5.1.1.2 assigns factors based on the number of loaded lanes, such that each lane load is reduced as more lanes are loaded. This factor accounts for the fact that the probability that all lanes will have the load in the extreme location for a given element drops as more lanes are loaded. The result is that an increase in the number of loaded lanes does not necessarily result in an increase in the extreme effect, even when the additional lane is contributing to the effect.

7.3.5 Live Load Optimization

In order to perform component design, the maximum and minimum live load force effects in the component must be determined. This requires the live loading to be placed on the bridge model in the positions which result in the extreme force effects. For some relatively simple structures the location of loads to maximize the force effects is intuitive and obvious, but for more complex structures influence lines or surfaces can be used to help determine these loading patterns.

Obtaining influence lines for a single girder with the appropriate boundary conditions and span lengths is sufficient for 1D models and can be useful in determining the approximate longitudinal position of live load on 2D and 3D bridge models. Most software packages can generate influence lines automatically, or they can be generated by the user. For very simple structures, handbook solutions exist.

One way to generate influence lines/surfaces is to use the Müller-Breslau principle which states that the influence lines of an action (force or moment) is a scaled form of the deflection that the structure displays after removing the restraint on the point where the action is evaluated and applying a concentrated load or moment at that point which causes a unit displacement. The major advantage to this method is that it only requires calculation of the specific influence ordinates desired. The main disadvantage is that it requires a modification of the model for every point of interest. If influence lines/surfaces are required for many points, it can be time-intensive.

A second way to generate influence lines/surfaces is to use a general “brute force” method, which entails solving the structural analysis of the model independently for a unit load at every single node on the influence surface. The effect of all the analyses at any point can be mapped to

the point of application of the unit load causing that effect to determine the influence surface. The major advantage of this method is that once all of the analyses have been performed an influence surface can be generated for any force effect at any point. The disadvantage is that it is computationally inefficient, especially when the influence surface contains many nodes and relatively few influence surfaces are desired.

Influence lines/surfaces can be generated by applying the principles above, and then loads applied to generate the extreme force effects. This consists of applying the Specification loads in the prescribed manner. For example, Figure 133 shows an influence surface generated for bending moment at a specific point, Node 24, in a three span curved bridge. In Figure 134, the influence ordinates are used to position the AASHTO Fatigue Truck loading to maximize the positive bending moment at Node 24.

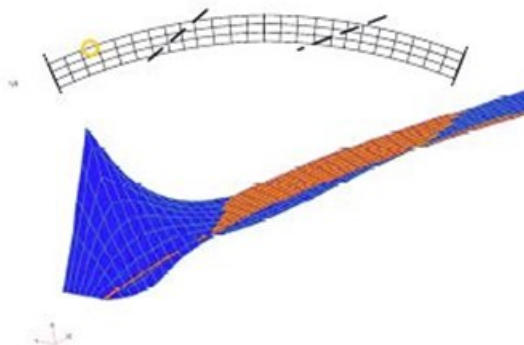


Figure 133. Illustration. Influence surface for vertical bending moment at the circled location, Node 24 (Grubb, 2011).

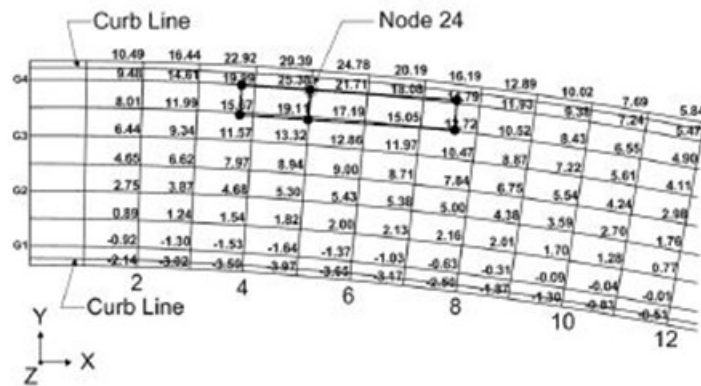


Figure 134. Illustration. Wheel-load model of the fatigue live load positioned on influence surface to maximize the positive vertical bending moment at Node 24 (Grubb, 2011).

Sometimes additional design live loads, such as permit or legal loads, are specified by the Owner. The configuration, loading, and manner in which permit loads are applied differs from Owner to Owner. Sometimes Owners may require that the design load occupy only one lane (Figure 135 Part A), two lanes (Figure 135 Part B), or all design lanes (Figure 135 Part C).

Some Owners may require that the permit load occupy one lane, with HL-93 loading in the remaining lanes (Figure 135 Part D). The reason for requiring multiple permit loads might be that certain routes carry a high number of permit vehicles. Placing HL-93 traffic in the remaining lanes with permit loading would account for cases when permit loads are present along with normal traffic. For more on live load placement see (Grubb, 2011).

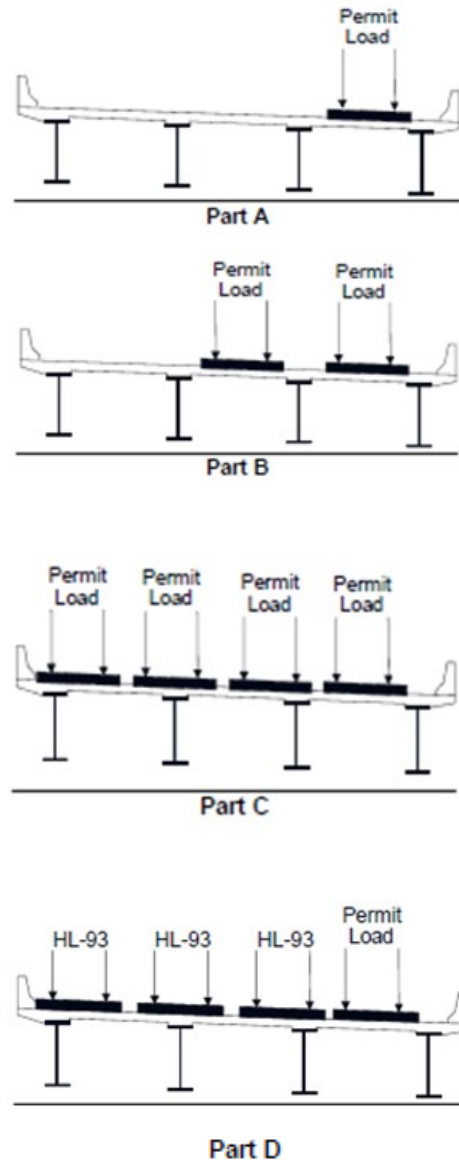


Figure 135. Illustration. Various permit lane and truck loading configurations (Grubb, 2011).

A trial and refinement approach would probably need to be utilized when applying loads based on influence surfaces, with the number of refinements required largely dependent on the required accuracy of the results, and the engineer's ability to estimate/understand the shape of the influence surface. *In order to reduce computational effort, during preliminary design or model verification, a relatively coarse mesh can be utilized and the vehicle placement increment can be*

relatively large, in the range of 4-6 feet. For final design, a finer mesh can be utilized and a vehicle placement increment of 1-3 feet both transversely and longitudinally is typically adequate. Judgment may be required based on the geometry of the structure in order to balance the level of accuracy versus the solution effort.

Even with a good understanding of the structural behavior of the system, difficulties can arise with multi-lane bridges due to the large number of variables, such as lane placement, truck placement within the lane, presence of a shared use path, multiple presence factors, etc., not to mention the effort involved in generating the influence surfaces.

In some cases, it may be simpler to dispense with the influence lines/surfaces completely, and use a “brute force” method of many load cases independently stepping the truck load and stepping a small patch of lane load “nose to tail” longitudinally along the structure in a transversely defined lane. The maximum load in a component would be the load case of the maximum truck load summed with all of the lane load cases that contribute to the maximum effect. This method is particularly attractive when a lateral distribution factor for the component is easily calculated, such that lateral placement of the load is not a variable. Additional “vehicle” loadings using various axle combinations can be included if there are cases where neglecting certain axles increases the maximum effect.

Some FEA packages, especially those tailored for bridge design, have the ability to generate influence lines/surfaces and to determine the placement of live loads to maximize/minimize the desired force effects automatically. This greatly simplifies the procedure for the user, but still generally requires a large computational effort. And as always, results should be verified.

7.3.6 Wind Loads

Section 3.8 of AASHTO LRFD prescribes the means to calculate design wind load pressures for bridge design. The specification also details how windward and leeward wind as well as skew effect should be applied.

To apply wind to surface or volume elements, the wind pressure can simply be applied to the appropriate surface. To apply wind loading to line elements, the depth of the projected wind areas of the members can be multiplied by the wind pressure to obtain a distributed force, which can then be applied to the member. Alternatively, the full projected area of an element can be multiplied by the wind pressure, and the resulting concentrated force divided appropriately among the element nodes.

Most of the time, even for 3D models, the full cross-sectional wind area is not explicitly modeled, i.e. parapets are not modeled with shell elements, and shell element deck height is not explicitly modeled. *Any combination of concentrated, distributed, or pressure loads can be used to apply the wind pressure, as long as a statically equivalent loading to the wind pressure results.*

To account for wind loading on vehicles, AASHTO LRFD prescribes an interruptible 0.10 klf force acting 6.0 ft. above the roadway. Usually there are not any nodes or elements located 6.0 ft. above the deck in a model, so the load is transformed into a statically equivalent loading of a transverse distributed force of 0.10 klf and a distributed moment of 0.60 k-ft/ft applied at deck

level. The distributed moment can be applied either by a direct moment or by a force couple, ideally at the wheel locations, depending on what is easiest.

The wind force on vehicles is interruptible because vehicles need not be present in all locations on the bridge, so the load should be conservatively applied only when it contributes to the extreme force effect in the component under consideration. Generally, the patch pattern of wind can be limited on a span basis, i.e. the wind is either present or not on each span of the bridge between supports to produce an extreme effect in an element. The LRFD specification details how to account for the skew effect of wind on vehicles as well, by adjusting the percentage of lateral and longitudinal force effects.

Article 3.8.2 of AASHTO LRFD details the magnitude of an upward acting longitudinal distributed load equal to 0.020 ksf times the width of the bridge applied at the windward quarter point of the deck. This load is easily applied as a distributed load on the model. Note that it is only applied in conjunction with wind loading acting perpendicular to the bridge.

The AASHTO LRFD prescribes wind tunnel tests to address aeroelastic instability and dynamic response to wind loadings when bridge span to width or depth ratio exceeds 30.

7.3.7 Centrifugal and Braking Forces

The lateral forces due to centrifugal and braking should be considered as well. The magnitudes of the centrifugal and braking forces are prescribed by AASHTO LRFD Articles 3.6.3 and 3.6.4, respectively. Similarly to wind forces acting on live load, the centrifugal and braking forces are applied 6.0 ft. above the deck surface. Again, like wind, the forces can be applied at deck level with in-plane forces and moments as necessary. The moments can be applied directly or as a force couple, ideally at the wheel locations.

Modeling the boundary conditions or the bearing elements connecting the superstructure to the substructure correctly is important when analyzing for centrifugal and braking load effects. A load path needs to be provided to carry these in-plane forces to the substructure, and the bearings are often the critical elements in this path.

7.3.8 Thermal Loads

The extremes of design uniform temperatures that are to be used for determining stresses and/or movements are prescribed by Article 3.12.2 of AASHTO LRFD. A uniform temperature increase or decrease loading in a finite element model is achieved by simply applying a uniform temperature change to every element comprising the model. Load effects and/or displacements can then be extracted from the model. *Where physical restraints exist, care should be taken to make sure appropriate boundary conditions are being utilized in the model, such that unintended restraint from idealized unyielding supports does not result in spurious forces/overstressed members or incorrect displacements.* Avoiding unintentional horizontal restraint can be particularly important in the analysis of significantly curved and skewed structures.

Article 3.12.3 of AASHTO LRFD prescribes the design temperature gradient for concrete deck on girder bridges. Note that the temperature gradient does not prescribe an absolute temperature, but the difference in temperature with depth. No stresses or reactions are produced in statically determinate structures when the temperature variation is linear, only changes in length or

curvature. When the temperature variation is nonlinear, self-equilibrating stresses are induced in individual cross-sections of statically determinate structures, but no reactions. When the structure is statically indeterminate, temperature variations can result in both reactions and internal forces in members. For cases where uniform temperature changes result in force effects in the structure, temperature gradients should be superimposed on uniform temperature changes to obtain extreme effects.

Article C4.6.6 of AASHTO LRFD provides some guidance on how to estimate the imposed deformations of a linear temperature gradient on a 1D beam. A linear temperature gradient analysis needs to consider axial extension, flexural deformation, and internal stresses. For more information and examples see (Ghali, 2009).

Because most FEA programs can only accommodate linear thermal gradients within beam and shell elements, in order to analyze a temperature gradient in a 2D PEB analysis, it is recommended that a nonlinear gradient over the cross-section be approximated by linear gradients applied to the elements of the model. Differing linear temperature gradients can be applied to the deck and the girder in order to achieve this.

For a full 3D analysis, the temperature gradient can either be applied as a series of linear gradients, or if the mesh is fine enough and/or the gradient is shallow enough, as a stepwise series of uniform temperature variations through the depth of the section, or some combination of the two methods. The application of a nonlinear temperature gradient can be made simpler by meshing the model with the assumed gradient in mind.

It is important that boundary conditions/bearings are modeled correctly in cases where thermal forces are developed in the superstructure and substructure of a bridge. Often an analysis is performed to verify that piers are flexible enough to tolerate thermal movements such that pinned rather than expansion bearings can be provided on the maximum number of piers. Integral piers will also need to be designed for force effects due to thermal loadings.

7.3.9 Loading Substructures

When the substructure is modeled along with the superstructure, extreme force effects due to live loading can be determined in a similar manner as for the superstructure. The stiffnesses of the superstructure/substructure interface elements will distribute the concurrent force effects automatically and design forces can be obtained directly utilizing influence lines/surfaces. When the substructure and superstructure are modeled independently, the extreme force effects at the superstructure/substructure interface, usually bearings, need to be determined in the superstructure model, then applied to the substructure model.

Depending on the geometry of the substructure, different strategies may need to be employed to obtain the force effects from the superstructure model to be applied to the substructure model in order to determine the substructure design force effects. Often five loadcases, maximizing the total axial force, total transverse and longitudinal bending moment, and total transverse and longitudinal shear on the substructure unit are sufficient. But for substructures that are unsymmetrical, skewed, or bents with interior columns, the loadings can be more complicated and more care should be exercised.

For most slab on girder bridges, modeling the substructure along with the superstructure is generally not complicated, and does not add many degrees of freedom to the model, meaning not much additional computing time is required. *If the analyst chooses to model the substructure, ensure that the modeled stiffness results in accurate, or at worst conservative bearing reactions.*

7.3.10 Verifying Live Loads

As stated previously, correct calculation of the effects of the moving live load requires the proper application of the AASHTO LRFD mandated number of design lanes, multiple presence factors, lane size and position of lanes and position of truck or patch load within the lane boundaries. Implementing this correctly for a general situation is quite a challenge. Add to this the variety and complexity of influence surface shapes for various force effects and the result is a very difficult programming problem. One might think that after decades of application all software gets this right, but two examples over twenty years apart will show that this is not the case. The analyst must still take the responsibility to confirm that the results are correct.

The relatively simple curved, single span bridge whose framing is shown in Figure 136 was analyzed circa 1980 using a commercial grid-based software package that had AASHTO live load processing. The designer modeled the bridge with nodes between diaphragms to more thoroughly define the live load force effect envelopes. Fortunately, the designer spent time to study the results before proceeding to proportion the girders. The results just looked odd. The moment envelopes were plotted for each girder and the results are shown in the top part of Figure 136. After discussions with the software vendor, it was discovered that the live load processor assumed that all nodes were connections between girders and diaphragms. The additional nodes added to better define the shape of the envelopes were not being processed correctly. Removal of some of the added nodes improved the results as shown in the lower part of Figure 136. This previously unreported problem was quickly addressed by the vendor, but was discovered only by the vigilance of the designer.

Twenty years later another problem in the application of the AASHTO live load was discovered in cutting edge commercial software. As in the example above, it was only the vigilance of a designer who could not believe that the large reported difference between traditional design methods and a three-dimensional analysis made sense. The shape of force effect envelopes looked fine; the difference in magnitude did not. One would expect some difference in magnitude but the reported difference just looked about 10 percent too great. After some test cases, it was found that the new software was applying the provisions for multiple presence incorrectly; a very subtle problem, but a problem nonetheless.

Another bug that has occasionally cropped up with automatic software optimization is that the methods are too general. For instance, trucks and tandems will be mixed, or different numbers of lane loads and truck loads will be used in the same load case. While not as worrisome as other errors, since presumably these types of bugs provide conservative results, the analyst should be aware of the possibility of odd loadings being generated by automatic optimizers.

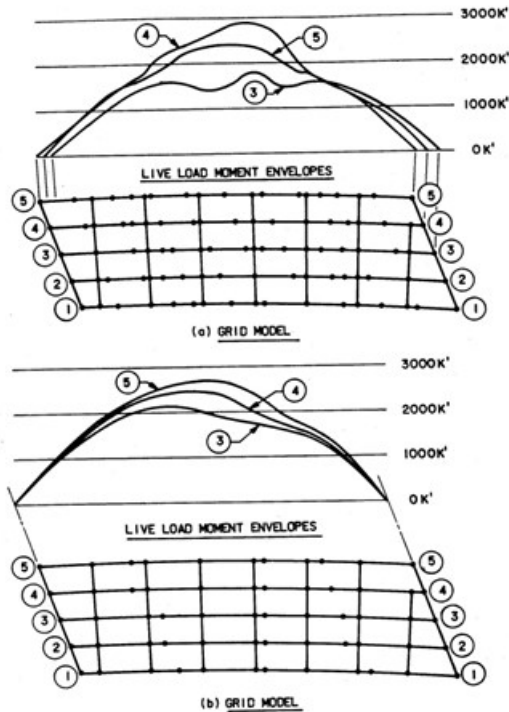


Figure 136. Illustration. Calculated moment envelopes.

As the above examples demonstrate, software cannot always be relied on to provide the correct answers, and user error is always a possibility as well. But simply examining the influence lines/surfaces, the placement of the loads, and the resulting force effects, is often sufficient to spot erroneous results. Sometimes the intuition of an experienced engineer is the best tool for detecting errors, and for many force effects the user should have a qualitative idea of what the loading should look like. Another approach to verifying results would be to spot check results manually, by using approximate methods, to confirm that the FEA automatic procedure was producing reasonably accurate results. A final verification method would be to independently generate the results with a different finite element program, and confirm that similar results were obtained.

7.4 Prestressing Loads

The AASHTO LRFD handles concrete prestressing on the resistance side of the equation. As such, it is not treated as a load subject to load factors, but as a contributor to the resistance subject to resistance factors. That being said, when analyzing prestressed concrete, the prestressing forces need to be accounted for in the model. There are typically two ways to model prestressing, the equivalent force method and the explicit modeling method. The equivalent force method replaces the steel bars/tendons with statically equivalent forces. The explicit modeling method models the bars/tendons at their correct geometry and then shortens them using the program to develop the appropriate tension. For more guidance on prestressed concrete modeling see Section 4.1.3.

7.5 Loading Nonlinear Models

Load Combinations in AASHTO LRFD typically take advantage of the ability to superimpose and factor (or extrapolate) multiple linear elastic analyses. *Nonlinear analyses results cannot be factored or superimposed.* All factoring and superposition must be done before performing the nonlinear analysis. Due to this limitation, performing multiple nonlinear analyses for load combinations such as moving vehicle loadings can become quite onerous, and is not recommended.

Performing nonlinear analyses should only be performed on a limited number of cases. Further, when using any automatic factoring or load combination features of any particular software package in conjunction with any nonlinear analysis, it is a good idea to confirm that the factoring and/or combining is indeed being performed prior to the nonlinear analysis.

For more guidance on nonlinear modeling, see Section 5.3.

CHAPTER 8. ANALYSIS TO DESIGN

8.1 Compatibility of Analysis and Specification Provisions

While analysis is a major part of bridge design, it is still just one of the steps in the multi-step process of designing a bridge based on AASHTO LRFD. Analysis as part of routine slab on girder bridge design typically entails a first-order linear elastic solution that provides load resultants based on member stiffness and connectivity. Bridge design is also an iterative process, requiring multiple analyses, often of multiple models, and for multiple load cases, as the design is optimized. After each analysis iteration bridge components must be checked to make sure they satisfy all limit states using the provisions of AASHTO LRFD as well as other applicable specifications.

Most FEA software only provides analysis results in the form of forces or stresses. Some software packages provide specification checking within the program, but as always, the designer should verify that the checks are being performed correctly, and that all relevant checks are being performed.

Ideally, bridge analysis methods and bridge design methods would be completely compatible, with a seamless integration of the two, making it a relatively easy proposition to check the load carrying capacities of bridge components as well as check all other limit states. This is not the case, due to a number of reasons, not the least of which is the AASHTO LRFD was not written with a specific analysis method in mind. The AASHTO LRFD also contains provisions that implicitly account for certain design factors, such as residual stresses or initial out-of-straightness, which need to be addressed if an alternative approach is substituted for the AASHTO strength design, such as determining the compression capacity of a member directly from the finite element analysis.

The AASHTO LRFD is mostly a component design specification. Given member properties and using the various provisions of AASHTO LRFD, individual member nominal ultimate capacities at the strength limit state, which often intrude into the non-linear realm of behavior, are generally calculated in the form of moments, shears and axial forces. Equations in the AASHTO LRFD such as the steel column resistance give results as forces. Flexural resistance of concrete girders is calculated as a moment due to the material non-linearity of concrete and reinforcing bars at the strength limit state. The concrete moment-axial interaction curve requires loads and resistances in forces.

In its current form, especially for the Strength Limit State, the AASHTO LRFD is most compatible with line element analyses, such as single girder analyses using the approximate distribution factors from Article 4.6.2, or basic grid analyses. In these cases, loads extracted from the linear elastic analyses are the factored shears, moments and axial forces that can be compared to factored resistances calculated by the LRFD Specification.

Making a model more discretized, and using plate, shell, volume, or combinations of elements provides the design engineer with the capabilities necessary to handle complex 3D analyses. However, generally the output from these elements is in the form of stresses or nodal forces, and in the case of volume elements, three-dimensional stress fields, not the component moments,

shears, and axial forces required for design. Additional 3D model complexity also often results in more complicated “book keeping” to account for the live load stresses.

In the cases where AASHTO LRFD provides for directly checking stresses, usually it is in one dimension, and often for Serviceability Limit States, where concrete behavior is assumed to be linear. Shear and normal stresses are typically addressed independently rather than looking at principal stresses. An example of a check in two dimensions is contained in Article 5.8.5 of AASHTO LRFD which details the service and construction load cases for which webs of segmental concrete bridges are subject to the principal stress check. Future versions of the AASHTO Bridge Design Specifications may incorporate additional principal stress checks, which can be calculated by hand using Mohr’s circle, or directly obtained from FEA analyses.

8.2 Analysis Results to Design Inputs

When the analysis results do not correspond to the required design inputs, additional post-processing steps are needed to obtain the values which are needed to perform the design checks required by the AASHTO LRFD. *Two different approaches are possible; the analysis results can be transformed into the form needed to apply specification checks, or the specification checks can be transformed into a form compatible with the analysis outputs.* An example of the former would be integrating stresses over a surface to determine forces, or summing force outputs of several elements, to calculate the design load resultants, or the demands on a given component, such as the shears, moments and axial forces necessary to compare to AASHTO LRFD limit states. An example of the latter would be using the section properties and the resistance forces to calculate the corresponding maximum stress for a given resistance, which would then be compared to the analysis stress.

When calculating a corresponding stress from an LRFD resistance, care should be taken such that the stress is the actual stress expected in a linear elastic member due to the given load, and not a notional stress. For instance, if one wished to check shear stress in the web of a steel member, calculating a notional stress using the shear force divided by the area of the web would not be appropriate for comparing to the parabolic shear stress expected from FEA shell element results.

Furthermore, it is not appropriate to conduct a geometric nonlinear analysis including geometric imperfections, or a full nonlinear analysis with or without geometric imperfections, and compare the corresponding results to the resistance equations in the Specifications. The Specifications often implicitly or explicitly include additional effects that have been empirically verified, such as creep and shrinkage, relaxation, or residual stresses. Failure to include all of the factors that affect resistance in a refined analysis can result in an unsafe overestimation of capacity. In such cases the analyst should strive to correlate analysis results with physical tests, preferably those used to calibrate the Specification being used.

Nominal section and material properties should also typically be used. The LRFD Specification is probability based, and takes the variability of members and materials used in construction of bridges into account. Unless a statically valid sample has been obtained for measurement and/or testing, “actual” section and material properties should not be used for design or rating.

8.2.1 Integrating Stresses

To obtain member force effects such as shears (V), moments (M), axial forces (P), and torsion (T) from the stress output generated by an FEA program, stresses can be integrated over the area of the component, such as the one in Figure . Alternatively, it may be possible to output membrane and plate force effects on a unit width basis for use in design calculations. Major-axis bending moments can be found from the output stresses by summing the integrated stresses about the centroid of the section.

These steps can be done outside of the finite element software program, for instance in a spreadsheet application, though this can quickly become a tedious undertaking. Some FEA programs have tools which will automatically slice through shell elements (or a combination of shell and beam elements) and sum the internal stresses and/or forces present to determine the effective total forces at the sliced locations, with an output that is similar to that of a beam or frame element.

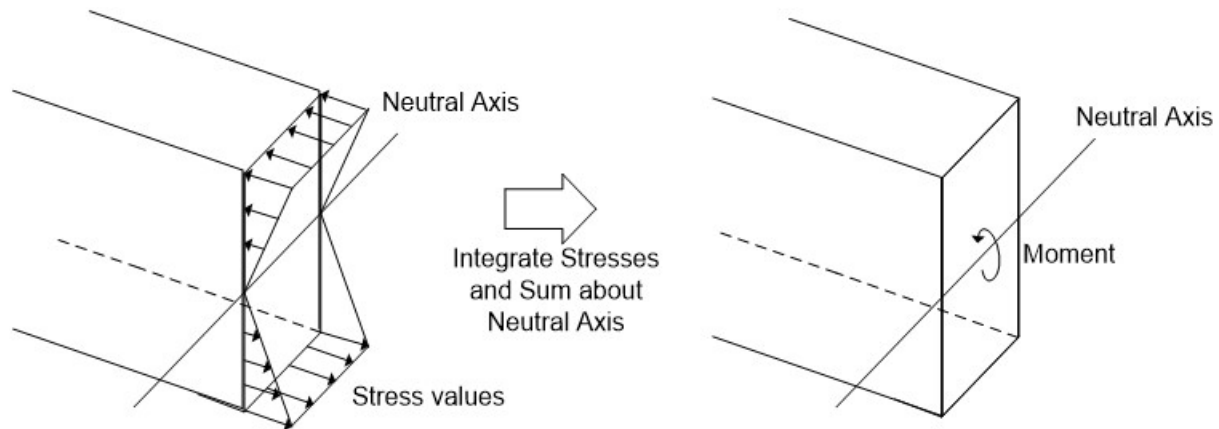


Figure 137. Illustration. Determining moments from FEA stress output.

Section 9.1.2.3.3 shows an example of integrating stresses over the area of a deck shell element and summing the forces. The general procedure is summarized as follows:

- Determine the geometric properties of the cross-section, including dimensions of all of the individual elements, centroid and shear center of the entire cross-section using a strength of materials approach, and “participating” width (see Section 8.2.3) of the deck, if necessary.
- Extract the forces for any beam elements that are part of the cross-section.
- Extract the stresses for all shell and/or solid elements that are part of the cross-section.
- From the extracted shear stresses and geometric properties, determine the equivalent shear forces and lines of action for all shell and/or solid elements.
- Transform the shear forces into major-axis and minor-axis components if necessary.
- Sum the major-axis shear forces and the minor-axis shear forces, including any beam element resultant to get the net major-axis shear and minor-axis shear forces, respectively.

- Sum the shear force resultants of all the elements, including any beam elements, times the distance from the shear center of the cross-section to get the net torsional force.
- Determine the equivalent normal forces and lines of action for all shell and/or solid elements from the extracted normal stresses and the geometric properties.
- Sum the normal forces on the cross-section to get the net axial force.
- Sum the moments from the equivalent normal forces times their distance from the centroid of the cross-section in both the major-axis and minor-axis planes along with any major-axis or minor-axis moments from beam elements to get the net major-axis and minor-axis moments on the cross-section. Note that if there is no net axial force on the cross-section, the moments can be summed about any arbitrary convenient point on the section, such as the neutral axis.

While this procedure can be time consuming when compared with extracting the force effects of lower order elements, the end result is that the shell elements can produce results which can be used for design in a form similar to those produced by beam elements. *Care must be taken to ensure that the coordinate axes of the slice are set-up properly and are understood prior to using the program output. Performing a simplified test case which can be checked by hand is always recommended.* For instance, Section 9.1.2.3.3 demonstrates a check of the moment/shear/axial force slicing capability of an FEA program.

8.2.2 Non-Composite Construction

Many concrete slab on girder highway bridges are non-composite for some, although typically not all, of the applied loads. Examples of non-composite loads would be the girder and deck weight of a bridge with an unshored cast-in-place concrete deck.

Non-composite girder loadings are relatively simple to model and design. The model force effects are based on the stiffnesses of the girders and diaphragms/cross-frames, and the design applies these force effects to the properties of the girder-only section. For 1D or 2D models, the design shears, moments and axial forces can be directly obtained. For 3D models, the design forces would need to be integrated as detailed in Section 8.2.1 before designing the girders according to AASHTO LRFD.

8.2.3 Composite Construction

When a composite section is loaded in bending, the axial stress in the deck is a maximum directly above the girder and then decreases as you move transversely away from the girder centerline due to shear lag. In calculating design capacity of composite sections, a simplification is usually employed. A notional “effective width” of deck is assigned, and the stress on this notional width is assumed to be uniform and equal to the maximum stress in the deck. The effective width of this uniform maximum stress is equal to the width required such that the total force is equal to the sum total force carried over the actual width of participating deck.

For refined analyses, knowledge of the effective width of deck is often not necessary and to some extent may be misleading. What is required for design is a calculation of the moment and shear (and possibly axial force) present in the composite girder. In order to determine these force

effects, the forces in the deck in the refined analysis must be proportioned correctly to each composite girder.

In situations where the analyst wishes to determine the effects of shear lag, such as the distribution of normal stresses in the deck, it is important that the mesh is sufficiently refined. A minimum of two elements between web lines is required to capture shear lag effects, but at least four elements is recommended.

When using a slicing utility of an FEA program that automatically integrates the stresses over the selected elements and returns the equivalent beam forces (M, V, P, T), something akin to an “effective width,” referred to here as “participating width,” must be employed in order to proportionally distribute the deck forces correctly among the girders. Often this participating width is simply halfway to the next girder, or the width that results in no net axial force in the composite section. Quantifying shear lag effects and identifying the participating width in more complicated situations can be a more difficult proposition.

A method to approximate an effective flange width for design purposes is provided in AASHTO LRFD Article 4.6.2.6 for various types of systems (concrete decks, box beams, orthotropic decks, etc.). In multi-girder bridges, typically the design effective flange width is taken to be equal to the tributary width of deck above the member, and the same participating width can be used for analysis purposes. However in some cases, effective width calculations can become complicated if the bridge geometry is not straight forward. For instance, in cases similar to what is depicted in Figure 138, in which the girders are not the same size, the tributary width assumption of AASHTO LRFD is not valid and its use may result in an unconservative design.

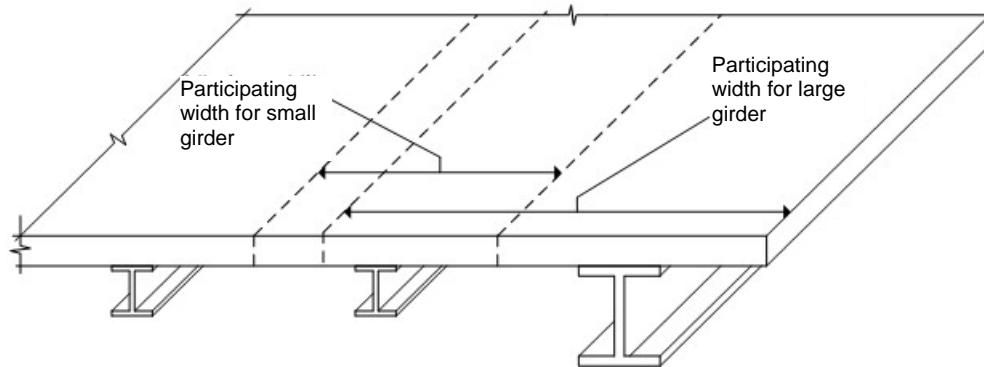


Figure 138. Illustration. Deck system in which the effective flange width set equal to the tributary width may result in an underestimation of force effects for the larger section.

The larger stiffness of the exterior beam will cause a larger width of deck to act compositely with it, so while the tributary width assumption would be conservative for use as a design section for the exterior beam, determining the analysis force effects using this effective width as the participating width would most likely underestimate the actual force effects. In a case such as this, sometimes the refined analysis can be used to determine the participating width which can then also be used as the design “effective width.” If the composite girders carry only moment and shear the effective width can be determined by finding the width resulting in no net axial force on the composite section.

One technique for determining the design forces is to integrate the stresses over an estimated participating width of deck slab, then sum the forces over the cross-section, as described in Section 8.2.1 of this manual. By iteratively adjusting the participating width of deck slab until there is no net axial force, the equivalent force effects can be determined. This method also has the advantage of producing a participating width of deck, which can then be used in determining the effective width of deck used for calculating resistance.

When little or no net axial force is present in the composite member, the participating width of deck is not required, and the composite force effects can be determined using the beam forces only. Assuming that the moment in the deck slab is negligible and the axial stress in the deck slab is uniform, the major-axis moment in the cross-section can be determined by adding the moment in the girder section to the moment due to the axial force couple between the deck slab and the girder section. To estimate the moment due to the couple, multiply the axial force in the girder section, which should be equal and opposite the axial force in the effective width of deck, times the arm between the girder centroid and the deck slab centroid.

When net axial forces are present in girders, engineering judgement may be required to determine girder design forces. This may entail estimating the distribution of axial force across the width of the bridge, or bounding the design forces, among the possible approaches.

This method can be used for any model where the beam forces can be isolated from the deck forces, and can also provide a quick check of an FEA slicing utility. The model should account for any Specification required effective modular ratio factors for permanent load effects. This shortcut is not valid when net axial forces are present in the girders, due to transverse bridge loadings or in curved or skewed bridges for instance. Even though the bridge cross-section may not have a net axial force, when individual girders have axial load the stresses must be integrated, unless those effects can be subtracted out prior to calculating the in-plane moment.

Once the equivalent beam force effects (M, V, P, T) have been determined, design can proceed using the AASHTO LRFD Specification as usual. For instance, normal stresses can be calculated using M/S , or shear at the composite interface can be calculated using the well known formula VQ/I as one step in the design of shear connectors for deck slabs. The change in axial force in the girder of a composite section is also equal to the interface shear, and can be used in place of, or as a check on the VQ/I method.

8.2.4 Concrete Girder Bridges

For typical design, per Article 4.5.2.2 of AASHTO LRFD, concrete components are generally modeled using gross (un-cracked) section properties to determine distribution of forces, even though those forces may be used to design a cracked section. Although cracked stiffness properties are seldom used in models for routine slab-girder bridge design, they might be utilized for more complex structures or when more accurate results are required.

As a consequence, the shell element stresses extracted from an analysis model are only valid if the stresses present would not result in cracking or crushing of the concrete. If the analysis shows that cracking occurs, the correct stresses would have to be found by applying the force effects from the model to the design section, accounting for the lack of participation of the cracked concrete in tension as illustrated in Figure 139.

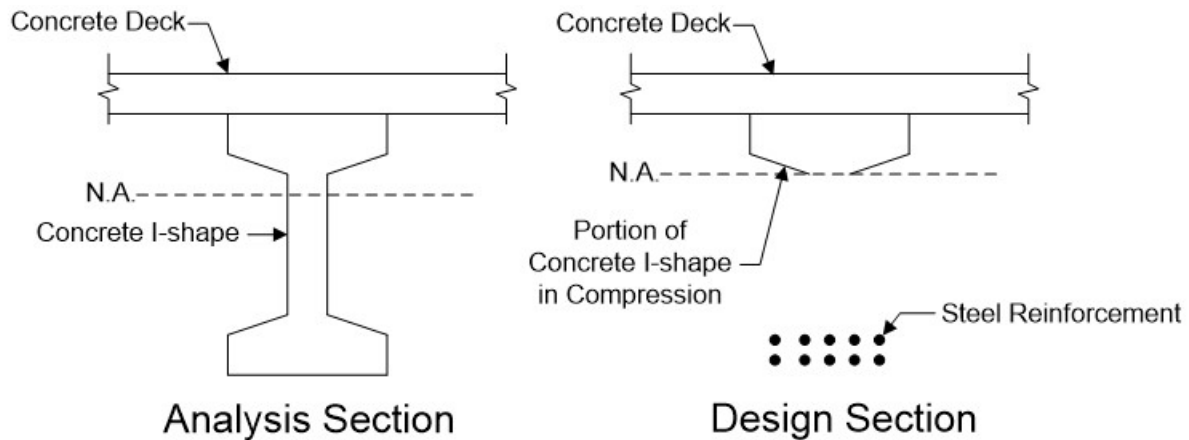


Figure 139. Illustration. Analysis and design section for a concrete member in positive bending.

In most circumstances, stresses extracted directly from an FEA model are not used to develop or check the design of concrete members at the strength limit state. Instead of stresses it is typically moment, axial force, or shear force values which are compared with resistances calculated per the AASHTO LRFD which are then used to determine the adequacy of the design. If the model is representative of the actual structure, concrete compressive strains should be limited to a maximum of 0.003.

On the other hand, the AASHTO LRFD provides stress limits for the Constructability and Serviceability Limit States, allowing these to be directly checked in an analysis. Care should be taken to make sure that the direction and location of the stress generated by the model corresponds to the limit state being checked. Models should also reflect the locations that are cracked, as well as the assumed effective modular ratio of $2n$ for permanent loads and prestress. The correct load and resistance factors also should be applied, either within the program or externally.

8.2.5 Steel Girder Bridges

Most concrete deck slab on steel girder bridges designed and constructed today take advantage of composite behavior by connecting the deck and the girders, although some new designs as well as some existing bridges are designed non-compositely. Non-composite steel girder bridges are simpler to analyze and design, as all loads are applied to a single steel-only model, and load resultants are easily factored and summed to be applied to the design of the steel girders, as detailed in Section 8.2.2.

As mentioned previously, per Articles 4.5.2.2 and C6.10.1.5 of AASHTO LRFD, analysis models for composite steel bending members typically allow tension in the deck concrete and assume composite action over the entire length of the bridge to determine distribution of forces, although some software packages allow the use of “partially composite” sections over the negative moment regions. Different section properties are then used in design, resulting in analysis model stresses not being equivalent to those which are used for design. Figure 140 depicts the assumed section properties to be used for analysis and design of a continuous composite steel girder.

For each step in the sequence of loading the correct associated stiffness must be used in the analysis; for bridges composite in the final condition, non-composite properties are used for loads applied prior to the hardening of the attached concrete deck, long-term composite properties are used for additional dead loads, and short-term composite properties are used for transient loads. Steel reinforcement is typically neglected when modeling composite decks in compression.

In positive moment regions, the section properties assumed for analysis are the same as the section properties assumed for design, and the stresses determined from the model can be used for all design checks which involve linear elastic loadings.

In negative moment regions the analysis and design sections are dissimilar due to the assumptions made about how the concrete deck behaves in tension. Per 6.10.1.1c of AASHTO LRFD, the tensile capacity of the concrete must be neglected in negative moment regions when determining resistance, but as described above it is not neglected when determining force effects. As a result, the process shown in Figure 141 must be used to determine the design stresses. The concrete deck slab longitudinal steel reinforcing can be used to resist the negative moment if the deck is composite and sufficient shear connectors are present to develop the reinforcing within the effective width.

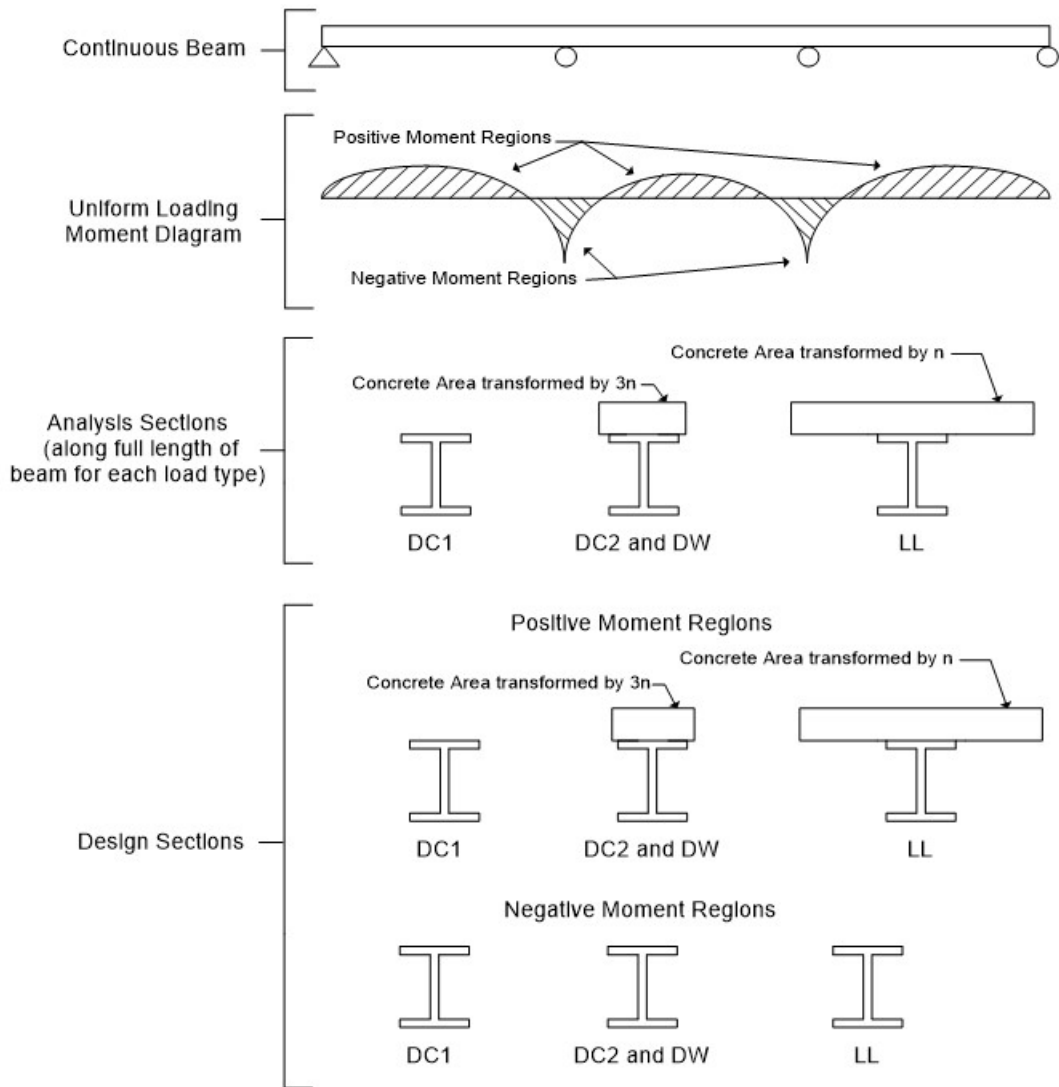


Figure 140. Illustration. Steel girder analysis and design sections (note that in some circumstances the longitudinal deck steel reinforcement which is not illustrated may be taken as part of the design section in negative moment regions).

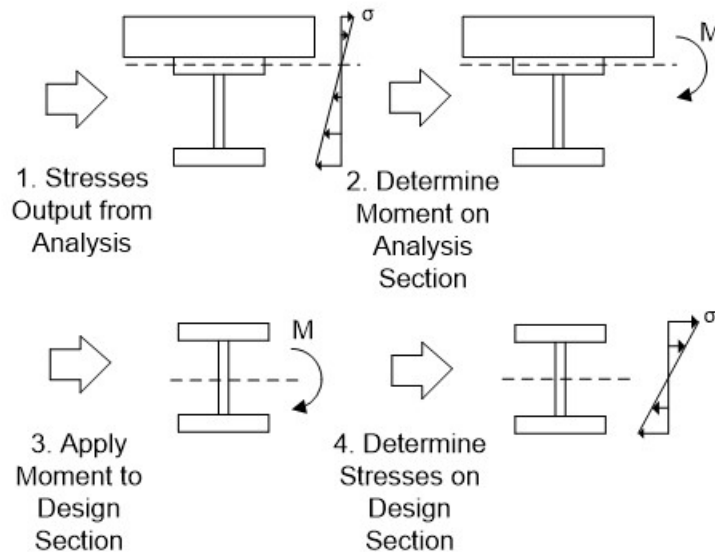


Figure 141. Illustration. Steps required to determine design stresses from stress output in negative moment regions

At strength limit states design inelastic behavior of composite steel girders is permitted. Depending on section criteria, which include local stability and ductility limits for steel sections, up to the full plastic section capacity can be achieved in both positive and negative bending. Plastic ultimate capacity is load sequence independent, and due to the nature of the composite member (compression carried by the deck as well as support of the top flange) achieving full plastic capacity in positive bending is not unusual, while achieving the full plastic capacity in negative bending is more difficult, and is generally not economical. Article 6.10.7.1.2 in AASHTO LRFD limits the maximum allowable positive moment capacity to $1.3M_y$ in continuous steel girder bridges, unless the ability to redistribute additional load to the negative moment regions is confirmed.

As with concrete, it is difficult to directly utilize the stresses from a 3D model for steel design at the Strength Limit State. Directly checking stress limits at the Constructability and Serviceability Limit States is generally easier, as long as the section properties of the analysis model are consistent with the section properties of the design section. As stated previously for concrete, care should be taken to make sure that the direction and location of the stress generated by the model corresponds to the limit state being checked and that correct load and resistance factors are applied, either within the program or externally.

When steel cross-frames participate in the lateral distribution of forces, for instance in curved or skewed bridges, the cross-frames need to be designed for the force resultants determined by the design model. For 3D models, where the elements are non-composite and explicitly modeled, the design forces can be directly obtained from the model. Composite top chords of cross-frames should be treated similarly to composite girders, as described in Section 8.2.3. For models such as grids using effective single element representations of cross-frames, the single element force resultants need to be transformed into the forces in the individual elements of the cross-frames.

To accomplish this transformation, the joint forces commonly are determined as shown in Figure 142. The V_i and V_j shears are essentially the same; the difference between them is equal to the weight of the cross-frame. The cross-frame weight is generally negligible, so the largest of these forces is typically selected and equally divided between the top and bottom nodes of the cross-frame (assuming an X-type cross-frame). For cross-frames with a single diagonal framing into the girders at each end of the cross-frame, the shear force is applied to the cross-frame node corresponding to the diagonal.

For a case of a V-type cross-frame with no top chord, the flexural stiffness of the cross-frame is highly dependent upon the stiffness of the combination of the bottom chord and any connection plates across the joint at the cross-frame mid-length. The distribution of the shear between the diagonal and the bottom chord in this case is statically indeterminate, but it is reasonable to assume that any shear is taken predominantly by the diagonal.

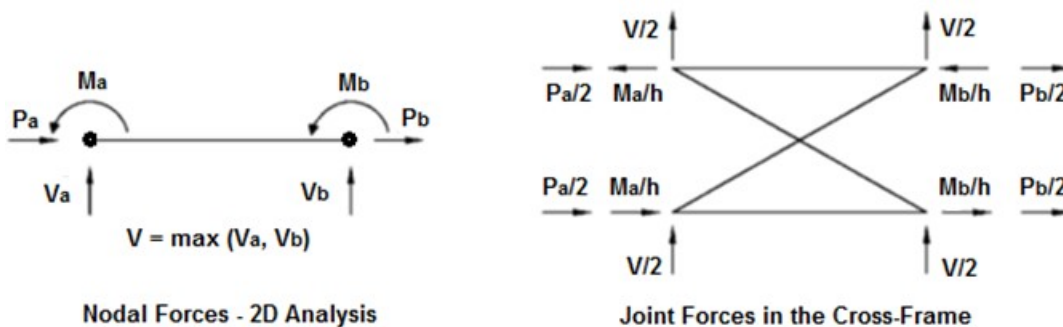


Figure 142. Illustration. Conventional practices for determination of cross-frame member forces from 2D-grid analysis results (adapted from White et al., 2012).

For most girder bridges, the axial forces, P_a and P_b , are negligible. In the case that they are not, they can be equally divided between the top and bottom joints in order to satisfy equilibrium, assuming that the reference axis of the equivalent beam element is located at the centroid of the cross-frame.

The left and right moments, M_a and M_b , are decomposed into force couples with magnitude equal to M/h , where h is the depth of the cross-frame, and applied as equal and opposite forces to the cross-frame joints. The forces in the chords and the diagonals can be obtained by statics assuming the cross-frame is a truss. For more information, see (White et al., 2012).

8.2.6 Spine Beam Models

The stress resultants from a spine beam model are the shears, moments (including torsion), and axial force at the selected design cross-sections of the bridge. AASHTO LRFD Article 5.8.2.1 provides an equation to determine if torsional effects need be investigated for concrete box girders. If torsion cannot be neglected, Article 5.8.2.1 also provides an equation for calculating the equivalent shear in the exterior web including the torsional shear, as illustrated in Figures 143 and 144. The torsional shear is added to the flexural shear, which is generally determined to be the flexural shear divided by the number of webs. Any inclination of webs should also be included, as illustrated in Figure 145. A similar approach is taken for calculating shear in the top

and bottom flanges of the box. Design proceeds according to the AASHTO LRFD Specifications for shear and flexure. For a complete design examples, see (Nutt et al., 2008) and (Corven, 2015).

Similar considerations apply to steel boxes. Article C6.11.1.1 provides an equation for shear flow due to torsion in a box section, from which shear in the flanges and webs can be determined.

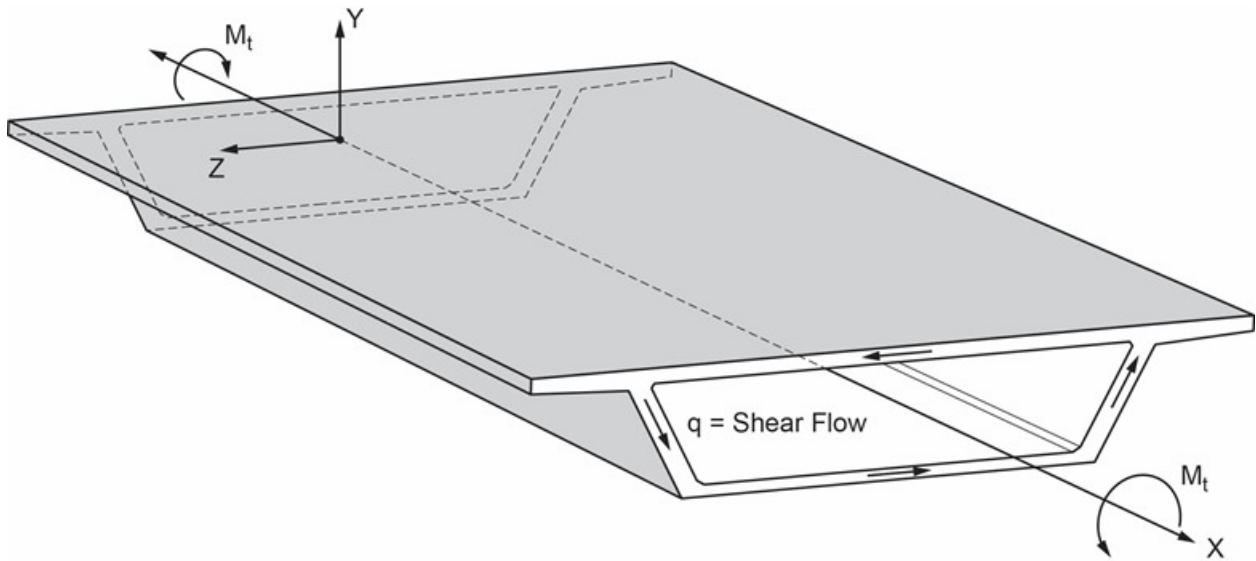


Figure 143. Illustration. Shear flow due to torsion in single cell box girder (Corven, 2015).

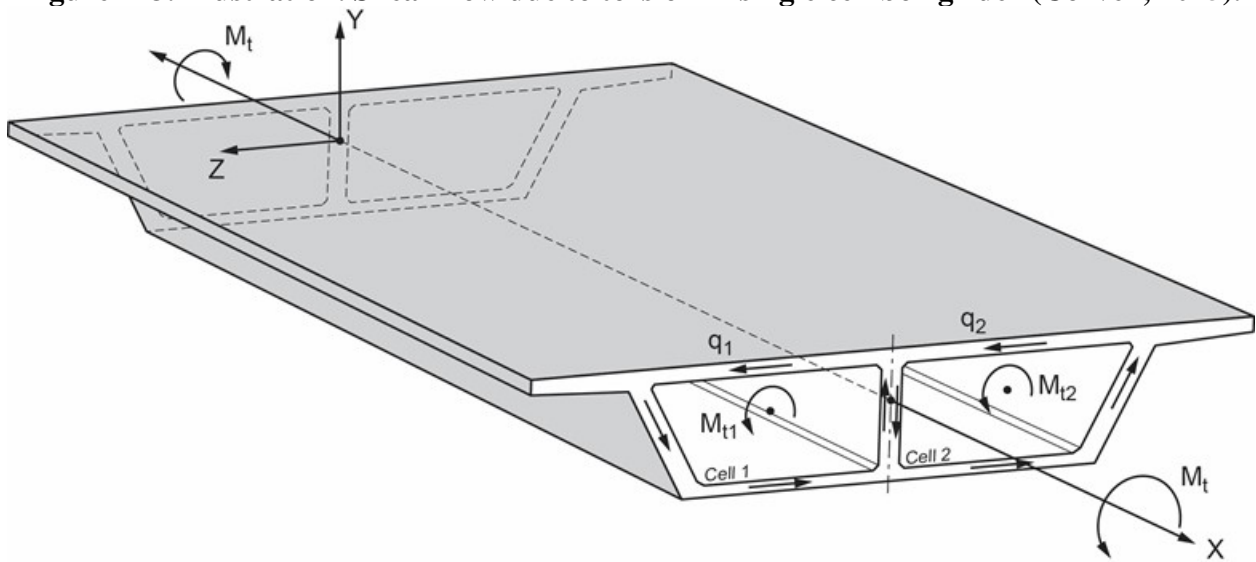


Figure 144. Illustration. Shear flow due to torsion in multicell box girder (Corven, 2015).

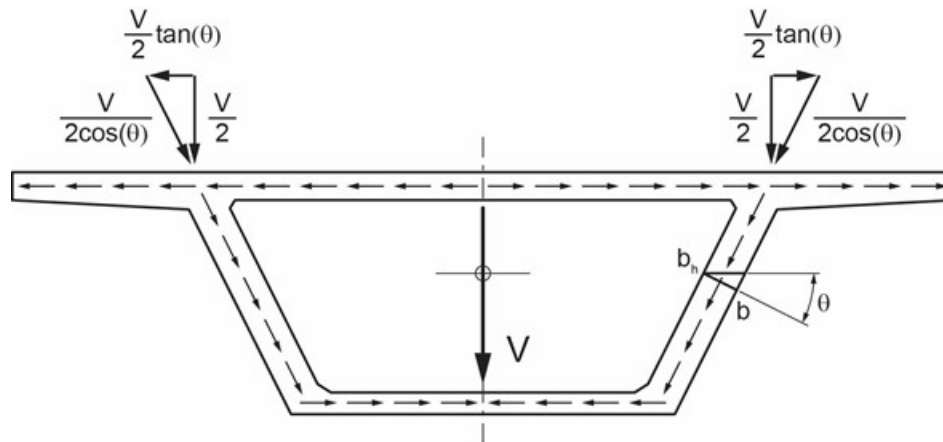


Figure 145. Illustration. Shear flow due to major-axis shear in single cell box girder with inclined webs (Corven, 2015)

8.2.7 Deflection and Camber

Refined analyses are excellent tools for calculating deflection and/or camber directly. *But the models used for deflection calculations often are completely different from the models used to calculate load effects.* The reason is that for strength design, the goal is obtaining load effects that are equal to or greater than the actual load effects. Being conservative is not inherently bad. For deflections or camber design, the goal is to be as accurate as possible. As such, deflection analyses should include all non-structural sources of stiffness, such as barriers and wearing surfaces.

For concrete bridges, getting the effective moment of inertia correct is important when calculating deflections. For prestressed girders, it is recommended that the uncracked gross concrete section be used. For mild reinforced concrete girders, an effective moment of inertia such as that provided in LRFD Article 5.7.3.6.2 should be used. For more advanced models where the reinforcement is modeled explicitly, concrete material with tensile cracking properties can be used, but will require a nonlinear analysis. The modulus of elasticity for concrete specified in LRFD Article 5.4.2.4 can be used in most cases, but for some structures, such as segmentally constructed bridges, the maturity of the concrete at the time of loading should be taken into account.

2D and 3D analyses are much better than 1D analyses for deflection/camber calculations. 1D analyses do not model the cross-frames and diaphragms that connect the girders and force the structure to deflect as a unit. If the dead load distribution is not properly approximated in a 1D analysis, the resulting errors in camber can lead to issues with haunch thickness and deck elevations. For 2D and 3D analyses, the dead load distribution is automatically performed based on the relative stiffnesses of the elements. As long as the stiffnesses are modeled correctly, good results for deflection/camber can be obtained.

8.2.8 Volume Elements

Volume elements suffer from many of the same issues as shell elements, if not more so, with respect to designing with AASHTO LRFD. If volume elements are used to model a component

such as a girder of a bridge, the designer would need to integrate over the surface and sum the results of all the volume and any other additional elements of the component in order to calculate the moment, shear, and axial force demands for design. *For this reason volume elements are more suited to analysis of local effects, where stresses can be directly checked.* In the future, as AASHTO LRFD evolves, and programs become more powerful, designers may be able to capacity check components directly, making shell and volume elements easier to use in bridge design analysis.

8.2.9 Nonlinear Behavior

Inelastic and/or nonlinear analyses are commonly used for determining the capacity of a given element or structural system under a specific loading scenario. Determining inelastic/nonlinear capacity can be useful in situations such as forensic analyses, or where post yield/post ultimate phenomenon is desired, for example in the evaluation of the pushover capacity of a bridge for seismic design or redundancy assessments of bridges with fracture critical members (FCMs). In particular, a redundancy analysis usually involves sophisticated elements and material models able to replicate the inelastic and nonlinear response of members along an alternative loading path activated after a FCM fails.

Analysis including geometric nonlinearities are useful to determine the second order effects, otherwise addressed with approximate equations in the Specifications. As mentioned previously in Section 5.3, when behavior is nonlinear, superposition and/or factoring of load effects no longer is valid. *Therefore, when using the results of nonlinear analyses for design according to a load-factor method such as LRFD, factoring should be performed prior to applying the loads in the nonlinear analysis.* This means that for situations with a large number of load cases, nonlinear analyses are not usually the best tool for the task. As an alternative, a number of representative nonlinear analyses can be performed, ratioed to their linear counterparts and then enveloped to determine an appropriate design amplification factor to be used for all design load cases. For more details on nonlinear analyses and corresponding modeling approaches, see Section 5.3.

8.2.10 Stability

8.2.10.1 Beam Columns

Compression members, such as columns or arches, are prone to undergo instability issues commonly referred to as buckling. This is a condition where the structure reaches a maximum or critical load and is unable to sustain any additional loading exhibiting instead a progressive deformation that can lead to collapse (Structural Stability Research Council, 2010). *Stability limit states in bridge design are a function of a number of variables, including the state of residual stress in the case of steel material, the initial out-of-straightness of the elements, eccentricity of load, time-dependent effects (i.e. creep in concrete), and the actual end-member restraints.*

For straight, constant cross-section members with commonly-defined end conditions, the LRFD Specification equations include design resistance equations that were calibrated to provide a conservative estimate of the capacity of typical columns, including the effects of residual stresses and an initial geometric imperfection of $L/1500$ (White, 2015, Griffis and White, 2013).

Therefore, these aspects do not need to be addressed in a refined analysis when the member capacities are determined according to the Specifications. When the behavior begins to include complexities such as curved elements, variable cross-sections, complex buckling modes or nonlinear end conditions, refined analysis can aid in accurately determining the member capacity. However, care must be taken to avoid neglecting the effects of initial geometric imperfections and residual stresses.

One way to approach refined analysis for stability member design is to determine the maximum elastic buckling load from a refined analysis. The maximum load resulting from the refined analysis is set as the Euler buckling load, or the elastic critical buckling resistance, P_e , of the member and substituted into the column equations from the Specifications to get the member capacities. The resultant critical buckling load can also be used to determine the effective slenderness ratio (KL/r) (or effective length, KL) from the P_e equation. The convenience of using KL/r (or KL) instead of the critical load directly is that it provides a better feel for the influence of the member end restraints on the buckling modes. Additionally, the slenderness ratio can be utilized in the approximate single step moment magnification equations in the Specifications to determine second order effects. The resulting amplification factor can then be used to increase the design moments determined from linear analyses, accordingly.

The key to calculating the slenderness ratio when analyzing concrete is to model the stiffness of the column accurately. Due to items such as variability in cracking, reinforcement, and creep along the length of concrete compression members, it is inappropriate to use the gross section moment of inertia to calculate the stiffness along the entire member. Various formulas have been developed to calculate an effective stiffness of concrete members in such situations. AASHTO LRFD Article 5.7.4.3 provides a method based on section properties and loading. ACI 318-14 Article 6.6.4.4 (ACI, 2014) utilizes the AASHTO equations as well as a third equation for calculating effective stiffness. The third equation in ACI is considered the most accurate but requires more information about the section. Additional discussion on reinforced concrete member stiffness can be found in various text (Wight and MacGregor 2012, Khuntia and Ghosh 2004a, Khuntia and Ghosh 2004b).

In practice, linear and nonlinear refined analyses are available to identify the critical loads where instability occurs. Elastic linear buckling analyses typically provide the eigenvalue solution, and result in a load factor which, when applied to the existing loads, provides the theoretical bifurcation point or critical load. Eigenvalue analyses are very attractive for design purposes since they are quick, easy to perform typically using a line (beam) element model, and provide a definite load for each buckling mode.

When conditions are outside the limits of the specifications, or more accurate results are needed, nonlinear load-deflection analyses may be more desirable to identify the early stages of buckling. Nonlinear load-deflection analyses, including time history, incremental, or step-wise nonlinear analyses, reformulate the stiffness of the system at each load step as the applied loads are factored up. These analyses can utilize appropriate stiffness reductions and geometric imperfections in the context of the AISC Direct Analysis Method (Chapter C) or Advanced Analysis Method (Appendix 1) (AISC, 2016). Although these analyses provide immediate magnified force effects at any load level, it can be more challenging to determine secondary

buckling modes, especially if they correspond to a particular live load deformation pattern or if there is an interaction of several buckling modes.

Regardless of the approach selected, the designer must ensure that the important effects of residual stresses and initial imperfections are accounted for in the design process, either through the use of the AASHTO capacity equations, or directly in the analysis.

With regard to the design of steel arch ribs, AASHTO LRFD includes some simplified guidelines to address the in-plane buckling but no recommendations are given to consider the out-of-plane behavior which may be the controlling mode for arches with minimal lateral bracing. Such a case would be a good candidate for a refined nonlinear analysis.

8.2.10.2 Lateral-Torsional Buckling

For design of typical concrete slab on girder bridges, girder stability can be an important issue. Stability of precast concrete girders can be critical during transportation and erection. Stability of positive moment regions of steel girders can be a concern during deck placement, prior to the slab curing. Most of the time, modeling lateral torsional buckling explicitly is unnecessary. *For routine design of typical concrete slab on girder bridges, using the AASHTO LRFD provisions to ensure stability based on the load effects from a linear elastic analysis is recommended.*

Determining the actual stability capacity of negative moment regions of steel girders with relatively long unbraced lengths in existing bridges can be challenging, *especially if loadings change causing ratings to decrease.* Quantifying the design benefits of an inflection point may be helpful in increasing ratings and avoiding costly repairs. This can be difficult, as considering inflection points to be fully braced can be unconservative. A full 3D shell model of the negative moment region of the girder can be used to determine the resistance based on AASHTO LRFD Article 6.10.8.2.3.

A procedure analogous to finding the elastic buckling load of a column as described in Section 8.2.10.1 can be used. In this case the elastic lateral torsional buckling stress F_{cr} is analogous to the elastic buckling load P_e , and the moment gradient modifier C_b times the web load shedding factor R_b is analogous to the effective length factor K . Because Article 6.10.8.2.3 utilizes stresses, the elastic buckling analysis results can be used directly to calculate $C_b R_b$.

8.2.11 Dynamic Behavior

According to Article 4.7 of the LRFD Specifications, dynamic analysis may be required to investigate wind or vehicle induced vibrations, the effects of seismic loads, or the effects of blast loads. *There are in general two methods available for dynamic analysis: response spectrum analysis and time-history analysis.* For seismic analyses, the LRFD Specifications provide guidance on when each method should be used. This depends on features of the structure, such as the number of spans, span length, horizontal curvature, overall complexity, operational classification, seismic zone, etc. The development of finite element analysis models for each method is similar, but the loadings and analysis techniques are different. *The time-history analysis is the more advanced of the two methods, since non-linear geometric and material effects can be considered, and its use is required to analyze structures of significant importance and complexity.* Once a refined dynamic analysis has been performed, the load effects can be

utilized directly by the LRFD Specification to perform member design. For guidance on modeling for dynamic analyses, see Section 5.4.

CHAPTER 9. EXAMPLES

Introduction

This chapter demonstrates the use of the manual contents in seven design examples: (1) a straight, three-span, composite precast concrete I-girder concrete deck slab bridge with square supports, simply supported for dead load made continuous for live load; (2) a straight, three-span continuous, composite steel I-girder concrete deck slab bridge with square supports; (3) a curved, three-span continuous, composite steel I-girder concrete deck slab bridge with skewed supports; (4) a curved, three-span continuous, concrete box girder spine beam; (5) dynamic analysis of a curved steel girder bridge; (6) stability analysis of a tall concrete pier column; and (7) a four-span continuous prestressed segmental concrete box girder bridge. The geometry for Example 1 comes from a bridge on the PennDOT ECMS website, geometry for Examples 2, 3, and 5 use information from NHI Course 130095, geometry for Example 4 is taken from Appendix B of NCHRP 620, and geometry for Examples 6 and 7 are from available plan sets. This chapter does not contain any new guidance regarding the use of the different analysis methods; instead, it provides examples of the implementation of the information provided in the previous chapters. For the first two examples, dead and live load moments, shears, and deflections are determined using 1D line girder, 2D plate and eccentric beam, and 3D finite element analysis methods. For the third example, dead and live load moments, shears, and deflections are determined using 2D plate and eccentric beam and 3D finite element analysis methods for the final condition, and 2D grid (since no slab is present during erection) and 3D finite element analysis methods for a steel only analysis. The 1D line girder analyses utilize PennDOT's Continuous Beam Analysis (CBA) program. The Spine Beam, 2D, and 3D analyses were performed using the FEA program LUSAS. The goal was to remain as software non-specific as possible; but in some cases the method used was specific to the software used and is stated as such.

For completeness, detailed calculations for the 1D models are provided as well. Some readers may choose to skip over these calculations to those dealing with the more refined methods of analysis.

9.1 Example 1 – Three-span, Precast Concrete I-Girder Bridge (Continuous for Live Load)

A three-span composite precast concrete I-girder concrete deck slab bridge made continuous for live load is the subject of Example 1. The cross-section consists of four (4) AASHTO Type VI precast concrete beams spanning 113 ft-3 inches when simply supported and spanning lengths of 114 ft-3 inches – 115 ft-3 inches – 114 ft-3 inches when continuous. The precast concrete beams utilize 8 ksi concrete. Intermediate diaphragms are placed at the centerline of each simple span; continuity diaphragms are placed at the piers to make the girders continuous for live load. Diaphragms are also present at each abutment. Figure 146 shows the Example 1 framing plan.

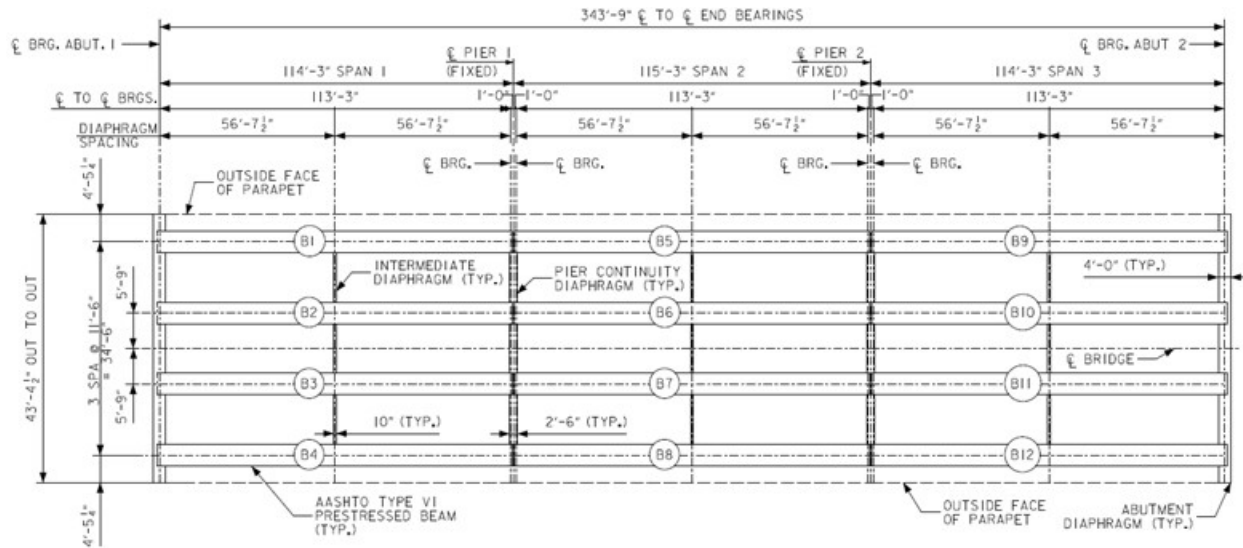


Figure 146. Illustration. Example 1 framing plan.

Figure 147 shows the Example 1 bridge cross-section. The composite concrete deck slab is 8½ inches thick including a ½ inch integral wearing surface; the deck slab utilizes 4 ksi concrete. The intermediate diaphragms are 10 inches wide by 3 ft-10 inches deep. The pier continuity diaphragms are 30 inches wide by approximately 7 ft-2¼ inches deep while the abutment diaphragms are 4 feet wide by approximately 6 ft-6 inches deep. The diaphragms utilize 3.5 ksi concrete.

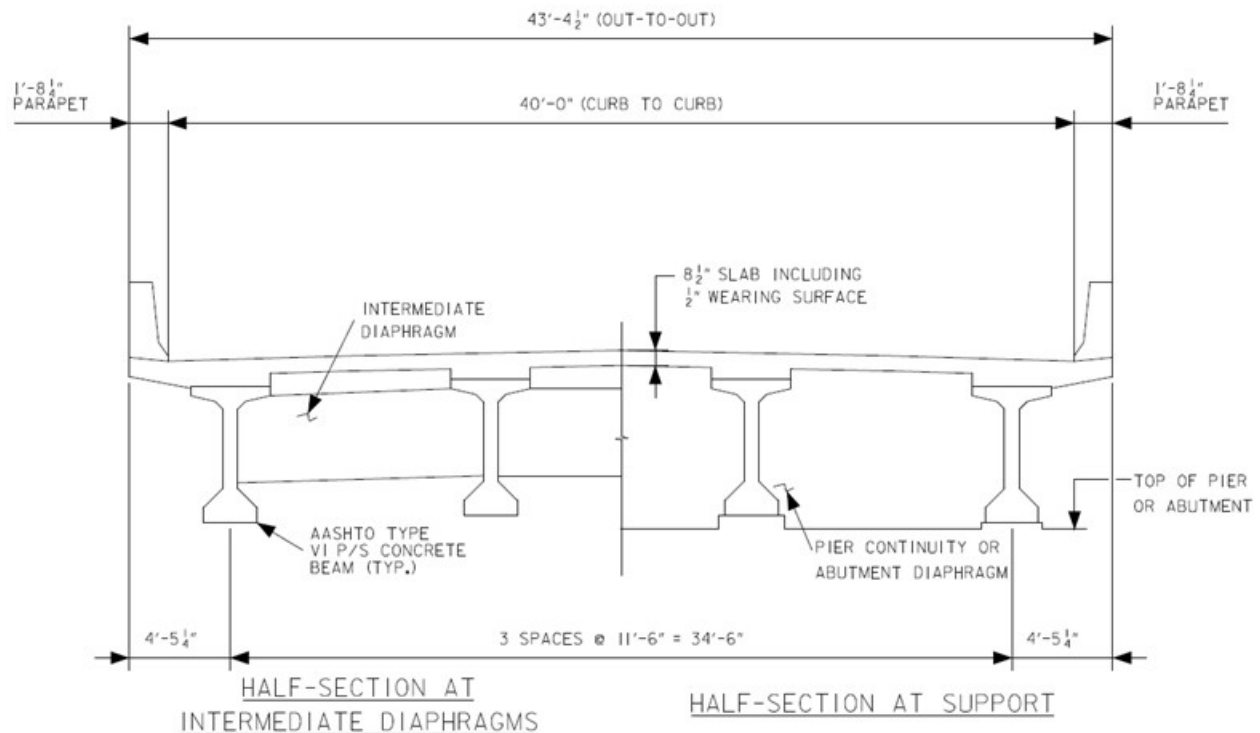


Figure 147. Illustration. Example 1 bridge cross-section.

9.1.1 1D Line Girder Analysis

The three simple spans shown in Figure 146 that are made continuous for composite dead loads and live loads are modeled with a 1D Line Girder Analysis. To adequately capture behavior in the different loading stages at least three separate models are required; one for non-composite dead loads, one for composite dead loads, and one for live load. Because simply supported and continuous support conditions are both considered for composite dead load and live load in these examples an additional two models are used. The 1D line girder analysis utilizes the approximate distribution factors contained in Article 4.6.2.2 of the AASHTO LRFD Bridge Design Specifications (AASHTO LRFD). The following steps are used to determine the dead and live load moments, shears, and deflections:

1. Determine non-composite and composite section properties for interior and exterior girders.
2. Calculate moment distribution factors for interior and exterior girders for one lane loaded and multiple lanes loaded.
3. Determine the dead loads due to girder self-weight, concrete deck slab, haunches, barriers, intermediate diaphragms, stay-in-place (SIP) forms, and future wearing surface (FWS).
4. Develop and run analysis models. (Notes: Depending on software, several models may have to be developed using the different section properties from Step 1; live load distribution factors from Step 2 may, depending on software, be included in the developed model and distributed moments will be provided as results)
5. Develop moment, shear, and deflection diagrams for non-composite dead load, composite dead load, and live load.

In this analysis, the following models are developed and used to determine the dead and live load moments, shears, and deflections:

- Non-composite section properties with non-composite dead loads applied;
 - These dead loads include the following: girder self-weight, SIP forms (if used), diaphragms, haunches, and concrete deck slab.
 - The non-composite dead loads are applied to a simply supported girder. Before the concrete deck hardens the girders span between bearings and act independently to resist loads.
- Composite section properties with composite dead loads applied;
 - Composite dead loads include the barriers and future wearing surface. Because these loads act in long-duration, variation in time-dependent material properties caused by factors such as creep must be accounted for. Depending on the level of complexity required, a thorough treatment of creep behavior and its resulting effects may be modeled; however, this is not done in these examples.
 - The composite dead loads are applied to both simply supported and continuous girders. As the concrete deck (including concrete placed between the ends of girders in adjacent spans) hardens and attains stiffness (and the ability to transmit load), the system becomes continuous. However, in the interest of conservatism,

some agencies require an assumed loss in continuity which reverts back to the previously stated simply supported condition. Though it is not the typical case, this is the methodology used in the examples herein. As a result the maximum force effects from either the simply supported or continuous girder are utilized.

- Composite section properties with live load applied.
 - Similarly to the composite dead load model, live loads are applied to both simply supported and continuous girders, utilizing the force effects of the worst condition.
 - Live loads considered in these examples include HL-93 Trucks as prescribed by AASHTO LRFD Section 3.6.1.2.1, but investigation of other project specific loads may also be required. Because live loads are considered short-duration loads, no consideration is given to time-dependent material properties.

9.1.1.1 Step 1 – Determine Non-Composite and Composite Section Properties

9.1.1.1.1 Non-Composite Section Properties – Interior and Exterior Girders

The non-composite section properties are calculated using basic mechanics of materials equations. These include equations for the moment of inertia about the centroidal axes of rectangles and triangles as well as the parallel axis theorem. These equations are shown as Equation (32) through Equation (34).

$$I_{Rectangle} = \frac{1}{12}bh^3 \quad (32)$$

$$I_{Triangle} = \frac{1}{36}bh^3 \quad (33)$$

$$Parallel\ Axis\ Theorem = I_{o,i} + A_i(y_i - y_{bar})^2 \quad (34)$$

The non-composite section properties for the AASHTO Type VI precast concrete beam are calculated below in Table with the different areas shown in Figure 148 and the dimensions shown in Figure 149. The second row of the table indicates the column number.

Table 9. Non-composite section property calculation.

Comp.	#	b (in)	h (in)	A (in ²)	y (in)	Ay (in ³)	d=(y-y _{bar}) (in)	Ad ² (in ⁴)	I _o (in ⁴)	I = I _o +Ad ² (in ⁴)	
(1)	(2)	(3)	(4)	(5)	(6)	(7)	(8)	(9)	(10)	(11)	
A1	1	42	5	210	69.5	14595.0	33.12	230347.25	437.5	230785	
A2	2	13	3	39	66	2574.0	29.62	34214.94	19.5	34234	
A3	2	4	3	24	65.5	1572.0	29.12	20350.48	18.0	20368	
A4	2	4	4	16	62.7	1002.7	26.29	11055.28	14.22	11069	
A5	1	8	59	472	37.5	17700.0	1.12	591.39	136919	137510	
A6	2	10	10	100	11.3	1133.3	-25.05	62736.78	555.56	63292	
A7	1	28	8	224	4	896.0	-32.38	234865.38	1194.67	236060	
				ΣA=	1085	ΣAy=	39473.0			I _x =	733320

$y_{bar} = \frac{\Sigma Ay}{\Sigma A} = \frac{39473.0}{1085} = 36.38$ inches
 $A = 1085$ in²
 $I_x = 733320.29$ in⁴

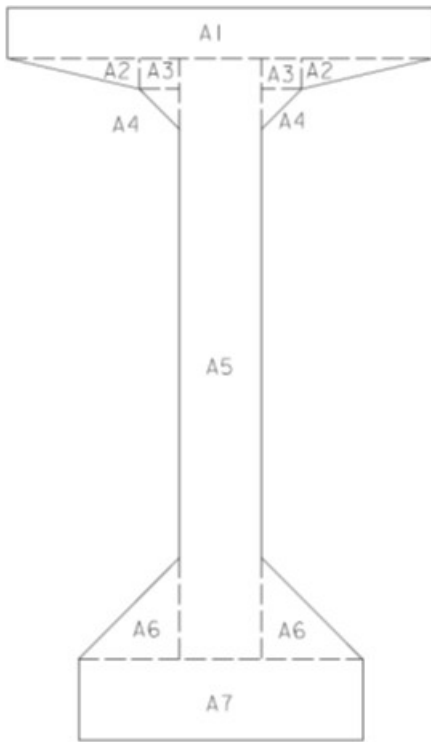


Figure 148. Illustration. Components of AASHTO Type VI prestressed beam.

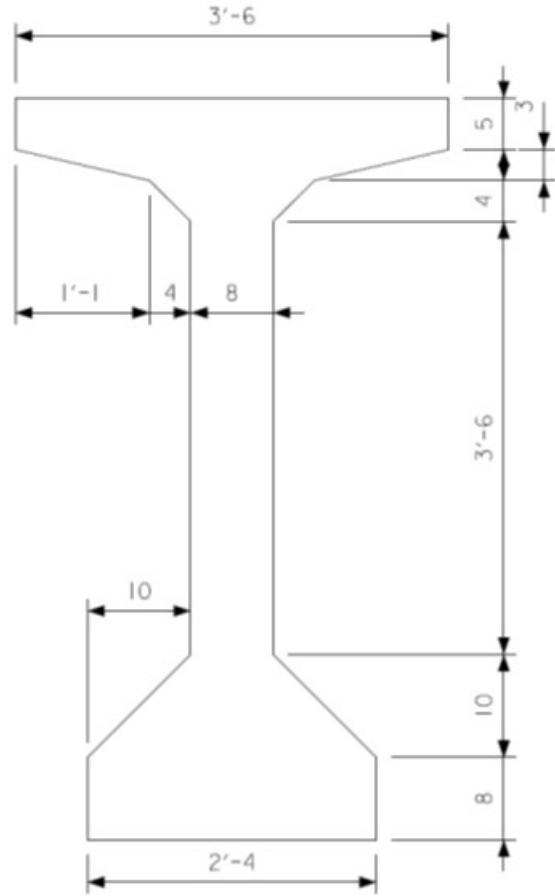


Figure 149. Illustration. Dimensions of AASHTO Type VI prestressed beam.

9.1.1.1.2 Composite Section Properties for Interior Girders

The composite section properties for the interior girders are calculated below. Because the deck slab and beam have different stiffness properties, the modular ratio must be calculated to create a transformed section and enforce the assumption that plane sections remain plane. The modular ratio is the ratio of modulus of elasticity for the beam to the modulus of elasticity of the deck slab. The modulus of elasticity of concrete with compressive strengths less than or equal to 5.0 ksi is calculated using the concrete compressive strength and AASHTO LRFD Equation C5.4.2.4-1, shown here as Equation (35). For concrete with compressive strength greater than 5 ksi, Equation (36) is used where w_c is given by Equation (37) and K_1 is taken equal to 1.0. The modulus of elasticity for the beam is determined to be 5314 ksi and for the deck slab is determined to be 3640 ksi, based on compressive strengths of 8 and 4 ksi respectively. The modular ratio, given by Equation (38), is 1.46.

$$E_c = 1820\sqrt{f'_c} \quad (35)$$

$$E_c = 33,000K_1w_c^{1.5}\sqrt{f'_c} \quad (36)$$

$$w_c = 0.140 + 0.001f'_c \quad (37)$$

$$n = \frac{E_{beam}}{E_{deck}} \quad (38)$$

The deck slab contribution depends on the effective flange width determined according to AASHTO LRFD Article 4.6.2.6. This section indicates that the center-to-center girder spacing should be used as the effective flange width for the interior girders. The depth of the haunch and the ½ inch integral wearing surface are conservatively not included in any of the section properties calculated in this example.

Table 10. Composite section property calculation – interior girder.

Comp.	b (in)	h (in)	A (in ²)	y (in)	Ay (in ³)	d=(y-y _{bar}) (in)	Ad ² (in ⁴)	I _o (in ⁴)	I = I _o +Ad ² (in ⁴)
(1)	(3)	(4)	(5)	(6)	(7)	(8)	(9)	(10)	(11)
Deck	94.52	8	756.2	76	57468.9	23.35	412198.0	4032.90	416230.9
Beam	-	-	1085	36.38	39473	-16.27	287273.2	733320.3	1020593.5
			ΣA= 1841.2		ΣAy= 96941.9			I _x =	1436824.3

$$y_{bar} = \frac{\Sigma Ay}{\Sigma A} = \frac{96941.9}{1841.2} = 52.65 \text{ inches}$$

$$A = 1841.2 \text{ in}^2$$

$$I_x = 1436824.3 \text{ in}^4$$

9.1.1.1.3 Composite Section Properties for Exterior Girders

The calculation is identical to that of the interior girders except that the effective flange width is different for exterior girders. AASHTO LRFD Article 4.6.2.6 indicates that one-half the center-to-center girder spacing plus the overhang width should be used as the effective flange width for exterior girders.

Table 11. Composite section property calculation – exterior girder.

Comp.	b (in)	h (in)	A (in ²)	y (in)	Ay (in ³)	d=(y-y _{bar}) (in)	Ad ² (in ⁴)	I _o (in ⁴)	I = I _o +Ad ² (in ⁴)
(1)	(3)	(4)	(5)	(6)	(7)	(8)	(9)	(10)	(11)
Deck	83.73	8	669.9	76	50909.9	24.50	401952.3	3572.6	405524.9
Beam	-	-	1085	36.38	39473	-15.12	248161.0	733320.3	981481.3
			ΣA= 1754.9		ΣAy= 90382.9			I _x =	1387006.2

$$y_{bar} = \frac{\Sigma Ay}{\Sigma A} = \frac{90382.9}{1754.9} = 51.50 \text{ inches}$$

$$A = 1754.9 \text{ in}^2$$

$$I_x = 1387006.2 \text{ in}^4$$

9.1.1.2 Step 2 – Determine Approximate Live Load Distribution Factors

9.1.1.2.1 Interior Girder Moment Distribution Factors

Equations for the approximate live load distribution factors, “g,” are provided in AASHTO LRFD Article 4.6.2.2. Different cross-section types are provided in AASHTO LRFD Table 4.6.2.2.1-1; comparing Figure 147 to those in the table, it is determined that cross-section “k” is similar. Using the cross-section type and AASHTO LRFD Table 4.6.2.2.2b-1, the equations for the moment distribution factors for interior girders can be found.

The distribution factor equations for live load moment in interior girders are shown as Equation (39) for one lane loaded and Equation (40) for multiple lanes loaded.

$$g_{SIM} = 0.06 + \left(\frac{S}{14}\right)^{0.4} \left(\frac{S}{L}\right)^{0.3} \left(\frac{K_g}{12.0Lt_s^3}\right)^{0.1} \quad (39)$$

$$g_{MIM} = 0.075 + \left(\frac{S}{9.5}\right)^{0.6} \left(\frac{S}{L}\right)^{0.2} \left(\frac{K_g}{12.0Lt_s^3}\right)^{0.1} \quad (40)$$

Where: S = girder spacing [ft]
 L = span length [ft]
 t_s = deck slab thickness [in]
 K_g = longitudinal stiffness parameter [in⁴] = n(I_x + Ae_g²)
 n = modular ratio
 A, I_x = area and moment of inertia for non-composite beam
 e_g = distance between centers of gravity of the non-composite beam and deck slab [in]
 g = distribution factor

The first step in determining the approximate distribution factors is to determine the value of K_g. This value is the same for both the interior and exterior girders as the same beam is used. The non-composite area and moment of inertia are found in Table 9. The value for “e_g” is determined using Equation (41) and found to be 39.62 inches.

$$e_g = D - y_{bar} + \frac{t_s}{2} \quad (41)$$

Substituting all values into the equation for K_g, determine that K_g is 3557176 in⁴.

$$K_g = n(I + Ae_g^2) = 1.46(733320.3in^4 + 1085in^2 \times (39.62in)^2) = 3557176in^4$$

The second step in determining the approximate distribution factors is to determine if the bridge characteristics satisfy the range of applicability listed in AASHTO LRFD Table 4.6.2.2.2b-1. These characteristics, the range of applicability, and the Example 1 bridge values are shown in Table 12.

Table 12. Bridge characteristics for distribution factor equations.

Characteristic	Range	Satisfied for Example 1
Girder spacing, S	3.5 ≤ S ≤ 16.0	S = 11.5, YES
Deck Slab thickness, t _s	4.5 ≤ t _s ≤ 12.0	t _s = 8, YES
Span length, L	20 ≤ L ≤ 240	L = 114.25 and 115.25, YES
Number of beams, N _b	N _b ≥ 4	N _b = 4, YES
Longitudinal Stiffness, K _g	10,000 ≤ K _g ≤ 7,000,000	K _g = 3557176, YES

Since all of the criteria are satisfied, the approximate distribution factors of Equations (39) and (40) can be used to calculate the moment distribution factors for the interior girders. The distribution factors depend on the span length; the center span of this bridge is slightly longer

than the side spans, therefore separate distribution factors will be calculated for the center span. Additionally for negative moment between dead load points of contraflexure (POCs), AASHTO LRFD indicates that the average of the two span lengths can be used (See AASHTO LRFD Table C4.6.2.2.1-1). Calculation of the moment distribution factor in an interior girder for one lane loaded is shown below, the others are similarly calculated and are shown in Table 13 below.

$$g_{SIM} = 0.06 + \left(\frac{S}{14}\right)^{0.4} \left(\frac{S}{L}\right)^{0.3} \left(\frac{K_g}{12.0Lt_s^3}\right)^{0.1}$$

$$= 0.06 + \left(\frac{11.5}{14}\right)^{0.4} \left(\frac{11.5}{114.25}\right)^{0.3} \left(\frac{3557176}{12 \times 114.25 \times 8^3}\right)^{0.1} = 0.61 \text{ lanes}$$

Table 13. Interior girder moment distribution factors.

Action	Lanes Loaded	Spans 1 and 3	Span 2
M+ and M- not between POCs	1	0.61	0.60
	2+	0.91	0.91
M- between POCs	1	0.61	
	2+	0.91	

9.1.1.2.2 Exterior Girder Moment Distribution Factors

AASHTO LRFD Table 4.6.2.2.2d-1 indicates that for one lane loaded, the lever rule should be used; for two or more lanes loaded, use the equation provided in AASHTO LRFD Table 4.6.2.2.2d-1. But in no case, for any number of lanes loaded, should the distribution factor be less than that calculated using AASHTO LRFD Eq. C4.6.2.2.2d-1 which assumes a rigid cross-section.

The lever rule uses statics to distribute the live load to the girders. The lever rule assumes that the deck slab is hinged at the interior girder and is therefore statically determinant transversely. Figure 150 shows the dimensions necessary to calculate the moment distribution factor via the lever rule. Using the lever rule also requires application of the multiple presence factor in AASHTO LRFD Table 3.6.1.1.2-1.

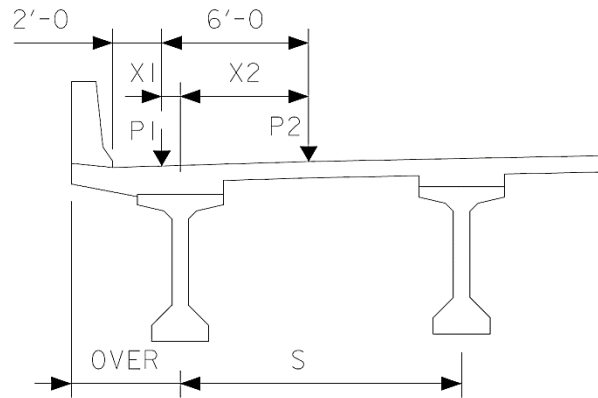


Figure 150. Illustration. Lever rule dimensions.

The dimensions shown in Figure 150 are defined as: S is the girder spacing, $OVER$ is the overhang width, $P1$ and $P2$ are the left and right wheel centerlines respectively, $X1$ is the distance from the left wheel to centerline of exterior girder, and $X2$ is the distance from the exterior girder centerline to the right wheel. $X1$ is determined using Equation (42), where “barrier” is the width of the barrier, and $X2$ is determined using Equation (43). $X1$ is negative if the wheel line is between the edge of the deck slab and the centerline of the exterior girder and positive if between girders. The distribution factor can then be calculated using Equation (44), where m is the multiple presence factor from AASHTO LRFD Table 3.6.1.1.2-1.

$$X1 = OVER - Barrier - 2' \quad (42)$$

$$X2 = 6' + X1 \quad (43)$$

$$g = \frac{m(S - X1 + S - X2)}{2S} \quad (44)$$

Using the dimensions in Figure 147 and Equations (42) and (43), $X1$ is determined to be -9 inches and $X2$ is determined to be 63 inches. Using Equation (44) and selecting the multiple presence factor from AASHTO LRFD Table 3.6.1.1.2-1 for one lane loaded, the distribution factor is calculated as 0.97 lanes.

$$g = \frac{m(S - X1 + S - X2)}{2S} = \frac{1.2(138'' - (-9'') + 138'' - 63'')}{2 \times 138''} = 0.97 \text{ lanes}$$

For multiple lanes loaded, AASHTO LRFD Table 4.6.2.2.2d-1 indicates to use the equation provided in the table. The moment distribution factor for multiple lanes loaded and exterior girders is given by Equation (45) and “ e ” is given by Equation (46).

$$g_{MEM} = e g_{MIM} \quad (45)$$

$$e = 0.77 + \frac{d_e}{9.1} \quad (46)$$

In Equation (46), d_e is the horizontal distance from the centerline of the web of the exterior girder to the interior face of the traffic barrier. Using Equation (47), d_e is determined. AASHTO LRFD Table 4.6.2.2.2d-1 indicates that the calculated value of d_e must be between -1.0 ft and 5.5

ft. Figure 147 indicates the overhang width to be 4 ft-5¼ inches and the barrier width to be 1 ft-8¼ inches, giving a value of d_e equal to 2.75 ft; this value is between -1.0 ft and 5.5 ft.

$$d_e = OVER - Barrier \quad (47)$$

Substituting d_e into Equation (46), “e” is determined to be 1.072. Table 14 shows the moment distribution factors determined using AASHTO LRFD Table 4.6.2.2.2d-1 for multiple lanes loaded.

Table 14. Exterior girder moment distribution factors.

Action	Lanes Loaded	Spans 1 and 3	Span 2
M+ and M- not between POCs	2+	0.97	0.97
M- between POCs	2+	0.97	

The final step to determine the moment distribution factor for the exterior girders is to consider the rigid cross-section analysis of AASHTO LRFD C4.6.2.2.2d. The live load distributed to the exterior girder is determined using Equation (48).

$$R = m \left(\frac{N_L}{N_b} + \frac{X_{ext} \sum_1^{N_L} e}{\sum_1^{N_b} x^2} \right) \quad (48)$$

- Where:
- R = reaction on exterior beam in terms of lanes
 - m = multiple presence factor, from AASHTO LRFD Table 3.6.1.1.2-1
 - N_L = number of loaded lanes under consideration
 - e = eccentricity of design truck or design lane load from center of gravity of the pattern of girders [ft]
 - x = horizontal distance from center of gravity of girder pattern to each girder [ft]
 - X_{ext} = horizontal distance from center of gravity of girder pattern to exterior girder [ft]
 - N_b = number of beams/girders

One Lane Loaded:

Multiple Presence Factor: (Table 3.6.1.1.2-1)

$$m = 1.2$$

First Term of Equation (48):

$$N_L = 1$$

$$N_b = 4$$

$$N_L/N_b = 0.25$$

Second Term of Equation (48):

$$X_{ext} = 1.5 \times 11.5 \text{ ft} = 17.25 \text{ ft}$$

$$e_1 = X_{ext} + OVER - \frac{Barrier}{12} - 2' - \frac{6'}{2} = 15 \text{ ft}$$

$$\Sigma e = 15 \text{ ft}$$

$$x_1, x_4 = 1.5 \times 11.5 \text{ ft} = 17.25 \text{ ft}$$

$$x_2, x_3 = 0.5 \times 11.5 \text{ ft} = 5.75 \text{ ft}$$

$$\Sigma x^2 = 2 \times (5.75 \text{ ft})^2 + 2 \times (17.25 \text{ ft})^2 = 661.25 \text{ ft}^2$$

Two Lanes Loaded:

Multiple Presence Factor: (Table 3.6.1.1.2-1)

$$m = 1.0$$

First Term of Equation (48):

$$N_L = 2$$

$$N_b = 4$$

$$N_L/N_b = 0.5$$

Second Term of Equation (48):

$$X_{ext} = 1.5 \times 11.5 = 17.25 \text{ ft}$$

$$e_1 = X_{ext} + OVER - \frac{Barrier}{12} - 2' - \frac{6'}{2} = 15 \text{ ft}$$

$$e_2 = e_1 - 12 \text{ ft} = 3 \text{ ft}$$

$$\Sigma e = 15 \text{ ft} + 3 \text{ ft} = 18 \text{ ft}$$

$$x_1, x_4 = 1.5 \times 11.5 \text{ ft} = 17.25 \text{ ft}$$

$$x_2, x_3 = 0.5 \times 11.5 \text{ ft} = 5.75 \text{ ft}$$

$$\Sigma x^2 = 2 \times (5.75 \text{ ft})^2 + 2 \times (17.25 \text{ ft})^2 = 661.25 \text{ ft}^2$$

$$\frac{x_{ext} \sum_1^{N_L} e}{\sum_1^{N_b} x^2} = \frac{17.25ft(15ft)}{661.25ft^2} = 0.39$$

Reaction on Exterior Beam:

$$R = m \left(\frac{N_L}{N_b} + \frac{x_{ext} \sum_1^{N_L} e}{\sum_1^{N_b} x^2} \right)$$

$$= 1.2 \times (0.25 + 0.39)$$

$$= 0.77 \text{ lanes}$$

$$\frac{x_{ext} \sum_1^{N_L} e}{\sum_1^{N_b} x^2} = \frac{17.25ft(18ft)}{661.25ft^2} = 0.47$$

Reaction on Exterior Beam:

$$R = m \left(\frac{N_L}{N_b} + \frac{x_{ext} \sum_1^{N_L} e}{\sum_1^{N_b} x^2} \right)$$

$$= 1.0 \times (0.50 + 0.47)$$

$$= 0.97 \text{ lanes}$$

The moment distribution factors for the exterior girders are summarized in Table 15. For one lane loaded, AASHTO LRFD Table 4.6.2.2d-1 resulted in a larger distribution factor than assuming a rigid cross-section; for multiple lanes loaded the opposite occurred. For the exterior girders, the moment distribution factor is 0.97.

Table 15. Exterior girder distribution factor summary.

	One Lane Loaded	Multiple Lanes Loaded
Table 4.6.2.2d-1	0.97	0.97
Rigid Cross-Section	0.77	0.97

9.1.1.3 Step 3 – Determine Dead Loads

9.1.1.3.1 Self-Weight of Girder, w_{sw}

The unit weight of concrete girders is assumed to be 150 pounds per cubic foot. The cross-section area is 7.54 ft². The self-weight of the girder, w_{sw} , is equal to $w_{sw} = 7.54 \text{ ft}^2 \times 150 \text{ lb/ft}^3 = 1,131 \text{ lb/ft} = 1.13 \text{ kip/ft}$.

9.1.1.3.2 Weight of Stay-in-Place Forms, w_{sip}

Stay-in-place forms with an assumed weight of 0.015 ksf are used. The weight includes the weight of the form as well as the concrete in the form valleys. For the interior girders, the weight for SIP forms is $0.015 \text{ ksf} \times 11.5 \text{ ft} = 0.17 \text{ k/ft}$. For the exterior girders, the SIP forms are used only between girders; therefore the weight of SIP forms is $0.015 \text{ ksf} \times 5.75 \text{ ft} = 0.086 \text{ k/ft}$.

9.1.1.3.3 Weight of Concrete Deck Slab, w_{deck}

For the interior girder, the tributary width is taken as one-half the girder spacing on each side of the girder while for the exterior girder, the tributary width is taken as the overhang plus one-half the girder spacing. The deck slab is 8½ inches thick, including a ½ inch integral wearing surface. The concrete deck slab unit weight is assumed to be 150 pounds per cubic foot. The weight of the concrete deck slab for the interior and exterior girders is determined below.

Interior Girder:

Tributary Width, t_w :

$$t_w = S/2 + S/2 = S$$

$$= 11.5 \text{ ft}$$

Deck Slab Thickness, t_s :

Exterior Girder:

Tributary Width, t_w :

$$t_w = S/2 + \text{Overhang}$$

$$= 11.5 \text{ ft}/2 + 4 \text{ ft}-5\frac{1}{4} \text{ inches} = 10.1875 \text{ ft}$$

Deck Slab Thickness, t_s :

$$t_s = 8.5 \text{ inches}$$

Concrete Unit Weight, γ_c :

$$\gamma_c = 150 \text{ lb/ft}^3$$

Interior Girder Deck Slab Weight

$$w_{\text{deck}} = 11.5\text{ft} \times 8.5 \text{ in}/12 \times 150 \text{ lb/ft}^3 = 1222 \text{ lb/ft}$$
$$= 1.22 \text{ k/ft}$$

$$t_s = 8.5 \text{ inches}$$

Concrete Unit Weight, γ_c :

$$\gamma_c = 150 \text{ lb/ft}^3$$

Exterior Girder Deck Slab Weight

$$w_{\text{deck}} = 10.1875\text{ft} \times 8.5 \text{ in}/12 \times 150 \text{ lb/ft}^3 = 1082 \text{ lb/ft}$$
$$= 1.08 \text{ k/ft}$$

9.1.1.3.4 Weight of Concrete Haunches

The weight of the haunch is determined using the cross-section area of the haunch and the unit weight of concrete. For the interior girders, the haunch depth is assumed to be $5^{3/8}$ inches.

The weight of the haunch on the interior girder, w_{hi} , is determined to be $(5^{3/8} \text{ inches} \times 42 \text{ inches}) / (144 \text{ in}^2/\text{ft}^2) \times 150 \text{ lb/ft}^3 = 0.24 \text{ k/ft}$.

For the exterior girders, the concrete in the overhang in excess of the deck slab thickness is included in the weight of the haunch. The haunch depth is $5^{3/4}$ inches at the centerline of the exterior girder.

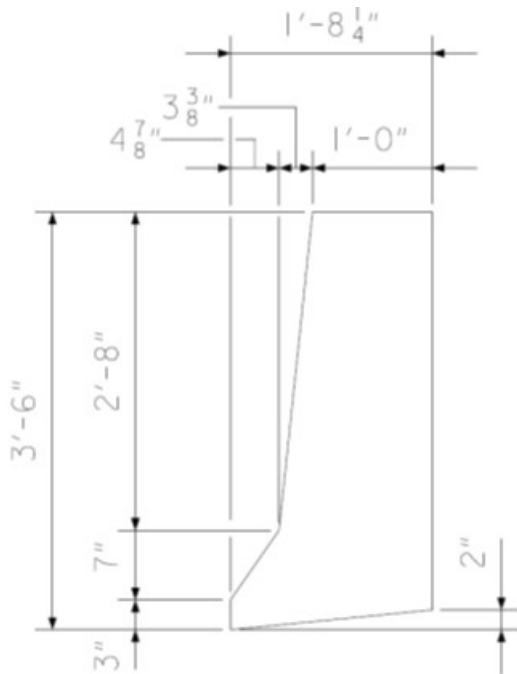
The weight of the haunch, including the concrete in the upturn and overhang, is determined to be 0.39 k/ft.

9.1.1.3.5 Weight of Intermediate Diaphragms

The intermediate diaphragm is located at the center of each span. The diaphragm is 10 inches wide and 46 inches deep and constructed of reinforced concrete. The diaphragm weight applied to the interior girders is 5.2 k and to the exterior girder is 2.44 k.

9.1.1.3.6 Weight of Barriers

The weight of the barrier is determined using available dimensions shown in Figure 151. The calculation of the barrier weight is also shown as part of Figure 151.



Total Barrier Height:
 $H = 42$ inches

Total Barrier Width:
 $W = 20.25$ inches

Total Area:
 $A = W \times H$
 $= 42 \text{ inches} \times 20.25 \text{ inches} = 850.5 \text{ in}^2$

Upturn Area:
 $A_{up} = 20.25 \text{ in}^2$

Sloped Face Area:
 $A_{face} = (32 \text{ inches} \times 4.875 \text{ inches}) + \frac{1}{2}(3.375 \text{ inches} \times 32 \text{ inches}) + \frac{1}{2}(7 \text{ inches} \times 4.875 \text{ inches}) = 227.0625 \text{ in}^2$

Barrier Area:
 $A_p = A - A_{up} - A_{face}$
 $= 850.5 \text{ in}^2 - 20.25 \text{ in}^2 - 227.06 \text{ in}^2$
 $= 603.2 \text{ in}^2 = 4.19 \text{ ft}^2$

Barrier Weight:
 $w_p = A_p \times \gamma_c = 4.19 \text{ ft}^2 \times 150 \text{ lb/ft}^3 = 628.5 \text{ lb/ft}$
 $= 0.63 \text{ k/ft}$

Figure 151. Illustration. Barrier dimensions and weight calculation.

The distribution of the barrier weight to the girders can be performed in several different ways: equally to all girders, to the exterior girder only, or by the lever rule to the exterior girder and first interior girder. For this example, the weight of the barriers will be assumed to be distributed equally to all girders, $w_p = 0.315 \text{ k/ft}$.

9.1.1.3.7 Weight of Future Wearing Surface

A 30 psf future wearing surface is considered in the design of the bridge. The weight of the wearing surface can be distributed equally to all girders or based on tributary width; this example assumes the weight is distributed based on tributary width. For the interior girders, the tributary width is equal to the girder spacing. For the exterior girders, the tributary width is equal to one-half the girder spacing plus the overhang distance minus the width of the barrier. The magnitude of the applied load to the interior girders is $0.030 \text{ ksf} \times 11 \text{ ft-6 inches} = 0.35 \text{ k/ft}$. The magnitude of the applied load to the exterior girders is $0.030 \text{ ksf} \times ((11 \text{ ft-6 inches})/2 + (4 \text{ ft-5} \frac{1}{4} \text{ inches} - 1 \text{ ft-8} \frac{1}{4} \text{ inches})) = 0.26 \text{ k/ft}$.

9.1.1.3.8 Summary of Dead Loads

A summary of the dead load magnitudes for the interior and exterior girders is shown in Table 16 below. The loads shown are on a per girder basis.

Table 16. Dead loads on a per girder basis.

Dead Load Component	Interior	Exterior
Girder Self-Weight, w_{sw} [k/ft]	1.130	1.130
Stay-in-Place Forms, w_{sip} [k/ft]	0.170	0.086
Concrete Deck Slab, w_{deck} [k/ft]	1.220	1.080
Concrete Haunch, w_h [k/ft]	0.240	0.390
Intermediate Diaphragms, P_d [k]	5.190	2.440
Barrier, w_p [k/ft]	0.315	0.315
Future Wearing Surface, w_{fws} [k/ft]	0.350	0.260

9.1.1.4 Step 4 – Develop Analysis Models

This step will be software specific in many of the details, but in general the following will need to be defined in the model:

- 1) Basic layout such as span lengths and support types
- 2) Properties of the cross-sections such as moment of inertia
- 3) Dead loads
- 4) Live loads

As part of this step the engineer needs to verify that the software is performing correctly. One simple test is to apply a known load and ensure that the reactions sum to the total load applied. In this case, the barrier load was applied as a test.

Barrier Load = 0.305 k/ft

Length of Bridge = 114.25ft + 115.25ft + 114.25ft = 343.75 ft

Total Applied Load = 0.315 k/ft × 343.75 ft = 108.28 k

Reactions from 1D Line Girder Analysis:

Abutment 1	Pier 1	Pier 2	Abutment 2	Total
14.38 k	39.76 k	39.76 k	14.38 k	108.28 k
∴ Sum of reactions is equal to applied load; model should be providing reasonable results. Additionally, the reactions are symmetric as would be expected.				

For further verification, an approximate check is made for the maximum negative live load moment. This calculation can be made in several ways, but a standard method used in the past, and used in this example, is with the tables from AISC Moments, Shears and Reactions for Continuous Highway Bridges.

For $N=1.0$ (approximately equal span lengths) and a total length of 343.75 ft the maximum negative moment for a design truck is interpolated as **-1356.97 k-ft/lane**. The lane load is given by $-0.10wL^2 = (-0.10)(0.64 \text{ k/ft})(114.25 \text{ ft})^2 = \text{-835.40 k-ft/lane}$.

Therefore, including impact and distribution, the maximum negative live load moment for an interior girder is given by $[(1.33)(-1356.97 \text{ k-ft/lane})+(-835.40 \text{ k-ft/lane})](0.91 \text{ lanes}) = \mathbf{-2402.55 \text{ k-ft}}$.

This is within 1 percent of the results provided by the analysis software, suggesting the program is operating as expected. In general, acceptable levels of accuracy should consider the complexity of the analysis and geometry being investigated, but ultimately depend on the discretion of the project manager.

9.1.1.5 Step 5 – Develop Moment, Shear, and Deflection Diagrams

After performing the analysis, moment, shear, and deflection diagrams are created using the analysis results. Diagrams can be developed for individual components or combined according to the type of applied load. Figures 152 through 157 show the moments, shears, and deflection calculated from the 1D line girder analysis. The following figures show the moment, shear, and deflection due to: non-composite dead loads including the beam self-weight, stay-in-place deck forms, diaphragms, haunches, and concrete deck slab, maximum and minimum (from continuity conditions) composite dead loads including the barrier and future wearing surface, and maximum positive and negative live load moments including 33 percent dynamic load allowance on the axles only.

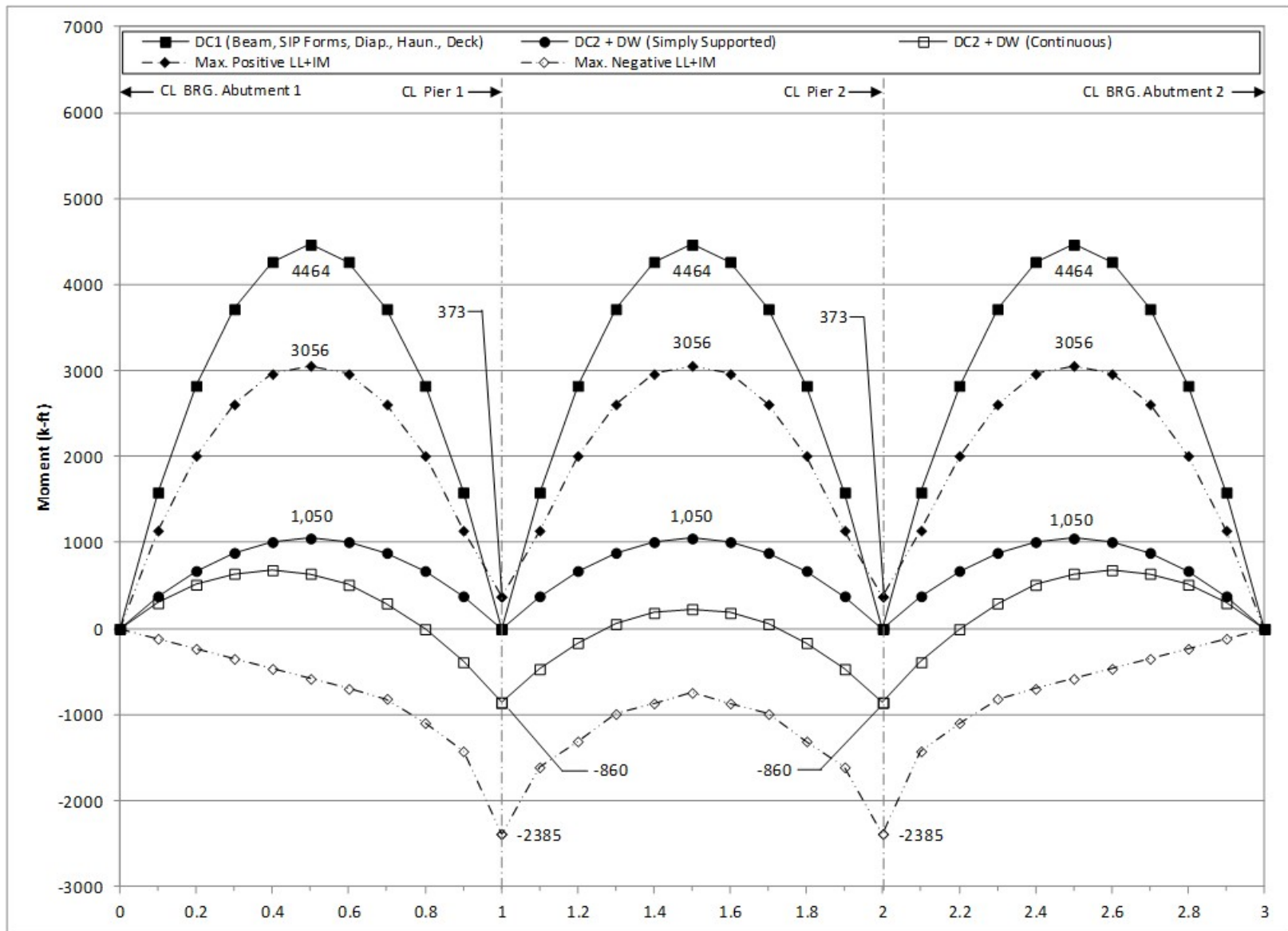


Figure 152. Graph. 1D moment diagram and live load envelope for interior girder.

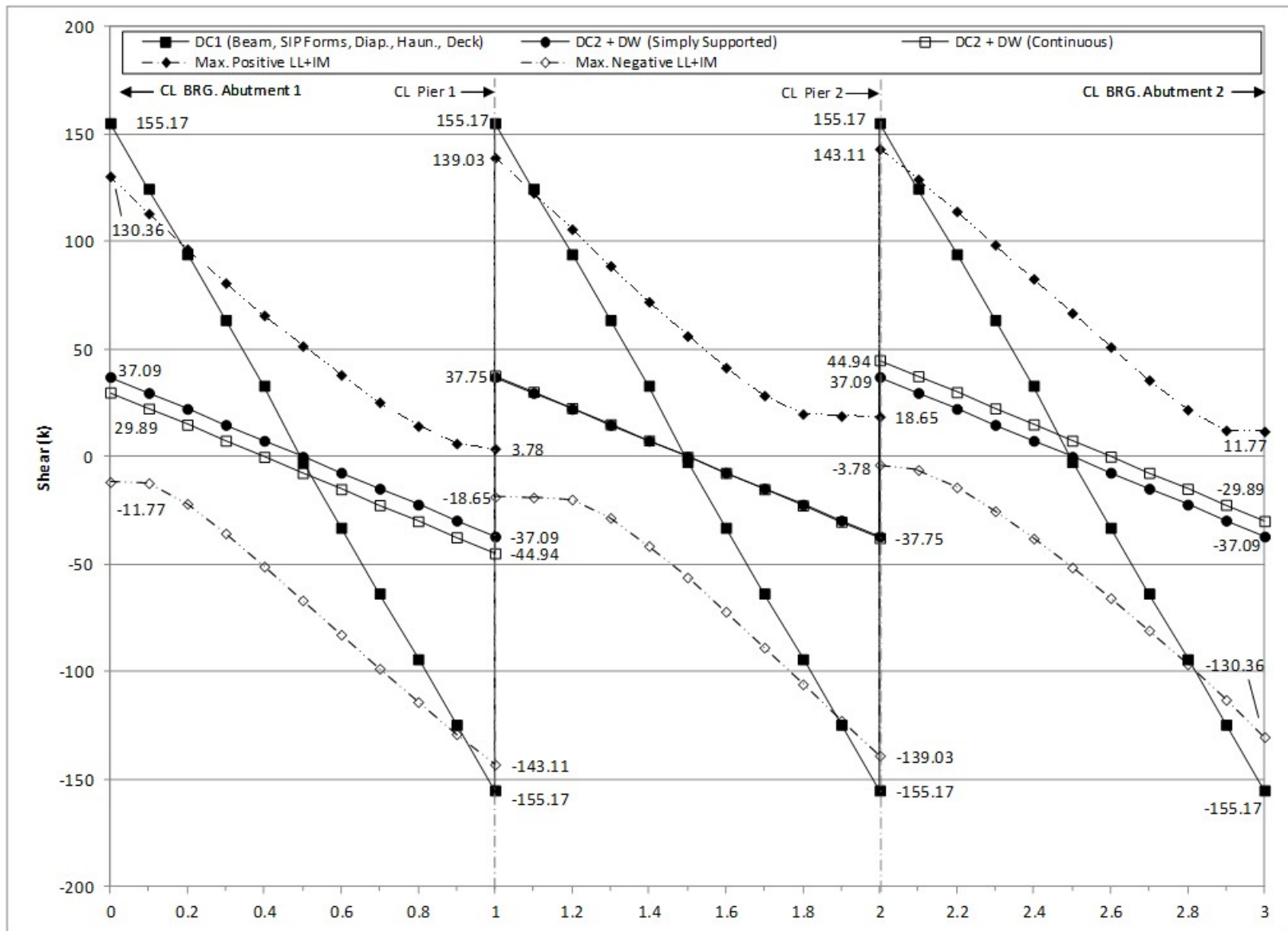


Figure 153. Graph. 1D shear diagram and live load envelope for interior girder.

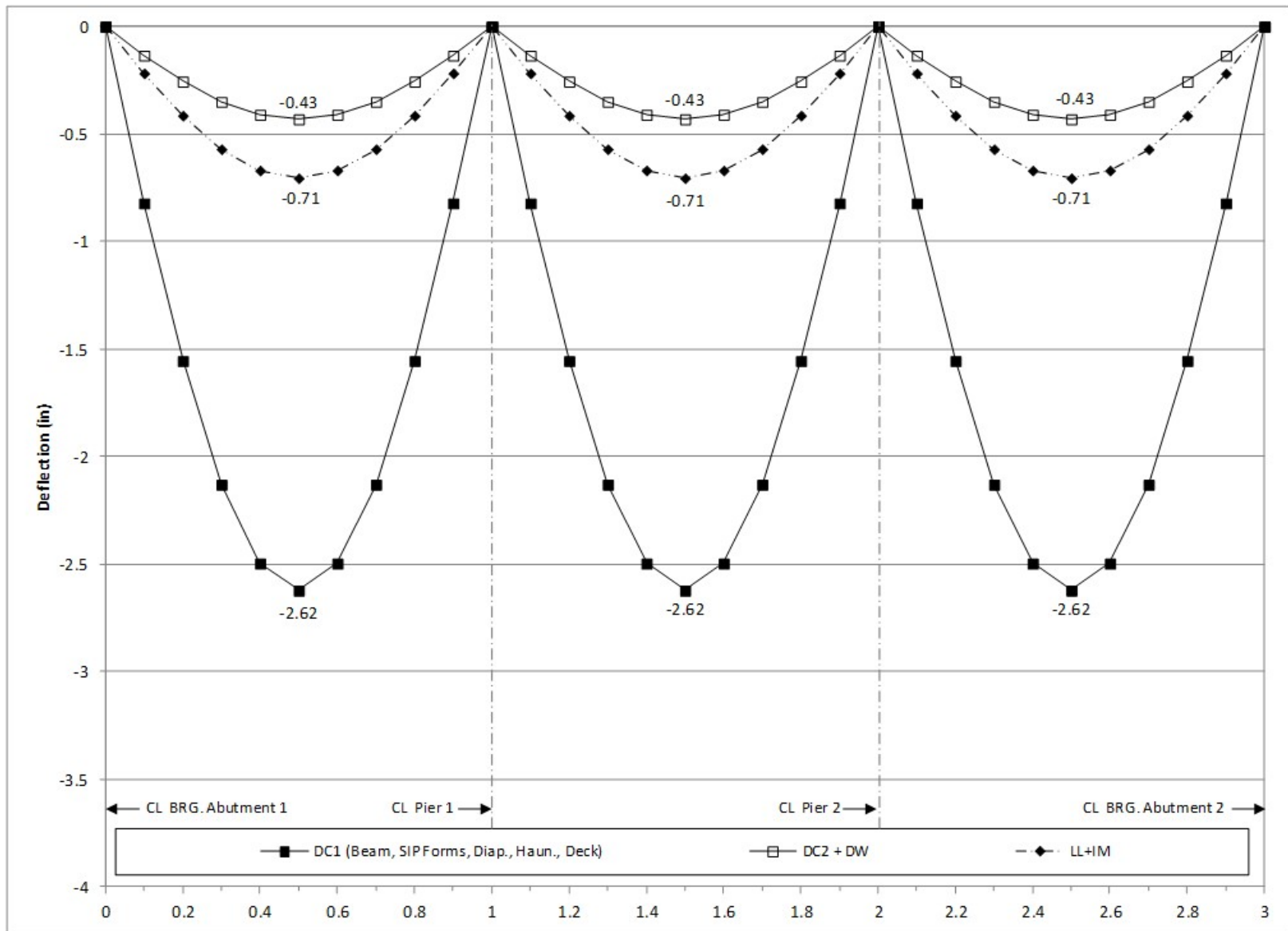


Figure 154. Graph. 1D deflection diagram for interior girder.

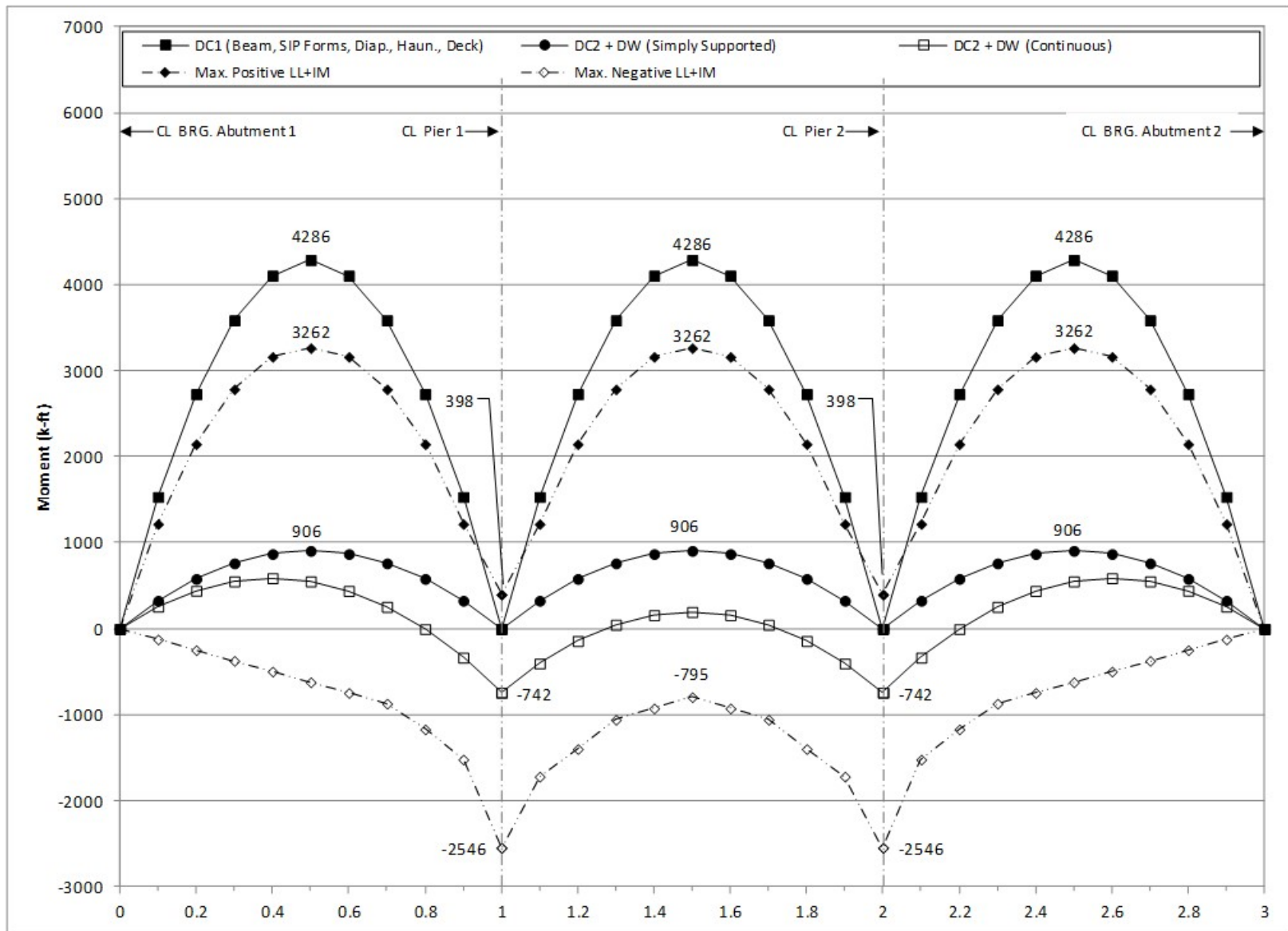


Figure 155. Graph. 1D moment diagram and live load envelope for exterior girder.

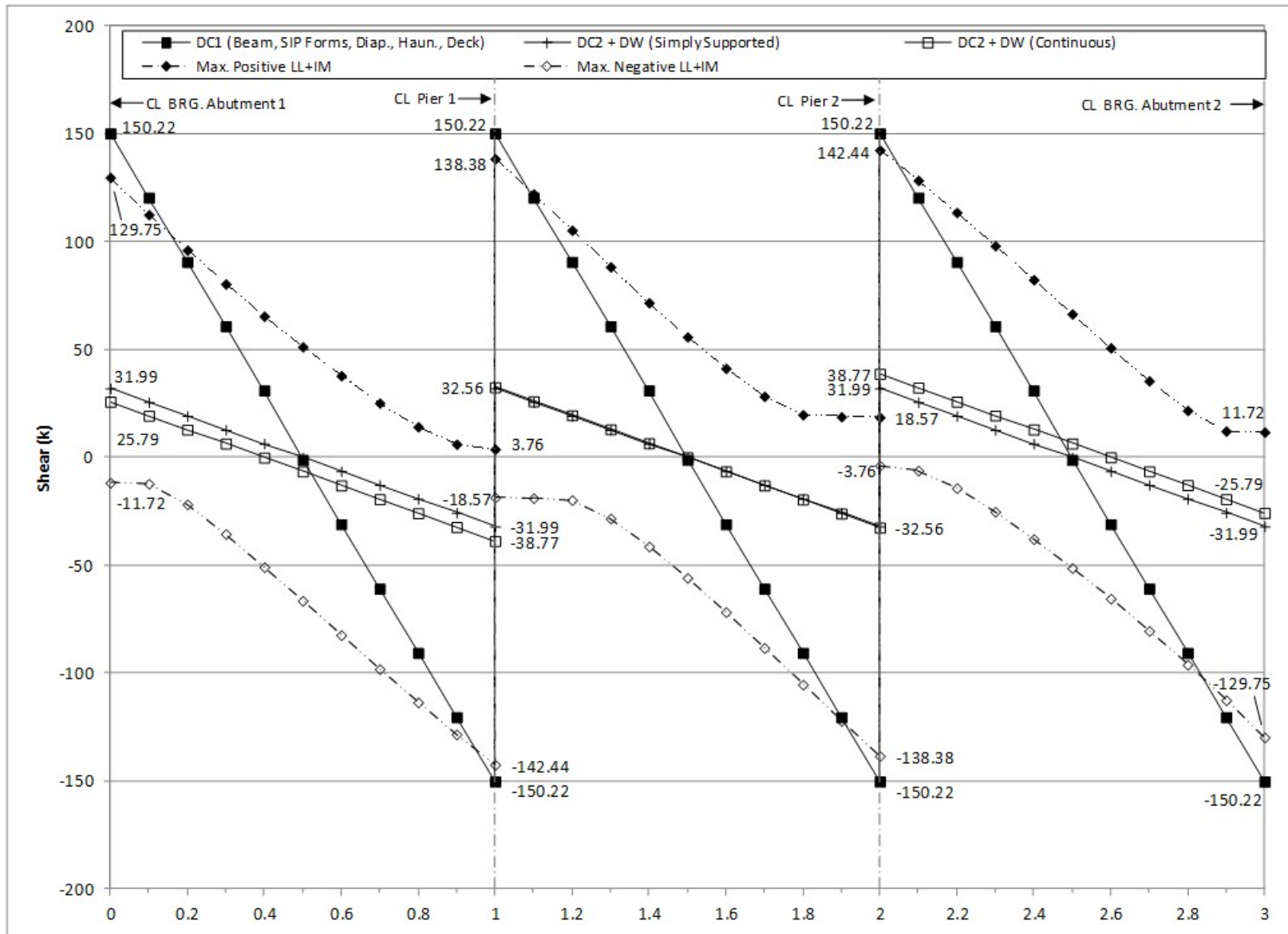


Figure 156. Graph. 1D shear diagram and live load envelope for exterior girder.

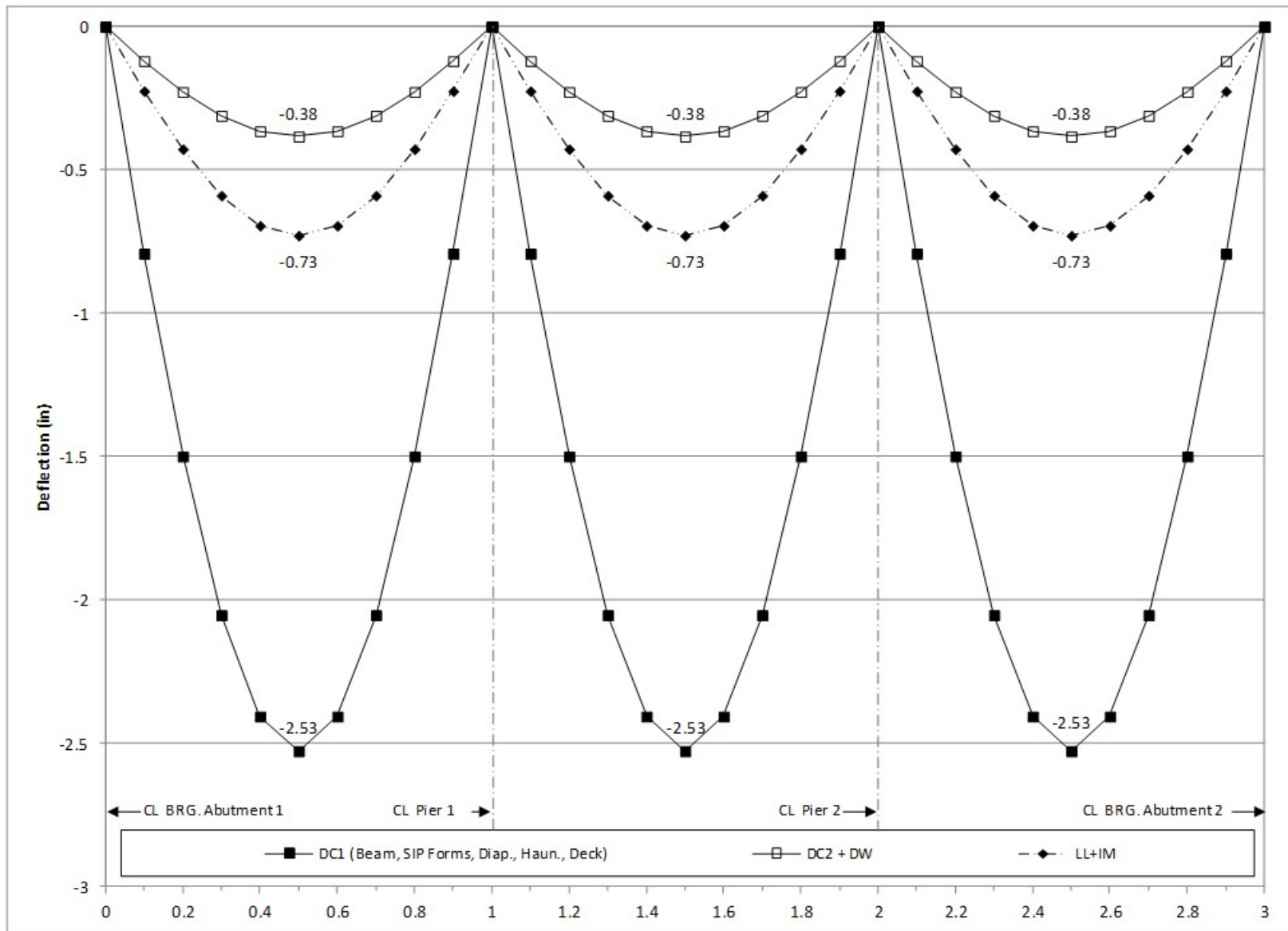


Figure 157. Graph. 1D deflection diagram for exterior girder.

9.1.2 Plate and Eccentric Beam Analysis

Taking the 1D analysis from the previous section one degree further in complexity, the three simple spans shown in Figure 146 that are made continuous for composite dead loads and live loads are modeled with a 2D Plate and Eccentric Beam. To adequately capture behavior in the different loading stages at least three separate models are required; one for non-composite dead loads, one for composite dead loads, and one for live load. Because simply supported and continuous support conditions are both considered for composite dead load and live load in these examples an additional two models are used. For this example, an automated utility within the analysis software was used to determine the location of the truck (or tandem) and lane load that resulted in the maximum positive and negative moments at each tenth point along the structure, but other methods of determining loading extremes (such as development and utilization of influence lines/surfaces) could also be used. All geometry is modeled at the centroid of the girders. The following steps are used to determine the dead and live load moments, shears, and deflections:

1. Create model for non-composite dead loads.
 - a. Define location of girders and intermediate diaphragms. Depending on software, the girder may have to be defined by multiple segments such that the intermediate diaphragm can be connected to the girders, see Figure 158. Between nodes used to define member ends it may also be necessary in this step to discretize the geometry (through addition of nodes) such that members are ultimately composed of a sufficient number of elements. The number of elements should be enough to capture the expected behavior of each component, but not so many that computational time becomes excessive. Consideration should also be given to where results are required, as additional nodes may need defined at these locations. In the analysis software used, elements are created through a meshing process, where an element size/number is specified and applied to the structural members. As elements are defined geometrically, it may also be necessary to choose element type. Further discussion of element definition and element types can be found in Section 3.7.

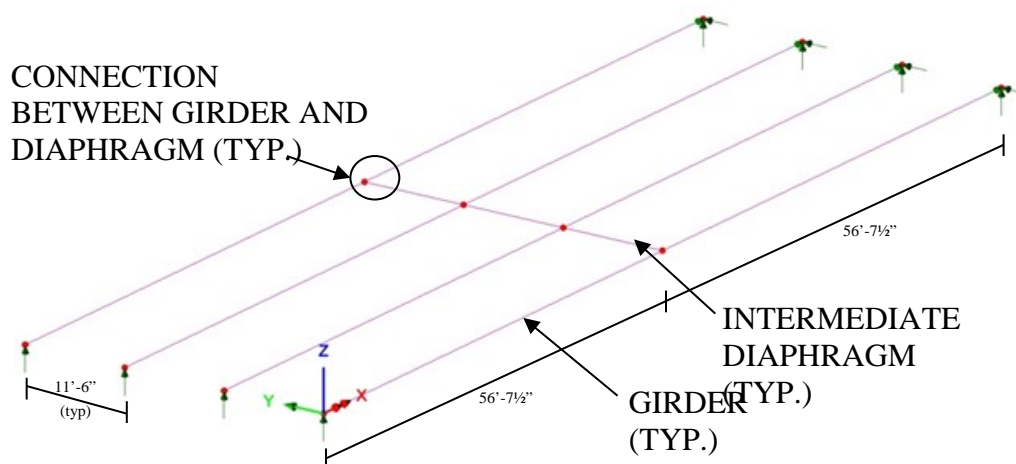


Figure 158. Illustration. Girder and intermediate diaphragm location.

- b. Define geometry of girder cross-section and intermediate diaphragm cross-section. Analysis software may have standard girder cross-sections stored internally; these can be used but the dimensions should be verified. (Note: ensure that the section properties and the model are using consistent units).
 - c. Define material properties for girders and intermediate diaphragms. Separate material properties are defined for the prestressed girders and intermediate diaphragms as different strength concretes are used. The analysis software may have material properties for commonly used materials stored internally; these can be used but should be verified.
 - d. Define support conditions.
 - e. Define loads applied to the non-composite structure.
 - i. For the members defined in the model, the girders and intermediate diaphragms, automatic dead load application can be used if mass density is assigned through material properties. Otherwise, concentrated or distributed loads that are statically equivalent to the weight of the members can be used.
 - ii. The other non-composite dead loads (SIP forms, haunches, deck slab) are applied as uniform line loads to each girder.
 - f. Define load cases.
 - g. Ensure correct attributes (geometric and material properties, support conditions, and non-composite dead loads) are assigned to appropriate components.
 - h. Run analysis; verify analysis results using simplified methods.
 - i. Extract required results from analysis software.
2. Create models for composite dead loads (continuation of the model created in Step 1).
- a. Define location of concrete deck slab and create appropriate surface elements (see Step 1a and Section 3.7.1.3 for more information). For the continuous beam model span lengths will require modification from those created in Step 1 and used for the simply supported case, but will otherwise be identical.
 - b. Define geometry and thickness of concrete deck slab. An eccentricity is applied to the deck such that it is at the appropriate elevation relative to the other members. Some elements support offsets internally, making assigning eccentricities easier. For elements that do not support eccentricities, rigid link constraints or rigid beam elements can be used to provide the required offset.
 - c. Define material properties concrete deck slab. (See Step 1c for more information).
 - d. Define loads applied to the composite structure.
 - i. The FWS is defined as a uniform load distributed over an area. If possible, the load should be applied over a partial width of the bridge, representing placement between barriers. However, if the area of loading does not coincide with the model geometry and partial width loading cannot be specified, either the geometry can be modified to facilitate load application or the load should be modified such that the total applied load remains the same, though the area over which it is spread may be different.

- ii. The weight of the barrier is defined as a uniform line load. Similarly to the FWS, if the barrier load cannot be precisely located due to geometric and loading constraints, either geometry can be modified or approximations can be made.
 - e. Define support conditions.
 - f. Define load cases.
 - g. Ensure correct attributes are assigned (geometric and material properties, support conditions, and loading) to appropriate components.
 - h. Run analysis; verify analysis results using simplified methods.
 - i. Extract required results from analysis software.
3. Create models for composite live loads (continuation of the models created in Step 2).
 - a. Determine optimized loading. The analysis software may have utilities that help in the determination. Influence surfaces can be developed to aid in loading generation.
 - b. Run analysis with optimized loadings and verify results
 - c. Extract required results from analysis software
 4. Combine analysis results extracted in Steps 1i, 2h, and 3c.

9.1.2.1 Step 1 – Create Non-Composite Dead Load Model

9.1.2.1.1 Step 1a – Define Girder and Intermediate Diaphragm Locations

From Figures 146 and 147, the location of the girders and intermediate diaphragms as well as the non-composite span length can be found. Assuming that the origin is located at the left end of girder B4 in Figure 146, the coordinates for the girder ends and intermediate diaphragm locations are shown in Table 17. Each girder is defined by two segments, one from $x = 0$ ft to $x = 56.625$ ft and the second from $x = 56.625$ ft to $x = 113.25$ ft. Since the software being used has elements that allow offsets to be defined, as the coordinates in Table 17 indicate, the nodes of all components lie on the same horizontal plane; in the physical structure, the component centroids do not all lie on the same plane.

Table 17. Coordinates for girder and intermediate diaphragm ends.

Component	Start			End		
	x (ft)	y (ft)	z (ft)	x (ft)	y (ft)	z (ft)
B1	0	34.5	0	113.25	34.5	0
B2	0	23.0	0	113.25	23.0	0
B3	0	11.5	0	113.25	11.5	0
B4	0	0	0	113.25	0	0
Int. Diaphragm B1-B2	56.625	23.0	0	56.625	34.5	0
Int. Diaphragm B2-B3	56.625	11.5	0	56.625	23.0	0
Int. Diaphragm B3-B4	56.625	0	0	56.625	11.5	0

Beam elements are used for modeling both the girders and intermediate diaphragms. In the software used, both Timoshenko and Euler beam elements are available. The Timoshenko formulation, which is capable of capturing shear deformations, is used. However, because shear deformations are insignificant in these members, Euler beam elements would be acceptable as

well, though there is a negligible computational penalty for utilizing the more complete formulation.

For the girders, each line is divided into five elements. This is done such that nodes are located at the girder tenth-points. For the intermediate diaphragms, three elements per line are specified.

9.1.2.1.2 Step 1b – Define Girder and Intermediate Diaphragm Cross-Sections

Refer to Section 9.1.1.1 for calculation of the girder properties.

The intermediate diaphragm is defined as a rectangle that is 46 inches deep and 10 inches wide. Table 18 shows the intermediate diaphragm section properties as calculated by the analysis software.

Because the centroid of the diaphragms is at a different height than the girder centroid a vertical offset is required. The centroid of the girder is 36.375 inches from the bottom of the girder while the centroid of the intermediate diaphragm is 44 inches from the bottom of the girder; therefore the intermediate diaphragm cross-section must be shifted up by 7.625 inches (or 0.635 ft) (see Figure 159). In the software used, this is entered as a negative value.

Table 18. Intermediate diaphragm section properties.

Section Property	Value
Cross-section Area (A) (ft^2)	3.194
Strong Axis Moment of Inertia (I_{yy}) (ft^4)	3.912
Weak Axis Moment of Inertia (I_{zz}) (ft^4)	0.185
Torsion Constant (J_{xx}) (ft^4)	0.638
Shear Area in y direction (A_{vy}) (ft^2)	2.662
Shear Area in z direction (A_{vz}) (ft^2)	2.662
Offset in z direction (R_z) (ft)	-0.635

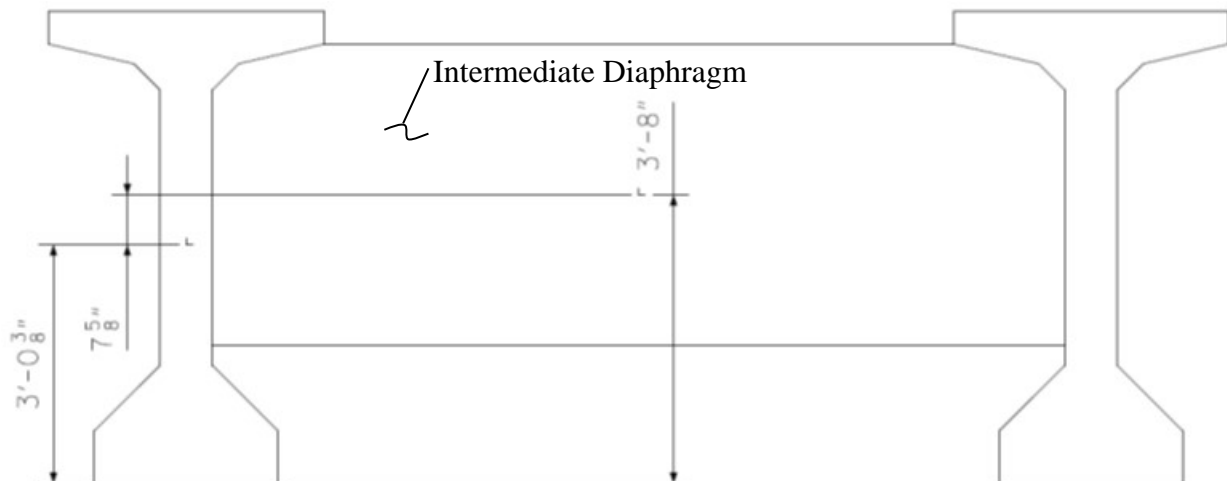


Figure 159. Illustration. Diaphragm eccentricity.

9.1.2.1.3 Step 1c – Define Material Properties for Girders and Intermediate Diaphragms

Material properties can be calculated by hand and input into the analysis software or defined using materials already included in the software. If specifying material properties directly from analysis software it should be verified that they conform to the design specifications. Based on the available information, the girders utilize concrete with a 28-day compressive strength of 8 ksi while the intermediate diaphragms utilize concrete with a 28-day compressive strength of 3.5 ksi. This example utilizes material properties shown in Table 19 calculated in accordance with Equations (36) and (37) in Section 9.1.1.1.2.

Table 19. Concrete material properties.

Material Property	Girder Concrete (8 ksi)	Int. Diaphragm Concrete (3.5 ksi)
Modulus of Elasticity (ksf)	765,216	490,307
Poisson's Ratio	0.2	0.2
Unit Weight (k/ft ³)	0.153	0.150
Thermal Expansion Coefficient (ft/ft/°F)	6.0E-6	6.0E-6

9.1.2.1.4 Step 1d – Define Support Conditions

The beams are simply supported before the continuity diaphragms at the piers are placed. One end of each girder is restrained in the vertical and transverse directions only. At the other end, each girder is restrained vertically, transversely, and longitudinally. In this model the supports are located vertically at the centroid of the girders. For dead load, modeling the supports at the girder centroid, rather than below the bottom of the girder should not have any effect on the results.

9.1.2.1.5 Step 1e – Define Non-Composite Loads

The non-composite dead loads in addition to self-weight (SIP forms, haunches, and deck slab) are applied as uniform line loads to each girder. The values previously calculated in Sections 9.1.1.3.2 through 9.1.1.3.4 for the SIP form weight, haunch weight, and deck slab weight are applied to the interior and exterior girders as uniformly distributed line loads.

9.1.2.1.6 Step 1f – Define Load Cases

The next step is to define different load cases. Since all loads in this model are non-composite, they are combined into a single load case.

9.1.2.1.7 Step 1g – Ensure Correct Attributes Are Assigned to Components

After defining the geometry, member properties, material properties, support conditions, and loads, these attributes must be assigned to the appropriate geometry within the model. The elements defining the girder are assigned the properties associated with the girders and the elements defining the intermediate diaphragms are assigned the properties associated with the intermediate diaphragms. Listed below are the different components and the attributes that must be assigned:

- Girders
 - Beam elements
 - Geometric cross-section
 - Concrete material properties, $f'_c = 8$ ksi in this example
 - Dead loads (including self-weight, SIP forms, haunches, and deck slab)
- Intermediate diaphragms
 - Beam elements
 - Geometric cross-section
 - Concrete material properties, $f'_c = 3.5$ ksi in this example
 - Dead load (self-weight)

When applying different loads, make sure that the load is applied to the correct load case.

9.1.2.1.8 Step 1h – Run Analysis and Verify Results using Simplified Methods

The next step is to run the analysis. Errors may exist such that the analysis cannot be finished, these must be corrected. Errors may also exist that do not prevent the analysis from finishing but may provide erroneous results. These errors are typically more difficult to detect. Viewing the deflected shape should always be the first step as it can often reveal obvious problems.

The analysis results can be verified using a variety of simplified methods. In this particular case, for a simply supported bridge, midspan moment or end reaction can be calculated using textbook equations. The results from the equations should be very similar to the results from the analysis. In this example, the reaction and midspan moment due to girder self-weight are verified.

From Section 9.1.2.1.2 and 9.1.2.1.3, the girder area (A) is 7.41 ft² and the unit weight of the concrete is 0.153 k/ft³. The weight per linear foot of the girder, w, is therefore 1.134 k/ft.

The midspan moment is calculated using the equation, $M = wL^2/8 = 1818.02$ k-ft. The reaction is calculated using the equation, $R = wL/2 = 64.21$ k.

	Textbook Equation	Analysis Software	% Difference
Midspan Moment (k-ft)	1818.02	1818.02	0.00%
End Reaction (k)	64.21	64.22	0.02%

Therefore, the model is producing reasonable results.

9.1.2.1.9 Step 1i – Extract Required Results from Analysis Software

After verifying that the results from the analysis are reasonable, the results of interest can be extracted and input into a spreadsheet for further use. For the non-composite analysis, the moments in the beam elements can be used directly.

9.1.2.2 Step 2 – Create Composite Dead Load Model

This will be a continuation of the model created in Step 1 above. The bridge is made continuous for composite loads by the pier diaphragms and deck slab. As the deck concrete hardens, including concrete which is placed between ends of adjacent girders, the composite girders will

span between the centerline of piers rather than between bearings. As a result, the continuous span lengths increase to 114 ft-3 inches, 115 ft-3 inches, and 114 ft-3 inches; the intermediate diaphragms are located at the center of the simple spans not at the center of the continuous spans.

9.1.2.2.1 Step 2a – Define Girder, Diaphragm, and Concrete Deck Slab Location

From Figures 146 and 147, the location of the girders, diaphragms (abutment, intermediate, and pier), concrete deck slab, barrier width, and composite span lengths can be found. Assuming that the origin is located at the lower, left corner of the deck slab in Figure 146, the coordinates for the girder supports and diaphragms are shown in Table 20. The pier diaphragms are used to make the girders continuous for composite loads.

Table 20. Coordinates for girder and diaphragm ends.

Component		Start			End		
		x (ft)	y (ft)	z (ft)	x (ft)	y (ft)	z (ft)
Abut. 1	Abut. 1 Diaphragm B1-B2	0	27.4375	0	0	38.9375	0
	Abut. 1 Diaphragm B2-B3	0	15.9375	0	0	27.4375	0
	Abut. 1 Diaphragm B3-B4	0	4.4375	0	0	15.9375	0
Span 1	B1	0	38.9375	0	114.25	38.9375	0
	B2	0	27.4375	0	114.25	27.4375	0
	B3	0	15.9375	0	114.25	15.9375	0
	B4	0	4.4375	0	114.25	4.4375	0
	Int. Diaphragm B1-B2	57.125	27.4375	0	57.125	38.9375	0
	Int. Diaphragm B2-B3	57.125	15.9375	0	57.125	27.4375	0
	Int. Diaphragm B3-B4	57.125	4.4375	0	57.125	15.9375	0
Pier 1	P1 Diaphragm B1-B2	114.25	27.4375	0	114.25	38.9375	0
	P1 Diaphragm B2-B3	114.25	15.9375	0	114.25	27.4375	0
	P1 Diaphragm B3-B4	114.25	4.4375	0	114.25	15.9375	0
Span 2	B5	114.25	38.9375	0	229.5	38.9375	0
	B6	114.25	27.4375	0	229.5	27.4375	0
	B7	114.25	15.9375	0	229.5	15.9375	0
	B8	114.25	4.4375	0	229.5	4.4375	0
	Int. Diaphragm B5-B6	171.875	27.4375	0	171.875	38.9375	0
	Int. Diaphragm B6-B7	171.875	15.9375	0	171.875	27.4375	0
	Int. Diaphragm B7-B8	171.875	4.4375	0	171.875	15.9375	0
Pier 2	P2 Diaphragm B1-B2	229.5	27.4375	0	229.5	38.9375	0
	P2 Diaphragm B2-B3	229.5	15.9375	0	229.5	27.4375	0
	P2 Diaphragm B3-B4	229.5	4.4375	0	229.5	15.9375	0
Span 3	B9	229.5	38.9375	0	343.75	38.9375	0
	B10	229.5	27.4375	0	343.75	27.4375	0
	B11	229.5	15.9375	0	343.75	15.9375	0
	B12	229.5	4.4375	0	343.75	4.4375	0
	Int. Diaphragm B9-B10	286.625	27.4375	0	286.625	38.9375	0
	Int. Diaphragm B10-B11	286.625	15.9375	0	286.625	27.4375	0
	Int. Diaphragm B11-B12	286.625	4.4375	0	286.625	15.9375	0
Abut. 2	Abut. 2 Diaphragm B1-B2	343.75	27.4375	0	343.75	38.9375	0
	Abut. 2 Diaphragm B2-B3	343.75	15.9375	0	343.75	27.4375	0
	Abut. 2 Diaphragm B3-B4	343.75	4.4375	0	343.75	15.9375	0

Consideration should be given to node location when defining the geometry. While it is desirable to model all components at their actual locations, sometimes models can be greatly simplified without compromising the results by modeling components in slightly shifted locations, where a node is already present for some other reason. As always, judgment should be exercised.

For this example, even though the intermediate diaphragms are not located at midspan of Spans 1 and 3 in the continuous structure, they were modeled at that location, 6 inches from their actual

location. This aligned them with the node location of one of the tenth-points, where critical force effects were desired. Alternatively, the actual diaphragm location could have been modeled, and the tenth-point results taken from those nodes or interpolated to their actual location. Combining these nodes makes meeting aspect ratio recommendations much easier, as otherwise a 6-inch long element between these two locations would have been required. Using the same assumptions as in Table 20, the coordinates for the corners of the concrete deck slab are shown in Table 21.

Table 21. Coordinates of concrete deck slab corners.

Corner	x (ft)	y (ft)	z (ft)
Upper, Left	0	43.375	0
Upper, Right	343.75	43.375	0
Lower, Right	343.75	0	0
Lower, Left	0	0	0

The elements defined for the girders and intermediate diaphragms in the non-composite model are also used in the composite model. Thick shell elements, a type of surface element capable of capturing shear deformations and membrane forces, are used to model the concrete deck slab.

9.1.2.2.2 Step 2b – Define Diaphragm Cross-Sections and Concrete Deck Slab Thickness

The definition of the girder and intermediate diaphragm cross-section is described in Section 9.1.2.1.2. The difference between the definitions in the composite model and the non-composite model is the presence of the concrete deck slab and diaphragms at the abutments and piers. The nodes defining the deck slab, girders, and diaphragms all lie on the same horizontal plane in the analytical model but in the actual structure they are not at the same elevation. To more accurately model the structure, an eccentricity is applied to the concrete deck slab (see Figure 160), pier diaphragms, and abutment diaphragms to shift the centroids vertically to the correct position relative to the girders and intermediate diaphragms (see Section 9.1.2.1.2). Cross-slope of the deck is neglected in the geometry of the model as its effect on load distribution and load effects is negligible, while it can add a nontrivial amount of preprocessing time.

The pier diaphragms are 30 inches wide and 7 ft-2¼ inches deep while the abutment diaphragms are 48 inches wide and 6.5 feet deep. The cross-section properties are shown in Table 22.

Table 22. Pier and abutment diaphragm section properties.

Section Property	Pier	Abutment
Cross-section Area (A) (ft ²)	17.98	26.00
Strong Axis Moment of Inertia (I _{yy}) (ft ⁴)	77.49	91.54
Weak Axis Moment of Inertia (I _{zz}) (ft ⁴)	9.36	34.67
Torsion Constant (J _{xx}) (ft ⁴)	29.26	85.55
Shear Area in y direction (A _{vy}) (ft ²)	14.98	21.67
Shear Area in z direction (A _{vz}) (ft ²)	14.98	21.67
Offset in z direction (R _z) (ft)	0.625	0.281

The only values required to define the concrete deck slab are the thickness and eccentricity. The deck slab thickness used in the model is the structural design thickness of 8 inches, which neglects stiffness contributions from the ½ inch integral wearing surface. To account for the weight of the omitted wearing surface thickness the material properties of the concrete deck slab will be modified in the following section. An eccentricity of 3.406 ft is applied to the deck slab.

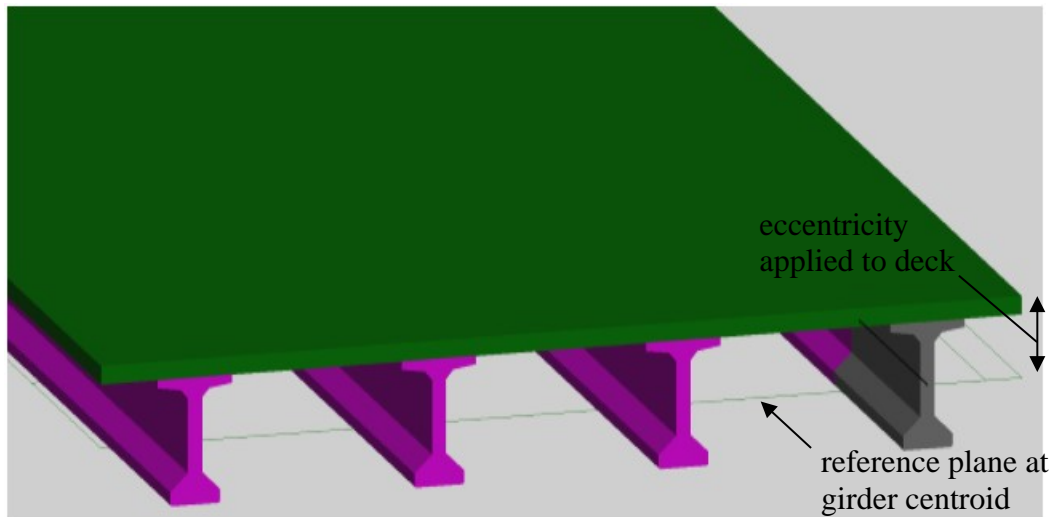


Figure 160. Illustration. PEB model.

9.1.2.2.3 Step 2c – Define Material Properties for the Concrete Deck Slab

The properties for the deck slab concrete are added to the model. The deck slab concrete has a 28 day compressive strength of 4 ksi. The 150 pcf unit weight is increased by the ratio of actual deck slab thickness (including wearing surface) to the modeled deck slab thickness. Table 23 shows the material properties for the concrete deck.

Table 23. Concrete material properties.

Material Property	Deck Slab Concrete (4 ksi)
Modulus of Elasticity (ksf)	524,757
Poisson's Ratio	0.2
Unit Weight (k/ft ³)	0.159
Thermal Expansion Coefficient (ft/°F)	6.0E-6

While the deck slab, girder, and diaphragms are expected to have differential creep behavior (as a function of variable mix design and age) which suggests the use of a modular ratio, this effect is generally negligible and no modular ratio is applied.

9.1.2.2.4 Step 2d – Define Support Conditions

The supports at the abutments and Pier 1 restrain movement in the vertical and transverse directions only. At Pier 2, the girders are restrained vertically, transversely, and longitudinally

against translation. Rotation about all three orthogonal axes is allowed at all bearing locations. Because of eccentricities applied in Section 9.1.2.2.2, the supports in this model are effectively located at the centroid of the girders. If desired, rigid links could be added to relocate the supports as they exist at the bottom of the girders.

9.1.2.2.5 Step 2e – Define Dead Loads Applied to Composite Structure

The future wearing surface (FWS) load is defined as a uniform load distributed over the bridge width. To account for the difference in modeled width and actual width (which spans only between barriers), the FWS load is reduced from 0.030 ksf (spread over 40.0 ft) to 0.028 ksf (spread over 43.375 ft).

The weight of the barrier, determined above in Section 9.1.1.3.6, is applied as a uniform line load.

9.1.2.2.6 Step 2f – Define Load Cases

Separate load cases are defined for the composite dead loads; in this analysis, the composite dead loads are simply added together as moment envelopes are being compared but if the force effects were to be used in design, the barrier would be a DC (component dead load) load while the future wearing surface would be a DW (wearing surface dead load) load with the appropriate load factors applied.

9.1.2.2.7 Step 2g – Ensure Correct Attributes Are Assigned to Components

After defining the geometry and elements, member properties, material properties, support conditions, and loads, these attributes must be assigned to the appropriate geometry within the model. The lines defining the girders, intermediate diaphragms, and pier diaphragms are assigned the properties for the respective component. The concrete deck slab surfaces are assigned the properties of the deck slab. Listed below are the different components and the attributes that must be assigned:

- Girders
 - Beam elements
 - Geometric cross-section
 - Concrete material properties, $f'_c = 8$ ksi in this example
- Intermediate Diaphragms
 - Beam elements
 - Geometric cross-section
 - Concrete material properties, $f'_c = 3.5$ ksi in this example
- Pier Diaphragms
 - Beam elements
 - Geometric cross-section
 - Concrete material properties, $f'_c = 3.5$ ksi in this example
- Concrete Deck Slab
 - Thick shell elements
 - Deck slab thickness
 - Concrete material properties, $f'_c = 4$ ksi in this example

- Future wearing surface and barrier loading

9.1.2.2.8 Step 2h – Run Analysis and Verify Results using Simplified Methods

After running the analysis moments and reactions can be calculated using published equations for uniform loads. For a three equal span continuous beam with uniform loading, the reaction at the end support is $0.4wl$ and the reaction at the interior support is $1.1wl$. Using tributary areas, an average span of 114 ft-7 inches, and the FWS load of 0.028 ksf the approximate reactions at the supports are listed below:

Location	Girder Line 1	Girder Line 2	Girder Line 3	Girder Line 4	Total
Abutment 1	13.07	14.76	14.76	13.07	55.66
Pier 1	35.95	40.59	40.59	35.95	153.08
Pier 2	35.95	40.59	40.59	35.95	153.08
Abutment 2	13.07	14.76	14.76	13.07	55.66
				Total	417.48

Compare these to the reactions from the PEB Model:

Location	Girder Line 1	Girder Line 2	Girder Line 3	Girder Line 4	Total
Abutment 1	12.16	15.63	15.63	12.16	55.58
Pier 1	33.53	43.05	43.05	33.53	153.16
Pier 2	33.53	43.05	43.05	33.53	153.16
Abutment 2	12.16	15.63	15.63	12.16	55.58
				Total	417.48

The reactions are very similar, verifying that the model is providing accurate results. Additionally, for uniform loads applied to the entire structure, the total applied load applied can be calculated and should equal the sum of the reactions from the analysis model.

Check reactions for FWS load versus applied load:

$$\text{Weight of FWS} = 0.028 \text{ ksf}$$

$$\text{Area over which FWS applied} = 43 \text{ ft-}4\frac{1}{2} \text{ inches} \times 343 \text{ ft-}9 \text{ inches} = 14910.16 \text{ ft}^2$$

$$\text{Total Weight of FWS} = 0.028 \text{ ksf} \times 14910.16 \text{ ft}^2 = 417.48 \text{ k}$$

The total applied FWS load is equal to the sum of the reactions from the model. Additionally, since the structure is symmetric the reactions should also be symmetric. The reactions are symmetric as expected.

9.1.2.2.9 Step 2i – Extract Required Results from Analysis Software

Since the results from the analysis appear reasonable, the results of interest can be extracted and input into a spreadsheet for further analysis or used within the analysis and design software. The results of interest are moments, shears, and deflections in the girders. For a PEB model, the moment due to composite dead load and live load in the girder is not just the moment directly from the beam element. Due to the multiple elements that make up the composite section and eccentricity of the beam elements (plate and eccentric beam), the actual moment in the composite design girder is equal to the moment at the center of gravity of the beam element plus the moment in the deck shell elements and the axial force couple between the deck shell elements and girder beam element. Alternatively, if the analysis software includes a numerical integration utility, the utility could be used to integrate the stresses from the shell elements and the forces/moments in the girder to determine the design moment. Example calculations are shown in Section 9.1.2.3.3.

9.1.2.3 Step 3 – Create Live Load Model

This model uses the same geometry as the model created in Step 2.

9.1.2.3.1 Step 3a – Determine Optimized Live Load

The analysis software may have utilities that help in the determination of optimum live load placement in order to produce extreme effects at chosen design cross-sections. For this example, the software used automatically generates the influence surfaces and then determines the load placement required for extreme effects. In the absence of such utilities, influence line/surfaces can be generated using classical analysis methods.

9.1.2.3.2 Step 3b – Run Analysis and Verify Results using Simplified Methods

After the optimized loadings for each location of interest have been determined, the analysis can be performed. As an example check, the results are verified by summing the reactions and comparing to the total applied load. A sample load case in which two HL-93 Design Trucks are applied was chosen, each truck weighs 72 k resulting in a total applied load of 144 k.

Reactions from Model:

Location	Girder Line 1	Girder Line 2	Girder Line 3	Girder Line 4	Total
Abutment 1	0.315	0.671	0.928	1.486	3.408
Pier 1	-1.557	-3.878	-6.592	-8.579	-20.606
Pier 2	3.049	18.721	43.299	50.852	115.922
Abutment 2	-1.030	8.875	14.559	22.880	45.284
				Total	144.000

The total applied load and the sum of the reactions are equal. The reactions along girder line 4 are greater than those along the other girder lines; this is expected since this load case was to determine the maximum moment in the exterior girder. The reactions are not expected to be symmetric as the loading is not symmetric. Therefore, the model appears to be providing reasonable results.

9.1.2.3.3 Step 3c – Extract Required Results from Analysis Software

The results needed to create the moment, shear, and deflection diagrams can be extracted from the model once the results have been verified. The design moments in the girder can be calculated by summing the moment in the beam element and the axial force in the beam element times the eccentricity. If the moment in the deck shell elements is assumed to be negligible, and there is no net axial forces on the cross-section, the composite design moment can be approximated by adding the moment in the girder beam element to the moment due to the couple between the axial force in the girder beam element and the axial force in the deck as described in Section 8.2.1 (sample calculation shown below). The deck eccentricity is determined in Section 9.1.2.2.2.

Shown in Figure 161, are the force effects at the four-tenths point of the center span in the exterior girder for the future wearing surface loading. The design moment in the girder is calculated by summing the moments about the centroid of the deck slab.

$$M = -[M_y + F_x \times e_{girder}] = -[-48.0 \text{ k-ft} + 7.4 \text{ k} \times (77.25 \text{ in} - 36.375 \text{ in})/12] \\ = 73.21 \text{ k-ft}$$

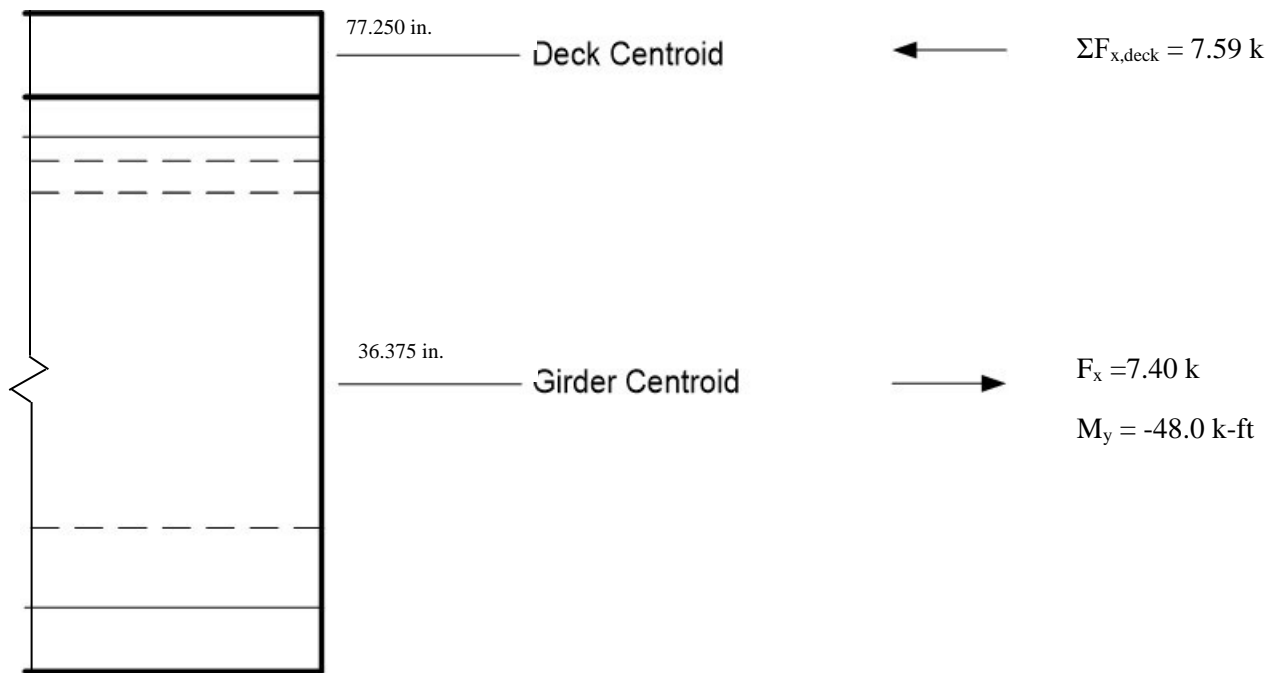


Figure 161. Illustration. PEB moment calculation.

Alternatively, this calculation can be performed as described in Section 8.2.1 manually, by integrating the shell stresses on the cross-section and summing the results. Some FEA software provides a utility that will integrate stresses over a cross-section automatically. Note that at the nodes the forces will appear to have a discontinuity due to the node also behaving as a shear connector. The moment calculated from the utility in this case is 73.68 k-ft, which is slightly different from values above due to rounding.

At this point, depending on the Owner's policy, it may be necessary to repeat Steps 2 and 3 for a simply supported girder bridge. This step was taken in this example. All the steps illustrated above remain the same, except that only a single span is analyzed. The continuous and simple span results were then enveloped.

9.1.2.4 Step 4 – Combine Analysis Results

Once the results of interest, in this case moments, shears, and deflections, have been extracted from the analysis software, they are combined into groups of non-composite dead loads, composite dead loads, and live loads.

The HL-93 Design Load consists of the maximum of the design truck or design tandem amplified by the dynamic load allowance plus the design lane load. The analysis software utility develops the critical vehicle and lane loadings separately, therefore the results must be combined. Similarly, for negative moment between dead load inflection points, the design truck train amplified by the dynamic load allowance and design lane must be combined. The analysis program includes the 0.9 factor for negative moment between dead load inflection points as well as the multiple presence factor. With some software, these steps will need to be done manually

Once the moments, shears, and deflections have been combined into appropriate groups using the results from the various analyses, graphs can be created to show the moment diagram and deflected shape. In this example, the envelope of maximum moments, shears, and deflections from either the simple or continuous girder models for composite dead load and live load are used. The analysis results are combined using the same groups as for the 1D analysis: non-composite dead loads (girder self-weight, diaphragms, SIP forms, haunches, and concrete deck slab), composite dead loads (barrier and FWS), and maximum and minimum live loads including dynamic load allowance. The moment, shear, and deflection diagrams from the PEB analysis are shown in Figures 162 through 167.

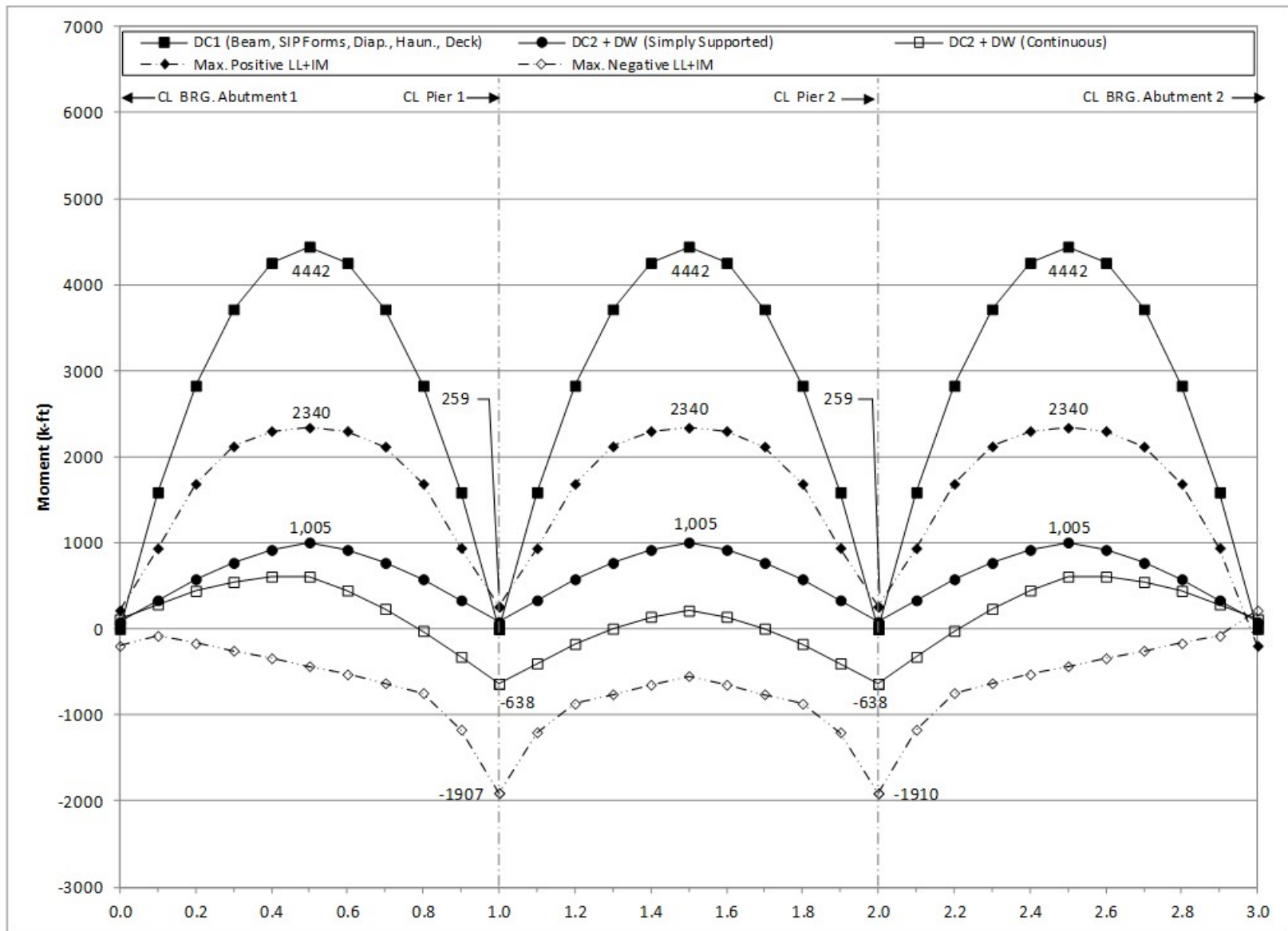


Figure 162. Graph. 2D moment diagram and live load envelope for interior girder.

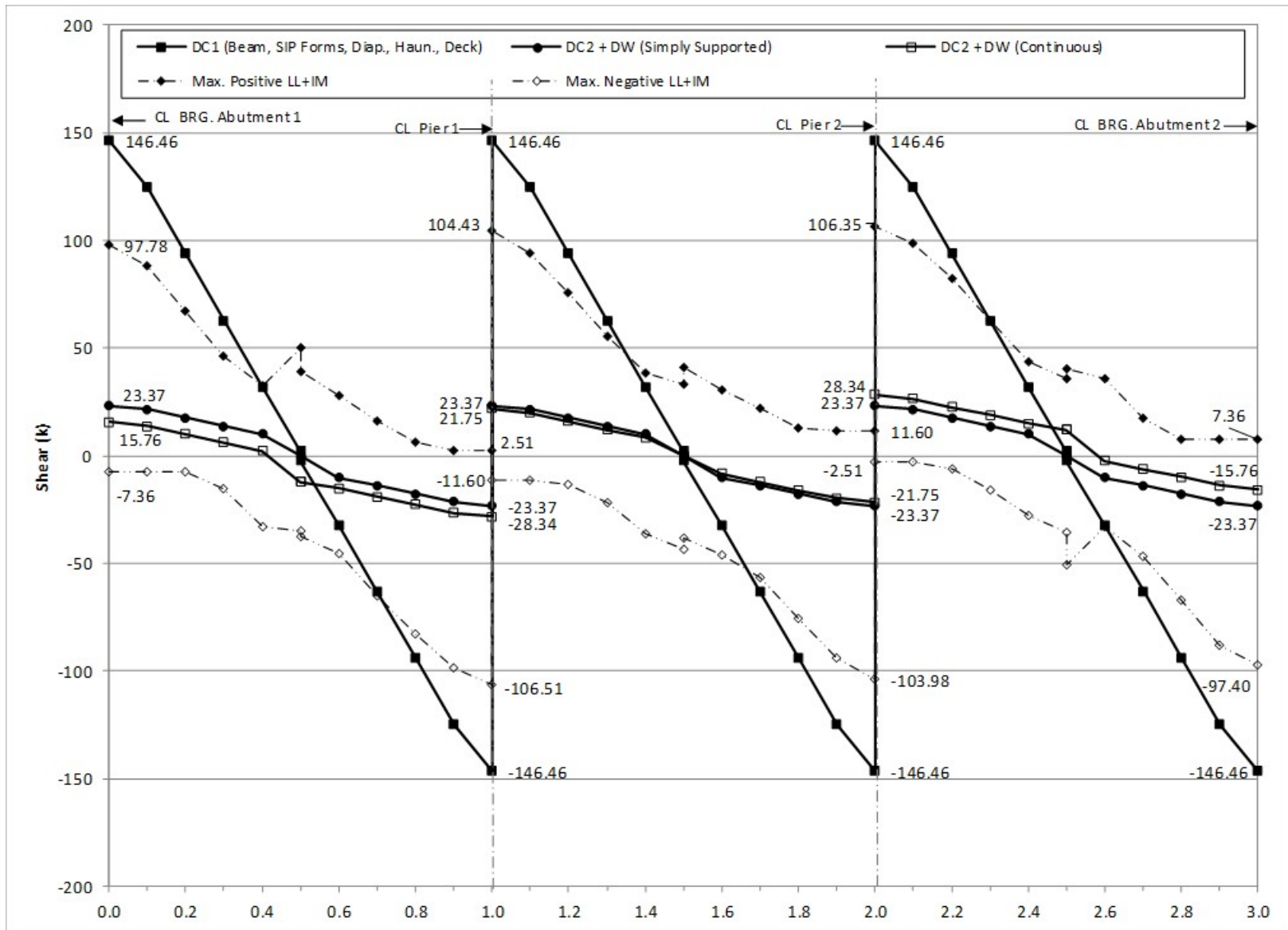


Figure 163. Graph. 2D shear diagram and live load envelope for interior girder.

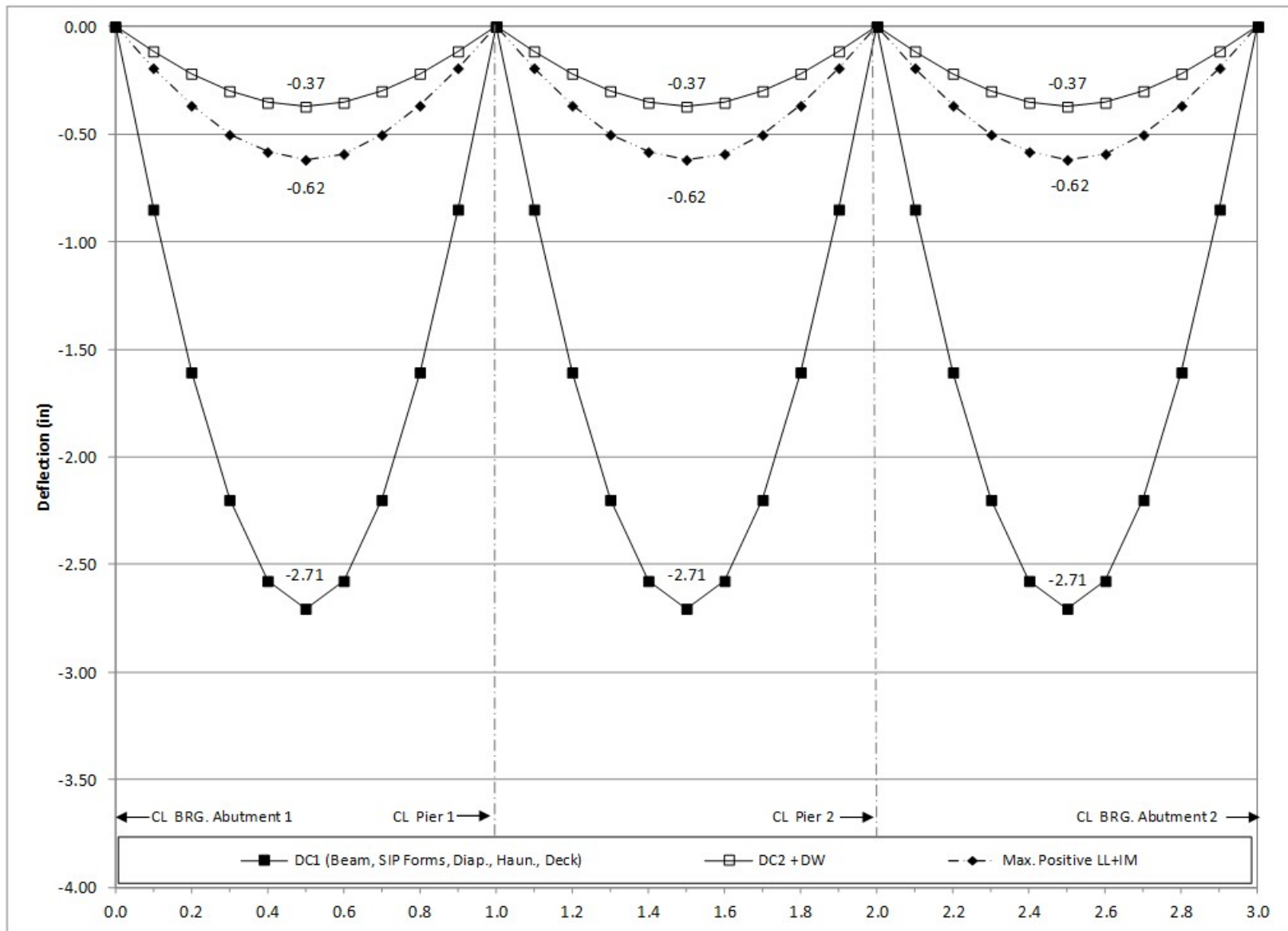


Figure 164. Graph. 2D deflection diagram for interior girder.

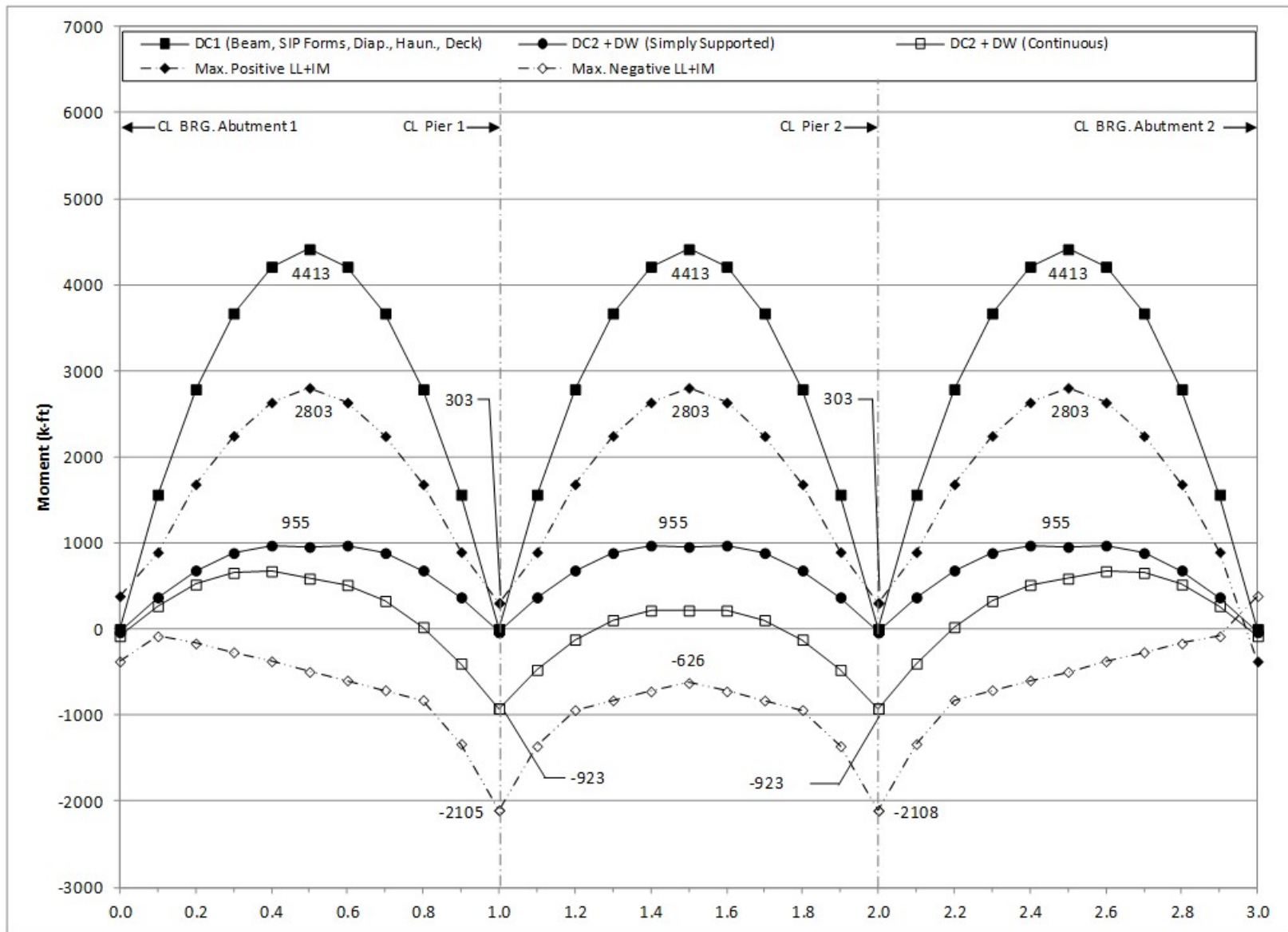


Figure 165. Graph. 2D moment diagram and live load envelope for exterior girder.

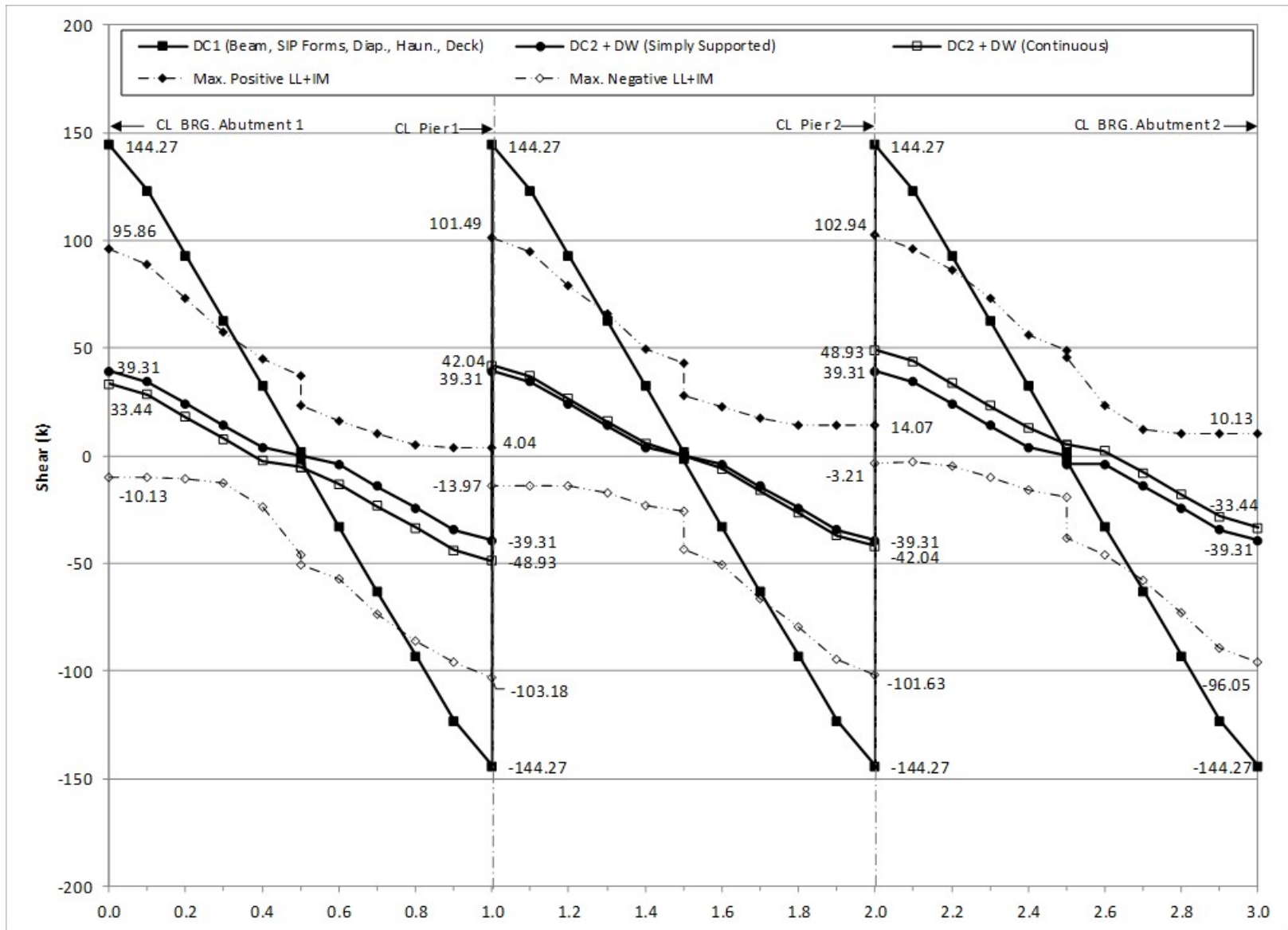


Figure 166. Graph. 2D shear diagram and live load envelope for exterior girder.

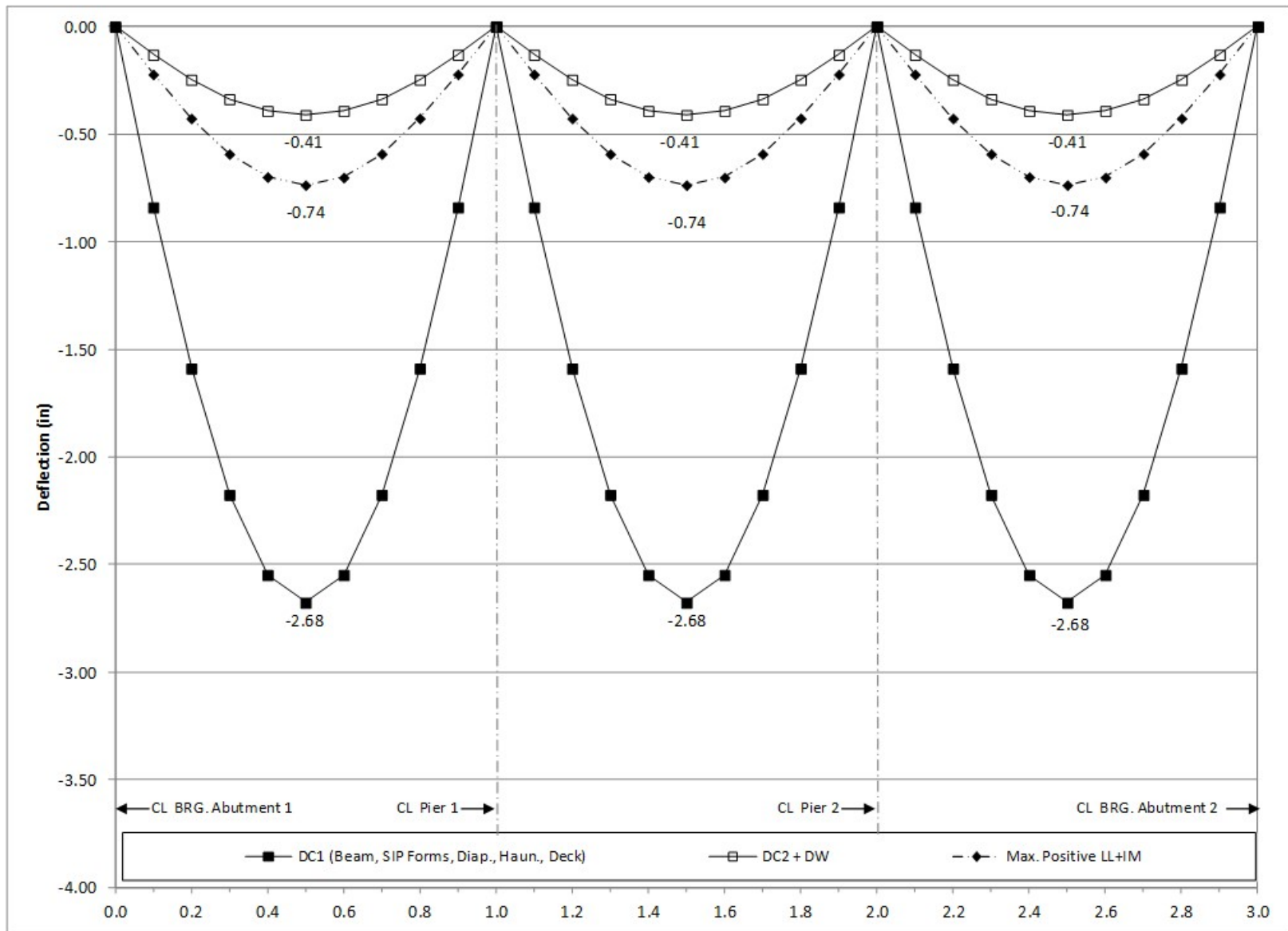


Figure 167. Graph. 2D deflection diagram for exterior girder.

9.1.3 Finite Element Model and Analysis

A full 3D FEA is more involved than the previous two methods presented. In a 3D FEA, the structure depth including supports is modeled explicitly unlike the PEB analysis where all components are modeled in the same plane and then are offset to the correct physical location. The stiffness of the girders and diaphragms are used to distribute non-composite loads and the stiffness of the girders, diaphragms, and deck slab are used to distribute composite dead loads and live loads. The approximate distribution factors in AASHTO LRFD Article 4.6.2.2 are *not* used. Similarly to the previous sections, a minimum of three separate models are required for the analysis.

The following steps are used to determine the dead and live load bending moments, shears, and deflections:

1. Create non-composite dead load model.
 - a. Define geometry for girders and intermediate diaphragms. Flanges of girders and diaphragms are modeled with beam elements, the girder webs with surface elements. Further guidance on modeling these members and discretizing them into an appropriate number of elements is provided in Section 3.7.
 - b. Define section properties for those components modeled with beam elements and thicknesses of those with shell elements.
 - c. Define material properties for girders and intermediate diaphragms.
 - d. Define support conditions.
 - e. Define loads applied to the non-composite structure.
 - i. For the members defined in the model, the girders and intermediate diaphragms, automatic dead load application can be used if mass density is assigned through material properties. Otherwise, concentrated or distributed loads that are statically equivalent to the weight of the members can be used.
 - ii. The other non-composite dead loads (SIP forms, haunches, deck slab) are applied as uniform line loads to each girder.
 - f. Define non-composite load cases.
 - g. Ensure correct attributes are assigned (geometric and material properties, support conditions, and non-composite dead loads) to appropriate components.
 - h. Run analysis; verify analysis results using simplified methods.
 - i. Extract required results from analysis software.
2. Create model for composite dead loads (will be a continuation of the model created in Step 1).
 - a. Define geometry for concrete deck slab. Similarly to Section 9.1.2, the concrete deck slab is modeled with surface elements.
 - b. Define thickness of concrete deck slab.
 - c. Define material properties for concrete deck slab.
 - d. Define support conditions.
 - e. Define loads applied to the composite structure.
 - i. The FWS is defined as a uniform load distributed over an area.
 - ii. The weight of the barrier is defined as a uniform line load.

- f. Define load cases for composite dead loads.
 - g. Ensure correct attributes are assigned (geometric and material properties, support conditions, and loading) to appropriate components.
 - h. Run analysis; verify analysis results using simplified methods.
 - i. Extract required results from analysis software.
3. Create model for live loads (continuation of the model created in Step 2).
 - a. Determine optimized loading. The analysis software may have utilities that help in the determination. Influence surfaces can be developed to aid in loading generation.
 - b. Run analysis with optimized loadings and verify results.
 - c. Extract required results from analysis software
 4. Combine analysis results extracted in Steps 1i, 2i, and 3c.

9.1.3.1 Step 1 – Develop Non-Composite Model

9.1.3.1.1 Step 1a – Define Geometry for Girders and Diaphragms

The girder geometry is defined by creating surface elements along the girder centerline. Four elements in cross-section are used to represent the girder webs while beam elements are used to represent the girder flanges at the top and bottom of the web. When defining the girders, nodes should be defined at the locations of the intermediate diaphragms to facilitate connections. The intermediate diaphragms are defined by beam elements connecting the points at midspan of each girder.

In a prestressed concrete girder bridge, the flanges represent a significant portion of the total girder depth; the vertical location of the supports varies depending on how the web is modeled. In this example, the shell elements defining the web are modeled to extend the full depth of the section, as recommended in Section 3.6.2.1 of the manual, and illustrated in Figure 168.

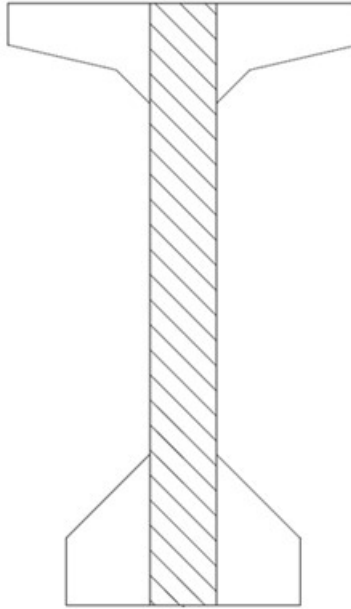


Figure 168. Illustration. Modeling of web depth.

The girder web surface elements utilize thick shells, a type of surface element capable of capturing shear deformations and membrane forces further discussed in Section 3.6.1.3. Thick beam elements, a beam element capable of capturing shear deformations, are used for the girder flanges and intermediate diaphragms and further discussed in Section 3.6.1.2.

Diaphragms could be modeled with surface elements similarly to the girder webs, but doing so significantly increases preprocessing and post-processing time for negligible improvements in accuracy. For preprocessing it requires consideration of matching node location for members with different height so that elements can be connected, while post-processing requires additional effort to extract force effects. Figure 169 shows an isometric view of the non-composite model.

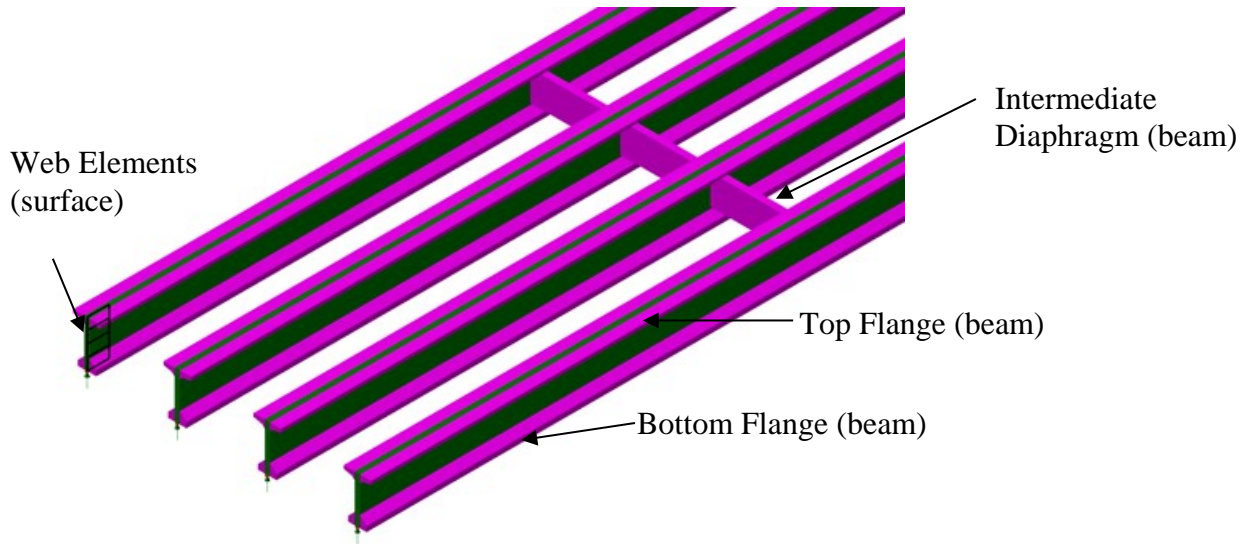


Figure 169. Illustration. Non-composite 3D FEA model.

9.1.3.1.2 Step 1b – Define Cross-Section Properties

The cross-section properties for the girder top and bottom flanges must be defined and the element located such that the section properties of the entire girder cross-section are correct. Figure 170 shows the dimensions for the top and bottom flanges; the section properties and centroid location were determined and are listed in Table 24. Because the flange beam elements are connected at the top and bottom of the web, offsets shown in the table are used to locate the flange beam elements at the centroid of each flange so they are at the correct height relative to the girder web.

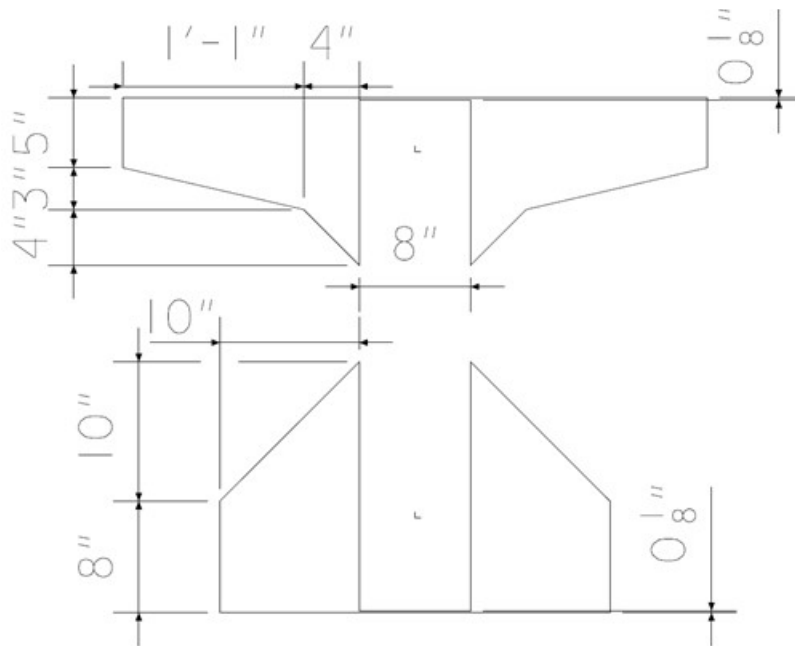


Figure 170. Illustration. Girder flanges for 3D FEA model.

Table 24. Girder flange section properties.

Section Property	Top Flange	Bottom Flange
Cross-section Area (A) (ft ²)	1.736	1.813
Strong Axis Moment of Inertia (I _{yy}) (ft ⁴)	0.075	0.230
Weak Axis Moment of Inertia (I _{zz}) (ft ⁴)	1.848	0.976
Torsion Constant (J _{xx}) (ft ⁴)	0.139	0.195
Shear Area in y direction (A _{vy}) (ft ²)	0.084	0.039
Shear Area in z direction (A _{vz}) (ft ²)	1.544	1.615
Offset in z direction (R _z) (ft)	0.323	-0.568

The intermediate diaphragms are 10 inches wide by 46 inches deep. In this example the diaphragm is connected at the top flange of the girder and offset such that it is in the correct location, but the member could be modeled at the correct location and attached via constraint equations or rigid links. The offset is equal to the distance between the top of the modeled girder web and the centroid of the diaphragm. The section properties for these intermediate diaphragms (which are modeled with beam elements) are the same as the previous section, except for the eccentricity (offset), which is now offset from the top of the web rather than centroid of the girder, a distance of 2.3125 feet.

The only geometric property needed for the girder web is the thickness, 8 inches.

9.1.3.1.3 Step 1c – Define Material Properties

Similar to the girder section properties, the material properties can be calculated by hand and input into the analysis software or defined using material properties already included in the software library. If the latter is used, the properties should be verified to conform with design specifications. This example utilizes material properties shown in Table 25. Based on the available information, the girders utilize concrete with a 28-day compressive strength of 8 ksi while the intermediate diaphragms utilize concrete with a 28-day compressive strength of 3.5 ksi.

Table 25. Concrete material properties.

Material Property	Girder Concrete (8 ksi)	Int. Diaphragm Concrete (3.5 ksi)
Modulus of Elasticity (ksf)	765,216	490,307
Poisson's Ratio	0.2	0.2
Unit Weight (k/ft ³)	0.153	0.150
Thermal Expansion Coefficient (ft/ft/°F)	6.0E-6	6.0E-6

9.1.3.1.4 Step 1d – Define Support Conditions

The same support conditions as the 2D model are used in this model, but are located at the actual elevation along the bottom flange.

9.1.3.1.5 Step 1e – Define Non-Composite Loads

Self-weight of members defined in the model, the girders and intermediate diaphragms, is applied using a body force.

The other non-composite dead loads (SIP forms, haunches, and deck slab) are applied as uniform line loads to each girder. The values previously calculated in Sections 9.1.1.1.2 through 9.1.1.1.4 for the SIP form weight, haunch weight, and deck slab weight are applied to the interior and exterior girders as uniformly distributed loads.

9.1.3.1.6 Step 1f – Define Load Cases

The next step is to define load cases. Since all loads in this model are non-composite they are combined into a single load case. If the results of this example were used for design, the loads could still be combined into a single load case because they carry the same load factors. In Section 9.1.3.1.8, the results are verified using a simplified method. To facilitate checking of the model it may be desirable to create a separate load case containing only one of the loads (e.g. girder self-weight or stay-in-place forms).

9.1.3.1.7 Step 1g – Ensure Correct Attributes Are Assigned to Components

The attributes assigned to each of the different components as shown below:

- Girders
 - Web
 - Thick Shell surface elements
 - Geometric surface cross-section
 - Concrete material properties, in this example, $f'_c = 8$ ksi
 - Body force acceleration (gravity)
 - Flanges
 - Thick beam elements
 - Flange cross-sections
 - Concrete material properties, in this example, $f'_c = 8$ ksi
 - Body force acceleration (gravity)
 - Other non-composite loads (to top flange only)
- Intermediate Diaphragms
 - Thick beam elements
 - Geometric cross-section
 - Concrete material properties, in this example, $f'_c = 3.5$ ksi
 - Body force acceleration (gravity)

9.1.3.1.8 Step 1h – Run Analysis and Verify Results

The next step is to run the analysis. The analysis results can be verified using a variety of simplified methods. Using the equations shown in Section 9.1.2.1.8 to calculate the midspan moment and the weight per linear foot from Section 9.1.1.1.1, the moment is 1789.2 k-ft. Determining the moment at midspan, by hand, from the 3D analysis model is more involved due

to using multiple beam and shell elements. The required element nodal forces and moments required to determine the design moment in the girder are shown in Figure 171. The shell element nodal “forces,” indicated as N_y in Figure 171, are equal to the stress at the node multiplied by the element thickness. A sample moment calculation is shown below Figure 171.

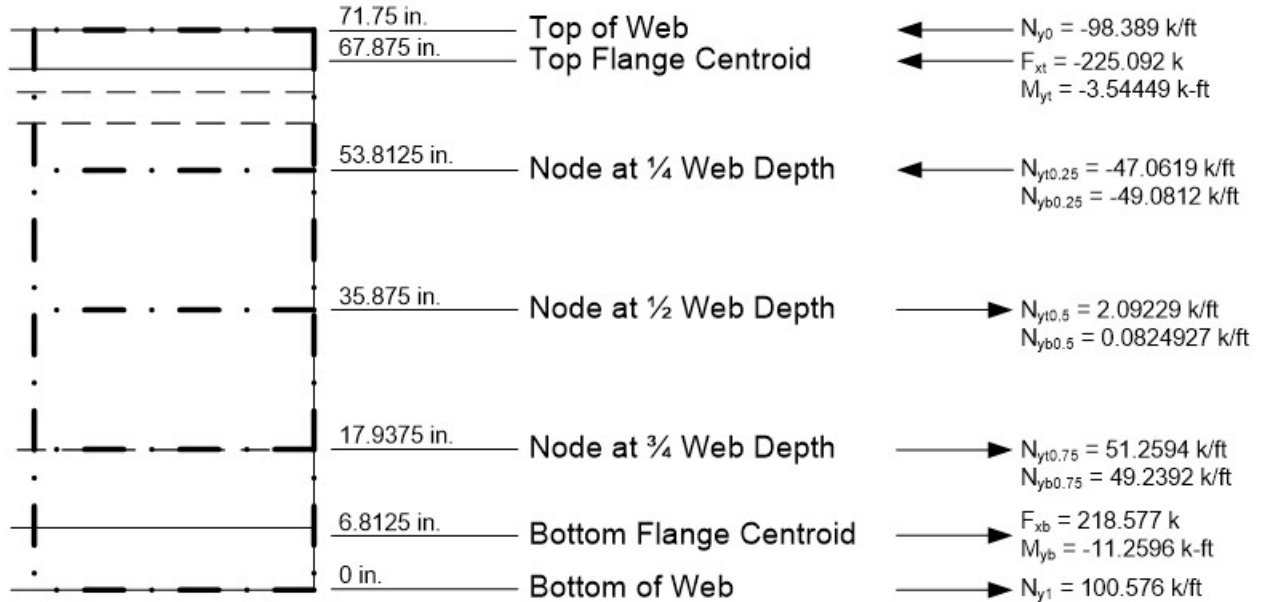


Figure 171. Illustration. Element force effects in non-composite concrete girder

Nodal Forces (from analysis software):

Shell Elements (4 Elements through web depth):

N_{y0}	= -98.389 k/ft	(upper node of top shell element)
$N_{yt0.25}$	= -47.062 k/ft	(lower node of top shell element)
$N_{yb0.25}$	= -49.081 k/ft	(upper node of second shell element)
$N_{yt0.50}$	= 2.092 k/ft	(lower node of second shell element)
$N_{yb0.50}$	= 0.082 k/ft	(upper node of third shell element)
$N_{yt0.75}$	= 51.259 k/ft	(lower node of third shell element)
$N_{yb0.75}$	= 49.239 k/ft	(upper node of bottom shell element)
N_{y1}	= 100.576 k/ft	(lower node of bottom shell element)

Beam Elements

F_{xt}	= -225.092 k	(axial force in top flange beam element)
M_{yt}	= -3.544 k-ft	(bending moment in top flange beam element)
F_{xb}	= 218.577 k	(axial force in bottom flange beam element)
M_{yb}	= -11.260 k-ft	(bending moment in bottom flange beam element)

Nodal Force Lever Arms from Bottom of Web:

E_{y0}	= 71.75 inches
E_{xt}	= 67.875 inches
$E_{yb/t0.25}$	= 53.8125 inches
$E_{yb/t0.50}$	= 35.875 inches
$E_{yb/t0.75}$	= 17.9375 inches
E_{xb}	= 6.8125 inches
E_{y1}	= 0 inches

Web Element height:

h_e	= 17.9375 inches
-------	------------------

Sum Moments about Bottom of Web:

$$\begin{aligned}
 M_{yt0.50} &= -(N_{y0} \times h_e/2 \times E_{y0} + F_{xt} \times E_{xt} + M_{yt} + (N_{yt0.25} + N_{yb0.25})/2 \times h_e \times E_{yb/t0.25} + \\
 &+ N_{yb0.50})/2 \times h_e \times E_{yb/t0.50} + (N_{yt0.75} + N_{yb0.75})/2 \times h_e \times E_{yb/t0.75} + F_{xb} \times E_{xb} + \\
 &+ N_{y1} \times h_e/2 \times E_{y1}) \\
 M_{yb} &= -(-98.389\text{k/ft} \times (17.9375\text{inches}/2)/(12\text{inches/ft}) \times 71.75\text{inches} + -225.092\text{k} \times \\
 &67.875\text{inches} + -3.544\text{ k-ft} \times 12\text{inches/ft} + (-47.062\text{k/ft} + -49.081\text{k/ft})/2 \times \\
 &17.9375\text{inches}/(12\text{inches/ft}) \times 53.8125\text{inches} + (2.092\text{k/ft} + 0.082\text{k/ft})/2 \times \\
 &17.9375\text{inches}/(12\text{inches/ft}) \times 35.875\text{inches} + (51.259\text{k/ft} + 49.239\text{k/ft})/2 \times \\
 &17.9375\text{inches}/(12\text{inches/ft}) \times 17.9375\text{inches} + 218.577\text{k} \times 6.8125\text{inches} + - \\
 &11.260\text{k-ft} \times 12\text{inches/ft} + 100.576\text{k/ft} \times (17.9375\text{inches}/2)/(12\text{inches/ft}) \times \\
 &0\text{inches}) \\
 &= 21704.05\text{ k-inches} = \mathbf{1808.67\text{ k-ft}}
 \end{aligned}$$

∴ OK, Moment from 3D model is within 1 percent of calculated value using equation. Model is providing reasonable results. (Note: If more elements were used, the difference would be even smaller). The moment from the software's internal numerical integration utility is 1808.53 k-ft.

Furthermore, axial loads are summed to verify there is no net axial force on the section.

Sum Axial Loads:

$$\begin{aligned}
 P &= -(N_{y0} \times h_e/2 + F_{xt} + (N_{yt0.25} + N_{yb0.25})/2 \times h_e + (N_{yt0.50} + N_{yb0.50})/2 \times h_e + (N_{yt0.75} \\
 + N_{yb0.75})/2 \times h_e + F_{xb} + N_{y1} \times h_e/2) \\
 &= -(-98.389\text{k/ft} \times (17.9375\text{inches}/2)/(12\text{inches/ft}) + -225.092\text{k} + (-47.0619\text{k/ft} + - \\
 &\quad 49.0812\text{k/ft})/2 \times 17.9375\text{inches}/(12\text{inches/ft}) + (2.09229\text{k/ft} + 0.0824927\text{k/ft})/2 \\
 &\quad \times 17.9375\text{inches}/(12\text{inches/ft}) + (51.2594\text{k/ft} + 49.2392\text{k/ft})/2 \times \\
 &\quad 17.9375\text{inches}/(12\text{inches/ft}) \times + 218.577\text{k} + 100.576\text{k/ft} \times \\
 &\quad (17.9375\text{inches}/2)/(12\text{inches/ft})) \\
 &= \mathbf{4.88 \text{ k}}
 \end{aligned}$$

∴ OK, Net axial force from 3D is approximately zero. It is expected that due to the 3D nature of the model that this net axial force should be small (for straight bridges), but nonzero. This force arises when behavior of the girders, which do not precisely conform to typical idealized assumptions (where girders act independently), is captured.

Check reactions due to stay-in-place forms. The weight per linear foot of girder for the stay-in-place forms is 0.17 k/ft for the interior girders and 0.086 k/ft for the exterior girders.

$$L = 113.25 \text{ ft}$$

$$R = 2 \times (0.17 \text{ k/ft} + 0.086 \text{ k/ft}) \times 113.25 \text{ ft} = \mathbf{57.984 \text{ k}}$$

Reactions from Model:

Location	Girder Line 1	Girder Line 2	Girder Line 3	Girder Line 4	Total
Left Support	6.003	8.493	8.493	6.003	28.992
Right Support	6.001	8.495	8.495	6.001	28.992
				Total	57.984
∴ OK, model is providing reasonable results					

9.1.3.1.9 Step 1i – Extract Required Results from Analysis Software

After verifying that the results from the analysis are reasonable, the results of interest can be extracted and input into a spreadsheet for further use. The analysis results required are typically moments and shears which are not readily available due to using multiple beam and/or shell elements. The moments can be determined as described in Section 8.2.1 and shown above, by integrating the shell stresses on the cross-section and summing the results. Some FEA software provides a utility that will integrate stresses over a cross-section automatically. Note that at the nodes where the deck is connected the forces will appear to have a discontinuity due to the node also behaving as a shear connector.

9.1.3.2 Step 2 – Create Composite Dead Load Model

Step 2 is a continuation of the model created in Step 1 above. As the girders are made composite and become continuous over piers, the span lengths change from 113 ft-3 inches between centerline of bearings for all three simple spans in the non-composite model to 114 ft-3 inches for Spans 1 and 3 and 115 ft-3 inches between centerline of abutments and piers for Span 2 in the continuous composite model.

9.1.3.2.1 Step 2a – Create Geometry for Girders, Diaphragms, and Deck Slab

Since critical force effects are desired at the tenth-points, nodes should be provided at these locations. As with the PEB model, even though the intermediate diaphragms are 6 inches away from midspan of Spans 1 and 3, modeling them at the tenth-point midspan node should not noticeably affect accuracy of results (Span 1 is shown in Figure 172):

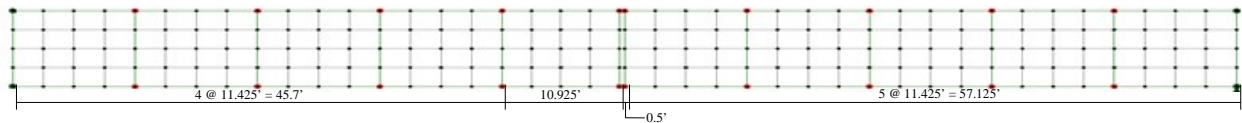


Figure 172. Illustration. Surface definitions for Span 1 of composite model.

The deck slab surface elements are defined using the points along the top edges of the previously defined girder webs. The slab geometry in the 3D finite element analysis is similar to that shown in Section 9.1.2.2.1 for the PEB analysis. Thick shell elements are used to model the deck slab. Elements that do not include through-thickness shear deformation can be used; the decrease in accuracy is not significant.

9.1.3.2.2 Step 2b – Define Cross-Sections for Girders, Diaphragms, and Concrete Deck Slab

The pier diaphragms are 30 inches wide and approximately 7 ft-2¼ inches deep and are connected to the concrete deck slab. The abutment diaphragms are 48 inches wide and approximately 6 ft-6 inches deep and are connected to the concrete deck slab. These diaphragms are connected to the concrete slab locations rather than at the centroid of girders for convenience, as no new nodes or lines are required. The cross-section properties for all diaphragms are shown in Table 26. Similar to Section 9.1.2.2.2, vertical offsets are made as necessary to correctly locate members relative to the centroid of the girder web. The offsets are different than those in the 2D example as components are connected at different points in space (for example, the deck sits at the top of the girder in the 3D model, instead of at the girder centroid).

Table 26. Abutment, intermediate, and pier diaphragm section properties.

Section Property	Abutment	Intermediate	Pier
Cross-section Area (A) (ft ²)	26.00	3.19	17.98
Strong Axis Moment of Inertia (I _{yy}) (ft ⁴)	91.54	3.91	77.49
Weak Axis Moment of Inertia (I _{zz}) (ft ⁴)	34.67	0.19	9.36
Torsion Constant (J _{xx}) (ft ⁴)	85.55	0.64	29.26
Shear Area in y direction (A _{vy}) (ft ²)	21.67	2.66	14.98
Shear Area in z direction (A _{vz}) (ft ²)	21.67	2.66	14.98
Offset in z direction (R _z) (ft)	2.77	2.31	3.14

The concrete deck slab is modeled with the 8 inches design thickness to neglect stiffness contributions of the integral wearing surface. An eccentricity of 0.781 ft, which includes haunches, is applied.

9.1.3.2.3 Step 2c – Define Material Properties for Girders, Diaphragms, and Deck Slabs

The material properties for the 4 ksi concrete used in the deck slab are added in the composite model and are shown in Table 27. The unit weight is modified to account for the ½ inch integral wearing surface that is not included in the deck thickness.

Table 27. Concrete material properties.

Material Property	Slab Concrete (4 ksi)
Modulus of Elasticity (ksf)	524,757
Poisson's Ratio	0.2
Unit Weight (k/ft ³)	0.159
Thermal Expansion Coefficient (ft/ft/°F)	6.0E-6

9.1.3.2.4 Step 2d – Define Support Conditions

The supports conditions used in the 3D composite dead load model are the same as those used in the 2D composite dead load model.

9.1.3.2.5 Step 2e – Define Loads Applied to Composite Structure

The FWS load is defined as a uniform load distributed over the bridge width. The magnitude of the FWS load is reduced from 0.030 ksf to 0.028 ksf to account for the fact that the FWS is being spread over the full bridge width instead of just between barriers.

The weight of the barrier, determined above in Section 9.1.1.1.6, is applied as a uniform line load.

9.1.3.2.6 Step 2f – Define Load Cases for Composite Dead Loads

Define load cases for the future wearing surface and barrier dead loads. Defining separate load cases is important for composite dead loads; in the design process, wearing surface loads and component dead loads have different load factors.

9.1.3.2.7 Step 2g – Ensure Correct Attributes Are Assigned to Components

The attributes assigned to each of the different components as shown below:

- Girders
 - Web
 - Thick shell surface elements
 - Geometric surface cross-section
 - Concrete material properties, in this example, $f'_c = 8$ ksi

- Flanges
 - Thick beam elements
 - Flange cross-section properties
 - Concrete material properties, in this example, $f'_c = 8$ ksi
- Abutment, Intermediate, and Pier Diaphragms
 - Thick beam elements
 - Geometric cross-section properties
 - Concrete material properties, in this example, $f'_c = 3.5$ ksi
- Concrete Deck Slab
 - Thick shell surface elements
 - Geometric surface cross-section
 - Concrete material properties, in this example, $f'_c = 4$ ksi
 - FWS and barrier loading

9.1.3.2.8 Step 2h – Run Analysis and Verify Results Using Simplified Methods

The next step is to run the analysis. The analysis results can be verified using a variety of simplified methods. For continuous span bridges, moments and reactions can be calculated using textbook equations for uniform loads. Additionally, for uniform loads applied to the entire structure, the total applied load applied can be calculated and should equal the sum of the reactions from the analysis model.

Check reactions for FWS load versus applied load:

Weight of FWS = 0.028 ksf

Area over which FWS applied = 43 ft-4½ inches × 343 ft-9 inches = 14910.16 ft²

Total Weight of FWS = 0.028 ksf × 14910.16 ft² = 417.48 k

Reactions from Model:

Location	Line 1 (B1-B5-B9)	Line 2 (B2-B6-B10)	Line 3 (B3-B7-B11)	Line 4 (B4-B8-B12)	Total
Abutment 1	12.744	14.976	14.976	12.744	55.440
Pier 1	32.850	43.800	43.800	32.850	153.300
Pier 2	32.849	43.799	43.805	32.847	153.300
Abutment 2	12.744	14.976	14.976	12.744	55.441
				Total	417.481

The calculated total applied load is equal to the sum of the reactions from the model. Additionally, the reactions are approximately symmetric as expected.

The next check of the results will be verifying the moment at the four-tenths point of Span 1 due to the FWS loading. Determining the moment by hand from the 3D analysis model is more involved due to using beam and shell elements. Shown in Figure 173, are the required element nodal forces in the assumed effective width of the concrete deck slab for the exterior girder. The total force in the deck slab is determined and shown in Figure 174. The shell element nodal

“forces,” indicated as N_x and N_y in Figures 173 and 174, are equal to the stress at the node multiplied by the element thickness. A sample moment calculation is shown below Figure 174.

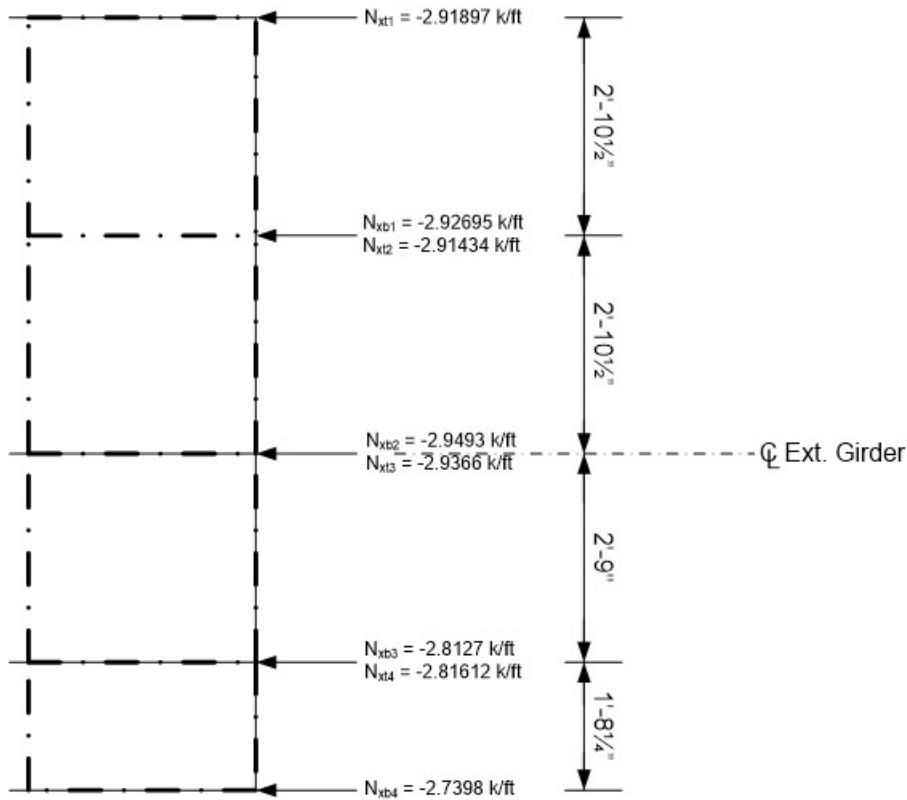


Figure 173. Illustration. Deck slab element forces in composite concrete girder.

Unaveraged Element Nodal Force/Length (from analysis software):

Shell Elements:

N_{xt1}	=	-2.919 k/ft	(upper node of top shell element)
N_{xb1}	=	-2.927 k/ft	(lower node of top shell element)
N_{xt2}	=	-2.914 k/ft	(upper node of second shell element)
N_{xb2}	=	-2.950 k/ft	(lower node of second shell element)
N_{xt3}	=	-2.937 k/ft	(upper node of third shell element)
N_{xb3}	=	-2.813 k/ft	(lower node of third shell element)
N_{xt4}	=	-2.816 k/ft	(upper node of bottom shell element)
N_{xb4}	=	-2.740 k/ft	(lower node of bottom shell element)

Element Width

W_{xt1}	=	1 ft-5 1/4 inches	(1/2 of 2 ft-10 1/2 inches)
$W_{xb1,xt2}$	=	2 ft-10 1/2 inches	
$W_{xb2,xt3}$	=	2 ft-9 3/4 inches	[1/2 of (2 ft-10 1/2 inches + 2 ft-9 inches)]
$W_{xb3,xt4}$	=	2 ft-2 5/8 inches	[1/2 of (2 ft-9 inches + 1 ft-8 1/4 inches)]
W_{xb4}	=	0 ft-10 1/8 inches	(1/2 of 1 ft-8 1/4 inches)

Element Nodal Forces

$$\begin{aligned}
 F_{xt1} &= N_{xt1} \times W_{xt1} = -2.919 \text{ k/ft} \times 1 \text{ ft}-5\frac{1}{4} \text{ inches} = -4.20 \text{ k} \\
 F_{xb1/t2} &= (N_{xb1} + N_{xt2})/2 \times W_{xb1/t2} = (-2.927\text{k/ft} + -2.914\text{k/ft})/2 \times 2 \text{ ft}-10\frac{1}{2} \\
 &\text{inches} \\
 &= -8.40 \text{ k} \\
 F_{xb2/t3} &= (N_{xb2} + N_{xt3})/2 \times W_{xb2/t3} = (-2.950\text{k/ft} + -2.937\text{k/ft})/2 \times 2 \text{ ft}-9\frac{3}{4} \\
 \text{inches} &= -8.28 \text{ k} \\
 F_{xb3/t4} &= (N_{xb3} + N_{xt4})/2 \times W_{xb3/t4} = (-2.813\text{k/ft} + -2.816\text{k/ft})/2 \times 2 \text{ ft}-2\frac{5}{8} \\
 \text{inches} &= -6.25 \text{ k} \\
 F_{xb4} &= N_{xb4} \times W_{xb4} = -2.740 \text{ k/ft} \times 0 \text{ ft}-10\frac{1}{8} \text{ inches} \\
 &= -2.31 \text{ k}
 \end{aligned}$$

Total Force Applied at Deck Slab Centroid = -29.41 k

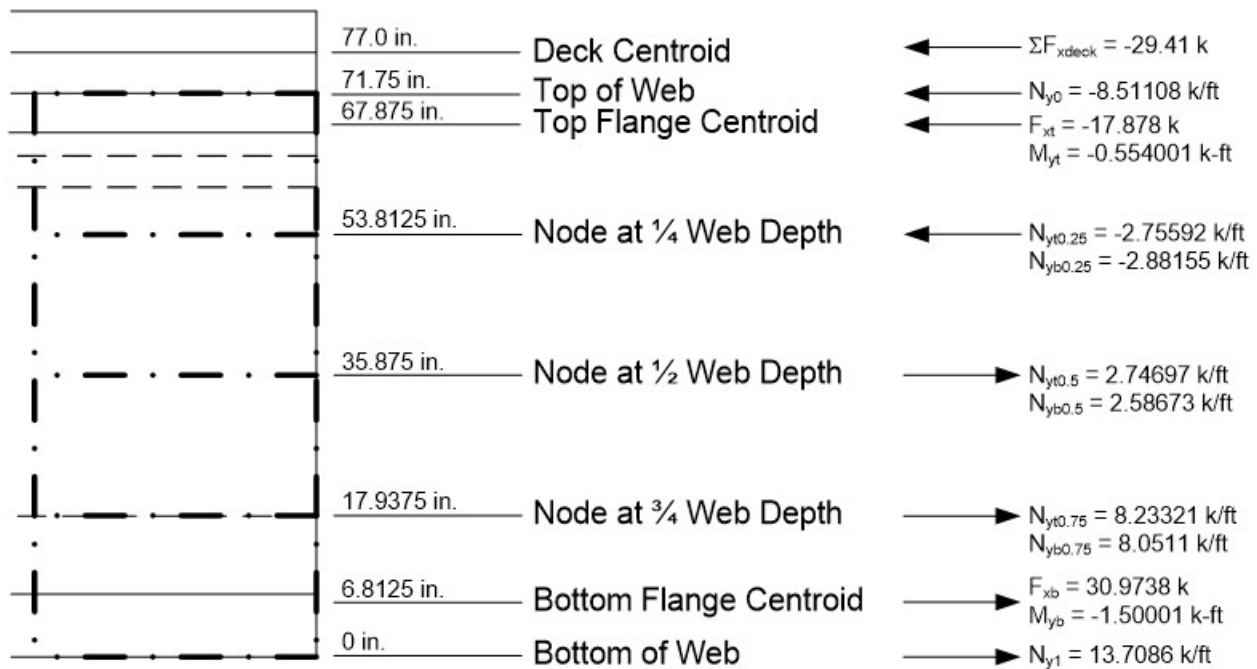


Figure 174. Illustration. Element force effects in composite concrete girder.

Nodal Forces (from analysis software):

Shell Elements (4 Elements through web depth):

N_{y0}	=	-8.511 k/ft	(upper node of top shell element)
$N_{yt0.25}$	=	-2.756 k/ft	(lower node of top shell element)
$N_{yb0.25}$	=	-2.882 k/ft	(upper node of second shell element)
$N_{yt0.50}$	=	2.747 k/ft	(lower node of second shell element)
$N_{yb0.50}$	=	2.587 k/ft	(upper node of third shell element)
$N_{yt0.75}$	=	8.233 k/ft	(lower node of third shell element)
$N_{yb0.75}$	=	8.051 k/ft	(upper node of bottom shell element)
N_{y1}	=	13.709 k/ft	(lower node of bottom shell element)

Beam Elements

$$\begin{aligned}
 F_{xt} &= -17.878 \text{ k} && \text{(axial force in top flange beam element)} \\
 M_{yt} &= -0.554 \text{ k-ft} && \text{(bending moment in top flange beam element)} \\
 F_{xb} &= 30.974 \text{ k} && \text{(axial force in bottom flange beam element)} \\
 M_{yb} &= -1.500 \text{ k-ft} && \text{(bending moment in bottom flange beam element)}
 \end{aligned}$$

Force in Deck Slab Elements

$$\Sigma F_{x\text{deck}} = -29.41 \text{ k}$$

Nodal Force Lever Arms from Centroid of Deck Slab:

$$\begin{aligned}
 E_{\text{Deck}} &= 0 \text{ inches} \\
 E_{y0} &= 5.25 \text{ inches} \\
 E_{xt} &= 9.125 \text{ inches} \\
 E_{yb/t0.25} &= 23.1875 \text{ inches} \\
 E_{yb/t0.50} &= 41.125 \text{ inches} \\
 E_{yb/t0.75} &= 59.0625 \text{ inches} \\
 E_{xb} &= 70.125 \text{ inches} \\
 E_{y1} &= 77 \text{ inches}
 \end{aligned}$$

Element height:

$$h_e = 17.9375 \text{ inches}$$

Sum Moments about Deck Slab Centroid:

$$\begin{aligned}
 M &= \Sigma F_{x\text{deck}} \times E_{\text{deck}} + N_{y0} \times h_e/2 \times E_{y0} + F_{xt} \times E_{xt} + M_{yt} + (N_{yt0.25} + N_{yb0.25})/2 \\
 \times & h_e \times E_{yb/t0.25} + (N_{yt0.50} + N_{yb0.50})/2 \times h_e \times E_{yb/t0.50} + (N_{yt0.75} + N_{yb0.75})/2 \times \\
 h_e & \times E_{yb/t0.75} + F_{xb} \times E_{xb} + M_{yb} + N_{y1} \times h_e/2 \times E_{y1} \\
 &= -29.41\text{k} \times 0\text{inches} + -8.51108\text{k/ft} \times (17.9375\text{inches}/2)/(12\text{inches/ft}) \times \\
 & 5.25\text{inches} + -17.878\text{k} \times 9.125\text{inches} + -0.554001 \text{ k-ft} \times 12\text{inches/ft} + (- \\
 & 2.75592\text{k/ft} + -2.88155\text{k/ft})/2 \times 17.9375\text{inches}/(12\text{inches/ft}) \times \\
 & 23.1875\text{inches} + (2.74697\text{k/ft} + 2.58673\text{k/ft})/2 \times 17.9375 \\
 & \text{inches}/(12\text{inches/ft}) \times 41.125\text{inches} + (8.23321\text{k/ft} + 8.0511\text{k/ft})/2 \times \\
 & 17.9375\text{inches}/(12\text{inches/ft}) \times 59.0625\text{inches} + 30.9738\text{k} \times 70.125\text{inches} \\
 & + -1.50001\text{k-ft} \times 12\text{inches/ft} + 13.7086\text{k/ft} \times \\
 & (17.9375\text{inches}/2)/(12\text{inches/ft}) \times 77\text{inches} \\
 &= 3524.86 \text{ k-inches} = \mathbf{293.74 \text{ k-ft}}
 \end{aligned}$$

Simple Calculation (assume that all three spans are of equal length)

$$M_{\text{max}} = 0.08wL^2 \text{ (see case 39 of AISC Manual of Steel Construction, 13}^{\text{th}} \text{ Edition)}$$

$$W = 0.255 \text{ k/ft} = 0.030 \text{ ksf} [(11 \text{ ft}-6 \text{ inches})/2 + 4 \text{ ft}-5\frac{1}{4} \text{ inches} - 1 \text{ ft}-8\frac{1}{4} \text{ inches}]$$

$$L = 114 \text{ ft}-7 \text{ inches} = [(114 \text{ ft}-3 \text{ inches} + 115 \text{ ft}-3 \text{ inches} + 114 \text{ ft}-3 \text{ inches})/3] \text{ (average span length)}$$

$$\begin{aligned}
 M_{\text{max}} &= 0.08 \times 0.255 \text{ k/ft} \times (114 \text{ ft}-7 \text{ inches})^2 \\
 &= \mathbf{267.84 \text{ k-ft}}
 \end{aligned}$$

∴ OK, Moment from 3D model is within 9 percent of value calculated using equation assuming equal span lengths. When a similar process is followed for an interior girder, the result from the analysis software and AISC equations are 327.09 k-ft and 362.37 k-ft, respectively. Therefore, considering the total moment between an interior and exterior girder, the difference is approximately 1.5 percent. This suggests better load sharing is occurring between girders than assumed by the equation and that the model is providing reasonable results.

Furthermore, axial loads are summed to verify there is no net axial force on the section.

Sum Axial Forces:

$$\begin{aligned}
 P &= \Sigma F_{x\text{deck}} + N_{y0} \times h_e/2 + F_{xt} + (N_{yt0.25} + N_{yb0.25})/2 \times h_e + (N_{yt0.50} + \\
 N_{yb0.50})/2 &\quad \times h_e + (N_{yt0.75} + N_{yb0.75})/2 \times h_e + F_{xb} + N_{y1} \times h_e/2 \\
 &= -29.41\text{k} + -8.511\text{k/ft} \times (17.9375\text{in}/2)/(12\text{in/ft}) + -17.878\text{k} + (-2.756\text{k/ft} + \\
 &\quad -2.882\text{k/ft})/2 \times 17.9375\text{inches}/(12\text{inches/ft}) + (2.747\text{k/ft} + 2.587\text{k/ft})/2 \times \\
 &\quad 17.9375\text{inches}/(12\text{inches/ft}) + (8.233\text{k/ft} + 8.051\text{k/ft})/2 \times \\
 &\quad 17.9375\text{inches}/(12\text{inches/ft}) + 30.974\text{k} + 13.709\text{k/ft} \times \\
 &\quad (17.9375\text{inches}/2)/(12\text{inches/ft}) \\
 &= \mathbf{-0.486\text{ k}}
 \end{aligned}$$

∴ OK, Net axial force from 3D is approximately zero. It is expected that due to the 3D nature of the model that this net axial force should be small (for straight bridges), but nonzero. This force arises when behavior of the girders, which do not precisely conform to typical idealized assumptions (where girders act independently), is captured.

9.1.3.2.9 Step 2i – Extract Analysis Results

After verifying that the results from the analysis are reasonable, the results of interest can be extracted and input into a spreadsheet for further analysis or used within the analysis and design software. Refer to Section 9.1.3.1.9 for further discussion.

At this point, depending on the Owner’s policy, it may be necessary to repeat Steps 2 and 3 for a simply supported girder bridge. This step was taken in this example. All the steps illustrated above remain the same, except that only a single span is analyzed. The continuous and simple span results were then enveloped.

9.1.3.3 Step 3 – Create Composite Live Load Model

This model uses the same geometry as the model created in Step 2. The deck slab thickness in this model should be equal to the design thickness of 8 inches.

9.1.3.3.1 Step 3a – Determine Optimized Live Load

In this example, critical moments at tenth-points along all spans for the interior and exterior girders (both positive and negative) about the transverse axis of the bridge are determined. Some FEA software has utilities that aid in the generation of influence surfaces and optimized loadings. In the absence of such utilities, influence lines/surfaces can be generated using

classical analysis methods. It is always a good idea to at least spot check the optimized loadings to make sure that they are reasonable. If the optimized loadings are reasonable, the analysis can then be run.

Once the optimized loading for each location is found, a check of the critical loadings should be performed to verify that the loadings are reasonable and make sense. As an example, the lane (Figure 175) and truck (Figure 176) loadings shown below were obtained for the maximum positive moment in an exterior girder at Pier 1 in this example. Loading Span 3 is exactly what would be expected if one was trying to maximize the positive moment at Pier 1.

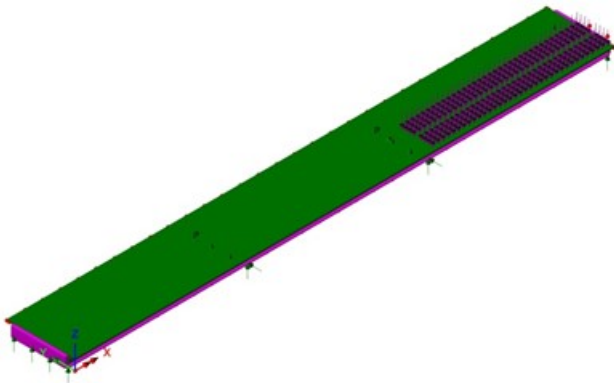


Figure 175. Illustration. Critical lane loading.

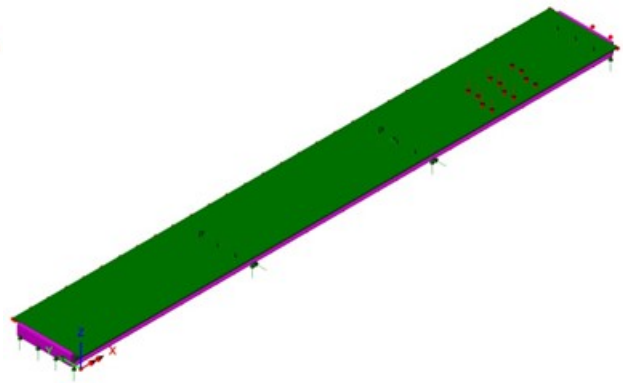


Figure 176. Illustration. Critical truck loading.

9.1.3.3.2 Step 3b – Run Analysis and Verify Results using Simplified Methods

After the optimized loadings for each location have been determined, the analysis can be performed. The results can be verified using simplified methods. As an example, the results are verified by summing the reactions and comparing to the total applied load for the loading shown in Figure 176. Two HL-93 Design Trucks are applied in this model, each truck weighs 72 k resulting in a total applied load of 144 k.

Reactions from Model:

Location	Line 1 (B1-B5-B9)	Line 2 (B2-B6-B10)	Line 3 (B3-B7-B11)	Line 4 (B4-B8-B12)	Total
Abutment 1	0.218	0.647	1.018	1.519	3.40
Pier 1	-0.627	-4.200	-7.010	-8.875	-20.71
Pier 2	-0.648	21.777	43.410	49.917	114.46
Abutment 2	0.136	8.650	14.903	23.167	46.86
				Total	144.0

The total applied load and the sum of the reactions are equal. The reactions along girder line 4 are greater than those along the other girder lines; this is expected since this load case was to determine the maximum moment in the exterior girder. The reactions are not expected to be

symmetric as the loading is not symmetric. The model appears to be providing reasonable results.

An additional check is made for the maximum positive moment in the first span. Because the maximum positive moment will occur in the simply supported case the span will be fully loaded with lane load. The truck will be placed such that the centroid of the load group is the same distance from one support as one of the loads is from the other. By inspection the design truck will control over the design tandem. The maximum moment for a simply supported beam with a 113.25 ft span is determined as follows:

Reaction at support 1:

$$R_1 = [(32 \text{ k})(113.25 \text{ ft} - 44.96 \text{ ft}) + (32 \text{ k})(113.25 \text{ ft} - 58.96 \text{ ft}) + (8 \text{ k})(113.25 \text{ ft} - 72.96 \text{ ft})] / (113.25 \text{ ft}) = 37.48 \text{ k}$$

$$M_{\text{max, truck/lane}} = (37.48 \text{ k})(44.96 \text{ ft}) + (5.48 \text{ k})(14 \text{ ft}) = 1761.82 \text{ k-ft/lane}$$

$$M_{\text{lane/lane}} = (0.64 \text{ k/ft})(58.96 \text{ ft})(113.25 \text{ ft} - 58.96 \text{ ft}) / 2 = 1024.30 \text{ k-ft/lane}$$

$$M_{\text{HL-93}} = (1761.82 \text{ k-ft/lane})(1.33) + (1024.30 \text{ k-ft/lane}) = 3367.71 \text{ k-ft/lane}$$

Using distribution factors for an interior girder from Section 9.1.1.2.1:

$$M_{\text{LL}} = (3367.71 \text{ k-ft/lane})(0.91 \text{ lanes}) = \mathbf{3064.62 \text{ k-ft}}$$

From the analysis, the maximum positive live moment was determined to be **2367.89 k-ft**. This is within 1 percent of the value from the 1D model, but 29 percent in the 3D model. The difference is accounted for by the fact that the distribution factors are a conservative estimate of how many design lanes each girder will receive. This level of conservatism demonstrates the advantage of refined analysis for design.

9.1.3.3.3 Step 3c – Extract Required Results from Analysis Model

After verifying that the results from the analysis are reasonable, the results of interest can be extracted and input into a spreadsheet for further analysis or used within the analysis and design software. Refer to Section 9.1.3.1.9 for further discussion. Similar to Section 9.1.3.2.9 the continuous and simple span results were enveloped.

9.1.3.4 Step 4 – Combine Analysis Results

Once the results of interest, in this case moments, shears, and deflections, have been extracted from the analysis software, they are combined into groups of non-composite dead loads, composite dead loads, and live loads.

Similar to Section 9.1.2.4 moment, shear, and deflection diagrams from the 3D finite element analysis are shown in Figures 177 through 182.

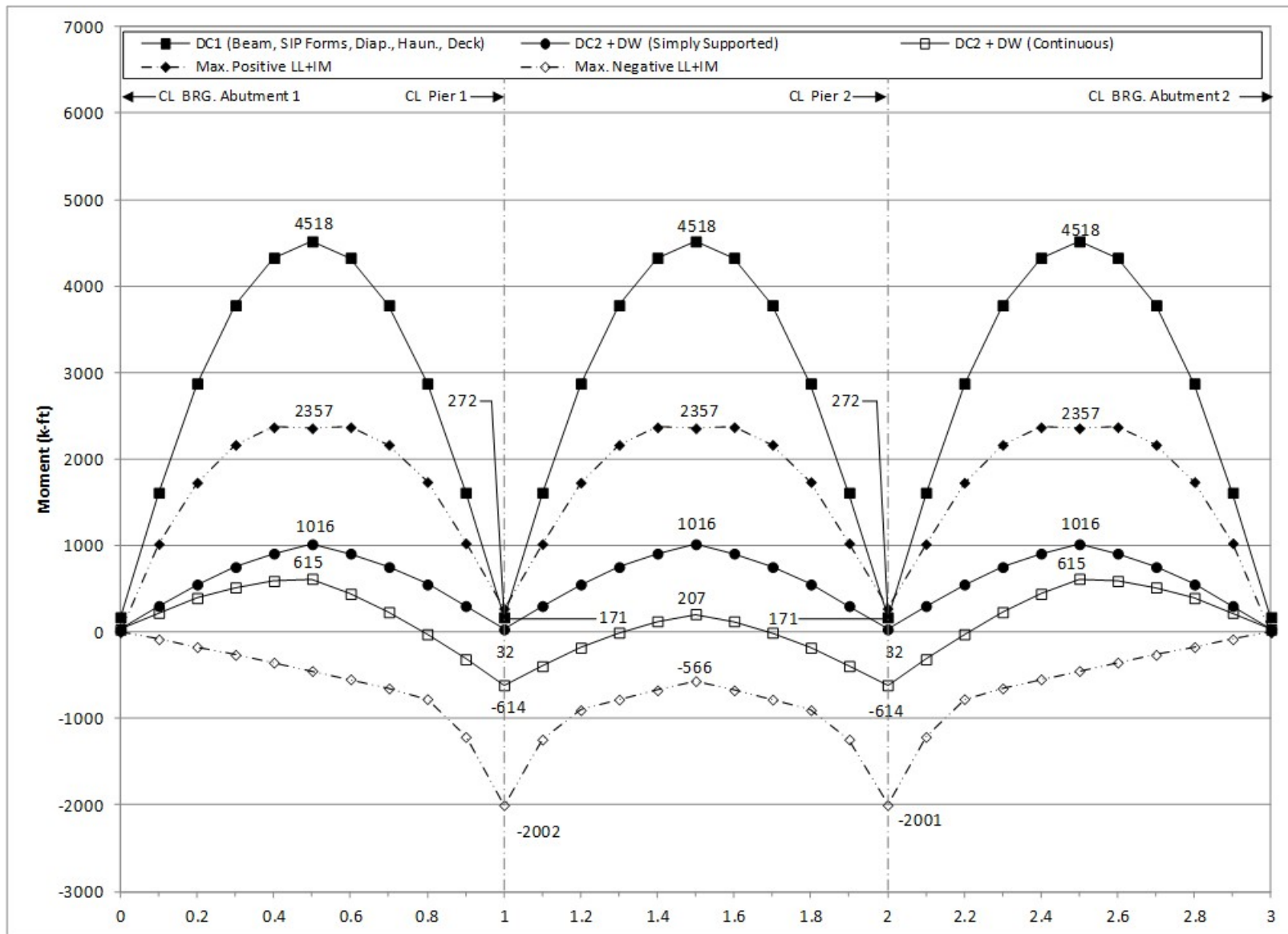


Figure 177. Graph. 3D moment diagram and live load envelope for interior girder.

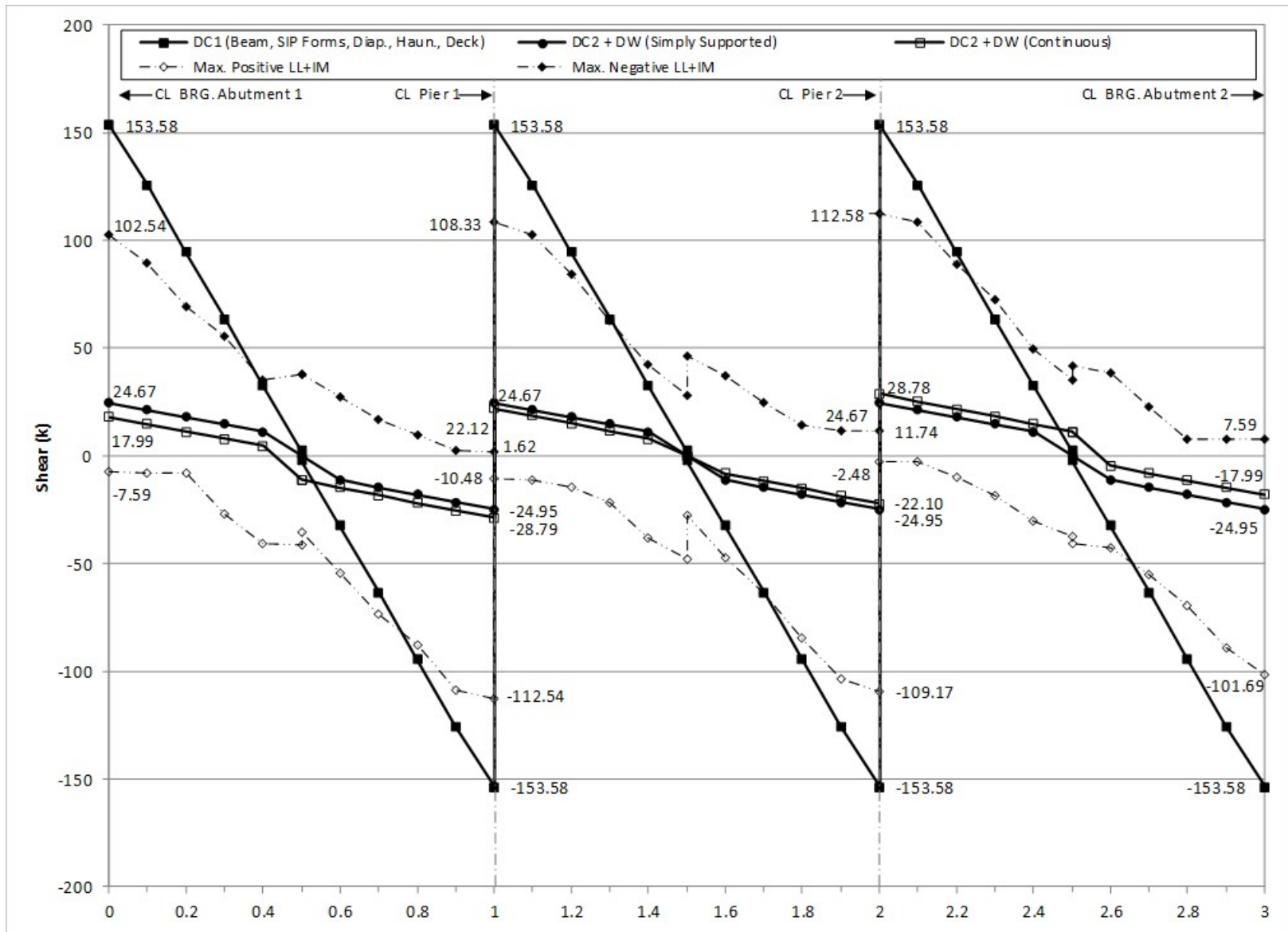


Figure 178. Graph. 3D shear diagram and live load envelope for interior girder.

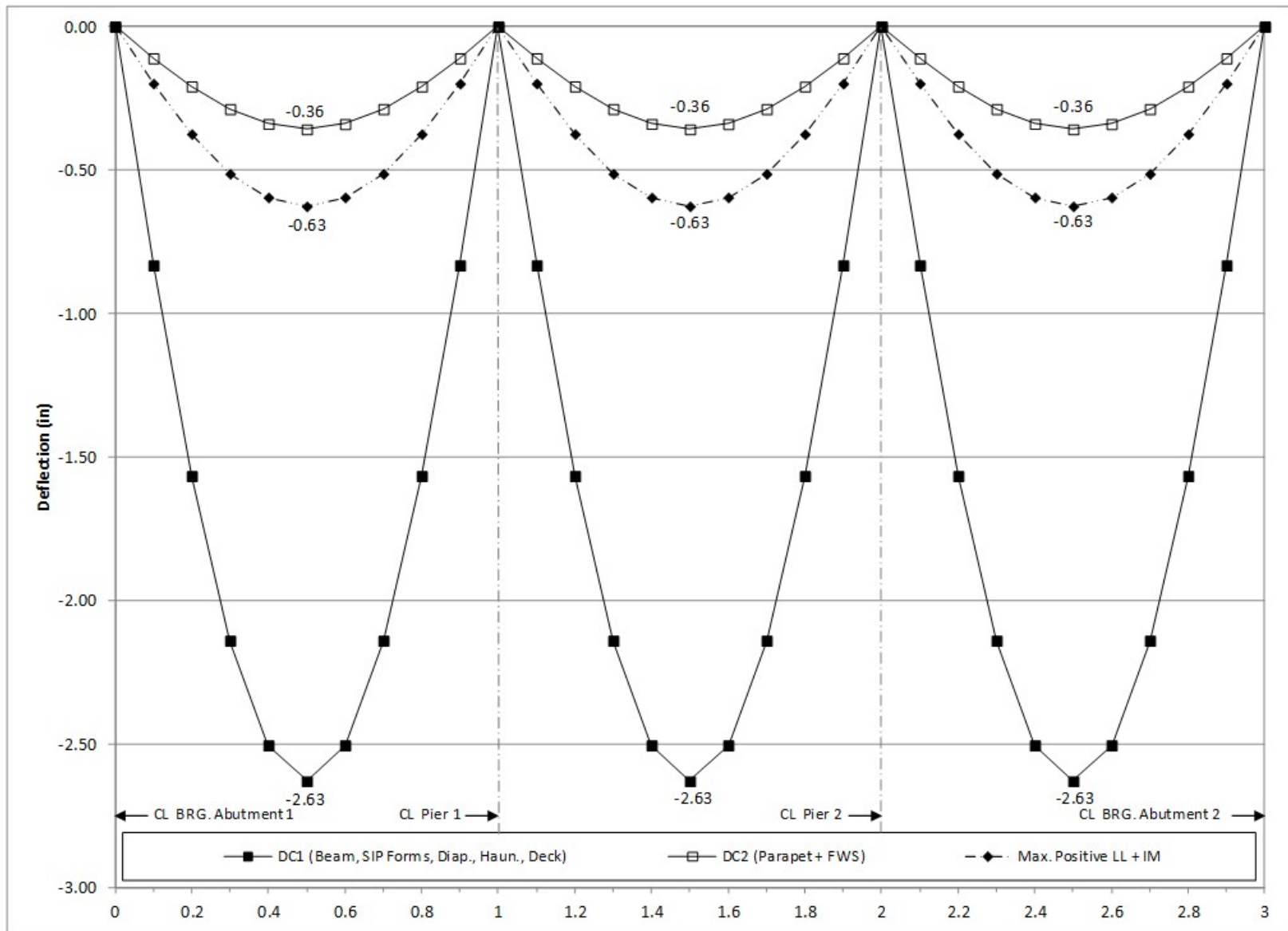


Figure 179. Graph. 3D deflection diagram for interior girder.

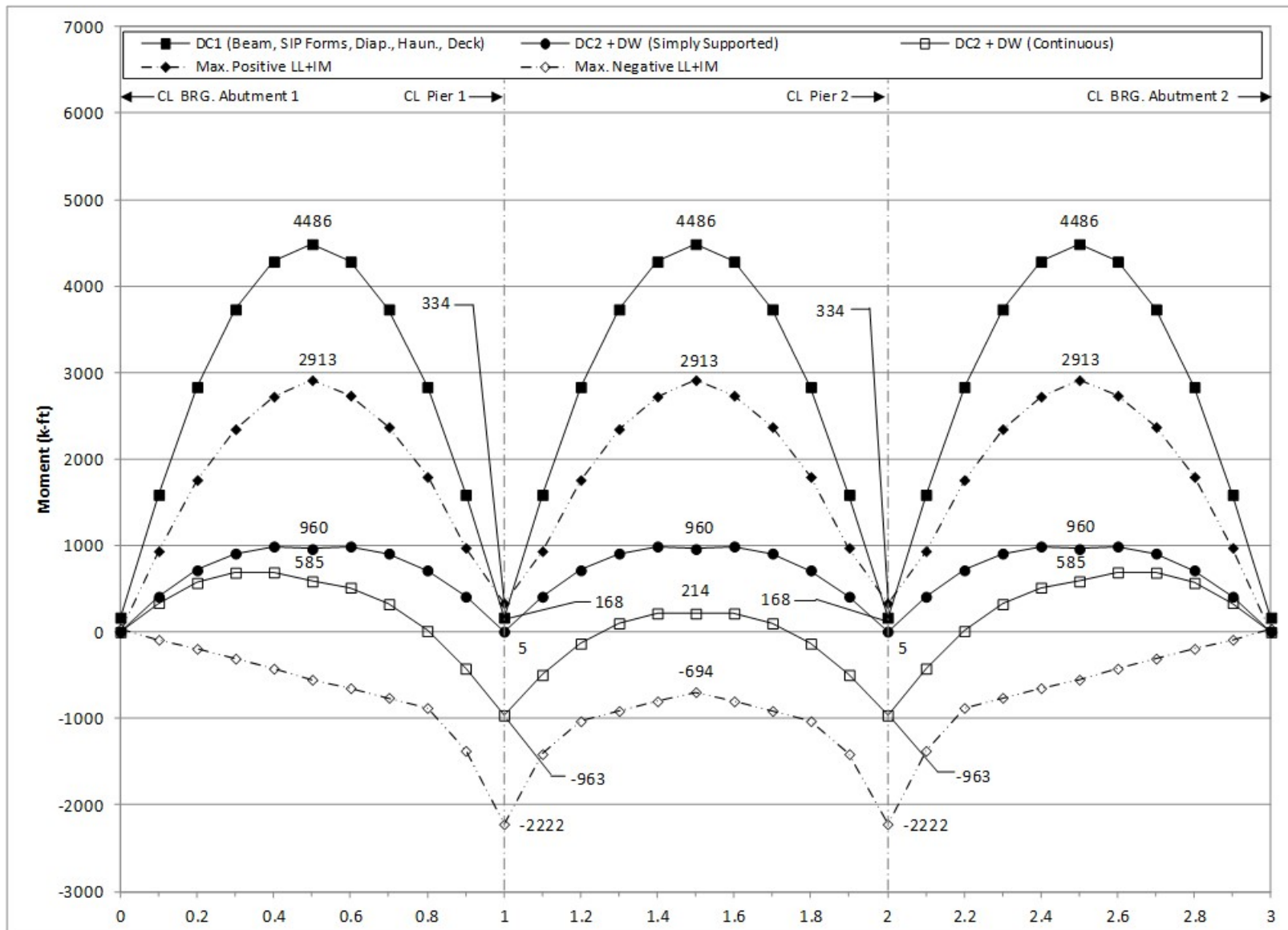


Figure 180. Graph. 3D moment diagram and live load envelope for exterior girder.

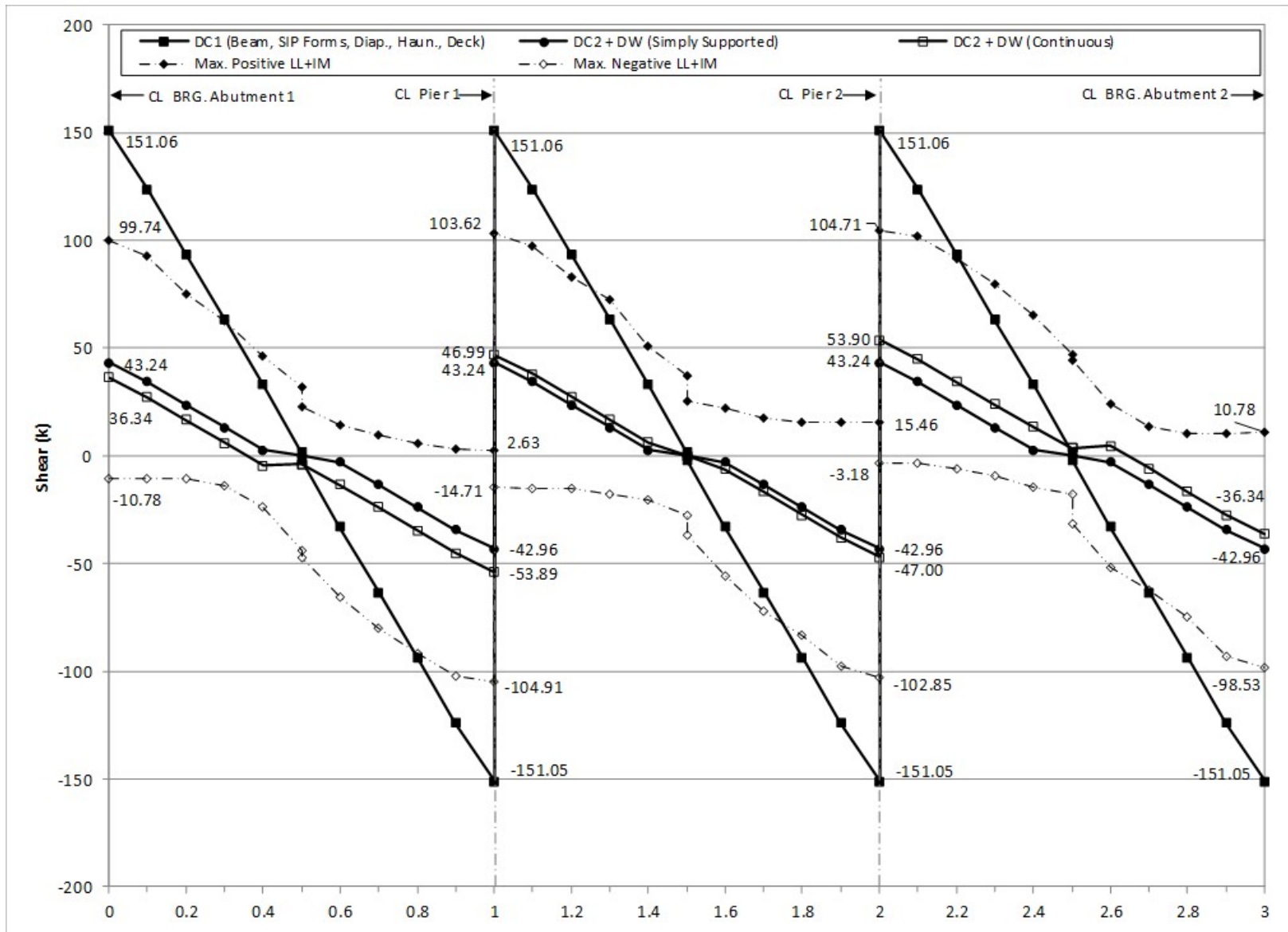


Figure 181. Graph. 3D shear diagram and live load envelope for exterior girder.

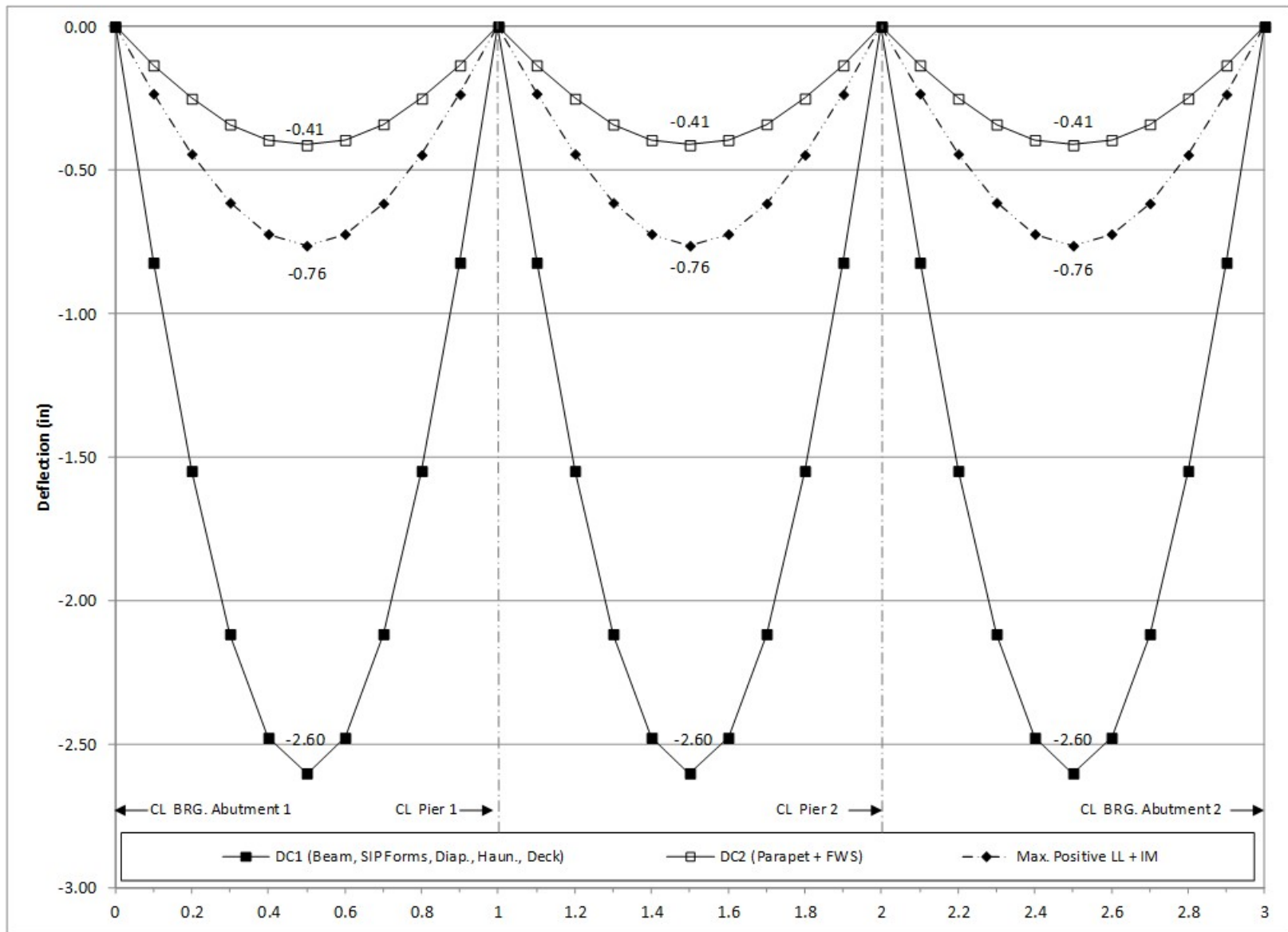


Figure 182. Graph. 3D deflection diagram for exterior girder.

9.1.4 Comparison of 1D, 2D, and 3D Analysis Results

The results from the 1D, 2D, and 3D analyses are compared in the following sections for both the interior and exterior girders. The 3D analysis is expected to provide the most accurate results.

9.1.4.1 Interior Girder

9.1.4.1.1 Moment

The moment results are compared in Figure 183. The figure shows that the 1D non-composite dead load moments are within 2 percent of the 3D non-composite dead load moments. The 1D composite dead load moments are typically from 5-25 percent greater than 3D composite dead load moments. The 1D live load moments are typically between 10-40 percent greater than the 3D live load moments.

The 2D non-composite dead load moments are within 2 percent of the 3D non-composite dead load moments. The 2D composite dead load and live load moments are typically less than 5 percent, but up to 10 percent greater than the 3D composite dead load moments.

The 1D non-composite dead load moments are very nearly equal to corresponding 2D moments. 1D composite dead load moments are typically 5-20 percent greater than 2D composite dead load moments. The 1D live load moments are typically 20-50 percent greater than 2D live load moments.

Figure 184 compares the factored Strength I moments from the 1D, 2D, and 3D models. The 1D model typically provides conservative design force effects when compared to the 2D and 3D models.

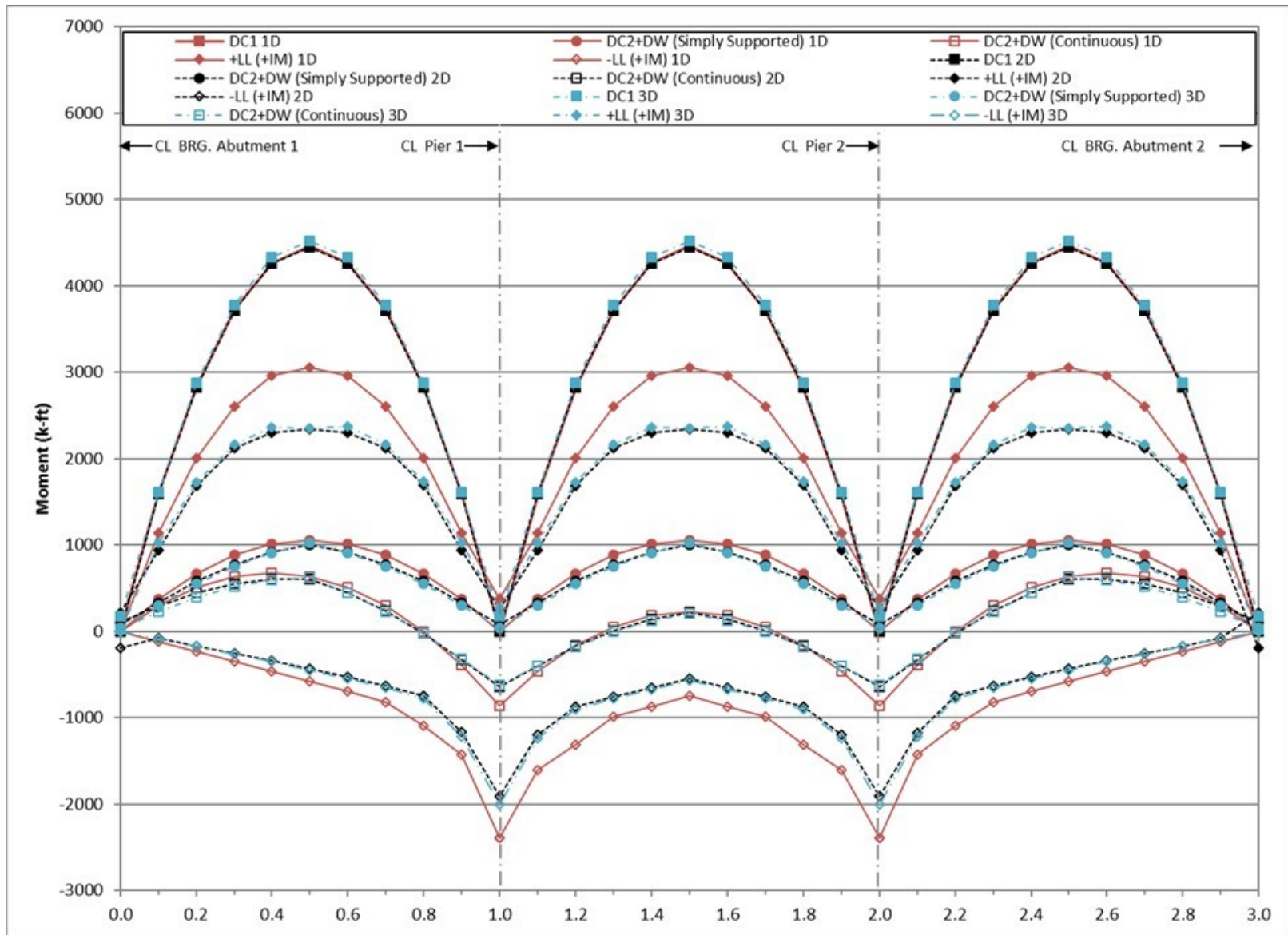


Figure 183. Graph. Comparison of moments for interior P/S concrete girder.

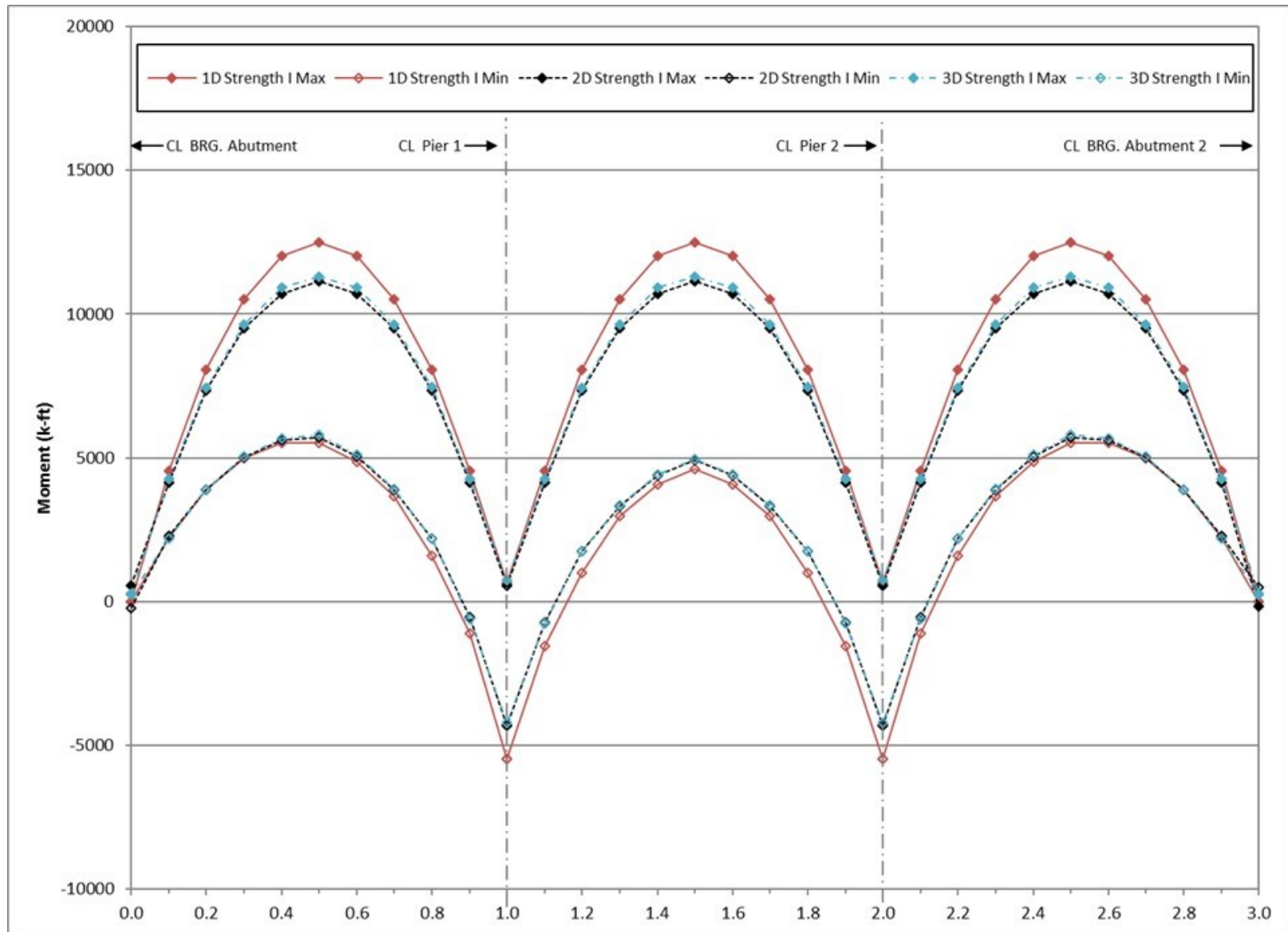


Figure 184. Graph. Comparison of factored moments for interior P/S concrete girder.

9.1.4.1.2 Shear

A comparison of shears is shown in Figure 185. With the exception of values near midspan, the 1D non-composite dead load shears are within 2 percent of the 3D shears. Due to the relatively small magnitude, the 1D composite dead load shears are different by 0-50 percent as compared to corresponding 3D values. The 1D live load shears are mostly within 25-30 percent of the 3D values, but vary inconsistently along the span.

The 2D dead load non-composite shears are mostly within 1 percent, but up to 5 percent smaller than 3D shears. Composite dead load shears are typically 10 percent smaller in the 2D case. The 2D live load shears are typically smaller than those from the 3D analysis, but vary significantly in magnitude along the span.

1D and 2D non-composite dead load shears are mostly within 2 percent but are approximately 6 percent greater in the 1D case at supports. Composite dead load shears are typically higher in 1D analysis, particularly at supports where they are 60-75 percent larger. The ratio of live load shears varies inconsistently along the span, but the 2D results are consistently enveloped by those from 1D analysis.

Figure 186 compares the factored Strength I shears for the 1D, 2D, and 3D models. Similar to the moments, the 1D model provides more conservative design forces when compared to the 2D and 3D models.

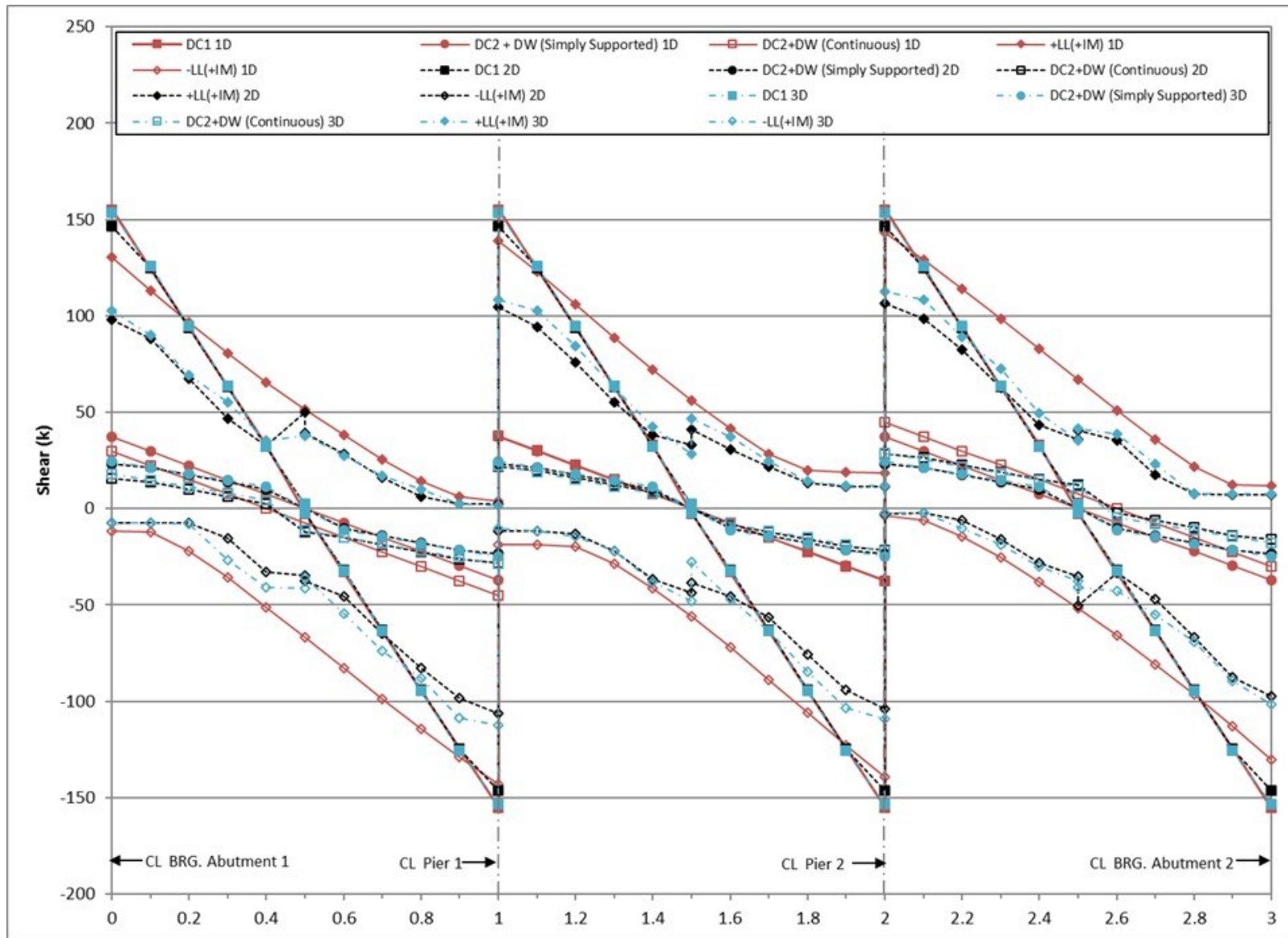


Figure 185. Graph. Comparison of shears for interior P/S concrete girder.

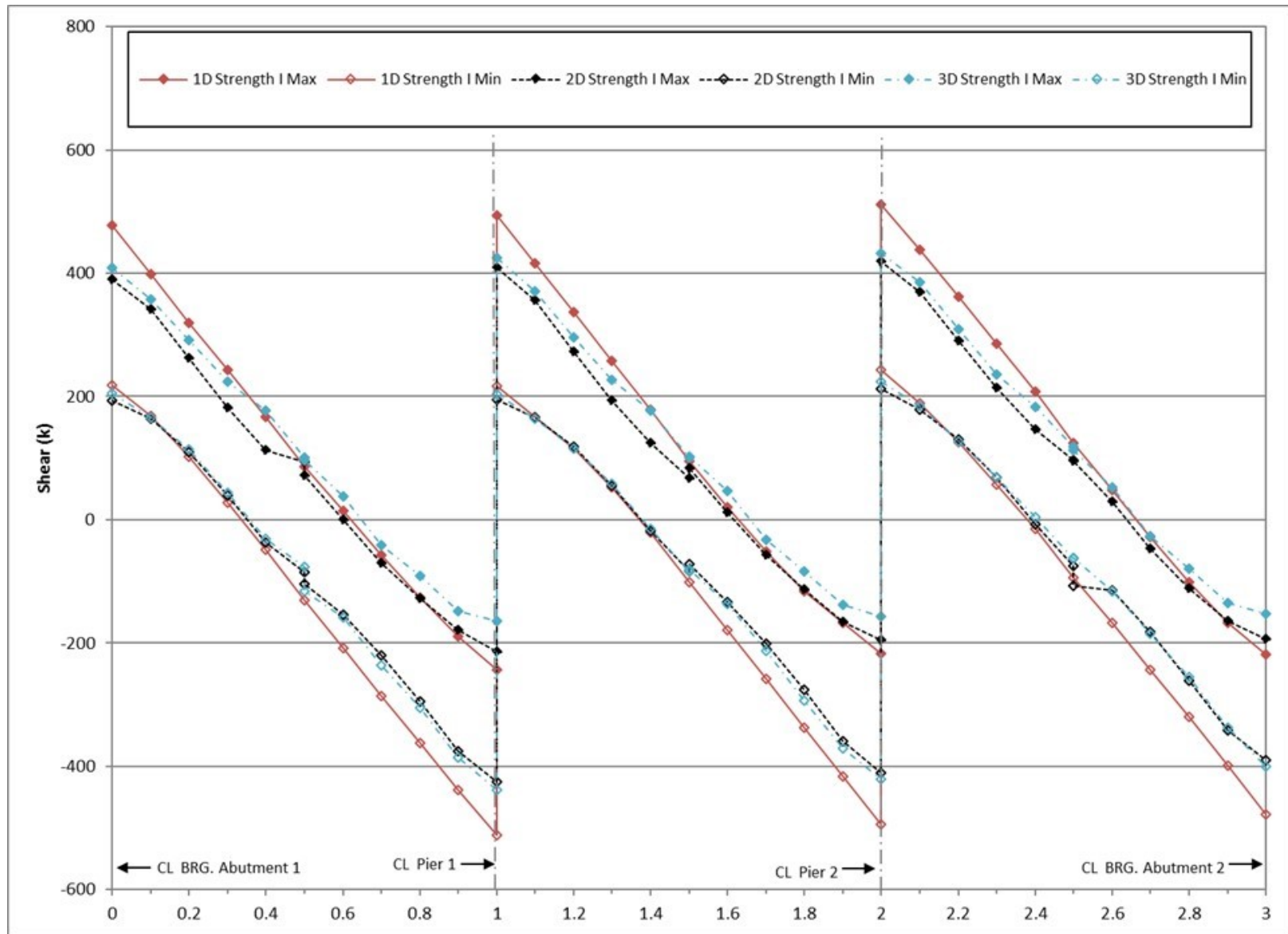


Figure 186. Graph. Comparison of factored shears for interior P/S concrete girder.

9.1.4.1.3 Deflection

A comparison of deflections is shown in Figure 187. The 1D non-composite dead load deflections are within 2 percent of the 3D non-composite dead load deflections. The 1D composite dead load deflections are typically 20-22 percent greater than those from the 3D analysis. The 1D live load deflections are typically 10 percent higher than the live load deflections from the 3D analysis.

The 2D dead load (both non-composite and composite) deflections are 2-5 percent higher than the 3D deflections. The live load deflections are generally 2 percent smaller than the 3D deflections.

1D non-composite dead load deflections are typically 4 percent smaller than 2D deflections, while composite dead load deflections are 15-17 percent greater. 1D live load deflections are 12-14 percent greater than those from the 2D analysis.

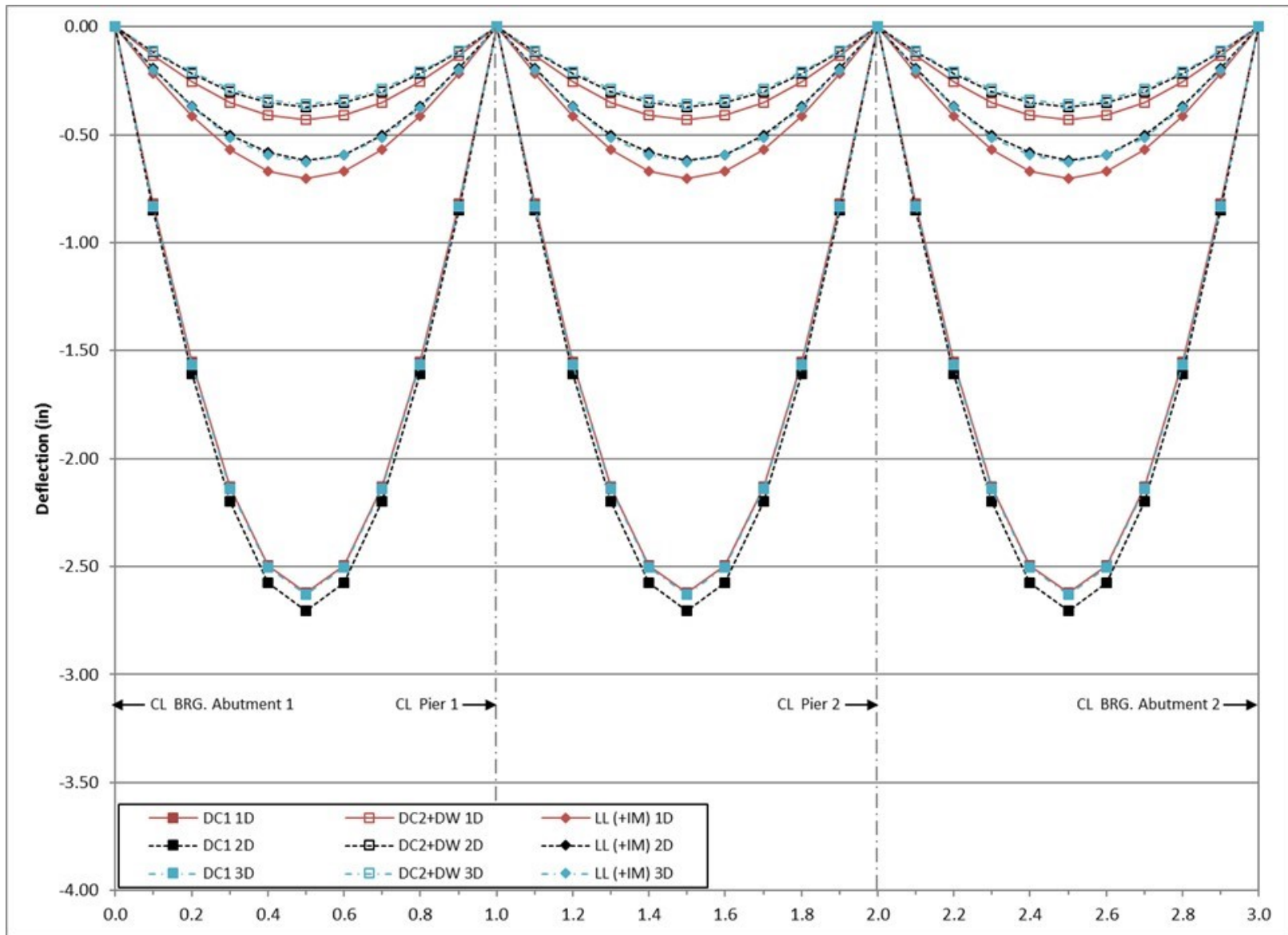


Figure 187. Graph. Comparison of deflections for interior P/S concrete girder.

9.1.4.2 Exterior Girder

9.1.4.2.1 Moment

Moments are compared in Figure 188. The non-composite dead load moments from the 1D analysis are approximately 3-5 percent less than the non-composite dead load moments from the 3D analysis. The 1D composite dead load moments are between 5-20 percent lower than the composite dead load moments from the 3D analysis. Similarly to the interior girder, the 1D live load moments are typically 10-40 percent greater than those from the 3D analysis.

The non-composite dead load moments are about 2 percent lower for the 2D analysis than the 3D analysis. The composite dead load moments from the 2D analysis are typically within 5 percent, but up to 10 percent smaller than 3D moments. The 2D positive live load moment is typically 5 percent less than the 3D positive live load moment while the 2D negative live load moment is typically 5-10 percent higher than the 3D negative live load moment.

1D non-composite dead load moments are within 3 percent of the 2D moments. Composite dead load moments from the 1D analysis are typically 15-20 percent lower than 2D composite dead load moments. Live load moments from 1D analysis are typically 20-50 percent greater than 2D live load moments.

Figure 189 compares the factored Strength I moments from the 1D, 2D, and 3D models. The 1D model typically provides conservative design force effects when compared to the 2D and 3D models.

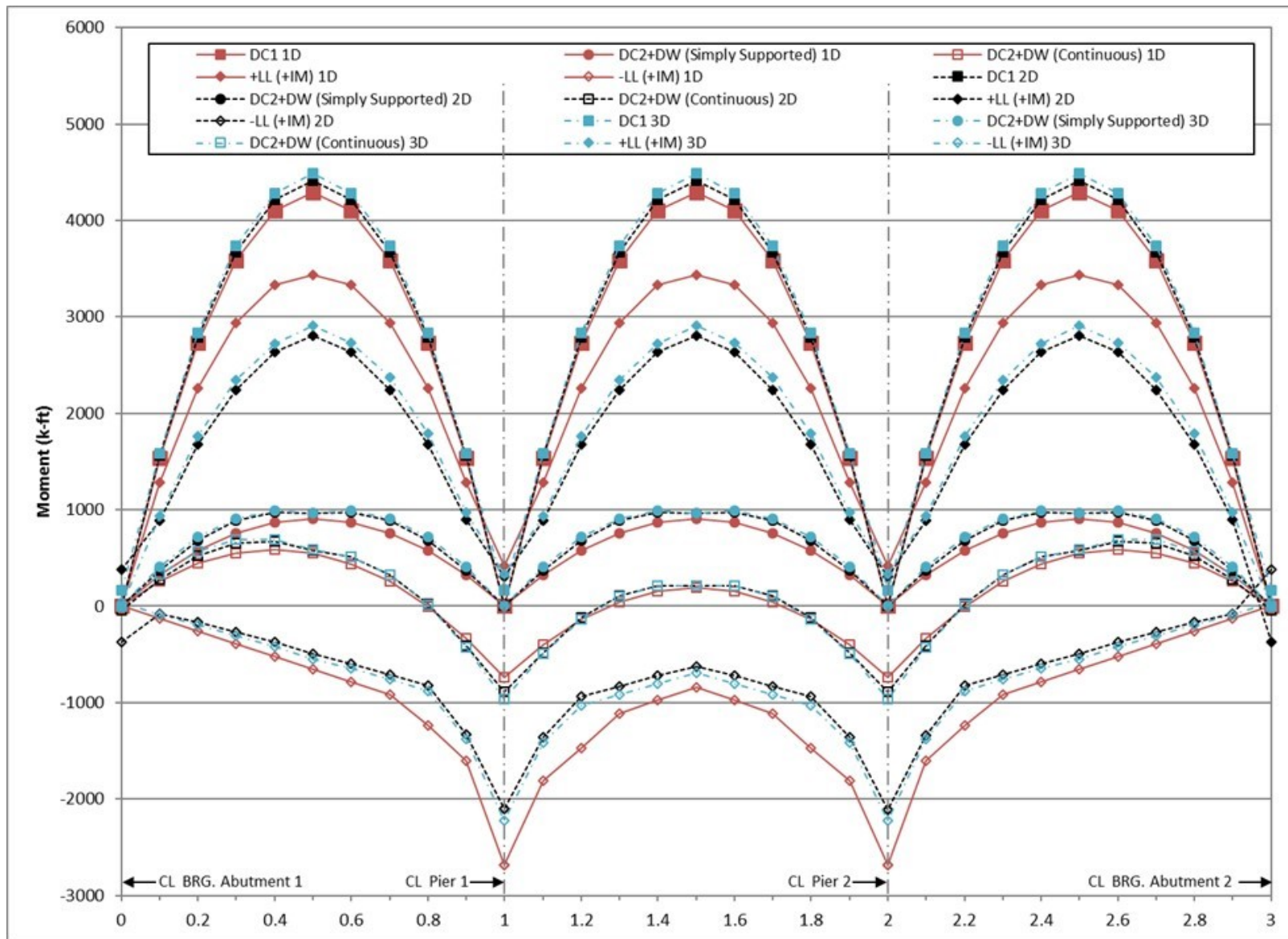


Figure 188. Graph. Comparison of moments for exterior P/S concrete girder.

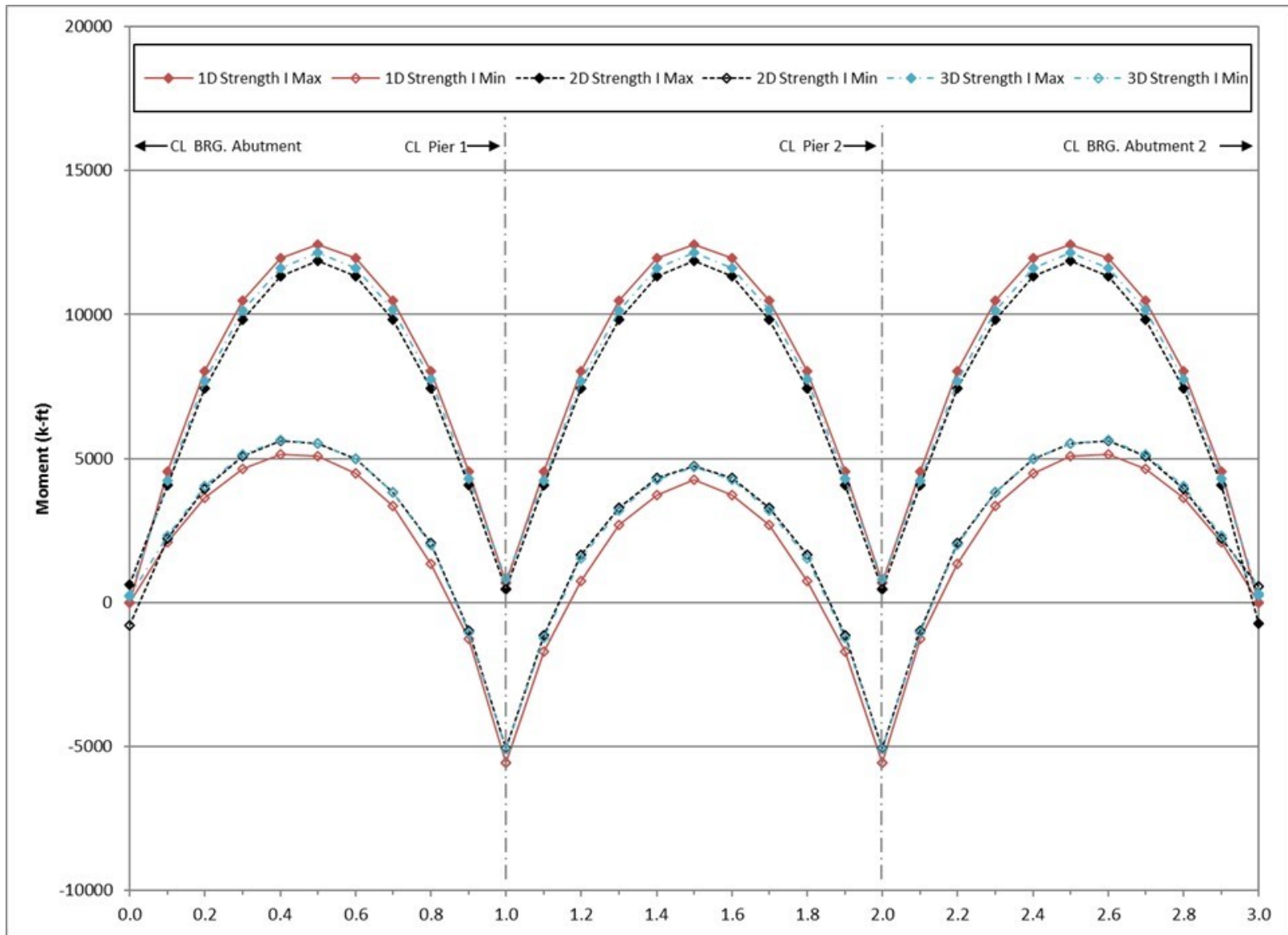


Figure 189. Graph. Comparison of factored moments for exterior P/S concrete girder.

9.1.4.2.2 Shear

Shears are compared in Figure 190. The shears due to non-composite dead loads are approximately 5 percent lower for the 1D analysis than for the 3D analysis and approximately 20-30 percent lower for the composite dead loads. The 1D maximum positive live load shears are mostly within 25 percent of corresponding 3D values, but are as much as 80 percent different in some cases. The ratio of minimum live load shears (maximum negative shears) are inconsistently related in terms of magnitude, but 1D results envelope those from the 3D analysis.

The 2D non-composite dead load shears are typically 0-5 percent lower than those from 3D analysis, and composite dead load shears are mostly 10 percent lower. The 2D minimum live load shears are typically 10 percent lower than corresponding 3D shears while the 2D maximum live load shears are typically considerably smaller and are enveloped by the 3D shears.

The 1D non-composite dead load shears are typically within 5 percent of those from the 2D analysis. Composite dead load shears are typically 20-30 percent smaller in the 1D case, but are larger in a few cases where values are small near midspan. 1D live load shears envelope the 2D results, and are typically greater by approximately 35 percent at supports.

Figure 191 compares the factored Strength I shears for the 1D, 2D, and 3D models. Similar to the moments, the 1D model provides more conservative design forces when compared to the 2D and 3D models.

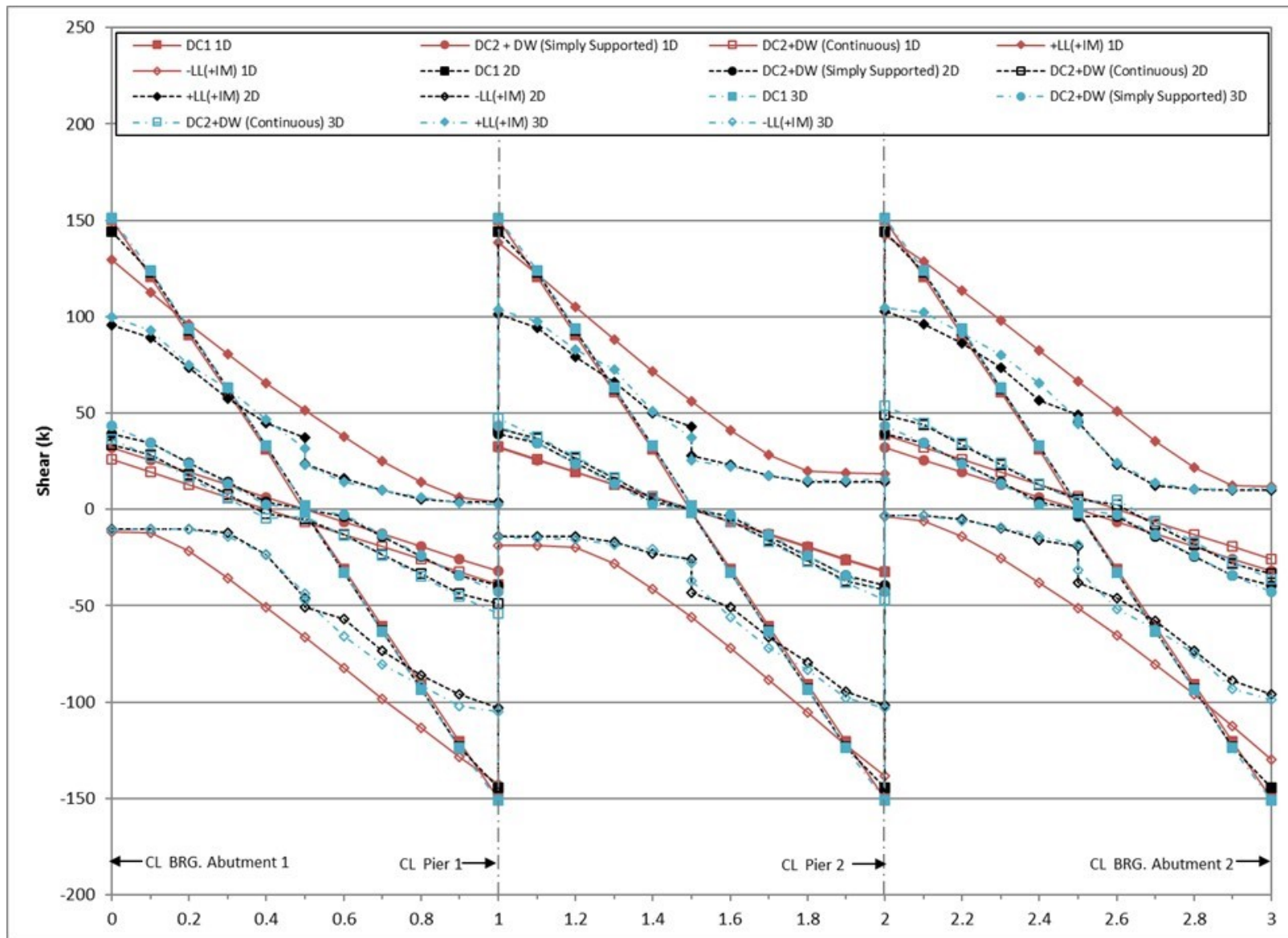


Figure 190. Graph. Comparison of shears for exterior P/S concrete girder.

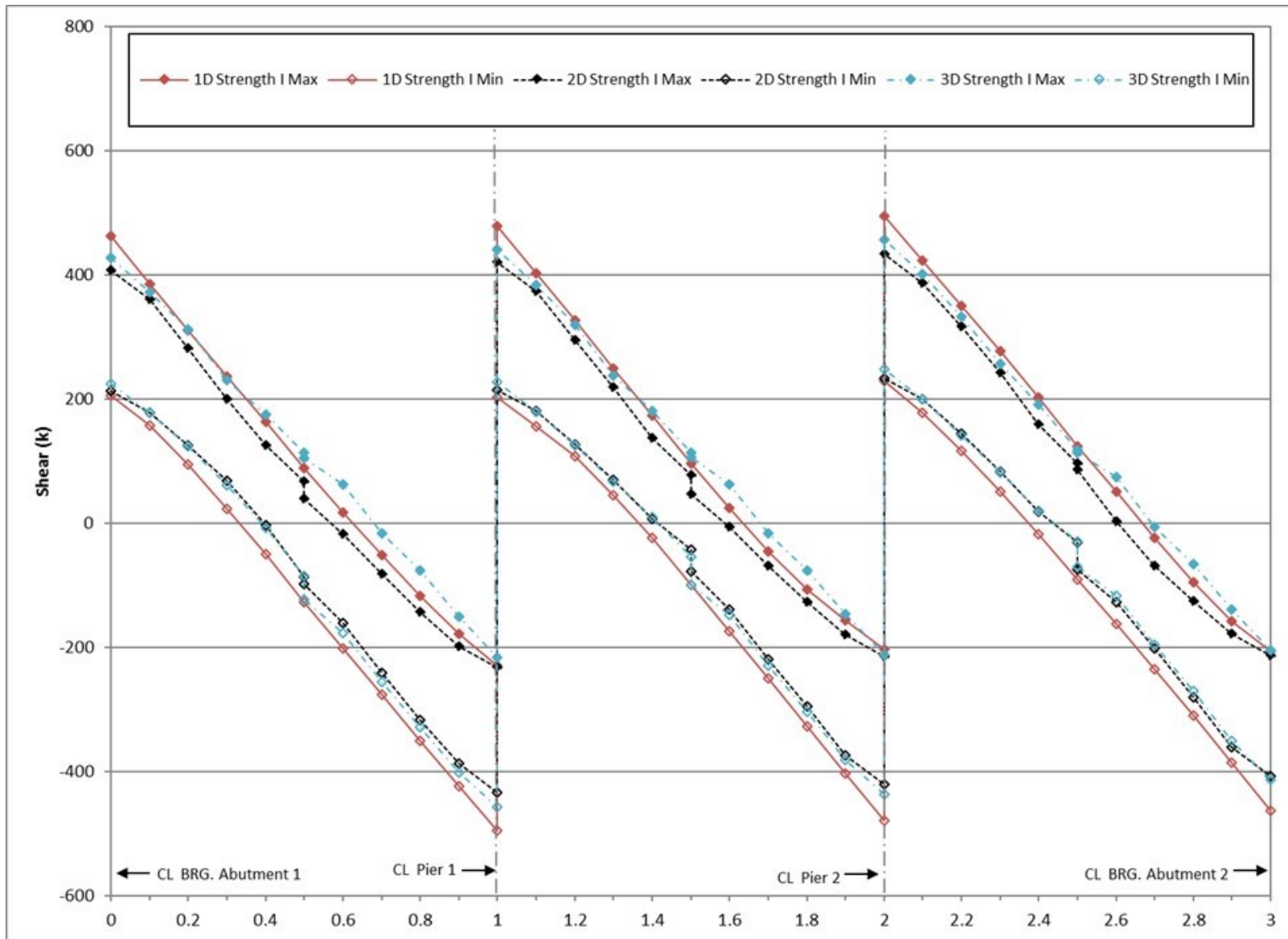


Figure 191. Graph. Comparison of factored shears for exterior P/S concrete girder.

9.1.4.2.3 Deflection

Deflections are compared in Figure 192. The deflections due to non-composite dead loads are approximately 3 percent lower for the 1D analysis than for the 3D analysis and approximately 10 percent lower for the composite dead loads. The 1D live load deflections are approximately 5 percent lower than the 3D deflections.

The deflections from the 2D non-composite dead load analysis exceed the 3D non-composite dead load deflections by less than 3 percent. The 2D composite dead load deflections are typically 3 percent lower than the 3D deflections. The live load deflections from the 2D analysis are generally 5 percent lower than those from the 3D analysis.

The 1D non-composite dead load deflections are typically 6 percent smaller than those from the 2D analysis, and 7-10 percent smaller for the composite dead load case. The 1D live load deflections are approximately equal to those from the 2D analysis.

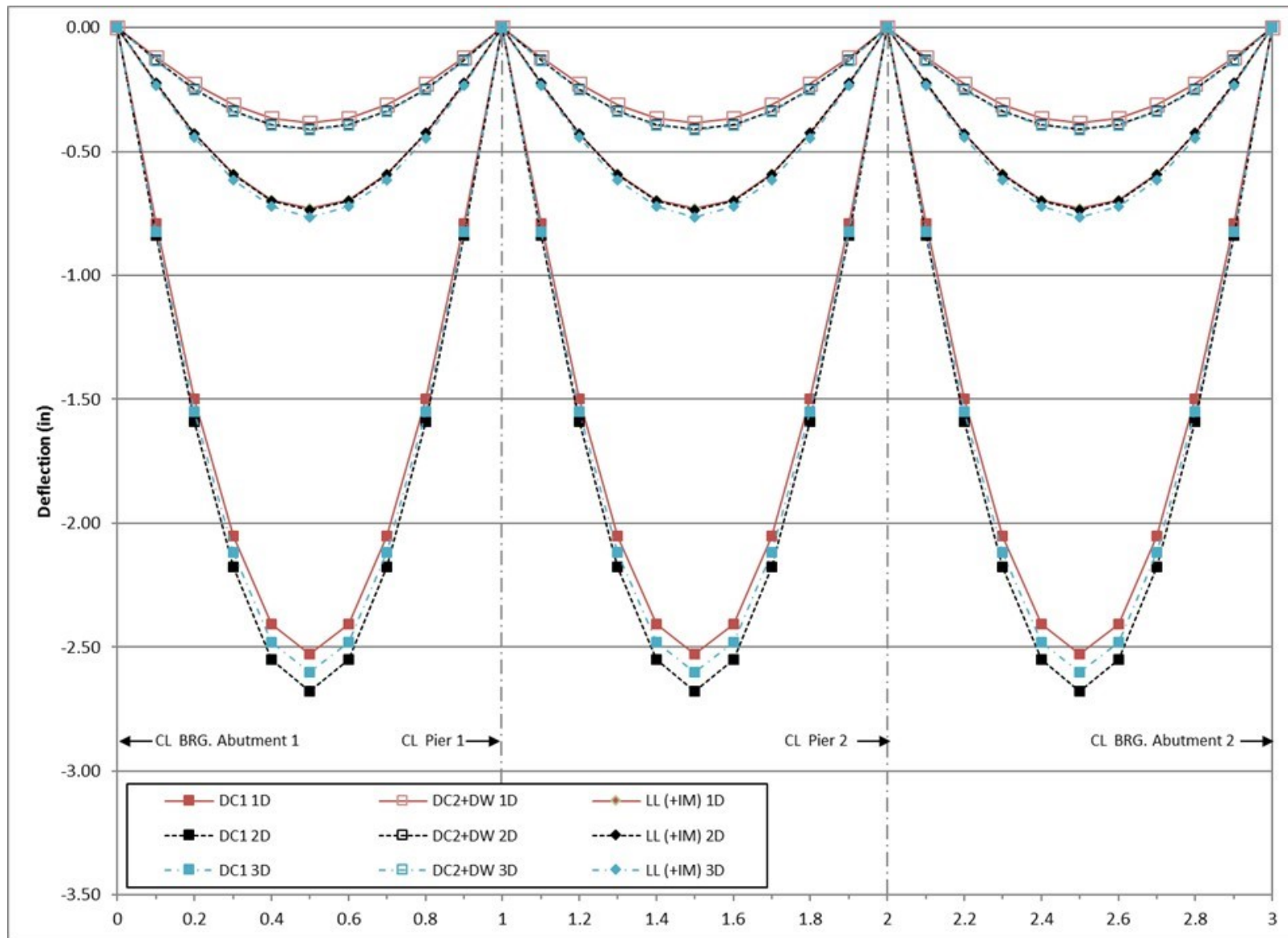


Figure 192. Graph. Comparison of deflections for exterior P/S concrete girder.

9.1.4.3 Conclusions

The 1D line girder analysis results in non-composite dead load moments that are typically within 5 percent of corresponding moments from 3D analysis for both interior and exterior girders. For the composite case the interior girder moments in the 1D analysis are typically 20 percent higher than 3D results, while the exterior girder moments are 20 percent lower. The exception is with midspan moments, where 1D results for the interior and exterior girders closely match those from 3D analysis. As would be expected, this suggests that the assumption of equal load sharing between interior and exterior girders in 1D analysis is most reasonable in areas away from supports. Live load moments are typically 10-40 percent greater for 1D line girder analysis than from the 3D analysis for both interior and exterior girders. This is a result of the live load distribution factors used in 1D analysis, which tend to overestimate the amount of load each girder takes.

Non-composite dead load shears from the 1D analysis are typically within 5 percent of those from the 3D analysis for interior girders and exterior girders. Similar to the moments, composite dead load shears tend to be over-predicted in the interior girder and under-predicted in the exterior girder on the order of 30-50 percent due to assumptions in load sharing. 1D live load shears are around 25-50 percent different than the 3D live load shears for interior girders and exterior girders. Differences tend to be greatest near midspan, where shear values are smallest and minor differences in magnitude result in larger error.

Non-composite dead load deflections from the 1D analysis are typically within 3 percent of 3D deflections for interior and exterior girders. For exterior girders, composite dead load deflections are typically 15-20 percent lower than corresponding 3D deflections, while interior girder deflections are 10 percent higher (for similar reasons to the difference in moments). 1D live load deflections are around 5 percent smaller than 3D live load deflections for the exterior girders and are 10 percent greater for the interior girders.

The Plate and Eccentric Beam method generally provides reasonable results when compared to the 3D Finite Element Method. The moments from the 2D analysis are generally within 10 percent of those from the 3D analysis for both dead and live loads. 2D shears are typically within 5 percent of the 3D dead load shears for interior girders and exterior girders. Similar to the 1D case, the largest disparities are observed where shear values are small, near midspan. 2D live load shears vary inconsistently with 3D live load shears for interior girders and exterior girders. 2D deflections are typically within 5 percent of the 3D deflections for both dead and live load and for both interior and exterior girders.

The 1D non-composite dead load moments are within 3 percent of the 2D results for both interior and exterior girders. The composite dead load interior moments are up to 20 percent greater and 20 percent lower in exterior girders from 1D to 2D, as a result of the assumption that the interior girders will carry an equal share of these loads, whereas items such as barriers are mostly going to be carried by the exterior girders. 1D live load moments are 20-50 percent greater than 2D moments, mostly as a result of the use of live load distribution factors.

The 1D non-composite dead load shears are typically within 5 percent of those from the 2D analysis for both interior and exterior girders. 1D composite dead load shears are typically higher in interior girders and smaller in exterior girders than corresponding 2D shears for reasons

similar to the moments. Similarly to the moments, the 1D live load shears are consistently larger than 2D shears as a result of the live load distribution factors.

The 1D deflections follow a similar pattern to the moments and shears for dead load. Non-composite dead load deflections are similar for the interior and exterior girders, while composite dead load shears are typically higher in the interior girders and lower in exterior girders. Live load deflections are closer between the two analyses as no distribution factors are applied.

Overall, the greatest improvements in terms of design benefits will typically come from refinement into a 2D model, particularly in the instance of live load where the conservative distribution factors are no longer applied. In most cases, it is typical that the 2D results sufficiently approach those from the 3D model.

9.2 Example 2 – Three-span Continuous Steel I-Girder Bridge

A three-span continuous steel I-girder bridge adapted from an example in NHI Course 130095 is the subject of Example 2. The cross-section consists of four welded steel plate girders spanning 160 ft-0 inches – 210 ft-0 inches – 160 ft-0 inches. Cross-frames are at 20 ft-0 inch centers in Spans 1 and 3 and 21 ft-0 inch centers in Span 2. Figure 193 shows the framing plan for Example 2.

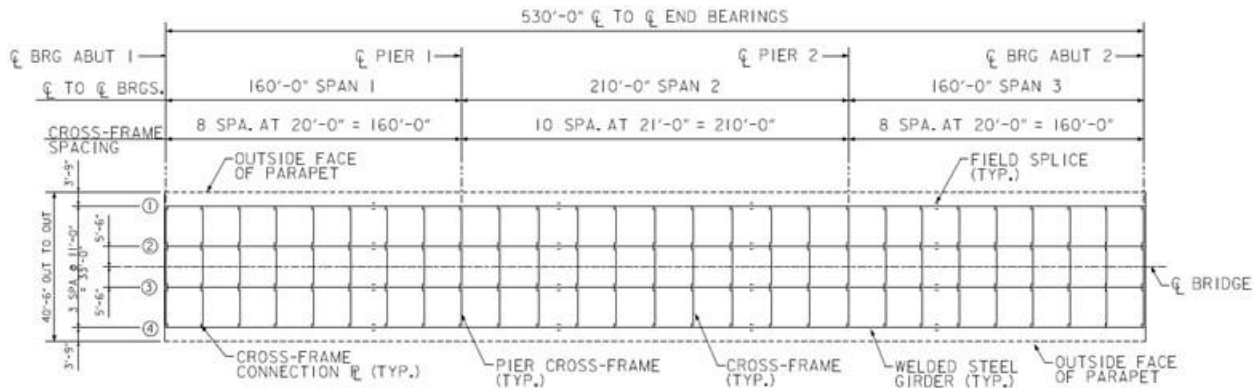


Figure 193. Illustration. Example 2 framing plan.

Figure 194 shows the bridge cross-section for Example 2. The concrete deck slab is 9½ inches thick including a ½ inch integral wearing surface; the deck slab is constructed with concrete having a compressive strength of 4 ksi. The intermediate cross-frames are composed of L5x5x½ top chords and WT6x22.5 diagonals and bottom chord. The cross-frames at the piers and abutments are composed of L8x8x¾ top chords and L5x5x⅝ diagonals and bottom chord. The welded steel girders have a 92-inch deep web. The top and bottom flange plate dimensions are shown in Figure 195.

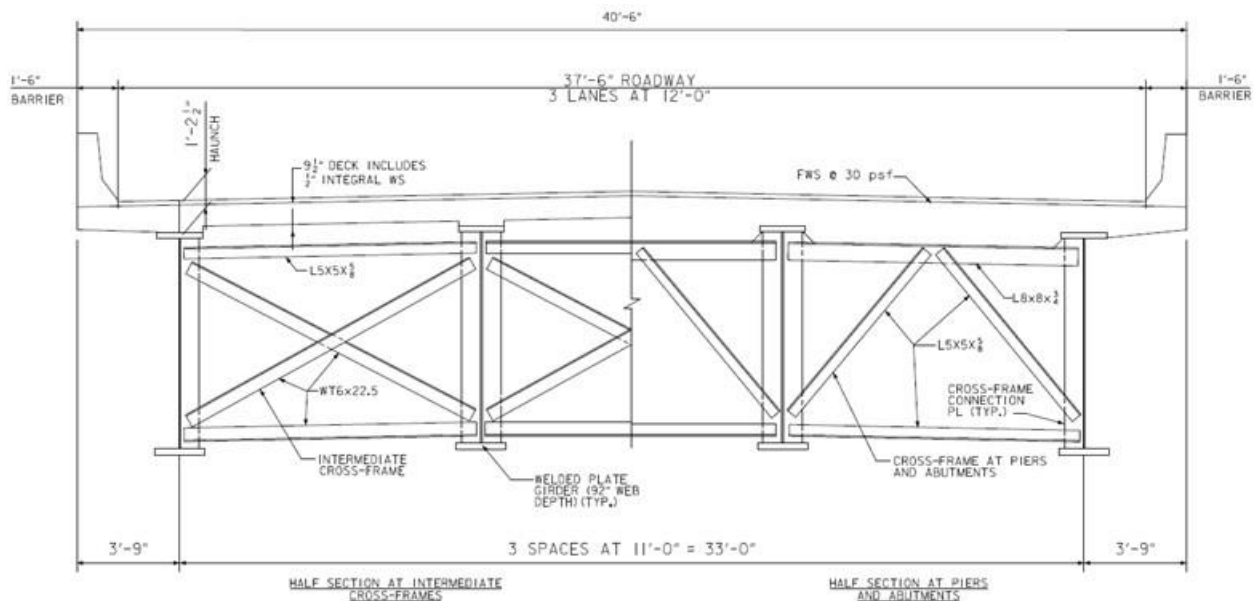


Figure 194. Illustration. Example 2 bridge cross-section.

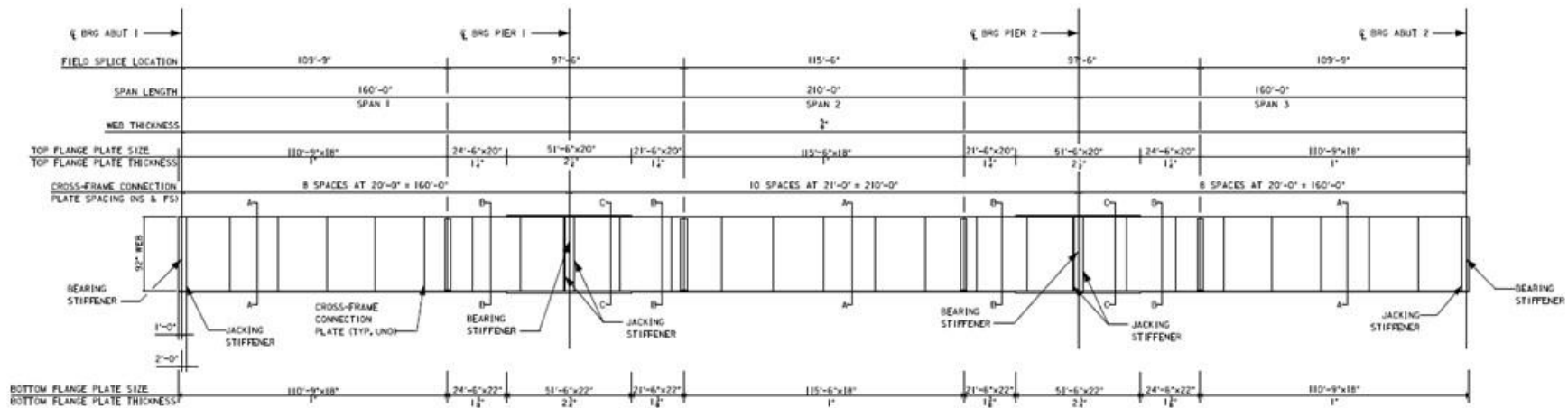


Figure 195. Illustration. Example 2 girder elevation.

9.2.1 1D Line Girder Analysis

1D line girder analysis utilizes the approximate distribution factors contained in Article 4.6.2.2 of the AASHTO LRFD Bridge Design Specifications (Specifications). The following steps are used to determine the dead and live load bending moments, shears, and deflections:

1. Determine non-composite and short- and long-term composite section properties for interior and exterior girders.
2. Calculate moment distribution factors for interior and exterior girders for one lane loaded and multi-lane loaded situations.
3. Determine and input magnitude (generally in kips or kips per foot) of dead loads due to girder self-weight, concrete deck slab, haunches, barrier, and cross-frames.
4. Develop and run analysis models. (Notes: Depending on software, several models may have to be developed using the different section properties from Step 1; live load distribution factors from Step 2 may, depending on software, be included in the developed model and distributed moments (and shears) will be provided as results)
5. Develop moment, shear, and deflection diagrams for non-composite dead load, composite dead load, and live load.

In this analysis, the following models are developed and used to determine the dead and live load bending moments, shears, and deflections:

- Non-composite section properties with non-composite dead loads applied;
 - The non-composite dead loads are applied to a continuous girder.
 - These dead loads include the following: girder self-weight, cross-frames, haunches, and concrete deck slab.
- Long-term composite section properties with composite dead loads applied; and
 - The composite dead loads are applied to a continuous girder.
 - Composite dead loads include the barrier and future wearing surface.
- Short-term composite section properties with live load applied.
 - The live load is applied to a continuous girder.

9.2.1.1 Step 1 – Determine Non-Composite and Various Composite Section Properties

9.2.1.1.1 Non-Composite Section Properties – Interior and Exterior Girders

The non-composite section properties are calculated using basic mechanics of materials equations and are shown in Table 28. For details, see Example 1.

Table 28. Example 2 non-composite section properties.

Section	Area (in ²)	Moment of Inertia (in ⁴)
Section A-A	93.50	118401
Section B-B	112.75	160309
Section C-C	168.00	286524

9.2.1.1.2 Long-Term Composite Section Properties for Interior Girders

The long-term composite section properties for the interior girders are calculated below. Due to the different materials used in the deck slab and beam, the modular ratio must be calculated. The modular ratio is the ratio of modulus of elasticity for the beam to the modulus of elasticity of the deck slab. The modulus of elasticity of concrete is calculated using the concrete compressive strength and AASHTO LRFD Equation C5.4.2.4-1, shown here as Equation (49). The modulus of elasticity for the beam is 29,000 ksi and for the deck slab is determined to be 3640 ksi, for a compressive strength of 4 ksi. The modular ratio, given by Equation (50), is then 29000 ksi divided by 3640 ksi which is equal to 7.96 (rounded to 8).

$$E_c = 1820\sqrt{f'_c} \quad (49)$$

$$n = \frac{E_{beam}}{E_{deck}} \quad (50)$$

The long-term section properties are shown in Table 29 using an effective modular ratio of 3n to account for the effects of creep. The effective modular ratio is used to convert the deck slab concrete into an equivalent area of steel. The deck slab contribution depends on the effective flange width determined according to AASHTO LRFD Article 4.6.2.6 which indicates that the center-to-center girder spacing should be used as the effective flange width for the interior girders. The depth of the haunch and the ½ inch integral wearing surface are, conservatively, not included in the section property calculation.

Table 29. Example 2 interior girder long-term composite section properties.

Section	Area (in ²)	Moment of Inertia (in ⁴)
Section A-A	143.00	204576
Section B-B	162.25	260717
Section C-C	217.50	406754

9.2.1.1.3 Short-Term Composite Section Properties for Interior Girders

The short-term section properties are calculated using the modular ratio as indicated previously and shown in Table 30. The center-to-center girder spacing is used for the effective flange width. Because there are no creep effects for loads of short duration no modification of the modular ratio is applied. To account for the different material properties, the effective flange width is divided by the modular ratio. As above, the depth of the haunch and the ½ inch integral wearing surface are, conservatively, not included in the section property calculation.

Table 30. Example 2 interior girder short-term composite section properties.

Section	Area (in ²)	Moment of Inertia (in ⁴)
Section A-A	242.00	271576
Section B-B	261.25	347766
Section C-C	316.50	534705

9.2.1.1.4 Long-Term and Short-Term Composite Section Properties for Exterior Girders

The long-term and short-term composite section properties for the exterior girders are shown in Tables 31 and 32, respectively. The calculation is identical to that of the interior girders except that the effective flange width is different for exterior girders. AASHTO LRFD Article 4.6.2.6 indicates that one-half the center-to-center girder spacing plus the overhang width should be used as the effective flange width for exterior girders. As above, the depth of the haunch and the ½ inch integral wearing surface are, conservatively, not included in the section property calculation.

Table 31. Example 2 exterior girder long-term composite section properties.

Section	Area (in ²)	Moment of Inertia (in ⁴)
Section A-A	135.13	195073
Section B-B	154.38	249036
Section C-C	209.63	391414

Table 32. Example 2 exterior girder short-term composite section properties.

Section	Area (in ²)	Moment of Inertia (in ⁴)
Section A-A	218.38	261051
Section B-B	237.63	333531
Section C-C	292.88	511988

9.2.1.2 Step 2 – Determine Approximate Live Load Distribution Factors

9.2.1.2.1 Interior Girder Distribution Factors

The approximate live load distribution factor equations are provided in AASHTO LRFD Article 4.6.2.2. Different cross-section types are provided in AASHTO LRFD Table 4.6.2.2.1-1; comparing Figure 194 to those in the table, it is determined that cross-section “a” is similar. The controlling distribution factors for the interior and exterior girders are summarized in Table 33. For detailed calculation of the distribution factors, refer to Appendix 9.A.

Table 33. Example 2 distribution factors.

Girder	Action	Spans 1 and 3			Span 2		
		A-A	B-B	C-C	A-A	B-B	C-C
Interior Girder	M+ and M- not between POCs	0.76	0.78	0.82	0.71	0.73	0.76
Exterior Girder		0.92	0.92	0.92	0.92	0.92	0.92
		A-A		B-B	C-C		
Interior Girder	M- between POCs	0.73		0.75	0.79		
Exterior Girder		0.92		0.92	0.92		
		A-A		B-B	C-C		
Interior Girder	Shear	1.02		1.02	1.02		
Exterior Girder		0.90		0.90	0.90		

9.2.1.3 Step 3 – Determine Dead Loads on a “Per Girder” Basis

9.2.1.3.1 Self-Weight of Girder, w_{sw}

The self-weight of the girder is calculated using the cross-section area and unit weight of the material. The values are summarized in Table 34.

Table 34. Example 2 girder self-weight.

Cross-Section	Lineal Weight (k/ft)
A-A	0.319
B-B	0.384
C-C	0.575

9.2.1.3.2 Weight of Stay-in-Place Forms, w_{sip}

Stay-in-place forms with an assumed weight of 0.015 ksf are used. The weight includes the weight of the form as well as the concrete in form valleys. For the interior girders, the weight for SIP forms is $0.015 \text{ ksf} \times 11 \text{ ft} = 0.17 \text{ k/ft}$. For the exterior girders, the weight of SIP forms is $0.015 \text{ ksf} \times 5.5 \text{ ft} = 0.083 \text{ k/ft}$.

9.2.1.3.3 Weight of Concrete Deck Slab, w_{deck}

The weight of the concrete deck slab is determined on a basis of tributary width for the interior and exterior girders. For the interior girder, the tributary width is taken as one-half the girder spacing on each side of the girder while for the exterior girder, the tributary width is taken as the overhang plus one-half the girder spacing. The resulting loads are 1.31 k/ft for interior girders and 1.10 k/ft for exterior girders.

9.2.1.3.4 Weight of Concrete Haunches

The weight of the haunch is determined using the cross-section area of the haunch and the unit weight of concrete. For the interior girders, the total depth (deck slab plus haunch) is 1 ft-2½ inches at the centerline of the girder with the deck slab having a 2 percent cross-slope.

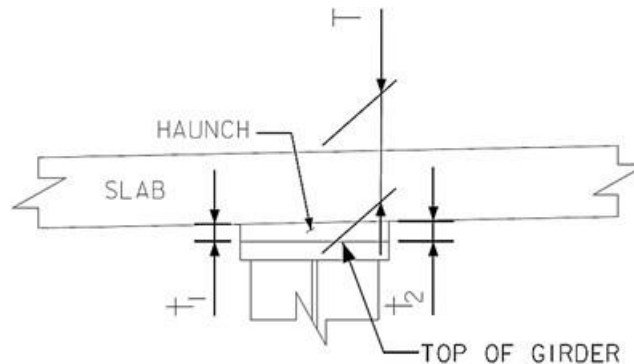


Figure 196. Illustration. Haunch area for interior girders.

The weight of the haunch on the interior girder, w_{hi} , is determined to be 0.075 k/ft for Section A-A, 0.078 k/ft for Section B-B, and 0.053 k/ft for Section C-C.

For the exterior girders, the concrete in the overhang in excess of the deck slab thickness is included in the weight of the haunch. The weight of the haunch, including the concrete in the upturn and overhang, is determined to be 0.155 k/ft for Section A-A, 0.152 k/ft for Section B-B, and 0.103 k/ft for Section C-C.

9.2.1.3.5 Weight of Intermediate Cross-Frames and Connection Plates

Intermediate cross-frames are located at equal spacing in each span. The cross-frames are composed of L5x5x $\frac{5}{8}$ top chords and WT6x22.5 diagonals and bottom chords. The weight of each cross-frame is determined using the steel section properties and member length. For the exterior girders, one-half of the cross-frame weight calculated for the interior girders is applied. The cross-frame weight applied to the interior girders is 1.25 k and to the exterior girder is 0.63 k.

9.2.1.3.6 Weight of Barrier

The weight of the barrier is determined to be 0.40 k/ft. The distribution of the barrier weight to the girders can be performed in several different ways: equally to all girders, to the exterior girder only, or by the lever rule to the exterior girder and first interior girder. The barrier weight is assumed to be distributed equally to all girders. Therefore, 0.20 k/ft is applied to each girder to represent the weight of the barrier.

9.2.1.3.7 Weight of Future Wearing Surface

A 30 psf future wearing surface is considered in the design of the bridge. The weight of the wearing surface can be distributed equally to all girders or based on tributary width; this example assumes the weight is distributed based on tributary width. For the interior girders, the tributary width is equal to the girder spacing. For the exterior girders, the tributary width is equal to one-half the girder spacing plus the overhang distance minus the width of the barrier. The magnitude of the applied load to the interior girders is 0.33 k/ft. The magnitude of the applied load to the exterior girders is 0.23 k/ft.

9.2.1.3.8 Summary of Dead Loads

A summary of the dead load magnitudes for the interior and exterior girders is shown in Table 35 below. The loads shown are on a “per girder” basis.

Table 35. Dead loads on a per girder basis.

Section	Self-Weight, w_{sw} [k/ft]	Cross-Frames, P [k]		SIP Forms, w_{sip} [k/ft]		Deck Slab, w_d [k/ft]		Haunch, w_h [k/ft]		Barrier, w_p [k/ft]	FWS [k/ft]	
		Int.	Ext.	Int.	Ext.	Int.	Ext.	Int.	Ext.		Int.	Ext.
A-A	0.319	1.25	0.63	0.17	0.083	1.31	1.10	0.075	0.155	0.20	0.33	0.23
B-B	0.384							0.078	0.152			
C-C	0.575							0.053	0.103			

9.2.1.4 Step 4 – Develop Analysis Models

This step will be software specific in many of the details, but in general the following will need to be defined in the model:

- 1) Basic layout such as span lengths and support types
- 2) Properties of the cross-sections such as moment of inertia
- 3) Dead loads
- 4) Live loads

As part of this step the engineer needs to verify that the software is performing correctly. For verification a check is made for the sum of deck slab dead load reactions. For an interior girder, the total applied load is $(1.31 \text{ k/ft})(530 \text{ ft}) = \mathbf{694.3 \text{ k}}$.

The reactions from the analysis software:

Location	Reaction (k)
Abutment 1	71.15
Pier 1	276
Pier 2	276
Abutment 2	71.15
Total	694.3

The sum of reactions matches the applied loading and as expected the reactions are symmetric. Therefore, the software is operating as anticipated. In general, acceptable levels of accuracy should consider the complexity of the analysis and geometry being investigated, but ultimately depend on the discretion of the project manager.

9.2.1.5 Step 5 – Develop Moment, Shear, and Deflection Diagrams

After performing the analysis, moment, shear, and deflection diagrams are created using the analysis results. Diagrams can be developed for individual components or combined according to the type of applied load. Figures 197 through 202 show the moments, shears, and deflections calculated from the 1D line girder analysis. The following figures show the moment, shear, and deflection due to: non-composite dead loads including the beam self-weight, stay-in-place deck forms, diaphragms, haunches, and concrete deck slab, composite dead loads including the barrier and future wearing surface, and maximum positive and negative live load moments including dynamic load allowance.

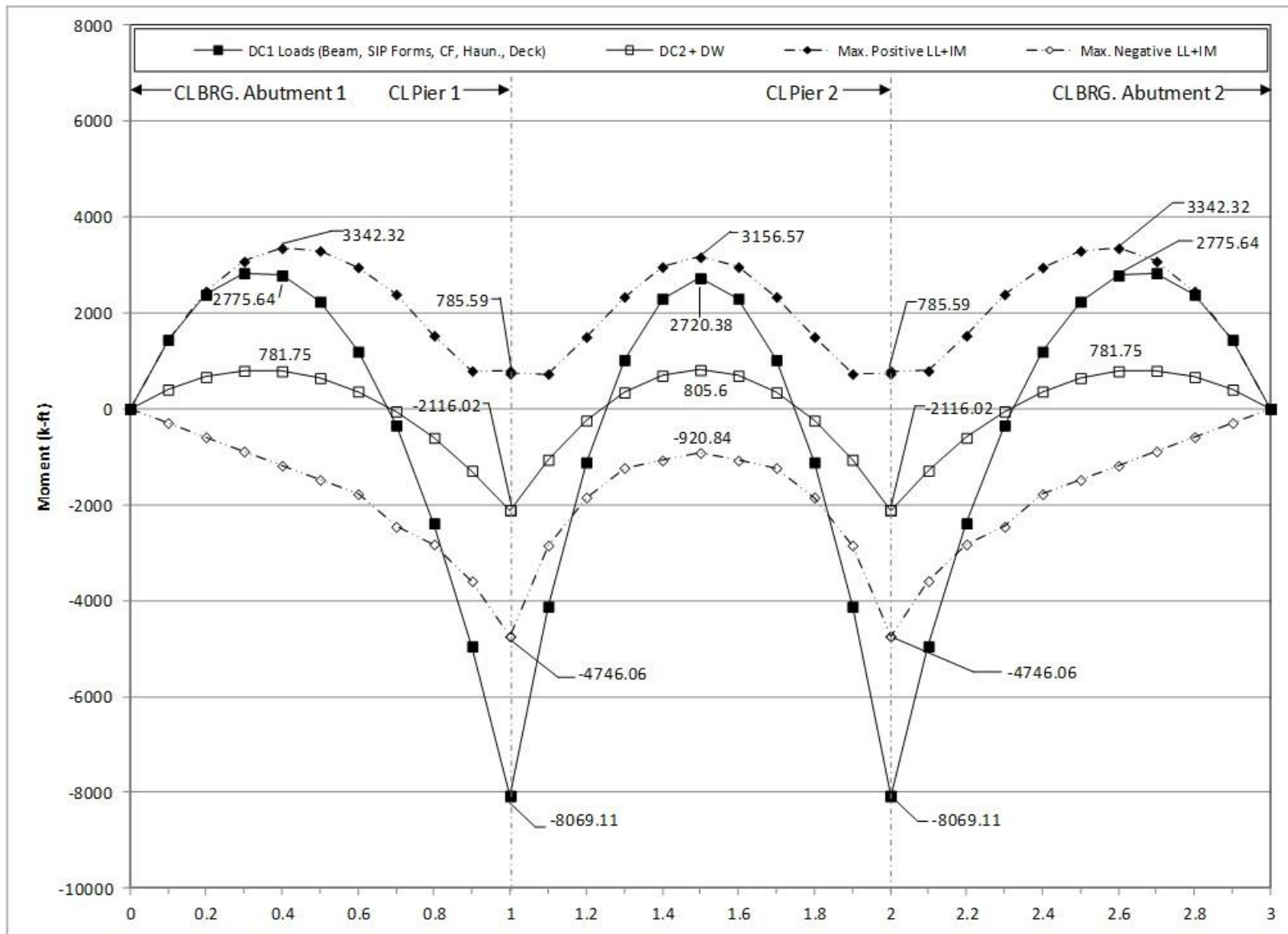


Figure 197. Graph. 1D moment diagram and live load envelope for interior girder.

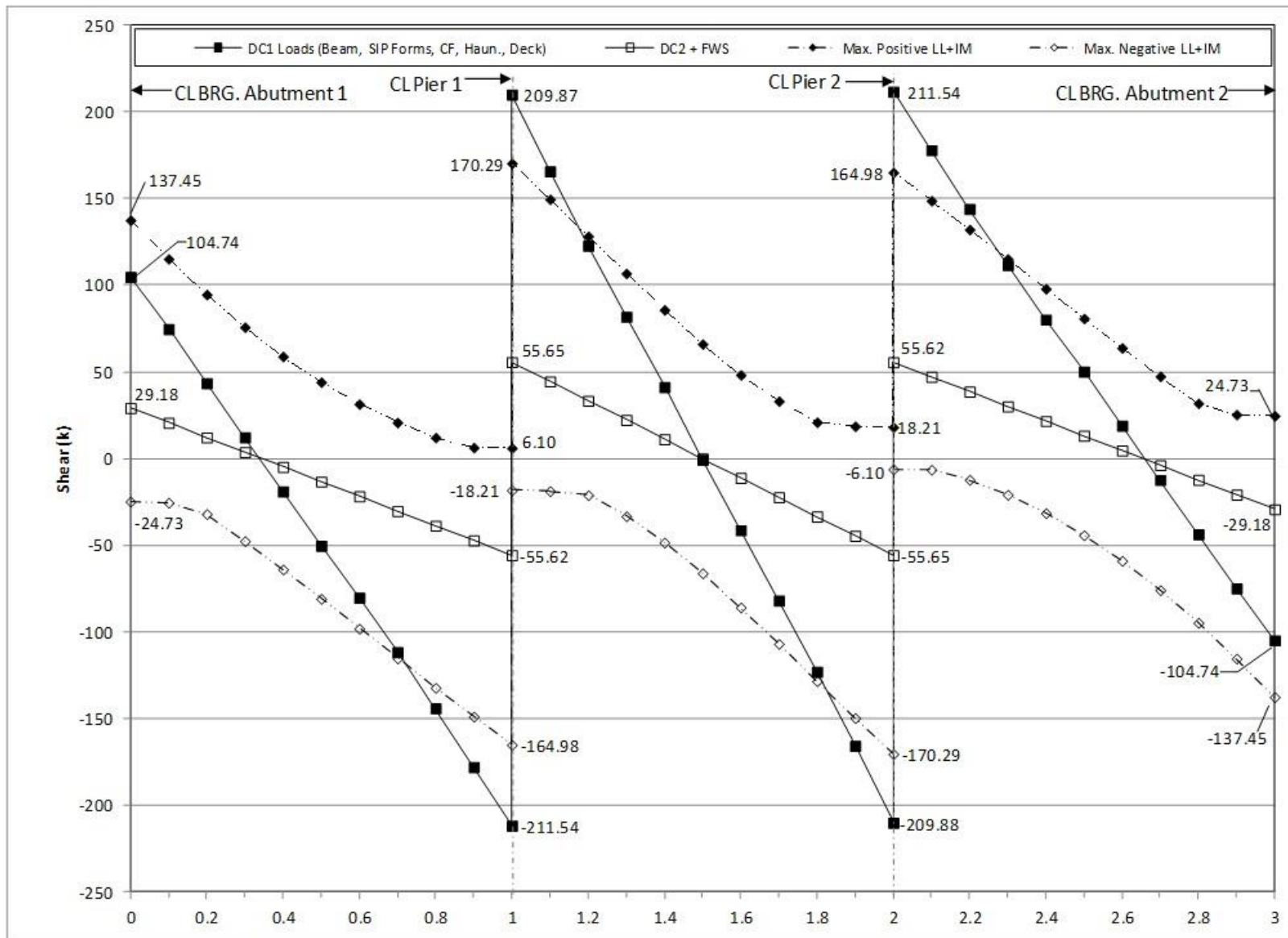


Figure 198. Graph. 1D shear diagram and live load envelope for interior girder.

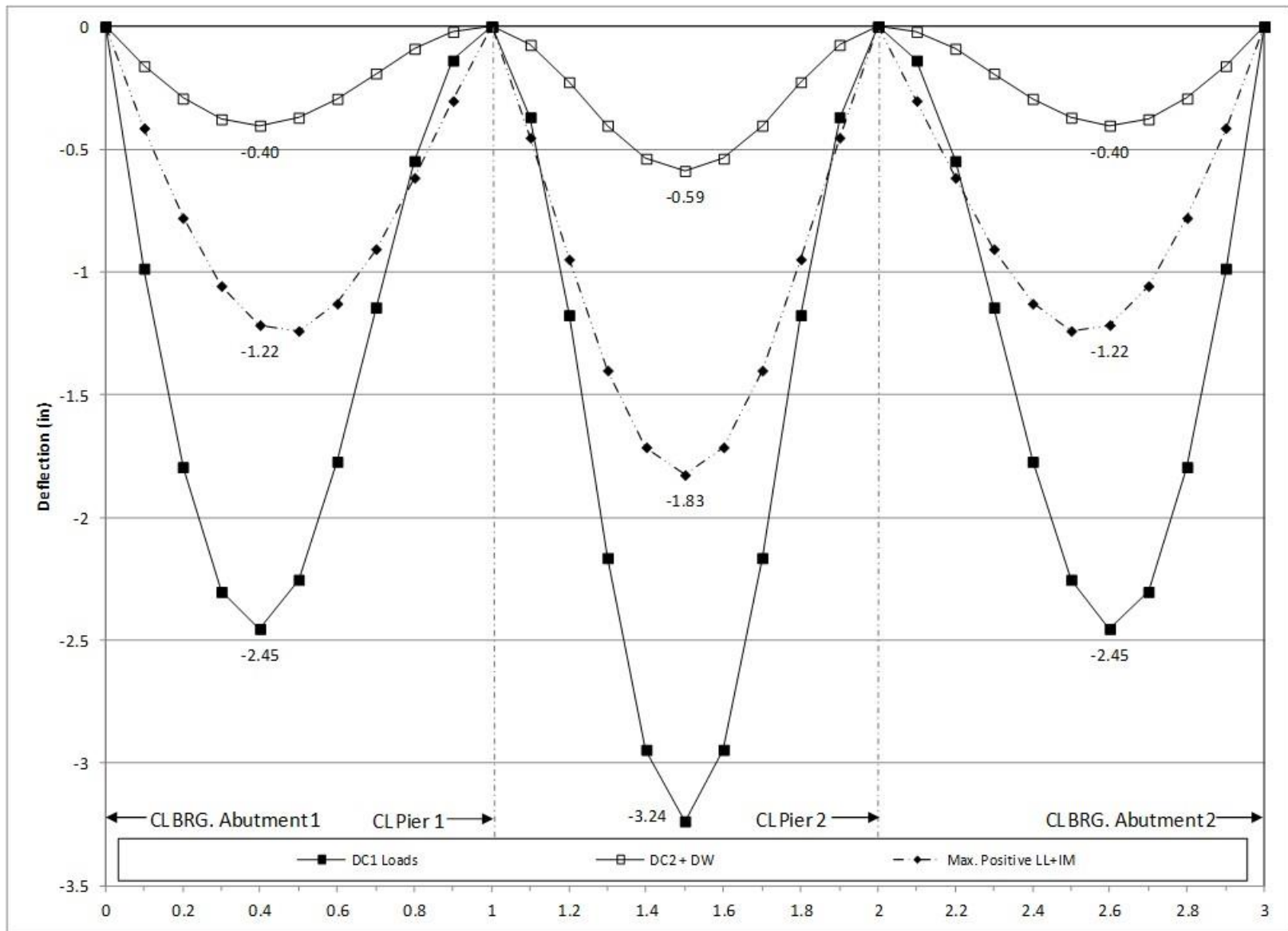


Figure 199. Graph. 1D deflection diagram for interior girder.

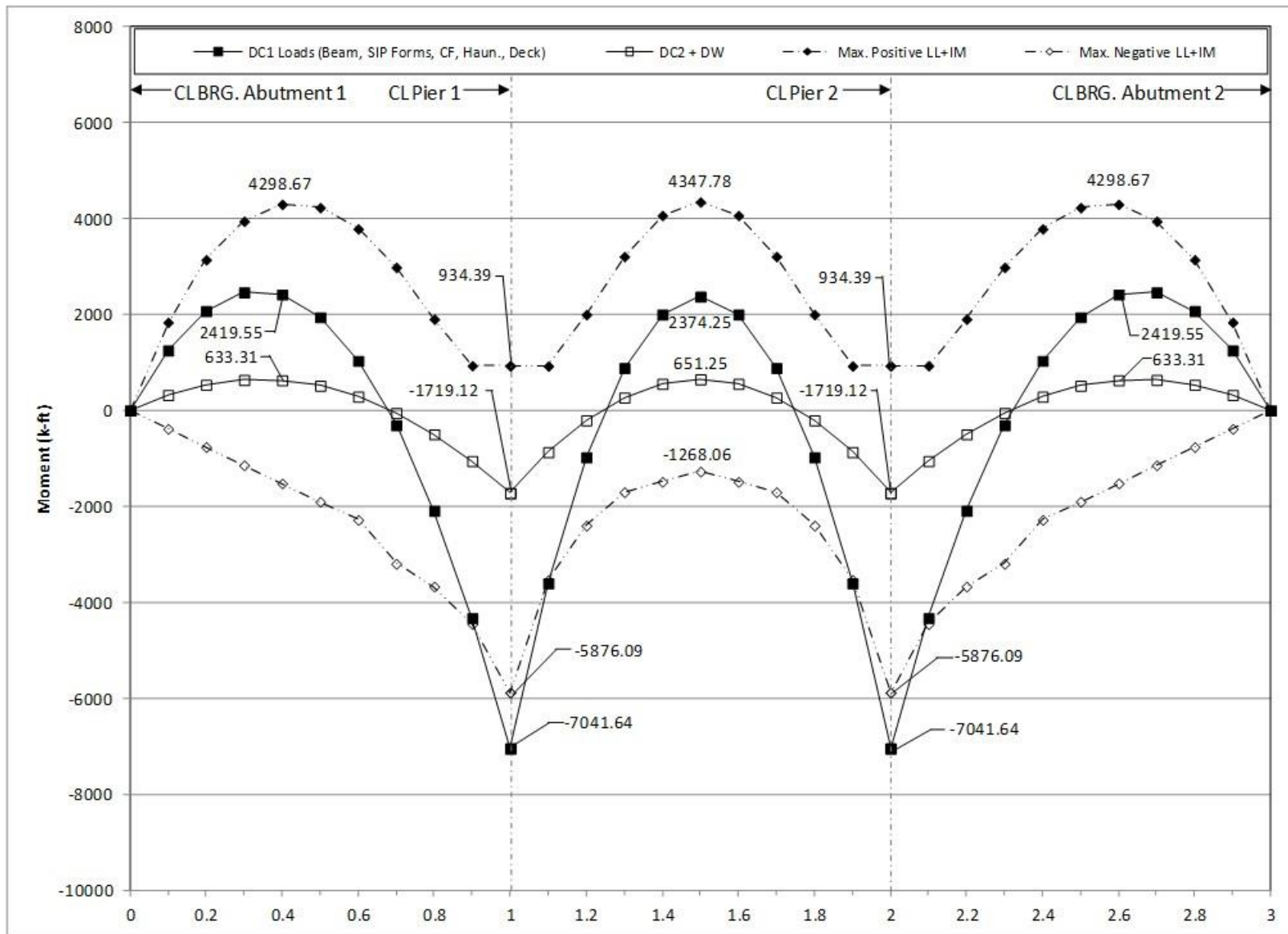


Figure 200. Graph. 1D moment diagram and live load envelope for exterior girder.

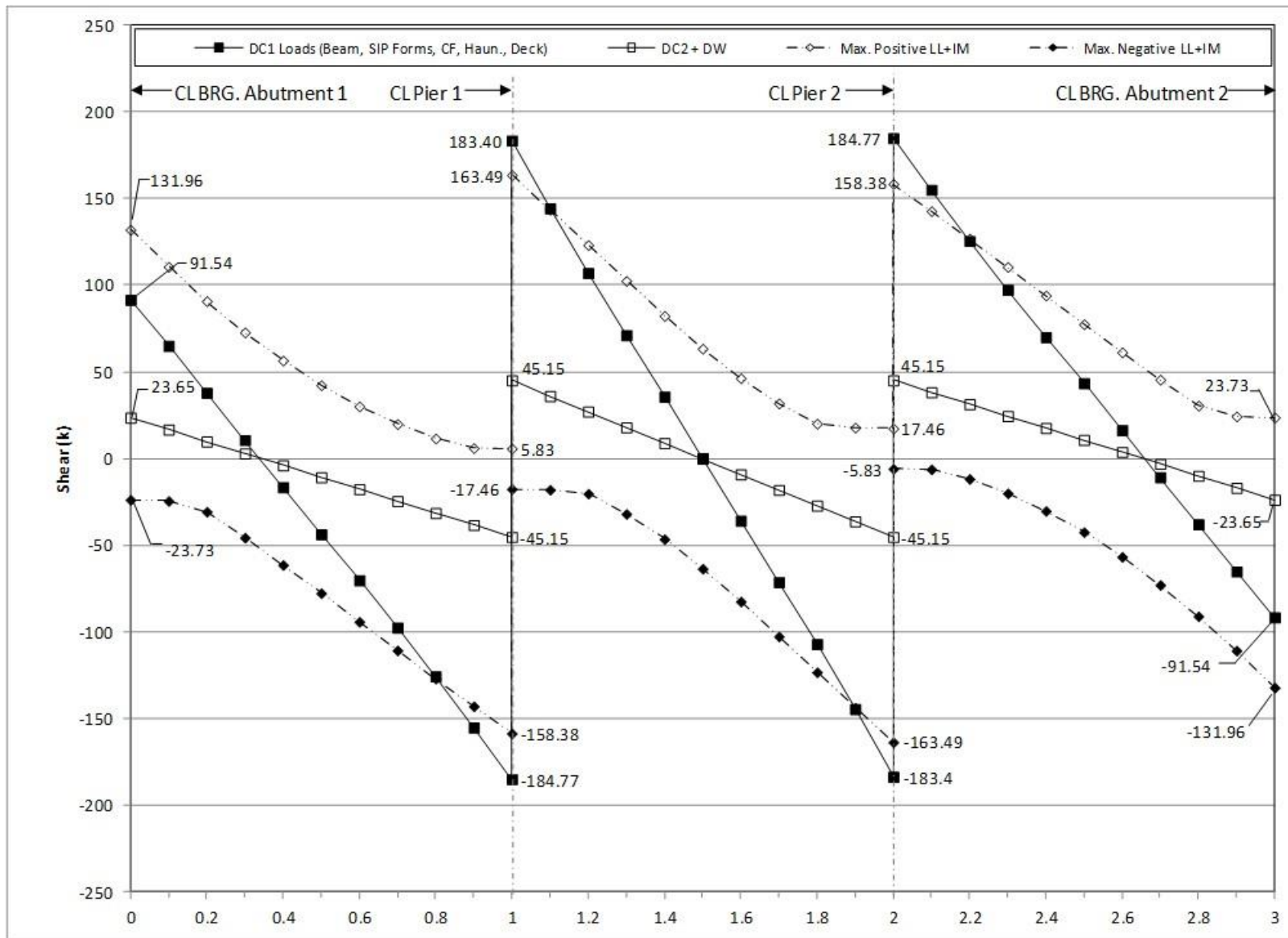


Figure 201. Graph. 1D shear diagram and live load envelope for exterior girder.

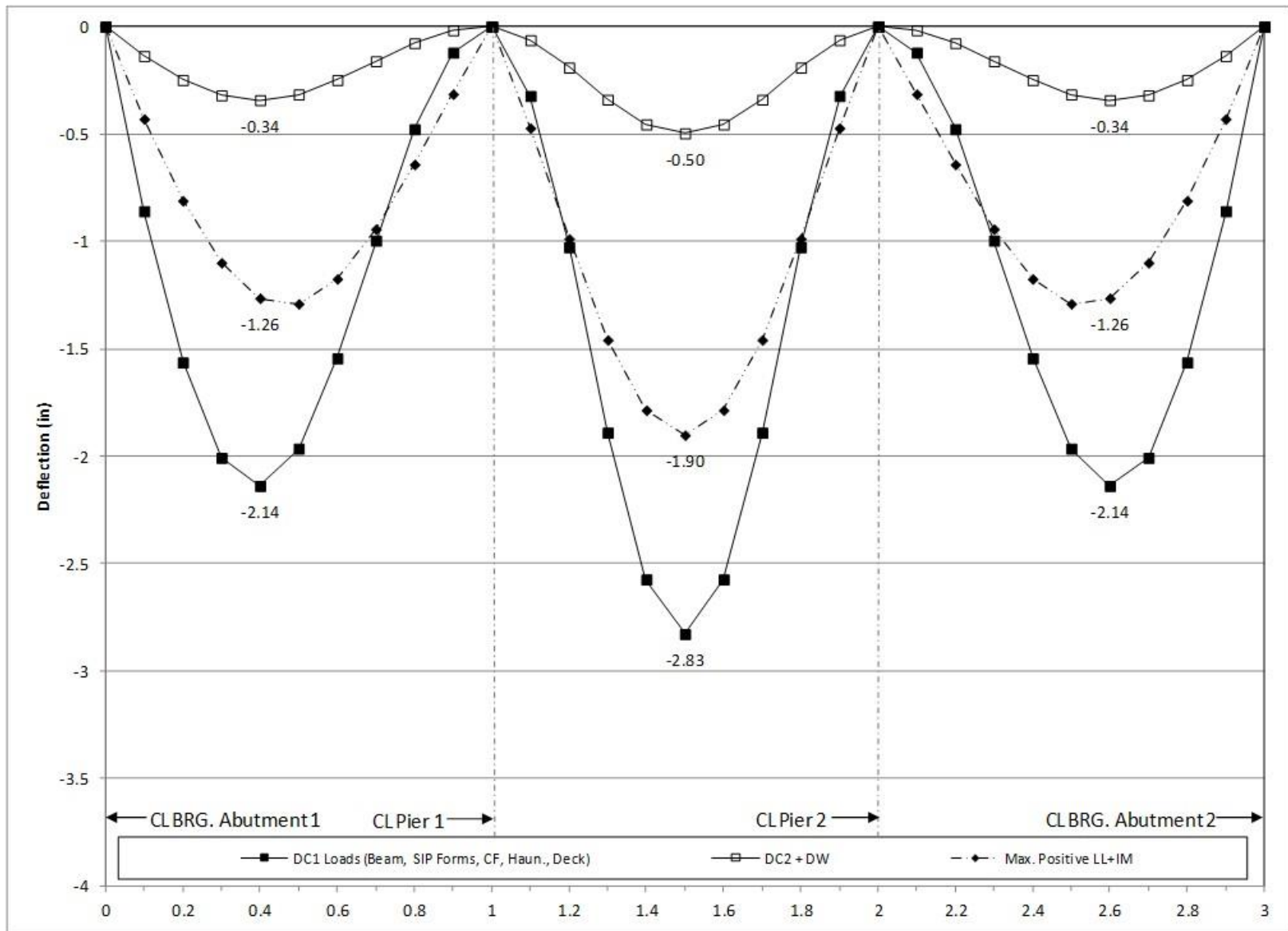


Figure 202. Graph. 1D deflection diagram for exterior girder.

9.2.2 Plate and Eccentric Beam Analysis

Similar to Section 9.1.2, the 1D analysis from the previous section is taken one degree further in complexity. A PEB analysis, which utilizes the stiffness of the girders and cross-frames to distribute the non-composite dead loads and the stiffness of the girders, cross-frames, and deck slab to distribute the composite dead loads and live loads, is used. The approximate distribution factors in AASHTO LRFD Article 4.6.2.2 are not used. Geometry is modeled at the centroid of the first girder section, Section A-A. The following steps are used to determine the dead and live load bending moments, shears, and deflections and are similar to those in Section 9.1.2:

1. Create model for non-composite dead loads.
 - a. Define location of girders and cross-frames. Depending on software, the girder may have to be defined by multiple segments such that the intermediate cross-frame can be connected to the girders, see Figure 203. Between nodes used to define member ends it may also be necessary in this step to discretize the geometry (through addition of nodes) such that members are ultimately composed of a sufficient number of elements. The number of elements should be enough to capture the expected behavior of each component, but not so many that computational time becomes excessive. Consideration should also be given to where results are required, as additional nodes may need defined at these locations. In the analysis software used, elements are created through a meshing process, where an element size/number is specified and applied to the structural members. As elements are defined geometrically, it may also be necessary to choose element type. Further discussion of element definition and element types can be found in Section 3.5.

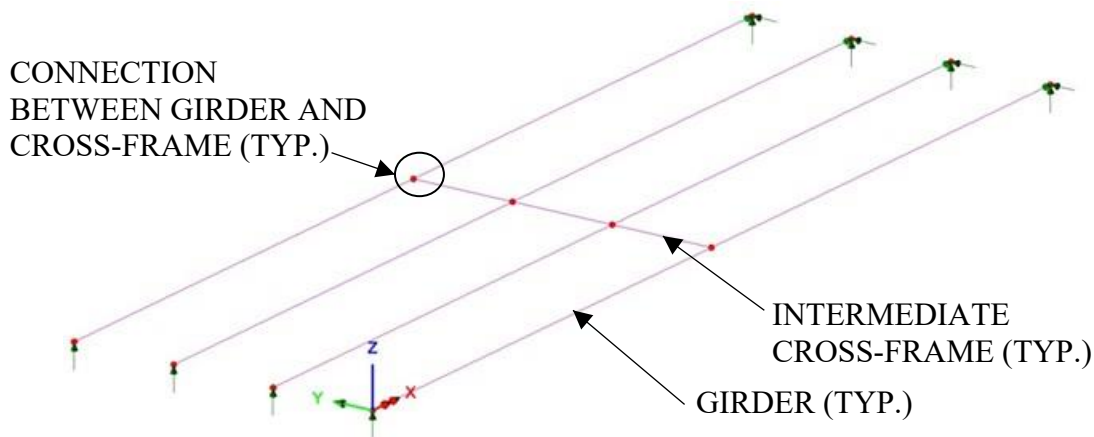


Figure 203. Illustration. Girder and intermediate cross-frame location.

- b. Define geometry of girder and intermediate cross-frame cross-sections. The girder in this example has several cross-sections along its length due to plate transitions; section properties may be calculated by hand as in Section 9.2.1.1.1 or the analysis software may require plate dimensions to be input from which the cross-section properties will be calculated. The cross-frames are composed of a

top chord, bottom chord, and two diagonals but will be represented by a single member in the PEB analysis. Therefore, the cross-section properties must be estimated. This process is further described below.

- c. Define material properties for girders and intermediate cross-frames. The analysis software may have material properties for commonly used materials stored internally; these can be used but should be verified.
 - d. Define support conditions.
 - e. Define loads applied to the non-composite structure.
 - i. For the members defined in the model, the girders and intermediate diaphragms, automatic dead load application can be used if mass density is assigned through material properties. Otherwise, concentrated or distributed loads that are statically equivalent to the weight of the members can be used.
 - ii. The other non-composite dead loads (SIP forms, haunches, deck slab) are applied as uniform line loads to each girder.
 - f. Define load cases.
 - g. Ensure correct attributes are assigned (geometric and material properties, support conditions, and non-composite dead loads) to appropriate components.
 - h. Run analysis; verify analysis results using simplified methods.
 - i. Extract required results from analysis software.
2. Create model for composite dead loads (continuation of the model created in Step 1).
- a. Define location of concrete deck slab and create appropriate surface elements (see Step 1a and Section 3.5.2.1 for more information).
 - b. Define geometry and thickness of concrete deck slab. An eccentricity is applied to the deck such that it is at the appropriate elevation relative to the other members. Some elements support offsets internally, making assigning eccentricities easier. For elements that do not support eccentricities, rigid link constraints or rigid beam elements can be used to provide the required offset.
 - c. Define material properties for concrete deck slab (See Step 1c above for more information). The stiffness is reduced by a factor of 3 for long-duration loading.
 - d. Define support conditions.
 - e. Define loads applied to the composite structure.
 - i. The FWS is defined as a uniform load distributed over an area. If possible, the load should be applied over a partial width of the bridge, representing placement between barriers. However, if the area of loading does not coincide with the model geometry and partial width loading cannot be specified, either the geometry can be modified to facilitate load application or the load should be modified such that the total applied load remains the same, though the area over which it is spread may be different.
 - ii. The weight of the barrier is defined as a uniform line load. Similar to the FWS, if the barrier load cannot be precisely located due to geometric and loading constraints, either geometry can be modified or approximations can be made.
 - f. Define load cases.

- g. Ensure correct attributes are assigned (geometric and material properties, support conditions, and loading) to appropriate components. Note that the stiffness of the concrete deck should be reduced by a factor of 3, either by adjusting the area of concrete or the modulus of elasticity of the concrete. This accounts for long-term stiffness reduction due to material behavior.
 - h. Run analysis; verify analysis results using simplified methods.
 - i. Extract required results from analysis software.
3. Create model for composite live load (continuation of the model created in Step 2).
 - a. Define material properties for concrete deck slab. Because live loading is short-duration the stiffness of the concrete deck is modified back to the normal stiffness of concrete.
 - b. Determine optimized loading. The analysis software may have utilities that help in the determination. Influence surfaces can be developed to aid in loading generation.
 - c. Run analysis with optimized loadings and verify results
 - d. Extract required results from analysis software
 4. Combine analysis results extracted in Steps 1i, 2i, and 3d.

9.2.2.1 Step 1 – Create Non-Composite Dead Load Model

9.2.2.1.1 Step 1a – Define Girder and Intermediate Cross-Frame Locations

From Figures Figure and 194, the location of the girders and cross-frames as well as the span lengths can be found. For detailed geometric information see Appendix 9.B. Beam elements used for both the girders and intermediate cross-frames are Timoshenko beam elements capable of capturing shear deformations, although the shear deformations in the girders are negligible and Euler beam elements would be acceptable as well. For the girders and cross-frame, four elements per segment is used; in some cases where the segments are short (such as between a cross-frame and a splice location), only one element is defined and used.

9.2.2.1.2 Step 1b – Define Girder and Cross-Frame Cross-Sections

Several cross-sections exist along the length of the bridge. Properties can be calculated manually (as shown in Section 9.1.1.1) and input into software, or some software has utilities that automatically calculate section properties. For this analysis, the girder cross-sections were defined using the utilities within the analysis software; the section properties used are shown in Table 36. Vertical offsets are used in Section B-B and Section C-C to correctly locate the members relative to the centroid of Section A-A.

Table 36. Girder section properties from the software.

Section Property	Section A-A	Section B-B	Section C-C
Cross-section Area (A) (ft ²)	0.649	0.783	1.167
Strong Axis Moment of Inertia (I _{yy}) (ft ⁴)	5.710	7.731	13.818
Weak Axis Moment of Inertia (I _{zz}) (ft ⁴)	0.047	0.100	0.198
Torsion Constant (J _{xx}) (ft ⁴)	0.933E-3	1.873E-3	0.012
Shear Area in y direction (A _{vy}) (ft ²)	0.250	0.384	0.767
Shear Area in z direction (A _{vz}) (ft ²)	0.408	0.411	0.422
Offset in z direction (R _z) (ft)	0.000	0.151	0.104

Because this is a straight bridge with no skew the contribution of warping stiffness from flange lateral bending is neglected and no modifications to the torsional stiffness are necessary.

9.2.2.1.2.1 Intermediate Cross-Frames

The cross-frames are composed of four members acting as a truss (a top and bottom chord and two diagonals) but in a PEB analysis, the cross-frame is represented by one member acting as a beam. The one member should represent the behavior of the actual cross-frame. Different methods exist (see Section 3.6.3 and White et al. 2012) for determining approximate equivalent section properties to represent the actual cross-frame with one member. The methods include: assume cross-frame is a pure flexure member and calculate an equivalent moment of inertia, assume cross-frame is a pure shear member and calculate an equivalent area, or assume cross-frame is somewhere between pure flexure and pure shear and approximate both the moment of inertia and the area. The model utilizes beam elements for the cross-frame members. Robust, thick beam elements (Timoshenko beam formulation), which are capable of capturing shear deformations, are used. Thin (Euler) beams could be used, but cross-frames generally exhibit substantial beam shear deformations when modeled using equivalent beam elements. Therefore, thick beams are significantly more accurate and only increase computational time a negligible amount.

In this example, it is assumed that the cross-frame is somewhere between a pure shear member and a pure flexure member. Using the method presented by White, et al in NCHRP Report 725, the flexural and shear stiffness are estimated. The first step is to assume that the cross-frame is subjected to flexure only. This is done by modeling the cross-frame as a cantilever subject to a unit force couple as shown in Figure 204.

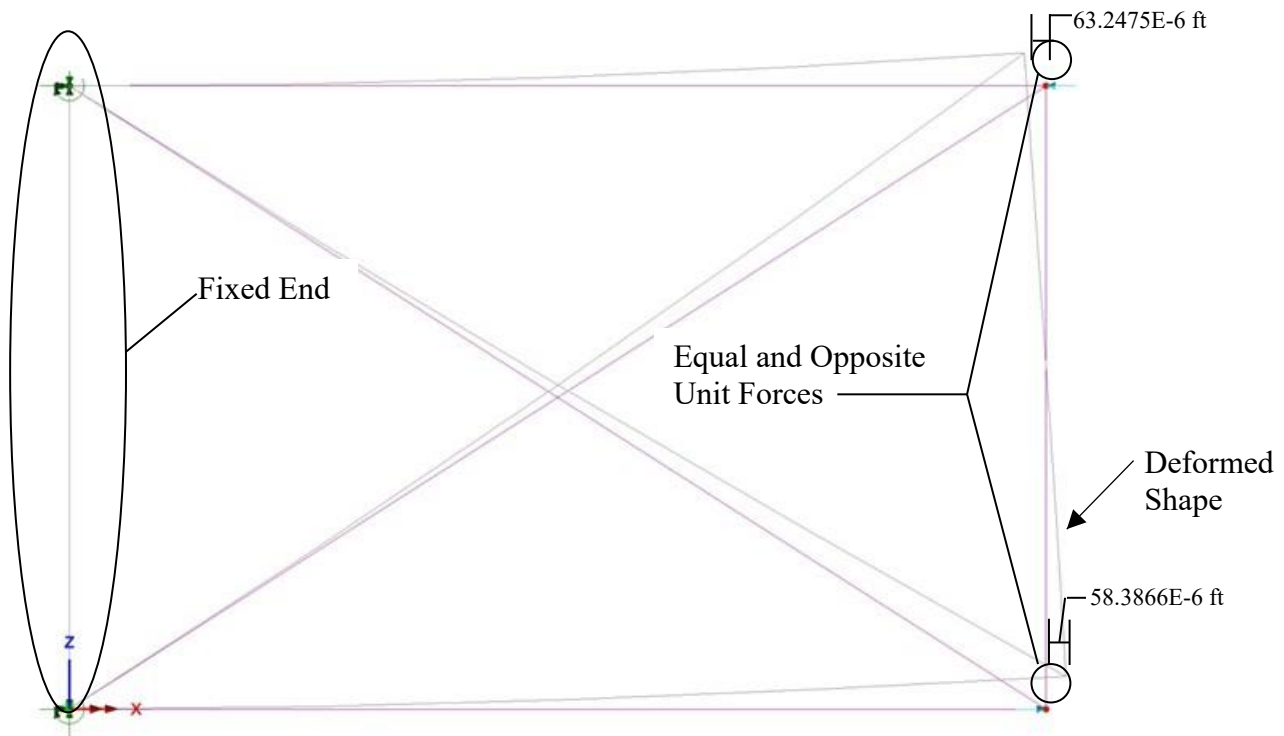


Figure 204. Illustration. Intermediate cross-frame model – flexural stiffness.

Equation (51) is used to determine the equivalent moment of inertia of the cross-frame shown in Figure 204. The rotation, θ , is calculated using the sum of the horizontal deflections (from the analysis model) divided by the height of the cross-frame; this is equal to $(63.2475E-6 + 58.3866E-6) \times 12/84 = 1.73763E-5$ radians. Substituting the values shown below into Equation (51), I_{eq} is determined to be 22004 in^4 (1.061 ft^4).

$$I_{eq} = \frac{ML}{E\theta} \quad (51)$$

where: I_{eq} = equivalent moment of inertia
 M = moment due to unit force couple = $1 \text{ k} \times 84 \text{ in} = 84 \text{ k-in}$
 L = length between girders = $11 \text{ ft-0 inches} = 132 \text{ in}$
 E = modulus of elasticity = $29,000 \text{ ksi}$
 θ = rotation due to unit force couple = $1.73763E-5$ radians

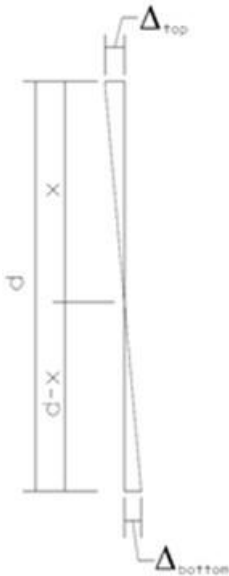
The centroid of the intermediate cross-frame can be determined using the horizontal displacements of the cross-frame ends from the analysis model created to determine the equivalent flexural properties of the cross-frame. Using the horizontal displacements and similar triangles, the centroid can be determined as shown in Table 37. Similar triangles are used to determine the centroid of the cross-frame as the section remains linear elastic.

Knowing the location of the intermediate cross-frame centroid, the vertical offset (the distance between the centroid of the girder cross-section and the centroid of the cross-frame) is determined. The cross-frame is centered vertically on the girder web; therefore the offset is

equal to the difference between the location of the centroid “x” and one-half the cross-frame depth. The offset is equal to $x - d/2 = 3.64 \text{ ft} - 7\text{ft}/2 = 0.14 \text{ ft}$ downward.

Table 37. Intermediate cross-frame centroid calculation.

$\Delta_{\text{top}} = 63.2475 \times 10^{-6} \text{ ft}$ (from analysis model)
 $\Delta_{\text{bottom}} = 58.3866 \times 10^{-6} \text{ ft}$ (from analysis model)
 $d = 7 \text{ ft}$ (distance between centroids of cross-frame chords)



Using similar triangles:

$$\frac{x}{\Delta_{\text{top}}} = \frac{d - x}{\Delta_{\text{bottom}}}$$

Solve for “x”:

$$x = \frac{\Delta_{\text{top}} \times d}{\Delta_{\text{top}} + \Delta_{\text{bottom}}}$$

Substitute in for Δ_{top} , Δ_{bottom} , and d:

$$x = \frac{(63.2475E - 6)\text{ft} \times 7\text{ft}}{(63.2475E - 6)\text{ft} + (58.3866E - 6)\text{ft}}$$

$$x = 3.64 \text{ ft}$$

The next step is to determine the equivalent shear area of the cross-frame. This is done by modeling the cross-frame as a cantilever with a unit load applied to the other end as shown in Figure 205.

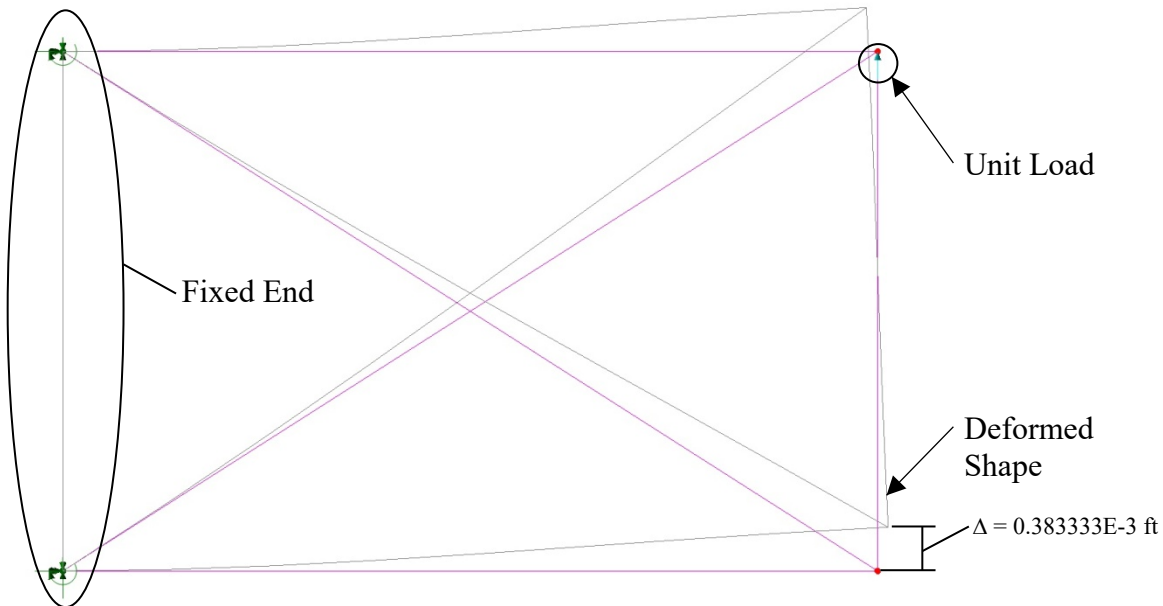


Figure 205. Illustration. Intermediate cross-frame model – shear stiffness.

The equivalent shear area is then calculated using Equation (52). Substituting in the values shown, the equivalent cross-frame shear area is 3.48 in² (0.0242 ft²).

$$A_{eq} = \frac{VL}{G \left(\Delta - \frac{VL^3}{3EI_{eq}} \right)} \quad (52)$$

where: A_{eq} = equivalent area
 Δ = deflection due to unit force = 0.0046 in.
 V = unit force = 1 k
 L = length between girders = 11 ft-0 inches = 132 in.
 E = modulus of elasticity = 29000 ksi
 I_{eq} = equivalent moment of inertia = 22004 in⁴
 G = shear modulus of elasticity = $E/[2 \times (1 + \nu)] = 29000/[2 \times (1 + 0.3)] = 11154$ ksi

The calculated values can be used to define the moment of inertia and major-axis shear area for the member representing the cross-frame. The next step is to determine the cross-sectional area (for axial stiffness). To calculate the appropriate cross-sectional area, equal (but not opposite) loads should be applied to the model and the correct area can be back-calculated from the resulting deflection. Moreover, the weight should match the actual weight of the members (including connection plates), which may require an adjustment to the unit weight of the material assigned, or application of weight as a separate load. The section properties are shown in Table 38.

To account for stiffness softening due to 2nd order effects of connections the specified modulus of elasticity is reduced to 65 percent of its actual value. Alternatively, the area could be similarly modified, but changes to the unit weight or applied load would be required. It should be noted that as long as the weight is correct, the area is only a concern in the composite models.

Table 38. Equivalent cross-frame properties.

Section Property	Value
Cross-section Area (A) (ft ²)	1.540
Strong Axis Moment of Inertia (I_{yy}) (ft ⁴)	1.061
Weak Axis Moment of Inertia (I_{zz}) (ft ⁴)	0.000
Torsion Constant (J_{xx}) (ft ⁴)	0.000
Shear Area in y direction (A_{vy}) (ft ²)	0.000
Shear Area in z direction (A_{vz}) (ft ²)	0.024
Offset in z direction (R_z) (ft)	0.140

9.2.2.1.2.2 Pier Cross-Frames

The same method used for the intermediate cross-frames above is used for the cross-frames located at the piers. For detailed calculations, refer to Appendix 9.C.

Table 39. Equivalent pier cross-frame properties.

Section Property	Value
Cross-section Area (A) (ft ²)	0.232
Strong Axis Moment of Inertia (I _{yy}) (ft ⁴)	1.323
Weak Axis Moment of Inertia (I _{zz}) (ft ⁴)	0.000
Torsion Constant (J _{xx}) (ft ⁴)	0.000
Shear Area in y direction (A _{vy}) (ft ²)	0.000
Shear Area in z direction (A _{vz}) (ft ²)	0.025
Offset in z direction (R _z) (ft)	-1.120

9.2.2.1.3 Step 1c – Define Material Properties for Girders and Cross-Frames

Material properties shown in Table 40 are specified.

Table 40. Steel material properties.

Material Property	Girder Steel	Intermediate Cross-Frame Steel	Pier Cross-Frame Steel
Modulus of Elasticity (ksf)	4,176,000	2,714,400	2,714,400
Poisson's Ratio	0.3	0.3	0.3
Unit Weight (k/ft ³)	0.490	0.074	0.490
Thermal Expansion Coefficient (ft/°F)	6.5E-6	6.5E-6	6.5E-6

9.2.2.1.4 Step 1d – Define Support Conditions

Girders are restrained vertically and transversely at all locations, and against longitudinal translation at Pier 2. Supports are modeled at the girder centroid. For dead load, modeling the supports at the girder centroid, rather than below the bottom of the girder should not have any effect on the results.

9.2.2.1.5 Step 1e – Define Non-Composite Loads

The non-composite dead loads in addition to self-weight (SIP forms, haunches, and deck slab) are applied as uniform line loads to each girder. The values previously calculated in Sections 9.2.1.3.2 through 9.2.1.3.4 for the SIP form weight, haunch weight, and deck slab weight are applied to the interior and exterior girders as uniformly distributed loads.

9.2.2.1.6 Step 1f – Define Load Cases

The next step is to define different load cases. Since all loads in this model are non-composite, they are combined into a single load case.

9.2.2.1.7 Step 1g – Ensure Correct Attributes Are Assigned to Components

After defining the geometry, member properties, material properties, support conditions, and loads, these attributes must be assigned to the appropriate geometry within the model. The elements defining the girder are assigned the properties associated with the girders and the elements defining the intermediate and pier cross-frames are assigned the properties associated

with the intermediate and pier cross-frames. Listed below are the different components and the attributes that must be assigned:

- Girders
 - Beam elements
 - Geometric cross-section
 - Girder steel material properties
 - Dead loads (including self-weight, SIP forms, haunches, and deck slab)
- Intermediate and Pier cross-frames
 - Beam elements
 - Geometric cross-section
 - Cross-frame steel material properties
 - Dead load (self-weight)

9.2.2.1.8 Step 1h – Run Analysis and Verify Results using Simplified Methods

After the analysis is run the results can be verified using a variety of simplified methods. For continuous span bridges, summing the reactions for one of the dead loads and comparing that value to the expected dead load can be used to verify that, in general, the results are correct. Additionally, if the bridge is symmetric, the dead load moments, shears, and deflections should be symmetric.

Check girder self-weight versus sum of reactions (slight variations can be expected due to rounding in hand calculations):

Area of Different Girder Cross-Sections (See Section 9.2.1.1.1):

$$\begin{aligned} A_{A-A} &= 93.50 \text{ in}^2 \\ A_{B-B} &= 112.75 \text{ in}^2 \\ A_{C-C} &= 168.00 \text{ in}^2 \end{aligned}$$

Unit Weight of Steel:

$$\gamma_s = 0.490 \text{ k/ft}$$

Weight per Linear Foot for Each Cross-Section:

$$\begin{aligned} w_{x-x} &= A \times \gamma_s / (144 \text{ in}^2/\text{ft}^2) \\ w_{A-A} &= 93.50 \text{ in}^2 \times 0.490 \text{ k/ft} / (144 \text{ in}^2/\text{ft}^2) = 0.318 \text{ k/ft} \\ w_{B-B} &= 112.75 \text{ in}^2 \times 0.490 \text{ k/ft} / (144 \text{ in}^2/\text{ft}^2) = 0.384 \text{ k/ft} \\ w_{C-C} &= 168.00 \text{ in}^2 \times 0.490 \text{ k/ft} / (144 \text{ in}^2/\text{ft}^2) = 0.572 \text{ k/ft} \end{aligned}$$

Length of Each Cross-Section (See Figure 195):

$$\begin{aligned} L_{A-A} &= 109 \text{ ft-9 inches} + 115 \text{ ft-6 inches} + 109 \text{ ft-9 inches} = 335 \text{ ft-0 inches} \\ L_{B-B} &= 24 \text{ ft-6 inches} + 21 \text{ ft-6 inches} + 21 \text{ ft-6 inches} + 24 \text{ ft-6 inches} = 92 \text{ ft-0 inches} \\ L_{C-C} &= 51 \text{ ft-6 inches} + 51 \text{ ft-6 inches} = 103 \text{ ft-0 inches} \end{aligned}$$

Total Girder Weight:

$$\begin{aligned} W &= W_{A-A} \times L_{A-A} + W_{B-B} \times L_{B-B} + W_{C-C} \times L_{C-C} \\ &= 0.318 \text{ k/ft} \times 335 \text{ ft} + 0.384 \text{ k/ft} \times 92 \text{ ft} + 0.572 \text{ k/ft} \times 103 \text{ ft} \\ &= 200.77 \text{ k} \end{aligned}$$

Reactions from Analysis Model:

$$\begin{aligned} R_1, R_4 &= 17.4467 \text{ k} \\ R_2, R_3 &= 83.0156 \text{ k} \end{aligned}$$

Sum of Reactions:

$$\begin{aligned} R &= R_1 + R_2 + R_3 + R_4 \\ &= 17.4467 \text{ k} + 83.0156 \text{ k} + 83.0156 \text{ k} + 17.4467 \text{ k} \\ &= 200.93 \text{ k} \end{aligned}$$

Compare W to R:

$$\begin{aligned} W &= 200.77 \text{ k} \\ R &= 200.93 \text{ k} \end{aligned} \quad \therefore \text{OK, model is producing reasonable results. Reactions from model are symmetric as would be expected.}$$

9.2.2.1.9 Step 1i – Extract Required Results from Analysis Software

After verifying that the results from the analysis are reasonable, the results of interest can be extracted and input into a spreadsheet for further use. It may be necessary to select only certain portions of the model to obtain the results wanted.

9.2.2.2 Step 2 – Create Composite Dead Load Model

9.2.2.2.1 Step 2a – Define Concrete Deck Slab Location

From Figures Figure and 194, the location of the girders, intermediate and pier diaphragms, concrete deck slab, barrier width as well as the span lengths can be found. Assuming that the origin is located at the left end of girder line 4 in Figure , the coordinates for the girder ends and cross-frame locations are shown in Appendix 9.B. Each girder is defined by segments that connect one cross-frame to the adjacent cross-frame; the segments are then split such that a node occurs at the tenth-points along the girder.

The coordinates for the corners of the concrete deck slab are shown in Table 41.

Table 41. Coordinates of concrete deck slab corners.

Corner	x (ft)	y (ft)	z (ft)
Upper, Left	0	36.75	0
Upper, Right	530.0	36.75	0
Lower, Right	530.0	-3.75	0
Lower, Left	0	-3.75	0

The elements defined for the girders and cross-frames in the non-composite model are also used in the composite model. Thick shell elements, a type of surface element capable of capturing shear deformations and membrane forces, are used to model the concrete deck slab.

9.2.2.2.2 Step 2b – Define Concrete Deck Slab Thickness

The composite model includes the concrete deck slab and requires the deck slab thickness and eccentricity to be defined. The deck slab thickness used in the model is the design thickness of 9 inches. The eccentricity is equal to the distance between the center of gravity of the deck slab and the center of gravity of girder Section A-A, which serves as the reference plane as shown in Figure 206. An eccentricity of 4.625 ft is applied to the deck.

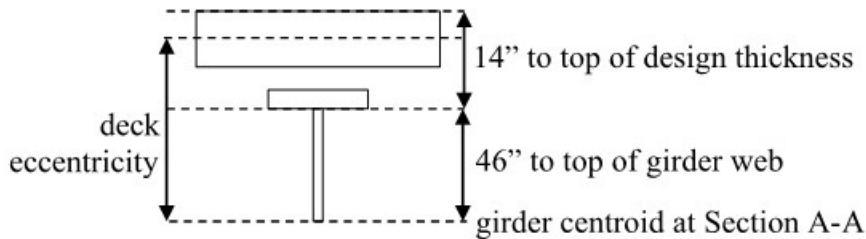


Figure 206. Illustration. Deck eccentricity.

9.2.2.2.3 Step 2c – Define Material Properties for Concrete Deck Slab

The material properties used for the girders and diaphragms in the non-composite model are also used in the composite model. Additionally, the properties for the concrete used in the deck slab are added to the model. The deck slab concrete has a 28-day compressive strength of 4 ksi. The 150 pcf unit weight is increased by the ratio of actual deck slab thickness (including wearing surface) to the modeled deck slab thickness. The modulus of elasticity is reduced by a factor of 3 for long-duration loading. Table 42 shows the material properties for the steel and concrete used in the analysis model.

Table 42. Material properties.

Material Property	Deck Slab Concrete (4 ksi)
Modulus of Elasticity (ksf)	174,919
Poisson's Ratio	0.2
Unit Weight (k/ft ³)	0.158
Thermal Expansion Coefficient (ft/°F)	6.0E-6

9.2.2.2.4 Step 2d – Define Support Conditions

The supports defined in Section 9.2.2.1.4 are also used for this model.

9.2.2.2.5 Step 2e – Define Loads Applied to Composite Structure

The future wearing surface (FWS) load is defined as a uniform load distributed over the bridge width. To account for the difference in modeled width and actual width (which spans only

between barriers), the FWS load is reduced from 0.030 ksf (spread over 37.50 ft) to 0.028 ksf (spread over 40.50 ft).

The weight of the barrier, determined above in Section 9.2.1.3.6, is applied as a uniform line load.

9.2.2.2.6 Step 2f – Define Load Cases

Separate load cases are defined for the composite dead loads; in this analysis, the composite dead loads are simply added together as moment envelopes are being compared but if the force effects were to be used in design the barrier would be a DC (component dead load) load while the future wearing surface would be a DW (wearing surface dead load) load.

9.2.2.2.7 Step 2g – Ensure Correct Attributes Are Assigned to Components

After defining the geometry and elements, member properties, material properties, support conditions, and loads, these attributes must be assigned to the appropriate geometry within the model. The lines defining the girders, intermediate cross-frames, and pier cross-frames are assigned the properties for the respective component. The concrete deck slab surfaces are assigned the properties of the deck slab.

Listed below are the different components and the attributes that must be assigned:

- Girders
 - Geometric cross-section
 - Girder steel material properties
 - Beam elements
- Intermediate and Pier Cross-Frames
 - Geometric cross-section
 - Cross-frame steel material properties
 - Beam elements
- Concrete Deck Slab
 - Deck slab thickness
 - 4 ksi concrete material properties, stiffness reduced by a factor of 3
 - Surface elements
 - FWS and barrier loading

9.2.2.2.8 Step 2h – Run Analysis and Verify Results using Simplified Methods

The analysis results can be verified using a variety of simplified methods. For continuous span bridges, moments and reactions can be calculated using equations available in textbooks for uniform loads. Additionally, for uniform loads applied to the entire structure, the total applied load applied can be calculated and should equal the sum of the reactions from the analysis model.

Check reactions for FWS load versus applied load:

Weight of FWS = 0.028 ksf

Area over which FWS applied = 40 ft-6 inches × 530 ft-0 inches = 21465 ft²

Total Weight of FWS = 0.028 ksf × 21465 ft² = 601.02 k

Reactions from Model:

Location	Line 1	Line 2	Line 3	Line 4	Total
Abutment 1	15.118	16.245	16.245	15.118	62.726
Pier 1	53.606	65.286	65.286	53.606	237.784
Pier 2	53.606	65.286	65.286	53.606	237.784
Abutment 2	15.118	16.245	16.245	15.118	62.726
				Total	601.020

The calculated total weight is equal to the sum of the reactions from the model. Additionally, since the structure is symmetric the reactions should also be symmetric. The reactions are symmetric as would be expected.

9.2.2.2.9 Step 2i – Extract Required Results from Analysis Software

After verifying that the results from the analysis are reasonable, the results of interest can be extracted and input into a spreadsheet for further use. It may be necessary to select only certain portions of the model to obtain the results wanted.

9.2.2.3 Step 3 – Create Live Load Model

This is a continuation of the model created in Step 2.

9.2.2.3.1 Step 3a – Define Material Properties for Concrete Deck Slab

The only change that needs to be made between this model and the previous one is that the normal modulus of elasticity of concrete should be used. Since live load is a short-duration load, no reduction of stiffness is necessary. Table 43 shows the properties of the concrete used in this model.

Table 43. Deck slab concrete material properties

Material Property	Deck Slab Concrete (4 ksi)
Modulus of Elasticity (ksf)	524,757
Poisson's Ratio	0.2
Unit Weight (k/ft ³)	0.158
Thermal Expansion Coefficient (ft/°F)	6.0E-6

9.2.2.3.2 Step 3b – Determine Optimized Live Load

To illustrate results from another method, a different process of live load optimization than the one in Example 1 is used. First, the AASHTO Design Truck, Design Tandem, Design Lane, and Design Truck Train loads are defined. Each of the loads is then moved through predefined paths representing design lanes along the bridge. This step is an automation of what could be done alternatively over a number of individual static steps, in which trucks are systematically placed at

various locations on the bridge and the effects at each point are observed. Ultimately, live load configurations which cause critical effects are determined in post-processing and envelopes of those critical effects can be made. The inclusion of multiple presence factors is manually included when determining force envelopes in spreadsheets outside of the analysis programs. Depending on the software used other methods may need to be applied, or may be able to be applied with greater efficiency.

9.2.2.3.3 Step 3c – Run Analysis and Verify Results using Simplified Methods

After the optimized loadings for each location of interest have been determined, the analysis can be performed. The results can be verified using simplified methods. As an example, the results are verified by summing the reactions and comparing to the total applied load. In this load case two HL-93 Design Trucks are applied (lane load applied separately), each truck weighs 72 k (impact is included in post-processing) resulting in a total applied load of 144 k.

Reactions from Model:

Location	Girder Line 1	Girder Line 2	Girder Line 3	Girder Line 4	Total
Abutment 1	0.315	0.671	0.928	1.486	3.408
Pier 1	-1.557	-3.878	-6.592	-8.579	-20.606
Pier 2	3.049	18.721	43.299	50.852	115.922
Abutment 2	-1.030	8.875	14.559	22.880	45.284
				Total	144.000

The total applied load and the sum of the reactions are equal. The reactions along girder line 4 are greater than those along the other girder lines; this is expected since this load case was to determine the maximum moment in the exterior girder. The reactions are not expected to be symmetric as the loading is not symmetric. Therefore, the model appears to be providing reasonable results.

9.2.2.3.4 Step 3d – Extract Required Results from Analysis Software

After verifying that the results from the analysis are reasonable, the results of interest can be extracted and input into a spreadsheet for further use. It may be necessary to select only certain portions of the model to obtain the results wanted.

9.2.2.4 Step 4 – Combine Analysis Results

Once the results of interest, in this case moments, shears, and deflections, have been extracted from the analysis software, they will most likely be combined into groups of non-composite dead loads, composite dead loads, and live loads.

Additionally, for a PEB model, the moment due to composite dead load and live load in the girder is not just the girder moment in the results. Due to the eccentricity between the deck slab and beam, the actual moment in the girder is equal to the moment plus the axial force times the girder eccentricity. Refer to previous sections for example calculations.

The HL-93 Design Load consists of the maximum of the design truck or design tandem amplified by the dynamic load allowance plus the design lane. Each load component was analyzed individually therefore the results must be combined. Similarly, for negative moment between dead load inflection points, the design truck train including the dynamic load allowance and design lane must be combined. Additionally, the results from the different live load models may have to be combined to determine the greatest live load force effect for each girder. Also for live load, the multiple presence factor in Table 3.6.1.1.2-1 of the Specifications must be applied.

Once the moments, shears, and deflections have been combined into appropriate groups using the results from the various analyses, graphs can be created to show the moment and shear diagrams, and deflected shape. The analysis results are combined using the same groups as for the 1D analysis: non-composite dead loads (girder self-weight, diaphragms, SIP forms, haunches, and concrete deck slab), composite dead loads (barrier and FWS), and maximum and minimum live loads including the dynamic load allowance. The moment, shear, and deflection diagrams from the PEB analysis are shown in Figures 207 through 212.

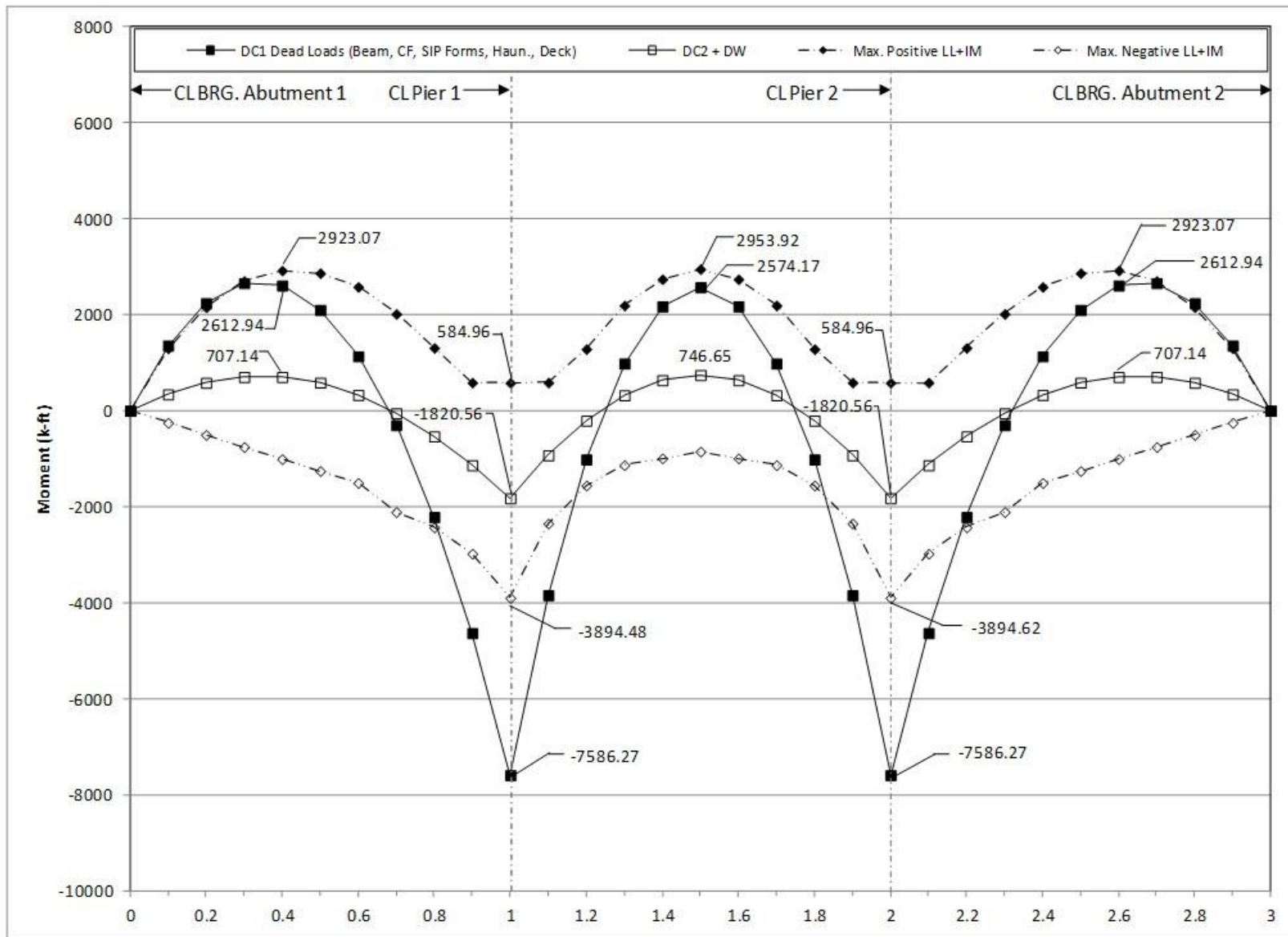


Figure 207. Graph. 2D moment diagram and live load envelope for interior girder.

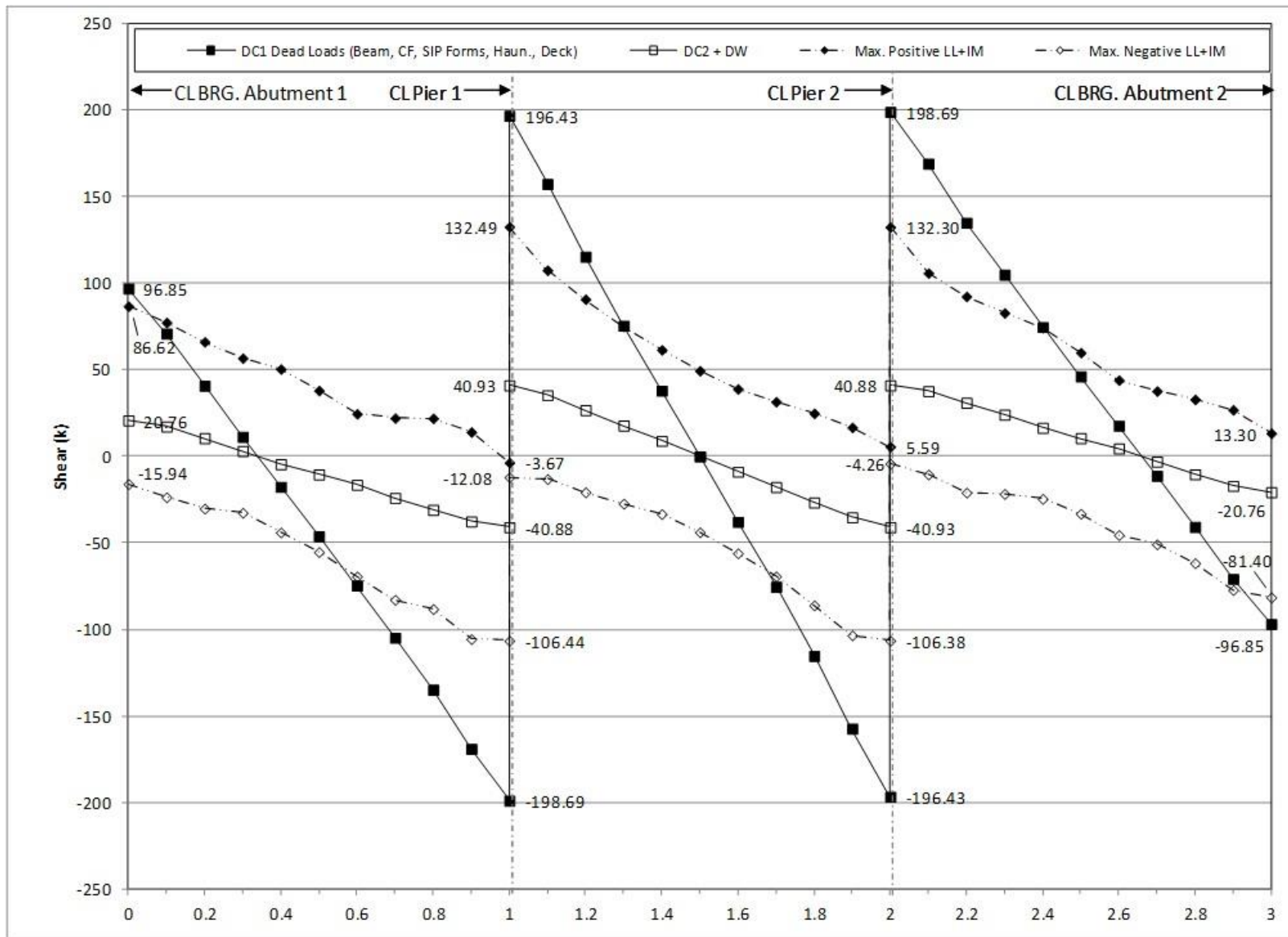


Figure 208. Graph. 2D shear diagram and live load envelope for interior girder.

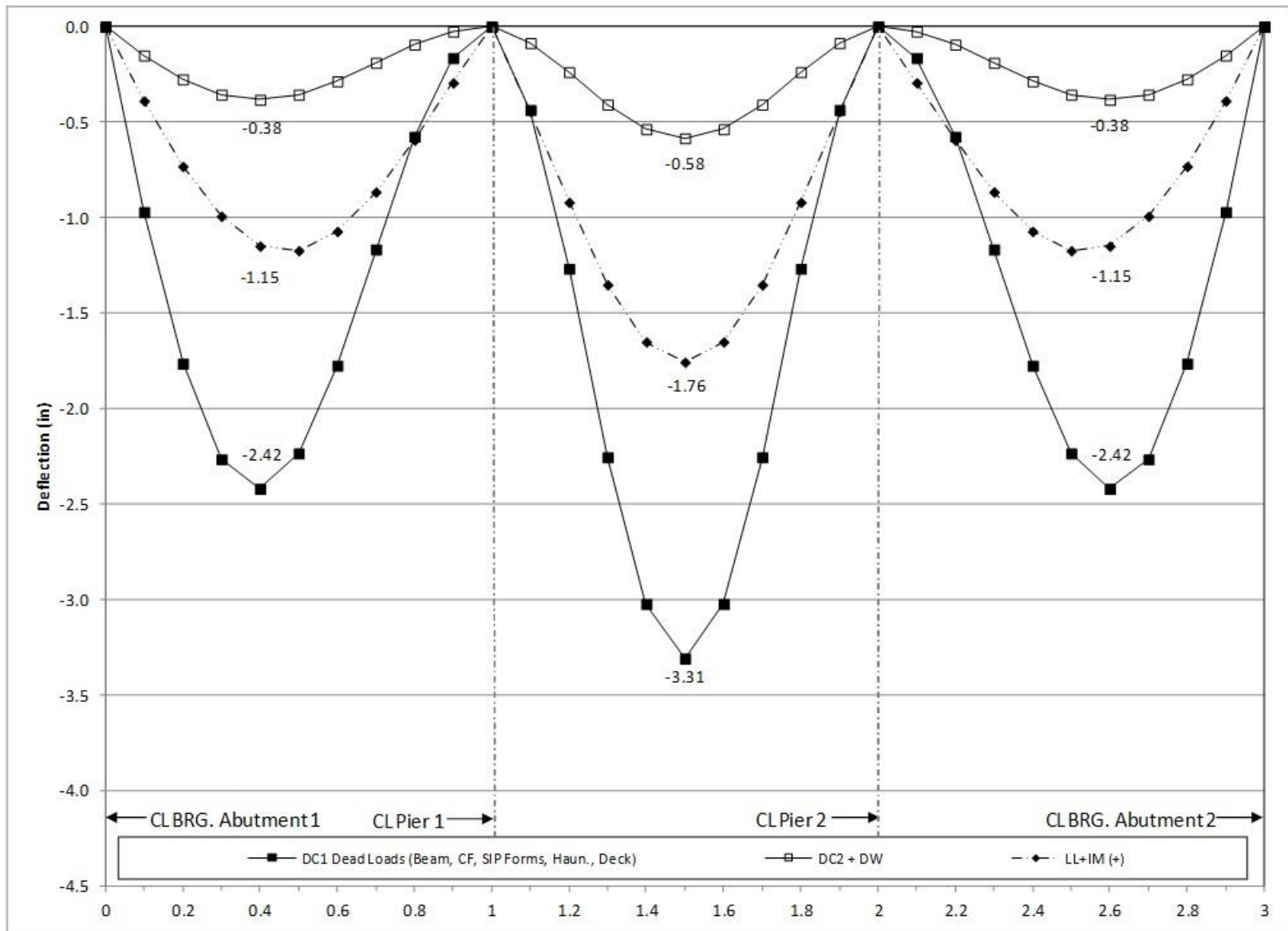


Figure 209. Graph. 2D deflection diagram for interior girder.

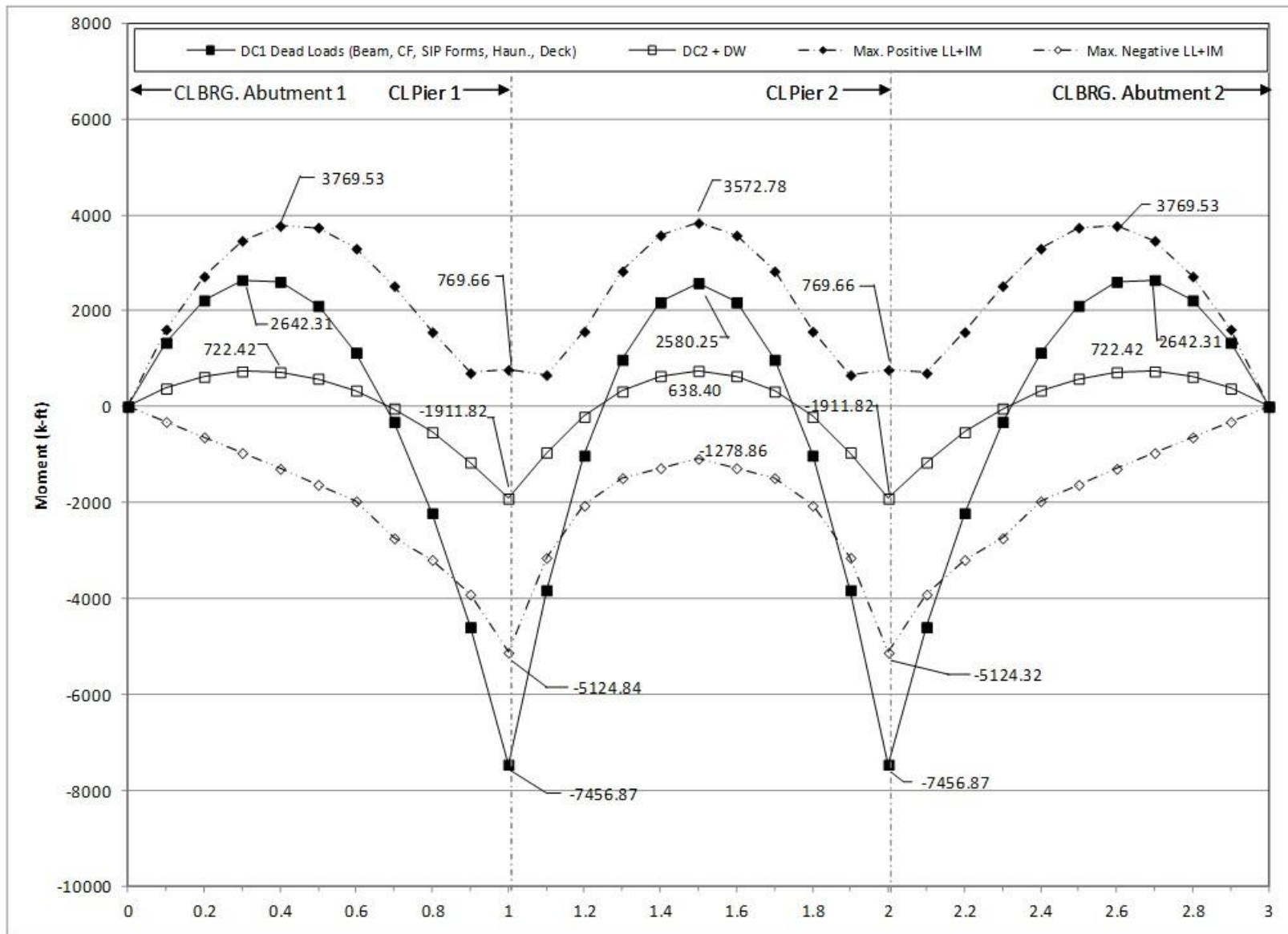


Figure 210. Graph. 2D moment diagram and live load envelope for exterior girder.

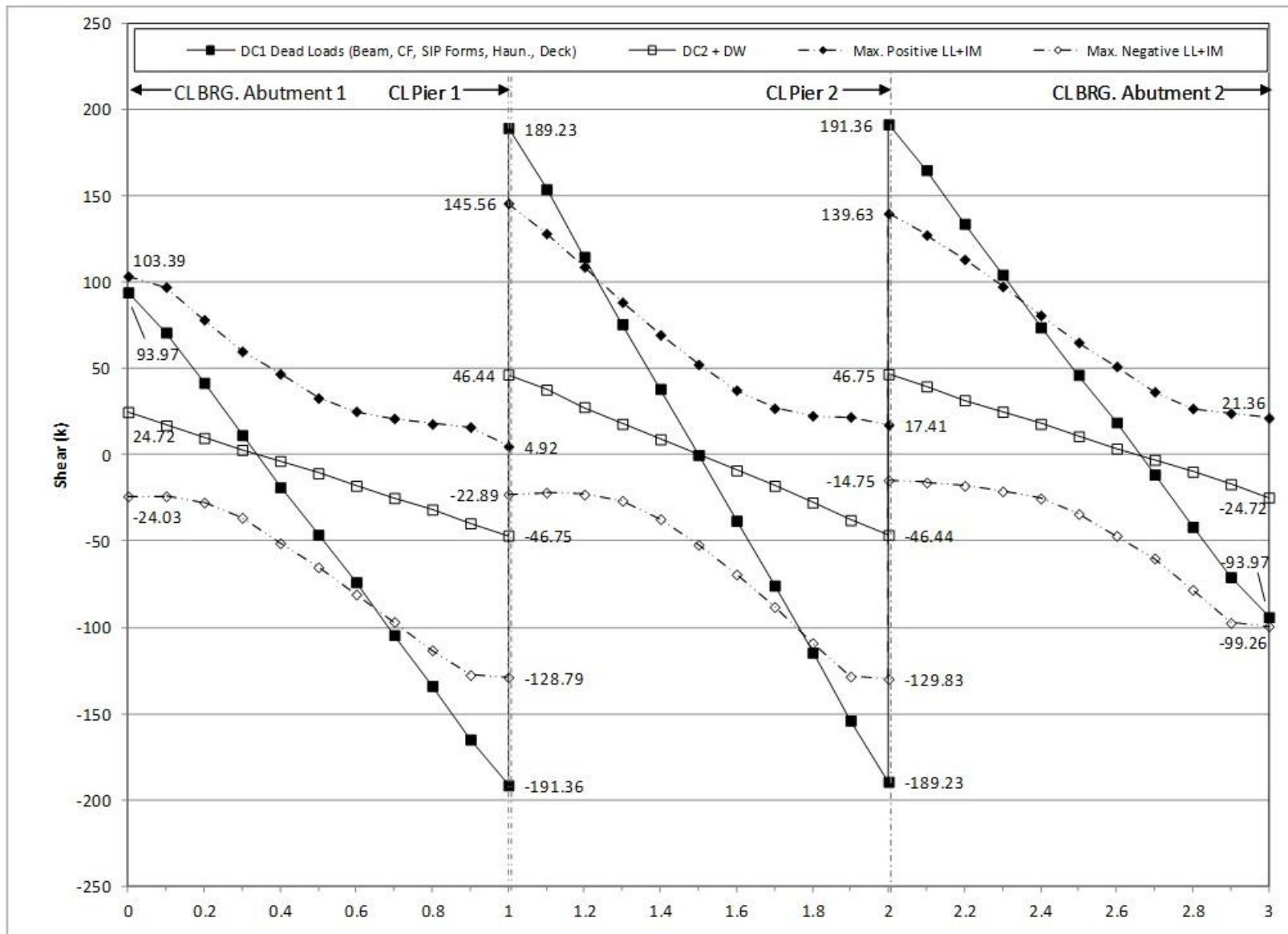


Figure 211. Graph. 2D shear diagram and live load envelope for exterior girder.

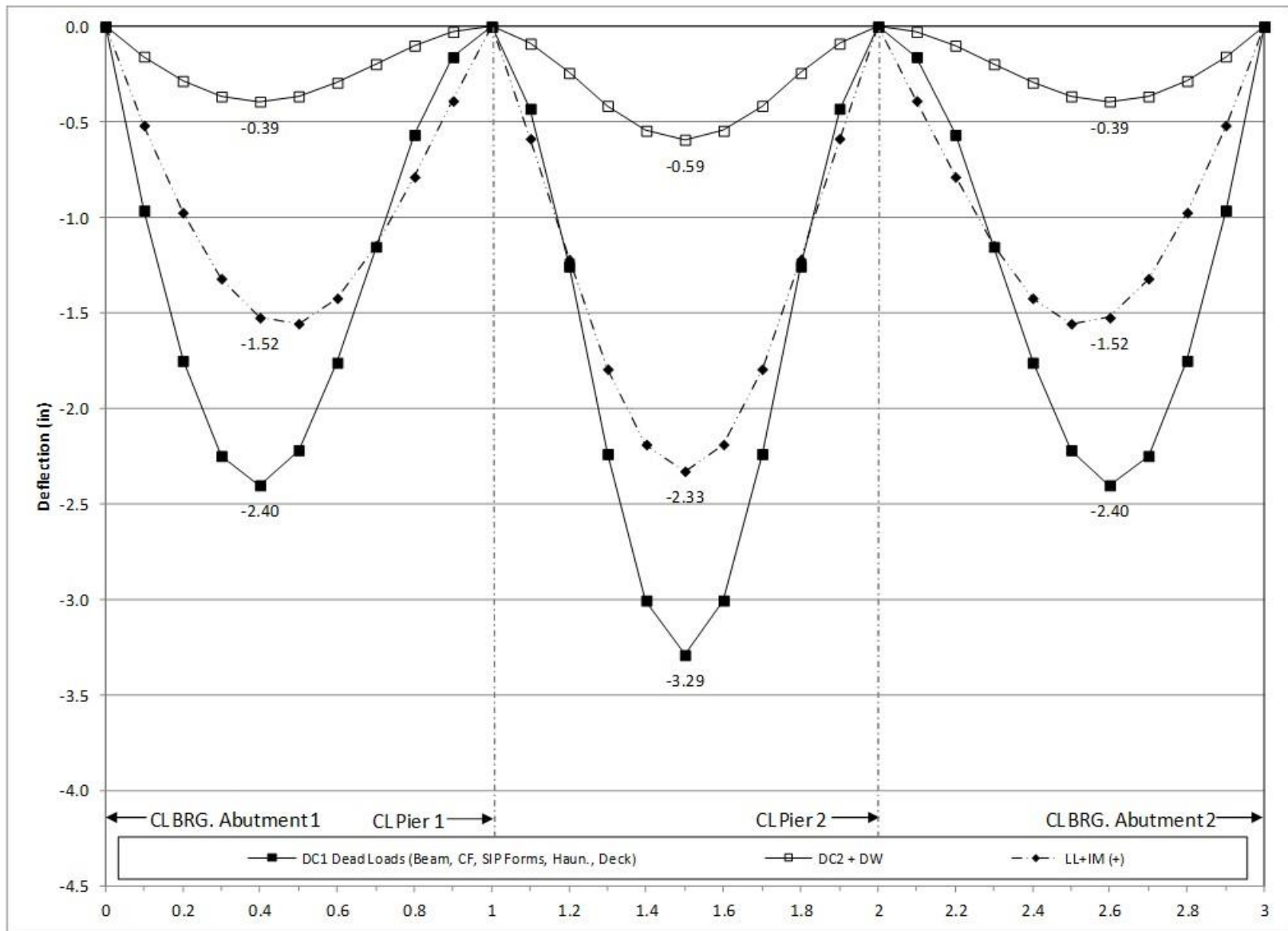


Figure 212. Graph. 2D deflection diagram for exterior girder.

9.2.3 3D Finite Element Analysis

Increasing the degree of complexity from the previous example, a full 3D FEA is presented. In a 3D FEA, the structure depth is modeled unlike the PEB analysis where it is assumed that all components lie on the same plane (prior to applying eccentricities). Modeling the structure depth results in the support conditions being at the actual physical location (i.e. the bottom of the girder) not at the girder centroid. The stiffness of the girders and cross-frames are used to distribute non-composite loads and the stiffness of the girders, cross-frames, and deck slab are used to distribute composite dead loads and live loads. The approximate distribution factors in AASHTO LRFD Article 4.6.2.2 are not used.

The following steps are used to determine the dead and live load bending moments, shears, and deflections:

1. Create non-composite dead load model.
 - a. Create geometry for girders and cross-frames. Flanges of girders and cross-frames are modeled with beam elements, the girder webs with surface elements. Further guidance on modeling these members and discretizing them into an appropriate number of elements is provided in Section 3.6.
 - b. Define section properties for those components modeled with beam elements and thicknesses of those with surface elements.
 - c. Define material properties for girders and cross-frames.
 - d. Define support conditions.
 - e. Define loads applied to the non-composite structure.
 - i. For the members defined in the model, the girders and intermediate cross-frames, automatic dead load application can be used if mass density is assigned through material properties. Otherwise, concentrated or distributed loads that are statically equivalent to the weight of the members can be used.
 - ii. The other non-composite dead loads (SIP forms, haunches, deck slab) are applied as uniform line loads to each girder.
 - f. Define non-composite load cases.
 - g. Ensure correct attributes are assigned (geometric and material properties, support conditions, and non-composite dead loads) to appropriate components.
 - h. Run analysis; verify analysis results using simplified methods.
 - i. Extract required results from analysis software.
2. Create model for composite dead loads (a continuation of the model created in Step 1).
 - a. Define geometry for concrete deck slab. Similarly to Section 9.2.2, the concrete deck slab is modeled with surface elements.
 - b. Define thickness of concrete deck slab.
 - c. Define material properties for concrete deck slab.
 - d. Define support conditions.
 - e. Define loads applied to the composite structure.
 - i. The FWS is defined as a uniform load distributed over an area.
 - ii. The weight of the barrier is defined as a uniform line load.
 - f. Define load cases for composite dead loads.

- g. Ensure correct attributes are assigned (geometric and material properties, support conditions, and loading) to appropriate components.
 - h. Run analysis; verify analysis results using simplified methods.
 - i. Extract required results from analysis software.
3. Create model for live loads (continuation of the model created in Step 2).
 - a. Define material properties for concrete deck slab. Because live loading is short-duration the stiffness of the concrete deck is modified back to the normal stiffness of concrete.
 - b. Determine optimized loading. The analysis software may have utilities that help in the determination. Influence surfaces can be developed to aid in loading generation.
 - c. Run analysis with optimized loadings and verify results
 - d. Extract required results from analysis software
 4. Combine analysis results extracted in Steps 1i, 2i, and 3d.

9.2.3.1 Step 1 – Create Non-Composite Dead Load Model

9.2.3.1.1 Step 1a – Create Geometry for Girders and Cross-Frames

The girder geometry is defined by creating surface elements along the girder centerline. These elements represent the girder webs, while beam elements are used to represent the girder flanges at the top and bottom of the web. To accommodate modeling of the cross-frames and cross-section changes, the girder is divided into segments evenly divisible by the distance between cross-frames or equal to the distance between a cross-frame and a cross-section change. The cross-frame members are located by creating lines between the two girders at that location. For simplicity, in this example the cross-frame members are assumed to connect at the flange-web intersection, while in actuality, they connect several inches from the flange-web intersection. It is up to the analyst to determine if modeling the cross-frames in their exact locations is necessary for any given design. Thick shell elements are used for the surface elements and thick (Timoshenko) beam elements are used for the beam elements. Both of these element types are capable of capturing shear deformations.

Figure 213 shows the non-composite geometry for the 3D finite element model visualized in three dimensions.

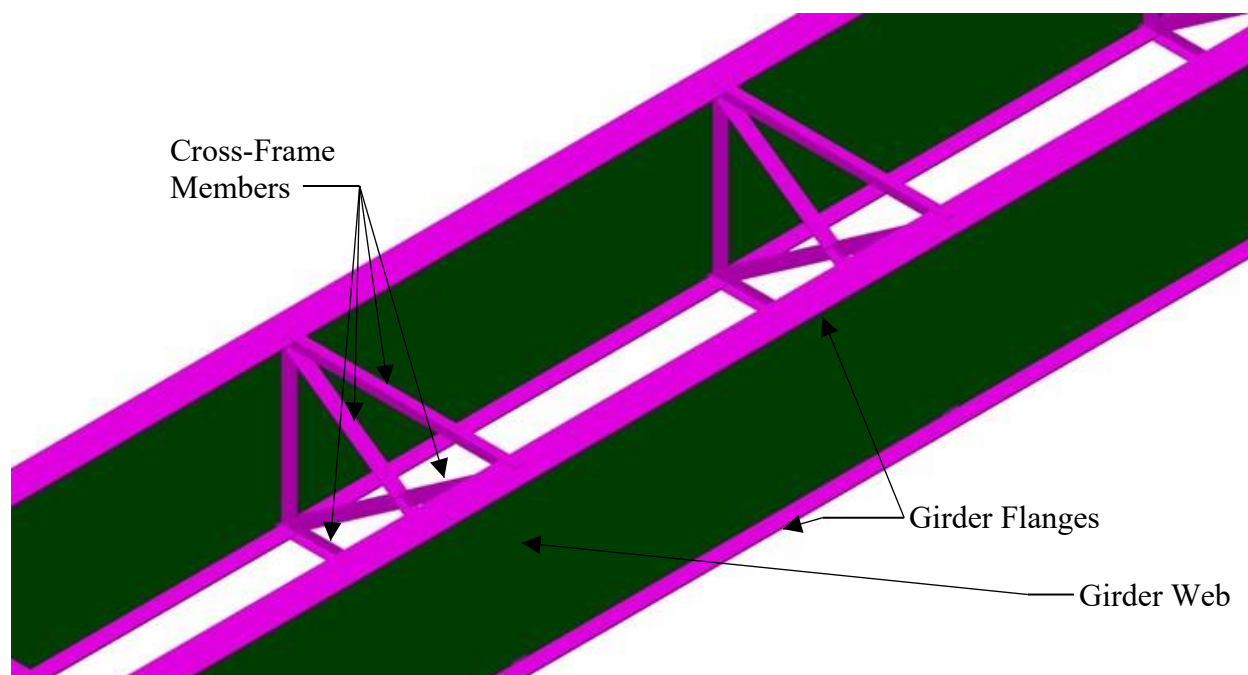


Figure 213. Illustration. 3D non-composite geometry visualized.

9.2.3.1.2 Step 1b – Define Cross-Section Properties

The thickness of the girder web is defined as 5/8 inches. The different flange plate properties are shown in Table 44. Offsets are given with respect to where each flange is connected, at the top and bottom of the girder web.

Table 44. Girder flange properties.

	Section A-A		Section B-B		Section C-C	
	Top Flange	Bottom Flange	Top Flange	Bottom Flange	Top Flange	Bottom Flange
Cross-Section Area (A) (ft ²)	0.125	0.125	0.174	0.210	0.347	0.420
Moment of Inertia (I _x) (ft ⁴)	72.34E-6	72.34E-6	0.157E-3	0.230E-3	1.256E-3	1.839E-3
Moment of Inertia (I _y) (ft ⁴)	0.0234	0.0234	0.040	0.059	0.080	0.118
Torsion Constant (J) (ft ⁴)	0.279E-3	0.279E-3	0.603E-3	0.883E-3	4.628E-3	6.776E-3
Shear Area (A _{vx}) (ft ²)	0.104	0.104	0.145	0.175	0.289	0.350
Shear Area (A _{vy}) (ft ²)	0.104	0.104	0.145	0.175	0.289	0.350
Offset in z direction (R _z) (ft)	-0.042	0.042	-0.052	0.057	-0.104	0.099

The cross-frame members are angles and WT shapes as indicated in Figure 194. The section properties are shown below in Table 45. To account for stiffness softening due to 2nd order effects of connections the modulus of elasticity will be reduced to 65 percent of its actual value. Alternatively, the area specified for cross-frame members could be similarly reduced, along with modification of the unit weight or applied loading.

Table 45. Cross-frame member section properties.

	Abutment/Pier Cross-Frames		Intermediate Cross-Frames	
	L5x5x5/8	L8x8x3/4	WT6x22.5	L5x5x5/8
Cross-Section Area (A) (ft ²)	0.041	0.079	0.046	0.041
Moment of Inertia (I _x) (ft ⁴)	0.656E-3	3.361E-3	0.801E-3	0.656E-3
Moment of Inertia (I _y) (ft ⁴)	0.656E-3	3.361E-3	1.206E-3	0.656E-3
Polar Moment of Inertia (ft ⁴)	0.385E-3	1.995E-3	0.000	0.385E-3
Torsion Constant (J) (ft ⁴)	38.680E-6	0.108E-3	31.640E-6	38.680E-6
Shear Area (A _{vx}) (ft ²)	0.022	0.042	0.032	0.022
Shear Area (A _{vy}) (ft ²)	0.022	0.042	0.014	0.022
Offset in z direction (R _z) (ft)	0.000	0.000	0.000	0.000

9.2.3.1.3 Step 1c – Define Material Properties for Girders and Cross-Frames

For the non-composite stage, all material is structural steel, however, as previously stated the cross-frame modulus is reduced to account for softening due to secondary effects. The material properties are shown in Table 46.

Table 46. Steel material properties.

Material Property	Girder Steel	Cross-Frame Steel
Modulus of Elasticity (ksf)	4,176,000	2,714,400
Poisson's Ratio	0.3	0.3
Unit Weight (k/ft ³)	0.490	0.490
Thermal Expansion Coefficient (ft/°F)	6.5E-6	6.5E-6

9.2.3.1.4 Step 1d – Define Support Conditions

The same support conditions as the 2D model (Section 9.2.2.1.4) are used in this model, but are located at the actual elevation along the bottom flange.

9.2.3.1.5 Step 1e – Define Non-Composite Dead Loads

Self-weight of the members is applied through the use of a body force.

The weight of the non-composite loads due to the SIP forms, haunches, and deck slab were calculated in Sections 9.2.1.3.2 through 9.2.1.3.4. The non-composite loads are defined as uniform line loads with the magnitude calculated previously specified.

9.2.3.1.6 Step 1f – Define Load Cases

The next step is to define load cases. Since all loads in this model are non-composite, they are combined into a single load case. If the results of this example were used for design, the loads could still be combined into a single load case because they carry the same load factors. In Section 9.2.3.1.8, the results are verified using a simplified method. To facilitate checking of the model it may be desirable to create a separate load case containing only one of the loads (e.g. girder self-weight or stay-in-place forms).

9.2.3.1.7 Step 1g – Ensure Correct Attributes Are Assigned to Components

The attributes assigned to each of the different components as shown below:

- Girders
 - Web
 - Geometric surface cross-section
 - Girder steel material properties
 - Thick shell surface elements
 - Dead load (self-weight)
 - Flanges
 - Flange cross-section
 - Girder steel material properties
 - Thick beam elements
 - Dead load (self-weight)
 - Other non-composite dead loads (to top edge only)
- Intermediate and Pier Cross-Frames
 - Geometric cross-section
 - Cross-frame steel material properties
 - Thick beam elements
 - Dead load (self-weight)

9.2.3.1.8 Step 1h – Run Analysis and Verify Results using Simplified Methods

The analysis results can be verified using a variety of simplified methods. For continuous span bridges, summing the reactions for one of the dead loads and comparing that value to the expected dead load can be used to verify that, in general, the results are correct. Additionally, if the bridge is symmetric, dead load moments, shears, and deflections should also be symmetric. Slight variation in symmetry is expected due to the supports not being symmetric.

Check girder self-weight versus sum of reactions (slight variations can be expected due to rounding in hand calculations):

Area of Different Girder Cross-Sections (See Section 9.2.1.1.1):

$$\begin{aligned}A_{A-A} &= 93.50 \text{ in}^2 \\A_{B-B} &= 112.75 \text{ in}^2 \\A_{C-C} &= 168.00 \text{ in}^2\end{aligned}$$

Unit Weight of Steel:

$$\gamma_s = 0.490 \text{ k/ft}^3$$

Weight per Linear Foot for Each Cross-Section:

$$w_{x-x} = A \times \gamma_s / (144 \text{ in}^2/\text{ft}^2)$$

$$w_{A-A} = 93.50 \text{ in}^2 \times 0.490 \text{ k/ft} / (144 \text{ in}^2/\text{ft}^2) = 0.318 \text{ k/ft}$$

$$w_{B-B} = 112.75 \text{ in}^2 \times 0.490 \text{ k/ft} / (144 \text{ in}^2/\text{ft}^2) = 0.384 \text{ k/ft}$$

$$w_{C-C} = 168.00 \text{ in}^2 \times 0.490 \text{ k/ft} / (144 \text{ in}^2/\text{ft}^2) = 0.572 \text{ k/ft}$$

Length of Each Cross-Section (See Figure 195):

$$L_{A-A} = 109 \text{ ft-9 inches} + 115 \text{ ft-6 inches} + 109 \text{ ft-9 inches} = 335 \text{ ft-0 inches}$$

$$L_{B-B} = 24 \text{ ft-6 inches} + 21 \text{ ft-6 inches} + 21 \text{ ft-6 inches} + 24 \text{ ft-6 inches} = 92 \text{ ft-0 inches}$$

$$L_{C-C} = 51 \text{ ft-6 inches} + 51 \text{ ft-6 inches} = 103 \text{ ft-0 inches}$$

Weight of Stiffeners

$$h = 92 \text{ in}$$

$$b = 8.5 \text{ in}$$

$$t = 0.625 \text{ in}$$

$$V = b \times h \times t$$

$$= 8.5 \text{ in} \times 92 \text{ in} \times 0.625 \text{ in} = 488.75 \text{ in}^3 = 0.283 \text{ ft}^3$$

$$w_{\text{stiff}} = V \times \gamma_s = 0.283 \text{ ft}^3 \times 0.490 \text{ k/ft}^3 = 0.139 \text{ k}$$

Total Exterior Girder Weight:

$$\begin{aligned} W_{\text{ext}} &= w_{A-A} \times L_{A-A} + w_{B-B} \times L_{B-B} + w_{C-C} \times L_{C-C} + N \times w_{\text{stiff}} \\ &= 0.318 \text{ k/ft} \times 335 \text{ ft} + 0.384 \text{ k/ft} \times 92 \text{ ft} + 0.572 \text{ k/ft} \times 103 \text{ ft} + 31 \times 0.139 \\ &= 205.08 \text{ k} \end{aligned}$$

Total Interior Girder Weight:

$$\begin{aligned} W_{\text{int}} &= w_{A-A} \times L_{A-A} + w_{B-B} \times L_{B-B} + w_{C-C} \times L_{C-C} + N \times w_{\text{stiff}} \\ &= 0.318 \text{ k/ft} \times 335 \text{ ft} + 0.384 \text{ k/ft} \times 92 \text{ ft} + 0.572 \text{ k/ft} \times 103 \text{ ft} + 54 \times 0.139 \\ &= 208.26 \text{ k} \end{aligned}$$

Total Girder Weight:

$$\begin{aligned} W &= 2 \times W_{\text{ext}} + 2 \times W_{\text{int}} \\ &= 2 \times 205.08 \text{ k} + 2 \times 208.26 \text{ k} \\ &= 826.68 \text{ k} \end{aligned}$$

Reactions (in kips) from Analysis Model:

	Girder 1	Girder 2	Girder 3	Girder 4
Abut. 1	18.221	18.338	18.407	18.467
Pier 1	85.700	85.070	83.943	85.595
Pier 2	85.026	85.341	85.413	85.241
Abut. 2	18.282	18.309	18.301	18.258
	207.23	207.06	206.064	207.561

Sum of Reactions:

$$\begin{aligned}
 R &= R_1 + R_2 + R_3 + R_4 \\
 &= 207.229 \text{ k} + 207.058 \text{ k} + 206.064 \text{ k} + 207.561 \text{ k} \\
 &= 827.912 \text{ k}
 \end{aligned}$$

Compare W to R:

$$\begin{aligned}
 W &= 826.680 \text{ k} \\
 R &= 827.912 \text{ k} \quad \therefore \text{OK, model is producing reasonable results.}
 \end{aligned}$$

Additional checks are made for the girder self-weight moment at an interior support and at midspan for the center span. To facilitate easier calculations, an average lineal weight of 0.370 k/ft is used. Table A3.3 from AISC Moments, Shears and Reactions for Continuous Highway Bridges is used.

For the moment over the interior support:

$$M = -0.1355wL^2 = (-0.1355)(0.370 \text{ k/ft})(160 \text{ ft})^2 = \mathbf{-1283.46 \text{ k-ft}}$$

For the midspan moment in the center span:

$$M = 0.0758wL^2 = (0.0758)(0.370 \text{ k/ft})(160 \text{ ft})^2 = \mathbf{717.98 \text{ k-ft}}$$

From the model the moments at the interior support and at midspan of the center span were determined to be **-1429.41 k-ft** and **461.42 k-ft**, respectively. Considering the analysis model has a more accurate weight and stiffness distribution it is unsurprising that the heavier, stiffer sections at and adjacent to piers result in larger negative moments and smaller positive moments than the values calculated using a uniformly distributed weight and equal stiffness. Therefore, though the moments are significantly different, the results, for which the total static moments are within 6 percent, are reasonable.

9.2.3.1.9 Step 1i – Extract Required Results from Analysis Software

After verifying that the results from the analysis are reasonable, the results of interest can be extracted and input into a spreadsheet for further use. Since both shell and beam elements are utilized in this model, moments (and shears) are not readily available as the shell element results are stresses not forces. The analysis software will typically have a numerical integration utility capable of determining the force effects (moments and shears) at a given cross-section which can be used to obtain force effects for design. It may be necessary to select only certain portions of the model to obtain the results wanted.

9.2.3.2 Step 2 – Create Composite Dead Load Model

9.2.3.2.1 Step 2a – Create Geometry for the Concrete Deck Slab

Continuing the development of the model created in Step 1, the geometry for the girders and cross-frames have already been defined but the concrete deck slab geometry must still be defined. The deck slab surface elements are defined using the points along the top edges of the previously defined girder webs. The deck slab geometry in the 3D finite element analysis is similar to that used in Section 9.1.3.2.1 for the PEB analysis. Shell elements are used to model the deck slab. Elements that include through-thickness shear deformation can be used, although the increase in accuracy is not significant.

9.2.3.2.2 Step 2b – Create Geometric Sections for the Concrete Deck Slab

The geometric sections required for the girders and cross-frames are shown in Section 9.2.3.1.2. The only property required is the deck slab thickness, which is defined as the structural thickness of 9 inches. For the composite dead load model, the modulus of elasticity is reduced by a factor of 3 to account for the effective modular ratio.

9.2.3.2.3 Step 2c – Define Material Properties for Steel and Concrete

The material properties for the structural steel were previously defined in Section 9.2.3.1.3. The concrete is assumed to have a compressive strength of 4 ksi and is defined using the material properties library in the analysis software. The concrete material properties are shown in Table 47.

Table 47. Concrete material properties.

Material Property	Concrete
Modulus of Elasticity (ksf)	174,720
Poisson's Ratio	0.2
Unit Weight (k/ft ³)	0.158
Thermal Expansion Coefficient (ft/°F)	6.0E-6

9.2.3.2.4 Step 2d – Define Support Conditions

The support conditions for the composite model are the same as those used for the non-composite model. See Section 9.2.3.1.4 for more information.

9.2.3.2.5 Step 2e – Define Composite Dead Loads

The future wearing surface (FWS) load is defined as a uniform load distributed over the bridge width. To account for the difference in modeled width and actual width (which spans only between barriers), the FWS load is reduced from 0.030 ksf (spread over 37.50 ft) to 0.028 ksf (spread over 40.50 ft).

The weight of the barrier is applied as a uniform line load of 0.400 k/ft.

9.2.3.2.6 Step 2f – Define Load Cases

Separate load cases are defined for the composite dead loads; in this analysis, the composite dead loads are simply added together as moment envelopes are being compared but if the force effects were to be used in design, as would typically be the case, the barrier would be a DC (component dead load) load while the future wearing surface would be a DW (wearing surface dead load) load.

9.2.3.2.7 Step 2g – Ensure Correct Attributes Are Assigned to Components

After defining the geometry and elements, member properties, material properties, support conditions, and loads, these attributes must be assigned to the appropriate geometry within the model. The lines defining the girders, intermediate cross-frames, and pier cross-frames are assigned the properties for the respective component. The concrete deck slab surfaces are assigned the properties of the deck slab. Listed below are the different components and the attributes that must be assigned:

- Girders
 - Web
 - Geometric surface cross-section
 - Girder steel material properties
 - Thick shell surface elements
 - Flanges
 - Flange cross-section
 - Girder steel material properties
 - Thick beam elements
- Intermediate and Pier Cross-Frames
 - Geometric cross-section
 - Cross-frame steel material properties
 - Beam elements
- Concrete Deck Slab
 - Deck slab thickness
 - 4 ksi concrete material properties, stiffness reduced by a factor of 3
 - Surface elements
 - FWS and barrier loading

9.2.3.2.8 Step 2h – Run Analysis and Verify Results with Simplified Methods

The analysis results can be verified using a variety of simplified methods. For continuous span bridges, summing the reactions for one of the dead loads and comparing that value to the expected dead load can be used to verify that, in general, the results are correct. Additionally, if the bridge is symmetric, dead load moments, shears, and deflections should also be symmetric.

The results are verified by summing the reactions for the future wearing surface as well as for one case where the entire design truck is on the bridge:

Check reactions for FWS load versus applied load:

Weight of FWS = 0.028 ksf

Area over which FWS applied = 40 ft-6 inches × 530 ft-0 inches = 21465 ft²

Total Weight of FWS = 0.028 ksf × 21465 ft² = 601.02 k

Reactions from Model:

Location	Line 1	Line 2	Line 3	Line 4	Total
Abutment 1	14.826	16.606	16.642	15.003	63.077
Pier 1	55.351	63.618	63.284	55.119	237.372
Pier 2	55.054	63.652	63.686	55.183	237.575
Abutment 2	14.888	16.602	16.605	14.902	62.997
				Total	601.021

9.2.3.2.9 Step 2i – Extract Required Results from Analysis Software

After verifying that the results from the analysis are reasonable, the results of interest can be extracted and input into a spreadsheet for further use. It may be necessary to select only certain portions of the model to obtain the relevant results.

9.2.3.3 Step 3 – Create Live Load Model

This is a continuation of the model created in Step 2.

9.2.3.3.1 Step 3a – Define Material Properties for Concrete Deck Slab

The only change that needs to be made between this model and the previous one is that the normal modulus of elasticity of concrete should be used. Since live load is a short-duration load, no reduction of stiffness is necessary. Table 48 shows the properties of the concrete used in this model.

Table 48. Deck slab concrete material properties.

Material Property	Deck Slab Concrete (4 ksi)
Modulus of Elasticity (ksf)	524,160
Poisson's Ratio	0.2
Unit Weight (k/ft ³)	0.158
Thermal Expansion Coefficient (ft/°F)	6.0E-6

9.2.3.3.2 Step 3b – Determine Optimized Live Load

Refer to Section 9.2.2.3 for an explanation of live load application used in this model.

9.2.3.3.3 Step 3c – Run Analysis and Verify Results using Simplified Methods

After the optimized loadings for each location of interest have been determined, the analysis can be performed. The results can be verified using simplified methods.

Reactions were checked against applied load for a sample load case in which one design truck was applied:

Weight of Design Truck only = 72 k

Reactions (in kips) from Model:

Location	Girder 1	Girder 2	Girder 3	Girder 4	Total
Abutment 1	0.725	-1.731	-3.074	-5.546	-9.630
Pier 1	-2.045	8.470	18.760	22.802	47.990
Pier 2	-4.858	6.131	15.937	25.052	42.262
Abutment 2	-4.633	-2.631	-1.676	0.311	-8.630
				Total	71.992

It should be noted that the manual method of live load application used applies multiple presence factors outside of the software, and therefore was not included in this check against analysis results.

9.2.3.3.4 Step 3d – Extract Required Results from Analysis Software

After verifying that the results from the analysis are reasonable, the results of interest can be extracted and input into a spreadsheet for further use. It may be necessary to select only certain portions of the model to obtain the results wanted.

9.2.3.4 Step 4 – Combine Analysis Results

Once the results of interest, in this case moments, shears, and deflections, have been extracted from the analysis software, they are combined into groups of non-composite dead loads, composite dead loads, and live loads.

The moments due to the composite dead loads and live loads can be used as extracted from the analysis software; no additional calculations are required. The utility within the analysis software integrates the stresses in the shell elements and then combines the force effects from the shell elements and the beam elements to determine the force effects on the composite section.

The HL-93 Design Load consists of the maximum of the design truck or design tandem amplified by the dynamic load allowance plus the design lane; each component was analyzed individually therefore the results must be combined. Similarly, for negative moment between dead load inflection points, the design truck train including the dynamic load allowance and design lane must be combined. Additionally, the results from the different live load models may have to be combined to determine the greatest live load force effect for each girder. Also for live load, the multiple presence factor in Table 3.6.1.1.2-1 of the Specifications must be applied.

Once the moments, shears, and deflections have been combined into appropriate groups using the results from the various analyses, graphs can be created to show the moment and shear diagrams, and deflected shape. The analysis results are combined using the same groups as for the 1D and 2D analyses: non-composite dead loads (girder self-weight, diaphragms, SIP forms, haunches, and concrete deck slab), composite dead loads (barrier and FWS), and maximum and

minimum live loads including the dynamic load allowance. The moment, shear, and deflection diagrams from the 3D finite element analysis are shown in Figures 214 through 219.

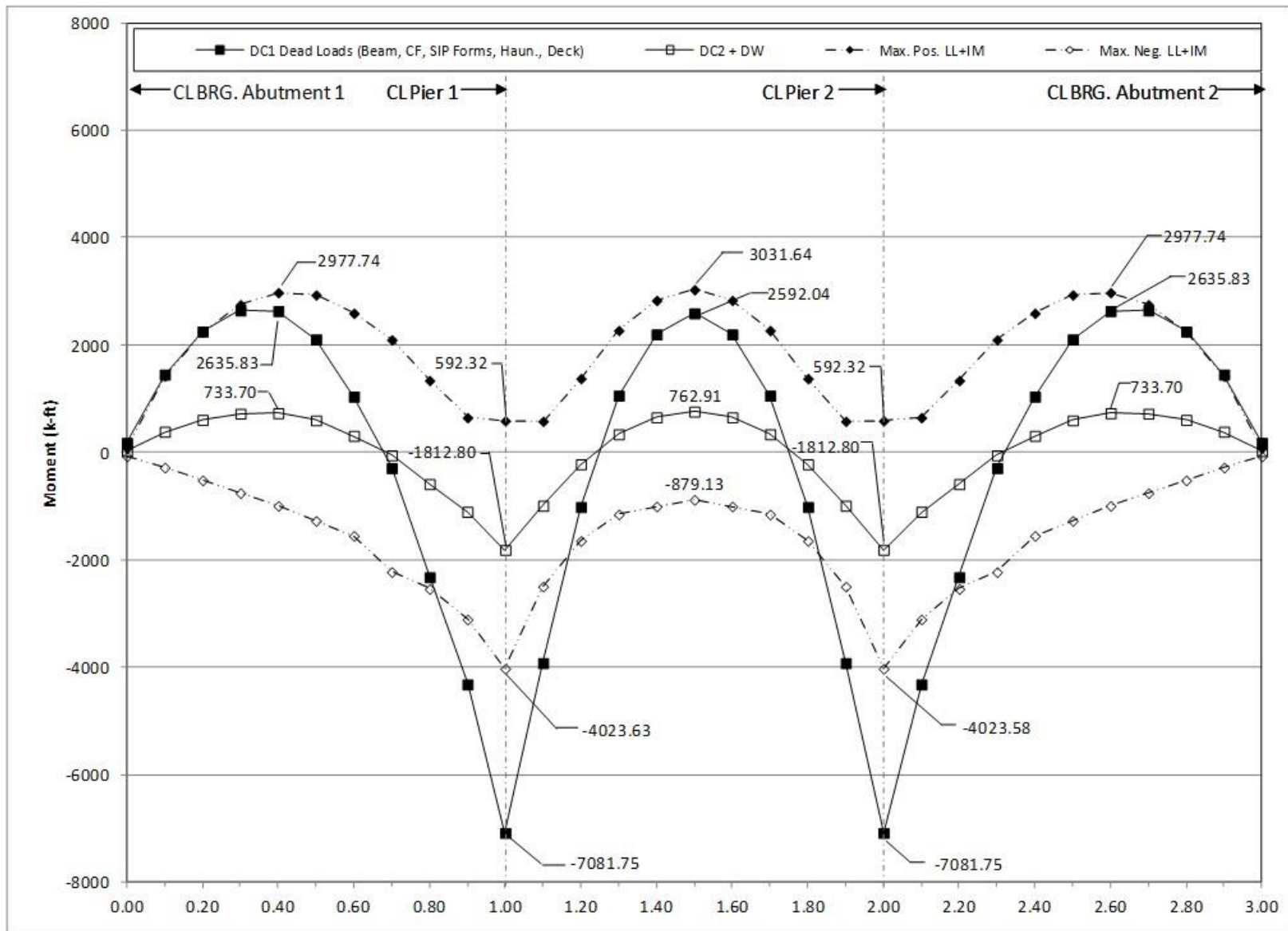


Figure 214. Graph. 3D moment diagram and live load envelope for interior girder.

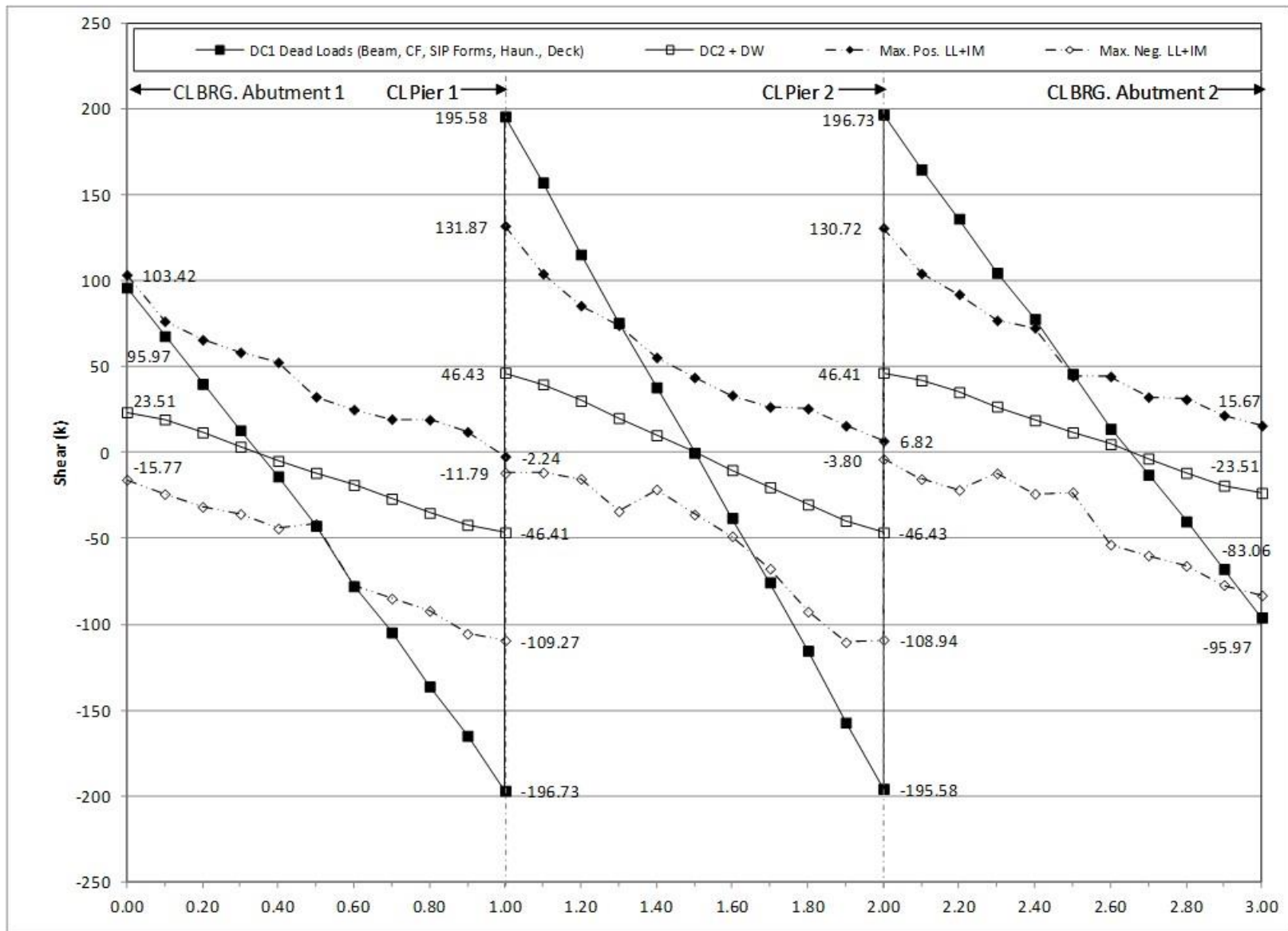


Figure 215. Graph. 3D shear diagram and live load envelope for interior girder.

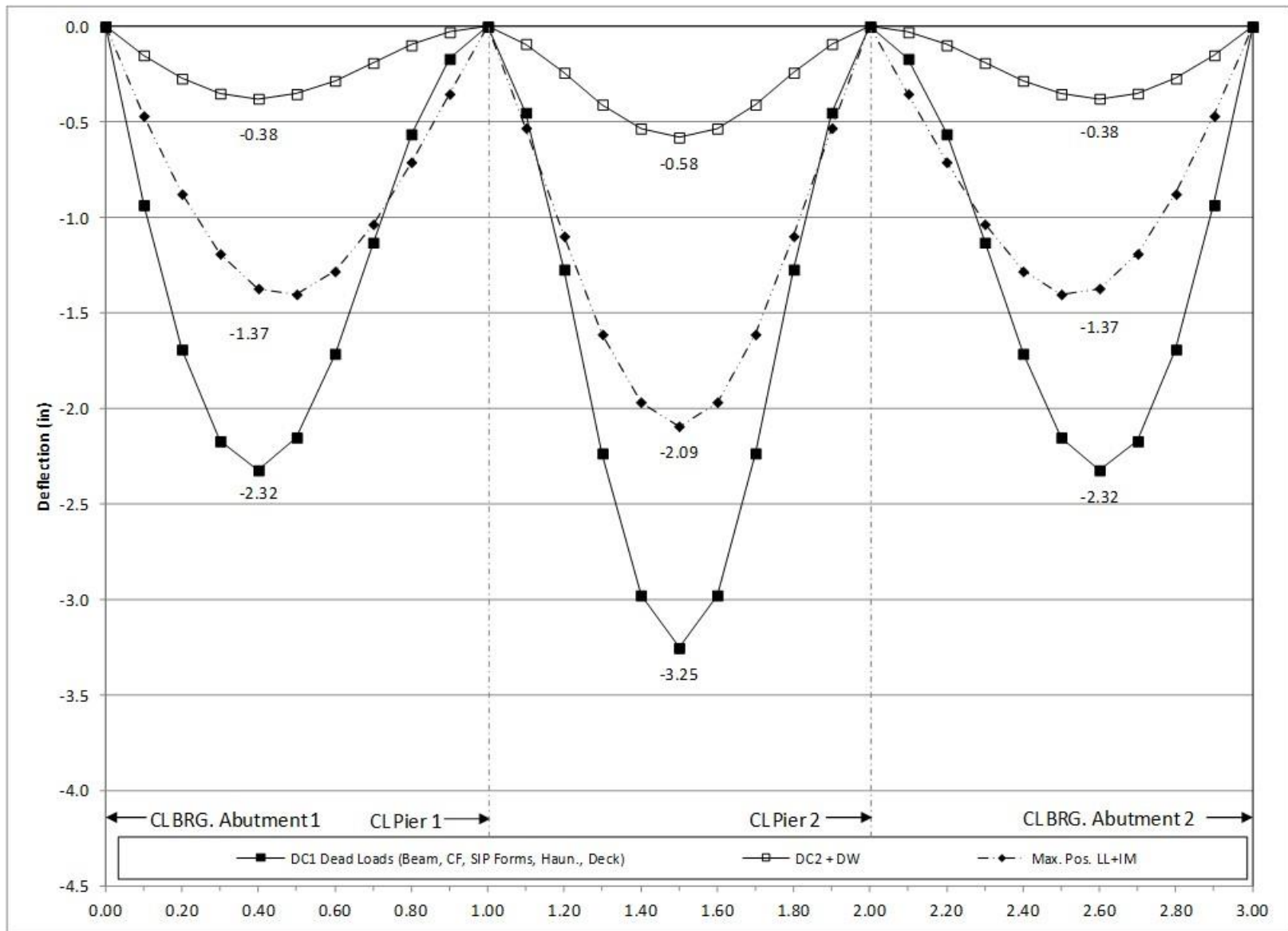


Figure 216. Graph. 3D deflection diagram for interior girder.

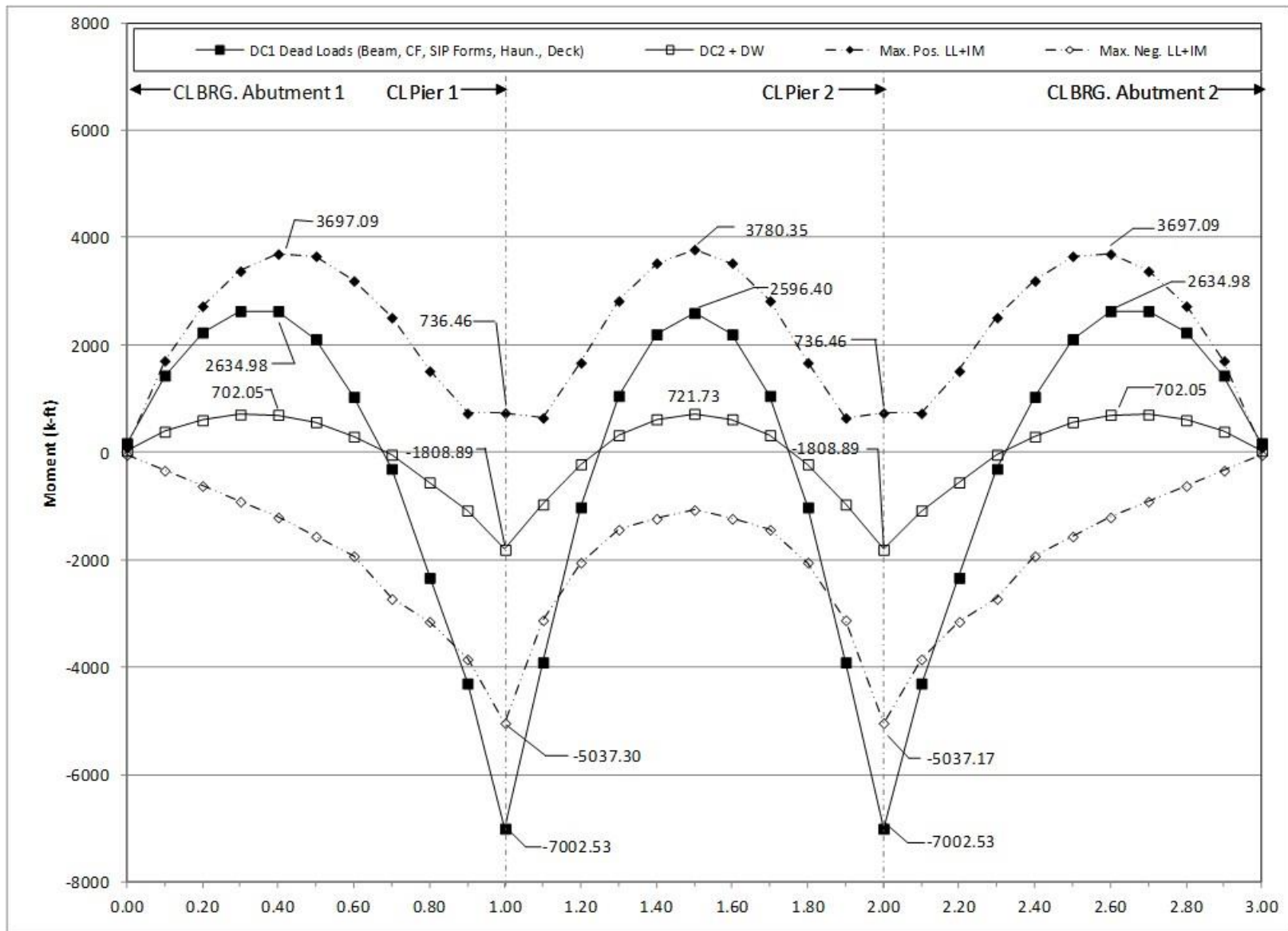


Figure 217. Graph. 3D moment diagram and live load envelope for exterior girder.

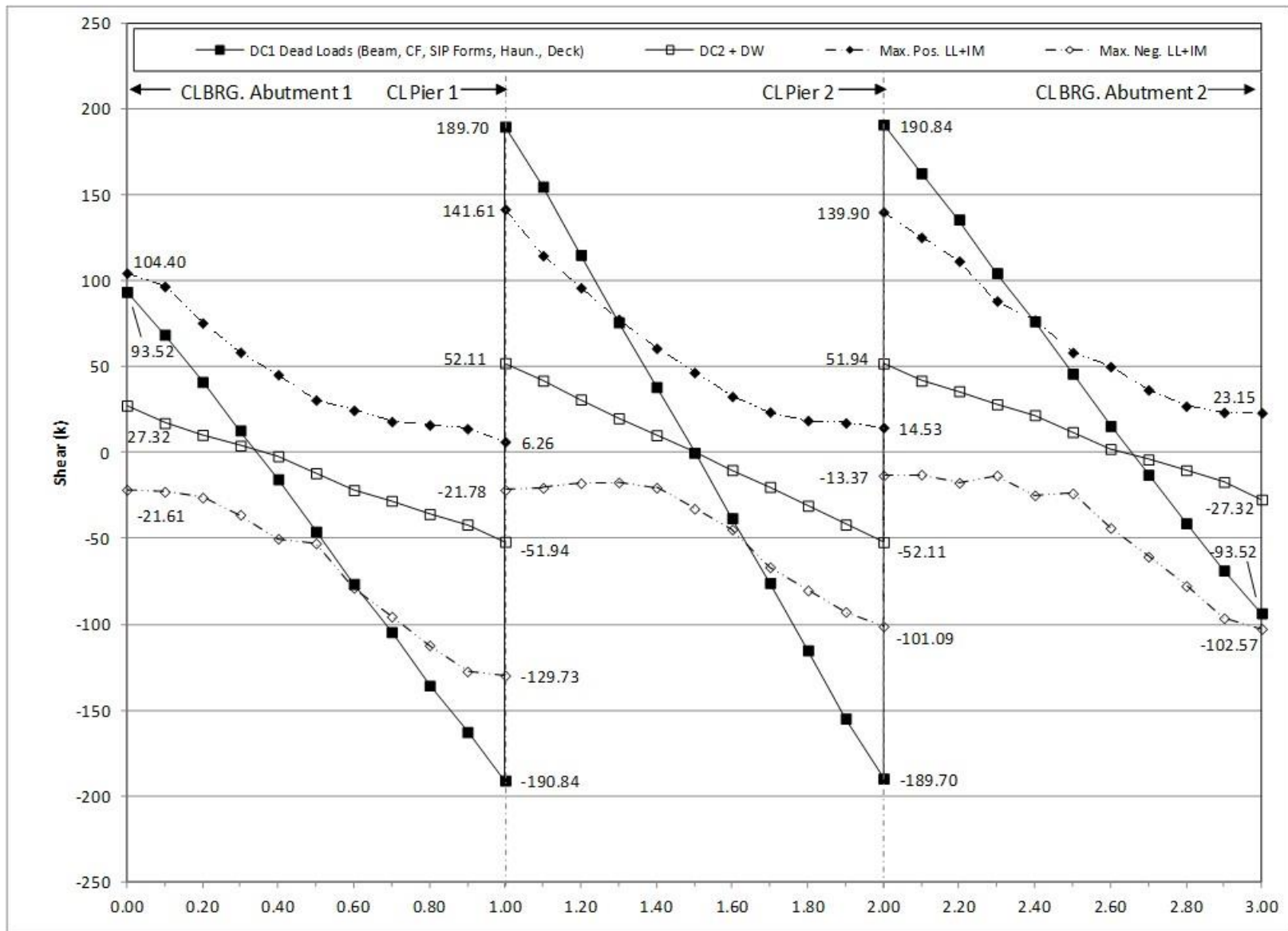


Figure 218. Graph. 3D shear diagram and live load envelope for exterior girder.

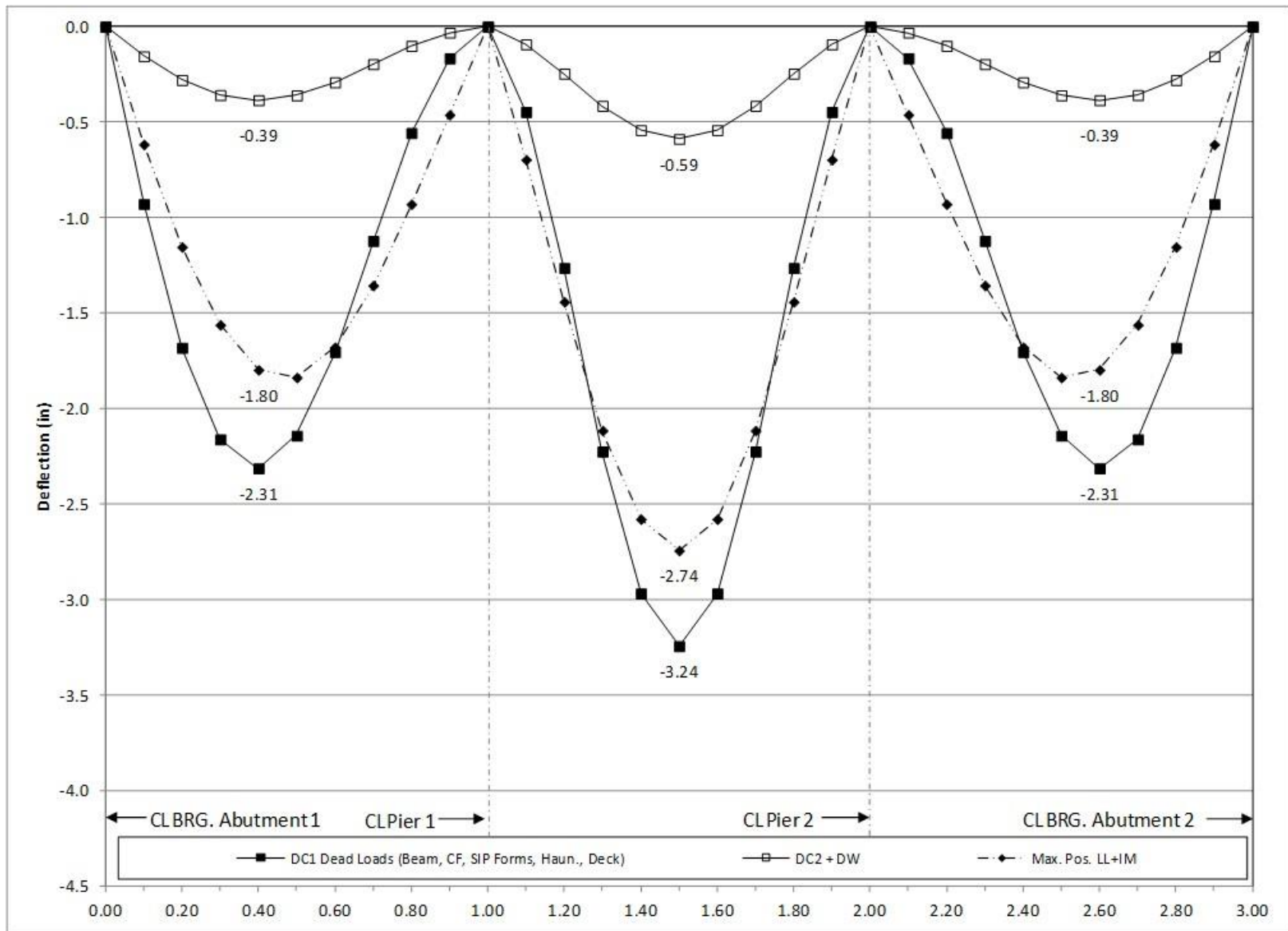


Figure 219. Graph. 3D deflection diagram for exterior girder.

9.2.4 Comparison of 1D, 2D, and 3D Analysis Results

The results from the 1D, 2D, and 3D analyses are compared in the following sections for both the interior and exterior girders. The 3D analysis is expected to provide the most accurate results.

9.2.4.1 Interior Girder

9.2.4.1.1 Moment

Moment results are compared in Figure 220. The figure shows that the 1D dead load moments are typically 5-15 percent greater than the 3D dead load moments. The 1D live load moments are typically 10-20 percent greater than the 3D live load moments.

The figure shows that the 2D dead load moments are within 10 percent of the 3D dead load moments. The 2D live load moments are typically within 10 percent of the 3D live load moments.

1D non-composite dead load moments are typically 5-10 percent higher than those from the 2D analysis, while composite dead load moments are typically 10-20 percent higher. 1D live load moments are typically 15-20 percent higher than 2D live load moments.

Figure 221 compares the factored Strength I moments from the 1D, 2D, and 3D models for the interior girders. The 2D and 3D models provided very similar results; the 1D model provides conservative results when compared to the 2D and 3D models.

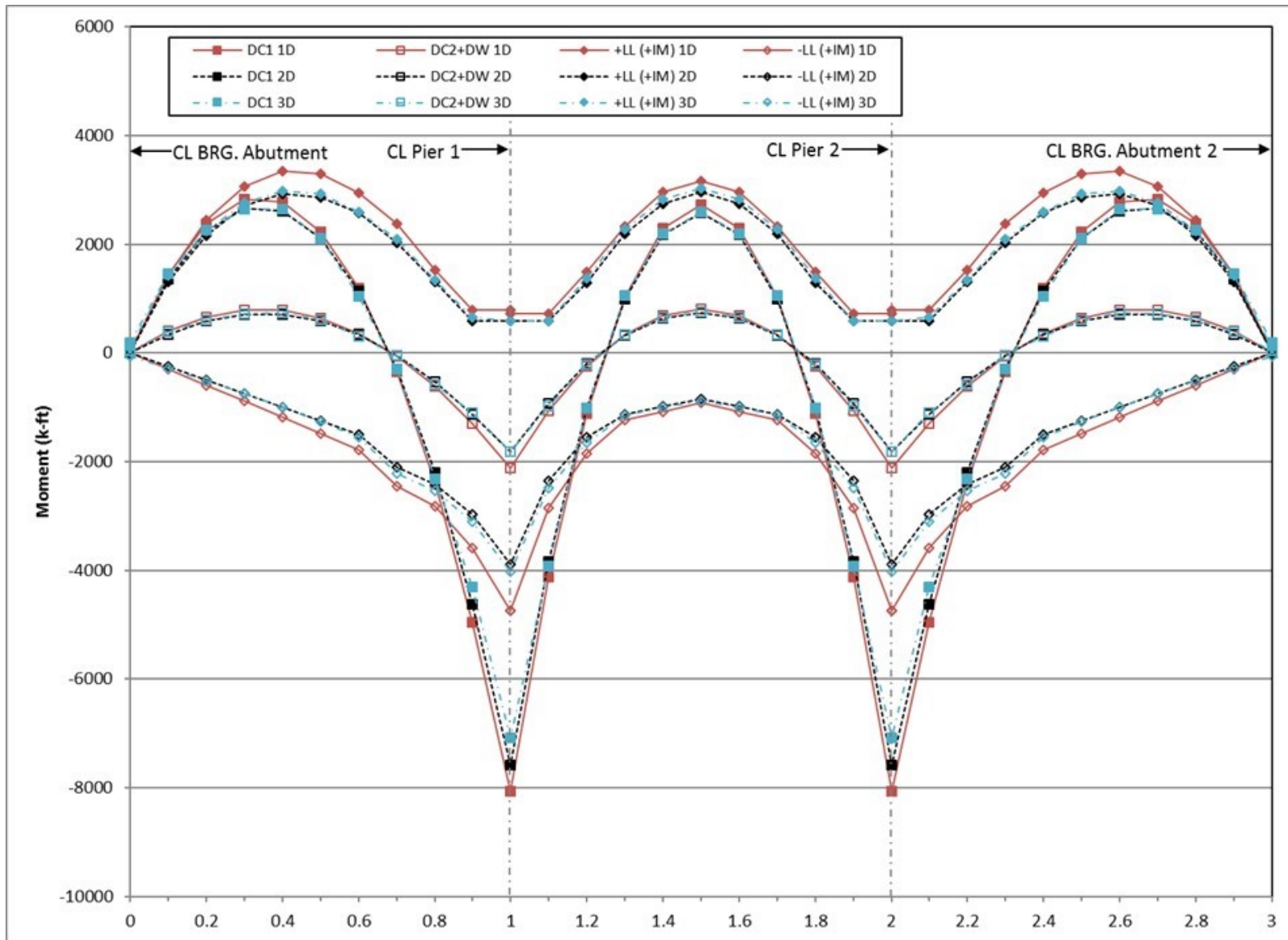


Figure 220. Graph. Comparison of moments for interior steel girder.

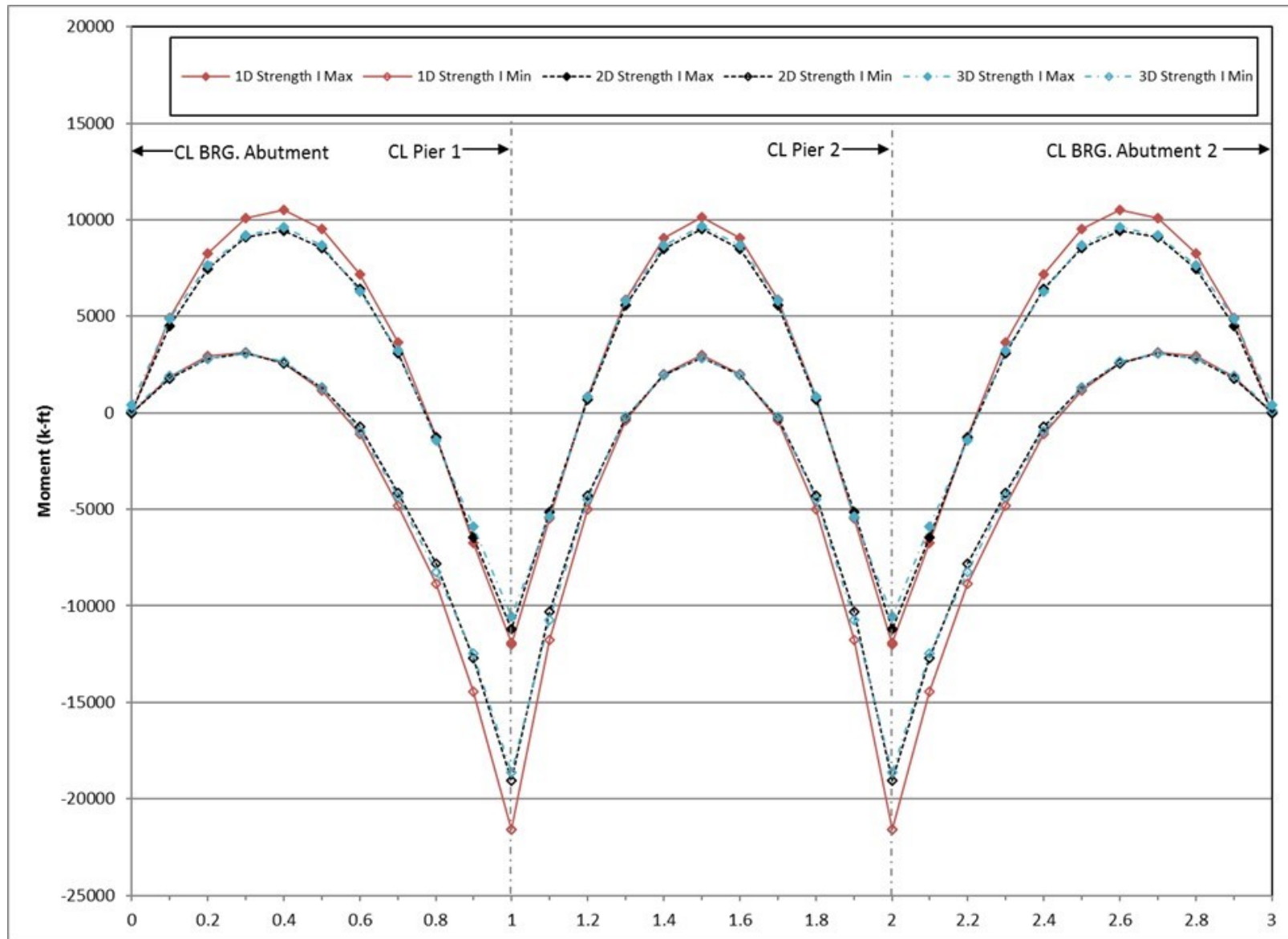


Figure 221. Graph. Comparison of factored moments for interior steel girder.

9.2.4.1.2 Shear

Shears are compared in Figure 222. The figure shows that the 1D non-composite and composite dead load shears are typically 10-15 percent greater than the 3D non-composite dead load shears. The 1D live load shears are approximately 30-50 percent greater than the 3D live load shears.

The figure shows that the 2D non-composite dead load shears are typically 0-4 percent greater than the 3D results. For composite dead load, the 2D shears are typically 10-12 percent lower than 3D shears. The 2D live load shears are generally within 15 percent and typically larger than the 3D live load shears.

1D non-composite dead load shears are typically 5-9 percent greater than the 2D results. For composite dead load 1D shears are typically 25 percent larger than those from the 2D analysis. 1D live load shears are generally 40 percent larger than 2D live load shears.

Figure 223 compares the factored Strength I shears from the 1D, 2D, and 3D models for an interior girder. The 1D model provides conservative design shears when compared to those from the 2D and 3D models.

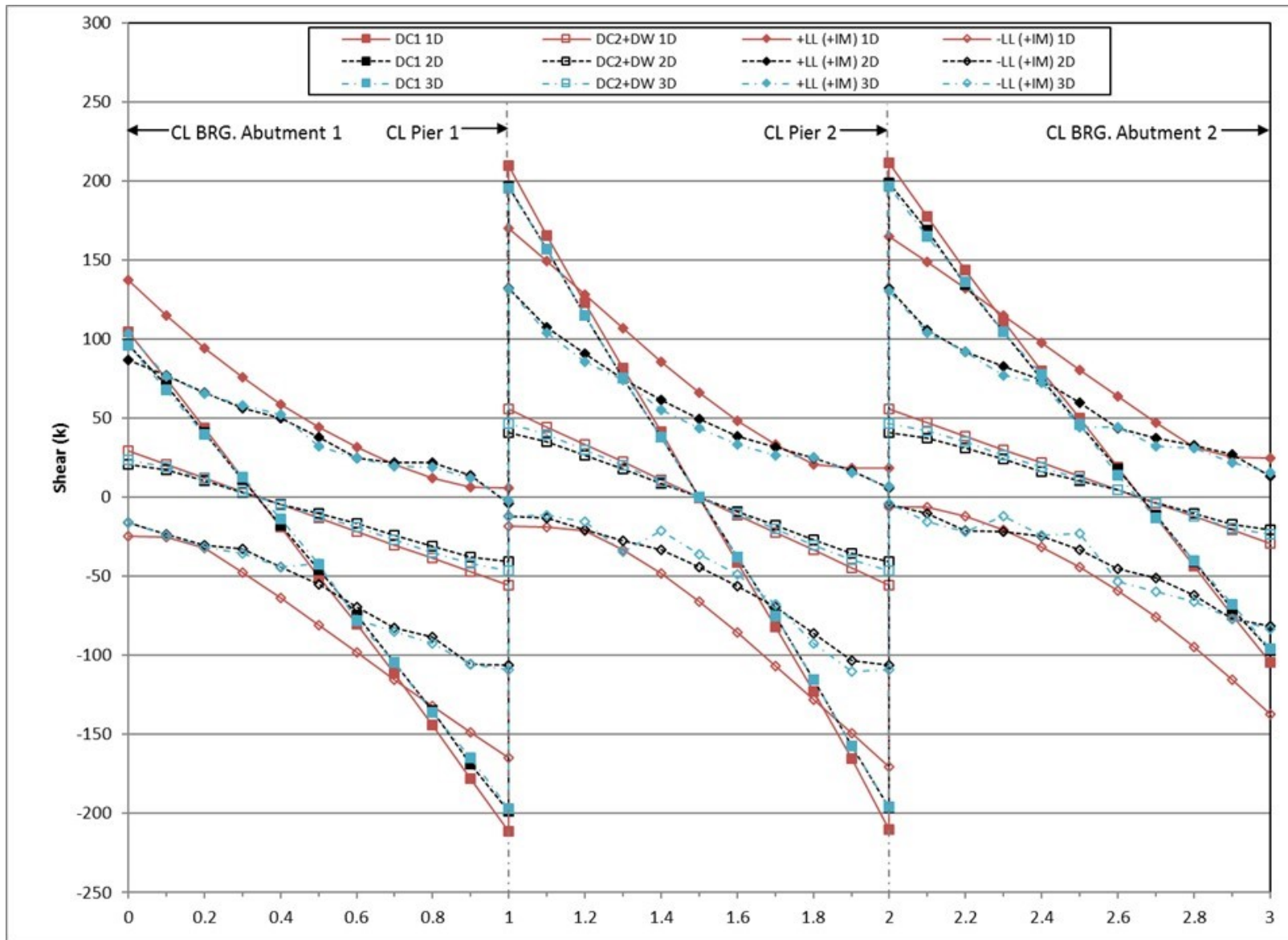


Figure 222. Graph. Comparison of shears for interior steel girder.

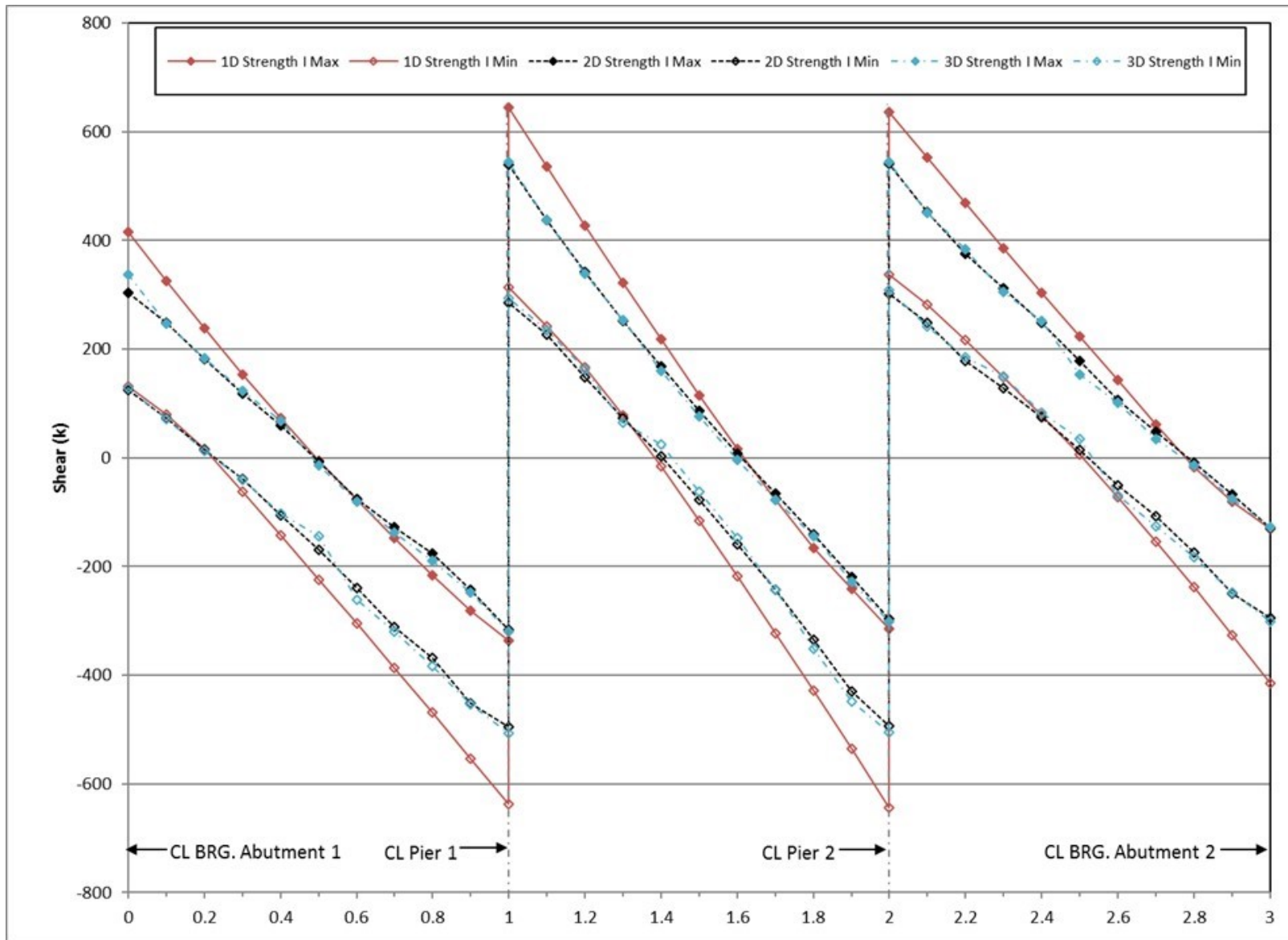


Figure 223. Graph. Comparison of factored shears for interior steel girder.

9.2.4.1.3 Deflection

Deflections are compared in Figure 224. The figure shows that the 1D non-composite and composite dead load deflections are typically within 10 percent of the 3D non-composite dead load deflections. The 1D live load deflection is approximately 10-15 percent smaller than the 3D live load deflection.

The figure shows that the 2D non-composite and composite dead load deflections are typically within 4 percent of the 3D non-composite dead load deflections. The 2D live load deflection is generally 15-17 percent of the 3D live load deflection.

1D non-composite dead load deflections are typically 0-5 percent smaller than those from the 2D analysis. 1D composite dead load deflections are typically within 6 percent of 2D results. The 1D live load deflections are typically 0-6 percent greater than 2D live load deflections.

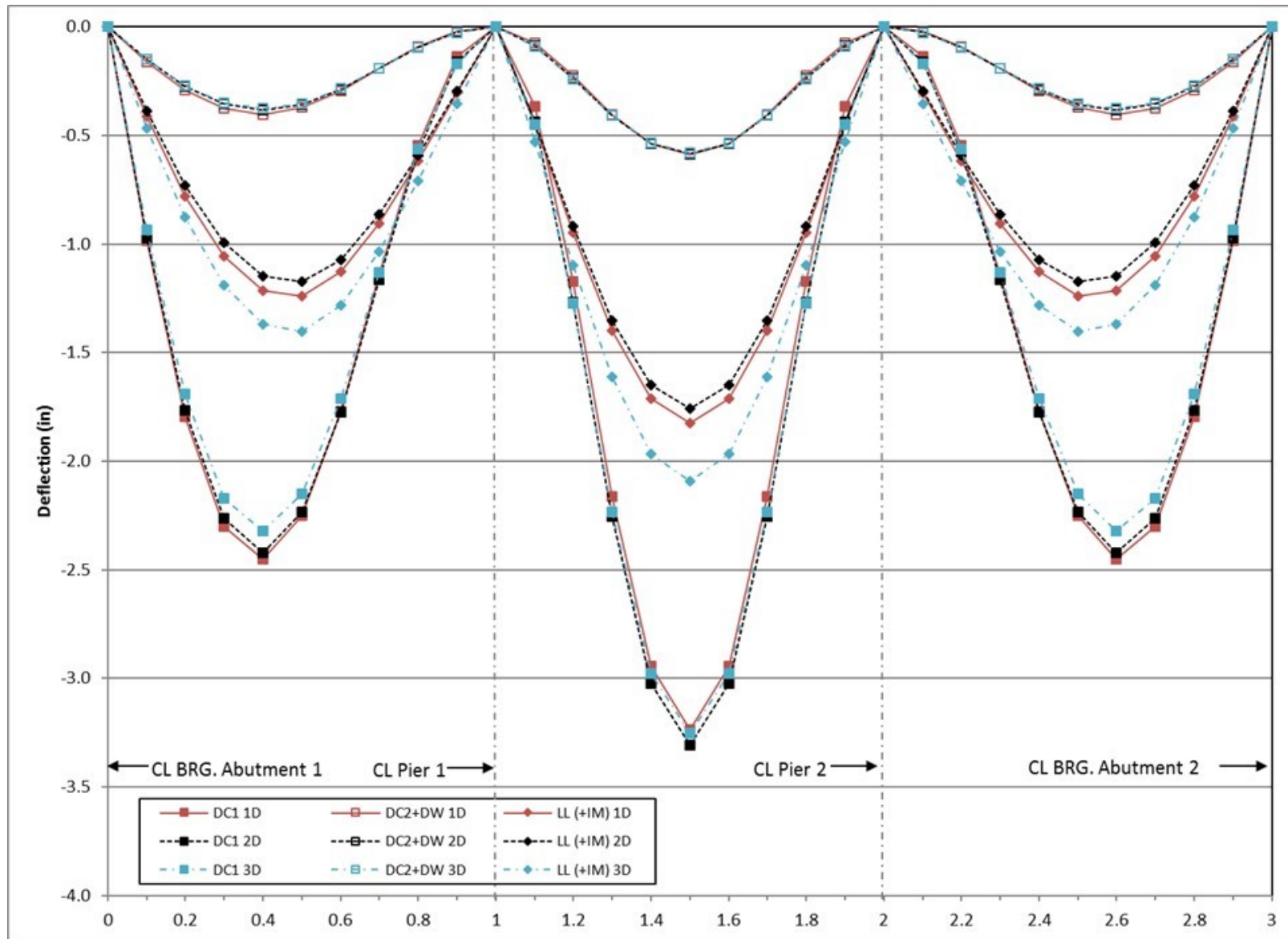


Figure 224. Graph. Comparison of deflections for interior steel girder.

9.2.4.2 *Exterior Girder*

9.2.4.2.1 Moment

Moment results are compared in Figure 225. The figure shows that the 1D dead load moments are typically 0-15 percent lower than the 3D dead load moments. The 1D live load moments are typically 15-30 percent greater than the 3D live load moments.

The figure shows that the 2D dead load moments are typically within 8 percent of the 3D moments. The 2D live load moments are typically within 5 percent of the 3D live load moments.

1D moments are typically 6-8 percent lower than 2D non-composite dead load moments. Composite dead load moments are 10-15 percent lower in the 1D analysis. 1D live load moments are typically 15-18 percent higher than those from the 2D analysis.

Figure 226 compares the factored Strength I moments from the 1D, 2D, and 3D models for an exterior girder. The design moments from the 1D model are conservative when compared to those from the 2D and 3D models.

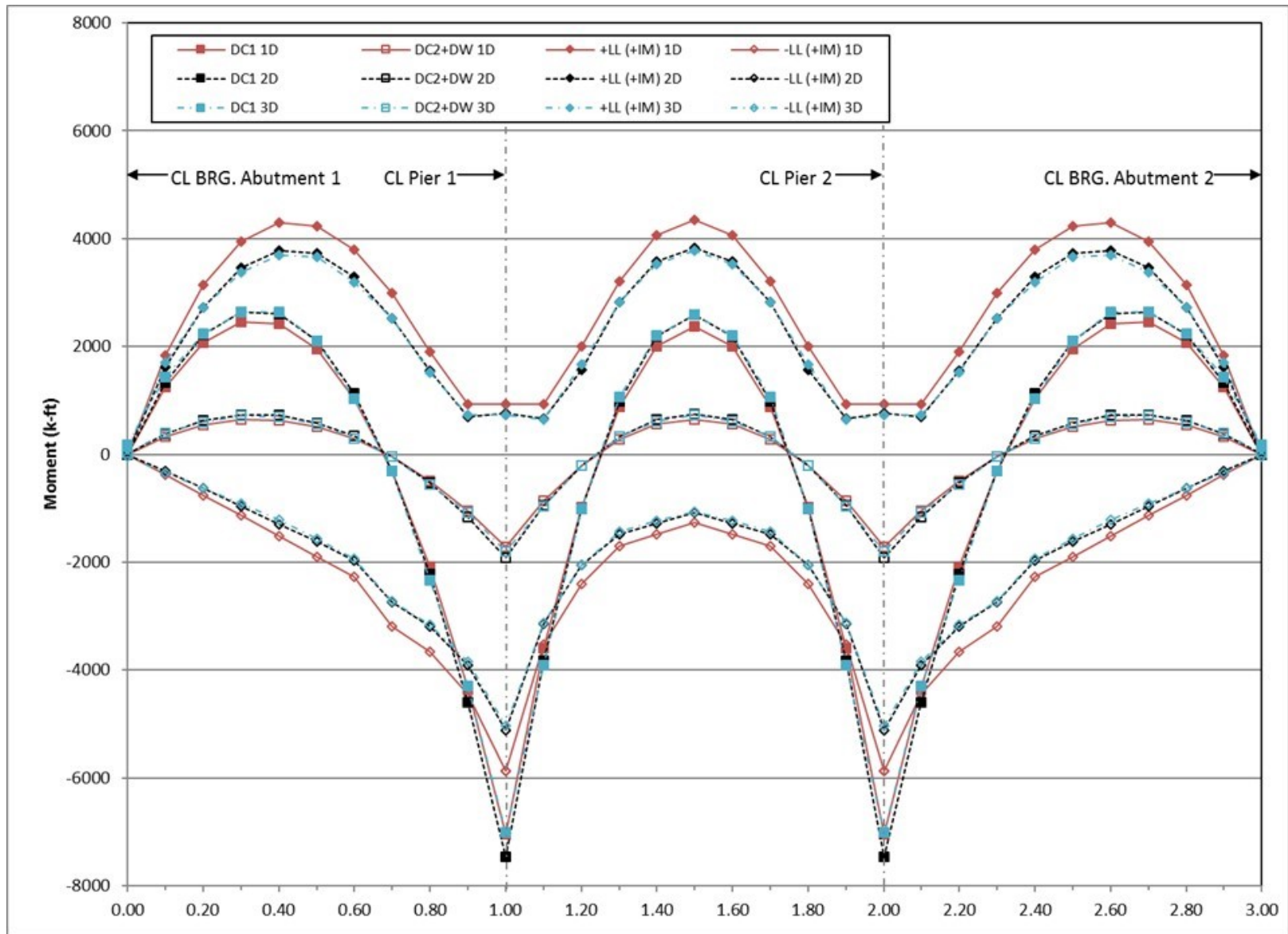


Figure 225. Graph. Comparison of moments for exterior steel girders.

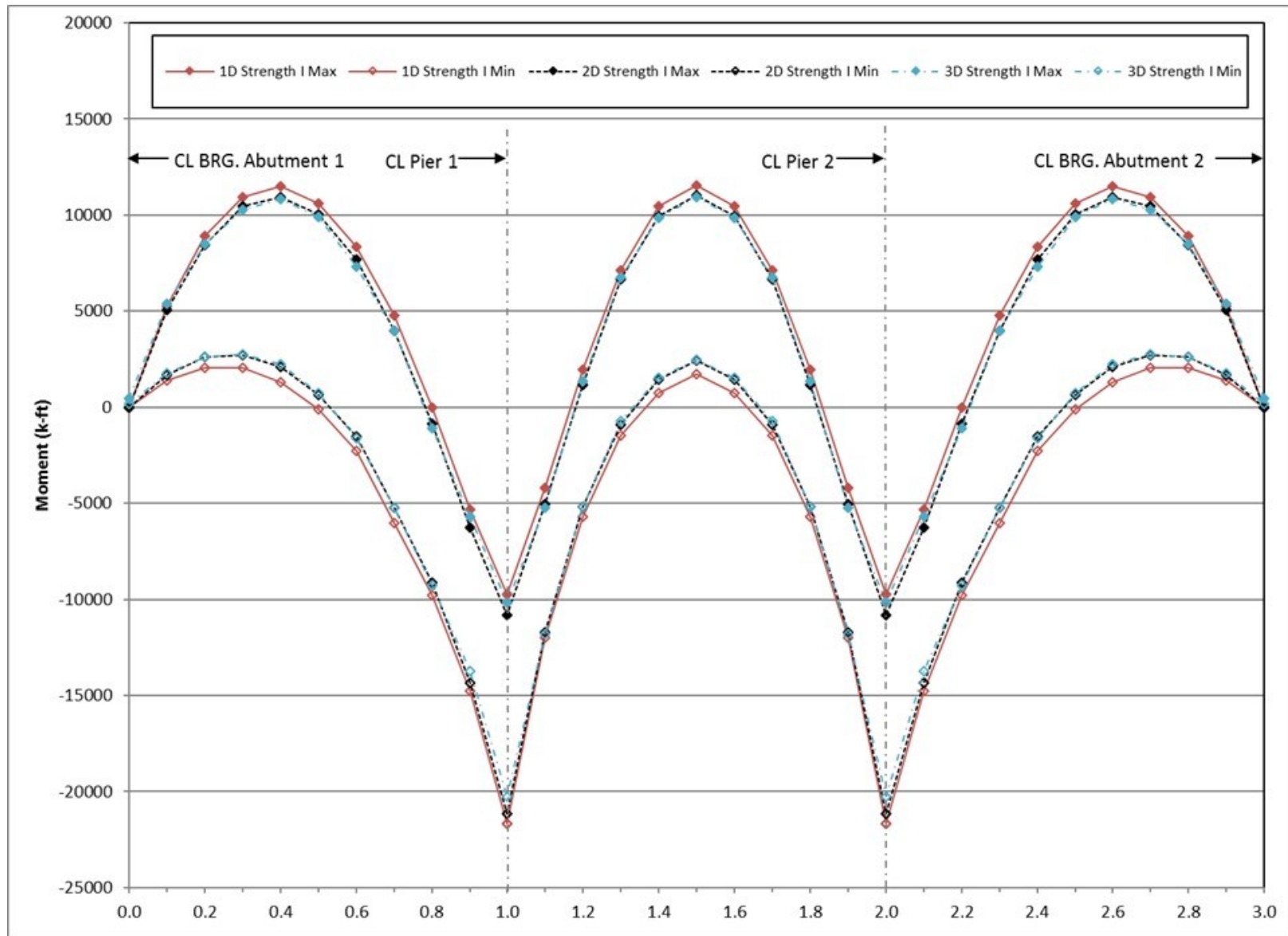


Figure 226. Graph. Comparison of factored moments for exterior steel girders.

9.2.4.2.2 Shear

Shears are compared in Figure 227. The figure shows that the 1D non-composite and composite dead load shears are 5-12 percent smaller than those from the 3D analysis. The 1D live load shears are typically 15-30 percent greater than the 3D live load shears.

The figure shows that the 2D non-composite dead load shears are typically within 4 percent of the 3D non-composite dead load shears. For composite dead load, the 2D shears are typically 10-12 percent smaller than the 3D shears. The 2D maximum live load shears are mostly 0-20 percent greater than the 3D shears, while the 2D minimum live load shears are typically 0-60 percent greater than the 3D shears.

1D non-composite dead load shears are typically 3-9 percent smaller than corresponding 2D shears. For composite dead load, 1D shears are typically between 3 percent smaller and 9 percent larger than those from the 2D analysis. 1D live load shears are typically 12-25 percent greater than 2D live load shears.

Figure 228 compares the factored Strength I shears for the 1D, 2D, and 3D models for an exterior girder. The design shears from the 1D model are conservative when compared to those from the 2D and 3D models.

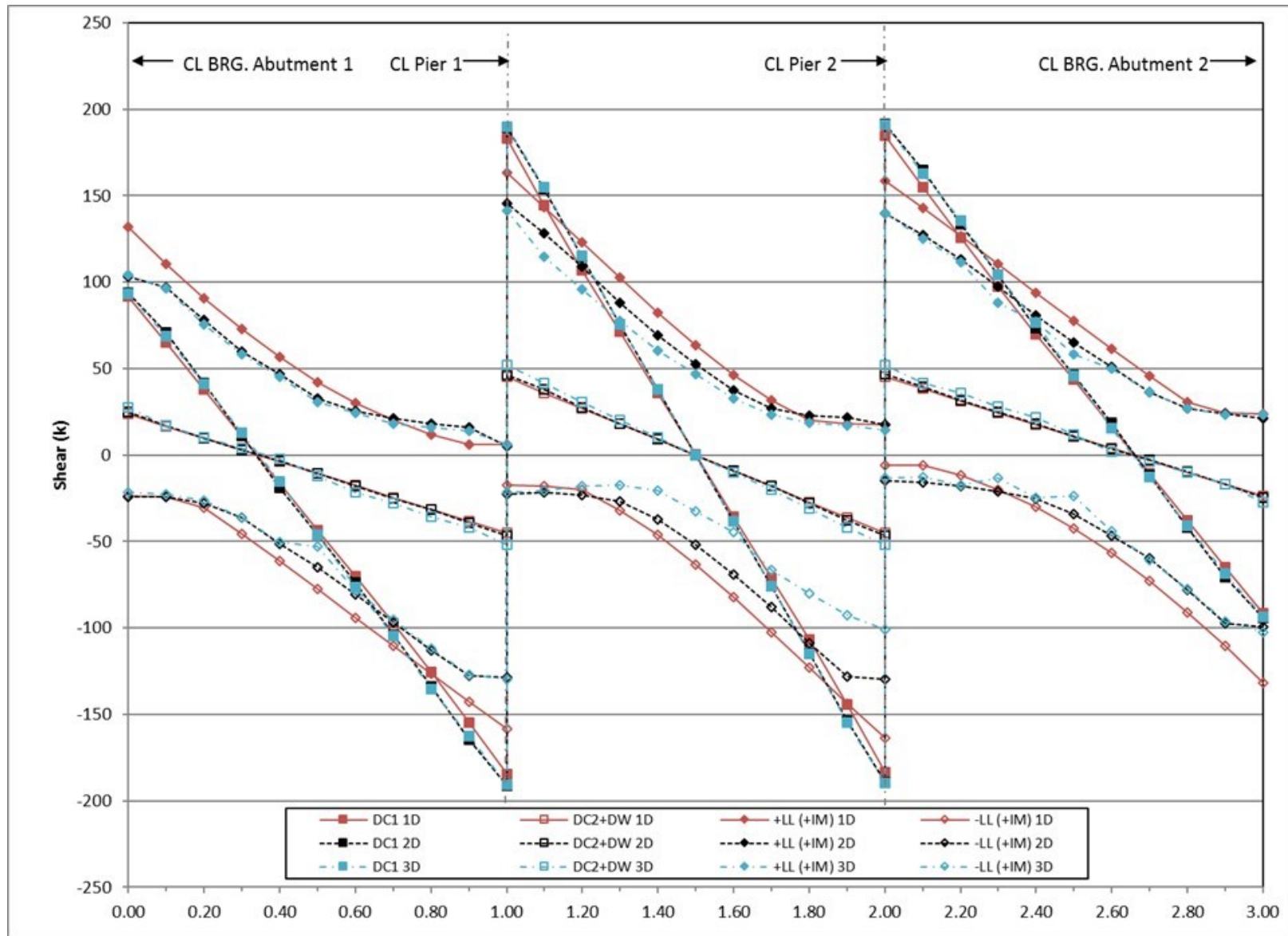


Figure 227. Graph. Comparison of shears for exterior steel girders.

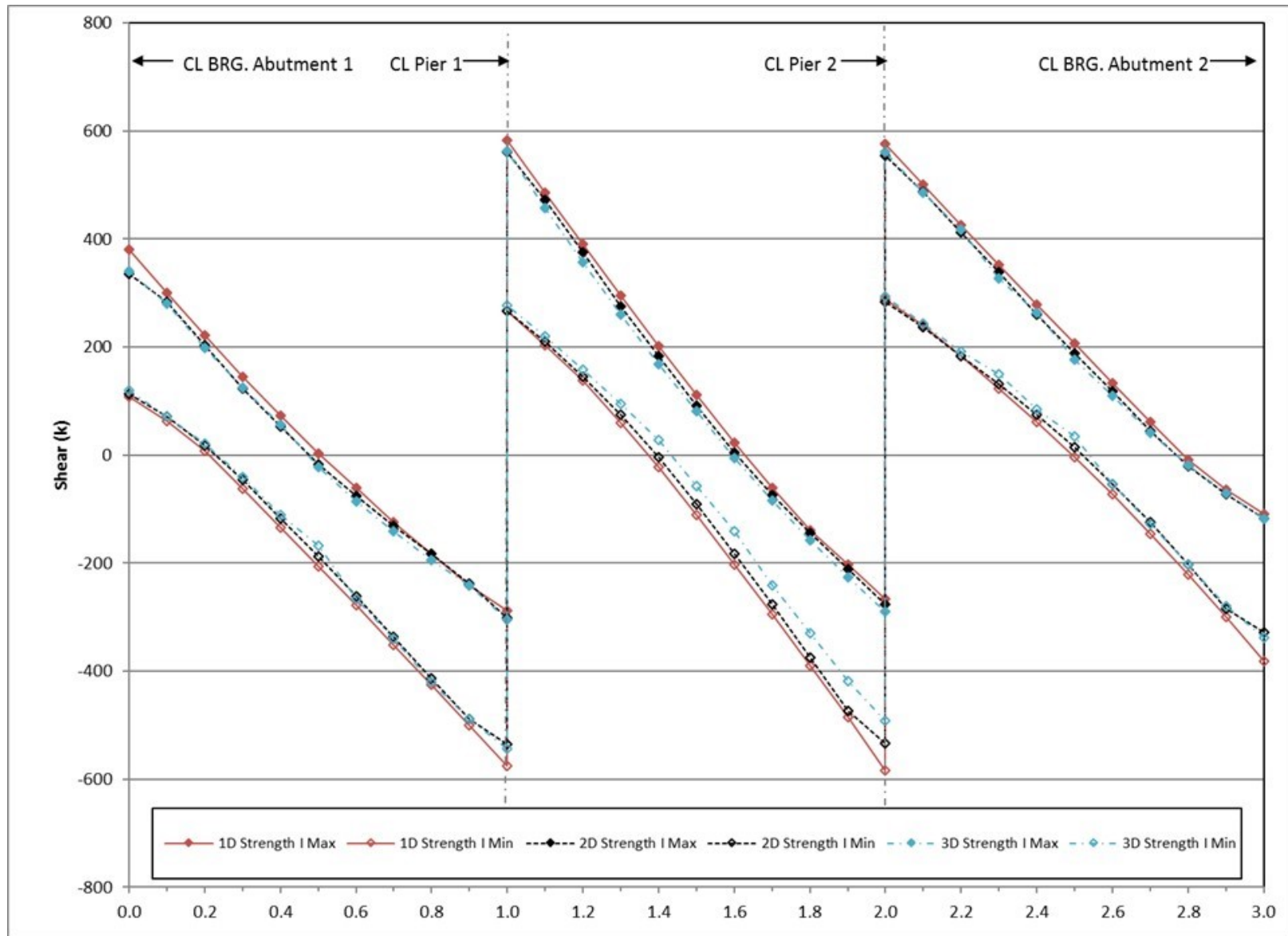


Figure 228. Graph. Comparison of factored shears for exterior steel girders.

9.2.4.2.3 Deflection

Deflections are compared in Figure 229. The figure shows that the 1D non-composite and composite dead load deflections are typically 10-15 percent smaller than corresponding 3D deflections. The 1D live load deflection is approximately 30 percent smaller than the 3D live load deflection.

The figure shows that the 2D non-composite and composite dead load deflections are typically 4 percent larger than the 3D dead load deflections, while the live load deflections are approximately 15 percent smaller.

1D dead load deflections are approximately 15-20 percent smaller than 2D deflections. 1D live load deflections are typically 17-19 percent lower than 2D results.

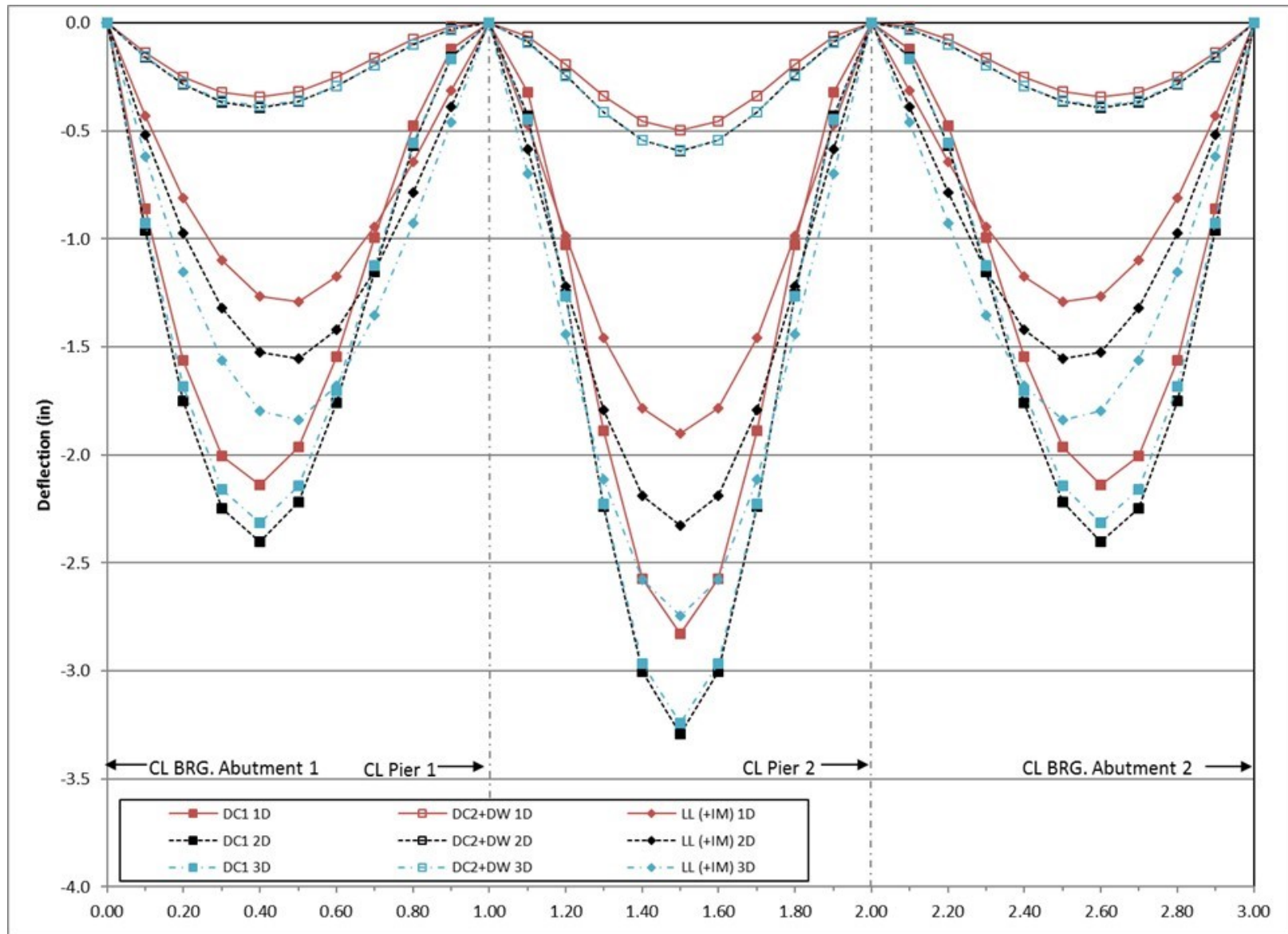


Figure 229. Graph. Comparison of deflections for exterior steel girder.

9.2.4.3 Conclusions

The 1D line girder analysis results in dead load moments that are typically within ± 15 percent of the dead load moments from the 3D analysis for both interior and exterior girders. Locations where the difference in dead load is greater than ± 10 percent are typically near points of contraflexure. Live load moments are typically 10-30 percent greater for 1D line girder analysis than from the 3D analysis for both interior and exterior girders. Dead load shears from the 1D analysis are typically within 15 percent of the dead load shears from the 3D analysis for interior girders and exterior girders. Differences tend to be greatest near midspan, where shear values are smallest. 1D live load shears are around 30-50 percent greater than the 3D live load shears for interior girders and exterior girders. The large differences are attributed to the use of distribution factors, which tends to overestimate the amount of load each girder takes. Dead load deflections from the 1D analysis are typically within ± 10 percent of the dead load deflections from the 3D analysis for interior girders and typically around 10 percent smaller than the 3D analysis deflections for exterior girders. 1D live load deflections are around 10 percent smaller than the 3D live load deflections for the interior girders and around 30 percent smaller than the 3D live load deflections for the exterior girders.

The Plate and Eccentric Beam method generally provides reasonable results when compared to the 3D Finite Element Method. The moments from the 2D analysis are generally within 10 percent of those from the 3D analysis for both dead and live loads; the locations where the moments are typically not within 10 percent are near points of contraflexure. 2D shears are typically within 10 percent of the 3D dead load shears for interior girders and exterior girders. Similar to the 1D case, the largest disparities are observed where shear values are small, near midspan. 2D live load shears are approximately 15-20 percent greater than 3D live load shears for interior girders and exterior girders. 2D dead load deflections are typically within 5 percent of the 3D dead load deflections for both interior and exterior girders, with those locations indicating more variation typically near the support. 2D live load deflections are approximately 15 percent smaller than the 3D live load deflections for both interior and exterior girders.

1D non-composite dead load moments are within 10 percent of 2D results for both interior and exterior girders. Similar to Example 1, as a result of the assumption of equal load sharing between all girders, 1D composite dead load moments in interior girders are higher than in the 2D case, while moments in exterior girders are lower. 1D live load moments are higher than 2D moments as a function of the application of live load distribution factors. 1D shears follow similar patterns with respect to the 2D results. 1D deflections for dead and live load are typically close to 2D deflections for interior girders, but are 15-20 percent smaller for exterior girders.

Overall, the greatest improvements in terms of economical design will typically come from refinement into a 2D model, particularly in the instance of appreciable live loads where the conservative distribution factors are no longer applied. In most cases, the 2D results will sufficiently capture behavior and not necessitate the use of a 3D model.

9.3 Example 3 – Three-span Continuous Curved Steel I-Girder Bridge with Skewed Supports

A three-span continuous curved steel I-girder bridge with skewed supports is the subject of Example 3. The centerline of the bridge is on a 700 foot radius with span lengths of 160 ft-0 inches – 210 ft-0 inches – 160 ft-0 inches along the centerline. The cross-section consists of four welded steel plate girders. Cross-frames are spaced as shown in **Figure 230**.

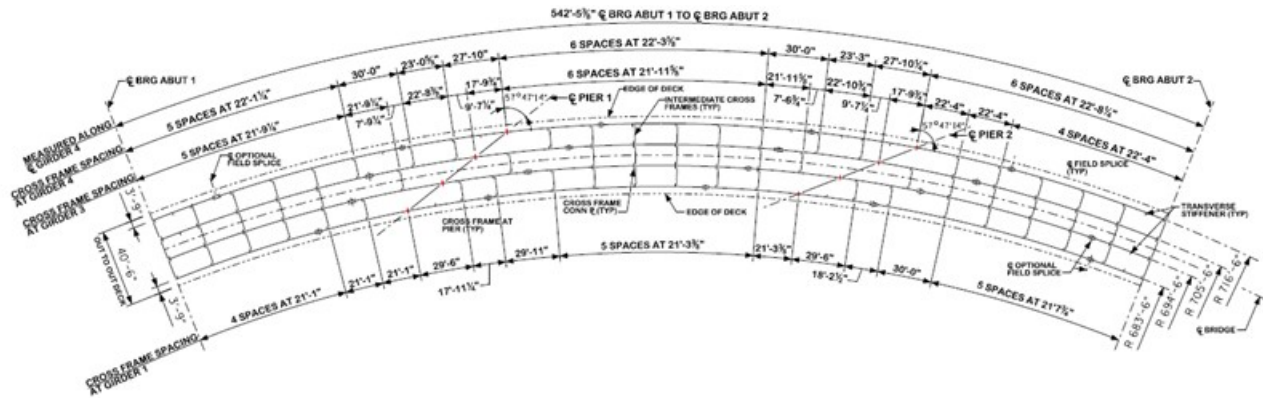


Figure 230. Illustration. Example 3 framing plan.

Figure 231 shows the cross-section for Example 3. The concrete deck slab is 9½ inches thick including a ½ inch integral wearing surface; the deck slab is constructed with concrete having a compressive strength of 4 ksi. The intermediate cross-frames are composed of L5x5x½ top chords and WT6x22.5 diagonals and bottom chord. The cross-frames at the piers and abutments are composed of L8x8x¾ top chords and L5x5x½ diagonals and bottom chord. The welded steel girders have a 92-inch deep web. The top and bottom flange plate dimensions are shown in Figures 232 through 235.

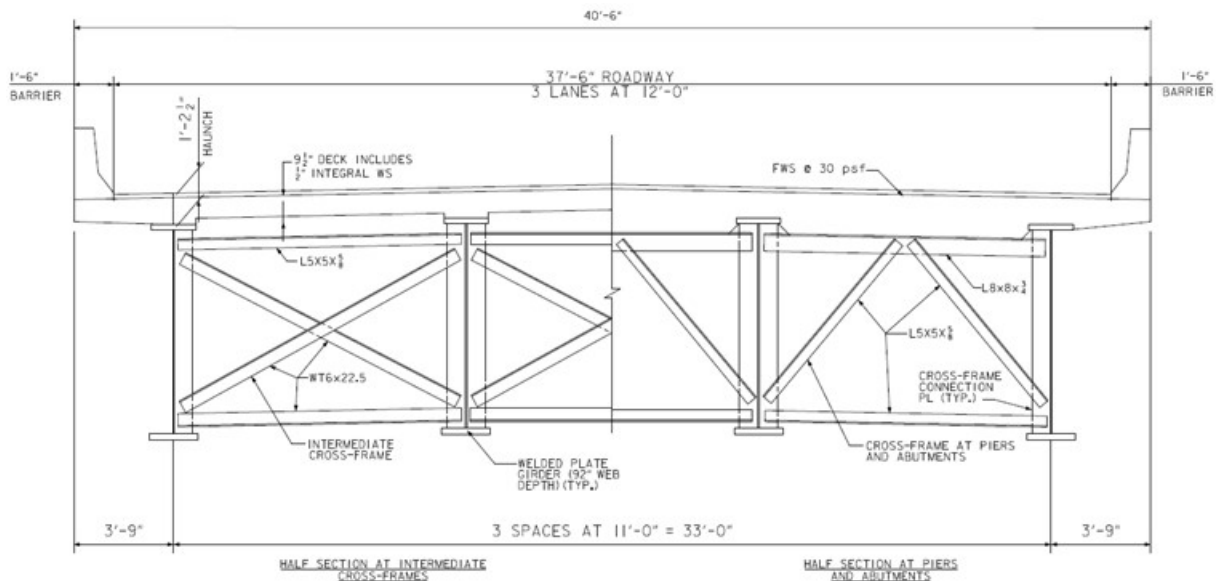


Figure 231. Illustration. Example 3 bridge cross-section.

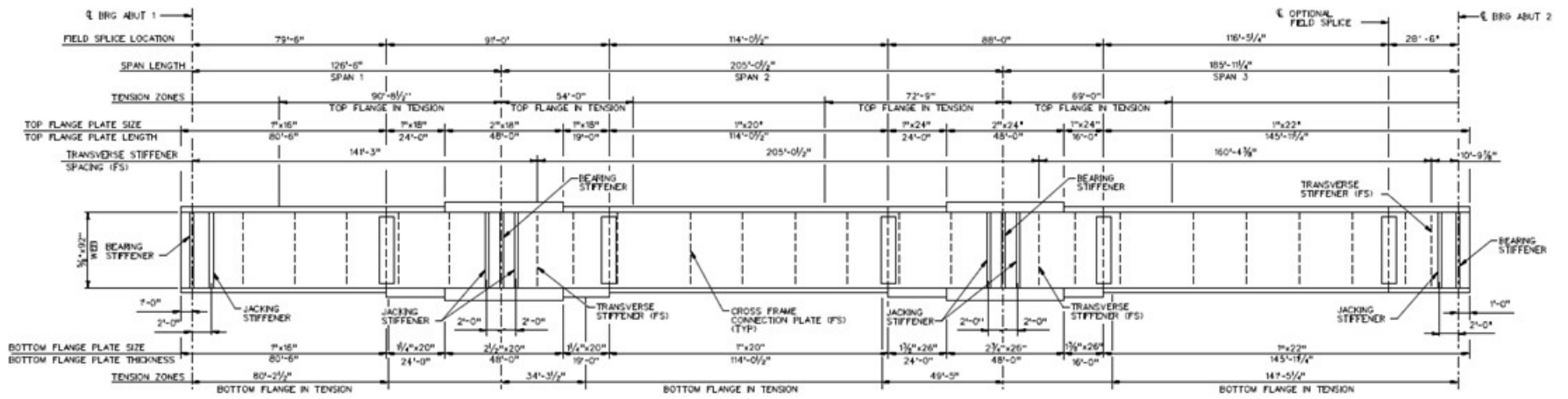


Figure 232. Illustration. Example 3 elevation of Girder 1 (G1).

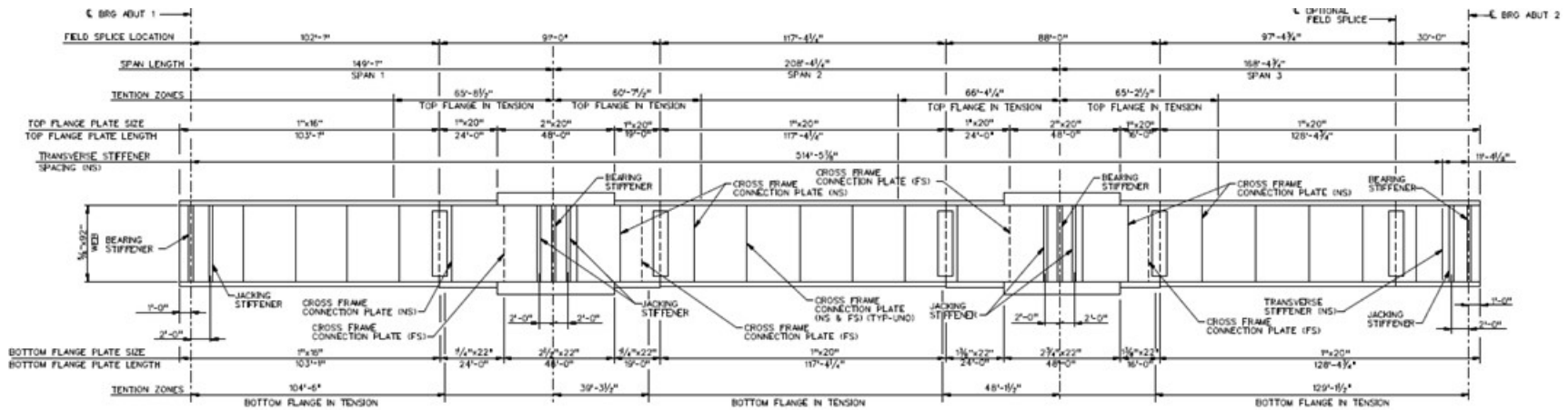


Figure 233. Illustration. Example 3 elevation of Girder 2 (G2).

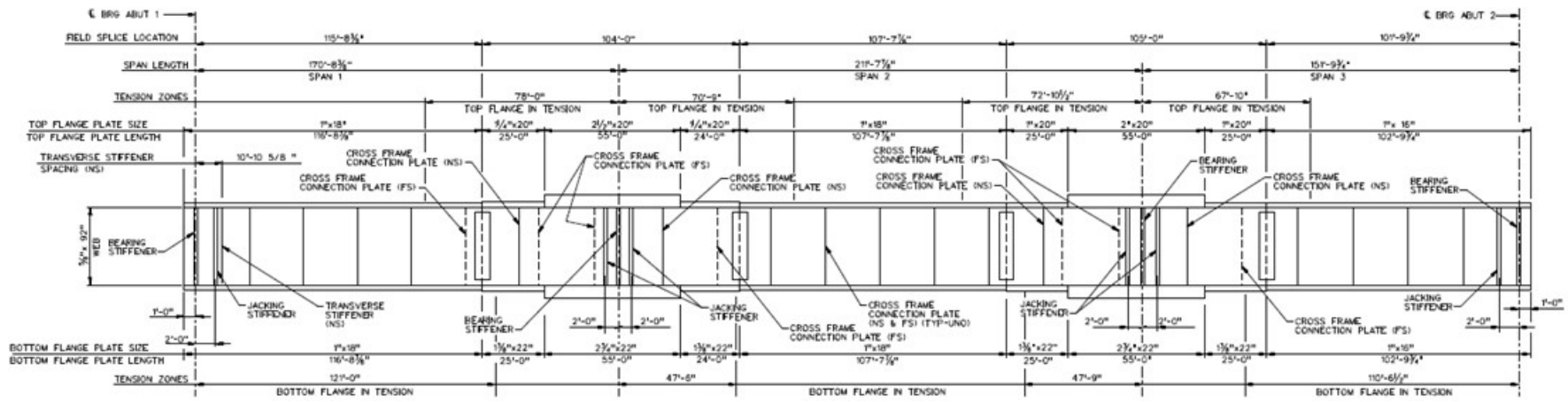


Figure 234. Illustration. Example 3 elevation of Girder 3 (G3).

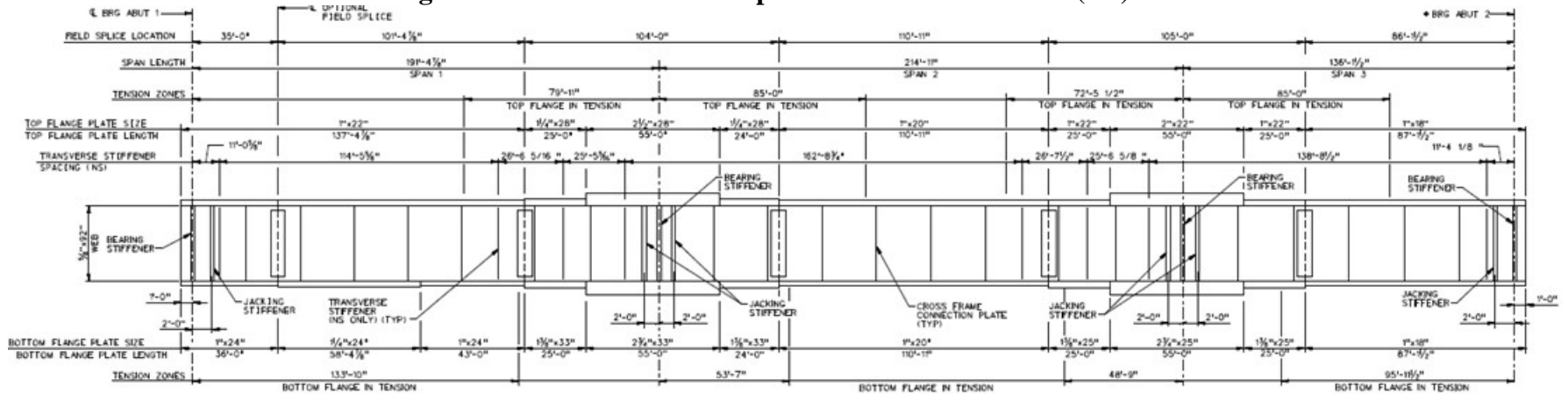


Figure 235. Illustration. Example 3 elevation of Girder 4 (G4).

9.3.1 1D Line Girder Analysis

Modeling of curved structures in 1D should be approached with caution. Idealizations made for 1D analysis forgo capturing several important effects and as a result require numerous subsequent calculations. Approximate methods, such as the V-load method exist to estimate lateral bending and cross-frame effects that arise from horizontal curvature. Lateral effects from overhang bracket loads and skew must also be accounted for (as well as any second order amplification effects), usually with coarse approximations.

9.3.2 2D Plate and Eccentric Beam Analysis

The 2D PEB analysis method explicitly considers the depth of the structure through the use of eccentric beams; while the depth is explicitly considered, geometry, including support conditions, is modeled at the centroid of the deck slab (or girder) not at the actual physical location. Equivalent cross-frame stiffness is accounted for using Timoshenko beam elements and an effective torsional stiffness is used to include warping. The approximate distribution factors in AASHTO LRFD Article 4.6.2.2 are NOT used. Three separate models are required; one for non-composite dead loads, one for composite dead loads, and one for live load. The following steps are used to determine the dead and live load moments, shears, and deflections:

1. Create model for non-composite dead loads.

The two major methods by which the non-composite dead load model can be constructed are explicit deck models and assumed tributary load models. An explicit deck model requires modeling of a flexible deck slab (wet concrete), which is used to distribute the weight of the concrete (which can be assigned as pressures on the surfaces or as body forces) as calculated by the software. The alternative is to assume a tributary width for each girder (typically half girder spacing in each direction for interior girders, half girder spacing and overhang width for exterior girders), then transform the surface pressures into line loads to be applied along each girder.

The explicit deck method, while more time intensive (both in pre-processing and analysis) has the advantage of establishing all of the necessary elements for development of composite models (with material and geometric properties to be modified as necessary) and more accurately capturing any complex behavior with respect to load distribution that may arise from irregular geometry and skew that will otherwise be approximated. It also facilitates calculations of eccentric effects from overhangs that may be of interest for construction analysis. However, the tributary load method is more efficient (with sufficient accuracy of global behavior) and with additional manual pre-processing can capture specific effects of interest. Because composite models are created in future steps an explicit deck model is used in this example. The general process for both methods is similar:

- a. Define location of girders and intermediate cross-frames, and deck slab (if applicable). Depending on software, the girder may have to be defined by multiple segments such that the intermediate cross-frames can be connected to the girders. Between nodes used to define member ends it may also be necessary in this step to discretize the geometry (through addition of nodes) such that members

are ultimately composed of a sufficient number of elements. The number of elements should be enough to capture the expected behavior of each component, but not so many that computational time becomes excessive. Consideration should also be given to where results are required, as additional nodes may need defined at these locations. In the analysis software used, elements are created through a meshing process, where an element size/number is specified and applied to the structural members. As elements are defined geometrically, it may also be necessary to choose an element type. Further discussion of element definition and element types can be found in Section 3.7.

- b. Define section properties of girder, intermediate cross-frame, and deck (if applicable). The girders in this example have several cross-sections along their length due to plate transitions; section properties may be calculated by hand as in previous examples, or analysis software may require plate dimensions to be input from which the cross-section properties will be calculated. Because the cross-frames are represented by a single member, effective section properties must be calculated. This process is further described in sections to follow. The deck slab is defined with a thickness and eccentricity.
 - c. Define material properties for girders, intermediate cross-frame, and deck slab (if applicable). If the deck slab is explicitly modeled, a small (generally a few orders of magnitude smaller than hardened concrete), but non-zero value should be specified for the elastic modulus of the material. As a general rule, zero stiffness assignments which can cause problems in numerical solution schemes should be avoided.
 - d. Define support conditions taking into account orientation and articulation.
 - e. Define loads applied to the non-composite structure.
 - i. For the members defined in the model, the girders and intermediate cross-frames (and deck if applicable), automatic dead load application can be used if mass density is assigned through material properties. Otherwise, concentrated or distributed loads that are statically equivalent to the weight of the members can be used.
 - ii. The other non-composite dead loads (SIP forms, haunches, deck slab if not explicitly modeled) are applied as uniform line loads to each girder.
 - f. Define load cases.
 - g. Ensure correct attributes are assigned (geometric and material properties, support conditions, and loading) to appropriate components.
 - h. Run analysis; verify analysis results using simplified methods and expected behavior (deflected shape, qualitative force distribution).
 - i. Extract required results from analysis software.
 - j. Perform supplemental hand calculations.
2. Create model for composite dead loads (continuation of the model created in Step 1).
 - a. Define location of concrete deck slab (if not performed in Step 1a) and create appropriate surface elements (refer to Section 3.5.2.1). Note that in typical design the haunch is assumed = 0 as it cannot be guaranteed to be present after construction. For existing structures, verified haunch depths can be included
 - b. Define properties of concrete deck slab (if not performed in Step 1b).

- c. Define (or modify) material properties for concrete deck slab. (See Step 1c for more information). The stiffness should consider long-term effects.
 - d. Define support conditions.
 - e. Define loads applied to the composite structure.
 - i. The FWS is defined as a uniform load distributed over an area.
 - ii. The weight of the barrier is defined as a uniform line load.
 - f. Define load cases.
 - g. Ensure correct attributes are assigned (geometric and material properties, support conditions, and loading) to appropriate components.
 - h. Run analysis; verify analysis results using simplified methods and expected behavior (deflected shape, qualitative force distribution).
 - i. Extract required results from analysis software.
 - j. Perform supplemental hand calculations.
3. Create model for composite live loads (continuation of model created in Step 2).
- a. Define material properties for concrete deck slab. Because live loading is short-duration the stiffness of the concrete deck is modified to the normal stiffness of concrete.
 - b. Define optimized loading. The analysis software may have utilities that help in the determination. Influence surfaces can be developed to aid in loading generation.
 - c. Run analysis with optimized loading and verify results using simplified methods and expected behavior (deflected shape, qualitative force distribution).
 - d. Extract required results from analysis software.
 - e. Perform supplemental hand calculations.
4. Combine analysis results extracted in Steps 1i, 1j, 2i, 2j, 3d, and 3e.

9.3.2.1 Step 1 – Create Non-Composite Dead Load Model (explicit deck)

9.3.2.1.1 Step 1a – Define Girder, Intermediate Cross-Frame, and Concrete Deck Slab Locations

From Figures 230 and 231, the location of the girders, intermediate cross-frames, can be found. To properly assign attributes, nodes must be defined at all member intersections and plate transitions (which are located using Figures 232 to 235). Beam elements are used for both girders and intermediate cross-frame members. The Timoshenko beam formulation, which is capable of capturing shear deformation, is specified. Mindlin-Reissner (“thick”) shell elements, which are also capable of capturing shear deformation (as well as membrane forces) are used to define the concrete deck slab.

9.3.2.1.2 Step 1b – Define Girder, Intermediate Cross-Frame, and Concrete Deck Slab Cross-Sections

Cross-section properties can be defined in several ways. One method is to generate properties using utilities within the analysis package. The second method is to calculate the section properties by hand and input them into software. This is necessary for generating cross-frame sections, which, in two-dimensions, must be defined using a line with effective properties representing the frame as it exists in space and in curved girders to account for the contribution

of warping torsional resistance (in lieu of Saint-Venant's resistance only). These extra steps are detailed below. Girder section properties are summarized in Appendix 9.D.

1. Warping Torsion Resistance in Girders

To enhance the response of the 2D girder system to the torsional effects resulting from overhang loading, skew, and curvature, modifications are made to the torsional constant, J. The equivalent torsional constant, J_{eq} , as proposed by White et al. (2012) for two sets of boundary conditions:

$$J_{eq} = J*[1-\sinh(pL)/pL+(\cosh(pL)-1)^2/pL\sinh(pL)]^{-1} \text{ (fixed-fixed)}$$

$$J_{eq} = J*[1-\sinh(pL)/pL\cosh(pL)]^{-1} \text{ (fixed-free)}$$

where L is the distance between cross-frames and p is related to the ratio of torsional stiffness (GJ) and warping stiffness (EC_w):

$$p^2 = GJ/EC_w$$

The fixed-fixed condition is assumed at interior segments (away from piers and abutments) where flanges are restrained by intermediate cross-frames, while the fixed-free condition is assumed at piers and abutments where member ends tend to provide less restraint.

A sample calculation for the first section along girder G1 is provided with section properties provided in Table 49:

Table 49. G1-1 section properties.

$b_{f,top}$ (in)	16
$t_{f,top}$ (in)	1
$b_{f,bottom}$ (in)	16
$t_{f,bottom}$ (in)	1
D (in)	92
t_w (in)	0.625

Given:

$$L = 21.083 \text{ ft}$$

$$E = 29000 \text{ ksi (steel)}$$

$$G = 11150 \text{ ksi (steel)}$$

Calculate p:

$$J \approx \sum bt^3/3 = [(16)(1^3)+(16)(1^3)+(92)(0.625^3)]/3 = 18.15 \text{ in}^4 = 0.000875 \text{ ft}^4$$

$$C_w \approx I_y h^2/4 = (684.54)(93^2)/4 = 1480146.62 \text{ in}^6$$

$$I_y = 2*(16^3)(1)/12+(92)(0.625^3)/12 = 684.54 \text{ in}^4$$

$$h = D+t_{f,top}/2+ t_{f,bottom}/2 = 93 \text{ in}$$

$$\text{Therefore, } p = ([(11150)(18.15)] / [(29000)(1480146.62)])^{1/2} = 0.00217 \text{ in}^{-1} = 0.026 \text{ ft}^{-1}$$

As an end section, G1-1 is represented by the fixed-free condition mentioned above:

$$\begin{aligned} \text{Therefore, } J_{eq} &= J*[1-\sinh(pL)/pL\cosh(pL)]^{-1} \\ &= (0.000875)*[1-\sinh(0.026*21.083)/(0.026*21.083*\cosh(0.026*21.083))]^{-1} \\ &= 0.00975 \text{ ft}^4 \end{aligned}$$

2. Effective Properties of Intermediate Cross-Frames

To model three-dimensional cross-frames with a single line, equivalent properties must be used. Per discussion in 3.5.3, when using Timoshenko beams an equivalent moment of inertia, I_{eq} , is used to represent the flexural stiffness and an equivalent shear area, A_{eq} , is used to represent the shear stiffness of the entire frame.

- a. Flexural stiffness - a separate model containing only the cross-frame (Figure 236) is created and a force couple is applied which gives rise to horizontal displacements at the top and bottom of the frame (related by a rotation angle, θ). The equivalent moment of inertia is given by:

$$I_{eq} = ML/E\theta$$

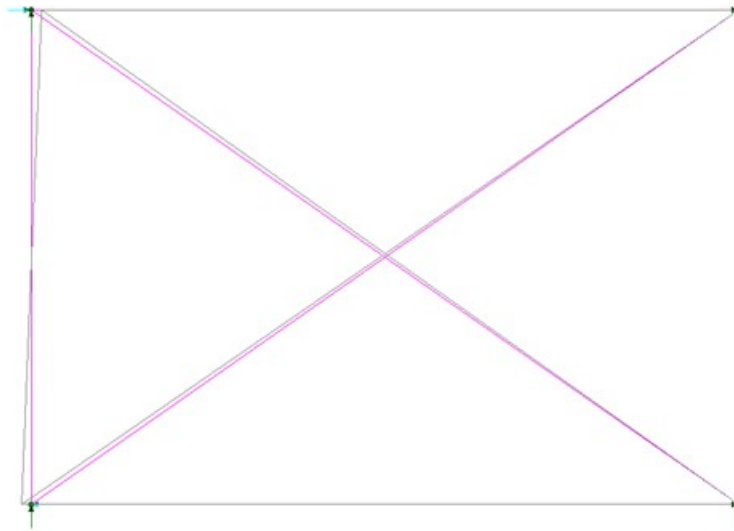


Figure 236. Illustration. Equivalent flexural stiffness model, example cross-frame (CF1).

The equivalent cross-frame inertia properties are summarized in Table 50.

Table 50. Example 3 cross-frame equivalent flexural stiffness

Cross-Frame Type	Δ_{top} (in)	Δ_{bot} (in)	θ (rad)	I_{eq} (ft ⁴)
CF1 (X Brace)	0.0476	0.0441	0.0010	2.0249
CF2 (V Brace)	0.0283	0.0486	0.0008	2.4163
CF3 (Inverted V Brace)	0.0297	0.0297	0.0007	3.1285

- b. Shear area – the models created in the previous step are modified per 3.6.3 as shown in Figure 237. A load is applied on the free end of the structure and the equivalent shear area is given by:

$$A_{eq} = VL/[G(\Delta-VL^3/3EI_{eq})]$$

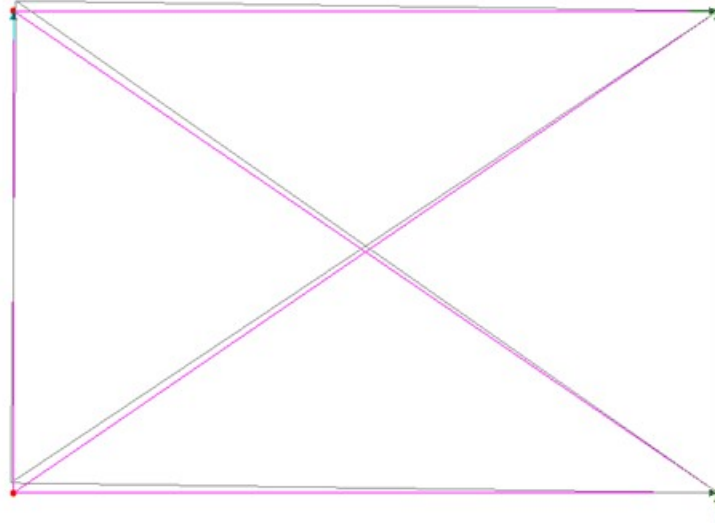


Figure 237. Illustration. Equivalent shear area model, example cross-frame (CF1).

The effective shear area properties are summarized in Table 51.

Table 51. Example 3 cross-frame equivalent shear area

Cross-Frame Type	Δ (in)	I_{eq} (ft ⁴)	A_{eq} (ft ²)
CF1 (X Brace)	0.2023	2.0249	0.0590
CF2 (V Brace)	0.1920	2.4163	0.0590
CF3 (Inverted V Brace)	0.1615	3.1285	0.0680

The concrete deck slab is defined using a geometric surface with a thickness of 9 inches (this is done so the integral wearing surface does not participate in the structural thickness for future models) and is given an eccentricity of 4.347 ft to correct locate its centroid relative to the centroid of the girder and cross-frames.

9.3.2.1.3 Step 1c – Define Material Properties for Girders, Intermediate Cross-Frames, and Concrete Deck Slab

Similar to the section properties, material properties can be calculated and input by hand or by using definitions in the software’s library. For the steel elements, typically assigned values shown in Table 52 are used. The concrete definition, however, must be modified to account for the lack of stiffness in wet concrete and also in a way to facilitate accounting for the actual weight of the deck slab (including the integral wearing surface). In this example the unit weight of the wet concrete is set to zero (pressures are applied to the surface), but if gravity were to be assigned to the deck slab a modified unit weight could be used (or alternatively, a load factor) to account for the difference in actual thickness and structural thickness.

Table 52. Example 3 non-composite material properties.

Material Property	Steel	Flexible Deck Slab Concrete
Modulus of Elasticity (ksf)	4,176,000	524.757E-3
Poisson's Ratio	0.3	0.2
Unit Weight (k/ft ³)	0.490	0.000
Thermal Expansion Coefficient (ft/°F)	6.5E-6	6.0E-6

9.3.2.1.4 Step 1d – Define Support Conditions

The girders are restrained at piers and abutments in local member directions for the conditions shown in Figure and summarized in Table 53. X, Y, and Z represent translational fixity in the longitudinal, transverse, and vertical directions, respectively. Note that in this example the restraints are aligned tangent to the girders. Typically, the expansion bearings would be aligned with the center of expansion, such that under a uniform temperature change, no thermal forces would be induced.

Table 53. Summary of Example 3 support conditions.

Location	<u>G1</u>	<u>G2</u>	<u>G3</u>	<u>G4</u>
Abutment 1	Z	Y, Z	Y, Z	Z
Pier 1	Z	Y, Z	Y, Z	Z
Pier 2	X, Z	X, Y, Z	X, Y, Z	X, Z
Abutment 2	Z	Y, Z	Y, Z	Z

9.3.2.1.5 Step 1e – Define Non-Composite Loads

Self-weight of members defined in the model, the girders and intermediate cross-frames, is applied using a body force. The body force uses the acceleration due to gravity, along with the unit weight and section properties, to determine the weight of the girders and intermediate diaphragms. The body force uses an acceleration of 32.2 ft/s².

The other non-composite dead loads are applied as uniform line loads (haunches) to girders and surface loads (SIP forms, deck slab weight) to the concrete deck slab.

9.3.2.1.6 Step 1f – Define Load Cases

The next step is to define load cases. Since all loads in this model are non-composite, they are combined into a single load case.

9.3.2.1.7 Step 1g – Ensure Correct Attributes Are Assigned to Components

After defining the geometry, member properties, material properties, support conditions, and loads, these attributes must be assigned to the appropriate geometry within the model. The elements defining the girder are assigned the properties associated with the girders and the elements defining the intermediate cross-frames are assigned the properties associated with the intermediate cross-frames. Listed below are the different components and the attributes that must be assigned:

- Girders
 - Beam elements
 - Geometric cross-section
 - Girder steel material properties
 - Dead loads (including self-weight, haunches)
- Cross-Frames
 - Beam elements
 - Geometric cross-section
 - Cross-Frame steel material properties
 - Dead load (self-weight)
- Concrete Deck Slab
 - Surface elements
 - Geometric cross-section
 - Flexible concrete material properties
 - Dead load (self-weight, SIP forms)

9.3.2.1.8 Step 1h – Run Analysis and Verify Results using Simplified Methods

The next step is to run the analysis. In addition to the qualitative inspection of deflected shapes, two simple quantitative checks are made to add confidence in the model.

Check 1: Sum of unfactored Concrete Deck Slab Reactions

Curb 1 Radius of Curvature, $R_1 = 679.75$ ft

Curb 2 Radius of Curvature, $R_2 = 720.00$ ft

Angle between Abutments, $\theta \approx 0.76$ radians

Therefore, total curb to curb area, $A = 0.5 \cdot (R_2^2 - R_1^2) \cdot \theta = 21326.92$ ft²

Surface pressure from 9½ inch thick reinforced concrete deck = $(9.5/12)(0.15 \text{ k/ft}^3) = 0.11875$ k/ft²

Total vertical reaction, $F_z = (0.11875 \text{ k/ft}^2)(21326.92 \text{ ft}^2) = 2532.57$ k

Table 54. Unfactored concrete deck slab reactions from 2D PEB model.

Location	X (ft)	Y (ft)	FZ (k)
G1-Abutment 1	0.00	3.75	28.97
G2-Abutment 1	0.00	14.75	78.63
G3-Abutment 1	0.00	25.75	52.90
G4-Abutment 1	0.00	36.75	91.33
G1-Pier 1	125.78	-7.92	204.84
G2-Pier 1	147.94	-1.19	272.89
G3-Pier 1	169.04	5.20	306.51
G4-Pier 1	189.14	11.34	220.65
G1-Pier 2	318.69	-75.10	263.18
G2-Pier 2	341.87	-75.22	286.38
G3-Pier 2	363.91	-75.35	281.51
G4-Pier 2	384.89	-75.41	173.69
G1-Abutment 2	469.44	-182.96	49.57
G2-Abutment 2	477.01	-174.99	90.51
G3-Abutment 2	484.57	-166.99	75.45
G4-Abutment 2	492.09	-158.97	53.29

Total vertical reaction from the analysis software, $F_z = 2530.30$ k

The percent difference between hand calculation and analysis software, $(2532.57-2530.30)/2532.57 = 0.09\%$, **therefore OK.**

Check 2: G2 Midspan Moment in Span 2 due to Self-Weight

The average weight of the G2 girder in Span 2 away from supports is 0.352 k/ft.

Though there are not easily accessible approximations for girder moments in horizontally curved bridges with skewed supports, unequal spans, and variable stiffness, some approximations are made to predict the order of moment that is to be expected. An interior girder is chosen since the span lengths are more symmetric on this bridge and the tributary width is expected to also be more symmetric about the girder centerline.

Treating G2 as a three span continuous beam and span length equal to the arc length between supports, and further approximating by using the three equal span moment equation:

$$M_{\text{midspan}} = 0.025wL^2 = 0.025*(0.352 \text{ klf})(208.354 \text{ ft})^2 = 382.02 \text{ k-ft}$$

From the analysis software, the midspan moment from G2 self-weight only in Span 2 is,

$$M_{\text{midspan}} = 403.11 \text{ k-ft}$$

The percent difference between hand calculation and analysis software, $(403.11-382.02)/382.02 = 5.52\%$, **therefore OK.**

In general, results for simple approximations of complicated structures should not be expected to be exact, and a discrepancy in the range of 10-20 percent is reasonable. When verifying a complex model it is often more helpful to use qualitative observations of deflected shapes and trends in forces (i.e. are moments increasing where they should, are there any unexpected jumps in shear). Acceptable levels of accuracy should consider the complexity of the analysis and geometry being investigated, but ultimately depend on the discretion of the project manager.

9.3.2.1.9 Step 1i – Extract Required Results from Analysis Software

After verifying that the results from the analysis are reasonable, the results of interest can be extracted and input into a spreadsheet for further use. It may be necessary to select only certain portions of the model to obtain the results wanted.

9.3.2.1.10 Step 1j – Perform supplemental hand calculations (flange lateral bending moments)

An equation from the *AASHTO LRFD Specifications* are used to approximate the flange lateral bending moments that arise due to horizontal curvature and cannot adequately be captured by the 2D representation of models. The flange lateral bending moments are given by:

$$M_{lat} = ML^2/NRD \text{ (AASHTO 4.6.1.2.4b-1)}$$

where M is the primary major-axis bending moment, L is the unbraced length of the span, N is a constant assumed to be 10 or 12 depending on the level of conservatism desired, R is the radius of curvature, and D is the web depth of the girder. A value of 12 (less conservative) has been assumed for this example in an attempt to provide a better comparison of behavior with the 3D FEA models.

9.3.2.2 Step 2 – Create Composite Dead Load Model

Building on the model in the previous step, the creation of a composite dead load model can be done through modification of the material properties of the concrete deck slab, by removing DC1 loads, and assigning the new loads of interest for DC2 and DW.

9.3.2.2.1 Step 2a – Define Location of Girders, Cross-Frames, and Concrete Deck Slab

The location of all bridge elements has been defined while creating the non-composite dead load model. Therefore, no modifications to geometry are required.

9.3.2.2.2 Step 2b – Define Section Properties for Girders, Cross-Frames, and Concrete Deck Slab

The cross-frames and deck slab have been defined while creating the non-composite dead load model. Therefore, no modifications to section properties are required.

9.3.2.2.3 Step 2c – Define Material Properties for Girders, Cross-Frames, and Concrete Deck Slab

To account for the cured concrete deck, the modulus of elasticity should be modified from the previously assumed flexible state. Because this model represents the long-term composite condition (in which the relative stiffness of the steel to concrete is assumed to increase as a result of concrete creep) the typical modulus of concrete is reduced by two-thirds ($E_c/3$). For 4 ksi concrete, the modulus is calculated per AASHTO Eq. 5.4.2.4-1 as 524.757E3 ksf, resulting in a long-term modulus of 174.919E3 ksf.

9.3.2.2.4 Step 2d – Define Support Conditions

As this model is a continuation of the previous model, support conditions have already been appropriately assigned.

9.3.2.2.5 Step 2e – Define Composite Dead Loads

The FWS load is defined as a uniform load distributed over the bridge width. To account for the difference in modeled width and actual width (which spans only between barriers), the FWS load is reduced from 0.030 k/ft² (spread over 37.50 ft) to 0.028 ksf (spread over 40.50 ft).

The weight of the barrier is applied as a uniform line load.

9.3.2.2.6 Step 2f – Define Load Cases

Separate load cases are defined for the composite dead loads; in this analysis the composite dead loads are simply added together, however, in a typical design the barrier would be a DC (component dead load) load while the future wearing surface would be a DW (wearing surface dead load) load. In Strength and Extreme Event load combinations these effects carry different load factors.

9.3.2.2.7 Step 2g – Ensure Correct Attributes Are Assigned to Components

After defining the geometry and elements, member properties, material properties, support conditions, and loads, these attributes must be assigned to the appropriate geometry within the model. The lines defining the girders, intermediate cross-frames, and pier cross-frames are assigned the properties for the respective component. The concrete deck slab surfaces are assigned the properties of the deck slab. Listed below are the different components and the attributes that must be assigned:

- Girders
 - Geometric cross-section
 - Girder steel material properties
 - Beam elements
- Intermediate and Pier Cross-Frames
 - Geometric cross-section
 - Cross-frame steel material properties
 - Beam elements

- Concrete Deck Slab
 - Deck slab thickness
 - 4 ksi concrete material properties, stiffness reduced by a factor of 3
 - Surface elements
 - FWS and barrier loading

9.3.2.2.8 Step 2h – Run Analysis and Verify Results using Simplified Methods

The next step is to run the analysis. Errors may exist and can be addressed as discussed in the preceding sections.

In addition to the qualitative inspection of deflected shapes, two simple quantitative checks are made to add confidence in the model.

Check 1: Sum of unfactored FWS Reactions

Similar to previous calculations (See Section 9.3.2.1.8),

Surface pressure from FWS = 0.028 k/ft²

Total vertical reaction, $F_z = (0.028 \text{ k/ft}^2)(21326.92 \text{ ft}^2) = 597.15 \text{ k}$

Table 55. Unfactored FWS reactions from 2D PEB model.

Location	X (ft)	Y (ft)	FZ (k)
G1-Abutment 1	0.00	3.75	10.00
G2-Abutment 1	0.00	14.75	14.05
G3-Abutment 1	0.00	25.75	16.47
G4-Abutment 1	0.00	36.75	19.95
G1-Pier 1	125.78	-7.92	46.63
G2-Pier 1	147.94	-1.19	65.92
G3-Pier 1	169.04	5.20	69.93
G4-Pier 1	189.14	11.34	54.21
G1-Pier 2	318.69	-75.10	64.52
G2-Pier 2	341.87	-75.22	59.43
G3-Pier 2	363.91	-75.35	67.08
G4-Pier 2	384.89	-75.41	45.39
G1-Abutment 2	469.44	-182.96	16.40
G2-Abutment 2	477.01	-174.99	16.40
G3-Abutment 2	484.57	-166.99	15.20
G4-Abutment 2	492.09	-158.97	15.56

Total vertical reaction from the analysis software, $F_z = 597.13 \text{ k}$

The percent difference between hand calculation and analysis software,

$(597.15-597.13)/597.15 = 0.003\%$, **therefore OK.**

Check 2: G2 Midspan Moment in Span 2 Due to FWS

Though there are not easily accessible approximations for girder moments in horizontally curved bridges with unequal spans and variable stiffness, some approximations are made to predict the order of moment that is to be expected from the FWS. An interior girder is chosen since the span lengths are more symmetric on this bridge and the tributary width is expected to also be more symmetric about the girder centerline.

Treating G2 as a three-span continuous beam with tributary width equal to 11 ft (girder spacing) and span length equal to the arc length between supports, and further approximating by using the three equal span moment equation:

$$M_{\text{midspan}} = 0.025wL^2 = 0.025*(0.028 \text{ ksf})(11 \text{ ft})(208.354 \text{ ft})^2 = 334.268 \text{ k-ft}$$

From the analysis software, the midspan moment from FWS only in Span 2 is,

$$M_{\text{midspan}} = 339.799 \text{ k-ft}$$

The percent difference between hand calculation and analysis software, $(334.268-339.799)/334.268 = 1.65\%$, **therefore OK**.

9.3.2.2.9 Step 2i – Extract Required Results from Analysis Software

After verifying that the results from the analysis are reasonable, the results of interest can be extracted and input into a spreadsheet for further use. It may be necessary to select only certain portions of the model to obtain these results.

9.3.2.2.10 Step 2j – Perform supplemental hand calculations (flange lateral bending moments)

Similar to Step 1j, additional calculations of flange lateral bending moments are made using AASHTO C4.6.1.2.4b-1.

9.3.2.3 Step 3 – Create Composite Live Load Model

Building on the model in the previous step, the creation of a composite live load model can be done through similar modification of the properties of the concrete deck slab, removing DC2 and DW loads, and assigning the new loads of interest for live load.

9.3.2.3.1 Step 3a – Define Material Properties for Concrete Deck Slab

Once again the stiffness of the concrete deck slab should be accounted for through modification of the modulus of elasticity. For 4 ksi concrete, a modulus of $524.757E3$ ksf is used per AASHTO Eq. 5.4.2.4-1.

9.3.2.3.2 Step 3b – Determine Optimized Live Load

Utilities within the analysis program are used to optimize loading conditions. Care should be taken in the definition of influence attributes of interest such that the correct orientation has been specified. Before running the analyses, the live load cases produced should be examined in a qualitative fashion to ensure they are logical. For this example, the software used automatically generates the influence surfaces and then determines the load placement required for extreme

effects. In the absence of such utilities, influence line/surfaces can be generated using classical analysis methods.

9.3.2.3.3 Step 3c – Run Analysis and Verify Results using Simplified Methods

The next step is to run the analysis. In addition to the qualitative inspection of deflected shapes and loading configurations for maximizing specific effects, a simple quantitative check is made to add confidence in the model.

Check 1: Vertical Reactions Under Sample Truck Loading Configuration

A live load truck configuration (Figure 238) was arbitrarily chosen to check vertical reactions. From the figure, the utility within the analysis program has produced a load case with three design trucks (HL-93 is used for design force effects).

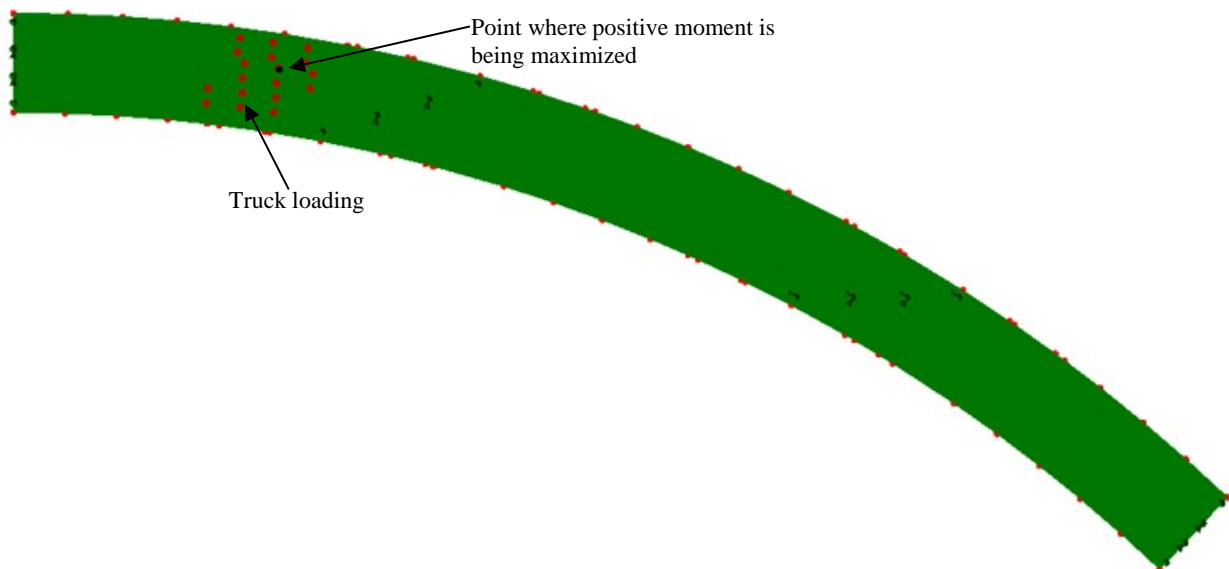


Figure 238. Illustration. Sample truck loading configuration.

Weight of three design trucks, $W = (3)(72 \text{ k}) = 216 \text{ k}$

Because this load case features three lanes of traffic, a multiple presence factor of 0.85, which is automatically applied by the analysis program, is required.

Applying the multiple presence factor, $W = (0.85)(216 \text{ k}) = 183.6 \text{ k}$

Table 56. Unfactored truck reactions (including multiple presence) from 2D PEB model.

Location	X (ft)	Y (ft)	FZ (k)
G1-Abutment 1	0.00	3.75	-0.71
G2-Abutment 1	0.00	14.75	5.90
G3-Abutment 1	0.00	25.75	11.74
G4-Abutment 1	0.00	36.75	22.53
G1-Pier 1	125.78	-7.92	0.06
G2-Pier 1	147.94	-1.19	91.88
G3-Pier 1	169.04	5.20	73.12
G4-Pier 1	189.14	11.34	1.85
G1-Pier 2	318.69	-75.10	-4.87
G2-Pier 2	341.87	-75.22	-23.43
G3-Pier 2	363.91	-75.35	-5.58
G4-Pier 2	384.89	-75.41	5.13
G1-Abutment 2	469.44	-182.96	1.68
G2-Abutment 2	477.01	-174.99	1.82
G3-Abutment 2	484.57	-166.99	1.03
G4-Abutment 2	492.09	-158.97	1.46

Total vertical reaction from the analysis software, $F_z = 183.60$ k

The percent difference between hand calculation and the analysis software, $(183.60-183.60)/183.60 = 0.00\%$, **therefore OK**.

9.3.2.3.4 Step 3d – Extract Required Results from Analysis Software

After verifying that the results from the analysis are reasonable, the results of interest can be extracted and input into a spreadsheet for further use. It may be necessary to select only certain portions of the model to obtain the results.

9.3.2.3.5 Step 3e – Perform supplemental hand calculations (flange lateral bending moments)

Similarly to Steps 1j and 2j, additional calculations of flange lateral bending moments are made using AASHTO C4.6.1.2.4b-1.

9.3.2.4 Step 4 – Combine Analysis Results

Once the results of interest, in this case moments, shears, and deflections, have been extracted from the analysis software, they will be combined into groups of non-composite dead loads, composite dead loads, and live loads so the resulting stresses can be combined using appropriate section properties.

For a 2D PEB model, the moment due to composite dead load and live load in the girder is not only the girder moment in the results. Due to the eccentricity between the deck slab and beam the actual moment in the girder is equal to the moment plus the axial force times the girder

eccentricity. The analysis program used herein has utilities that allow these moments to be extracted directly, but manual calculations integrating stresses may be required when other software is used (sample calculations appear in previous example problems).

The HL-93 Design Load consists of the maximum of the design truck or design tandem amplified by the dynamic load allowance plus the design lane. Each load component was analyzed individually therefore the results must be combined. Similarly, for negative moment between dead load inflection points, the design truck train including the dynamic load allowance and design lane must be combined. Additionally, the results from the different live load models may have to be combined to determine the greatest live load force effect for each girder. Also for live load, the multiple presence factor in Table 3.6.1.1.2-1 of the Specifications must be applied. The software used has a feature that incorporates multiple presence as a default.

Once the moments, shears, and deflections have been combined into appropriate groups using the results from the various analyses, graphs can be created to show the moment and shear diagrams and deflected shape. The analysis results are combined using the following groups: non-composite dead loads (girder self-weight, diaphragms, SIP forms, haunches, and concrete deck slab), composite dead loads (barrier and FWS), and maximum and minimum live loads including the dynamic load allowance. The moment and shear diagrams and deflected shapes from the 2D PEB analysis are shown in Figures 239 through 250.

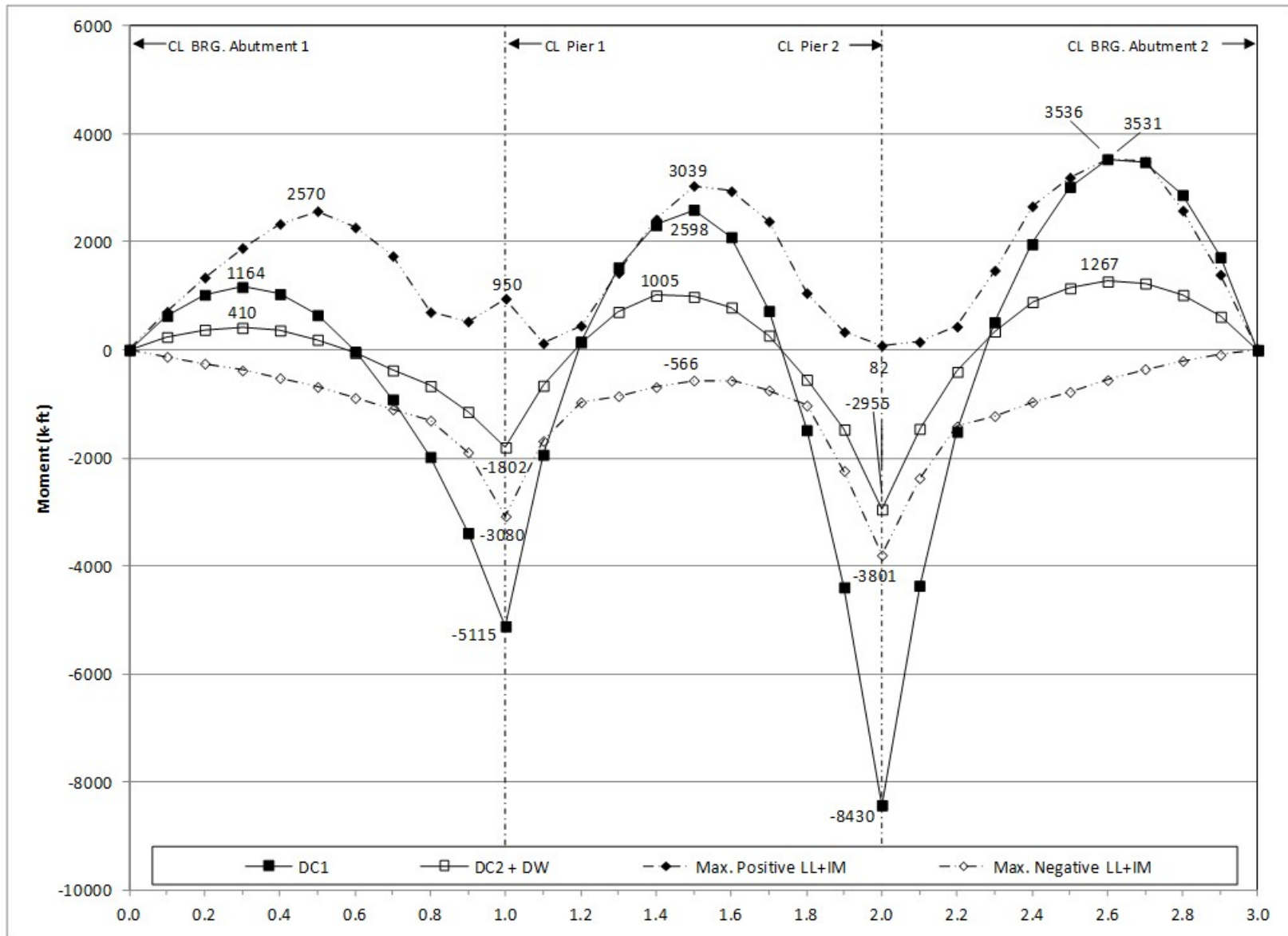


Figure 239. Graph. 2D moment diagram and live load envelope for Girder 1.

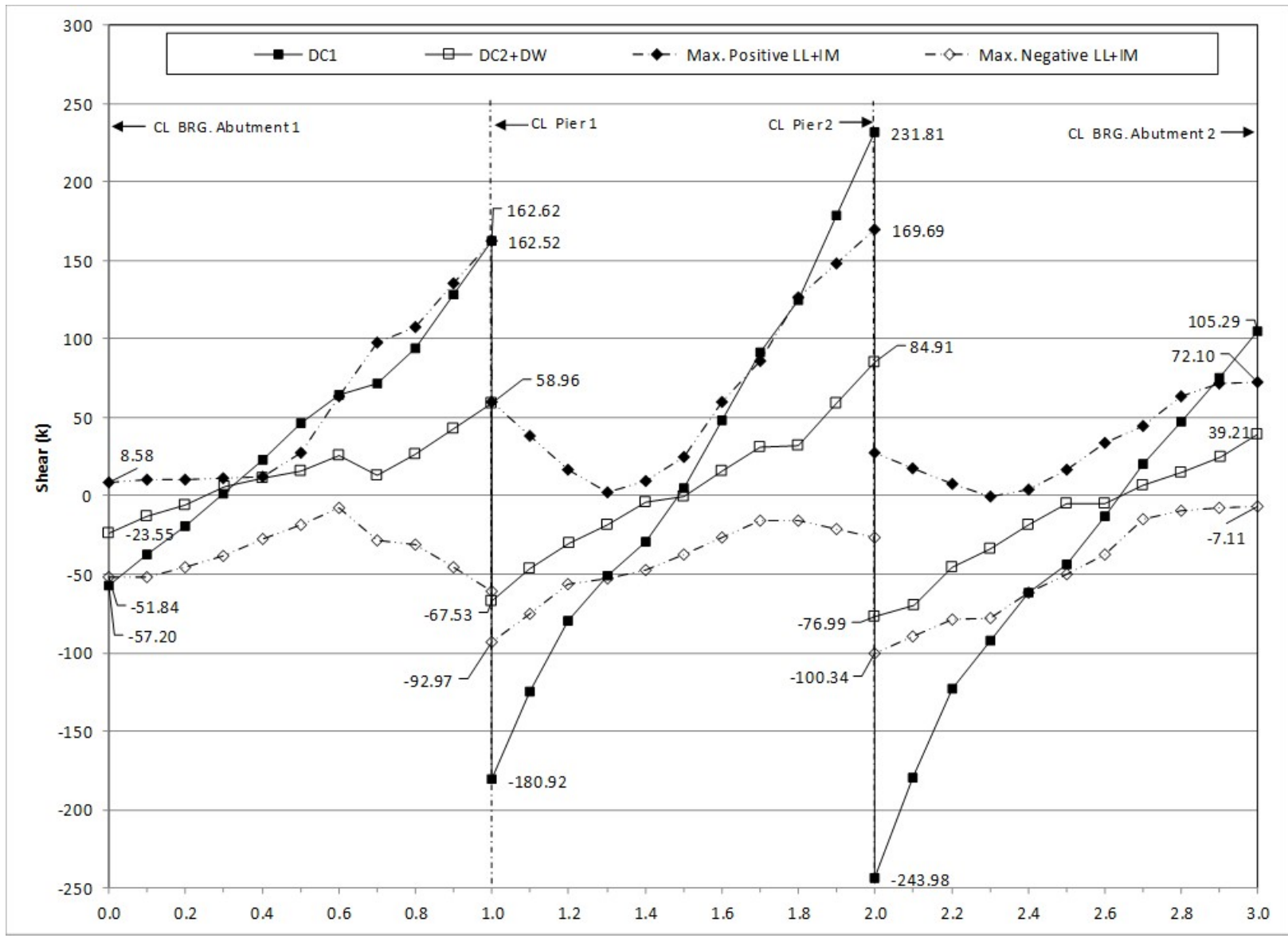


Figure 240. Graph. 2D shear diagram and live load envelope for Girder 1.

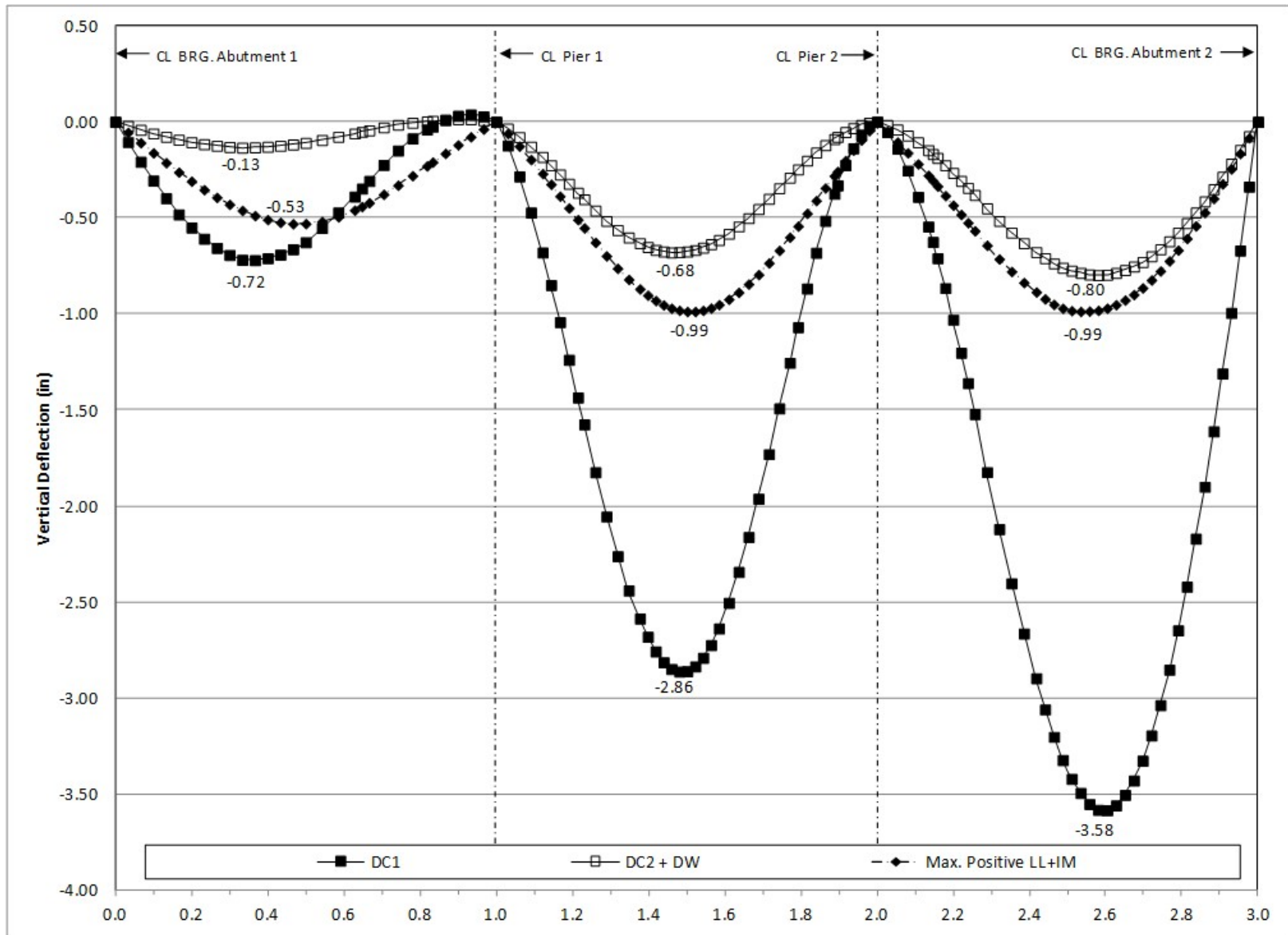


Figure 241. Graph. 2D deflection diagram for Girder 1.

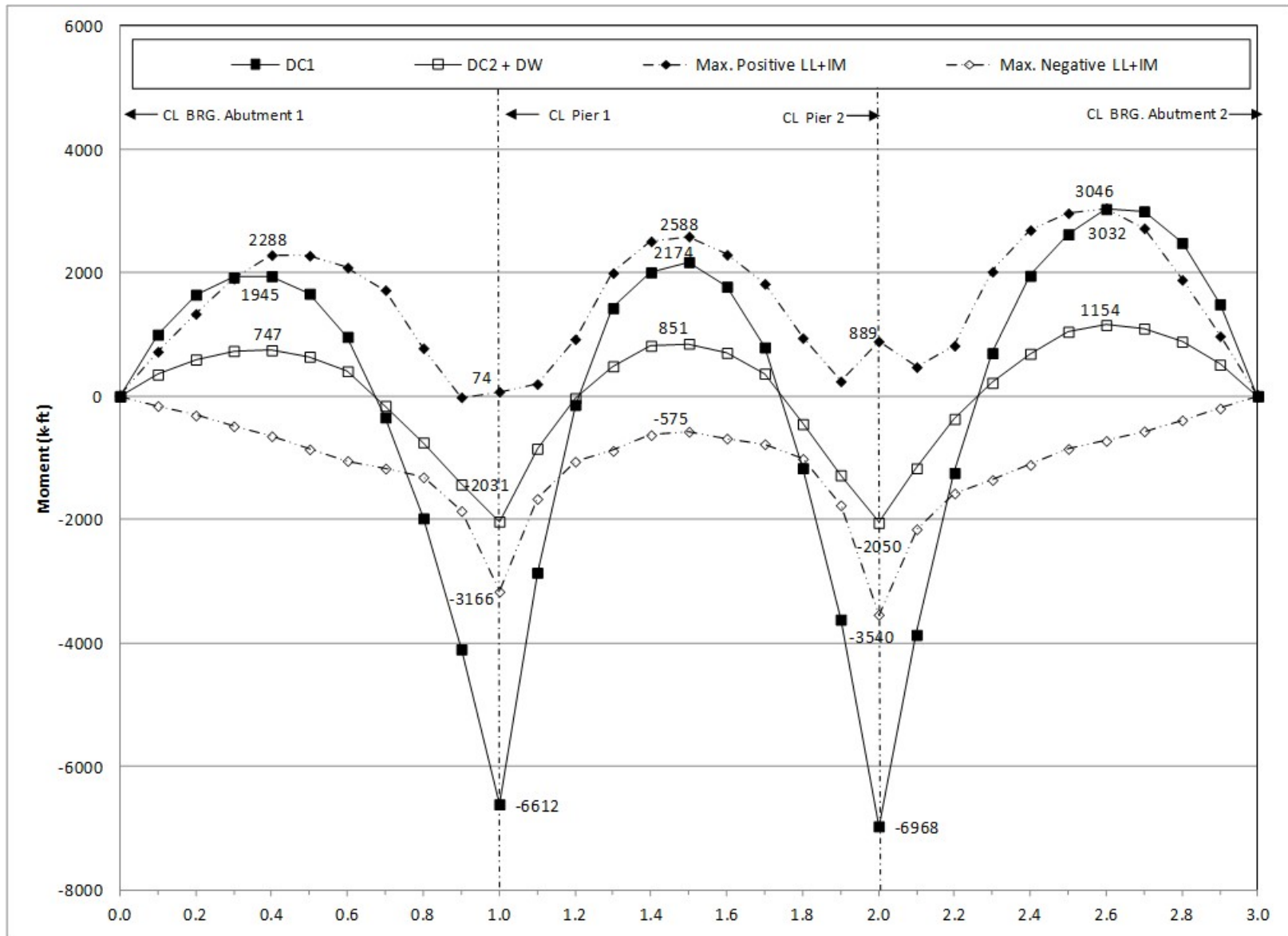


Figure 242. Graph. 2D moment diagram and live load envelope for Girder 2.

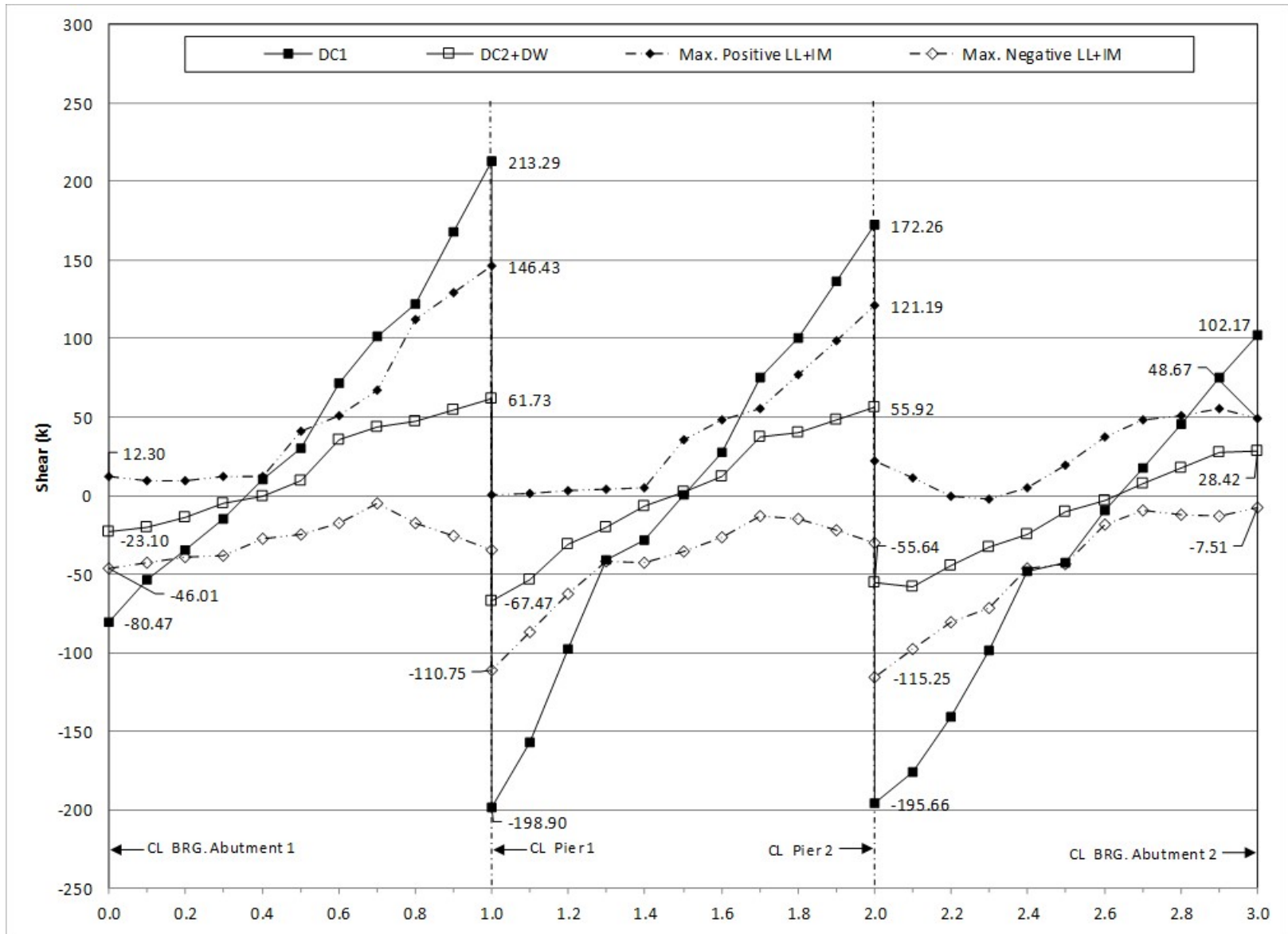


Figure 243. Graph. 2D shear diagram and live load envelope for Girder 2.

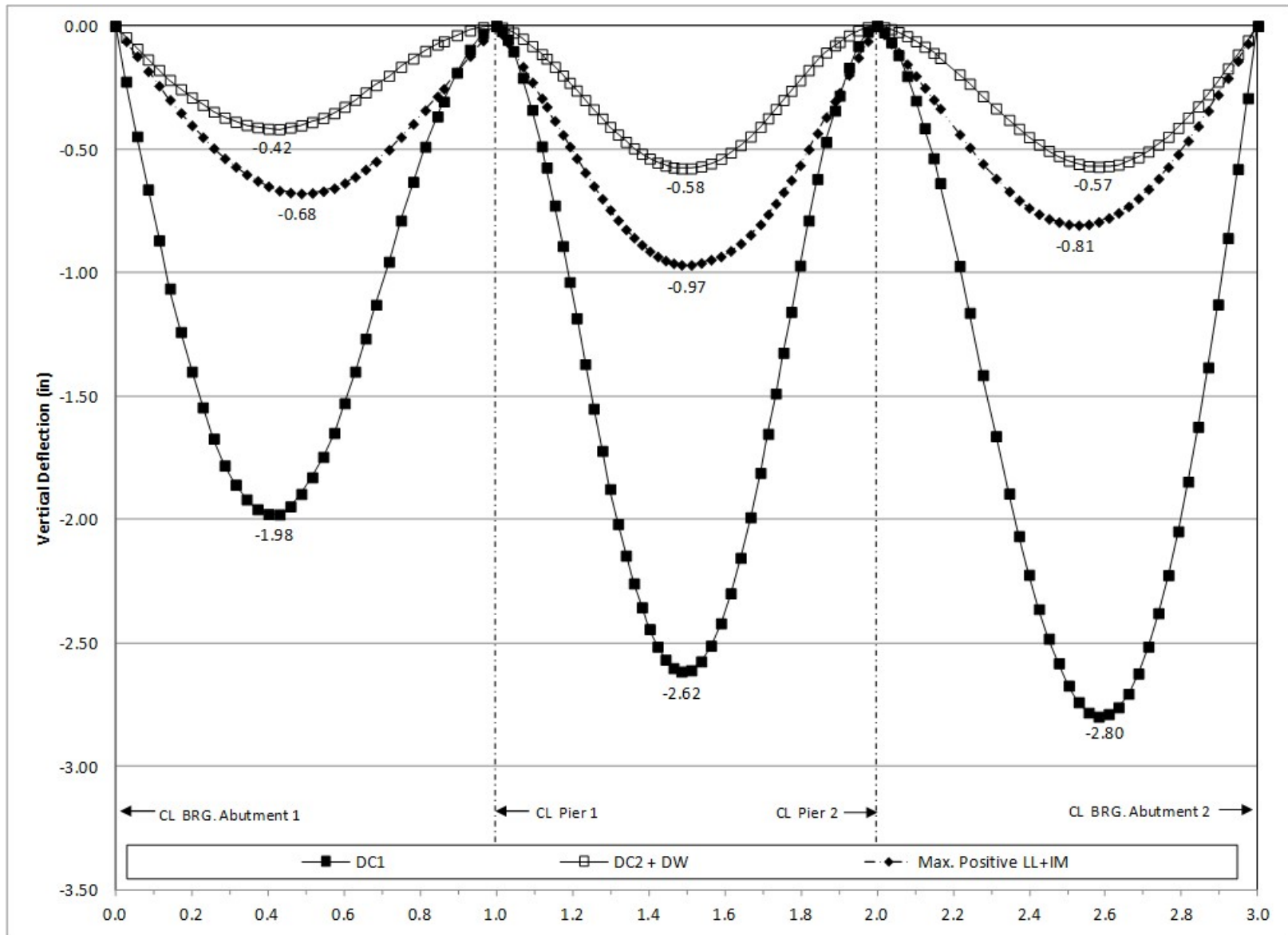


Figure 244. Graph. 2D deflection diagram for Girder 2.

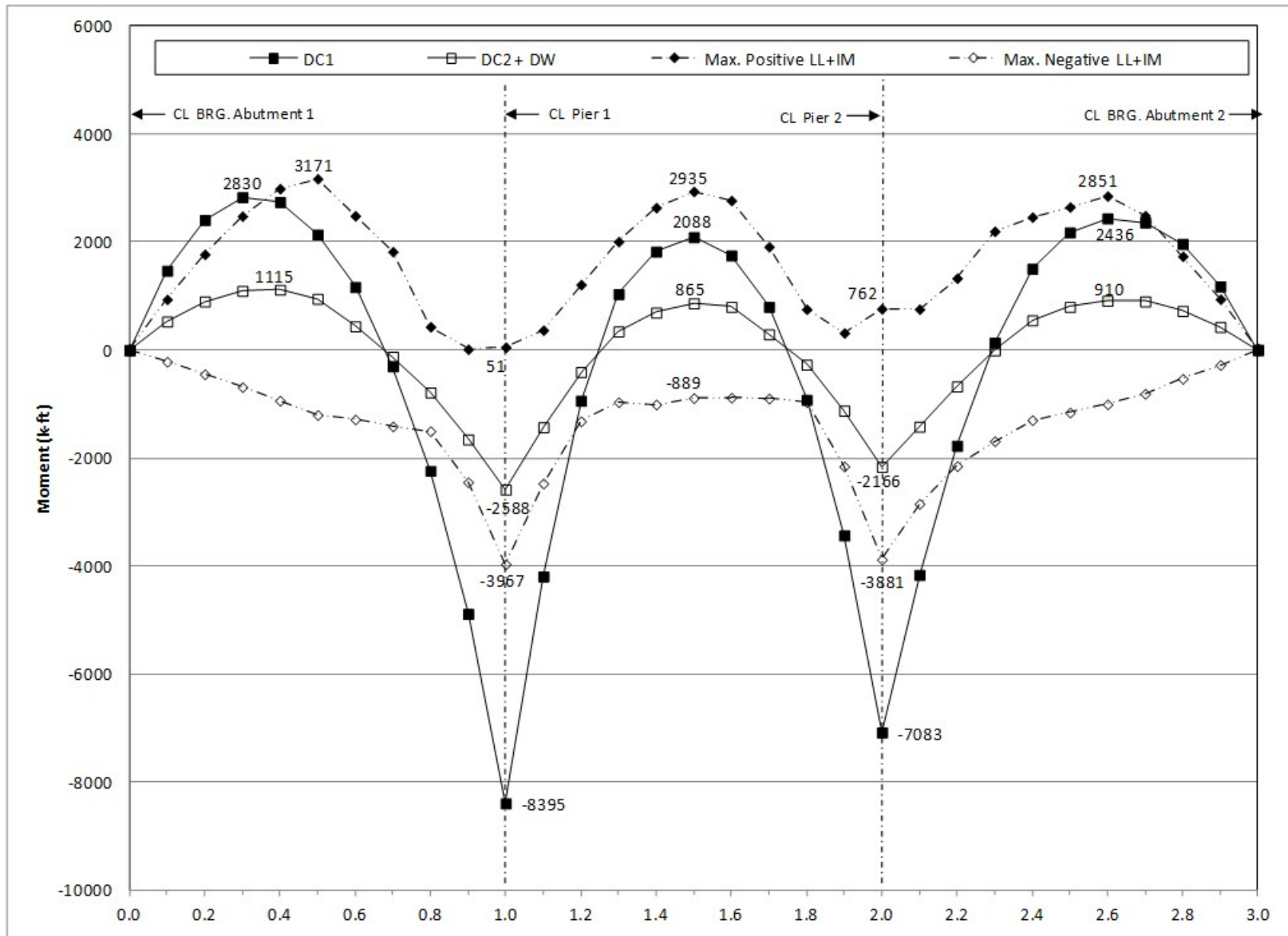


Figure 245. Graph. 2D moment diagram and live load envelope for Girder 3.

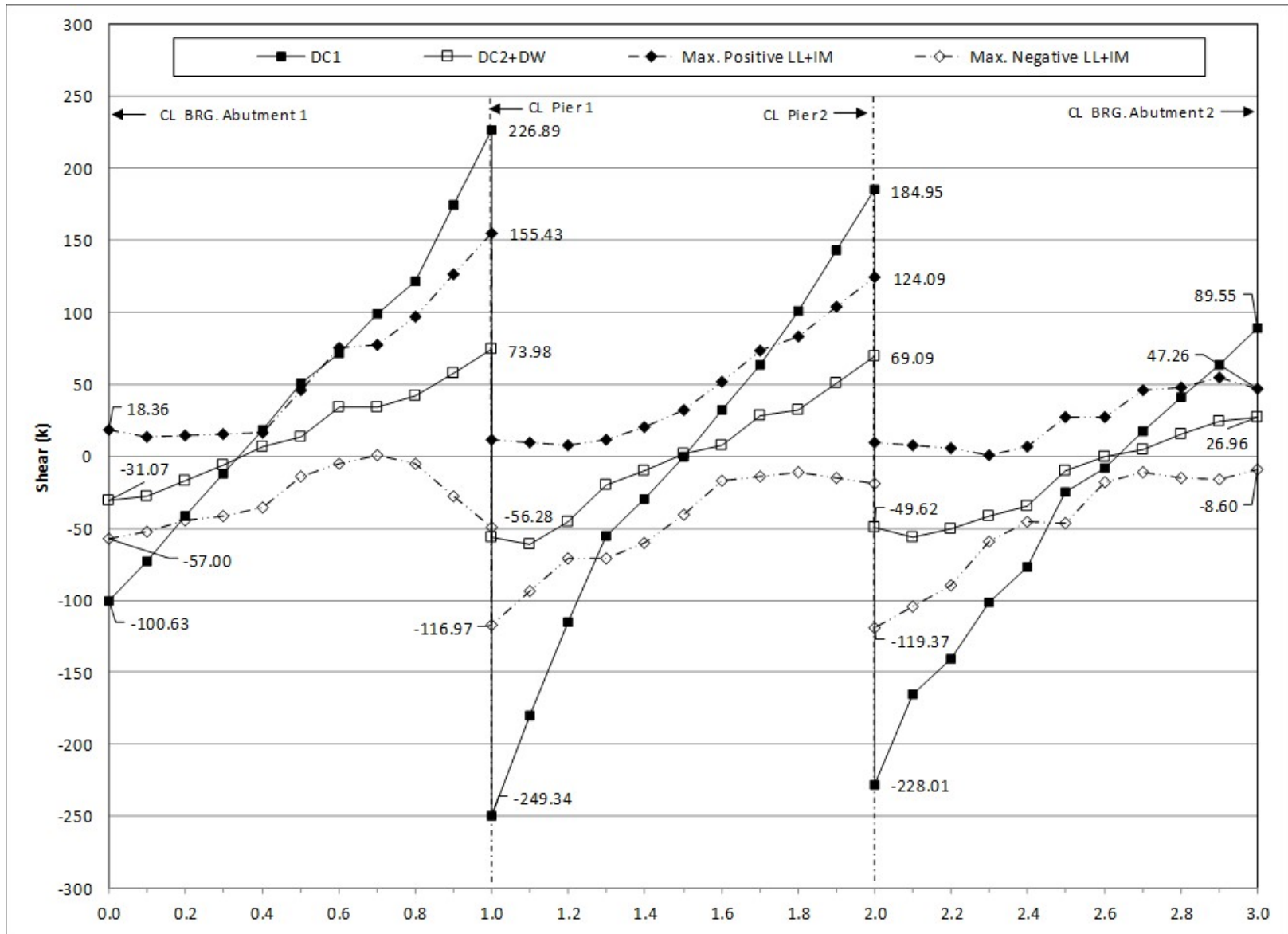


Figure 246. Graph. 2D shear diagram and live load envelope for Girder 3.

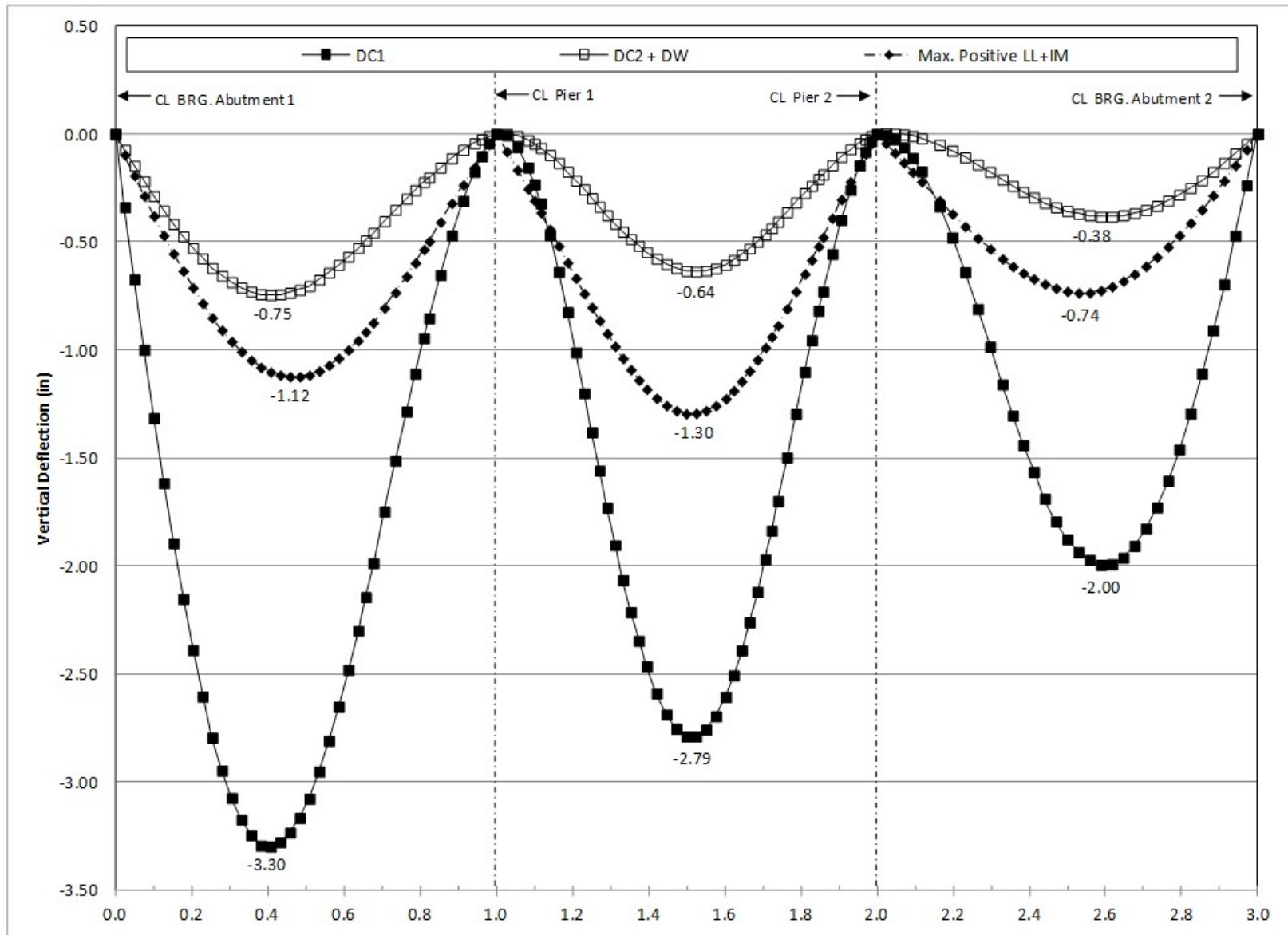


Figure 247. Graph. 2D deflection diagram for Girder 3.

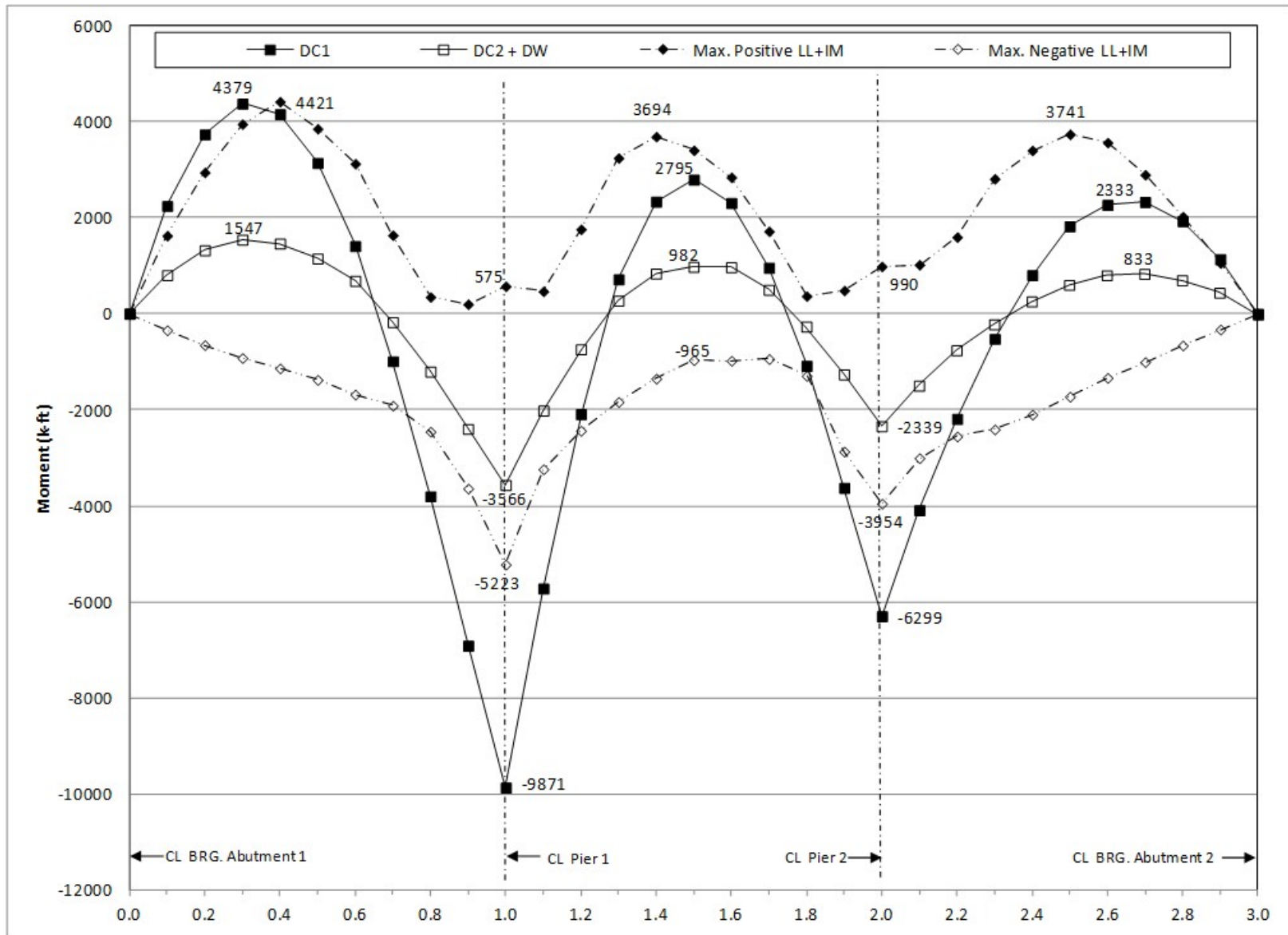


Figure 248. Graph. 2D moment diagram and live load envelope for Girder 4.

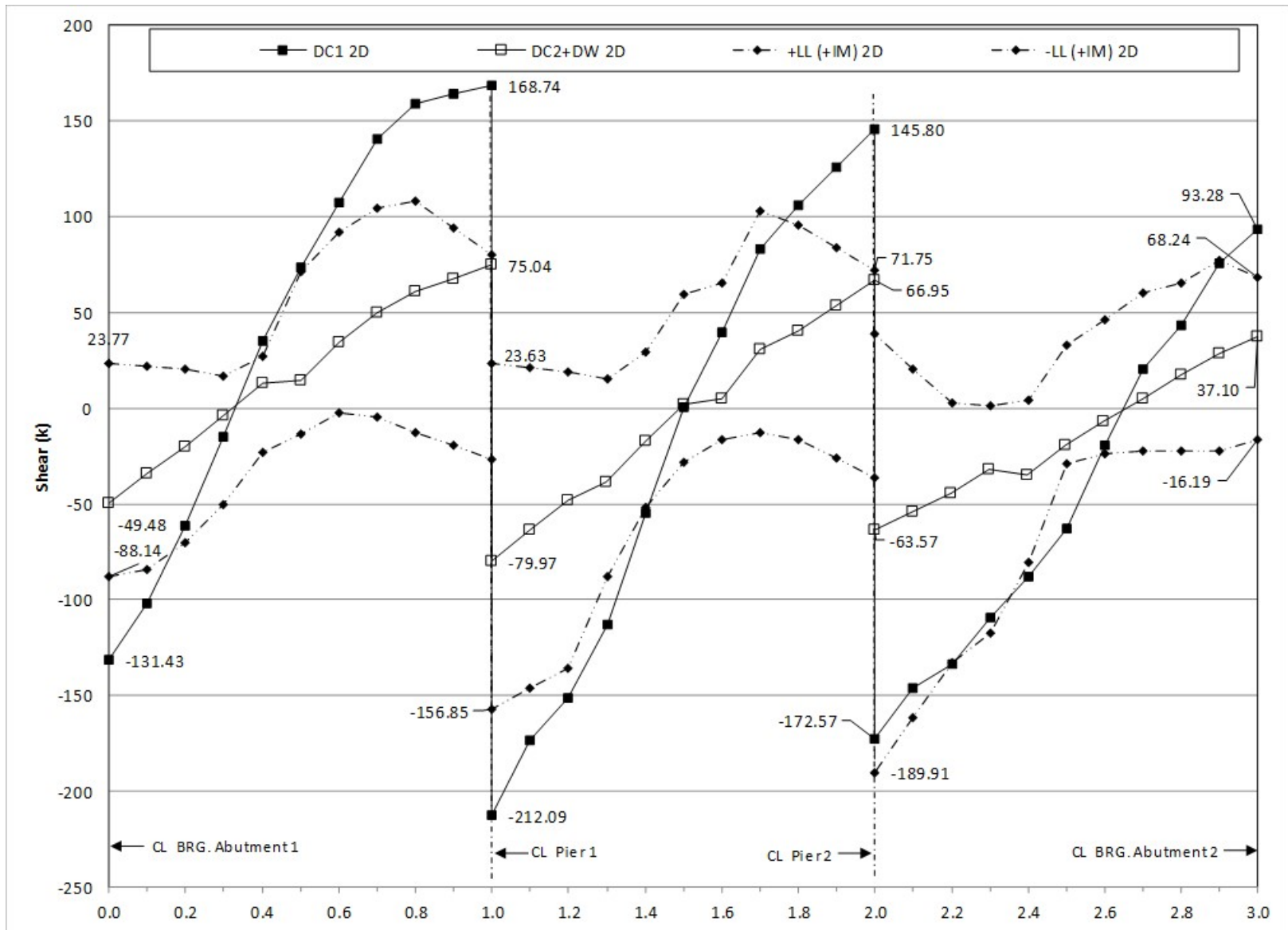


Figure 249. Graph. 2D shear diagram and live load envelope for Girder 4.

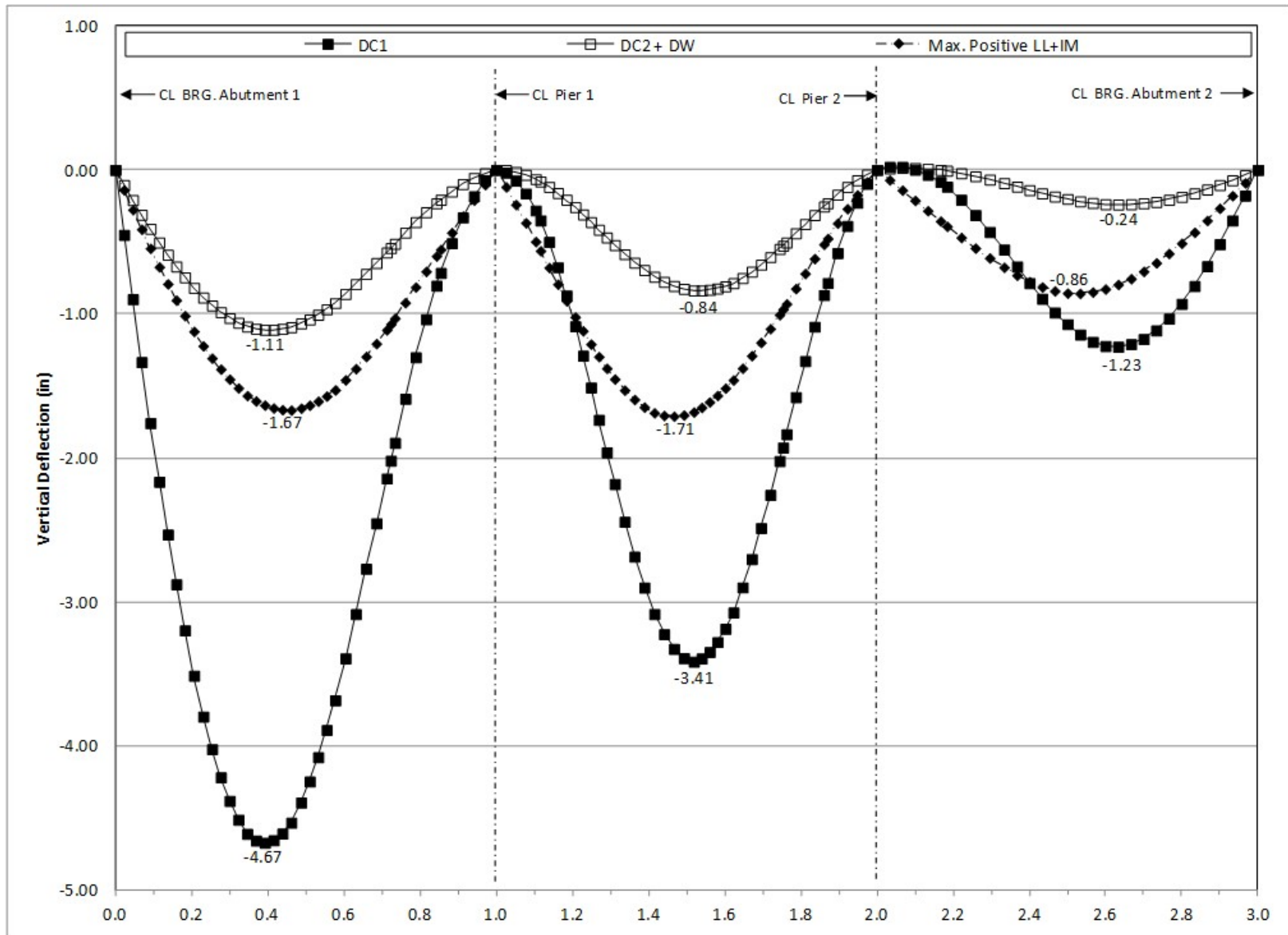


Figure 250. Graph. 2D deflection diagram for Girder 4.

9.3.3 3D Finite Element Model and Analysis

3D FEA is more involved than the previous method presented. In a 3D FEA components are located where they exist in physical space. Modeling the structure depth results in the support conditions being at the actual physical location instead of at the centroid of the deck slab or girder. The approximate distribution factors in AASHTO LRFD Article 4.6.2.2 are *not* used. Similar to the 2D PEB models, three separate models are required for analysis; one for non-composite dead loads, one for composite dead loads, and one for live load. The following steps are used to determine the dead and live load moments, shears, and deflections:

1. Create non-composite dead load model.

Similar to the 2D dead load models, the deck slab can be modeled explicitly or its weight can be accounted for by applying a line load (in this case along the top flange). Refer to Section 9.3.2 for additional information:

- a. Create geometry for girders, cross-frames, and concrete deck slab (if applicable). Flanges of girders and cross-frame elements are modeled with beam elements, girder webs and the concrete deck slab with surface elements. Further guide on modeling these members and discretizing them into an appropriate number of elements is provided in Section 3.6.
 - b. Define section properties for those components modeled with beam elements and thicknesses for those with surface elements.
 - c. Define material properties for girders, intermediate cross-frames, and concrete deck slab (if applicable).
 - d. Define support conditions.
 - e. Define loads applied to the non-composite structure.
 - i. For the members defined in the model, the girders, intermediate cross-frames, and concrete deck slab automatic dead load application can be used if mass density is assigned through material properties. Otherwise, concentrated or distributed loads that statically equivalent to the weight of the members can be used.
 - ii. The other non-composite dead loads (SIP forms, haunches) are applied as uniform line loads to each girder.
 - f. Define non-composite load cases.
 - g. Ensure correct attributes are assigned (geometric and material properties, support conditions, and loading) to appropriate components.
 - h. Run analysis; verify analysis results using simplified methods and expected behavior (deflected shape, qualitative force distribution).
 - i. Extract required results from analysis software.
2. Create model for composite dead loads (continuation of model created in Step 1).
 - a. Create geometry for concrete deck slab if not completed in Step 1a. The concrete deck slab is modeled with surface elements.
 - b. Define thickness of concrete deck slab if not completed in Step 1b.
 - c. Define or modify material properties for concrete deck slab.
 - d. Define support conditions.
 - e. Define loads applied to the composite structure.

- i. The FWS is defined as a uniform load distributed over an area.
 - ii. The weight of the barrier is defined as a uniform line load.
 - f. Define load cases for composite dead loads.
 - g. Ensure correct attributes are assigned (geometric and material properties, support conditions, and loading) to appropriate components.
 - h. Run analysis; verify analysis results using simplified methods and expected behavior (deflected shape, qualitative force distribution).
 - i. Extract required results from analysis software.
- 3. Create model for live loads (continuation of model created in Step 2).
 - a. Define material properties for concrete deck slab. Because live loading is short-duration the stiffness of the concrete deck is modified to the normal stiffness of concrete.
 - b. Define optimized loading. The analysis software may have utilities that help in the determination. Influence surfaces can be developed to aid in loading generation.
 - c. Run analysis with optimized loading and verify analysis results using simplified methods and expected behavior (deflected shape, qualitative force distribution).
 - d. Extract required results from analysis software.
- 4. Combine analysis results extracted in Steps 1i, 2i, and 3d.

9.3.3.1 Step 1 – Create Non-Composite Dead Load Model

9.3.3.1.1 Step 1a – Create Geometry for Girders, Cross-Frame, and Concrete Deck Slab

The girder geometry is created by defining surface elements at the girder centerline. These elements represent the girder webs, while beam elements are used to represent the girder flanges at the top and bottom of the web. To accommodate modeling of the cross-frames and cross-section changes, the web is divided into segments equal to the distance between cross-frames or equal to the distance between a cross-frame and a cross-section change. The cross-frame members are located by creating lines between adjacent girders at the location of the cross-frame members. The concrete deck slab geometry is set using surface elements in coordination with Figure 230. Thick shell elements are used for the surface elements and thick (Timoshenko) beam elements are used for the beam elements. Both of these element types are capable of capturing shear deformations.

9.3.3.1.2 Step 1b – Define Cross-Section Properties

The girder web thickness is a constant 5/8 inch. The girder flanges are defined by their width and thickness as shown in Figures 230 to 235; a section property calculator within the analysis software is used, though they could alternatively be calculated by hand and manually input.

The cross-frame members are angles and WT shapes as indicated in Figure 231. The analysis software includes the section properties for common rolled shapes in a section property database; these section properties are utilized for this example. As recommended in Section 3.5.3 per AASHTO LRFD Article C4.6.3.3.4, to account for stiffness softening due to 2nd order effects of connections, the modulus of elasticity for these elements will be reduced to 65 percent of its actual value.

The concrete deck slab is conservatively defined by its structural thickness of 9 inches so no benefit of stiffness provided by the integral wearing surface is taken into account.

9.3.3.1.3 Step 1c – Define Material Properties

Material properties assigned in this model are identical to those assigned in the 2D PEB model. See Section 9.3.2.1.3 for more detail.

9.3.3.1.4 Step 1d – Define Support Conditions

Support conditions used in the 3D FEA model are similar to those used for the 2D PEB model, however, the support is assigned only along the bottom flange. Refer to Table 53 in Section 9.3.2.1.4 for support definitions.

9.3.3.1.5 Step 1e – Define Non-Composite Dead Loads

Self-weight of members defined in the model, the girders and intermediate cross-frames, is applied using a body force. The body force uses the acceleration due to gravity, along with the unit weight and section properties, to determine the weight of the girders and intermediate diaphragms. The body force uses an acceleration of 32.2 ft/s^2 .

The other non-composite dead loads are applied as uniform line loads (haunches) to girders and surface loads (SIP forms, deck slab weight) to the concrete deck slab.

9.3.3.1.6 Step 1f – Define Load Cases

Since all loads in the model carry the same load factors and are applied to the same non-composite section they are combined into a single load case.

9.3.3.1.7 Step 1g – Ensure Correct Attributes Are Assigned to Components

The attributes assigned to each of the different components as shown below:

- Girders
 - Web
 - Geometric surface cross-section
 - Girder steel material properties
 - Thick shell surface elements
 - Dead load (self-weight)
 - Flanges
 - Flange cross-section
 - Girder steel material properties
 - Thick beam elements
 - Dead load (self-weight)
 - Other non-composite dead loads (haunches)
- Intermediate and Pier Cross-Frames
 - Geometric cross-section
 - Cross-frame steel material properties
 - Thick beam elements

- Dead load (self-weight)
- Concrete Deck Slab
 - Geometric cross-section
 - Flexible concrete material properties
 - Thick shell surface elements
 - Dead load (self-weight, SIP forms)

9.3.3.1.8 Step 1h – Run Analysis and Verify Results using Simplified Methods

The next step is to run the analysis. In addition to the qualitative inspection of deflected shapes, two simple quantitative checks are made to add confidence in the model.

Check 1: Sum of Concrete Deck Slab Reactions

From Section 9.3.2.1.8, the total vertical reaction, $F_z = 2532.57$ k

Table 57. Unfactored concrete deck slab reactions from 3D FEA model.

Location	X (ft)	Y (ft)	FZ (k)
G1-Abutment 1	0.00	3.75	41.44
G2-Abutment 1	0.00	14.75	55.33
G3-Abutment 1	0.00	25.75	68.74
G4-Abutment 1	0.00	36.75	86.25
G1-Pier 1	125.78	-7.92	216.64
G2-Pier 1	147.94	-1.19	252.08
G3-Pier 1	169.04	5.20	304.44
G4-Pier 1	189.14	11.34	232.32
G1-Pier 2	318.69	-75.10	291.98
G2-Pier 2	341.87	-75.22	243.05
G3-Pier 2	363.91	-75.35	273.74
G4-Pier 2	384.89	-75.41	196.36
G1-Abutment 2	469.44	-182.96	72.27
G2-Abutment 2	477.01	-174.99	69.17
G3-Abutment 2	484.57	-166.99	61.52
G4-Abutment 2	492.09	-158.97	64.97

Total vertical reaction from the analysis software, $F_z = 2530.30$ k

The percent difference between hand calculation and analysis software, $(2532.57-2530.30)/2532.57 = 0.09\%$, **therefore OK.**

Check 2: G2 Midspan Moment in Span 2 due to Self-Weight

From Section 9.3.2.1.8, $M_{\text{midspan}} = 382.02$ k-ft

From the analysis software, the midspan moment from G2 self-weight only in Span 2 is, $M_{\text{midspan}} = 394.88$ k-ft

The percent difference between hand calculation and analysis software, $(382.02-394.88)/382.02 = 3.37\%$, **therefore OK**.

9.3.3.1.9 Step 1i – Extract Required Results from Analysis Software

After verifying that the results from the analysis are reasonable, the results of interest can be extracted and input into a spreadsheet for further use. It may be necessary to select only certain portions of the model to obtain the results.

9.3.3.2 Step 2 – Create Composite Dead Load Model

9.3.3.2.1 Step 2a – Create Geometry for Girders and Cross-Frames

The location of all bridge elements has been defined while creating the non-composite dead load model. No modifications to geometry are required.

9.3.3.2.2 Step 2b – Define Cross-Section Properties

The girders, cross-frames, and concrete deck slab have already been defined while creating the non-composite dead load model. No modifications to section properties are required.

9.3.3.2.3 Step 2c – Define Material Properties

Material properties assigned in this model are the same as those assigned in the 2D PEB model. See Section 9.3.2.2.3 for more detail.

9.3.3.2.4 Step 2d – Define Support Conditions

As this model is a continuation of the previous model, support conditions have already been assigned. Refer to Table 53 in Section 9.3.2.1.4 for support definitions.

9.3.3.2.5 Step 2e – Define Composite Dead Loads

The composite dead loads and the method with which they are assigned are identical to those in the 2D PEB model. See Section 9.3.2.2.5 for more detail.

9.3.3.2.6 Step 2f – Define Load Cases

Separate load cases are defined for the composite dead loads; in this analysis the composite dead loads are simply added together, however, in a typical design the barrier would be a DC (component dead load) load while the future wearing surface would be a DW (wearing surface dead load) load. In Strength and Extreme Event load combinations these effects carry different load factors.

9.3.3.2.7 Step 2g – Ensure Correct Attributes are Assigned to Components

After defining the geometry and elements, member properties, material properties, support conditions, and loads, these attributes must be assigned to the appropriate geometry within the model. The lines defining the girders, intermediate cross-frames, and pier cross-frames are assigned the properties for the respective component. The concrete deck slab surfaces are

assigned the properties of the deck slab. Listed below are the different components and the attributes that must be assigned:

- Girders
 - Web
 - Geometric surface cross-section
 - Girder steel material properties
 - Thick shell surface elements
 - Flanges
 - Flange cross-section
 - Girder steel material properties
 - Thick beam elements
- Intermediate and Pier Cross-Frames
 - Geometric cross-section
 - Cross-frame steel material properties
 - Beam elements
- Concrete Deck Slab
 - Deck slab thickness
 - 4 ksi concrete material properties, stiffness reduced by a factor of 3
 - Surface elements
 - FWS and barrier loading

9.3.3.2.8 Step 2h – Run Analysis and Verify Results using Simplified Methods

The next step is to run the analysis. In addition to the qualitative inspection of deflected shapes, two simple quantitative checks are made to add confidence in the model.

Check 1: Sum of Unfactored FWS Reactions

From Section 9.3.2.2.8, the total vertical reaction, $F_z = 597.15$ k

Table 58. Unfactored FWS reactions from 3D FEA model.

Location	X (ft)	Y (ft)	FZ (k)
G1-Abutment 1	0.00	3.75	10.18
G2-Abutment 1	0.00	14.75	14.40
G3-Abutment 1	0.00	25.75	16.40
G4-Abutment 1	0.00	36.75	19.71
G1-Pier 1	125.78	-7.92	41.82
G2-Pier 1	147.94	-1.19	71.59
G3-Pier 1	169.04	5.20	72.45
G4-Pier 1	189.14	11.34	50.41
G1-Pier 2	318.69	-75.10	58.47
G2-Pier 2	341.87	-75.22	67.27
G3-Pier 2	363.91	-75.35	70.06

Location	X (ft)	Y (ft)	FZ (k)
G4-Pier 2	384.89	-75.41	40.97
G1-Abutment 2	469.44	-182.96	16.02
G2-Abutment 2	477.01	-174.99	16.54
G3-Abutment 2	484.57	-166.99	15.67
G4-Abutment 2	492.09	-158.97	15.15

Total vertical reaction from the analysis software, $F_z = 597.12$ k

The percent difference between hand calculation and the analysis software, $(597.15-597.12)/597.15 = 0.01\%$, **therefore OK**.

Check 2: G2 Midspan Moment in Span 2 Due to FWS

Similar assumptions and approximations are made as in Section 9.3.2.2.8.

$M_{\text{midspan}} = 358.14$ k-ft

From the analysis software, the midspan moment from FWS only in Span 2 is, $M_{\text{midspan}} = 363.30$ k-ft

The percent difference between hand calculation and the analysis software, $(358.14-363.30)/358.14 = 1.44\%$, **therefore OK**.

9.3.3.2.9 Step 2i – Extract Required Results from Analysis Software

After verifying that the results from the analysis are reasonable, the results of interest can be extracted and input into a spreadsheet for further use. It may be necessary to select only certain portions of the model to obtain the results.

9.3.3.3 Step 3 – Create Live Load Model

9.3.3.3.1 Step 3a – Define Material Properties for Concrete Deck Slab

The only property change that is required from the model created in the previous section is that the normal modulus of elasticity of concrete should be used. For 4 ksi concrete, a modulus of $524.757E3$ ksf is used per AASHTO Eq. 5.4.2.4-1.

9.3.3.3.2 Step 3b – Define Optimized Live Load

Refer to Section 9.3.2.3.2 for an explanation of live load application used in this model.

9.3.3.3.3 Step 3c – Run Analysis and Verify Results using Simplified Methods

The next step is to run the analysis. In addition to the qualitative inspection of deflected shapes and loading configurations for maximizing specific effects, a simple quantitative check is made to add confidence in the model.

Check 1: Vertical Reactions Under Sample Truck Loading Configuration

A live load truck configuration (Figure 251) was arbitrarily chosen to check vertical reactions. From the figure, the autoloader has produced a load case with two design trucks. Because this load case features two lanes of traffic, a multiple presence factor of 1.00 is used in the check.

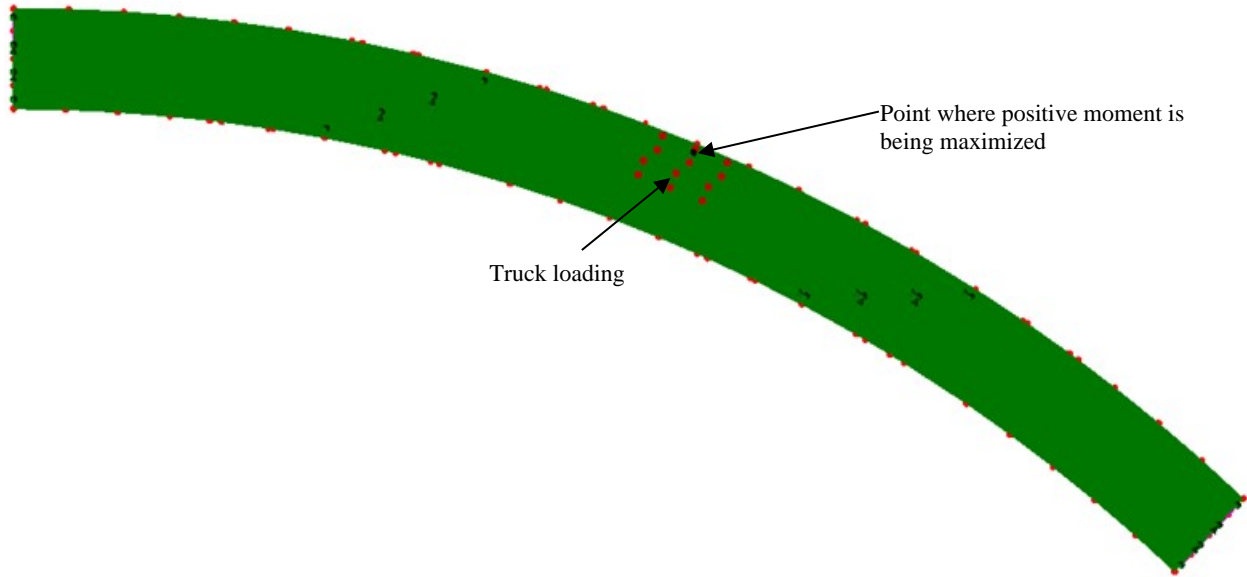


Figure 251. Illustration. Sample truck loading configuration.

Weight of two design trucks, $W = (2)(72 \text{ k}) = 144.00 \text{ k}$

Applying the multiple presence factor, $W_{mpf} = (1.0)(144 \text{ k}) = 144.00 \text{ k}$

Table 59. Unfactored truck reactions (including multiple presence) from 3D FEA model.

Location	X (ft)	Y (ft)	FZ (k)
G1-Abutment 1	0.00	3.75	6.17
G2-Abutment 1	0.00	14.75	-1.38
G3-Abutment 1	0.00	25.75	-5.37
G4-Abutment 1	0.00	36.75	-13.21
G1-Pier 1	125.78	-7.92	19.41
G2-Pier 1	147.94	-1.19	-10.27
G3-Pier 1	169.04	5.20	-7.67
G4-Pier 1	189.14	11.34	80.62
G1-Pier 2	318.69	-75.10	-2.18
G2-Pier 2	341.87	-75.22	49.85
G3-Pier 2	363.91	-75.35	46.29
G4-Pier 2	384.89	-75.41	0.32
G1-Abutment 2	469.44	-182.96	-9.40
G2-Abutment 2	477.01	-174.98	-5.52

Location	X (ft)	Y (ft)	FZ (k)
G3-Abutment 2	484.57	-166.99	-3.22
G4-Abutment 2	492.09	-158.97	-0.45

Total vertical reaction from the analysis software, $F_z = 144.00$ k

The percent difference between hand calculation and the analysis software, $(144.00-144.00)/144.00 = 0.00\%$, **therefore OK**.

9.3.3.3.4 Step 3d – Extract Required Results from Analysis Software

After verifying that the results from the analysis are reasonable, the results of interest can be extracted and input into a spreadsheet for further use. It may be necessary to select only certain portions of the model to obtain the results.

9.3.3.4 Step 4 – Combine Analysis Results

Once the results of interest, in this case moments, shears, and deflections, have been extracted from the analysis software, they are combined into groups of non-composite dead loads, composite dead loads, and live loads.

The moments due to the composite dead loads and live loads can be used as extracted from the analysis software; no additional calculations are required. The utility within the analysis software integrates the stresses in the shell elements and then combines the force effects from the shell elements and the beam elements to determine the force effects on the composite section.

The HL-93 Design Load consists of the maximum of the design truck or design tandem amplified by the dynamic load allowance plus the design lane; each component was analyzed individually therefore the results must be combined. Similarly, for negative moment between dead load inflection points, the design truck train including the dynamic load allowance and design lane must be combined. Additionally, the results from the different live load models may have to be combined to determine the greatest live load force effect for each girder.

Once the moments, shears, and deflections have been combined into appropriate groups using the results from the various analyses, graphs can be created to show the moment and shear diagrams, and deflected shape. The analysis results are combined using the same groups as for the 2D analyses: non-composite dead loads (girder self-weight, diaphragms, SIP forms, haunches, and concrete deck slab), composite dead loads (barrier and FWS), and maximum and minimum live loads including the dynamic load allowance. The moment, shear, and deflection diagrams from the 3D finite element analysis are shown in Figures 252 through 263.

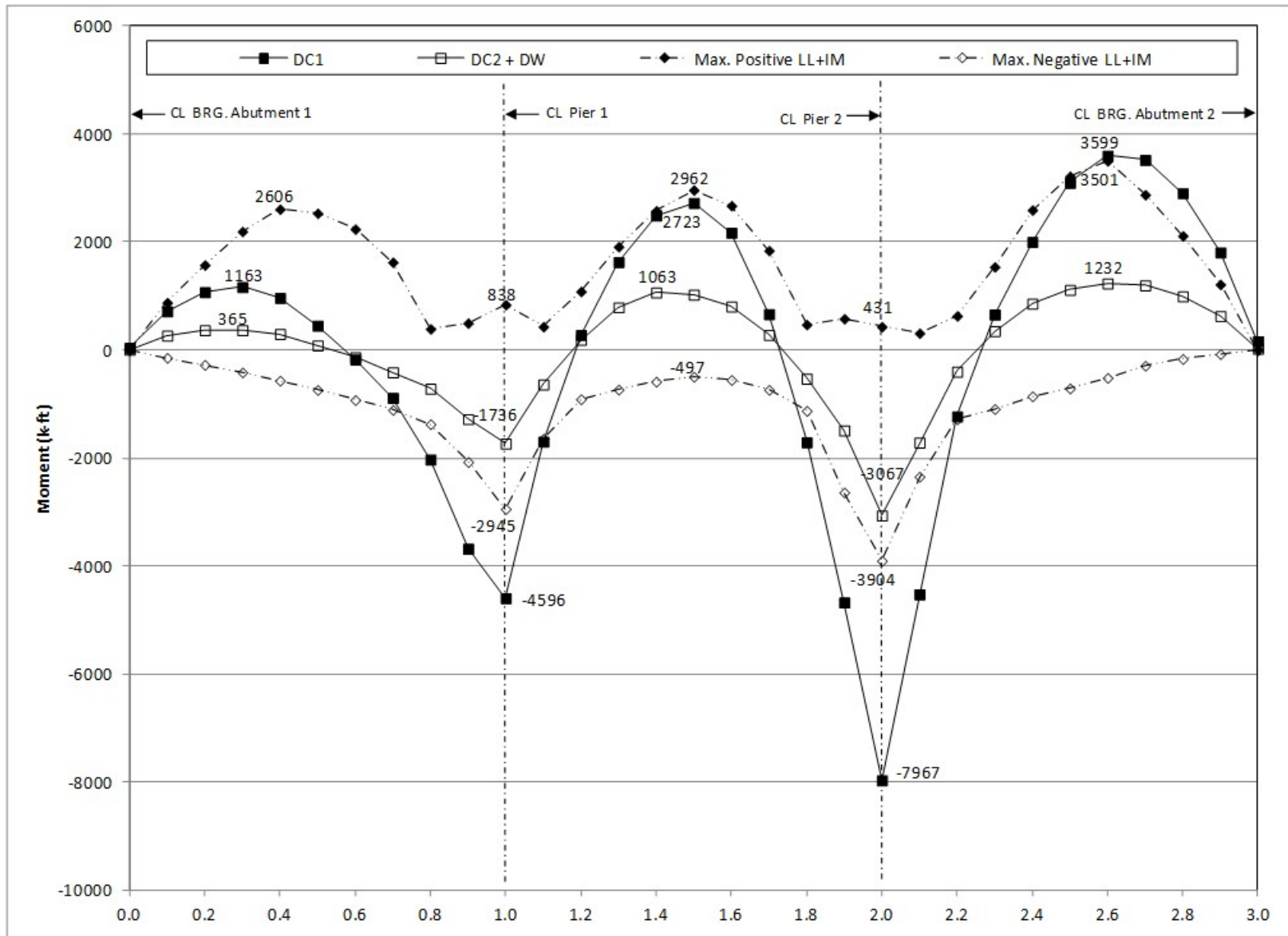


Figure 252. Graph. 3D moment diagram and live load envelope for Girder 1.

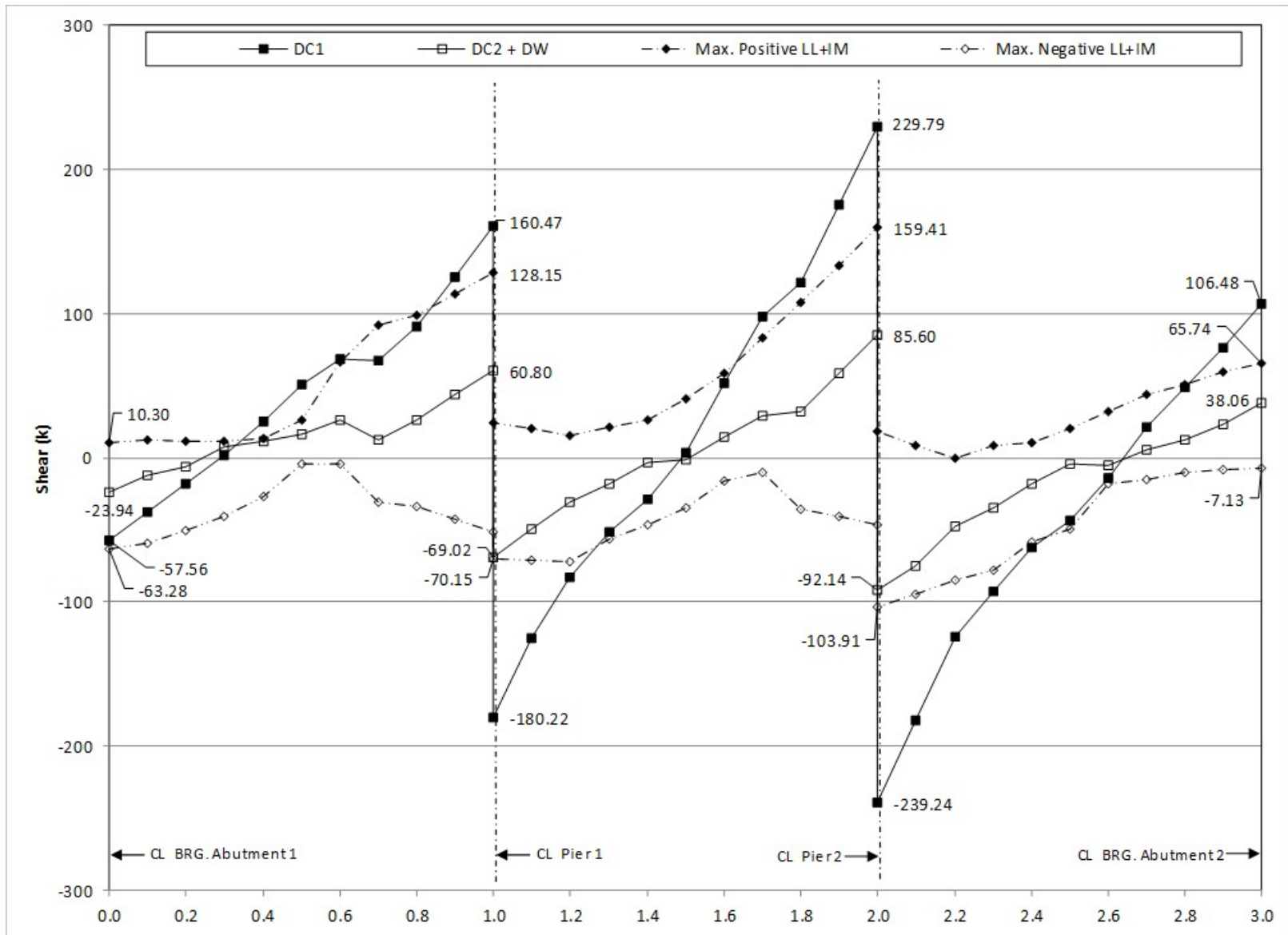


Figure 253. Graph. 3D shear diagram and live load envelope for Girder 1.

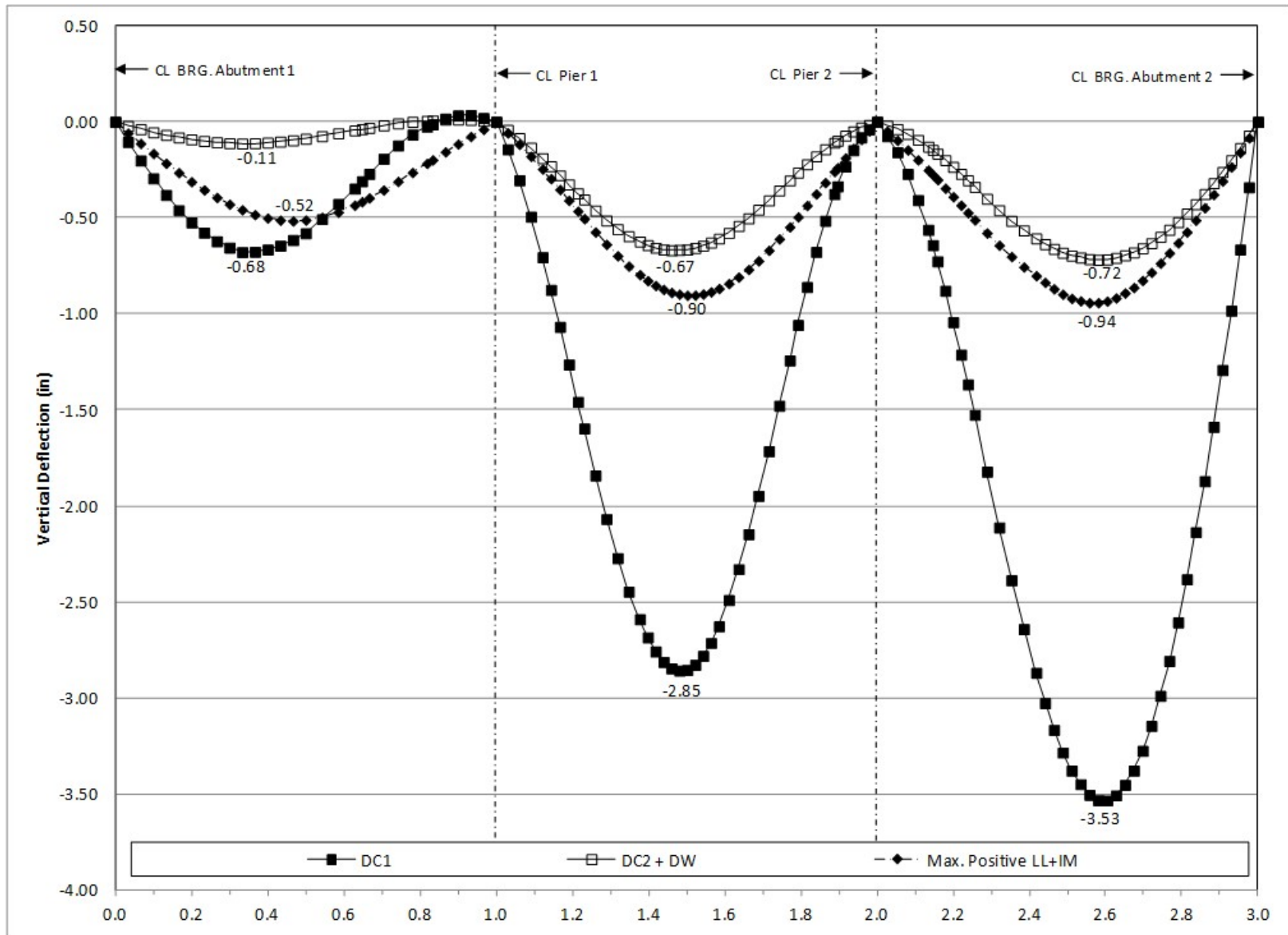


Figure 254. Graph. 3D deflection diagram for Girder 1.

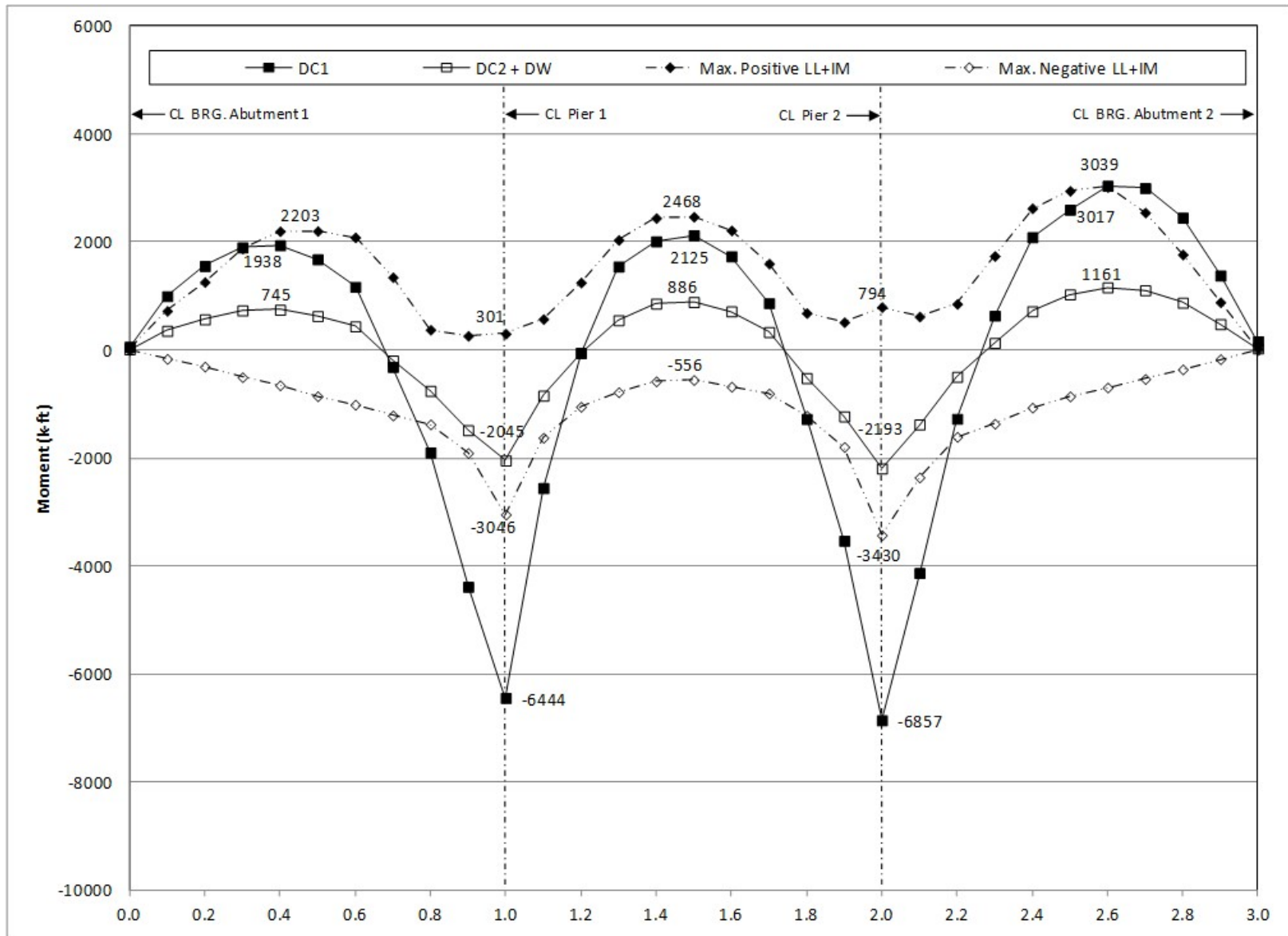


Figure 255. Graph. 3D moment diagram and live load envelope for Girder 2.

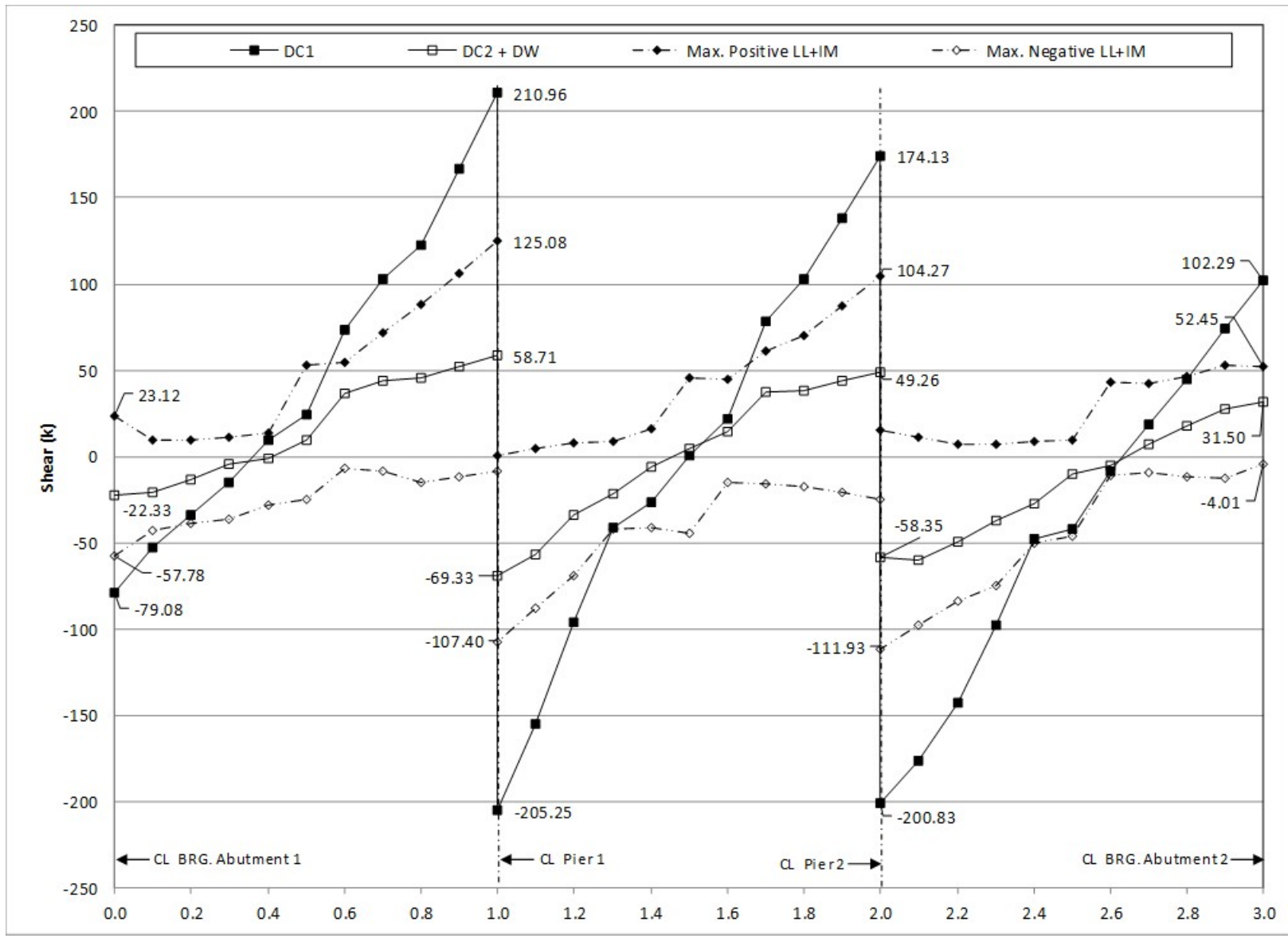


Figure 256. Graph. 3D shear diagram and live load envelope for Girder 2.

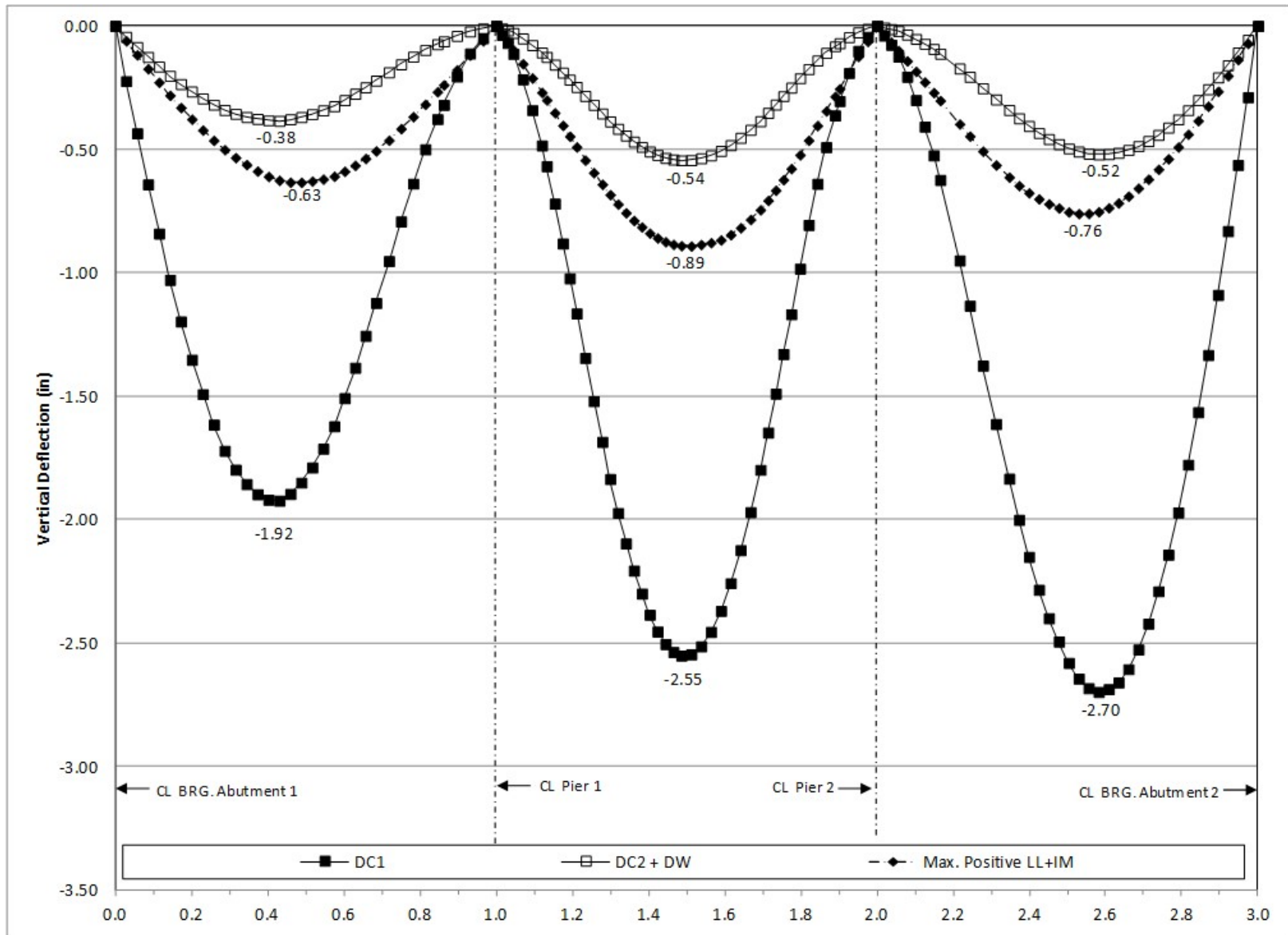


Figure 257. Graph. 3D deflection diagram for Girder 2.

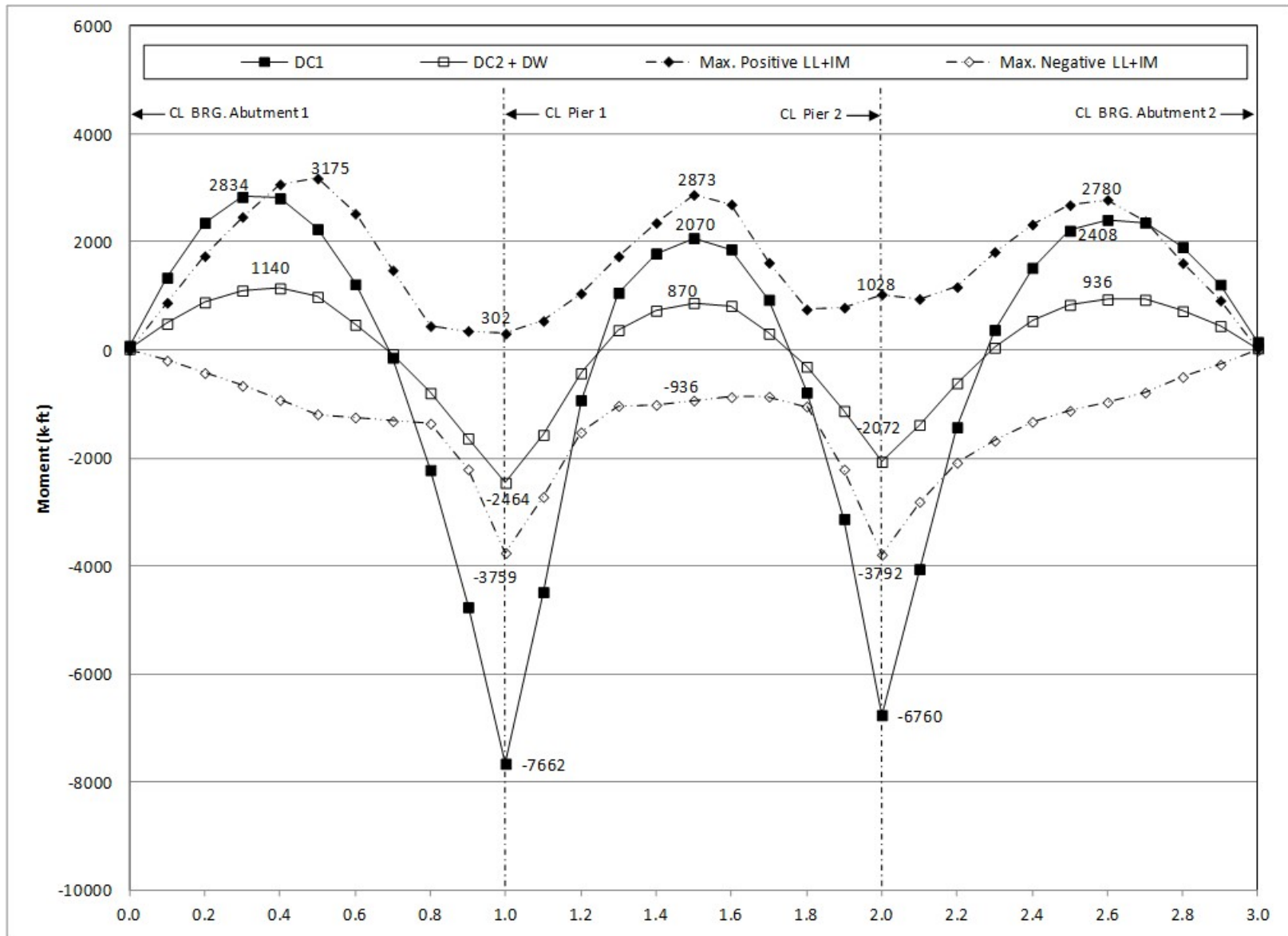


Figure 258. Graph. 3D moment diagram and live load envelope for Girder 3.

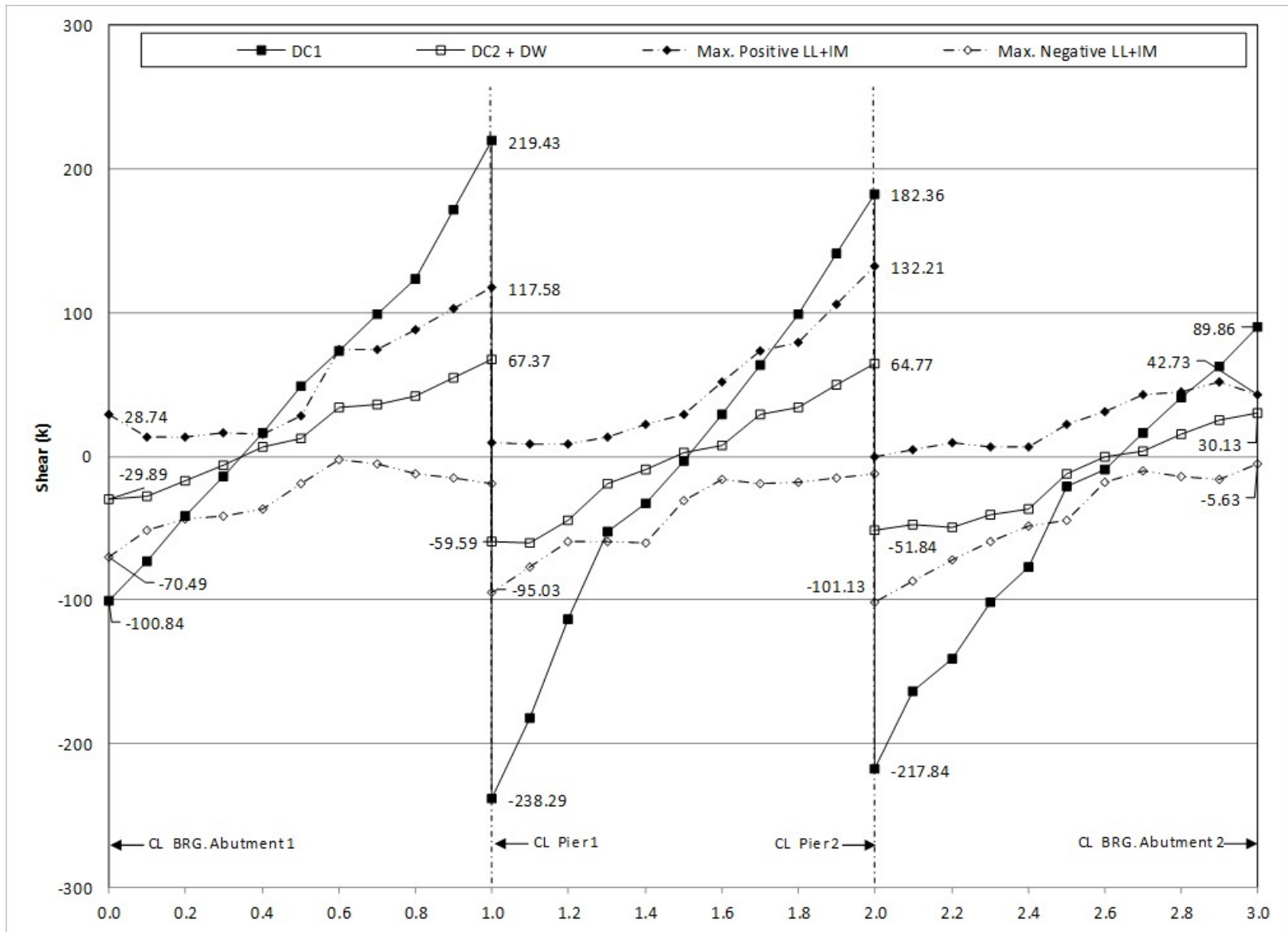


Figure 259. Graph. 3D shear diagram and live load envelope for Girder 3.

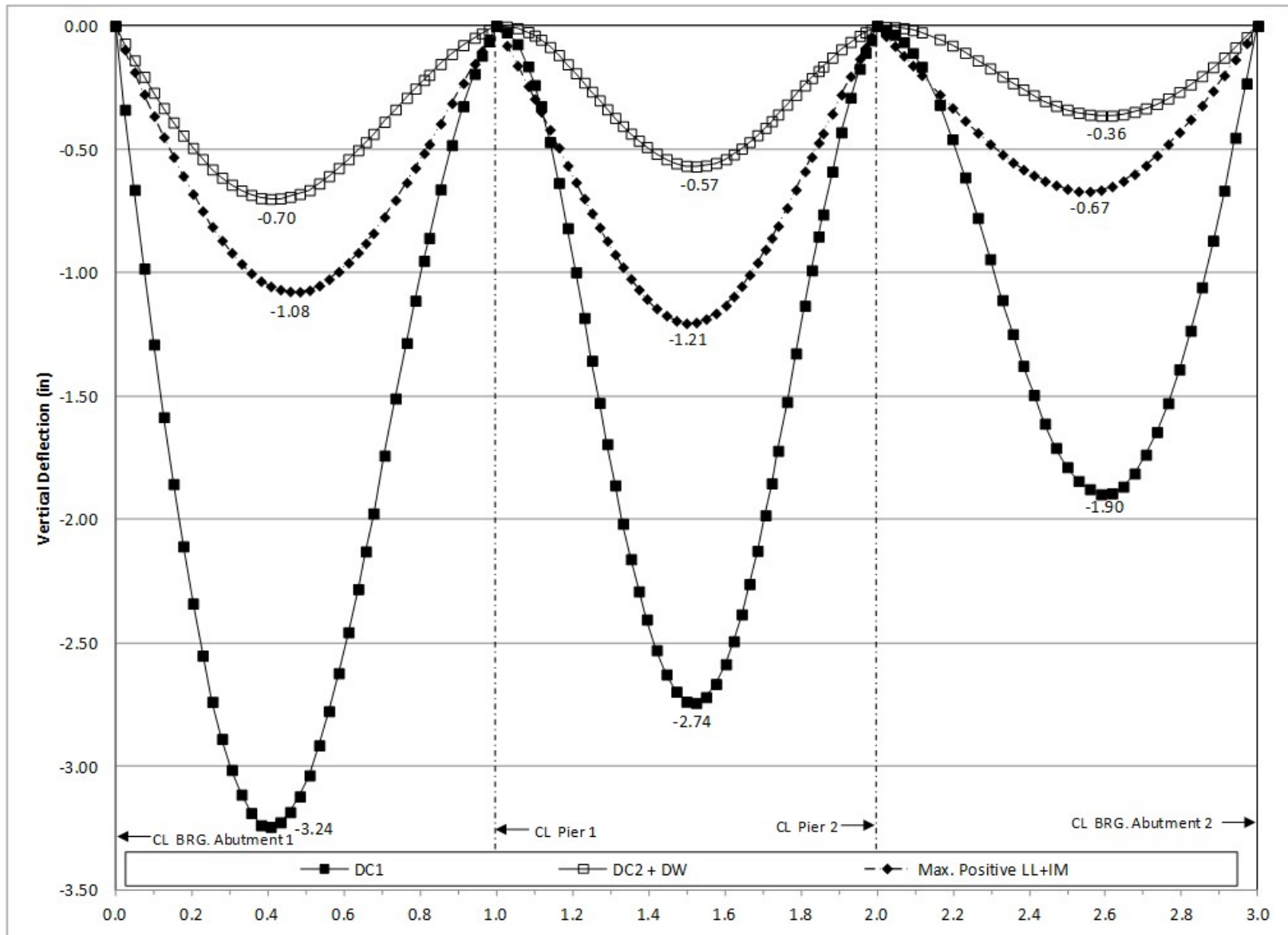


Figure 260. Graph. 3D deflection diagram for Girder 3.

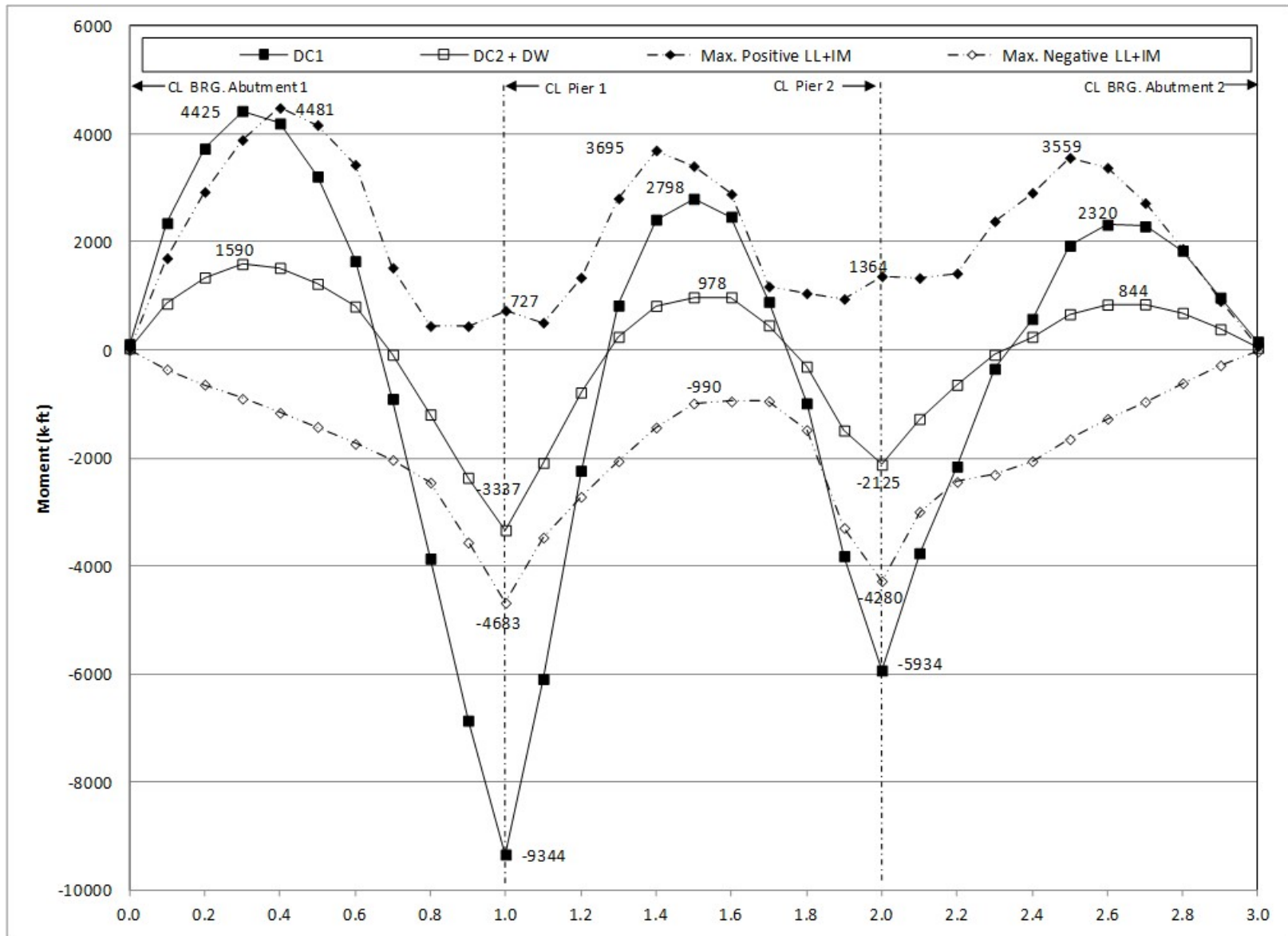


Figure 261. Graph. 3D moment diagram and live load envelope for Girder 4.

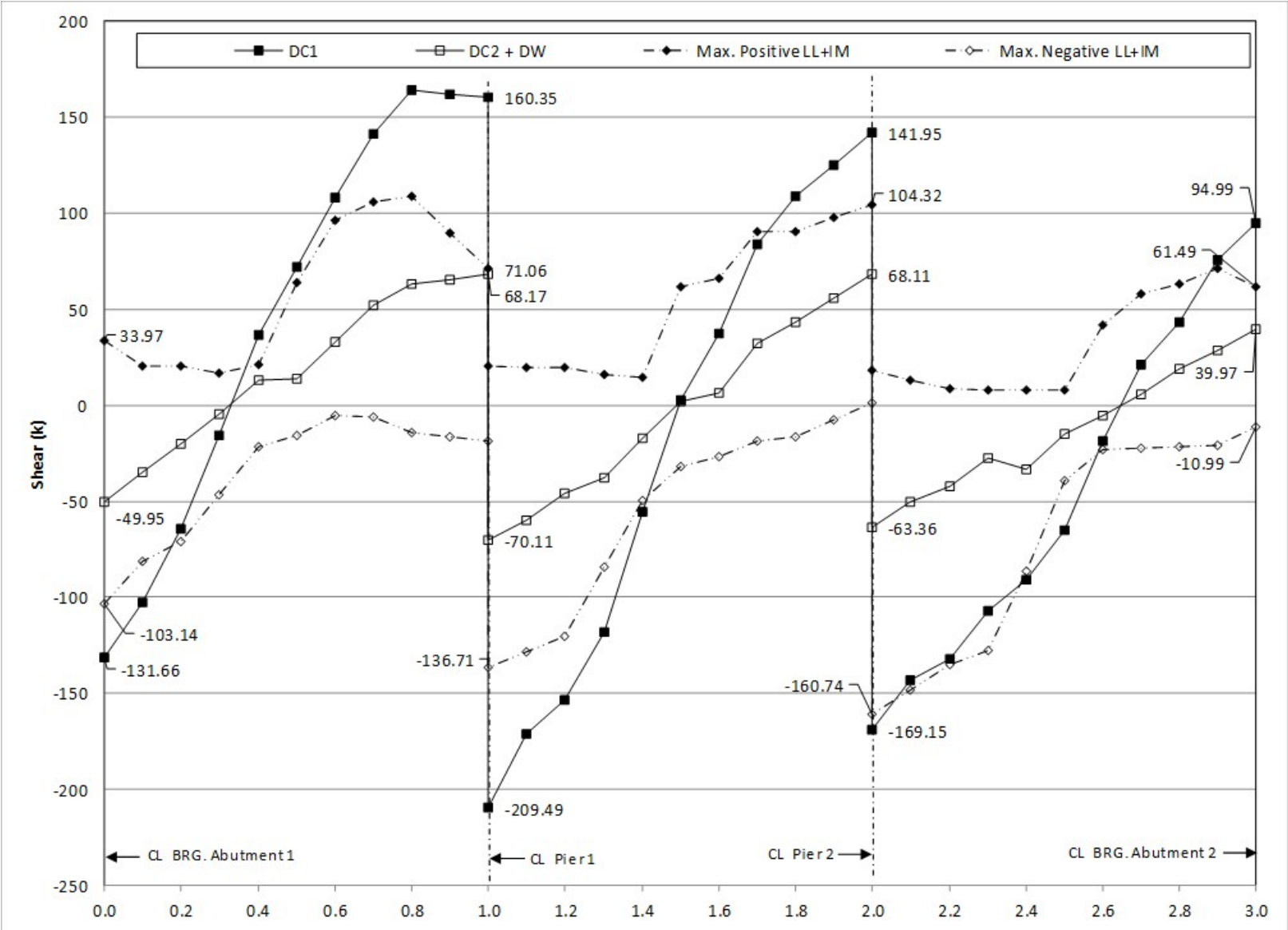


Figure 262. Graph. 3D shear diagram and live load envelope for Girder 4.

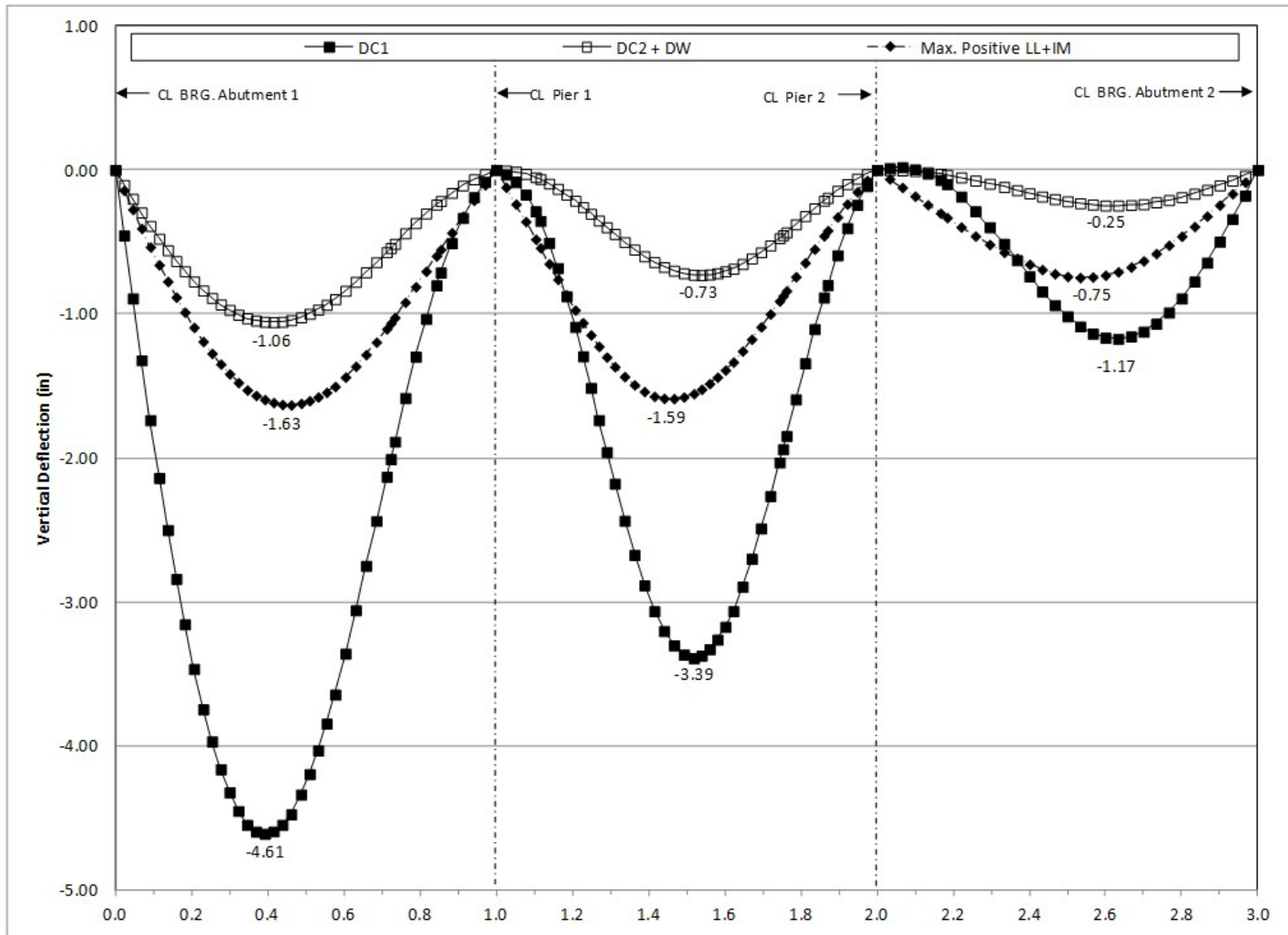


Figure 263. Graph. 3D deflection diagram for Girder 4.

9.3.4 Comparison of 2D and 3D Analysis Results

9.3.4.1 Girders

The results from the two analysis methods are compared on the following pages as Figures 264 through 287. Due to the presence of small values at several locations, the results from the 2D method are plotted along with the 3D results in absolute rather than normalized terms. Trivial variations between the two analyses otherwise cause outliers that obfuscate comparison.

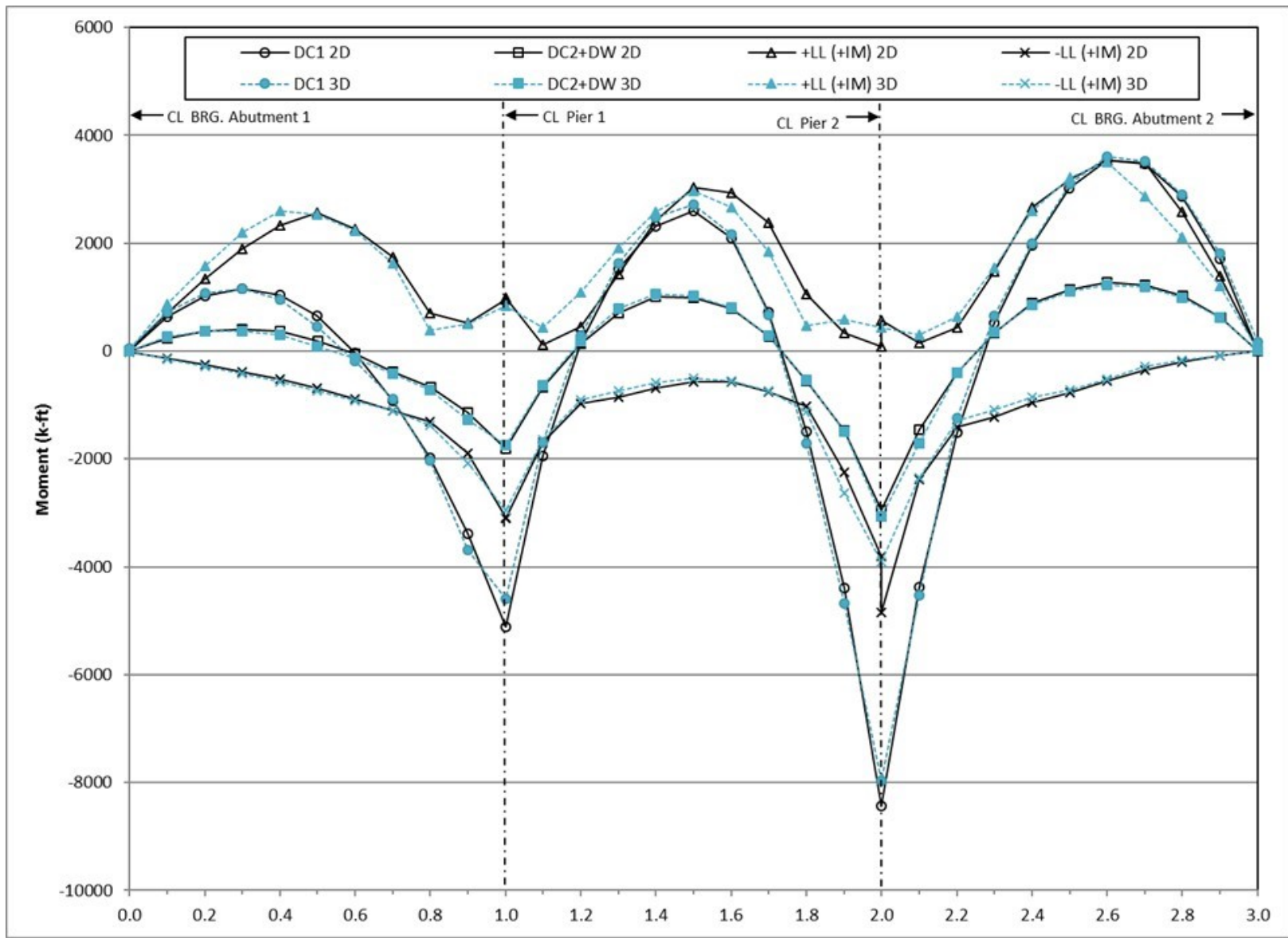


Figure 264. Graph. Comparison of 2D moments to 3D moments for Girder 1.

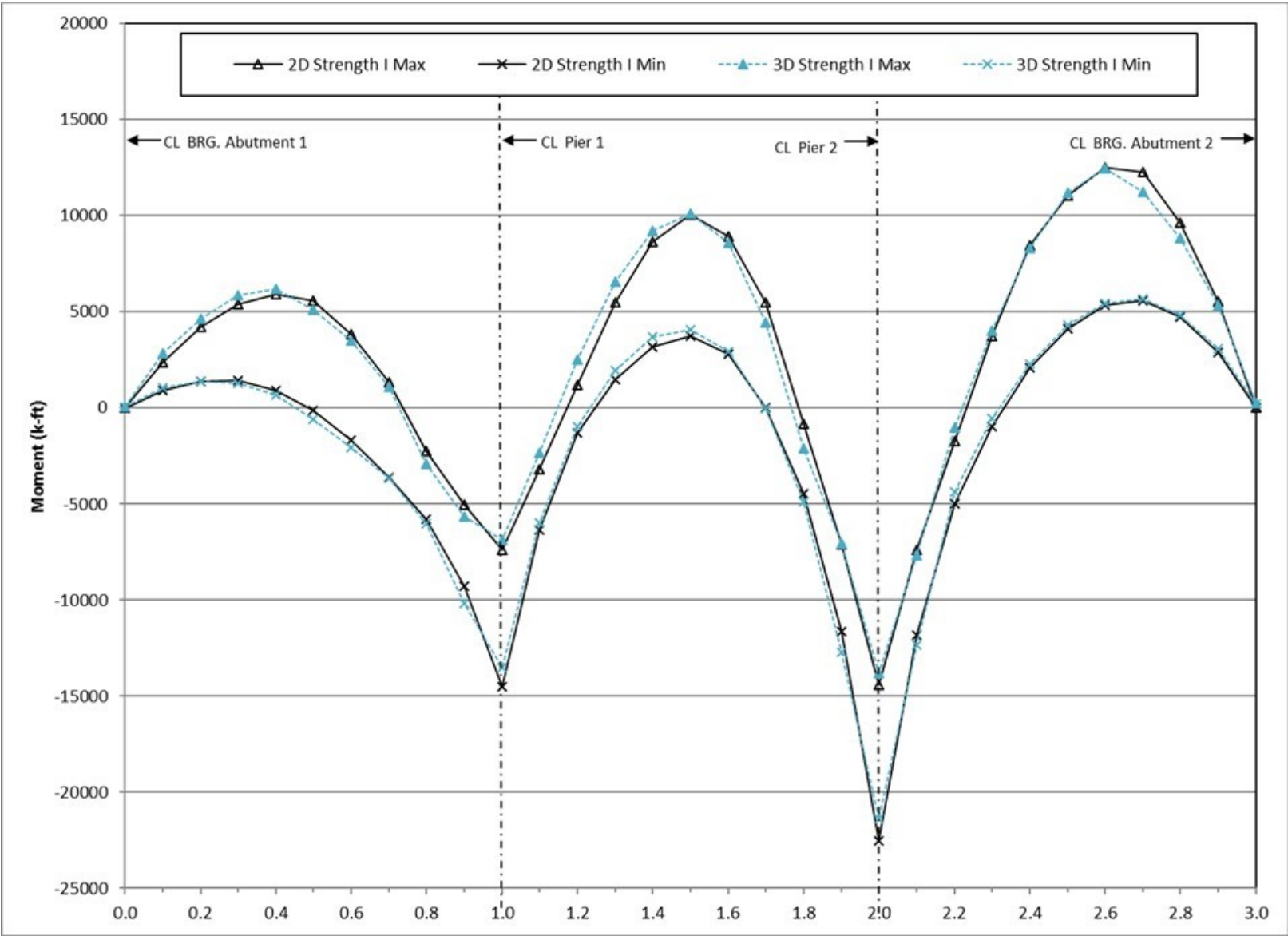


Figure 265. Graph. Comparison of factored moments for Girder 1.

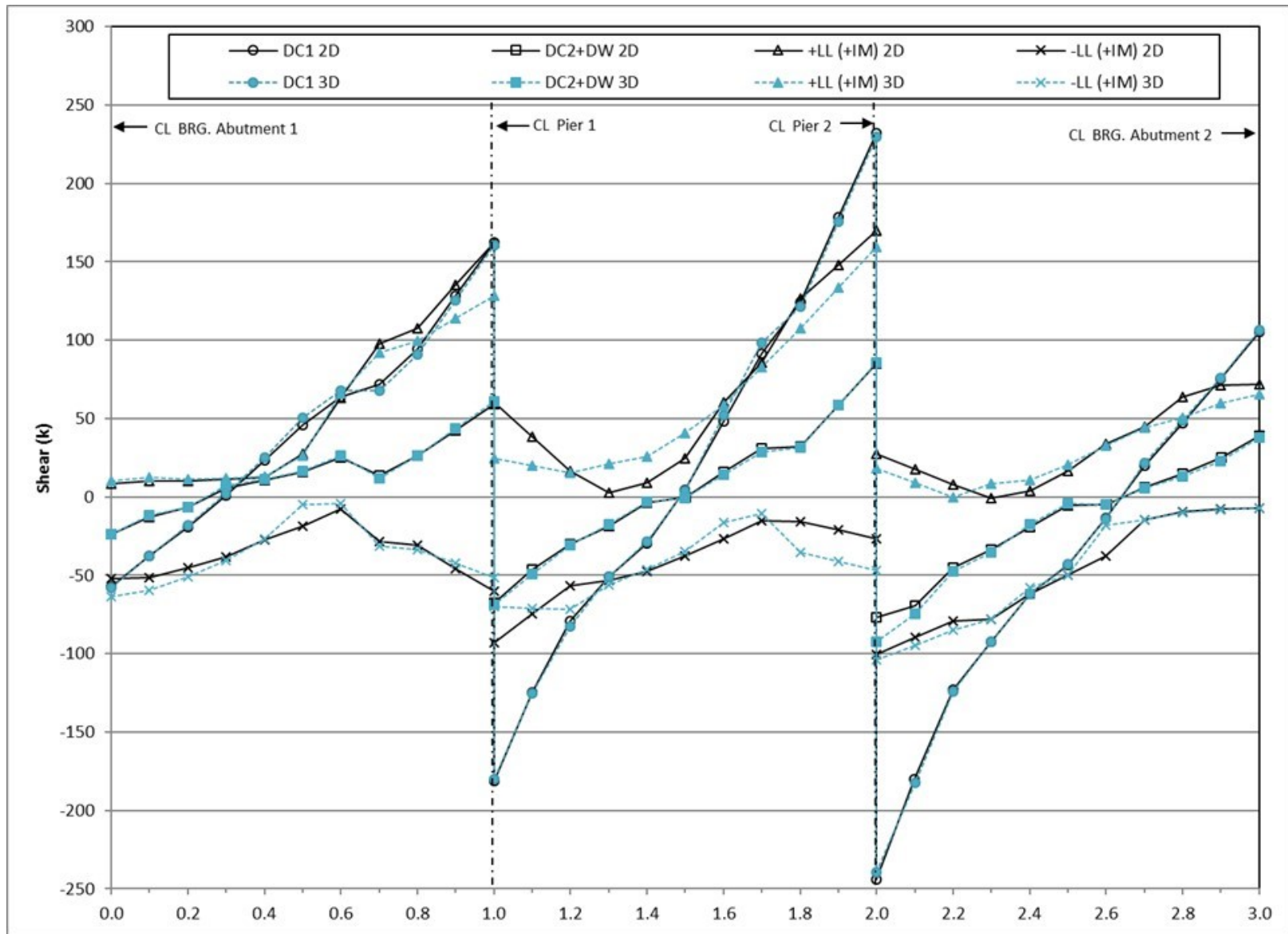


Figure 266. Graph. Comparison of 2D shears to 3D shears for Girder 1.

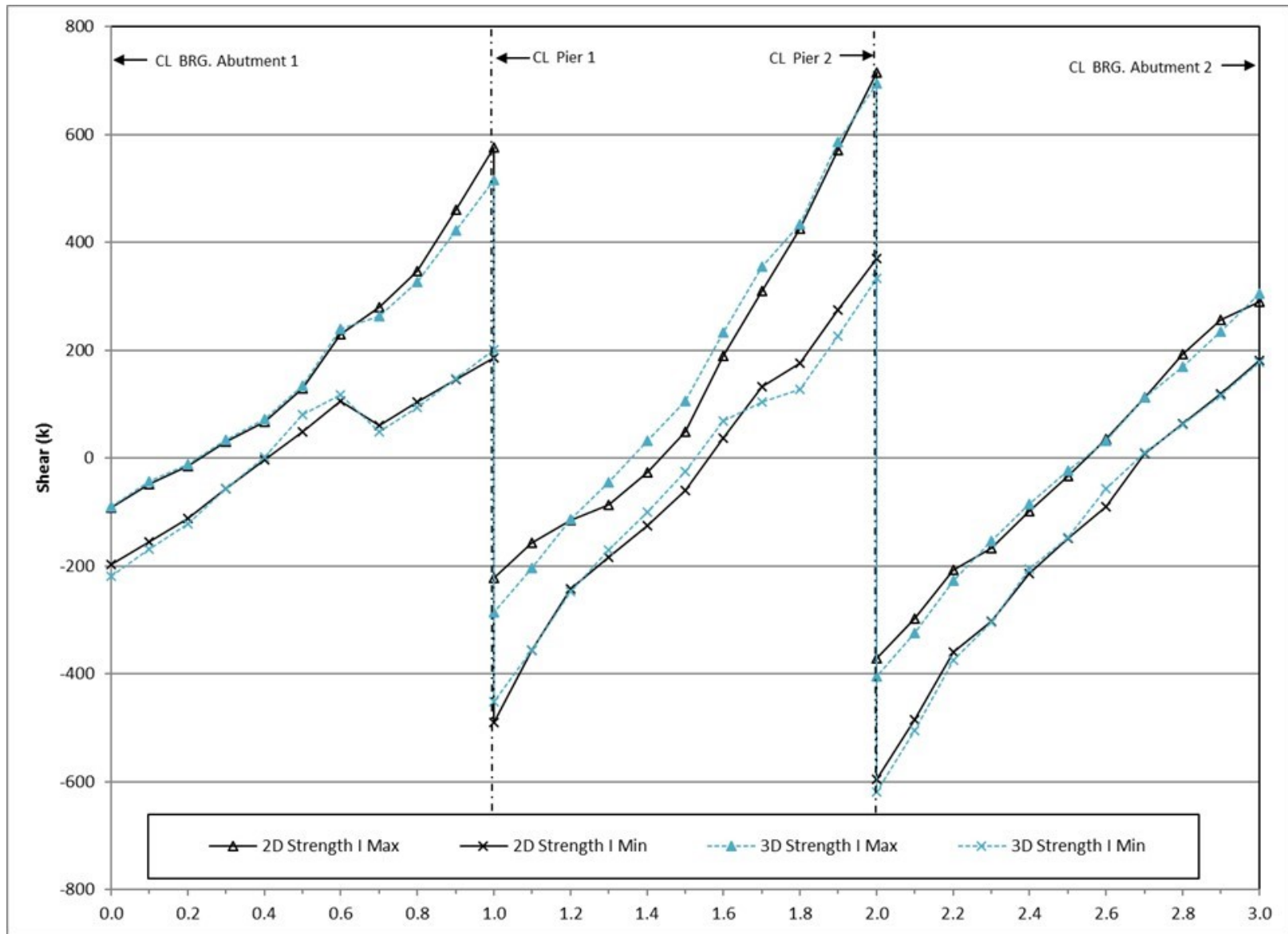


Figure 267. Graph. Comparison of factored shears for Girder 1.

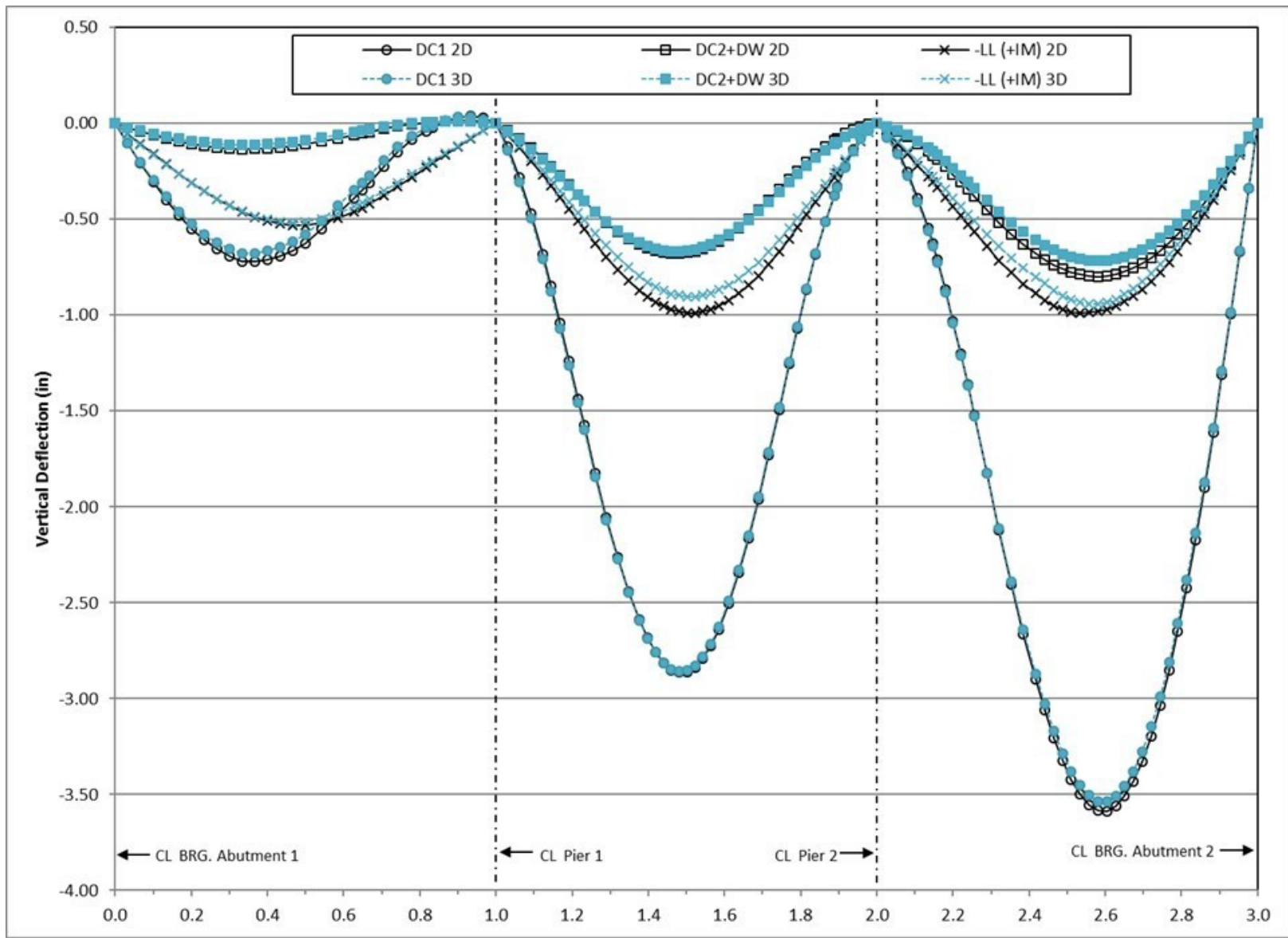


Figure 268. Graph. Comparison of 2D deflections to 3D deflections for Girder 1.

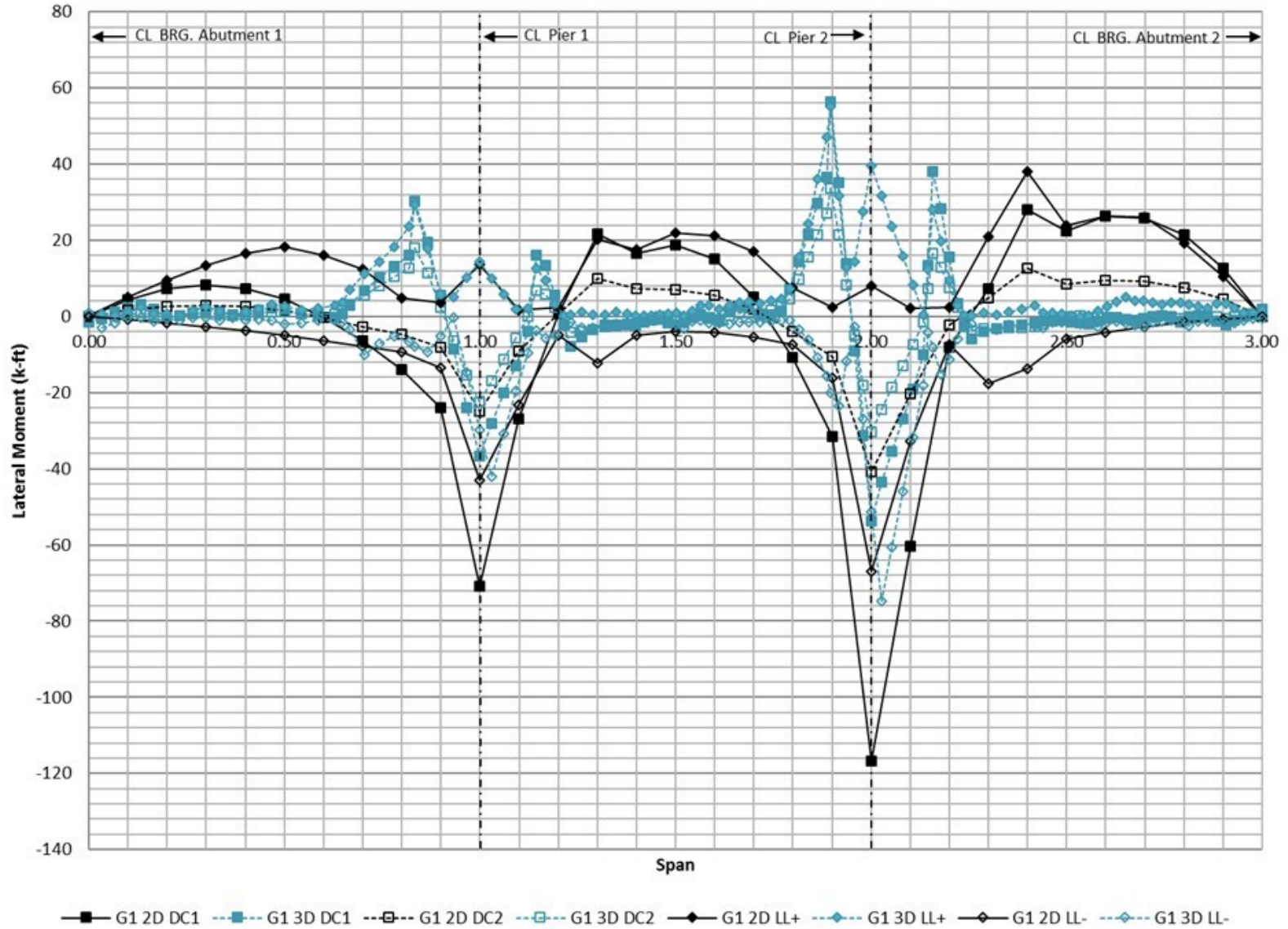


Figure 269. Graph. Comparison of 2D flange lateral bending moments to 3D flange lateral bending moments for Girder 1.

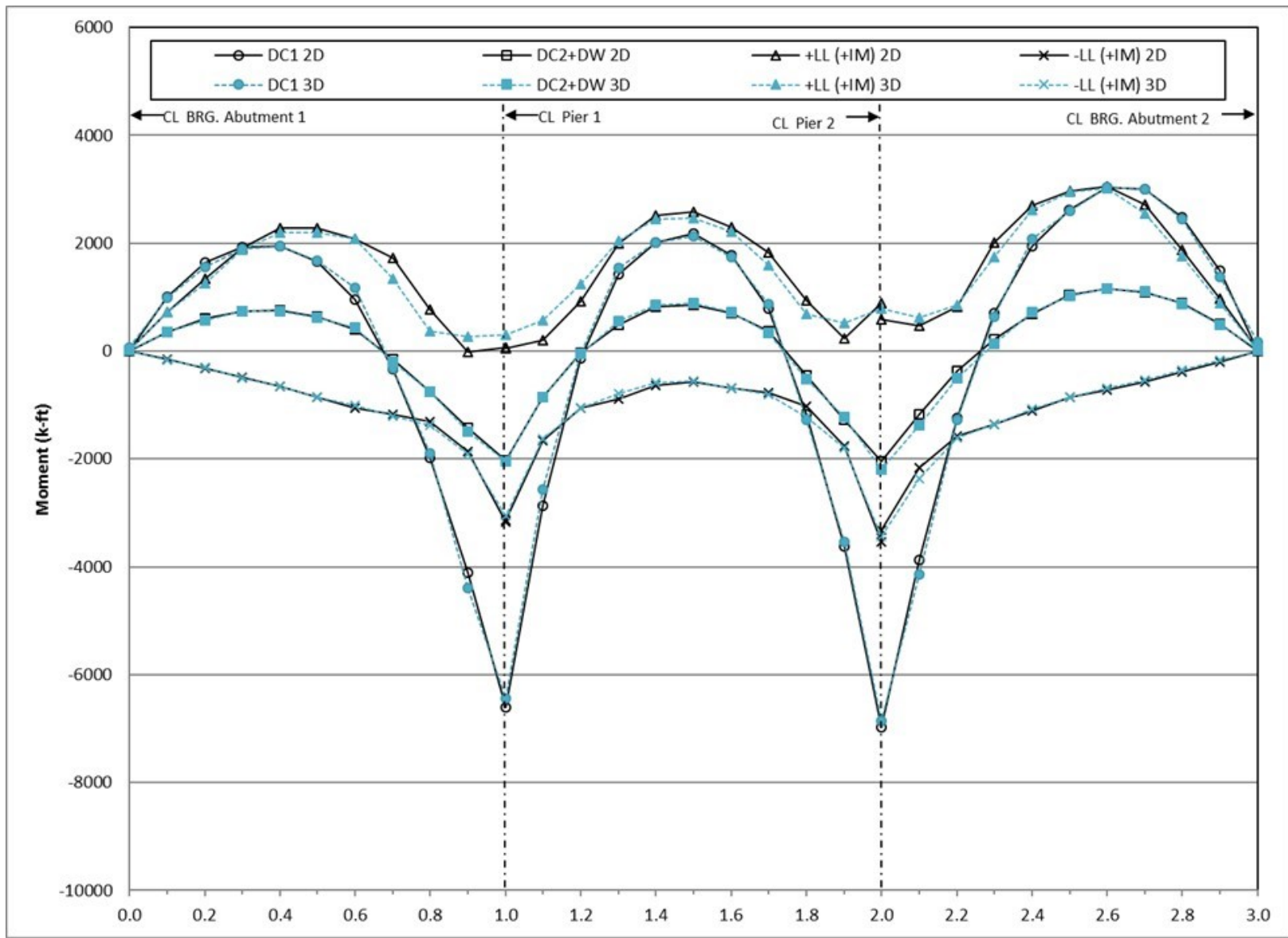


Figure 270. Graph. Comparison of 2D moments to 3D moments for Girder 2.

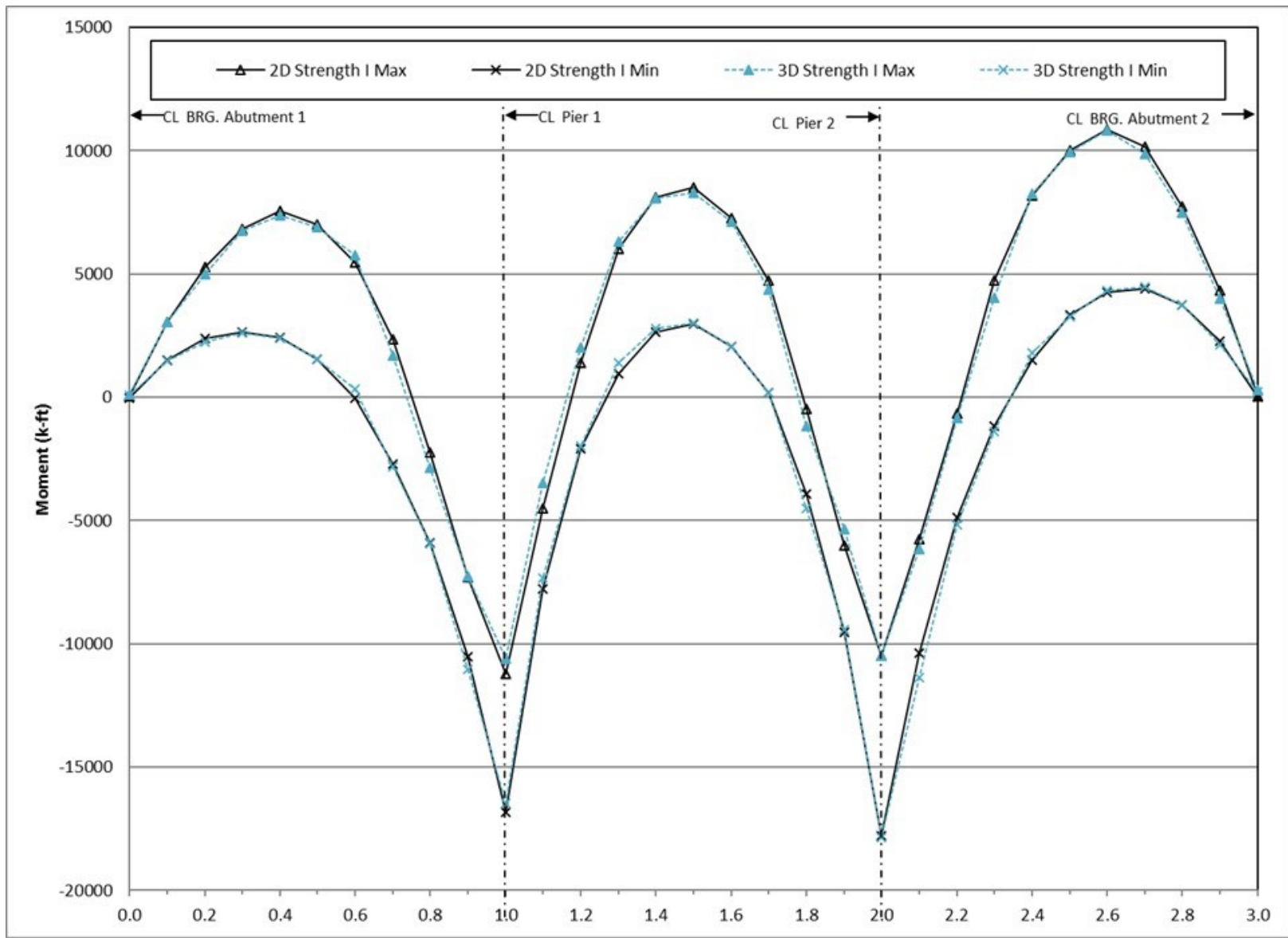


Figure 271. Graph. Comparison of factored moments for Girder 2.

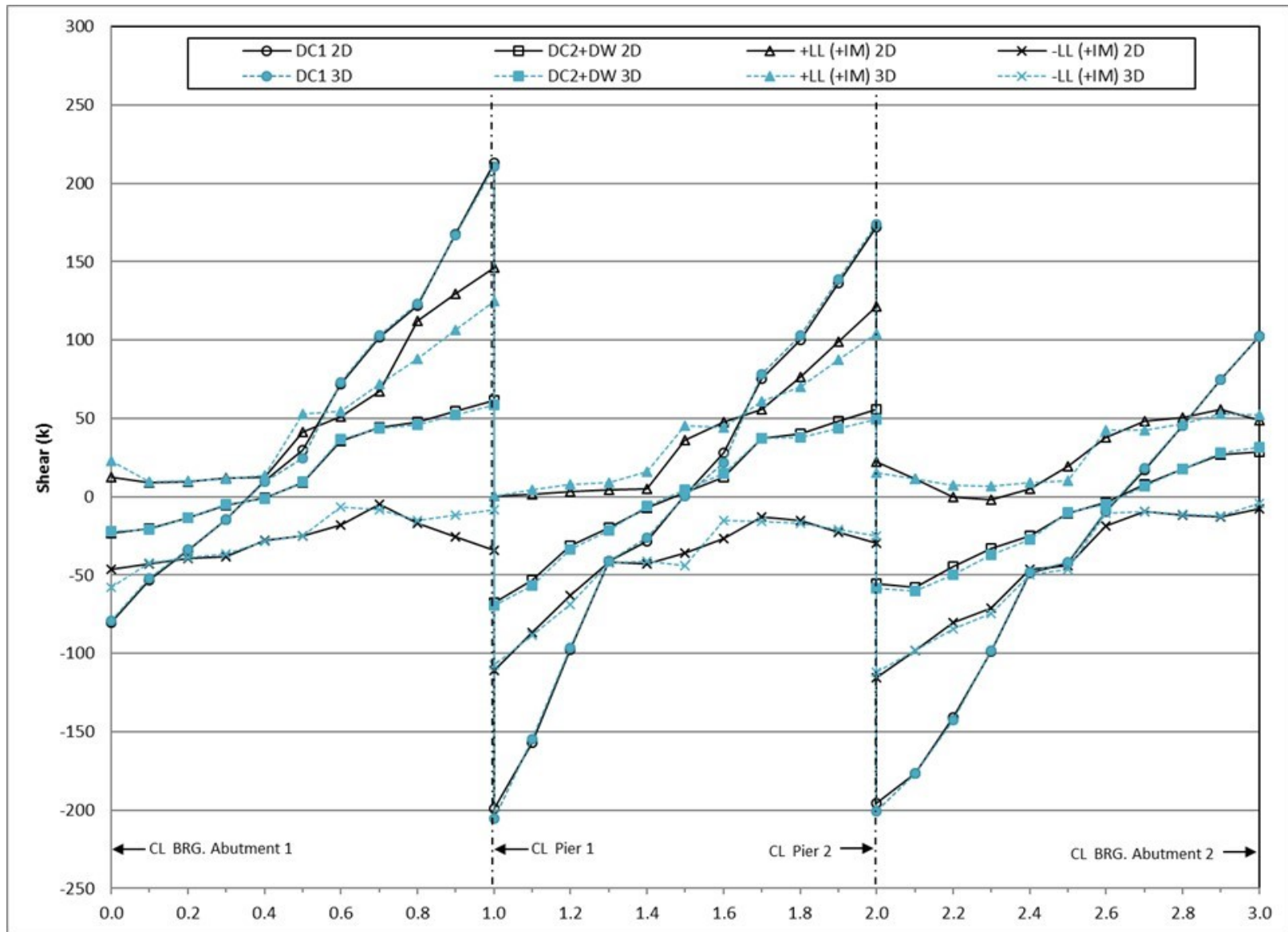


Figure 272. Graph. Comparison of 2D shears to 3D shears for Girder 2.

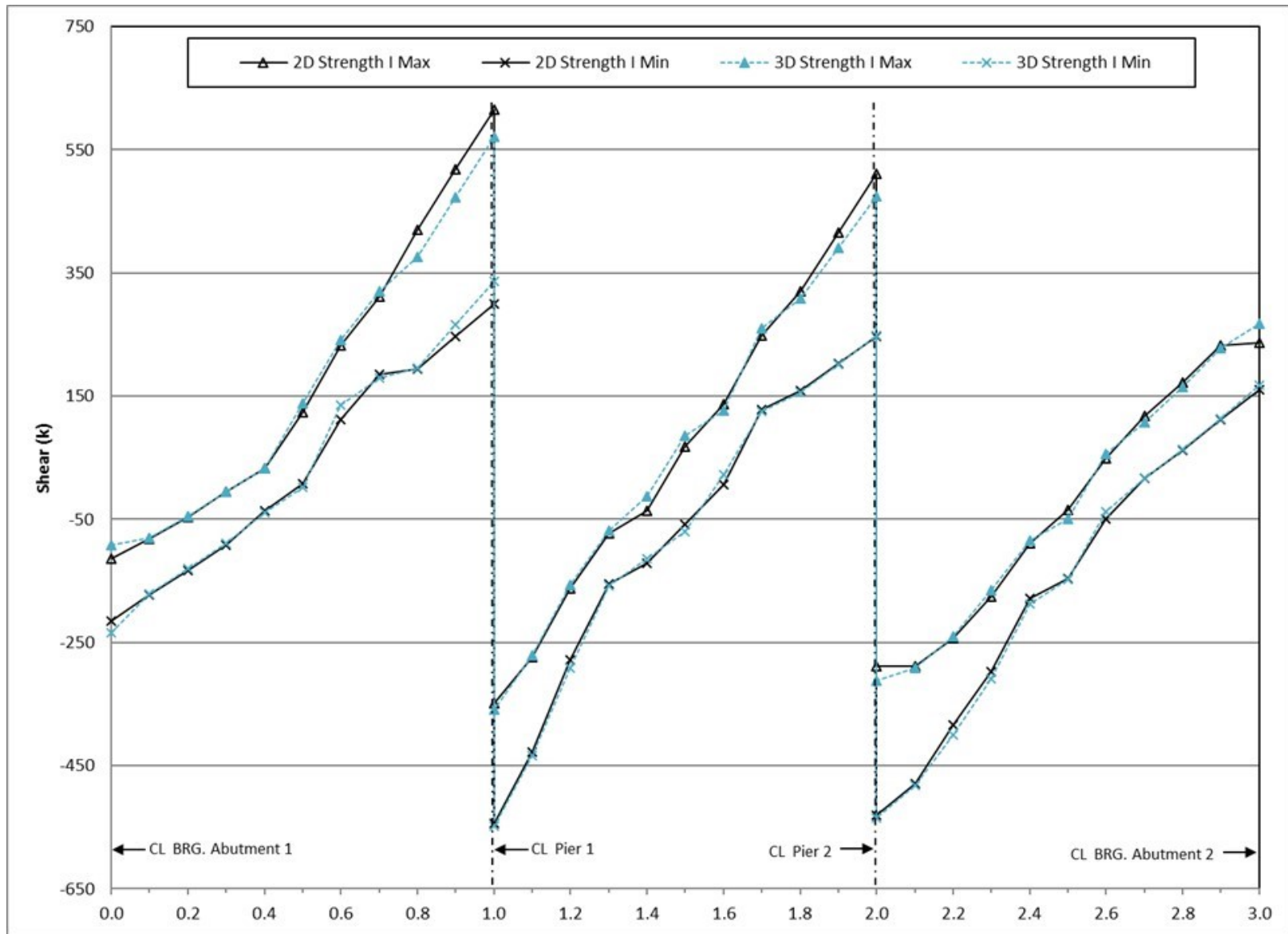


Figure 273. Graph. Comparison of factored shears for Girder 2.

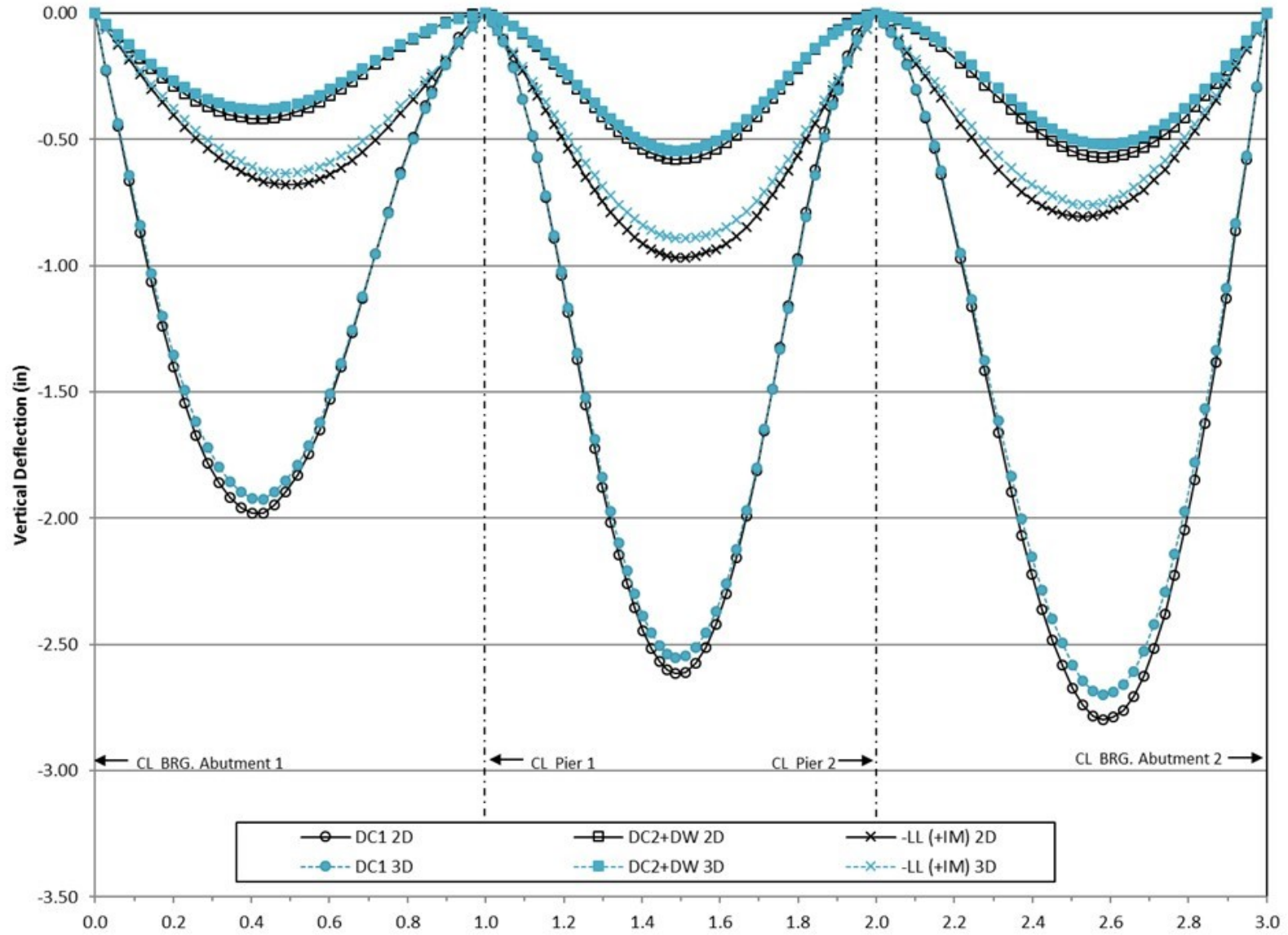


Figure 274. Graph. Comparison of 2D deflections to 3D deflections for Girder 2.

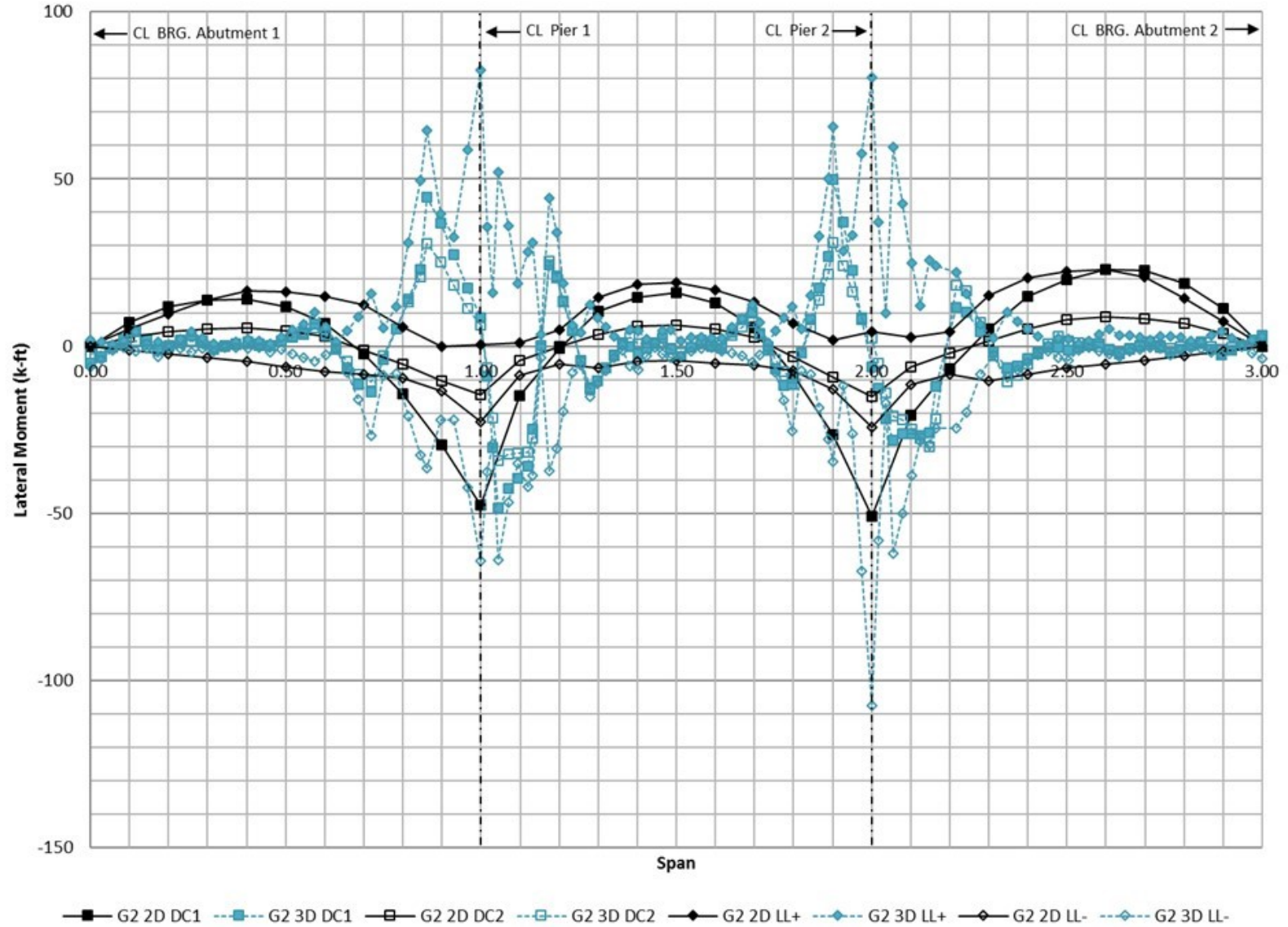


Figure 275. Graph. Comparison of 2D flange lateral bending moments to 3D flange lateral bending moments for Girder 2.

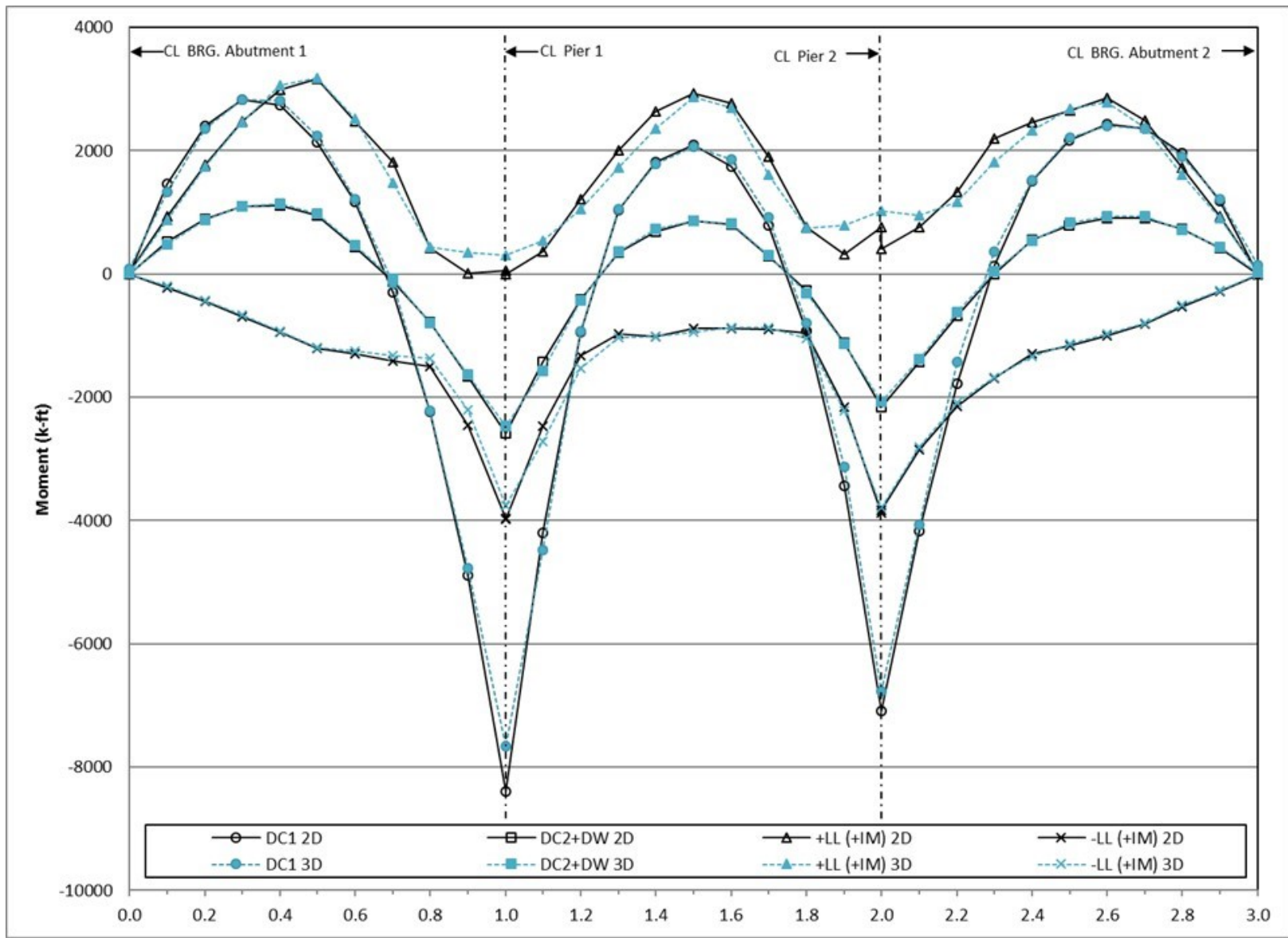


Figure 276. Graph. Comparison of 2D moments to 3D moments for Girder 3.

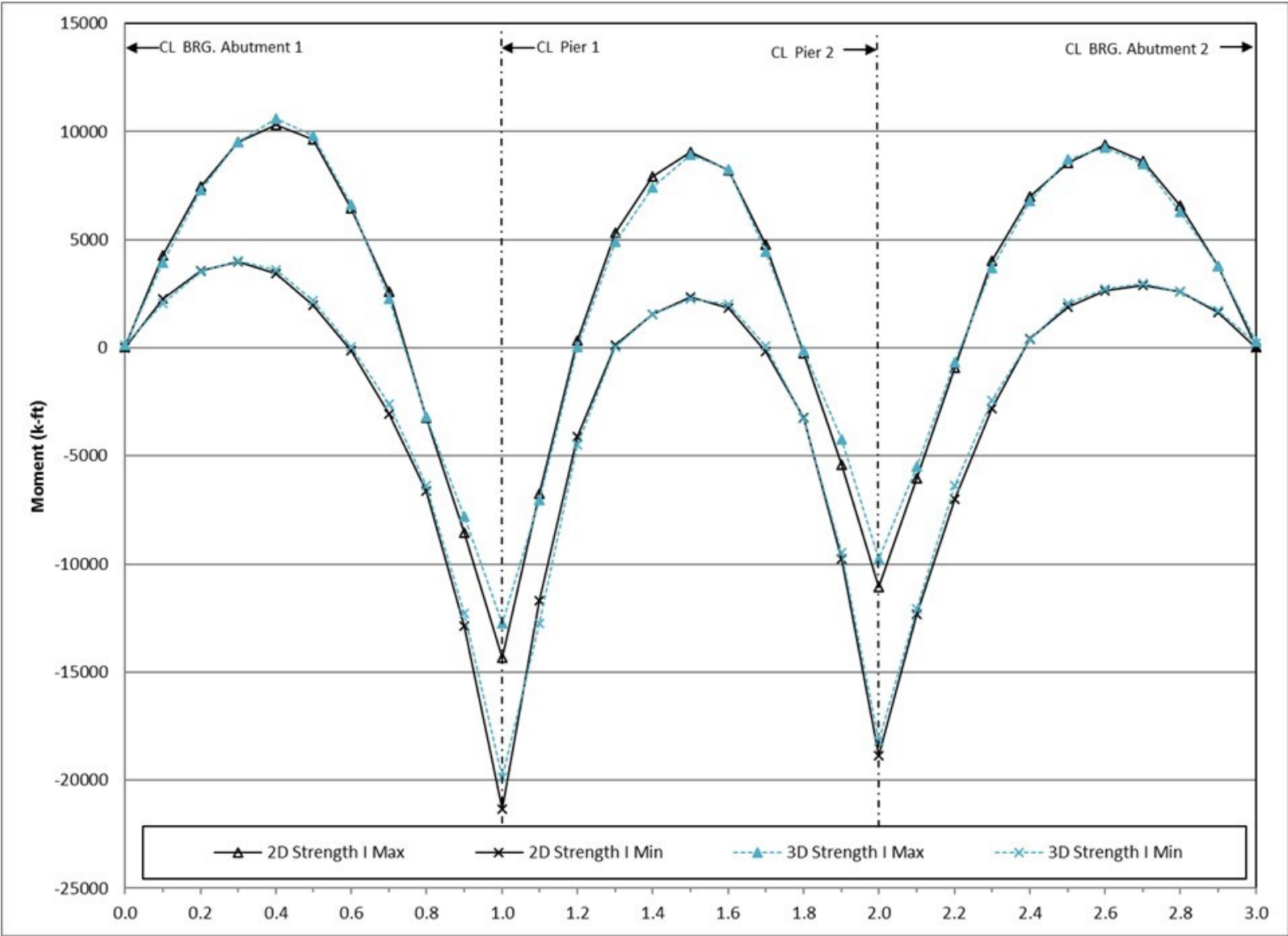


Figure 277. Graph. Comparison of factored moments for Girder 3.

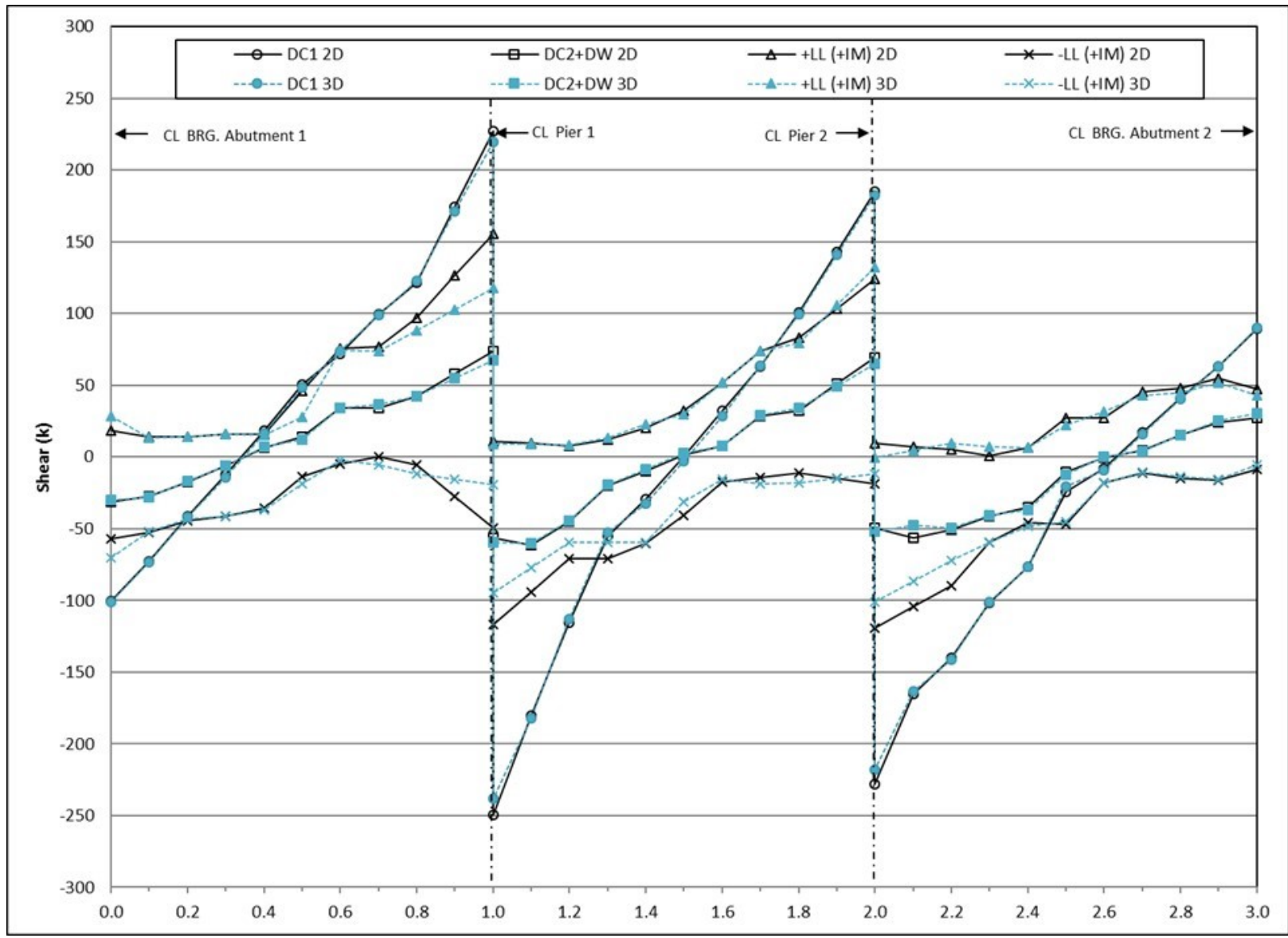


Figure 278. Graph. Comparison of 2D shears to 3D shears for Girder 3.

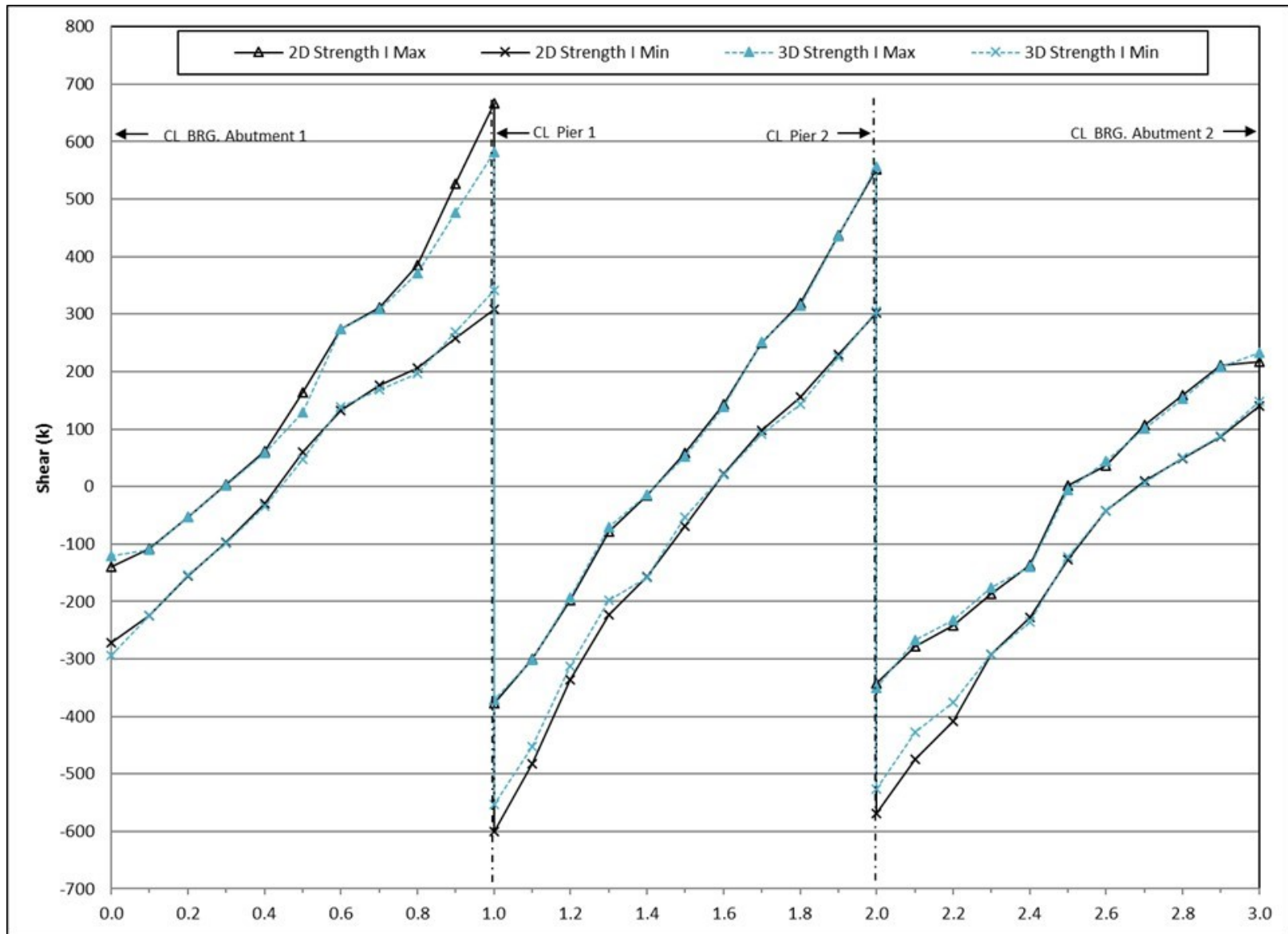


Figure 279. Graph. Comparison of factored shears for Girder 3.

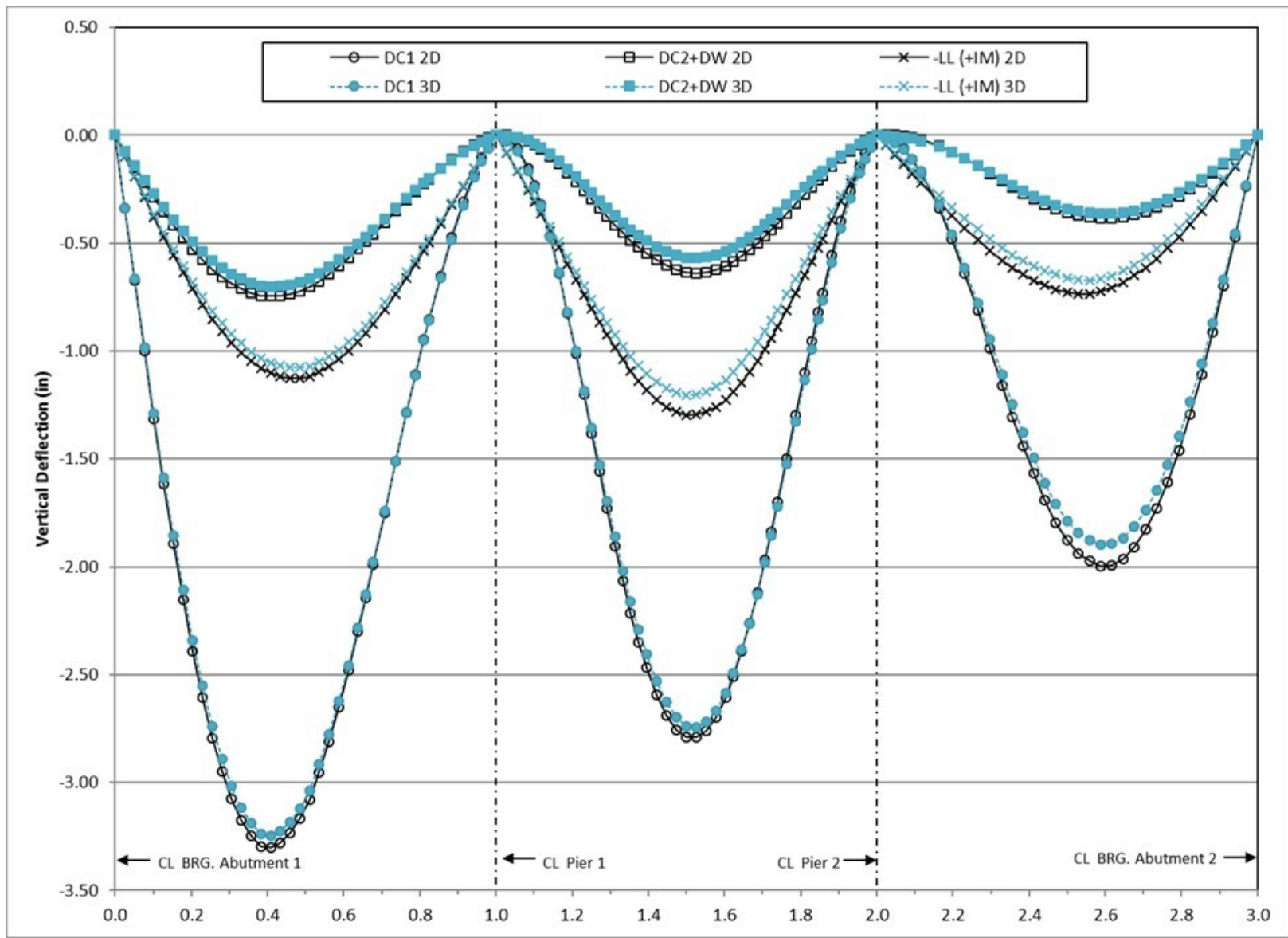


Figure 280. Graph. Comparison of 2D deflections to 3D deflections for Girder 3.

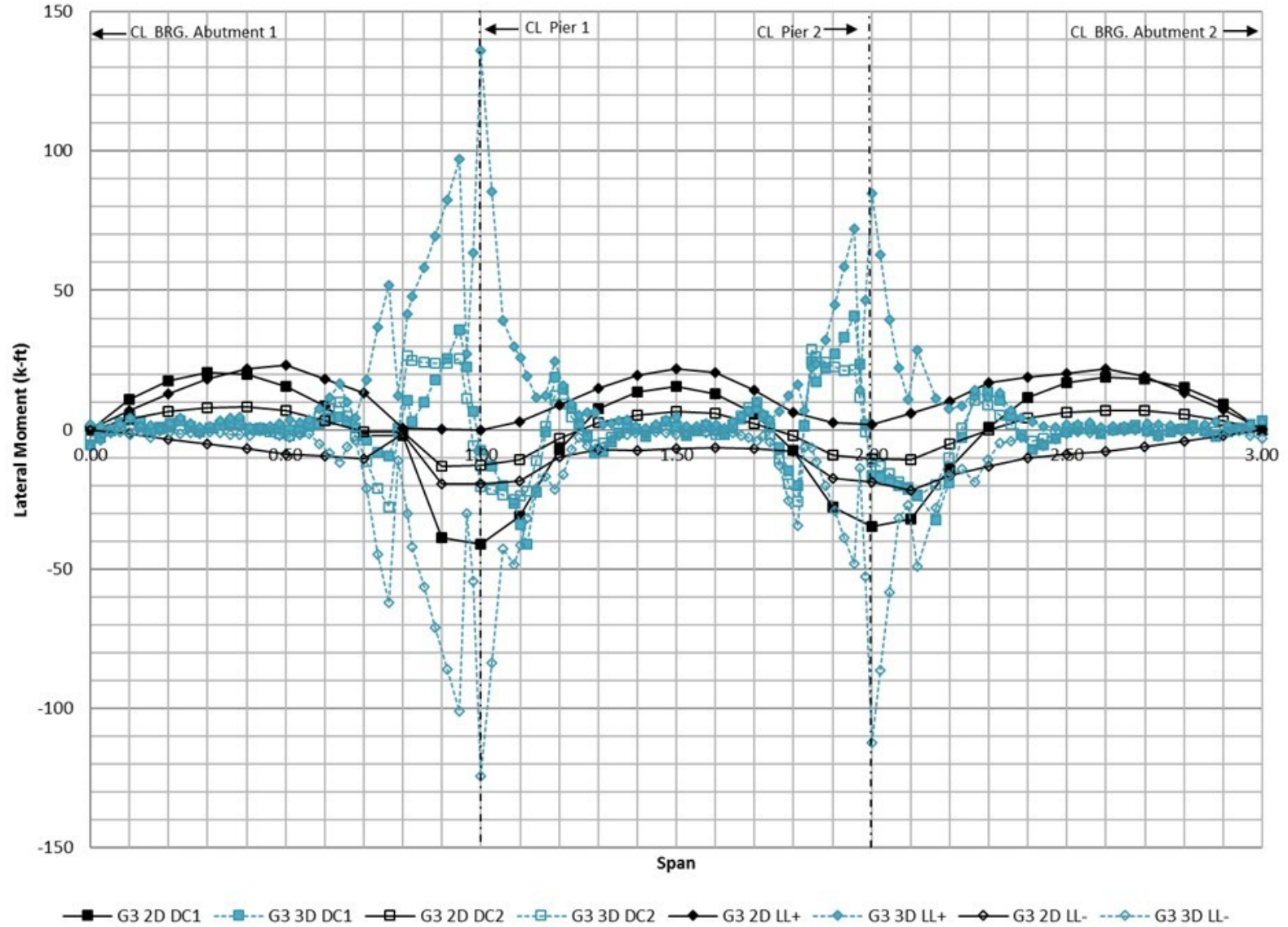


Figure 281. Graph. Comparison of 2D flange lateral bending moments to 3D flange lateral bending moments for Girder 3.

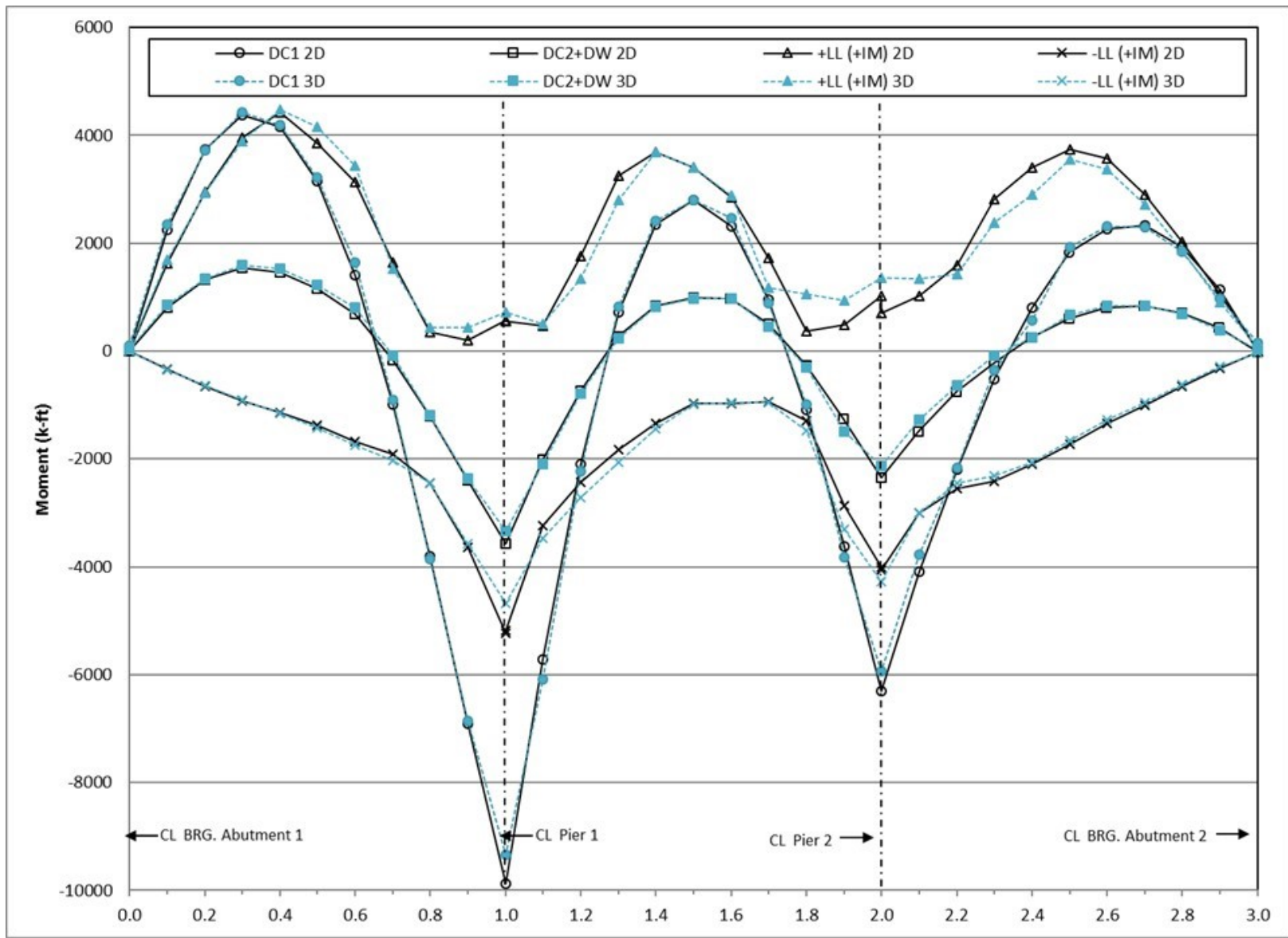


Figure 282. Graph. Comparison of 2D moments to 3D moments for Girder 4.

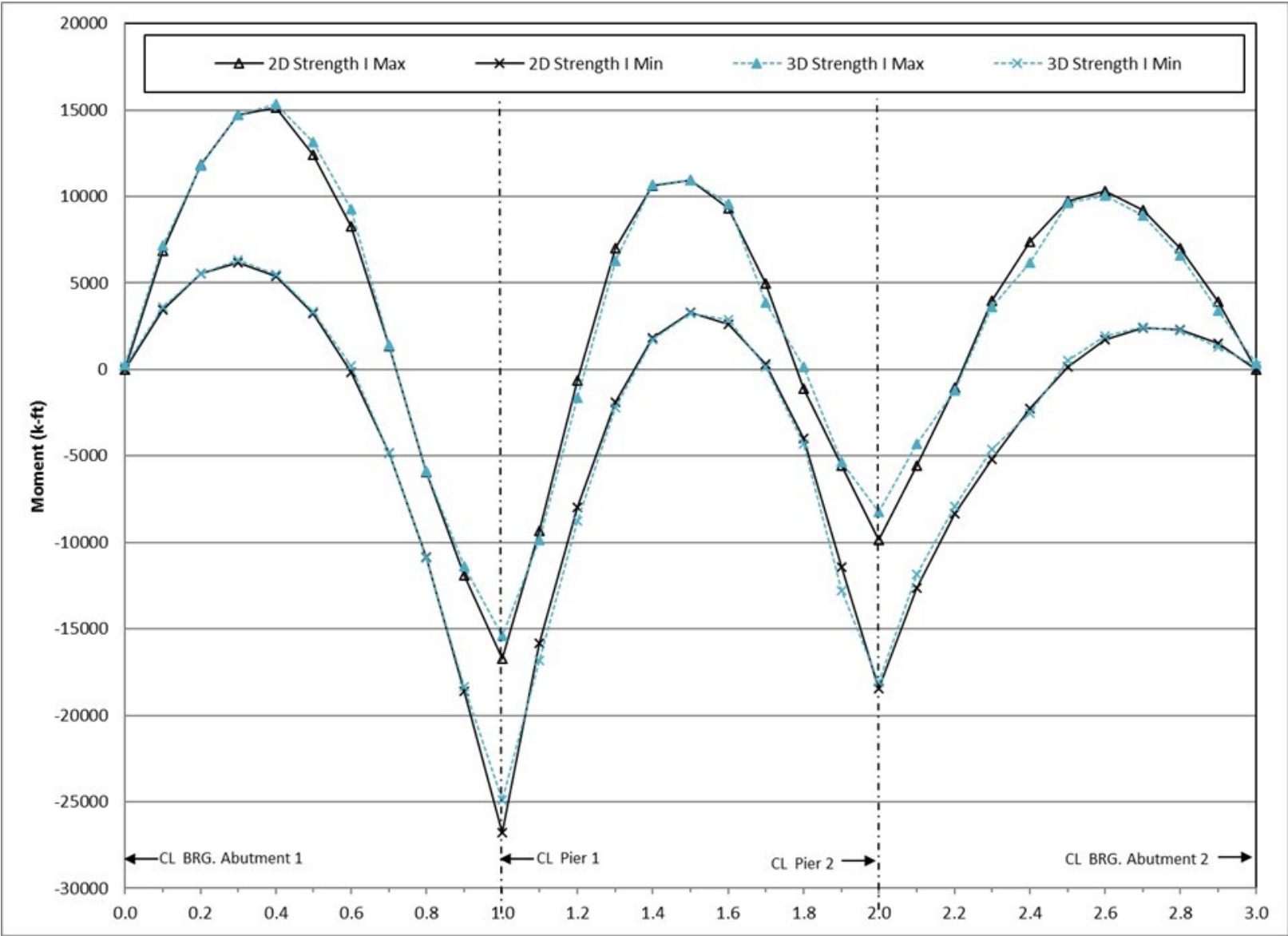


Figure 283. Graph. Comparison of factored moments for Girder 4.

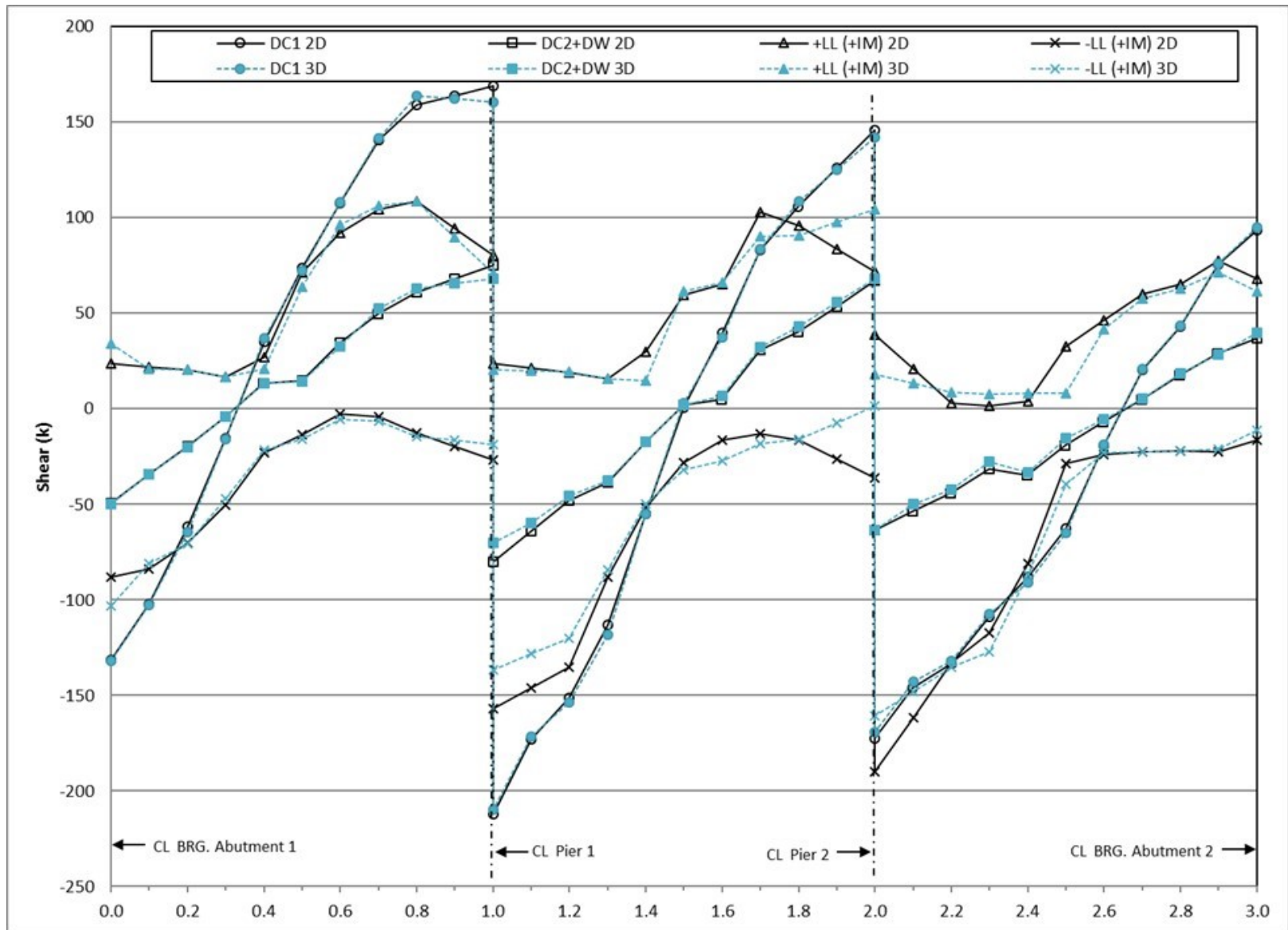


Figure 284. Graph. Comparison of 2D shears to 3D shears for Girder 4.

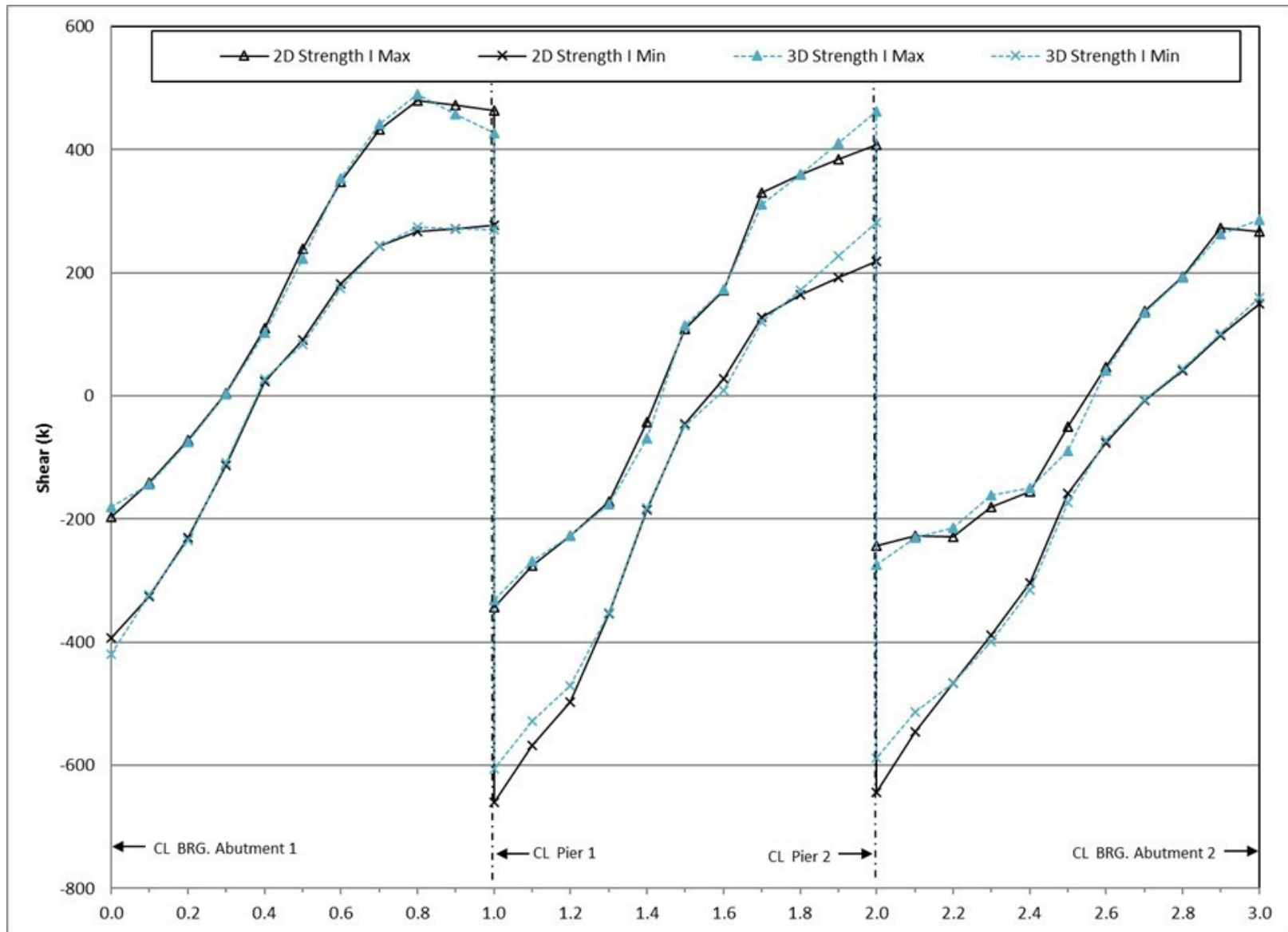


Figure 285. Graph. Comparison of factored shears for Girder 4.

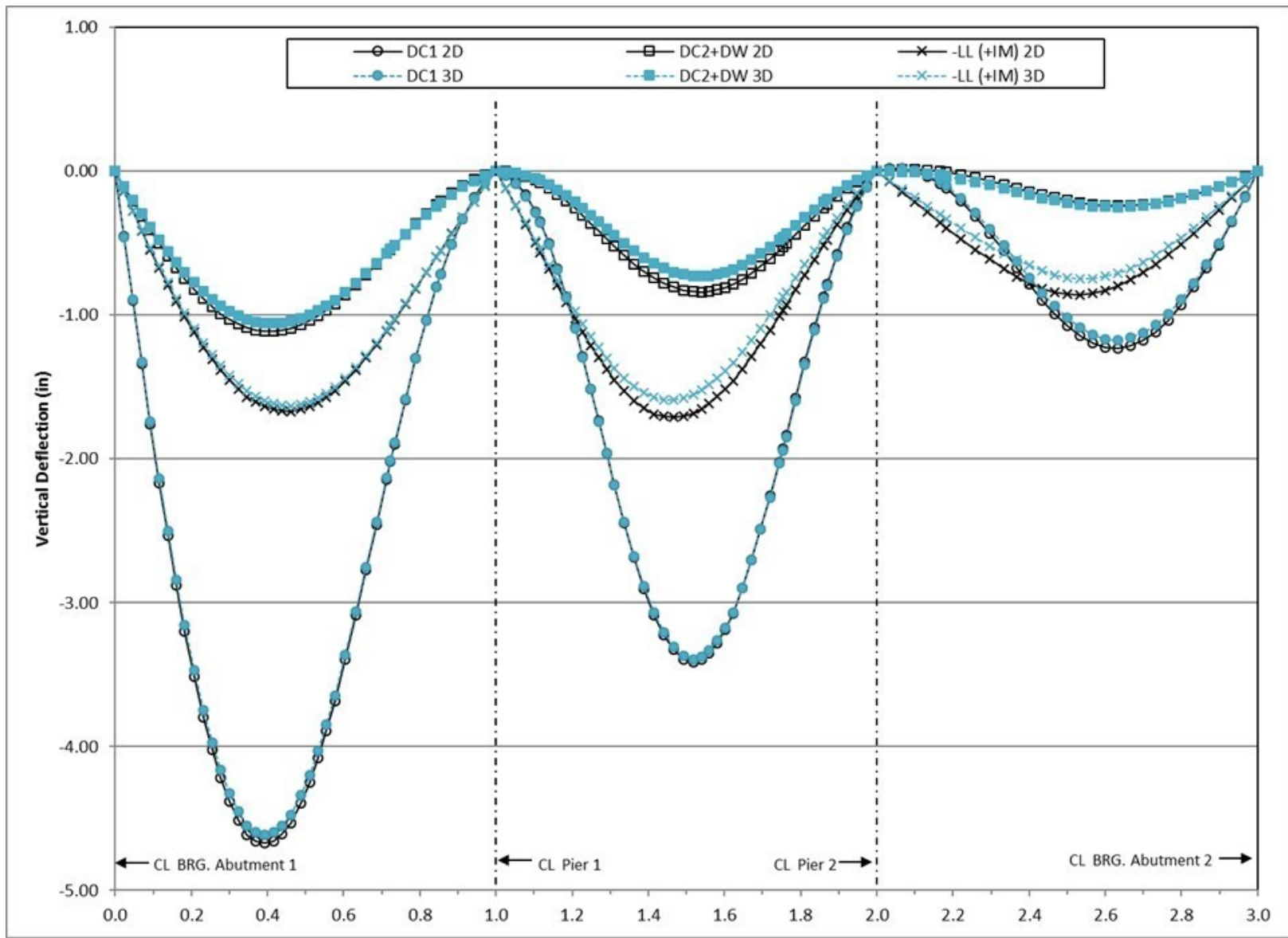


Figure 286. Graph. Comparison of 2D deflections to 3D deflections for Girder 4.

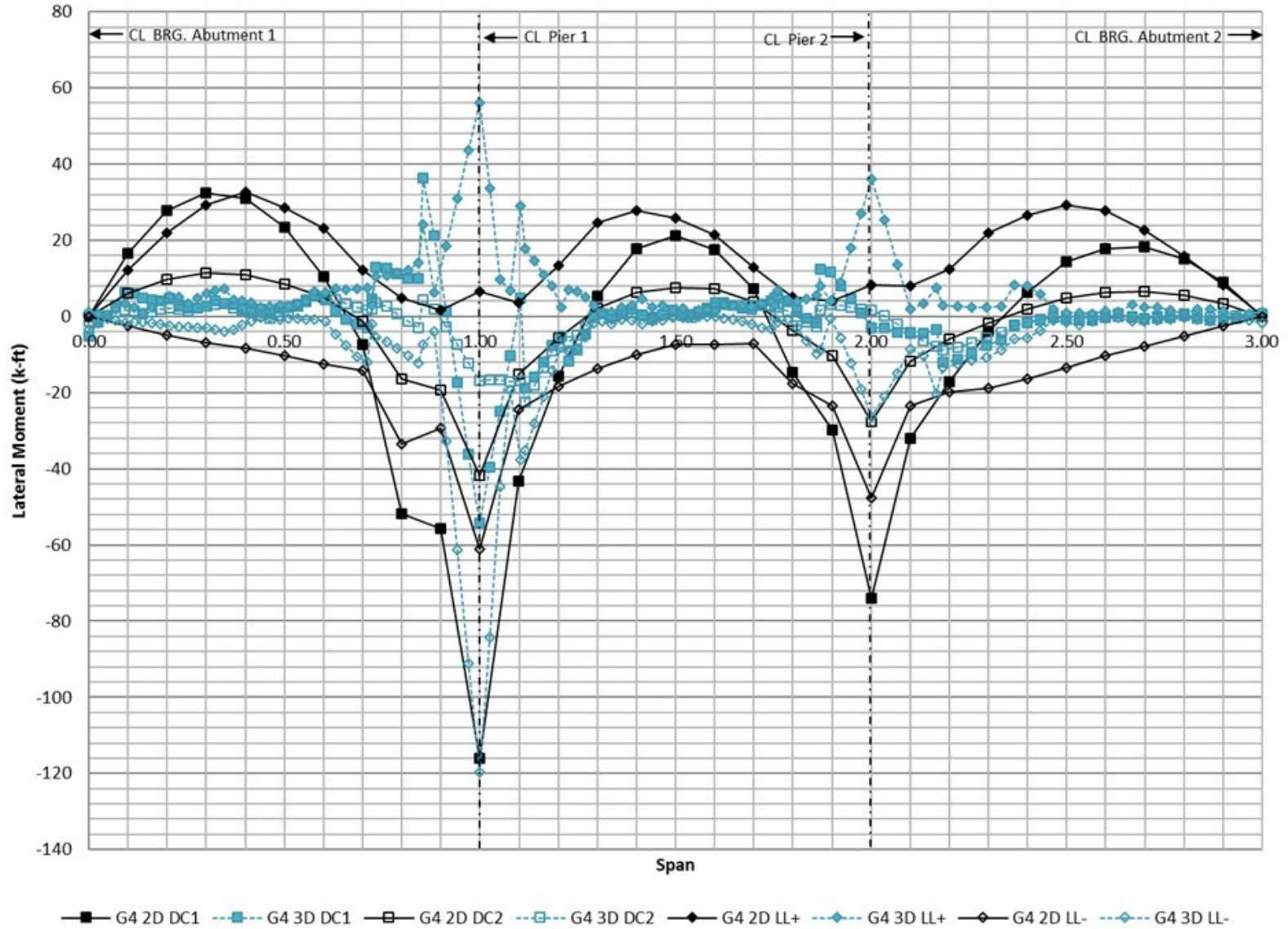


Figure 287. Graph. Comparison of 2D flange lateral bending moments to 3D flange lateral bending moments for Girder 4.

9.3.4.2 Cross-Frames

9.3.4.2.1 Cross-Frame Forces

One of the principal differences between the two- and three-dimensional models is how the cross-frames are handled. The forces developed in the cross-frames are a function of load distribution, torsional and lateral behavior captured in the model. Axial forces, shears, and moments at the cross-frame ends are tabulated and compared for the two- and three-dimensional cases. Cross-frames are numbered starting from the left abutment in Figure 230; interior pier locations are also noted on each figure.

9.3.4.2.1.1 Net Axial Force

In the two-dimensional models the axial force shown is simply the axial force in the equivalent cross-frame. In the three-dimensional models the forces shown in this and subsequent sections, are the sum of forces taken at a section near the ends of the cross-frame (i.e. sum of forces in the chords and diagonals). Figures 288 through 290 compare the net axial force in the cross-frames due to non-composite dead loads. The net axial force in the cross-frames from the 2D model is essentially zero. From the 3D model, the net axial force is essentially zero for all cross-frames except for those at the pier and abutment locations.

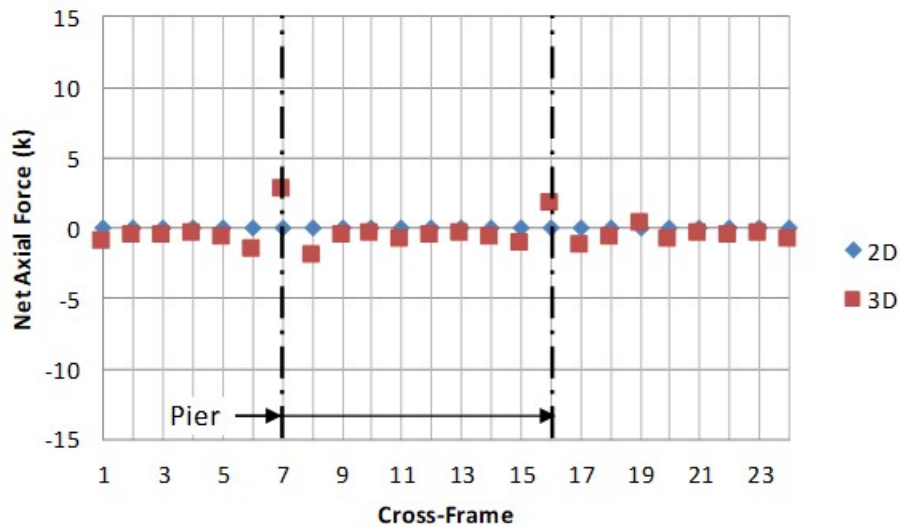


Figure 288. Graph. Comparison of cross-frame DC1 forces – G1-G2 cross-frames.

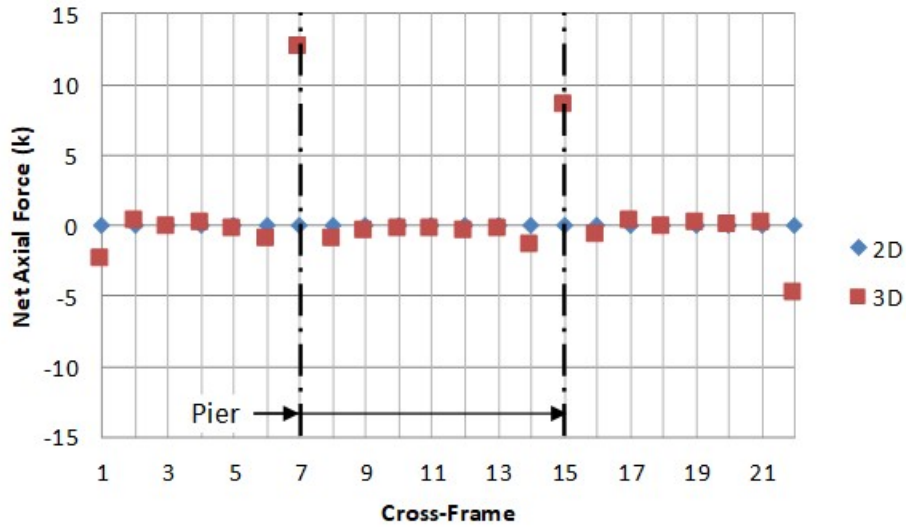


Figure 289. Graph. Comparison of cross-frame DC1 forces – G2-G3 cross-frames.

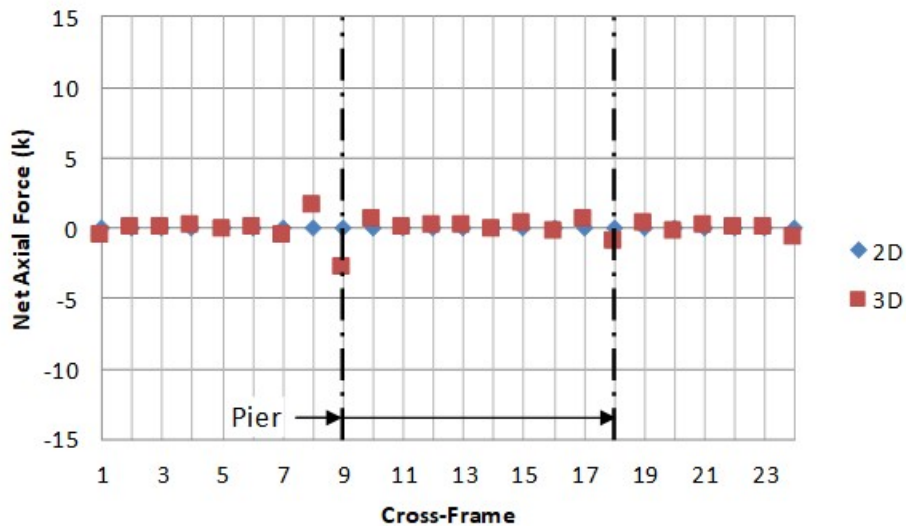


Figure 290. Graph. Comparison of cross-frame DC1 forces – G3-G4 cross-frames.

Figures 291 through 293 show the net axial force in the cross-frames due to composite dead load and the wearing surface. The net axial force from the 3D model is typically larger than the net axial force from the 2D model for the cross-frames between G1 and G2 (Figure 291) as well as between G3 and G4 (Figure 293) except at the pier locations where the 3D model provides smaller net axial forces than the 2D model. For the cross-frames between girders G2 and G3 (Figure 292), the results from the 2D and 3D models are very similar at all cross-frame locations.

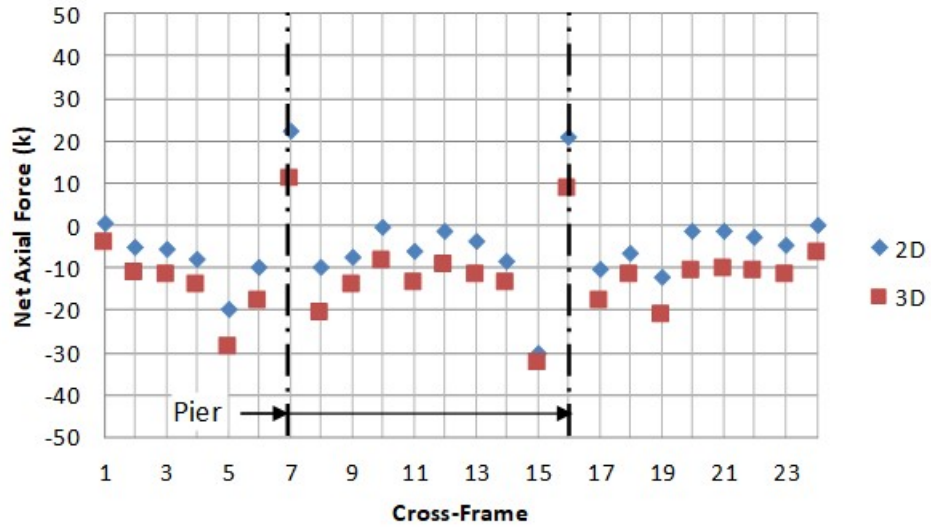


Figure 291. Graph. Comparison of cross-frame DC2+DW forces – G1-G2 cross-frames.

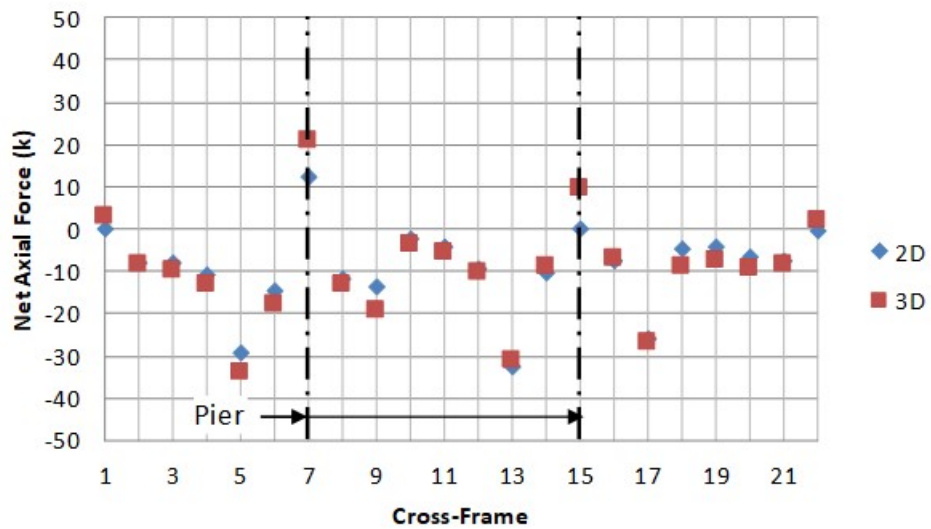


Figure 292. Graph. Comparison of cross-frame DC2+DW forces – G2-G3 cross-frames.

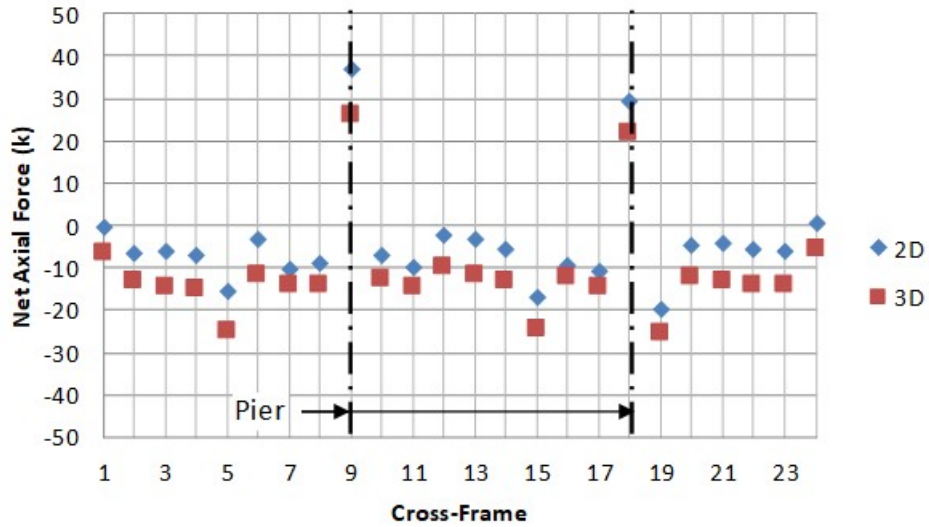


Figure 293. Graph. Comparison of cross-frame DC2+DW forces – G3-G4 cross-frames.

Figures 294 through 296 compare the minimum and maximum net axial live load force in the cross-frames for the 2D and 3D models. The force effects from the 2D model are typically greater than the force effects determined from the 3D model. The 3D model live load force effects are generally closer to zero than the 2D model live load force effects. At the abutment and pier locations, the forces in the 3D model are of similar magnitude to those from the 2D model.

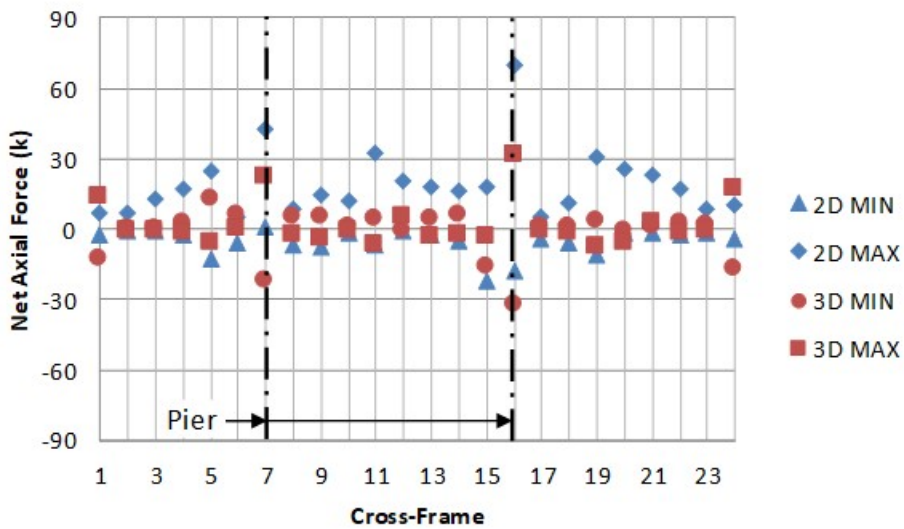


Figure 294. Graph. Comparison of cross-frame LL forces – G1-G2 cross-frames.

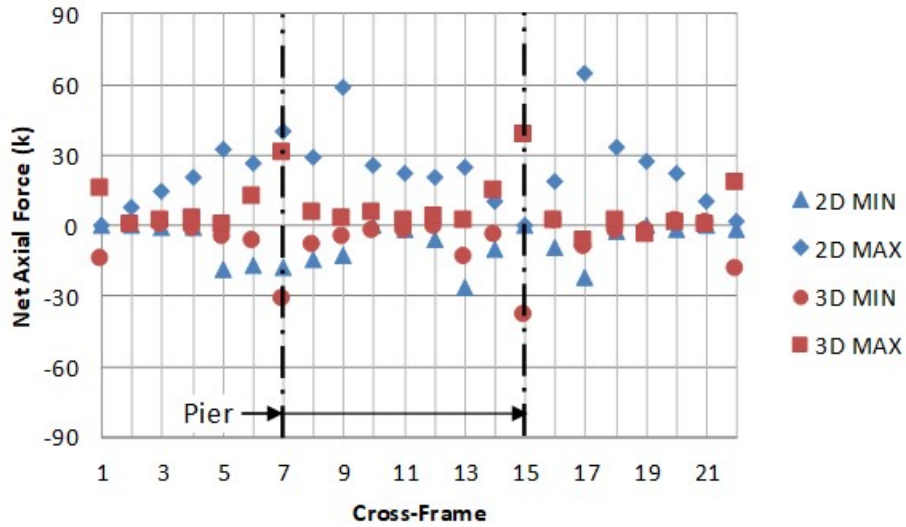


Figure 295. Graph. Comparison of cross-frame LL forces – G2-G3 cross-frames.

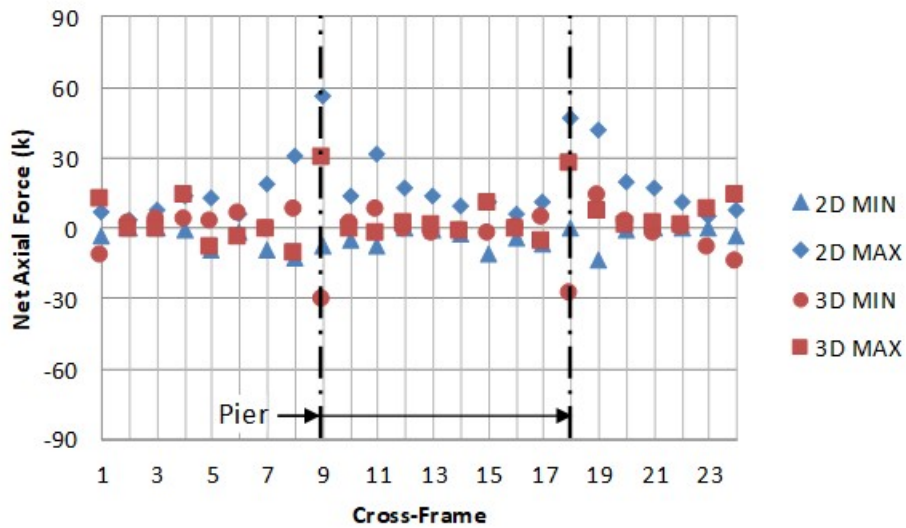


Figure 296. Graph. Comparison of cross-frame LL forces – G3-G4 cross-frames.

9.3.4.2.1.2 Shear

Figures 297 through 299 show the shear force in the cross-frames due to non-composite dead loads for both the 2D and 3D models. The cross-frame forces are very similar for the 2D and 3D models with the 3D model typically providing slightly smaller negative shears and slightly larger positive shears.

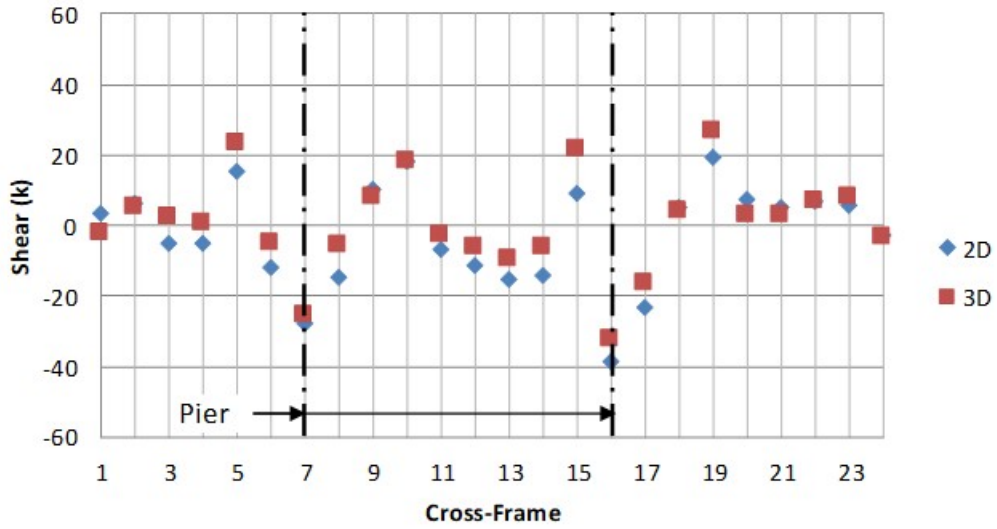


Figure 297. Graph. Comparison of cross-frame DC1 forces – G1-G2 cross-frames.

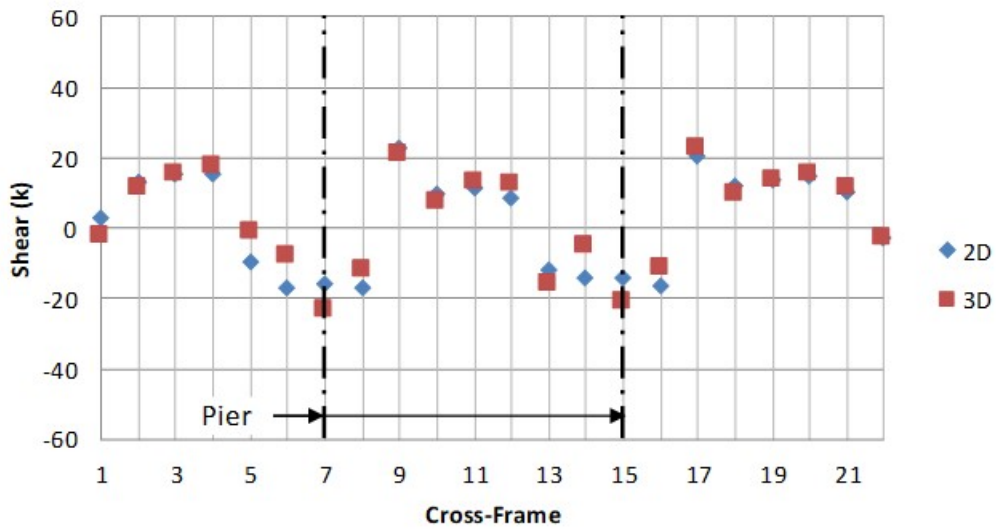


Figure 298. Graph. Comparison of cross-frame DC1 forces – G2-G3 cross-frames.

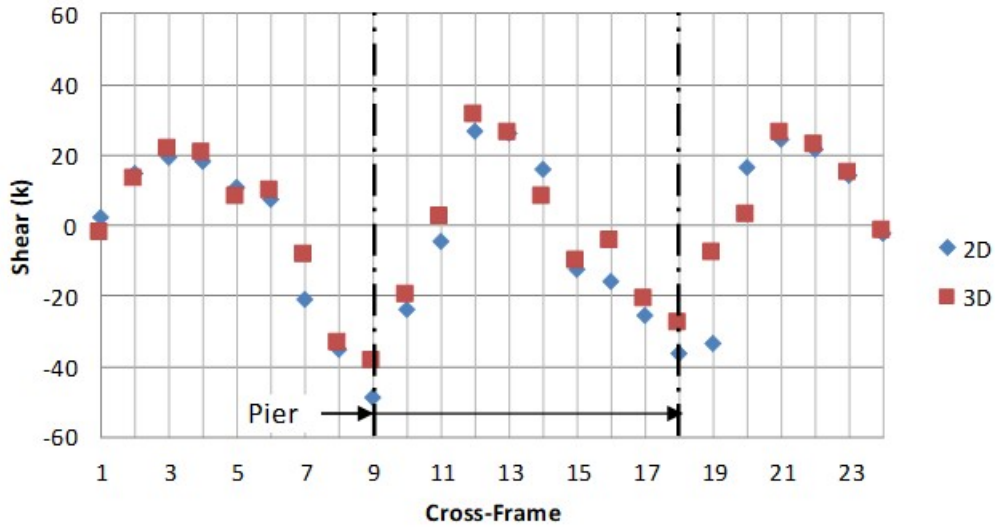


Figure 299. Graph. Comparison of cross-frame DC1 forces – G3-G4 cross-frames.

Figures 300 through 302 compare the shear force in the cross-frames due to composite dead loads from the 2D and 3D models. The cross-frame shear forces generally follow the same trend for both the 2D and 3D models between Girders 1 and 2 as well as between Girders 3 and 4; the equivalent force effects determined using the individual member forces for the 3D model are typically larger than the force effects from the 2D model. The force effects for the cross-frames between Girders 2 and 3 are nearly identical for all cross-frames.

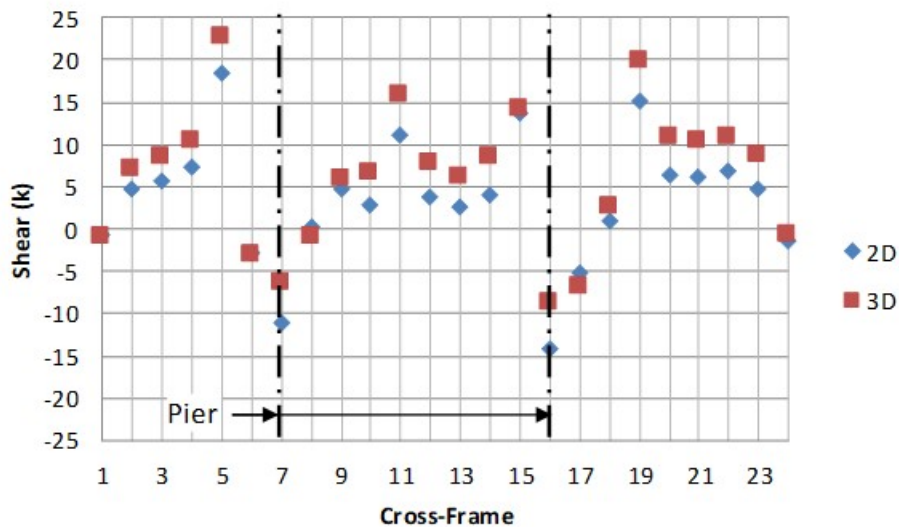


Figure 300. Graph. Comparison of cross-frame DC2+DW forces – G1-G2 cross-frames.

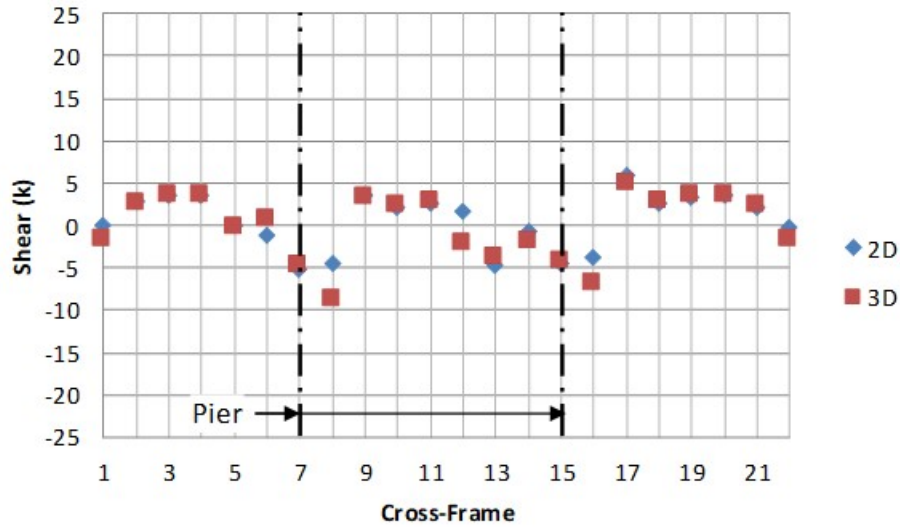


Figure 301. Graph. Comparison of cross-frame DC2+DW forces – G2-G3 cross-frames.

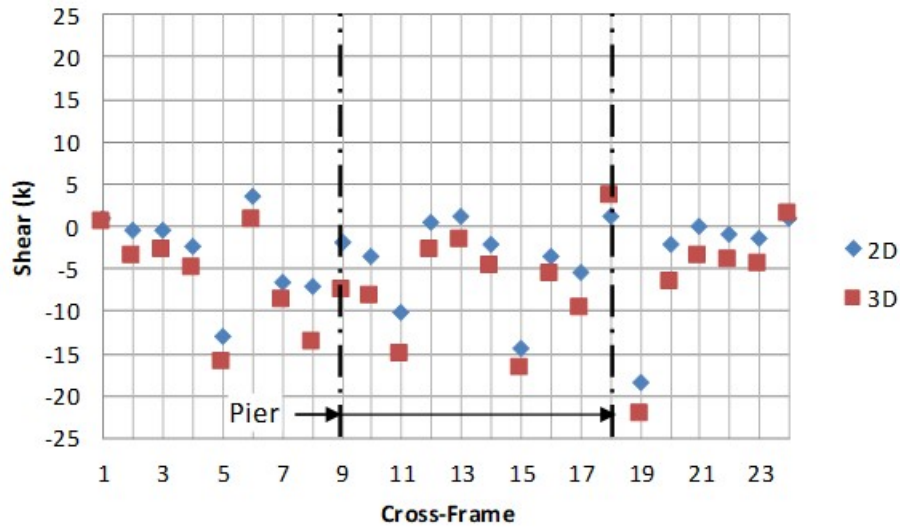


Figure 302. Graph. Comparison of cross-frame DC2+DW forces – G3-G4 cross-frames.

Figures 303 through 305 show the cross-frame shear forces due to live load from the 2D and 3D models. The cross-frame shear forces from the 2D and 3D models are generally similar in magnitude to those from the 3D model.

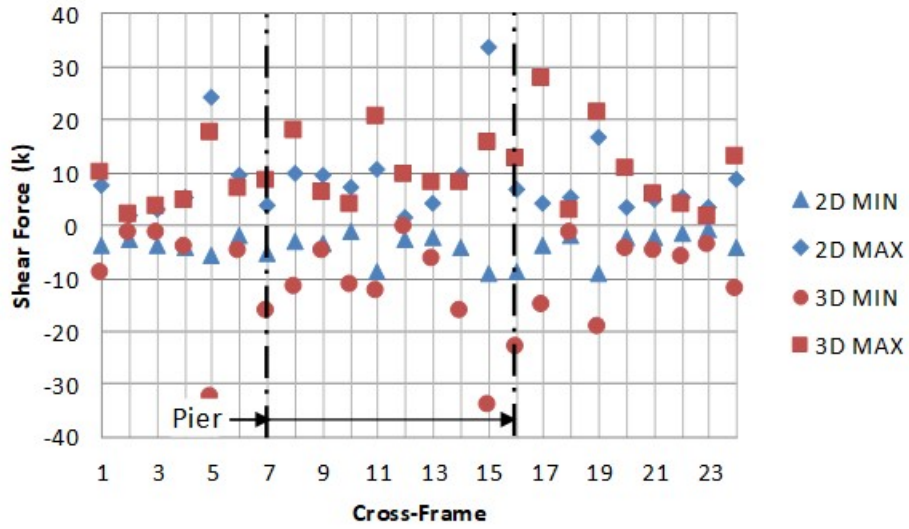


Figure 303. Graph. Comparison of cross-frame LL forces – G1-G2 cross-frames.

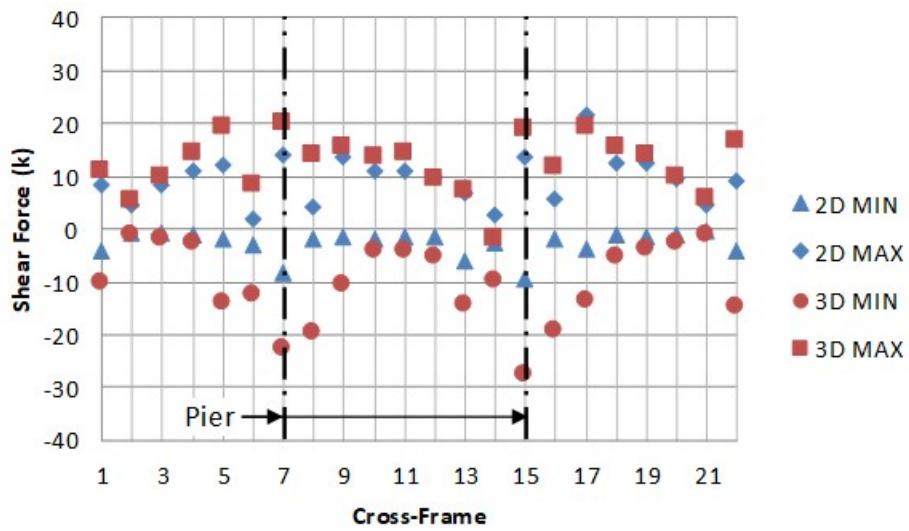


Figure 304. Graph. Comparison of cross-frame LL forces – G2-G3 cross-frames.

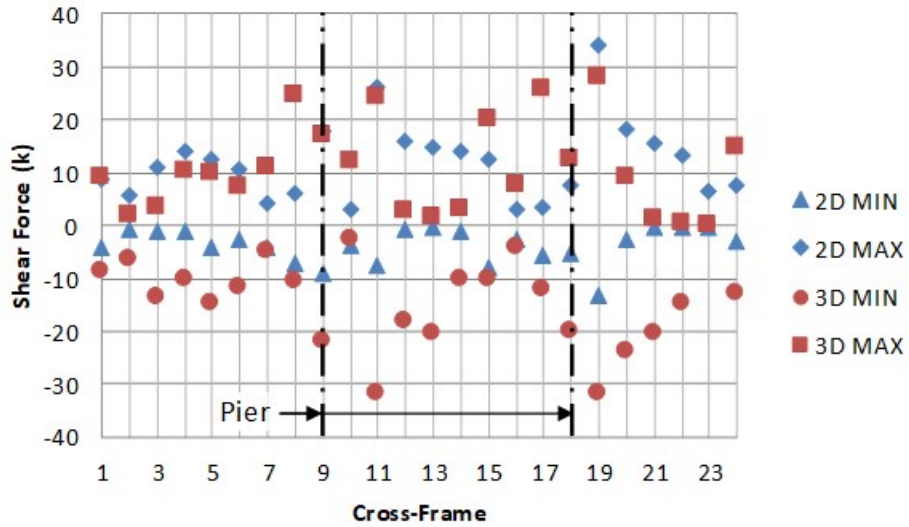


Figure 305. Graph. Comparison of cross-frame LL forces – G3-G4 cross-frames.

9.3.4.2.1.3 Moment

Figures 306 through 308 show the cross-frame moments due to non-composite dead loads. The extreme moments generally occur in the cross-frames near the interior skewed supports. As expected, the results from the 2D and 3D models are generally very similar.

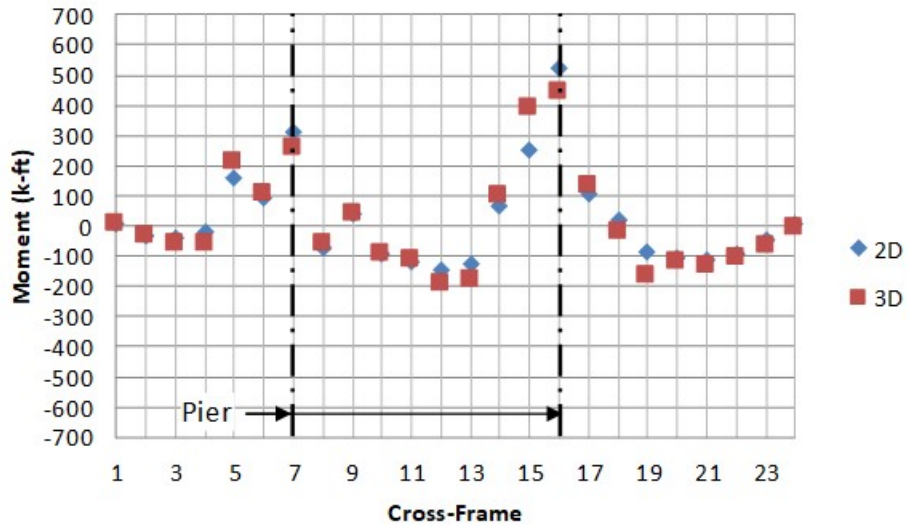


Figure 306. Graph. Comparison of cross-frame DC1 forces – G1-G2 cross-frames.

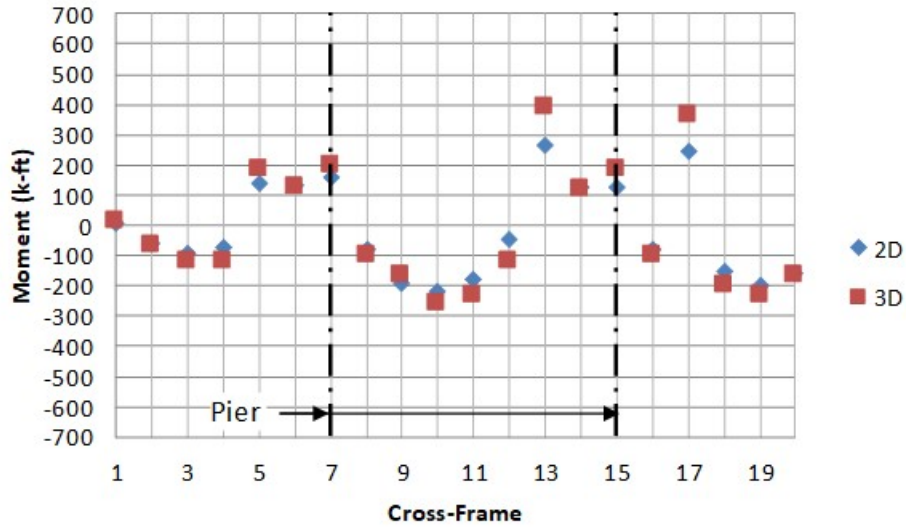


Figure 307. Graph. Comparison of cross-frame DC1 forces – G2-G3 cross-frames.

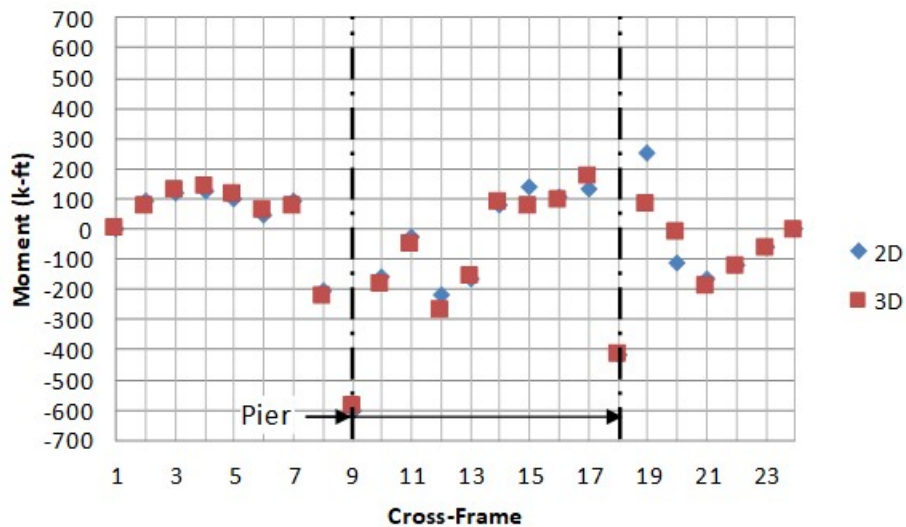


Figure 308. Graph. Comparison of cross-frame DC1 forces – G3-G4 cross-frames.

Figures 309 through 311 show the cross-frame moments due to composite dead loads for both the 2D and 3D models. The moments determined from the 3D model are similar to the moments in the 2D model at most cross-frame locations. Where the cross-frames are aligned, the results of the two models are very similar; larger variation occurs at the locations on either side of the pier where the cross-frames are staggered due to the skew.

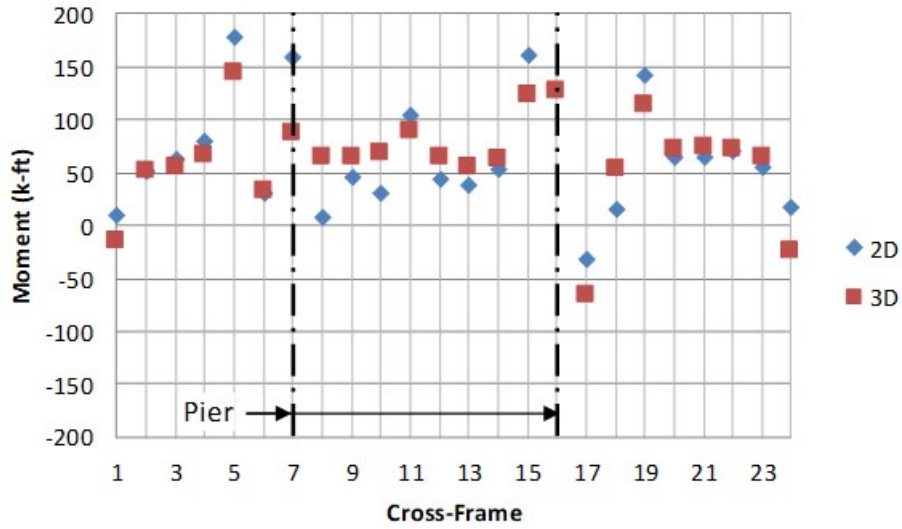


Figure 309. Graph. Comparison of cross-frame DC2+DW forces – G1-G2 cross-frames.

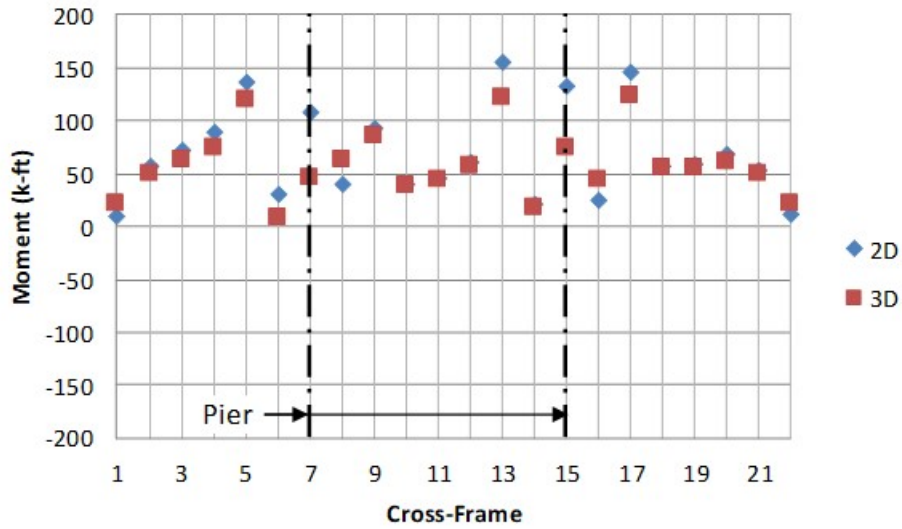


Figure 310. Graph. Comparison of cross-frame DC2+DW forces – G2-G3 cross-frames.

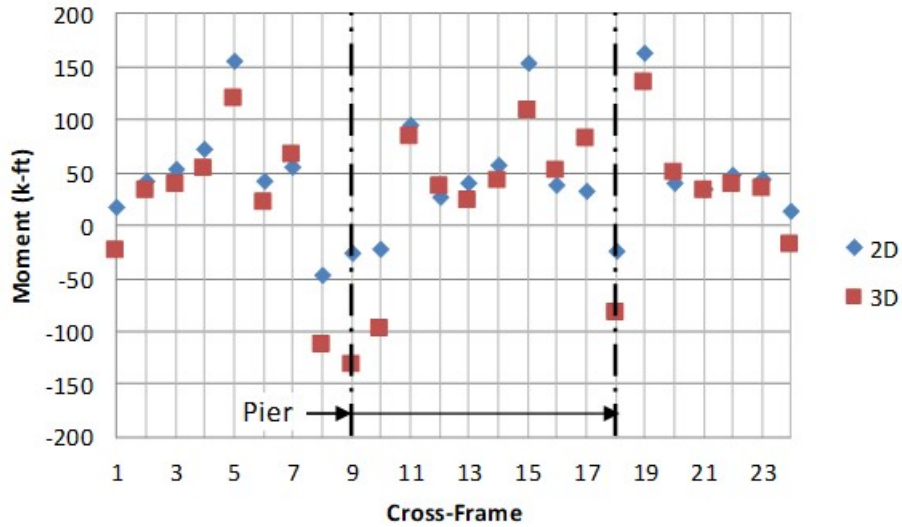


Figure 311. Graph. Comparison of cross-frame DC2+DW forces – G3-G4 cross-frames.

Figures 312 through 314 show the cross-frame moments due to live load for both the 2D and 3D models. The results from the 2D and 3D models are similar and generally follow the same trends.

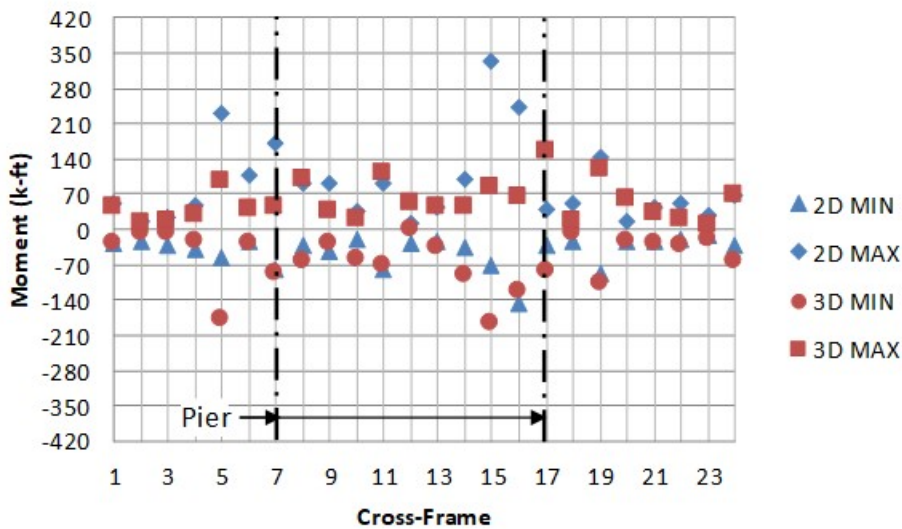


Figure 312. Graph. Comparison of cross-frame LL forces – G1-G2 cross-frames.

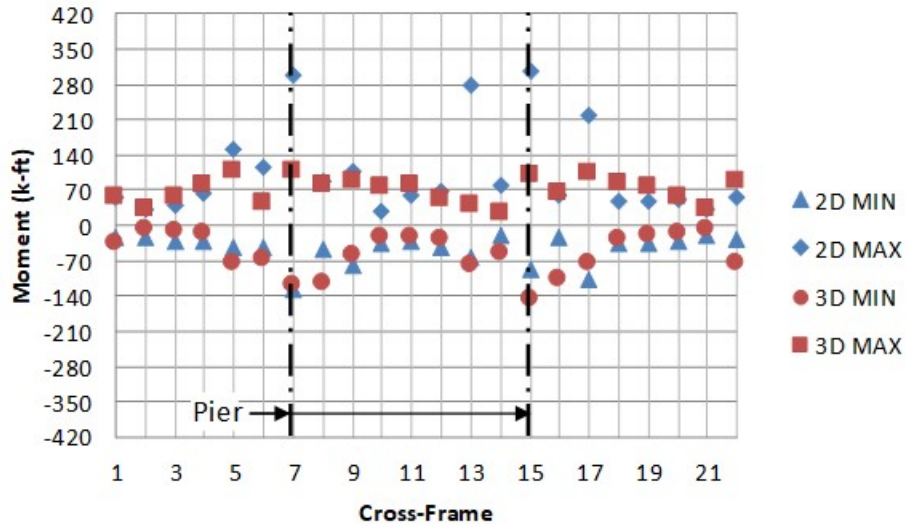


Figure 313. Graph. Comparison of cross-frame LL forces – G2-G3 cross-frames.

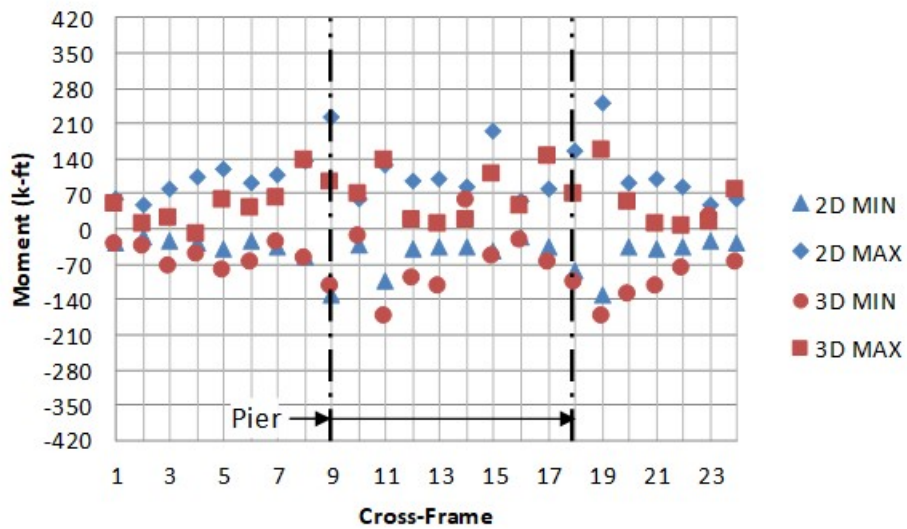


Figure 314. Graph. Comparison of cross-frame LL forces – G3-G4 cross-frames.

9.3.4.3 Conclusions

Of the effects studied, major-axis moment, shear and deflection showed the best agreement, while there was significant variability in the lateral moments. The level of accuracy observed for all but lateral moments were in a range of reasonable acceptability (within 10 percent in most cases). From Tables 60 and 61, major-axis bending moment results between the two- and three-dimensional cases are within 12 percent.

Table 60. 2D/3D ratios for maximum positive major-axis bending moment.

	G1			G2			G3			G4		
	Span 1	Span 2	Span 3	Span 1	Span 2	Span 3	Span 1	Span 2	Span 3	Span 1	Span 2	Span 3
DC1	1.00	0.95	0.98	1.00	1.02	1.00	1.00	1.01	1.01	0.99	1.00	1.01
DC2+DW	1.12	0.95	1.03	1.00	0.96	0.99	0.98	0.99	0.97	0.97	1.00	0.99
LL	0.99	1.03	1.01	1.04	1.05	1.01	1.00	1.02	1.03	0.99	1.00	1.05

Table 61. 2D/3D ratio for maximum negative major-axis bending moment.

	G1			G2			G3			G4		
	Span 1	Span 2	Span 3	Span 1	Span 2	Span 3	Span 1	Span 2	Span 3	Span 1	Span 2	Span 3
DC1	1.11	1.06	1.06	1.03	1.02	1.02	1.10	1.10	1.05	1.06	1.06	1.06
DC2+DW	1.04	0.96	0.96	0.99	0.93	0.93	1.05	1.05	1.05	1.07	1.07	1.10
LL	0.96	1.03	1.03	0.96	0.97	0.97	0.95	0.98	0.98	0.90	0.90	1.08

Table 62 shows the ratio of the 2D model to the 3D model for shear in each span. The results for shear are similar to those for major-axis bending moment, with most results from the two models being within 10 percent, but with a few cases in the 20-25 percent range. If the 2D model were used for design, the design live loads would, in most cases, be conservative. The exceptions would be Span 3 for Girder G1, Span 2 for Girder G3, and Span 1 for Girder G4.

Table 62. 2D/3D ratios for shear.

	G1			G2			G3			G4		
	Span 1	Span 2	Span 3	Span 1	Span 2	Span 3	Span 1	Span 2	Span 3	Span 1	Span 2	Span 3
DC1	1.00	1.02	1.02	0.97	0.97	0.97	1.05	1.05	1.05	1.01	1.01	1.02
DC2+DW	0.98	0.84	0.84	0.97	0.97	0.96	0.98	1.02	1.09	0.97	0.93	1.00
LL	1.19	1.11	0.95	1.21	1.01	1.00	1.23	0.98	1.14	0.80	1.10	1.10

From Table 63 it can be seen that the vertical system of the two-dimensional model is effectively slightly more flexible than the three-dimensional case. For non-composite dead load the results are mostly within 5 percent, however, as composite action develops the variation in deflection increases. Ideally the modifications made to the two-dimensional cross-frame elements would perfectly capture the stiffness of the three-dimensional system, but they are approximate methods and do a satisfactory job for a complex case.

Table 63. 2D/3D ratios for deflection.

	G1			G2			G3			G4		
	Span 1	Span 2	Span 3	Span 1	Span 2	Span 3	Span 1	Span 2	Span 3	Span 1	Span 2	Span 3
DC1	1.06	1.00	1.02	1.03	1.03	1.04	1.02	1.02	1.05	1.01	1.01	1.05
DC2+DW	1.19	1.02	1.11	1.09	1.06	1.10	1.06	1.12	1.05	1.05	1.15	0.97
LL	1.03	1.10	1.09	1.07	1.09	1.08	1.04	1.08	1.10	1.02	1.08	1.14

In general lateral behavior is not well predicted in two-dimensional models and agreement with actual behavior varies widely between bridges. The approximate equation which appears in AASHTO and is given by the V-Load method provides variable accuracy, which typically diminishes further when there are skewed supports, variable stiffness between girders, and away from cross-frame locations.

Table 64. 2D/3D ratios for flange lateral bending moment.

	G1			G2			G3			G4		
	Span 1	Span 2	Span 3	Span 1	Span 2	Span 3	Span 1	Span 2	Span 3	Span 1	Span 2	Span 3
DC1	0.33	0.49	3.59	3.40	1.13	2.76	6.85	2.56	2.52	3.60	3.02	2.87
DC2+DW	1.71	1.12	5.67	0.25	0.54	1.10	2.78	0.78	2.00	1.66	1.75	6.21
LL	10.46	5.13	4.85	4.36	1.54	2.59	4.78	5.87	4.73	2.69	5.29	6.97

The cross-frame forces compare reasonably well between the 2D and 3D models as shown in the previous section.

9.4 Example 4 – Three Span Continuous Concrete Box Girder Spine Beam

As stated in Section 3.5 of this manual, per AASHTO 4.6.1.2.3, horizontally curved, torsionally stiff, single girder and multi-cell concrete box girders may be analyzed with a single spine beam. Spine beam analysis is a specific case of space frame analysis in which the superstructure is modeled as a series of straight, chorded beam elements located along the centerline of the superstructure. Section properties of the spine beam are based on the entire cross-section they represent. As also stated in Section 3.5 of this manual, AASHTO limits the central angle for this analysis type to 34° within one span, while NCHRP 620 suggests accuracy is sufficient up to 46° . Further, both AASHTO and NCHRP 620 advise limiting each element within a span to 3.5° .

To illustrate this type of analysis, a brief example based on the geometry and section used in NCHRP Report 620 Appendix B for a curved three span continuous concrete box girder bridge with spans of 200 ft–300 ft–200 ft and central angles of 28.65° and 42.97° is reproduced below. Plan and elevation views are shown in Figure 315.

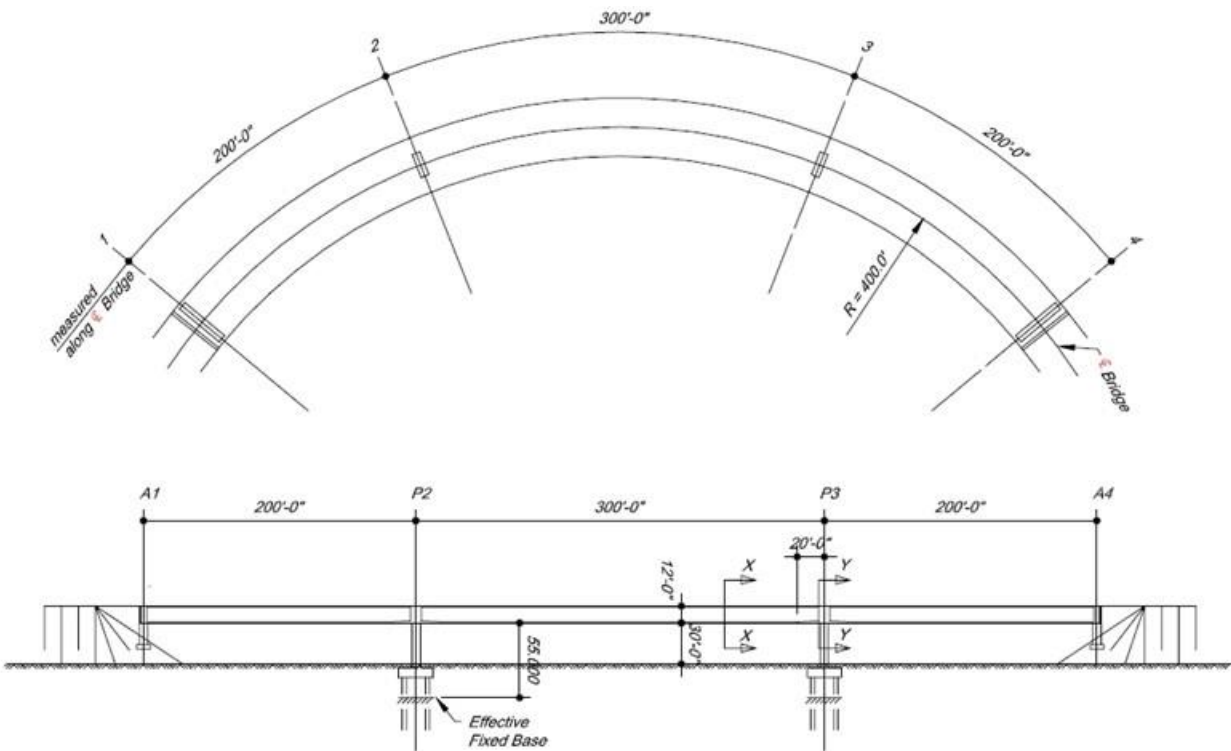


Figure 315. Illustration. NCHRP 620 comprehensive example (Nutt et al., 2008).

To avoid creating segments with arcs greater than 3.5° , each span in the analysis model (Figure 316) is split into 20 equal length elements, resulting in arcs of 1.43° (Spans 1 and 3) and 2.15° (Span 2). Columns are assumed fixed at piers and integral with the box girder, while abutments restrain translation laterally and vertically, and against torsional rotation.

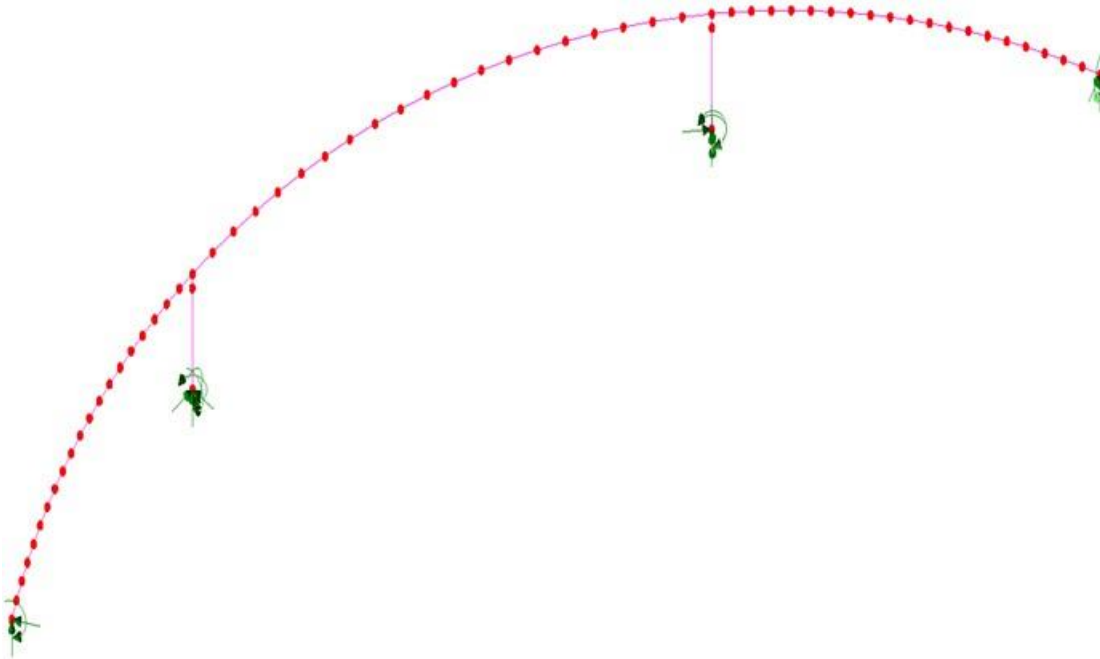


Figure 316. Illustration. Analysis model geometry.

Figure 317 shows the typical section for the two cell concrete box beam used in the model, while Figure 318 shows the section at pier locations. Properties for the two sections, which represent the full width of the bridge are calculated and shown in Table 65. An offset of 1.312 ft is given to the pier section to locate the section properly relative to the centroid of the typical section, which serves as the reference plane for the model.

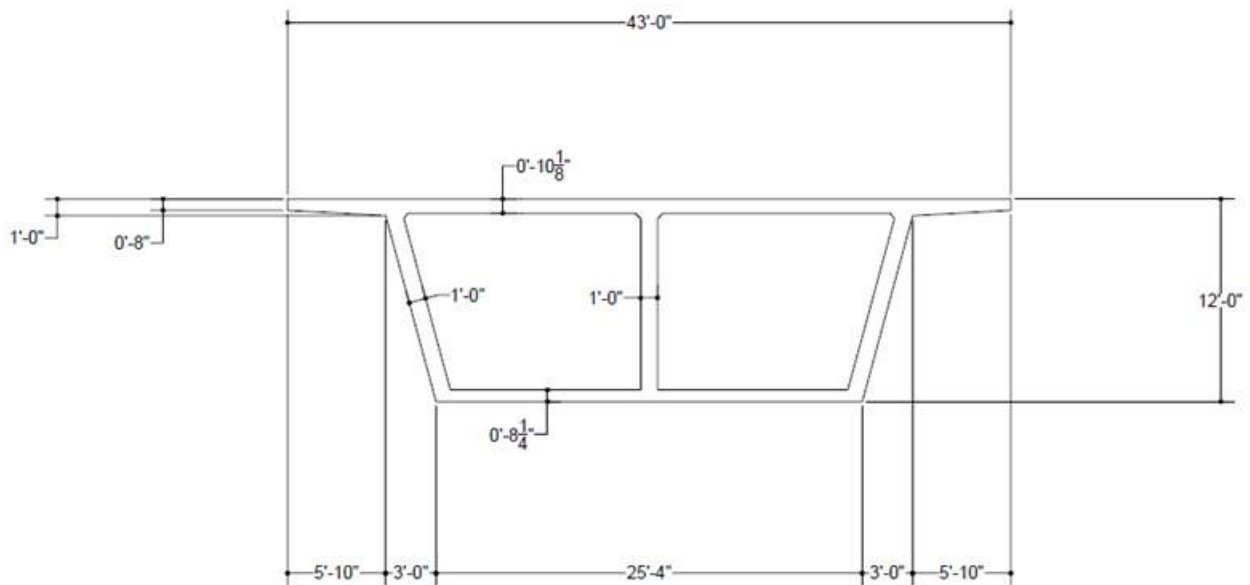


Figure 317. Illustration. Typical section, Section X-X (Nutt et al., 2008).

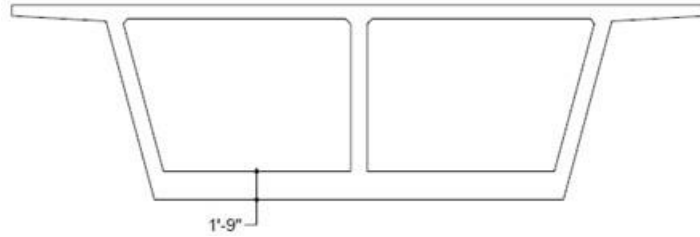


Figure 318. Illustration. Pier section, Section Y-Y (Nutt et al., 2008).

Table 65. Spine beam section properties.

	Section X-X (typical)	Section Y-Y (at piers)
A (ft ²)	85.87	110.23
I _x (ft ⁴)	1866.68	2539.10
I _y (ft ⁴)	10557.20	11769.80
J (ft ⁴)	4027.39	4841.01
A _{sx} (ft ²)	53.58	80.49
A _{sy} (ft ²)	36.88	36.88
Offset (ft)	0.00	1.312

The piers consist of 6 ft-0 inch x 18 ft-0 inch rectangular columns. The section properties of the piers are shown in Table 66.

Table 66. Column section properties.

	Pier
A (ft ²)	108.00
I _x (ft ⁴)	324.00
I _y (ft ⁴)	2916.00
J (ft ⁴)	1024.12
A _{sx} (ft ²)	90.00
A _{sy} (ft ²)	90.00

The loads considered in this analysis consist of dead and live loads only. Dead loads include self-weight of the members, a 3 inch 140 pcf overlay and concrete barriers. The barriers are assumed to weigh 0.5 k/ft. HL93 loading is considered for live load; a utility within the analysis program is used to automatically generate live load truck and lane configurations for one lane, then a distribution factor is used to determine the full live load effects.

The live load distribution factor (LLDF) is calculated in accordance with AASHTO 4.6.2.2.1, including multiple presence:

$$\text{LLDF} = (3 \text{ lanes})(0.85) = 2.55 \text{ lanes}$$

The shear, moment, and torsion results from the analyses are shown in Figures 319 through 321.

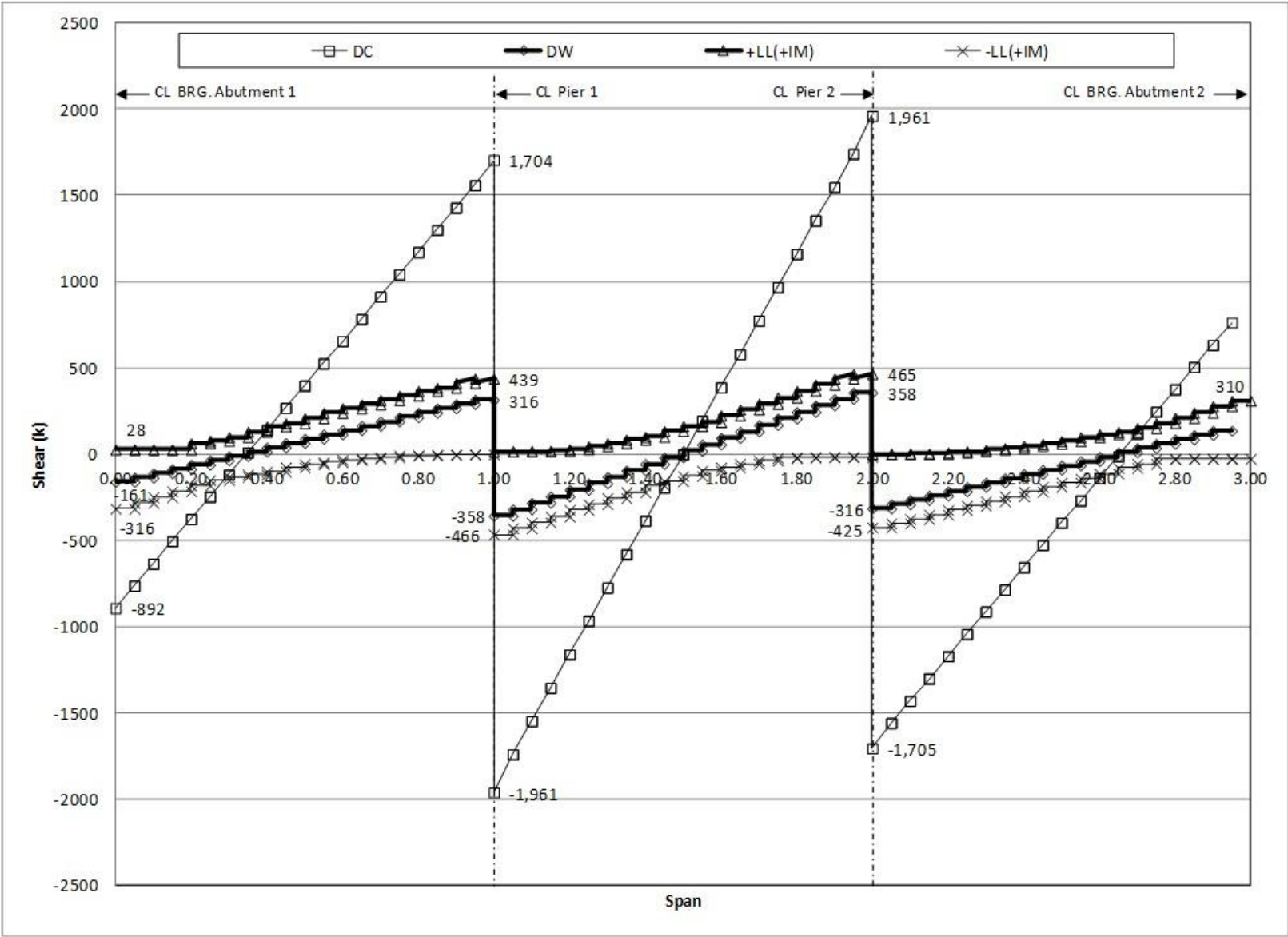


Figure 319. Graph. Spine beam shear.

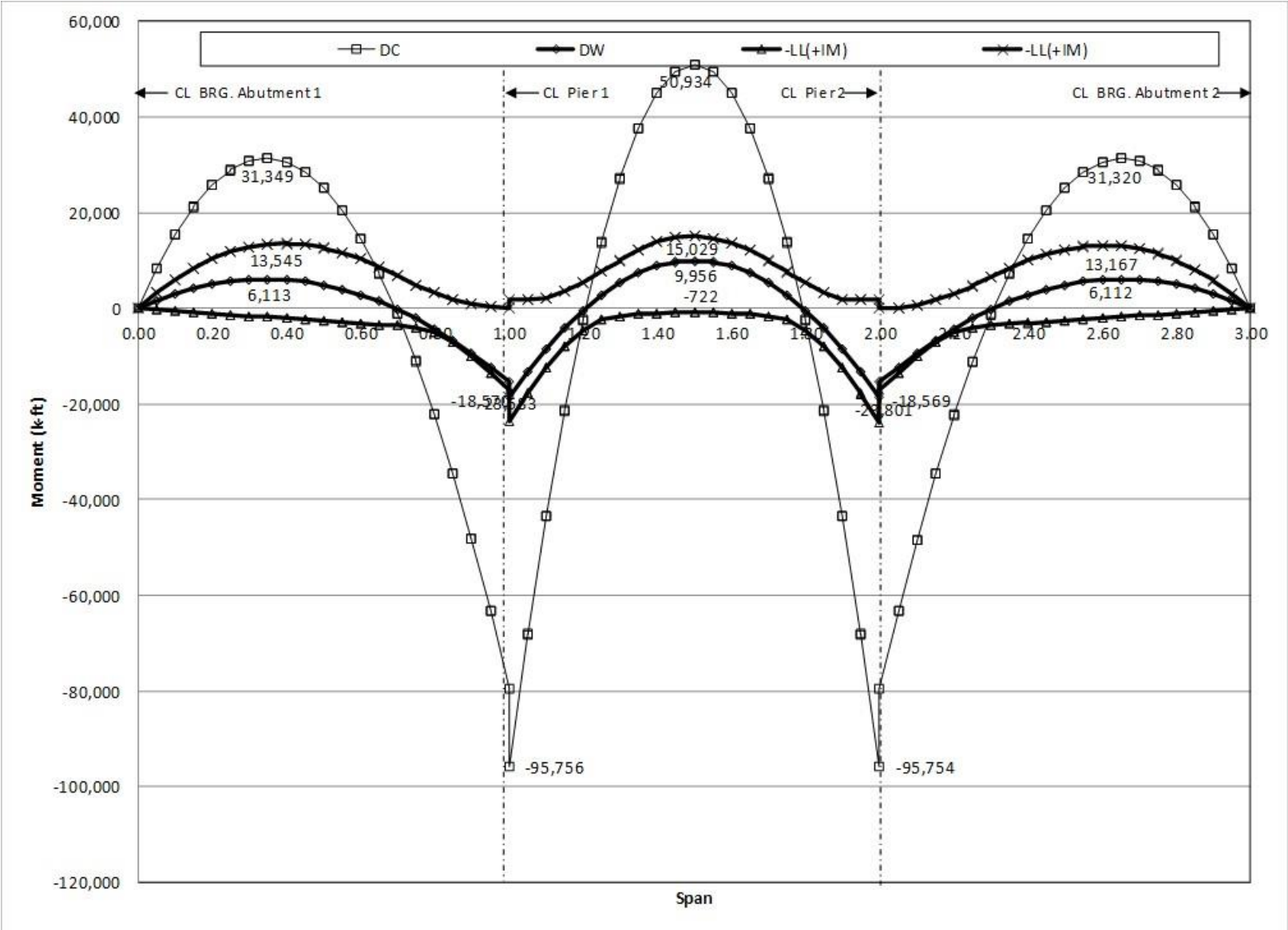


Figure 320. Graph. Spine beam moment.

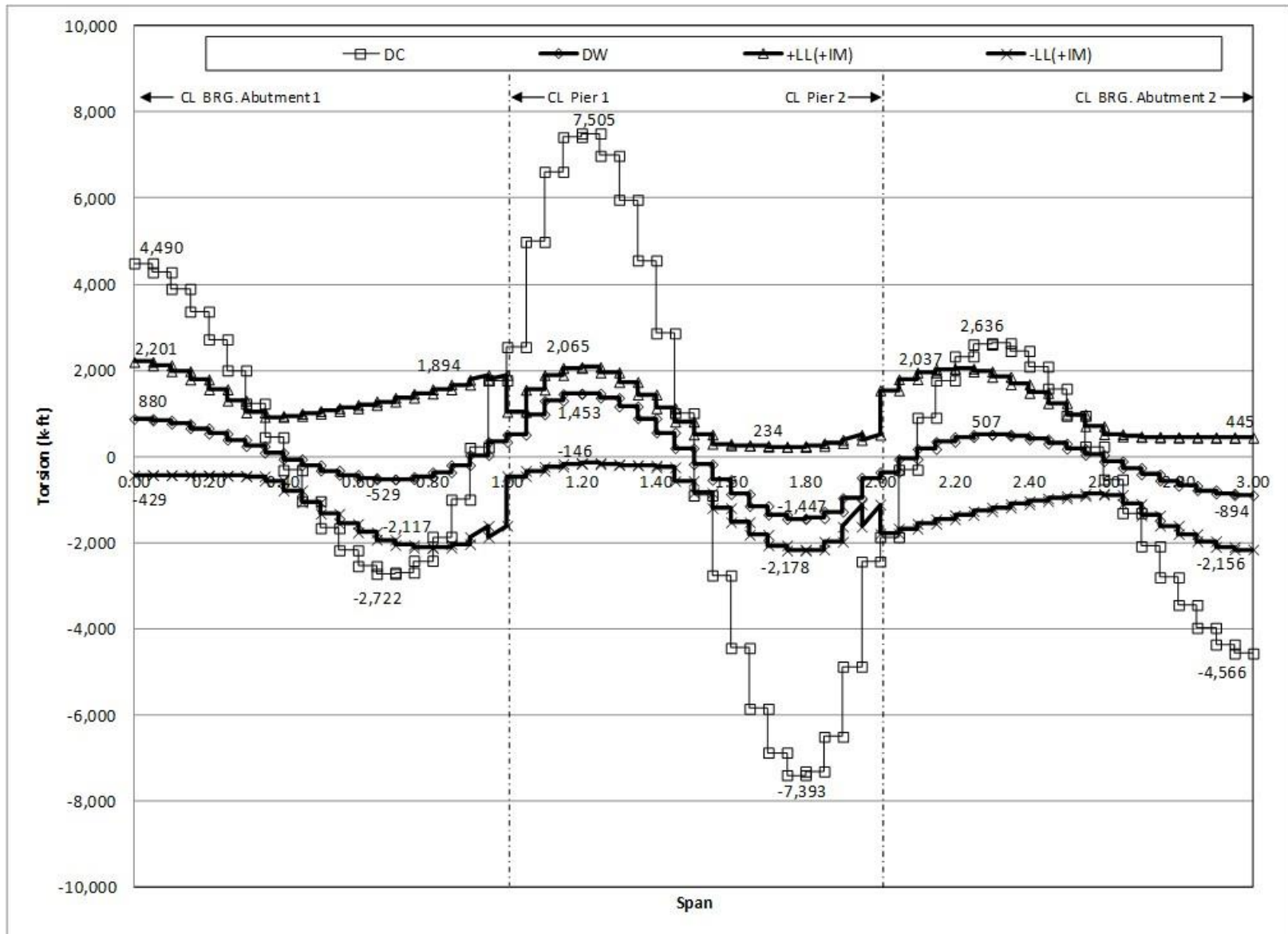


Figure 321. Graph. Spine beam torsion.

9.5 Example 5 – Dynamic analysis of a curved steel girder bridge

Example 5 involves a dynamic analysis of the curved steel girder bridge from Example 3. The framing plan, bridge cross-section, and girder details are the same as previously presented in Figures 230 through 235. The spans are supported by skewed concrete piers, while the ends are supported on concrete stub abutments. The piers consist of three columns that are integral with the bent cap as shown in Figure 322. The bent columns are 5 ft – 0 inches in diameter with a 1.5 percent reinforcing ratio and are 37 ft – 0 inches tall. The bent caps are 7 ft – 0 inches wide, 5 ft – 0 inches deep, and 74 ft – 0 inches long.

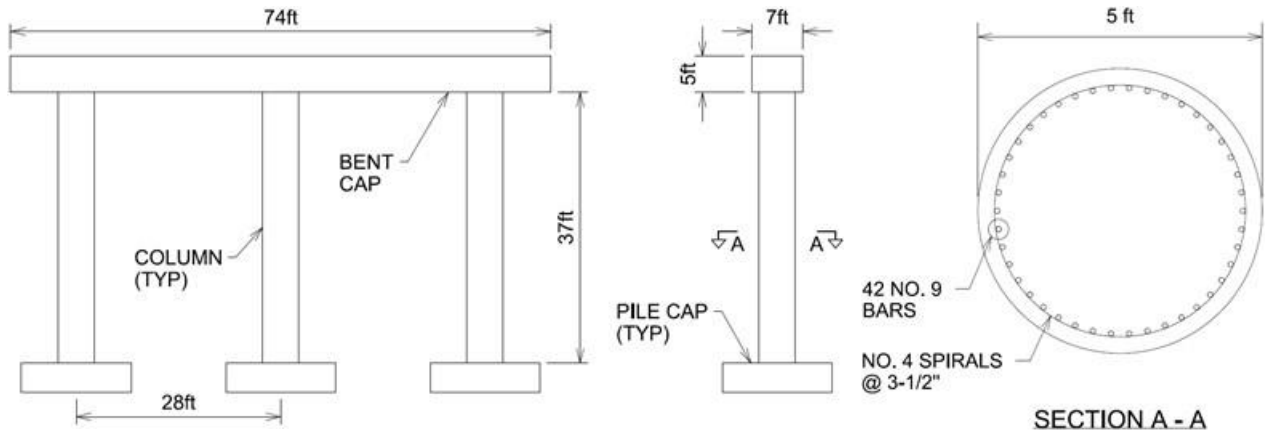


Figure 322. Illustration. Pier details.

The bridge is supported on pile foundations consisting of steel HP12x53 piles that are 40 ft – 0 inches long in a 3x3 pattern under the bent columns and a 2x9 pattern under the abutments, as detailed in Figure 323. The pile caps are 11 ft – 0 inches square and 5 ft – 0 inches in depth. The piles are embedded 1 ft – 0 inches into the pile caps and abutments. The abutments are 51 ft – 0 inches long with cross-section dimensions given in Figure 323. The assumed soil profile consists of a dense sand, with properties as given in Table 67. The soil properties were chosen such that the bridge would be assigned to a seismic zone that requires a multi-mode analysis.

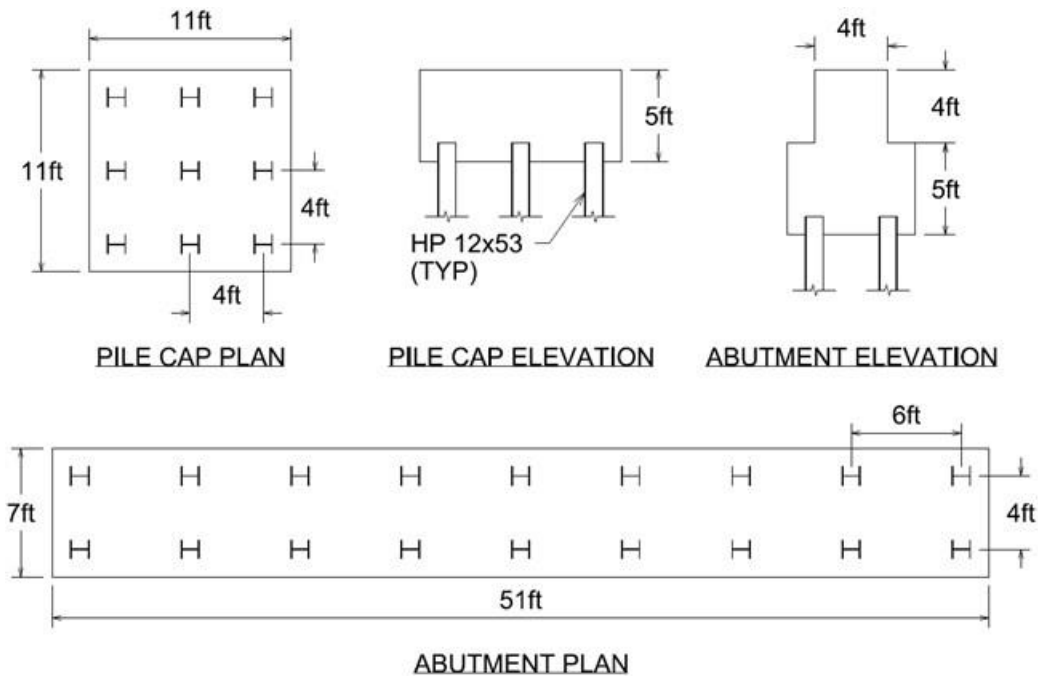


Figure 323. Illustration. Foundation details.

Table 67. Soil properties.

Soil Property	Symbol	Units	Value
Unit Weight	γ	lb/ft ³	130
Internal Friction Angle	ϕ	Degrees	39
Poisson's Ratio	ν	-	0.35
Corrected SPT Blow Count	N ₆₀	-	55

All substructure and foundation concrete is normal weight with a compressive strength of 5000 psi and all steel reinforcement is AASHTO M31 Grade 60. All steel piles are ASTM A572 Grade 60.

9.5.1 Methodology

The focus of Example 5 is the dynamic behavior of the bridge under seismic loading. The plate on eccentric beam (PEB) model from Example 3 is used as a starting point for modeling. The model is expanded to include the concrete substructure, which is modeled using beam elements. The soil-structure interaction behavior is calculated outside of the finite element program using a separate foundation analysis program that allows for the stiffness of the foundations to be determined. The foundation stiffness is then incorporated back into the finite element program at the footings and abutments.

The dynamic deflections of the superstructure are computed via an elastic multi-mode response spectra analysis and compared to allowable specification values. In addition, a pushover analysis is performed to determine the displacement capacities of the piers, in which plastic hinges form at the top and bottom of the bent columns. The calculated displacement capacities are compared

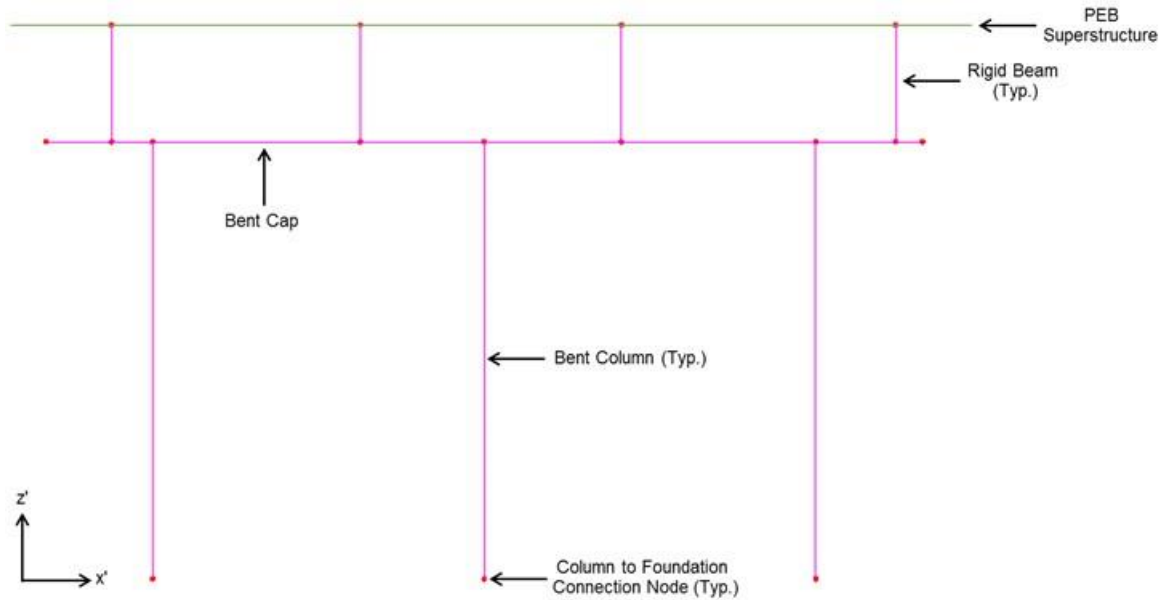
to the dynamic deflection values from the multi-mode response spectra analysis to assess the adequacy of the columns.

9.5.2 Step 1 – Model for Dynamic Analysis

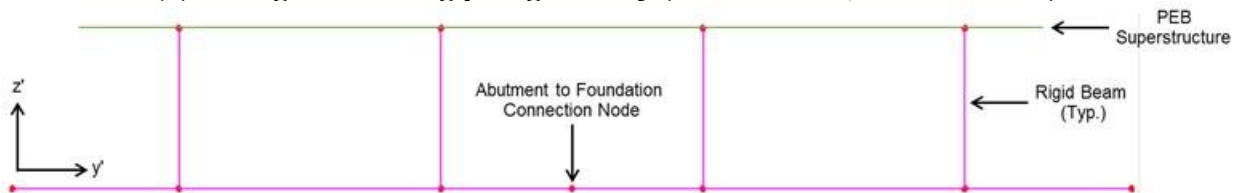
See Example 3 for guidance on the creation of the PEB model. Example 5 focuses on the modeling of the substructure, foundations, and connection of the superstructure to substructure. In order to correctly perform a dynamic analysis, all sources of mass must be included. Therefore, if any components were represented as applied loads in the original PEB model (e.g., barrier, future wearing surface), the model should be modified such that these sources of mass are accounted for. In this example, the barrier weight, which was modeled as an applied load in Example 3, is modeled by assigning the geometric and material properties of the barrier to the beam elements along the edge of the deck.

9.5.2.1 Step 1a - Model Geometry and Mesh

The piers and abutments need to be added to the previously created PEB model of the superstructure. The piers are defined according to the geometry shown in Figure 324. The skew angles of the piers are given in Figure 230. The piers are offset vertically from the PEB portion of the model such that the superstructure and pier members are at their correct locations vertically relative to one another. Beam elements with geometric non-linear capabilities are used for the bent caps and bent columns. Mesh densities are assigned such that there are 8 elements per line segment for the bent caps and 37 elements per line segment for the bent columns (i.e., 1 ft-0 inch element length). Nodes are defined along the length of the bent cap at locations corresponding to the locations of the bearings. Rigid beam elements are used to connect the girders to the bent caps at the location of bearing. A similar procedure is used to model the abutments. The pier and abutment geometries are shown in Figure 324.



(a) Subfigure showing pier geometry (Pier 1 shown, Pier 2 similar).



(b) Subfigure showing abutment geometry (Abutment 1 shown, Abutment 2 similar)

Figure 324. Illustrations. Compound figure showing substructure geometry.

9.5.2.2 Step 1b – Cross Section Properties

The member section properties can be calculated by hand and input into the analysis software or defined using utilities within the analysis program, if available. Using the dimensions provided in Figure 322, the section properties listed in Table 68 are calculated and input for the substructure members within the model.

For the reinforced concrete bent columns, effective section properties are used to reflect the degree of cracking within the member prior to reaching the idealized yield limit state (AASHTO 2011). The *AASHTO Guide Specifications for LRFD Seismic Bridge Design* (herein AASHTO Guide Specifications) require effective flexural and torsional moments of inertia, I_{eff} and J_{eff} respectively, to be used when performing a multi-mode spectra analysis. I_{eff} is determined in accordance with Article 5.6.2 of the AASHTO Guide Specifications using either a moment-curvature relationship or a nomograph approach; the nomograph approach was chosen for this example. For reference, the appropriate nomograph for circular sections is shown in Figure 325. The nomograph uses the axial load ratio and the reinforcement ratio of a column to determine the elastic stiffness ratio, I_{eff}/I_g , and subsequently the effective moment of inertia, I_{eff} . J_{eff} is calculated according to Section 5.6.5 of the AASHTO Guide Specifications.

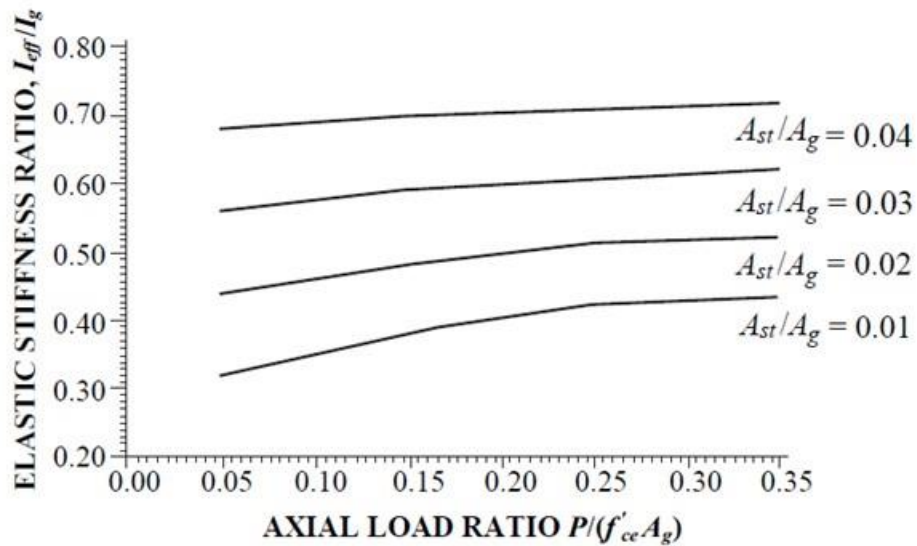


Figure 325. Chart. Effective flexural stiffness of cracked reinforced concrete circular sections (AASHTO Guide Specifications for LRFD Seismic Design, 2011).

Table 68. Substructure section properties.

Section Property	Units	Bent Cap	Bent Column (Effective)	Abutment
Cross-section Area (A)	ft ²	35.0	19.63	51.0
Strong Axis Moment of Inertia (I _{yy})	ft ⁴	72.92	11.91	316.60
Weak Axis Moment of Inertia (I _{zz})	ft ⁴	142.92	11.91	164.25
Torsion Constant (J _{xx})	ft ⁴	163.54	12.27	293.16
Shear Area in y Direction (A _{vy})	ft ²	29.17	16.82	38.95
Shear Area in z Direction (A _{vz})	ft ²	29.17	16.82	38.38
Offset in y Direction (e _y)	ft	0.0	0.0	0.0
Offset in z Direction (e _z)	ft	0.0	0.0	0.0

9.5.2.3 Step 1c – Material Properties

The material properties can be selected from the software’s library, if available, or input manually by the user. Along with the section properties, material properties may be adjusted to provide effective properties to members in the model. The material properties for the piers and abutments are shown in Table 69. The properties for the bent caps, columns, pile caps, and abutments are based on a specified 28-day compressive strength of 5000 psi. For the abutments, the Young’s modulus used in the finite element model should be chosen such that the abutments are made to be sufficiently rigid. This is done because the abutment stiffness is accounted for outside of the finite element model using a foundation analysis program.

The focus of this example is the dynamic deflection of the superstructure and piers. Within the finite element model, the abutment members are used solely to facilitate the connection between the superstructure and the foundation. The abutment is a very stiff member and, therefore, should not affect the behavior of the superstructure and piers. If the focus was on the pile behavior, then the stiffness of the abutment would be important. The unit weight of the abutment

concrete is set to zero such that the mass participation of the abutments is not included in the dynamic analysis.

Table 69. Concrete material properties.

Material Property	Units	Bents	Abutments
Modulus of Elasticity	ksf	586,697	586,697
Poisson's Ratio	-	0.2	0.2
Unit Weight	k/ft ³	0.150	0.0
Thermal Expansion Coefficient	ft/ft/°F	6E-6	6E-6

9.5.2.4 Step 1d – Boundary Conditions

The girder support conditions are the same as previously defined in Example 3. However, the addition of the substructure causes the method in which the support conditions are defined to change, depending on software. For the particular software used, the girder support conditions are defined using joint elements with specified spring stiffness for each degree of freedom, as recommended in Section 3.7.3. Restrained degrees of freedom are accounted for by assigning a large spring stiffness (e.g., 1E9). The joint elements are located at the end of each rigid beam that connects the girder to the bent cap to replicate the bearings on the girder end of the rigid beam. The bearings are oriented tangent to the girder lines at the bents; therefore, the joint elements should have the same orientation.

Boundary conditions are also defined at the base of the bent columns and at the abutments using restraints. Initially, all degrees of freedom are fully restrained. The support conditions will be changed at a later step to accommodate variations in support stiffness due to soil-structure interaction behavior. Therefore, the type of restraint chosen needs to be able to accommodate different spring stiffness values for each degree of freedom. The process for varying the support stiffness to account for soil-structure interaction is discussed in Step 1g.

9.5.2.5 Step 1e – Natural Frequency Analysis

An eigenvalue analysis is performed assuming an undamped unforced system to determine the natural frequencies and corresponding mode shapes of the bridge. The complete response of the structure is determined by combining the results of each mode shape. The response from all mode shapes do not need to be subsequently used in the response spectra analysis. The number of modes to consider is based on the total percent of mass participation in each direction, which should be greater than 90 percent. In addition, AASHTO LRFD 4.7.4.3.3 requires the number of modes included in a multi-mode spectral analysis to be at least three times the number of spans in the model. Refer to Section 5.4.2.2 for guidance on the solution to a natural frequency analysis.

For the initial analysis, the number of eigenvalues to consider is set to 20, and is adjusted as needed. The results of the final iteration of the natural frequency analysis are shown later in Step 1g, due to the iterative procedure associated with the soil-structure interaction.

9.5.2.6 Step 1f – Response Spectrum Analysis

The design response spectrum represents the relationship between acceleration and period and is the primary input to a response spectrum analysis. The design response spectrum is constructed according to AASHTO LRFD 3.10.4.1 and 3.10.4.2 and is shown below in Figure 326. Refer to Section 5.4.3.1 for guidance on response spectrum construction.

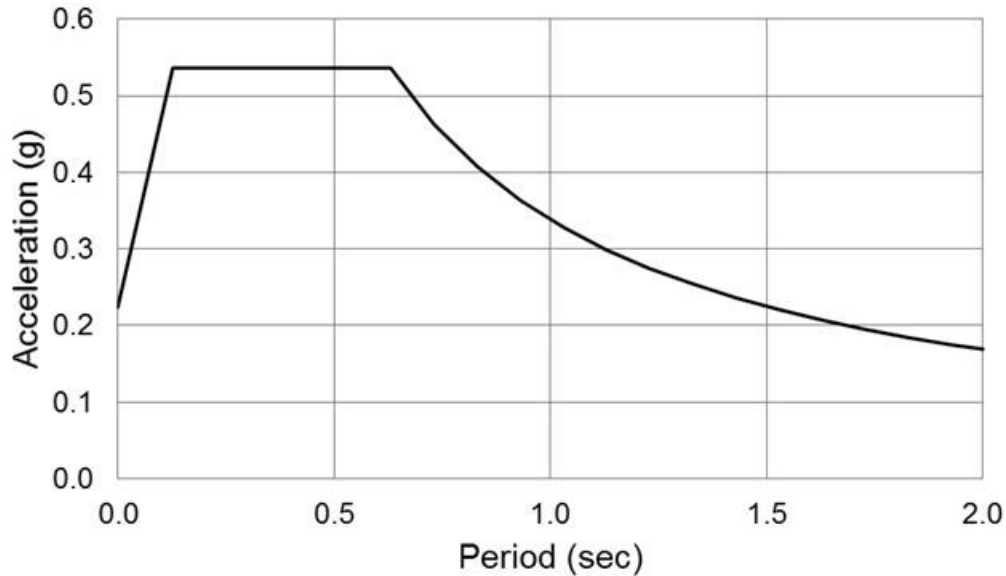


Figure 326. Graph. Design response spectrum.

The analysis method to be used for the seismic analysis is determined by the operational classification of the bridge and the Seismic Zone. The operational classification categories are defined in AASHTO LRFD 3.10.5 and are analogous to the importance of the bridge. For the purposes of this example, the bridge is classified as essential. The bridge is categorized in Seismic Zone 3 per AASHTO LRFD 3.10.6. The Seismic Zone in AASHTO LRFD is equivalent to the Seismic Design Category in the AASHTO Guide Specifications. Using the operational classification and seismic zone, the analysis method is determined in AASHTO LRFD 4.7.4.3 for multi-span bridges. The bridge is considered to be irregular based on the requirements of AASHTO LRFD 4.7.4.3.1. Therefore, using Table 4.7.4.3.1-1 for an essential irregular bridge in Seismic Zone 3, a multimode spectral analysis is required at minimum. AASHTO LRFD 4.7.4.3.3 outlines the procedure for performing a multimode spectral analysis, and includes the use of the previously constructed design response spectrum from Figure 326. In addition, the total seismic response is determined by combining the response quantities from individual modes using the Complete Quadratic Combination (CQC) method. The minimum number of modes to include in the total response is determined as described above in Step 1e.

The multimode response spectrum analysis is performed for this example by first incorporating the response spectrum from Figure 326 as the earthquake excitation in the finite element program. For the analysis program used for this example, the response spectrum is input in terms of acceleration versus period. Seismic excitation is assumed to act in the direction of each of the orthogonal axes of the bridge (i.e., transverse and longitudinal) in accordance with AASHTO LRFD 3.10.7.2; therefore, two seismic load cases are defined within the program: one for the transverse direction and one for the longitudinal direction. For a curved bridge, the

longitudinal axis can be taken as the chord between centerlines of abutments per AASHTO LRFD C3.10.7.2. For each load case, the support motion excitation is input as an acceleration defined by the previously input response spectrum. The direction of support excitation for the two load cases is input using a user defined vector that transforms the excitation direction from the global axes to the local axis of interest (transverse or longitudinal). The results requested from the analysis are the spectral results, and the modal responses are combined using the CQC method. No damping is defined within the load case because damping is already accounted for in the response spectrum. The number of modes included in the total response combination is selected such that 90 percent of the mass participates in each direction as shown in Step 1h below.

9.5.2.7 Step 1g – Soil Structure Interaction

The effects of soil-structure interaction (SSI) are included in the analysis using the substructure-iterative method as discussed in Section 5.2.2. In this method, the stiffness of the foundation members (e.g., piles and pile cap) and surrounding soil is represented by a stiffness matrix at the base of each substructure member (i.e., columns and abutments) within the finite element model. A separate foundation analysis program is used to model the foundation members and soil. Reactions from the finite element model along the local axes of the bent are input into the foundation program. The foundation is then analyzed for the displacements and rotations at a node of interest. Because the stiffness of the foundation depends on the magnitude of the loadings (i.e., nonlinear behavior), an iterative approach is required. A stiffness matrix is generated for each foundation by dividing the applied force by the associated displacement or rotation at the node of interest. The node at which the stiffness matrix is generated should match the foundation support location within the finite element model (e.g., base of the column/top of the pile cap). The stiffness matrix is then assigned to the appropriate support node from Step 1d within the finite element model and the structural analysis is re-run. A number of iterations are performed with updated loads and stiffness matrices until the results converge. Detailed guidance on soil-structure interaction is included in Section 5.2.

For this example, two separate models are created using the foundation program: one for the pier foundations and one for the abutment foundations. The models are defined using the details from Figure 323 and the soil properties from Table 67. Load cases are created for each direction of earthquake excitation (transverse and longitudinal) to match the finite element analysis results. In addition, load cases are created for each foundation location since the loads on each pier and abutment are different. Therefore, twelve load cases are needed for the pier foundation model (six columns with two load directions each) and four load cases are needed for the abutment foundation model (two abutments with two load directions each). The stiffness of the abutment backwall is ignored in this example. This stiffness is mobilized when the superstructure displaces enough to engage the soil behind the backwall. It is conservative to ignore the backwall stiffness when checking the adequacy of the bents, which is the main focus of this example.

The diagonal terms of the stiffness matrix are determined by dividing the applied force by the calculated displacement or rotation from the foundation analysis software at the node of interest. For this example, the off-diagonal terms, which account for cross-coupling of the degrees of freedom, were neglected. If the off-diagonal terms significantly influence behavior, such as

when battered piles are used, cross-coupling should be included. The naming convention of the abutments and columns is shown in Figure 327 with the corresponding diagonal terms of the stiffness matrices for the final iteration included in Table 70. For this example, iterations were performed until the change in stiffness at each degree of freedom was less than 10 percent between two consecutive iterations. However, this should not be considered a rule of thumb. The level of refinement required will vary on a case-by-case basis. Degrees of freedom 1 through 3 are the translations in the local x' , y' , and z' directions respectively, while degrees of freedom 4 through 6 are the rotations about the local x' , y' , and z' directions respectively. The pier and abutment local coordinates are included in Figure 324.

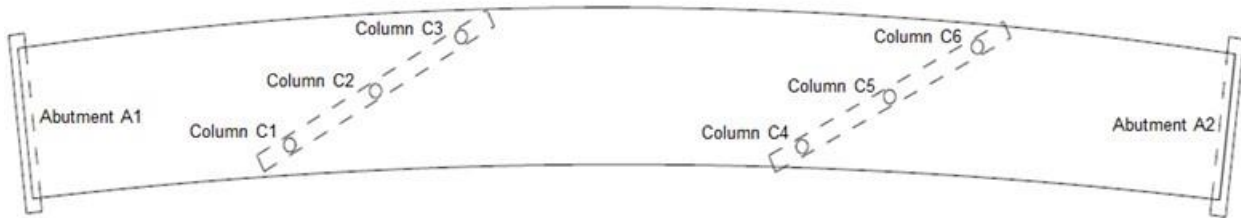


Figure 327. Illustration. Support member naming convention.

Table 70. Support stiffness matrices for final SSI iteration.

K	Units	A1	C1	C2	C3	C4	C5	C6	A2
Transverse Seismic Load									
K_{11}	k/ft	0	7.259E4	7.057E4	6.023E4	8.510E4	9.986E4	9.292E4	4.033E4
K_{22}	k/ft	9.527E4	7.624E3	7.596E3	7.451E3	8.501E3	8.606E3	7.860E3	9.802E4
K_{33}	k/ft	6.111E4	3.390E4	2.252E4	3.540E4	4.522E4	2.843E4	5.034E4	5.814E4
K_{44}	k-ft/rad	4.936E6	7.055E5	6.856E5	6.652E5	6.447E5	6.767E5	6.854E5	4.939E6
K_{55}	k-ft/rad	0	8.638E5	8.428E5	8.113E5	8.654E5	9.051E5	9.110E5	2.910E5
K_{66}	k-ft/rad	0	6.814E5	6.849E5	6.898E5	6.131E5	6.487E5	6.953E5	7.443E6
Longitudinal Seismic Load									
K_{11}	k/ft	0	1.201E5	1.336E5	1.121E5	4.693E4	6.122E4	4.568E4	5.049E4
K_{22}	k/ft	1.020E5	1.125E4	1.134E4	1.115E4	5.183E3	5.574E3	5.237E3	1.015E5
K_{33}	k/ft	3.144E4	4.957E4	2.861E4	5.568E4	3.565E4	2.041E4	3.521E4	4.868E4
K_{44}	k-ft/rad	4.963E6	7.992E5	8.106E5	7.833E5	4.485E5	4.772E5	4.433E5	4.965E6
K_{55}	k-ft/rad	0	1.026E6	1.037E6	1.008E6	6.636E5	7.235E5	6.556E5	3.204E5
K_{66}	k-ft/rad	0	8.536E5	8.390E5	8.436E5	5.640E5	5.972E5	5.583E5	7.269E6

A sample calculation of the substructure-iterative method is shown below to demonstrate how the stiffness matrix is generated for each foundation. The foundation supporting Column C1 is used for the calculation, subject to the transverse seismic load case. From the results of the initial seismic analysis using the model with fixed column support conditions, the reactions at the base of Column C1 are as follows (subscript values indicate degree of freedom numbering).

$$\begin{aligned}
 F_1 &= 57 \text{ kips} \\
 F_2 &= 103 \text{ kips} \\
 F_3 &= 104 \text{ kips} \\
 M_4 &= 3909 \text{ k-ft} \\
 M_5 &= 1065 \text{ k-ft} \\
 M_6 &= 46 \text{ k-ft}
 \end{aligned}$$

These reactions are input into the foundation analysis program at the node corresponding to the connection of the pile cap to the column. Analyzing the foundation for the applied loads given above, results in the following displacements and rotations at the node of interest.

$$\begin{aligned}\Delta_1 &= 0.0016 \text{ ft} \\ \Delta_2 &= 0.0168 \text{ ft} \\ \Delta_3 &= 0.0038 \text{ ft} \\ \theta_4 &= 0.0064 \text{ rad} \\ \theta_5 &= 0.0015 \text{ rad} \\ \theta_6 &= 0.0001 \text{ rad}\end{aligned}$$

The stiffness matrix is then calculated by dividing the reactions by the corresponding displacement or rotation.

$$[K] = \begin{bmatrix} \frac{F_1}{\Delta_1} & 0 & 0 & 0 & 0 & 0 \\ 0 & \frac{F_2}{\Delta_2} & 0 & 0 & 0 & 0 \\ 0 & 0 & \frac{F_3}{\Delta_3} & 0 & 0 & 0 \\ 0 & 0 & 0 & \frac{M_4}{\theta_4} & 0 & 0 \\ 0 & 0 & 0 & 0 & \frac{M_5}{\theta_5} & 0 \\ 0 & 0 & 0 & 0 & 0 & \frac{M_6}{\theta_6} \end{bmatrix}$$

$$[K] = \begin{bmatrix} \frac{57 \text{ kips}}{0.0016 \text{ ft}} & 0 & 0 & 0 & 0 & 0 \\ 0 & \frac{103 \text{ kips}}{0.0168 \text{ ft}} & 0 & 0 & 0 & 0 \\ 0 & 0 & \frac{104 \text{ kips}}{0.0038 \text{ ft}} & 0 & 0 & 0 \\ 0 & 0 & 0 & \frac{3909 \text{ k-ft}}{0.0064 \text{ rad}} & 0 & 0 \\ 0 & 0 & 0 & 0 & \frac{1065 \text{ k-ft}}{0.0015 \text{ rad}} & 0 \\ 0 & 0 & 0 & 0 & 0 & \frac{46 \text{ k-ft}}{0.0001 \text{ rad}} \end{bmatrix}$$

$$[K] = \begin{bmatrix} 34.8 & 0 & 0 & 0 & 0 & 0 \\ 0 & 6.12 & 0 & 0 & 0 & 0 \\ 0 & 0 & 27.7 & 0 & 0 & 0 \\ 0 & 0 & 0 & 608 & 0 & 0 \\ 0 & 0 & 0 & 0 & 718 & 0 \\ 0 & 0 & 0 & 0 & 0 & 656 \end{bmatrix} \times 10^3 \begin{bmatrix} \text{k/ft} \\ \text{k/ft} \\ \text{k/ft} \\ \text{k-ft/rad} \\ \text{k-ft/rad} \\ \text{k-ft/rad} \end{bmatrix}$$

The structural analysis is then repeated using the updated Column C1 support stiffness calculated above. Updated support reactions are determined and a new iteration is performed until the convergence criteria is met. An identical procedure is performed for the other columns and for the longitudinal seismic load case.

9.5.2.8 Step 1h – Run Analysis

Once the SSI convergence criteria is met, the final eigenvalue analysis and response spectrum analysis are performed. The results of the final iteration of the eigenvalue analysis are shown in Table 71, and include the frequency, period, and mass participation associated with each mode. As shown for both seismic load cases (transverse and longitudinal), the total mass participation percentage exceeds 90 percent at Mode 14. Therefore, the first 14 modes are selected to be included in the response spectrum results combination.

There are two sets of modes and associated frequencies included in Table 71 due to the SSI analysis. The SSI analysis requires the foundation stiffness to be calculated for seismic loads applied in both the transverse and longitudinal directions. The calculated stiffness for each direction of loading is slightly different, resulting in the two sets of natural frequencies.

Table 71. Natural frequency analysis results.

Mode No.	Frequency (Hz)	Period (sec)	Σ Mass Participation, Transverse (%)	Σ Mass Participation, Longitudinal (%)
Transverse Seismic Load				
1	0.55	1.83	28.0	56.1
2	0.81	1.23	85.1	78.5
3	1.24	0.81	85.5	78.8
4	1.82	0.55	85.8	80.4
5	1.86	0.54	85.8	91.3
6	2.06	0.49	85.8	93.4
7	2.31	0.43	86.5	94.1
8	2.37	0.42	86.6	94.1
9	2.76	0.36	86.7	94.1
10	2.83	0.35	86.7	94.2
11	3.29	0.30	86.7	94.2
12	3.91	0.26	87.4	94.9
13	4.20	0.24	87.5	95.4
14	4.39	0.23	93.7	96.1
15	4.84	0.21	93.9	96.1
16	5.19	0.19	93.9	96.1
17	5.65	0.18	94.1	96.2
18	6.04	0.17	94.2	96.3
19	6.66	0.15	94.3	96.5
20	7.24	0.14	94.3	96.5

Table 71 (continued). Natural frequency analysis results.

Mode No.	Frequency (Hz)	Period (sec)	ΣMass Participation, Transverse (%)	ΣMass Participation, Longitudinal (%)
Longitudinal Seismic Load				
1	0.52	1.93	26.8	57.1
2	0.81	1.24	85.0	78.8
3	1.23	0.81	85.5	79.1
4	1.82	0.55	85.7	80.4
5	1.91	0.52	85.8	90.1
6	2.07	0.48	85.8	93.8
7	2.31	0.43	86.3	94.2
8	2.37	0.42	86.7	94.2
9	2.78	0.36	86.7	94.3
10	2.84	0.35	86.7	94.3
11	3.31	0.30	86.7	94.3
12	3.86	0.26	87.4	94.6
13	4.23	0.24	87.8	95.5
14	4.41	0.23	93.6	96.1
15	4.83	0.21	93.9	96.1
16	5.28	0.19	93.9	96.2
17	5.63	0.18	94.1	96.3
18	5.98	0.17	94.3	96.3
19	6.69	0.15	94.3	96.5
20	7.00	0.14	94.5	96.6

9.5.2.9 Step 1i – P-Δ Check

The capacity of each bent column, in terms of displacement, is checked according to specification requirements. AASHTO LRFD 4.7.4.5 requires that the displacement of any column satisfy Equation (53).

$$\Delta P_u \leq 0.25\phi M_n \quad (53)$$

where Δ is the displacement of the point of contraflexure of the column relative to the foundation point of fixity, P_u is the factored axial load on the column, ϕ is the flexural resistance factor, and M_n is the nominal flexural strength of the column. Δ is defined in AASHTO LRFD 4.7.4.5 and is a function of the displacement of the point of contraflexure from the elastic seismic analysis, Δ_e . P_u is a combination of the axial dead load, live load, and seismic load on the column. The dead load and live load are taken from the results of Example 3 while the seismic load is taken from the results of the response spectrum analysis. Values of P_u for each column are listed in Table 72.

Table 72. Factored axial load on columns.

Column No.	C1	C2	C3	C4	C5	C6
P_u (kips)	1477	1397	1785	2161	1343	2003

The nominal moment capacity, M_n , is determined by developing an interaction diagram for the axial load and bending moment. Development of the interaction diagram is not included in this example but guidance can be found in text books on reinforced concrete (e.g, Wight and MacGregor 2012). The interaction diagram for the bent columns is shown in Figure 328.

The elastic seismic displacement of the point of contraflexure, Δ_e , is summarized in Table 73, and includes the combination provisions of AASHTO LRFD 3.10.8. The point of contraflexure can be determined from the results of the response spectrum analysis and the associated displacement can be calculated. Care should be taken to ensure that the displacements are in the local coordinates of the pier. A sample calculation for the P- Δ check from Equation (53) is shown below for Column C1. The procedure is similar for the other columns.

Table 73. Elastic seismic displacement demands on columns.

Column No.	Δ_e transverse (in)	Δ_e longitudinal (in)
1	1.65	3.65
2	1.71	3.84
3	1.75	3.97
4	2.48	5.87
5	2.47	5.84
6	2.49	5.81

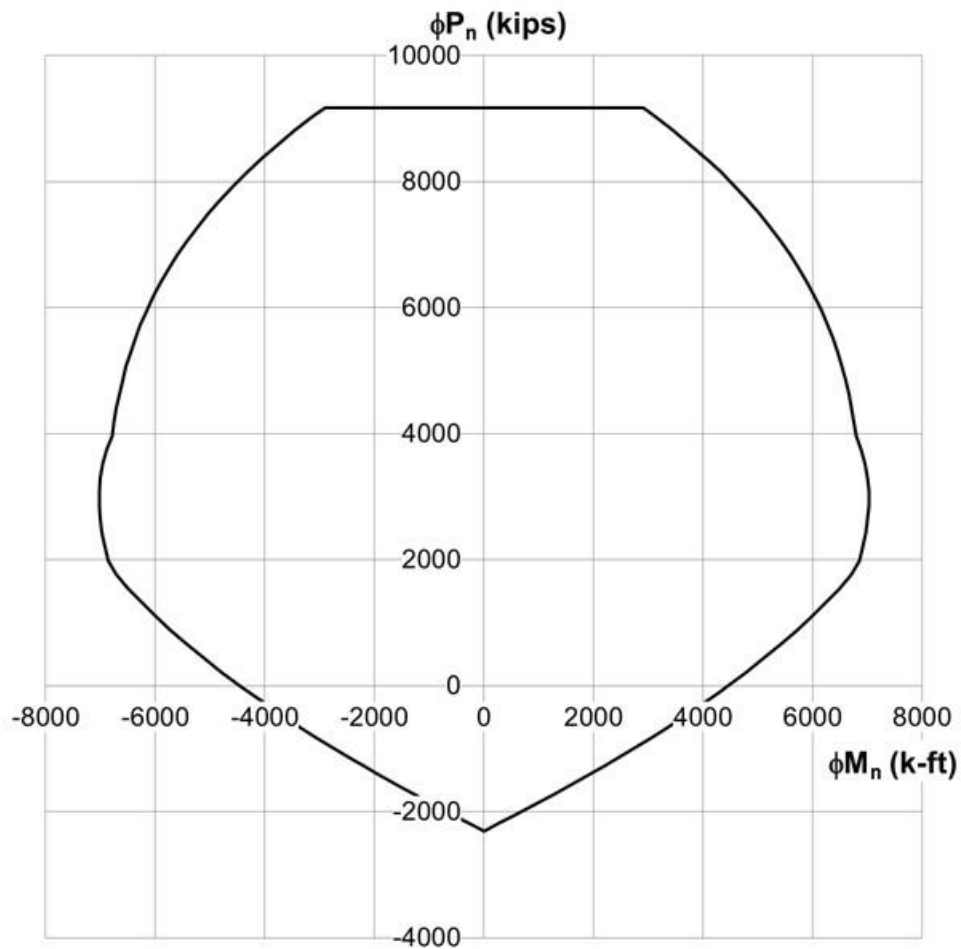


Figure 328. Graph. Bent column interaction diagram.

From Table 72 and Figure 328, P_u and ϕM_n for Column C1 are taken as

$$P_u = 1477 \text{ kips}$$

$$\phi M_n = 6361 \text{ k-ft}$$

The displacement Δ is then calculated according to AASHTO LRFD 4.7.4.5, using Δ_e from Table 73 and factored by R_d , which accounts for inelastic action.

$$\begin{aligned} \Delta_{e \text{ transverse}} &= 1.65 \text{ inches} \\ \Delta_{e \text{ longitudinal}} &= 3.65 \text{ inches} \end{aligned}$$

$$T_s = 0.63 \text{ sec}$$

$$\begin{aligned} 1.25 T_s &= 1.25(0.63 \text{ sec}) \\ &= 0.79 \text{ sec} \end{aligned}$$

$$T_{\text{transverse}} = 1.83 \text{ sec} > 1.25 T_s$$

$$T_{\text{longitudinal}} = 1.93 \text{ sec} > 1.25 T_s$$

$$R_{d \text{ transverse}} = 1.0$$

$$R_{d \text{ longitudinal}} = 1.0$$

$$\Delta_{\text{transverse}} = (1)(1.65 \text{ inches})$$

$$= 1.65 \text{ inches}$$

$$\Delta_{\text{longitudinal}} = (1)(3.65 \text{ inches})$$

$$= 3.65 \text{ inches}$$

Equation (53) is rearranged to check the adequacy of the column.

$$\Delta P_u / \phi M_n \leq 0.25$$

$$\Delta_{\text{transverse}} P_u / \phi M_n = (1.65 \text{ inches})(1477 \text{ kips}) / (6361 \text{ k-ft})$$

$$= 0.03$$

$$\leq 0.25 \quad \text{OK}$$

$$\Delta_{\text{longitudinal}} P_u / \phi M_n = (3.65 \text{ inches})(1477 \text{ kips}) / (6361 \text{ k-ft})$$

$$= 0.07$$

$$\leq 0.25 \quad \text{OK}$$

The P-Δ check for all of the columns is summarized in Table 74. As shown, all columns meet the P-Δ requirements.

Table 74. Column P-Δ check summary.

Column No.	C1	C2	C3	C4	C5	C6
$\Delta_{\text{transverse}} P_u / \phi M_n$	0.03	0.03	0.04	0.07	0.04	0.06
$\Delta_{\text{longitudinal}} P_u / \phi M_n$	0.07	0.07	0.09	0.15	0.11	0.14

9.5.3 Step 2 – Model for Pushover Analysis

A pushover analysis is a nonlinear static analysis method that is used to determine an ultimate strength and/or displacement capacity of a bridge or subcomponent of a bridge (e.g., pier). In a pushover analysis, the nonlinear behavior of the bent columns is explicitly considered in the model, including material properties and soil effects. The pier is incrementally “pushed” laterally in one of the principal axis directions (i.e., transverse or longitudinal) until a collapse mechanism forms, which defines the capacity of the structure, in terms of displacement and/or strength. The displacement capacity can be compared to the displacement demand, which is determined from the results of the response spectrum analysis.

9.5.3.1 Step 2a – Calculate Displacement Demand

The values of interest are the displacements at the tops of the bent columns (i.e., at the bent caps) from the elastic response spectrum analysis. These displacements are listed in Table 75. The

displacements are factored by a magnification factor, R_d , similar to the P- Δ check from Step 1i. The R_d factor is defined in Article 4.3.3 of the AASHTO Guide Specifications. Using the previously determined values for fundamental period, T , and corner period, T_s , from Step 1, the magnification factor can be calculated as shown below for Column 1. The displacement demands for all columns are summarized in Table 75.

Table 75. Seismic displacement demands at the top of the columns.

Column No.	$\Delta_{D \text{ transverse}}^L$ (in)	$\Delta_{D \text{ longitudinal}}^L$ (in)
1	2.49	3.65
2	2.59	3.84
3	2.67	3.97
4	4.93	5.87
5	4.93	5.84
6	4.92	5.81

$$\begin{aligned} \Delta_{e \text{ transverse}} &= 2.49 \text{ inches} \\ \Delta_{e \text{ longitudinal}} &= 3.65 \text{ inches} \end{aligned}$$

$$T_s = 0.63 \text{ sec}$$

$$\begin{aligned} 1.25 T_s &= 1.25(0.63 \text{ sec}) \\ &= 0.79 \text{ sec} \end{aligned}$$

$$\begin{aligned} T_{\text{transverse}} &= 1.83 \text{ sec} > 1.25 T_s \\ T_{\text{longitudinal}} &= 1.93 \text{ sec} > 1.25 T_s \end{aligned}$$

$$\begin{aligned} R_{d \text{ transverse}} &= 1.0 \\ R_{d \text{ longitudinal}} &= 1.0 \end{aligned}$$

$$\begin{aligned} \Delta_{\text{transverse}} &= (1)(2.49 \text{ inches}) \\ &= 2.49 \text{ inches} \end{aligned}$$

$$\begin{aligned} \Delta_{\text{longitudinal}} &= (1)(3.65 \text{ inches}) \\ &= 3.65 \text{ inches} \end{aligned}$$

9.5.3.2 Step 2b – Model Geometry and Mesh

The model from Step 1 can be copied as a starting point for the pushover analysis. The piers are the focus of the pushover analysis and, therefore, all other members can be deleted. Only the bent cap and bent columns of the piers need to be modeled. For consistency, the foundation stiffness from the final SSI iteration are used for the pushover analysis. Nodes are inserted at the expected location of plastic hinging within the bent columns. The approximate plastic hinge length, shown as Equation (54), is given in Article 4.11.6 of the AASHTO Guide Specifications as

$$L_p = 0.08L + 0.15f_{ye} d_{bl} \geq 0.3f_{ye} d_{bl} \quad (54)$$

where L is the length of the column from the point of maximum moment to the point of moment contraflexure, f_{ye} is the expected yield strength of the longitudinal column reinforcing steel bars, and d_{bl} is the nominal diameter of longitudinal column reinforcing steel bars. Using the column details provided in Figure 322 and the steel properties from Table 8.4.2-1 of the AASHTO Guide Specifications (Table 6), the plastic hinge length is calculated as shown below.

$$\begin{aligned} L &= h/2 \\ &= (37 \text{ ft } 0 \text{ inches})/2 \\ &= 222 \text{ inches} \end{aligned}$$

$$f_{ye} = 68 \text{ ksi}$$

$$d_{bl} = 1.128 \text{ inches}$$

$$\begin{aligned} L_p &= 0.08(222 \text{ inches}) + 0.15(68 \text{ ksi})(1.128 \text{ inches}) \geq 0.3(68 \text{ ksi})(1.128 \text{ inches}) \\ &= 29.27 \text{ inches} \geq 23.01 \text{ inches} \\ &= 29.27 \text{ inches} \end{aligned}$$

The centers of the plastic hinges are offset $L_p/2$ from the ends of the columns; therefore, nodes are inserted within the existing column members at a distance equal to $L_p/2$ from the column ends, as shown in Figure 329. Joint elements are assigned at the nodes corresponding to the center of the plastic hinge. The joint elements have nonlinear capabilities such that the moment-rotation relationship can be assigned to the elements.

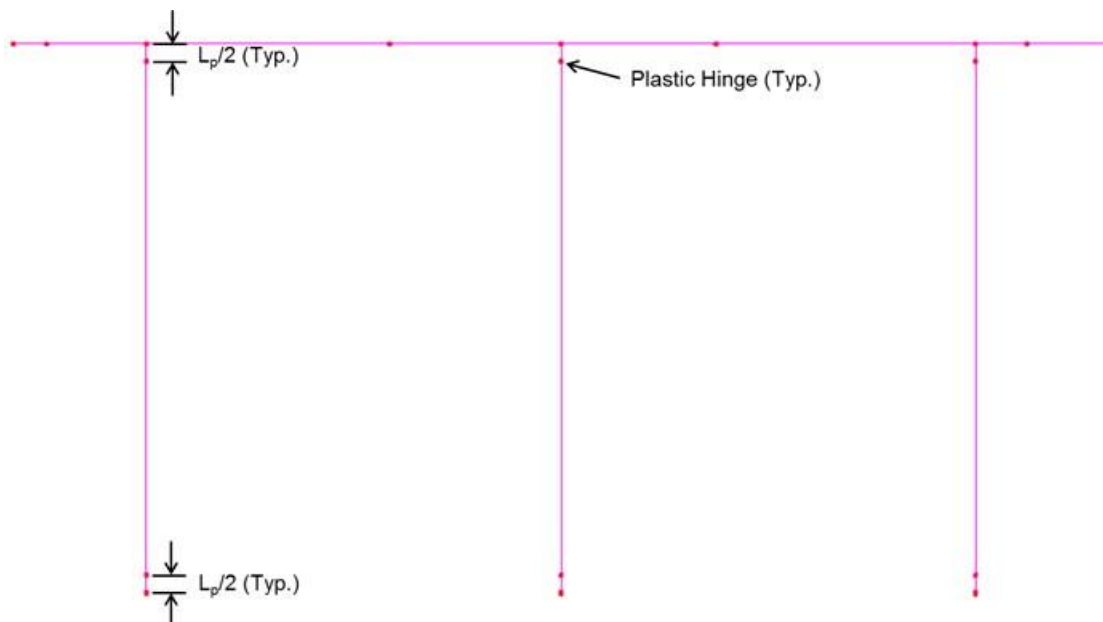


Figure 329. Illustration. Location of column plastic hinge nodes.

9.5.3.3 Step 2c – Column Plastic Moment Capacity

The plastic moment capacity of the reinforced concrete bent columns is calculated in accordance with Article 8.5 of the AASHTO Guide Specifications. A moment-curvature analysis is

performed to determine the plastic moment capacity, and includes the influence of axial forces due to dead load as well as overturning. Expected material properties for concrete and steel are used for the moment-curvature analysis. The moment-curvature relationship is idealized as elastic-perfectly plastic, with the elastic portion of the curve passing through the point corresponding to first yielding of the reinforcement. The plastic moment capacity (plateau of the curve) is determined by equating the areas between the actual and idealized moment-curvature curves beyond the point of first yielding of the reinforcement, as shown in Article 8.5 of the AASHTO Guide Specifications.

The axial forces due to overturning are considered in the moment-curvature analysis according to Articles 4.11.2 through 4.11.4 of the AASHTO Guide Specifications. The stress-strain models for the expected material properties of reinforcing steel and concrete are provided in Articles 8.4.2 and 8.4.4 of the AASHTO Guide Specifications, respectively. The reinforcing steel stress-strain model includes an elastic section, a yield plateau, and a strain-hardening region as shown in Figure 96 (Section 5.3.2.1). The values for properties that define the stress-strain model are included in Table 6. The AASHTO Guide Specifications allow for the Engineer to choose the specific model for the reinforcement stress-strain relationship, as long as it conforms to the shape and properties in Figure 96. For this example, the reinforcement stress-strain model proposed by Raynor et al. (2002) is used. The concrete model used for the expected concrete material properties is Mander's stress-strain model for confined and unconfined concrete, as defined in Figure 101 (Section 5.3.2.1) and Article 8.4.4 of the AASHTO Guide Specifications.

The moment-curvature relationship is computed using a strain compatibility approach, as outlined in Mander et al. (1998). The actual moment-curvature relationship is determined using expected material properties. An idealized bi-linear moment-curvature relationship is equated based on the actual moment-curvature relationship, as outlined in Article 8.5 of the AASHTO Guide Specifications. Examples of the actual and idealized curves for one of the columns is shown in Figure 330. The idealized moment-curvature relationship and corresponding moment-rotation relationship of each column in the transverse and longitudinal direction is summarized in Table 76. The elastic-perfectly plastic moment-rotation relationship is assigned to the joint elements at the plastic hinge locations from Step 2b. For the software used to model this example, a joint material property definition is used to define the moment-rotation relationship. The material property chosen allows for any piecewise linear curve to be defined for a given degree of freedom.

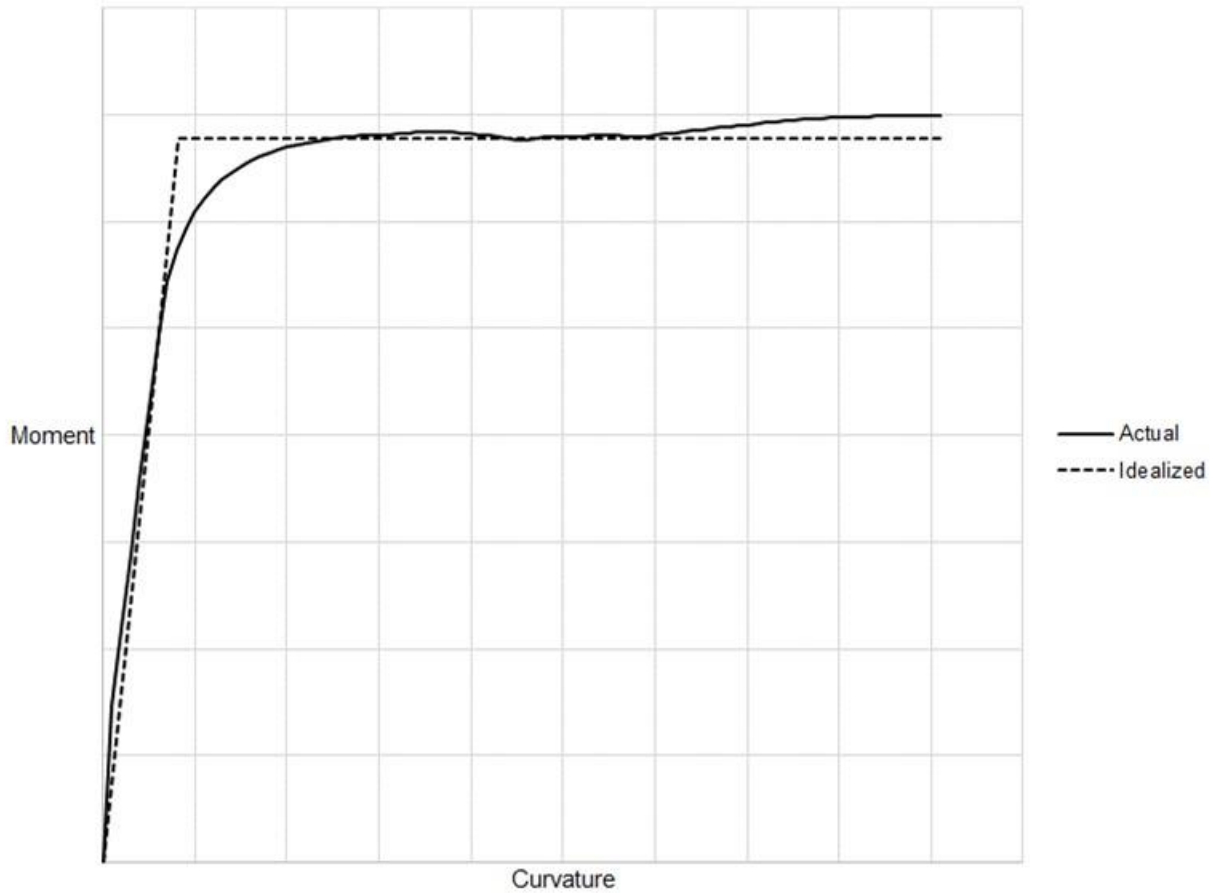


Figure 330. Graph. Reinforced concrete moment-curvature model.

Table 76. Column moment-curvature model values.

Column No.	M_p (k-ft)	ϕ_{yi} ($\times 10^{-4}$ 1/ft)	ϕ_u ($\times 10^{-4}$ 1/ft)	θ_{yi} ($\times 10^{-3}$ rad)	θ_u ($\times 10^{-3}$ rad)
Transverse Direction					
C1	6775	9.89	109.20	6.10	18.21
C2	7065	9.78	103.20	6.03	17.42
C3	8815	9.16	74.40	5.65	13.60
C4	6540	9.98	114.00	6.15	18.84
C5	6990	9.80	104.40	6.05	17.58
C6	8830	9.96	76.80	6.14	14.29
Longitudinal Direction					
C1	7005	9.80	104.40	12.09	23.63
C2	7065	9.78	103.20	12.06	23.45
C3	7145	9.75	102.00	12.02	23.27
C4	7205	10.28	100.80	12.67	23.71
C5	6990	9.80	104.40	12.09	23.63
C6	7005	9.80	104.40	12.09	23.62

9.5.3.4 Step 2d – Pushover Analysis

A pushover analysis is performed on each pier in each principal axis direction. An equivalent lateral load is applied at the top of the center column of each pier. Since the majority of the mass of the bridge acts at the center of gravity of the superstructure, an equivalent moment is necessary for the transverse pushover analyses to account for the difference between the center of gravity and the load application point. The center of gravity of the superstructure is 13 ft – 0 ¾ inches above the top of the columns. A point load with a magnitude of 100 kips is chosen for the equivalent lateral load. For the transverse pushover analyses, a force couple that accounts for the overturning effect is applied to the exterior columns in addition to the lateral point load.

The column moment-curvature analyses from Step 2c consider the axial dead load in each column. Therefore, the dead load in each column also needs to be included in the pushover analysis. Since the entire bridge is not modeled in the pushover analysis, equivalent point loads are used to model the axial dead load in the columns.

The response for each pushover analysis is solved for using two stages. In the first stage, the axial dead load in the columns is applied in a single loading increment. The response is stored and is used as the starting point for the second stage of the analysis. For the second stage, a geometric non-linear analysis is performed in which the lateral loads are increased over a given number of increments and the non-linear response is iteratively solved for within each increment. Although it was previously shown that all columns pass P-Δ checks, the P-Δ effects are included here for completeness. Refer to Section 5.3 and appropriate program documentation for guidance on non-linear analysis controls.

9.5.3.5 Step 2e – Displacement Demand vs. Capacity Check

The displacement capacity from the pushover analysis is checked against the displacement demand from the elastic seismic analysis according to Equation (55) as provided in AASHTO Guide Specifications 4.8.

$$\Delta_D^L \leq \Delta_C^L \quad (55)$$

where Δ_D^L is the displacement demand along the local principal axis of the member and Δ_C^L is the displacement capacity taken along the same principal axis as Δ_D^L . The displacement demand, Δ_D^L , is taken from the elastic seismic response spectrum analysis from Step 1. The displacement capacity, Δ_C^L , is determined from the results of the pushover analysis and can be defined as the displacement at which the first plastic hinge reaches its ultimate rotation, θ_u (see Table 76). To highlight the progression of plastic hinging in a pier, Figures 331 through 340 show the deformed shape of Pier 1 subject to a transverse load at increments of 2, 4, 6, 8, 10, 11, 12, 12.23, 12.31, and 12.35 respectively. The rotation at each plastic hinge location is included in the figures, along with colored contours defining the yield moment in each hinge. As shown, Columns 1 and 2 are the first to undergo plastic deformations, occurring in the hinge at the top of the columns at a load factor of 11.0 (Figure 336). A plastic hinge forms at the top of Column 3 at a load factors of 12.0 (Figure 337). The columns begin to approach their ultimate rotation capacities, θ_u , at load factors of 12.23 and 12.31 (Figures 338 and 339). At the subsequent load

increment of 12.35 (Figure 340), the plastic hinges at the top of Column 2 and 3 exceed their plastic rotation capacities. This load increment defines the displacement capacity of the pier.

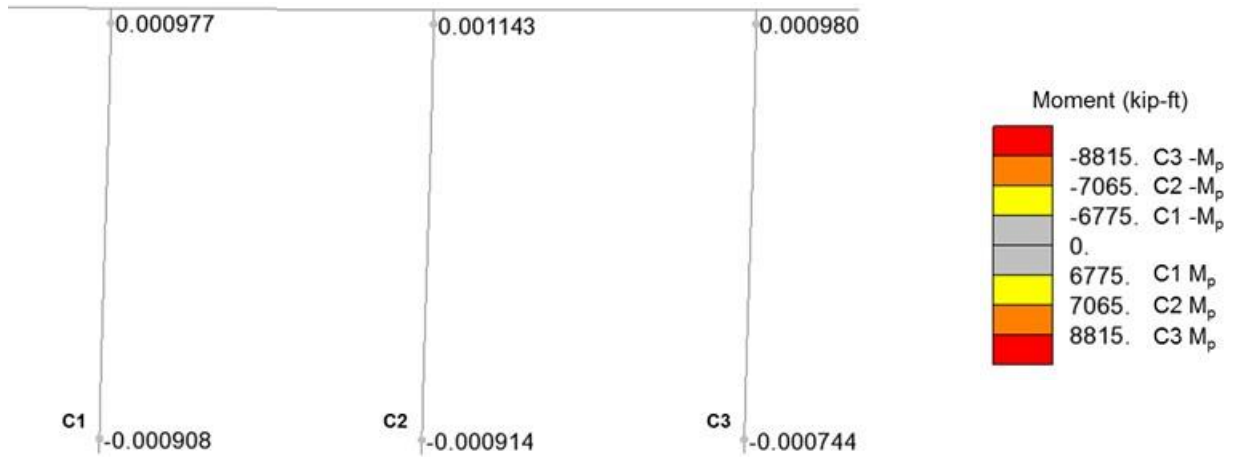


Figure 331. Illustration. Pier 1 transverse pushover deformed shape at load factor = 2.0.

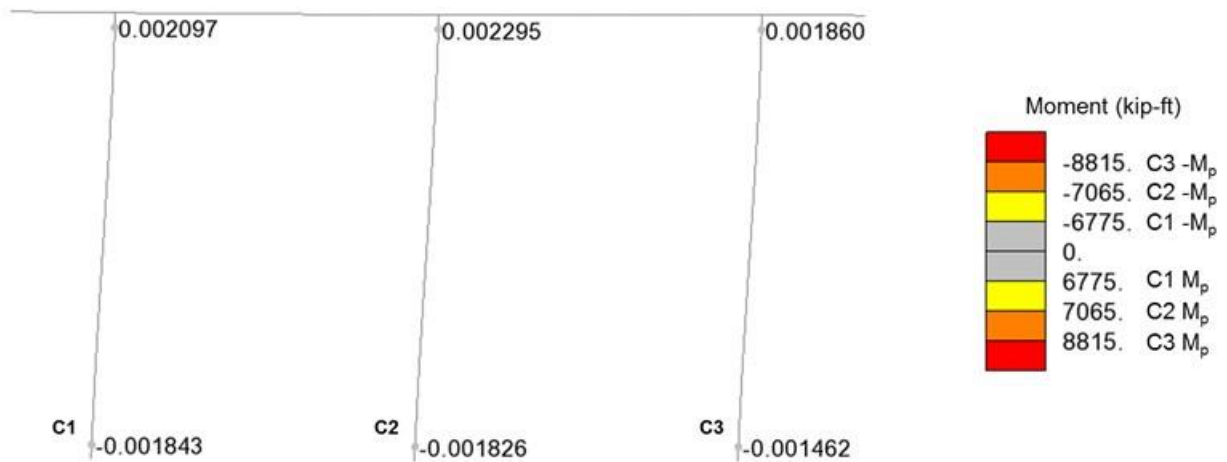


Figure 332. Illustration. Pier 1 transverse pushover deformed shape at load factor = 4.0.

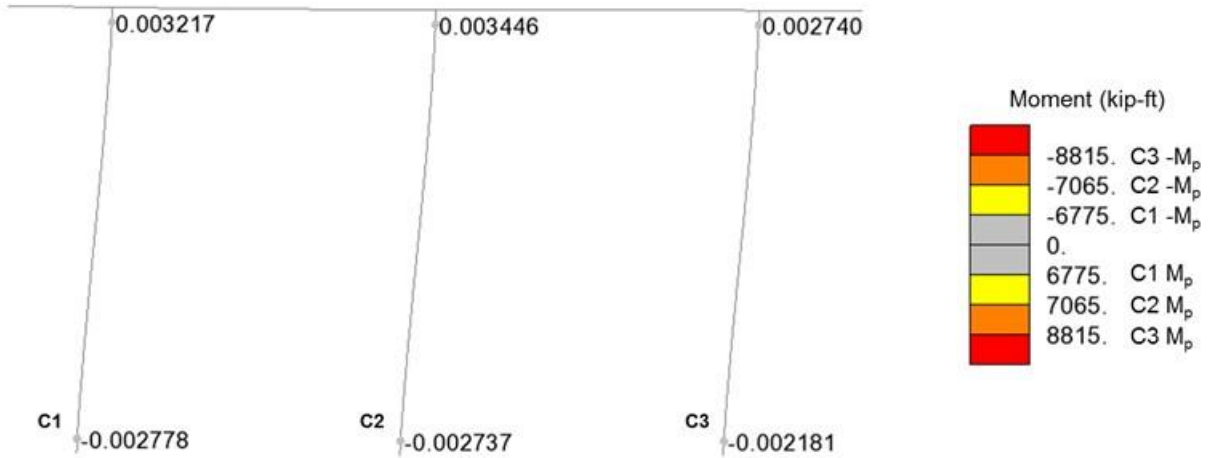


Figure 333. Illustration. Pier 1 transverse pushover deformed shape at load factor = 6.0.

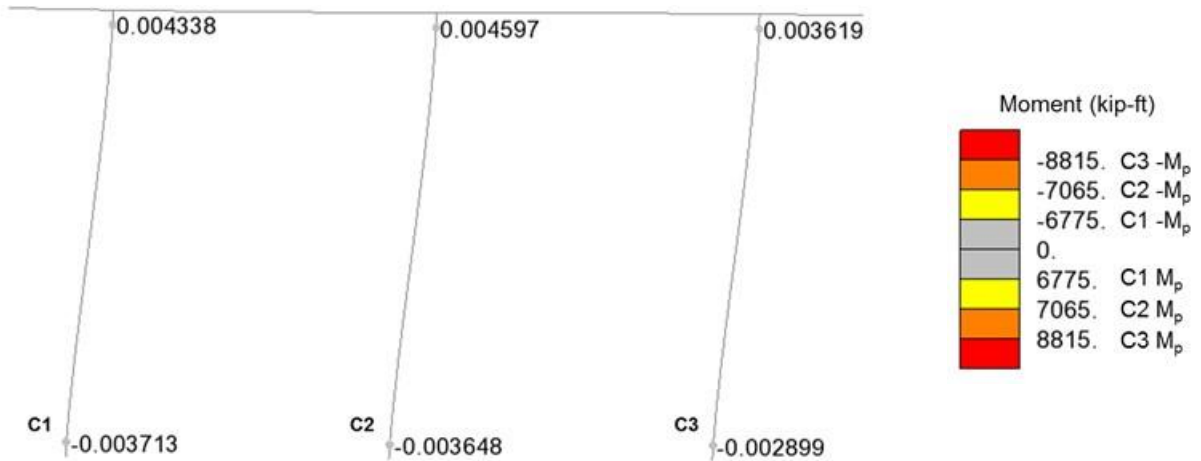


Figure 334. Illustration. Pier 1 transverse pushover deformed shape at load factor = 8.0.

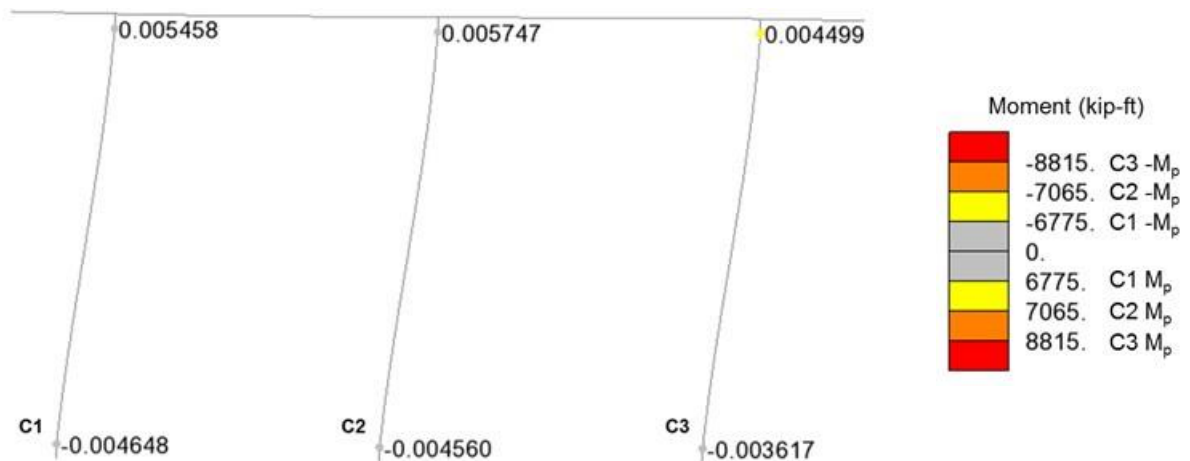


Figure 335. Illustration. Pier 1 transverse pushover deformed shape at load factor = 10.0.

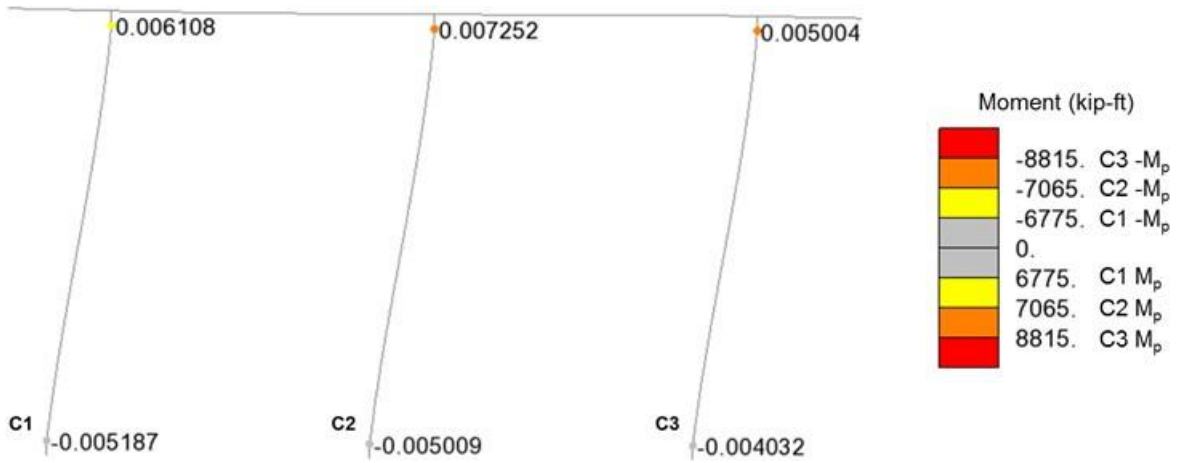


Figure 336. Illustration. Pier 1 transverse pushover deformed shape at load factor = 11.0.

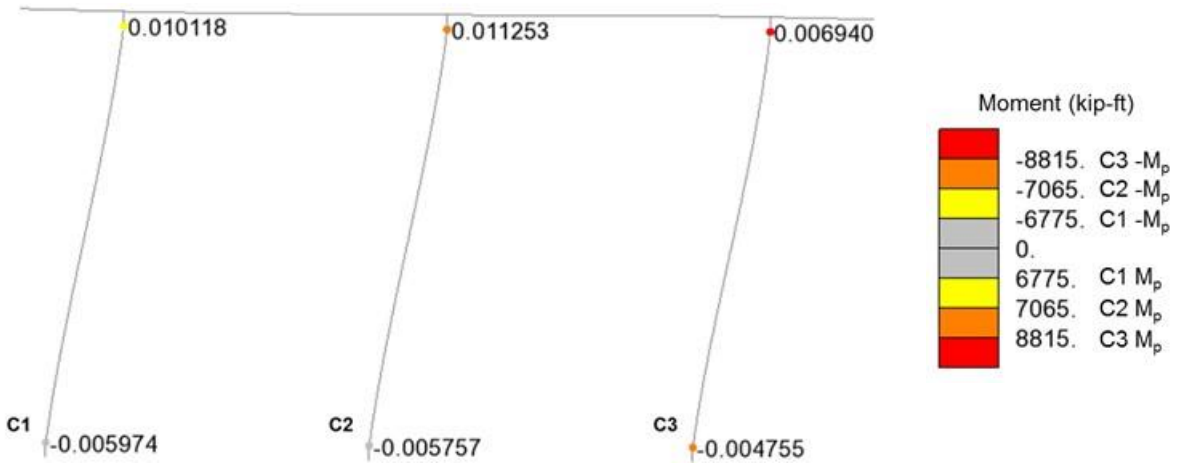


Figure 337. Illustration. Pier 1 transverse pushover deformed shape at load factor = 12.0.

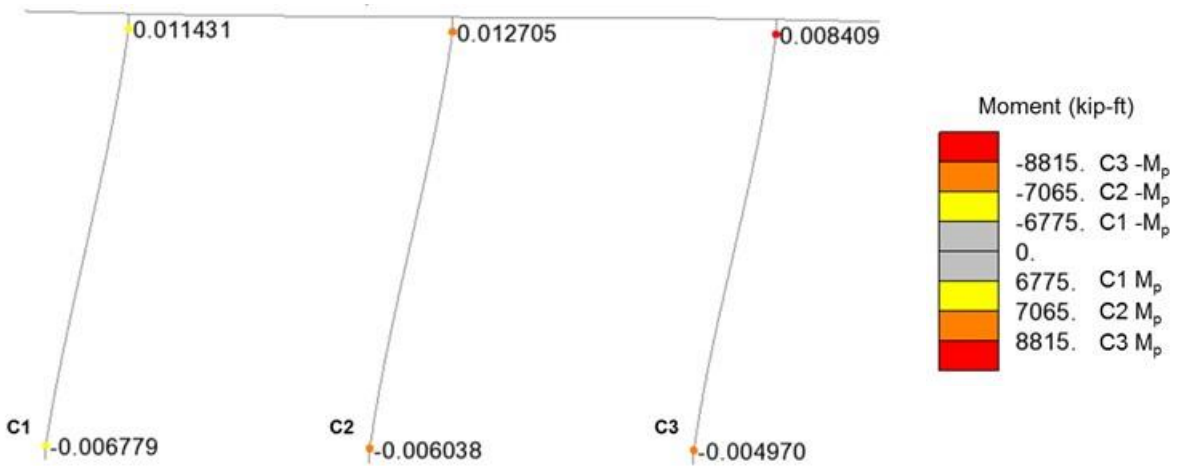


Figure 338. Illustration. Pier 1 transverse pushover deformed shape at load factor = 12.23.

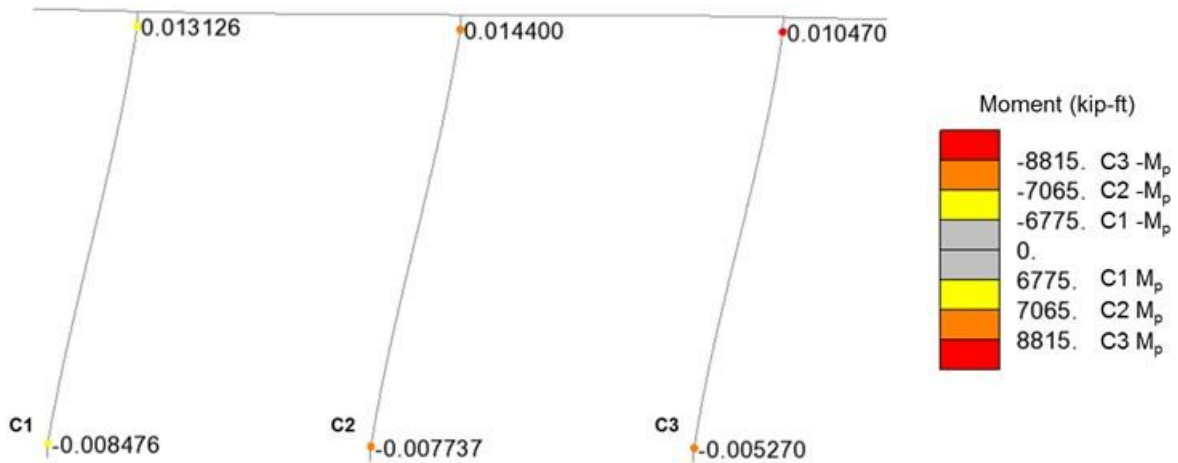


Figure 339. Illustration. Pier 1 transverse pushover deformed shape at load factor = 12.31.

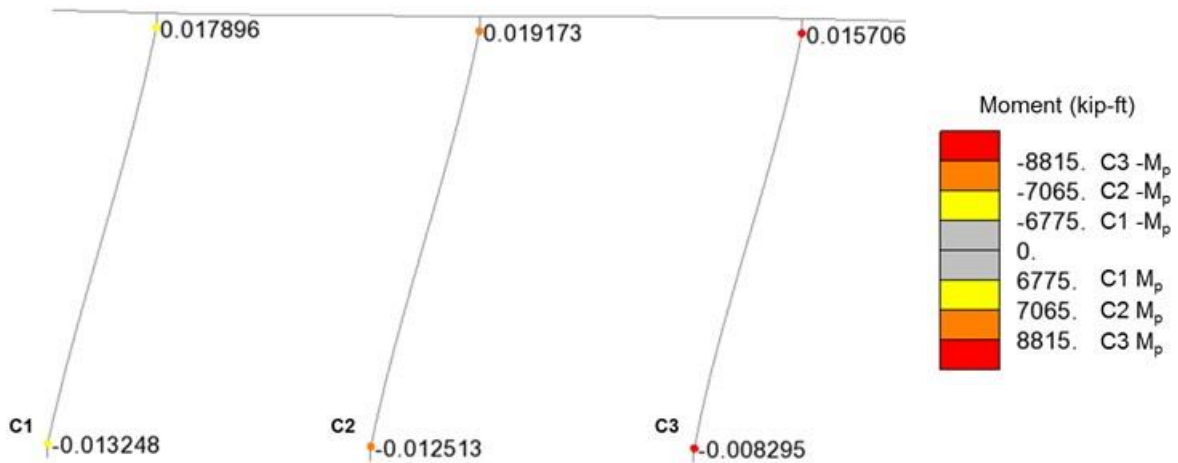


Figure 340. Illustration. Pier 1 transverse pushover deformed shape at load factor = 12.35.

The displacement capacity of each column is shown in Table 77 for the transverse and longitudinal pushover analyses, as well as the corresponding displacement demand that was previously calculated in Step 2a. As shown, the displacement capacity exceeds the displacement demand for all columns in both directions. Therefore, the column design is adequate to resist the seismic induced displacements.

Table 77. Column displacement capacity check.

Column No.	Transverse		Longitudinal	
	Δ^L_C (in)	Δ^L_D (in)	Δ^L_C (in)	Δ^L_D (in)
1	11.44	2.49	16.05	3.65
2	9.49	2.59	16.21	3.84
3	9.46	2.67	16.04	3.97
4	10.01	4.93	21.66	5.87
5	10.04	4.93	21.78	5.84
6	10.00	4.92	21.61	5.81

9.5.3.6 Step 2f – Results Verification

The next step is to verify the results using an available approximate method. The transverse pushover analysis of Pier 1 is chosen to illustrate one such approximate method, and can be similarly applied to the other pushover analyses.

From the results of the pushover analysis of Pier 1, the collapse mechanism forms at an applied lateral load of 1235 kips when the first plastic hinge failure (i.e., when the rotation capacity is exceeded) occurs in the top hinge of Column C3. The deformed shape of Pier 1 at failure is shown in Figure 341.

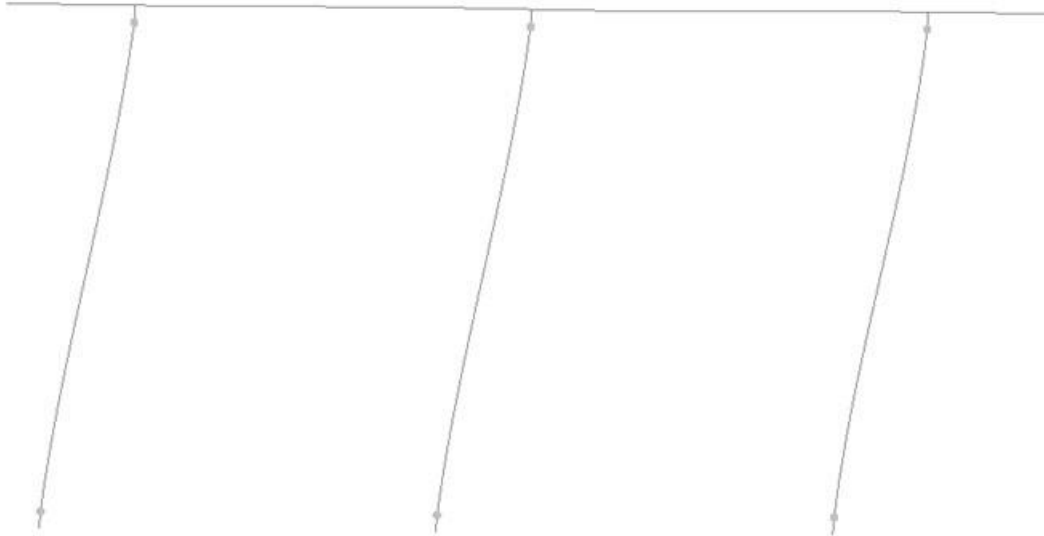


Figure 341. Illustration. Deformed shape for the transverse pushover analysis of Pier 1 at failure.

In order to verify the load at failure and corresponding plastic hinge location, the pier is idealized as a frame with a fixed support boundary condition at the base of each column. The assumed collapse mechanism is shown in Figure 342, with plastic hinges forming in each of the columns.

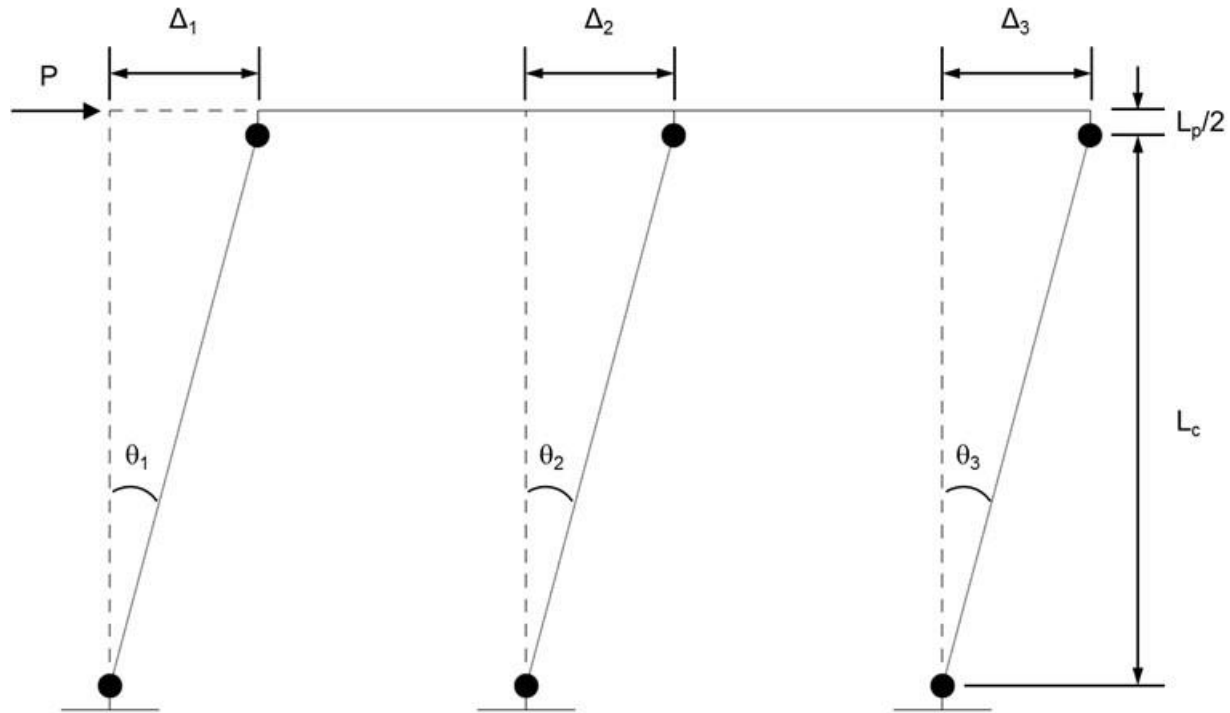


Figure 342. Illustration. Assumed transverse collapse mechanism of Pier 1.

The rotation of a plastic hinge at failure, θ_p , is defined in Equation (56).

$$\theta_p = \phi_p L_p \quad (56)$$

where ϕ_p is the plastic curvature capacity of the hinge and L_p is the plastic hinge length previously defined in Equation (54). The plastic displacement, Δ_p , corresponding to θ_p is defined in Equation (57).

$$\Delta_p = \theta_p L_c \quad (57)$$

where L_c is the distance between plastic hinges. Using the previously calculated plastic hinge length of 29.3 in and the plastic curvature capacities from Table 76, the plastic rotations and displacements are calculated as shown in Table 78.

Table 78. Pier 1 transverse plastic rotation and displacement capacities.

Column No.	θ_p ($\times 10^{-2}$ rad)	Δ_p (in)
1	2.422	10.04
2	2.278	9.45
3	1.591	6.60

Column 3 has the smallest plastic rotation capacity (and displacement capacity) and, therefore, will control the collapse mechanism. The principle of virtual work can be used to solve for the

load, P , at which the controlling displacement capacity is reached. The external work done on the frame is due to the externally applied load, P .

$$\text{External Virtual Work, EVW} = P\Delta_p$$

The internal virtual work is defined by the rotation of the plastic hinges at the collapse mechanism. The rotation of the three columns at the collapse mechanism is assumed to be equal to the controlling plastic rotation capacity, which is defined by Column 3. At this rotation value ($\theta = 1.591 \times 10^{-2}$ rad) all three of the columns have yielded (see Table 76); therefore, all columns have reached their plastic moment capacities.

$$\text{Internal Virtual Work, IVW} = (2M_{p1} + 2M_{p2} + 2M_{p3})\theta_p$$

Next, the External Virtual Work is set equal to the Internal Virtual Work and the load, P , is solved for.

$$\begin{aligned} \text{EVW} &= \text{IVW} \\ P\Delta_p &= (2M_{p1} + 2M_{p2} + 2M_{p3})\theta_p \\ P &= [(2M_{p1} + 2M_{p2} + 2M_{p3})\theta_p]/\Delta_p \\ P &= \{[2(6775 \text{ k-ft})+2(7065 \text{ k-ft})+2(8815 \text{ k-ft})](1.591 \times 10^{-2} \text{ rad})\}/(6.60 \text{ in}) \\ P &= 1311 \text{ kips} \end{aligned}$$

The approximate collapse load, P , of 1311 kips is close to the value of 1235 kips determined from the pushover analysis. Therefore, the results of the pushover analysis are reasonable. A similar procedure can be performed for the longitudinal pushover direction.

9.5.4 Conclusions

This example outlines the procedure for performing a multi-mode response spectra analysis using a PEB finite element model. The substructure iterative method was used to include the effects of soil-structure interaction. Pier column displacements from the response spectra analysis were acceptable when compared to allowable specification values. In addition, a pushover analysis was performed on each pier as an alternate method to compute displacement capacities. All columns had sufficient displacement capacities to resist the applied elastic displacements from the response spectra analysis. This example was not a comprehensive design of the bridge substructure, as the main purpose was to highlight the response spectra analysis procedure, soil-structure interaction, and the pushover analysis. Other capacity checks should be investigated according to the appropriate specification(s).

9.6 Example 6 – Stability Analysis of a Tall Concrete Pier Column

Example 6 consists of analyzing the stability of a tall concrete pier column that is part of a 3-span continuous multi-girder bridge. The bridge cross-section consists of 5 steel plate girders supporting an 8 inch composite concrete deck slab. The out-to-out deck width is 52 ft – 0 inches and the curb-to-curb width is 50 ft – 0 inches. The depth of the superstructure is 10 ft – 1½ inches from the top of the deck to the top of the pier cap. The bridge length is 660 ft with span lengths of 190ft-0 inches – 280 ft-0 inches – 190 ft-0 inches. The spans are supported by single column concrete piers, as shown in Figure 343. The piers consist of varying depth reinforced concrete pier caps (i.e., hammerhead caps) integral with the pier shafts. The pier shaft spans from the pier cap down through soil via a drilled shaft and into rock by means of a rock socket.

The pier of interest for this example is Pier 2. The pier is assumed to be supporting fixed bearings, such that moments due to longitudinal reactions from braking are present. The remaining pier and abutments of the bridge are assumed to support expansion bearings, such that the effective length of the Pier 2 column is that of a cantilever.

The cross section and reinforcement details of Pier 2 are shown in Figure 343. The cap is 7 ft – 0 inches wide, 52 ft – 6 inches long, and varies in depth from 15 ft – 5 inches at the face of the column to 6 ft – 5 inches at the ends. The pier shaft is 117 ft – 8½ inches tall from the top of the cap to the top of the drilled shaft. The drilled shaft extends 31 ft – 0 inches through a layer of dense granular soil to the top of the rock socket, which extends 25 ft – 0 inches into the rock layer. A constant diameter of 10 ft – 6 inches is used for the pier shaft, drilled shaft, and rock socket. There is a 3 inch architectural façade on the exterior of the pier shaft. The pier shaft is reinforced with 88 No. 11 bars longitudinally, while the drilled shaft and rock socket are reinforced with 132 No. 11 bars. All ties are No. 6 bars spaced at 6 inches. The steel reinforcement is AASHTO M31 Grade 60 and all concrete is normal weight with a compressive strength of 4,500 psi.

9.6.1 Methodology

Compression members in structures are typically designed using specification provided equations that implicitly account for slenderness effects caused by factors such as initial out-of-straightness and eccentricities. Compressive axial forces acting together with these eccentricities amplify the out of plane deformation of a member. The result is a reduction in the stiffness of the member, and is referred to as a second order effect. The slenderness ratio, Kl/r , of a member is typically used by the specifications to determine if second order effects are to be considered in an analysis. For many structures, second order effects are negligible and can be neglected when the Kl/r of a member is below a specification limit. Additionally, within certain bounds of Kl/r , second order effects can be conservatively approximated using a moment magnification factor calculated according to the specification. When Kl/r falls outside the limits of the specification, a refined analysis should be used to analyze stability and second-order-effects. For more information on stability refer to Section 8.2.10.

Example 6 consists of performing a second order analysis to account for secondary bending effects using (1) the moment magnification procedure from AASHTO LRFD and (2) a large deflection non-linear analysis. A moment magnification factor is determined from the results of the non-linear analysis and compared to the value calculated according to the specifications. The

column capacity is calculated using the specification equations. The moments calculated from both the moment magnification procedure and the non-linear analysis are checked against the column capacity. It is acknowledged that this example is a simple application of a second order analysis, where the section of the column is constant and the boundary conditions are easily defined. The results are easily checked using hand calculations. It is useful in demonstrating the general procedure, however, for cases that are more complicated, such as varying section properties and more complicated boundary conditions.

For simplicity, only the pier of interest is modeled. Rather than modeling the superstructure and all other piers, all reactions on the pier from the superstructure are applied at the bearing locations.

9.6.2 Step 1 – Model Description

A beam line element model of Pier 2 is created based on the materials and dimensions illustrated in Figure 343 and used to perform a stability analysis. A base model is created to define the geometry, finite element mesh, section properties, materials, boundary conditions, and loads. The base model is subsequently modified as necessary for the linear static analysis, eigenvalue buckling analysis, and large deflection non-linear analysis.

9.6.2.1 Step 1a – Model Geometry and Mesh

The Pier 2 geometry is modeled using beam elements approximately 2 ft in length, which provide accurate analysis results (see verification sections later). Refer to Section 3 of the Manual for more information on mesh refinement. The beam elements used have geometric non-linear capabilities. When creating the geometry, in addition to a sufficiently refined mesh, nodes should be defined at locations that facilitate connections and load application, as shown in Figure 344. For the pier caps, nodes should be defined at each of the bearing locations (see Figure 343) so that superstructure reactions can be applied. Additional nodes are defined at the pier cap to pier shaft connection and pier shaft to drilled shaft connection.

9.6.2.2 Step 1b – Material Properties

The same class of concrete is used for all pier members and, therefore, only one material property needs to be defined. The appropriate concrete material properties are listed in Table 79, and are based on a concrete with a specified 28-day compressive strength of 4,500 psi. The modulus of elasticity is calculated according to AASHTO LRFD.

Table 79. Material properties.

Material Property	Units	Pier Concrete
Compressive Strength	psi	4,500
Modulus of Elasticity	k/f	556,589
Poisson's Ratio	-	0.2
Unit Weight	k/ft ³	0.145
Thermal Expansion Coefficient	ft/ft/°F	6E-6

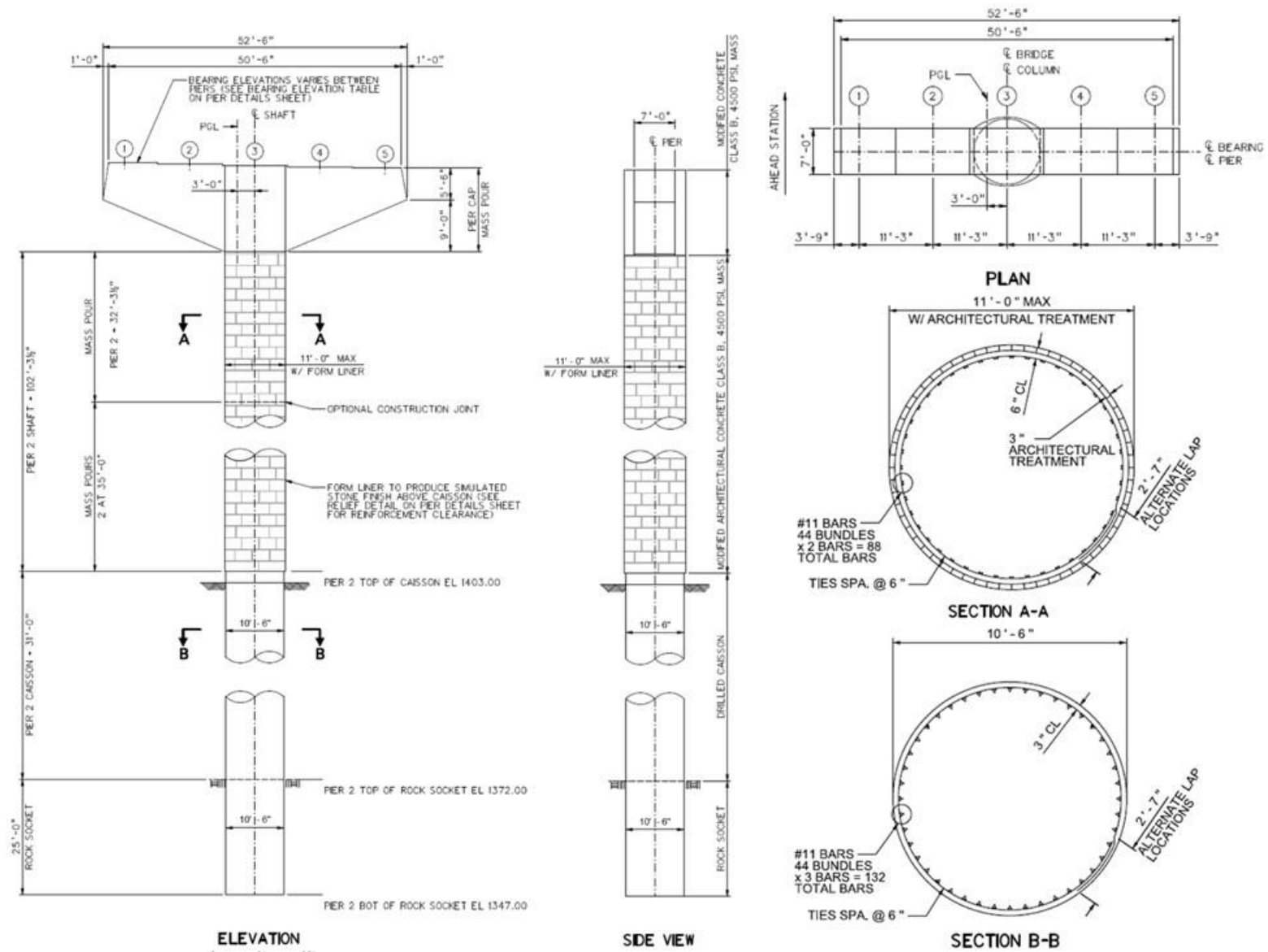


Figure 343. Illustration. Pier plan, elevation, and reinforcement details.

9.6.2.3 Step 1c – Cross-Section Properties

The member section properties can be calculated by hand and input into the analysis software or defined using the software section property library or section property calculator, if available. Using the dimensions provided in Figure 343, the gross section properties listed in Table 80 are calculated and input for the appropriate members within the model. The 3 inch architectural façade is not included in the dimensions of the pier shaft when calculating sections properties because it is assumed to not provide structural resistance. However, the façade does add weight to the structure and is accounted for in the application of dead load.

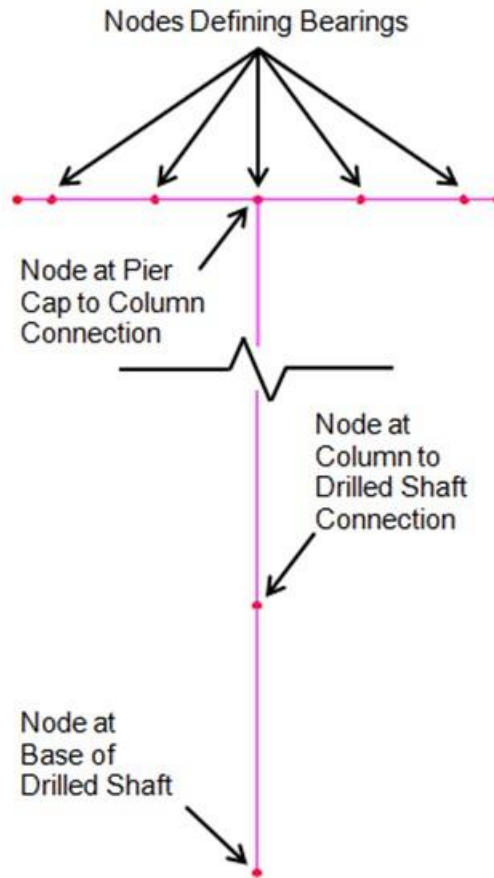


Figure 344. Illustration. User defined nodes.

Table 80. Gross section properties.

Section Property	Units	Drilled Shaft	Pier Shaft	Pier Cap (@ Column)	Pier Cap (@ End)
Cross-section Area (A)	ft ²	86.6	86.6	107.9	44.9
Strong Axis Moment of Inertia (I_{yy})	ft ⁴	596.7	596.7	2137.4	154.1
Weak Axis Moment of Inertia (I_{zz})	ft ⁴	596.7	596.7	440.7	183.4
Torsion Constant (J_{xx})	ft ⁴	1193.3	1193.3	1260.2	281.4
Shear Area in y Direction (A_{vy})	ft ²	77.9	77.9	89.9	37.4
Shear Area in z Direction (A_{vz})	ft ²	77.9	77.9	89.9	37.4
Offset in y Direction (e_y)	ft	0.0	0.0	0.0	0.0
Offset in z Direction (e_z)	ft	0.0	0.0	7.708	3.208

When evaluating a reinforced concrete member for slenderness effects the gross member properties should not typically be used to determine the stiffness of the member. Rather, an effective stiffness representative of the stiffness just prior to failure, taking into account the degree of cracking, creep, and the variation in stiffness along the length of the member (i.e., not just the most highly loaded or cracked section) should be utilized, as discussed in 8.2.10. However, there is not a stiffness value that comprehensively covers all possible failure modes of a column (e.g., material failure, stability failure). AASHTO LRFD Article 5.7.4.3 provides the following expressions for the effective stiffness of concrete compression members (AASHTO LRFD Eqs. 5.7.4.3-1 and 5.7.4.3-2) when evaluating for slenderness effects, taken as the greater of Equation (58) and Equation (59).

$$EI = \frac{\frac{E_c I_g}{5} + E_s I_s}{1 + \beta_d} \quad (58)$$

$$EI = \frac{\frac{E_c I_g}{2.5}}{1 + \beta_d} \quad (59)$$

where β_d is the ratio of maximum factored permanent load moments to maximum factored total load moments, I_g is the moment of inertia of the gross concrete section about the centroidal axis, I_s is the moment of inertia of the longitudinal steel about the centroidal axis, and E_c and E_s are the modulus of elasticity of concrete and steel, respectively. ACI 318-14 also allows for the use of Equation (58) and Equation (59) when calculating the Euler buckling load for the moment magnification procedure, but provides a third equation (ACI 318-14 Eq. 6.6.4.4c) for effective stiffness given as

$$EI = \frac{E_c I}{1 + \beta_d} \quad (60)$$

where I is the effective moment of inertia determined according to ACI Table 6.6.3.1.1(b) for columns.

$$I = 0.35I_g \leq \left(0.80 + 25 \frac{A_{st}}{A_g}\right) \left(1 - \frac{M_u}{P_u h} - 0.5 \frac{P_u}{P_0}\right) I_g \leq 0.875I_g \quad (61)$$

where A_{st} is the area of longitudinal reinforcement, A_g is the gross area of the cross-section, h is the height of the cross-section, M_u is the factored moment, P_u is the factored axial load, and P_0 is the nominal axial strength at zero eccentricity, given as

$$P_0 = 0.85f'_c(A_g - A_{st}) + f_y A_{st} \quad (62)$$

where f'_c is the specified 28 day concrete compressive strength and f_y is the specified yield strength of the steel reinforcement. The expression for the effective moment of inertia given in Equation (61) was developed by Khuntia and Ghosh (2004a, 2004b) and considers the axial load,

eccentricity, reinforcement ratio, and concrete compressive strength. The effective stiffness calculated using Equations (60) and (61) (herein “ACI expressions”) is considered to be more accurate than that determined from Equations (58) or (59) (herein “AASHTO expressions”), but requires more information about the section size, reinforcement, and loading on the member. The AASHTO expressions are typically used during preliminary design stages when member sizes and reinforcement arrangements are estimated, which explains why AASHTO allows their use “in lieu of a more precise calculation.” For this example, the effective stiffness is calculated using both the AASHTO and ACI expressions and comparisons are made to highlight the differences between the methods.

When performing a first-order or second-order elastic analysis using the ACI expressions for effective stiffness, Khuntia and Ghosh (2004a, 2004b) recommend performing an initial analysis with the stiffness assumed as $0.70E_cI_g$ for columns ($0.35E_cI_g$ for beams), which corresponds to a column with a 1.5 percent reinforcement ratio, an eccentricity ratio, e/h (or M_u/P_uh), of 0.20, and $P_u/P_0 = 0.40$. The results of the analysis are then used to calculate a new effective stiffness using the expression for moment of inertia given in Equation (61). The effective stiffness changes due to the updated eccentricity ratio calculated from the analysis results. If the new effective stiffness differs from the previous value by more than 15 percent, the analysis should be re-run with the new effective stiffness (Khuntia and Ghosh 2004b).

Using the details provided in Figure 343 and the concrete material properties from Table 79, the effective stiffness of the pier shaft and drilled shaft are calculated for both the AASHTO and ACI expressions. For the purpose of modeling, the effective stiffness is accounted for through an effective moment of inertia, $I_{effective}$ (e.g., EI from Equations (58) and (59) is divided by E from Table 79 to obtain $I_{effective}$). $I_{effective}$ values for the drilled shaft and pier shaft are included in Table 81. As shown in Table 80, the strong and weak axis moment of inertia are equal and, therefore, only one moment of inertia value is shown in Table 81 for brevity. The moment of inertia values shown in Table 81 for the ACI expressions are based on the results (i.e., M_u and P_u) of the linear static analysis (see Step 2a). Later sections of the example discuss the consequences that the assumed effective stiffness has on the results of the analysis.

Table 81. Effective section properties.

Section Property	Units	Drilled Shaft	Pier Shaft
Effective Moment of Inertia – AASHTO Expressions ($I_{effective\ AASHTO}$)	ft ⁴	247.0	238.7
Effective Moment of Inertia – ACI Expressions ($I_{effective\ ACI}$)	ft ⁴	522.1	500.5

The hammerhead pier cap is modeled with elements that allow the varying depth of the section to be explicitly defined. Alternatively, the pier cap can be modeled as a constant-depth section and applied loads can be used to account for the difference in dead load between the model geometry and the actual structure. In addition, the pier cap is assigned eccentricities in the vertical direction in order to align the top face of the cap with the top of the column. If the eccentricities are not used or properly defined, section properties can be incorrectly modeled as shown in Figure 345(a). If eccentricities cannot be used to correctly define elevations, an alternative is to model the cap elements along the centerline of the hammerhead cap and use rigid links to connect the cap to the bearing locations.

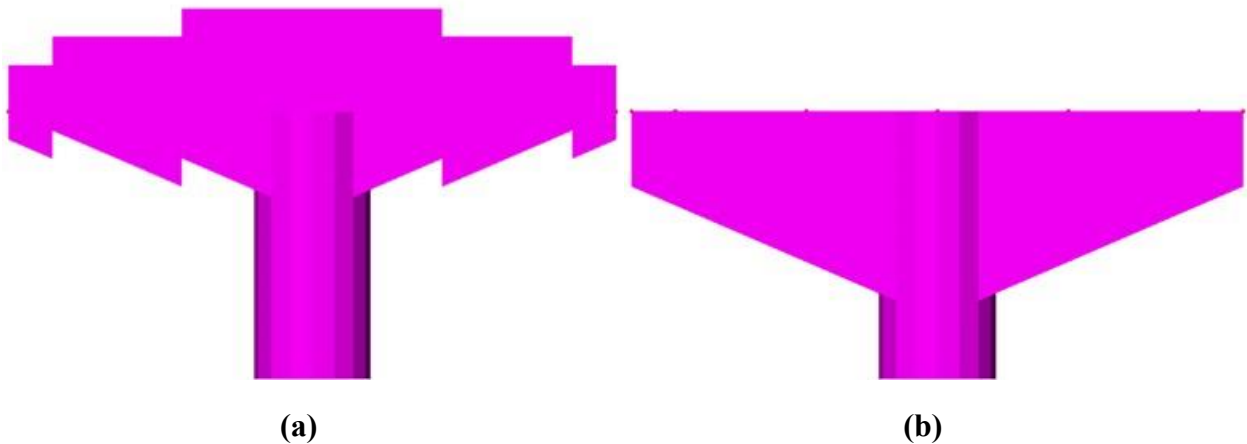


Figure 345. Illustration. (a) Incorrect and (b) correct definition of pier cap cross section vertical eccentricity.

9.6.2.4 Step 1d – Boundary Conditions

The interaction of the drilled shaft and rock socket with the surrounding soil is accounted for using the depth to fixity method. This method is considered overly simplistic and is not the most accurate for modeling soil-structure interaction. However, the purpose of this example is to study the behavior of a slender column considering second order effects, not the interaction of the foundation elements with the soil. Guidance on the use of more accurate methods to account for the soil-structure interaction are provided in Section 5.2 and in Example 5. The depth to fixity below ground for piles and drilled shafts in sands is given by Equation (63) from AASHTO LRFD Article C10.7.3.13.4 as

$$1.8 \left[\frac{E_p I_w}{n_h} \right]^{0.2} \quad (63)$$

where E_p is the modulus of elasticity of the drilled shaft (ksi), I_w is the weak axis moment of inertia (ft^4), and n_h is the rate of increase of soil modulus with depth. Based on the soil being a dense, granular sand and assuming it is submerged, n_h is taken as 1.39 ksi/ft from Table C10.4.6.3-2 of AASHTO LRFD. Using the material and section properties from Tables 79 and 80 respectively, the depth to fixity is calculated as:

$$\begin{aligned} &= 1.8[(3861 \text{ ksi})(597 \text{ ft}^4)/1.39]^{0.2} \\ &= 31.6 \text{ ft} \end{aligned}$$

Which is approximately equal to the top of rock elevation (31 ft – 0 inches below the top of ground). Therefore, for this example, the depth to fixity is taken as the top of rock at 31 ft – 0 inches and the drilled shaft is modeled to this depth. A boundary condition is assigned at the point of fixity restraining all translations and rotations.

Although the superstructure is not explicitly modeled, its interaction with the pier should be considered. The superstructure is not integral with the pier and since the pier supports fixed bearings, there are no rotational restraints at the top of the pier. It is assumed that the

superstructure provides sufficient restraint in the transverse direction. This behavior is idealized by restraining transverse translation at the top of the pier. Since the remaining pier and abutments have expansion bearings, longitudinal translation is modeled as unrestrained at the top of the pier.

9.6.2.5 Step 1e – Loads

For this example, the loads of interest are the dead load, vertical live load, and longitudinal braking force from the live load. For brevity, the dead load and vertical live load calculations are omitted, but are calculated similarly to Examples 1 through 3. The braking force is calculated according to AASHTO LRFD Article 3.6.4 and is taken as the greater of:

- 25 percent of the axle weights of the design truck or design tandem or,
- 5 percent of the design truck plus lane load or 5 percent of the design tandem plus lane load

Pier 2 is the only pier of the bridge with fixed bearings and therefore resists all of the braking force. Based on the curb-to-curb deck width, the bridge can accommodate up to 4 lanes of traffic. Vehicular traffic is conservatively assumed to travel in the same direction. Detailed calculations of the braking force are shown below.

The vehicle weights for use in the braking force calculations are as follows, taken from AASHTO LRFD Article 3.6.1.2:

$$\begin{aligned} W_{\text{truck}} &= \text{weight of the design truck} \\ &= 72 \text{ kips} \end{aligned}$$

$$\begin{aligned} W_{\text{tandem}} &= \text{weight of the design tandem} \\ &= 50 \text{ kips} \end{aligned}$$

$$\begin{aligned} W_{\text{lane}} &= \text{distributed lane load} \\ &= 0.64 \text{ k/ft} \end{aligned}$$

Sum the span lengths and multiply with the distributed lane load.

$$\begin{aligned} \sum L_{\text{span}} &= \text{sum of the span lengths} \\ &= 190 \text{ ft} + 280 \text{ ft} + 190 \text{ ft} \\ &= 660 \text{ ft} \end{aligned}$$

$$\begin{aligned} W_{\text{lane}} &= \text{weight of the lane load} \\ &= W_{\text{lane}} * \sum L_{\text{span}} \\ &= (0.64 \text{ k/ft})(660 \text{ ft}) \\ &= 422.4 \text{ kips} \end{aligned}$$

Determine which vehicle combination controls the braking force.

$$\begin{aligned} F_1 &= 25\% \text{ of the weight of the design truck or tandem} \\ &= 0.25[\text{Max}(W_{\text{truck}}, W_{\text{tandem}})] \\ &= 0.25[\text{Max}(72 \text{ kips}, 50 \text{ kips})] \end{aligned}$$

$$= 18.0 \text{ kips}$$

$$\begin{aligned} F_2 &= 5\% \text{ of the design truck or tandem plus lane load} \\ &= 0.05[\text{Max}(W_{\text{truck}}, W_{\text{tandem}}) + W_{\text{lane}}] \\ &= 0.05[\text{Max}(72 \text{ kips}, 50 \text{ kips}) + 422.4 \text{ kips}] \\ &= 24.7 \text{ kips} \end{aligned}$$

Account for the number of lanes and multiple presence factor to determine the braking force.

$$\begin{aligned} F_{BR1} &= \text{Braking force for one lane loaded} \\ &= \text{Max}(F_1, F_2)(\text{No. of lanes})(\text{MPF}) \\ &= \text{Max}(18 \text{ kips}, 25 \text{ kips})(1 \text{ lane})(1.2) \\ &= 29.7 \text{ kips} \end{aligned}$$

Repeat the calculations for two, three, and four lanes loaded. The braking force calculations are summarized as follows.

No. of Lanes	1	2	3	4	
MPF	1.20	1.00	0.85	0.65	
F ₁	18.0	36.0	54.0	72.0	kips
F ₂	24.7	49.4	74.2	98.9	kips
Controlling Force, F _{BRi}	29.7	49.4	63.0	64.3	kips

Therefore, four lanes loaded controls the braking force. Determine the braking force reaction on each bearing so that the reactions can be applied within the model. Assume an equal distribution of the braking force to each bearing.

$$\begin{aligned} n &= \text{No. of bearings per pier} \\ &= 5 \end{aligned}$$

$$\begin{aligned} F_{BR} &= \text{braking force} \\ &= 64.3 \text{ kips} \\ &= 12.9 \text{ kips/bearing} \end{aligned}$$

The braking force is applied as a horizontal force at each bearing location at the top of the pier.

The unfactored reactions on the pier from the superstructure are shown in Table 82, separated for exterior and interior bearings. The self-weight of the pier is accounted for by defining an acceleration in the downward vertical direction equal to the acceleration due to gravity (32.17 ft/s²). The analysis software uses the defined gravitational acceleration and previously defined material mass density to calculate the self-weight force of each member. Many analysis software programs provide various methods to account for the self-weight of members. The analyst should make sure they understand what assumptions the software makes, and ensure the gravity loads are correctly calculated.

Table 82. Unfactored bearing reactions.

Load Type	Exterior Bearing	Interior Bearing
Non-composite Dead Load (kips)	501	471
Composite Dead Load (kips)	34.1	29.6
Wearing Surface (kips)	64.8	64.8
Live Load (kips)	281	329
Braking (kips)	12.9	12.9

The additional weight of the pier shaft due to the architectural façade is accounted for by applying an equivalent distributed load along the length of the pier shaft. Using the provided dimensions from Figure 343, the façade load is calculated as

$$\begin{aligned}
 A_{\text{total}} &= \text{total cross-sectional area including façade} \\
 &= (\pi d^2)/4 \\
 &= \pi(11 \text{ ft} - 0 \text{ inches})^2/4 \\
 &= 95.0 \text{ ft}^2
 \end{aligned}$$

$$\begin{aligned}
 A_{\text{shaft}} &= \text{cross-sectional area of pier shaft} \\
 &= (\pi d^2)/4 \\
 &= \pi(10 \text{ ft} - 6 \text{ inches})^2/4 \\
 &= 86.6 \text{ ft}^2
 \end{aligned}$$

$$\begin{aligned}
 A_{\text{façade}} &= \text{cross-sectional area of façade} \\
 &= A_{\text{total}} - A_{\text{shaft}} \\
 &= 8.44 \text{ ft}^2
 \end{aligned}$$

$$\begin{aligned}
 W_{\text{façade}} &= \text{façade distributed load} \\
 &= W_{\text{concrete}} A_{\text{façade}} \\
 &= (0.145 \text{ kcf})(8.44 \text{ ft}^2) \\
 &= 1.53 \text{ k/ft}
 \end{aligned}$$

The applied loads must be factored prior to defining them in the model since a large deflection non-linear analysis is performed. Superposition is not valid in a non-linear analysis because the loads are not proportional to the displacements. Therefore, all loads must be factored and applied in a single analysis. For the purpose of this example, only the Strength I load combination from AASHTO LRFD Table 3.4.1-1 is shown. The factored reactions on the pier are shown in Table 83 along with the appropriate Strength I load combination factors. There are several ways to factor the self-weight load of the pier, even if the program is applying gravity automatically. The important thing is to make sure the load is factored prior to the analysis, rather than to the load effects post-analysis. In this case it is accomplished by applying a load factor (1.25 for Strength I dead load) to the acceleration due to gravity, resulting in a factored gravitational acceleration of 40.22 ft/s².

Table 83. Strength I load combination factored loads.

Load Type	Load Factor	Exterior Bearing (kips)	Interior Bearing (kips)
Non-composite Dead Load (kips)	1.25	626	589
Composite Dead Load (kips)	1.25	42.6	37.0
Wearing Surface (kips)	1.50	97.1	97.1
Live Load (kips)	1.75	492	576
Braking (kips)	1.75	22.5	22.5

The factored reaction forces are applied to the nodes corresponding to the location of the bearings, as previously defined in Figure 344. The non-composite dead load, composite dead load, wearing surface, and live load are applied in the vertical direction, and the braking force is applied in the longitudinal direction, as shown in Figure 346.

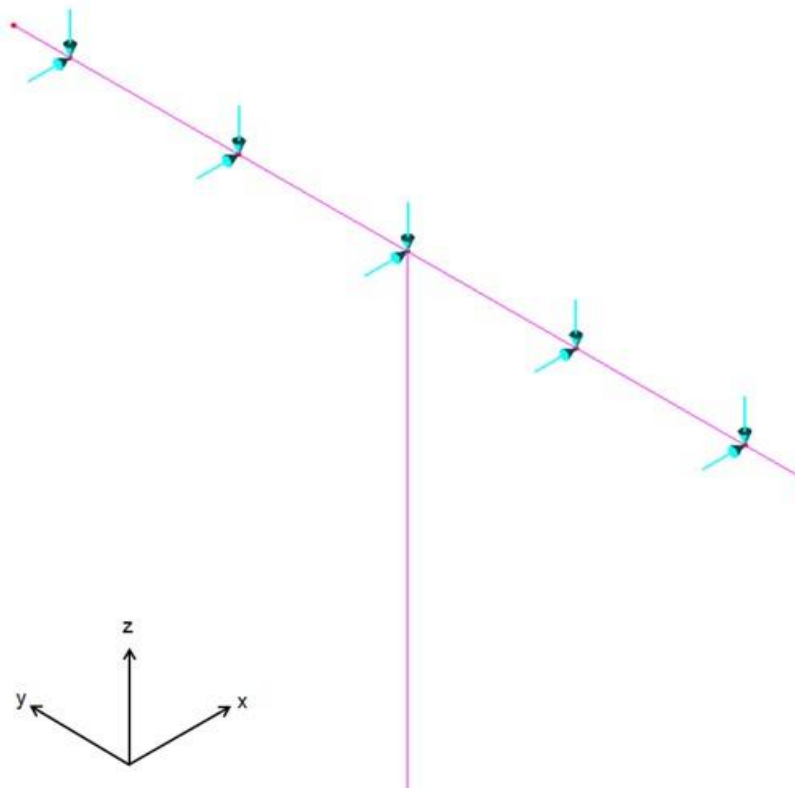


Figure 346. Illustration. Application of bearing reactions on the pier cap for linear static analysis.

9.6.3 Step 2 – Moment Magnification Procedure

The magnified moments resulting from second order effects are calculated as specified in AASHTO LRFD Article 4.5.3.2.2b. A linear static finite element analysis is performed to obtain the member forces of the column. The effective length factor of the column is determined using an eigenvalue buckling analysis and compared to the value presented in the Specifications. A

moment magnifier is then calculated according the Specifications and applied to the moments obtained from the linear static analysis.

9.6.3.1 Step 2a – Linear Static Analysis

A linear static analysis is performed first in order to (1) confirm that the model is capturing the correct behavior of the structure and (2) to obtain member force effects that will later be used to calculate a moment magnifier. The previously described base model is used for the linear static analysis with modifications as described in subsequent sections.

9.6.3.1.1 Load Cases

The results of the linear static analysis are used in the approximate moment magnification procedure of AASHTO LRFD Article 4.5.3.2.2b. In order to utilize the procedure, member force effects must be separated by “sway” and “nonsway” loads. Sway loads are defined as lateral or gravity loads that result in sidesway greater than $l_u/1500$ as calculated by a first order elastic analysis, where l_u is the unsupported length of the member. Nonsway loads are gravity loads that result in no appreciable sidesway as calculated by a first order elastic analysis. In addition, the loads must also be separated by those that are permanent (e.g., dead load) and those that are not permanent (e.g., live load). Therefore, for the linear static analysis, the loads are separated into four load cases, as shown in Table 84. It is expected that the only loads that cause sidesway of the column are the braking forces. All other loads should result in minimal sidesway. However, this must be confirmed by the analysis results. The braking force and live load are the only transient loads. There are no permanent sway loads (based on initial assumptions), but the load case is shown in Table 84 for completeness.

Table 84. Linear static analysis load cases.

Load Case	Applicable Loads
Nonsway – permanent	<ul style="list-style-type: none"> • Self-Weight • Non-composite Dead Load • Composite Dead Load • Wearing Surface
Nonsway – transient	<ul style="list-style-type: none"> • Live load
Sway – permanent	[none]
Sway – transient	<ul style="list-style-type: none"> • Braking

9.6.3.1.2 Analysis and Results Verification

The next step is to run the analysis and verify the results. A qualitative method of verification is to confirm that the deflected shape is reasonable based on the applied loads and boundary conditions. An additional option is to calculate a member force effect or reaction and compare to the analysis output. For this example, the reactions at the base of the drilled shaft are approximated by hand calculations and compared to the results of the linear static analysis.

A comparison of the hand calculated base reactions to the results of the finite element analysis is shown below. The vertical reaction is the sum of the applied vertical bearing reactions from Table 83 and the self-weight of the pier.

$$\begin{aligned}
R_{\text{bearing}} &= \text{factored vertical bearing reactions} \\
&= (626 \text{ kips} + 43 \text{ kips} + 97 \text{ kips} + 492 \text{ kips})(2 \text{ exterior bearings}) + (589 \text{ kips} \\
&\quad + 37 \text{ kips} + 97 \text{ kips} + 576 \text{ kips})(3 \text{ interior bearings}) \\
&= 6413 \text{ kips}
\end{aligned}$$

$$\begin{aligned}
R_{\text{pier cap}} &= \text{self-weight of the pier cap} \\
&= \left\{ (1/2)[(26 \text{ ft}-3 \text{ inches}) - (5 \text{ ft}-3 \text{ inches})](9 \text{ ft}) + [(26 \text{ ft}-3 \text{ inches}) - (5 \text{ ft}-3 \text{ inches})](6 \text{ ft}-5 \text{ inches}) \right\} \times (7 \text{ ft})(2)(0.145 \text{ k/ft}^3) \\
&= 469 \text{ kips}
\end{aligned}$$

$$\begin{aligned}
R_{\text{column}} &= \text{self-weight of the column} \\
&= [\pi(10 \text{ ft} - 6 \text{ inches})^2/4](31 \text{ ft})(0.145 \text{ k/ft}^3) + [\pi(11 \text{ ft}-0 \text{ inches})^2/4](102 \text{ ft}-3 \frac{1}{2} \text{ inches} + 15 \text{ ft}-5 \text{ inches}) \times (0.145 \text{ k/ft}^3) \\
&= 2011 \text{ kips}
\end{aligned}$$

$$\begin{aligned}
R_{\text{sw}} &= \text{factored self-weight of the pier} \\
&= 1.25[R_{\text{pier cap}} + R_{\text{column}}] \\
&= 1.25(469 \text{ kips} + 2011 \text{ kips}) \\
&= 3100 \text{ kips}
\end{aligned}$$

$$\begin{aligned}
R &= \text{factored vertical reaction} \\
&= R_{\text{bearing}} + R_{\text{sw}} \\
&= 6413 \text{ kips} + 3100 \text{ kips} \\
&= 9513 \text{ kips}
\end{aligned}$$

The longitudinal reaction is the sum of the horizontal forces which, in this case, is comprised only of the braking force reactions on the bearings. The moment about the transverse axis at the base of the pier is a result of the longitudinal braking force.

$$\begin{aligned}
F_{x \text{ bearing}} &= \text{Factored longitudinal bearing reaction} \\
&= (22.5 \text{ kips})(5 \text{ bearings}) \\
&= 112.5 \text{ kips}
\end{aligned}$$

$$\begin{aligned}
V_{x \text{ base}} &= \text{shear at the base of the column in the longitudinal direction} \\
&= F_{x \text{ bearing}} \\
&= 112.5 \text{ kips}
\end{aligned}$$

$$\begin{aligned}
M_{y \text{ base}} &= \text{moment at the base of the column about the transverse axis} \\
&= (F_{x \text{ bearing}})(\text{moment arm}) + M_{y \text{ bearing}} + R_{\text{bearing}}(\text{eccentricity}) \\
&= (112.5 \text{ kips})(31 \text{ ft} + 102 \text{ ft}-3 \frac{1}{2} \text{ inches} + 15 \text{ ft}-5 \text{ inches}) \\
&= 16730 \text{ k-ft}
\end{aligned}$$

A comparison of the base reactions calculated by hand to those obtained from the linear static analysis show good agreement.

Base Reactions	Hand Calculated	Analysis Software	% Difference
Vertical reaction (k)	9,513	9,726	2.2%
Longitudinal Shear (k)	112.5	112.5	0.0%
Moment about Transverse Axis (k-ft)	16,730	16,730	0.0%

The hand calculated values and the values from the analysis software for the base reactions are all within 2 percent of each other. The 2 percent difference in the vertical reaction between the analysis software and the hand calculation can be attributed to the pier cap and column elements overlapping at the top of the column within the model, as shown in Figure 347. Therefore, the linear static analysis is producing reasonable results.

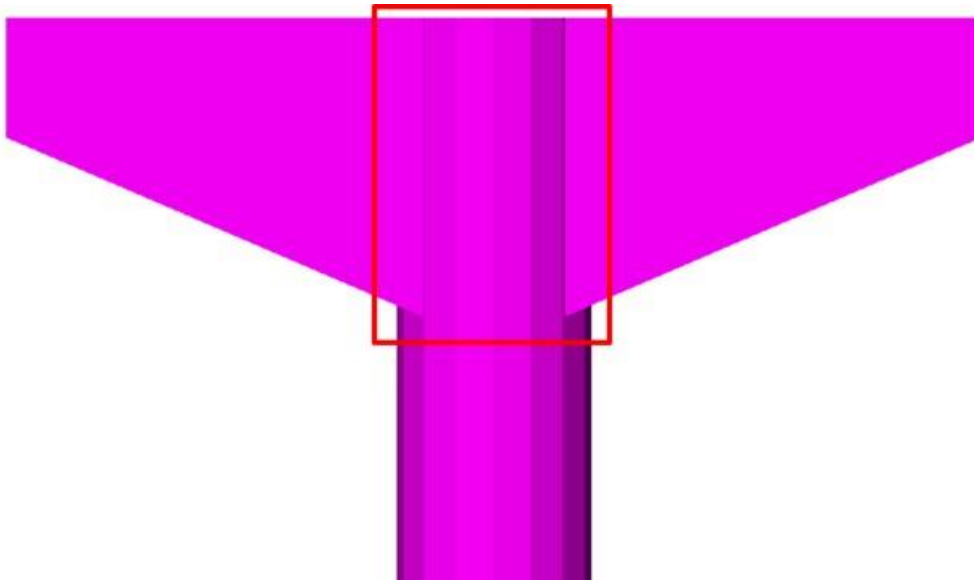
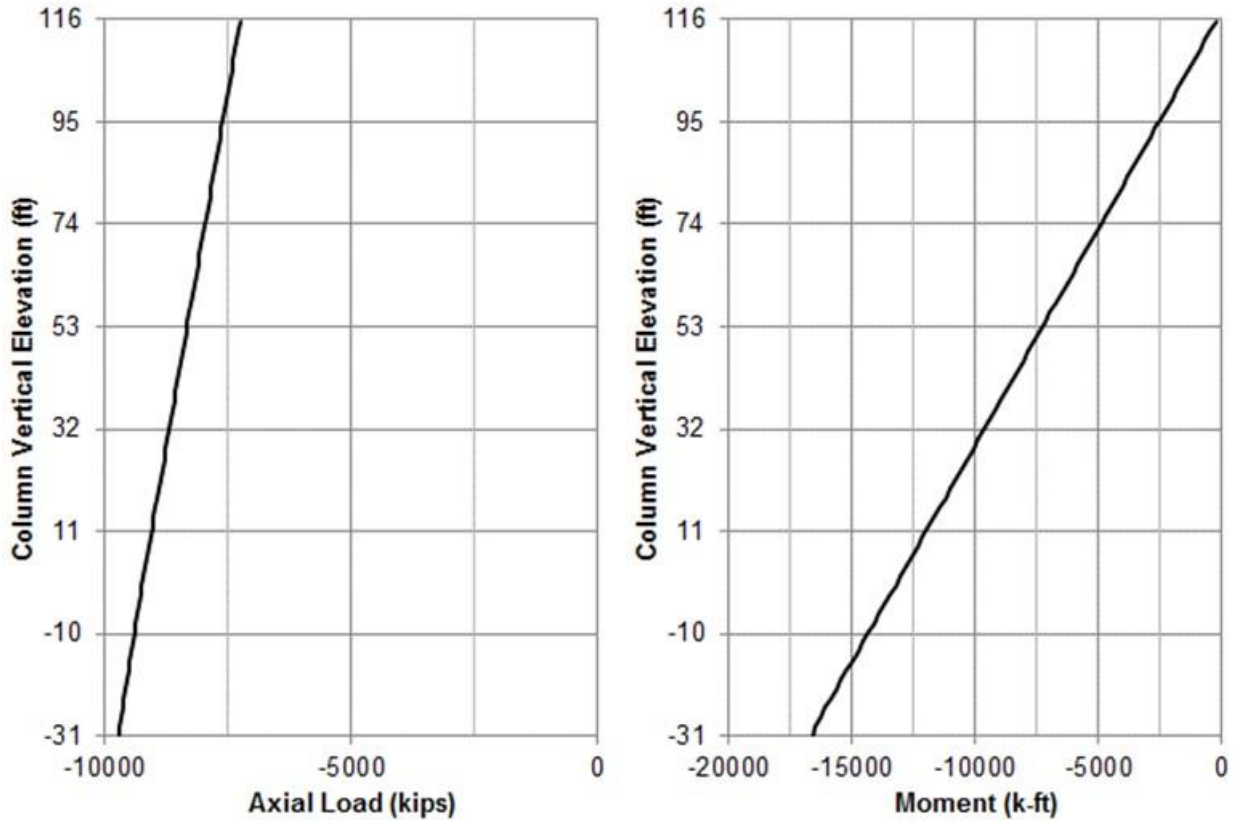


Figure 347. Illustration. Overlap of pier cap and column elements.

9.6.3.1.3 Results

The force effects in the column and drilled shaft along the member length, in particular the axial force and bending moment about the transverse axis, are the results of interest for this example. Graphs of the axial load and bending moment along the length of the member are shown in Figure 348. The axial load at the top of the column is about 7,000 kips in compression, which is approximately equal to the self-weight of the pier cap plus the vertical bearing reactions. The axial load increases with depth due to the self-weight of the column to a maximum value of nearly 10,000 kips in compression at the base of the column. The moment diagram is that of a cantilever beam. The maximum moment occurs at the base of the column and is approximately equal to 17,000 kip-ft.



(a) Subfigure showing axial load from linear static analysis.

(b) Subfigure showing bending moment from linear static analysis.

Figure 348. Graphs. Compound figure showing axial load and bending moment diagrams from the linear static analysis.

9.6.3.2 Step 2b – Eigenvalue Analysis

Stability and second order effects can be evaluated using an eigenvalue analysis and a large displacement analysis (discussed later). An eigenvalue analysis provides the theoretical critical buckling load, also referred to as the Euler buckling load, of a section without consideration of imperfections such as out-of-straightness. The Euler buckling load, P_e , is given as Equation (64).

$$P_e = \frac{\pi^2 EI}{(Kl_u)^2} \quad (64)$$

where E is the material modulus of elasticity, I is the moment of inertia of the section about the axis under consideration, K is the effective length factor, and l_u is the unbraced length of the member. The I used to calculate the Euler buckling load is the $I_{effective}$ from Table 81, in order to account for the stiffness at failure. For comparison, the eigenvalue analysis is performed twice: once with the AASHTO expressions for effective moment of inertia and a second time using the ACI expressions for effective moment of inertia. The effective length factor relates the buckled shape of the member to that of the Euler pinned end column. Many specifications provide

effective length factors for columns with idealized support conditions, such as AASHTO LRFD Article 4.6.2.5. The effective length factor can also be calculated for a given column by performing an eigenvalue analysis to determine the Euler buckling load and solving for the effective length factor using Equation (64).

For this example, an effective length factor is calculated using the results of an eigenvalue analysis and compared to the theoretical value presented in the specifications.

9.6.3.2.1 Loads

The purpose of the eigenvalue analysis is to determine the Euler buckling load and subsequently the effective length factor. An eigenvalue buckling analysis accounts for the effective decrease in bending stiffness caused by axial loads. Therefore, only loads which induce axial forces theoretically need to be applied for the eigenvalue analysis. The results of an eigenvalue analysis are factors that, when multiplied by the applied axial load, give the Euler buckling load. Therefore, the magnitude of the applied loading can be arbitrary, but the relationships, i.e. ratios, between the loads applied do need to be correct. Often, as is the case with this example, a unit load is chosen for the applied axial load such that the lowest eigenvalue will be equal to the Euler buckling load. In this example, a downward vertical load is applied at the node corresponding to the pier cap to column connection with a magnitude of 1 kip, as shown in Figure 349.

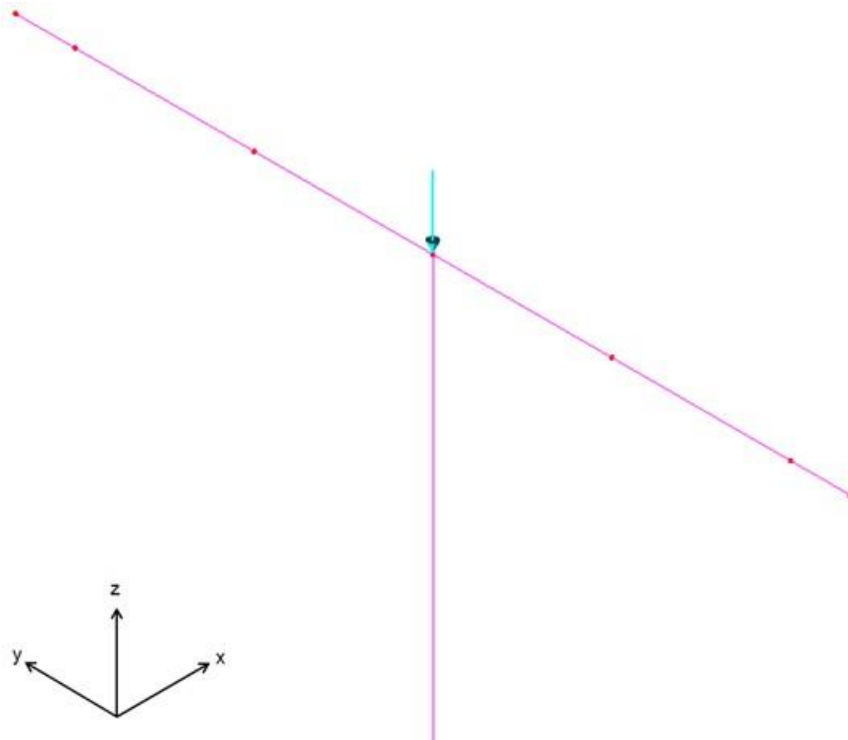


Figure 349. Illustration. Applied loads on the pier cap for eigenvalue analysis.

9.6.3.2.2 Analysis and Results Verification

The procedure for running an eigenvalue analysis often varies between programs and software documentation should be consulted for specific instructions. There are typically user options for

analysis methods of solution, which buckling modes to consider, and the number of buckling modes to solve for. For a buckling analysis, as is the case with this example, the mode of interest is the first mode. This mode corresponds to the lowest eigenvalue, or the lowest load that results in elastic buckling.

The results of the eigenvalue analysis are verified prior to calculating the effective length factor. The deflected shape of the column corresponding to the first eigenvalue, or Euler buckling load, is shown in Figure 350. As expected, the deflected shape is that of a buckled cantilevered column subject to axial load.

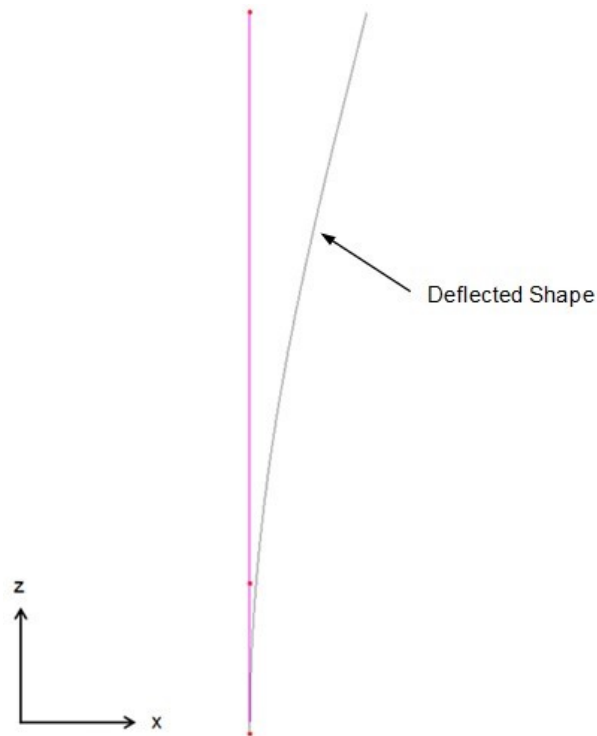


Figure 350. Illustration. Deflected shape of the column (in grey) corresponding to the Euler buckling load.

As an additional verification, the Euler buckling load is calculated and compared to the value obtained from the finite element eigenvalue analysis. First, the theoretical Euler buckling load is determined using Equation (64), the appropriate material properties from Table , and the AASHTO effective moment of inertia values Table 81. Since the effective moment of inertia is not constant over the length of the column, a weighted average is used to approximate the effective moment of inertia.

$$\begin{aligned} E &= \text{concrete modulus of elasticity} \\ &= 556589 \text{ ksf} \end{aligned}$$

$$\begin{aligned}
I_{\text{effective AASHTO}} &= \text{effective moment of inertia} \\
&= [(238.7 \text{ ft}^4)(117 \text{ ft}-8\frac{1}{2} \text{ inches})+(247.0 \text{ ft}^4)(31 \text{ ft}-0 \text{ inches})]/[(117 \text{ ft}-8\frac{1}{2} \text{ inches})+(31 \text{ ft}-0 \text{ inches})] \\
&= 240.4 \text{ ft}^4 \\
\\
l_u &= \text{unbraced length} \\
&= 148 \text{ ft } 8 \frac{1}{2} \text{ inches} \\
\\
K &= \text{effective length factor (theoretical)} \\
&= 2 \\
\\
P_e &= \text{Euler buckling load} \\
&= [\pi^2(556589 \text{ ksf})(240.4 \text{ ft}^4)]/[2(148 \text{ ft } 8 \frac{1}{2} \text{ inches})]^2 \\
&= 14931 \text{ kips}
\end{aligned}$$

The Euler buckling load from the eigenvalue analysis is 15,014 kips when using the AASHTO expressions for effective stiffness. The calculation is performed a second time using the ACI expressions for effective stiffness.

$$\begin{aligned}
E &= \text{concrete modulus of elasticity} \\
&= 556589 \text{ ksf} \\
\\
I_{\text{effective ACI}} &= \text{effective moment of inertia} \\
&= [(500.5 \text{ ft}^4)(117 \text{ ft}-8\frac{1}{2} \text{ inches})+(522.1 \text{ ft}^4)(31 \text{ ft}-0 \text{ inches})]/[(117 \text{ ft}-8\frac{1}{2} \text{ inches})+(31 \text{ ft}-0 \text{ inches})] \\
&= 505.0 \text{ ft}^4 \\
\\
l_u &= \text{unbraced length} \\
&= 148 \text{ ft } 8\frac{1}{2} \text{ inches} \\
\\
K &= \text{effective length factor (theoretical)} \\
&= 2 \\
\\
P_e &= \text{Euler buckling load} \\
&= [\pi^2(556589 \text{ ksf})(500.5 \text{ ft}^4)]/[2(148 \text{ ft } 8 \frac{1}{2} \text{ inches})]^2 \\
&= 31361 \text{ kips}
\end{aligned}$$

The Euler buckling load calculated from the eigenvalue analysis using the ACI effective stiffness expressions is 31553 kips. There is good agreement between the eigenvalue analysis and the hand calculations based on theory, with a difference of about 0.5 percent between the values when using either the AASHTO or ACI effective stiffness expressions.

9.6.3.2.3 Effective Length Factor

The effective length factor, K , is calculated based on the results of the eigenvalue analysis and compared to the theoretical value. Rearranging Equation (64) and solving for K gives

$$K = [(\pi^2 EI/P_e)^{1/2}]/l_u$$

Using the AASHTO expressions for effective stiffness, K is calculated as

$$\begin{aligned} K &= \{[(\pi^2(556589 \text{ ksf})(240.4 \text{ ft}^4)/(15014 \text{ kips}))^{1/2}]/(148 \text{ ft } 8 \frac{1}{2} \text{ inches}) \\ &= 1.99 \end{aligned}$$

Similarly, the K value calculated using the ACI expressions for effective stiffness is given as

$$\begin{aligned} K &= \{[(\pi^2(556589 \text{ ksf})(505.0 \text{ ft}^4)/(31553 \text{ kips}))^{1/2}]/(148 \text{ ft } 8 \frac{1}{2} \text{ inches}) \\ &= 1.99 \end{aligned}$$

There is a negligible difference between the theoretical K value and the value calculated from the eigenvalue analysis using both the AASHTO and ACI expressions for effective stiffness.

9.6.3.3 Step 2c – Moment Magnification

The AASHTO LRFD Specifications allow for second order effects to be approximated using a moment magnifier when the slenderness ratio, Kl_u/r , falls within certain limits. Per AASHTO LRFD Article 5.7.4.3, second order effects can be neglected when Kl_u/r is less than 22. In addition, when Kl_u/r is less than 100, the moment magnification procedure may be used to approximate the second order effects. The moment magnification procedure outlined in AASHTO LRFD Article 4.5.3.2.2b determines the factored moment including second order effects, M_c , by applying magnifiers to the linear static moments as shown in Equation (65).

$$M_c = \delta_b M_{2b} + \delta_s M_{2s} \quad (65)$$

where M_{2b} is the moment on the member due to factored gravity loads that result in no appreciable sidesway calculated by first order analysis, M_{2s} is the moment on the member due to factored lateral or gravity loads that result in sidesway greater than $l_u/1500$ calculated by first order analysis, and δ_b and δ_s are the moment magnifiers for the braced and unbraced deflection modes, respectively. The moment magnifiers are calculated according to Equations (66) and (67), respectively.

$$\delta_b = \frac{C_m}{1 - \frac{P_u}{\phi_k P_e}} \quad (66)$$

$$\delta_s = \frac{1}{1 - \frac{\Sigma P_u}{\phi_k \Sigma P_e}} \quad (67)$$

where C_m is the moment gradient coefficient, P_u is the factored axial load, ϕ_k is the stiffness reduction factor (taken as 0.75 for concrete members and 1.0 for steel and aluminum members), and P_e is the Euler buckling load as given by Equation (64). The summation terms given in Equation (67) are used when the sidesway of a structure is resisted by more than one compression member.

Calculation of the moment magnification procedure is included below. The procedure is first performed using the AASHTO expressions, then repeated using the ACI expressions. Typically, the location(s) of maximum force effects is a point of interest and, therefore, the node at the base of the drilled shaft where maximum axial load and bending moment in the column occur was chosen for the sample calculation.

From the results of the linear elastic analysis, the loads at the base of the column are

$$P_u = -9726 \text{ kips}$$

$$M_{2b \text{ perm}} = 0 \text{ k-ft}$$

$$M_{2b \text{ trans}} = 0 \text{ k-ft}$$

$$M_{2s \text{ perm}} = 0 \text{ k-ft}$$

$$M_{2s \text{ trans}} = -16730 \text{ k-ft}$$

Check the slenderness ratio of the column and compare to the limits from the specifications.

$$K = 1.99$$

$$l_u = 148 \text{ ft } 8 \frac{1}{2} \text{ inches}$$

$$\begin{aligned} r &= \text{radius of gyration} = \text{diameter}/4 \\ &= (10 \text{ ft}-6 \text{ inches})/4 \\ &= 2 \text{ ft}-7 \frac{1}{2} \text{ inches} \end{aligned}$$

$$\begin{aligned} Kl_u/r &= (1.99)(148 \text{ ft}-8 \frac{1}{2} \text{ inches})/(2 \text{ ft}-7 \frac{1}{2} \text{ inches}) \\ &= 113.0 \end{aligned}$$

The column slenderness ratio of 113.0 is greater than the limit of 100 imposed by AASHTO LRFD Article 5.7.4.3 for the use of the moment magnification procedure. However, for the purpose of this example, the moment magnification procedure will still be used in order to compare the results of the procedure to those from a non-linear analysis.

First, determine the values of the variables needed to calculate the stiffness using the AASHTO expressions.

$$\begin{aligned} A_{st} &= \text{area of longitudinal reinforcing steel} \\ &= (1.56 \text{ in}^2/\text{bar})(44 \text{ bundles})(3 \text{ bars per bundle}) \\ &= 205.9 \text{ in}^2 \end{aligned}$$

$$\begin{aligned} \gamma h &= \text{center-to-center of longitudinal reinforcement} \\ &= (\text{column diameter}) - (\text{clear cover}) - (\text{ties}) - (\text{one bar diameter}) \\ &= 126 \text{ in} - 2(3 \text{ in}) - 2(3/4 \text{ inches}) - 1.41 \text{ in} \end{aligned}$$

$$= 117.1 \text{ in}$$

$$\begin{aligned} I_s &= \text{Moment of inertia of longitudinal steel about centroidal axis} \\ &= 0.125A_{st}(\gamma h)^2 \text{ for a circular column (MacGregor and White 2012)} \\ &= 0.125(205.9 \text{ in}^2)(117.1 \text{ in})^2 \\ &= 352897 \text{ in}^4 \\ &= 17.02 \text{ ft}^4 \end{aligned}$$

The ratio β_d accounts for creep and is calculated for the braced mode as

$$\begin{aligned} \beta_{db} &= (M_{2b \text{ perm}})/(M_{2b} + M_{2s}) \\ &= (0 \text{ k-ft})/[(0 \text{ k-ft}) + (0 \text{ k-ft}) + (0 \text{ k-ft}) + (-16621 \text{ k-ft})] \\ &= 0.0 \end{aligned}$$

Substituting the variables into (58) and (59) gives

$$\begin{aligned} EI &= [(556589 \text{ ksf})(596.7 \text{ ft}^4)/5 + (4176000 \text{ ksf})(17.02 \text{ ft}^4)]/(1.0) \\ &= 1.375 \times 10^8 \text{ kip-ft}^2 \end{aligned}$$

$$\begin{aligned} EI &= [(5565894 \text{ ksf})(596.7 \text{ ft}^4)/2.5]/(1.0) \\ &= 1.328 \times 10^8 \text{ k-ft}^2 \end{aligned}$$

Per AASHTO LRFD Article 5.7.4.3, the larger value calculated from Equations (58) and (59) is to be used; therefore, the stiffness calculated per Equation (58) controls. The stiffness is then substituted into Equation (64) to calculate the Euler buckling load. Two separate calculations are made for the Euler buckling load: one for the calculation of δ_b with the factor K for braced frames and one for the calculation of δ_s with the factor K for unbraced frames.

$$K_b = 0.7 \quad \text{(braced)}$$

$$K_s = 1.99 \quad \text{(unbraced)}$$

$$\begin{aligned} P_e &= [\pi^2(1.375 \times 10^8 \text{ k-ft}^2)]/[0.7(148 \text{ ft } 8 \frac{1}{2} \text{ inches})]^2 \quad \text{(braced)} \\ &= 125227 \text{ kips} \end{aligned}$$

$$\begin{aligned} P_e &= [\pi^2(1.375 \times 10^8 \text{ k-ft}^2)]/[1.99(148 \text{ ft } 8 \frac{1}{2} \text{ inches})]^2 \quad \text{(unbraced)} \\ &= 15427 \text{ kips} \end{aligned}$$

Next, the moment magnifiers are calculated using Equation (66) and Equation (67).

$$\begin{aligned} \delta_b &= 1/\{1 - 9726 \text{ kips}/[(0.75)(125227 \text{ kips})]\} \\ &= 1.12 \end{aligned}$$

$$\begin{aligned} \delta_s &= 1/\{1 - 9726 \text{ kips}/[(0.75)(15427 \text{ kips})]\} \\ &= 6.28 \end{aligned}$$

The magnified moment is then calculated using Equation (65).

$$\begin{aligned} M_c &= 1.12(0 \text{ k-ft}) + 6.27(-16730 \text{ k-ft}) \\ &= -104991 \text{ k-ft} \end{aligned}$$

The large value for δ_s indicates the column is close to the stability failure limit. This is due to the factored axial load being close in magnitude to the Euler buckling load. The Euler buckling load is significantly influenced by the stiffness, EI , of the section. The relationships for the stiffness presented in the AASHTO expressions are only accurate for certain eccentricity ratios and axial load values (ACI 318-14) and, for this example, result in an effective stiffness that is approximately 41 percent of the gross stiffness.

The moment magnifiers are recalculated using the ACI expressions. The initial analysis assumes an initial stiffness of $0.70E_cI_g$ for the column per the recommendation of Khuntia and Ghosh (2004a, 2004b). Since the pier is a determinate first-order elastic system, the effective stiffness need only be calculated once using Equation (60). The linear elastic analysis is then repeated using the effective stiffness from Equation (60) in order to check deflections.

$$\begin{aligned} P_0 &= 0.85F_c'(A_g - A_{st}) + f_y A_{st} \\ &= 0.85(648 \text{ ksf})(86.59 \text{ ft}^2 - 1.43 \text{ ft}^2) + (8640 \text{ ksf})(1.43 \text{ ft}^2) \\ &= 59261 \text{ kips} \\ I &= 0.35I_g \leq (0.8 + 25A_{st}/A_g)[1 - M_u/(P_u h) - 0.5P_u/P_0]I_g \leq 0.875I_g \\ &= 0.35(596.7 \text{ ft}^4) \leq [0.8 + 25(1.43 \text{ ft}^2)/(86.59 \text{ ft}^2)]\{1 - (16730 \text{ k-ft})/[(9726 \text{ kips})(10.5 \text{ ft})] - 0.5(9726 \text{ kips})/(59261 \text{ kips})\}(596.7 \text{ ft}^4) \leq 0.875(596.7 \text{ ft}^4) \\ &= 208.8 \text{ ft}^4 \leq 545.7 \text{ ft}^4 \leq 522.1 \text{ ft}^4 \\ &= 522.1 \text{ ft}^4 \end{aligned}$$

For the sway mode, the ratio β_d is zero because there are no permanent sway loads.

$$\begin{aligned} \beta_{ds} &= (M_{2s \text{ perm}})/(M_{2b} + M_{2s}) \\ &= (0 \text{ k-ft})/[(0 \text{ k-ft}) + (0 \text{ k-ft}) + (0 \text{ k-ft}) + (-16730 \text{ k-ft})] \\ &= 0.0 \end{aligned}$$

Using the variables calculated above, the effective stiffness, Euler buckling loads, and moment magnifiers are determined as

$$\begin{aligned} EI &= [(556589 \text{ ksf})(522.1 \text{ ft}^4)]/(1.0) \\ &= 2.906 \times 10^8 \text{ k-ft}^2 \\ P_e &= [\pi^2(2.906 \times 10^8 \text{ k-ft}^2)]/[0.7(148 \text{ ft } 8 \frac{1}{2} \text{ inches})^2] && \text{(braced)} \\ &= 264669 \text{ kips} \\ P_e &= [\pi^2(2.906 \times 10^8 \text{ k-ft}^2)]/[1.99(148 \text{ ft } 8 \frac{1}{2} \text{ inches})^2] && \text{(unbraced)} \\ &= 32605 \text{ kips} \\ \delta_b &= 1/\{1 - 9726 \text{ kips}/[(0.75)(264669 \text{ kips})]\} \\ &= 1.05 \end{aligned}$$

$$\begin{aligned}\delta_s &= 1/\{1 - 9726 \text{ kips}/[(0.75)(32605 \text{ kips})]\} \\ &= 1.66\end{aligned}$$

The moment magnifiers are smaller than those previously calculated due to the increase in stiffness using the refined moment of inertia given in Equation (61). The effective stiffness calculated using the ACI expressions is approximately 88 percent of the gross stiffness, compared to the 41 percent previously calculated using the AASHTO expressions. The magnified moment at the base of the column is calculated using Equation (65).

$$\begin{aligned}M_c &= 1.05(0 \text{ k-ft}) + 1.66(-16730 \text{ k-ft}) \\ &= -27779 \text{ k-ft}\end{aligned}$$

Finally, the deflections are checked for the assumed nonsway load cases from Table 84. The nonsway deflection limit is 1.19 inches ($l_u/1500$) calculated per AASHTO LRFD 4.5.3.2.2b. From the results of the analysis, there is no longitudinal deflection at the top of the column caused by the nonsway loads. Therefore, it is not necessary to revise the previously assumed nonsway loads into sway loads.

Note that for this example the summation terms in Equation (67) are only comprised of those for Pier 2 because it is the only support that resists sidesway and, therefore, acts independently from the other pier and the abutments. If an additional support resisted sidesway, then the summations of the factored axial loads and Euler buckling loads of both columns would be used in Equation (67). The procedure for calculating the magnified moment at other nodes along the length of the column is similar.

9.6.4 Step 3 – Large Deflection Non-linear Analysis

A large deflection non-linear analysis is performed to account for second order effects that the column is subjected to as a result of the applied loads and deformations. Unlike an eigenvalue analysis, a geometric non-linear analysis accounts for the effect of deformations on the structural behavior. The deflected shape and corresponding magnitudes of deformations from the previously performed eigenvalue analysis are used as initial inputs for the non-linear analysis. The non-linear response of the column is then solved for through an iterative solution.

9.6.4.1 Step 3a – Non-linear Analysis Model

9.6.4.1.1 Member Stiffness

Similar to the moment magnification procedure, the stiffness of the concrete members used in the model should reflect the expected stiffness of the pier at a given load level (e.g., strength or service). The stiffness of a concrete member often varies along the length due to variable degrees of cracking, changes in the cross-section, and different amounts of reinforcement. To account for the aforementioned variations and simplify the analysis, an effective stiffness is applied to the member along its entire length. For this example, the effective column stiffness is accounted for using both the AASHTO and ACI expressions in order to be consistent with the moment magnification procedure. The effective moment of inertia values for the column members are shown in Table 85. As was done for the linear static analysis, an initial analysis is performed with an effective column stiffness of $0.70E_cI_g$ when using the ACI expressions. The

results of the initial analysis are then used to calculate a new effective stiffness using the expression for moment of inertia given in Equation (61). The effective stiffness changes because Equation (61) is dependent on the force effects, M_u and P_u , from the results of the analysis, which are in turn dependent on the stiffness used in the analysis. The final member force effects are obtained by iteratively solving for the effective stiffness using Equation (61) until the final value for effective stiffness is within 15 percent of the previous value. For reference, the ACI effective stiffness values from the final iteration are listed in Table 85 along with the previously calculated effective stiffness from the AASHTO expressions.

Table 85. Effective moment of inertia values of the column.

Section Property	Units	Drilled Shaft	Pier Shaft
Effective Moment of Inertia – AASHTO Expressions (Eq. 1 and 2)	ft ⁴	247.0	238.7
Initial Effective Moment of Inertia – ACI Expressions ($0.7I_g$)	ft ⁴	417.7	417.7
Final Effective Moment of Inertia – ACI Expressions (Eq. 4)	ft ⁴	502.1 ($0.84I_g$)	462.5 ($0.78I_g$)

9.6.4.1.2 Loads and Load Cases

The factored loads that were used in the linear static analysis are also used in the non-linear analysis. Note that the nonlinear analysis must use the full factored loads, as superposition and factoring of results is not appropriate.

9.6.4.1.3 Non-linear Controls

Analysis programs often offer a variety of controls when it comes to solving the non-linear problem. For a large deflection non-linear analysis, the controls of interest are typically related to the application of load and convergence. Depending on the analysis program, load incrementation and convergence tolerances can be controlled by the user, automatically controlled by the program, or there may be options for both.

For additional information on non-linear controls refer to Section 5.3.2 and the appropriate program documentation.

9.6.4.1.4 Analysis and Results Verification

Once the appropriate changes have been made for the non-linear model, the analysis can be performed. The execution of the analysis should be monitored for errors, particularly those related to convergence problems.

The results are verified by comparing the moment at the base of the drilled shaft from the non-linear analysis to that obtained from the linear analysis and the moment magnification procedure, as shown in Table 86. For reference, the effective stiffness that was used for each analysis is included in Table 86.

Table 86. Moment and stiffness comparison at the base of the drilled shaft.

	Linear Analysis	Moment Magnification – AASHTO expressions	Moment Magnification – ACI expressions	Non-linear Analysis – AASHTO expressions	Non-linear Analysis – ACI expressions
Moment about Transverse Axis (k-ft)	-16,730	-104,991	-27,779	-33,916	-21,793
Effective Stiffness	1.00E _c I _g	0.41E _c I _g	0.88E _c I _g	0.41E _c I _g	0.84E _c I _g

As expected, the column base moments from the non-linear analyses are greater than the value from the linear analysis. The linear analysis produces the least conservative results for this type of problem. The moment magnification procedure using the AASHTO expressions for stiffness gives the largest column base moment due to the conservative approximation of the member stiffness. The ACI expressions for stiffness result in a magnified column base moment slightly greater in magnitude than that from the non-linear analysis with a similar effective stiffness. The moments calculated in accordance with the moment magnification procedure using both the AASHTO and ACI expressions for effective stiffness are greater in magnitude than their non-linear counterparts. This is expected as the moment magnification procedure has built in assumptions that result in conservative approximations. In addition, the moment magnification procedure is accurate within certain limits for Kl/r . As calculated previously, Kl/r of the column falls outside the limits specified by the specifications; therefore, moments calculated using the moment magnification procedure are expected to be less accurate and more conservative for this example.

A calculation of the theoretical column base moment is performed to more accurately verify the results of the non-linear analyses. The moment including second order effects, M_c , derived based on elastic buckling theory can be expressed in terms of the first order moment, M_o , is given as Equation (68).

$$M_c = \frac{M_o \left(1 + \frac{CP_u}{P_e}\right)}{1 - \frac{P_u}{P_e}} \quad (68)$$

where C is a coefficient that is a function of the shape of the M_o diagram and P_u and P_e are the previously defined factored axial load and Euler buckling load, respectively. P_u at the base of the column and the corresponding P_e calculated using the AASHTO expressions for effective stiffness are used for the sample calculation. M_o at the base of the column is taken from the results of the linear analysis.

$$P_u = 9,726 \text{ kips}$$

$$P_e = 15,427 \text{ kips}$$

$$M_o = -16,730 \text{ k-ft}$$

For a column with a triangular moment diagram with M_o at one end and zero moment at the other end (i.e., a cantilever), C is taken as -0.38 (Wight and MacGregor 2012). The second order moment, M_c , is then calculated as follows.

$$\begin{aligned} M_c &= (-16730 \text{ k-ft})[1-0.38(9726 \text{ kips})/(15427 \text{ kips})]/[1-(9726 \text{ kips})/(15427 \text{ kips})] \\ &= -34428 \text{ k-ft} \end{aligned}$$

As shown in Table 86, M_c from the non-linear analysis using the AASHTO stiffness expressions is -33,916 k-ft. There is about a 1.5 percent difference between the value from the non-linear analysis and the hand calculated values. One source of the difference is that P_e is calculated assuming constant axial load, whereas the nonlinear analysis accounts for the increasing axial load along the column due to selfweight. Therefore, the non-linear analysis is producing reasonable results. A similar verification can be performed for the non-linear analysis that utilizes the ACI expressions for effective stiffness.

9.6.5 Step 4 – Comparison of Results

The results of the linear static analysis, the approximate moment magnification procedures, and the large displacement non-linear analyses are compared to illustrate the differences between analysis methods.

9.6.5.1 Step 4a – Magnified Moment

A graph of the bending moment along the height of the column from the linear static analysis, the magnified moment procedures, and the non-linear analysis are shown in Figure 351. The magnitudes of the moments from the linear analysis are the lowest of all the analysis methods because the non-linear second order effects are not captured in the analysis.

A difference in the moment diagrams is also observed when comparing the assumed effective stiffness. For this example, the smaller effective stiffness calculated using the AASHTO expressions results in larger second order moments in comparison to those calculated using the ACI expressions. A smaller stiffness produces larger deflections and, in turn, the $P-\Delta$ effects are magnified. For the moment magnification procedure, this effect is accounted for through the Euler buckling load (Equation (64)) and subsequently the moment magnifiers (Equations (66) and (67)). For a non-linear analysis, the $P-\Delta$ effects are explicitly accounted for in the analysis.

The differences in bending moment magnitudes between the moment magnification procedure and the non-linear analyses are due to inherent assumptions within the moment magnification procedure. The equations for the moment magnifiers in Equations (66) and (67) are simplified versions of the theoretical expression given in Equation (68). The differences between the equations are Equation (68) includes the $(1+CP_u/P_e)$ term and the stiffness reduction factor, ϕ_k , is added to Equations (66) and (67). Equations (66) and (67) were developed for columns with pinned end conditions ($C = 0.23$) and values of P_u/P_e between -0.18 and 0.25, which results in the $(1+CP_u/P_e)$ term being approximately equal to 1.0 (Wight and MacGregor 2012). Therefore, this term was omitted from Equations (66) and (67). ϕ_k is included in Equations (66) and (67) to account for the variability in the Euler buckling load (Wight and MacGregor 2012). These two modifications to the originally derived Equation (68) result in conservative amplifications of the true second order moment.

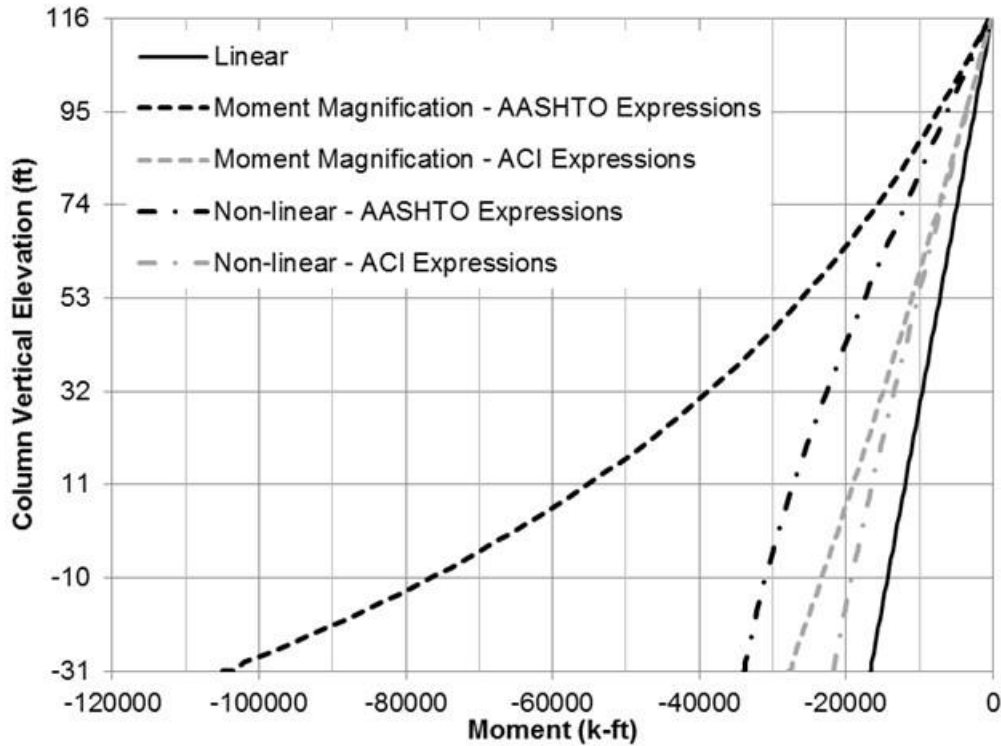
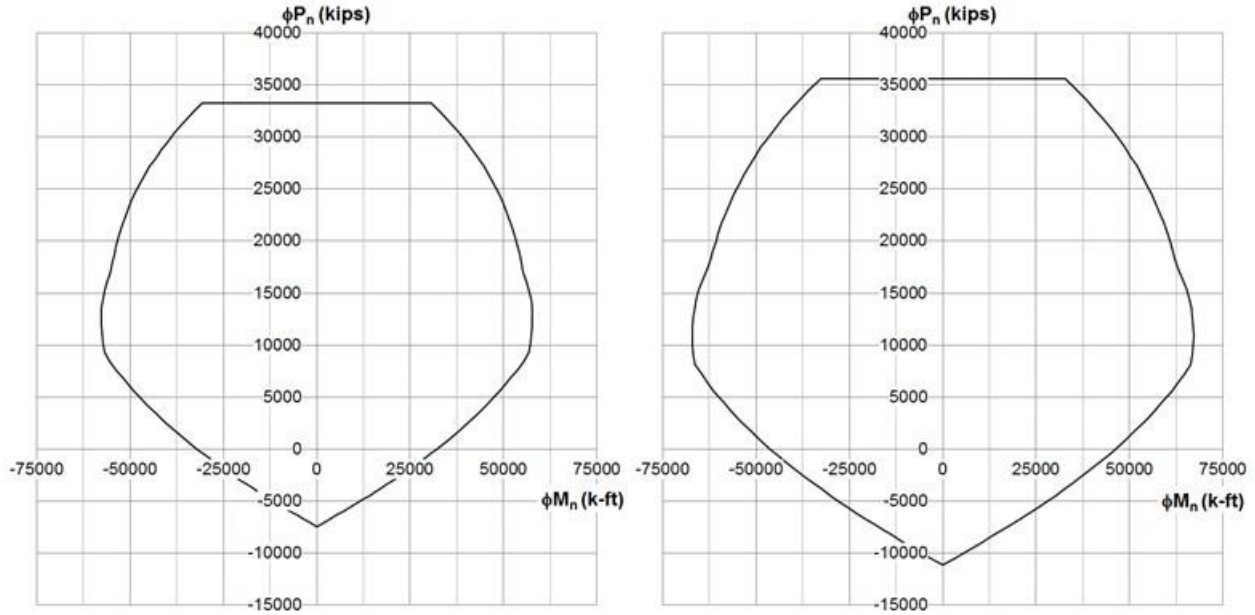


Figure 351. Graph. Comparison of column bending moments from linear static analysis, magnified moment procedure, and non-linear analysis.

9.6.6 Step 5 – Capacity

The capacity of the column is calculated according to the specifications in order to check the adequacy of the column to carry the applied loads. The column carries both axial load and bending moment. Therefore, the interaction of these two force effects needs to be considered when determining the capacity.

The column interaction diagram is calculated following the assumptions of AASHTO LRFD Article 5.7.2. The design axial resistance under axial compression alone is determined per Article 5.7.4.4 of AASHTO LRFD. Other points on the interaction diagram are determined using strain compatibility. Separate interaction diagrams are calculated for the pier shaft and drilled shaft sections of the column due to the differences in longitudinal reinforcement. Development of the interaction diagrams is not included in this example for brevity, but guidance can be found in reinforced concrete text books (e.g., Wight and MacGregor 2012). The complete interaction diagrams are shown in Figure 352.

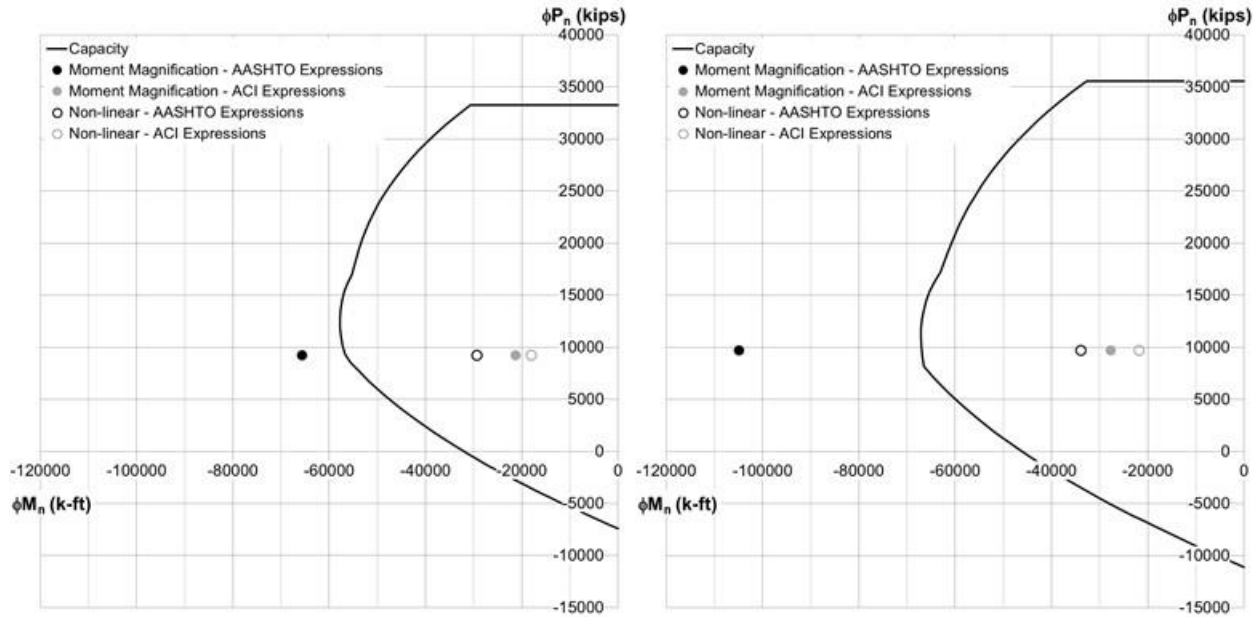


(a) Subfigure showing axial load - moment interaction diagram for pier shaft. (b) Subfigure showing axial load – moment interaction diagram for drilled shaft.

Figure 352. Graphs. Compound figure showing interaction diagrams for the pier shaft and drilled shaft.

9.6.6.1 Step 5b – Capacity vs. Demands

The adequacy of the column to carry the applied loads is checked using the previously calculated second order moments and the interaction diagrams. The controlling demands determined from the moment magnification procedure and the non-linear analyses are plotted with the interaction diagrams in Figure 353. The controlling demand using the moment magnification procedure with the AASHTO expressions for effective stiffness exceeds the capacity for both the pier shaft and drilled shaft sections of the column. The column does meet capacity requirements for the demands determined from the moment magnification procedure with the ACI expressions for effective stiffness and the non-linear analyses using both the AASHTO and ACI effective stiffness expressions, as the demands are well within the limits of the interaction diagrams. As the non-linear analysis is the most accurate of the methods studied in this example, the column is considered to have adequate capacity to carry the applied loads for the load combination analyzed.



(a) Subfigure showing the capacity and demand for the pier shaft.

(b) Subfigure showing the capacity and demand for the drilled shaft.

Figure 353. Graphs. Compound figure comparing the capacity and demand for the (a) pier shaft and (b) drilled shaft.

9.6.7 Conclusions

This example analyzed a slender column with a slenderness ratio outside of AASHTO specification bounds. A second order analysis was performed to account for secondary bending effects using (1) the moment magnification procedures from AASHTO LRFD and ACI 318 and (2) a large deflection non-linear analysis. The bending moments calculated using the moment magnification procedure varied significantly depending on the equation used to calculate the effective stiffness. Table 87 compares the moment calculated at the base of the drilled shaft using the different analysis methods (i.e., linear, moment magnification, and nonlinear) and the different expressions for effective stiffness (i.e., AASHTO, ACI). The most conservative expressions for effective stiffness, the AASHTO expressions, resulted in magnified moments that were more than six times greater than the moments determined from the linear static analysis; while the moments calculated using a more accurate expression for effective stiffness, the ACI expressions, were about 65 percent greater than those determined from the linear static analysis. The non-linear analysis with the AASHTO effective stiffness produced moments that were over two times greater than the linear analysis. When the ACI expressions for effective stiffness were used, the non-linear analysis produced second order moments upwards of 30 percent of those from the linear analysis. In addition, magnified moments calculated using the AASHTO expressions for effective stiffness were more than 3 times greater than the moments determined from the corresponding non-linear analysis. In comparison, the moments calculated using the ACI expressions for effective stiffness were within 30 percent of those determined from the non-linear analysis with a similar stiffness. These differences in second order moments highlight the effect that particular assumptions have on the results of each analysis. The different stiffness values calculated when using the AASHTO and ACI expressions for effective stiffness

result in large variations in second order moments when using the moment magnification procedure. Similarly, inherent assumptions within the moment magnification procedure in relation to the shape of the moment diagram and the variability of the Euler buckling load result in a conservative amplification of the true second order moment.

Table 87. Comparison of calculated moments at the base of the drilled shaft.

Moment Ratio	AASHTO Expressions	ACI Expressions
M_c moment magnification/ M_c linear	6.28	1.66
M_c non-linear/ M_c linear	2.03	1.30
M_c moment magnification/ M_c non-linear	3.09	1.28

This example also emphasizes the need to assess the applicability of a particular analysis method prior to its use. The moment magnification procedure is intended for use in the analysis of slender columns within certain limits for the slenderness ratio (kl_u/r). As calculated previously, the slenderness ratio of the column from this example is 113.0, which is greater than the limit of 100 imposed by AASHTO LRFD. Therefore, caution should be taken when applying the method outside of the specified limits. In addition, the moment magnification procedure becomes less accurate and more impractical as the magnifiers become larger. It is not practical to design the pier in this example for the moment due to the previously calculated sway magnifier, δ_s , of 6.28. Rather, a refined analysis should be performed in lieu of the moment magnification procedure or the section will have to be revised such that the design is more efficient.

The capacity of the column was calculated according to AASHTO LRFD. Interaction diagrams were determined using a strain compatibility approach. The moments calculated from both the moment magnification procedure and the non-linear analyses were checked against the column capacity. The demands calculated using the moment magnification procedure in conjunction with the AASHTO expressions for effective stiffness exceeded the capacity of the column, while the column capacity was adequate to carry the applied loads for the non-linear analyses using both expressions for stiffness as well as the moment magnification procedure using the more accurate ACI expression for effective stiffness.

9.7 Example 7 – Four-Span Continuous, Precast Segmental Concrete Box Girder Bridge

A four-span, precast segmental concrete box girder bridge with eight (8) external post-tensioning tendons is the subject of Example 7. The cross-section consists of one – 39 ft-6 inches wide precast box with span lengths of 165 ft-0 inches between pier centerlines. The precast segments utilize 6.5 ksi concrete. Each external post-tensioning tendon consists of 22-0.6 inches dia. low-relaxation strands with an ultimate strength of 270 ksi; the tendons are symmetrical about the centerline of the cross-section. The typical cross-section is shown in Figure 354 while the section for the deviator segments is shown in Figure 355. Figure 356 shows the cross-section at the pier diaphragm and the location of the external post-tensioning tendon anchorages while Figure 357 shows the expansion pier segment and tendon anchorage locations. Figure 358 shows an elevation view of the pier segments and the crossover of the external post-tensioning tendons. The girder elevations for Spans 1 and 2 are shown in Figures 359 and 360, respectively. Spans 3 and 4 are assumed to be symmetric to Spans 1 and 2.

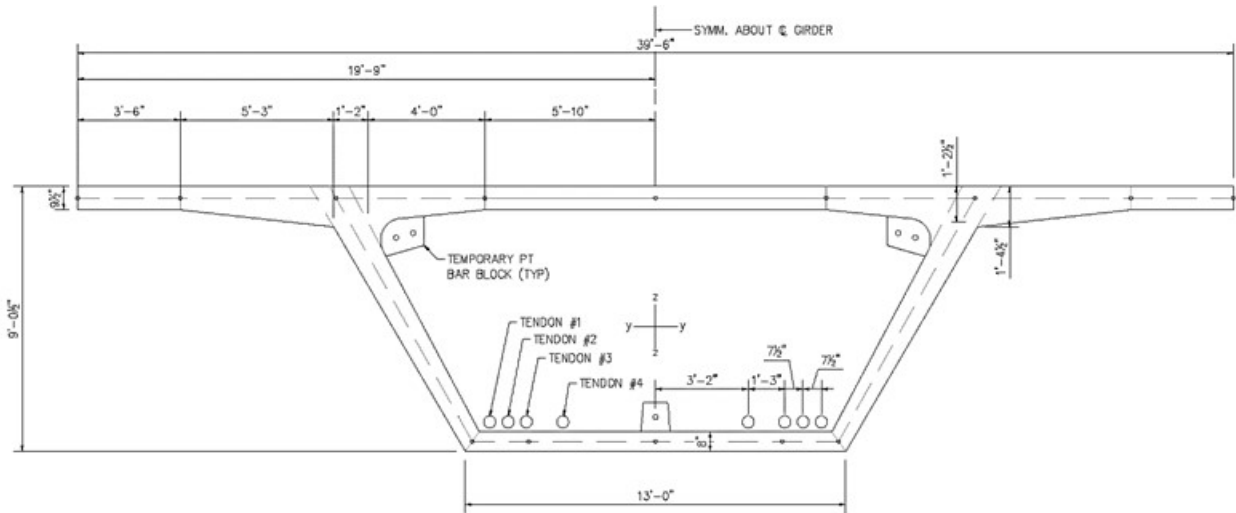


Figure 354. Illustration. Typical segment cross-section.

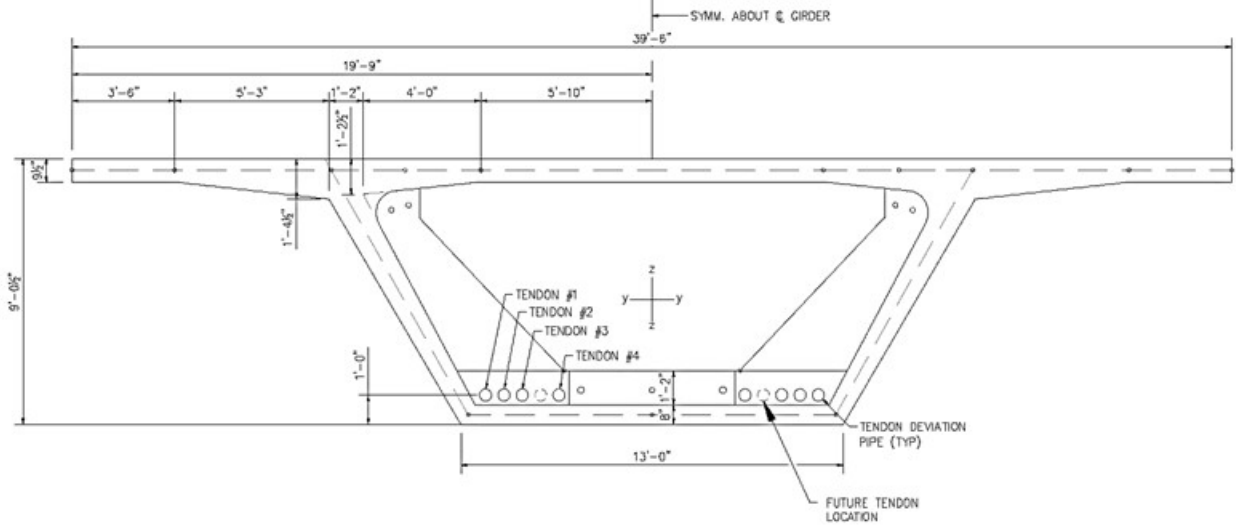


Figure 355. Illustration. Deviator segment cross-section.

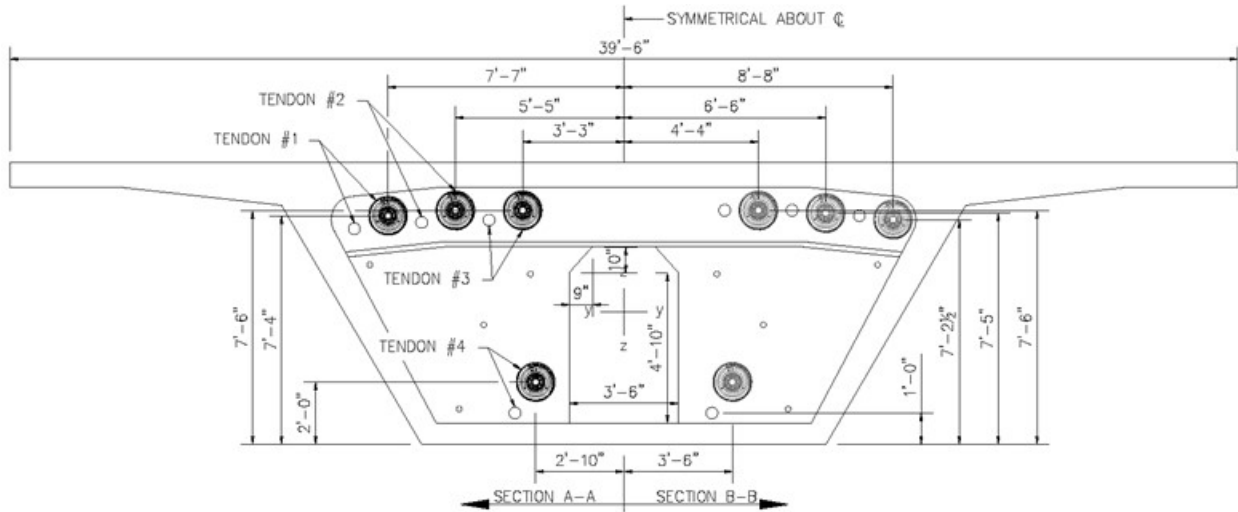


Figure 356. Illustration. Continuity pier segment cross-section.

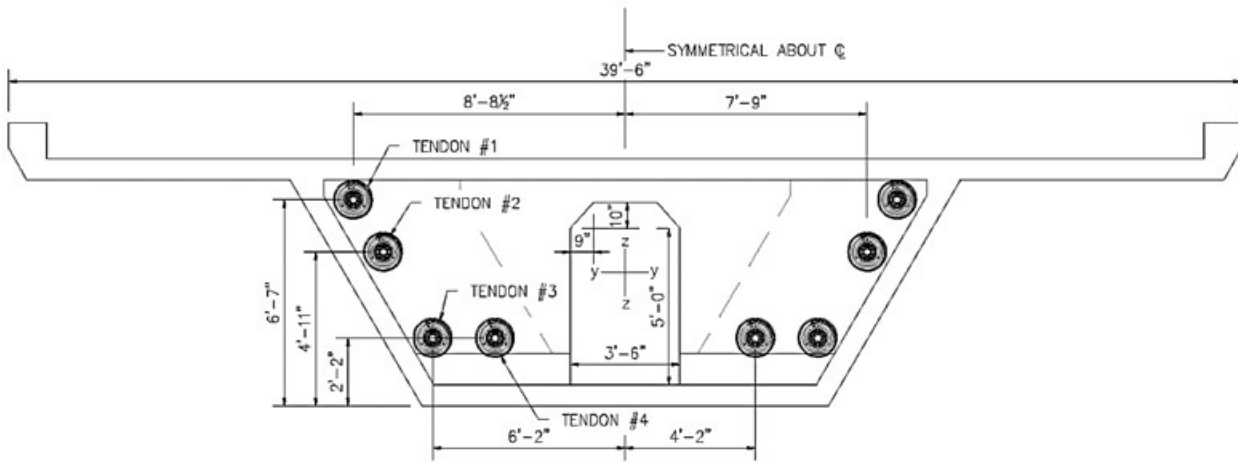


Figure 357. Illustration. Expansion pier segment cross-section.

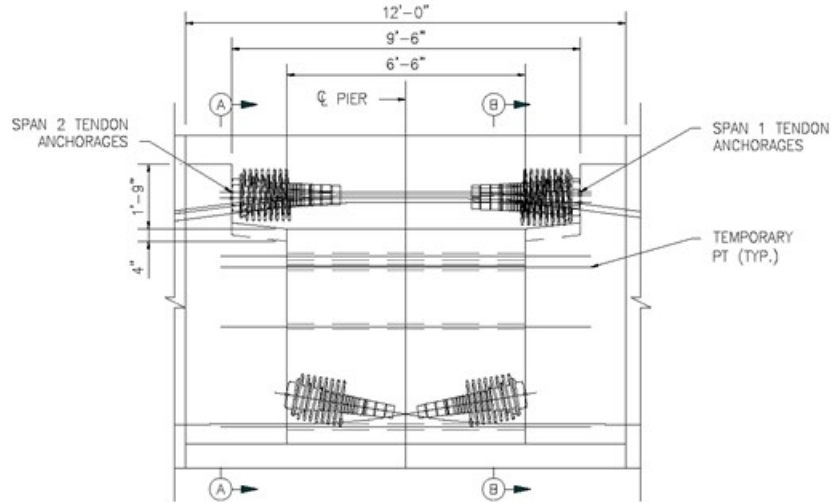


Figure 358. Illustration. Elevation view of pier segments.

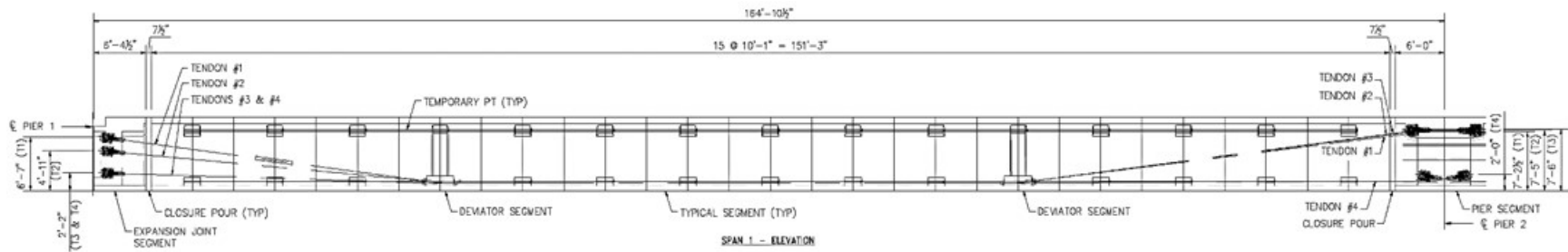


Figure 359. Illustration. Span 1 elevation.

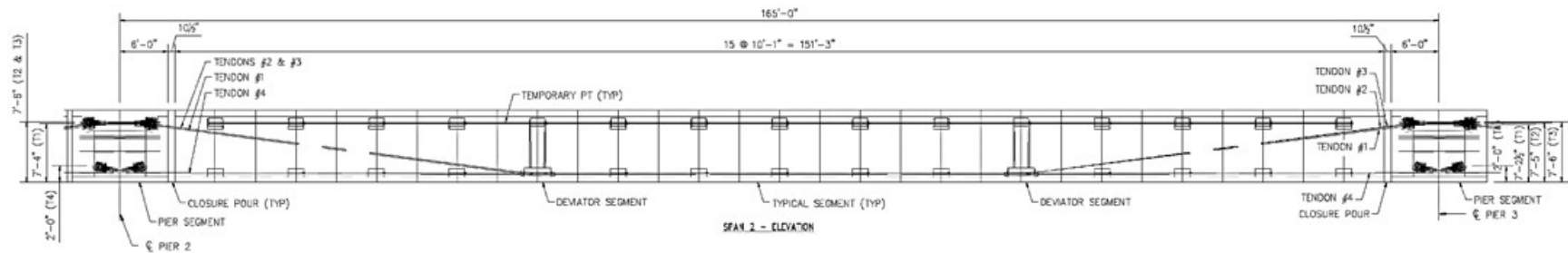


Figure 360. Illustration. Span 2 elevation.

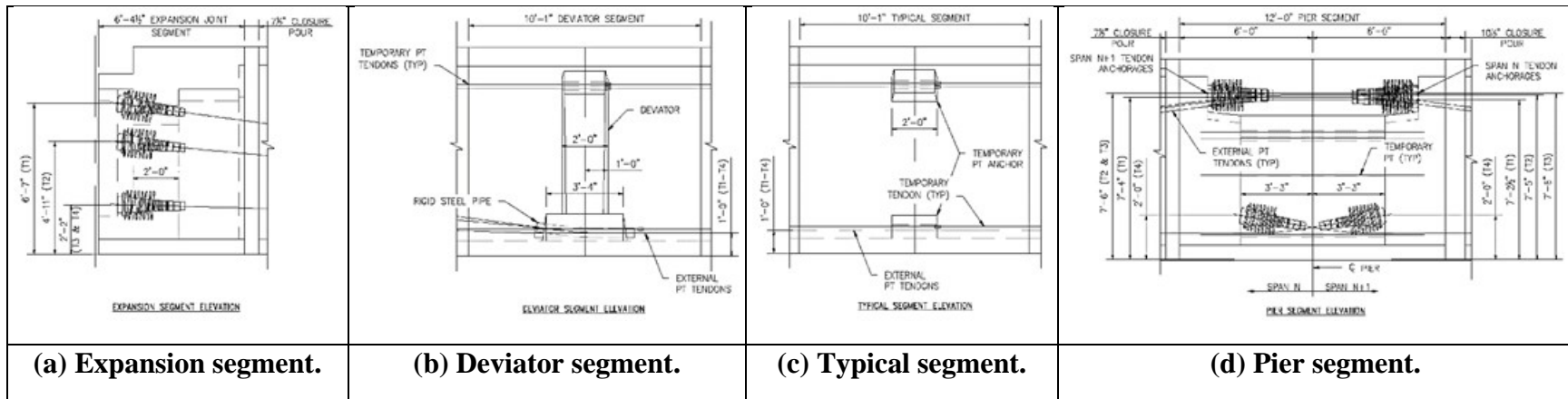


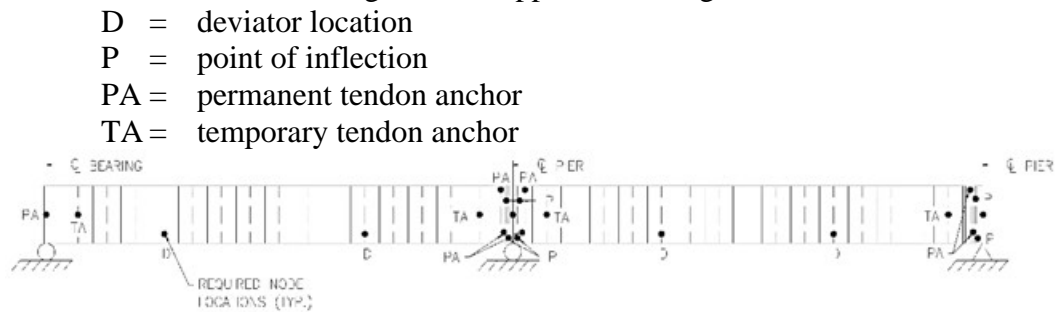
Figure 361. Illustration. Segment elevations.

In this example, Strength I moments will be determined at the mid-point of each span and over the interior supports and Strength I shears will be determined at a distance “d” away from interior and end supports, where “d” is the distance between the extreme compression fiber and the centroid of the tension steel. Only longitudinal force effects are considered in this example; in an actual design, the transverse effects due to self-weight, wearing surface, utilities, and live load would also need to be considered. The longitudinal force effects are found for a spine beam model with the post-tensioning applied using equivalent loads and compared to a shell element model where the tendons are explicitly modeled. The effects of creep and shrinkage are included in both the spine beam and shell element models. In the spine beam model, the effect of creep due to post-tensioning is considered by calculating equivalent loads for each stage of the analysis. The effect of creep due to dead load is accounted for using a non-linear material property for the concrete that considers creep and shrinkage. In the shell element model, the effect of creep under both dead load and post-tensioning is accounted for using a non-linear material property that accounts for creep and shrinkage. The creep and shrinkage of the concrete affects the force in the tendons since they are explicitly modeled.

9.7.1 Spine Beam Model Analysis – Using Equivalent Load Method

The following steps are used to determine the dead and live load moments and shears as well as the moments and shears due to post-tensioning (PT):

1. Create a dead load model. This example differs from the previous examples in that all loads (dead, live, and PT) are applied to the non-composite cross-section; however, separate models are used for dead, PT, and live loads as dead loads are applied to a model that considers creep and shrinkage, PT loads are applied to a model that only considers creep, and live load is applied to a model that does not consider creep or shrinkage.
 - a. Define the location of the box girder. Between nodes used to define the member ends, additional nodes are required to ensure that a sufficient number of elements are present. Additional nodes may also be needed to accommodate changes in cross-section as well as to obtain results at desired locations or for applying various loads. The following notation applies to the figure below:



- b. Define the geometry of the girder cross-section. Cross-section properties can either be calculated by hand as shown in Section 9.1.1.1 or the analysis software used may have the capability to determine cross-section properties based on input provided by the user.
 - c. Define material properties for the girder. The analysis software may have material properties for commonly used materials stored internally; these can be used but should be verified.
 - d. Define support conditions.

- e. Define loads applied to the structure.
 - i. For the members defined in the model, automatic dead load application can be used if the density or unit weight is assigned through the material properties. Alternatively, concentrated or distributed loads that are statically equivalent to the member weight can be used.
 - ii. The barrier dead load is applied as a uniformly distributed load.
 - f. Model construction staging for segmental construction method.
 - g. Run analysis; verify results using simplified methods.
 - h. Extract required results from analysis software.
2. Create post-tensioning model.
 - a. Copy model from Step 1 and save with new name for post-tensioning analysis.
 - b. Modify concrete material properties to remove effects of shrinkage.
 - c. Determine equivalent loads to represent post-tensioning effects including losses and apply to model.
 - d. Run analysis; verify results using simplified methods.
 - e. Extract required results from analysis software.
 3. Create model for live load analysis; this will be the same model as created in Step 1 but will utilize linear elastic material properties for the concrete.
 - a. Copy model from Step 1 or 2 and save with new name to perform live load analysis.
 - b. Change concrete material properties to a linear-elastic material that does not consider creep and shrinkage. Remove construction staging process from analysis.
 - c. Determine the live load pattern for various extreme design load effects. The analysis software may have utilities that help in the determination of the live load placement. Influence lines can be developed to aid in loading generation.
 - d. Run analysis; verify results using simplified methods.
 - e. Extract required results from analysis software.
 4. Combine analysis results for different load cases.

9.7.1.1 Step 1 – Dead Load Model

9.7.1.1.1 Step 1a – Define Girder Location

From Figures 359 and 360, the girder span lengths are shown as 164 ft-10½ inches for Span 1 and 165 ft-0 inches for Span 2; Spans 3 and 4 are assumed to be symmetric about the centerline of Pier 3. The elements used for the girders are beam elements capable of capturing shear deformations. The mesh definition specified elements two feet long; where necessary, such as for the closure pours, shorter elements were used.

9.7.1.1.2 Step 1b – Define Girder Cross-Sections

Several cross-sections exist along the length of the bridge; in this example, only the typical section is used in the analysis. The diaphragm and deviator section properties are provided as the tendon eccentricity depends on the cross-section. In this example, the cross-section properties were determined using a utility within the software used; the section properties are listed in Table 88. Vertical offsets are not required in this example since the girder is assumed to

be prismatic. Element axes are shown in Figures 354 through 357; the element x-axis is in and out of the page.

Table 88. Girder section properties from software.

Section Property	Typical Section	Diaphragm Section	Deviator Section
Cross-section Area (A) (ft ²)	63.2	164.4	109.1
Strong Axis Moment of Inertia (I _{yy}) (ft ⁴)	631.2	1173.2	1070.7
Weak Axis Moment of Inertia (I _{zz}) (ft ⁴)	6584	9225	8217
Torsion Constant (J _{xx}) (ft ⁴)	1275	1385	15404
Shear Area in y direction (A _{vy}) (ft ²)	47.9	83.4	64.4
Shear Area in z direction (A _{vz}) (ft ²)	19.6	133.9	69.1
Offset in z direction (R _z) (ft)	0.00	0.00	0.00
Neutral Axis Location – from Bottom of Section (ft)	6.39	5.52	5.18

9.7.1.1.3 Step 1c – Define Material Properties for Girders

The material properties shown in Table 89 are specified for the girder concrete. In this analysis, the concrete is assumed to be an “ageing linear visco-elastic” material which considers the effects of creep and shrinkage. The analysis software used for this example includes the CEB-FIP Model Code 1990 for modeling creep and shrinkage effects; other software may or may not include this specific concrete model. Table 89 presents the information used in the software (per CEB-FIP notation) and the equivalent AASHTO LRFD parameters that were used for independent checks.

The CEB-FIP Model Code 1990 assumes that concrete is an “ageing linear visco-elastic material.” In other words, creep is assumed to be linearly related to stress. This assumption is valid if the compressive stress is kept below 40 percent of the compressive strength at time of loading. The 1990 CEB-FIP prediction model for creep and shrinkage is valid for “ordinary structural concrete” (260 ksf < f_c < 1700 ksf) and exposed to a mean relative humidity in the range of 40-100 percent at mean temperatures ranging from 40 °F to 90 °F. The prediction model is not applicable for structural lightweight aggregate concrete. The CEB-FIP model assumes that “for variable stresses or strains, the principle of superposition is valid.”

Table 89. Concrete material properties – dead load model.

Material Property	Girder Concrete
CEB-FIP Tangent Modulus of Elasticity, E_{ci} (ksf)	741343
AASHTO Modulus of Elasticity (ksf)	717957
Poisson's Ratio	0.2
Mass Density (10^3 slugs/ft ³)	0.004718
Coefficient of Thermal Expansion(1/°C)	10E-6
Mean Compressive Strength at 28 Days, f'_{cm} (CEB-FIP), f'_c (AASHTO) (ksf)	936
CEB-FIP Cement Type	Normal or Rapid Hardening
Relative Humidity	70
Internal Perimeter Factor	0.5
Include Shrinkage	Yes
Automatically calculate nominal size from section dimensions	Yes – Specify internal perimeter factor
AASHTO V/S	6.73 in

The “nominal size” in Table 89 for the CEB-FIP Model Code is similar to the V/S (volume-to-surface area) ratio in AASHTO; the term “nominal size” is from the software used in this analysis and is equivalent to the “notational size” term used in the CEB-FIP Model Code. The nominal, or notational, size is used to relate the member cross-section to the perimeter of the same member that is in contact with the atmosphere. For beam elements, the software calculates this factor using the cross-section definition and the internal perimeter factor located in Table 2. The internal perimeter factor specifies the percentage of the interior perimeter used in calculating the value of the “nominal size.”

9.7.1.1.4 Step 1d – Define Support Conditions

In the final condition, the girder is restrained vertically and transversely at all bearing locations. The longitudinal support is located at Pier 3. The support conditions are shown in Figure 362. Supports are modeled at the girder centroid; this should not have a significant effect on the results.



Figure 362. Illustration. Support conditions.

The support type and location varies during the different construction stages; one example is when the pier segments are erected, each segment is individually supported but once they are connected and the bearing plinth cast, the entire assembly is set down on the bearings as shown in Figure 363.

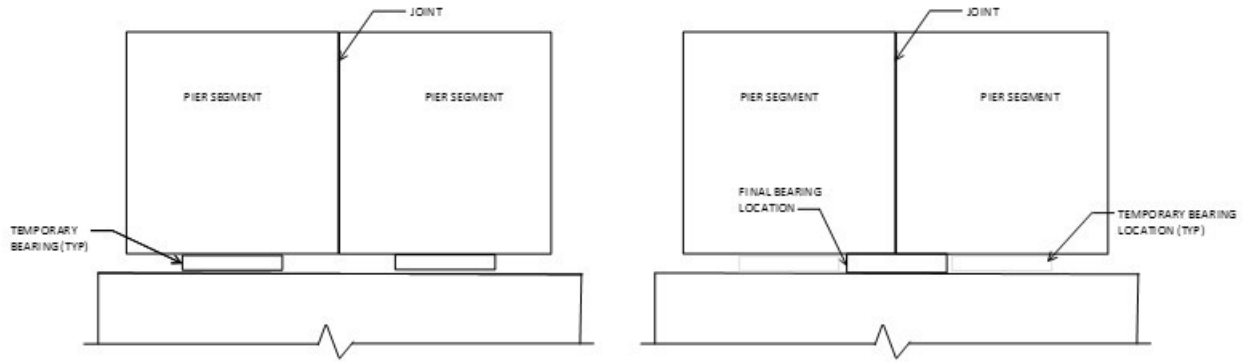








Figure 363. Illustration. Changing support conditions.

9.7.1.1.5 Step 1e – Define Dead Loads Applied to Structure

Girder self-weight is applied using the mass density and applying gravitational acceleration to the member. Note that the erection truss carries the weight of the girder until it is released or the post-tensioning causes the girder to camber up off of the truss, this results in limited bending effects in the longitudinal direction prior to releasing the erection truss. Other dead loads include the weight of the barrier on each side; the specified barrier has a weight per linear foot of 0.376 kips/foot. Since there are two barriers per cross section, a uniform load of 0.752 kips/foot is applied to the girder.

Since the typical section is used at all locations, the weight of the deviators, diaphragms, and temporary PT anchors are not accounted for in the section properties. The weight of these components is accounted for by applying point loads with magnitude equal to the weight of the component being considered. The weight of each component is calculated in Table 90 assuming a concrete unit weight of 0.15 k/ft^3 with sketches showing the different regions provided in Figures 364 and 365.

Table 90. Diaphragm, deviator, and anchor block weights.

Component		Area (ft ²)	Thickness (ft)	Volume (ft ³)	Weight (k)
Temporary PT Anchor Block		$2 \times 1.55 + 0.92 = 4.01$	2	8.02	1.21
Deviators	Bottom Flange	14.77	3'-8"	54.17	8.13
	Web	$2 \times 14.61 = 29.22$	2	58.43	8.77
					16.90
Pier Diaphragm	Top Flange 	32.36	9'-6"	307.39	46.1
	Web/Bottom 	$2 \times 32.52 = 65.04$	6'-6"	422.75	63.4
					109.5
Expansion Diaphragm	Shear Tongue 	$2 \times 4.66 = 9.32$	1'-6"	13.99	2.1
	Expansion Side 	$2 \times 24.23 = 48.46$	8"	32.31	4.9
	At Bearing 	99.7644	2	199.53	29.9
	Span Side 	71.73	2'-7½"	188.29	28.2
					65.1

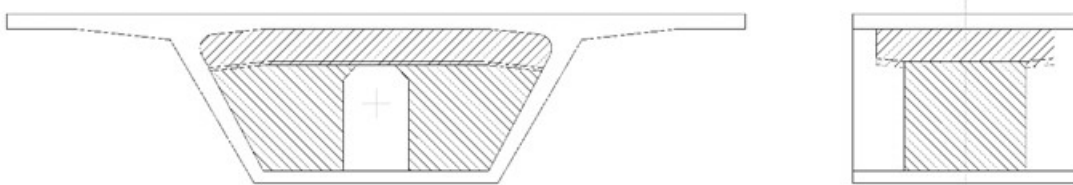


Figure 364. Illustration. Pier diaphragm areas.

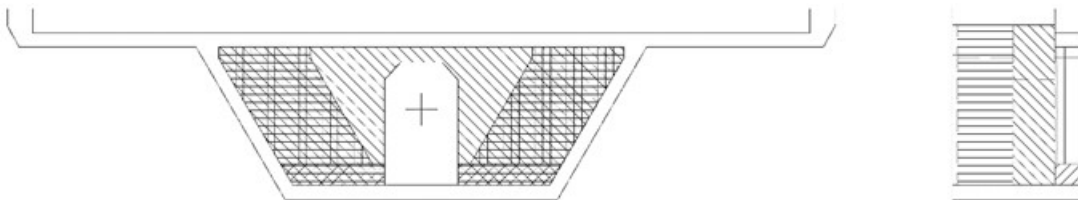


Figure 365. Illustration. Expansion diaphragm areas.

9.7.1.1.6 Step 1f – Model Staged Construction

In this example, the structure is constructed using the span-by-span method where one span is completed prior to starting erection of the next span. The construction sequence is described below using both words and figures. The following assumptions are made:

- an erection truss is used to erect the segments but is not shown in the figures for clarity; the erection truss is assumed to be appropriately cambered such that when all segments are erected, they are at the appropriate geometric relation to each other.
- all segments are 60 days old when erected
- each span takes four days to erect and post-tension
 - Day 1 – erect typical segments onto erection truss and connect segments,
 - Day 2 – erect and connect pier segments, cast bearing plinths,
 - Day 3 – install and stress tendons T1 and T4 to 100 kips, cast closure pours, and
 - Day 4 – install tendons T2 and T3 and post-tension all tendons

Stage #1 (Day 61) (Figure 366)

Erect all Span 1 typical and deviator segments on the erection truss (a). Align the first segment at the correct location. Align second segment with first segment, apply epoxy to each face, pull the two segments tight, and then stress temporary PT bars (b). Repeat process until all segments are connected coupling temporary PT bars to those from previous segment (c).

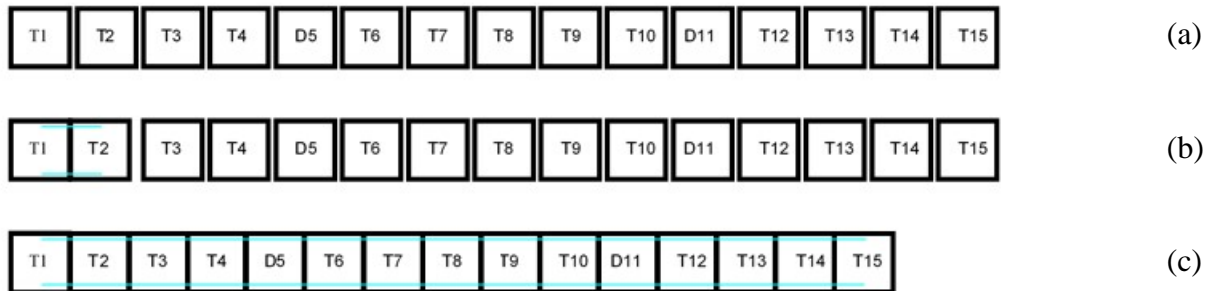


Figure 366. Illustration. Stage #1.

In the analysis model, connecting each individual segment was not modeled due to the relatively short time over which this occurs. Instead, it was assumed that the typical and deviator segments would be connected in a single time step. Each of the typical and deviator segments are connected using five temporary post-tensioning bars; each temporary post-tensioning bar is stressed to 94 kips. The force imposed by the temporary post-tensioning bars was applied using equivalent loads. At this stage, the analysis model only considered the elements representing the typical and deviator segments.

Stage #2 (Day 62) (Figure 367)

Erect Span 1 pier segments and set on temporary jacks over the pier (a). Align pier segments, apply epoxy to matching faces, pull segments tight together, and stress with temporary PT bars (b). Cast bearing plinth above bearing and once cured, release temporary jacks to transfer load to bearing (c). The pier segments are connected using eight post-tensioning bars; each post-

tensioning bar is stressed to 94 kips. In addition to the elements representing the typical and deviator segments, the elements representing the pier segments are included in the analysis at this stage.



Figure 367. Illustration. Stage #2.

Stage #3 (Day 63) (Figure 368)

In this stage, blocking devices are cast between the pier segments and the typical segments (a). The external PT ducts and Tendons T1 and T4 are installed; Tendons T1 and T4 are stressed to 100 kips once the blocking devices have reached strength (b). The closure pours are then formed and cast (c). The elements representing the casting blocks/closure pours are included in the analysis; the force from the temporary post-tensioning bars and Tendons T1 and T4 are applied as equivalent loads.

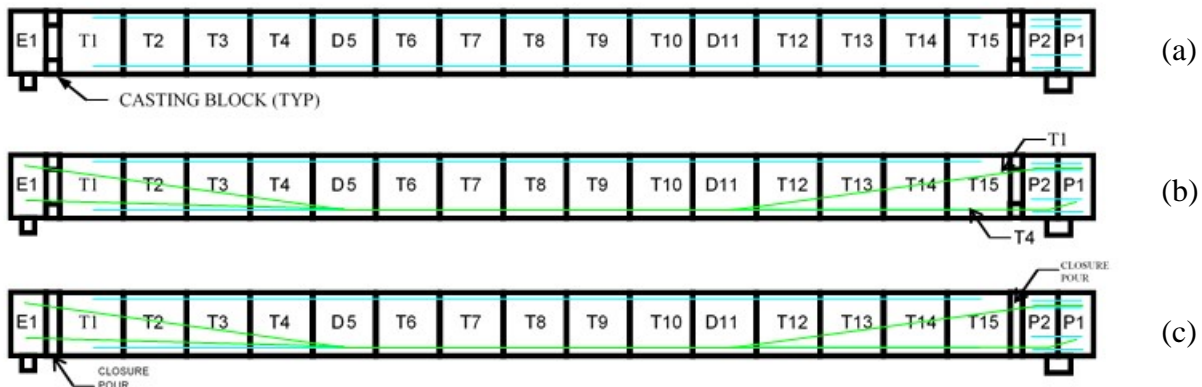


Figure 368. Illustration. Stage #3.

Stage #4 (Day 64) (Figure 369)

The remaining tendons are installed. All tendons are stressed to the jacking load after the concrete closure pour reaches the minimum specified strength; the jacking load is 993 kips for Tendons T1 and T2 and 967 kips for Tendons T3 and T4. The tendons are stressed from the right end only (a). Temporary PT bars may be removed after stressing operations are complete (b). In this stage, the equivalent loads for Tendons T1 and T4 are modified from those applied in Stage #3 and the equivalent loads for Tendons T2 and T3 are applied.

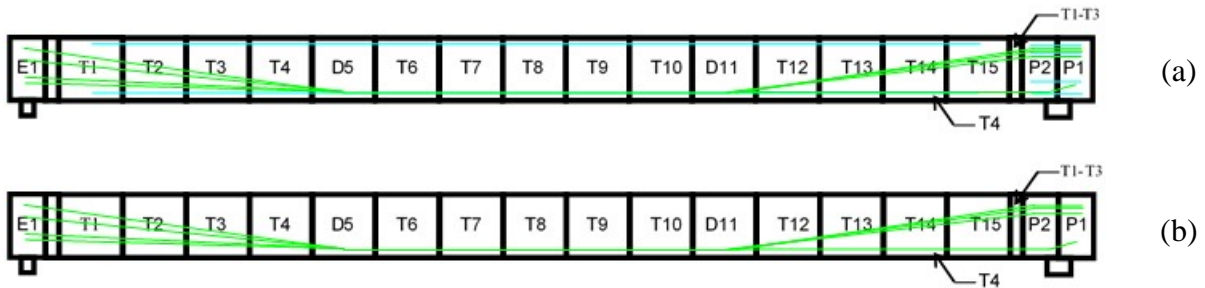


Figure 369. Illustration. Stage #4.

Stage #5 (Day 65) (Figure 370)

Release erection truss from Span 1 and move to Span 2. Erect all Span 2 typical and deviator segments on erection truss (a). Align the first segment at the correct location. Align second segment with the first segment, apply epoxy to each face, pull the two segments tight, and then stress temporary PT bars (b). Repeating this process until all segments are connected, coupling temporary PT bars to those from previous segment (c). Each segment is connected to the previous segment using five post-tensioning bars; each bar is stressed to 94 kips. The elements representing the typical and deviator segments for Span 2 are considered in this stage of the analysis.

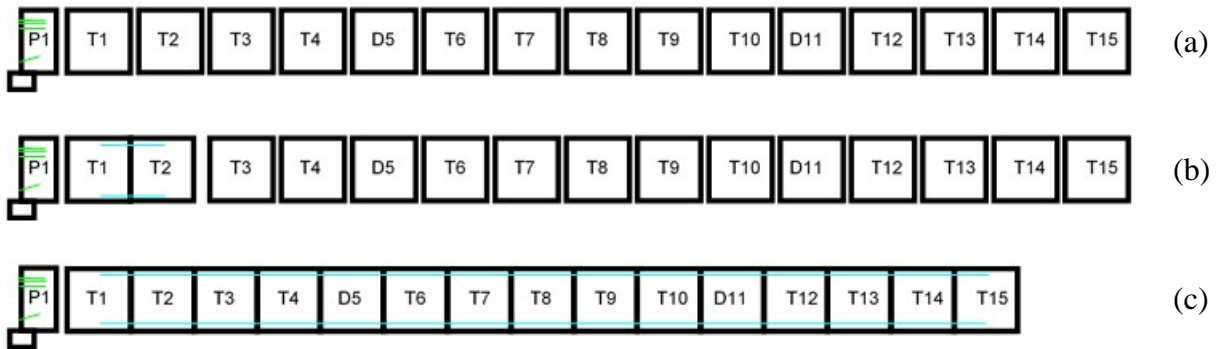


Figure 370. Illustration. Stage #5.

As mentioned in Stage #1, connecting each individual segment was not modeled.

Stage #6 (Day 66) (Figure 371)

Erect Span 2 pier segments and set on temporary jacks over the pier (a). Align pier segments, apply epoxy to matching faces, pull segments tight together, and stress with temporary PT bars (b). Cast bearing plinth above bearing and once cured, release temporary jacks to transfer load to bearing (c). The pier segments are connected using eight post-tensioning bars; each post-tensioning bar is stressed to 94 kips. The elements representing the pier segments at the middle pier are considered in the analysis.

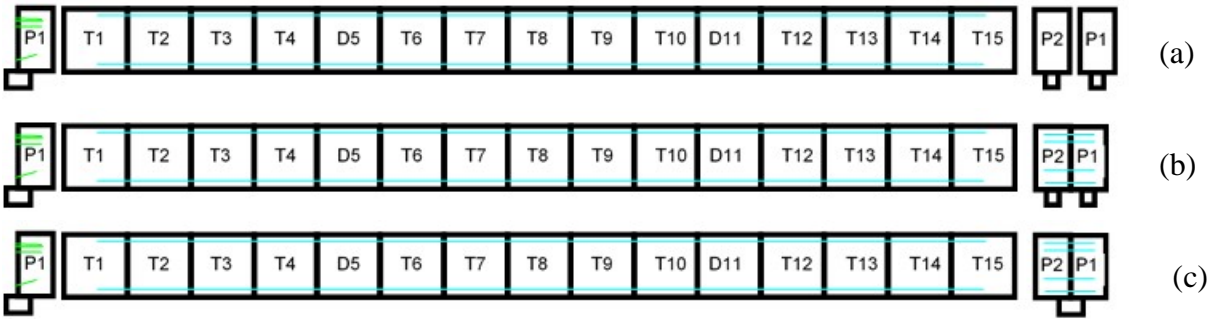


Figure 371. Illustration. Stage #6.

Stage #7 (Day 67) (Figure 372)

In this stage, blocking devices are cast between the pier segments and the typical segments (a). The external PT ducts and Tendons T1 and T4 are installed; Tendons T1 and T4 are stressed to 100 kips once the blocking devices have reached strength (b). The closure pours are then formed and cast (c). Similar to Stage #3, the elements representing the closure pours in Span 2 are considered in the analysis and the equivalent loads from Tendons T1 and T4 in Span 2 are included in the analysis.

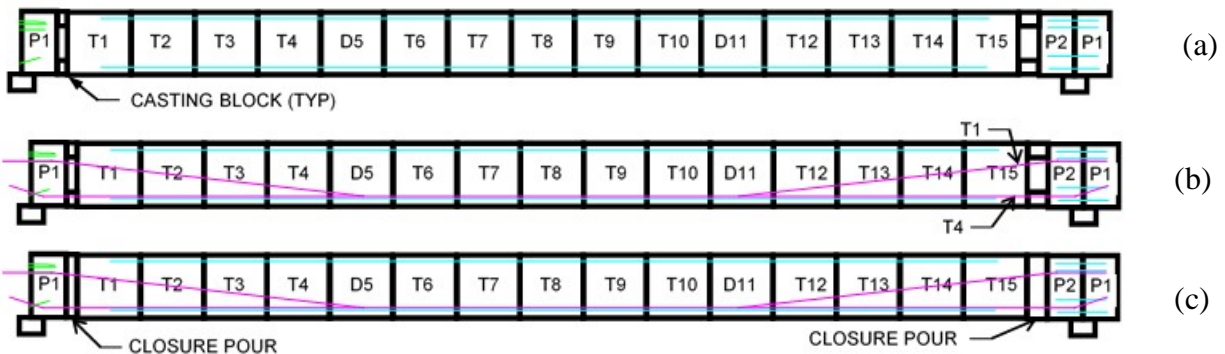


Figure 372. Illustration. Stage #7.

Stage #8 (Day 68) (Figure 373)

The remaining tendons are installed. All tendons are stressed to the jacking load after the concrete closure pour reaches the minimum specified strength; the jacking load is 1018 kips for Tendons T1 through T3 and 1005 kips for Tendon T4 (a). The tendons are stressed from the right end only. Temporary PT bars may be removed after stressing operations are complete (b).



Figure 373. Illustration. Stage #8.

Stages #9-#12 (Days 69-72)

Release erection truss from Span 2 and move to Span 3.

Stages #13-#16 (Days 73-76)

Release erection truss from Span 3 and move to Span 4.

Stage #17 (Days 77-90)

Age structure prior to casting barrier.

Stage #18 (Days 91-100)

Cast the barriers; in the analysis model, the barrier is applied as a uniformly distributed load. Apply any other superimposed dead loads, such as wearing surfaces and utilities, if applicable.

Stage #19 (Days 101 – 1,000) & Stage #20 (Days 1,001 – 10,000)

The structure continues to experience the effects of creep and shrinkage until the end of its life span. For the purposes of this analysis, the effects of creep and shrinkage are assumed to have ended by 10,000 days.

9.7.1.1.7 Step 1g – Run Analysis and Verify Results

The next step is to run the analysis. The analysis results can be verified using a variety of simplified methods. For continuous span bridges, moments and reactions can be calculated using textbook equations for uniform loads. Additionally, for uniform loads applied to the entire structure, the total applied load applied can be calculated and should equal the sum of the reactions from the analysis model.

Check reactions for bridge self-weight and barriers load versus applied load:

Weight of Barrier = 0.376 klf Weight of Girder = 9.61 klf

Length over which Barrier is applied = $2 \times 330 \text{ ft-0 inches} = 660 \text{ ft}$

Total Weight of Barriers and Girder = $0.376 \text{ klf} \times 660 \text{ ft-0 inches} + 9.61 \text{ klf} \times 330 \text{ ft-0 inches} = 3419.6 \text{ k}$

Weight of Temporary PT Anchor Blocks = $1.21 \text{ k/location} \times 26 \text{ locations} = 31.46 \text{ k}$

Weight of Deviators = $16.9 \text{ k/deviator} \times 4 \text{ locations} = 67.6 \text{ k}$

Weight of Pier Diaphragm = $109.5 \text{ k/location} \times 1.5 \text{ locations} = 164.25 \text{ k}$

Weight of Expansion Diaphragm = 65.1 k

Total Reaction = 3748.0 kips

Reactions from Model:

Location	Reaction (Dead Load)
Pier 1	761.626
Pier 2	2159.41
Pier 3	826.942
Total	3747.978

The calculated total applied load is equal to the sum of the reactions from the model. Additionally, the reactions are approximately symmetric as expected.

9.7.1.1.8 Step 1h – Extract Required Results from Software

After verifying that the results from the analysis are reasonable, the results of interest can be extracted and input into a spreadsheet for further use. Since the model utilizes beam elements, bending moments and shears can be extracted directly from the analysis model and used in the design. Note that negative moment values result in compression on the top face and tension on the bottom face.

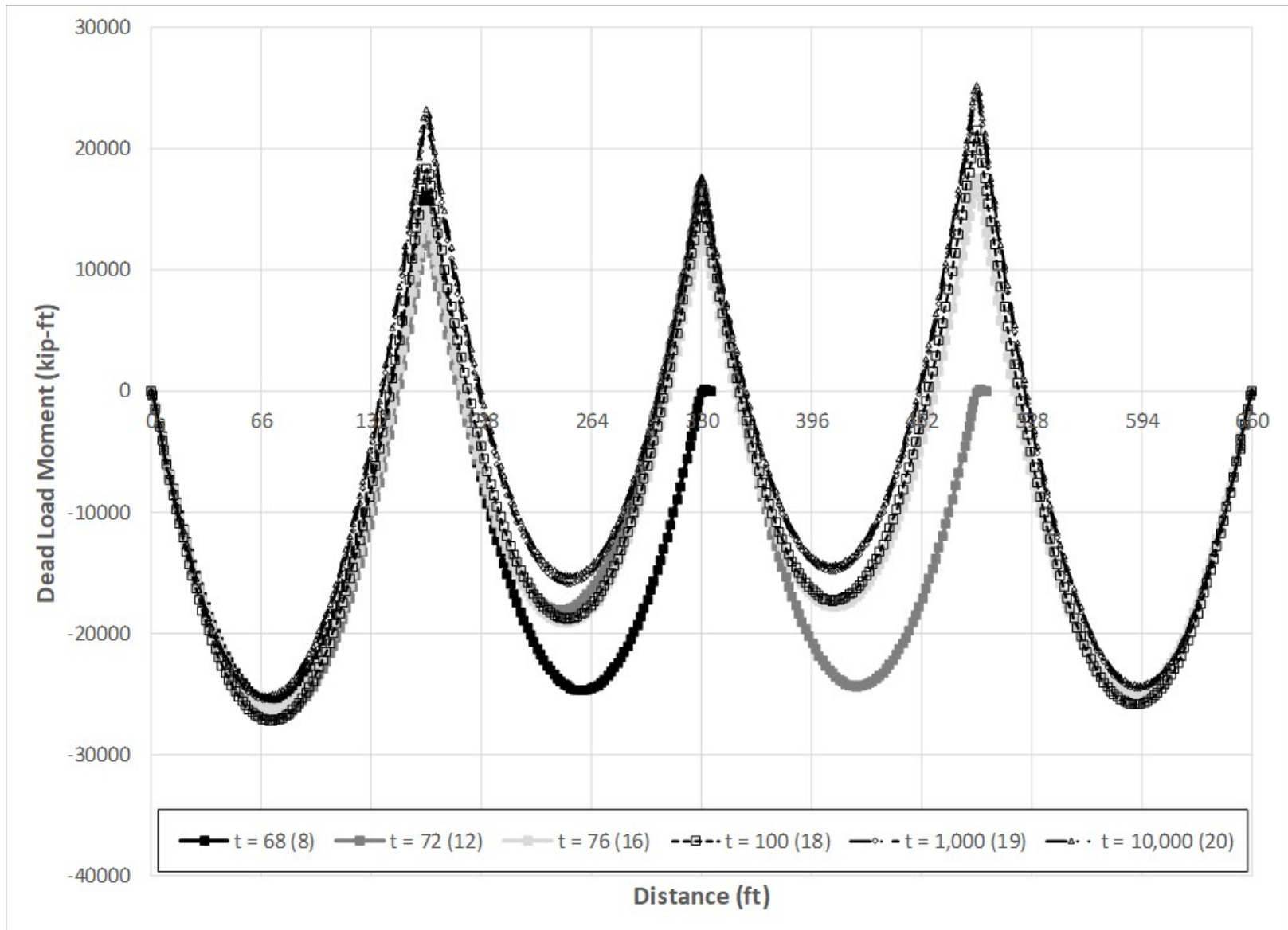


Figure 374. Graph. Dead load moment vs. distance along span for various construction stages.

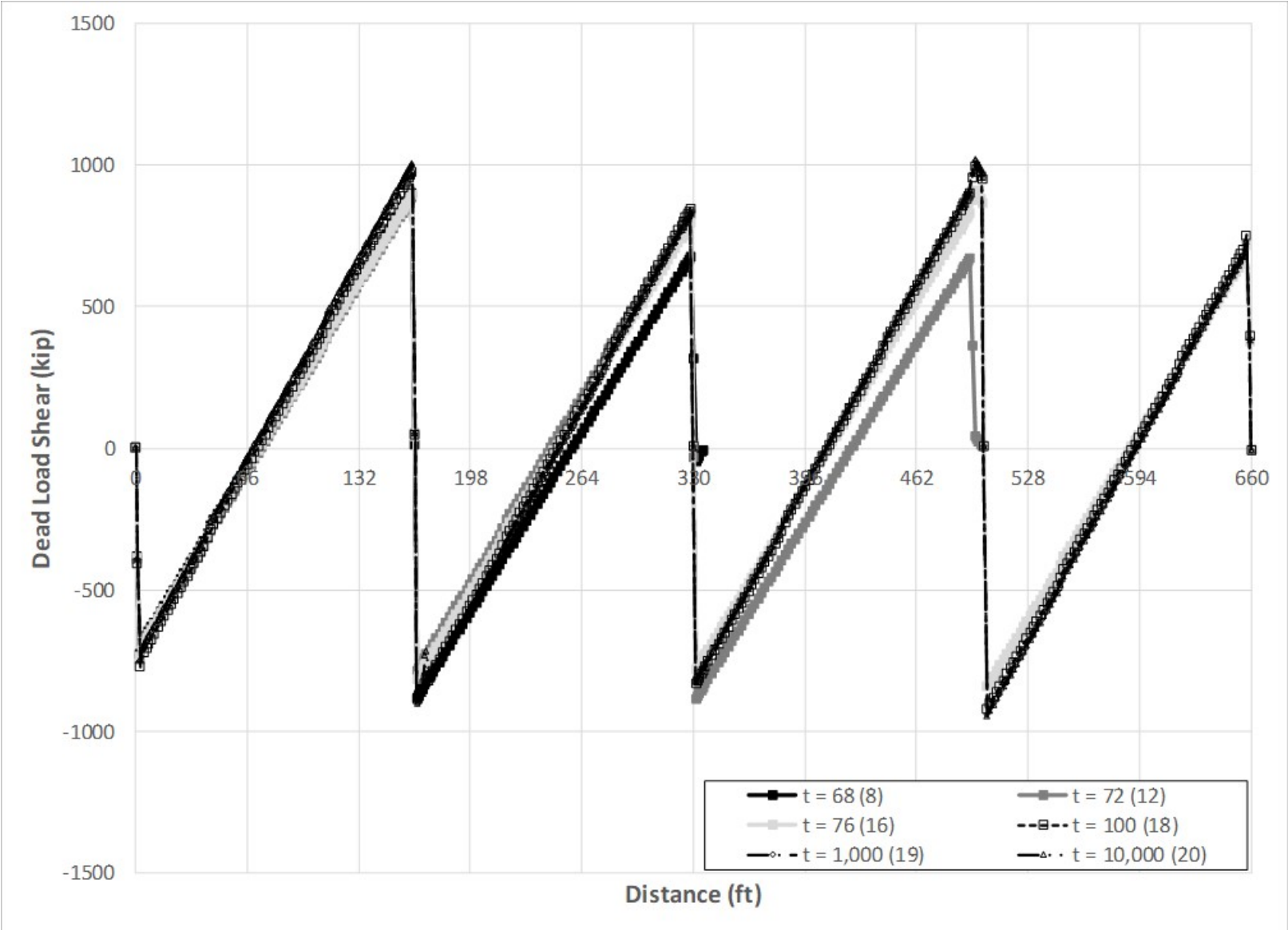


Figure 375. Graph. Dead load shear vs. distance along span for various construction stages.

9.7.1.2 Step 2 - Post-Tensioning Model

Starting with the model from Step 1, modify the model to determine the effects of the post-tensioning.

9.7.1.2.1 Step 2a – Modify Material Properties

The material properties for the concrete shown in Table 2 are modified to remove the effects of shrinkage (i.e. in this case simply uncheck the “include shrinkage” box within the software) as shrinkage is not dependent upon the applied load and was previously accounted for in the dead load model.

This example uses equivalent loads to model the effects of the temporary and permanent post-tensioning tendons; therefore, no tendon material property definitions are required within the analysis model. However, the material properties are necessary to calculate the equivalent loads and are provided in Table 91.

Table 91. PT material properties.

Property	PT Bars	Strand
Modulus of Elasticity (ksi)	30,000	28,500
f_{pu} (ksi)	150	270
Friction coefficient, μ	0.00	0.25
Wobble Coefficient, K (1/foot)	0.00	0.00
Anchor Set (inch)	0.00	0.375

9.7.1.2.2 Step 2b – Tendon Section Properties

This example utilizes equivalent loads to model the effects of the temporary and permanent post-tensioning; therefore, no tendon section properties are required within the analysis model. The section properties are required to determine the equivalent loads and are provided in Table 92.

Table 92. PT section properties.

	Temporary	Permanent (Continuity)
Diameter (in)	1.25	0.6
Number	1	22
Area (in ²)	1.227	4.774

9.7.1.2.3 Step 2c – Calculate and Define Post-Tensioning Equivalent Loads

The prestressing losses due to anchor set, friction and wobble, elastic shortening and strand relaxation are calculated according to AASHTO LRFD Article 5.9.4. Prestressing losses due to creep and shrinkage are calculated according to AASHTO LRFD Article 5.9.5. Note that the tendon losses and forces below are for a single tendon. In the spine beam analysis model, the equivalent loads are multiplied by two since the tendons are in pairs.

9.7.1.2.3.1 Friction Losses

Friction losses occur when the tendon changes directions at deviators and inflection points. The loss due to friction for external tendons is calculated using Equation (69) (AASHTO LRFD Eq. 5.9.5.2.2b-2).

$$\Delta F_{pF} = F_{pj} (1 - e^{-\mu(\alpha + 0.04)}) \quad (69)$$

where:

- ΔF_{pF} = losses due to friction (ksi or kips)
- F_{pj} = stress in the prestressing steel at jacking (ksi or kips)
- μ = coefficient of friction
- α = sum of the absolute values of angular change of prestressing steel path from jacking end (rad.)

The 0.04 radians shown in Equation (69) represents an inadvertent angle change that may occur due to larger tolerances in deviator pipe placement. For this example, the 0.04 radians is included in calculating the friction losses at the deviator locations.

The friction losses in Tendon T1 of Span 2 are calculated in Table 93 below. In Table 93, there are three columns of angular change shown. The first column, α_v , is the angle change due to the change in vertical location of the tendon. The second column, α_h , is the angle change due to the change in horizontal location of the tendon. The third column, α , is calculated using Equation (70).

$$\alpha = \sqrt{(\alpha_v)^2 + (\alpha_h)^2} \quad (70)$$

The friction losses for the tendons in Span 1 are summarized in Table 94 and in Table 95 for the tendons in Span 2. For all tendons, jacking is assumed to occur at the right end of the span (point ①). Figure 376 shows a general tendon schematic and the changes in angle that the tendon goes through between its two anchorage points. Points ① and ⑥ represent the tendon anchorages while Points ③ and ④ represent the deviator locations. Points ② and ⑤ represent the inflection points of the tendon.



Figure 376. Illustration. Tendon schematic.

Givens: $\mu = 0.25$
 $F_{pj} = 1018$ kips

Table 93. Friction losses in Span 2 Tendon T1.

Segment	X (ft)	Y (ft)	Z (ft)	α_v (rad)	α_h (rad)	α (rad)	$\mu(\alpha+0.04)$	$\Sigma\mu(\alpha+0.04)$	$e^{-\Sigma\mu(\alpha+0.04)}$	$1-e^{-\Sigma\mu(\alpha+0.04)}$	ΔF_{pF} (kips)
⑥ to ⑤	167.33	7.58	7.33	0.127	0.038	0.132	0.033	0.155	0.856	0.144	146.5
⑤ to ④	217.29	5.67	1.00	0.127	0.038	0.132	0.043	0.122	0.885	0.115	117.1
④ to ③	277.79	5.67	1.00	0.124	0.060	0.138	0.045	0.079	0.924	0.076	77.4
③ to ②	327.67	8.67	7.21	0.124	0.060	0.138	0.035	0.035	0.966	0.034	34.6
② to ①	330.00	8.67	7.21	0.000	0.000	0.000	0.000	0.000	1.000	0.000	0.00

Table 94. Friction and wobble losses for Span 1.

Segment	Span 1 Tendon T1 ($F_{pJ} = 993$ k)		Span 1 Tendon T2 ($F_{pJ} = 993$ k)		Span 1 Tendon T3 ($F_{pJ} = 967$ k)		Span 1 Tendon T4 ($F_{pJ} = 967$ k)	
	ΔF_{pF} (k)	α (rad)	ΔF_{pF} (k)	α (rad)	ΔF_{pF} (k)	α (rad)	ΔF_{pF} (k)	α (rad)
⑥ to ④	118.353	0.150	106.557	0.112	90.164	0.050	75.059	0.036
④ to ③	75.862	0.139	72.189	0.129	70.315	0.131	57.907	0.000
③ to ②	33.901	0.139	32.378	0.133	31.155	0.131	48.770	0.207
② to ①	0.000	0.000	0.000	0.000	0.000	0.000	0.000	0.000

Table 95. Friction and wobble losses for Span 2.

Segment	Span 2 Tendon T1 ($F_{pJ}=1018$ k)		Span 2 Tendon T2 ($F_{pJ} = 1018$ k)		Span 2 Tendon T3 ($F_{pJ} = 1018$ k)		Span 2 Tendon T4 ($F_{pJ} = 1005$ k)	
	ΔF_{pF} (k)	α (rad)	ΔF_{pF} (k)	α (rad)	ΔF_{pF} (k)	α (rad)	ΔF_{pF} (k)	α (rad)
⑥ to ⑤	146.474	0.132	142.789	0.130	142.904	0.132	119.677	0.207
⑤ to ④	117.133	0.132	113.804	0.130	113.502	0.132	72.655	0.007
④ to ③	77.444	0.138	74.471	0.132	73.716	0.130	61.736	0.007
③ to ②	34.583	0.138	33.030	0.132	32.636	0.130	50.686	0.207
② to ①	0.000	0.000	0.000	0.000	0.000	0.000	0.000	0.000

9.7.1.2.3.2 Anchor Set Losses

Anchor set losses occur when the strand slips to engage the wedges at the anchor locations. The losses are a function of how far the strand slips; this distance is referred to as the anchor set and varies depending on the type of anchorage. In this example, the anchor set is assumed to be 3/8 inch. Anchor set losses are calculated for two cases, one assuming friction and wobble are zero and one assuming friction and wobble are non-zero.

Anchor Set Losses without Friction

In the case where friction losses are assumed to be zero, the tendon is assumed to behave elastically and the stress loss is constant over the entire length of the tendon. From Hooke's Law, Equation (71) relates the applied axial load to the deformation of the member. By rearranging Equation (71), the change in force, ΔF_{pA} , can be determined as a function of the anchor set as shown in Equation (72).

$$\delta = \frac{\Delta F_{pA} L}{E_p A_{ps}} \quad (71)$$

$$\Delta F_{pA} = \frac{\delta E_p A_{ps}}{L} \quad (72)$$

where:

ΔF_{pA}	=	losses due to anchor set (kips)
δ	=	anchor set (in.)
E_p	=	modulus of elasticity of prestressing steel (ksi)
A_{ps}	=	area of tendon (in. ²)
L	=	length of tendon (in.)

The anchor set losses in Tendon 1 of Span 2 are calculated below. The anchor set losses for all tendons are summarized in Table 96 below; the values for δ , E_p , and A_{ps} are constant for all tendons. The tendon length, L , is approximated as shown below.

Givens:

δ	=	0.375 in. (from PT supplier)
E_p	=	28,500 ksi
A_{ps}	=	22 strands \times 0.217 in ² = 4.774 in ²
L	=	$\sum \sqrt{(x_i - x_j)^2 + (y_i - y_j)^2 + (z_i - z_j)^2} = 2104.56$ in.

Substituting into Equation (72) to find ΔF_{pA} :

$$\Delta F_{pA} = \frac{0.375 \text{ in.} \times 28,500 \text{ ksi} \times 4.774 \text{ in}^2}{2104.56 \text{ in.}} = 24.24 \text{ kips}$$

Table 96. Anchor set losses for Spans 1 and 2 without friction.

	Span 1		Span 2	
	Tendon Length (inches)	ΔF_{pA} (kips)	Tendon Length (inches)	ΔF_{pA} (kips)
Tendon T1	2036.64	25.05	2104.56	24.24
Tendon T2	2033.76	25.09	2103.96	24.25
Tendon T3	2031.12	25.12	2104.08	24.25
Tendon T4	2009.04	25.40	2060.28	24.76

Anchor Set Losses with Friction

As shown in Figure 377, the tendon force varies along the length due to friction losses with the maximum tendon force, F_{pj} , occurring at the jacking end. After the tendon is anchored, the force at the jacking end is reduced by an amount ΔF_{pA} , the loss due to anchor set. Moving away from the anchorage zone, the force in the tendon increases due to friction, up until the point where the force in the tendon after anchor set is equal to the force before anchor set. The point where this occurs is at a distance, L_{set} , from the jacking end. The area between the two curves, indicated by the hatching in Figure 377, divided by E_p times A_{ps} should equal the anchor set length provided by the PT supplier.

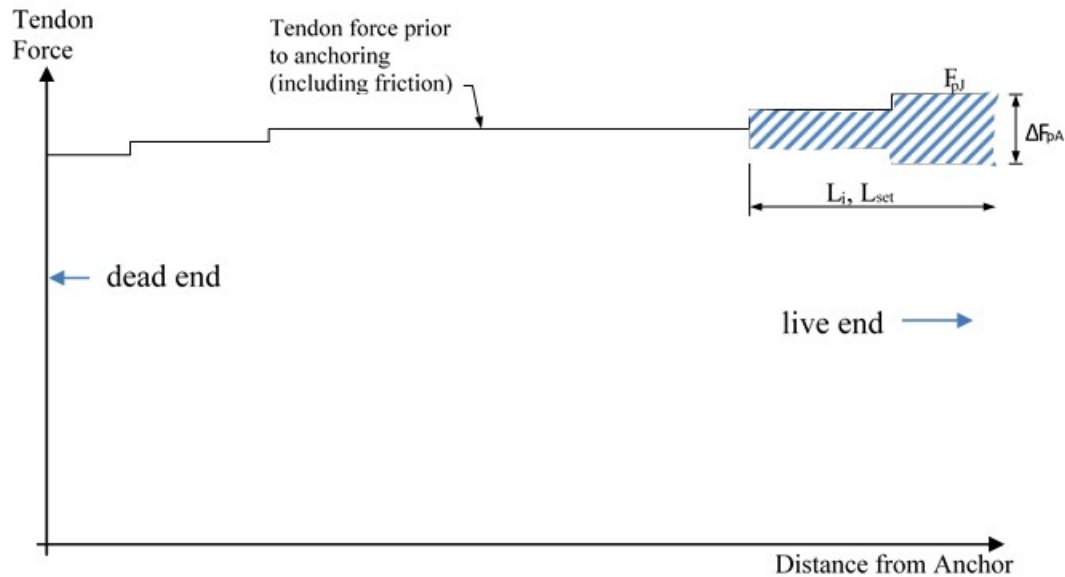


Figure 377. Illustration. Tendon force variation.

The procedure to determine L_{set} is an iterative process as the exact location depends on several variables. The steps to determine L_{set} are described below:

1. Calculate the slope of the line describing the force in the tendon prior to anchorage occurring, p , according to Equation (73). ΔF_{pF} is the loss due to friction between the jacking end and L_i , where L_i is assumed for the first iteration.

$$p = \frac{\Delta F_{pF}}{L_i} \quad (73)$$

2. Calculate L_{set} according to Equation (74) by substituting in the known values for δ , A_{ps} , E_p and p calculated in Step 1.

$$L_{set} = \sqrt{\frac{\delta A_{ps} E_p}{p}} \quad (74)$$

3. Compare L_{set} calculated from Equation (74) to L_i assumed in Step 1. If the two values are similar, the anchorage set loss can be calculated using Equation (75). Otherwise, the value for L_{set} can be input back into Equation (73) and the process repeated. This iterative process can be automated using Excel's Solver add-in or Goal Seek.

$$\Delta F_{pA} = 2pL_{set} \quad (75)$$

The anchorage loss is calculated for Span 2 Tendon T1 using the procedure above. In this example, the tendon force changes at discrete locations. Therefore, p is calculated assuming that the force changes uniformly between the anchorage location and L_i . Since the distance between the anchorage location and the first kink is relatively short, assume that L_i is at the second kink in the tendon for the first iteration.

Given: $\Delta F_{pF} = 77.4$ kips (See Table 95 Segment ④ to ③)

$L_i = 52.25$ ft = 627 in. (assumed at Point ③)

From Equation (73), calculate p :

$$p = \frac{\Delta F_{pF}}{L_i} = \frac{77.4 \text{ kip}}{627 \text{ in.}} = 0.123 \text{ kip/in}$$

From Equation (74), calculate L_{set} :

$$L_{set} = \sqrt{\frac{\Delta_{set} A_{ps} E_{ps}}{p}} = \sqrt{\frac{0.375 \text{ in} (4.774 \text{ in}^2) (28500 \text{ ksi})}{0.123 \text{ kip/in}}} = 644.1 \text{ in.}$$

Compare L_{set} to L_i . The calculated value of L_{set} is 644.1 in. while the assumed value was 627 in. For this example, Excel's Goal Seek was used to iterate until L_{set} and L_i are equal. Using the method described above for Span 2 Tendon 1, the anchor set loss was calculated as 154.9 kips and an associated L_{set} value of 658.8 in.

As the distance from the jacking end increases, the anchor set loss decreases. As shown in Figure 377, the force in the tendon increases from $(F_{pj} - \Delta F_{pA})$ to $(F_{pj} - \Delta F_{pA} + \Delta F_{pF})$ until the point where the force before anchor set equals the force after anchor set. The anchor set losses are shown along the length of Span 2 Tendon #1 in Table 97.

Table 97. Anchor set losses for Span 2 with friction.

Location	Span 2 Tendon T1
	ΔF_{pA} (k)
⑥ to ⑤	0.00
⑤ to ④	0.00
④ to ③	85.7
③ to ②	154.9
② to ①	154.9

Comparing the anchor set losses for Span 2 Tendon T1, without friction, the loss is a uniform 24.25 kips (Table 96) along the entire length of the tendon, and with friction, the loss is concentrated near the live end with a loss of 154.9 kips (Table 97). For the case with friction, the large loss is quickly reduced due to friction. One design implication is the amount of anchorage zone reinforcement required. For the case where friction is considered in the anchor set loss, the force in the tendon is, for Span 2 Tendon T1, approximately 125 kips lower than if the anchor set loss does not consider friction.

9.7.1.2.3.3 Elastic Shortening Losses

Elastic shortening losses occur when a series of tendons is stressed. The first tendon is stressed to F_{pj} . As subsequent tendons are stressed, the force in the previously stressed tendons is reduced due to the axial shortening of the member caused by jacking the next tendon. Elastic shortening losses can be calculated using AASHTO LRFD Eq. 5.9.5.2.3b-1 or Eq. C5.9.5.2.3b-1 shown below as Equations (76) and (77), respectively.

$$\Delta f_{pES} = \frac{N - 1}{2N} \frac{E_p}{E_{ci}} f_{cgp} \quad (76)$$

$$\Delta f_{pES} = \frac{N - 1}{2N} \frac{A_{ps} f_{pbt} (I_g + e_m^2 A_g) - e_m M_g A_g}{A_{ps} (I_g + e_m^2 A_g) + \frac{A_g I_g E_{ci}}{E_p}} \quad (77)$$

where: N = number of identical prestressing strands
 E_p = modulus of elasticity of prestressing strands (ksi)
 E_{ci} = modulus of elasticity of concrete at transfer (ksi)
 f_{cgp} = sum of concrete stresses at the center of gravity of prestressing tendons due to the prestressing force after jacking and the self-weight of the member at the section (ksi); the value used for f_{cgp} in calculating the elastic shortening was an average value along the member length.

$$= \frac{(M_g + M_{PT}) y_{PT} + \sum P_e}{I_g} + \frac{\sum P_e}{A_g}$$

A_{ps} = area of prestressing steel (in²)
 A_g = gross area of section (in²)
 f_{pbt} = stress in prestressing steel immediately prior to transfer (ksi)
 I_g = moment of inertia of gross concrete section (in.⁴)
 e_m = average eccentricity at midspan (in.)
 M_g = moment due to member self-weight (kip-in)
 M_{PT} = moment due to post-tensioning (kip-in)
 P_e = effective force (including friction losses) after jacking (kips)
 y_{pt} = distance between center of gravity of concrete and center of gravity of post-tensioning (in)

The losses due to elastic shortening are calculated for Span 2 Tendon T1 using Equation (76).

Given: $N = 8$
 $E_p = 28,500$ ksi (see Table 4)
 $E_{ci} = 717957$ ksf = 4985 ksi (see Table 2)
 $\sum P_e = 2(P_{T1} + P_{T2} + P_{T3} + P_{T4}) = 7543.3$ k
 $A_g = 63.23$ ft² = 9104.5 in² (see Table 1)
 $I_g = 631.2$ ft⁴ = 13088563 in⁴ (see Table 1)
 $\bar{y}_{pt} = 3.5$ ft = 42 in. (average eccentricity of tendons)
 $M_g = 16480$ k-ft = 197760 k-in
 $M_{PT} = -40670$ k-ft = -488050 k-in

Calculate f_{cgp} :

$$f_{cgp} = \frac{(197760k \cdot in - 488050k \cdot in) \times -42 in}{13088563 in^4} + \frac{7543.3k}{9104.5 in^2} = 1.76ksi$$

Substituting in to Equation (76)

$$\Delta f_{pES} = \frac{8 - 1}{2(8)} \left(\frac{28,500ksi}{4985 ksi} \right) 1.76ksi = 4.40 ksi$$

9.7.1.2.3.4 Relaxation Losses

Relaxation losses occur when strand is subjected to a constant strain for a long period of time. AASHTO LRFD 5.9.5.4.2c specifies the relaxation loss for low-relaxation tendons as 1.2 ksi for the time between transfer of prestress and casting the deck and AASHTO LRFD 5.9.5.4.3c specifies an additional 1.2 ksi loss between the time the deck is cast and the life of the structure. For post-tensioned tendons, the loss occurs between the time of stressing and the life of the structure. For this example, the relaxation is assumed to occur in two equal increments of 1.2 ksi, one occurring in Stage 12 and the second in Stage 13. This corresponds to a total, uniform reduction in force (ΔF_{pR}) of 11.46 kips (2.4 ksi \times 4.774 in²) along the length of the tendon.

9.7.1.2.3.5 Creep Losses

Creep losses occur due to load-induced volumetric strains in the concrete as described in Section 4.1.2. Due to the applied loads, the concrete shortens resulting in prestress losses in the tendons. These losses are calculated according to AASHTO LRFD 5.4.2.3.2 and 5.9.5. Equations (78)

through (82) are AASHTO LRFD Eq. 5.4.2.3.2-1 through Eq. 5.4.2.3.2-5, respectively. Equation (83) is AASHTO LRFD Eq 5.9.5.4.3b-1. K_{df} in Equation (83) is provided as (87) in the section regarding shrinkage losses.

$$\Psi(t, t_i) = 1.9k_s k_{hc} k_f k_{td} t_i^{-0.118} \quad (78)$$

$$k_s = 1.45 - 0.13 \left(\frac{V}{S} \right) \geq 1.0 \quad (79)$$

$$k_{hc} = 1.56 - 0.008H \quad (80)$$

$$k_f = \frac{5}{1 + f_{ci}} \quad (81)$$

$$k_{td} = \left(\frac{t}{61 - 4f_{ci}' + t} \right) \quad (82)$$

$$\Delta f_{pCD} = \frac{E_p}{E_{ci}} f_{cgp} [\Psi_b(t_f, t_i) - \Psi_b(t_d, t_i)] K_{df} + \frac{E_p}{E_c} \Delta f_{cd} \Psi_b(t_f, t_d) K_{df} \quad (83)$$

where:

- H = relative humidity (%) from AASHTO LRFD Figure 5.4.2.3.3-1
- k_s = factor for the effect of the volume-to-surface ratio of the component
- k_{hc} = humidity factor for creep
- k_f = factor for the effect of concrete strength
- k_{td} = time development factor
- t = maturity of concrete (day), defined as age of concrete between time of loading for creep calculations and time being considered for analysis of creep effects.
- t_i = age of concrete at time of load application (day)
- V/S = volume-to-surface ratio (in.)
- f_{ci}' = specified compressive strength of concrete at time of initial loading
- $\Psi_b(t_d, t_i)$ = girder creep coefficient at time of deck placement due to loading introduced at transfer
- t_d = age at deck placement (days)
- Δf_{cd} = change in concrete stress at centroid of prestressing strands due to long-term losses between transfer and deck placement, combined with deck weight and superimposed loads (ksi)
- $\Psi_b(t_f, t_d)$ = girder creep coefficient at final time due to loading at deck placement
- $\Psi_b(t_f, t_i)$ = girder creep coefficient at final time due to loading at transfer
- K_{df} = transformed section coefficient accounting for time-dependent interaction between concrete and steel in section being considered.

The losses due to creep are calculated for Span 2 Tendon T1 at Day 72 using Equation (83) below.

Givens:

Material Properties:

$$f_{ci}' = 6.5 \text{ ksi}$$

$$E_p = 28,500 \text{ ksi}$$

$$E_{ci} = 4985 \text{ ksi}$$

Section Properties:

$$A_g = 9104.5 \text{ in}^2$$

$$P_o = 89.43 \text{ ft}$$

$$P = \text{perimeter of cross-section} = P_o + 0.5P_i = 1351.9 \text{ in}$$

Time:

$$t_i, t_d = 68 \text{ days}$$

$$t_f = 72 \text{ days}$$

$$I_c = 13088563 \text{ in}^4$$

$$P_i = 46.47 \text{ ft}$$

$$t = 4 \text{ days (for } t_i = 68 \text{ to } t_f = 72)$$

$$t = 0 \text{ days (for } t_i = 68 \text{ to } t_d = 68)$$

Factors for creep and shrinkage calculations:

$$H = 70 \%$$

$$V/S = \frac{A_g}{P} = \frac{9104.5 \text{ in}^2}{1351.9 \text{ in}} = 6.73 \text{ in}$$

$$k_s = \max\left(1.45 - 0.13\left(\frac{V}{S}\right), 1.0\right) = \max(1.45 - 0.13 \times 6.73 = 0.57, 1.0) = 1.0$$

$$k_{hc} = 1.56 - 0.008H = 1.56 - 0.008 \times 70 = 1.0$$

$$k_f = \frac{5}{1+f'_{ci}} = \frac{5}{1+6.5} = 0.67$$

$$k_{td} = \left(\frac{t}{61-4f'_{ci}+t}\right) = \frac{4}{61-4 \times 6.5+4} = 0.103 \text{ for } (t_f, t_d) \text{ and } (t_f, t_i)$$

$$k_{td} = \left(\frac{t}{61-4f'_{ci}+t}\right) = \frac{0}{61-4 \times 6.5+0} = 0.000 \text{ for } (t_d, t_i)$$

Creep Coefficients:

$$\Psi(t_f, t_d) = \Psi(t_f, t_i) = 1.9k_s k_{hc} k_f k_{td} t_i^{-0.118} = 1.9 \times 1.0 \times 1.0 \times 0.67 \times 0.103 \times 68^{-0.118} = 0.079$$

$$\Psi(t_d, t_i) = 1.9k_s k_{hc} k_f k_{td} t_i^{-0.118} = 1.9 \times 1.0 \times 1.0 \times 0.67 \times 0.000 \times 68^{-0.118} = 0.000$$

Creep Losses:

$$f_{cgp} = 2.26 \text{ ksi}$$

$$\Delta f_{cd} = 0.001 \text{ ksi}$$

$$K_{df} = \frac{1}{1 + \frac{28500 \text{ ksi}}{4985 \text{ ksi}} \frac{38.2 \text{ in}^2}{9104.5 \text{ in}^2} \left(1 + \frac{9104.5 \text{ in}^2 (64.7 \text{ in})^2}{13088563 \text{ in}^4}\right) [1 + 0.7(0.079)]} = 0.910$$

$$\begin{aligned} \Delta f_{pCD} &= \frac{E_p}{E_{ci}} f_{cgp} [\Psi_b(t_f, t_i) - \Psi_b(t_d, t_i)] K_{df} + \frac{E_p}{E_c} \Delta f_{cd} \Psi_b(t_f, t_d) K_{df} \\ &= \frac{28500 \text{ ksi}}{4985 \text{ ksi}} (2.26 \text{ ksi}) [0.079 - 0.000] (0.910) + \frac{28500 \text{ ksi}}{4985 \text{ ksi}} (0.001 \text{ ksi}) (0.079) (0.910) \\ &= 0.929 \text{ ksi} \end{aligned}$$

The losses due to creep for various stages are shown in Figures 378 and 379 for Span 1 and Span 2 respectively. In Figure 378, the creep losses that occur from the time Span 1 is post-tensioned until just prior to Span 2 being post-tensioned are essentially symmetrical with slight peaks occurring at the deviator locations. As construction continues, the creep losses are no longer symmetric with those at the deviator near 115 feet being larger than those at the deviator near 45 feet. The larger losses at the second deviator are due to the change in statical system, from simple span to two-span continuous and, eventually, three- and four-span continuous.

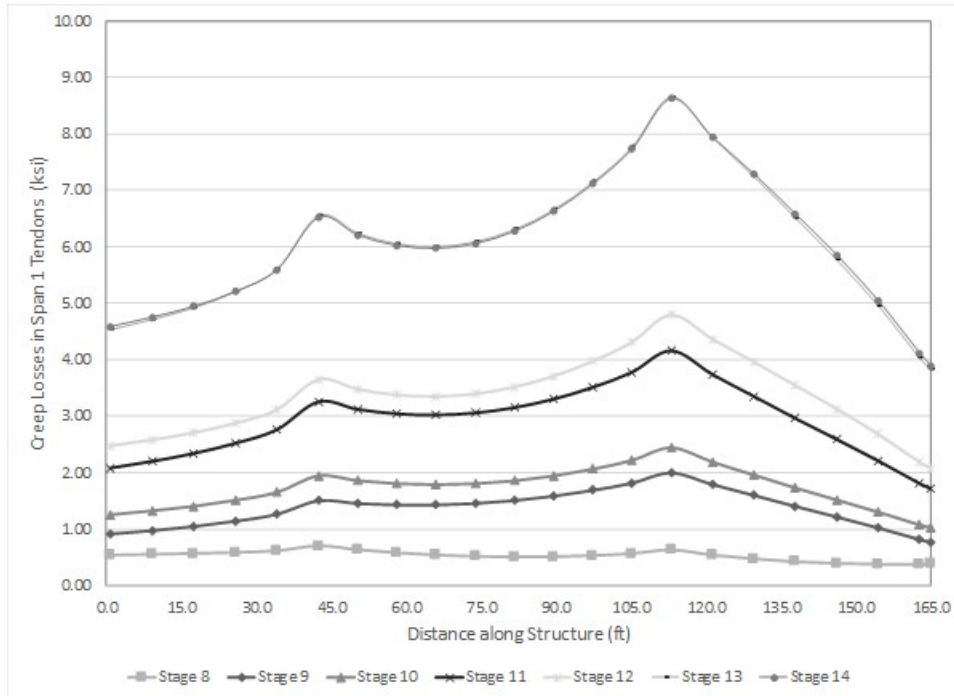


Figure 378. Graph. Creep losses at different stages vs. location – Span 1 tendons.

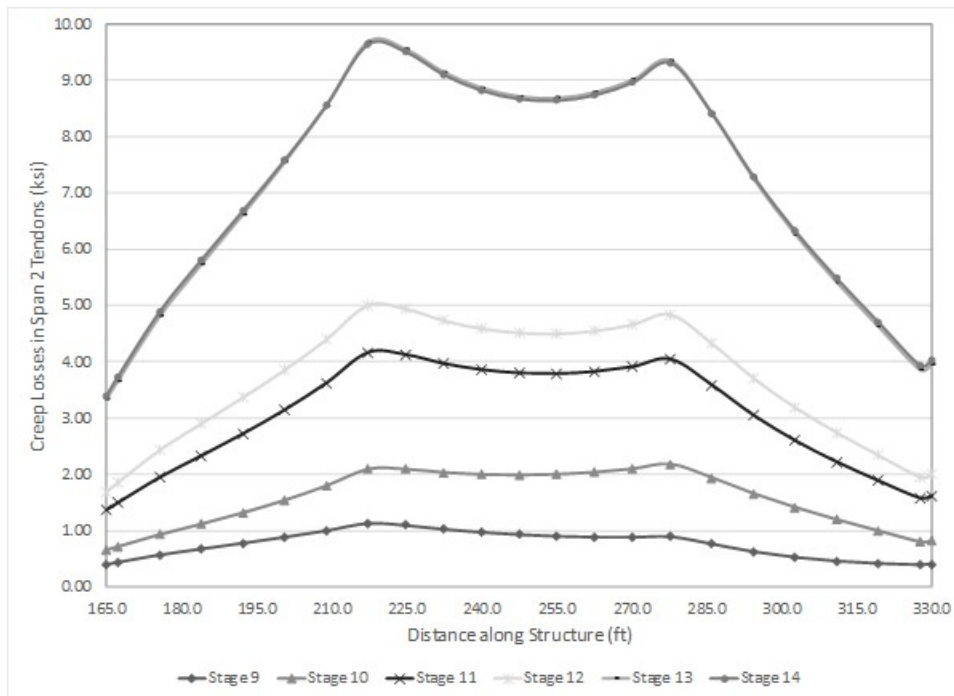


Figure 379. Graph. Creep losses at different stages vs. location - Span 2 tendons.

9.7.1.2.3.6 Shrinkage Losses

Shrinkage losses occur due to non-load-induced volumetric strains in the concrete as described in Section 4.1.3.1.6. Due to the loss of water from the concrete, the concrete shortens resulting in prestress losses in the tendons. These losses are calculated according to AASHTO LRFD

5.4.2.3.3 and 5.9.5. Equation (84) and (85) are AASHTO LRFD Eq. 5.4.2.3.3-1 and Eq. 5.4.2.3.3-2, respectively. Equation (86) and (87), are AASHTO LRFD Eqs. 5.9.5.4.3a-1 and 5.9.5.4.3a-2, respectively.

$$\varepsilon_{sh} = k_s k_{hs} k_f k_{td} 0.48 \times 10^{-3} \quad (84)$$

$$k_{hs} = (2.00 - 0.014H) \quad (85)$$

$$\Delta f_{pSD} = \varepsilon_{bdf} E_p K_{df} \quad (86)$$

$$K_{df} = \frac{1}{1 + \frac{E_p}{E_{ci}} \frac{A_{ps}}{A_c} \left(1 + \frac{A_c e_{pc}^2}{I_c}\right) [1 + 0.7\Psi_b(t_f, t_i)]} \quad (87)$$

where:

- ε_{sh} = strain due to shrinkage
- k_{hs} = humidity factor for shrinkage
- Δf_{pSD} = prestress loss due to shrinkage of girder concrete between time of deck placement and final time
- ε_{bdf} = strain due to shrinkage between deck placement and final time
- e_{pc} = eccentricity of prestressing force with respect to centroid of composite girder (in.)
- $\Psi_b(t_f, t_i)$ = girder creep coefficient at final time due to loading introduced at transfer
- t = maturity of concrete (day), defined as age of concrete between end of curing and time being considered for analysis of shrinkage effects.
- t_f = time being considered for analysis (days)
- t_i = age at end of curing (days)
- K_{df} = transformed section coefficient that accounts for time-dependent interaction between concrete and bonded steel in the section being considered for time between deck placement and time being considered for analysis
- e_{pc} = eccentricity of prestressing force with respect to centroid of composite section (in.)
- A_c = area of section calculated using the gross composite concrete section properties of the girder and the deck and the deck-to-girder modular ratio (in²)
- I_c = moment of inertia of section calculated using the gross composite concrete section properties of the girder and the deck and the deck-to-girder modular ratio (in⁴)

The losses due to shrinkage are calculated below for Span 2 Tendon 1 using Equation (86) for a section at the center of the span at $t = 72$ days.

Givens:

Time:

$t_i = 3$ days (end of moist curing)

$t_{f,2} = 72$ days (end of Stage 9)

$t_{f,1} = 68$ days (end of Stage 8)

$t = 69$ days (for $t_i = 3$ to $t_{f,2} = 72$)

$t = 65$ days (for $t_i = 3$ to $t_{f,1} = 68$)

Factors for creep and shrinkage calculations:

$$H = 70 \%$$

$$k_s = 1.0$$

$$k_{hs} = 2.00 - 0.014H = 2.00 - 0.014 \times 70 = 1.02$$

$$k_f = 0.67$$

$$k_{td} = \left(\frac{t}{61 - 4f'_{ci} + t} \right) = \frac{69}{61 - 4 \times 6.5 + 69} = 0.663$$

$$k_{td} = \left(\frac{t}{61 - 4f'_{ci} + t} \right) = \frac{65}{61 - 4 \times 6.5 + 65} = 0.650$$

$$V/S = \frac{A_g}{P} = \frac{9104.5 \text{ in}^2}{1351.9 \text{ in}} = 6.73 \text{ in}$$

$$\text{For } t_i = 3 \text{ to } t_{f,2} = 72$$

$$\text{For } t_i = 3 \text{ to } t_{f,1} = 68$$

Shrinkage Strains:

For $t_i = 3$ to $t_{f,2} = 72$:

$$\varepsilon_{bdf} = k_s k_{hs} k_f k_{td} 0.48 \times 10^{-3} = 1.0 \times 1.02 \times 0.67 \times 0.663 \times 0.48 \times 10^{-3} = 0.000217$$

For $t_i = 3$ to $t_{f,1} = 68$:

$$\varepsilon_{bdf} = k_s k_{hs} k_f k_{td} 0.48 \times 10^{-3} = 1.0 \times 1.02 \times 0.67 \times 0.650 \times 0.48 \times 10^{-3} = 0.000212$$

Shrinkage Coefficients:

For $t_i = 3$ to $t_{f,2} = 72$:

$$\Psi(t_f, t_i) = 1.9 k_s k_{hs} k_f k_{td} t_i^{-0.118} = 1.9 \times 1.0 \times 1.02 \times 0.67 \times 0.663 \times 3^{-0.118} = 0.738$$

For $t_i = 3$ to $t_{f,1} = 68$:

$$\Psi(t_d, t_i) = 1.9 k_s k_{hs} k_f k_{td} t_i^{-0.118} = 1.9 \times 1.0 \times 1.02 \times 0.67 \times 0.650 \times 68^{-0.118} = 0.723$$

Transformed Section Coefficient, K_{df} :

For $t_i = 3$ to $t_{f,2} = 72$:

$$K_{df} = \frac{1}{1 + \frac{28500 \text{ ksi}}{4985 \text{ ksi}} \frac{38.2 \text{ in}^2}{9104.5 \text{ in}^2} \left(1 + \frac{9104.5 \text{ in}^2 (64.7 \text{ in})^2}{13088563 \text{ in}^4} \right) [1 + 0.7(0.738)]} = 0.875$$

For $t_i = 3$ to $t_{f,1} = 68$:

$$K_{df} = \frac{1}{1 + \frac{28500 \text{ ksi}}{4985 \text{ ksi}} \frac{38.2 \text{ in}^2}{9104.5 \text{ in}^2} \left(1 + \frac{9104.5 \text{ in}^2 (64.7 \text{ in})^2}{13088563 \text{ in}^4} \right) [1 + 0.7(0.723)]} = 0.876$$

Shrinkage Losses:

For $t_i = 3$ to $t_{f,2} = 72$:

$$\Delta f_{pSD2} = \varepsilon_{bdf} E_p K_{df} = 0.000217 \times 28500 \text{ ksi} \times 0.875 = 5.403 \text{ ksi}$$

For $t_i = 3$ to $t_{f,1} = 68$:

$$\Delta f_{pSD1} = \varepsilon_{bdf} E_p K_{df} = 0.000212 \times 28500 \text{ ksi} \times 0.876 = 5.298 \text{ ksi}$$

The shrinkage loss in the tendon is the difference between Δf_{pSD2} and Δf_{pSD1} as Δf_{pSD1} occurs prior to the tendons being stressed.

$$\Delta f_{pSD} = \Delta f_{pSD2} - \Delta f_{pSD1} = 5.403 \text{ ksi} - 5.298 \text{ ksi} = 0.105 \text{ ksi}$$

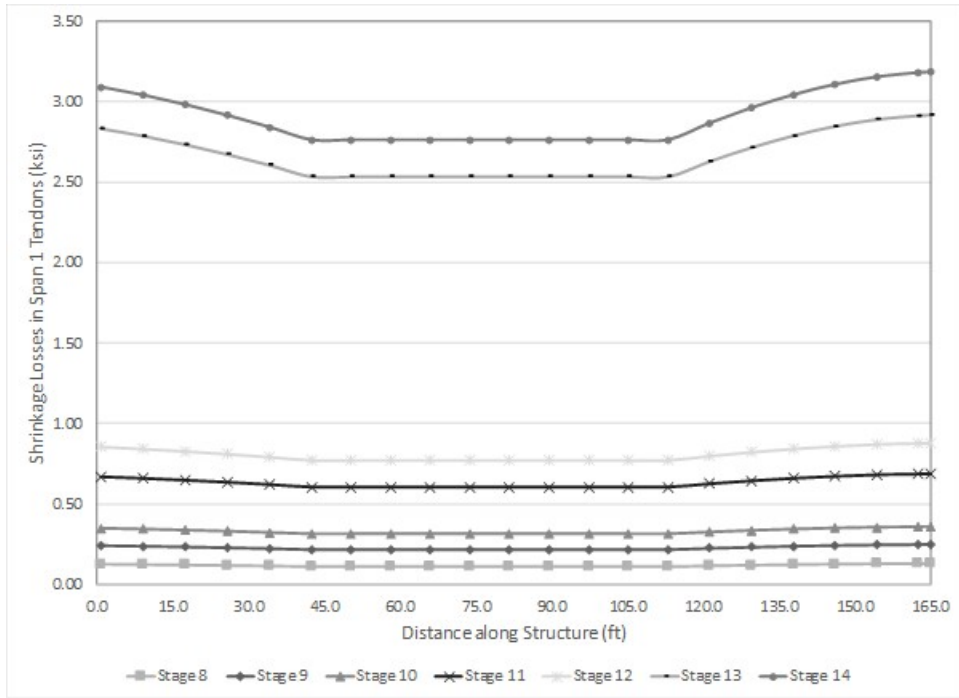


Figure 380. Graph. Shrinkage losses at different stages vs. location - Span 1 tendons.

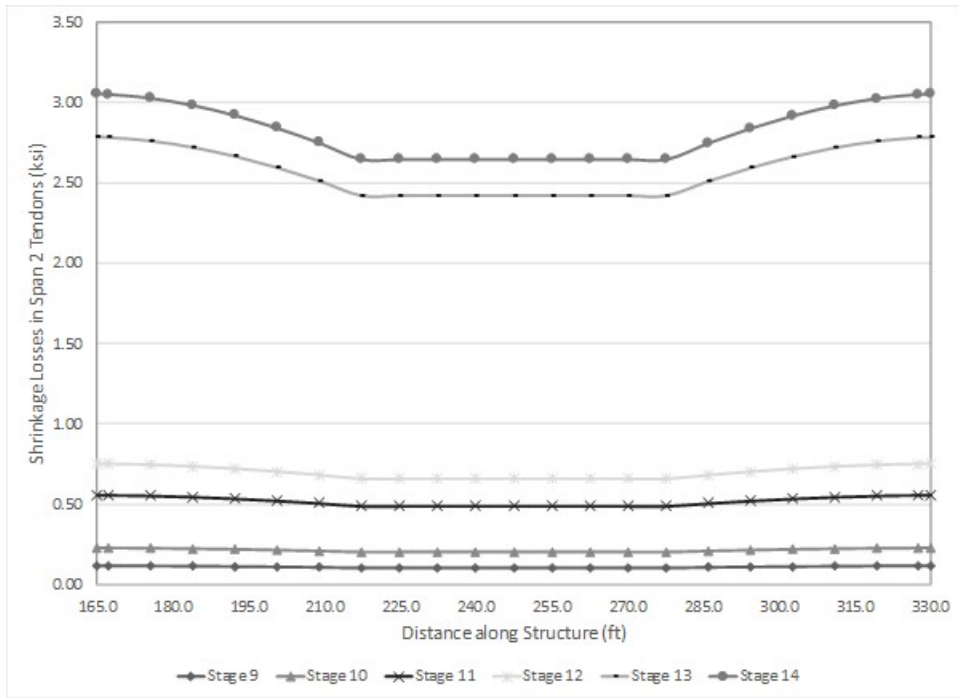


Figure 381. Graph. Shrinkage losses at different stages vs. location - Span 2 tendons.

9.7.1.2.3.7 Tendon Forces after Losses

The force remaining in the tendon after losses have occurred is given by Equation (88). The losses due to creep and shrinkage vary with time. Therefore, the force in each tendon is provided at several different points in time.

$$F = F_{pJ} - (\Delta F_{pF} + \Delta F_{pA} + \Delta F_{pR} + \Delta F_{pES} + \Delta F_{pCR} + \Delta F_{pSH}) \quad (88)$$

Tables 98 through 105 provide the tendon forces for each continuity tendon in Spans 1 and 2 during the various construction stages. The values provided for Stage 4 include the effects of friction, elastic shortening, and anchor set losses.

Table 98. Span 1 tendon T1 forces.

Segment	Stage 4	Stage 8	Stage 9	Stage 10	Stage 11	Stage 12	Stage 13	Stage 14
⑥ to ④	834.7	831.4	828.5	826.3	820.3	811.9	786.4	785.1
④ to ③	877.2	874.0	868.8	866.5	858.8	850.4	822.4	821.5
③ to ②	919.2	916.3	910.8	908.7	900.9	891.6	862.0	860.6
② to ①	953.1	950.6	948.1	946.3	941.4	933.0	908.9	907.3

Table 99. Span 1 tendon T2 forces.

Segment	Stage 4	Stage 8	Stage 9	Stage 10	Stage 11	Stage 12	Stage 13	Stage 14
⑥ to ④	846.5	843.2	840.2	838.0	832.0	823.7	798.2	796.9
④ to ③	880.8	877.6	872.2	869.9	862.0	853.5	825.1	824.1
③ to ②	915.0	912.2	913.2	911.2	904.2	895.1	866.8	865.3
② to ①	953.0	950.6	948.2	946.4	941.5	933.2	909.4	907.8

Table 100. Span 1 tendon T3 forces.

Segment	Stage 4	Stage 8	Stage 9	Stage 10	Stage 11	Stage 12	Stage 13	Stage 14
⑥ to ④	836.8	833.5	830.6	828.4	822.4	814.0	788.5	787.2
④ to ③	856.7	853.4	848.0	845.6	837.7	829.1	800.4	799.4
③ to ②	895.8	893.3	888.9	886.9	880.3	871.2	843.6	842.1
② to ①	927.0	924.5	922.1	920.4	915.5	907.2	883.4	881.8

Table 101. Span 1 tendon T4 forces.

Segment	Stage 4	Stage 8	Stage 9	Stage 10	Stage 11	Stage 12	Stage 13	Stage 14
⑥ to ④	851.7	848.4	845.4	843.2	837.2	828.9	803.3	802.1
④ to ③	878.0	874.9	869.8	867.6	860.0	851.3	822.9	821.8
③ to ②	878.0	874.9	869.8	867.6	860.0	851.3	822.9	821.8
② to ①	926.7	924.3	921.9	920.1	915.2	906.9	883.1	881.5

Table 102. Span 2 tendon T1 forces.

Segment	Stage 4	Stage 8	Stage 9	Stage 10	Stage 11	Stage 12	Stage 13	Stage 14
⑥ to ⑤	-	826.3	823.8	821.9	816.8	808.5	784.8	783.3
⑤ to ④	-	855.6	851.1	847.6	838.8	829.1	797.6	796.2
④ to ③	-	895.3	890.3	884.6	874.3	864.2	829.3	828.4
③ to ②	-	938.2	935.1	930.8	923.7	914.5	885.5	884.0
② to ①	-	972.8	970.3	967.8	962.4	953.9	929.2	927.5

Table 103. Span 2 tendon T2 forces.

Segment	Stage 4	Stage 8	Stage 9	Stage 10	Stage 11	Stage 12	Stage 13	Stage 14
⑥ to ⑤	-	830.0	827.4	825.6	820.5	812.2	788.5	786.9
⑤ to ④	-	858.9	854.4	850.9	842.2	832.4	800.9	799.5
④ to ③	-	898.3	893.3	887.5	877.2	867.1	832.2	831.3
③ to ②	-	939.7	936.7	932.3	925.3	916.0	887.0	885.5
② to ①	-	972.8	970.3	967.8	962.4	953.9	929.1	927.5

Table 104. Span 2 tendon T3 forces.

Segment	Stage 4	Stage 8	Stage 9	Stage 10	Stage 11	Stage 12	Stage 13	Stage 14
⑥ to ⑤	-	829.8	827.3	825.5	820.4	812.1	788.4	786.8
⑤ to ④	-	859.3	854.7	851.2	842.5	832.7	801.2	799.8
④ to ③	-	899.0	894.0	888.3	878.0	867.9	833.0	832.1
③ to ②	-	940.1	937.1	932.7	925.7	916.4	887.4	885.9
② to ①	-	972.8	970.3	967.8	962.4	953.9	929.1	927.5

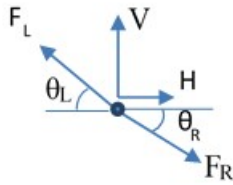
Table 105. Span 2 tendon T4 forces.

Segment	Stage 4	Stage 8	Stage 9	Stage 10	Stage 11	Stage 12	Stage 13	Stage 14
⑥ to ⑤	-	839.6	837.0	835.2	830.1	821.8	798.1	796.5
⑤ to ④	-	886.6	882.0	878.6	869.8	860.0	828.5	827.1
④ to ③	-	897.5	892.5	886.7	876.5	866.4	831.5	830.6
③ to ②	-	908.6	905.5	901.1	894.1	884.9	855.9	854.4
② to ①	-	959.2	956.7	954.2	948.9	940.4	915.6	914.0

9.7.1.2.3.8 Equivalent Loads Applied to Beam Elements

The equivalent loads to be applied to the beam elements are calculated using the tendon forces in Tables 98 through 105 above. The equivalent loads are calculated for Span 2 Tendon T1 for Stage 8; the procedure is repeated for each tendon at each stage. The equivalent loads for each tendon are summarized in Table 106 below; note that in the analysis model, the values used are two times that shown in Table 106 as there are two of each tendon. Figure 382 shows the free-

body diagram for a node where the tendon profile changes; the reactions, V and H, are the equivalent loads that are applied to the concrete beam elements. The angles, θ_L and θ_R , are positive in a counter-clockwise direction from the horizontal.



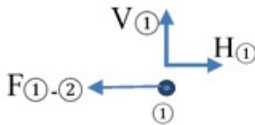
$$H = -F_L \cos(\theta_L) + F_R \cos(\theta_R)$$

$$V = F_L \sin(\theta_L) - F_R \sin(\theta_R)$$

Figure 382. Illustration. Equivalent load free-body diagram.

Right End of Beam

The free-body diagram of Point ① is shown in Figure 383. For equilibrium, the equivalent horizontal load is equal to F_1 but opposite in sign and there is no equivalent vertical load necessary.



$$F_{①-②} = 972.8 \text{ kips}$$

$$\theta_{①-②} = 0.00 \text{ rad}$$

$$\Sigma F_x = 0:$$

$$\begin{aligned} H_{①} &= -F_{①-②} \cos(\theta_{①-②}) \\ &= -972.8 \cos(0.00 \text{ rad}) \\ &= -972.8 \text{ k} \end{aligned}$$

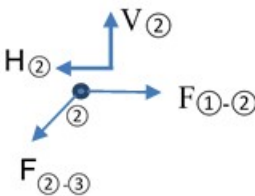
$$\Sigma F_z = 0:$$

$$\begin{aligned} V_{①} &= F_{①-②} \sin(\theta_{①-②}) \\ &= 972.8 \sin(0.00 \text{ rad}) \\ &= 0.0 \text{ k} \end{aligned}$$

Figure 383. Illustration. Free-body diagram - Point ①.

Right Inflection Point

The free-body diagram of Point ② is shown in Figure 384. To maintain equilibrium at Point ②, both horizontal and vertical reactions are necessary; these reactions are the equivalent loads that will be applied to the concrete beam elements.



$$F_{①-②} = 972.8 \text{ kips}$$

$$\theta_{①-②} = 0.0 \text{ rad}$$

$$F_{②-③} = 938.2 \text{ kips}$$

$$\theta_{②-③} = -0.12 \text{ rad}$$

$$\Sigma F_x = 0:$$

$$\begin{aligned} H_{②} &= -F_{②-③} \times \cos(\theta_{②-③}) + F_{①-②} \cos(\theta_{①-②}) \\ &= -938.2 \cos(-0.12 \text{ rad}) + 972.8 \cos(0.0 \text{ rad}) \\ &= 41.8 \text{ kips} \end{aligned}$$

$$\Sigma F_z = 0:$$

$$\begin{aligned} V_{②} &= F_{②-③} \times \sin(\theta_{②-③}) - F_{①-②} \sin(\theta_{①-②}) \\ &= 938.2 \sin(-0.12 \text{ rad}) - 972.8 \sin(0.0 \text{ rad}) \\ &= -116.5 \text{ kips} \end{aligned}$$

Figure 384. Illustration. Free-body diagram - Point ②.

Right Deviation Point

The free-body diagram of Point ③ is shown in Figure 385. To maintain equilibrium both horizontal and vertical reactions are necessary; these reactions are the equivalent loads that will be applied to the concrete beam elements.

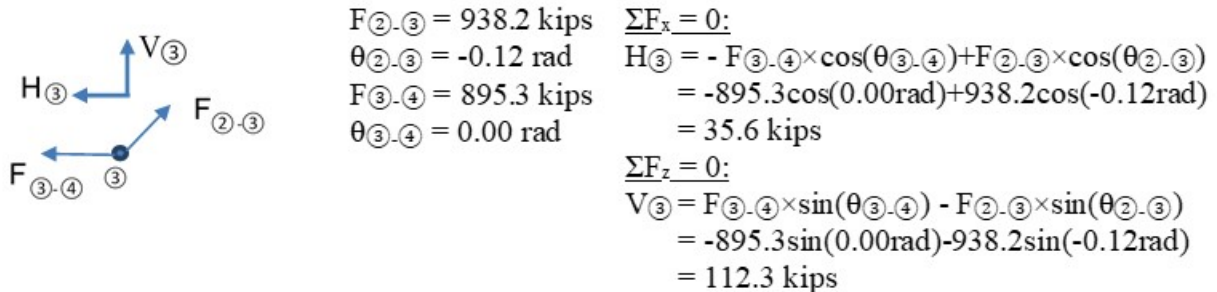


Figure 385. Free-body diagram - Point ③.

Left Deviation Point

The free-body diagram of Point ④ is shown in Figure 386. To maintain equilibrium both horizontal and vertical reactions are necessary; these reactions are the equivalent loads that will be applied to the concrete beam elements.

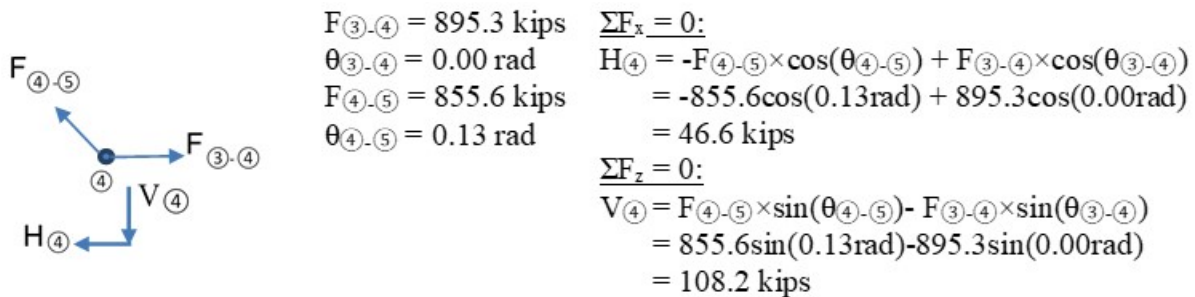


Figure 386. Illustration. Free-body diagram - Point ④.

Left Inflection Point

The free-body diagram of Point ⑤ is shown in Figure 387. To maintain equilibrium both horizontal and vertical reactions are necessary; these reactions are the equivalent loads that will be applied to the concrete beam elements.

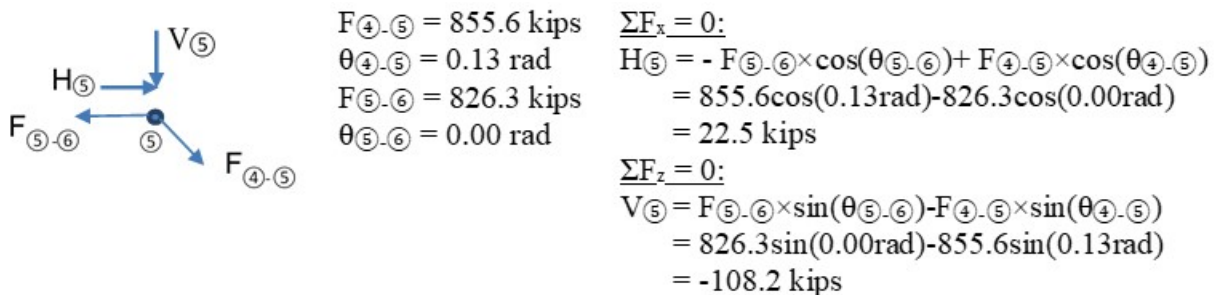
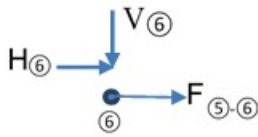


Figure 387. Illustration. Free-body diagram - Point ⑤.

Left End of Beam

The free-body diagram of Point ⑥ is shown in Figure 388. To maintain equilibrium both horizontal and vertical reactions are necessary; these reactions are the equivalent loads that will be applied to the concrete beam elements.



The free-body diagram shows a central point labeled ⑥. Three force vectors originate from this point: a horizontal arrow pointing left labeled $H_{⑥}$, a vertical arrow pointing down labeled $V_{⑥}$, and a horizontal arrow pointing right labeled $F_{⑤-⑥}$.

$$F_{⑤-⑥} = 826.3 \text{ kips}$$
$$\theta_{⑤-⑥} = 0.00 \text{ rad}$$
$$\underline{\Sigma F_x} = 0:$$
$$H_{⑥} = F_{⑤-⑥} \times \cos(\theta_{⑤-⑥})$$
$$= 826.3 \cos(0.00 \text{ rad})$$
$$= 826.3 \text{ kips}$$
$$\underline{\Sigma F_z} = 0:$$
$$V_{⑥} = -F_{⑤-⑥} \times \sin(\theta_{⑤-⑥})$$
$$= -826.3 \sin(0.00 \text{ rad})$$
$$= 0.00 \text{ kips}$$

Figure 388. Illustration. Free-body diagram - Point ⑥.

Table 106. Equivalent loads for model.

Stage	Tendon	Left End		Left Inflection Point		Left Deviator		Right Deviator		Right Inflection Point		Right End	
		H (k)	V (k)	H (k)	V (k)	H (k)	V (k)	H (k)	V (k)	H (k)	V (k)	H (k)	V (k)
Stage 4	Span 1 - T1	827.51	-109.45	-	-	49.70	109.45	34.78	114.69	41.08	-114.69	-953.07	0.00
	Span 1 - T2	842.88	-77.97	-	-	37.97	77.97	26.49	117.98	45.70	-117.98	-953.04	0.00
	Span 1 - T3	836.52	-22.99	-	-	20.16	22.99	31.49	117.01	38.83	-117.01	-927.00	0.00
	Span 1 - T4	851.35	-23.40	-	-	26.61	23.40	0.00	0.00	29.01	190.37	-906.96	-190.37
	Span 2 - T1	-	-	-	-	-	-	-	-	-	-	-	-
	Span 2 - T2	-	-	-	-	-	-	-	-	-	-	-	-
	Span 2 - T3	-	-	-	-	-	-	-	-	-	-	-	-
	Span 2 - T4	-	-	-	-	-	-	-	-	-	-	-	-
Stage 8	Span 1 - T1	824.23	-109.02	-	-	49.74	109.02	35.19	114.34	41.48	-114.34	-950.63	0.00
	Span 1 - T2	839.58	-77.67	-	-	38.02	77.67	26.96	117.62	46.01	-117.62	-950.57	0.00
	Span 1 - T3	833.21	-22.90	-	-	20.21	22.90	32.20	116.67	38.91	-116.67	-924.54	0.00
	Span 1 - T4	848.03	-23.31	-	-	26.88	23.31	0.00	0.00	29.64	189.87	-904.55	-189.87
	Span 2 - T1	826.28	0.00	22.48	-108.18	46.55	108.18	35.60	116.48	41.84	-116.48	-972.76	0.00
	Span 2 - T2	829.96	0.00	21.73	-111.44	46.59	111.44	33.67	120.57	40.80	-120.57	-972.75	0.00
	Span 2 - T3	829.85	0.00	22.14	-111.48	47.05	111.48	33.11	122.17	40.61	-122.17	-972.75	0.00
	Span 2 - T4	821.65	-172.47	64.93	172.47	10.92	0.00	11.05	0.00	30.23	197.05	-938.78	-197.05
Stage 9	Span 1 - T1	821.32	-108.63	-	-	47.46	108.63	34.93	113.65	44.36	-113.65	-948.08	0.00
	Span 1 - T2	836.66	-77.40	-	-	35.54	77.40	33.41	117.76	42.55	-117.76	-948.17	0.00
	Span 1 - T3	830.28	-22.82	-	-	17.67	22.82	33.31	116.09	40.87	-116.09	-922.13	0.00
	Span 1 - T4	845.11	-23.23	-	-	24.67	23.23	0.00	0.00	32.42	189.37	-902.20	-189.37
	Span 2 - T1	823.76	0.00	20.50	-107.61	46.03	107.61	37.60	116.10	42.38	-116.10	-970.27	0.00
	Span 2 - T2	827.43	0.00	19.75	-110.85	46.07	110.85	35.67	120.17	41.34	-120.17	-970.26	0.00
	Span 2 - T3	827.32	0.00	20.17	-110.89	46.52	110.89	35.10	121.78	41.15	-121.78	-970.26	0.00
	Span 2 - T4	819.18	-171.95	62.86	171.95	10.43	0.00	13.02	0.00	30.85	196.54	-936.34	-196.54
Stage 10	Span 1 - T1	819.14	-108.34	-	-	47.37	108.34	35.05	113.38	44.77	-113.38	-946.33	0.00
	Span 1 - T2	834.47	-77.20	-	-	35.43	77.20	33.71	117.49	42.82	-117.49	-946.42	0.00
	Span 1 - T3	828.08	-22.76	-	-	17.56	22.76	33.68	115.84	41.06	-115.84	-920.38	0.00
	Span 1 - T4	842.90	-23.17	-	-	24.67	23.17	0.00	0.00	32.92	189.01	-900.49	-189.01
	Span 2 - T1	821.91	0.00	18.89	-107.17	43.76	107.17	38.99	115.56	44.21	-115.56	-967.77	0.00
	Span 2 - T2	825.59	0.00	18.14	-110.40	43.79	110.40	37.07	119.61	43.17	-119.61	-967.76	0.00
	Span 2 - T3	825.48	0.00	18.56	-110.44	44.25	110.44	36.50	121.21	42.98	-121.21	-967.76	0.00
	Span 2 - T4	817.38	-171.57	61.19	171.57	8.18	0.00	14.38	0.00	32.77	196.02	-933.90	-196.02

Stage	Tendon	Left End		Left Inflection Point		Left Deviator		Right Deviator		Right Inflection Point		Right End	
		H (k)	V (k)	H (k)	V (k)	H (k)	V (k)	H (k)	V (k)	H (k)	V (k)	H (k)	V (k)
Stage 11	Span 1 - T1	813.17	-107.55	-	-	45.63	107.55	35.09	112.42	47.46	-112.42	-941.35	0.00
	Span 1 - T2	828.48	-76.64	-	-	33.53	76.64	34.67	116.59	44.86	-116.59	-941.54	0.00
	Span 1 - T3	822.07	-22.59	-	-	15.60	22.59	35.08	114.97	42.75	-114.97	-915.50	0.00
	Span 1 - T4	836.89	-23.00	-	-	23.13	23.00	0.00	0.00	35.69	188.01	-895.71	-188.01
	Span 2 - T1	816.80	0.00	15.32	-106.06	42.15	106.06	42.33	114.69	45.79	-114.69	-962.39	0.00
	Span 2 - T2	820.47	0.00	14.58	-109.26	42.18	109.26	40.41	118.72	44.73	-118.72	-962.38	0.00
	Span 2 - T3	820.36	0.00	14.99	-109.30	42.64	109.30	39.85	120.30	44.54	-120.30	-962.38	0.00
	Span 2 - T4	812.37	-170.52	57.44	170.52	6.65	0.00	17.67	0.00	34.51	194.92	-928.63	-194.92
Stage 12	Span 1 - T1	804.91	-106.46	-	-	45.50	106.46	34.21	111.25	48.36	-111.25	-932.98	0.00
	Span 1 - T2	820.18	-75.87	-	-	33.32	75.87	34.10	115.41	45.63	-115.41	-933.23	0.00
	Span 1 - T3	813.74	-22.37	-	-	15.33	22.37	34.69	113.79	43.44	-113.79	-907.20	0.00
	Span 1 - T4	828.56	-22.77	-	-	22.71	22.77	0.00	0.00	36.31	186.30	-887.58	-186.30
	Span 2 - T1	808.52	0.00	13.89	-104.82	41.76	104.82	43.24	113.54	46.51	-113.54	-953.92	0.00
	Span 2 - T2	812.20	0.00	13.15	-107.99	41.78	107.99	41.33	117.53	45.45	-117.53	-953.91	0.00
	Span 2 - T3	812.08	0.00	13.56	-108.03	42.24	108.03	40.77	119.10	45.26	-119.10	-953.91	0.00
	Span 2 - T4	804.27	-168.82	55.75	168.82	6.34	0.00	18.51	0.00	35.48	193.18	-920.34	-193.18
Stage 13	Span 1 - T1	779.60	-103.11	-	-	42.84	103.11	32.80	107.56	53.69	-107.56	-908.94	0.00
	Span 1 - T2	794.76	-73.52	-	-	30.31	73.52	34.54	111.77	49.80	-111.77	-909.41	0.00
	Span 1 - T3	788.22	-21.66	-	-	12.14	21.66	36.06	110.19	46.96	-110.19	-883.38	0.00
	Span 1 - T4	803.04	-22.07	-	-	19.88	22.07	0.00	0.00	41.35	181.41	-864.27	-181.41
	Span 2 - T1	784.83	0.00	6.32	-100.84	38.13	100.84	49.34	109.94	50.53	-109.94	-929.15	0.00
	Span 2 - T2	788.51	0.00	5.60	-103.91	38.14	103.91	47.44	113.81	49.46	-113.81	-929.15	0.00
	Span 2 - T3	788.39	0.00	6.01	-103.95	38.60	103.95	46.89	115.33	49.26	-115.33	-929.15	0.00
	Span 2 - T4	781.08	-163.95	47.42	163.95	2.96	0.00	24.38	0.00	40.25	188.09	-896.11	-188.09
Stage 14	Span 1 - T1	778.33	-102.95	-	-	43.17	102.95	32.35	107.38	53.45	-107.38	-907.31	0.00
	Span 1 - T2	793.48	-73.41	-	-	30.64	73.41	33.98	111.58	49.71	-111.58	-907.82	0.00
	Span 1 - T3	786.94	-21.63	-	-	12.45	21.63	35.46	109.98	46.93	-109.98	-881.79	0.00
	Span 1 - T4	801.76	-22.04	-	-	20.00	22.04	0.00	0.00	40.95	181.08	-862.71	-181.08
	Span 2 - T1	783.25	0.00	6.53	-100.66	38.59	100.66	48.78	109.75	50.36	-109.75	-927.52	0.00
	Span 2 - T2	786.93	0.00	5.81	-103.73	38.61	103.73	46.88	113.62	49.29	-113.62	-927.52	0.00
	Span 2 - T3	786.82	0.00	6.22	-103.77	39.06	103.77	46.32	115.13	49.09	-115.13	-927.52	0.00
	Span 2 - T4	779.54	-163.63	47.59	163.63	3.44	0.00	23.81	0.00	40.13	187.76	-894.51	-187.76

Depending on the analysis software, it may be possible to apply the equivalent loads as eccentric point loads where the eccentricity is equal to the distance from the tendon location to the neutral axis of the cross-section. In LUSAS this can be done using “Discrete Point Loads”; when defining the load effects, the physical location of the force is also defined as shown in Table 107. In this example, the discrete point load is applied to a node at the location of the anchorage; each component of the discrete point load is then applied at a location described by the X, Y, and Z distances shown in Table 107. Note that Z should account for the difference eccentricity between the center of gravity of the typical section and the center of gravity of the section at the anchorage and diaphragm locations. For example, if the node that the discrete point load was assigned to is located at (0, 0, 0) then the load described by the first line of data in Table 107 would be located at (160 ft 3 inches, 0, 11.3 inches).

Table 107. Discrete point load definition for Span 2 – Tendon T1 (Stage 8).

X	Y	Z	PX	PY	PZ
160 ft 3 inches	0	11.3 inches	826.3	0.0	0.0
167 ft 4 inches	0	11.3 inches	22.5	0.0	-108.2
217 ft 3.5 inches	0	-5 ft 4.7 inches	46.6	0.0	108.2
277 ft 9.5 inches	0	-5 ft 4.7 inches	35.6	0.0	116.5
327 ft 8 inches	0	9.8 inches	41.8	0.0	-116.5
330 ft 0 inches	0	9.8 inches	-972.8	0.0	0.0

If the analysis software does not include a similar load definition, the moment due to the tendon eccentricity should be calculated at each location as $P \times e$ where P is the tendon force and e is the eccentricity.

9.7.1.2.4 Step 2d – Run Analysis and Verify Results

Moment and shear diagrams are reviewed to make sure that the results are reasonable. Shown in Figure 389 is the shear diagram for the first PT model. There are several significant peaks in the shear diagram that do not appear reasonable with regards to the applied loads. The reason for these peaks is that the applied loads are not located at the same location as a node. The analysis software splits the forces between nodes and applies moments and shears necessary to enforce equilibrium and compatibility. The shear diagram for the revised model, with nodes at the locations of the applied loads, is shown in Figure 390. The fictitious peaks previously seen in the shear diagram no longer occur.

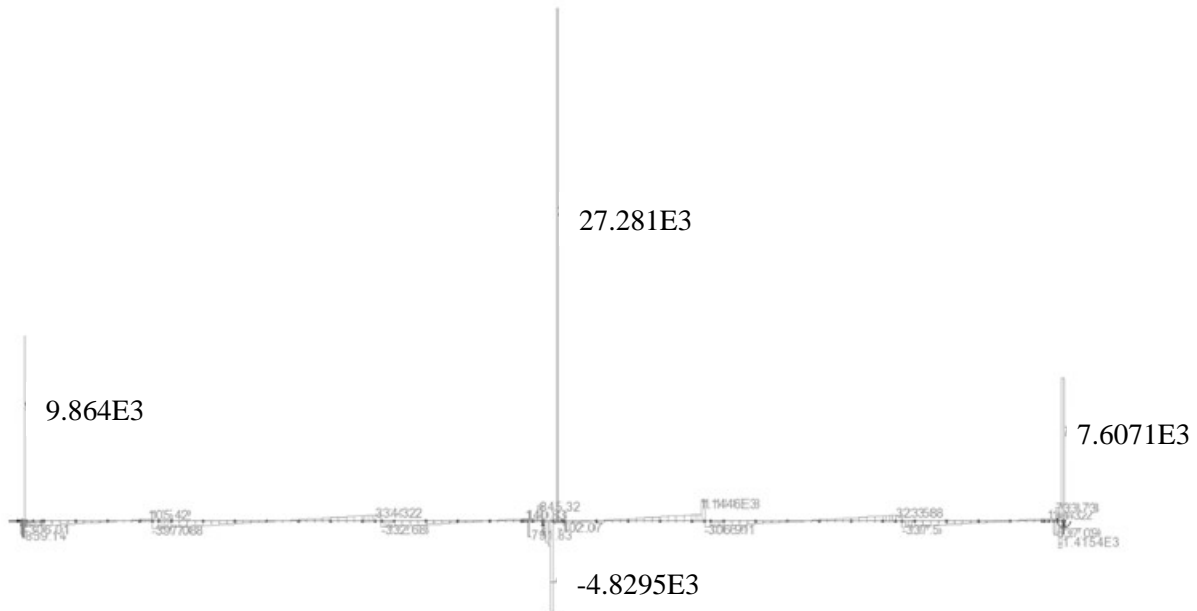


Figure 389. Illustration. Shears due to PT and dead loads - Model 1.

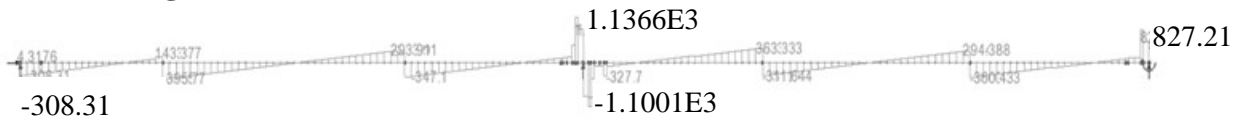


Figure 390. Illustration. Shears due to PT and dead loads - Model 2.

9.7.1.2.5 Step 2e – Extract Required Results from Software

After verifying that the results from the analysis are reasonable, the results of interest can be extracted and input into a spreadsheet for further use. Since the model utilizes beam elements, bending moments and shears can be extracted directly from the analysis model and used in the design. Figure 391 shows the moment and Figure 393 shows the shear due to post-tensioning for various construction stages; note that the PT moments shown in the figure below are not included in the determination of the design moment, M_u . The effects of the post-tensioning are not included on the load side of the equation, instead they are included in determining the resistance. In Figure 391 and Figure 392, positive moments result in tension on the top surface of the beam and negative moments result in compression on the top surface of the beam.

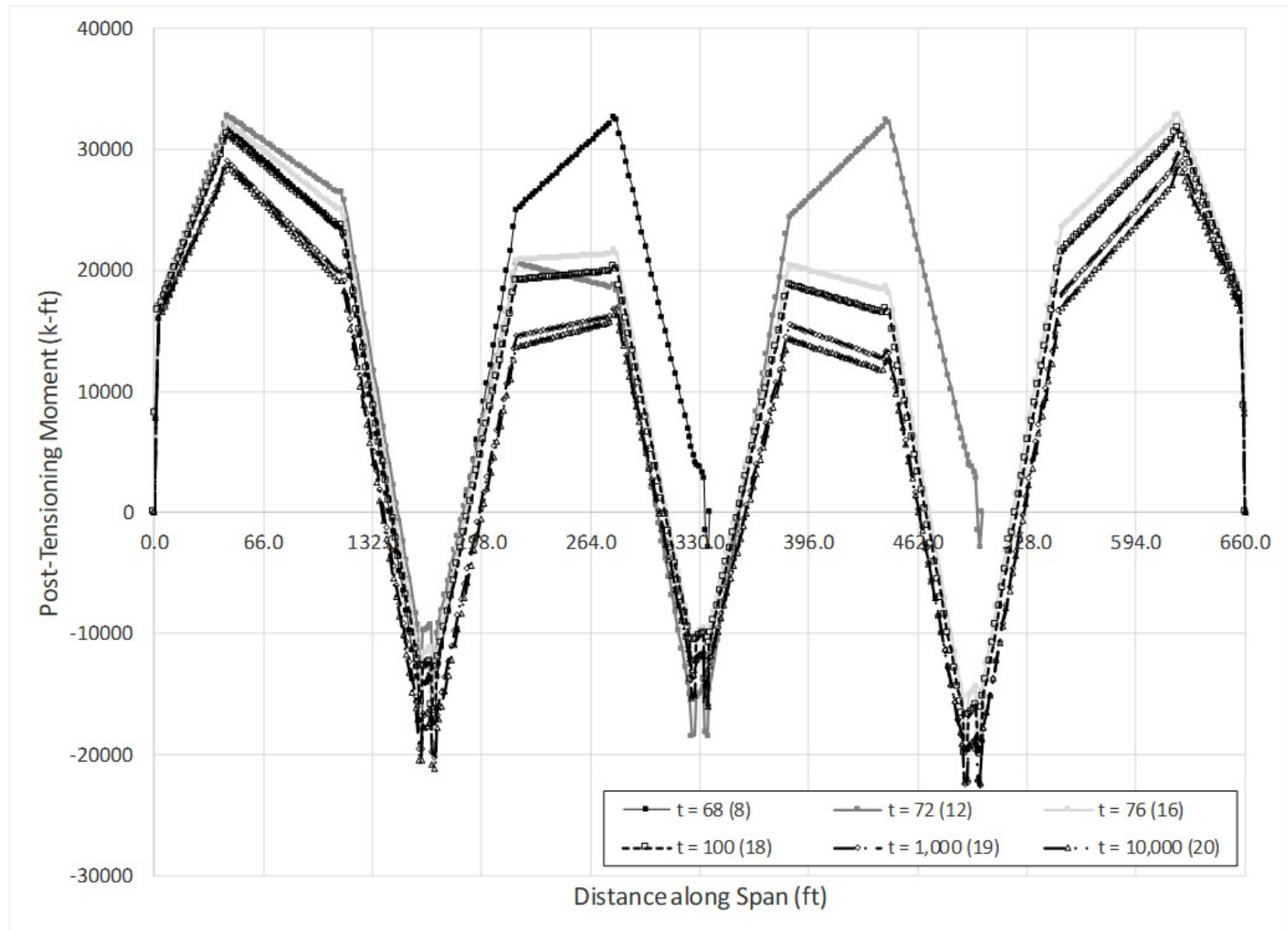


Figure 391. Graph. Moment due to post-tensioning vs. distance along span for various construction stages.

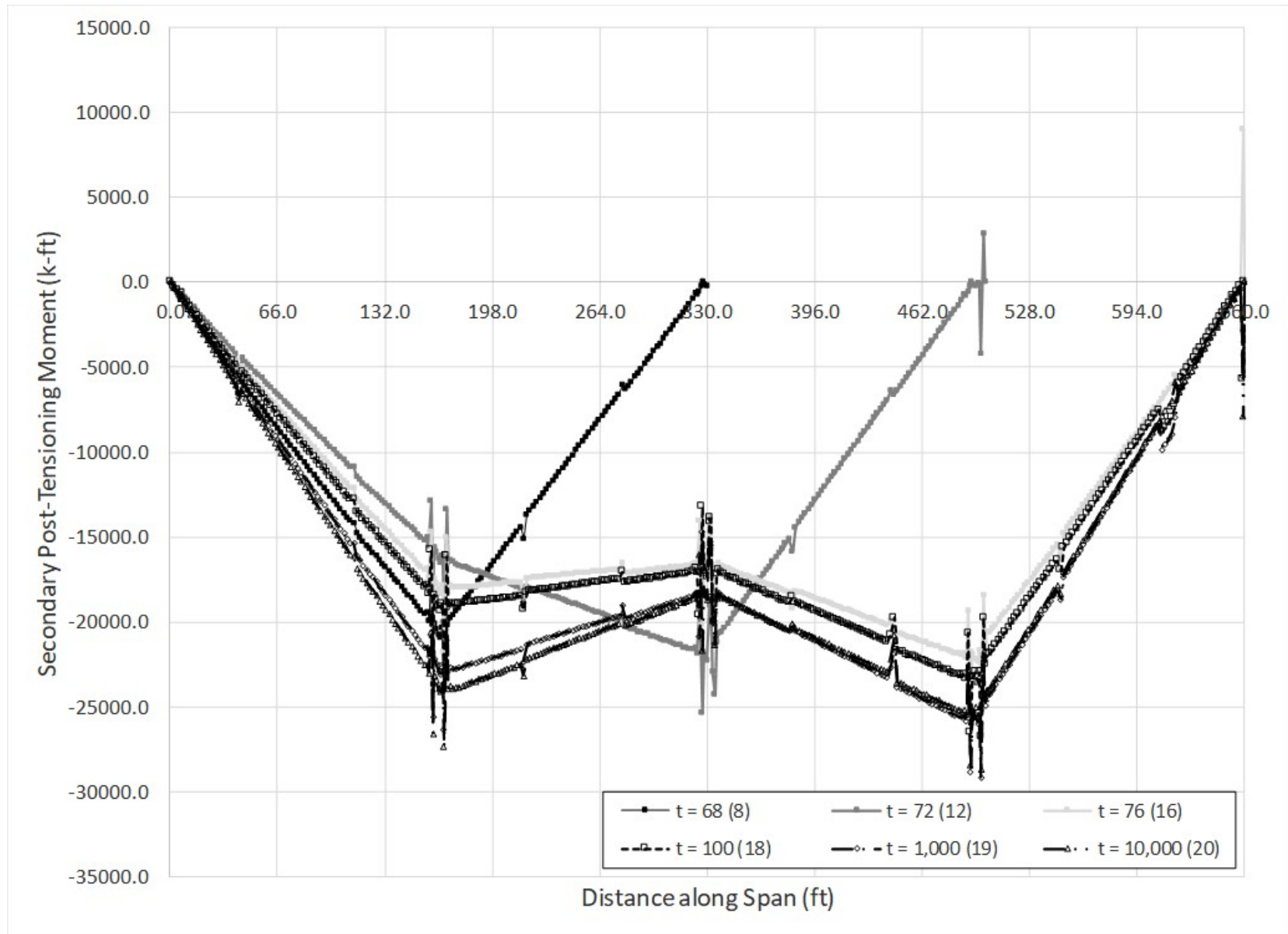


Figure 392. Graph. Secondary PT moments vs. distance along span for various construction stages.

The design moment, M_u , should include the secondary moments. An example of determining the secondary moment is shown below for mid-span of Span 2 at 10,000 days. The moment from the equivalent loads applied to the beam in the final condition, M_{res} , is 16,616.4 kip-ft. The primary moment, $M_{primary}$, is calculated as the sum of P times e , where P is the force in the tendon and e is the eccentricity between the centroid of the girder and the centroid of the tendon.

$$\begin{aligned} M_{primary} &= \sum P_i e_i = (2(828.4k + 831.3k + 832.1k + 830.6k)) \times 64.7in \\ &= 429919 \text{ kip-inches} \\ &= 35826.5 \text{ kip-ft} \end{aligned}$$

$$\begin{aligned} e_i &= 64.7 \text{ inches} \\ P_i &= \text{comes from Table 102 through Table 105} \\ P_1 &= 828.4 \text{ k} \\ P_2 &= 831.3 \text{ k} \\ P_3 &= 832.1 \text{ k} \\ P_4 &= 830.6 \text{ k} \end{aligned}$$

$$M_{2nd} = M_{res} - M_{primary} = 16616.4 \text{ k-ft} - 35826.5 \text{ k-ft} = -19,210.1 \text{ k-ft}$$

Figure 393 shows the shear in the beam elements due to the equivalent loads and Figure 394 shows the shear due to the secondary PT moments. The design shear force, V_u , includes the shear forces due to post-tensioning as well as those resulting from the secondary bending moments. The secondary PT shears were determined using Equation (89). It was assumed that the secondary moments are linear between anchorages; this is not exactly the case but is a reasonable, simplifying assumption based on the moment diagram shown in Figure 392. A sample calculation is shown below for $t = 10,000$ days.

$$V_{2nd} = \frac{\Delta M_{2nd}}{\Delta X} \tag{89}$$

For Span 1:

$$\begin{aligned} \Delta M_{2nd} &= -24,152 \text{ k-ft} \\ \Delta X &= 159 \text{ ft } 5 \text{ inches (from Span 1 left anchorage to Span 2 left anchorage)} \\ V_{2nd} &= \frac{\Delta M_{2nd}}{\Delta X} = \frac{-24152kft}{159.42ft} = -152.7k \end{aligned}$$

For Span 2:

$$\begin{aligned} \Delta M_{2nd} &= 9,802 \text{ k-ft} \\ \Delta X &= 157 \text{ ft } 0 \text{ inches (from Span 2 right anchorage to Span 3 left anchorage)} \\ V_{2nd} &= \frac{\Delta M_{2nd}}{\Delta X} = \frac{9802kft}{157ft} = 62.9k \end{aligned}$$

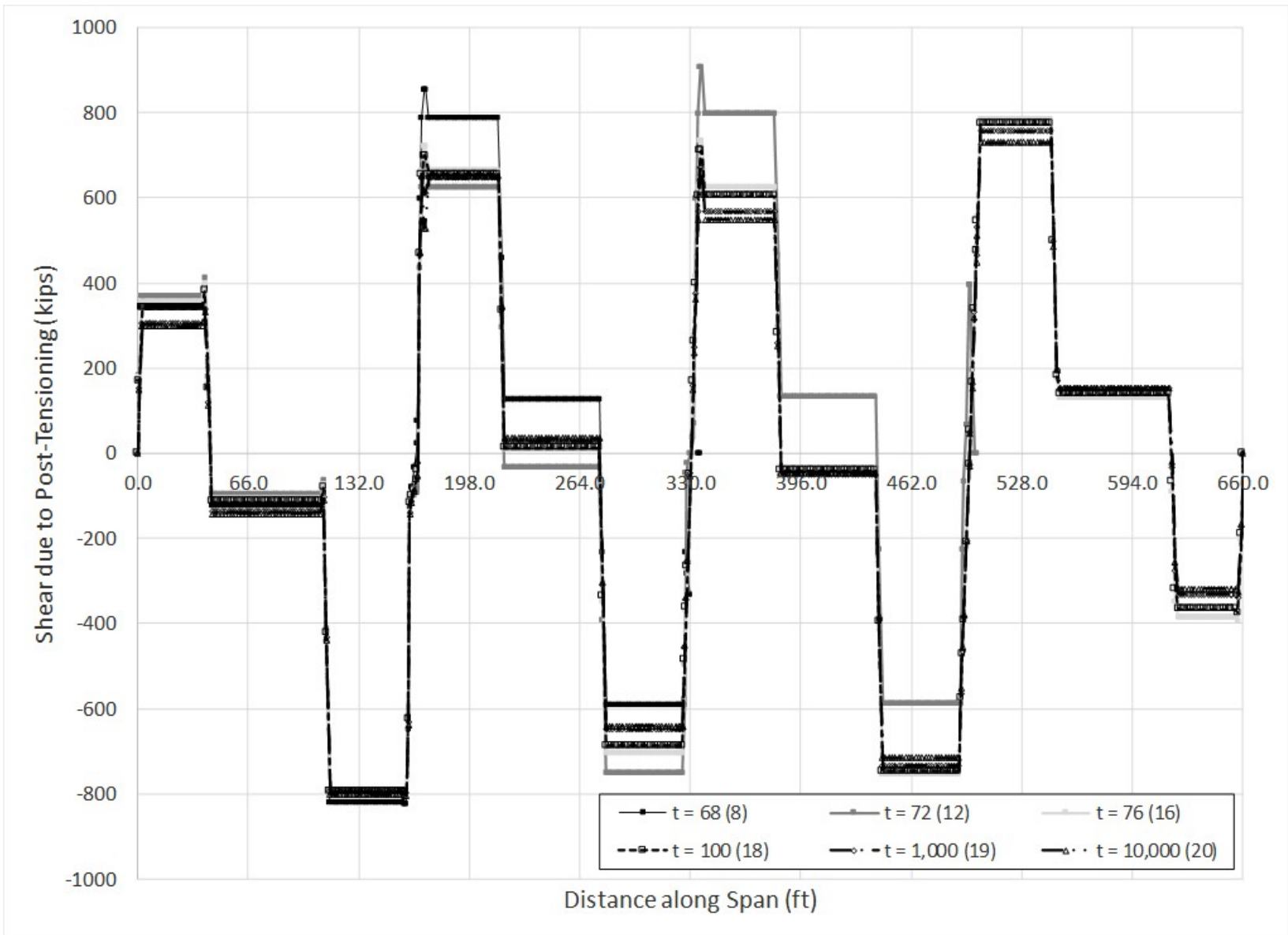


Figure 393. Graph. Shear due to post-tensioning vs. distance along span for various construction stages.

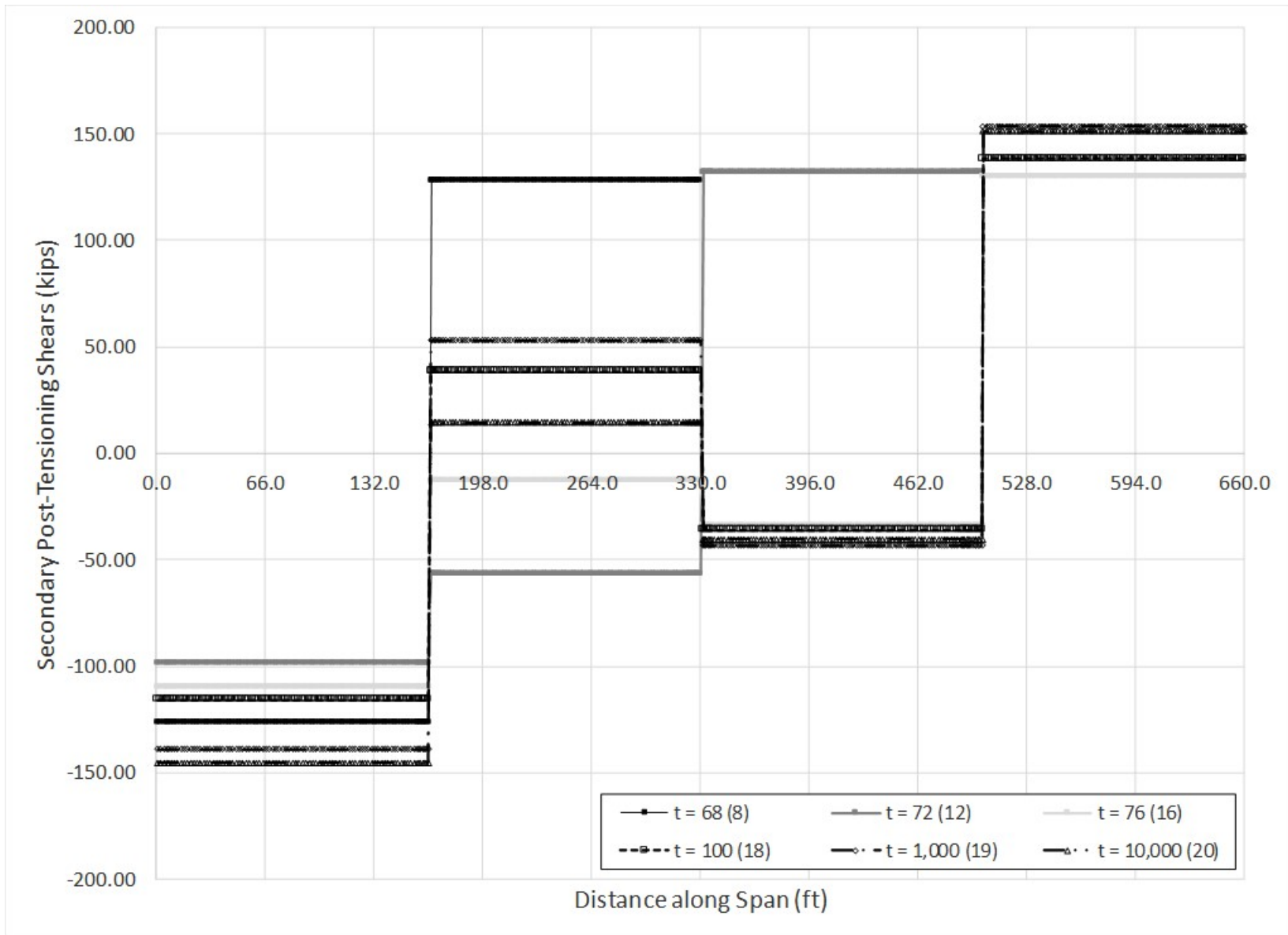


Figure 394. Graph. Secondary PT shears vs. distance along span for various construction stages.

9.7.1.3 Step 3 – Live Load Analysis

9.7.1.3.1 Step 3a – Create Live Load Analysis Model

Make a copy of the model created in Step 1 or 2 and save with a new name.

9.7.1.3.2 Step 3b – Modify Model for Linear-Elastic Analysis

Since live loads are applied for a very short period of time, this analysis is performed on a linear-elastic model that does not consider the effects of creep and shrinkage. The model used is identical to that used in Steps 1 and 2 except that the material definition for the concrete is now a linear-elastic concrete material model instead of the CEB-FIP90 creep model.

The construction staging process is also removed from this analysis model as we are assuming that live load is only applied to the completed structure.

9.7.1.3.3 Step 3c – Determine Optimized Live Loads

In this example, maximum bending moments (along the span length) are determined at mid-span of each span as well as over the interior support. Maximum vertical shears are also determined at a distance “d” away from each support where d is the depth from the extreme compression flange to the centroid of tension reinforcement. Some FEA software has utilities that aid in the generation of influence surfaces and optimized loadings. In the absence of such utilities, influence lines/surfaces can be generated using classical analysis methods. For this example, the software used automatically generates the influence surfaces and then determines the load placement required to obtain extreme effects. It is always a good idea to qualitatively spot check the optimized loadings to make sure that they are reasonable. As an example, Figure 395 shows the loading determined using the analysis software resulting in maximum negative moment over Pier 2. Qualitatively, the loading appears reasonable; it is known that the maximum negative moment at an interior support occurs when both adjacent spans are fully loaded and any point loads are located near the middle of the adjacent spans.

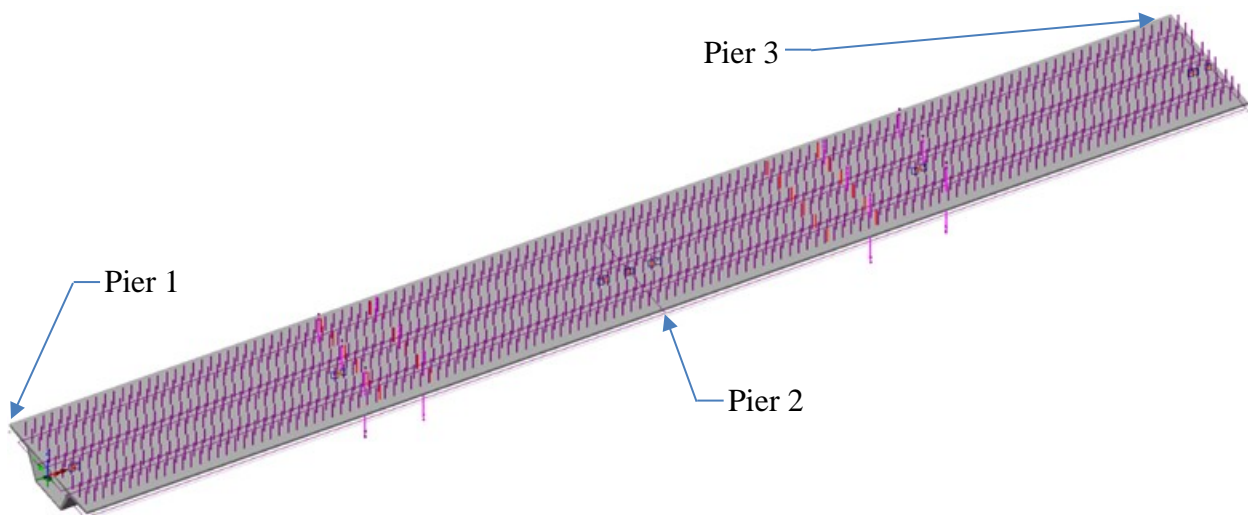


Figure 395. Illustration. Optimized loading for maximum moment over Pier 2.

9.7.1.3.4 Step 3d – Run Analysis and Verify Results

The next step is to run the analysis. In addition to the qualitative inspection of deflected shapes and loading configurations for maximizing specific effects, a simple quantitative check is made to add confidence in the model.

Vertical Reactions for Three Lanes Loaded in Span 1

As a check, the reaction for the loading causing the maximum positive bending moment in the first span will be compared to that calculated by hand.

Weight of three design trucks: $W_{DT} = (3) (72 \text{ k}) = 216 \text{ k}$

Weight of three design lanes: $W_{DL} = (3) (0.64 \text{ kip/ft}) (165 \text{ ft}) = 316.8 \text{ k}$

Total Reaction including Impact: $W = 1.33W_{DT} + W_{DL} = 1.33 \times 216 \text{ k} + 316.8 \text{ k} = 604.1 \text{ k}$

The analysis software includes the multiple presence factor in the live load analysis. For three lanes loaded, the multiple presence factor is 0.85.

Applying the multiple presence factor the total reaction is $W_{mpf} = 0.85 \times 604.1 \text{ k} = 513.468 \text{ kips}$.

Location	X (ft)	Y (ft)	FZ (k)
Pier 1	0	0	219.023
Pier 2	165	0	359.706
Pier 3	330	0	-65.260
		Total =	513.469

The reactions calculated by hand (513.468 kips) and that from the analysis software (513.469 kips) are essentially identical. Therefore, the results from the analysis software appear reasonable.

9.7.1.3.5 Step 3e – Extract Required Results from Analysis Software

After verifying that the results from the analysis are reasonable, the results of interest can be extracted and input into a spreadsheet for further use. Linear elastic results for post-tensioning and dead load should also be extracted from this model.

9.7.1.4 Step 4 – Combine Analysis Results

Once the results of interest, in this case moments and shears, have been extracted from the analysis software, they are factored according to the appropriate limit state. In this case, the Strength I limit state is being considered. From AASHTO LRFD Tables 3.4.1-1, 3.4.1-2, and 3.4.1-3, the Strength I load factors are:

$$\gamma_{DC} = 1.25 \text{ (AASHTO LRFD Table 3.4.1-2)}$$

$$\gamma_{LL} = 1.75 \text{ (AASHTO LRFD Table 3.4.1-1)}$$

$$\gamma_{PS} = 1.0 \text{ (AASHTO LRFD Table 3.4.1-3)}$$

$$\gamma_{CR,SH} = 1.25 \text{ (AASHTO LRFD Table 3.4.1-2 via Table 3.4.1-3)}$$

The effects of creep due to dead load and shrinkage are included in the dead load model from Step 1 using the CEB-FIP material model. The post-tensioning model in Step 2 also uses the CEB-FIP material model and the equivalent loads are calculated at various time steps to account

for the change in post-tensioning force due to creep and shrinkage. Secondary post-tensioning effects as described in Section 4.1.3 are included in the calculation of the factored load. Section 9.7.1.2.5 provides an example of calculating the secondary effects.

The individual component moments for PT, dead load, and live load are summarized in Table 108 for mid-span Span 1, at Pier 2, and at mid-span Span 2. The Strength I design moment is also shown for these three locations. Figure 396 shows the nodal locations in the model.

Table 108. Flexure results for selected locations at 10,000 days.

Node	X (ft)	M_{yPT} (kip-ft)	M_{yDL} (kip-ft)	M_{LL} (kip-ft)	Strength I Moment (kip-ft)
44	82.5	12015	24142	10998	61439
88	165	23941	-23216	-11397	-25023
132	247.5	21112	15197	7258	52810

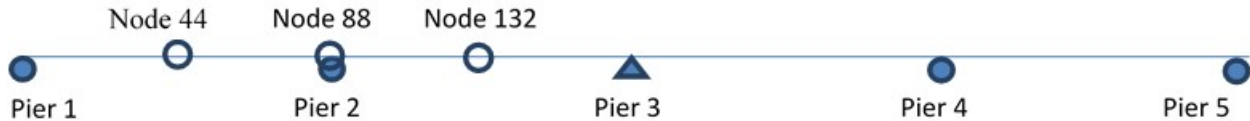


Figure 396. Illustration. Selected locations for design moments.

The individual component shears for PT, dead load, and live load are summarized in Table 109 for Pier 1 and both sides of Pier 2. The Strength I design shear is also shown for these three locations. Figure 397 shows the approximate nodal locations in the model.

Table 109. Shear results for selected locations at 10,000 days.

Node	X (ft)	F_{zPT} (kip)	F_{zDL} (kip)	F_{zLL} (kip)	Strength I Shear (kip)
7	9.1	-152	644.2	317.9	1210
81	156.4	946.1	-931.9	-384.7	-891.9
95	173.8	-667	823.2	352.6	978.9

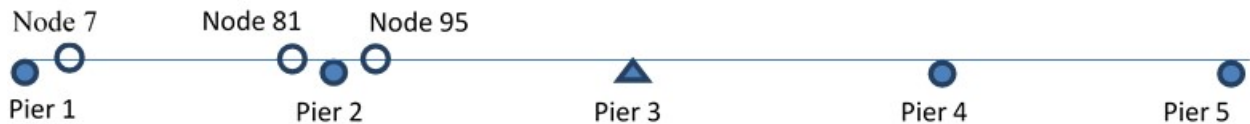


Figure 397. Illustration. Selected locations for design shears.

9.7.2 Shell Element Model Analysis – Using Explicitly Modeled Tendons

The following steps are used to determine the dead and live load moments and shears as well as the moments and shears due to post-tensioning:

1. Create model for dead load with creep and shrinkage.

- a. Create geometry for girders and tendons. Girder webs, flanges, and diaphragms are modeled with shell elements. Tendons are modeled with beam elements with end releases to prevent moments from developing.
 - b. Define section properties for the tendons and thicknesses for the girder webs and flanges.
 - c. Define material properties for girders, diaphragms, and tendons.
 - d. Define support conditions.
 - e. Define loads applied to the structure.
 - i. For the members defined in the model, the girders, diaphragms, and tendons, automatic dead load application can be used if the mass density is assigned through material properties. Otherwise, concentrated or distributed loads that are statically equivalent to the weight of the members can be used.
 - f. Define staged construction steps. The steps in this model are the same as those used for the spine beam analysis in Section 9.7.1.1.6.
 - g. Assign appropriate material and geometric properties to girder and tendon components. Assign loads and activate various members in the appropriate analysis stage.
 - h. Run analysis; verify analysis results using simplified methods.
 - i. Extract required results from analysis software.
2. Create model for post-tensioning analysis including creep.
 - a. Copy model from Step 1 and save with new name to perform analysis of post-tensioning loads.
 - b. Remove dead loads from model.
 - c. Define post-tensioning loads – in this example, the tendons are explicitly modeled, therefore, thermal loads are used to stress the tendons.
 - d. Assign post-tensioning loads to the tendon elements in the appropriate construction stage.
 - e. Run analysis; verify analysis results using simplified methods.
 - f. Extract required results from analysis software.
 3. Create model for live load analysis; this will be the same model used in Steps 1 and 2 but will utilize linear elastic material properties for the concrete.
 - a. Copy model and save with new name to perform live load analysis.
 - b. Modify concrete material properties to be linear-elastic and remove construction staging process from analysis.
 - c. Determine extreme design live load effects for the selected locations. The analysis software may have utilities that help in the determination of the live load placement. Influence lines can be developed to aid in loading generation.
 - d. Run analysis; verify results using simplified methods.
 - e. Extract required results from analysis software.
 4. Combine analysis results for different load cases.

9.7.2.1 Step 1 – Dead Load Model

9.7.2.1.1 Step 1a – Create Geometry for Girders, Tendons, and Diaphragms

Define girder and tendon geometry. The girder geometry is defined by creating shell elements along the centerline of the webs and flanges of the cross-section as shown in Figure 398. In the transverse direction, nodes are indicated by the solid circles shown in Figure 398. Figure 398 shows the basic node locations required to define the shell elements as well as the different shell element thicknesses. Areas ① and ② represent the constant thickness portion of the top slab and bottom slab, respectively. Areas ③, ④, and ⑤ represent the webs, the haunched portion outside the webs, and the haunched portion inside the webs, respectively. The thickness for areas ③, ④, and ⑤ represents an average thickness for the web and haunched portions of the top flange.

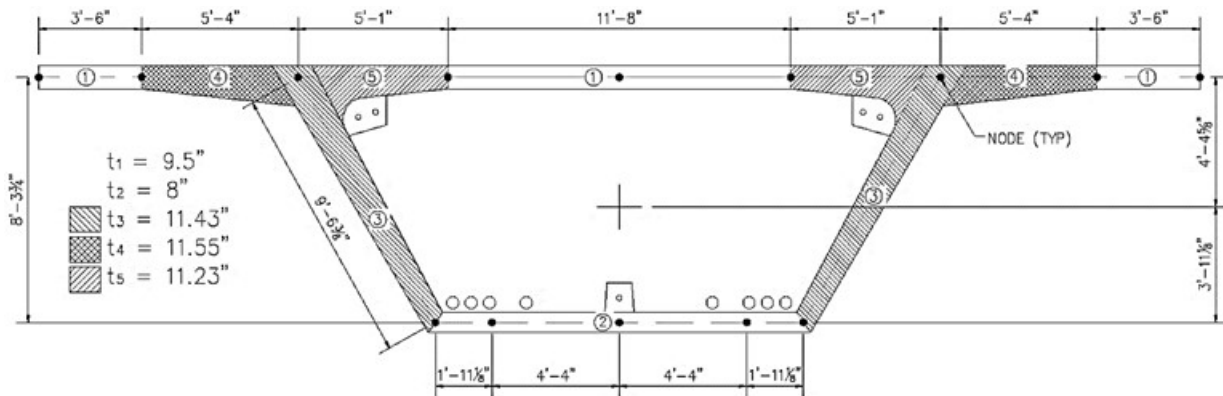


Figure 398. Illustration. Point locations.

Diaphragm geometry is defined by creating shell elements along the centerline of the diaphragm. To provide adequate restraint for the temporary PT anchor blocks (shown as A₁ and A₄ in Section 9.7.2.1.7), additional shell elements (A₂ in Section 9.7.2.1.7) are defined to prevent the anchor block elements from behaving as cantilevers under the post-tensioning load. Additional diaphragms are defined at tendon anchorage locations and points of inflection. See Section 4.1.1.5 for more information regarding diaphragms.

In the longitudinal direction, nodes are defined at the location of the diaphragms and deviation blocks as well as at the locations where the tendons are anchored. The tendons are defined by line elements along the centerline of the duct with nodes at each anchorage location as well as nodes at the location where the tendon changes direction. In this example, beam elements are used to model the tendons. Since the tendons only carry axial load, element end releases are utilized to prevent the tendons from carrying any moment.

9.7.2.1.2 Step 1b – Define Section Properties

For shell elements, the thickness and, if necessary, an eccentricity are defined. An eccentricity is used to align shell elements of different thickness. Shown in Figure 398 are the thicknesses assigned to the different regions of the girder; the thickness and eccentricity for each region are shown in Table 110.

Table 110. Girder shell section properties.

Surface Region	①	②	③	④	⑤
Thickness (in)	9.5	8.0	11.43	11.55	11.23
Eccentricity (in)	0.0	0.0	0.0	1.024	0.865

Additional shell section properties are defined for the diaphragm and deviator cross-sections, see Figure 361. These properties are listed in Table 111. The anchorage diaphragms are assigned an arbitrary thickness to prevent deformation under the applied load from the tendons.

Table 111. Diaphragm section properties.

	Expansion Diaphragm	Deviator	Pier Diaphragm	Anchorage Diaphragms
Thickness (in)	24	24	78	18
Eccentricity (in)	0	0	0	0

The temporary and continuity tendons are defined using beam elements; end releases are used to prevent moments from developing in the tendons. Cross-section properties are calculated using the analysis software for the different tendon types. Only the cross-section areas are shown in Table 112.

Table 112. Tendon section properties.

		Area (in ²)
Temporary Tendons	1 - 1¼ inches ϕ PT Bar	1.227
Continuity Tendons	22 - 0.6 inch ϕ Grade 270 LR Strand	4.774

9.7.2.1.3 Step 1c – Define Material Properties

The material properties for the girder concrete are the same as those defined in Table 89 for the spine beam model with two exceptions. The first exception is that the “nominal size” must be calculated by hand for the shell element model; for the spine beam model, the analysis software uses the beam cross-section to automatically calculate this size. The “nominal size” is determined using Equation (90).

$$Nominal\ Size = \frac{2A_c}{U} = \frac{2(63.2257\ ft^2)}{112.6613\ ft} = 1.12\ ft \quad (90)$$

where: A_c = area of cross-section (ft²)
 U = perimeter (ft), taken here as the outside perimeter plus ½ the inside perimeter as shown in Figure 399

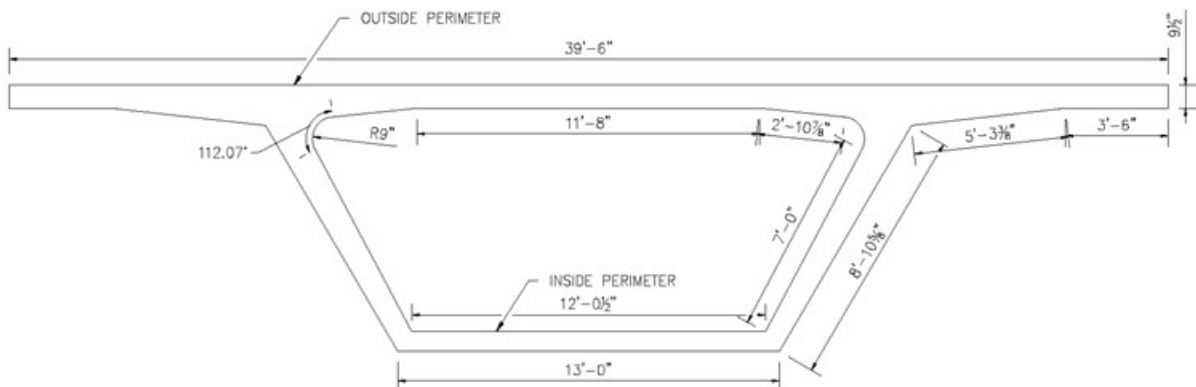


Figure 399. Illustration. Perimeter definition.

In this analysis, the concrete material is a non-linear material which considers the effects of creep and shrinkage according to CEB-FIP Model Code 90. The second exception is that shrinkage is not included in the dead load shell element model but is instead included in the PT model such that the tendons experience the losses due to shrinkage. This material property is included in the software used in the analysis.

The anchorage diaphragms utilize a weightless, isotropic material property to provide the stiffness of the diaphragm but without contributing any load to the structure as the pier diaphragm definition accounts for the weight of the diaphragm.

9.7.2.1.4 Step 1d – Define Support Conditions

The girder is supported by an erection truss until the tendons are stressed and the erection truss moved forward to the next span. The longitudinal support is located at the left end of Span 1. Since only half of the unit is modeled, the right end is restrained against rotation about the transverse axis of the bridge. Supports are located at their approximate physical location since the depth of the girder is modeled, see Figure 400.

The support type and location varies during the different construction stages; one example is when the pier segments are erected each segment is individually supported but once they are connected and the bearing plinth cast, the assembly is set on the permanent bearings. Figure 363 and Figure 400 show an example of this situation; restraints are provided at individual nodes to represent the bearing locations. The actual bearings would distribute the reaction over an area instead of at a single point.

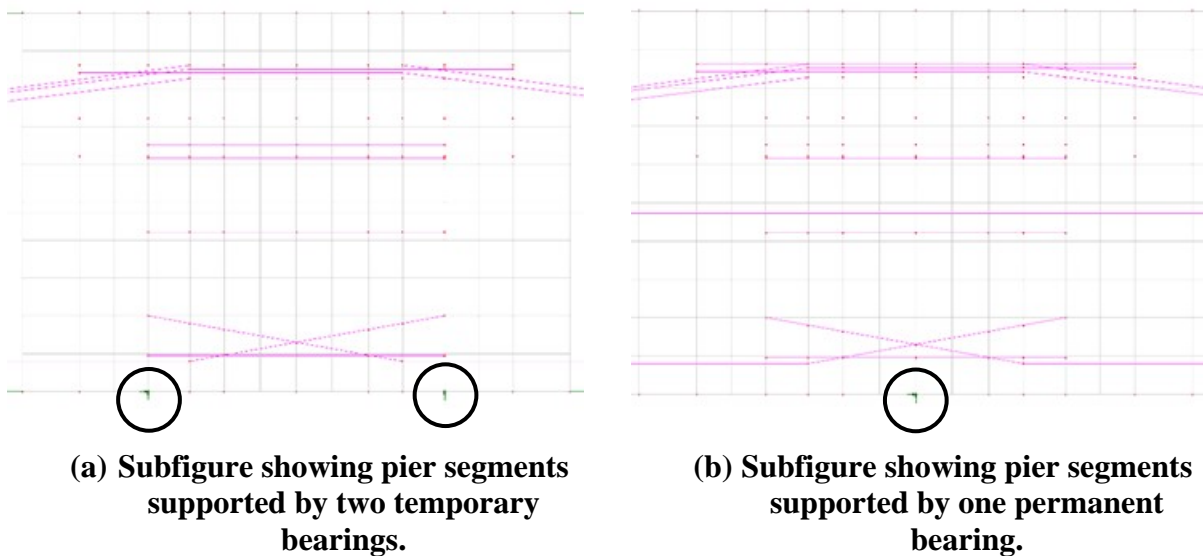


Figure 400. Illustrations. Compound figure showing varying support conditions.

9.7.2.1.5 Step 1e – Define Dead Loads applied to Structure

The self-weight of the girder is applied using the mass density and applying gravitational acceleration to the member. Note that the erection truss carries the weight of the girder until the

erection truss is released, this results in limited bending effects in the longitudinal direction prior to releasing the erection truss. Other dead loads include the weight of the barrier on each side; the specified barrier has a weight per linear foot of 0.376 kips/foot. The weight of the barrier is applied as a uniformly distributed line load to the girder flange tips.

9.7.2.1.6 Step 1f – Model Staged Construction

The construction staging for the shell element model is the same as for the spine beam model described in Section 9.7.1.1.6. One exception is that the temporary tendons are removed from the analysis in the same stage that the continuity tendons are stressed. This is done to prevent the tendons from carrying loads in compression; this could also be done through the use of tension only elements.

9.7.2.1.7 Step 1g – Run Analysis and Verify Results

The next step is to run the analysis. The analysis results can be verified using a variety of simplified methods. For continuous span bridges, moments and reactions can be calculated using textbook equations for uniform loads. Additionally, for uniform loads applied to the entire structure, the total applied load applied can be calculated and should equal the sum of the reactions from the analysis model.

Check reactions for bridge self-weight and barriers load versus applied load:

Barriers:

$$\text{Weight of Barrier} = 0.376 \text{ klf}$$

$$\text{Length over which Barrier is applied} = 2 \times 330 \text{ ft} = 660 \text{ ft}$$

$$\text{Total Weight of Barriers} = 0.376 \text{ klf} \times 660 \text{ ft} = 248.16 \text{ k}$$

Bridge Self-Weight:

Typical Section:

$$\text{Area of Typical Section} = 61.06 \text{ ft}^2 \text{ (calculated using dimensions and thicknesses in Figure 398)}$$

$$\text{Weight of Typical Section} = 9.22 \text{ k/ft}$$

$$\text{Bridge Length} = 330 \text{ ft}$$

$$\text{Total Weight of Typical Section} = 9.22 \text{ k/ft} \times 330 \text{ ft} = 3042.44 \text{ k}$$

Tendons:

$$\text{Total Length of Tendons} = 2708.03 \text{ ft}$$

$$\text{Area of Tendon} = 4.774 \text{ in}^2 = 0.033 \text{ ft}^2$$

$$\text{Weight of Tendons} = 2708.03 \text{ ft} \times 0.033 \text{ ft}^2 \times 0.49 \text{ k/ft}^3 = 44.00 \text{ k}$$

Pier Diaphragms:

$$\text{Area} = 122.41 \text{ ft}^2$$

$$\text{Pier 1 Thickness} = 2 \text{ ft}$$

$$\text{Pier 2 Thickness} = 6.5 \text{ ft}$$

$$\text{Pier 3 Thickness} = 3.25 \text{ ft (actual diaphragm is 6.5 ft thick, only half of diaphragm included in model)}$$

$$\text{Diaphragm Volume} = 122.41 \text{ ft}^2 (2 \text{ ft} + 6.5 \text{ ft} + 3.25 \text{ ft}) = 1438.33 \text{ ft}^3$$

$$\text{Diaphragm Weight} = 1438.33 \text{ ft}^3 \times 0.15 \text{ k/ft}^3 = 215.75 \text{ k}$$

Deviators (Figure 401):

$$\text{Area} = 2A_1 + 2A_2 + A_3 + A_4 = 2(2.38 \text{ ft}^2) + 2(16.33 \text{ ft}^2) + 24.55 \text{ ft}^2 + 1.44 \text{ ft}^2 = 63.41 \text{ ft}^2$$

Deviator Thickness = 2 ft

$$\text{Volume per Deviator} = 63.41 \text{ ft}^2 \times 2 \text{ ft} = 126.82 \text{ ft}^3$$

$$\text{Weight per Deviator} = 126.82 \text{ ft}^3 \times 0.15 \text{ k/ft}^3 = 19.02 \text{ k}$$

Number of Deviators = 4

$$\text{Total Deviator Weight} = 19.02 \text{ k} \times 4 \text{ deviators} = 76.08 \text{ k}$$

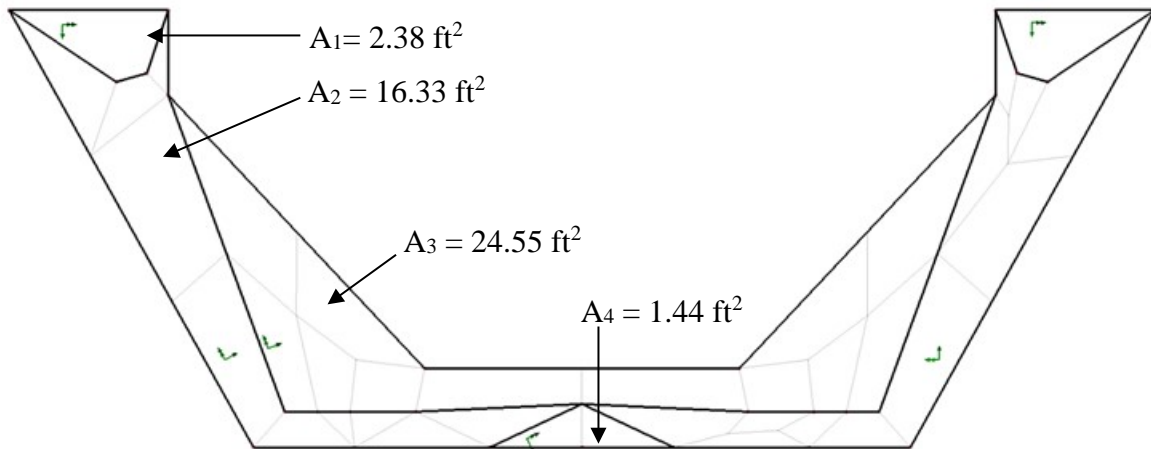


Figure 401. Illustration. Deviator areas for weight calculations.

Temporary PT Anchor Blocks:

$$\text{Area} = 2A_1 + 2A_2 + A_4 = 2(2.38 \text{ ft}^2) + 2(16.33 \text{ ft}^2) + 1.44 \text{ ft}^2 = 38.86 \text{ ft}^2$$

Temporary PT Anchor Block Thickness = 2 ft

$$\text{Volume per PT Anchor Block} = 38.86 \text{ ft}^2 \times 2 \text{ ft} = 77.72 \text{ ft}^3$$

$$\text{Weight per PT Anchor Block} = 77.72 \text{ ft}^3 \times 0.15 \text{ k/ft}^3 = 11.66 \text{ k}$$

Number of PT Anchor Blocks = 30

$$\text{Total Weight of PT Anchor Blocks} = 11.66 \text{ k} \times 26 = 303.16 \text{ k}$$

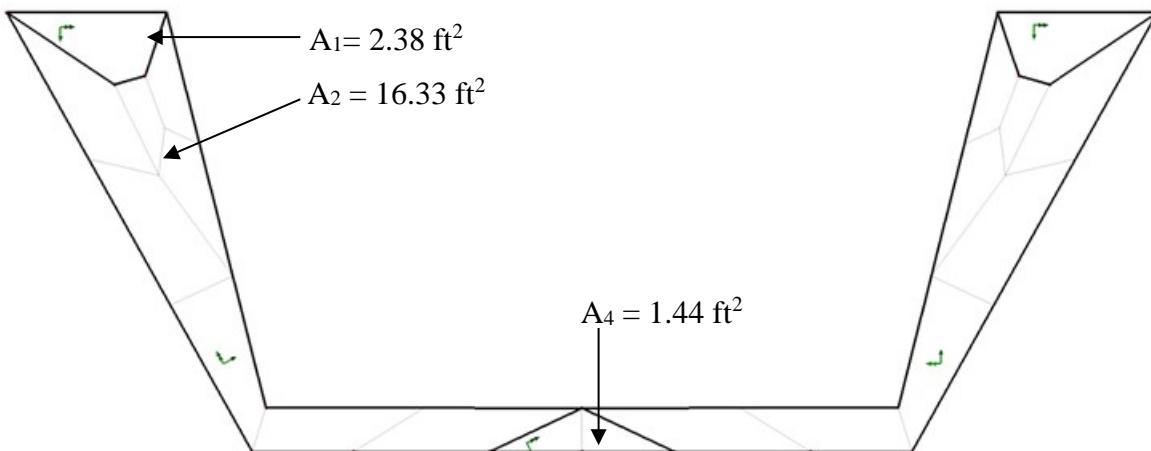


Figure 402. Illustration. Temporary PT anchor block areas for weight calculations.

Temporary PT:

$$\text{Area} = 1.227 \text{ in}^2 = 0.009 \text{ ft}^2$$

$$\text{Length} = 2 \times 5 \times 14 \times 10 \text{ ft-1 inches} + 8 \times 6 \text{ ft-6 inches} + 8 \times 3 \text{ ft-3 inches} = 1489 \text{ ft-8 inches}$$

$$\text{Total Volume} = 0.009 \text{ ft}^2 \times 1489 \text{ ft-8 inches} = 12.6 \text{ ft}^3$$

$$\text{Total Weight} = 12.6 \text{ ft}^3 \times 0.49 \text{ k/ft}^3 = 6.22 \text{ k}$$

Summing up the total weight of each component above:

$$W = 248.16 \text{ k} + 3042.44 \text{ k} + 44.00 \text{ k} + 215.75 \text{ k} + 76.08 \text{ k} + 303.16 \text{ k} + 6.22 \text{ k} = 3935.81 \text{ k}$$

Reactions from Model:

Location	Dead Load Reaction (k)		
	Left Bearing	Right Bearing	Total (Left + Right)
Pier 1	388.86	389.39	778.26
Pier 2	1113.72	1112.26	2225.98
Pier 3	465.63	466.96	932.59
		Total	3936.83

The calculated total applied load is within 1 percent of the sum of the reactions from the model.

Additionally, the reactions are approximately symmetric about Pier 2. Since the reactions appear reasonable, the other results from the model are expected to be reasonable as well. Note that the total reaction from this model is slightly larger than that shown for the spine beam model; this difference can be attributed to where the shell elements overlap slightly and as well as how the temporary anchor blocks were modeled in this analysis.

9.7.2.1.8 Step 1h – Extract Required Results from Software

After verifying that the results from the analysis are reasonable, the results of interest can be extracted for further use. Since the model utilizes shell elements, design bending moments and shears are typically not directly available from the analysis model. There are several options available to determine the bending moments and shears. One technique to determine design force effects is demonstrated in Example 1 Section 9.1.3.1.8 and involves integrating the stresses by hand over the depth of the cross-section. A second method, which should be used if available, is to use a built-in slicing utility within the analysis software. A slicing utility automatically integrates the stresses at specific planar cross-sections as requested by the engineer.

Figures 403 and 404 show the dead load moments and shears for various construction stages. In Figure 403, the plot labeled “Continuous w/o Creep” are from the spine beam model without consideration of the staged construction. The figure shows that the dead load moments are creeping towards the continuous final condition of the structure.

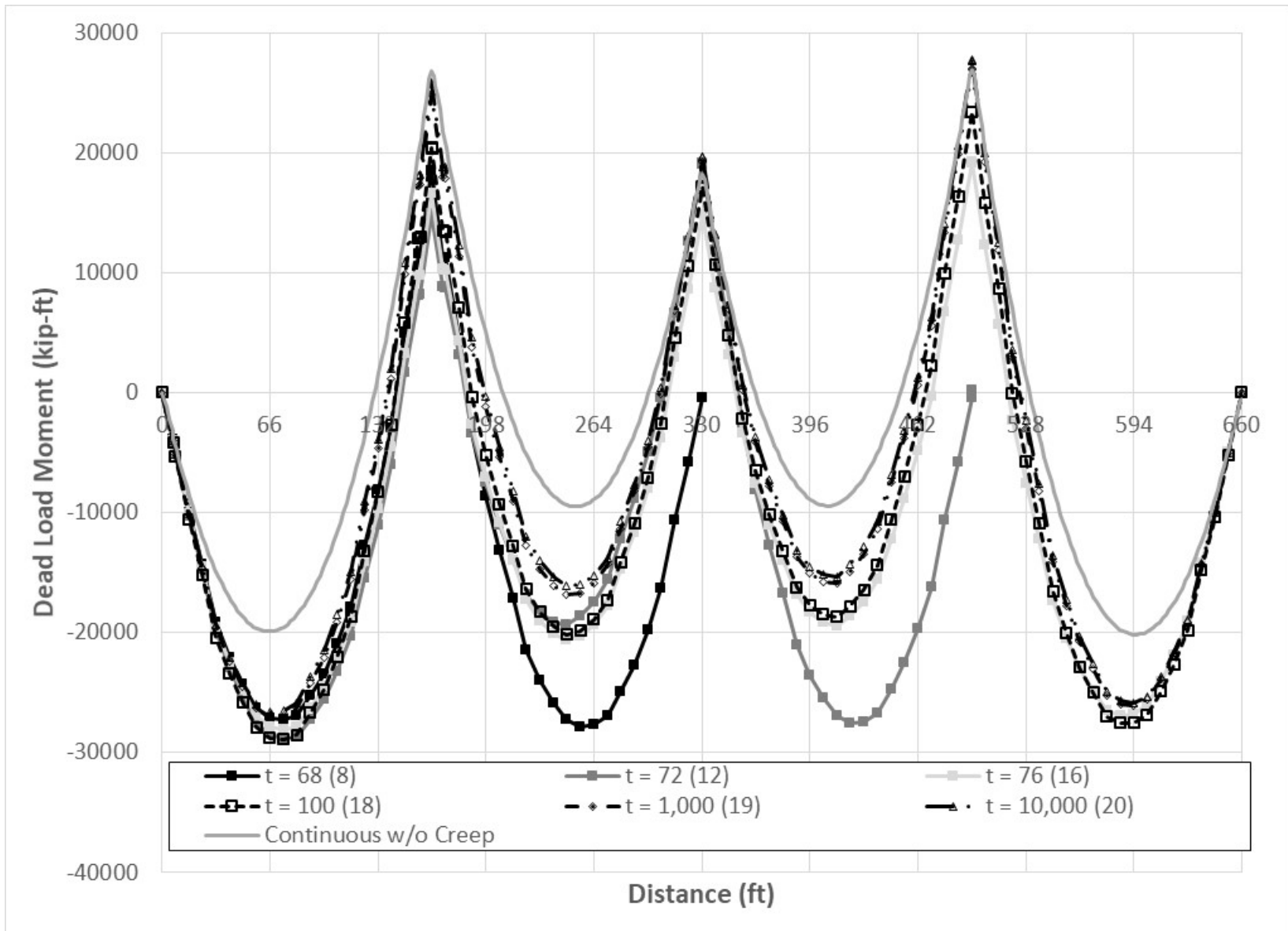


Figure 403. Graph. Dead load moment vs. distance for various construction stages.

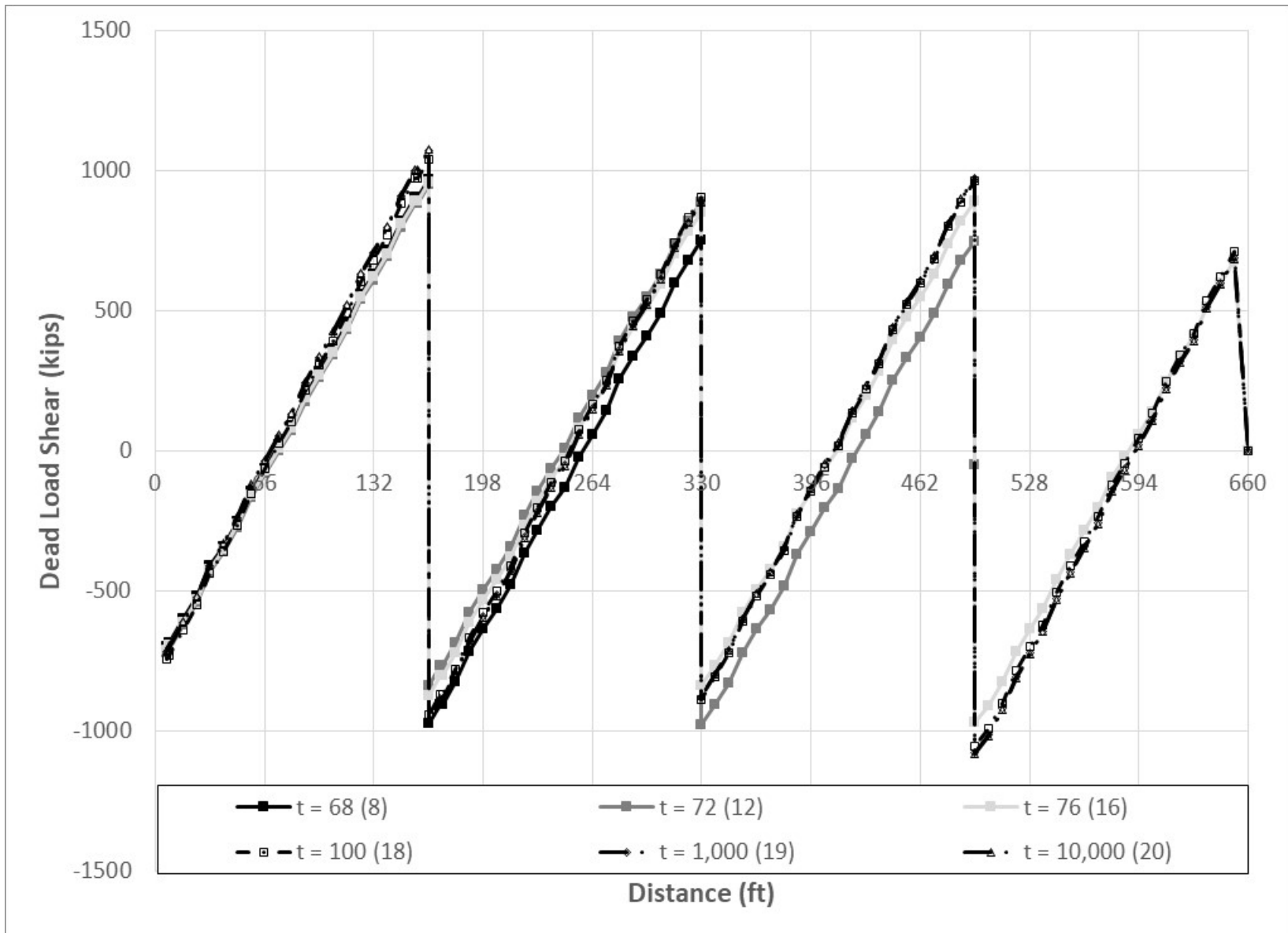


Figure 404. Graph. Dead load shear vs. distance for various construction stages.

9.7.2.2 Step 2 – Post-Tensioning Model

9.7.2.2.1 Step 2a – Create Analysis Model for Post-Tensioning Loads

Make a copy of the model created in Step 1, saving with a new name.

9.7.2.2.2 Step 2b – Modify Material Properties

As described in the spine beam example, the material properties for the concrete are modified such that shrinkage is considered in this model such that the shrinkage losses are experienced by the tendons. The tendon material properties are provided in Table 91.

9.7.2.2.3 Step 2c – Calculate and Define Post-Tensioning Loads

The post-tensioning losses were calculated in Section 9.7.1.2.3 for the spine beam model. The losses for anchor set, relaxation, friction, and elastic shortening are used to determine the forces applied to each tendon segment. The tendon forces immediately after jacking that are used in this analysis are shown in Tables 113 and 114.

Table 113. Tendon forces for Span 1.

Segment	Span 1 Tendon T1	Span 1 Tendon T2	Span 1 Tendon T3	Span 1 Tendon T4
	F (k)	F (k)	F (k)	F (k)
⑥ to ④	823.3	835.0	825.4	840.2
④ to ③	865.6	869.4	845.2	866.5
③ to ②	907.7	903.5	884.4	866.5
② to ①	941.6	941.6	915.6	915.3

Table 114. Tendon forces for Span 2.

Segment	Span 2 Tendon T1	Span 2 Tendon T2	Span 2 Tendon T3	Span 2 Tendon T4
	F (k)	F (k)	F (k)	F (k)
⑥ to ⑤	814.8	818.5	818.4	828.1
⑤ to ④	844.2	847.5	847.8	875.1
④ to ③	883.8	886.8	887.6	886.0
③ to ②	926.7	928.3	928.7	897.1
② to ①	961.3	961.3	961.3	947.8

Since the tendons are explicitly modeled in this analysis, there are several methods in which the tendon forces can be included in the analysis as described in Section 4.1.3.2 of the manual. One method is to calculate a temperature change that corresponds to the required tensile force in the tendon utilizing Equation (91) where the variables are defined in Section 4.1.3.2.

$$\Delta T = -\frac{P}{\alpha E_p A_{ps}} \quad (91)$$

Using Equation (91), the temperature changes necessary to induce the tendon forces shown in Tables 113 and 114 was calculated. The following values were used: $\alpha = 11.7 \times 10^{-6} / ^\circ\text{C}$, $E_p = 28,500$ ksi, $A_{ps} = 4.774$ in²; note that α must use the same temperature units as used in the model. The calculated temperature changes are shown in Tables 115 and 116.

Table 115. Temperature changes for Span 1.

Segment	Span 1 Tendon T1	Span 1 Tendon T2	Span 1 Tendon T3	Span 1 Tendon T4
	ΔT ($^\circ\text{C}$)	ΔT ($^\circ\text{C}$)	ΔT ($^\circ\text{C}$)	ΔT ($^\circ\text{C}$)
⑥ to ④	-517.2	-524.6	-518.5	-527.8
④ to ③	-543.9	-546.1	-531.0	-544.3
③ to ②	-570.2	-567.6	-555.6	-544.3
② to ①	-591.5	-591.5	-575.1	-575.0

Table 116. Temperature changes for Span 2.

Segment	Span 2 Tendon T1	Span 2 Tendon T2	Span 2 Tendon T3	Span 2 Tendon T4
	ΔT ($^\circ\text{C}$)	ΔT ($^\circ\text{C}$)	ΔT ($^\circ\text{C}$)	ΔT ($^\circ\text{C}$)
⑥ to ⑤	-511.9	-514.2	-514.4	-520.2
⑤ to ④	-530.3	-532.34	-532.6	-549.7
④ to ③	-555.2	-557.1	-557.6	-556.6
③ to ②	-582.2	-583.1	-583.4	-563.5
② to ①	-603.9	-603.9	-603.9	-595.4

As mentioned in Section 4.1.3.2, it may be necessary utilize an iterative approach to obtain the correct force in the tendons. Note that the prestressing forces tabulated in Tables 113 and 114 are valid only for the stage when the tendons are stressed i.e., Stage 4 for Span 1 and Stage 8 for Span 2, respectively. After the tendons are stressed, creep and shrinkage losses begin to occur and the stress in the tendons is reduced.

9.7.2.2.4 Step 2d – Run Analysis and Verify Results

For the shell element model, verifying the analysis results for the post-tensioning is not necessarily as straightforward as for the beam element model since shell elements do not directly provide moments and shears. One method of verifying the analysis results is to calculate the stresses at the extreme cross-section fibers due to the post-tensioning by hand using beam theory and compare them to the stresses from the analysis model. An example of this is shown below at mid-span of Span 1 immediately after the tendons are stressed before any creep and shrinkage losses occur.

The stresses due to post-tensioning are calculated using Equation (92).

$$\sigma = \frac{P}{A} \pm \frac{Pey}{I} \quad (92)$$

where: P = post-tensioning force in all tendons at time, t (kips)
A = cross-section area of girder (ft²)
e = tendon eccentricity (ft)

- y = distance from neutral axis of cross-section to top or bottom edge of girder (ft)
 I = moment of inertia of girder (ft⁴)

From Table 113, the effective force in each tendon after jacking is found for Segment ③-④ and shown below:

- $P_1 = 865.6$ kips
 $P_2 = 869.4$ kips
 $P_3 = 845.2$ kips
 $P_4 = 866.5$ kips

The tendon forces are added together to determine P .

$$P = 2 \times (P_1 + P_2 + P_3 + P_4) = 2 \times (865.6k + 869.4k + 845.2k + 866.5k) = 6893.4 \text{ kips}$$

The cross-section area, A , moment of inertia, I , and distance from the bottom of the section to the neutral axis, y_b , are found in Table 88 for the typical cross-section. The distance to the top of the section, y_t , is found by subtracting y_b from the total girder depth of 9 ft- 0½ inches

- $A = 63.2257$ ft²
 $I = 631.2$ ft⁴
 $y_b = 6.391$ ft
 $y_t = -2.65$ ft

The tendon eccentricity is the distance between the centroid of the tendon and the centroid of the girder. At mid-span, the tendon centroid is located 1 ft-0 inches from the bottom of the girder. This results in an eccentricity, e , of 5.391 ft. Substituting in the values for P , A , e , y , and I , the stresses are calculated using Equation (92). Negative values indicate tensile stresses and positive values indicate compressive stresses.

$$\sigma_t = \frac{P}{A} + \frac{Pe y_t}{I} = \frac{6893.4k}{63.23 \text{ ft}^2} + \frac{6893.4k \times 5.391 \text{ ft} \times -2.65 \text{ ft}}{631.2 \text{ ft}^4} = -47.0 \text{ ksf}$$

$$\sigma_b = \frac{P}{A} + \frac{Pe y_b}{I} = \frac{6893.4k}{63.23 \text{ ft}^2} + \frac{6893.4k \times 5.391 \text{ ft} \times 6.391 \text{ ft}}{631.2 \text{ ft}^4} = 485.3 \text{ ksf}$$

From the analysis model, the maximum stresses near Span 1 midspan are:

$\sigma_t = -11.0$ ksf
 $\sigma_b = 400.0$ ksf

The stresses calculated by hand are reasonable approximations of those from the model considering that the analysis model includes the effects of shear lag as described in Section 4.1.1.4 and shear lag is not considered in the hand calculations.

9.7.2.2.5 Step 2e – Extract Analysis Results

As discussed in Section 9.7.2.1.8, design moments and shears are not directly available from the shell element model. A slicing utility in the software was used to determine design moments and shears at twentieth-points along the span. For the analysis software used in this example, it is necessary for the results from the beam element representing the tendons to be neglected by the

slicing utility. If the beam element results are considered, the compression force in the concrete and tension force in the tendons cancel each other out resulting in incorrect moments and shears from the slicing utility.

Figure 405 shows the moment due to the post-tensioning for various construction stages. As discussed for the spine beam model above, the moments shown in Figure 405 are not used to calculate the design moment, M_u . Instead, the secondary moments, shown in Figure 406, are used in calculating the design moment. In Figure 405 and Figure 406, positive moments result in tension on the top surface of the beam and negative moments result in compression on the top surface of the beam.

Figure 407 shows the shear forces for the various construction stages and Figure 408 shows the shear due to the secondary moments. As mentioned above for the spine beam model, the design shear force, V_u , includes the shear forces due to post-tensioning as well as those caused by the secondary bending moments. The secondary PT shears were determined using the same method as shown for the spine beam model.

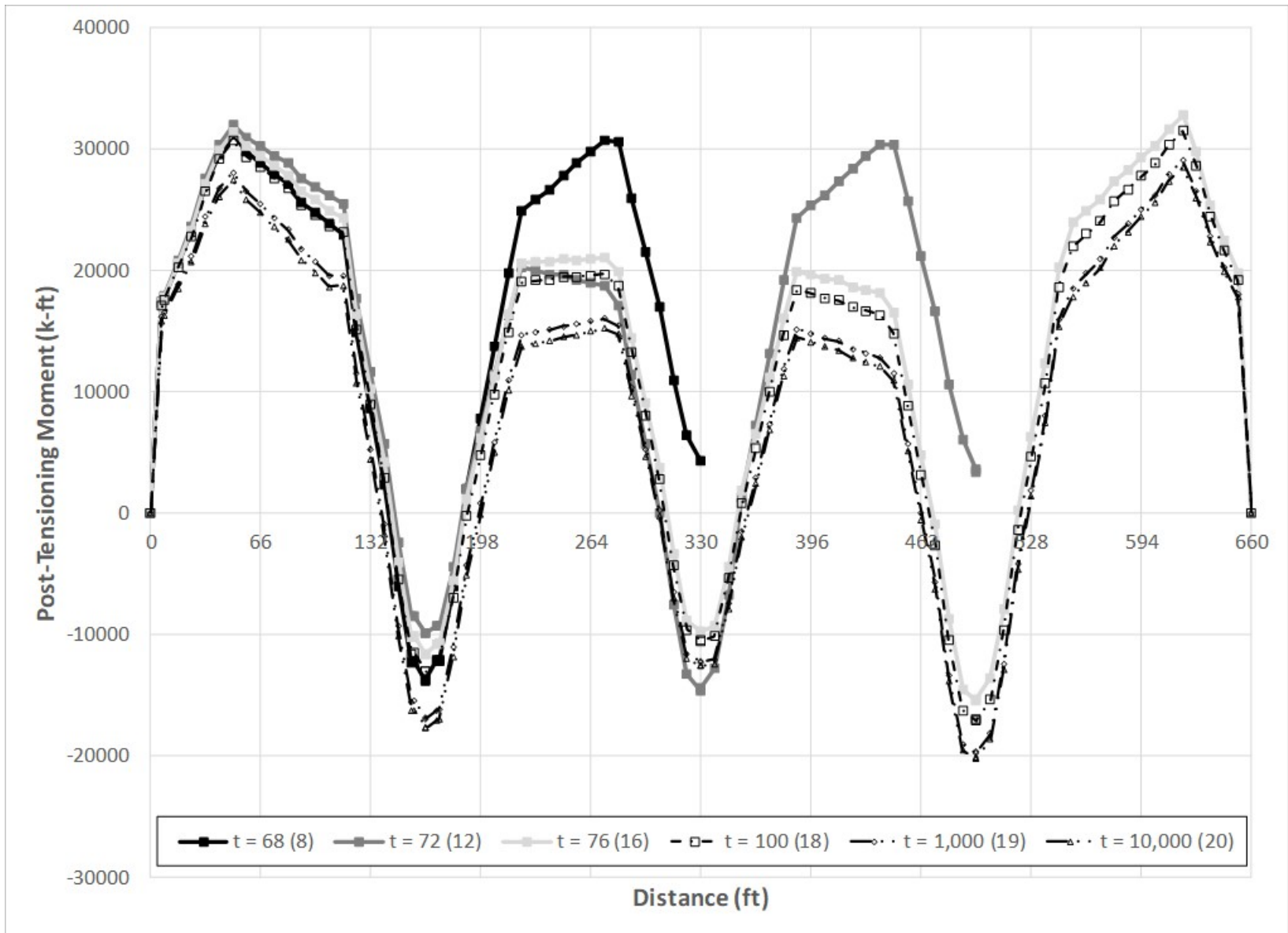


Figure 405. Graph. Post-tensioning moments vs. distance for various construction stages.

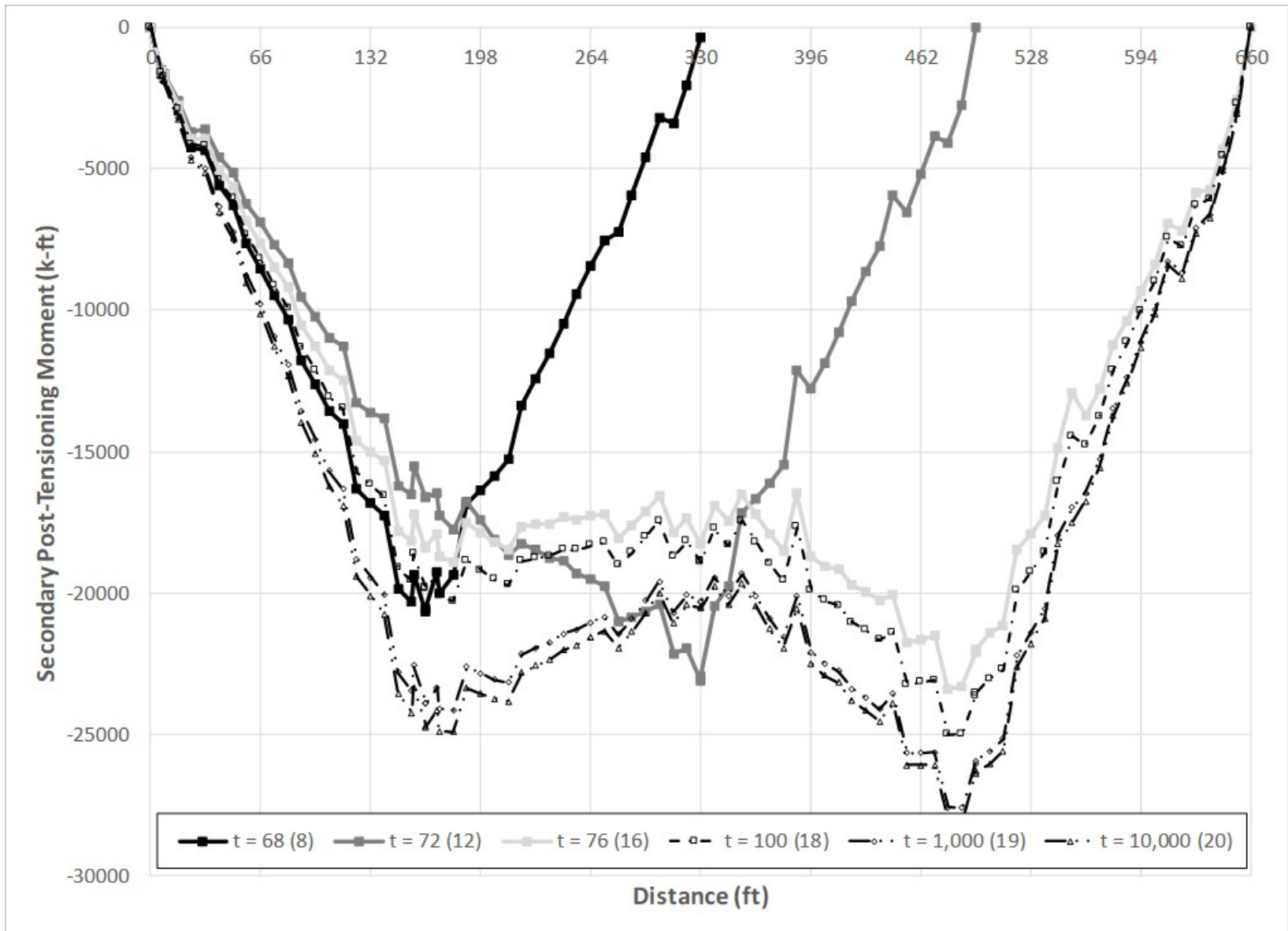


Figure 406. Graph. Secondary post-tensioning moments vs. distance for various construction stages.

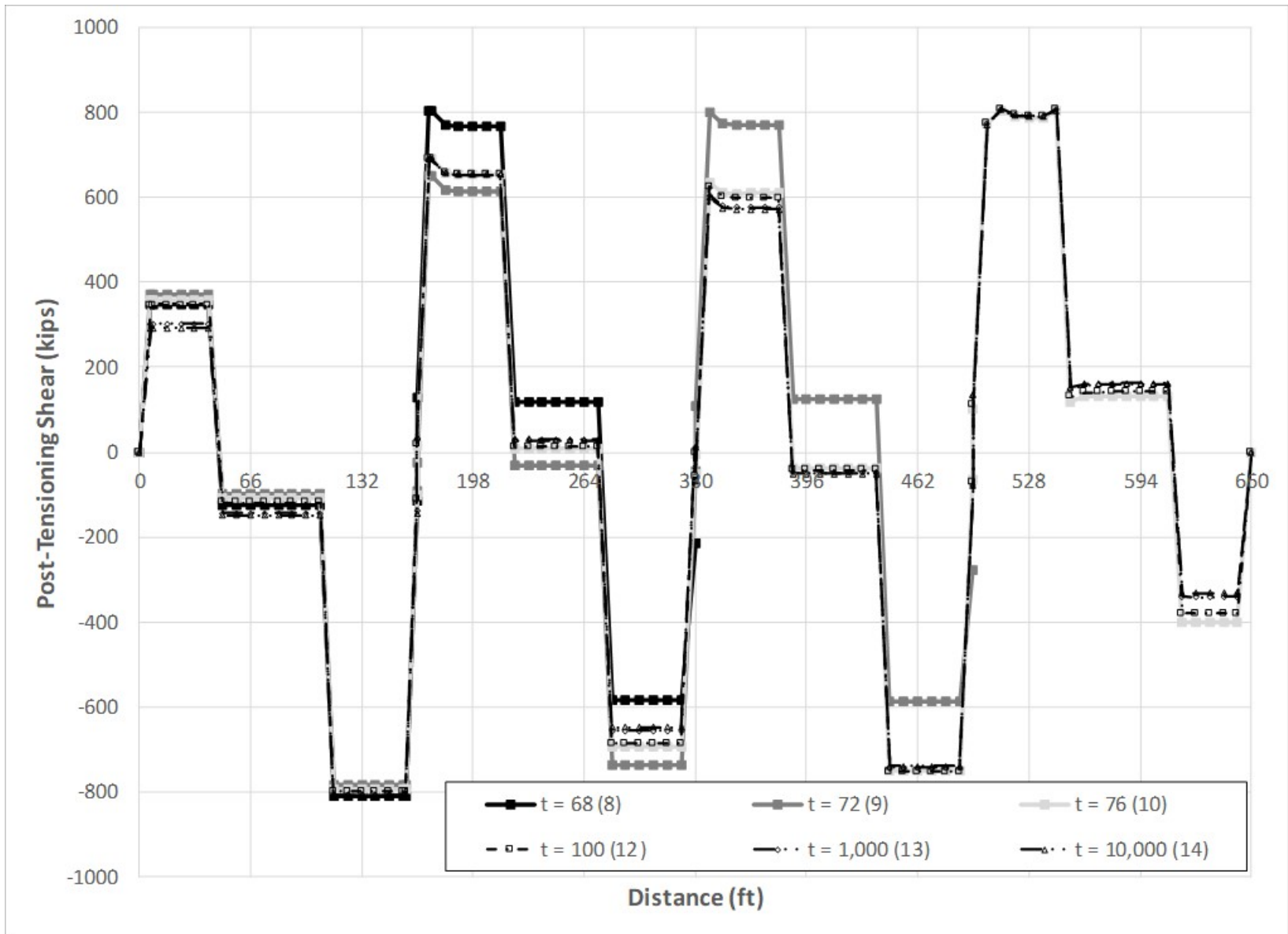


Figure 407. Graph. Shears due to post-tensioning vs. distance for various construction stages.

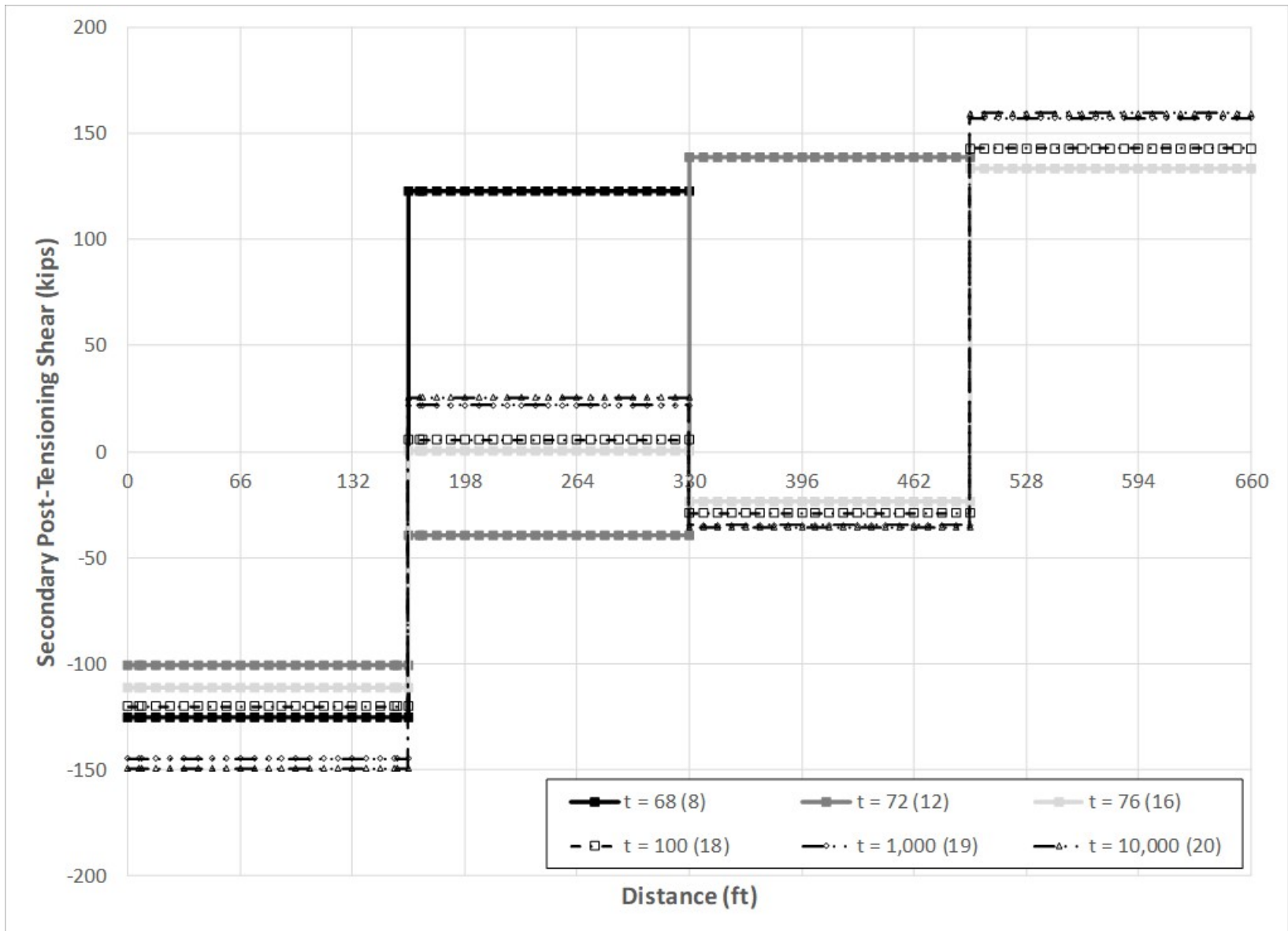


Figure 408. Graph. Shears due to secondary PT moment vs. distance for various construction stages.

9.7.2.3 Step 3 – Live Load Analysis

9.7.2.3.1 Step 3a – Create Live Load Analysis Model

Make a copy of the model created in Step 1 or Step 2 and save with a new name.

9.7.2.3.2 Step 3b – Modify Model for Linear-Elastic Analysis

Since live loads are short term and intermittent, this analysis is performed on a linear-elastic model that does not consider long term effects such as creep and shrinkage. The model used is identical to those used above except that the material definition for the concrete is now a linear-elastic material model instead of the CEB-FIP90 material model.

The construction staging process is also removed from this analysis model as live load is only applied to the completed structure.

9.7.2.3.3 Step 3c – Determine Optimized Live Loads

Maximum design bending moments (along the span length) are desired at mid-span of each span as well as over the interior support. Maximum design vertical shears are desired at a distance approximately equal to “d” away from each support where “d” is the depth from the extreme compression flange to the centroid of tension reinforcement. Since shell elements are being used, determining the optimized live load pattern is not as straightforward as it was for the beam element model since moments and shears are not directly calculated. Determining the optimized live load pattern resulting in the design moment at each location can be done by finding the loading that maximizes the tension stress in the longitudinal direction on the extreme tension surface of the shell element. For shear, determining the maximum loading is more complicated since the desired loading would maximize the total shear in the section but the optimization feature can only consider the shear in one web at a time. For this example, the shear loading from the spine beam model was applied to the shell element model to determine the design shear load effects.

9.7.2.3.4 Step 3d – Run Analysis and Verify Results

The next step is to run the analysis. In addition to the qualitative inspection of deflected shapes and loading configurations for maximizing specific force effects, a simple quantitative check is made to add confidence in the model.

Vertical Reactions for Three Lanes Loaded in Span 1

As a check, the reaction for the loading causing the maximum positive bending moment in the first span will be compared to that calculated by hand.

Weight of three design trucks: $W_{DT} = (3) (72 \text{ k}) = 216.0 \text{ k}$

Weight of three design lanes: $W_{DL} = (3) (0.64 \text{ kip/ft}) (165 \text{ ft}) = 316.8 \text{ k}$

Total Reaction including Impact: $W = 1.33W_{DT} + W_{DL} = 1.33 \times 216 \text{ k} + 316.8 \text{ k} = 604.1 \text{ k}$

The analysis software includes the multiple presence factor in the live load analysis. For three lanes loaded, the multiple presence factor is 0.85.

Applying the multiple presence factor the total reaction is $W_{mpf} = 0.85 \times 604.1 \text{ k} = 513.5 \text{ kips}$.

Location	X (ft)	FZ (k)		Total
		Left Bearing	Right Bearing	
Pier 1	0	83.8	109.1	192.9
Pier 2	165	173.9	208.1	382.0
Pier 3	330	-31.6	-31.4	-63.0
				511.9

The reactions calculated by hand (513.5 kips) and that from the analysis software (511.9 kips) are similar. Therefore, the results from the analysis software appear reasonable.

9.7.2.3.5 Step 3e – Extract Required Results from Analysis Software

After verifying that the results from the analysis are reasonable, the results of interest can be extracted and input into a spreadsheet for further use. The results of interest are the moments at the midspan locations of Spans 1 and 2 as well as the moment at the first interior support. Also of interest are the shears near each support. The moments and shears at each location are found using the slicing utility.

9.7.2.4 Step 4 – Combine Analysis Results

Once the results of interest, in this case moments and shears, have been extracted from the analysis software, they are factored according to the appropriate limit state. In this case, the Strength I limit state is being considered. From AASHTO LRFD Tables 3.4.1-1, 3.4.1-2, and 3.4.1-3, the Strength I load factors are:

$$\begin{aligned}\gamma_{DC} &= 1.25 \text{ (AASHTO LRFD Table 3.4.1-2)} \\ \gamma_{LL} &= 1.75 \text{ (AASHTO LRFD Table 3.4.1-1)} \\ \gamma_{PS} &= 1.0 \text{ (AASHTO LRFD Table 3.4.1-3)} \\ \gamma_{CR,SH} &= 1.25 \text{ (AASHTO LRFD Table 3.4.1-2 via Table 3.4.1-3)}\end{aligned}$$

The force effects due to creep and shrinkage are included in the post-tensioning model. Creep is also included in the dead load model such that the effects due to creep from the dead load are determined.

The individual component moments for PT, dead load, and live load are summarized in Table 117 for mid-span Span 1, at Pier 2, and at mid-span Span 2 as shown in Figure 409. The Strength I design moment is also shown for these three locations. Figure 410 shows the locations where the maximum moment was determined. Distances are indicated with respect to the left end of the structure.

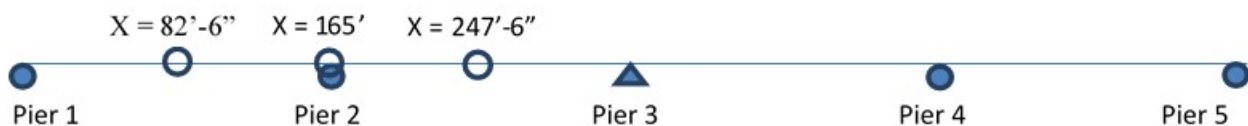


Figure 409. Illustration. Selected design moment locations.

Table 117. Flexure results for selected locations at 10,000 days.

Location	X (ft)	M_{yPT} (kip-ft)	M_{yDL} (kip-ft)	M_{LL} (kip-ft)	Strength I Moment (kip-ft)
Span 1 Mid-Span	82.5	12319	25832	10332	56233
Pier 2	165.0	24700	-25800	-10271	-25524
Span 2 Mid-Span	247.5	22021	16143	6076	52833

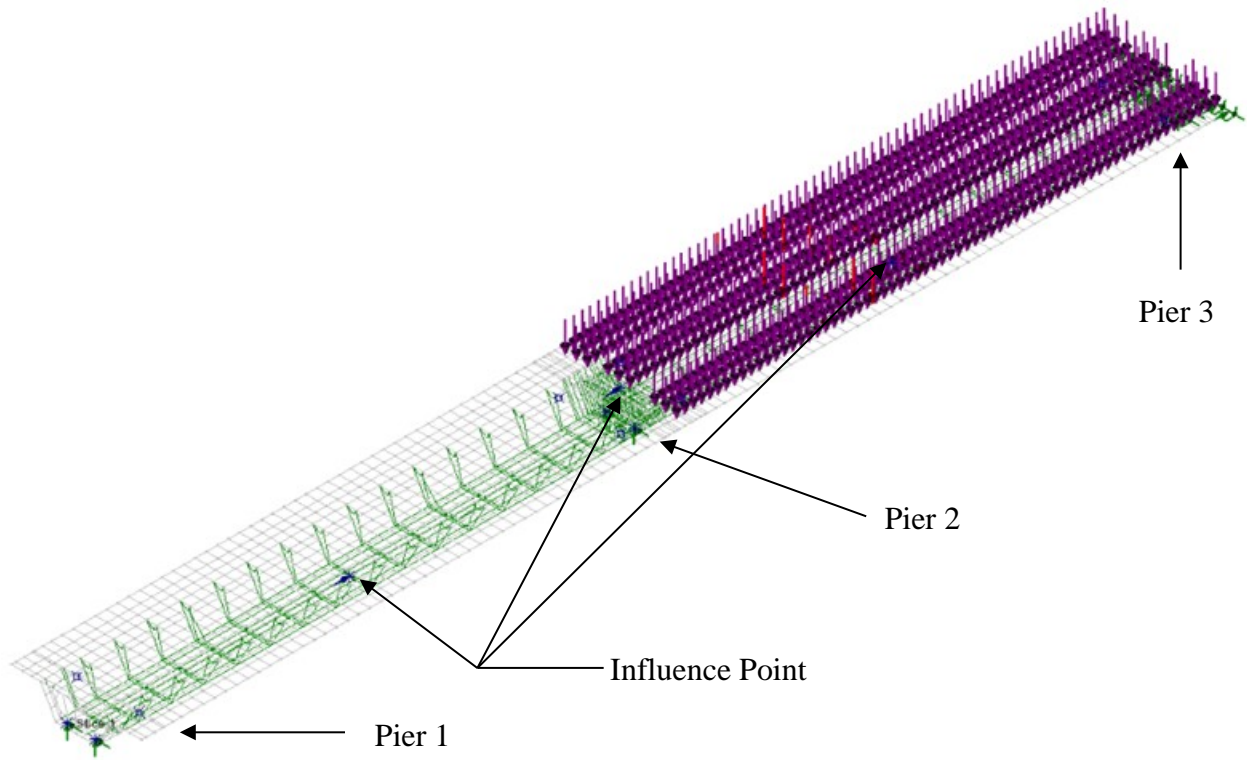


Figure 410. Illustration. Selected locations for design moments and live load for Span 2 maximum positive moment.

The individual component shears for PT, dead load, and live load are summarized in Table 118 for Pier 1 and both sides of Pier 2 as shown in Figure 411. The Strength I design shear is also shown for these three locations. Figure 412 shows the truck loading for the maximum shear near the first support; lane loading is not shown for clarity.



Figure 411. Illustration. Selected design shear locations.

Table 118. Shear results for selected locations at 10,000 days.

Location	X (ft)	F_{zPT} (kip)	F_{zDL} (kip)	F_{zLL} (kip)	Strength I Shear (kip)
Pier 1	7	-143	713	301	1275
Pier 2 – Left	158	958	-1004	-383	-967
Pier 2 – Right	172	-716	887	352	1009

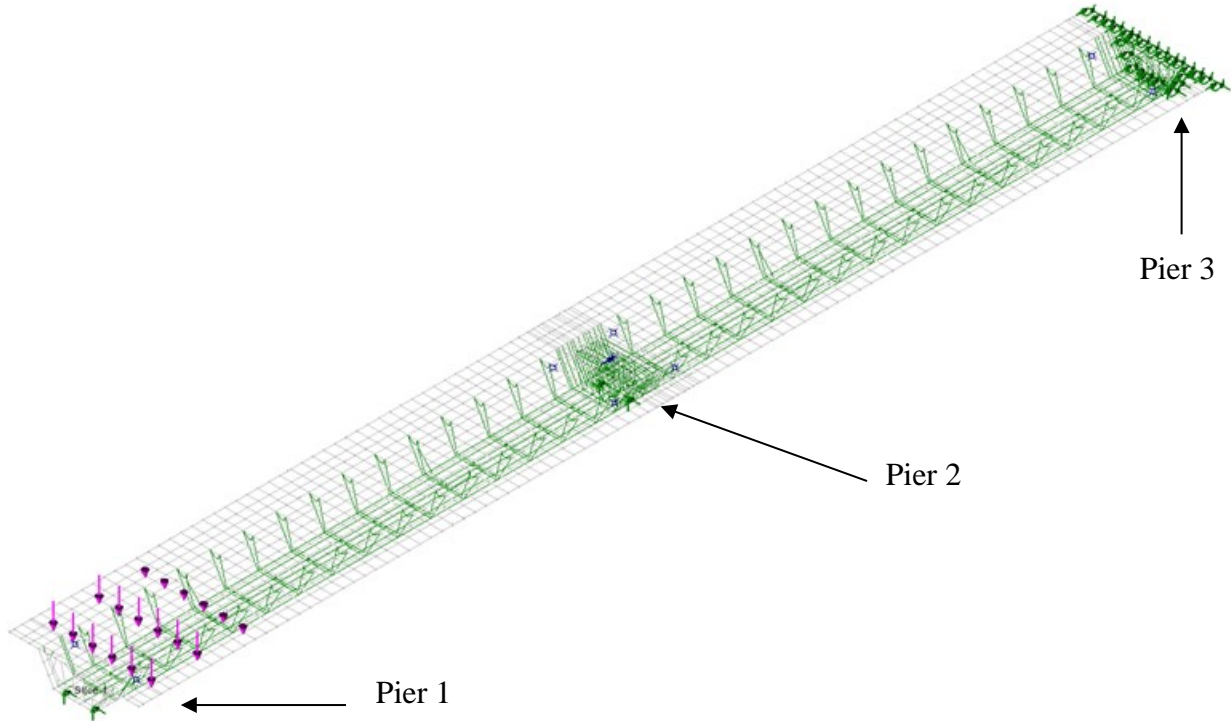


Figure 412. Illustration. Selected locations for design shears and truck loading for maximum shear near Pier 1.

9.7.3 Comparison of Spine Beam and Shell Element Model Results

The results from the spine beam model and the shell element model are compared in the following sections. Comparisons are shown for $t = 100$ days – the stage where the barrier is assumed to be cast, $t = 1,000$ days – an intermediate stage, and $t = 10,000$ days – the stage where creep is assumed to have plateaued.

9.7.3.1 Moment

Figures 413 through 415 compare the dead load and post-tensioning moments from the spine beam and shell element models for $t = 100$ days, $t = 1,000$ days, and $t = 10,000$ days, respectively. As shown in the figures, the results from the two models are very similar. The shell element analysis results in slightly larger dead load moments near midspan of each span and over each pier and results in slightly lower post-tensioning moments. The results from the two models are generally within 5 percent of each other.

9.7.3.2 Shear

Figures 416 through 418 compare the dead load and post-tensioning shears from the spine beam and shell element models for $t = 100$ days, $t = 1,000$ days, and $t = 10,000$ days, respectively. As shown in the figures, the results from the two models are very similar. The shell element analysis results in slightly larger dead load shears and post-tensioning shears.

9.7.3.3 Comparison of Strength I Factored Loads

Using the results provided in Sections 9.7.1.4 and 9.7.2.4, the Strength I factored loads are provided in Table 119. The results from the two models are within 10 percent of each other.

Table 119. Comparison of Factored Strength I Loads.

X (ft)	Spine Beam Moment	Shell Element Moment	X (ft)	Spine Beam Shear	Shell Element Shear
82.5	61439	56233	9.1	1210	1275
165	-25023	-25524	156.4	-892	-967
247.5	52810	52833	173.8	979	1009

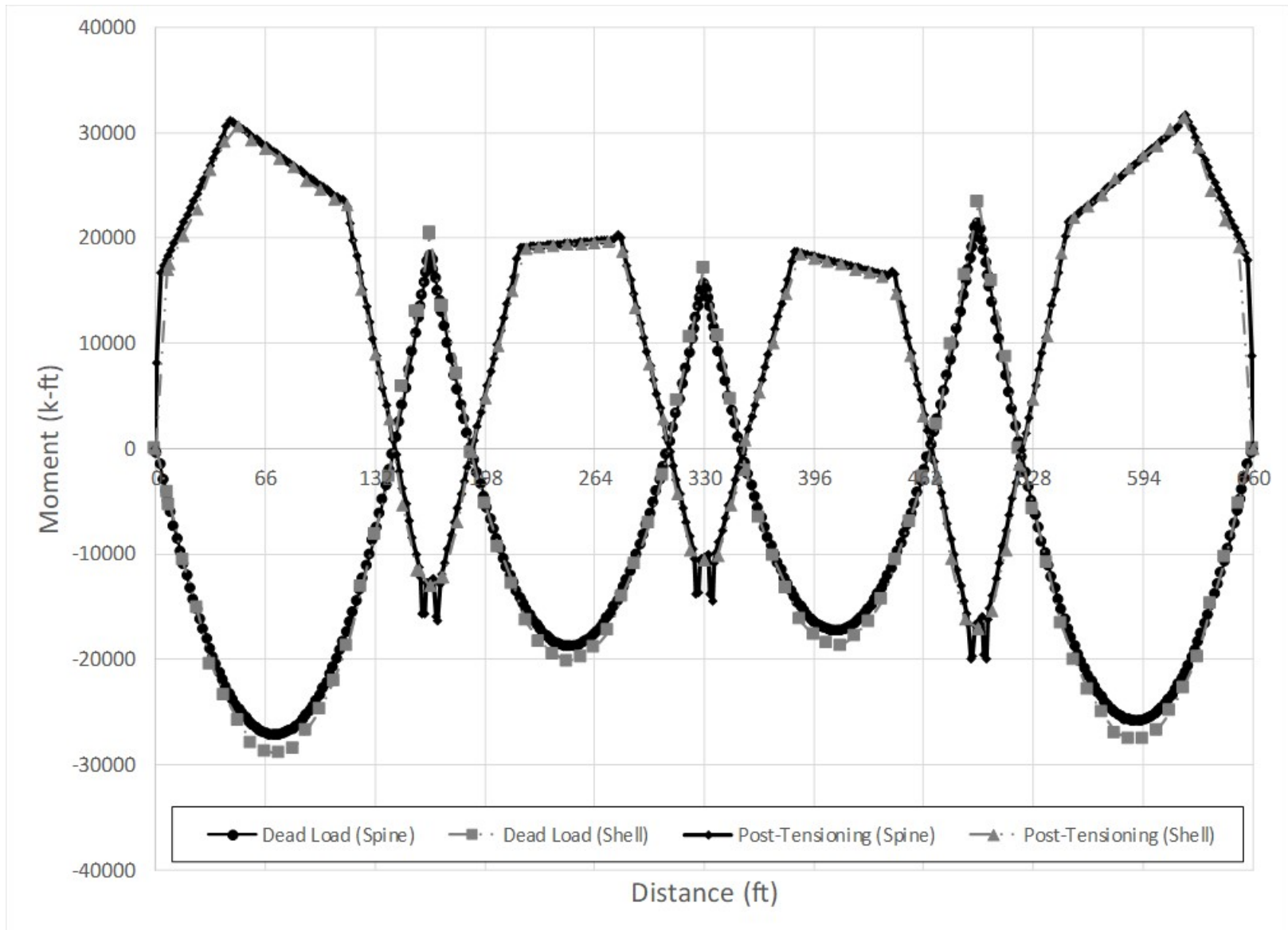


Figure 413. Graph. Comparison of dead load and post-tensioning moments from spine beam and shell element models at t = 100 days.

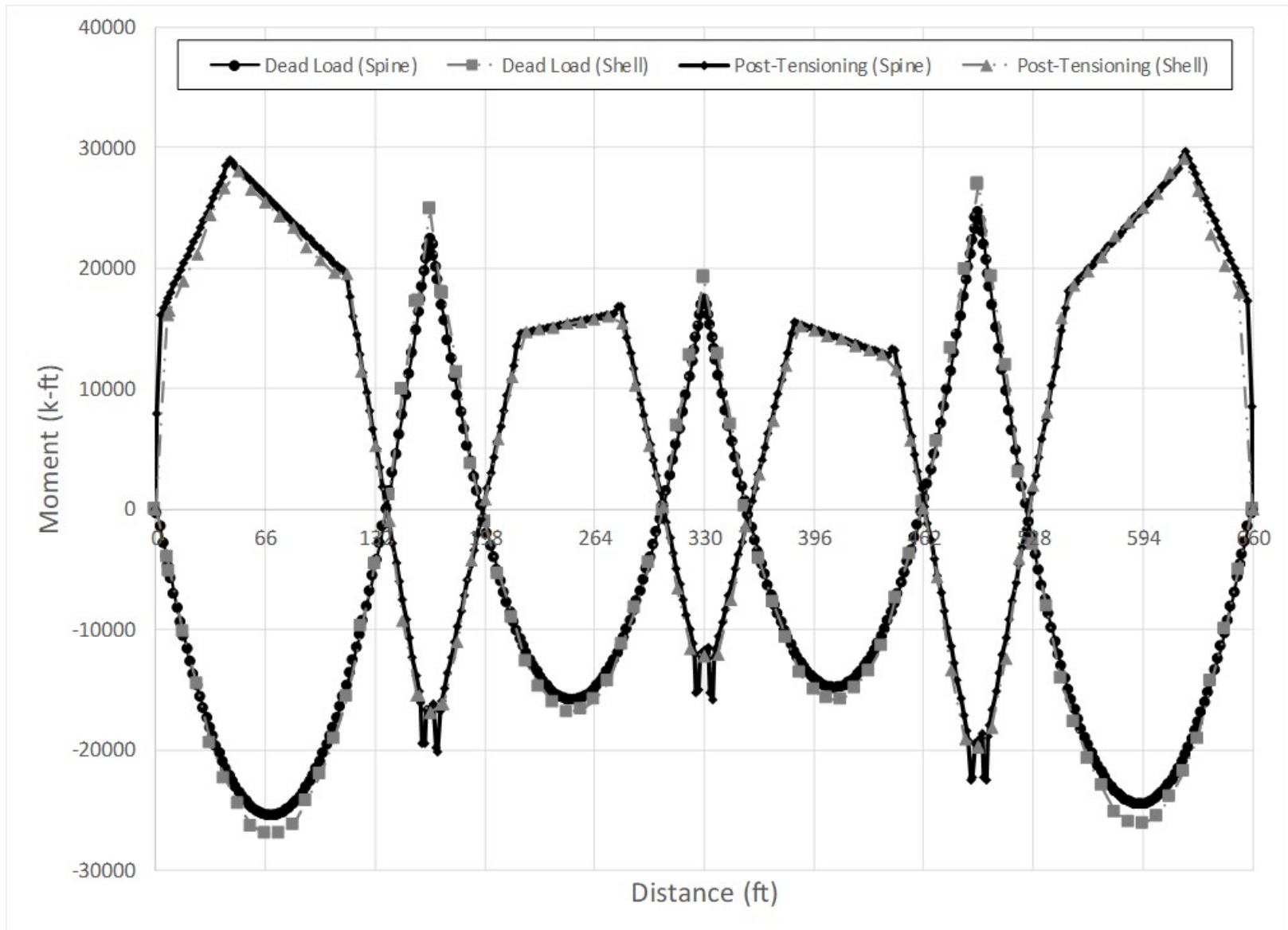


Figure 414. Graph. Comparison of dead load and post-tensioning moments from spine beam and shell element models at t = 1,000 days.

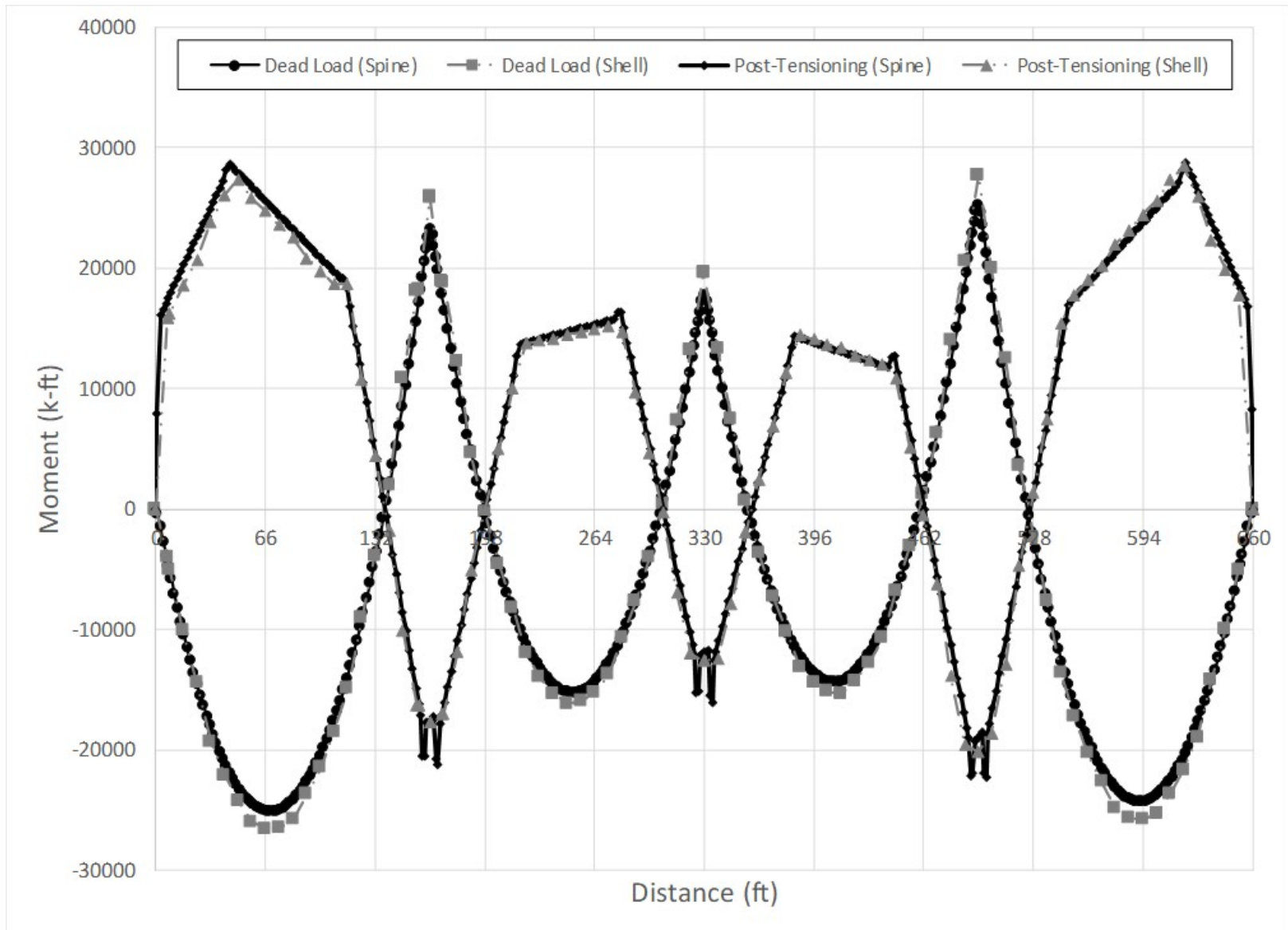


Figure 415. Graph. Comparison of dead load and post-tensioning moments from spine beam and shell element models at t = 10,000 days.

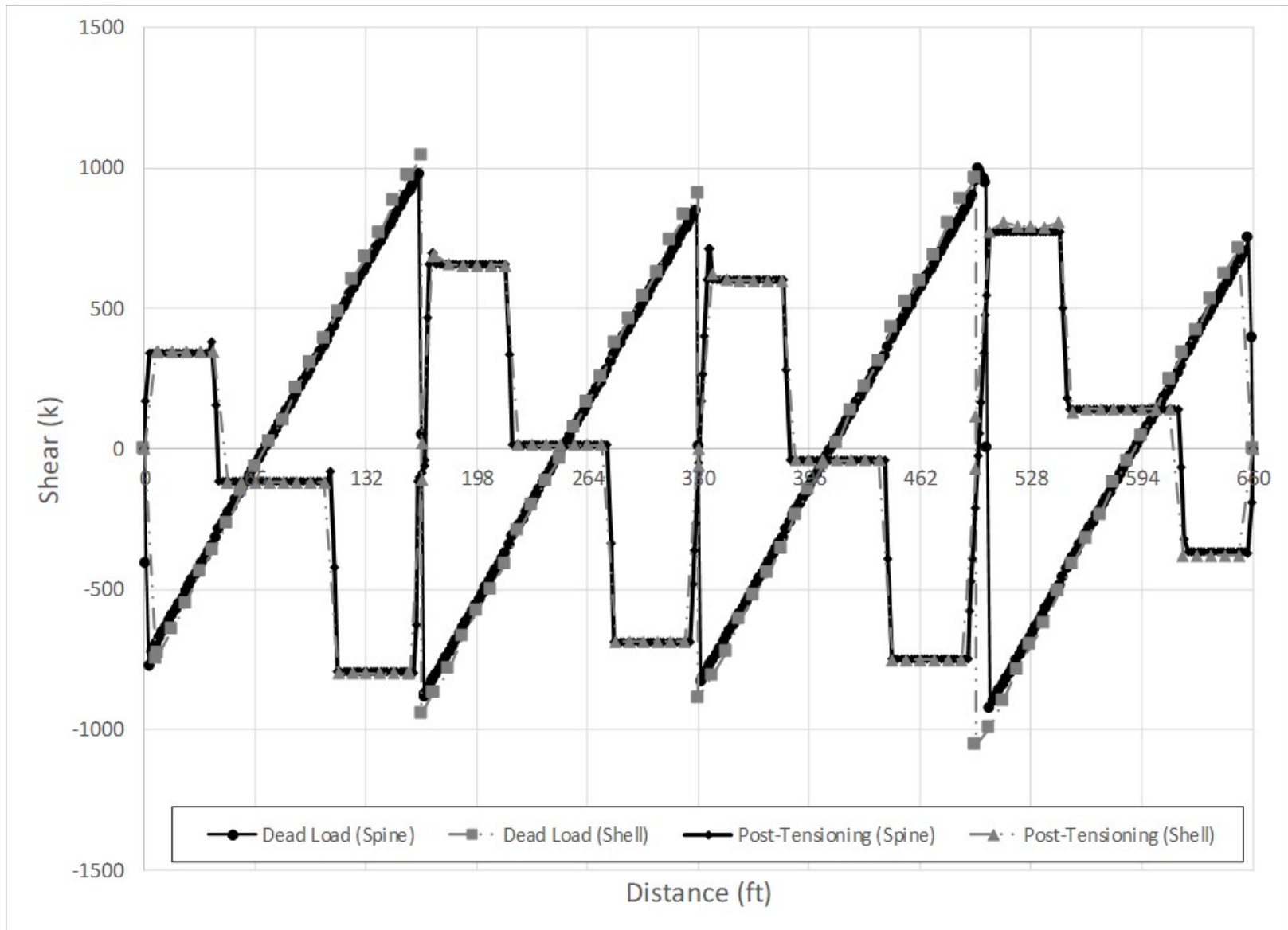


Figure 416. Graph. Comparison of dead load and post-tensioning shears from spine beam and shell element models at t = 100 days.

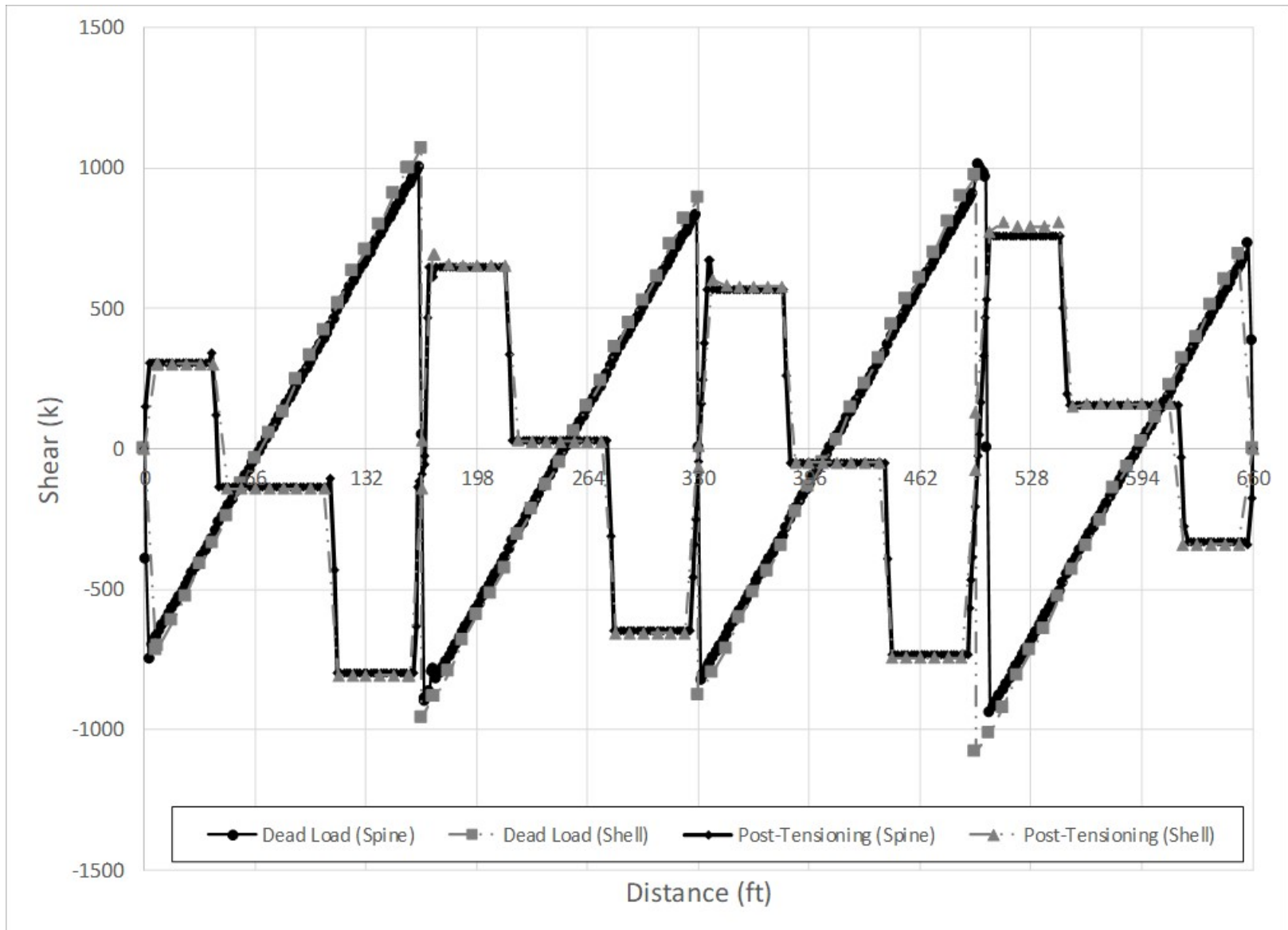


Figure 417. Graph. Comparison of dead load and post-tensioning shears from spine beam and shell element models at t = 1,000 days.

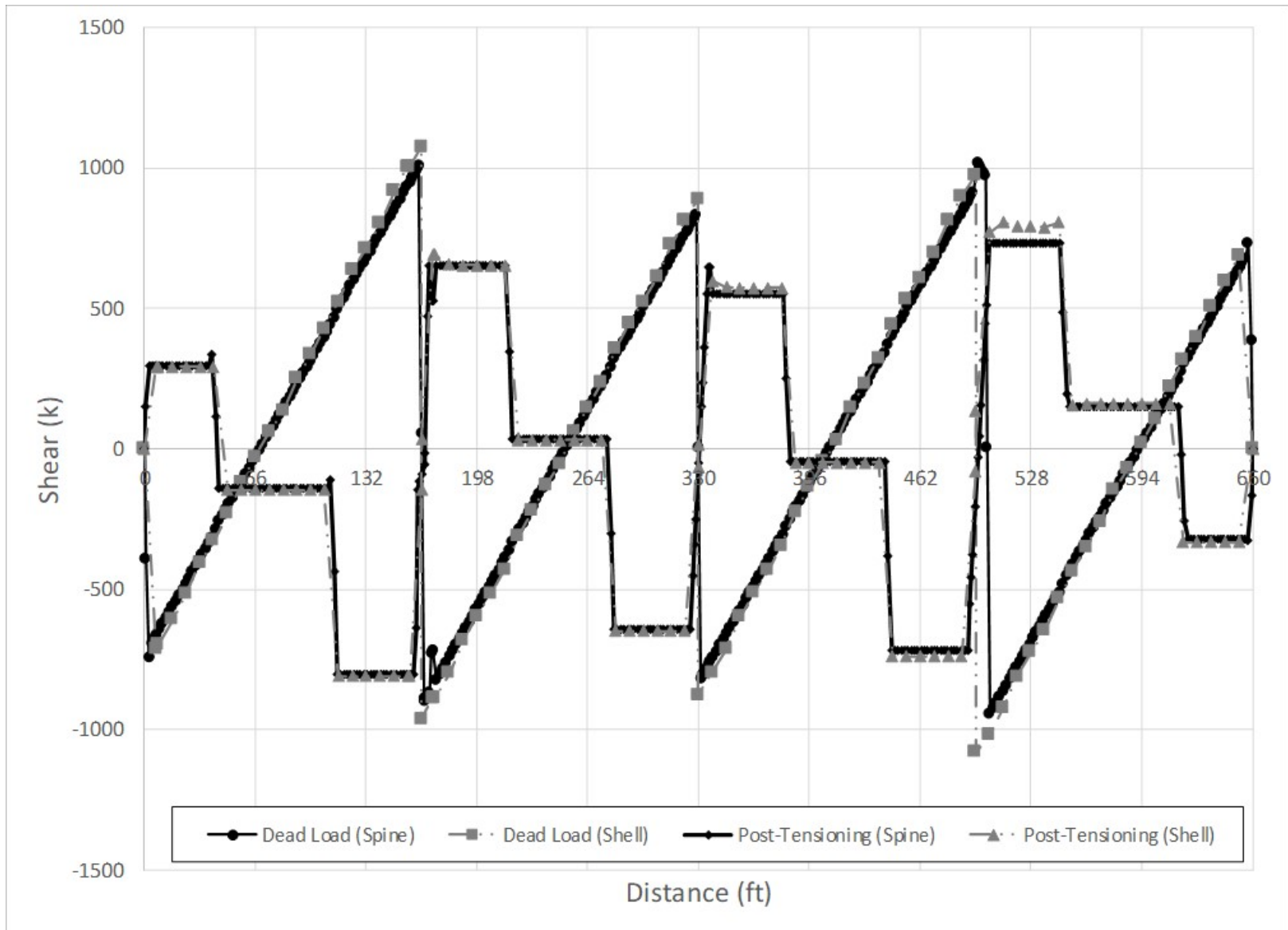


Figure 418. Graph. Comparison of dead load and post-tensioning shears from spine beam and shell element models at t = 10,000 days

REFERENCES

Aalami, Bijan O. "Structural Modeling of Posttensioned Members." *ASCE Journal of Structural Engineering*, Vol. 126, No. 2, February 2000, pp. 157-162.

AASHTO Guide Specifications for LRFD Seismic Bridge Design, 2nd Edition, American Association of State Highway and Transportation Officials, Washington, D.C., 2011.

AASHTO Guide Specifications for Seismic Isolation Design, 3rd Edition, American Association of State Highway and Transportation Officials, Washington, D.C., 2010.

AASHTO LRFD Bridge Design Specifications, 7th Edition, American Association of State Highway and Transportation Officials, Washington, D.C., 2014.

AASHTO Manual for Bridge Evaluation, 2th Edition, American Association of State Highway and Transportation Officials, Washington, D.C., 2011.

AASHTO/NSBA Steel Bridge Collaboration, *G 13.1 Guidelines for Steel Girder Bridge Analysis*, 2nd Edition, 2014.

ACI Committee 318, Building Code Requirements for Structural Concrete and Commentary. American Concrete Institute, Farmington Hills, MI, 2014.

AISC, Specification for Structural Steel Buildings, American Institute of Steel Construction, 130 East Randolph Street, Suite 2000, Chicago, IL, 60601-6204, July 7, 2016.

Anger, Georg, *Ten-division Influence Lines for Continuous Beams*, F. Ungar Publishing Company, Madison, WI, 1956.

Aviram, Ady, Mackie, Kevin R., Stojadinović, Božidar, *Guidelines for nonlinear analysis of bridge structures in California*, Berkeley, CA: Pacific Earthquake Engineering Research Center, 2008.

Bathe, Klaus-Jurgen, *Finite Element Procedures*, Prentice-Hall, Pearson Education Inc., Watertown, MA, 2006.

Bathe, K.J., and Wilson, E.O., *Numerical Methods in Finite Element Analysis*, Prentiss-Hall Civil Engineering and Engineering Mechanics Series, Englewood Cliffs, NJ, 1976.

Beckman, F., Chavel, B., Coletti, D., Cooper, J., Frank, K., Grubb, M., Fraser, G., Kozy, B., Medlock, R., Murray, G., Nguyen, T., Russo, F., Wallace, D., Walsh, S, White, D., and Yadlosky, J., *Skewed and Curved Steel I-Girder Bridge Fit*, NSBA Technical Subcommittee, Full Document, August, 2016.

Beer, F., Johnston Jr., E.R., Mazurek, D., Cornwell, P., and Self, B., *Vector Mechanics for Engineers: Statics and Dynamics*, 11th Edition, McGraw-Hill, 2016.

British Stainless Steel Association (BSSA), <https://www.bssa.org.uk/topics.php?article=125>, 2018.

- Chavel, B., Coletti, D., Frank, K., Grubb, M., McEleney, B., Medlock, R., and White, D., *Skewed and Curved Steel I-Girder Bridge Fit*, Fit Task Force, NSBA Technical Subcommittee, Summary Document, August, 2016.
- Chopra, Anil K., *Dynamics of Structures – Theory and Applications to Earthquake Engineering, 5th Edition*, Pearson, 2017.
- Clough, R.W., “The Finite Element Method, in Plane Stress Analysis”, Proc. 2nd A.S.C.E. Conf: on Electronic Comp., Pittsburgh, PA, 1960.
- Coletti, D., Chavel, B., and Gatti, W.J., *The Challenges of Skew*, TRB 2011 Annual Meeting.
- FHWA Steel Bridge Design Handbook, Bracing System Design, Publication No. FHWA-IF-12-052 – Vol. 13, November 2012B.
- Cook, Robert D., Malkus, David S., Plesha, Michael E., and Witt, Robert J., *Concepts and Applications of Finite Element Analysis, Fourth Edition*, John Wiley & Sons, Inc., 2002.
- Crawford, Sherwood F., and Kulak, Geoffrey L., *Eccentrically Loaded Bolted Connections*, Proceedings of the American Society of Civil Engineers Journal of the Structural Division, Vol. 97, No. ST3, March 1971, pp. 765-783.
- Felippa, C. A., A Historical Outline of Matrix Structural Analysis: A Play in Three Acts, *Computers and Structures*, vol. 79, no. 14, pp. 131-1324, 2001.
- FHWA *Load Rating Guidance and Examples for Bolted and Riveted Gusset Plates in Truss Bridges*, Publication No. FHWA-IF-09-014, February 2009.
- FHWA, *Manual for Design, Construction, and Maintenance of Orthotropic Steel Deck Bridges*, Publication No. FHWA-IF-12-027, February 2012.
- FHWA, *Manual for Repair and Retrofit of Fatigue Cracks in Steel Bridges*, Publication No. FHWA-IF-13-020, March 2013.
- FHWA, *Seismic Retrofitting Manual for Highway Structures: Part I Bridges*, Publication No. FHWA-HRT-06-032, US Department of Transportation, Federal Highway Administration, January 2006.
- Ghali, A., Neville, A. M., and Brown, T. G., *Structural Analysis – A Unified Classical and Matrix Approach*, 6th Edition, Taylor and Francis Publishers, New York, NY, 2009.
- Griffis, L. G., and White, D. W., *Stability Design of Steel Buildings—Design Guide 28*, American Institute of Steel Construction, Chicago, IL, 2013.
- Grubb, Michael A. et al., *Analysis and Design of Skewed and Curved Steel Bridges with LRFD – Reference Manual*, NHI Course No. 130095, Publication No. FHWA-NHI-10-087, February 2011.
- Hambly, Edmund C., *Bridge Deck Behavior*, John Wiley and Sons, Inc., New York, NY, 1976.
- Hewson, Nigel R. *Prestressed Concrete Bridges: Design and Construction*. London: Thomas Telford Publishing, 2003.

- Hida, S., Ibrahim, F.I.S., Capers, H.A., Bailey, G.L., Freidland, I.M., Kapur, J., Martin, B.T., Mertz, D.R., Perfetti, G.R., Saad, T., Sivakumar, B., *Assuring Bridge Safety and Serviceability in Europe*, Report No. FHWA-PL-10-014, International Technology Scanning Program, U.S. Department of Transportation, Federal Highway Administration, August 2010.
- Homberg, H, and Ropers, W., *Kragplatten mit verandlicher Dicke*, Beton and Stahlberonbau, March, 1963.
- Homberg, H, *Fahrbahnplatten mit Verandlicher Dicke*, Springer-Verlag, NY, 1968
- Hu, Hsuan-Teh, Huang, Chiung-Shiann, Wu, Ming-Hsien, and Wu, Yih-Min, *Nonlinear Analysis of Axially Loaded Concrete-Filled Tube Columns with Confinement Effect*, ASCE Journal of Structural Engineering, Vol. 129, No. 10, October 2003.
- Hughes, Thomas J. R., *The Finite Element Method: Linear Static and Dynamic Finite Element Analysis*, Courier Corporation, 2012.
- International Institute of Welding (IIW), *Recommendations for Fatigue Design of Welded Joints and Components* IIW document IIW-1823-07 ex XIII-2151r4-07/XV-1254r4-07 December 2008.
- Kaehler, Richard C., White, Donald W., and Kim, Yoon Duk, *Steel Design Guide 25 – Frame Design Using Web-Tapered Members*, American Institute of Steel Construction (AISC)/Metal Building Manufacturers Association(MBMA), March 2015.
- Khuntia, M., and Ghosh, S.K. (2004a). Flexural Stiffness of Reinforced Concrete Columns and Beams: Analytical Approach. *ACI Structural Journal*, Vol. 101, No. 3, pp. 351-363.
- Khuntia, M., and Ghosh, S.K. (2004b). Flexural Stiffness of Reinforced Concrete Columns and Beams: Experimental Verification. *ACI Structural Journal*, Vol. 101, No. 3, pp. 364-374.
- Krupicka, G., and Poellot, W.N., *Nuisance Stiffness*, HDR Bridgeline, Vol. 4, No. 1, HDR Inc., Omaha, NE, 1993.
- Kulicki, J.M., Mertz, D.R., and Murphy, R.E., *Dynamic response and subsequent retrofit of a tied-arch bridge*, 13th IABSE Congress Report, 1988.
- Kulicki, J., Z. Prucz, C. Clancy, D. Mertz, and A. Nowak. 2007. *Updating the Calibration Report for AASHTO LRFD Code*. Report on NCHRP 20-7/186. Transportation Research Board of the National Academies, Washington, D.C.
- Liao, F.Y., and Huang, Z. “Using XFEM for modeling localized fracture of reinforced concrete beams.” in *Computational Modeling of Concrete Structures*, ed. Nenad Bicanic, Herbert Mang, Gunther Meschke, and René de Borst, 552-553. London: Taylor & Francis Group, LLC, 2014.
- Lin, T.Y., and Burns, Ned H., *Design of Prestressed Concrete Structures*. NY: John Wiley and Sons, 1981.
- MacGregor, J.G., and Wight, J.K., *Reinforced Concrete Mechanics and Design*. NJ: Pearson Education, Inc., 2012.

- Mander, J.B., Dutta, A., and Goel, P. (1998). Capacity Design of Bridge Piers and the Analysis of Overstrength. Technical Report MCEER-98-0003, State University of New York at Buffalo.
- Mander, J.B., M.J.N. Priestley, and R. Park. *Theoretical Stress-Strain Model for Confined Concrete*. Journal of Structural Engineering. ASCE. 114(8). 1804-1826. 1988.
- Mander, J.B., Priestly, M.J.N., and Park, R., *Observed Stress-Strain Behavior of Confined Concrete*, Journal of the Structural Division, ASCE, Vol. 114, No. 8, August 1988b.
- Naaman, Antoine E. *Prestressed Concrete Analysis and Design Fundamentals*. Ann Arbor, MI: Techno Press 3000, 2004.
- NHI, LRFD Seismic Analysis and Design of Transportation Geotechnical Features and Structural Foundations, NHI Course No. 130094 Reference Manual*, Publication No. FHWA-NHI-11-032, August 2011.
- Nowak, A. 1999. *NCHRP Report 368: Calibration of LRFD Bridge Design Code*. TRB, National Research Council, Washington, D.C.
- Nutt et al., "Development of Design Specifications and Commentary for Horizontally Curved Concrete Box-Girder Bridges", *NCHRP Report 620*, Transportation Research Board, 2008.
- O'Brien, Eugene K., and Keogh, Damien L., *Bridge Deck Analysis*, Routledge, New York, NY, 1999.
- Ocel, Justin, *NCHRP Web-Only Document 197: Guidelines for the Load and Resistance Factor Design and Rating of Riveted and Bolted Gusset-Plate Connections for Steel Bridges*, Federal Highway Administration Turner-Fairbank Highway Research Center McLean, VA, February, 2013.
- PCI, *Precast Prestressed Concrete Bridge Design Manual*, Third Edition, 2011.
- Priestly, M.J.N, Seible, F., and Calvi, G.M (1996). *Seismic Design and Retrofit of Bridges*. John Wiley and Sons, New York, NY.
- Pucher, A, *Einflussfelder elastischer Platten: Influence Surfaces of Elastic Plates*, Springer-Verlag Wien, 1977.
- Rackwitz, R. and Fiessler, B., 1978, "Structural Reliability under Combined Random Load Sequences", *Computer and Structures*, 9, (1978) pp. 489-494. Meek, J.L., *Matrix Structural Analysis*, McGraw-Hill, 1971, pp142-145.
- Raynor, D. J., Lehman, D. L., and Stanton, J. F., *Bond-slip Response of Reinforcing Bars Grouted in Ducts*, ACI Structural Journal, Vol. 99, No. 5, September-October 2002, pp. 568–576.
- Scordelis, A. C., "A Matrix Formulation of the Folded Plate Equations", *Journal of the Structural Division – Proceedings of the American Society of Civil Engineers*, Vol.86, No. ST10, October 1960, pp. 1-23.

Structural Stability Research Council. (2010). *Guide to Stability Design Criteria for Metal Structures* (Sixth ed.). (R. D. Ziemian, Ed.) Lewisburg, PA, USA: John Wiley & Sons, Inc.

Vercher, J., Gil, E., Mas, A., and Cubel, F., *Analysis of the Residual Safety Level in RC Slabs with Severe Joist Corrosion*, ASCE Journal of Performance of Constructed Facilities, Vol 29, No. 4, August 2015.

Wang, W.H., Battistini, A.D., Helwig, T.A., Engelhardt, M.D. and Frank, K.H. (2012), “Cross Frame Stiffness Study by Using Full Size Laboratory Test and Computer Models,” Proceedings of the Annual Stability Conference, Structural Stability Research Council, Grapevine, TX, April 18-21, 11 pp.

White, D. (2012). Structural Behavior of Steel. In FHWA, *Steel Bridge Design Handbook*. Washington, D.C., USA: Federal Highway Administration.

White, D. *Steel Bridge Design Handbook: Structural Behavior of Steel*. Federal Highway Administration. Publication No. FHWA-HIF-16-002 - Vol. 4. Washington, D.C. 2015.

White, D. W. et al., “Guidelines for Analysis Methods and Construction Engineering of Curved and Skewed Steel Girder Bridges”, *NCHRP Report 725*, Transportation Research Board, 2012.

White, D., Nguyen, T., Coletti, D., Chavel, B., Grubb, M., and Boring, C., NCHRP Project 20-07/Task 355, *Guidelines for Reliable Fit-Up of Steel I-Girder Bridges*, Final Report prepared for the AASHTO Subcommittee on Bridges and Structures, T-14 Structural Steel, October 26, 2015.

Wilson, E. L. (2002). *Three-Dimensional Static and Dynamic Analysis of Structures*. Berkeley, California, USA: Computer and Structures, Inc.

Wong, Wai Tak, *Basic Refined Analysis Workshop*, Augusta, ME, July 8, 2010.

Yousif, Z. and Hindi, B., “Live Load Distribution for Beam-and-Slab Bridges: Limitations and Applicability”, *Journal of Bridge Engineering*, American Society of Civil Engineers, Vol. 12, No. 6, November/December 2007.

Zienkiewicz, O.C., Taylor, R.L., and Zhu, J.Z., *The Finite Element Method: Its Basis and Fundamentals 6th Edition*, Butterworth-Heinemann, 2005.

Zokaie, T., “AASHTO-LRFD Live Load Distribution Specifications”, *Journal of Bridge Engineering*, American Society of Civil Engineers, Vol. 5, No. 2, May 2000.

APPENDIX 2A – REFERENCES TO REFINED ANALYSIS IN AASHTO LRFD

List of references to refined analysis found in the 7th Edition of AASHTO LRFD.

Keywords such as "analysis", "methods", "software", and "finite" were used.

ARTICLE	CONTEXT	FORCE EFFECTS?	SECTION EFFECTS?	FEA CANDIDATE?	OTHER REFINED ANALYSIS?	GUIDANCE FOR FEA?	ADDITIONAL GUIDANCE PROVIDED
2.5.2.6.1	If dynamic analysis is used to determine deformations, it shall comply with Article 4.7.	-	-	X	X	X	Reference to Article 4.7 (See below).
3.4.1	If refined analysis is used for concrete substructures, use 1.0 for γ_{TU} with a partially cracked moment of inertia.	-	X	X	X	X	Use partially cracked moment of inertia for thermal loadings of concrete substructures.
3.6.1.4.3a	Where the bridge is analyzed by any refined method, as specified in Article 4.6.3, a single design truck shall be positioned transversely and longitudinally to maximize stress range at the detail under consideration.	X	-	X	X	X	Position of design truck.
Table 3.10.3.2-1	Site-specific geotechnical investigation and dynamic site response analysis should be performed for all sites in Site Class F.	-	X	-	X	-	-
4.1	States that methods of analysis based on documented material characteristics that satisfy equilibrium and compatibility, including inelastic analyses, may be used.	-	-	X	X	-	-
C4.1	States that the limitations and assumptions of refined and complex analyses are described in this section.	-	-	X	X	-	-
4.4	Bulleted list of acceptable methods for structural analysis.	-	-	X	X	-	-
C4.4	Warns the reader to be aware of assumptions embedded in computer program code. Also provides some verification methods.	-	-	X	X	X	Suggests some verification methods for computer programs.

ARTICLE	CONTEXT	FORCE EFFECTS?	SECTION EFFECTS?	FEA CANDIDATE?	OTHER REFINED ANALYSIS?	GUIDANCE FOR FEA?	ADDITIONAL GUIDANCE PROVIDED
4.5.1	Provides modeling guidance.	X	X	X	X	X	<p>Mathematical models shall include loads, geometry, and material behavior of the structure, and, where appropriate, response characteristics of the foundation. The choice of model shall be based on the limit states investigated, the force effect being quantified, and the accuracy required.</p> <p>Unless otherwise permitted, consideration of continuous composite barriers shall be limited to service and fatigue limit states and to structural evaluation. The stiffness of structurally discontinuous railings, curbs, elevated medians, and barriers shall not be considered in structural analysis.</p> <p>For the purpose of this section, an appropriate representation of the soil and/or rock that supports the bridge shall be included in the mathematical model of the foundation.</p> <p>In the case of seismic design, gross soil movement and liquefaction should also be considered.</p> <p>If lift-off is indicated at a bearing, the analysis shall recognize the vertical freedom of the girder at that bearing.</p>
C4.5.1	Provides modeling guidance, including that very flexible bridges should be analyzed using nonlinear elastic methods.	X	X	X	X	X	<p>Gives guidance as to when elastic modeling is sufficient, and when inelastic modeling is more appropriate. Also provides guidance on when a more rigorous treatment of boundary conditions is warranted.</p>
4.5.2.2 C4.5.2.2	Elastic behavior - states that behavior of concrete shall be based upon cracked and/or uncracked sections consistent with anticipated behavior.	-	X	X	X	X	<p>Studies indicate that cracking of concrete has little effect on the global behavior of bridges, so generally the effects can be safely neglected in modeling concrete for structural analysis.</p>

ARTICLE	CONTEXT	FORCE EFFECTS?	SECTION EFFECTS?	FEA CANDIDATE?	OTHER REFINED ANALYSIS?	GUIDANCE FOR FEA?	ADDITIONAL GUIDANCE PROVIDED
4.5.2.3 C4.5.2.3	Inelastic behavior - gives guidance on how to account for inelastic behavior in models.	X	X	X	X	X	States that unintended overstrength of components should be considered. Large deformations should be taken into account. Expected inelastic behavior should be validated by tests. Plane sections should remain plane. Shear deformations shall be considered. Concrete strain limits should not be exceeded. Inelastic behavior of compression components shall be taken into account.
C4.5.3.1	States that a second-order analysis may be necessary for determination of deflections. Provides guidance of large- vs. small-deflection theory.	X	X	X	X	-	-
4.5.3.2.1 C4.5.3.2.1	Large deflection theory - should be used if the deformation of a structure results in a significant change in force effects. Important in stability analyses. Out-of-straightness, time- and stress-dependent material characteristics shall be considered. The order of load application is important, and superposition is not valid.	X	X	X	X	X	In modeling large deflection problems, iterative solutions are typically applied. Order of loading is important, and superposition is not valid. The analyst should be aware of the characteristics of the elements employed, the assumptions upon which they are based, and the numerical procedures used in the computer code. Suggests it is prudent to start with a linear analysis for a baseline, then proceed to a simple nonlinear problem that can be hand verified, such as a cantilever beam, before proceeding to more complex nonlinear problems.
4.5.3.2.3	Refined methods of analysis for large deflections shall be based upon the concept of forces satisfying equilibrium in a deformed position.	X	X	X	X	-	-
4.5.4 C4.5.4	Modeled boundary conditions should accurately reflect actual characteristics.	X	X	X	X	X	Suggests that if accurate assessment of boundary conditions cannot be made, their effects may be bounded.

ARTICLE	CONTEXT	FORCE EFFECTS?	SECTION EFFECTS?	FEA CANDIDATE?	OTHER REFINED ANALYSIS?	GUIDANCE FOR FEA?	ADDITIONAL GUIDANCE PROVIDED
4.5.5 C4.5.5	States that non-prismatic members can be modeled using prismatic members. Either use a series of prismatic members with varying properties, or a single equivalent stiffness prismatic member. Alternatively, a non-prismatic element can simply be utilized.	X	X	X	X	X	Guidance is provided on the number of elements to use dependent on the behavior being modeled. Eight elements per span are suggested for forces in beams with smoothly varying cross sections. Fewer elements are proposed for deflection and frequency analyses.
4.6.1.1	Provides guidance on when a spine beam model may apply.	X	X	X	X	X	If the span length of a superstructure with torsionally stiff closed cross-sections exceeds 2.5 times its width, the superstructure may be idealized as a single-spine beam. The following dimensional definitions shall be used to apply this criterion: <ul style="list-style-type: none"> • Width—the core width of a monolithic deck or the average distance between the outside faces of exterior webs. • Length for rectangular simply supported bridges—the distance between deck joints. • Length for continuous and/or skewed bridges—the length of the longest side of the rectangle that can be drawn within the plan view of the width of the smallest span, as defined herein. The length-to-width restriction specified above does not apply to cast-in-place multicell box girders concrete box girder bridges.
4.6.1.2.1 C4.6.1.2.1	For curved girders, finite element analyses that model the actual cross-section shape of the I- or box girders can recognize cross-section distortion and its effect on structural behavior. Provides general guidance on modeling.	X	X	X	X	X	Recognizes that the integrated behavior of all structural elements, including cross-braces, is important in curved structures. Use FEA when distortion of cross-section is important.

ARTICLE	CONTEXT	FORCE EFFECTS?	SECTION EFFECTS?	FEA CANDIDATE?	OTHER REFINED ANALYSIS?	GUIDANCE FOR FEA?	ADDITIONAL GUIDANCE PROVIDED
4.6.1.2.3 C4.6.1.2.3	Concrete box girder bridges with high curvatures or unusual plan geometry require a method of analysis that utilizes sophisticated three-dimensional computer models.	X	X	X	X	-	-
4.6.1.2.4a C4.6.1.2.4a	Recommends when horizontally curved bridges can be analyzed as grids or continuums with straight segments for major axis bending.	X	X	X	X	X	Guidance on when using straight segments to model horizontally curved structures is appropriate.
C4.6.1.2.4b	Recommends use of refined analysis for I-girder bridges with varying girder stiffnesses. Also suggests using a refined analysis for conditions that produce torsion in curved girders.	X	X	X	X	-	-
C4.6.2.1.7	Suggests using a three-dimensional analysis for larger structures with integral decks.	X	-	X	X	-	-
4.6.2.1.9	States that the inelastic finite element analysis or yield line analysis may be permitted by the Owner for decks.	-	-	X	X	-	-
4.6.2.2.1	Gives option to use refined analysis method for curved bridges.	X	-	X	X	-	-
C4.6.2.2.1	Suggests using a refined method of analysis for Strength Load Combination II with a heavy permit load to reduce conservatism.	X	-	X	X	-	-
4.6.2.2.2b	For interior beams with concrete decks, refined analysis shall be used if criteria is met.	X	X	X	X	-	-
C4.6.2.2.4	For exceptional loadings of curved steel bridges, a more refined analysis is required.	X	X	X	X	-	-
4.6.2.4	Limits on "pin-connected" truss analogy.	X	X	X	X	X	Allows trusses to be modeled as pin-connected for given loads

ARTICLE	CONTEXT	FORCE EFFECTS?	SECTION EFFECTS?	FEA CANDIDATE?	OTHER REFINED ANALYSIS?	GUIDANCE FOR FEA?	ADDITIONAL GUIDANCE PROVIDED
4.6.2.5	<i>In the absence of a more refined analysis</i> , the effective length factor in the braced plane, K, for the compression members in triangulated trusses, trusses, and frames may be taken as described herein.	-	X	-	-	-	-
4.6.2.6.1	The slab effective flange width should be determined by a refined analysis when criteria herein are met.	X	X	X	X	-	-
C4.6.2.6.1	Approximate tributary width for main girders or truss chords may lead to an underestimation of shear connector requirements. To utilize a larger slab width, a refined analysis should be considered. Refined analysis shall be used for slab effective width of composite tied arches and cable stayed bridges.	X	X	X	X	-	-
4.6.2.6.2	For segmental concrete box beams and single-cell CIP box beams, the section properties for normal forces due primarily to anchorage of post-tensioning tendons may be based on the pattern according to Figure 4.6.2.6.2-4 or determined by more rigorous analysis.	X	X	X	X	-	-
4.6.2.6.4 C4.6.2.6.4	For orthotropic steel decks, the effective width need not be determined when using refined analysis. For service and fatigue limit states in regions of high shear, the effective deck width or orthotropic decks can be determined by refined analysis or other accepted approximate methods.	-	X	X	X	-	-

ARTICLE	CONTEXT	FORCE EFFECTS?	SECTION EFFECTS?	FEA CANDIDATE?	OTHER REFINED ANALYSIS?	GUIDANCE FOR FEA?	ADDITIONAL GUIDANCE PROVIDED
C4.6.2.7.1	<i>Unless a more refined analysis is made</i> , the wind force, wind moment, horizontal force to be transmitted by diaphragms and cross-frames, and horizontal force to be transmitted by lateral bracing may be calculated as indicated herein.	X	-	X	X	-	-
4.6.2.8.3	<i>Unless a more refined seismic analysis is made</i> , an approximate load path shall be assumed as described herein.	X	-	X	X	-	-
C4.6.2.9.1	Analysis of segmental concrete bridges requires consideration of variation of design parameters with time as well as a specific construction schedule and method of erection. Generally requires a computer analysis.	X	X	X	X	-	-
4.6.2.9.3	The section properties for normal forces of segmental girders may be as described herein or determined by more rigorous analysis.	-	X	X	X	-	-
C4.6.2.10.4	For box culverts not meeting the requirements herein, and <i>in lieu of a more rigorous design method</i> , specified reduced distribution widths shall be used.	X	X	X	X	-	-
4.6.3 (all sections)	Provides guidelines for refined methods of analysis.	X	X	X	X	X	Most of the text in these sections (too large to copy here).
4.6.4.2	Provides refined method for negative moment sections of continuous beams.	X	X	X	X	X	The negative moments over the support, as established by linear elastic analysis, may be decreased by a redistribution process considering the moment rotation characteristics of the cross-section or by a recognized mechanism method. The moment rotation relationship shall be established using material characteristics, as specified herein, and/or verified by physical testing.

ARTICLE	CONTEXT	FORCE EFFECTS?	SECTION EFFECTS?	FEA CANDIDATE?	OTHER REFINED ANALYSIS?	GUIDANCE FOR FEA?	ADDITIONAL GUIDANCE PROVIDED
4.6.5	The investigation of stability shall utilize the large deflection theory.	X	X	X	X	-	
4.7 (all sections)	Provides guidelines for dynamic analyses.	X	X	X	X	X	Much of the text in these sections (too large to copy here).
C5.7.2.2	If a more refined estimate of flexural capacity for sections that consist of a beam with a composite slab of different concrete strength, and the compression block includes both types of concrete, is warranted, a more rigorous analysis method should be used.	-	X	X	X	-	-
5.7.3.5	In lieu of a more refined analysis, the provisions of this article, for negative moment redistribution at internal supports, may be used.	X	X	X	X	-	-
5.7.3.6.2	In the absence of a more comprehensive analysis, instantaneous deflections may be computed using the modulus of elasticity for concrete as specified in Article 5.4.2.4 and taking the moment of inertia as either the gross or effective moment of inertia. Unless a more exact determination is made, the long term deflection may be taken as the factored instantaneous deflection.	X	X	X	X	-	-
5.7.4.1	In lieu of a more refined procedure, nonprestressed columns with the slenderness ratio $KL/r < 100$, may be designed by the approximate procedure specified in Article 5.7.4.3	X	X	X	X	-	-

ARTICLE	CONTEXT	FORCE EFFECTS?	SECTION EFFECTS?	FEA CANDIDATE?	OTHER REFINED ANALYSIS?	GUIDANCE FOR FEA?	ADDITIONAL GUIDANCE PROVIDED
5.7.4.5	In lieu of an analysis based on equilibrium and strain compatibility for biaxial flexure, noncircular members subjected to biaxial flexure and compression may be proportioned using the following approximate expressions.	X	X	X	X	-	-
C5.8.3.1	An appropriate nonlinear finite element analysis or a detailed sectional analysis would satisfy the requirements of this Article.	X	X	X	X	-	More information on appropriate procedures and a computer program that satisfies these requirements are given by Collins and Mitchell (1991). One possible approach to the analysis of biaxial shear and other complex loadings on concrete members is outlined in Rabbat and Collins (1978), and a corresponding computer-aided solution is presented in Rabbat and Collins (1976).
5.8.6.2	<i>In lieu of a more refined analysis</i> , the torsional loading from a slab may be assumed as linearly distributed along the member.	X	-	X	X	-	-
5.8.6.3	<i>In lieu of a more refined analysis</i> , effective width may be calculated as described herein.	-	X	X	X	-	-
5.9.5.1 C5.9.5.1	<i>In lieu of more detailed analysis (i.e. time-step method)</i> , prestress losses in members may be calculated as described herein.	X	-	X	X	-	-
5.10.9.3.1	Three-dimensional effects in post-tensioned anchorage zones may be analyzed using three-dimensional analysis procedures or may be approximated.	X	X	X	X	-	-

ARTICLE	CONTEXT	FORCE EFFECTS?	SECTION EFFECTS?	FEA CANDIDATE?	OTHER REFINED ANALYSIS?	GUIDANCE FOR FEA?	ADDITIONAL GUIDANCE PROVIDED
C5.10.11.4.1b	Limiting the flexural resistance factor to 0.9 is considered justified <i>in lieu of a more rigorous analysis</i> because the LRFD provisions are force-based and ductility demand is not calculated. See Seismic Guide Spec and NCHRP 12-49 for alternatives.	-	X	X	X	-	-
C5.14.2.3.10d	If in a single cell box the limit of depth to width ratio is exceeded, a more rigorous analysis is required and longitudinal edge beams at the tip of the cantilever may be required to distribute loads acting on the cantilevers. An analysis for shear lag should be made in such cases. Transverse load distribution is not substantially increased by the use of three or more cells.	X	X	X	X	-	-
C5.14.2.3.11	Design of segmental concrete superstructures should take into account inelastic hinging in the pier columns.	X	X	X	X	X	Recommends pushover analysis.
5.14.3.2	<i>In lieu of a rigorous analysis</i> for arch ribs, the effective length for buckling may be estimated as described herein.	-	X	X	X	-	-
5.14.4.1	The distribution of live load in CIP solid slab superstructures may be determined by a refined analysis or as specified in Article 4.6.2.3.	X	-	X	X	-	-
5.14.4.2.3 C5.14.4.2.3	<i>In the absence of more refined analysis</i> , the solid sections of the CIP voided slab may be analyzed as a transverse beam distributing forces to bridge bearings and to post-tensioning anchorages. For deep and narrow decks, a three-dimensional analysis or use of a strut-and-tie model is advisable.	X	X	X	X	-	-

ARTICLE	CONTEXT	FORCE EFFECTS?	SECTION EFFECTS?	FEA CANDIDATE?	OTHER REFINED ANALYSIS?	GUIDANCE FOR FEA?	ADDITIONAL GUIDANCE PROVIDED
C6.6.1.2.1	Where force effects in cross-frames or diaphragms are obtained through analysis, it may be desirable to check fatigue-sensitive details on a bracing member.	X	X	X	X	-	-
C6.6.1.3.1	Suggestion to determine diaphragm forces for curved or skewed bridges by analysis.	X	X	X	X	-	-
6.6.2	Unless a rigorous analysis with assumed hypothetical cracked components confirms the strength and stability of the hypothetically damaged structure, the location of all FCMs shall be clearly delineated on the contract plans.	X	X	X	X	-	-
C6.6.2	The criteria for a refined analysis used to demonstrate that part of a structure is not fracture-critical has not yet been codified. Therefore, the loading cases to be studied, location of potential cracks, degree to which the dynamic effects associated with a fracture are included in the analysis, and fineness of models and choice of element type should all be agreed upon by the Owner and the Engineer. The ability of a particular software product to adequately capture the complexity of the problem should also be considered and the choice of software should be mutually agreed upon by the Owner and the Engineer.	X	X	X	X	X	The loading cases to be studied, location of potential cracks, degree to which the dynamic effects associated with a fracture are included in the analysis, and fineness of models and choice of element type should all be agreed upon by the Owner and the Engineer. The ability of a particular software product to adequately capture the complexity of the problem should also be considered and the choice of software should be mutually agreed upon by the Owner and the Engineer. Relief from the full factored loads associated with the Strength I Load Combination of Table 3.4.1-1 should be considered, as should the number of loaded design lanes versus the number of striped traffic lanes.

ARTICLE	CONTEXT	FORCE EFFECTS?	SECTION EFFECTS?	FEA CANDIDATE?	OTHER REFINED ANALYSIS?	GUIDANCE FOR FEA?	ADDITIONAL GUIDANCE PROVIDED
C6.7.4.2	Refined analysis is recommended for cross-frame forces, lateral bearing reactions, and lateral flange bending whenever removal of diaphragms or cross-frames along and/or in the vicinity of severely skewed interior support lines is considered.	X	X	X	X	-	-
C6.7.4.3	For box section members, refined analysis of internal diaphragms at supports is desirable because these primary members are necessary for the integrity of the bridge.	X	X	X	X	-	-
C6.7.5.3	<i>In the absence of a more refined analysis</i> , Fan and Helwig provide an approach for estimating the flexural forces in the top lateral bracing members.	X	X	X	X	-	-
6.8.2.2	<i>In the absence of more refined analysis</i> or tests, the reduction factors specified herein may be used to account for shear lag in connections.	-	X	X	X	-	-
6.9.2.2	Moments to calculate compressive resistance may be determined by second-order elastic analysis.	-	X	X	X	X	A second-order elastic analysis that accounts for the magnification of moment caused by the factored axial load
C6.9.4.1.1	The resistance equations herein may be used to calculate P_n when a refined buckling analysis is employed to assess the stability of trusses, frames or arches in lieu of utilizing an effective length factor approach.	X	X	X	X	X	The resistance equations herein may be used to calculate P_n when a refined buckling analysis is employed to assess the stability of trusses, frames or arches in lieu of utilizing an effective length factor approach.
C6.9.4.1.3	C_w may be calculated using equations provided herein <i>in lieu of a more precise analysis</i> .	X	X	X	X	-	-

ARTICLE	CONTEXT	FORCE EFFECTS?	SECTION EFFECTS?	FEA CANDIDATE?	OTHER REFINED ANALYSIS?	GUIDANCE FOR FEA?	ADDITIONAL GUIDANCE PROVIDED
C6.10.1	Although the use of refined analysis methods is not required in order to fulfill the requirements of the provisions for I-section flexural members, these methods, when utilized, do allow for consideration of flange lateral bending.	X	-	X	X	-	-
C6.10.1.6	<i>In lieu of a more refined analysis</i> , Article C6.10.3.4 gives approximate equations for calculation of the maximum flange lateral bending moments due to eccentric concrete deck overhang loads acting on cantilever forming brackets placed along exterior members. When the flange second-order lateral bending effects are significant, the Engineer may wish to consider a direct geometric nonlinear analysis to more accurately determine the second-order effects within the superstructure.	X	-	X	X	-	-
C6.10.3.4	<i>In the absence of a more refined analysis</i> for deck placement, the equations herein may be used to estimate the maximum flange lateral bending moments due to the eccentric loadings. Refined analysis of the noncomposite bridge for these loads provides more accurate lateral moments and may identify any rotation of the overhang that could potentially affect the elevation of the screed when finishing the deck.	X	X	X	X	-	-
C6.10.10.1.2	For shear connectors and <i>in lieu of a refined analysis</i> , F_{rc} may be taken as 25.0 kips for an exterior girder.	X	X	X	X	-	-

ARTICLE	CONTEXT	FORCE EFFECTS?	SECTION EFFECTS?	FEA CANDIDATE?	OTHER REFINED ANALYSIS?	GUIDANCE FOR FEA?	ADDITIONAL GUIDANCE PROVIDED
C6.11.1.1	For live load distribution, box-section flexural members not satisfying one or more of the restrictions provided herein should be investigated using one of the available methods of refined structural analysis, or other acceptable methods of approximate structural analysis as specified in Articles 4.4 or 4.6.2.2.4.	X	-	X	X	-	-
C6.11.2.3	For bridges with box-section flexural members and support skew or horizontal curvature, a more rigorous analysis of stresses is necessary using one of the available methods of refined structural analysis. For straight portions of bridges that satisfy these restrictions, but that also contain horizontally curved segments, a refined analysis is also recommended. Although not required, refined structural analysis methods may also be used for bridges satisfying the restrictions of this Article, if desired.	X	X	X	X	-	-
C6.11.3.2	<i>In lieu of a more refined analysis</i> , the maximum flange lateral bending moments in the outermost top flange of a tub due to eccentric loadings may be estimated using equations herein. The maximum lateral flange bending moments due to transverse load in box sections with inclined webs can be estimated using equations herein in lieu of a more refined analysis.	X	-	X	X	-	-

ARTICLE	CONTEXT	FORCE EFFECTS?	SECTION EFFECTS?	FEA CANDIDATE?	OTHER REFINED ANALYSIS?	GUIDANCE FOR FEA?	ADDITIONAL GUIDANCE PROVIDED
6.11.5	Unless adequate strength and stability of a damaged structure can be verified by refined analysis, in cross-sections comprised of two box sections, only the bottom flanges in the positive moment regions should be designated as fracture-critical.	X	X	X	X	-	-
6.14.3.2.3 C6.14.3.2.3	For orthotropic decks, the critical buckling stress of the strut shall be determined in accordance with Article 6.9.4 or by methods of refined analysis as defined in Article 4.6.3.2.3. For orthotropic decks, refined analysis may be used for a more accurate assessment of panel buckling strength with full consideration of the orthogonal stiffening behavior.	X	X	X	X	-	-
B6.6.1 CB6.6.1	The Engineer is also provided the option to use a refined method in which a direct shakedown analysis is conducted at the service and/or strength limit states. (see also 4.6.4.2)	X	X	X	X	X	This analysis requires the simultaneous satisfaction of continuity and moment-rotation relationships at all interior-pier sections from which moments are redistributed. If software that handles this type of calculation along with the determination of the elastic moment envelopes does not exist, significant manual work is required in conducting the analysis calculations. The Engineer can gain some additional benefit when using direct analysis in that the restriction that all interior-pier sections within the member satisfy the requirements of Article B6.2.1 is relaxed. Also, the directly calculated inelastic rotations at the interior pier sections will tend to be smaller than the upper-bound values that the equations in Articles B6.3 through B6.5 are based upon.

ARTICLE	CONTEXT	FORCE EFFECTS?	SECTION EFFECTS?	FEA CANDIDATE?	OTHER REFINED ANALYSIS?	GUIDANCE FOR FEA?	ADDITIONAL GUIDANCE PROVIDED
7.9.4 (2012 Agenda)	For aluminum members in combined axial compression and flexure, the moments about the axes of symmetry may be determined by a second-order analysis that accounts for the magnification of moment caused by the factored axial load.	-	X	X	X	-	-
9.6.1	States that refined methods specified in Article 4.6.3.2 may be used to design deck slabs.	X	-	X	X	-	-
C9.7.1.3	Suggestion to use one of the refined methods described in 4.6.3.2 if less conservative reinforcement quantity desired for skewed deck slabs.	X	-	X	X	-	-
C9.7.3.1	States that the live load force effects in the slab may be determined using the refined methods of Article 4.6.3.2.	X	-	X	X	-	-
C9.8.3.4.1	States that refined analysis for orthotropic decks will add engineering cost and potentially limit use for routine span arrangements. Describes 3 Levels of design. Level 1 design requires little or no structural analysis, but uses proven details. Level 2 design utilizes simplified one- or two-dimensional analyses and nominal stresses, for instance using the Pelikan-Esslinger method. Level 3 design is based on refined three-dimensional analysis of the panel to quantify the local stresses to the most accurate extent reasonably expected from a qualified design engineer experienced in refined analysis.	X	X	X	X	X	Research has demonstrated that a Level 3 evaluation of the local stress range with AASHTO Category C provides a reliably conservative assessment of the probability of weld toe cracks of orthotropic deck panels. Suggests the mesh size for a Level 3 shell or solid element analysis should be t (length) by t (width) where t is the thickness of the connected component. For more information, see <i>Recommendations for Fatigue Design of Welded Joints and Components</i> (International Institute of Welding, Paris, France, 2007), and <i>Manual for Design, Construction, and Maintenance of Orthotropic Steel Bridges</i> (in development).
9.8.3.4.3c	Level 2 Design: For decks with closed ribs the Pelikan-Esslinger method may be used.	X	X	-	X	-	-

ARTICLE	CONTEXT	FORCE EFFECTS?	SECTION EFFECTS?	FEA CANDIDATE?	OTHER REFINED ANALYSIS?	GUIDANCE FOR FEA?	ADDITIONAL GUIDANCE PROVIDED
9.8.3.4.4	Level 3 Design: Provides option for using finite element analyses as defined in Article 4.6.3.2.3 and for fatigue analysis of orthotropic decks.	X	X	X	X	X	For fatigue analysis, the structural modeling techniques shall include: <ul style="list-style-type: none"> • Use of shell or solid elements with acceptable formulation to accommodate steep stress gradients, • Mesh density of $t \times t$, where t is the thickness of the plate component, and • Local structural stresses shall be determined as specified below For fatigue design, the local structural stress shall be used for comparison to the nominal fatigue resistance. Local structural stress at welded connections shall be measured perpendicular to the weld toe and is determined using reference points in the finite element model and extrapolation as shown in Figure 9.8.3.4.4-1. The reference points shall be located at the surface of elements at a distance of $0.5 t$ and $1.5 t$ measured perpendicular from the weld toe, respectively, with the local structural stress f_{lss} determined in accordance with Eq. 9.8.3.4.4-1.
C9.8.3.5.2d	For Level 1 design, test loads should be representative of the fatigue truck factored for the Fatigue I load combination and the critical details of the test specimen(s) should simulate both the expected service conditions and the appropriate boundary conditions; verification of these details is sufficient <i>in lieu of a detailed refined fatigue analysis</i> .	X	X	X	X	-	-
C10.5.4.2	Article dealing with liquefaction of soils. Addresses nonlinear inelastic response in soil liquefaction behavior and hinging in both pier columns and subsurface elements.	X	X	X	X	X	Recommends pushover analysis for pier columns.

ARTICLE	CONTEXT	FORCE EFFECTS?	SECTION EFFECTS?	FEA CANDIDATE?	OTHER REFINED ANALYSIS?	GUIDANCE FOR FEA?	ADDITIONAL GUIDANCE PROVIDED
C11.8.6.4	States that pseudostatic or dynamic finite element or finite difference procedures in computer programs can also be used to evaluate the seismic response of nongravity cantilever walls during seismic loading.	X	X	X	X	X	For two-dimensional models, it may be necessary to “smear” the stiffness of the structural section below the excavation level to adjust the model to an equivalent two-dimensional representation if the below-grade portion of the wall is formed from discrete piles (e.g., soldier piles).
12.8.9.3.2	Requires analysis of deep corrugated structures using finite element analysis.	X	X	X	-	X	Structures designed under the provisions of this Article shall be analyzed by accepted finite element analysis methods that consider both the strength and stiffness properties of the structural plate and the soil. The analysis shall produce thrust and moments for use in design. The analysis must consider all applicable combinations of construction, earth, live, and other applicable load conditions. Springline thrust due to earth load used in wall resistance, buckling, and seam resistance design shall not be less than 1.3 times the earth load thrust computed in accordance with Article 12.7.2.2.
C12.9.4.2	For structural plate box structures that do not meet the requirements herein, finite element modeling that employs soil-structure interaction may be performed.	X	X	X	-	-	-
C12.11.2.3	States that a refined analysis may be beneficial for distribution of loads to bottom slab of box culvert.	X	X	X	X	-	-
13.1	For use beyond the design of barrier test specimens similar to those herein, a rigorous yield line solution or a finite element solution should be developed.	X	X	X	X	-	-
C14.8.1	States that finite element analysis for design of masonry plates is preferable, but may not be practical.	X	X	X	-	-	-

**Please note that a search of the Appendices was not performed.

APPENDIX 2B – REFERENCES TO REFINED ANALYSIS IN AASHTO MBE

List of references to refined analysis found in the 2nd Edition of AASHTO MBE.

Keywords such as "analysis", "methods", "software", and "finite" were used.

ARTICLE	CONTEXT	FORCE EFFECTS?	SECTION EFFECTS?	FEA CANDIDATE?	OTHER REFINED ANALYSIS?	GUIDANCE FOR FEA?	ADDITIONAL GUIDANCE PROVIDED
4.2.3	Suggests using refined analysis to supplement Damage Inspections.	-	-	X	X	-	-
6.1.6	States that special analysis methods and/or procedures may be required for complex structures.	-	-	X	X	-	-
6.1.9	States that if a computer model is used, the input data file shall be retained for future use.	-	-	X	X	-	-
C6A.3.1	States that the evaluator has the option of using a more refined approach for improved accuracy.	-	X	X	X	-	-
C6A.3.2	States that refined methods of analysis should be considered for structures with loading parameters falling outside of the specified ranges.	X	X	X	X	-	-
6A.3.3 C6A.3.3	Entire section devoted to utilizing refined methods of analysis for bridges with insufficient load capacity when analyzed using approximate methods and bridges or loading conditions for which accurate live load distribution formulas are not readily available.	X	X	X	X	-	-
C6A.4.4.2.2	States that more refined site-specific load factors may be estimated if more detailed traffic and truck load data are available for the site.	X	-	X	X	-	-
6A.4.5.4.2b	States that a refined analysis may be used to determine a one-lane distribution factor for special permit review.	X	-	X	X	-	-

ARTICLE	CONTEXT	FORCE EFFECTS?	SECTION EFFECTS?	FEA CANDIDATE?	OTHER REFINED ANALYSIS?	GUIDANCE FOR FEA?	ADDITIONAL GUIDANCE PROVIDED
6A.4.5.4.2c (2013 Interim)	Entire section devoted to permit checks using refined analysis.	-	-	X	X	-	-
C6A.6.4.2.2	States that, for existing structures that are curved in plan, either approximate methods or refined analysis methods may be used for the Service II limit state check.	X	-	X	X	-	-
6A.9.1.2	Suggests using a more refined analysis to establish a more accurate safe load capacity for arches.	X	X	X	X	-	-
C6B.6.7.2	Permits the investigator to use either the relatively simple methods of the AASHTO Bridge Standard Specifications or the more complex analysis procedures described in the AASHTO Specifications for Seismic Design.	X	-	X	X	X	Recommends multimodal spectral method for more thorough results.
6B.7.2 C6B.7.2	Defines AASHTO Legal Vehicle loadings. States that a posting analysis for single-unit multi-axle trucks should be performed for bridges with RF < 1.0 for the Notional Rating Load (NRL) loading.	X	-	X	X	-	-
7.1	States that distortion-induced fatigue can only be calculated using very refined methods of analysis.	-	X	X	X	-	-
7.2.1	States that refined analysis results in increased certainty in stresses allowing use of lower partial load factors.	X	-	X	X	-	-
7.2.1	States that if cracks are detected a complex fracture mechanics approach for load-induced fatigue-damage is required instead of the procedure specified herein.	-	X	X	X	-	-

ARTICLE	CONTEXT	FORCE EFFECTS?	SECTION EFFECTS?	FEA CANDIDATE?	OTHER REFINED ANALYSIS?	GUIDANCE FOR FEA?	ADDITIONAL GUIDANCE PROVIDED
C7.2.1	States that the stress-range estimate for the infinite-life check should be refined before the more complex procedures of the finite-life fatigue evaluation are considered.	X	-	X	X	-	-
Table 7.2.2.1-1	Provides the partial load factors for refined analyses.	X	-	X	X	-	-
7.2.2.1.1	Provides the calculation for R_{sa} if effective stress range is calculated through refined analysis.	X	-	X	X	-	-

**Please note that a search of the Appendices was not performed.

APPENDIX 7A – REFERENCES TO REFINED ANALYSIS IN AASHTO LRFD

Provisions related to the magnitude and application of live load in refined analyses - Seventh Edition of AASHTO LRFD

**Keywords such as "analysis", "refined", "methods", "software", and "finite" were used.

ARTICLE	CONTEXT	GUIDANCE FOR LIVE LOAD PROVIDED
2.5.2.6.1	If dynamic analysis is used to determine deformations, it shall comply with Article 4.7.	Reference to Article 4.7 (See below).
3.6.1.3.3	When refined methods are used in design of decks, deck systems, and top slabs of box culverts, describes live loading to be used depending on the primary direction the deck spans.	When deck spans primarily in the transverse direction, only the axles of the design truck of Article 3.6.1.2.2 or design tandem of Article 3.6.1.2.3 shall be applied. When the deck spans primarily in the longitudinal direction, all of the loads of Article 3.6.1.2 shall be applied.
3.6.1.4.3a	Where the bridge is analyzed for fatigue by any refined method, as specified in Article 4.6.3, a single design truck shall be positioned transversely and longitudinally to maximize stress range at the detail under consideration.	Where the bridge is analyzed for fatigue by any refined method, as specified in Article 4.6.3, a single design truck shall be positioned transversely and longitudinally to maximize stress range at the detail under consideration.
4.6.2.4	Limits on "pin-connected" truss analogy.	Allows truss to be modeled as pin-connected for live loads
4.6.3 (all sections)	Provides guidelines for refined methods of analysis.	Most of the text in these sections (too large to copy here).
4.7 (all sections)	Provides guidelines for dynamic analyses.	Guidance on determining dynamic load allowance.
5.14.4.1	The distribution of live load in CIP solid slab superstructures may be determined by a refined analysis or as specified in Article 4.6.2.3.	Distribution of live load can be determined by refined analysis.
C6.6.1.2.1	Where force effects in cross-frames or diaphragms are obtained through analysis, it may be desirable to check fatigue-sensitive details on a bracing member.	An additional load factor of 0.75 is recommended when the stress range is maximized by the passage of the factored fatigue load in two different transverse positions on the bridge.
C6.11.1.1	For live load distribution, box-section flexural members not satisfying one or more of the restrictions provided herein should be investigated using one of the available methods of refined structural analysis, or other acceptable methods of approximate structural analysis as specified in Articles 4.4 or 4.6.2.2.4.	Distribution of live load can be determined by refined analysis.
C9.7.3.1	States that the live load force effects in the slab may be determined using the refined methods of Article 4.6.3.2.	See 4.6.3.2 (too much to list here).

APPENDIX 7B – REFERENCES TO REFINED ANALYSIS IN AASHTO MBE

Provisions related to the magnitude and application of live load in refined analyses - *Manual for Bridge Evaluation, 2nd Edition*.

**Keywords such as "analysis", "refined", "methods", "software", and "finite" were used.

ARTICLE	CONTEXT	GUIDANCE FOR LIVE LOAD PROVIDED
C6A.4.4.2.2	States that more refined site-specific load factors may be estimated if more detailed traffic and truck load data are available for the site.	States that more refined site-specific load factors may be estimated from detailed traffic and truck load data from the site.
6A.4.5.4.2b	States that a refined analysis may be used to determine a one-lane distribution factor for special permit review.	States that refined analysis can be used for one lane distribution
6A.4.5.4.2c (2013 Interim)	Entire section devoted to permit checks using refined analysis.	Describes load factors to be applied.
6B.7.2 C6B.7.2	Defines AASHTO Legal Vehicle loadings. States that a posting analysis for single-unit multi-axle trucks should be performed for bridges with RF < 1.0 for the Notional Rating Load (NRL) loading.	Provides Legal Vehicle axle spacings and loadings.
Table 7.2.2.1-1	Provides the partial load factors for refined fatigue analyses.	Provides for lower partial load factors for refined fatigue analyses.
7.2.2.1.1	Provides the calculation for R_{sa} if effective fatigue stress range is calculated through refined analysis.	Provides the calculation for R_{sa} if effective fatigue stress range is calculated through refined analysis.

APPENDIX 9A - EXAMPLE 2 LIVE LOAD DISTRIBUTION FACTORS

Interior Girder Distribution Factors

The distribution factor equations for live load moment in interior beams are shown as Equation (93) for one lane loaded and Equation (94) for multiple lanes loaded.

$$g_{SIM} = 0.06 + \left(\frac{S}{14}\right)^{0.4} \left(\frac{S}{L}\right)^{0.3} \left(\frac{K_g}{12.0Lt_s^3}\right)^{0.1} \quad (93)$$

$$g_{MIM} = 0.075 + \left(\frac{S}{9.5}\right)^{0.6} \left(\frac{S}{L}\right)^{0.2} \left(\frac{K_g}{12.0Lt_s^3}\right)^{0.1} \quad (94)$$

where: S = girder spacing [ft]
 L = span length [ft]
 t_s = deck slab thickness [inches]
 K_g = longitudinal stiffness parameter [in⁴] = n(I + Ae_g²)
 n = modular ratio
 A, I = area and moment of inertia for non-composite beam
 e_g = distance between centers of gravity of the non-composite beam and deck slab [inches]
 g = distribution factor

The first step in determining the approximate distribution factors is to determine the value of K_g for each girder cross-section. This value is the same for both the interior and exterior girders as the same beam is used. The non-composite area and moment of inertia are found in Table 28. The value for “e_g” is determined using Equation (95). The calculation herein neglected the ½ inch integral wearing surface and the haunch depth in calculating “e_g.” Using Equation (95), “e_g” is determined to be 51.50 inches for Section A-A, 53.94 inches for Section B-B, and 56.00 inches for Section C-C.

$$e_g = D - y_{bar} + \frac{t_s}{2} \quad (95)$$

From Section 9.2.1.1.2, the modular ratio, n, is 8.0. As calculated above, the distance between centers of gravity of the non-composite beam and deck slab, e_g, is 51.50 inches for Section A-A, 53.94 inches for Section B-B, and 56.00 inches for Section C-C. Inserting all values into the equation for K_g, determine that K_g is 2,931,088.33 in⁴ for Section A-A, 3,906,645.20 in⁴ for Section B-B, and 6,506,699.75 in⁴ for Section C-C.

$$K_{gA-A} = n(I + Ae_g^2) = 8(118400.7in^4 + 93.5in^2 \times (51.50in)^2) = 2931088.33in^4$$

$$K_{gB-B} = n(I + Ae_g^2) = 8(160308.90in^4 + 112.75in^2 \times (53.94in)^2) = 3906645.20in^4$$

$$K_{gC-C} = n(I + Ae_g^2) = 8(286524.47in^4 + 168.0in^2 \times (56.00in)^2) = 6506699.75in^4$$

The second step in determining the approximate distribution factors is to determine if the bridge characteristics satisfy the range of applicability listed in AASHTO LRFD Table 4.6.2.2.2b-1. These characteristics and the range of applicability are shown in Table 120 as well as if the

Example 2 bridge satisfies the criteria. Since all of the criteria are satisfied, Equations (93) and (94) can be used to calculate the moment distribution factors for the interior girders.

Table 120. Bridge characteristics for distribution factor equations.

Characteristic	Range	Satisfied for Example 2
Girder spacing, S	$3.5 \leq S \leq 16.0$	$S = 11.0$, YES
Deck slab thickness, t_s	$4.5 \leq t_s \leq 12.0$	$t_s = 9$, YES
Span length, L	$20 \leq L \leq 240$	$L = 160$ and 210 , YES
Number of beams, N_b	$N_b \geq 4$	$N_b = 4$, YES
Longitudinal Stiffness, K_g	$10,000 \leq K_g \leq 7,000,000$	$K_{gA-A} = 2,931,088.33$, YES $K_{gB-B} = 3,906,645.20$, YES $K_{gC-C} = 6,506,699.75$, YES

As all the characteristics of this bridge meet the requirements to use the approximate distribution factors, the next step is to calculate the distribution factors. The distribution factors depend on the span length; the center span of this bridge is longer than the side spans, therefore separate distribution factors will be calculated for the center span. Additionally, for negative moment between dead load points of contraflexure (POCs), AASHTO LRFD indicates that the average of the two span lengths can be used (See AASHTO LRFD Table C4.6.2.2.1-1). The values shown in Table 120, are inserted into Equations (93) and (94) to determine the distribution factors for positive moment in the side and center span and for negative moment in the side and center span when not between POCs. For negative moment between POCs, the average of the two span lengths is used. Calculation of the distribution factor for moment in an interior girder for one lane loaded is shown below, the others are calculated similarly and are shown in Table 121.

$$g_{SIM} = 0.06 + \left(\frac{S}{14}\right)^{0.4} \left(\frac{S}{L}\right)^{0.3} \left(\frac{K_g}{12.0Lt_s^3}\right)^{0.1} = 0.06 + \left(\frac{11.0}{14}\right)^{0.4} \left(\frac{11.0}{160.0}\right)^{0.3} \left(\frac{2931088.33}{12 \times 160.0 \times 9^3}\right)^{0.1}$$

$$= 0.50 \text{ lanes}$$

Table 121. Interior girder moment distribution factors.

Action	Lanes Loaded	Spans 1 and 3			Span 2		
		A-A	B-B	C-C	A-A	B-B	C-C
M+ and M- not between POCs	1	0.50	0.51	0.53	0.45	0.46	0.49
	2+	0.76	0.78	0.82	0.71	0.73	0.76
		A-A		B-B		C-C	
M- between POCs	1	0.47		0.49		0.51	
	2+	0.73		0.75		0.79	

Exterior Girder Distribution Factors

Once the distribution factors for the interior girder have been determined, the distribution factors for the exterior girders can be calculated. AASHTO LRFD Table 4.6.2.2.2d-1 indicates that for one lane loaded, the lever rule should be used; for two or more lanes loaded, use the equation provided in AASHTO LRFD Table 4.6.2.2.2d-1. But in no case, for any number of lanes loaded, should the distribution factor be less than that calculated using AASHTO LRFD Eq. C4.6.2.2.2d-1 assuming a rigid cross-section.

The lever rule uses a static distribution to distribute the live load to the girders. The lever rule assumes that the deck slab is simply supported between girders; for exterior girders, the deck slab is continuous with the overhang. Figure 419 shows the various dimensions necessary to calculate the distribution factor via the lever rule. Using the lever rule also requires application of the multiple presence factors in AASHTO LRFD Table 3.6.1.1.2-1 for one lane loaded.

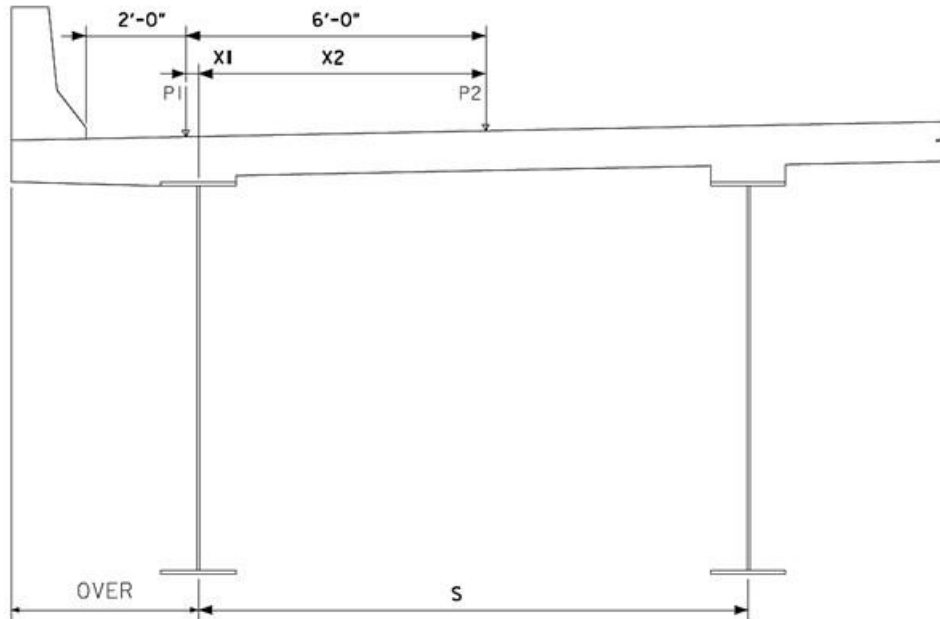


Figure 419. Illustration. Lever rule dimensions.

The dimensions shown in Figure 419 are defined as: S is the girder spacing, $OVER$ is the overhang width, $P1$ and $P2$ are the left and right wheel centerlines respectively, $X1$ is the distance from the left wheel to centerline of exterior girder, and $X2$ is the distance from the exterior girder centerline to the right wheel. $X1$ is determined using Equation (96), where “barrier” is the width of the barrier, and $X2$ is determined using Equation (97). $X1$ is negative if the wheel line is between the edge of the deck slab and the centerline of the girder and positive if between girders. The distribution factor can then be calculated using Equation (98), where m is the multiple presence factor from AASHTO LRFD Table 3.6.1.1.2-1.

$$X1 = OVER - Barrier - 2' \quad (96)$$

$$X2 = 6' + X1 \quad (97)$$

$$g = \frac{m(S - X1 + S - X2)}{2S} \quad (98)$$

Using the dimensions in Figure 194 and Equations (96) and (97), $X1$ is determined to be -3 inches and $X2$ is determined to be 69 inches. Using Equation (98) and selecting the appropriate multiple presence factor ($m = 1.2$) from AASHTO LRFD Table 3.6.1.1.2-1, the distribution factor is calculated as 0.90 lanes for one lane loaded.

$$g = \frac{m(S - X1 + S - X2)}{2S} = \frac{1.2(132'' - (-3'') + 132'' - 69'')}{2 \times 132''} = 0.90 \text{ lanes}$$

For multiple lanes loaded, AASHTO LRFD Table 4.6.2.2.2d-1 indicates to use the equation provided in the table. The moment distribution factor for multiple lanes loaded and exterior girders is given by (99) and “e” is given by (100).

$$g_{MEM} = e g_{MIM} \quad (99)$$

$$e = 0.77 + \frac{d_e}{9.1} \quad (100)$$

In Equation (100), d_e is the horizontal distance from the centerline of the web of the exterior girder to the interior face of the traffic barrier. Using Equation (101), d_e can be determined. AASHTO LRFD Table 4.6.2.2.2d-1 indicates that the calculated value of d_e must be between -1.0 ft and 5.5 ft. Figure 194 indicates the overhang width to be 3 ft-9 inches and the barrier width to be 1 ft-6 inches, giving a value of d_e equal to 2.25 ft; this value is between -1.0 ft and 5.5 ft.

$$d_e = \text{OVER} - \text{Barrier} \quad (101)$$

Substituting d_e into Equation (100), “e” is determined to be 1.02. Then substituting “e” into Equation (99) and using the previously calculated distribution factors for the interior girders and multiple lanes loaded from Table 121, the distribution factors for the exterior girders are determined. Table 122 shows the distribution factors determined using AASHTO LRFD Table 4.6.2.2.2d-1 for multiple lanes loaded.

Table 122. Exterior girder moment distribution factors based on AASHTO LRFD Table 4.6.2.2.2d-1.

Action	Lanes Loaded	Spans 1 and 3			Span 2		
		A-A	B-B	C-C	A-A	B-B	C-C
M+ and M- not between POCs	1	0.90			0.90		
	2+	0.78	0.80	0.83	0.72	0.74	0.78
		Section B-B			Section C-C		
M- between POCs	1	0.90			0.90		
	2+	0.77			0.79		

The final step to determine the live load distribution factor for the exterior girders is to consider the rigid cross-section analysis in AASHTO LRFD C4.6.2.2.2d. The live load distributed to the exterior girder can be determined using Equation (102).

$$R = m \left(\frac{N_L}{N_b} + \frac{X_{ext} \sum_1^{N_L} e}{\sum_1^{N_b} x^2} \right) \quad (102)$$

where: R = reaction on exterior beam in terms of lanes
m = multiple presence factor, from Table 3.6.1.1.2-1
 N_L = number of loaded lanes under consideration
e = eccentricity of design truck or design lane load from center of gravity of the pattern of girders [ft]

x = horizontal distance from center of gravity of girder pattern to each girder [ft]
 X_{ext} = horizontal distance from center of gravity of girder pattern to exterior girder [ft]
 N_b = number of beams/girders

One Lane Loaded:

Multiple Presence Factor:

$$m = 1.2$$

First Term of Equation (102):

$$N_L = 1$$

$$N_b = 4$$

$$N_L/N_b = 0.25$$

Second Term of Equation (102):

$$X_{ext} = 1.5 \times 11.0 \text{ ft} = 16.5 \text{ ft}$$

$$e_1 = X_{ext} + \text{OVER} - \frac{\text{Barrier}}{12} - 2\text{ft} - \frac{6\text{ft}}{2}$$

$$= 13.75 \text{ ft}$$

$$\Sigma e = 13.75 \text{ ft}$$

$$x_1, x_4 = 1.5 \times 11 \text{ ft} = 16.5 \text{ ft}$$

$$x_2, x_3 = 0.5 \times 11 \text{ ft} = 5.5 \text{ ft}$$

$$\Sigma x^2 = 2 \times (5.5 \text{ ft})^2 + 2 \times (16.5 \text{ ft})^2 = 605.0 \text{ ft}^2$$

$$\frac{X_{ext} \sum_1^{N_L} e}{\sum_1^{N_b} x^2} = \frac{16.5 \text{ ft}(13.75 \text{ ft})}{605 \text{ ft}^2} = 0.375$$

Reaction on Exterior Beam:

$$R = m \left(\frac{N_L}{N_b} + \frac{X_{ext} \sum_1^{N_L} e}{\sum_1^{N_b} x^2} \right)$$

$$= 1.2 \times (0.25 + 0.375)$$

$$= 0.75 \text{ lanes}$$

Two Lanes Loaded:

Multiple Presence Factor:

$$m = 1.0$$

First Term of Equation (102):

$$N_L = 2$$

$$N_b = 4$$

$$N_L/N_b = 0.5$$

Second Term of Equation (102):

$$X_{ext} = 1.5 \times 11.0 \text{ ft} = 16.5 \text{ ft}$$

$$e_1 = X_{ext} + \text{OVER} - \frac{\text{Barrier}}{12} - 2\text{ft} - \frac{6\text{ft}}{2}$$

$$= 13.75 \text{ ft}$$

$$e_2 = e_1 - 12 \text{ ft} = 1.75 \text{ ft}$$

$$\Sigma e = 13.75 \text{ ft} + 1.75 \text{ ft} = 15.5 \text{ ft}$$

$$x_1, x_4 = 1.5 \times 11 \text{ ft} = 16.5 \text{ ft}$$

$$x_2, x_3 = 0.5 \times 11 \text{ ft} = 5.5 \text{ ft}$$

$$\Sigma x^2 = 2 \times (5.5 \text{ ft})^2 + 2 \times (16.5 \text{ ft})^2 = 605 \text{ ft}^2$$

$$\frac{X_{ext} \sum_1^{N_L} e}{\sum_1^{N_b} x^2} = \frac{16.5 \text{ ft}(15.5 \text{ ft})}{605 \text{ ft}^2} = 0.423$$

Reaction on Exterior Beam:

$$R = m \left(\frac{N_L}{N_b} + \frac{X_{ext} \sum_1^{N_L} e}{\sum_1^{N_b} x^2} \right)$$

$$= 1.0 \times (0.5 + 0.423)$$

$$= 0.92 \text{ lanes}$$

For one lane loaded, AASHTO LRFD Table 4.6.2.2.d-1 resulted in a larger distribution factor than assuming a rigid cross-section; for multiple lanes loaded the opposite occurred. For the exterior girders, the distribution factor to be used in distribution the live load is 0.92.

Table 123. Exterior girder moment distribution factor summary.

	One Lane Loaded	Multiple Lanes Loaded					
		Spans 1 and 3			Span 2		
		A-A	B-B	C-C	A-A	B-B	C-C
M+ and M- (not between POC)							
Table 4.6.2.2.d-1	0.90	0.78	0.80	0.83	0.72	0.74	0.78
Rigid Cross-Section	0.75	0.92	0.92	0.92	0.92	0.92	0.92
M- (Between POC)							
		Section B-B			Section C-C		
Table 4.6.2.2.d-1	0.90	0.77	0.77	0.77	0.79	0.79	0.79
Rigid Cross-Section	0.75	0.92	0.92	0.92	0.92	0.92	0.92

APPENDIX 9B – EXAMPLE 2 GEOMETRY

Assuming that the origin is located at the left end of girder line 4 in Figure 193, the coordinates for the girder ends and cross-frames are shown in Tables 124 through 126. Each girder is defined by several segments with (at least) one between each cross-frame; changes in cross-section must also be included.

Table 124. Coordinates for girder and cross-frame ends – Span 1.

Component	Start			End		
	x (ft)	y (ft)	z (ft)	x (ft)	y (ft)	z (ft)
G1	0.0	33.0	0.0	160.0	33.0	0.0
G2	0.0	22.0	0.0	160.0	22.0	0.0
G3	0.0	11.0	0.0	160.0	11.0	0.0
G4	0.0	0.0	0.0	160.0	0.0	0.0
Cross-Frame 1-1 G1-G2	0.0	33.0	0.0	0.0	22.0	0.0
Cross-Frame 1-1 G2-G3	0.0	22.0	0.0	0.0	11.0	0.0
Cross-Frame 1-1 G3-G4	0.0	11.0	0.0	0.0	0.0	0.0
Cross-Frame 1-2 G1-G2	20.0	33.0	0.0	20.0	22.0	0.0
Cross-Frame 1-2 G2-G3	20.0	22.0	0.0	20.0	11.0	0.0
Cross-Frame 1-2 G3-G4	20.0	11.0	0.0	20.0	0.0	0.0
Cross-Frame 1-3 G1-G2	40.0	33.0	0.0	40.0	22.0	0.0
Cross-Frame 1-3 G2-G3	40.0	22.0	0.0	40.0	11.0	0.0
Cross-Frame 1-3 G3-G4	40.0	11.0	0.0	40.0	0.0	0.0
Cross-Frame 1-4 G1-G2	60.0	33.0	0.0	60.0	22.0	0.0
Cross-Frame 1-4 G2-G3	60.0	22.0	0.0	60.0	11.0	0.0
Cross-Frame 1-4 G3-G4	60.0	11.0	0.0	60.0	0.0	0.0
Cross-Frame 1-5 G1-G2	80.0	33.0	0.0	80.0	22.0	0.0
Cross-Frame 1-5 G2-G3	80.0	22.0	0.0	80.0	11.0	0.0
Cross-Frame 1-5 G3-G4	80.0	11.0	0.0	80.0	0.0	0.0
Cross-Frame 1-6 G1-G2	100.0	33.0	0.0	100.0	22.0	0.0
Cross-Frame 1-6 G2-G3	100.0	22.0	0.0	100.0	11.0	0.0
Cross-Frame 1-6 G3-G4	100.0	11.0	0.0	100.0	0.0	0.0
Cross-Frame 1-7 G1-G2	120.0	33.0	0.0	120.0	22.0	0.0
Cross-Frame 1-7 G2-G3	120.0	22.0	0.0	120.0	11.0	0.0
Cross-Frame 1-7 G3-G4	120.0	11.0	0.0	120.0	0.0	0.0
Cross-Frame 1-8 G1-G2	140.0	33.0	0.0	140.0	22.0	0.0
Cross-Frame 1-8 G2-G3	140.0	22.0	0.0	140.0	11.0	0.0
Cross-Frame 1-8 G3-G4	140.0	11.0	0.0	140.0	0.0	0.0

Table 125. Coordinates for girder and cross-frame ends – Span 2.

Component	Start			End		
	x (ft)	y (ft)	z (ft)	x (ft)	y (ft)	z (ft)
G1	160.0	33.0	0.0	370.0	33.0	0.0
G2	160.0	22.0	0.0	370.0	22.0	0.0
G3	160.0	11.0	0.0	370.0	11.0	0.0
G4	160.0	0.0	0.0	370.0	0.0	0.0
Cross-Frame 2-1 G1-G2	160.0	33.0	0.0	160.0	22.0	0.0
Cross-Frame 2-1 G2-G3	160.0	22.0	0.0	160.0	11.0	0.0
Cross-Frame 2-1 G3-G4	160.0	11.0	0.0	160.0	0.0	0.0
Cross-Frame 2-2 G1-G2	181.0	33.0	0.0	181.0	22.0	0.0
Cross-Frame 2-2 G2-G3	181.0	22.0	0.0	181.0	11.0	0.0
Cross-Frame 2-2 G3-G4	181.0	11.0	0.0	181.0	0.0	0.0
Cross-Frame 2-3 G1-G2	202.0	33.0	0.0	202.0	22.0	0.0
Cross-Frame 2-3 G2-G3	202.0	22.0	0.0	202.0	11.0	0.0
Cross-Frame 2-3 G3-G4	202.0	11.0	0.0	202.0	0.0	0.0
Cross-Frame 2-4 G1-G2	227.4375	33.0	0.0	227.4375	22.0	0.0
Cross-Frame 2-4 G2-G3	227.4375	22.0	0.0	227.4375	11.0	0.0
Cross-Frame 2-4 G3-G4	227.4375	11.0	0.0	227.4375	0.0	0.0
Cross-Frame 2-5 G1-G2	244.0	33.0	0.0	244.0	22.0	0.0
Cross-Frame 2-5 G2-G3	244.0	22.0	0.0	244.0	11.0	0.0
Cross-Frame 2-5 G3-G4	244.0	11.0	0.0	244.0	0.0	0.0
Cross-Frame 2-6 G1-G2	265.0	33.0	0.0	265.0	22.0	0.0
Cross-Frame 2-6 G2-G3	265.0	22.0	0.0	265.0	11.0	0.0
Cross-Frame 2-6 G3-G4	265.0	11.0	0.0	265.0	0.0	0.0
Cross-Frame 2-7 G1-G2	286.0	33.0	0.0	286.0	22.0	0.0
Cross-Frame 2-7 G2-G3	286.0	22.0	0.0	286.0	11.0	0.0
Cross-Frame 2-7 G3-G4	286.0	11.0	0.0	286.0	0.0	0.0
Cross-Frame 2-8 G1-G2	307.0	33.0	0.0	307.0	22.0	0.0
Cross-Frame 2-8 G2-G3	307.0	22.0	0.0	307.0	11.0	0.0
Cross-Frame 2-8 G3-G4	307.0	11.0	0.0	307.0	0.0	0.0
Cross-Frame 2-9 G1-G2	328.0	33.0	0.0	328.0	22.0	0.0
Cross-Frame 2-9 G2-G3	328.0	22.0	0.0	328.0	11.0	0.0
Cross-Frame 2-9 G3-G4	328.0	11.0	0.0	328.0	0.0	0.0
Cross-Frame 2-10 G1-G2	349.0	33.0	0.0	349.0	22.0	0.0
Cross-Frame 2-10 G2-G3	349.0	22.0	0.0	349.0	11.0	0.0
Cross-Frame 2-10 G3-G4	349.0	11.0	0.0	349.0	0.0	0.0

Span 2

Table 126. Coordinates for girder and cross-frame ends – Span 3.

Component	Start			End		
	x (ft)	y (ft)	z (ft)	x (ft)	y (ft)	z (ft)
G1	370.0	33.0	0.0	530.0	33.0	0.0
G2	370.0	22.0	0.0	530.0	22.0	0.0
G3	370.0	11.0	0.0	530.0	11.0	0.0
G4	370.0	0.0	0.0	530.0	0.0	0.0
Cross-Frame 3-1 G1-G2	370.0	33.0	0.0	370.0	22.0	0.0
Cross-Frame 3-1 G2-G3	370.0	22.0	0.0	370.0	11.0	0.0
Cross-Frame 3-1 G3-G4	370.0	11.0	0.0	370.0	0.0	0.0
Cross-Frame 3-2 G1-G2	390.0	33.0	0.0	390.0	22.0	0.0
Cross-Frame 3-2 G2-G3	390.0	22.0	0.0	390.0	11.0	0.0
Cross-Frame 3-2 G3-G4	390.0	11.0	0.0	390.0	0.0	0.0
Cross-Frame 3-3 G1-G2	410.0	33.0	0.0	410.0	22.0	0.0
Cross-Frame 3-3 G2-G3	410.0	22.0	0.0	410.0	11.0	0.0
Cross-Frame 3-3 G3-G4	410.0	11.0	0.0	410.0	0.0	0.0
Cross-Frame 3-4 G1-G2	430.0	33.0	0.0	430.0	22.0	0.0
Cross-Frame 3-4 G2-G3	430.0	22.0	0.0	430.0	11.0	0.0
Cross-Frame 3-4 G3-G4	430.0	11.0	0.0	430.0	0.0	0.0
Cross-Frame 3-5 G1-G2	450.0	33.0	0.0	450.0	22.0	0.0
Cross-Frame 3-5 G2-G3	450.0	22.0	0.0	450.0	11.0	0.0
Cross-Frame 3-5 G3-G4	450.0	11.0	0.0	450.0	0.0	0.0
Cross-Frame 3-6 G1-G2	470.0	33.0	0.0	470.0	22.0	0.0
Cross-Frame 3-6 G2-G3	470.0	22.0	0.0	470.0	11.0	0.0
Cross-Frame 3-6 G3-G4	470.0	11.0	0.0	470.0	0.0	0.0
Cross-Frame 3-7 G1-G2	490.0	33.0	0.0	490.0	22.0	0.0
Cross-Frame 3-7 G2-G3	490.0	22.0	0.0	490.0	11.0	0.0
Cross-Frame 3-7 G3-G4	490.0	11.0	0.0	490.0	0.0	0.0
Cross-Frame 3-8 G1-G2	510.0	33.0	0.0	510.0	22.0	0.0
Cross-Frame 3-8 G2-G3	510.0	22.0	0.0	510.0	11.0	0.0
Cross-Frame 3-8 G3-G4	510.0	11.0	0.0	510.0	0.0	0.0
Cross-Frame 3-8 G1-G2	530.0	33.0	0.0	530.0	22.0	0.0
Cross-Frame 3-8 G2-G3	530.0	22.0	0.0	530.0	11.0	0.0
Cross-Frame 3-8 G3-G4	530.0	11.0	0.0	530.0	0.0	0.0

APPENDIX 9C - EXAMPLE 2 EQUIVALENT PIER CROSS-FRAME CALCULATIONS

Figures 420 and 421 show the models created and analyzed to estimate the flexural and shear stiffness.

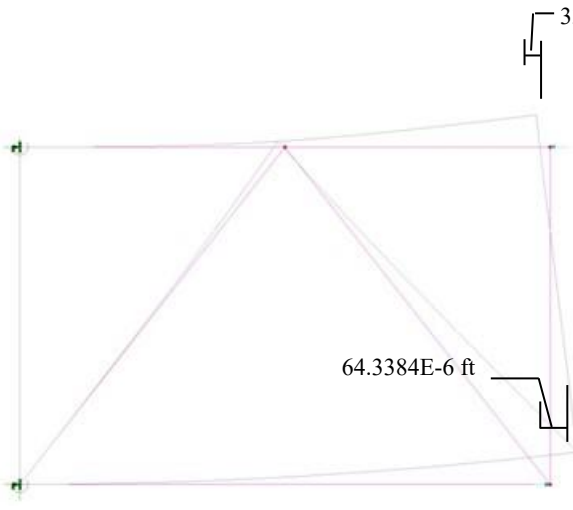


Figure 420. Illustration. Pier cross-frame - flexural stiffness model.

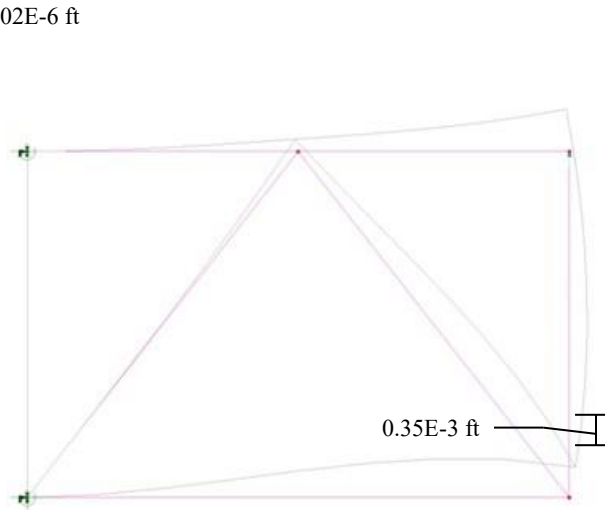


Figure 421. Illustration. Pier cross-frame - shear stiffness model.

Determine rotation at free end of cross-frame:

$$\theta = \frac{(\Delta_{top} + \Delta_{bottom}) \frac{12in}{ft}}{d} = \frac{((33.2402E-6)ft + (64.3384E-6)ft) \frac{12in}{ft}}{84in} = 1.39398 \times 10^{-5} \text{ radians}$$

Determine equivalent moment of inertia:

$$I_{eq} = \frac{ML}{E\theta} = \frac{84k-in \times 132in}{29000ksi \times 1.39398 \times 10^{-5}rad} = 27428.3in^4 = 1.323ft^4$$

Determine cross-frame centroid:

$$\Delta_{top} = 63.2475 \times 10^{-6} \text{ ft (from analysis model)}$$

$$\Delta_{bottom} = 58.3866 \times 10^{-6} \text{ ft (from analysis model)}$$

$$d = 7 \text{ ft (distance between centroids of cross-frame chords)}$$

Using similar triangles:

$$\frac{x}{\Delta_{top}} = \frac{d-x}{\Delta_{bottom}}$$

Solve for "x":

$$x = \frac{\Delta_{top} \times d}{\Delta_{top} + \Delta_{bottom}}$$

Substitute in for Δ_{top} , Δ_{bottom} , and d :

$$x = \frac{(33.2402 \times 10^{-6})ft \times 7ft}{(33.2402 \times 10^{-6})ft + (64.3384 \times 10^{-6})ft} = 2.38ft$$

Determine cross-frame offset:

$$Offset = x - \frac{d}{2} = 2.38ft - \frac{7ft}{2} = -1.12ft$$

Determine equivalent shear area:

$$A_{eq,v} = \frac{VL}{G\left(\Delta - \frac{VL^3}{3EI_{eq}}\right)} = \frac{1kip \times 132in}{11154ksi\left(0.0042in - \frac{1kip \times (132in)^3}{3 \times 29000ksi \times 27428.3in^4}\right)} = 3.66in^2$$

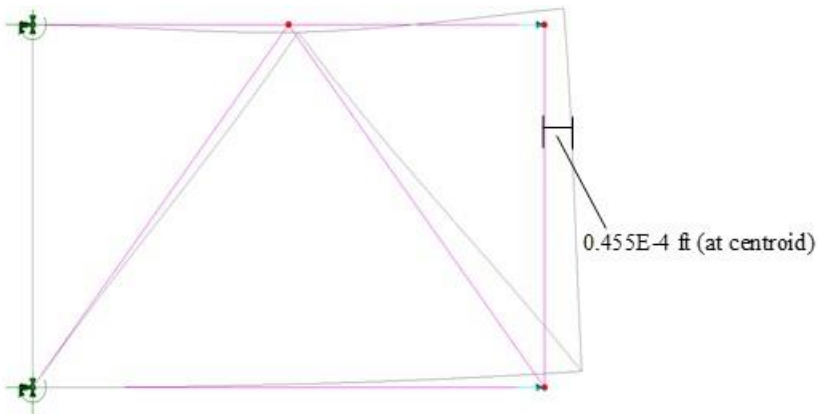


Figure 422. Illustration. Pier cross-frame - axial stiffness model.

Figure 422 shows the model created and analyzed to estimate the axial stiffness.

$$A_{eq,p} = \frac{2PL}{E\Delta} = \frac{2kip \times 132in}{29000ksi(0.455 \times 10^{-4}ft \times 12in/ft)} = 33.346in^2 = 0.232ft^2$$

Determine weight of cross-frame components:

- Top Chord (L8×8×¾)
 $W_{L8 \times 8 \times 3/4} = 38.9 \text{ lb/ft}$, $L = 10.5 \text{ ft}$, $W_{TC} = 38.9 \text{ lb/ft} \times 10.5 \text{ ft} = 408.5 \text{ lbs}$
- Bottom Chord (L5×5×⅝)
 $W_{L5 \times 5 \times 5/8} = 20 \text{ lb/ft}$, $L = 10.5 \text{ ft}$, $W_{BC} = 20 \text{ lb/ft} \times 10.5 \text{ ft} = 210 \text{ lbs}$
- Diagonals (L5×5×⅝)
 $W_{L5 \times 5 \times 5/8} = 20 \text{ lb/ft}$, $L = 8.75 \text{ ft}$, $W_{BC} = 20 \text{ lb/ft} \times 8.75 \text{ ft} = 175 \text{ lbs}$
- Connection Plate (⅜ inch x 8.5 inches x 92 inches)
 $V_{CP} = 5/8 \text{ inch} \times 8.5 \times 92 \text{ inches} = 488.75 \text{ in}^3 = 0.283 \text{ ft}^3$

$$W_{CP} = V_{CP} \times \gamma_{\text{steel}} = 0.283 \text{ ft}^3 \times 490 \text{ lb/ft}^3 = 138.6 \text{ lbs}$$

Determine weight of cross-frame:

$$\begin{aligned} W_{CF} &= W_{TC} + W_{BC} + 2 \times W_D + 2 \times W_{CP} \\ &= 408.5 \text{ lbs} + 210 \text{ lbs} + 2 \times 175 \text{ lbs} + 2 \times 138.6 \text{ lbs} = 1246 \text{ lbs} \\ &= 1.25 \text{ kips} \end{aligned}$$

Determine equivalent area of cross-frame:

$$A_{cf} = \frac{W_{CF}}{\gamma_s L} = \frac{1.25 \text{ kips}}{0.490 \frac{\text{kip}}{\text{ft}^3} \times 11 \text{ ft}} = 0.232 \text{ ft}^2$$

Therefore, modify the unit weight,

$$\gamma_{cf} = \frac{A_{cf}}{A_{eq,p}} \gamma = \frac{0.232 \text{ ft}^2}{0.232 \text{ ft}^2} 0.490 \text{ k/ft}^3 = 0.490 \text{ k/ft}^3$$

APPENDIX 9D - EXAMPLE 3 GIRDER SECTION PROPERTIES

Table 127. Example 3 Girder G1 section properties.

Location Along Span (ft)	Cross-section Area (A) (ft ²)	Strong Axis Moment of Inertia (I _{yy}) (ft ⁴)	Weak Axis Moment of Inertia (I _{zz}) (ft ⁴)	Eff. Torsion Constant (J _{xx}) (ft ⁴)	Shear Area in y direction (A _{vy}) (ft ²)	Shear Area in z direction (A _{vz}) (ft ²)	Offset in z direction (R _z) (ft)
0.000	0.622	5.293	0.033	0.010	0.222	0.399	0.000
79.500	0.698	6.402	0.064	0.069	0.299	0.399	0.000
103.500	0.997	11.025	0.127	0.147	0.597	0.399	0.000
151.500	0.698	6.402	0.064	0.036	0.299	0.399	0.000
170.500	0.677	6.127	0.064	0.095	0.278	0.399	0.000
284.542	0.814	8.091	0.153	0.161	0.415	0.399	0.000
308.542	1.229	14.462	0.305	0.340	0.830	0.399	0.000
356.542	0.814	8.091	0.153	0.085	0.415	0.399	0.000
372.542	0.705	6.544	0.086	0.122	0.306	0.399	0.000

Table 128. Example 3 Girder G2 section properties.

Location Along Span (ft)	Cross-section Area (A) (ft ²)	Strong Axis Moment of Inertia (I _{yy}) (ft ⁴)	Weak Axis Moment of Inertia (I _{zz}) (ft ⁴)	Eff. Torsion Constant (J _{xx}) (ft ⁴)	Shear Area in y direction (A _{vy}) (ft ²)	Shear Area in z direction (A _{vz}) (ft ²)	Offset in z direction (R _z) (ft)
0.000	0.622	5.293	0.033	0.009	0.222	0.399	0.000
102.083	0.729	6.868	0.086	0.089	0.330	0.399	0.000
126.083	1.059	11.977	0.171	0.190	0.660	0.399	0.000
174.083	0.729	6.868	0.086	0.123	0.330	0.399	0.000
193.083	0.677	6.127	0.064	0.092	0.278	0.399	0.000
310.438	0.748	7.117	0.091	0.094	0.349	0.399	0.000
334.438	1.097	12.471	0.182	0.200	0.698	0.399	0.000
382.438	0.748	7.117	0.091	0.127	0.349	0.399	0.000
398.438	0.677	6.127	0.064	0.064	0.278	0.399	0.000

Table 129. Example 3 Girder G3 section properties.

Location Along Span (ft)	Cross-section Area (A) (ft ²)	Strong Axis Moment of Inertia (I _{yy}) (ft ⁴)	Weak Axis Moment of Inertia (I _{zz}) (ft ⁴)	Eff. Torsion Constant (J _{xx}) (ft ⁴)	Shear Area in y direction (A _{vy}) (ft ²)	Shear Area in z direction (A _{vz}) (ft ²)	Offset in z direction (R _z) (ft)
0.000	0.649	5.710	0.047	0.013	0.250	0.399	0.000
115.698	0.783	7.731	0.099	0.101	0.384	0.399	0.000
140.698	1.167	13.818	0.198	0.202	0.767	0.399	0.000
195.698	0.783	7.731	0.099	0.099	0.384	0.399	0.000
219.698	0.649	5.710	0.047	0.047	0.250	0.399	0.000
327.354	0.748	7.117	0.091	0.091	0.349	0.399	0.000
352.354	1.097	12.471	0.182	0.180	0.698	0.399	0.000
407.354	0.748	7.117	0.091	0.088	0.349	0.399	0.000
432.354	0.622	5.293	0.033	0.032	0.222	0.399	0.000

Table 130. Example 3 Girder G4 section properties.

Location Along Span (ft)	Cross-section Area (A) (ft ²)	Strong Axis Moment of Inertia (I _{yy}) (ft ⁴)	Weak Axis Moment of Inertia (I _{zz}) (ft ⁴)	Eff. Torsion Constant (J _{xx}) (ft ⁴)	Shear Area in y direction (A _{vy}) (ft ²)	Shear Area in z direction (A _{vz}) (ft ²)	Offset in z direction (R _z) (ft)
0.000	0.719	6.749	0.098	0.025	0.319	0.399	0.000
35.000	0.760	7.333	0.112	0.110	0.361	0.399	0.000
93.406	0.719	6.749	0.098	0.096	0.319	0.399	0.000
136.406	0.957	10.313	0.309	0.165	0.558	0.399	0.000
161.406	1.516	19.102	0.618	0.586	1.116	0.399	0.000
216.406	0.957	10.313	0.309	0.296	0.558	0.399	0.000
240.406	0.677	6.127	0.064	0.062	0.278	0.399	0.000
351.323	0.791	7.720	0.129	0.070	0.391	0.399	0.000
376.323	1.182	13.687	0.258	0.245	0.783	0.399	0.000
431.323	0.791	7.720	0.129	0.120	0.391	0.399	0.000
456.323	0.649	5.710	0.047	0.044	0.250	0.399	0.000

GLOSSARY OF TECHNICAL TERMS

1D Analysis – a simple analysis type characterized by replacing the structure with a single series of line elements along the structure’s length. To account for the transverse distribution of load, which is not explicitly considered, assumptions must be made with respect to tributary widths, and live load distribution factors must be applied.

2D Analysis – an analysis that explicitly considers the transverse distribution of load by incorporating structure width in addition to its length. As a result, live load distribution factors are not applied. Types of 2D analysis include grid/grillage analysis and plate and eccentric beam (PEB) analysis.

3D Analysis – an analysis that considers the full geometry of the structure, including member depth. Depending on the application, any combination of beam elements, shell elements, or solid elements may be used.

Approximate Methods – In the context of this report, approximate methods refer to the methods of design detailed in the LRFD Bridge Design Specification. These simplified methods generally can be performed by hand, provide conservative results, and despite having a limited range of applicability, are applicable in many typical cases such as straight unskewed multigirder bridges.

Aspect Ratio – Ratio of the length to width of a rectangle.

Boundary Condition – Restraints assigned to nodes in a model to represent support/restraint provided by unmodeled structure/supports.

Bounded Solution – Approach to solving a problem when exact conditions may not be known. Usually involves applying alternate assumptions such that the actual solution lies between two bounds created by those assumptions.

Central Angle – Angle between the two radii connected to the ends of a curved girder.

Closed Form Solution – One or more equations, including those based on convergent series, that permit calculation of force effects by the direct introduction of loads and structural parameters.

Compatibility – The geometrical equality of movement at the interface of joined components.

Composite – A combination of two or more materials acting together to form a single component.

Constraint – A way of connecting two or more nodes such that they have a defined relationship for a given degree of freedom.

Contact Element – Similar to a one way element, an element that only transmits forces when the nodes are in contact.

Cracked Concrete Section – A section where properties are based on the compression area of the concrete and the transformed area of the reinforcing steel.

Creep – Phenomenon where the strain in a material continues to increase over time under constant stress.

Degrees of Freedom – Number of translations or rotations required to define the movement of a node.

Dilatancy – The volume expansion observed in granular materials when they are subjected to shear deformations. Due to dilatancy, the angle of friction increases as the confinement increases until it reaches a peak value.

Direct Stiffness Method – The matrix analysis method that is the basis for most finite element analysis programs, structures are discretized into a number of elements, element stiffness matrices are generated in local reference systems, then transformed to a global reference system and directly assembled together to create the overall structure stiffness matrix. The stiffness matrix is inverted and multiplied by the structure force matrix to solve for the unknown displacements.

Distortion Induced Fatigue – Fatigue due to stresses induced by deflections, typically unintentional, rather than directly applied loads.

Distribution Factor – A factor determining how much of a design lane is carried by any particular girder or stringer.

Disturbed Regions – Regions in a concrete structure near concentrated loads or abrupt section changes where stresses do not follow beam section behavior.

Effective Width – A notional width of deck over which the stress is assumed to be uniform and equal to the maximum stress in the deck. The width is approximated such that the total force is equal to the sum total force carried over the actual width of participating deck.

Effective Shear Area – Also known as the shear form factor, the area in a given plane assigned to a Timoshenko beam element which is effective in resisting shear deformation.

Element – A point, line, surface, or volume used to provide connectivity between nodes in a finite element analysis.

Euler-Bernoulli Beam – Beam element formulation that excludes shear deformation.

Finite Element Method – A method of analysis in which a structure is discretized into elements connected at nodes, and structural analysis performed utilizing the direct stiffness method.

First-Order Analysis – An analysis in which the equilibrium conditions are formulated on the undeformed geometry.

Flexibility Method – A solution method wherein the member forces are treated as the unknowns, and are solved for. Also called the method of consistent deformations Its modern version formulated in terms of the members' flexibility matrices also has the name **Matrix Force Method**.

Force Effect – A deformation, stress, or stress resultant, i.e., axial force, shear force, flexural or torsional moment caused by applied loads, imposed deformations, or volumetric changes.

Gap Element – Element used to represent a gap, where for a certain range of values of relative displacement across the element, no stiffness is present.

Gauss Numerical Integration – Also known as Gaussian Quadrature, a numerical integration technique that minimizes internal integration points and locates them so as to minimize integration error when the integrand is a general polynomial.

Gauss Points – Points within an element at which Gaussian Quadrature or Gauss numerical integration solutions are performed.

GIGO – Garbage In = Garbage Out.

Grid Method – Analysis consisting of concentrating the longitudinal and transverse stiffness properties of the bridge structure into a network of line elements in a plane.

Grillage Method – See **Grid Method**.

Gross Concrete Section – Section properties are based on the concrete dimensions and generally neglect any internal reinforcing.

Hot Spot Stress – The value of the stress at a defined location near a point of stress concentration. Also see **Local Structural Stress**.

Ill-conditioned matrix – A matrix is ill-conditioned if the Condition Number, the ratio C of the largest to smallest singular value in the singular value decomposition of a matrix, is large. With an ill-conditioned matrix a small change in an input parameter can result in a large change in an output parameter.

Influence Line/Surface – A line or surface that shows the effect of a unit load applied at the locations along the line or surface on a specific force effect at a specific point.

Kirchoff-Love Shell – Shell element formulation that excludes through-thickness shear deformations.

Legal Load – Refers to provisions which vary by state governing the limiting weights and dimensions for trucks permitted to travel without permits in the normal traffic flow.

Limit State – A condition beyond which the bridge or component ceases to satisfy the provisions for which it was designed.

Line Girder – A single idealized girder which approximates the behavior of the girder as a part of the bridge.

Local Structural Stress – The value of the stress at a defined location near a point of stress concentration. Also see **Hot Spot Stress**.

Lower Bound – The lowest value of a solution to a problem given the range of starting assumptions.

McHenry Lattice – A technique where a lattice of beam elements can be used to approximate the behavior of a shell structure.

Mesh – A series of discrete elements connected at nodes.

Mindlin-Reissner Shell – Shell element formulation that includes through thickness shear deformations.

Mode Shape – Shape a structure takes for a given mode of vibration. A function of the stiffness and mass, and its distribution, of a structure.

Modular Ratio – The modulus of elasticity of one material divided by the modulus of elasticity of a second material.

Mohr's Circle – A two-dimensional graphical representation of the transformation law for the stress tensor.

M/R Method – An approximate method in which curved box girders are represented by equivalent straight girders to calculate flexural effects and as a corresponding straight conjugate beam to calculate the concomitant Saint-Venant torsional moments due to curvature.

Müller-Breslau Principle – The influence lines of an action (force or moment) is a scaled form of the deflection that the structure displays after removing the restraint on the point where the action is evaluated and applying a concentrated load or moment at that point which causes a unit displacement.

Multiple Presence Factor – A factor applied to account for the reduced probability that multiple lanes are maximally loaded simultaneously.

Node – Point at which elements are connected in a finite element analysis.

No Load Fit – Fit-up of steel cross-frames is based on the undeflected shape.

Nuisance Stiffness – Generally refers to the effects of cross-frames in bridges with high width-to-span-length ratios and severe skew. The cross-frames which frame toward the obtuse corners of the bridge can provide a transverse load path with significant stiffness, attracting significant loads, which can also result in increased shear, end reactions, and flange lateral bending in the girders.

One-way Element – Element that only has stiffness in one direction.

Patch Load – Specified load acting in a specified direction applied over an area.

Permit Vehicle – Any vehicle whose right to travel is administratively restricted in any way due to its weight or size.

Plastic Hinge – A yielded zone which forms in a structural member when the plastic moment is attained. The member is then assumed to rotate as if hinged, except that the plastic moment capacity is maintained within the hinge.

Plastic Moment – The resisting moment of a fully yielded cross-section.

Plate and Eccentric Beam (PEB) Model – a specific kind of 2D analysis that incorporates the use of eccentricities to locate the bridge deck and supporting members to their correct relative position in space. Shell elements are used to model the deck and beam elements are used to model the girders.

Principal Stress – A principal stress is any one of three orthogonal components of the stress tensor when the basis is changed in such a way that the shear stress components become zero.

Primary Prestressing Moment – Moment induced due the eccentricity of the tendon in a prestressed member.

Redundant Forces – Forces whose removal result in a statically determinate structure.

Restraint – Usually refers to the degrees of freedom that are defined to develop reactions at boundary conditions.

Rigid Link – Connection between nodes that results in the nodes deflecting as a rigid unit through all degrees of freedom.

Saint-Venant Torsion – That portion of the internal resisting torsion in a member producing only pure shear stresses on a cross-section; also referred to as pure torsion or uniform torsion.

Second-Order Analysis - An analysis in which the equilibrium conditions are formulated based on the deformed geometry.

Second-Order Stiffness Softening – Refers to the fact that second order effects due to compression can sometimes be modeled as a first order reduction in stiffness.

Secondary Prestressing Moment – Moment induced due to prestressing and enforced compatibility in an indeterminate structure such as a continuous beam.

Shape Functions – Polynomial function approximations of the deflected shape of an element between nodes.

Shear Lag – Nonlinear distribution of normal stress across a component due to shear distortion.

Shear Locking – Also known as “parasitic shear”. The problem manifests itself when shear strains become vanishingly small compared to bending strains, such as in cases of pure bending, and results in overly stiff behavior of the elements.

Shrinkage – Phenomenon where changes in pore water content can cause significant volume changes in concrete in load-free specimens.

Site-Specific Load – A load that is unique to a given geographical location.

Skew Angle – Angle between the centerline of a support and a line normal to the roadway centerline.

Small Deflection Theory – A basis for methods of analysis where the effects of deformation upon force effects in the structure are neglected

Software Bug – An error in the code of the software.

Solver – The specific technique used by the finite element program to solve the simultaneous equations.

Spine Beam Analysis – a special case of 1D analysis for use in torsionally stiff, closed cross-sections with spans at least 2.5 times their widths. The superstructure, typically composed of horizontally curved concrete box girders, is replaced with a single series of line elements called a “spine beam.” See Sections 2.4.2, 3.5, and 9.4 for further discussion.

Statically Equivalent Loadings – Loadings that produce the equivalent force effects.

Stiffness Method – A traditional structural analysis method that uses member displacements as the primary unknowns. Its modern version formulated in terms of the members' stiffness matrices also has the name **Matrix Displacement Method**.

Steel Dead Load Fit – Fit-up of steel cross-frames is based on the deflected shape of the steel dead load only.

Stress Integration – Integration of stresses over a cross-sectional area in order to find the equivalent stress resultants, or forces.

Stress Tensor – Also known as the Cauchy Stress Tensor, is a second order tensor with nine components that completely define the state of stress at a point.

Strut and Tie – An analysis technique which idealizes a concrete member as a truss made up of concrete compression struts and steel ties.

Submodeling/Substructuring – Technique of using a larger coarse mesh model to determine the global forces and/or displacements at the boundaries of a smaller finer mesh model.

Superposition – The situation where the force effect for one loading can be added to the force effect of another loading. Only applicable when the stress-strain relation is linear elastic and small deflection theory is valid.

Time Dependent Analysis – Analysis that takes into account the changes in properties over time.

Time History Analysis – Analysis of a given structure under a time dependent loading over a specified time interval.

Timoshenko Beam – Beam element formulation that includes shear deformation.

Total Dead Load Fit – Fit-up of steel cross-frames is based on the deflected shape under total dead load.

Transformed Section – A method of converting a member consisting of two dissimilar materials into an equivalent section consisting of a single material using elastic modular ratios.

Transition Mesh – The region of mesh between a fine portion and a coarse portion of a mesh.

Upper Bound – Highest possible value to the solution to a problem.

Validation – The process of ensuring that the refined analysis accurately represents the behavior of an actual structure.

Verification – The process of ensuring that the refined analysis is providing correct results.

V-Load Method – An approximate method in which curved I-girders are represented by equivalent straight girders and the effects of curvature are represented by vertical and lateral forces applied at the cross-frame locations. Flange lateral bending at brace points due to curvature is estimated.

Warping Torsion – That portion of the internal resisting torsion that produces normal stresses and distortion of the cross-section.

Winkler Springs – An idealization that represents soil as a system of identical but mutually independent, closely spaced, discrete, springs. Analogous to a beam on elastic foundation.

Wobble Friction – The friction caused by the deviation of a tendon duct or sheath from its specified profile.



U.S. Department of Transportation
Federal Highway Administration

FHWA-HIF-18-046